DOT/FAA/TC-25/1

Federal Aviation Administration
William J. Hughes Technical Center
Aviation Research Division
Atlantic City International Airport
New Jersey 08405

Frost Thickness and Roughness Evolution on Cold Soaked, Fuel-Laden Wings

March 2026

Final report

U.S. Department of Transportation
Federal Aviation Administration

NOTICE

This document is disseminated under the sponsorship of the U.S. Department of Transportation in the interest of information exchange. The U.S. Government assumes no liability for the contents or use thereof. The U.S. Government does not endorse products or manufacturers. Trade or manufacturers' names appear herein solely because they are considered essential to the objective of this report. The findings and conclusions in this report are those of the author(s) and do not necessarily represent the views of the funding agency. This document does not constitute FAA policy. Consult the FAA sponsoring organization listed on the Technical Documentation page as to its use.

This report is available at the Federal Aviation Administration William J. Hughes Technical Center's Full-Text Technical Reports page: actlibrary.tc.faa.gov in Adobe Acrobat portable document format (PDF).

Technical Report Documentation Page

Form DOT F 1700.7 (8-72) Reproduction of completed page authorized

1. Report No.	2. Government Accession No.	3. Recipient's Catalog No.
DOT/FAA/TC-25/1		

4. Title and Subtitle	5. Report Date
Frost Thickness and Roughness Evolution on Cold-Soaked, Fuel-Laden Wings	March 2026
	6. Performing Organization Code

7. Author(s)	8. Performing Organization Report No.
Stephen T. McClain, Dennis L. O'Neal, Tongxin Zhang, Taber Miyauchi, Nicholas Forslund	

9. Performing Organization Name and Address	10. Work Unit No. (TRAIS)
Baylor University One Bear Place 97360 Waco, TX 76798-7360	11. Contract or Grant No. 17-G-011

12. Sponsoring Agency Name and Address	13. Type of Report and Period Covered
Federal Aviation Administration (FAA)	14. Sponsoring Agency Code AFS-200

15. Supplementary Notes

16. Abstract

Frost that forms on the surface of wings with fuel remaining in integrated fuel tanks following a flight is referred to as *cold soaked fuel frost*. Frost roughness was characterized using two experimental facilities which provided different methods for capturing the thermodynamic environment representing the cold soaked fuel frost growth process. A photogrammetric approach was developed to measure frost roughness and used in each facility. Modeling approaches were developed to predict the evolution of cold-soaked fuel frost roughness characteristics.

17. Key Words	18. Distribution Statement
Frost, Cold-soaked fuel frost, Frost Modeling	This document is available to the U.S. public through the National Technical Information Service (NTIS), Springfield, Virginia 22161. This document is also available from the Federal Aviation Administration William J. Hughes Technical Center at actlibrary.tc.faa.gov.

19. Security Classif. (of this report)	20. Security Classif. (of this page)	21. No. of Pages	19. Security Classif. (of this report)
Unclassified	Unclassified	532	Unclassified

Contents

1 Introduction 1

2 Frost evolution background 2

3 Baylor Frost Tunnel 4

4 Baylor Climatic Chamber and Aviation Frost Facility 6

4.1 Climatic chamber 7

4.2 Wing-tank thermal model and primary coolant system 8

4.3 Wind tunnel 9

4.4 Wing skin design 10

4.5 Testing procedure 13

5 Photogrammetric frost measurements 15

5.1 Photogrammetry approach in the Baylor Frost Tunnel 17

5.2 Photogrammetry approach in CAFF 19

5.3 Point cloud statistical reduction 24

6 Summary of Baylor Frost Tunnel frost measurements 25

6.1 Analysis of variance study of Miyauchi et al. 26

6.2 Roughness, thickness, and surface temperature study of Zhang et al. 30

6.2.1 Roughness variations in the sample regions 31

6.2.2 Thickness and roughness measurements 34

6.2.3 Surface temperature measurements 36

6.2.4 Empirical correlation development 37

7 Summary of Climatic Chamber and Aviation Frost Facility frost measurements 39

7.1 Climatic Chamber and Aviation Frost Facility measurements on painted aluminum skins 40

7.1.1 Measurements without rib structure 40

7.1.2 Measurements with aluminum rib 43

7.2 Climatic Chamber and Aviation Frost Facility measurements on painted carbon fiber skins 48

7.2.1 Measurements without rib structure 48

7.2.2 Measurements with aluminum rib 54

8 Carbon fiber skin thermal conductivity 60

8.1 Thermal conductivity apparatus 60

8.2 Thermal conductivity measurement procedure 61

8.3 Carbon fiber thermal conductivity results 63

9 Frost and roughness evolution modeling 64

9.1 Cold soaked fuel frost thermal and mass transfer circuits 64

9.2 Fuel or fuel surrogate thermal properties 65

9.3 Internal convective heat transfer coefficient 66

9.4 Skin thermal conductivity 66

9.5 Moist air properties 67

9.6 External convective heat transfer 68

9.7 Frost density and thermal conductivity 69

9.8 Instantaneous frost growth model 69

9.9 Heat transfer and frost temperature algorithm 70

9.10 Instantaneous frost roughness model 70

9.11 Application to selected cases 71

10 Summary 75

11 References 76

A Appendix A: Baylor Frost Tunnel case reports using an unpainted aluminum coupon A-1

B Appendix B: CAFF test reports using an aluminum skin without a structural rib ... B-1

C Appendix C: CAFF test reports using an aluminum skin with structural rib C-1

D Appendix D: CAFF test reports using a carbon fiber skin without structural rib D-1

E Appendix E: CAFF test reports using a carbon fiber skin with aluminum structural rib E-1

Figures

Figure 1. Schematic of the BFT 4
Figure 2. Detailed schematic of the BFT test section 5
Figure 3. Assembled and exploded view of the BFT thermal stage 6
Figure 4. Climatic Chamber and Aviation Frost Facility (CAFF) layout 7
Figure 5. Image from inside the CAFF showing most major equipment 8
Figure 6. Wing-tank thermal model: (a) top view and (b) isometric view 9
Figure 7. Wing tank and wind tunnel configuration for frost measurement 10
Figure 8. Skin design and access layout 11
Figure 9. Photo of aluminum skin with thermocouple bulkhead feedthrough and expansion tank connection 11
Figure 10. (a) Aluminum skin with rib and (b) instrumentation attached 12
Figure 11. Carbon fiber skin with aluminum rib structure during instrumentation construction . 12
Figure 12. View of the test section: (a) with foam covering prior to test, (b) immediately following foam removal, and (c) following frost testing 14
Figure 13. Time-lapse video images from CAFF test 091621: (a) image immediately following foam removal and (b) image following 120 min. of frost growth 15
Figure 14. BFT photogrammetric setup 18
Figure 15. Photogrammetric model of a scale bar with constraining control points and slope 18
Figure 16. Percent difference of photogrammetric method with increasing roughness and a detailed height distribution comparison 19
Figure 17. View of the test section from above, demonstrating the three-axis stepper-controlled photogrammetry system 20
Figure 18. Camera locations and image overlap 21
Figure 19. Error report for camera locations 22
Figure 20. Aligned camera locations and surface tie points 23
Figure 21. Example surface point cloud 24
Figure 22. Roughness topography map for Case 052318.01 27
Figure 23. RMS roughness height variation for ANOVA cases from Miyauchi, McClain, Zhang, and O'Neal 28
Figure 24. Surface skewness variation for ANOVA cases from Miyauchi, McClain, Zhang, and O'Neal 28
Figure 25. Calculated equivalent sand-grain roughness height variation for ANOVA cases from Miyauchi, McClain, Zhang, and O'Neal 29

Figure 26. Demonstration of the influence of various factors affecting frost roughness 30
Figure 27. Example frost morphology and feature variations along the BFT sample 32
Figure 28. Example roughness evolution on BFT surface (T_s = -10 C, T_{air} = 12 C, RH = 70%, V_{air} = 1 m/s): a) RMS roughness height; b) skewness; and c) equivalent sand-grain roughness height 33
Figure 29. Demonstration of frost thickness measurements in the BFT 34
Figure 30. RMS roughness measurements from the cases in the BFT 35
Figure 31. Calculated equivalent sand-grain roughness measurements from the cases in the BFT 35
Figure 32. Frost thickness measurements from the cases in the BFT 36
Figure 33. Infrared thermometer installation on the BFT for frost surface temperature measurements 36
Figure 34. Frost surface temperature measurements in the BFT 37
Figure 35. Correlation of BFT measured quantities: a) frost thickness and b) frost surface temperature 38
Figure 36. Comparison of experimental roughness and correlation predictions: a) RMS roughness and b) equivalent sand-grain roughness 39
Figure 37. CAFF measurements of frost roughness using aluminum skin without rib structure at x = 20.75 in. from leading edge: a) RMS roughness, b) skewness, c) predicted equivalent sand-grain roughness, and d) peak-to-valley height 42
Figure 38. Frost surrounding rib screw head following 031820 frost test 44
Figure 39. CAFF measurements of frost roughness using aluminum skin with a rib structure at x = 11.75 in. from leading edge: a) RMS roughness; b) skewness; c) predicted equivalent sand-grain roughness; and d) peak-to-valley height 45
Figure 40. CAFF measurements of frost roughness using aluminum skin with a rib structure at x = 14.75 in. from leading edge: a) RMS roughness; b) skewness; c) predicted equivalent sand-grain roughness; and d) peak-to-valley height 46
Figure 41. CAFF measurements of frost roughness using aluminum skin with a rib structure at x = 20.75 in. from leading edge: a) RMS roughness; b) skewness; c) predicted equivalent sand-grain roughness; and d) peak-to-valley height 47
Figure 42. Images from partial test cases or cases that ended early: a) 03/03/21 and (b) 03/31/21 49
Figure 43. CAFF measurements of frost roughness using carbon fiber skin without rib structure at x = 12.0 in. from leading edge: a) RMS roughness; b) skewness; c) predicted equivalent sand-grain roughness; and d) peak-to-valley height 51

Figure 44. CAFF measurements of frost roughness using carbon fiber skin without rib structure at x = 17.5 in. from leading edge: a) RMS roughness; b) skewness; c) predicted equivalent sand-rain roughness; and d) peak-to-valley height 52
Figure 45. CAFF measurements of frost roughness using carbon fiber skin without rib structure at x = 20.8 in. from leading edge: a) RMS roughness; b) skewness; c) predicted equivalent sand-grain roughness; and d) peak-to-valley height 53
Figure 46. Images following tests using the carbon fiber composite skin 55
Figure 47. CAFF measurements of frost roughness using carbon fiber skin with rib structure at x = 12.0 in. from leading edge: a) RMS roughness; b) skewness; c) predicted equivalent sand-grain roughness; and d) peak-to-valley height 57
Figure 48. CAFF measurements of frost roughness using carbon fiber skin with rib structure at x = 17.0 in. from leading edge: a) RMS roughness; b) skewness; c) predicted equivalent sand-grain roughness; and d) peak-to-valley height 58
Figure 49. CAFF measurements of frost roughness using carbon fiber skin with rib structure at x = 21.0 in. from leading edge: a) RMS roughness; b) skewness; c) predicted equivalent sand-grain roughness; and d) peak-to-valley height 59
Figure 50. The schematic of the carbon fiber thermal conductivity apparatus 60
Figure 51. Views of the as-built carbon fiber thermal conductivity apparatus: a) apparatus without Balsa top insulation and b) fully assembled apparatus 61
Figure 52. Time history for a carbon fiber thermal conductivity measurement 62
Figure 53. Three-minute average temperature slope identifying measurement periods 63
Figure 54. Measured carbon fiber sample thermal conductivity for two power settings 64
Figure 55. CSFF thermal and mass circuits 65
Figure 56. Thermal conductivity of Al 6061-T6 from 4K to 300K [https://www.nist.gov/] 67
Figure 57. Model implementation example results for the aluminum skin without a rib (Case 12/06/19): a) RMS roughness evolution; b) equivalent sand-grain roughness evolution; and c) thickness or peak-to-valley height 73
Figure 58. Model implementation example results for the carbon fiber composite skin without a rib (Case 04/23/21): a) RMS roughness evolution; b) equivalent sand-grain roughness; and c) thickness or peak-to-valley height 74

Tables

Table 1. Summary of roughness and thickness case conditions from Miyauchi, McClain, Zhang, and O'Neal (2019) 26
Table 2. Case conditions for combined roughness, thickness, and frost surface temperature measurements 31
Table 3. Nominal Test Conditions for Wing Tank Thermal Model with an Aluminum Skin without a Structural Rib 41
Table 4. Nominal test conditions for wing tank thermal model with an aluminum skin and a structural rib at three locations 43
Table 5. Nominal test conditions for wing tank thermal model with a carbon fiber skin without a structural rib 48
Table 6. Summary of nominal test conditions for wing tank thermal model with a carbon fiber skin and an aluminum structural rib 54

Acronyms

Acronym	Definition
ANOVA	Analysis of variance
BFT	Baylor Frost Tunnel
CAFF	Climatic Chamber and Aviation Frost Facility
CSFF	Cold soaked fuel frost
FAA	Federal Aviation Administration
RMS	Root mean square

Executive summary

Under certain atmospheric conditions, frost may form on the top surface of a wing with integrated fuel tanks if fuel remains in the tanks following a flight. The frost that forms under these conditions is called *cold soaked fuel frost* (CSFF). If CSFF is present on aircraft wings, 14 CFR Part 121 requires de-icing and anti-icing of critical surfaces before takeoff. However, aircraft manufacturers may apply for exemptions for takeoff with cold soaked fuel frost for each model of aircraft they manufacture. To assist the FAA in exemption requests for CSFF, frost roughness was characterized using two experimental facilities which provided different methods for capturing the thermodynamic environment representing the CSFF evolution process. A photogrammetric approach was developed to measure frost roughness and used in each facility. One of the facilities employed a wing-tank thermal model that captured the internal convection using a fuel surrogate and that captured the conduction through representative wing skins. Aluminum and carbon fiber skins using relevant aviation coatings were used in the measurements. Additionally, modeling concepts for the frost evolution process are also presented. The modeling concepts and details of the experimental measurements are intended to assist industry engineers in the development and validation of proprietary models.

1 Introduction

Commercial airlines and parcel delivery companies must fly into and out of airports that may be remote from a central hub airport. Typically, aircraft only fly with sufficient fuel for each leg of a trip, plus enough to meet diversion requirements. This mode of operation requires refueling the aircraft upon landing. Depending on the remoteness of the airport and the climate, fuel costs at the airport may be high enough that the airplane operator would rather bring enough fuel with them from the central hub airport for both the departure and return legs.

However, when an aircraft operator carries enough fuel for both legs of the flight, the aircraft must sit on the tarmac while cargo is unloaded and loaded onto the aircraft. Because the extra fuel is carried in the wing tanks, the fuel and wing surfaces may be below -10 °C after cruising at altitudes around 10,000 m (33,000 ft). In certain times of the year at some airports, temperatures and humidity levels will form what is referred to as *cold soaked fuel frost* (CSFF) on the aircraft wings over the fuel tanks.

The FAA has restricted the takeoff of an aircraft with frost contamination on the upper surface of a wing, unless an exemption is granted for an aircraft model. The roughness of the frost surface can degrade the lift of the wing during takeoff. Most aircraft are required to take off under the Federal Aviation Regulation 14 CFR Part 135.227 (14 CFR Part 135.227 - Icing Conditions: Operating Limitations). This regulation requires that an airplane is free of frost, ice, or snow contamination. Otherwise, a de-icing or alternative procedure must be used to clean aircraft surfaces before takeoff. Therefore, aircraft operators are required to clean the aircraft wings if CSFF forms. Because CSFF can form at any time during the year, de-icing equipment may not be readily available when CSFF forms on the wing surface. As a consequence, other time-consuming options, such as emptying and refilling the fuel tanks, must be employed.

Because of operator demands, aircraft manufacturers may determine a need for an exemption for an aircraft to takeoff with frost contamination on wings aft of the leading edge. To provide guidance to aircraft manufacturers regarding requests for exemptions for aircraft for takeoff with frost accumulation aft of the wing leading edge and to evaluate such requests, the FAA desires 1) a public database of CSFF thickness and roughness evolution and 2) a thermodynamic prediction model for CSFF evolution.

To address the needs of the FAA and the aviation community, this work included 1) expanded characterizations of frost evolution on aviation wing-skin surfaces and in CSFF conditions in the Baylor Climatic Chamber and Aviation Frost Facility (CAFF), 2) measurements of the thermal properties of the composite wing-skin material, and 3) continued analytical model development

and refinement for frost thickness and roughness evolution on fuel-laden wings following flights. The proposed effort also involved 1) continued measurements of frost roughness and thickness evolution in the Baylor Frost Tunnel (BFT) relevant to analytical model development and 2) expanded development of a public database of frost evolution on cold soaked aviation surfaces.

2 Frost evolution background

The dependence of frost growth on different atmospheric and surface conditions has been investigated extensively, specifically on flat plates. Air humidity, air velocity, wall temperature, and air temperature are known as the primary variables affecting the microstructure and properties of frost deposited on a cold surface (O'Neal & Tree, 1985). Generally, frost formation on a cold surface usually starts with condensation of water droplets and the subsequent freezing of these super-cooled droplets (Wu, Dai, Xu, & Tang, 2007). Initial frost crystals then emerge on the frozen condensate droplets. These crystals vary in shapes that correspond to the ambient cold wall temperature and air humidity (Lee, Shin, Ha, Choi, & and Lee, 2004; Yun, Kim, & Min, 2002). As the frost crystals continue to grow and connect with each other, a porous frost layer eventually forms. The type of frost crystals on the top of the frost layer might change from feather-shaped to needle-shaped, then flake-shaped or even irregular-shaped during frost formation (Zhang, O'Neal, & McClain, Impact of Environmental Conditions on Frost Crystal Structure, 2020). Additionally, the different shapes of frost crystals propagating from the frost surface can produce a range of frost roughness. During the frost growth process, moist air either deposits on the frost surface to increase the frost thickness or diffuses into the frost layer to increase the frost density (Brian, Reid, & and Shah, 1970).

Several frost growth predictive methods have been presented and reviewed in the literature. These include empirical correlations obtained from experimental data and mathematical models based on the analysis of the conservation of mass and energy in the frost layer. Most studies focused on estimating frost thickness and density. The models developed required many simplifying assumptions to predict either frost thickness or density. Breque and Nemer (2016) investigated the effects of different assumptions and concluded that improving correlations for the convective heat and mass transfer coefficients was one approach to increasing the accuracy of frost growth models. The heat and mass transfer coefficients were not only dependent on frost thickness and frost density, but also frost surface roughness. It was not acceptable to assume that the frost layer was a smooth wall. Data on frost surface roughness was essential to better estimate the heat and mass transfer to and from the frost layers. Furthermore, a predictive model of frost roughness is essential for estimating the impact of frost on the pressure drop in heat transfer equipment and the aerodynamic performance of surfaces with frost.

Although researchers have investigated the modeling of frost formation for many years, few studies have focused on estimating or measuring frost roughness. Chen and Rohsenow (1964) provided a relationship between frost thickness and frost equivalent sand roughness. The authors obtained the frost roughness data via visual comparisons between frost images and sand grain sizes. According to their results, frost roughness was proportional to frost thickness when frost first initially formed on the surface and gradually climbed to a plateau as the frost continued to grow.

Yun, Kim, and Min (2002) developed a model that estimated frost roughness based on experiments on a flat plate (128 mm wide and 500 mm long) at subfreezing temperatures. In their study, frost roughness was defined as the height difference between frost peaks and valleys. It was measured under magnification using a micrometer with a thin needle to ensure the needle tip/frost contact. Because the micrometer tip made contact with frost surface, it could have damaged the frost surface during the measurement. They identified two different types of frost crystals on the surface: column-type and plate-type. The column-type crystals mainly grew along their axial direction, while the plate-type crystals had a smaller upward growth rate. The authors indicated that column-type crystals grew almost normal to the frost surface so that a rougher frost was formed with these crystals. In contrast, plate-type crystals made the frost layer denser and smoother than with column crystals. By calculating the average frost roughness under different test conditions, the authors developed an empirical equation for frost roughness as a function of time, which is presented in Equation 1.

$$y(t) = 3.92 \times 10^{-3} + 0.069t - 0.0023t^2 + 2.84 \times 10^{-5}t^3 - 1.28 \times 10^{-7}t^4 \quad (1)$$

The resulting correlation demonstrates that frost roughness peaked at about 25 minutes, then decreased over time.

Yun, Kim, and Min's frost roughness correlation had several limitations due to the small range of experimental conditions and its high standard deviation (±29%). The roughness data were based on one local measurement (250 mm away from the leading edge of the 500 mm-long flat plate), which limited the ability to obtain other information of frost surface roughness, such as root-mean-square (RMS) height and surface skewness. Furthermore, the correlation was given only as a function of time, but the frost roughness was known to be strongly influenced by locations on a surface and environmental conditions, such as air temperature, wall temperature, air velocity, and air humidity.

3 Baylor Frost Tunnel

The Baylor Frost Tunnel (BFT) was used for the CSFF roughness measurements on a polished aluminum surface maintained at a constant temperature. The BFT is a closed-loop psychrometric wind tunnel (Zhang, O'Neal, & McClain, Analysis of frost thickness and roughness growth from the perspective of frost crystal structure, 2020). Figure 1 presents the schematic drawing of the BFT, which is composed of four sections: the humidity control module with a humidifier and a dry gas injection system; the circulation module with an adjustable electronically commutated motor blower; an air temperature control module with two cooling coils and a duct heater; and a test section.

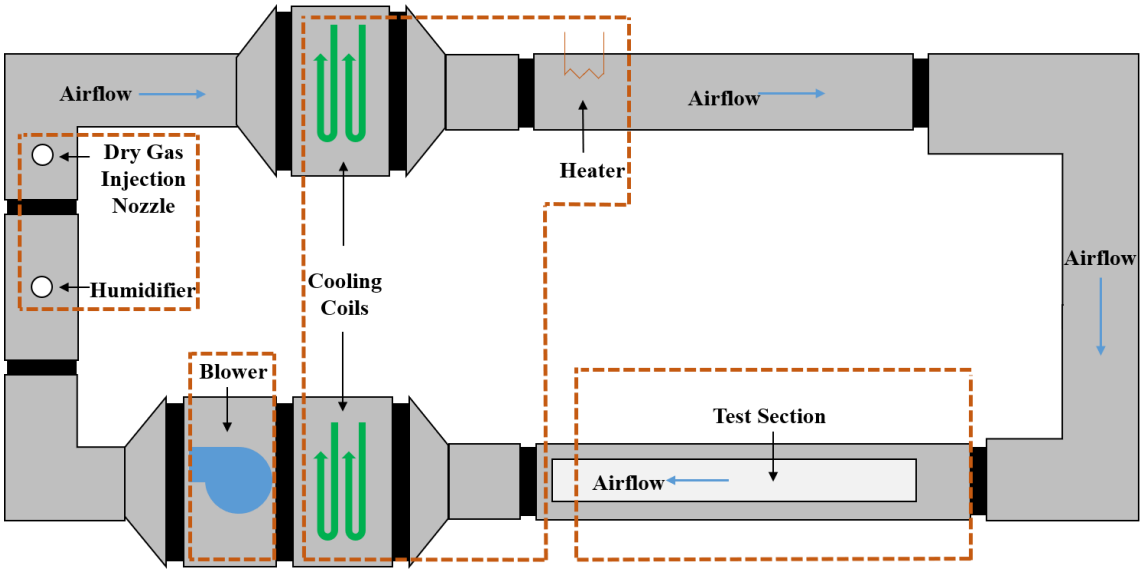

Figure 1. Schematic of the BFT

A 120-VAC centrifugal blower drives air through the entire wind tunnel while manually controlled with a silicon-controlled rectifier (SCR). The moisture is produced using an ultrasonic, dial-adjustable humidifier with a water reservoir of 3.5 L. Crossflow cooling coils with a single-phase glycol/water mixture reservoir are located downstream and upstream of the blower. The chiller can produce temperatures of -5 °C while maintaining bulk air stream temperatures as low as 10 °C for air velocities at 0.5 m/s. If necessary, humidity can be reduced through the injection of zero-grad nitrogen (N_2) gas directly into the wind tunnel.

A Vaisala HMT-333 series relative humidity sensor and a type-T thermocouple, mounted upstream from the test surface, are used for the measurement of the relative humidity and air temperature, respectively. A TSI 1750 constant-temperature hot-wire anemometer (model 1201

sensor probe) was located downstream from the test surface for the measurement of the air velocity.

The central component to the wind tunnel was the test section module. Figure 2 provides a more detailed schematic of the test section module. Within the module there were two parallel ducts: a test duct with a thermal stage and a bypass duct. Just within the test duct is a bank of 1.5 mm diameter and 20 mm long flow straighteners. The test duct was manufactured out of acrylic panels. An optical view port for capturing top-down micro photographs was machined out of the acrylic panel and allowed for in-situ image acquisition. A double pane of optical quality, 0.17 mm thick glass was sealed over the view port to ensure clarity for viewing frost while preserving the air temperature.

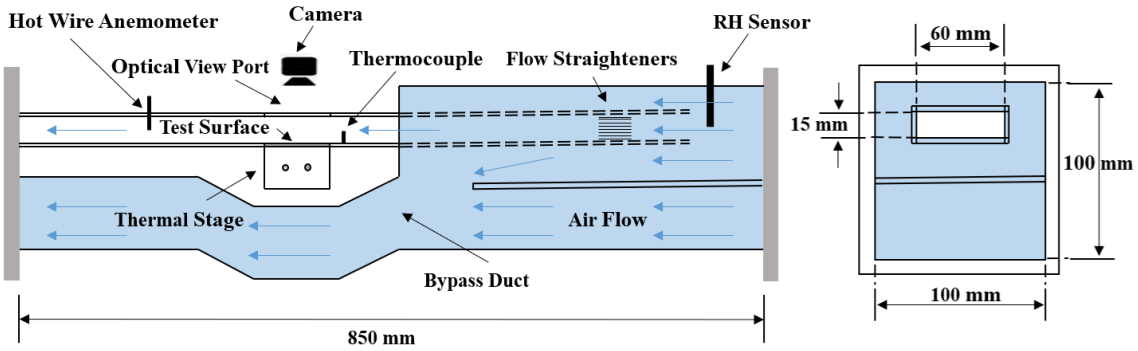

Figure 2. Detailed schematic of the BFT test section

A thermal stage mounted at the bottom of the test section was used to control the test surface temperature. The stage was composed of a type-T thermocouple, a thermoelectric cooler, and a copper heat sink. A 3-cm by 3-cm polished aluminum test surface was bonded with the thermal stage by a 0.254 mm thick thermally conductive material. A detailed exploded view of the thermal stage is presented in Figure 3.

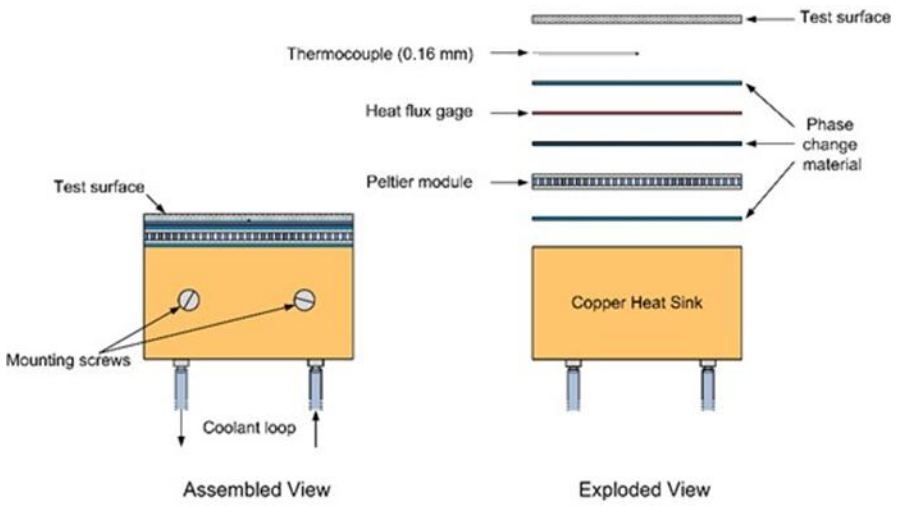

Figure 3. Assembled and exploded view of the BFT thermal stage

The BFT was an excellent facility for quickly setting frost conditions and obtaining frost measurements. The acrylic test section provided optical access for photogrammetry measurements and frost thickness measurements from the side of the tunnel. Additionally, an infrared thermometer could be mounted into the test section ceiling to provide frost surface temperature measurements.

While the BFT is a well-controlled and versatile facility, the BFT was constructed to represent heat pump frost conditions. Consequently, the BFT does not capture some aspects of CSFF. Specifically, the construction and control of the thermal stage allows the measurement of frost with a precisely controlled surface temperature. However, in a CSFF situation, the internal convection through the fuel and the conduction through the skin and surface treatment are not captured in the BFT.

4 Baylor Climatic Chamber and Aviation Frost Facility

The Climatic Chamber and Aviation Frost Facility (CAFF) was developed as an extension of the BFT studies for large-scale testing of aviation frost conditions and evolution. The facility is composed of a climatic chamber, a wing tank thermal model, a wind tunnel to impose known thermodynamic conditions on the wing skin surface, and an automated photogrammetry system used to characterize frost roughness (McClain, et al., 2020).

4.1 Climatic chamber

The climatic chamber was constructed using a 3.0-m by 4.3-m (10-ft by 14-ft) walk-in freezer. The refrigeration system has a cooling rating of 7-kW (2-ton) system using R-404a with a minimum temperature of -23 °C (-10 °F). Humidity control is performed using an industrial dehumidifier and two ultrasonic humidifiers. A top view of the climatic chamber is shown in Figure 4. Additionally, Figure 5 presents an image from inside the CAFF.

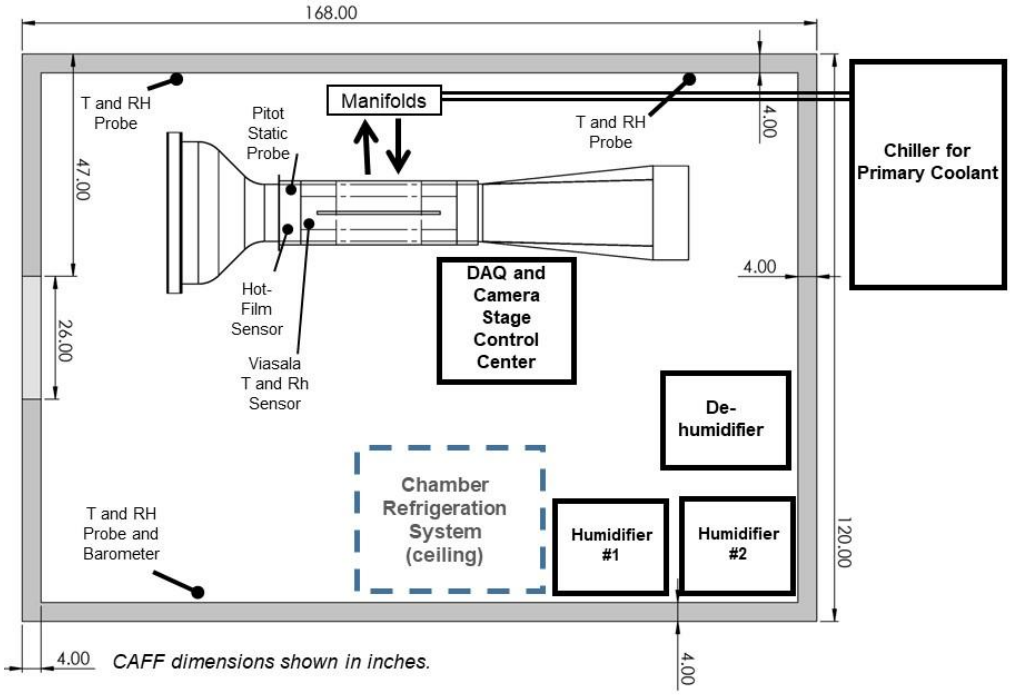

Figure 4. Climatic Chamber and Aviation Frost Facility (CAFF) layout

Figure 5. Image from inside the CAFF showing most major equipment

4.2 Wing-tank thermal model and primary coolant system

The wing-tank thermal model was constructed using 2.54-cm (1-in.) thick aluminum 6061 for the side walls. The floor is 0.95 cm (3/8-in.) thick 6061 aluminum plate. The tank is 83.82 cm (33-in.) long and 50.8 cm (20-in.) wide. The interior of the tank is 11.43-cm (4.5-in.) tall. Figure 6 presents a top view and an isometric view of the wing-tank thermal model. When assembled, the wing tank thermal model is filled with a 60%-40% propylene glycol and deionized water solution to act as a surrogate for jet fuel.

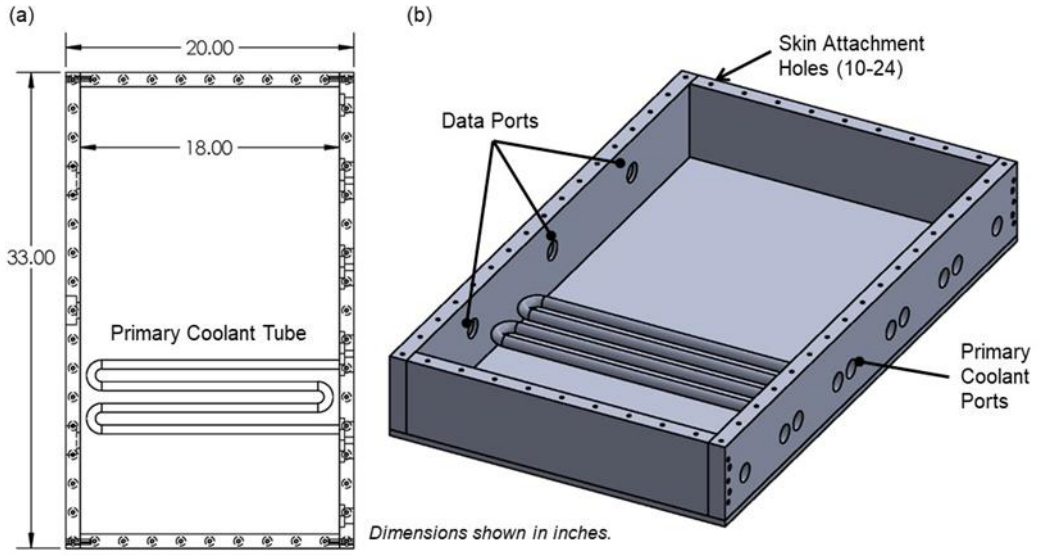

Figure 6. Wing-tank thermal model: (a) top view and (b) isometric view

The wing tank thermal model was designed to allow replaceable wing skins enabling the study of different wing skin constructions as well as the influence of ribs and wing-internal structures on CSFF evolution. A chiller and primary coolant system were used to cold soak the wing tank thermal model. The chiller delivered four gallons per minute of primary coolant, which was a 60%-40% solution of propylene glycol and deionized water. The primary coolant was pumped to a manifold. The manifold split the primary coolant flow into five tubes in the wing tank, and each tube made four passes in the wing tank thermal model.

4.3 Wind tunnel

The wind tunnel used for the frost facility has a 30.48-cm by 30.48-cm by 106.7-cm (12-in. by 12-in. by 42-in.) test section. The wind tunnel is a low-speed wind tunnel that was originally designed and constructed in 2016 for an undergraduate laboratory at Baylor University. The wind tunnel was not used for aerodynamic investigations in this study. It was present to impose a known freestream speed on the frost surface and to cycle air through the test section to avoid water vapor depletion as frost developed on the wing skin surface. The wind tunnel and wing tank thermal model are depicted in Figure 7.

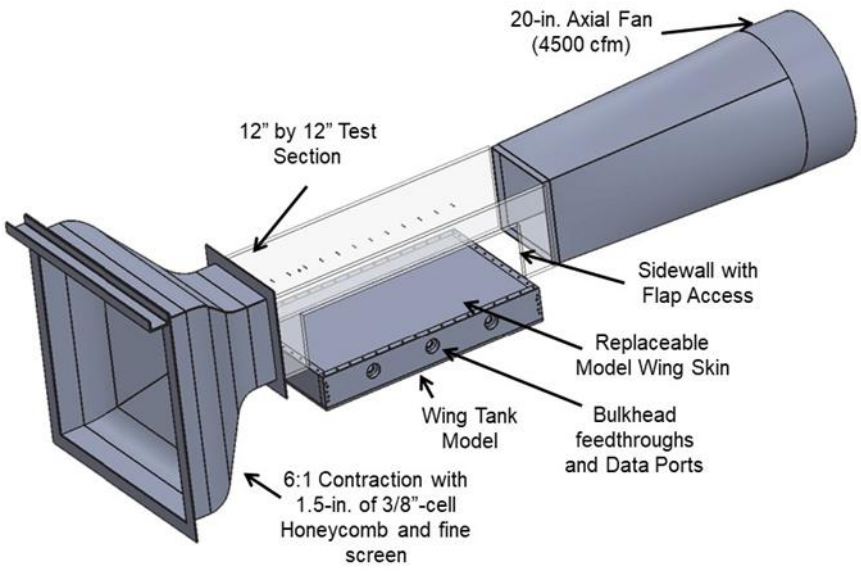

Figure 7. Wing tank and wind tunnel configuration for frost measurement

4.4 Wing skin design

Four wing skins were created for testing in the CAFF. Two of the skins were aluminum, and two of the skins were carbon fiber. For the initial tests, the wing skins were constructed of 0.04-in. aluminum 6061 sheet. For the following tests, the wing skins were constructed of 3-mm (0.121-in.) carbon fiber with a 0-90 layup. For each wing skin material, two skins were created: a skin without an attached rib and a skin with an aluminum rib attached to the skin.

The wing tank thermal model was designed to allow replaceable wing skins, which enables the study of different wing skin constructions as well as the influence of ribs and wing-internal structures on CSFF evolution. Each wing skin contains a data port for the attachment of bulkhead thermocouple connectors and a port for the attachment of tubing to a fuel surrogate expansion tank. The mechanical design for the skins is presented in Figure 8. Figure 9 shows the aluminum skin without a rib on the wing tank model without the wind tunnel installed. The thermocouple bulkhead connector and the expansion tank connection are shown. When the wind tunnel is

installed above the wing-tank model, the thermocouple bulkhead connector and the expansion tank connector are outside the wind tunnel test section.

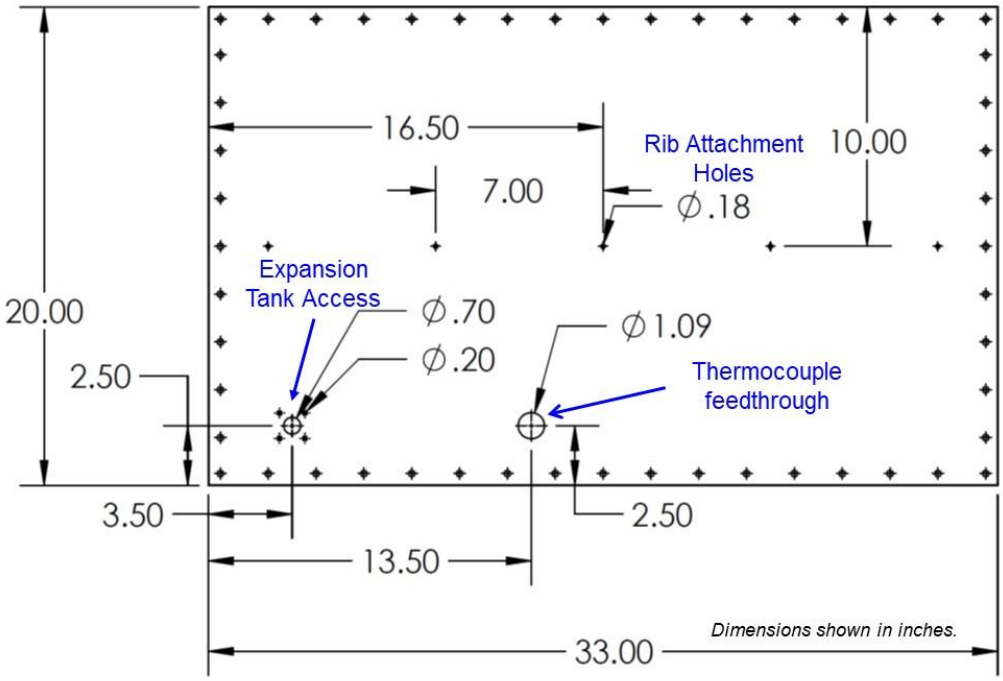

Figure 8. Skin design and access layout

Figure 9. Photo of aluminum skin with thermocouple bulkhead feedthrough and expansion tank connection

One aluminum and one carbon fiber skin were constructed using an aluminum rib. While the member was referred to as a "rib," the feature for both skins was more like a stringer in terms of the thermal mass present. However, the rib feature performed the same effect as a true rib in that the rib interacted with cooler fuel surrogate than was present in the immediate vicinity of the skin. The rib for the aluminum skin was constructed using a 1.5-in. by 1.5-in. by 3/16-in. structural T-member. Figure 10 shows the aluminum skin with rib and the thermocouple instrumentation after construction.

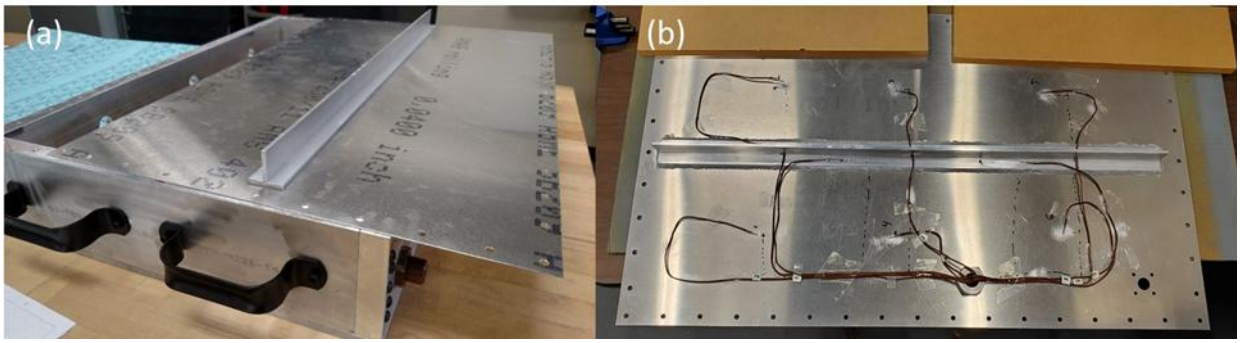

Figure 10. (a) Aluminum skin with rib and (b) instrumentation attached

The carbon fiber skin with a rib structure is shown in Figure 11. The rib used for the carbon fiber was also a 1.5 in by 1.5 in. by 3/16 in structural member, but the shape was an "L" profile instead of a "T" profile. This choice of profile was made because of the slightly easier attachment using inside washers instead of blind taps into the "T" profile.

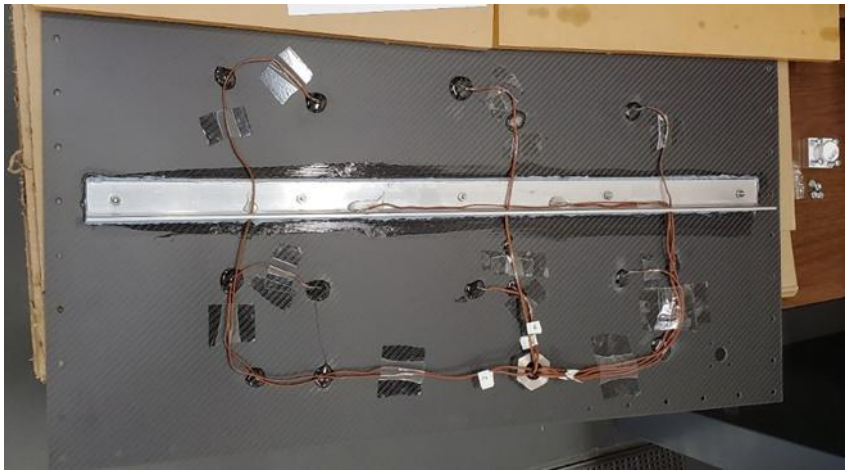
Figure 11. Carbon fiber skin with aluminum rib structure during instrumentation construction

The ribs were attached using silicon-based adhesives. With the exception of the type of adhesives used, the guidelines in AIR4069C “Sealing of Integral Fuel Tanks” were followed. AIR4069C generally covers the surface preparation, adhesive application, and the addition of adhesive beads surrounding the structural members (SAE AMS G9 Aerospace Sealing Committee , 2016).

Each skin was painted using aviation coatings. Each surface received two coats of Desoprime and two coats of light gray Desothane HD. The color gray was chosen to provide contrast with the clear or white ice crystals.

4.5 Testing procedure

The testing procedure began the day prior to the test. The dehumidifiers were turned on and allowed to operate overnight. On the day of the test, the set point temperature for the CAFF was entered, and the primary coolant chiller was started. To keep frost from forming on the test surface (skin), a 25.4-mm (1-in.) thick piece of foam board was placed on top of the test surface and weighted down using acrylic plates. Figure 12(a) shows the test section with the foam covering and acrylic weights.

The CAFF and chiller were run for approximately five hours until the wing-tank and the skin thermocouples reached steady state. After negligible changes in temperature were observed (less than 0.02 °C/min) in the wing-tank and skin thermocouples, the dehumidifiers were turned off, the humidifiers were turned on, and the automatic humidity control system was started.

Once the desired CAFF test relative humidity was reached, the foam sheet was removed from the test skin surface. The removal of the foam sheet designated the start of a frost test. The typical appearance of the test surface following removal of the foam sheet is presented in Figure 12(b). Some frost can be observed at the very front and very rear of the test section. Frost can also be seen at the side edges of the test section surface, which occurs because the foam sheet does not cover the entire surface inside the wind-tunnel test section. The foam sheet covered 93% of the surface and kept frost from forming on the test surface.

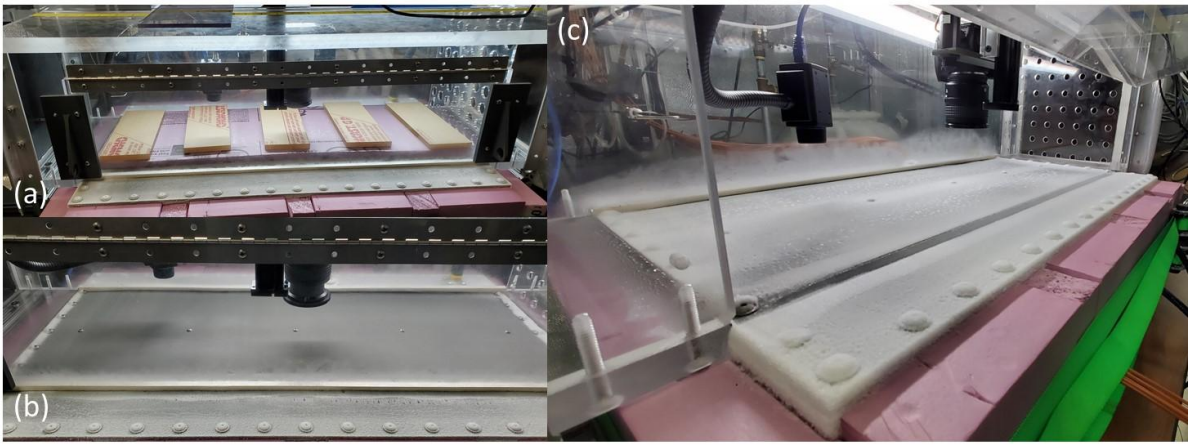

Figure 12. View of the test section: (a) with foam covering prior to test, (b) immediately following foam removal, and (c) following frost testing

Once the foam sheet was removed, the camera and lighting system were initiated. Once the camera was focused, the photogrammetry system was used to measure the frost topography on the wing skin surface. For each topography measurement, a seven-image (streamwise) by four-image (spanwise) array of images was acquired using the photogrammetry system with 80% overlap of the images in each direction. Following the first photogrammetry measurements, image sets were acquired at regular intervals, which were typically every 20 minutes. The last image set was typically taken following 140 minutes of frost growth. **Error! Reference source not found.**(c) demonstrates the level of frost on the wing tank model skin following a test.

During testing, a LabVIEW program on the primary CAFF PC monitored the important environmental conditions and recorded the conditions at a rate of one sample from every instrument approximately every three seconds. Additionally, because most environmental conditions were controlled from outside the CAFF, four cameras were used to monitor the conditions and equipment inside the CAFF. Figure 13 presents two screen captures at the beginning of a test and at the end of a test. To monitor and document test procedures, screen captures are acquired every 2.5 seconds. Video records of each test were made based on the screen captures.

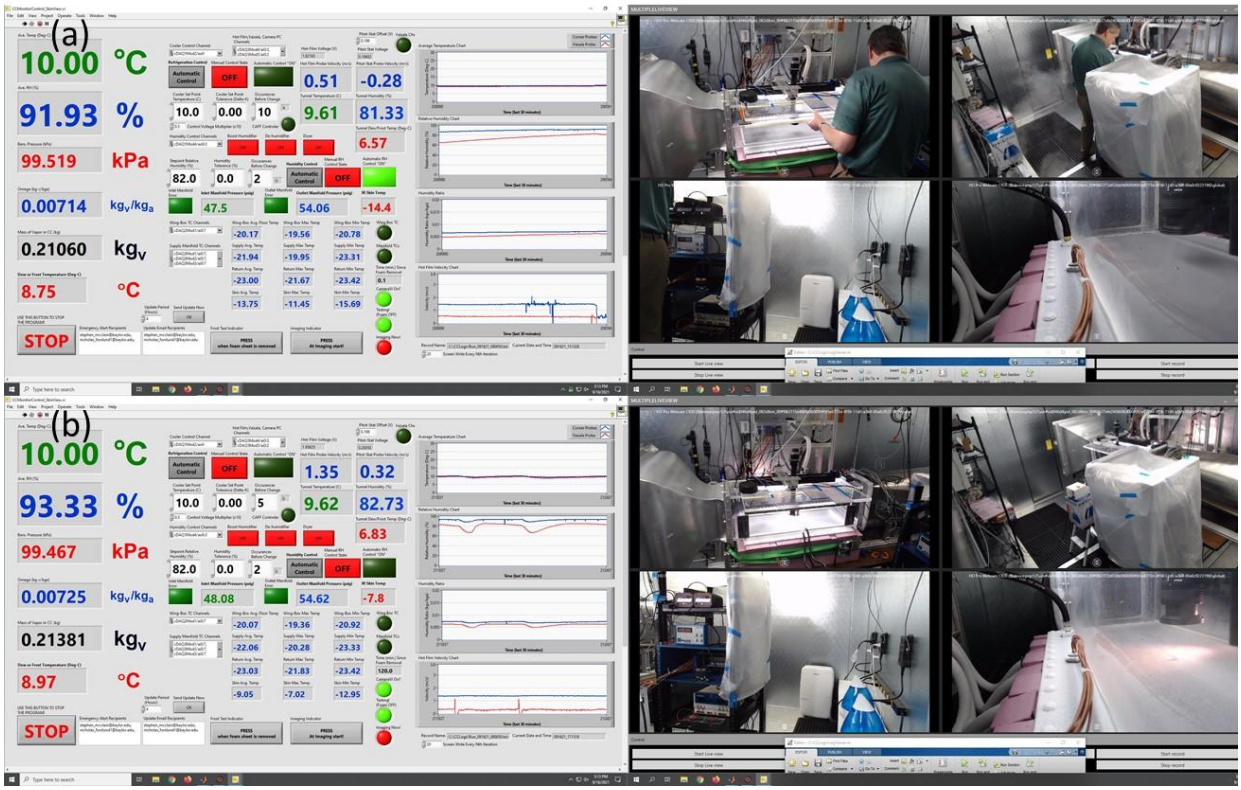

Figure 13. Time-lapse video images from CAFF test 091621: (a) image immediately following foam removal and (b) image following 120 min. of frost growth

After the final image set, the chiller, photogrammetry system, and automatic humidity system were stopped, and the dehumidifier was turned on. The CAFF temperature set point was typically increased to 16 °C, and the system was allowed to dry for a minimum of 36 hours before the next test.

5 Photogrammetric frost measurements

The brittle nature of frost dendrites and the optical properties of frost present challenges when attempting to characterize roughness. Therefore, a method to accurately measure frost surface roughness was established.

Several researchers have measured frost roughness. Lawrysyn (1989) utilized a polyvinyl formal plastic material dissolved in ethylene dichloride to cast a model of frost formed on cold-soaked plates overnight. The frost model height was measured using a profilometer type device. The method of Lawrysyn cannot be used because it cannot measure transient frost formation.

Yun, Kim, and Min (2002) performed experiments in a closed-loop wind tunnel by measuring frost height on a refrigerated test plate using a pin-needle micrometer and a magnifier to check for contact. Because frost crystals are fragile, any technique that requires physical contact with the frost surface may damage the surface and affect the measurement. Thus, the technique used by Yun, Kim, and Min may introduce inaccuracies in the measurement due to physical contact with the frost. In addition, the frost surface resembles more the canopy of a forest and would require extensive measurements of the "hills and valleys" in the canopy to accurately characterize the roughness.

The most similar surface to frost roughness that has accurately and repeatedly been measured is ice accretion on wing models. At the NASA Glenn Icing Research Tunnel, several methods for measuring ice roughness have been established (Lee, Broeren, Kreeger, Potapczuk, & and Utt, 2014). The most advanced method uses a laser scanner to obtain a 3D model of the ice shape. However, this method requires the wind tunnel tests to be halted for a white paint to be applied to the transparent ice. Since an airbrush system would be used to paint the ice, this approach damages the dendrites and changes the frost surface characteristics during painting.

The most favorable method for measuring frost roughness evolution is photogrammetry. Photogrammetry is the science of deriving the spatial and geometrical information of objects through the evaluation of recorded images (Linder, 2003). In a 2D image, depth of field is lost. By capturing multiple 2D images of a surface, the light rays that create the pixels in each image can be intersected and used to calculate height at various locations (Schenk, 2005). These multiple perspectives can be captured by moving the camera between images, which is a method known as *structure-from-motion*.

An important distinction of photogrammetry is that it functions solely off of non-contact optical images, unlike laser scanners (Vosselman & and Maas, 2010) or interferometers (Hariharan, 2003), which require light beams to be directed at the surface. Since frost can be transparent and/or reflective, photogrammetry can be used with various light setups to capture the frost surface with detail. Collier, Dixon, Fontana, Payne, and Pearson (1999) used close-range photogrammetry for 3D modeling of ice on an airfoil because it was premised on global measurements and enabled flexibility in capturing data in tight fit areas. They concluded that photogrammetry is the best method for measuring ice accretion because it allows for maximum data acquisition in the shortest amount of time and at minimal cost.

Recently, Soinne, Rosnell, and Vilijanen (2017) compared a photogrammetry technique to NASA's established laser scanning method by measuring frost on an aircraft wing. The frost was generated in the method as described by Koivisto (2015). Once frost had formed, a small target

was laid upon the frost, and a total of 47 to 54 images at different orientations were captured around the target. However, reorienting the camera between captured images required up to one hour for the total set of images, which is excessive because of the rapid evolution of frost on a cold surface.

5.1 Photogrammetry approach in the Baylor Frost Tunnel

Photogrammetry was the selected method of characterizing frost roughness in the BFT because it captures global, in-situ, non-contact measurements, and can be performed very quickly (Miyauchi, McClain, Zhang, & O'Neal, 2019). The photogrammetric instrumentation involved a camera in a top-down orientation above the frosted test surface as shown in Figure 14. The photographic setup included a Nikon D3400 DSLR camera and an AF Micro Nikkor 60mm f/2.8D lens. A key feature of this lens was the 1.0x magnification with a working distance of 73 mm, providing standoff distance from the top surface of the wind tunnel. The camera was traversed in micrometrical increments through the use of a multi-axial traversing system. This system incorporated a telescoping boom stand and two positioning slide plates to traverse the camera in the x and y directions and focus the camera in the z direction. A scale bar was designed to meet the requirements of not interfering with the airflow and presenting microscopic photographical targets to specify control points for scaling the model on the x and y planes. Additionally, the scale bar was sloped for a two-fold purpose: to present targets at increasing focal heights as the frost thickness increased and to scale the model in the z direction based on the difference in angle between the physical model and the photogrammetric model. A halogen light, directed through fiber optic guides, illuminated the frost and the scale bar to clearly depict details without creating a flat light setting.

Figure 14. BFT photogrammetric setup

For each surface measurement, a total of 40 images were collected in a serpentine pattern during a short time span of 45 seconds. The images were processed using the commercial photogrammetric software Agisoft Photoscan Pro. The process resulted in a 3D dense point cloud of the scale bar and frost surface. This photogrammetric model was geometrically scaled on the x and y plane by importing the horizontal distance between two calibrated target points from the scale bar. The point cloud was then exported to MATLAB and the model was correctly scaled in the z direction. A numerical method was used to iteratively increase a z-scaling factor applied to the point cloud of the scale bar's slope until it matched the physical model's slope. This z-scaling factor was then applied to the frost surface model, resulting in a point cloud that was correctly scaled in all three directions. Figure 15 depicts the constraints used on the scale bar to correctly scale the photogrammetric frost model.

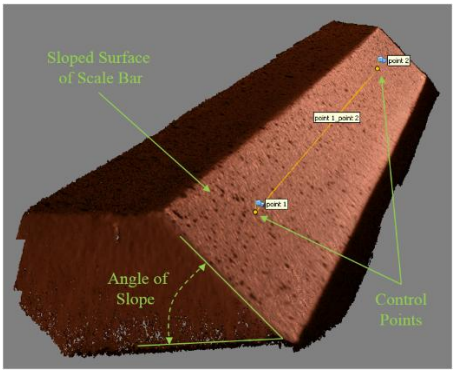

Figure 15. Photogrammetric model of a scale bar with constraining control points and slope

A set of validation measurements was required for the photogrammetry approach. For the validation measurements, plastic matte-white surfaces with artificial roughness, similar in magnitude to frost RMS roughness values, were fabricated. The photogrammetry measurements of the artificial surfaces were compared with measurements from a Keyence VR3000 structured-light profilometer. The Keyence VR3000 could not be used directly for the frost measurements because of the reflectance of real frost. A total of seven validation surfaces were created with the following RMS roughness values: 21.68, 54.46, 102.81, 131.89, 232.04, 311.09, and 458.01 µm. The photogrammetric measurements were repeated three times, and percent differences compared to the Keyence are presented in Figure 16. The percent differences were less than 7% for RMS roughness values greater than 100 µm.

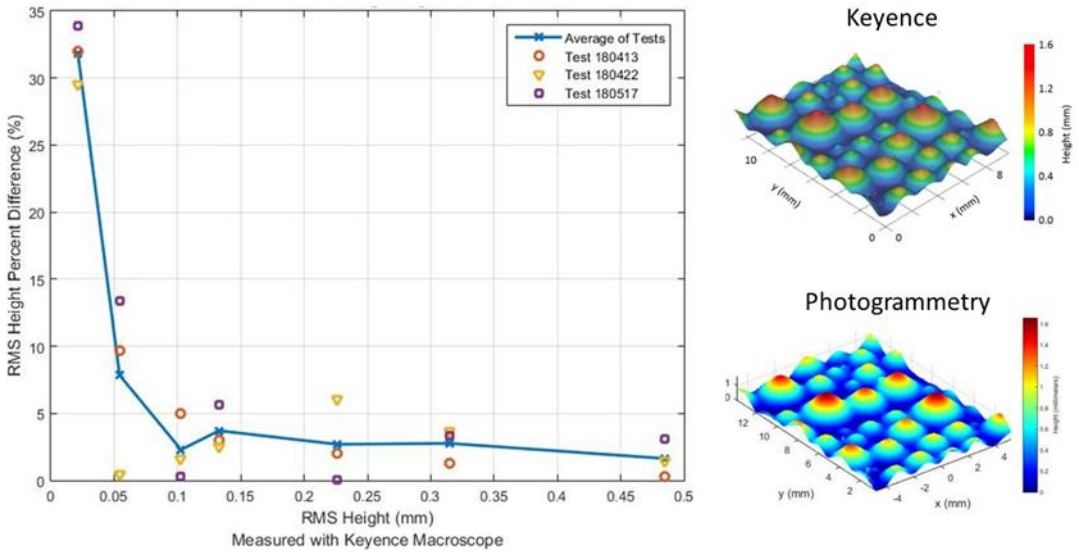

Figure 16. Percent difference of photogrammetric method with increasing roughness and a detailed height distribution comparison

5.2 Photogrammetry approach in CAFF

Following the work of Miyauchi, McClain, Zhang, and O'Neal (2019) for the BFT measurements, close-up photogrammetry using a 60-mm macro-lens and a Nikon D3400 DSLR camera was also employed for surface roughness measurements. To avoid intrusions into the climatic chamber during a test, the camera was mounted on a stepper motor-driven three-axis positioning system that could be controlled using a PC and data acquisition software. The photogrammetry system is shown in Figure 17 as installed on the wind tunnel in the climatic chamber.

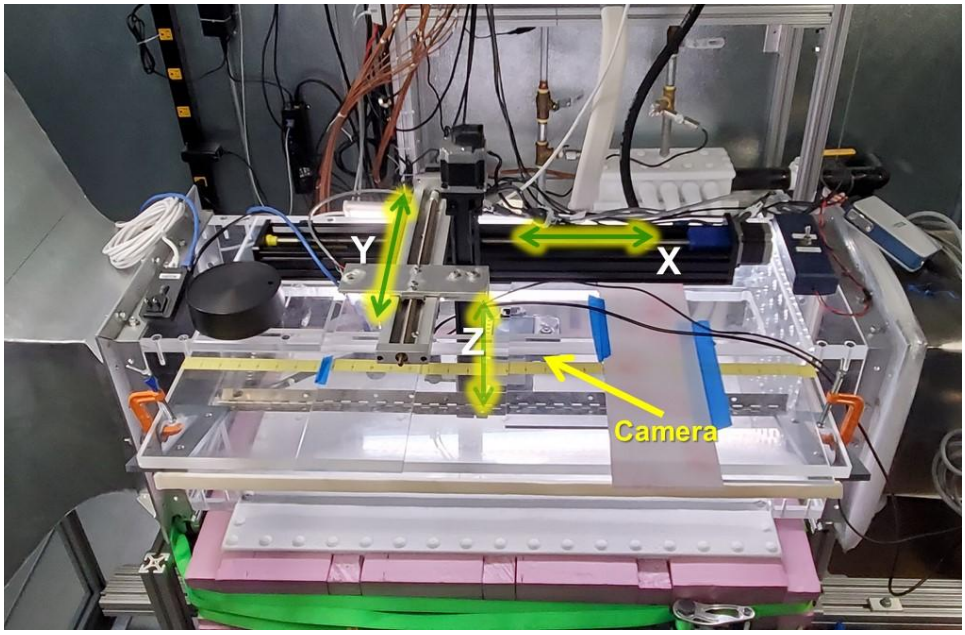

Figure 17. View of the test section from above, demonstrating the three-axis stepper-controlled photogrammetry system

For a single test, the photogrammetry system was positioned over an 8-cm by 3.5-cm (3.15-in. by 1.37-in.) section of the wing skin and shows that section for the duration of the test. At set time intervals, the camera was then moved to 28 different positions to create a map of images that have 60% overlap. While the location of the camera is moved for the photogrammetry measurements, the angle of the camera relative to the skin surface is not changed during the imaging sequence. Figure 18 presents a visualization of the 28 image locations used during a photogrammetry measurement and the overlap of the images. In Figure 18, the different colors correspond to the number of images which contain a region on the surface of the frost.

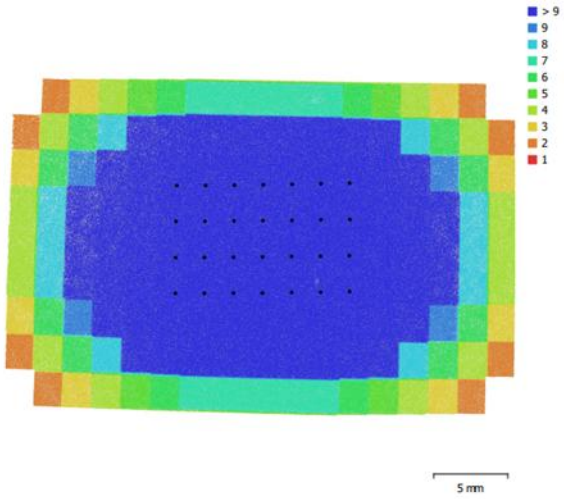

Figure 18. Camera locations and image overlap

Because of the time sensitivity of frost growth, only one location on the frosted plate was viewed in a single test. Therefore, to study variation due to the location on the plate, the same environmental conditions were run on multiple days, with each day viewing a different location on the plate.

Following completion of a test, the 28 images were brought into Agisoft Metashape for processing. Agisoft Metashape is a professional photogrammetry software that produces 3D point clouds and surfaces based on the geometry of the provided images. The camera positions relative to one another were known for each test and were programmed into the Agisoft Metashape model to assist with the photo alignment process. The procedure for developing the Agisoft Model included importing the 28 images, uploading the camera reference file, aligning the photos using a high accuracy setting, and finally developing a 3D density cloud based on the aligned photos.

The first step was photo alignment, in which Metashape identified tie points between the cameras and aligned the camera locations to one another. A high accuracy setting for the alignment process was used to ensure that the locations of the tie points were accurate. Also, the reference preselection option was set to *source*, meaning that the predefined camera locations from the reference file were used. An example of the camera location error report is presented in Figure 19.

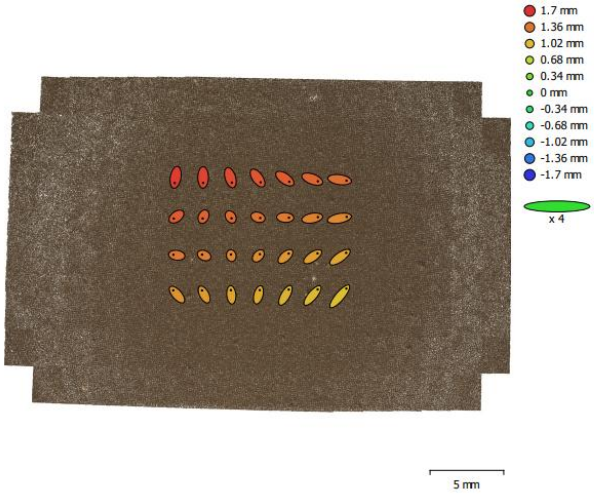

Fig. 3. Camera locations and error estimates.
Z error is represented by ellipse color. X,Y errors are represented by ellipse shape.
Estimated camera locations are marked with a black dot.

X error (mm)	Y error (mm)	Z error (mm)	XY error (mm)	Total error (mm)
0.130938	0.126157	1.32362	0.181825	1.33605

Table 3. Average camera location error.

Figure 19. Error report for camera locations

The Agisoft Metashape software used defined camera locations from the camera reference file as a starting point in determining exact locations of the cameras and the respective tie points for each of the images. The *key point limit* setting was set to the standard 40,000 value. The key point limit was the maximum number of points to be used in determining image locations relative to one another. For all the CAFF measurements, the *tie point limit* was set to 4,000. The tie point limit was the maximum number of points that could be used to attach the photos to one another. In other words, the tie point limit was how the images were stitched together. Figure 20 presents a top view of the refined camera location and the surface tie points for an example case.

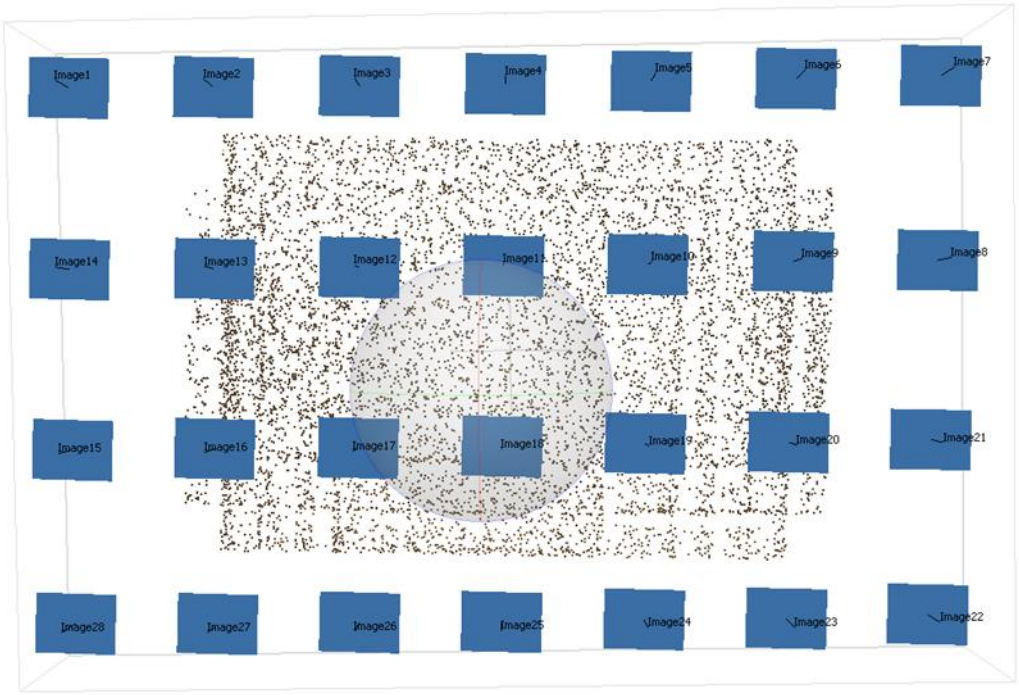

Figure 20. Aligned camera locations and surface tie points

The next step was building the dense point cloud, which created a map of the entire 3D surface. The quality of the dense cloud generation was set to medium. A higher quality setting could be used, but it would result in a significant increase in the associated processing time. The use of a high alignment setting paired with the fact that the region of interest was in the middle of the density cloud (where it was most accurate) allowed for a lower quality setting to be used for the dense point cloud generation. The depth filtering setting was also set to mild. Depth filtering was necessary to determine height information of the frosted surface. Using a mild filter was the best option to retain the small details in the surface, as the small depth elements were the most important part of the photogrammetry model. Last, the 3D density cloud was exported as X, Y, and Z coordinates to be used in post-processing. An example dense point cloud is shown in Figure 21. Because of the high accuracy and resolution of the images, each batch of 28 photos took about 30 hours to complete.

Figure 21. Example surface point cloud

The Agisoft Metashape software generated reports for each data set. The report generated an overview of the camera overlaps and their respective error estimates across the plate. As demonstrated in Figure 19, the error was calculated in the region that had the most overlap of images. The center region had the highest accuracy because there were tie points and image overlaps in every direction. The sources of error within the Agisoft Metashape model can be primarily attributed to the variations in camera height above the measured surface. The camera had a fixed focus setting, and the physical height of the camera had to be adjusted to focus the image. Also, the given accuracy was for the entirety of the plate. Because the measurements were most accurate in the middle of the imaged region, the region of interest used for all the statistical values reported was a 1-cm by 1-cm section in the middle of the 83.82-cm by 50.8-cm plate.

5.3 Point cloud statistical reduction

Once the dense point clouds were generated for the BFT and CAFF photogrammetry measurements, the root-mean-square (RMS) roughness, skewness, and equivalent sand-grain roughness were calculated. The RMS roughness, or the mean-square roughness (R_q), represents the standard deviation and is evaluated using Equation 2.

$$R_q = \left[\frac{1}{N_P}\sum_{i=1}^{N_P}(Z_i - \bar{Z})^2\right]^{\frac{1}{2}} \quad 2$$

In Equation 2, the mean elevation, $\bar{Z}$, is defined as the average of the surface measurements in the interrogation area for each set of photogrammetry measurements. The mean elevation is defined in Equation 3.

$$\bar{Z} = \frac{1}{N_P}\sum_{i=1}^{N_P} Z_i \quad 3$$

The skewness, Skw, is a dimensionless value that represents the symmetric distribution of the surface. A positive skewness indicates a surface heavily dispersed with frost peaks. The skewness was calculated using Equation 4.

$$Skw = \frac{1}{{R_q}^3}\left[\frac{1}{N_P}\sum_{i=1}^{N_P}(Z_i - \bar{Z})^3\right] \quad 4$$

Based solely the RMS roughness and the surface skewness, Flack and Schultz (2010) presented a correlation that predicts the equivalent sand-grain roughness height (k_s), shown in Equation 5.

$$k_s = 4.43R_q(1 + Skw)^{1.37} \quad 5$$

The correlation of Flack and Schultz (2010) is not the only correlation available for predicting the equivalent sand-grain roughness of a frost surface. However, the particular correlation was chosen because it is one of few correlations that only depend on statistical properties of a roughness surface. Flack, Schultz, Barros, and Kim (2016) present an alternate correlation for surfaces with highly negative skewness, indicating more prominent valleys than peaks. The alternate correlation of Flack, Schultz, Barros, and Kim (2016) was not used in this study, because only a few photogrammetry measurements resulted in skewness values outside the computation limits of Equation 5.

Finally, the peak-to-valley roughness was determined using Equation 6.

$$R_{PV} = \max(Z) - \min(Z) \quad 6$$

In Equation (6), Z is the matrix of all elevation measurements along the surface in the region of interest.

6 Summary of Baylor Frost Tunnel frost measurements

To acquire sufficient information for model development and implementation, experiments were performed in both the BFT and the CAFF. The BFT measurements were important because the surface temperature was selected and controlled during the frost measurements. The CAFF measurements were important because the internal convection of the fuel surrogate and the

conduction through the wing skin and surface treatment were captured. While the fuel surrogate used for the investigations, which was a 60% propylene glycol and 40% deionized water solution, did not match the properties of jet fuel, the measurements were intended to validate models which captured the physics of CSFF and could be employed for simulations or predictions for true aviation CSFF situations. The resulting measurements from the BFT are summarized in the following sections. The details of the measured atmospheric conditions and the tabular frost measurement results are presented in Appendix A for the BFT measurements.

6.1 Analysis of variance study of Miyauchi et al.

The first roughness study in the BFT was presented in Miyauchi, McClain, Zhang, and O'Neal (2019) and in Miyauchi (2018). In that study, an analysis of variance (ANOVA) study was performed to determine if any of the variables could be isolated or fixed during more extensive investigations of CSFF. The formation and evolution of frost was known to depend on four primary properties: the air temperature, T_∞; the surface temperature, T_s; the relative humidity of the air, *%RH* or ϕ; and the velocity of the air passing over the surface, V. The ANOVA tests were used to determine which four variables were dominant in the measurements and if any of the measurements could be neglected or frozen with constant values in the subsequent measurements.

To perform the ANOVA tests, a square test matrix of four parameters and two predetermined values was constructed for the ANOVA study. Table 1 presents the complete test matrix for the ANOVA investigation. The conditions were based on T_∞, set to 16 °C or 10 °C, T_s set to -10 °C or -25 °C, *%RH* set to 76% or 85%, and the velocity of the air set to 0.5 or 1.5 m/s.

Table 1. Summary of roughness and thickness case conditions from Miyauchi, McClain, Zhang, and O'Neal (2019)

Roughness Case ID	**T_∞ (°C)**	**T_s (°C)**	**%RH**	**V (m/s)**
042518	16	-10	76	0.5
050818.01	16	-10	76	1.5
050818.02	16	-25	76	1.5
051718.01	10	-10	76	1.5
051718.02	10	-10	85	0.5
051918	10	-10	76	0.5
052318.01	10	-10	85	1.5
052318.02	10	-25	85	1.5

Roughness Case ID	T_∞ (°C)	T_s (°C)	%RH	V (m/s)
052818	16	-10	85	1.5
052918.01	16	-25	85	0.5
052918.02	16	-25	85	1.5
060418.01	10	-25	76	0.5
060418.02	10	-25	85	0.5
060618.01	16	-10	85	0.5
060618.02	16	-25	76	0.5
061118	10	-25	76	1.5

Another objective of the Miyauchi (2018) and Miyauchi, McClain, Zhang, and O'Neal (2019) was to develop and validate the photogrammetry measurements reported in Section 5. An example roughness topography measurement of the validated photogrammetry approach is presented in Figure 22 (Miyauchi T. S., 2018).

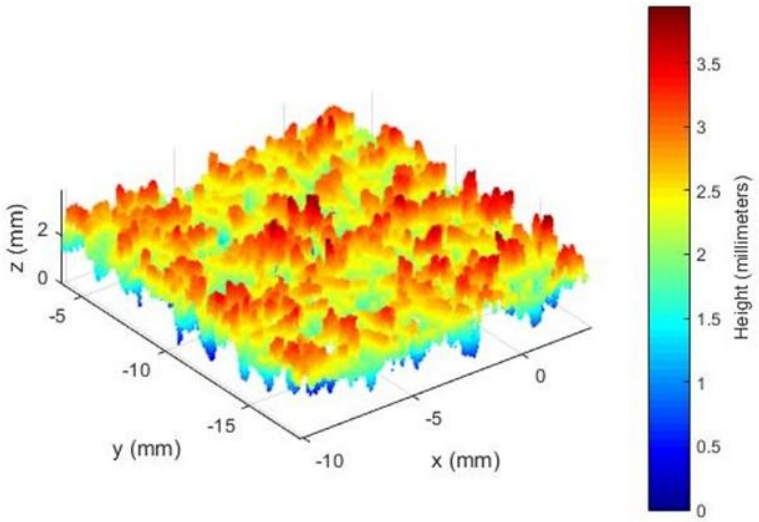

Figure 22. Roughness topography map for Case 052318.01

For each case of Table 1, the roughness properties were measured using the photogrammetry approach in 15-minute intervals over the span of 120 minutes. Figure 23 presents the RMS roughness measurements from the ANOVA investigation of RMS roughness height variation for ANOVA cases from Miyauchi, McClain, Zhang, and O'Neal (2019). The surface skewness measurements are presented in Figure 24, and the resulting calculated equivalent sand-grain roughness values are shown in Figure 25.

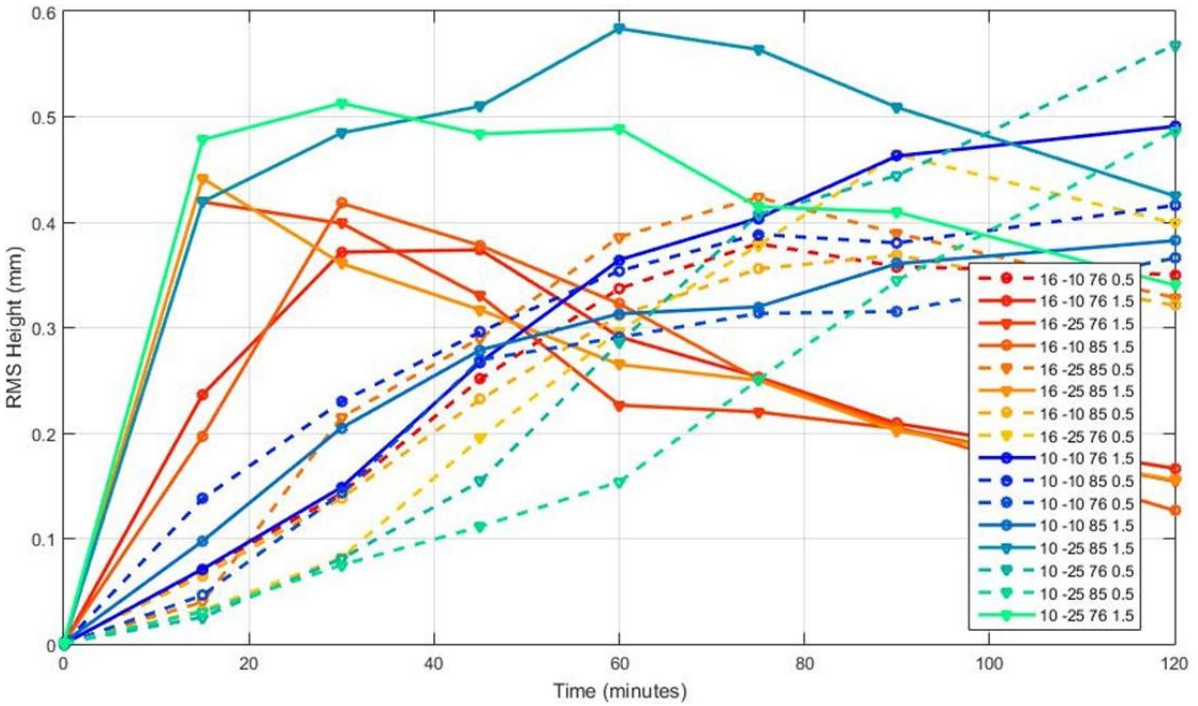

Figure 23. RMS roughness height variation for ANOVA cases from Miyauchi, McClain, Zhang, and O'Neal

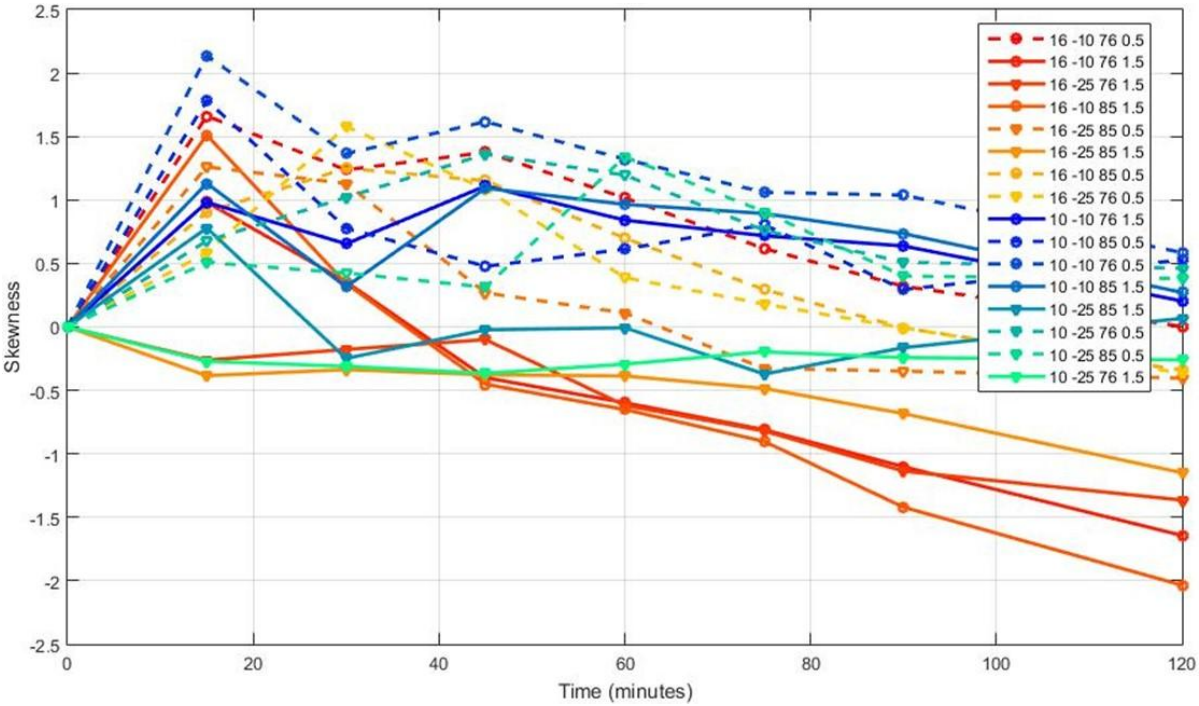

Figure 24. Surface skewness variation for ANOVA cases from Miyauchi, McClain, Zhang, and O'Neal

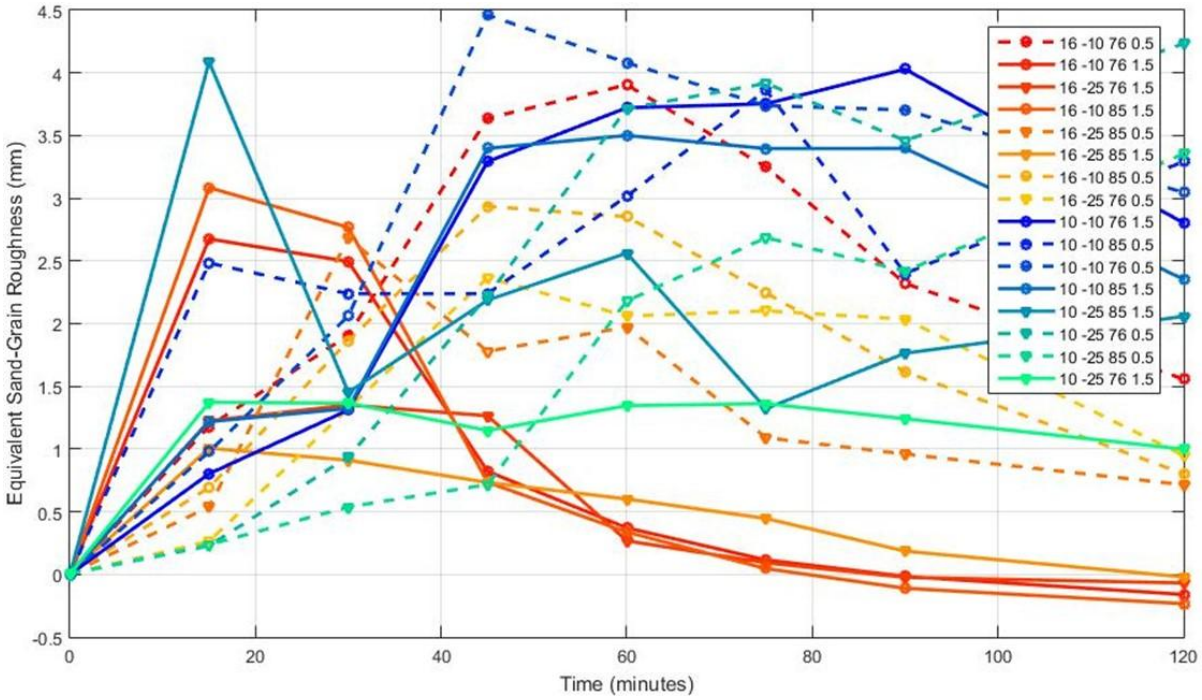

Figure 25. Calculated equivalent sand-grain roughness height variation for ANOVA cases from Miyauchi, McClain, Zhang, and O'Neal

As shown in Figure 23, Figure 24, and Figure 25, identifying trends in the measurements was non-trivial. Most of the ANOVA cases exhibited some period of increasing roughness followed by decreasing roughness, which was evidence of the initial crystal growth phase, the densification phase, and the melting phase that was commonly observed by investigators. Consequently, the ANOVA approach focused on the roughness parameter growth or rates of change in the short time periods (0-30 minutes) and the intermediate time periods (30-75 minutes).

The overall result was that the least important parameter affecting the rates of frost growth in the representative conditions used was the relative humidity of the air. The lack of significance of the relative humidity was surprising, but it is explained by the abundance of water vapor in the air above the saturation humidity ratio at the frost surface temperature. That is, since the humidity ratio of the air was much greater than the saturation humidity ratio of the frost surface temperature for all cases used, the mass transfer from the air to the frost surface was not the limiting or controlling factor in the frost growth for the ANOVA cases.

Figure 26 presents a demonstration of the importance of the air temperature, air velocity, and time following test initiation on the resulting frost topography (Miyauchi T. S., 2018). For each case in Figure 26, the surface temperature was held at -10 °C, and the relative humidity was 76%.

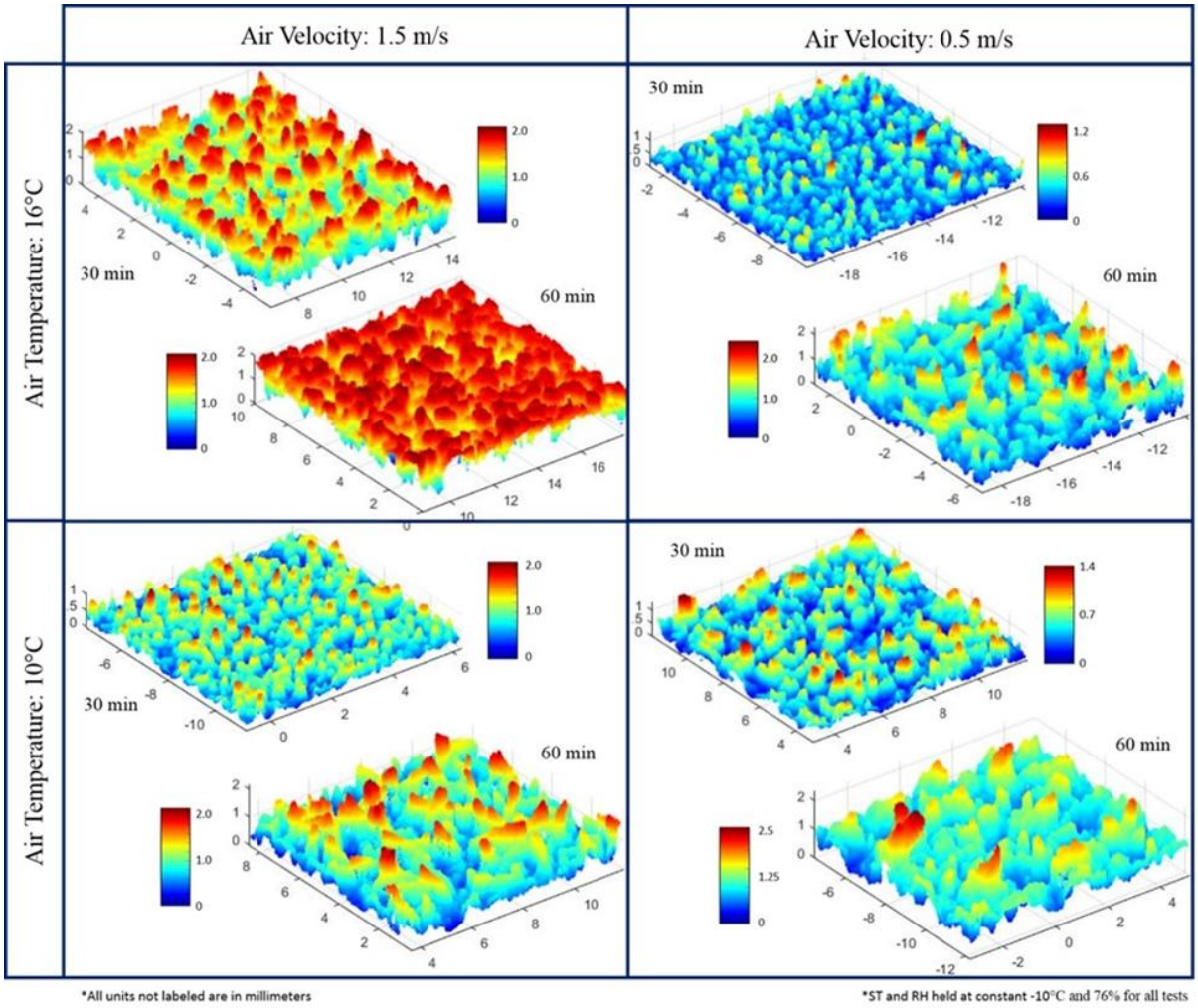

Figure 26. Demonstration of the influence of various factors affecting frost roughness

6.2 Roughness, thickness, and surface temperature study of Zhang et al.

Following the ANOVA study of Miyauchi (2018) and Miyauchi, McClain, Zhang, and O'Neal (2019), a series of experiments were performed to investigate the spatial variations in roughness along the BFT specimens to relate thickness measurements to roughness characteristics of the frost and to relate the mean surface temperature of the frost to the roughness characteristics.

Environmental and surface conditions used for the follow-up investigations by Zhang, O'Neal, and McClain (Analysis of frost thickness and roughness growth from the perspective of frost crystal structure, 2020; Zhang, O'Neal, & McClain, Impact of Environmental Conditions on Frost Crystal Structure, 2020; Zhang, O'Neal, & McClain, Variation of Frost Roughness on a Flat Plate Under Forced Convection, 2021) are presented in Table 2.

Table 2. Case conditions for combined roughness, thickness, and frost surface temperature measurements

Roughness Case ID	**Thickness Case ID**	T_∞ **(°C)**	T_s **(°C)**	**%RH**	**Velocity (m/s)**
042518	102219.01	16	-10	76	0.5
072318	101619.01	16	-10	76	1.0
061118	101619.02	16	-10	76	1.5
070218.01	101519.01	16	-10	61	0.5
070218.02	101519.02	16	-10	91	0.5
062518.01	102319	16	-5	76	0.5
062518.02	102219.02	16	-15	76	0.5
081418	102119	8	-10	76	0.5
062718	101819	12	-10	76	0.5
110719.01	010720.01	8	-15	70	1.0
110619.01	010620.01	12	-10	70	1.0
111219.01	010820.01	12	-15	60	1.0
111119.01	010720.02	12	-15	70	0.5
110619.02	010620.02	12	-15	70	1.0
111119.02	010820.02	12	-15	70	1.5
111319	010720.03	12	-15	70	2.5
111219.02	010820.03	12	-15	80	1.0
110619.03	010620.03	12	-20	70	1.0
110719.02	010920	16	-15	70	1.0

6.2.1 Roughness variations in the sample regions

The study of Zhang, O'Neal, and McClain (2021) was performed to investigate variations in the roughness properties along the surface distance of the BFT specimen. In the measurements of Miyauchi, McClain, Zhang, and O'Neal (2019), some variations along the 60-mm length of the

BFT measurement region in the streamwise direction were observed. Subsequently, ten cases out of Table 2 were used more fully characterize these variations.

An example image from above the BFT measurement region following test 110719.02 is shown in Figure 27. The front 20 mm, the center 20 mm, and the rear 20 mm regions are identified in Figure 27, and differences in the size, spacing, and morphology of the frost are apparent. The differences were caused by the abrupt change in heat and mass transfer boundary condition. Additionally, as the flow moved over the upstream frost, the roughness was postulated as causing a new boundary layer to form which transitions and grows. As the boundary layer grew and the convection and mass transfer coefficients decreased along the test sample, the frost grew taller into the flow.

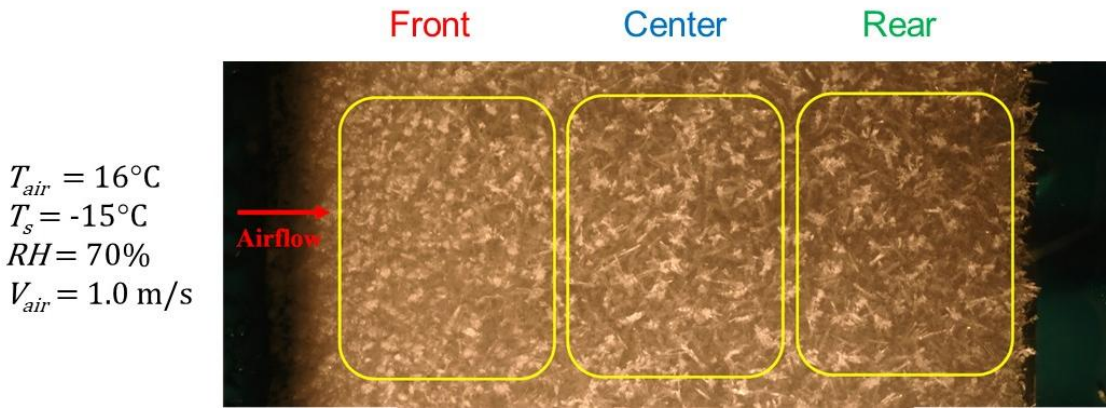

Figure 27. Example frost morphology and feature variations along the BFT sample

While the frost appeared taller at the leading-edge region, the RMS roughness heights did not always follow the appearance captured in Figure 27. Figure 28 presents the roughness evolution variations from case 110619.01 for each of the three regions of the BFT test section. Figure 28 demonstrates that the RMS roughness grew similarly over each of the three regions of the BFT test section. However, because the roughness features were more sparsely spaced in the downstream regions leading to higher values of skewness, the predicted equivalent sand-grain roughness values were larger than in the front or upstream region, especially in the middle (40-100 minute) range of the test.

a.

b.

c.

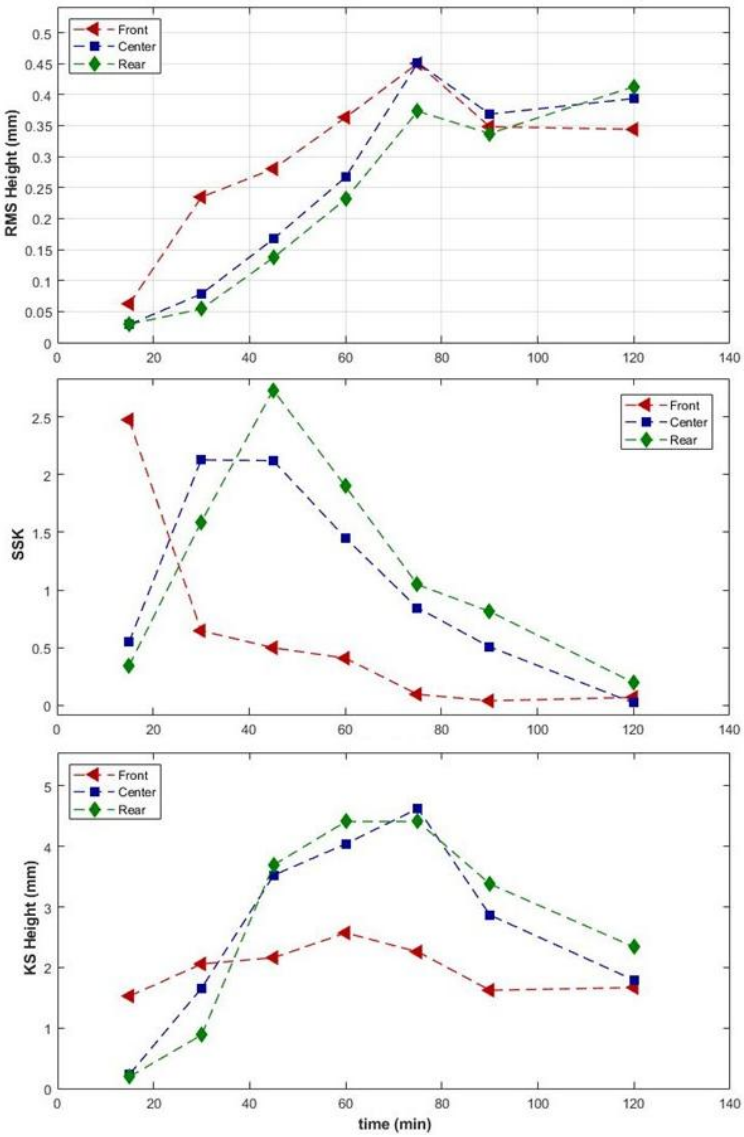

Figure 28. Example roughness evolution on BFT surface (T_s = -10 C, T_{air} = 12 C, RH = 70%, V_{air} = 1 m/s): a) RMS roughness height; b) skewness; and c) equivalent sand-grain roughness height

The effort of Zhang, O'Neal, and McClain (2021) illuminated the importance of the location of the measurements in producing the roughness characteristics based on the relative size of the thermal and velocity boundary layers. Because of the findings of Zhang, O'Neal, and McClain (2021), subsequent frost measurements in the CAFF were performed at three streamwise distance locations when possible.

6.2.2 Thickness and roughness measurements

Because the roughness measurement statistics and peak-to-valley height were bounded by the frost thickness, an approach to relate the roughness characteristics to the frost thickness was performed by Zhang (2020). For each roughness case listed in Table 2, a case was also identified where the thickness variation was measured under the same conditions as used for the roughness case.

For the thickness measurements, the camera was mounted to view the BFT test section from the side, as shown in **Error! Reference source not found.** (Zhang, 2020). An image was acquired before the beginning of frost measurements. At each time used for the roughness measurements, the frost thickness was measured from the side view. For all of the cases in Table 2, the RMS measurements and the equivalent sand-grain roughness predictions are presented in Figure 30 and Figure 31, respectively (2020). The thickness measurements for all of the cases of Table 2 are shown in **Error! Reference source not found.** (Zhang, 2020).

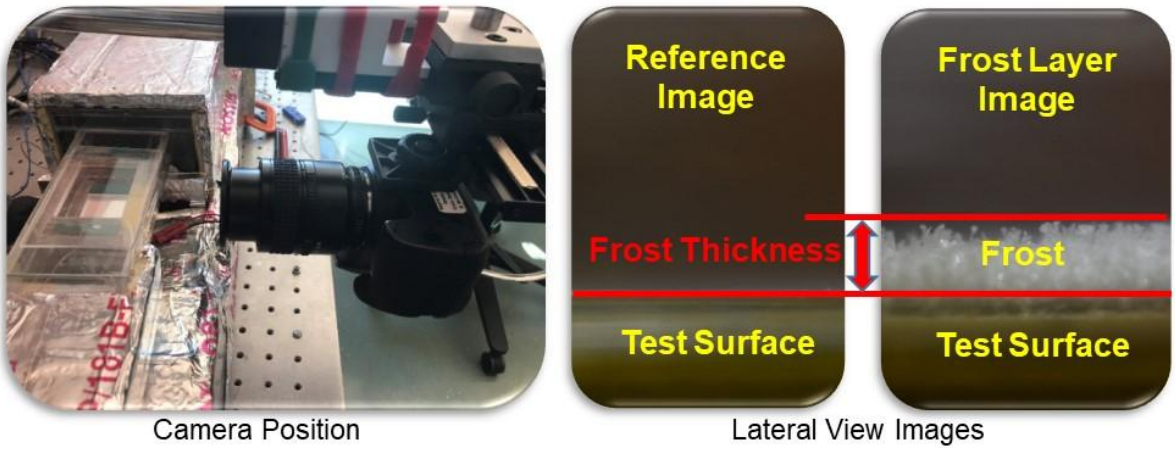

Figure 29. Demonstration of frost thickness measurements in the BFT

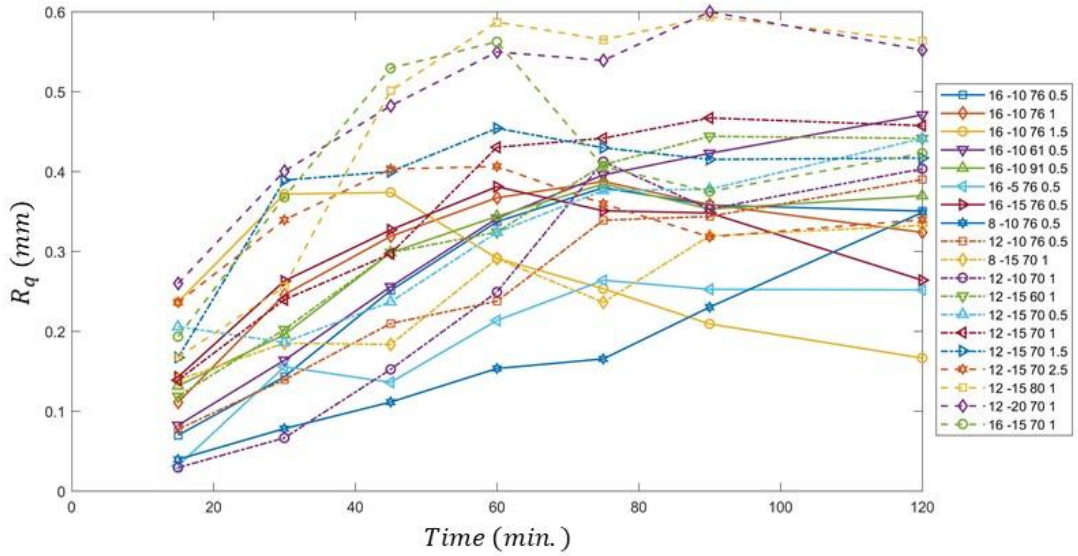

Figure 30. RMS roughness measurements from the cases in the BFT

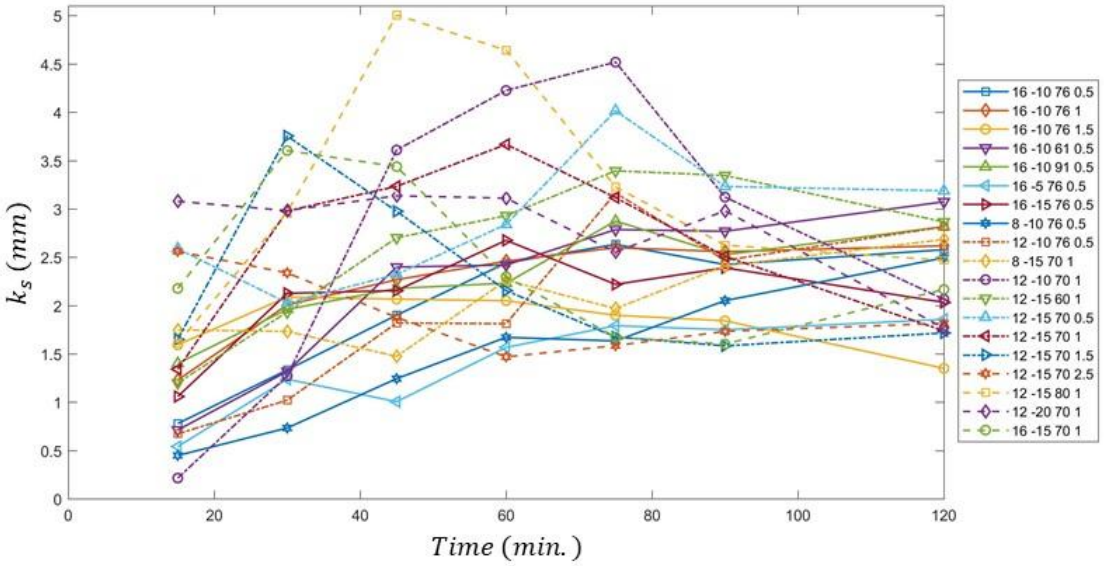

Figure 31. Calculated equivalent sand-grain roughness measurements from the cases in the BFT

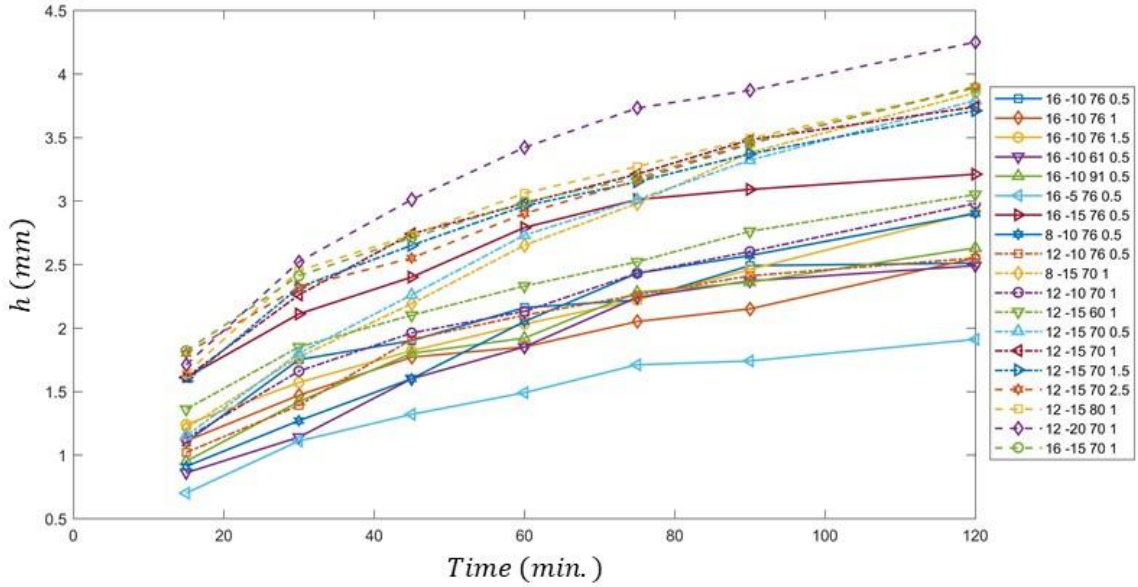

Figure 32. Frost thickness measurements from the cases in the BFT

6.2.3 Surface temperature measurements

In addition to the frost and roughness measurements in the BFT, a third set of tests were performed at each case in Table 2. As depicted in Figure 33 (Zhang, O'Neal, McClain, & Riley, 2021), an infrared thermometer was mounted on the ceiling of the BFT test section and used to monitor the frost surface temperature as a function of time during each test.

Figure 33. Infrared thermometer installation on the BFT for frost surface temperature measurements

The resulting frost surface temperature variations for the cases of Table 2 are presented in Figure 34 (Zhang, 2020). For each case, the temperature began close to the thermoelectric cooler set point temperature and then increased as the time increased. The increase in frost temperature demonstrated the increasing thickness of the frost and the increasing thermal resistance of the frost layer.

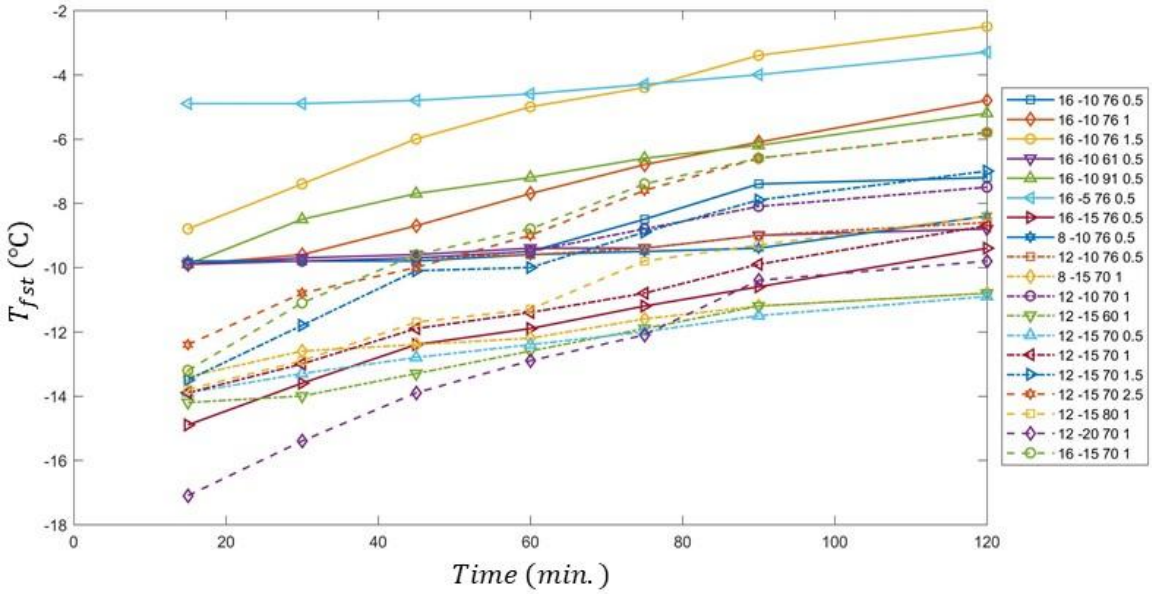

Figure 34. Frost surface temperature measurements in the BFT

6.2.4 Empirical correlation development

The nineteen cases listed in Table 2 with roughness, thickness, and frost surface temperature measurements at seven different times for each case provided 133 conditions with which to construct new correlations for frost roughness evolution. The correlations were developed by fitting multiple least square regression equations to the frost property data. Before developing the predictive models of frost roughness, the correlations of frost surface temperature and thickness were generated. These two parameters were employed as independent variables in the resulting frost roughness correlations.

The environmental properties were expressed as functions of dimensionless parameters, including Fourier number (Fo), absolute humidity (w_a), Reynolds number (Re_D), and dimensionless temperatures (T^*). Equations 7 through 10 provide the Fourier number, Reynolds number, dimensionless wall temperature, and dimensionless air temperature. In Equations 9 and

10, the temperatures are in absolute units (K), and (T_o) is the triple point temperature of water (273.15 K).

$$Fo = \frac{t\ \alpha}{D^2} \quad (7)$$

$$Re_D = \frac{V_{air}\ D}{\mu} \quad (8)$$

$$T_s^* = \frac{T_o - T_s}{T_o} \quad (9)$$

$$T_{air}^* = \frac{T_{air} - T_o}{T_o} \quad (10)$$

Based on the dimensionless groups of Equations 7-10, the equation for frost thickness (h_f) is shown in Equation 11. The frost thickness values are in mm units.

$$h_f = (1.759mm)(Fo)^{0.445}\ (\omega_a)^{0.221}\ (Re_D)^{0.092}\ (T_s^*)^{0.653}\ (T_{air}^*)^{-0.174} \quad (11)$$

The equation for the frost surface temperature is presented in Equation 12.

$$T_{fst}^* = \frac{T_{air} - T_o}{T_{air} - T_{fst}} = 0.770(Fo)^{0.087}(\omega_a)^{0.226}(Re_D)^{0.104}(T_s^*)^{-0.273}(T_{air}^*)^{0.390} \quad (12)$$

A comparison between measured and predicted thickness and between measured and predicted frost surface temperature is presented in Figure 35. The R^2 value for the frost thickness correlation is 0.94, and the R2 value for the frost surface temperature correlation is 0.95.

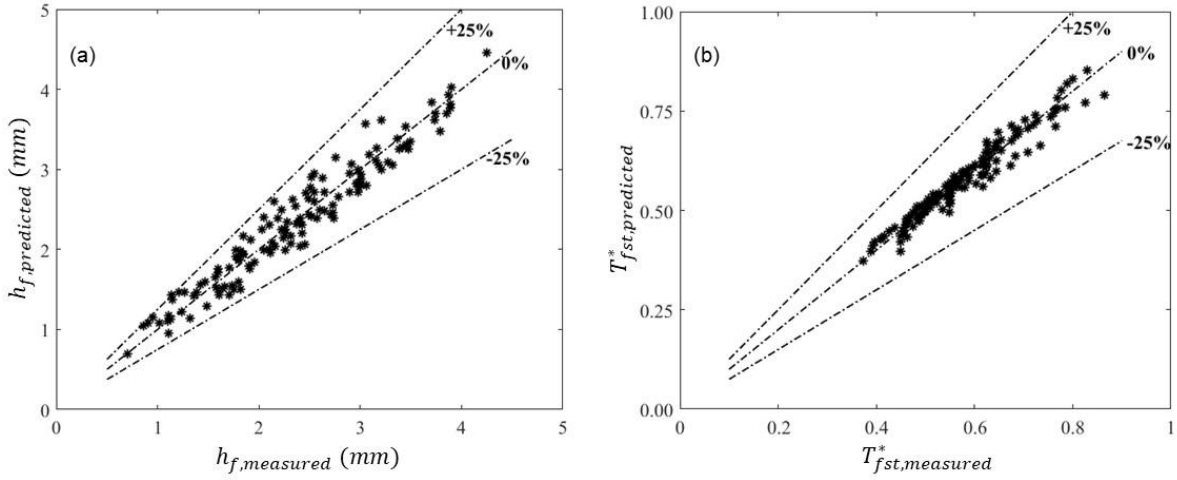

Figure 35. Correlation of BFT measured quantities: a) frost thickness and b) frost surface temperature

The resulting RMS roughness correlation is presented in Equation 13, and the resulting equivalent stand-grain roughness prediction is presented in Equation 14.

$$R_q^* = \frac{R_q}{h_f} = 2.123(w_a)^{-0.023}(Re_D)^{0.065}\left(\frac{T_{air}-T_o}{T_o}\right)^{0.790}\left(\frac{T_o-T_s}{T_o-T_{fst}}\right)^{-1.227}\left(\frac{T_{fst}-T_s}{T_o-T_s}\right)^{0.342} \quad 13$$

$$k_s^* = \frac{k_s}{h_f} = 0.029(w_a)^{0.367}(Re_D)^{0.150}\left(\frac{T_{fst}-T_s}{T_o}\right)^{0.342}\left(exp\left(\frac{T_{air}-T_{fst}}{T_{air}-T_s}\right)\right)^{6.716} \quad 14$$

Each of the roughness correlations are presented in terms of non-dimensional thicknesses and are made relative to the frost thickness. Equation 14 was created by correlating the calculated equivalent sand-grain roughness parameters from the correlation of Flack and Schultz (2010) from Equation 5.

Figure 36 presents a comparison of the correlation predictions for the roughness parameters compared to the values from the experiments. The correlations of Equations 13 and 14 demonstrate significant scatter compared to the frost thickness and temperature correlations. The R^2 values for the RMS roughness and k_s correlations are 0.57 and 0.534, respectively.

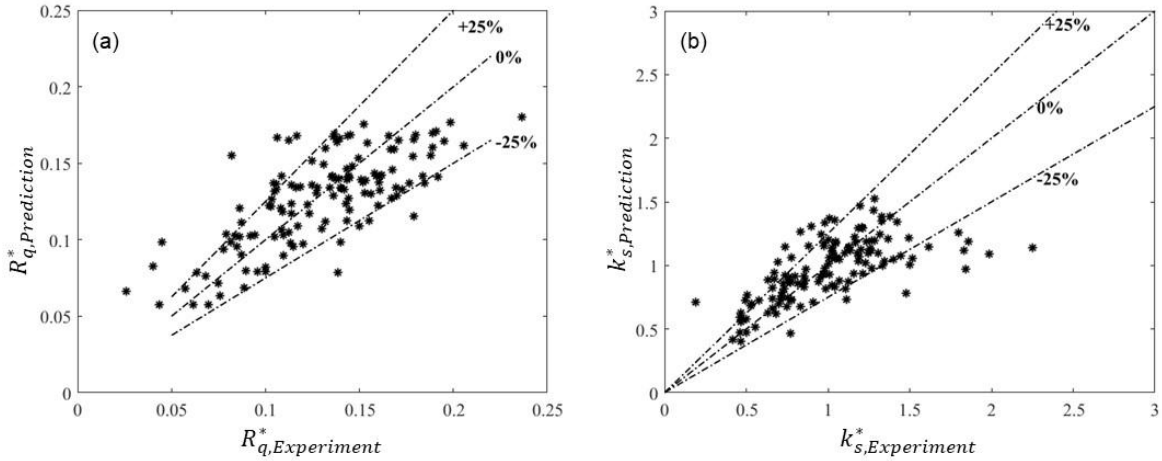

Figure 36. Comparison of experimental roughness and correlation predictions: a) RMS roughness and b) equivalent sand-grain roughness

7 Summary of Climatic Chamber and Aviation Frost Facility frost measurements

While the BFT measurements provide substantial data for model development and validation, the thermoelectric cooler approach did not replicate the fuel convection and wing-skin conduction

that are part of real CSFF conditions. The objective of the CAFF measurements was to study the frost evolution on the top surfaces of integrated wing fuel tanks with aviation representative surface coatings. Additionally, the CAFF investigations used models of appropriate wing scale sizes. However, jet fuel could not be used in the wing tank thermal model. A 60% propylene glycol and 40% deionized water mixture was used in the wing tank thermal model as a "fuel surrogate."

For each skin configuration and at each measurement location from the leading edge of the wing tank model, a series of tests were performed using three air set point temperatures (5 °C, 10 °C, or 16 °C), two air speeds (generally set points of 0.4 m/s or 1.4 m/s), one relative humidity (typically 82%), and as many as three locations along the wing skin surface in the airflow streamwise direction. The chiller set point for the primary coolant was typically -27 °C.

7.1 Climatic Chamber and Aviation Frost Facility measurements on painted aluminum skins

CSFF tests were performed using two aluminum skins. The first skin did not have a rib structure, but the second skin had five holes placed down the centerline of the wind tunnel in the flow direction to attach an internal aluminum beam. The purpose of the rib structure was to replicate how internal ribs or stringers interact with colder fluid away from the aircraft skin. The aluminum structures are highly thermally conductive and essentially cool the skin locally near the temperature of the coldest fluid with which the rib/stringer interacts.

7.1.1 Measurements without rib structure

Table 3 presents the cases and set point conditions used for the tests on the aluminum skin without a rib structure. The primary coolant temperature was not the standard value of -27 °C, and the relative humidity set point was 87%. The tests on the skin with the aluminum surface without a rib were performed first, and while CAFF shakedown tests were completed, the test matrix was being refined. During the initial cases with T_{PC} = -28 °C, the primary coolant became sufficiently viscous to cause vibration in the chiller pump. The coldest setpoint identified that avoided chiller pump vibration was T_{PC} = -27 °C. During the first set of CAFF tests, the high humidity values were found to cause condensation on the camera lens. One of the operators would periodically need to enter the CAFF and use a lens cloth to clear the condensation. Subsequent tests were performed at set points of 82% to avoid condensation on the photogrammetry camera lens and reduce entry into the CAFF during testing.

Table 3. Nominal Test Conditions for Wing Tank Thermal Model with an Aluminum Skin without a Structural Rib

Date	T_{PC} (°C)	$T_{air,set}$ (°C)	RH (%)	V (m/s)	x_{img} (in.)	Notes
11/15/19	-28	10	87	1.0	20.75	20 min. int.
11/21/19	-28	6	87	1.0	20.75	20 min. int.
12/06/19	-28	14	87	1.0	20.75	20 min. int.
12/18/19	-25	10	87	0.3	20.75	20 min. int.
12/20/19	-25	6	87	0.3	20.75	20 min. int.
12/23/19	-25	15	87	0.3	20.75	20 min. int.

Only one x-location from the leading edge was used for photogrammetry measurements on the aluminum skin without a rib. When the aluminum skin without a rib was attached to the wing tank thermal model and the tank was filled with the fuel surrogate, the skin flexed outward. To compensate for the changes in density of the fuel surrogate, an expansion tank was created and provided approximately 40 in. of head pressure on the fuel surrogate. This head pressure was sufficient to bend the skin without a structural rib. Additionally, the photogrammetry approach each of the images used for surface triangulation was focused and at the same plane. The location chosen for the aluminum skin without a rib was a location near the middle of the skin where the bend was sufficiently small that the photogrammetry images acquired in one plane were all in focus.

The resulting frost measurements and statistics for the aluminum skin without a structural rib are presented in Figure 37. The RMS roughness height is presented in Figure 37(a), the surface skewness values are presented in Figure 37(b), the predicted equivalent sand-grain roughness values are reported in Figure 37(c), and the peak-to-valley roughness heights are shown in Figure 37(d). The details of the measured atmospheric conditions, the tabular frost measurement results, and the frost topographies from the photogrammetry images are presented in Appendix B for the aluminum skin without a rib.

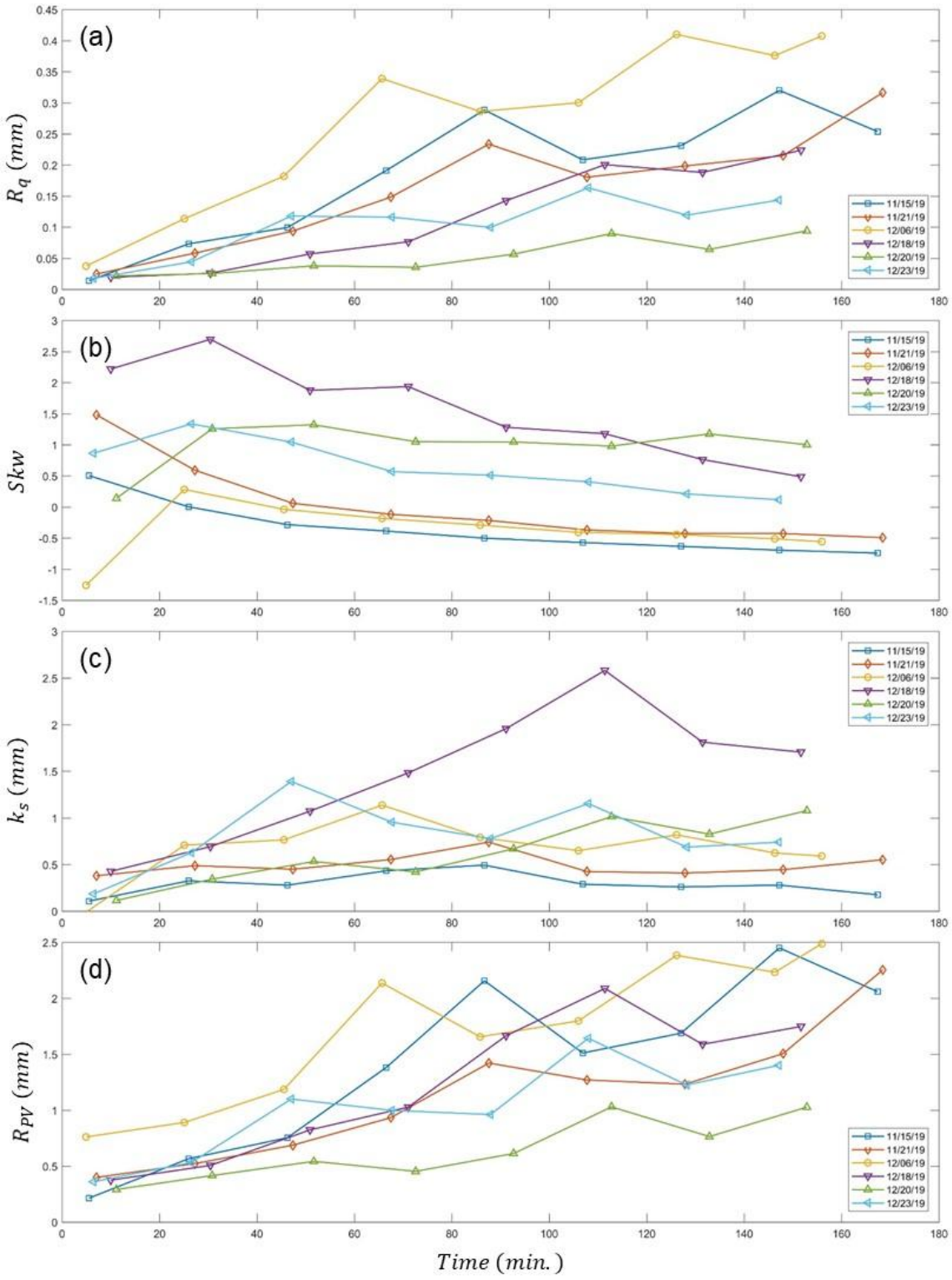

Figure 37. CAFF measurements of frost roughness using aluminum skin without rib structure at x = 20.75 in. from leading edge: a) RMS roughness, b) skewness, c) predicted equivalent sand-grain roughness, and d) peak-to-valley height

7.1.2 Measurements with aluminum rib

The nominal conditions for tests at three locations using the aluminum skin with an aluminum rib are presented in Table 4. The three locations were chosen based on distance from the screw heads used to attach the rib structure to the skin. The lateral location of the screw heads was on the centerline of the skin. The location of the photogrammetry measurements was selected to be either approximately two inches upstream or three inches downstream, and the lateral location was selected such that the roughness characterization was approximately 0.5 in. from the centerline. Because the screw heads protruded from the skin, the circulation and reattachment flows created a wake region downstream of the screw heads. Figure 38 presents an image following the complete 03/18/20 test indicating the presence of the enhanced frost roughness caused by the screw head. The streamwise locations of the photogrammetry measurements were selected to avoid the frost enhancement regions caused by the screw heads while remaining on the skin region above the rib structure.

Table 4. Nominal test conditions for wing tank thermal model with an aluminum skin and a structural rib at three locations

Date	**T_{PC} (°C)**	**$T_{air,set}$ (°C)**	**RH (%)**	**V (m/s)**	**x_{img} (in.)**	**Notes**
2/26/20	-27	16	82	1.3	20.75	20 min. int.
3/04/20	-27	16	82	0.4	20.75	20 min. int.
3/09/20	-27	10	82	0.4	20.75	20 min. int.
3/18/20	-27	10	82	1.3	20.75	20 min. int.
3/20/20	-27	5	82	1.3	20.75	20 min. int.
3/23/20	-27	5	82	0.4	20.75	20 min. int.
7/29/20	-27	16	82	0.4	11.75	10 min. int.
8/3/20	-27	16	82	1.3	11.75	10 min. int.
8/5/20	-27	10	82	1.3	11.75	10 min. int.
8/8/20	-27	5	82	1.3	11.75	10 min. int.
8/11/20	-27	10	82	0.4	11.75	10 min. int.
8/14/20	-27	5	82	0.4	11.75	10 min. int.
8/28/20	-27	16	82	1.4	14.75	10 min. int.
9/24/20	-27	10	82	1.4	14.75	10 min. int.

Date	T_{PC} (°C)	$T_{air,set}$ (°C)	RH (%)	V (m/s)	x_{img} (in.)	Notes
9/29/20	-27	5	82	1.4	14.75	10 min. int.
10/1/20	-27	10	82	0.4	14.75	10 min. int.
10/6/20	-27	5	82	0.4	14.75	10 min. int.
10/8/20	-27	16	82	0.4	14.75	10 min. int.

Figure 38. Frost surrounding rib screw head following 031820 frost test

The resulting frost measurements and statistics for the aluminum skin with a structural rib are presented in Figure 39, Figure 40, and Figure 41. The RMS roughness height is presented in Figure 39(a)-Figure 41(a), the surface skewness values are presented in Figure 39(b)-Figure 41(b), the predicted equivalent sand-grain roughness values are reported in Figure 39(c)-Figure 41(c), and the peak-to-valley roughness heights are shown in Figure 39-Figure 41(d). The details of the measured atmospheric conditions, the tabular frost measurement results, and the frost topographies from the photogrammetry images are presented in Appendix C for the aluminum skin with a rib. In addition to the cases reported in Figure 39, Figure 40, and Figure 41, Appendix C includes multiple repeatability cases and three cases from a fourth photogrammetry measurement location in the streamwise direction.

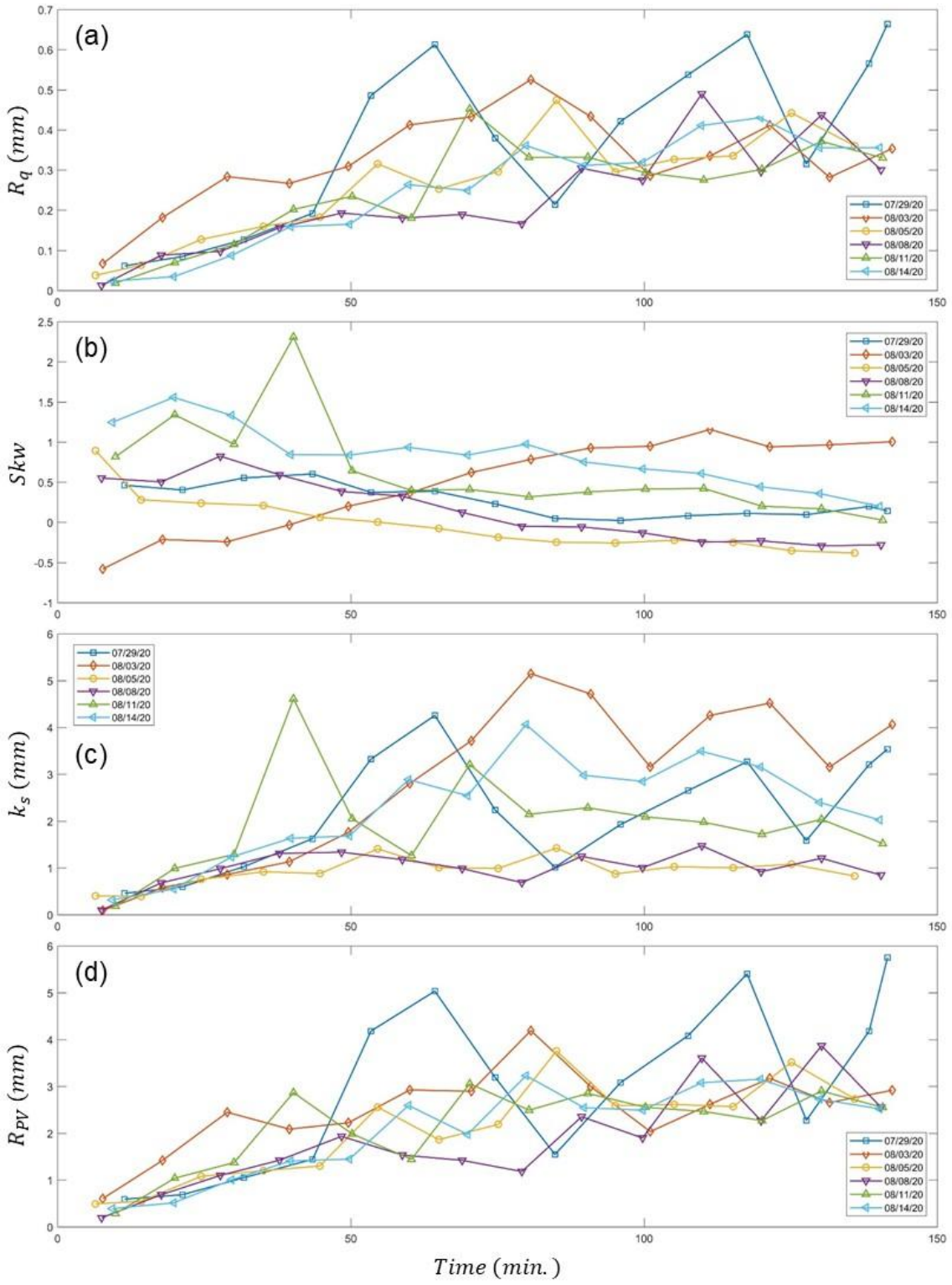

Figure 39. CAFF measurements of frost roughness using aluminum skin with a rib structure at x = 11.75 in. from leading edge: a) RMS roughness; b) skewness; c) predicted equivalent sand-grain roughness; and d) peak-to-valley height

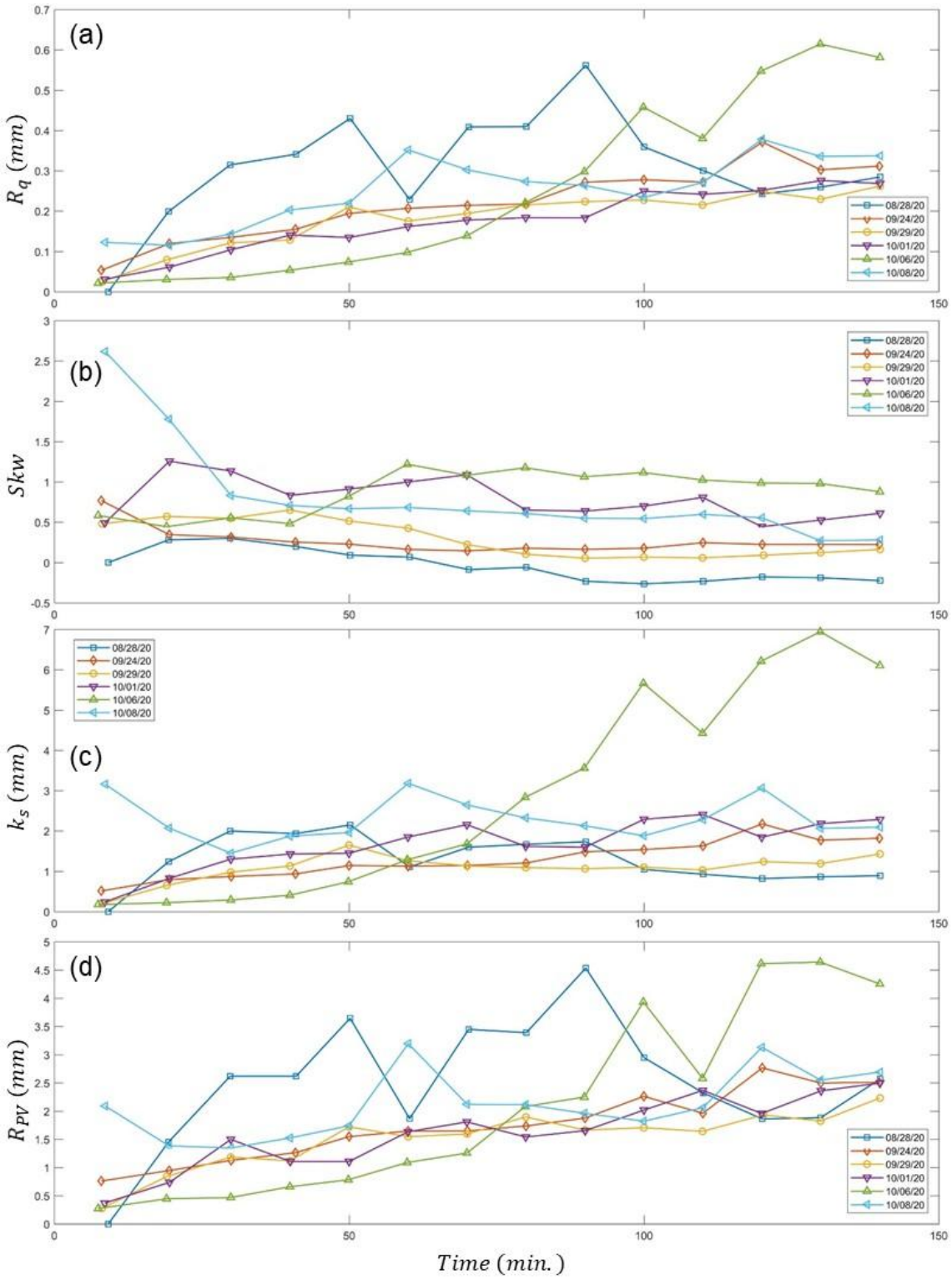

Figure 40. CAFF measurements of frost roughness using aluminum skin with a rib structure at x = 14.75 in. from leading edge: a) RMS roughness; b) skewness; c) predicted equivalent sand-grain roughness; and d) peak-to-valley height

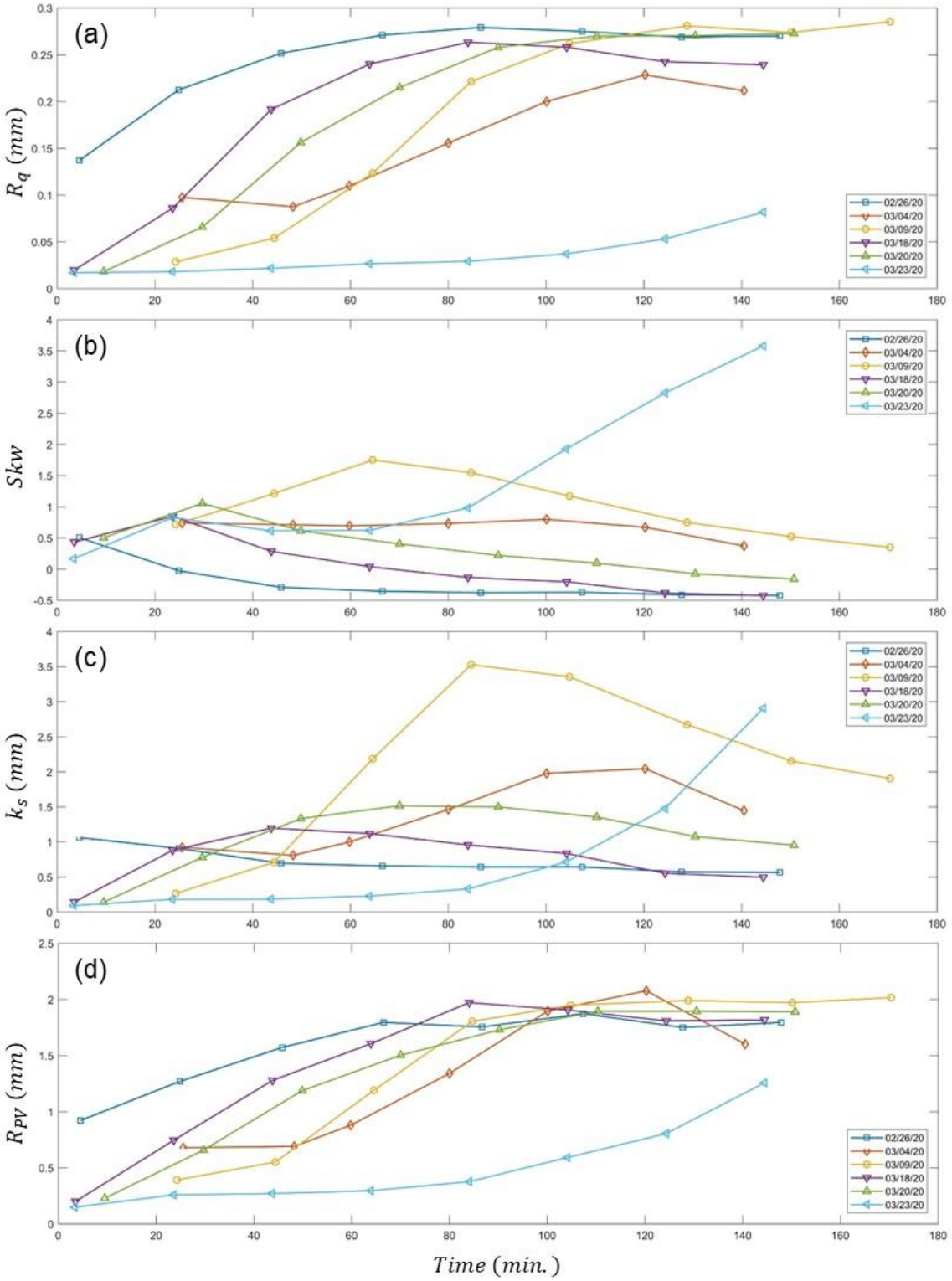

Figure 41. CAFF measurements of frost roughness using aluminum skin with a rib structure at x = 20.75 in. from leading edge: a) RMS roughness; b) skewness; c) predicted equivalent sand-grain roughness; and d) peak-to-valley height

7.2 Climatic Chamber and Aviation Frost Facility measurements on painted carbon fiber skins

CSFF tests were also performed using two carbon fiber composite skins. The first carbon fiber skin did not have a rib structure, but the second skin had five holes placed down the centerline of the wind tunnel in the flow direction. Screws were threaded through these holes to attach an internal aluminum beam.

7.2.1 Measurements without rib structure

The nominal conditions for tests at three locations using the carbon fiber composite skin without a rib are presented in Table 5. The streamwise locations differed from those used for the aluminum skin with a rib, but the locations were within 10 cm. The locations for the fiber composite skin were shifted because of slight imperfections in the paint that we thought might influence the frost roughness evolution.

Table 5. Nominal test conditions for wing tank thermal model with a carbon fiber skin without a structural rib

Date	T_{PC} (°C)	$T_{air,set}$ (°C)	RH (%)	V (m/s)	x_{img} (in.)	Notes
03/03/21	-27	16	82	1.4	17.5	10 min. int., frost formed then quickly melted
03/08/21	-27	10	82	1.4	17.5	10 min. int.
03/10/21	-27	5	82	1.4	17.5	10 min. int.
03/24/21	-27	5	82	0.4	17.5	10 min. int.
03/26/21	-27	10	82	0.4	17.5	10 min. int.
03/31/21	-27	16	82	0.4	17.5	10 min. int., frost formed then melted, test ended at 70 min.
04/12/21	-27	5	82	0.4	12.0	10 min. int.
04/14/21	-27	10	82	0.4	12.0	10 min. int.
04/16/21	-27	5	82	1.4	12.0	10 min. int.
04/19/21	-27	10	82	1.4	12.0	10 min. int.
04/21/21	-27	5	82	1.4	20.8	10 min. int.
04/23/21	-27	10	82	1.4	20.8	10 min. int.
04/26/21	-27	16	82	0.4	20.8	10 min. int.

Date	T_{PC} (°C)	$T_{air,set}$ (°C)	RH (%)	V (m/s)	x_{img} (in.)	Notes
04/28/21	-27	10	82	0.4	20.8	10 min. int.
04/30/21	-27	5	82	0.4	20.8	10 min. int.

Some of the cases using the carbon fiber skin failed to generate frost at the highest CAFF set point air temperature (16 °C). As shown in Table 5, two of the cases at the 17.5-in. photogrammetry location ended before the full 140 minutes of testing time was completed. Figure 42 presents images from the incomplete tests identified in Table 5. In Figure 42(a), the camera was clearly not at the correct location indicated in Table 5. For Case 03/03/21, frost initially formed on the skin then melted in a line progressing from the leading edge to the trailing edge. Once this behavior was observed, the camera was moved in an attempt to capture images in the vicinity of the thawing front. Three other cases were not characterized because of the lack of frost during the tests.

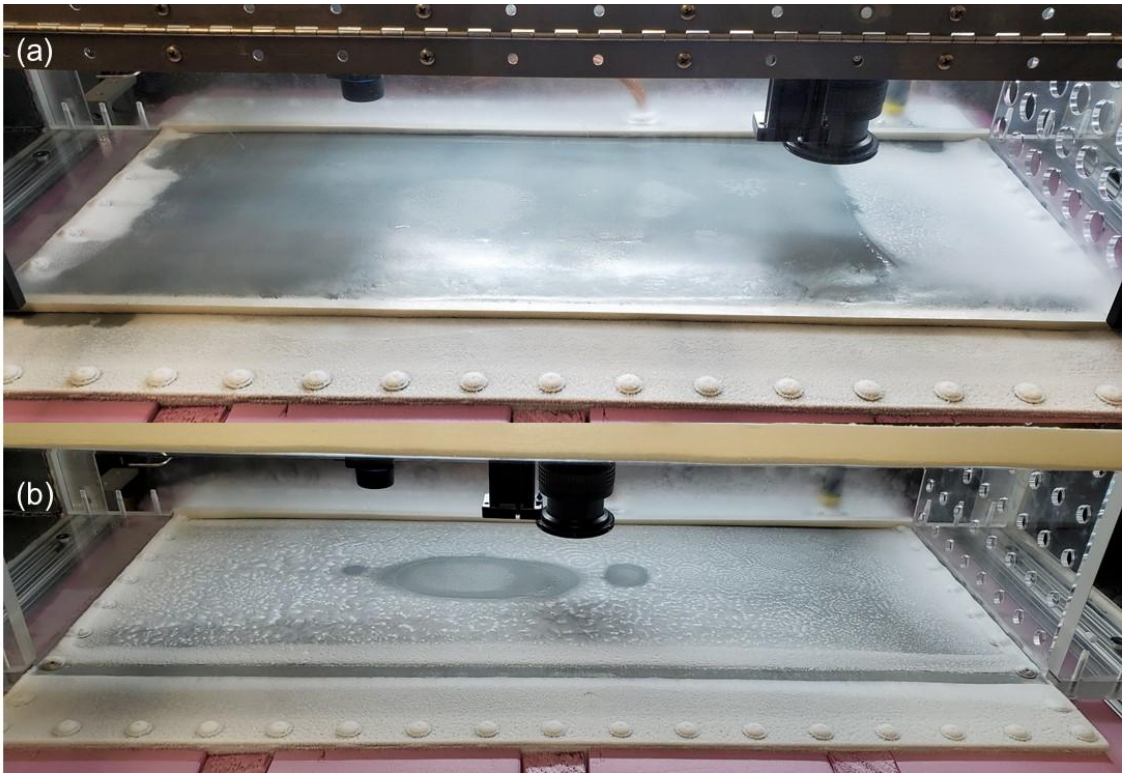

Figure 42. Images from partial test cases or cases that ended early: a) 03/03/21 and (b) 03/31/21

The resulting frost measurements and statistics for the carbon fiber composite skin without a structural rib are presented in Figure 43, Figure 44, and Figure 45. The RMS roughness height is presented in Figure 43(a)-Figure 45(a), the surface skewness values are presented in Figure 43(b)-**Error! Reference source not found.**(b), the predicted equivalent sand-grain roughness values are reported in Figure 43(c)-Figure 45(c), and the peak-to-valley roughness heights are shown in Figure 43(d)-Figure 45(d). The details of the measured atmospheric conditions, the tabular frost measurement results, and the frost topographies from the photogrammetry images are presented in Appendix D for the carbon fiber composite skin without a rib.

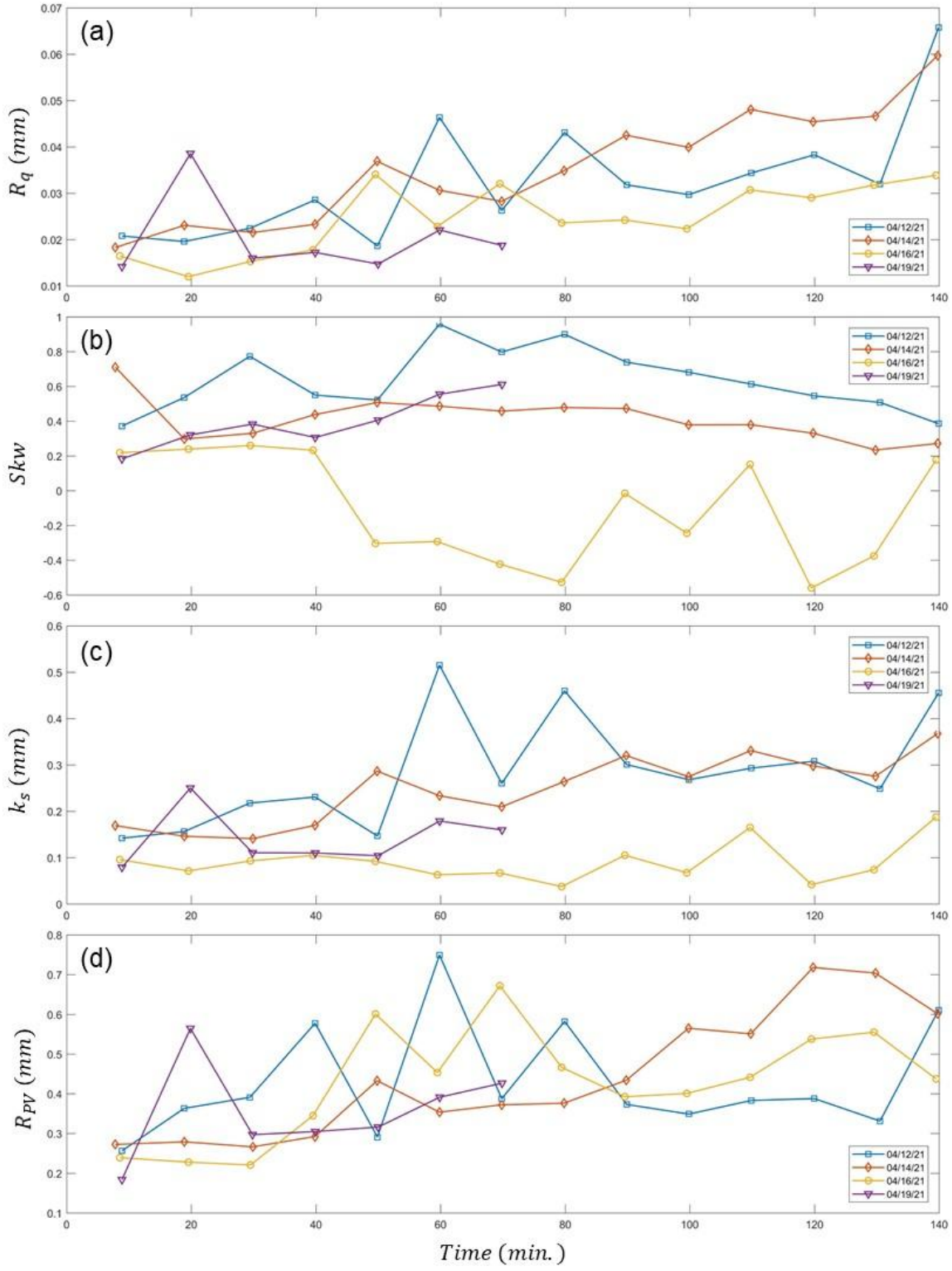

Figure 43. CAFF measurements of frost roughness using carbon fiber skin without rib structure at x = 12.0 in. from leading edge: a) RMS roughness; b) skewness; c) predicted equivalent sand-grain roughness; and d) peak-to-valley height

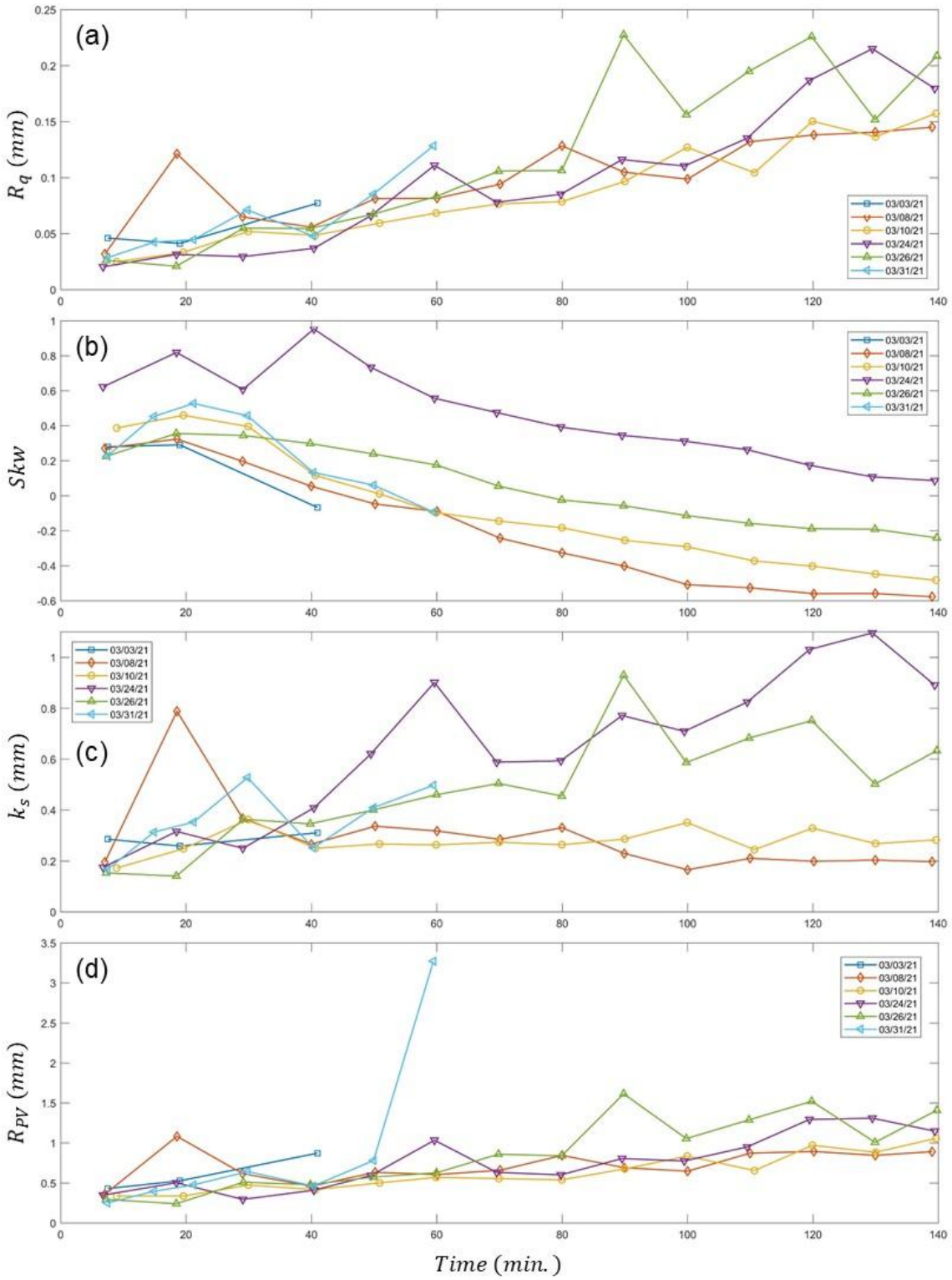

Figure 44. CAFF measurements of frost roughness using carbon fiber skin without rib structure at x = 17.5 in. from leading edge: a) RMS roughness; b) skewness; c) predicted equivalent sand-rain roughness; and d) peak-to-valley height

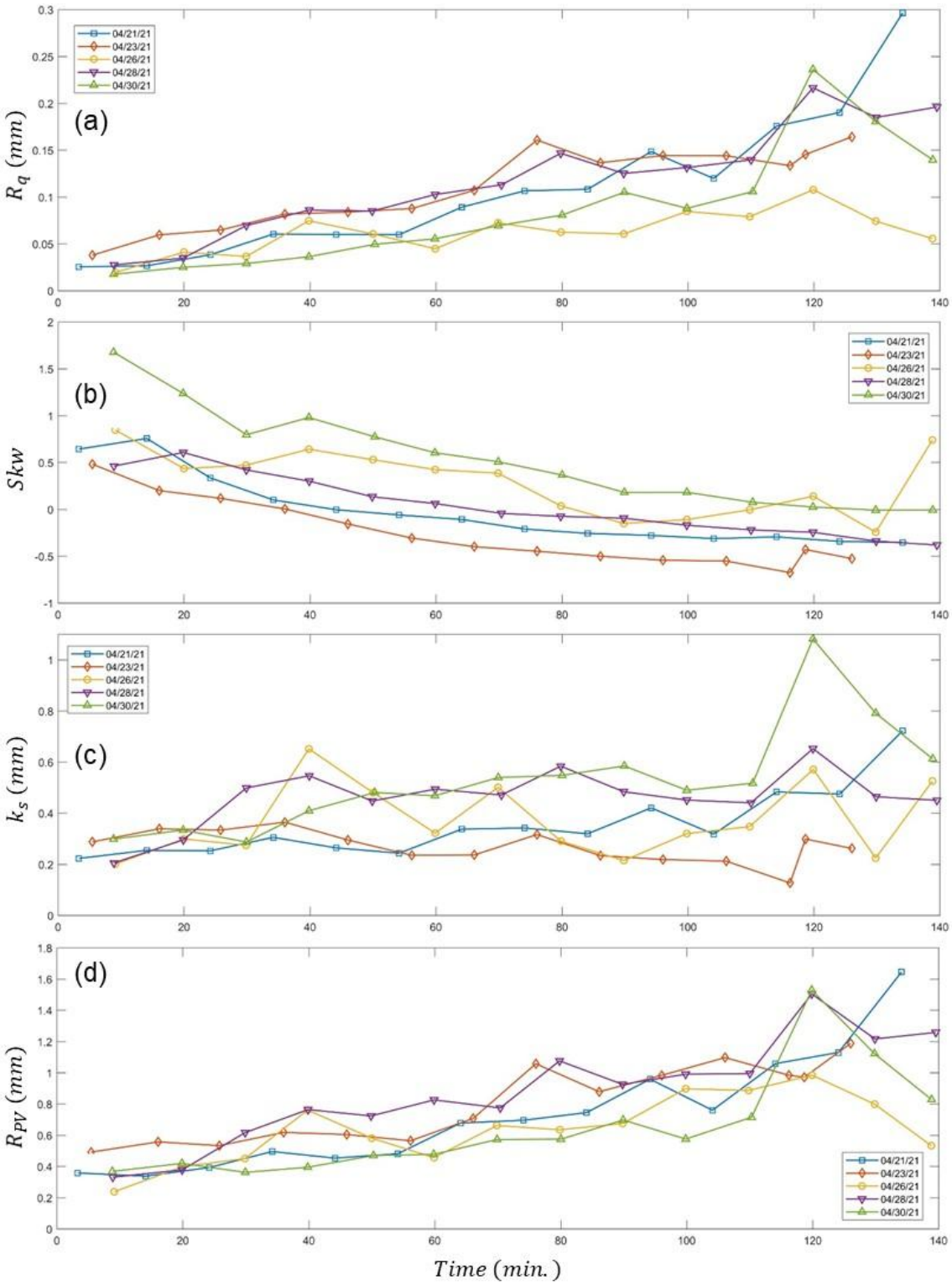

Figure 45. CAFF measurements of frost roughness using carbon fiber skin without rib structure at x = 20.8 in. from leading edge: a) RMS roughness; b) skewness; c) predicted equivalent sand-grain roughness; and d) peak-to-valley height

7.2.2 Measurements with aluminum rib

The nominal conditions for tests at three locations using the carbon fiber composite skin with an aluminum structural rib are presented in Table 6. The streamwise locations used were not exactly the same as for the aluminum skin with a rib or the carbon fiber composite skin without a rib, but the locations were within 10 cm. The locations were shifted because of slight imperfections in the paint that were thought to influence the frost roughness evolution or because of the presence of the screw heads on the top surface of the skin.

Table 6. Summary of nominal test conditions for wing tank thermal model with a carbon fiber skin and an aluminum structural rib

Date	**T_{PC} (°C)**	**$T_{air,set}$ (°C)**	**RH (%)**	**V (m/s)**	**x_{img} (in.)**	**Notes**
06/19/21	-27	16	82	1.3	21.0	10 min. int.
06/21/21	-27	10	82	1.3	21.0	10 min. int.
06/23/21	-27	5	82	1.3	21.0	10 min. int.
06/25/21	-27	5	82	1.5	21.0	10 min. int.
06/28/21	-27	16	82	0.3	21.0	10 min. int.
06/30/21	-27	10	82	0.3	21.0	10 min. int.
07/02/21	-27	5	82	0.3	21.0	10 min. int.
07/06/21	-27	5	82	0.3	12.0	10 min. int.
07/30/21	-27	16	82	0.3	12.0	10 min. int.
08/03/21	-27	10	82	0.3	12.0	10 min. int.
08/12/21	-27	5	82	0.3	12.0	10 min. int.
08/16/21	-27	5	82	1.4	12.0	10 min. int.
08/18/21	-27	10	82	1.4	12.0	10 min. int.
08/21/21	-27	16	82	1.4	12.0	10 min. int.
09/04/21	-27	5	82	1.4	17.0	10 min. int.
09/07/21	-27	10	82	1.4	17.0	10 min. int.
09/10/21	-27	16	82	1.4	17.0	10 min. int.
09/14/21	-27	5	82	0.3	17.0	10 min. int.
09/16/21	-27	10	82	0.3	17.0	10 min. int.
08/18/21	-27	16	82	0.3	17.0	10 min. int.

The importance of the rib was noticeable during the tests. Figure 46 presents images following complete frosts tests using the carbon fiber skin with a rib. In Figure 46(a) a low air speed case, Case 07/30/21, is depicted that does not exhibit evidence of flow separation and reattachment downstream of the screw heads as observed in Figure 38. However, the taller and denser frost near the rib is evident. A higher speed case at the highest temperature, Case 08/21/21, is shown in Figure 46(b). Outside the rib region on the carbon fiber composite skin, the frost mostly melted by the end of the 08/21/21 test.

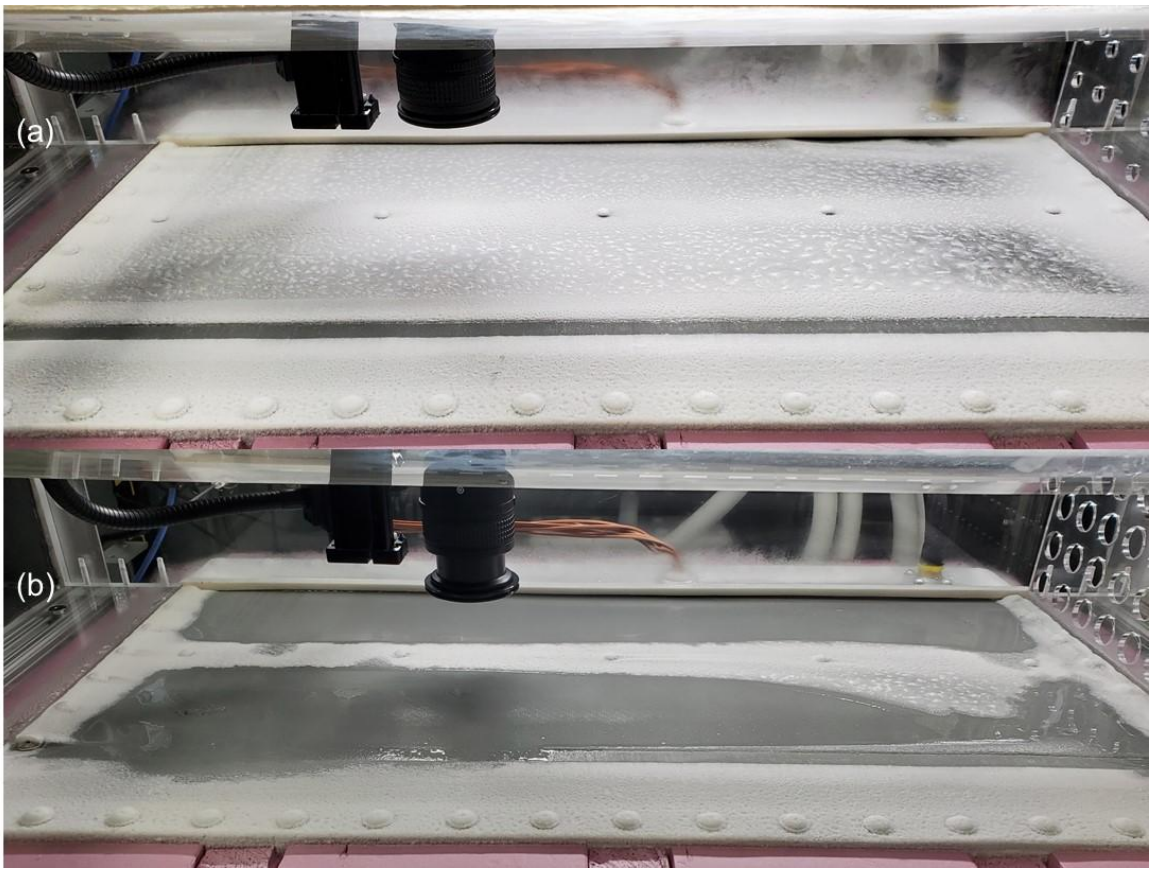

Figure 46. Images following tests using the carbon fiber composite skin

The resulting frost measurements and statistics for the carbon fiber composite skin with an aluminum structural rib are presented in Figure 47, Figure 48, and Figure 49. The RMS roughness height is presented in Figure 47(a)-Figure 49(a), the surface skewness values are presented in Figure 47(b)-Figure 49(b), the predicted equivalent sand-grain roughness values are reported in Figure 47(c)-Figure 49(c), and the peak-to-valley roughness heights are shown in Figure 47(d)-Figure 49(d). The details of the measured atmospheric conditions, the tabular frost

measurement results, and the frost topographies from the photogrammetry images are presented in Appendix D for the carbon fiber composite skin with an aluminum structural rib.

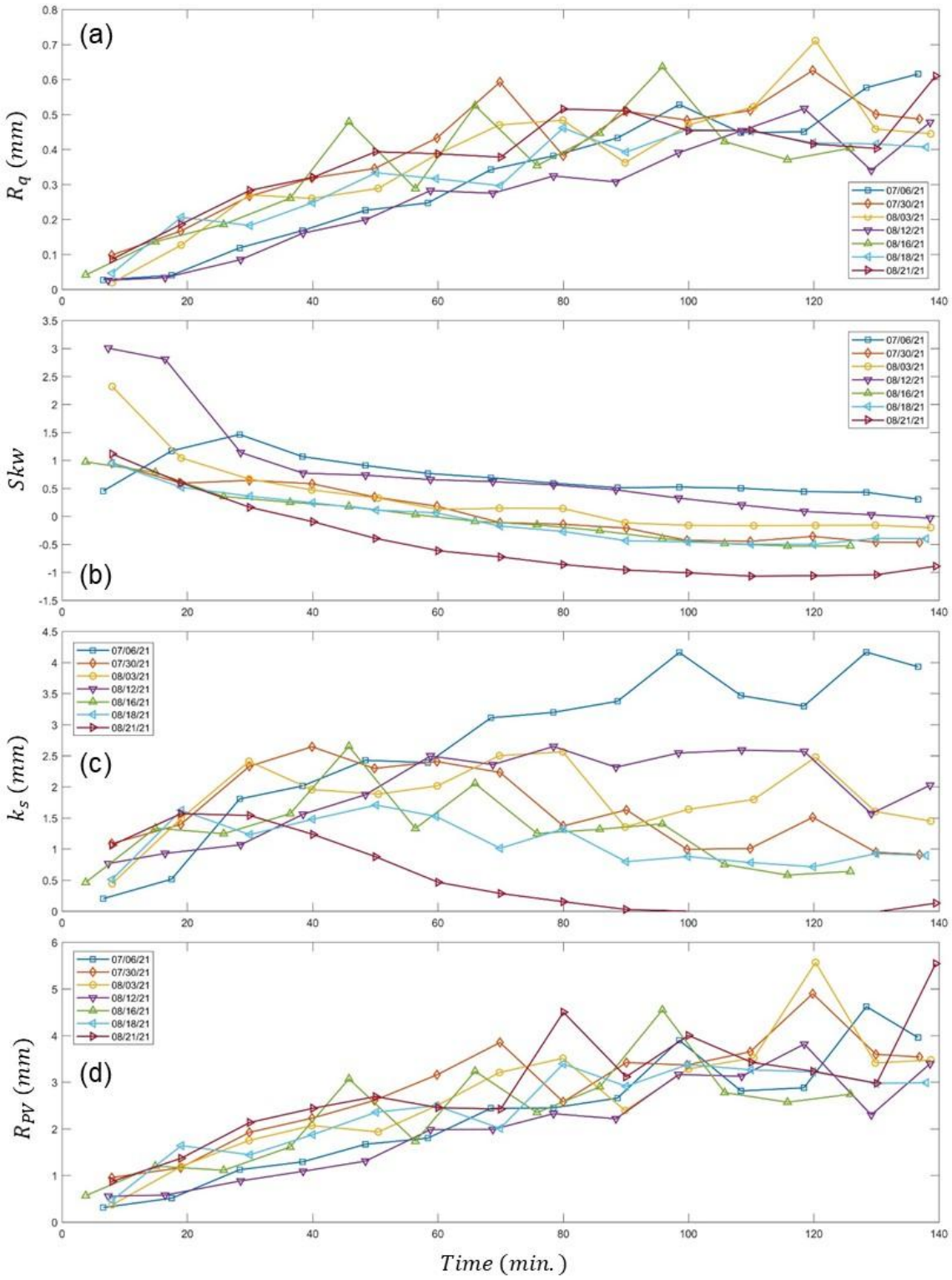

Figure 47. CAFF measurements of frost roughness using carbon fiber skin with rib structure at x = 12.0 in. from leading edge: a) RMS roughness; b) skewness; c) predicted equivalent sand-grain roughness; and d) peak-to-valley height

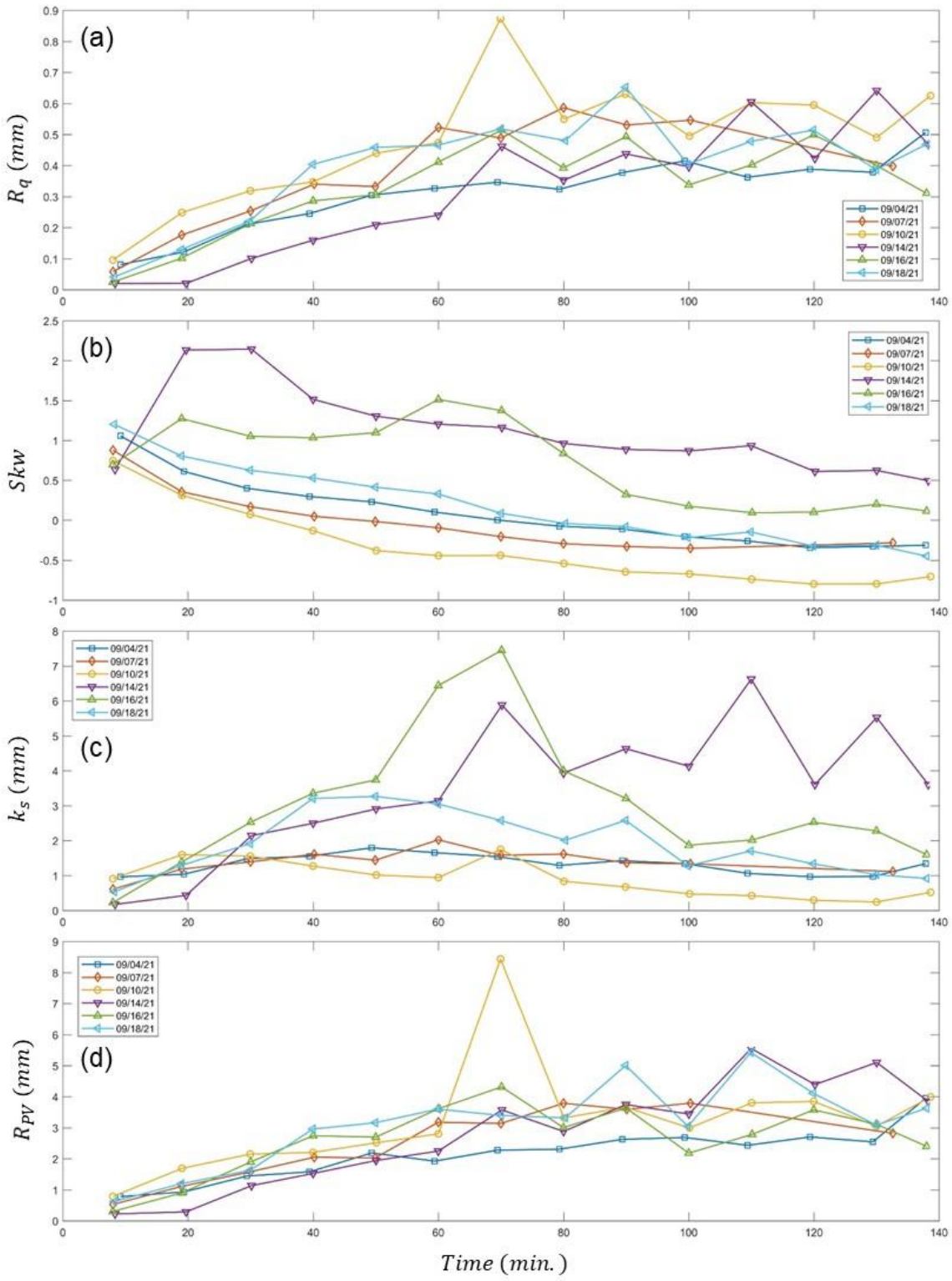

Figure 48. CAFF measurements of frost roughness using carbon fiber skin with rib structure at x = 17.0 in. from leading edge: a) RMS roughness; b) skewness; c) predicted equivalent sand-grain roughness; and d) peak-to-valley height

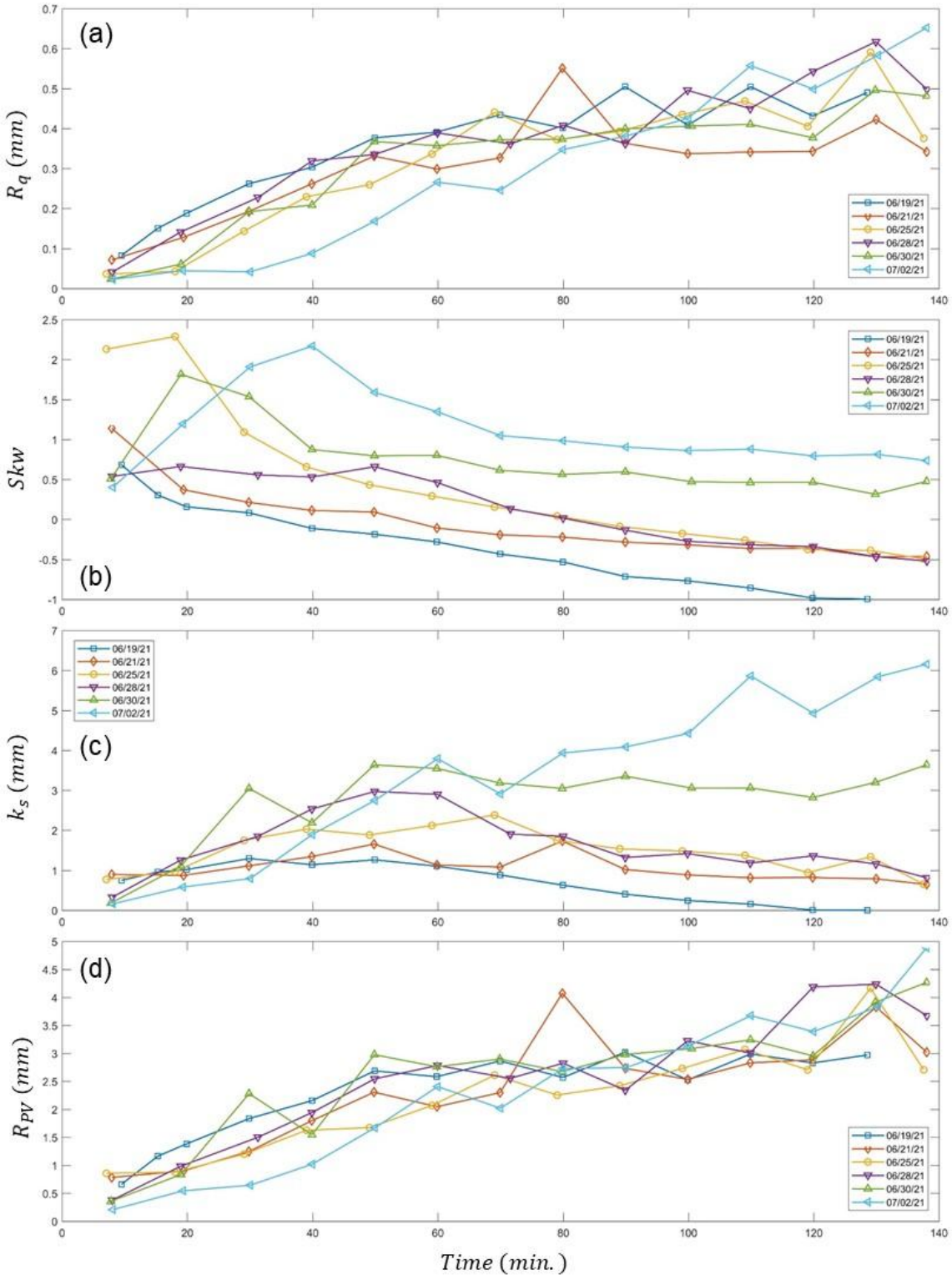

Figure 49. CAFF measurements of frost roughness using carbon fiber skin with rib structure at x = 21.0 in. from leading edge: a) RMS roughness; b) skewness; c) predicted equivalent sand-grain roughness; and d) peak-to-valley height

8 Carbon fiber skin thermal conductivity

The thermal conductivity of the wing skin is a critical thermal parameter to capture when modeling the CSFF process. Variability may exist in the creation of carbon fiber composites based on the carbon fiber used, procedures followed in the layup of the different carbon fiber sheets, and the exact epoxy composition used in bonding. Because of the variability, sections from the sheet used to cut the carbon fiber skins for the CAFF testing were created and tested in a custom apparatus.

8.1 Thermal conductivity apparatus

The apparatus was based on the ASTM C177-19 (2019), with the exception that the guard heaters were not used, and the heat losses were mitigated using Balsa wood as insulation to surround the apparatus. The schematic of the apparatus is shown in Figure 50 and was constructed to split the energy consumed by a 350-Ω resistance heater in opposite directions along the same axis. Copper sheets with a thickness of 1 mm were then used to evenly distribute the energy from the heater. The carbon fiber specimens with thermocouples attached to each side were then placed after the copper plates. Finally, 2-in. finned aluminum heat sinks were placed on the outside of the carbon fiber specimens. Cooling fans, which are not shown in Figure 50, were placed on either side of the apparatus to enhance heat transfer from the aluminum sinks. The apparatus is shown in Figure 51.

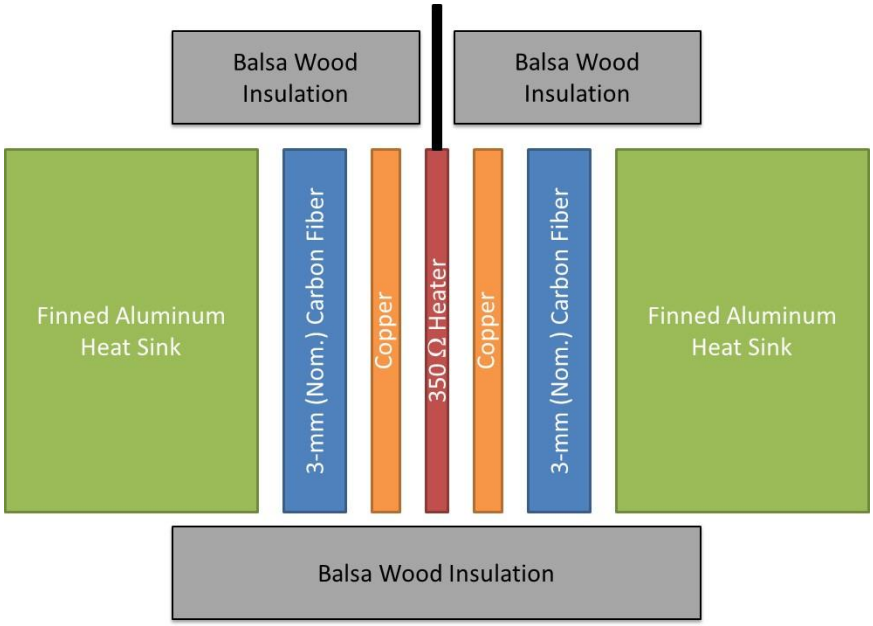

Figure 50. The schematic of the carbon fiber thermal conductivity apparatus

Figure 51. Views of the as-built carbon fiber thermal conductivity apparatus: a) apparatus without Balsa top insulation and b) fully assembled apparatus

The carbon fiber coupons used in the measurements were 2 in. by 2 in. The thickness of the coupons used for the thermal conductivity measurements was measured twenty times using a set of Fowler micrometers with a resolution of 0.0001 in. The mean coupon thickness was measured to be 0.122 in.

8.2 Thermal conductivity measurement procedure

Carbon fiber composite structures are known to have varying thermal conductivity with temperature. Consequently, the thermal conductivity of the carbon fiber coupons was characterized over the same temperature range as experienced during the CSFF measurements. The apparatus shown in Figure 51 was installed in the CAFF, and the temperature of the CAFF was controlled so that the resulting coupon temperatures bounded the range of temperatures observed during the frost measurements.

For the thermal conductivity measurements, the voltage across the resistive heating element was set. The desired air temperature was then set on the CAFF controller. Approximately two hours were required for the thermocouples to reach a quasi-equilibrium state. The term *quasi-*

equilibrium was used to describe the process, because the thermal cycling of the CAFF controller created a situation in which the temperatures of carbon fiber coupons was cyclic but not steady.

Figure 52 presents a time history of the thermocouple measurements during the thermocouple conductivity test with the voltage across the heating element set to 30 V. In Figure 52, the four thermocouples on the sides of the coupons, the CAFF temperature, and the CAFF set point temperature are presented as a function of time during a thermal conductivity test. For the tests depicted in Figure 52, four measurements were performed at different air temperature set points. The four shaded regions indicate the regions where the test conditions were averaged for the thermal conductivity measurements. The cyclic nature of the test temperatures caused by the CAFF temperature control system is evident in Figure 52.

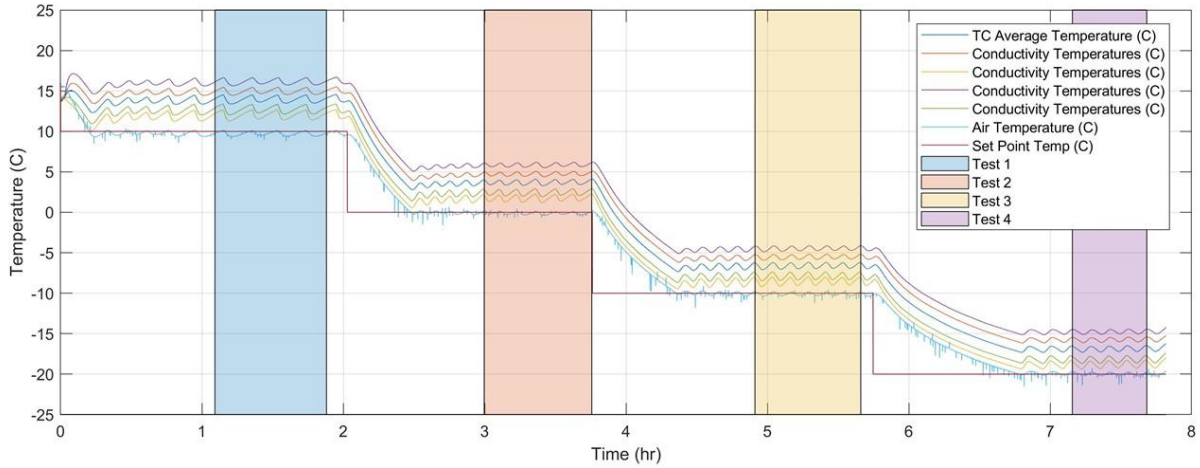

Figure 52. Time history for a carbon fiber thermal conductivity measurement

Because of the cycling of the CAFF temperature controller, the measurement averaging regions were constructed to create an integer number of complete cycles. To identify the integer number of complete cycles for each measurement, the mean temperature of the four carbon fiber coupon thermocouples was determined. The three-minute rolling slope of the temperature was then used to identify integer values of cycles. Figure 53 presents the three-minute slope of the carbon fiber coupon average temperature. The start of each test was initiated based on the following conditions: (1) at least an hour had to pass after a set point temperature change, and (2) the slope of the average temperature had to pass through 0 °C/min. with a rising slope. The end of the test was set after at least 30 minutes of testing when the slope of the average temperature again passed through 0 °C/min. with a rising slope.

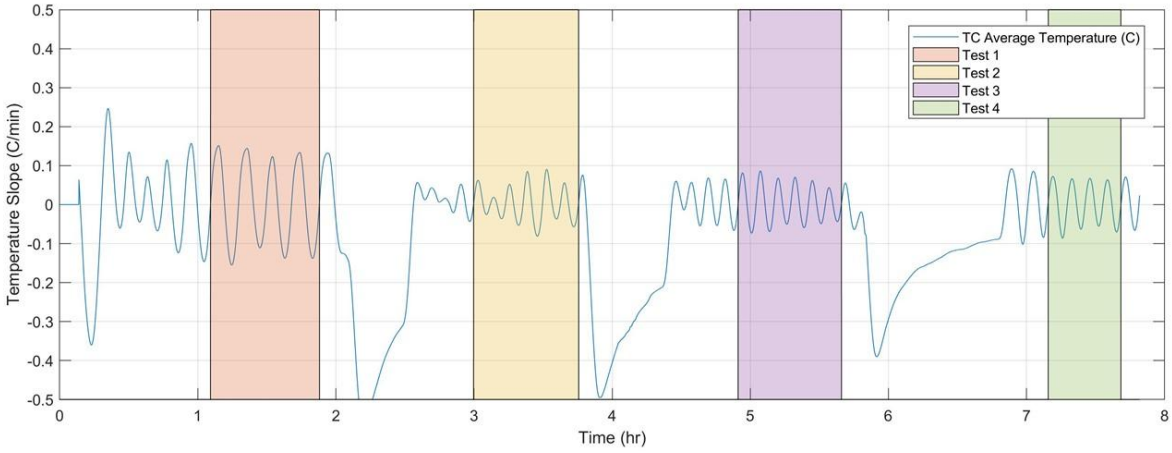

Figure 53. Three-minute average temperature slope identifying measurement periods

For each measurement or averaging period in Figure 53, the average temperatures from the sides of the carbon fiber coupons were determined. Based on Fourier's law, the thermal conductivity was calculated using Equation 15 for each measurement region identified in Figure 53.

$$k = \frac{V^2 t_C}{RA[(\overline{T_1} - \overline{T_3}) + (\overline{T_2} - \overline{T_4})]} \quad 15$$

The uncertainty of the resulting thermal conductivity values was determined using the approach of Coleman and Steele (1999).

8.3 Carbon fiber thermal conductivity results

Figure 54 presents the measured thermal conductivity of the carbon fiber over the range of -18 °C to 15 °C. A linear fit to the data shown in Figure 54 had an intercept of 0.4805 W/(m·K) and a slope of 0.000336 W/(m·K^2). However, the uncertainties of the measurements were larger than the observed range of the measurements. Consequently, an average value of 0.48 W/(m·K) ± (0.015 W/(m·K)) would also be acceptable for the value of the thermal conductivity of the carbon fiber coupons over the range of temperatures investigated. The trend of increasing thermal conductivity with temperature and the average value were in agreement with reported trends for thermal conductivity for carbon fiber composite panels measured at higher temperatures (Joven, Das, Ahmed, Roozbehjavan, & Minaie, 2012; Sweeting & Liu, 2004).

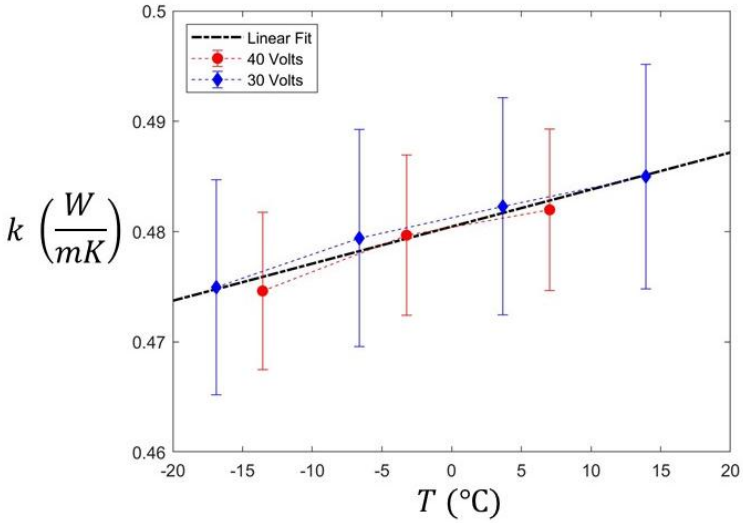

Figure 54. Measured carbon fiber sample thermal conductivity for two power settings

9 Frost and roughness evolution modeling

Many computational, analytical, and semi-empirical approaches to modeling CSFF and roughness evolution are available. The objectives of this section are 1) to identify critical physical aspects that should be captured using a CSFF model and 2) present an example approach. Because several modeling concepts were created based on the BFT measurements, the modeling results focus on applications to the CAFF measurements.

9.1 Cold soaked fuel frost thermal and mass transfer circuits

The formation of frost in a CSFF situation involves a net heat transfer from the fuel to the surrounding environment and a net mass transfer of water from the atmosphere to the frost layer. The heat and mass transfer processes in CSFF can be represented as thermal and mass circuits, as shown in Figure 55. As noted in the figure, the measurements made in the BFT did not capture the heat transfer that occurs between the fuel and the wing skin. The heat and mass transfer from/to the skin and environment was captured in the BFT. However, to properly model CSFF, the full model should include the heat transfer between the fuel and the skin. In the following sections, an example approach is presented and described based on the correlations developed in the BFT.

For the example approach, two simplifications were used. First, the correlation for frost thickness in Equation 11 directly considered the water accumulation in the frost layer and was dependent on the humidity ratio, which drives the frost process. Consequently, Equation 11 captured the mass transfer circuit depicted in Figure 55. Second, Figure 55 shows the latent energy release of

the liquid melt layer and the direct vapor-solid phase change in the dendrite layer. The latent energy process may either absorb energy, such as during a melt and frost densification period, or the process may reject energy to the air stream during the frost crystal formation. For the example modeling approach, the amount latent energy release or absorption was neglected.

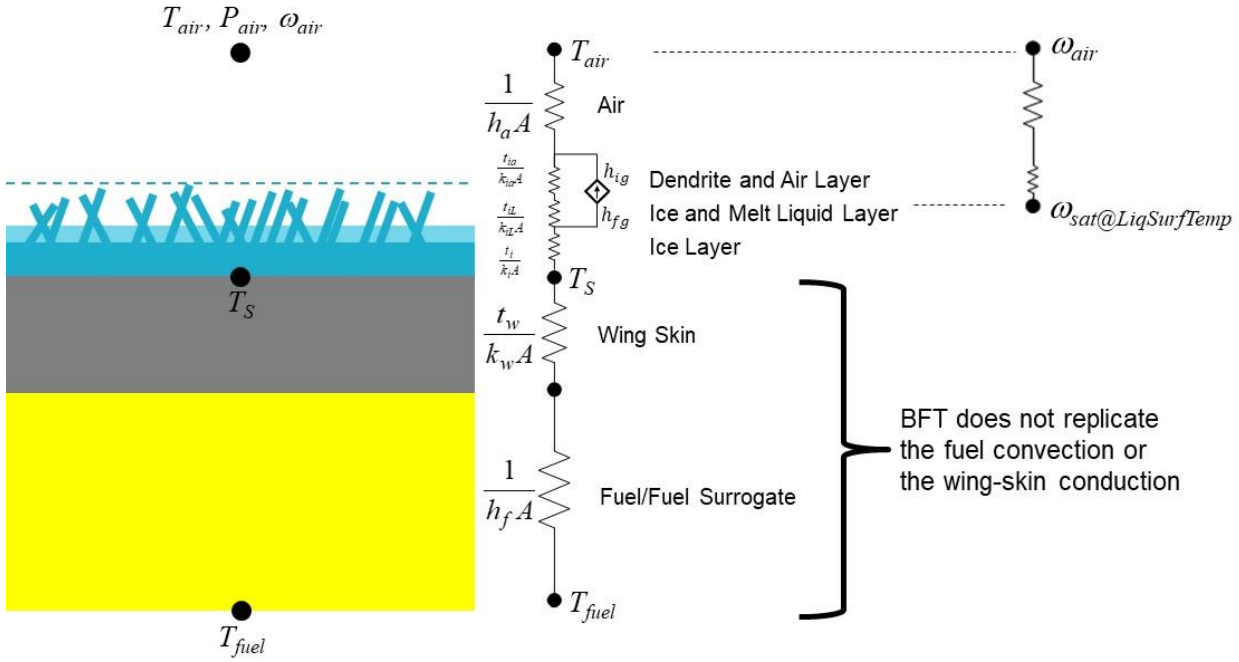

Figure 55. CSFF thermal and mass circuits

9.2 Fuel or fuel surrogate thermal properties

The thermal properties of the fuel or fuel surrogate when validating models using CAFF measurements were critical aspects of the thermal circuit. The fuel surrogate used for the CAFF measurements was a 60%-40% propylene glycol mixture with deionized water and corrosion inhibitor. The properties used for 60%-40% propylene glycol mixture were based on a Dynalene publication (Dynalene, Inc., 2014), which contained properties for propylene glycol-deionized water mixtures ranging from 20% to 60% propylene glycol. Example 60%-40% propylene glycol mixture thermal properties at -15 C (5 F) are:

$$\rho_{PG} = 1067 \frac{kg}{m^3}$$

$$\mu_{PG} = 94.6 \times 10^{-3} \frac{N \cdot s}{m^2}$$

$$k_{PG} = 0.309 \frac{W}{m \cdot K}$$

$$c_{p,PG} = 3.398 \frac{kJ}{kg \cdot K}$$

The following were important propylene glycol mixture properties that were calculated based on the basic information reported by Dynalene (2014).

$$\beta_{PG} = \frac{1}{\rho_{PG}} \left(\frac{\partial \rho_{PG}}{\partial T} \right)_{P=const.} = 3.783 \times 10^{-4} \frac{1}{K}$$

$$\nu_{PG} = \frac{\mu_{PG}}{\rho_{PG}} = 8.866 \times 10^{-5} \frac{m^2}{s}$$

$$\alpha_{PG} = \frac{k_{PG}}{\rho_{PG} c_{p,PG}} = 8.522 \times 10^{-8} \frac{m^2}{s}$$

9.3 Internal convective heat transfer coefficient

The propylene glycol mixture properties were important for the determination of the convection coefficient on the internal surface of the skin. In the example modeling approach, the Rayleigh number was calculated using Equation 16.

$$Ra_L = \frac{g \beta_{PG} \left(T_{s,l} - T_{PG} \right) L^3}{\nu_{PG} \alpha_{PG}} \quad 16$$

In Equation 16, the length scale, L, was defined as the area of the liquid surface contact divided by the perimeter of contact as shown in Equation 17.

$$L = \frac{A_s}{P_s} \quad 17$$

For a surface pointed downwards, that is, with a fluid naturally convecting to the surface from below, the convection coefficient was then calculated based on the correlation from Janna (1986).

$$h_{PG} = \frac{k_{PG}}{L} 0.27 Ra_L^{\frac{1}{4}} \quad 18$$

9.4 Skin thermal conductivity

The thermal conductivity of aluminum varies as a function of temperature. NIST reports a function for the thermal conductivity of Al 6061-T6 that was used for modeling the CAFF measurements with an aluminum skin. Figure 56 from the NIST website shows the variation in the thermal conductivity of Al 6061 over the range of 4K to 300K (NIST, 2021). In the range of

skin temperatures measured for the aluminum skins in the CAFF, a typical value for the aluminum skin thermal conductivity was 150 W/(mK).

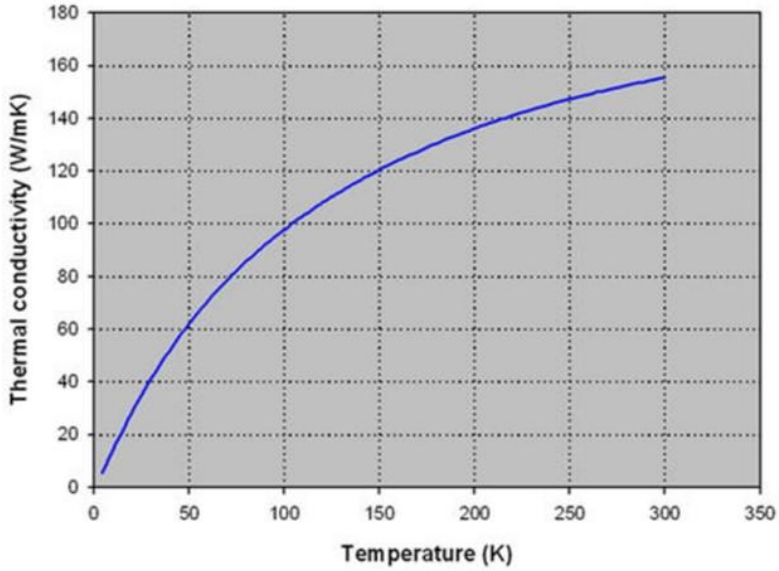

Figure 56. Thermal conductivity of Al 6061-T6 from 4K to 300K [https://www.nist.gov/]

When the skin was the carbon fiber composite skin, the results from Section 8 for the measured thermal conductivity were employed. Because the uncertainties form Section 8 were larger than the variation in the thermal conductivity with temperature, the constant value of 0.48 W/(m·K) was used for the model implementation when the experiments used the carbon fiber skin.

9.5 Moist air properties

The properties of moist air were calculated using a computer program which was based upon a standard published by the International Association for the Properties of Water and Steam (IAPWS) (Wagner & Prub, 2002). In the computer program, the properties of saturated vapor water were determined using the IAPWS expressions, and the program uses Sutherland's Law (Sutherland, 1893) for the ideal properties of air. The moist air properties were determined using Wilke's equation for gas mixtures (Wilke, 1950). Values for the properties of moist air calculated at 10 °C, 82% relative humidity, and one atmospheric pressure were:

$$\omega_a = 0.00624 \frac{kg_v}{kg_{da}}$$

$$\rho_{air} = 1.242 \frac{kg}{m^3}$$

$$c_{p,air} = 1.007 \frac{kJ}{kg \cdot K}$$

$$\mu_{air} = 18.12 \times 10^{-6} \frac{N \cdot s}{m^2}$$

$$k_{air} = 0.025 \frac{W}{m \cdot K}$$

9.6 External convective heat transfer

The convection coefficient from the frost layer to the air was evaluated by treating the air as creating a boundary layer over the frost. Because the frost surface was rough and there was a lip at the transition from the wind tunnel to the wing-box model and skin surface, the boundary layer over the photogrammetry location was assumed to be turbulent, even though the speeds employed in the CAFF were very low.

For the modeling, the Reynolds number based on the distance from the skin starting location and the photogrammetry location was calculated using Equation 19.

$$Re_x = \frac{\rho_{air} V_\infty x_{PM}}{\mu_{air}} \quad 19$$

The boundary layer thickness was then calculated using Equation 20.

$$\delta_{PM} = 0.37 Re_x^{-\frac{1}{5}} \quad 20$$

The skin friction coefficient was calculated using Equation 21 simply because it was used in the correlation for the Stanton number.

$$C_{f,x} = \frac{0.455}{[ln(0.06Re_x)]^2} \quad 21$$

The Colburn analogy from Equation 22 was then used to determine the Stanton number at the photogrammetry location.

$$St_x = \frac{C_{f,x}/2}{1+13(Pr^{0.667}-1)\left(C_{f,x}/2\right)^{0.5}} \quad 22$$

Finally, the convection coefficient was determined using Equation 23.

$$h_{air} = St_x \rho_{air} V_\infty c_{p,air} \quad 23$$

9.7 Frost density and thermal conductivity

Many models for the density and thermal conductivity of the frost-sublayer, the frost-liquid region, and the frost structure-air layer exists in the literature (O'Neal, 1982). These models predict widely varying values of the relationship between the density and thermal conductivity. For the modeling approach, a simple method was to assume an overall density of the frost structure (20% ice) and treat the frost and the air as a parallel conducting structure, as shown in Equation 24.

$$k_{fst} = \left(\frac{1}{0.2k_{ice}} + \frac{1}{0.8k_{air}}\right)^{-1} \quad 24$$

For the example simulations below, $k_{ice} = 2.3\ W/(m \cdot K)$.

9.8 Instantaneous frost growth model

When applying the correlations developed from the BFT measurements to the CAFF measurements or generalized CSFF situations, two primary differences must be addressed. The first issue is that the BFT measurements and the resulting correlations were based on the hydraulic diameter of the test section. In the CAFF and in generalized CSFF situations, the flow will be a boundary layer over an exposed surface. To address the flow geometry change, the hydraulic diameter used in the frost thickness and roughness correlations may be implemented as twice the boundary layer thickness.

$$D_{CAFF} = 2\delta_{PM} \quad 25$$

The second difference between the BFT and CAFF measurements is related to the skin top surface temperature and the frost surface temperatures. For the BFT, the skin surface temperature remained constant throughout the test. For the CAFF, the propylene glycol/water temperature remained constant, but the skin surface temperature could vary. In both cases, the surface temperature of the frost changed as the frost thickness increased. Consequently, applying Equation 11 from the BFT directly at each time during a simulation of the CAFF required some modifications in the simulation approach. To better capture the evolution process, a roughness growth model was employed based on simple numerical integration of Equation 11 when differentiated to create an instantaneous growth model.

For the first time step, Equation 11 was directly implemented using Equation 25 for the length scale. For subsequent iterations, the derivative of the Equation 11 with respect to time was evaluated using Equation 26.

$$\frac{\partial h_f}{\partial t} = 0.445(1.759mm)(Fo)^{-0.555}(w_a)^{0.221}\,(Re_{2\delta_{PM}})^{0.092}\,(T_s^*)^{0.653}\,(T_{air}^*)^{-0.174}\,\frac{\alpha_{air}}{(2\delta_{PM})^2} \quad 26$$

Since Equations 11 and 26 were based on the frost surface temperature, which was based on the instantaneous energy balance, the integration approach was more appropriate than direct implementation of Equation 11 at each simulation time. Following the evaluation of the frost thickness at each time step, *n*, the thickness at the subsequent time step, *n*+1, was determined using Equation 27.

$$h_{f,n+1} = h_{f,n} + \left(\frac{\partial h_f}{\partial t}\right)_n \Delta t \quad 27$$

9.9 Heat transfer and frost temperature algorithm

Referring to Figure 55, following the new thickness calculated for the next time step, the temperature of the frost was calculated by performing a steady-state energy balance, as shown in Equation 28.

$$q'' = \frac{T_{air} - T_{PG}}{R_{eq}} \quad 28$$

In Equation 28, the equivalent resistance of the circuit was determined by neglecting the latent energy released by the water during the frost process, as demonstrated in Equation 29.

$$R_{eq} = \frac{1}{h_{PG}} + \frac{t_s}{k_s} + \frac{h_f}{\left(\frac{1}{0.2k_{ice}} + \frac{1}{0.8k_{air}}\right)^{-1}} + \frac{1}{h_{air}} \quad 29$$

Based on the energy balance of Equation 28, the temperature skin on the frost side and the temperature of the frost surface were then predicted using Equations 30 and 31.

$$T_s = T_{PG} + \frac{q''}{h_{PG}} + q''\frac{t_s}{k_s} \quad 30$$

$$T_{fst} = T_{PG} + \frac{q''}{h_{PG}} + q''\frac{t_s}{k_s} + q''\frac{h_f}{\left(\frac{1}{0.2k_{ice}} + \frac{1}{0.8k_{air}}\right)^{-1}} \quad 31$$

9.10 Instantaneous frost roughness model

Following the calculation of the skin surface temperature, T_s, and the frost surface temperature, T_{fst}, Equations 32 and 33 could be used along with Equations 13 and 14 from the BFT tests to

predict the RMS roughness and the equivalent sand-grain roughness. In Equations 32 and 33, the Reynolds number was cast in terms of the boundary layer thickness using Equation 25.

$$R_q^* = \frac{R_q}{h_f} = 2.123(\omega_a)^{-0.023}\left(Re_{2\delta_{PM}}\right)^{0.065}\left(\frac{T_{air}-T_o}{T_o}\right)^{0.790}\left(\frac{T_o-T_s}{T_o-T_{fst}}\right)^{-1.227}\left(\frac{T_{fst}-T_s}{T_o-T_s}\right)^{0.342} \quad 32$$

$$k_{s,CAFF}^* = \frac{k_s}{h_f} = 0.029(\omega_a)^{0.367}\left(Re_{2\delta_{PM}}\right)^{0.150}\left(\frac{T_{fst}-T_s}{T_o}\right)^{0.342}\left(exp\left(\frac{T_{air}-T_{fst}}{T_{air}-T_s}\right)\right)^{6.716} \quad 33$$

9.11 Application to selected cases

Summarizing the approach, at each time step, the thickness was determined using either Equation 11 for the first time step or Equations 26 and 27 for subsequent time steps. Then, the skin outer surface temperature and the frost surface temperature were predicted using Equations 30 and 31 based on the ice density and thermal conductivity assumption from Equation 24. The roughness parameters were then predicted using Equations 32 and 33.

One aluminum skin set of measurements and one carbon fiber skin set of measurements were used to demonstrate the application of the frost evolution approach. Both cases selected were for the skins without a rib or stringer structure.

The aluminum skin case used was the case performed on 12/06/19. For the 12/06/19 case, T_{air} = 14 °C, RH = 87%, V_∞ = 1 m/s, and x_{PM} = 52.7 cm (20.75 in.). For this case, the free-floating thermocouples indicated a fuel surrogate temperature of -18 °C. The comparison of the model predictions to the measurements for case 12/06/19 are presented in **Error! Reference source not found.**. The RMS roughness evolution is presented in **Error! Reference source not found.**(a), and the equivalent sand-grain roughness prediction is presented in **Error! Reference source not found.**(b). In the CAFF, the frost thickness was not measured directly. To provide an indirect comparison, **Error! Reference source not found.**(c) compares the predicted thickness evolution to the measured peak-to-valley roughness. Without the presence of a dense ice sublayer, the peak-to-valley roughness should be on similar or slightly less than the predicted thickness of the frost. Figure 57 demonstrates that the model under-predicted the RMS roughness beyond the 50 minute mark, but the trends and magnitudes of the equivalent sand-grain roughness and thickness were generally captured by the model implementation.

The carbon fiber composite skin case used was the case performed on 04/23/21. For the 04/23/21 case, T_{air} = 10 °C, RH = 82%, V_∞ = 1.4 m/s, and x_{PM} = 52.8 cm (20.8 in.). For this case, the free-floating thermocouples indicated a fuel surrogate temperature of -14 °C. The comparison of the

model predictions to the measurements for case 04/23/21 are presented in Figure 58. The RMS roughness evolution is presented in Figure 58(a), and the equivalent sand-grain roughness prediction is presented in Figure 58(b). Figure 58(c) compares the predicted thickness evolution to the measured peak-to-valley roughness. Figure 58 demonstrates that for the carbon-fiber skin, the model captured the magnitudes and trends of the RMS roughness and frost thickness. However, the model over-predicted equivalent sand-grain roughness evolution during the test.

The differences in the predictions and the measured values are likely caused by the simplistic treatment of the density of the frost. However, the level of agreement was not unexpected based on the low R2 values of the correlations of Equations 13 and 14.

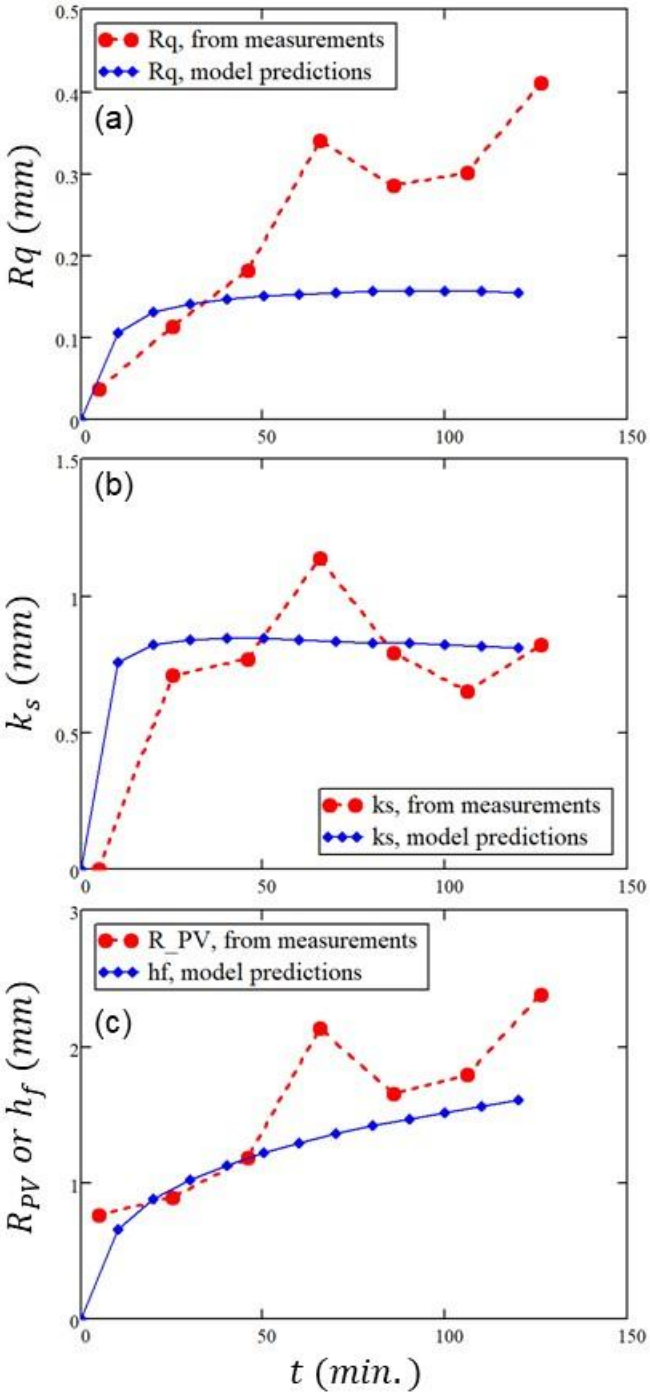

Figure 57. Model implementation example results for the aluminum skin without a rib (Case 12/06/19): a) RMS roughness evolution; b) equivalent sand-grain roughness evolution; and c) thickness or peak-to-valley height

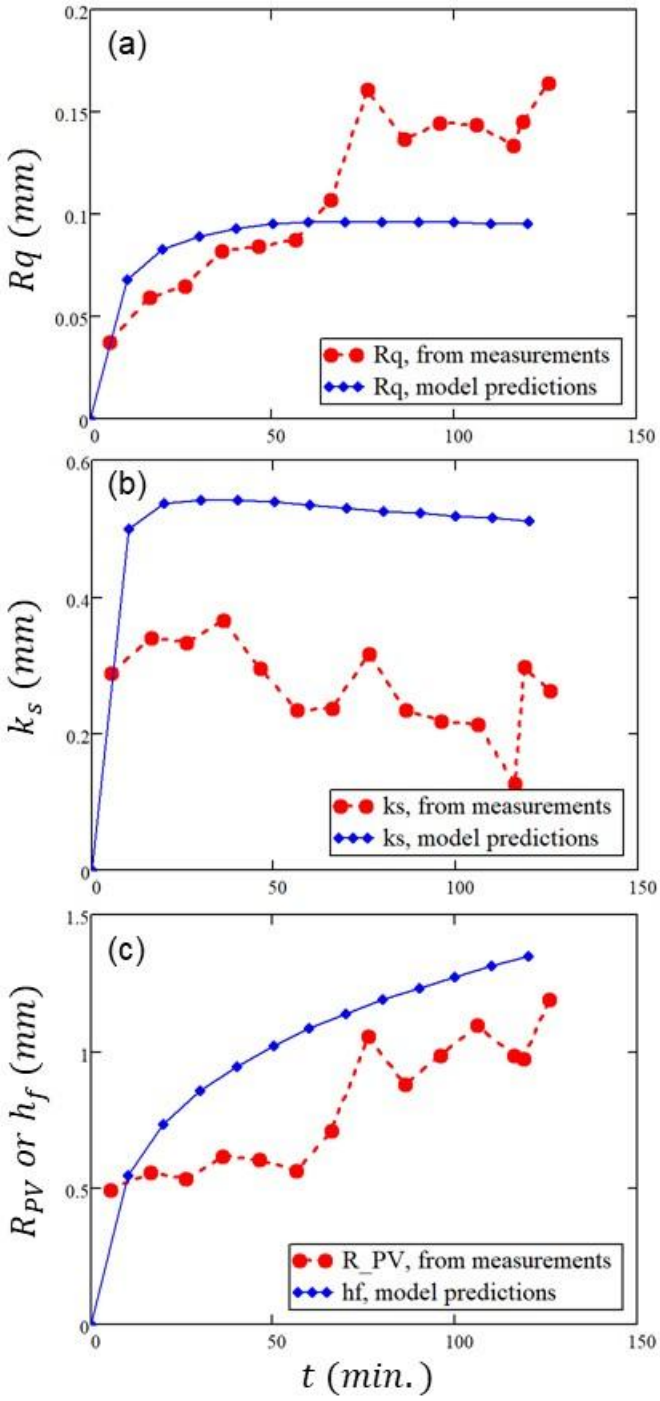

Figure 58. Model implementation example results for the carbon fiber composite skin without a rib (Case 04/23/21): a) RMS roughness evolution; b) equivalent sand-grain roughness; and c) thickness or peak-to-valley height

For the example cases provided, the fuel surrogate temperature was set based on the free-floating thermocouples in the wing tank thermal model. When applying the current approach to the skins with aluminum rib or stringer structures, the coldest thermocouple measurements from the skin thermocouples would be imposed on the bottom side of the skin in the thermal circuit, which would in essence treat the rib as a perfectly conducting part of the thermal circuit. Additionally, the internal convection coefficient term, h_{PG} from Equations 29 through 31, would be removed from the modeling approach.

10 Summary

CSFF is frost that forms on the surfaces of integrated fuel tanks when fuel remains in aircraft fuel tanks following a flight at typical commercial aviation altitudes. CSFF must be removed or allowed to melt prior to returning to flight, unless the vehicle model has a certification exemption for takeoff with CSFF. To help the FAA assess future exemption requests, the activities of this grant focused on 1) acquiring frost roughness evolution measurements in apparatuses with varying levels of complexity compared to a real CSFF situation; 2) developing a frost roughness evolution model based on the measurements acquired as part of the grant; 3) identifying requisite model components that must be addressed when aircraft manufacturers seek CSFF exemptions for takeoff.

As part of the grant activities, a photogrammetry approach to measuring frost roughness in the laboratory environment was developed and validated. Approximately 238 roughness measurements were performed using the photogrammetry approach with 34 distinct environmental conditions in a small frost wind tunnel. The measurements in the small frost wind tunnel were used to identify the most important atmospheric conditions to capture in the frost measurements and to develop the correlations for important frost thickness and roughness parameters.

A new facility was then used to create situations that capture aspects of the CSFF physics that could not be captured in the small frost tunnel. The facility consisted of an environmental chamber, a thermal model of an integrated fuel tank, and a wind tunnel to circulate humid air over the wing tank thermal model. The wing tank thermal model was created so that different skins could be attached and used to investigate wing skin composition and support rib and stringer construction on frost evolution. The skins were primed and painted using appropriate aviation paints. Using the new facility, an automated photogrammetry system was developed. Four distinct skins were used, and more than 58 environmental cases were investigated. The

result was more than 700 measurements of CSFF roughness that may be used to develop and refine models created and used by aircraft manufacturers.

Using the correlations developed in the small frost tunnel, a modeling approach was presented that captures important aspects of the CSFF process. The model was applied to one case in the new facility using an aluminum skin and one case using a carbon fiber composite skin. Opportunities to improve the modeling approach were described, but the purpose of the effort was to identify relevant physics that should be considered when proprietary models are developed by aircraft manufacturers for certification or exemption documentation.

11 References

14 CFR Part 135.227 - Icing Conditions: Operating Limitations. (n.d.). In *Federal Register - Aeronautics and Space.* Washington, DC: Office of the Federal Register, National Archives and Records Administration.

(2019). *ASTM C117-19: Standard Test Method for Steady-State Heat Flux Measurements and Thermal Transmission Properties by Means of the Guarded-Hot-Plate Apparatus.* ASTM International.

Breque, F., & Nemer, M. (2016, Sept.). Frosting Modeling on a Cold Flat Plate: Comparison of the Different Assumptions and Impacts on Frost Growth Predictions. *International Journal of Refrigeration, 69*, 340-360.

Brian, P., Reid, R., & and Shah, Y. (1970). Frost Deposition on Cold Surfaces. *Industrial & Engineering Chemistry Fundamentals, 9*(3), 375-380.

Chen, M., & Rohsenow, W. (1964). Heat, Mass, and Momentum Transfer inside Frosted Tubes - Experiment and Theory. *Journal of Heat Transfer, 86*(3), 334-340.

Coleman, H., & Steele, W. (1999). *Experimentation and Uncertainty Analysis for Engineers* (2nd ed.). New York: Wiley.

Collier, P., Dixon, L., Fontana, D., Payne, D., & Pearson, A. (1999). The Use of Close Range Photogrammetry for Studying Ice Accretion on Aerofoil Sections. *The Photogrammetric Record, 16*(94), 671-684.

Dynalene, Inc. (2014). *Dynalene Propylene Glycol Series: Engineering Guide.* Whitehall, PA.

Flack, K., & Schultz, M. (2010). Review of Hydraulic roughness Scales in the Fully Rough Regime. *Journal of Fluids Engineering, 132*(4), 041203.

Flack, K., Schultz, M., Barros, J., & Kim, Y. (2016, October). Skin-Friction Behavior in the Transitionally-Rough Regime. *International Journal of Heat and Fluid Flow, 61*(A), 21-30.

Hariharan, P. (2003). *Optical Interferometry.* Academic Press.

Janna, W. (1986). *Engineering Heat Transfer.* Boston: PWS Engineering.

Joven, R., Das, R., Ahmed, A., Roozbehjavan, P., & Minaie, B. (2012). Thermal properties of carbon fiber-epoxy composites with different fabric weave. *SAMPE International Symposium Proceedings*, (p. 14). Charleston.

Koivisto, P. (2015). *Effects of Cold Soaked Fuel Frost on Lift Degradation during Simulated Take-Off.* Aalto University and Finish Transportation Safety Agency.

Lawrysyn, M. (1989). *Aerodynamic Characteristics of Frost Roughness.* Carleton University.

Lee, H., Shin, J., Ha, S., Choi, B., & and Lee, J. (2004). Frost Formation on a Plate with Different Surface Hydrophilicity. *International Journal of Heat and Mass Transfer, 47*(22), 4881-4893.

Lee, S., Broeren, A., Kreeger, R., Potapczuk, M., & and Utt, L. (2014). Implementation and Validation of a 3-D Ice Accretion Measurement Methodology. *AIAA Aviation Forum and Exposition.* Atlanta, GA: AIAA-2014-2613.

Linder, W. (2003). *Digital Photogrammetry: Theory and Applications.* New York: Springer.

McClain, S., Zhang, T., Ahmed, A., Stafford, G., Cornejo, J., & and O'Neal, D. (2020). A Climatic Facility and Apparatus for Investigations of Cold Soaked Fuel Frost Evolution. *2020 AIAA Aviation Forum.* AIAA-2020-2808.

Miyauchi, T. S. (2018). *A Photogrammetric Method for Measuring Transient Frost Surface Roughness.* Baylor University, Department of Mechanical Engineering, M.S. Thesis.

Miyauchi, T., McClain, S. T., Zhang, T., & O'Neal, D. (2019). Photogrammetric Frost Roughness Measurements in Cold-Soaked Conditions. *SAE International*, SAE 2019-01-1970.

NIST. (2021, June 2). *Aluminum 6061-T6 (UNS AA96061)*. Retrieved from https://www.nist.gov/mml/acmd/aluminum-6061-t6-uns-aa96061

O'Neal, D. (1982). *The Effect of Frost Formation on the Performance of a Parrallel Plate Heat Exchanger.* Ph.D. Dissertation. Purdue University.

O'Neal, D., & Tree, D. (1985). A Review of Frost Formation in Simple Geometries. *ASHRAE Transactions*, 267-281.

SAE AMS G9 Aerospace Sealing Committee . (2016). *AIR4069C: Sealing of Integral Fuel Tanks.* SAE International. doi:https://doi.org/10.4271/AIR4069C

Schenk, T. (2005). *Introduction to Photogrammetry.* Columbus, OH: Ohio State University Department of Civil and Environmental Engineering.

Soinne, E., Rosnell, T., & Vilijanen, N. (2017). *Aerodynamic, Laser and Photogrammetry Measurements on CRM Wing Model with Frost.* Finish Transportation Safety Agency.

Sutherland, W. (1893). LII. The viscosity of gases and molecular forc. *Philosophical Magazine Series 5, 36*(233), 507-531.

Sweeting, R., & Liu, X. (2004). Measurement of thermal conductivity for fibre-reinforced composites. *Composites Part A: Applied Science and Manufacturing, 35*(7-8), 933-938.

Vosselman, G., & and Maas, H.-G. (2010). *Airborne and Terrestrial Laser Scanning.* Whittles Publishing.

Wagner, W., & Prub, A. (2002). The IAPWS Formulation 1995 for the Thermodynamic Properties of Ordinary Water Substance for General and Scientific Use. *Journal of Physical and Chemical Reference Data, 31*, 287-535.

Wilke, C. (1950). A Viscosity Equation for Gas Mixtures. *The Journal of Chemical Physics, 18*, 517-519.

Wu, X., Dai, W., Xu, W., & Tang, L. (2007). Mesoscale Investigation of Frost Formation on a Cold Surface. *Experimental Thermal and Fluid Science, 18*, 1043-1048.

Yun, R., Kim, Y., & Min, M.-K. (2002). Modeling of Frost Growth and Frost Properties with Airfoil over a Flat Plate. *International Journal of Refrigeration, 25*(3), 362-371.

Zhang, T. (2020). *A Study of Frost Growth and Roughness on a Cold Flat Plate under Forced Convection.* Baylor University, Department of Mechanical Engineering, Ph.D. Dissertation.

Zhang, T., O'Neal, D., & McClain, S. (2020). Analysis of frost thickness and roughness growth from the perspective of frost crystal structure. *International Journal of Refrigeration, 112*(2), 314-323.

Zhang, T., O'Neal, D., & McClain, S. (2020). Impact of Environmental Conditions on Frost Crystal Structure. *International Journal of Air Conditioning and Refrigeration, 28*(2), 2050014.

Zhang, T., O'Neal, D., & McClain, S. (2021). Variation of Frost Roughness on a Flat Plate Under Forced Convection. *Journal of Thermal Science and Engineering Applications, 13*(2), 011020.

Zhang, T., O'Neal, D., McClain, S., & Riley, J. (2021). Dimensionless Model of Frost Roughness on Cold Flat Plate Under Forced Convection. *Journal of Aircraft, 58*(6), 1375-1385.

A Appendix A: Baylor Frost Tunnel case reports using an unpainted aluminum coupon

Table A- 1. Summary of roughness and thickness case conditions from Miyauchi (2018) A-3
Table A- 2. Summary of roughness and thickness case conditions from Zhang (Zhang, 2020) A-4
Table A- 3. Frost roughness and thickness in Baylor Frost Tunnel: Cases 042518 and 102219, T_{air} = 16 °C, T_{surf} = -10 °C, RH = 76%, V_{air} = 0.5 m/s A-5
Table A- 4. Frost roughness measurements in Baylor Frost Tunnel: Case 050818.01, T_{air} = -10 °C, T_{surf} = -10 °C, RH = 76%, V_{air} = 1.5 m/s A-5
Table A- 5. Frost roughness measurements in Baylor Frost Tunnel: Case 050818.02, T_{air} = -16 °C, T_{surf} = -25 °C, RH = 76%, V_{air} = 1.5 m/s A-6
Table A- 6. Frost roughness measurements in Baylor Frost Tunnel: Case 051718.02, T_{air} = 10 °C, T_{surf} = -10 °C, RH = 85%, V_{air} = 1.5 m/s A-6
Table A- 7. Frost roughness measurements in Baylor Frost Tunnel: Case 051718.02, T_{air} = 10 °C, T_{surf} = -10 °C, RH = 85%, V_{air} = 0.5 m/s A-7
Table A- 8. Frost roughness measurements in Baylor Frost Tunnel: Case 051918, T_{air} = 10 °C, T_{surf} = -10 °C, RH = 76%, V_{air} = 0.5 m/s A-7
Table A- 9. Frost roughness measurements in Baylor Frost Tunnel: Case 052318.01, T_{air} = 10 °C, T_{surf} = -10 °C, RH = 85%, V_{air} = 1.5 m/s A-8
Table A- 10. Frost roughness measurements in Baylor Frost Tunnel: Case 052318.02, T_{air} = 10 °C, T_{surf} = -25 °C, RH = 85%, V_{air} = 1.5 m/s A-8
Table A- 11. Frost roughness measurements in Baylor Frost Tunnel: Case 052818, T_{air} = 16 °C, T_{surf} = -10 °C, RH = 85%, V_{air} = 1.5 m/s A-9
Table A- 12. Frost roughness measurements in Baylor Frost Tunnel: Case 052918.01, T_{air} = 16 °C, T_{surf} = -25 °C, RH = 85%, V_{air} = 0.5 m/s A-9
Table A- 13. Frost roughness measurements in Baylor Frost Tunnel: Case 052918.02, T_{air} = 16 °C, T_{surf} = -25 °C, RH = 85%, V_{air} = 1.5 m/s A-10
Table A- 14. Frost roughness measurements in Baylor Frost Tunnel: Case 060418.01, T_{air} = 10 °C, T_{surf} = -25 °C, RH = 76%, V_{air} = 0.5 m/s A-10
Table A- 15. Frost roughness measurements in Baylor Frost Tunnel: Case 060418.02, T_{air} = 10 °C, T_{surf} = -25 °C, RH = 85%, V_{air} = 0.5 m/s A-11
Table A- 16. Frost roughness measurements in Baylor Frost Tunnel: Case 060618.01, T_{air} = 16 °C, T_{surf} = -10 °C, RH = 85%, V_{air} = 0.5 m/s A-11
Table A- 17. Frost roughness measurements in Baylor Frost Tunnel: Case 060618.02, T_{air} = 16 °C, T_{surf} = -25 °C, RH = 76%, V_{air} = 0.5 m/s A-12

Table A- 18. Frost roughness measurements in Baylor Frost Tunnel: Case 061118.01, T_{air} = 10 °C, T_{surf} = -25 °C, RH = 76%, V_{air} = 1.5 m/s A-12
Table A- 19. Frost roughness and thickness measurements in Baylor Frost Tunnel: Cases 072318 and 101619.01, T_{air} = 16 °C, T_{surf} = -10 °C, RH = 76%, V_{air} = 1.0 m/s A-13
Table A- 20. Frost roughness and thickness measurements in Baylor Frost Tunnel: Cases 061118.02 and 101619.02, T_{air} = 16 °C, T_{surf} = -10 °C, RH = 76%, V_{air} = 1.5 m/s A-13
Table A- 21. Frost roughness and thickness measurements in Baylor Frost Tunnel: Cases 070218.01 and 101519.01, T_{air} = 16 °C, T_{surf} = -10 °C, RH = 61%, V_{air} = 0.5 m/s A-14
Table A- 22. Frost roughness and thickness measurements in Baylor Frost Tunnel: Cases 070218.02 and 101519.02, T_{air} = 16 °C, T_{surf} = -10 °C, RH = 91%, V_{air} = 0.5 m/s A-14
Table A- 23. Frost roughness and thickness measurements in Baylor Frost Tunnel: Cases 062518.01 and 102319, T_{air} = 16 °C, T_{surf} = -5 °C, RH = 76%, V_{air} = 0.5 m/s A-15
Table A- 24. Frost roughness and thickness measurements in Baylor Frost Tunnel: Cases 062518.02 and 102219.02, T_{air} = 16 °C, T_{surf} = -15 °C, RH = 76%, V_{air} = 0.5 m/s A-15
Table A- 25. Frost roughness and thickness measurements in Baylor Frost Tunnel: Cases 081418 and 102119, T_{air} = 8 °C, T_{surf} = -10 °C, RH = 76%, V_{air} = 0.5 m/s A-16
Table A- 26. Frost roughness and thickness measurements in Baylor Frost Tunnel: Cases 062718 and 101819, T_{air} = 12 °C, T_{surf} = -10 °C, RH = 76%, V_{air} = 0.5 m/s A-16
Table A- 27. Frost roughness and thickness measurements in Baylor Frost Tunnel: Cases 110719.01 and 010720.01, T_{air} = 8 °C, T_{surf} = -15 °C, RH = 70%, V_{air} = 1.0 m/s A-17
Table A- 28. Frost roughness and thickness measurements in Baylor Frost Tunnel: Cases 110619.01 and 010620.01, T_{air} = 12 °C, T_{surf} = -10 °C, RH = 70%, V_{air} = 1.0 m/s A-17
Table A- 29. Frost roughness and thickness measurements in Baylor Frost Tunnel: Cases 111219.01 and 010820.01, T_{air} = 12 °C, T_{surf} = -15 °C, RH = 60%, V_{air} = 1.0 m/s A-18
Table A- 30. Frost roughness and thickness measurements in Baylor Frost Tunnel: Cases 111119.01 and 010720.02, T_{air} = 12 °C, T_{surf} = -15 °C, RH = 70%, V_{air} = 0.5 m/s A-18
Table A- 31. Frost roughness and thickness measurements in Baylor Frost Tunnel: Cases 110619.02 and 010620.02, T_{air} = 12 °C, T_{surf} = -15 °C, RH = 70%, V_{air} = 1.0 m/s A-19
Table A- 32. Frost roughness and thickness measurements in Baylor Frost Tunnel: Cases 111119.02 and 010820.02, T_{air} = 12 °C, T_{surf} = -15 °C, RH = 70%, V_{air} = 1.5 m/s A-19
Table A- 33. Frost roughness and thickness measurements in Baylor Frost Tunnel: Cases 111319 and 010720.03, T_{air} = 12 °C, T_{surf} = -15 °C, RH = 70%, V_{air} = 2.5 m/s A-20
Table A- 34. Frost roughness and thickness measurements in Baylor Frost Tunnel: Cases 1112.19.02 and 010820.03, T_{air} = 12 °C, T_{surf} = -15 °C, RH = 78%, V_{air} = 1.0 m/s A-20
Table A- 35. Frost roughness and thickness measurements in Baylor Frost Tunnel: Cases 110619.03 and 010620.03, T_{air} = 12 °C, T_{surf} = -20 °C, RH = 70%, V_{air} = 1.0 m/s A-21

Table A- 36. Frost roughness and thickness measurements in Baylor Frost Tunnel: Cases 111219.02 and 010820.03, T_{air} = 12 °C, T_{surf} = -15 °C, RH = 80%, V_{air} = 1.0 m/s A-21

Table A- 1. Summary of roughness and thickness case conditions from Miyauchi (2018)

Roughness Case ID	T_∞ **(°C)**	***Ts*** **(°C)**	**%RH**	**Velocity (m/s)**
042518	16	-10	76	0.5
050818.01	16	-10	76	1.5
050818.02	16	-25	76	1.5
051718.01	10	-10	76	1.5
051718.02	10	-10	85	0.5
051918	10	-10	76	0.5
052318.01	10	-10	85	1.5
052318.02	10	-25	85	1.5
052818	16	-10	85	1.5
052918.01	16	-25	85	0.5
052918.02	16	-25	85	1.5
060418.01	10	-25	76	0.5
060418.02	10	-25	85	0.5
060618.01	16	-10	85	0.5
060618.02	16	-25	76	0.5
061118	10	-25	76	1.5

Table A- 2. Summary of roughness and thickness case conditions from Zhang (Zhang, 2020)

Roughness Case ID	Thickness Case ID	T∞ (°C)	Ts (°C)	%RH	Velocity (m/s)
042518*	102219.01	16	-10	76	0.5
072318	101619.01	16	-10	76	1.0
061118	101619.02	16	-10	76	1.5
070218.01	101519.01	16	-10	61	0.5
070218.02	101519.02	16	-10	91	0.5
062518.01	102319	16	-5	76	0.5
062518.02	102219.02	16	-15	76	0.5
081418	102119	8	-10	76	0.5
062718	101819	12	-10	76	0.5
110719.01	010720.01	8	-15	70	1.0
110619.01	010620.01	12	-10	70	1.0
111219.01	010820.01	12	-15	60	1.0
111119.01	010720.02	12	-15	70	0.5
110619.02	010620.02	12	-15	70	1.0
111119.02	010820.02	12	-15	70	1.5
111319	010720.03	12	-15	70	2.5
111219.02	010820.03	12	-15	80	1.0
110619.03	010620.03	12	-20	70	1.0
110719.02	010920	16	-15	70	1.0

*Case roughness measurements were reported by Miyauchi (2018) is dually listed in Table A- 1

Table A- 3. Frost roughness and thickness in Baylor Frost Tunnel: Cases 042518 and 102219, T_{air} = 16 °C, T_{surf} = -10 °C, RH = 76%, V_{air} = 0.5 m/s

Time (min)	R_q **(mm)**	***Skw***	R_{PV} **(mm)**	***h*** **(mm)**	T_{FS} **(mm)**
15	0.069739	1.6611	0.77895	1.10	-9.9
30	0.14293	1.2375	1.3341	1.75	-9.8
45	0.251	1.3751	1.9008	1.90	-9.7
60	0.33704	1.0171	2.4408	2.16	-9.5
75	0.37962	0.61737	2.6332	2.22	-8.5
90	0.35794	0.32029	2.4245	2.49	-7.4
120	0.35026	0.003024	2.5782	2.51	-7.2

Table A- 4. Frost roughness measurements in Baylor Frost Tunnel: Case 050818.01, T_{air} = -10 °C, T_{surf} = -10 °C, RH = 76%, V_{air} = 1.5 m/s

Time (min)	R_q **(mm)**	***Skw***	R_{PV} **(mm)**
15	0.23652	0.98232	1.5939
30	0.37162	0.35469	2.089
45	0.3737	-0.4	2.067
60	0.29127	-0.59716	2.0502
75	0.2532	-0.81	1.9
90	0.20911	-1.1013	1.8425
120	0.16643	-1.6429	1.3508

Table A- 5. Frost roughness measurements in Baylor Frost Tunnel: Case 050818.02, T_{air} = -16 °C, T_{surf} = -25 °C, RH = 76%, V_{air} = 1.5 m/s

Time (min)	$\boldsymbol{R_q}$ **(mm)**	***Skw***	$\boldsymbol{R_{PV}}$ **(mm)**
15	0.41914	0.77908	2.3158
30	0.48463	-0.24815	3.3127
45	0.5099	-0.02316	3.3886
60	0.58358	-0.0067	4.0334
75	0.56371	-0.37127	4.7152
90	0.50887	-0.16375	3.9308
120	0.42492	0.067142	3.5671

Table A- 6. Frost roughness measurements in Baylor Frost Tunnel: Case 051718.02, T_{air} = 10 °C, T_{surf} = -10 °C, RH = 85%, V_{air} = 1.5 m/s

Time (min)	$\boldsymbol{R_q}$ **(mm)**	***Skw***	$\boldsymbol{R_{PV}}$ **(mm)**
15	0.071036	0.98151	0.53329
30	0.14853	0.65422	1.0414
45	0.2672	1.1101	1.7826
60	0.36414	0.84082	2.1754
75	0.40368	0.71798	2.7019
90	0.46269	0.63768	2.9702
120	0.4908	0.20384	3.1628

Table A- 7. Frost roughness measurements in Baylor Frost Tunnel: Case 051718.02, T_{air} = 10 °C, T_{surf} = -10 °C, RH = 85%, V_{air} = 0.5 m/s

Time (min)	$\boldsymbol{R_q}$ **(mm)**	***Skw***	$\boldsymbol{R_{PV}}$ **(mm)**
15	0.13779	1.7849	0.95252
30	0.22975	0.77787	1.4129
45	0.29608	0.47728	1.9191
60	0.35385	0.61249	2.6373
75	0.38852	0.80415	3.1708
90	0.38032	0.29496	2.8326
120	0.41585	0.52774	3.0939

Table A- 8. Frost roughness measurements in Baylor Frost Tunnel: Case 051918, T_{air} = 10 °C, T_{surf} = -10 °C, RH = 76%, V_{air} = 0.5 m/s

Time (min)	$\boldsymbol{R_q}$ **(mm)**	***Skw***	$\boldsymbol{R_{PV}}$ **(mm)**
15	0.046137	2.1363	0.53167
30	0.14314	1.3647	1.2058
45	0.26952	1.6173	1.9253
60	0.29073	1.3204	2.3634
75	0.31343	1.0606	2.3028
90	0.31532	1.0377	2.2852
120	0.36578	0.58515	2.5635

Table A- 9. Frost roughness measurements in Baylor Frost Tunnel: Case 052318.01, T_{air} = 10 °C, T_{surf} = -10 °C, RH = 85%, V_{air} = 1.5 m/s

Time (min)	$\boldsymbol{R_q}$ **(mm)**	***Skw***	$\boldsymbol{R_{PV}}$ **(mm)**
15	0.09758	1.1301	0.78253
30	0.20495	0.31653	1.7106
45	0.27881	1.0931	2.3872
60	0.31314	0.96527	2.8303
75	0.31966	0.8936	2.7785
90	0.3606	0.7346	3.0767
120	0.38246	0.27134	2.9401

Table A- 10. Frost roughness measurements in Baylor Frost Tunnel: Case 052318.02, T_{air} = 10 °C, T_{surf} = -25 °C, RH = 85%, V_{air} = 1.5 m/s

Time (min)	$\boldsymbol{R_q}$ **(mm)**	***Skw***	$\boldsymbol{R_{PV}}$ **(mm)**
15	0.41914	0.77908	2.3158
30	0.48463	-0.24815	3.3127
45	0.5099	-0.02316	3.3886
60	0.58358	- 0.0067	4.0334
75	0.56371	- 0.37127	4.7152
90	0.50887	- 0.16375	3.9308
120	0.42492	0.067142	3.5671

Table A- 11. Frost roughness measurements in Baylor Frost Tunnel: Case 052818, T_{air} = 16 °C, T_{surf} = -10 °C, RH = 85%, V_{air} = 1.5 m/s

Time (min)	R_q **(mm)**	***Skw***	R_{PV} **(mm)**
15	0.19723	1.5107	1.587
30	0.41794	0.34121	2.175
45	0.37776	-0.45141	2.1754
60	0.32262	-0.65109	2.2288
75	0.2511	-0.90189	2.1036
90	0.20598	-1.4202	1.9515
120	0.12647	-2.0352	1.3795

Table A- 12. Frost roughness measurements in Baylor Frost Tunnel: Case 052918.01, T_{air} = 16 °C, T_{surf} = -25 °C, RH = 85%, V_{air} = 0.5 m/s

Time (min)	R_q **(mm)**	***Skw***	R_{PV} **(mm)**
15	0.039839	1.2608	0.60225
30	0.21486	1.1296	2.2661
45	0.29016	0.26807	2.1978
60	0.38594	0.11023	2.7974
75	0.42347	-0.32718	3.1402
90	0.38938	-0.34802	3.2814
120	0.32836	-0.40439	2.7541

Table A- 13. Frost roughness measurements in Baylor Frost Tunnel: Case 052918.02, T_{air} = 16 °C, T_{surf} = -25 °C, RH = 85%, V_{air} = 1.5 m/s

Time (min)	$\boldsymbol{R_q}$ **(mm)**	***Skw***	$\boldsymbol{R_{PV}}$ **(mm)**
15	0.44144	-0.38414	2.8458
30	0.36081	-0.3368	3.1343
45	0.31677	-0.3771	2.8284
60	0.26505	-0.38629	2.0782
75	0.24999	-0.48489	2.1516
90	0.20215	-0.68311	1.6432
120	0.15549	-1.1488	1.3636

Table A- 14. Frost roughness measurements in Baylor Frost Tunnel: Case 060418.01, T_{air} = 10 °C, T_{surf} = -25 °C, RH = 76%, V_{air} = 0.5 m/s

Time (min)	$\boldsymbol{R_q}$ **(mm)**	***Skw***	$\boldsymbol{R_{PV}}$ **(mm)**
15	0.025399	0.67725	0.3605
30	0.080815	1.0205	0.782
45	0.1544	1.3613	1.7551
60	0.28555	1.1956	2.1101
75	0.40721	0.76087	3.126
90	0.44422	0.5097	2.6054
120	0.56808	0.46177	3.6202

Table A- 15. Frost roughness measurements in Baylor Frost Tunnel: Case 060418.02, T_{air} = 10 °C, T_{surf} = -25 °C, RH = 85%, V_{air} = 0.5 m/s

Time (min)	$\boldsymbol{R_q}$ **(mm)**	***Skw***	$\boldsymbol{R_{PV}}$ **(mm)**
15	0.030542	0.50792	0.43806
30	0.074842	0.42445	0.63276
45	0.11136	0.31334	0.91189
60	0.15368	1.3394	1.7293
75	0.25036	0.90703	1.8681
90	0.34445	0.39968	2.4017
120	0.48658	0.38098	3.5271

Table A- 16. Frost roughness measurements in Baylor Frost Tunnel: Case 060618.01, T_{air} = 16 °C, T_{surf} = -10 °C, RH = 85%, V_{air} = 0.5 m/s

Time (min)	$\boldsymbol{R_q}$ **(mm)**	***Skw***	$\boldsymbol{R_{PV}}$ **(mm)**
15	0.064713	0.90364	0.64064
30	0.13852	1.2492	1.3428
45	0.23191	1.152	1.8657
60	0.31141	0.69928	2.2037
75	0.35565	0.2954	2.6478
90	0.36872	-0.0083681	2.4739
120	0.32119	-0.34111	2.6372

Table A- 17. Frost roughness measurements in Baylor Frost Tunnel: Case 060618.02, T_{air} = 16 °C, T_{surf} = -25 °C, RH = 76%, V_{air} = 0.5 m/s

Time (min)	$\boldsymbol{R_q}$ **(mm)**	***Skw***	$\boldsymbol{R_{PV}}$ **(mm)**
15	0.031781	0.58476	0.36474
30	0.081733	1.5785	1.2588
45	0.19512	1.0849	1.6265
60	0.29675	0.38839	2.8518
75	0.37791	0.1807	2.4864
90	0.46416	-0.0073928	2.8224
120	0.39881	-0.365	2.9759

Table A- 18. Frost roughness measurements in Baylor Frost Tunnel: Case 061118.01, T_{air} = 10 °C, T_{surf} = -25 °C, RH = 76%, V_{air} = 1.5 m/s

Time (min)	$\boldsymbol{R_q}$ **(mm)**	***Skw***	$\boldsymbol{R_{PV}}$ **(mm)**
15	0.47812	-0.27134	2.6352
30	0.51287	-0.31041	3.2862
45	0.48354	-0.36561	3.6871
60	0.48875	-0.29321	3.8687
75	0.41473	-0.19631	3.5101
90	0.40956	-0.24189	3.8116
120	0.34029	-0.25945	2.9884

Table A- 19. Frost roughness and thickness measurements in Baylor Frost Tunnel: Cases 072318 and 101619.01, T_{air} = 16 °C, T_{surf} = -10 °C, RH = 76%, V_{air} = 1.0 m/s

Time (min)	R_q **(mm)**	***Skw***	R_{PV} **(mm)**	***h (mm)***	T_{FS} ***(mm)***
15	0.1109	1.4677	1.2300	1.11	-9.9
30	0.2457	1.4357	2.0071	1.47	-9.6
45	0.3188	0.8453	2.2676	1.77	-8.7
60	0.3670	0.4931	2.4596	1.85	-7.7
75	0.3874	0.2529	2.5992	2.05	-6.8
90	0.3584	-0.0305	2.5578	2.15	-6.1
120	0.3237	-0.2158	2.6181	2.55	-4.8

Table A- 20. Frost roughness and thickness measurements in Baylor Frost Tunnel: Cases 061118.02 and 101619.02, T_{air} = 16 °C, T_{surf} = -10 °C, RH = 76%, V_{air} = 1.5 m/s

Time (min)	R_q **(mm)**	***Skw***	R_{PV} **(mm)**	***h (mm)***	T_{FS} ***(mm)***
15	0.2365	0.9823	1.5939	1.24	- 8.8
30	0.3716	0.3547	2.0890	1.57	- 7.4
45	0.3737	-0.4000	2.0670	1.82	- 6.0
60	0.2913	-0.5972	2.0502	2.03	-5.0
75	0.2532	-0.8100	1.9000	2.22	-4.4
90	0.2091	-1.1013	1.8425	2.46	-3.4
120	0.1664	-1.6429	1.3508	2.91	-2.5

Table A- 21. Frost roughness and thickness measurements in Baylor Frost Tunnel: Cases 070218.01 and 101519.01, T_{air} = 16 °C, T_{surf} = -10 °C, RH = 61%, V_{air} = 0.5 m/s

Time (min)	R_q **(mm)**	***Skw***	R_{PV} **(mm)**	***h (mm)***	T_{FS} ***(mm)***
15	0.0822	1.3590	0.7129	0.86	-9.9
30	0.1636	0.9976	1.3184	1.14	-9.7
45	0.2557	1.1595	2.3981	1.60	-9.6
60	0.3413	1.0083	2.4197	1.85	-9.4
75	0.3957	0.6886	2.7861	2.24	-9.4
90	0.4226	0.5229	2.7686	2.37	-9.0
120	0.4707	0.2580	3.0740	2.49	-8.8

Table A- 22. Frost roughness and thickness measurements in Baylor Frost Tunnel: Cases 070218.02 and 101519.02, T_{air} = 16 °C, T_{surf} = -10 °C, RH = 91%, V_{air} = 0.5 m/s

Time (min)	R_q **(mm)**	***Skw***	R_{PV} **(mm)**	***h (mm)***	T_{FS} ***(mm)***
15	0.1316	1.2257	1.4018	0.95	-9.9
30	0.1958	1.5184	1.9599	1.42	-8.5
45	0.2982	1.0960	2.1775	1.80	-7.7
60	0.3438	0.6561	2.2316	1.92	-7.2
75	0.3842	0.2478	2.8746	2.28	-6.6
90	0.3528	0.1940	2.5252	2.36	-6.2
120	0.3696	-0.3062	2.8170	2.63	-5.2

Table A- 23. Frost roughness and thickness measurements in Baylor Frost Tunnel: Cases 062518.01 and 102319, T_{air} = 16 °C, T_{surf} = -5 °C, RH = 76%, V_{air} = 0.5 m/s

Time (min)	R_q **(mm)**	***Skw***	R_{PV} **(mm)**	***h* *(mm)***	T_{FS} ***(mm)***
15	0.0315	1.7686	0.5423	0.70	-4.9
30	0.1554	0.5665	1.2377	1.11	-4.9
45	0.1360	-0.3137	1.0057	1.32	-4.8
60	0.2134	0.2482	1.5673	1.49	-4.6
75	0.2637	0.0151	1.7917	1.71	-4.3
90	0.2524	-0.1915	1.7495	1.74	-4.0
120	0.2517	0.0497	1.8577	1.91	-3.3

Table A- 24. Frost roughness and thickness measurements in Baylor Frost Tunnel: Cases 062518.02 and 102219.02, T_{air} = 16 °C, T_{surf} = -15 °C, RH = 76%, V_{air} = 0.5 m/s

Time (min)	R_q **(mm)**	***Skw***	R_{PV} **(mm)**	***h* *(mm)***	T_{FS} ***(mm)***
15	0.1426	0.6264	1.0589	1.61	-14.9
30	0.2628	0.8981	2.1271	2.11	-13.6
45	0.3269	0.7046	2.1554	2.40	-12.4
60	0.3809	0.3504	2.6751	2.79	-11.9
75	0.3507	-0.2902	2.2194	3.01	-11.2
90	0.3480	-0.3741	2.3908	3.09	-10.6
120	0.2638	-0.6310	2.0330	3.21	-9.4

Table A- 25. Frost roughness and thickness measurements in Baylor Frost Tunnel: Cases 081418 and 102119, T_{air} = 8 °C, T_{surf} = -10 °C, RH = 76%, V_{air} = 0.5 m/s

Time (min)	R_q **(mm)**	***Skw***	R_{PV} **(mm)**	***h (mm)***	T_{FS} ***(mm)***
15	0.0395	0.8485	0.4489	0.91	-9.8
30	0.0780	1.1971	0.7335	1.27	-9.8
45	0.1113	1.2094	1.2440	1.60	-9.8
60	0.1533	1.4105	1.6714	2.05	-9.6
75	0.1653	1.3059	1.6341	2.43	-9.5
90	0.2301	1.1486	2.0510	2.57	-9.4
120	0.3486	0.4729	2.4934	2.90	-8.4

Table A- 26. Frost roughness and thickness measurements in Baylor Frost Tunnel: Cases 062718 and 101819, T_{air} = 12 °C, T_{surf} = -10 °C, RH = 76%, V_{air} = 0.5 m/s

Time (min)	R_q **(mm)**	***Skw***	R_{PV} **(mm)**	***h (mm)***	T_{FS} ***(mm)***
15	0.0771	0.8499	0.6727	1.02	-9.9
30	0.1392	0.8917	1.0212	1.39	-9.8
45	0.2096	0.9559	1.8200	1.91	-9.7
60	0.2376	0.9049	1.8124	2.10	-9.6
75	0.3389	0.8964	3.1647	2.26	-9.4
90	0.3437	0.5467	2.4673	2.41	-9.0
120	0.3898	0.0859	2.8156	2.55	-8.6

Table A- 27. Frost roughness and thickness measurements in Baylor Frost Tunnel: Cases 110719.01 and 010720.01, T_{air} = 8 °C, T_{surf} = -15 °C, RH = 70%, V_{air} = 1.0 m/s

Time (min)	R_q **(mm)**	***Skw***	R_{PV} **(mm)**	***h (mm)***	T_{FS} ***(mm)***
15	0.1388	1.1505	1.7483	1.21	-13.4
30	0.1851	0.7288	1.7325	1.77	-12.6
45	0.1834	0.5449	1.4741	2.19	-12.4
60	0.2907	0.5083	2.2619	2.65	-12.2
75	0.2362	0.5838	1.9693	2.98	-11.6
90	0.3193	0.4726	2.4101	3.38	-11.2
120	0.3325	0.5502	2.6841	3.85	-10.8

Table A- 28. Frost roughness and thickness measurements in Baylor Frost Tunnel: Cases 110619.01 and 010620.01, T_{air} = 12 °C, T_{surf} = -10 °C, RH = 70%, V_{air} = 1.0 m/s

Time (min)	R_q **(mm)**	***Skw***	R_{PV} **(mm)**	***h (mm)***	T_{FS} ***(mm)***
15	0.0293	0.4446	0.2153	1.13	-9.9
30	0.0664	1.8586	1.2720	1.66	-9.8
45	0.1522	2.4288	3.6098	1.96	-9.7
60	0.2491	1.6771	4.2258	2.13	-9.5
75	0.4122	0.9460	4.5186	2.43	-8.8
90	0.3529	0.6610	3.1220	2.60	-8.1
120	0.4033	0.1078	2.0642	2.98	-7.5

Table A- 29. Frost roughness and thickness measurements in Baylor Frost Tunnel: Cases 111219.01 and 010820.01, T_{air} = 12 °C, T_{surf} = -15 °C, RH = 60%, V_{air} = 1.0 m/s

Time (min)	R_q **(mm)**	***Skw***	R_{PV} **(mm)**	***h (mm)***	T_{FS} ***(mm)***
15	0.1184	0.8290	1.1994	1.36	-14.2
30	0.2021	0.7545	1.9337	1.85	-14.0
45	0.2984	0.6845	2.7015	2.10	-13.3
60	0.3241	0.6851	2.9298	2.33	-12.6
75	0.4083	0.5815	3.3942	2.52	-11.9
90	0.4439	0.4737	3.3459	2.76	-11.2
120	0.4413	0.3199	2.8660	3.05	-10.8

Table A- 30. Frost roughness and thickness measurements in Baylor Frost Tunnel: Cases 111119.01 and 010720.02, T_{air} = 12 °C, T_{surf} = -15 °C, RH = 70%, V_{air} = 0.5 m/s

Time (min)	R_q **(mm)**	***Skw***	R_{PV} **(mm)**	***h (mm)***	T_{FS} ***(mm)***
15	0.2056	1.1481	2.5889	1.15	-13.9
30	0.1860	0.9286	2.0267	1.80	-13.3
45	0.2368	0.7882	2.3241	2.26	-12.8
60	0.3238	0.6406	2.8390	2.73	-12.4
75	0.3762	0.8976	4.0156	3.01	-12.0
90	0.3777	0.6201	3.2324	3.32	-11.5
120	0.4413	0.4274	3.1872	3.79	-10.9

Table A- 31. Frost roughness and thickness measurements in Baylor Frost Tunnel: Cases 110619.02 and 010620.02, T_{air} = 12 °C, T_{surf} = -15 °C, RH = 70%, V_{air} = 1.0 m/s

Time (min)	R_q **(mm)**	***Skw***	R_{PV} **(mm)**	***h* *(mm)***	T_{FS} ***(mm)***
15	0.1387	0.7699	1.3419	1.61	-13.9
30	0.2393	1.1248	2.9790	2.26	-13.0
45	0.2970	0.9315	3.2338	2.74	-11.9
60	0.4302	0.6144	3.6682	2.98	-11.4
75	0.4415	0.4026	3.1168	3.21	-10.8
90	0.4669	0.1495	2.5089	3.48	-9.9
120	0.4573	-0.1078	1.7387	3.74	-8.7

Table A- 32. Frost roughness and thickness measurements in Baylor Frost Tunnel: Cases 111119.02 and 010820.02, T_{air} = 12 °C, T_{surf} = -15 °C, RH = 70%, V_{air} = 1.5 m/s

Time (min)	R_q **(mm)**	***Skw***	R_{PV} **(mm)**	***h* *(mm)***	T_{FS} ***(mm)***
15	0.1669	0.7946	1.6496	1.58	-13.5
30	0.3890	0.7657	3.7537	2.32	-11.8
45	0.3997	0.4606	2.9753	2.65	-10.1
60	0.4540	0.0517	2.1547	2.96	-10.0
75	0.4296	-0.0934	1.6739	3.15	-8.9
90	0.4150	-0.1112	1.5833	3.37	-7.9
120	0.4167	-0.0514	1.7172	3.71	-7.0

Table A- 33. Frost roughness and thickness measurements in Baylor Frost Tunnel: Cases 111319 and 010720.03, T_{air} = 12 °C, T_{surf} = -15 °C, RH = 70%, V_{air} = 2.5 m/s

Time (min)	R_q **(mm)**	***Skw***	R_{PV} **(mm)**	***h* *(mm)***	T_{FS} ***(mm)***
15	0.2360	0.9261	2.5605	1.80	-12.4
30	0.3393	0.3787	2.3382	2.32	-10.8
45	0.4030	0.0352	1.8778	2.55	-10.0
60	0.4062	-0.1342	1.4697	2.90	-9.0
75	0.3594	0.0000	1.5860	3.16	-7.6
90	0.3180	0.1638	1.7331	3.45	-6.6
120	0.3395	0.1481	1.8169	3.90	-5.8

Table A- 34. Frost roughness and thickness measurements in Baylor Frost Tunnel: Cases 1112.19.02 and 010820.03, T_{air} = 12 °C, T_{surf} = -15 °C, RH = 78%, V_{air} = 1.0 m/s

Time (min)	R_q **(mm)**	***Skw***	R_{PV} **(mm)**	***h* *(mm)***	T_{FS} ***(mm)***
15	0.1673	0.7646	1.6095	1.64	-13.8
30	0.2557	1.0196	2.9658	2.45	-12.9
45	0.5011	0.8091	5.0061	2.73	-11.7
60	0.5870	0.5264	4.6426	3.06	-11.3
75	0.5648	0.2026	3.2264	3.27	-9.8
90	0.5936	-0.0013	2.6249	3.49	-9.3
120	0.5632	-0.0122	2.4680	3.89	-8.4

Table A- 35. Frost roughness and thickness measurements in Baylor Frost Tunnel: Cases 110619.03 and 010620.03, T_{air} = 12 °C, T_{surf} = -20 °C, RH = 70%, V_{air} = 1.0 m/s

Time (min)	***R_q* (mm)**	***Skw***	***R_{PV}* (mm)**	***h* *(mm)***	***T_{FS}* *(mm)***
15	0.2596	1.0526	3.0790	1.71	-17.1
30	0.4003	0.4631	2.9825	2.52	-15.4
45	0.4821	0.3246	3.1358	3.01	-13.9
60	0.5496	0.1963	3.1113	3.42	-12.9
75	0.5389	0.0500	2.5545	3.73	-12.1
90	0.5998	0.0872	2.9803	3.87	-10.4
120	0.5519	-0.2127	1.7682	4.25	-9.8

Table A- 36. Frost roughness and thickness measurements in Baylor Frost Tunnel: Cases 111219.02 and 010820.03, T_{air} = 12 °C, T_{surf} = -15 °C, RH = 80%, V_{air} = 1.0 m/s

Time (min)	***R_q* (mm)**	***Skw***	***R_{PV}* (mm)**	***h* *(mm)***	***T_{FS}* *(mm)***
15	0.1931	0.9628	2.1770	1.82	-13.2
30	0.3677	0.7887	3.6035	2.41	-11.1
45	0.5292	0.3223	3.4375	2.71	-9.6
60	0.5623	-0.0574	2.2981	2.99	-8.8
75	0.4058	-0.0510	1.6737	3.18	-7.4
90	0.3749	-0.0253	1.6015	3.46	-6.6
120	0.4227	0.1117	2.1667	3.89	-5.8

B Appendix B: CAFF test reports using an aluminum skin without a structural rib

Table B- 1. Summary of nominal test conditions for wing tank thermal model with an aluminum skin and a structural rib

Date	T_{PC} (°C)	$T_{air,set}$ (°C)	RH (%)	V (m/s)	x_{img} (in.)	Notes
11/15/19	-28	10	87	1.0	20.75	20 min. int.
11/21/19	-28	6	87	1.0	20.75	20 min. int.
12/06/19	-28	14	87	1.0	20.75	20 min. int.
12/18/19	-25	10	87	0.3	20.75	20 min. int.
12/20/19	-25	6	87	0.3	20.75	20 min. int.
12/23/19	-25	15	87	0.3	20.75	20 min. int.

CAFF Conditions Report - Case Date: 111519

Table 111519.01: Summary of Measured Test Variables

Variable	Mean	St. Dev.	Rand. Unc.
T_air (C)	9.0704	0.4927	0.0177
Rh (%)	78.3800	4.8241	0.1736
Omega (kg_v/kg_da)	0.00561491	0.00038751	0.00001394
V_air (m/s)	0.9964	0.0547	0.0020
T_skin (C)	-17.4618	0.0848	0.0031
T_floor (C)	-20.4580	0.0305	0.0011

Figure 111519.01: Temperature and Voltage Control Time History

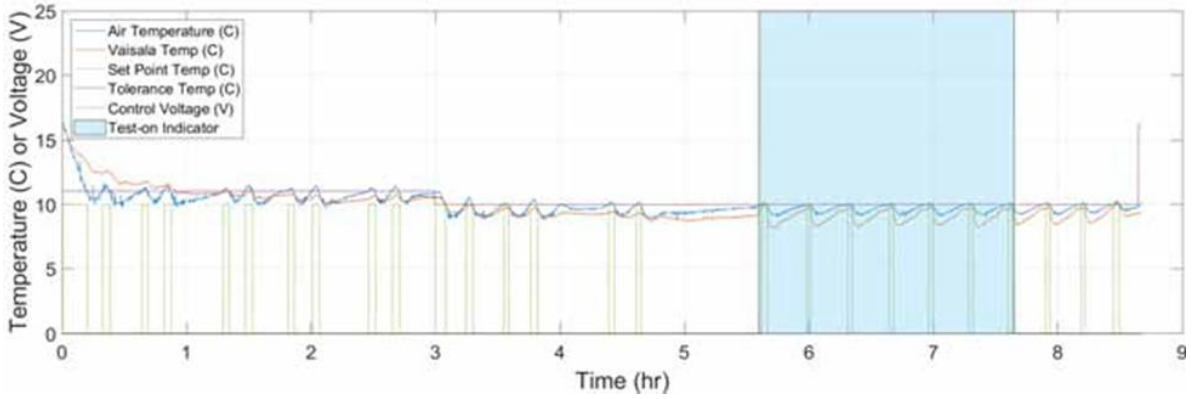

Figure 111519.02: Relative Humidity Time History

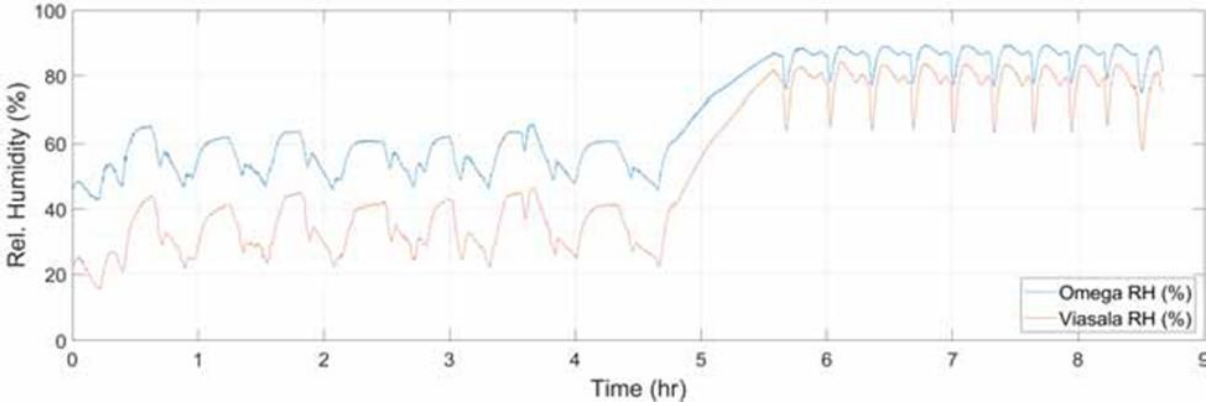

Figure 111519.03: Velocity Time History

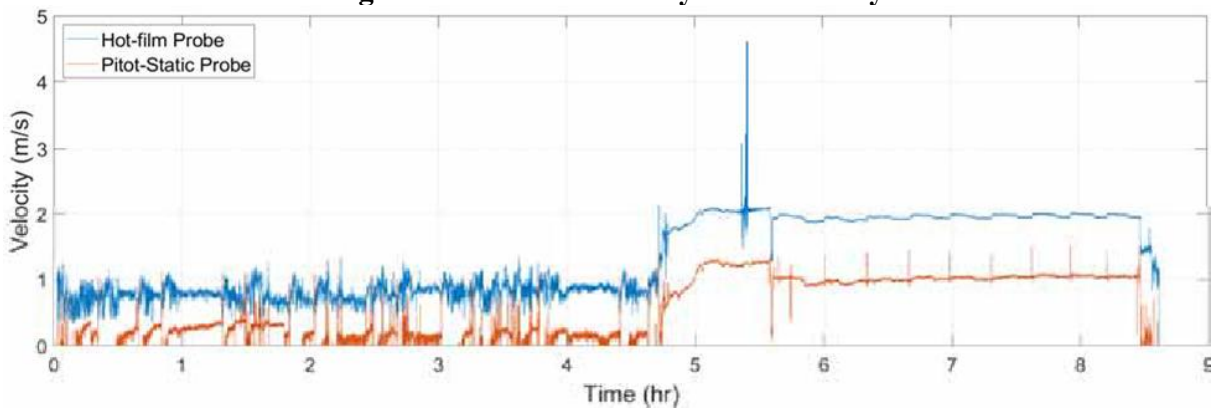

Figure 111519.04: Coolant Return Temperature Time History

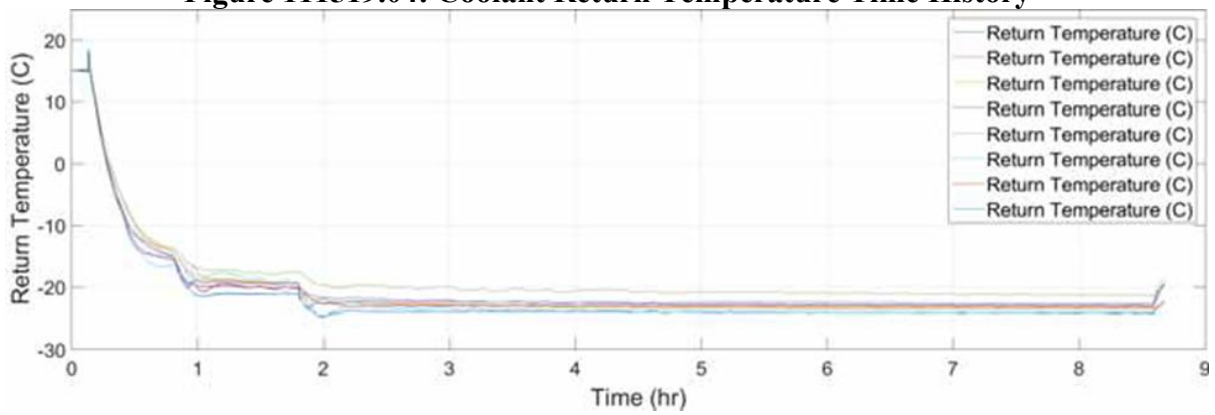

Figure 111519.05: Coolant Supply Temperature Time History

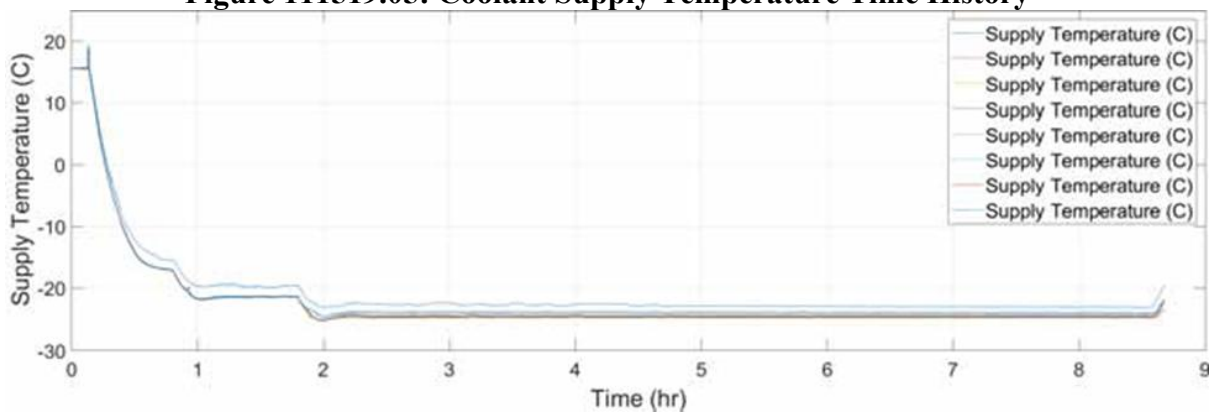

Figure 111519.06: Skin Temperature Time History

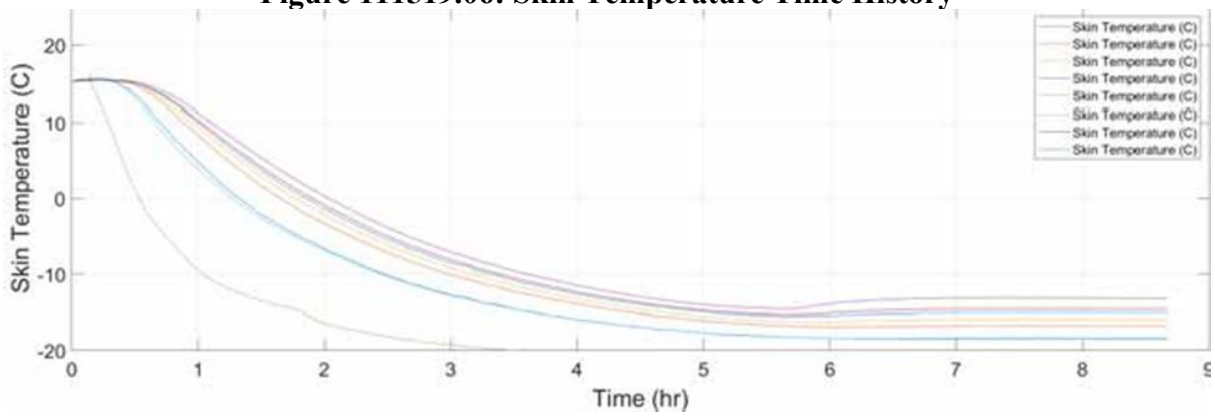

Figure 111519.07: Floor Temperature Time History

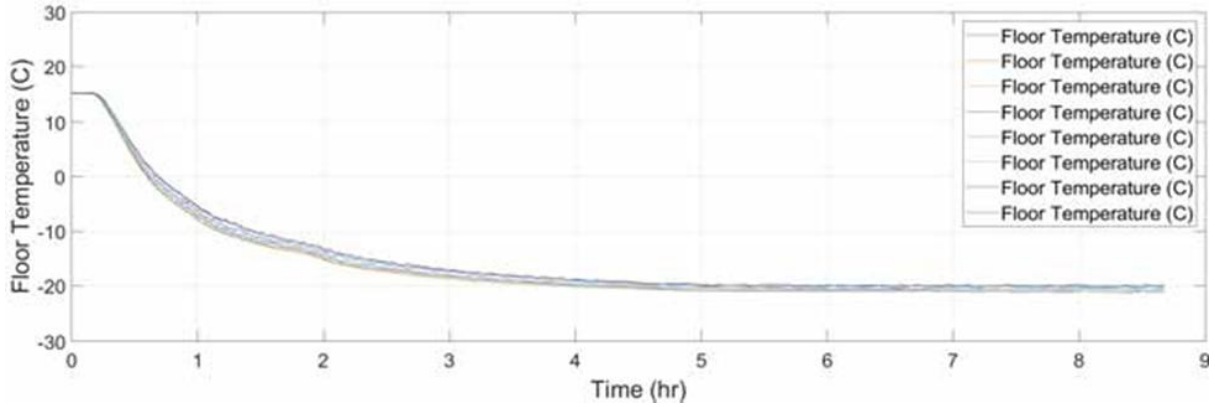

Figure 111519.08: Skin Temperature Slope Time History

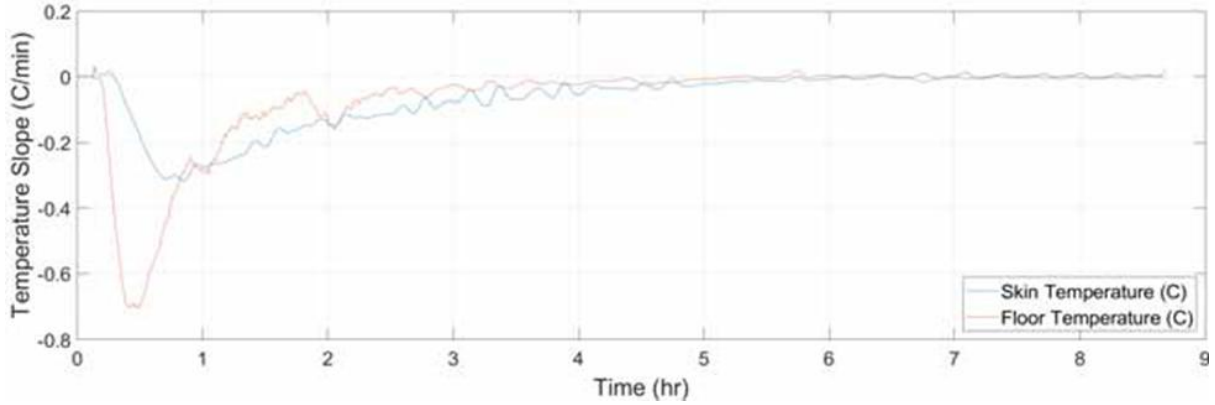

Figure 111519.09: RMS Height Evolution

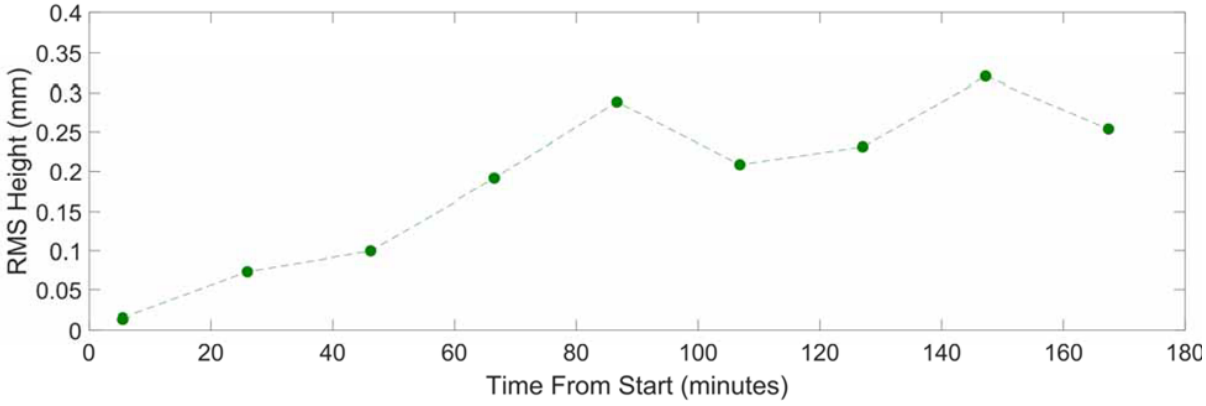

Figure 111519.10: Skewness Evolution

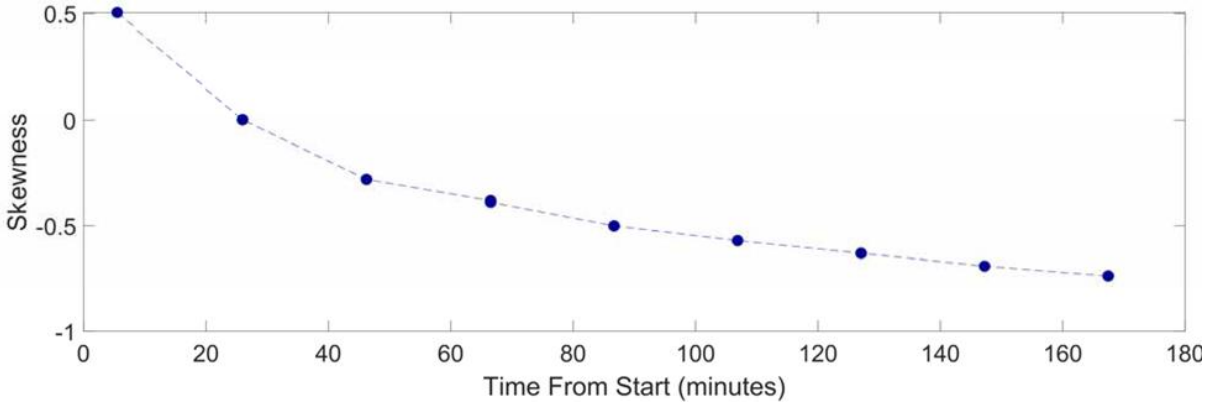

Figure 111519.11: Peak to Valley Evolution

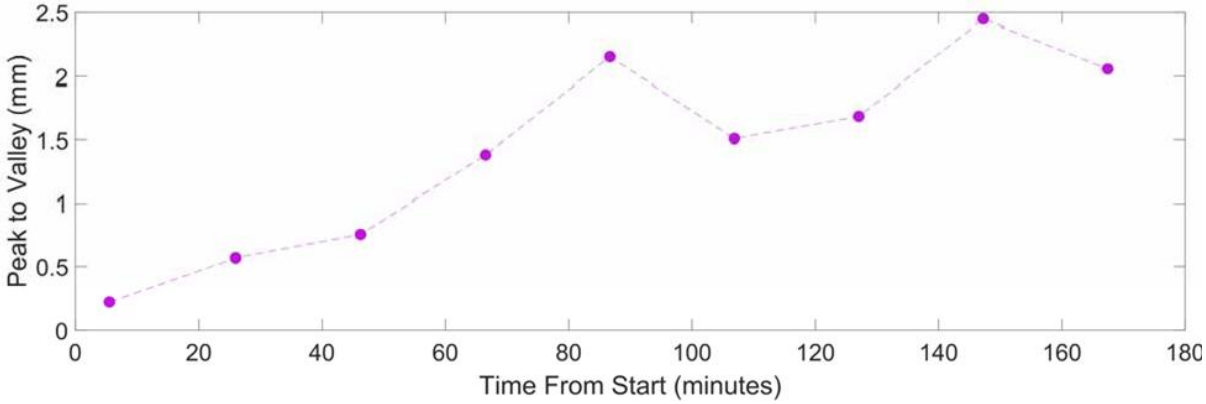

Figure 111519.12: Equivalent Roughness Evaluation

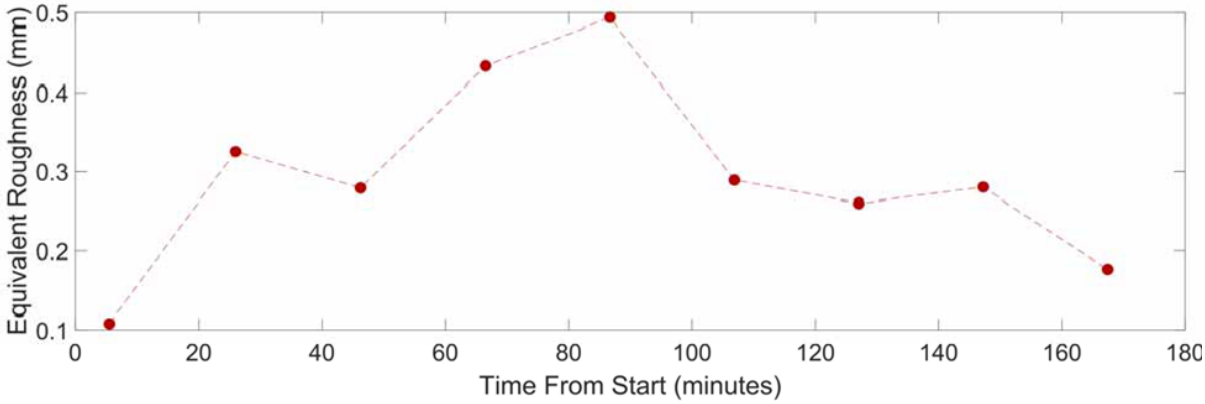

Table 111519.02: Summary of Roughness Parameters

Time (min.)	RMS (mm)	Skewness	Peak to Valley (mm)	ks,Flack-Schultz (mm)
5.5000	0.0139	0.5053	0.2137	0.1078
25.9667	0.0732	0.0028	0.5665	0.3254
46.2333	0.0995	-0.2840	0.7538	0.2788
66.5167	0.1911	-0.3867	1.3813	0.4333
86.6833	0.2886	-0.5007	2.1561	0.4936
106.8667	0.2083	-0.5716	1.5106	0.2889
127.0500	0.2312	-0.6325	1.6880	0.2599
147.2333	0.3200	-0.6940	2.4493	0.2799
167.4167	0.2537	-0.7414	2.0582	0.1762

Figure 111519.13: Frost Topography at 00:05:30

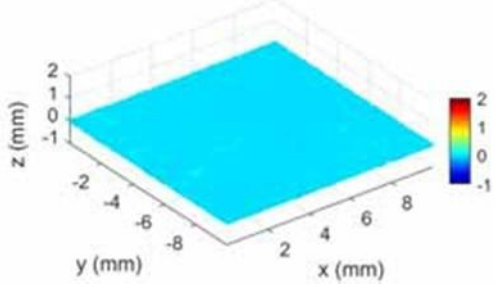

Figure 111519.14: Frost Topography at 00:25:58

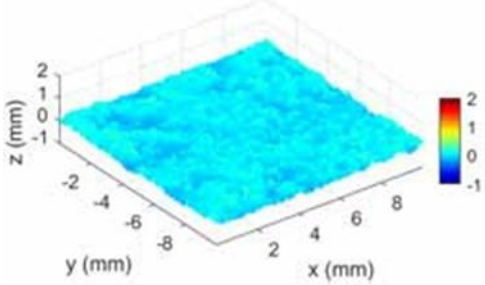

Figure 111519.15: Frost Topography at 00:46:14

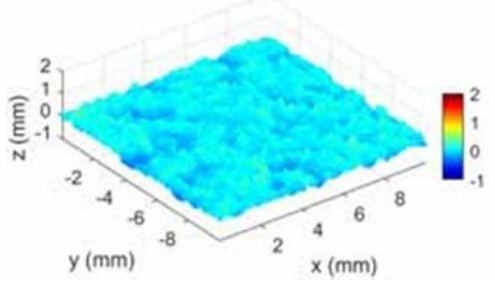

Figure 111519.16: Frost Topography at 01:06:31

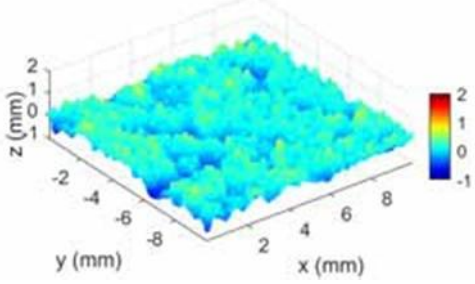

Figure 111519.17: Frost Topography at 01:26:41

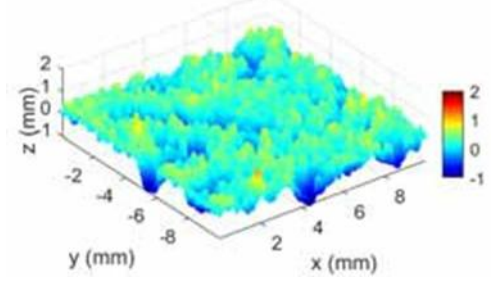

Figure 111519.18: Frost Topography at 01:46:52

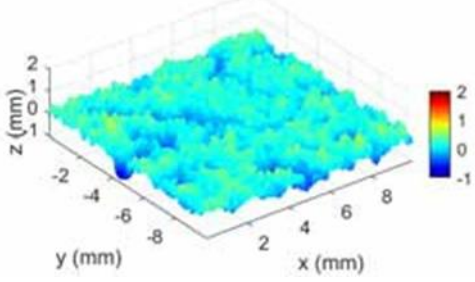

Figure 111519.19: Frost Topography at 02:07:03

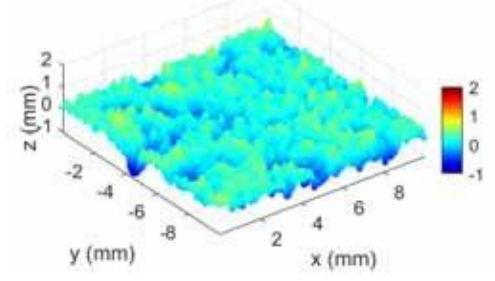

Figure 111519.20: Frost Topography at 02:27:14

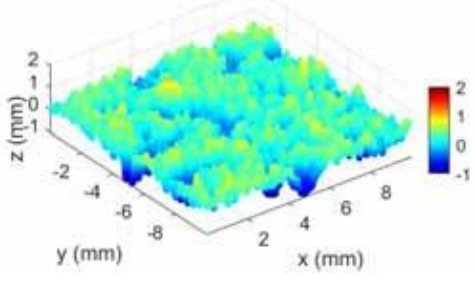

Figure 111519.21: Frost Topography at 02:47:25

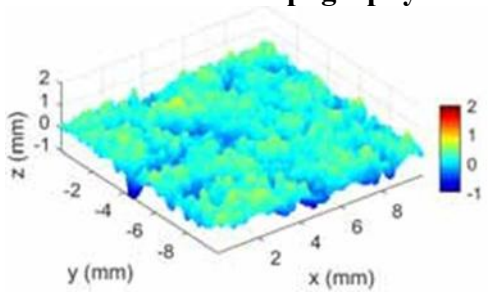

CAFF Conditions Report – Case Date: 112119

Table 112119.01: Summary of Measured Test Variables

Variable	Mean	St. Dev.	Rand. Unc.
T_air (C)	5.1074	0.2989	0.0091
Rh (%)	78.6198	5.4521	0.1668
Omega (kg_v/kg_da)	0.00434575	0.00035183	0.00001076
V_air (m/s)	1.0397	0.0624	0.0019
T_skin (C)	-18.1481	0.0051	0.0002
T_floor (C)	-20.9298	0.0625	0.0019

Figure 112119.01: Temperature and Voltage Control Time History

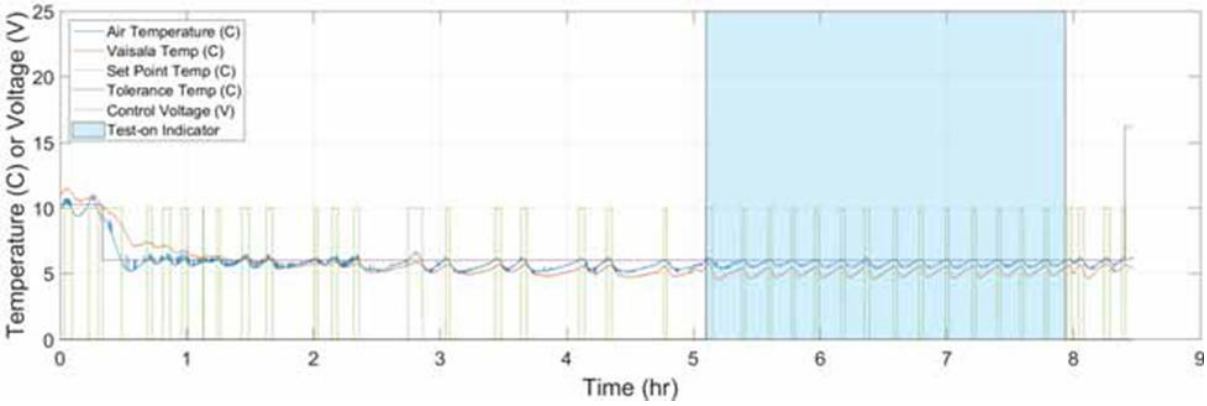

Figure 112119.02: Relative Humidity Time History

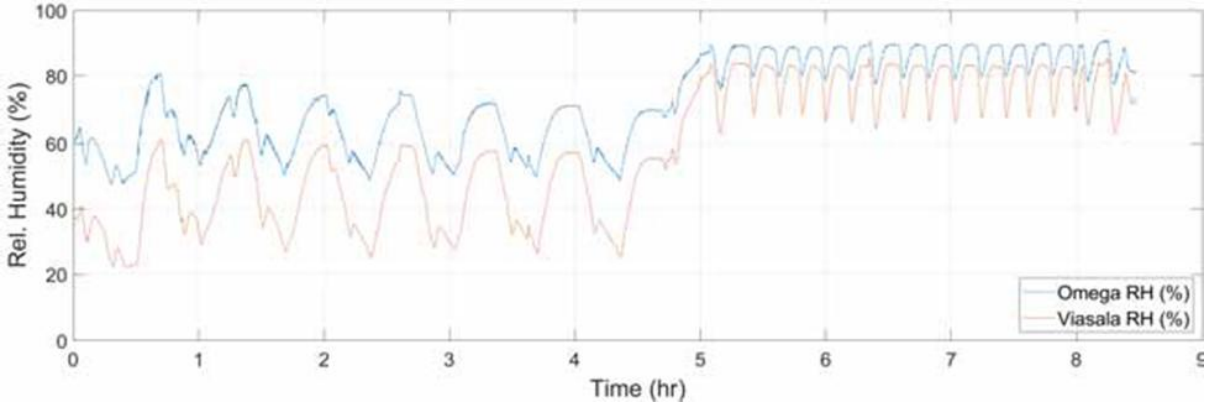

Figure 112119.03: Velocity Time History

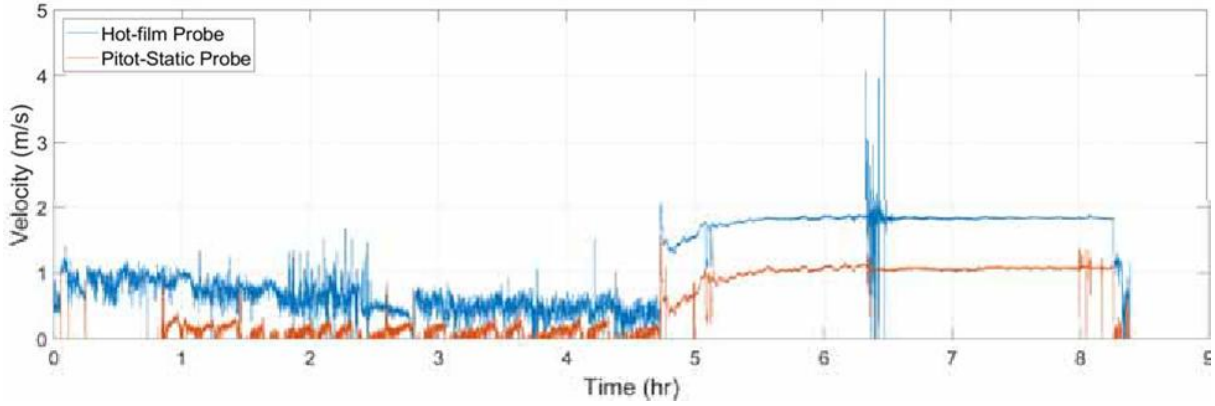

Figure 112119.04: Coolant Return Temperature Time History

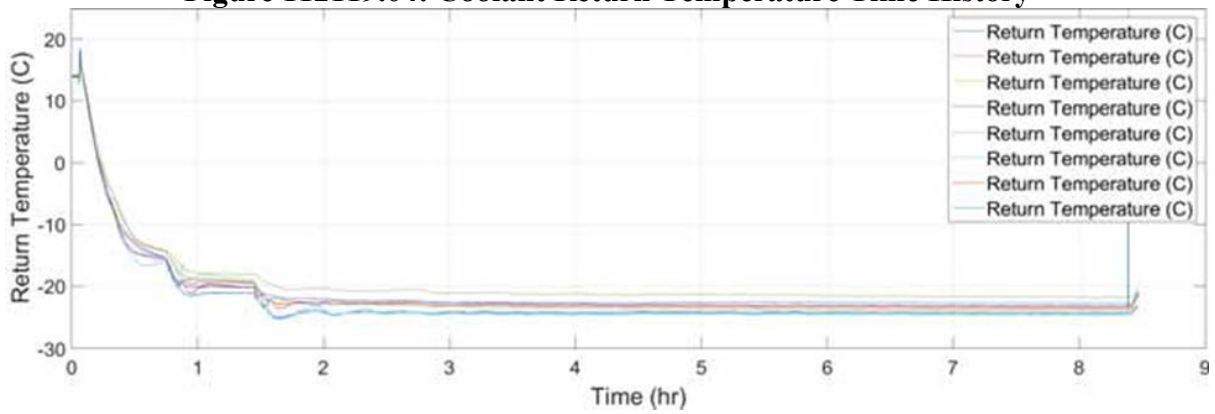

Figure 112119.05: Coolant Supply Temperature Time History

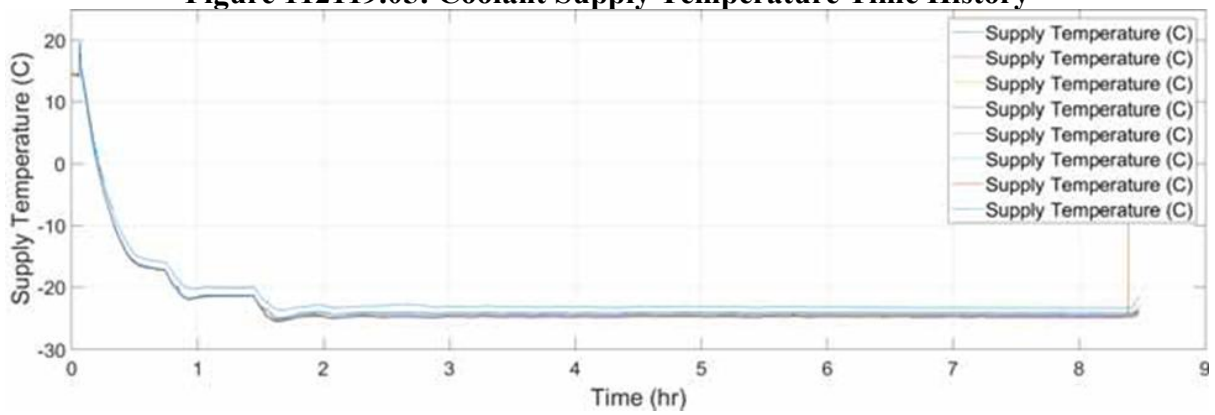

Figure 112119.06: Skin Temperature Time History

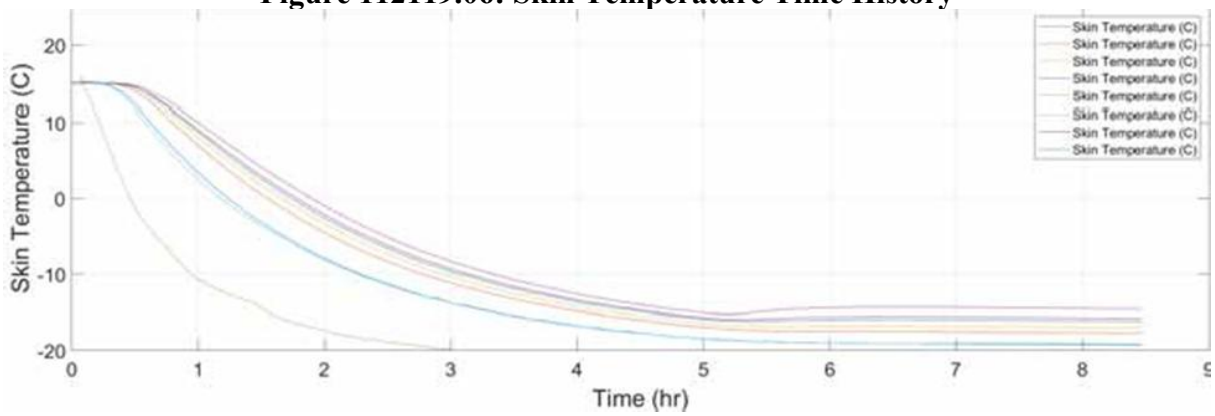

Figure 112119.07: Floor Temperature Time History

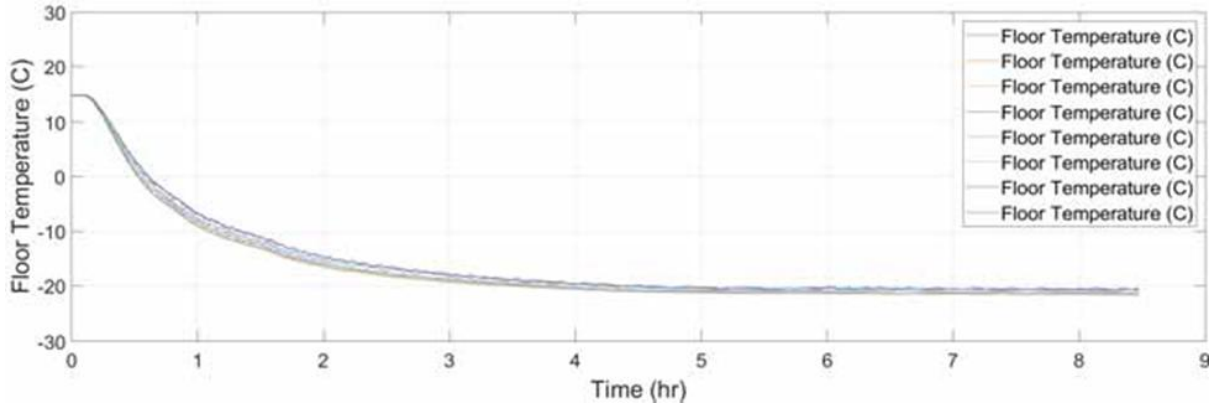

Figure 112119.08: Skin Temperature Slope Time History

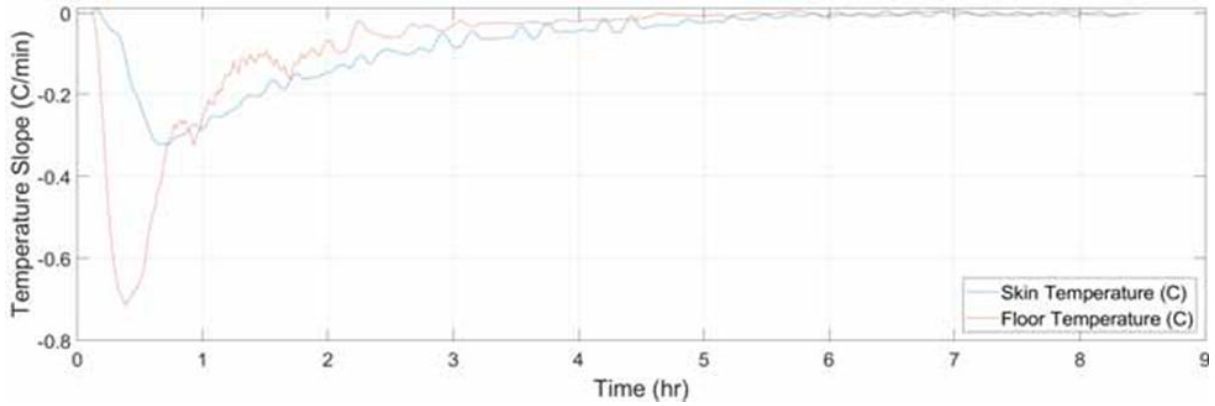

Figure 112119.09: RMS Height Evolution

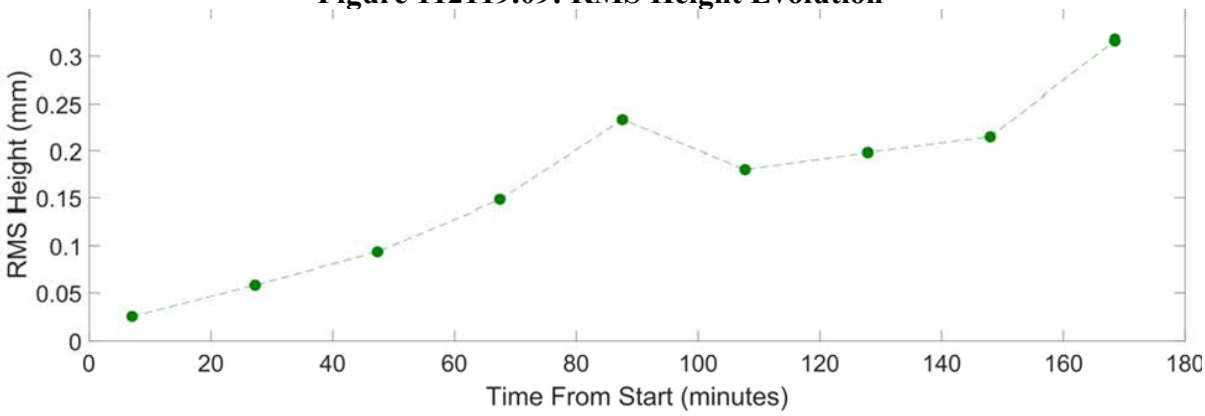

Figure 112119.10: Skewness Evolution

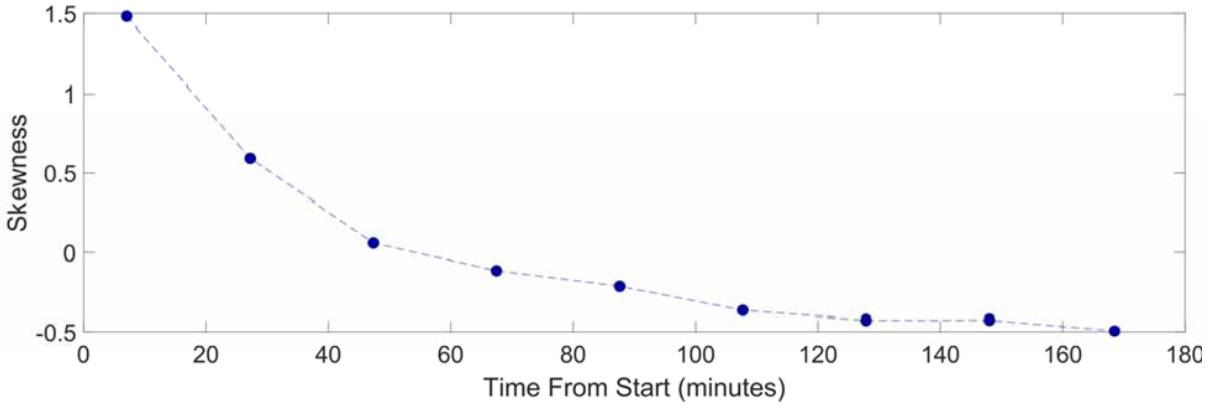

Figure 112119.11: Peak to Valley Evolution

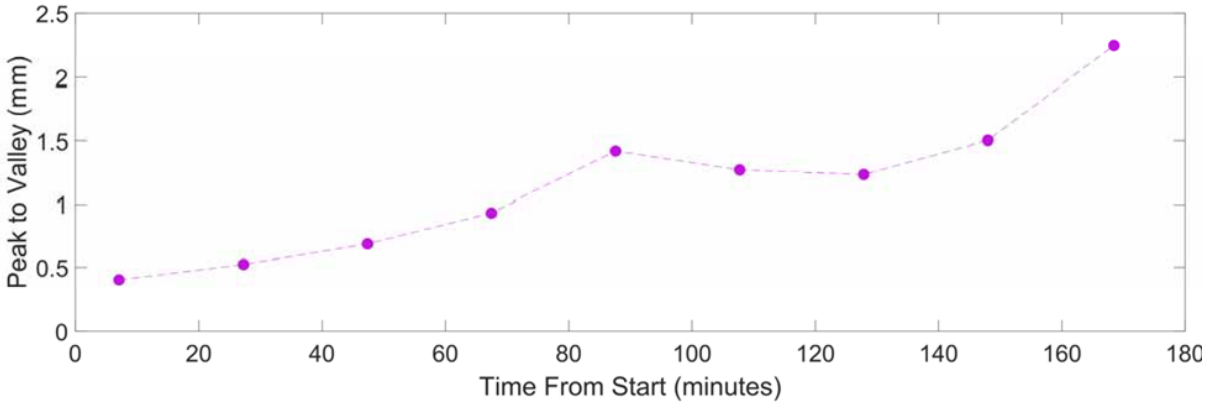

Figure 112119.12: Equivalent Roughness Evolution

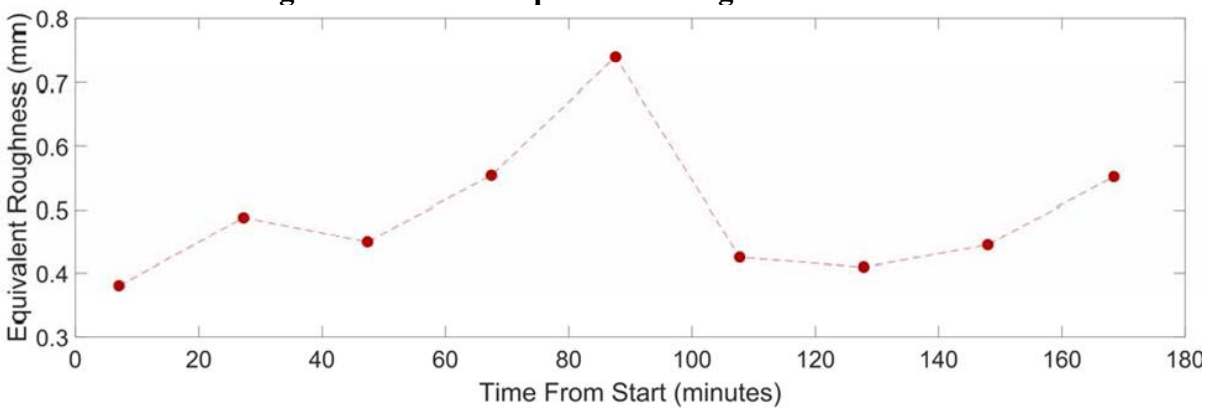

Table 112119.02: Summary of Roughness Parameters

Time (min.)	RMS (mm)	Skewness	Peak to Valley (mm)	ks,Flack-Schultz (mm)
7.0480	0.0247	1.4818	0.3994	0.3797
27.2480	0.0583	0.5915	0.5230	0.4882
47.3480	0.0937	0.0595	0.6873	0.4495
67.4647	0.1484	-0.1175	0.9330	0.5538
87.5980	0.2335	-0.2164	1.4210	0.7407
107.7313	0.1804	-0.3691	1.2697	0.4251
127.8647	0.1984	-0.4276	1.2323	0.4093
147.9980	0.2152	-0.4265	1.5051	0.4450
168.4480	0.3164	-0.4937	2.2534	0.5517

Figure 112119.13: Frost Topography at 00:07:02

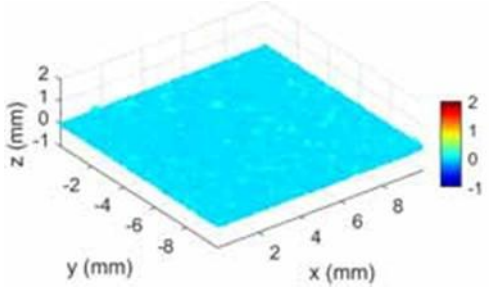

Figure 112119.14: Frost Topography at 00:27:14

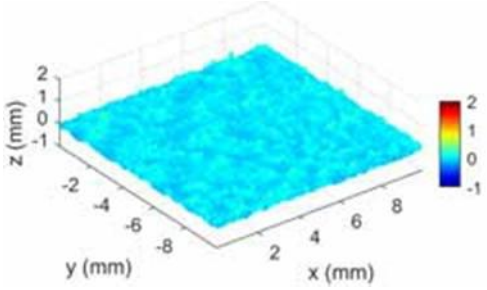

Figure 112119.15: Frost Topography at 00:47:20

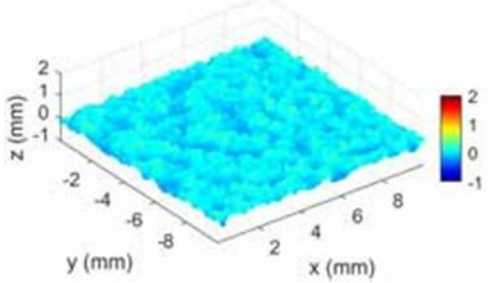

Figure 112119.16: Frost Topography at 01:07:27

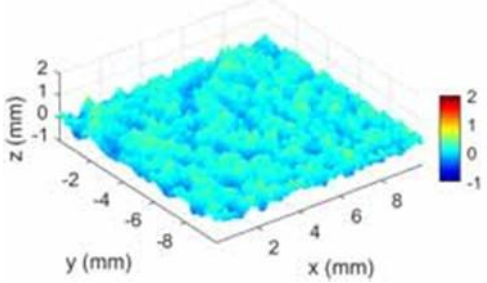

Figure 112119.17: Frost Topography at 01:27:35

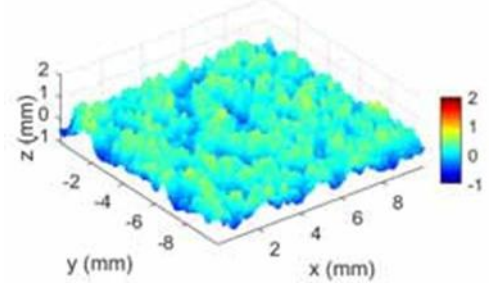

Figure 112119.18: Frost Topography at 01:47:43

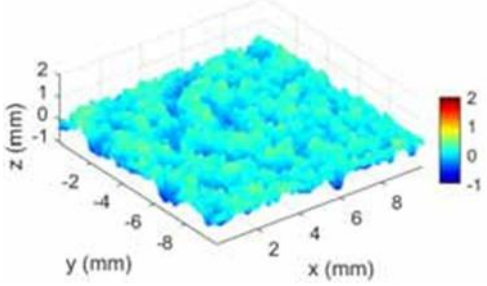

Figure 112119.19: Frost Topography at 02:07:51

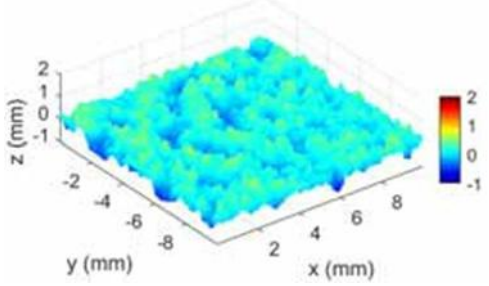

Figure 112119.20: Frost Topography at 02:27:59

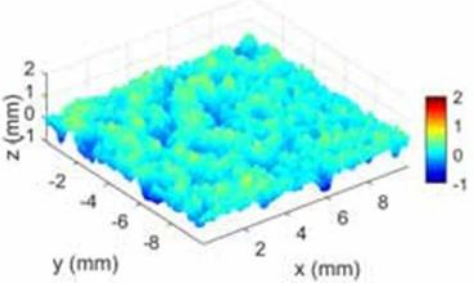

Figure 112119.21: Frost Topography at 02:48:26

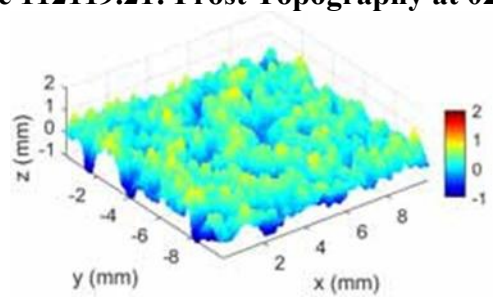

CAFF Conditions Report – Case Date: 120619

Table 120619.01: Summary of Measured Test Variables

Variable	Mean	St. Dev.	Rand. Unc.
T_air (C)	13.0325	0.4026	0.0135
Rh (%)	81.4353	2.4976	0.0835
Omega (kg_v/kg_da)	0.00764540	0.00033419	0.00001117
V_air (m/s)	0.7449	0.0307	0.0010
T_skin (C)	-17.1532	0.2493	0.0083
T_floor (C)	-20.2105	0.0716	0.0024

Figure 120619.01: Temperature and Voltage Control Time History

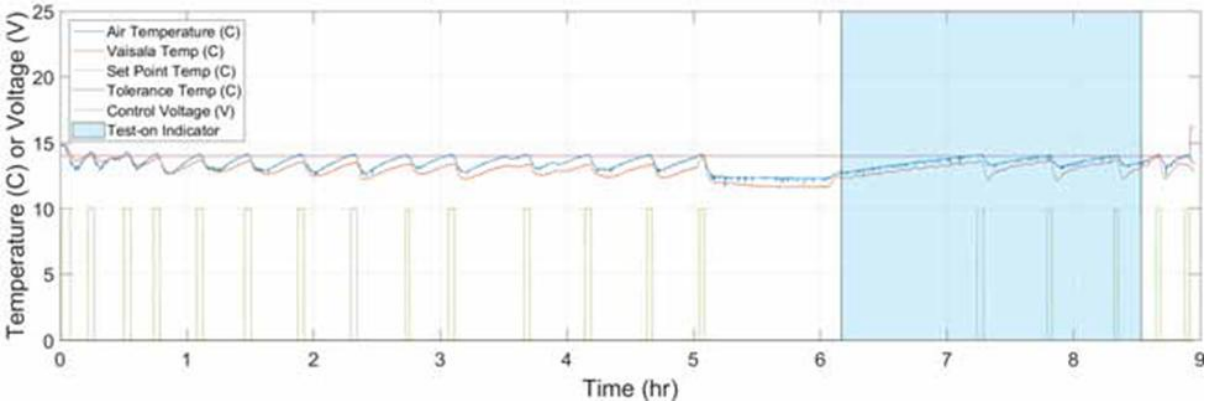

Figure 120619.02: Relative Humidity Time History

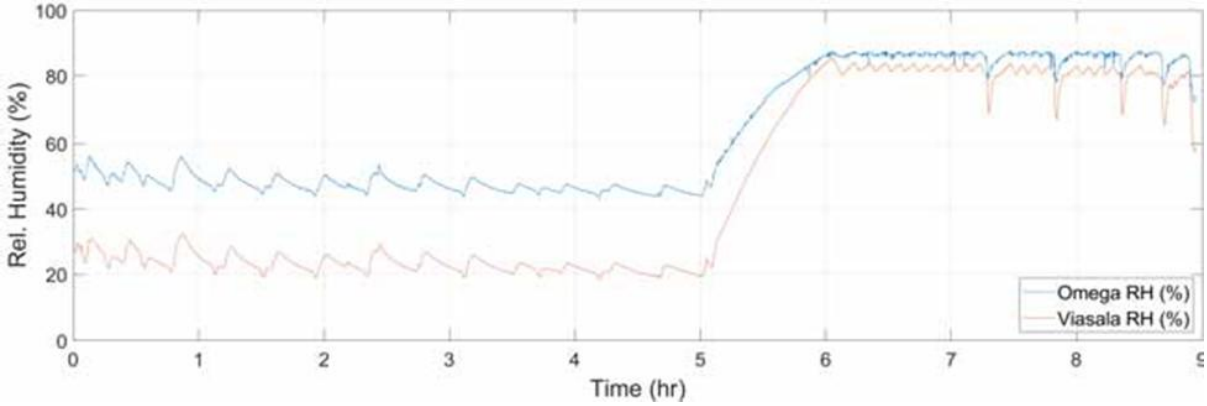

Figure 120619.03: Velocity Time History

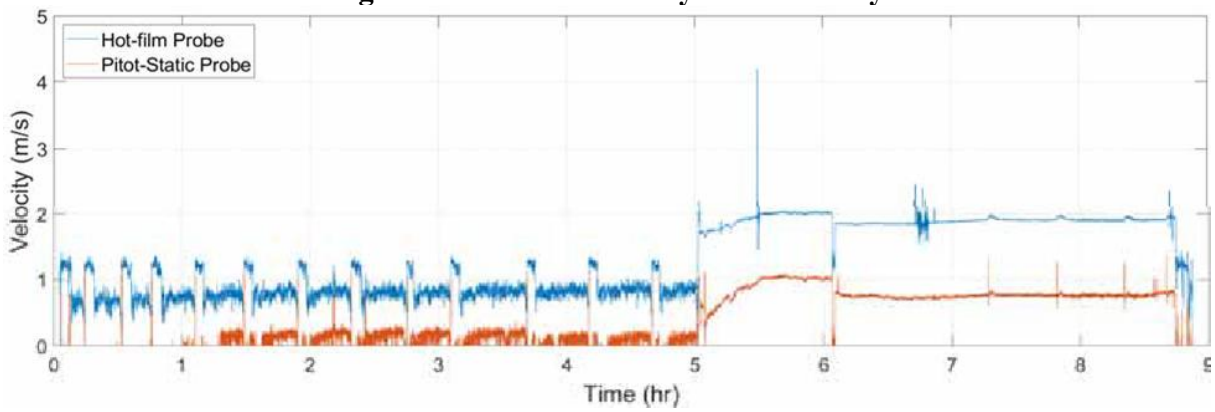

Figure 120619.04: Coolant Return Temperature Time History

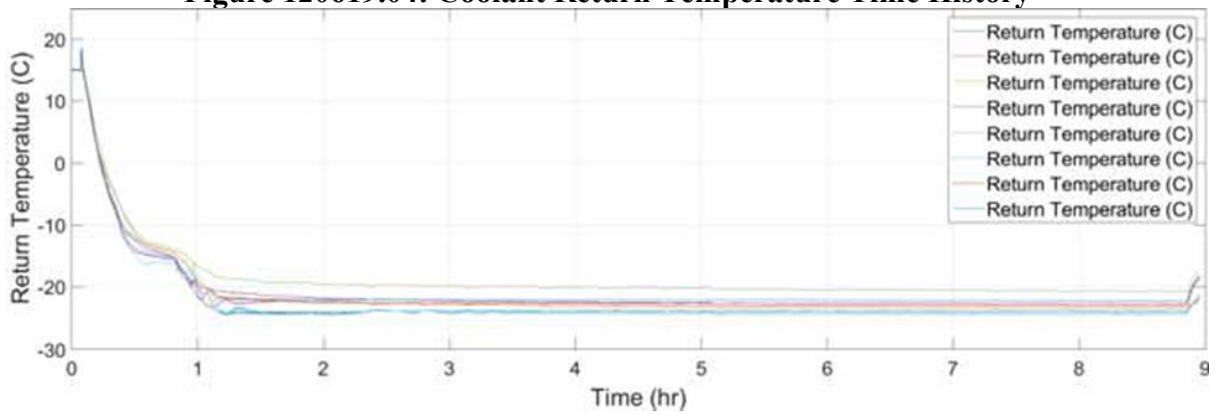

Figure 120619.05: Coolant Supply Temperature Time History

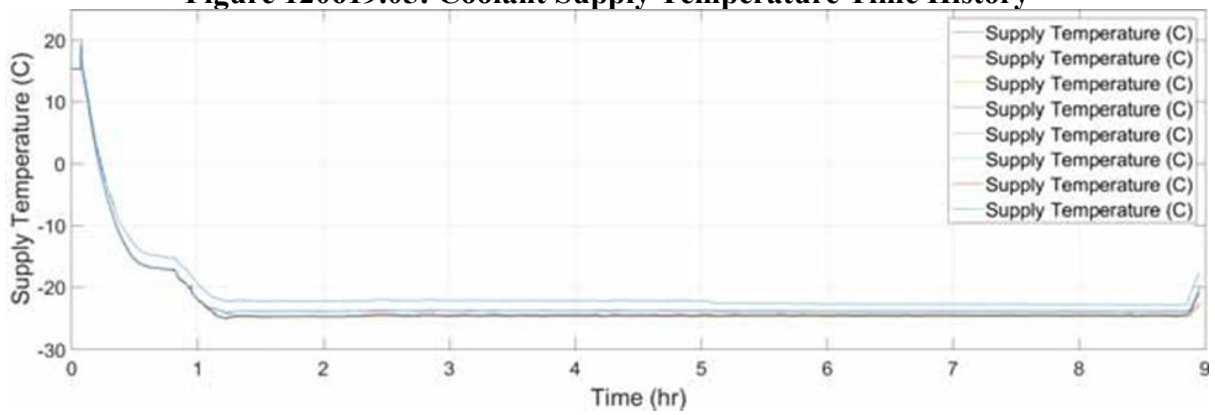

Figure 120619:06: Skin Temperature Time History

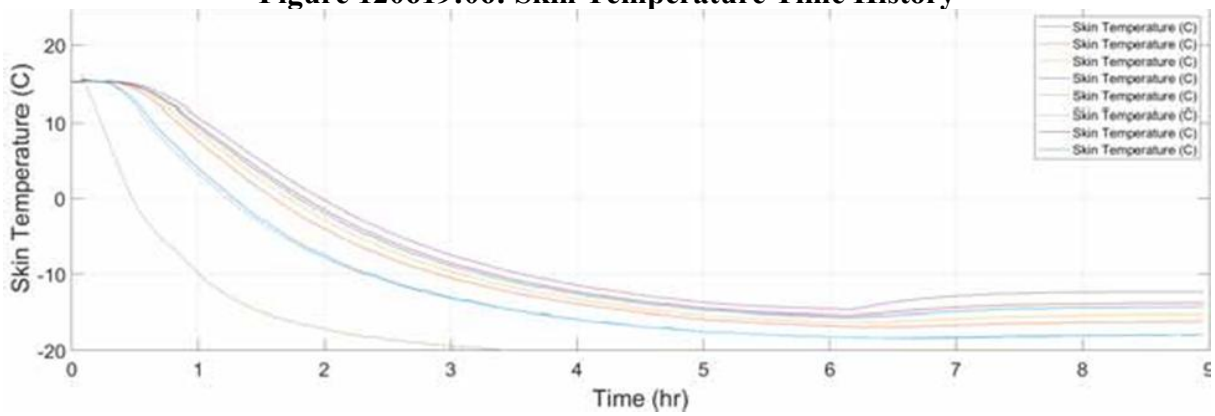

Figure 120619.07: Floor Temperature Time History

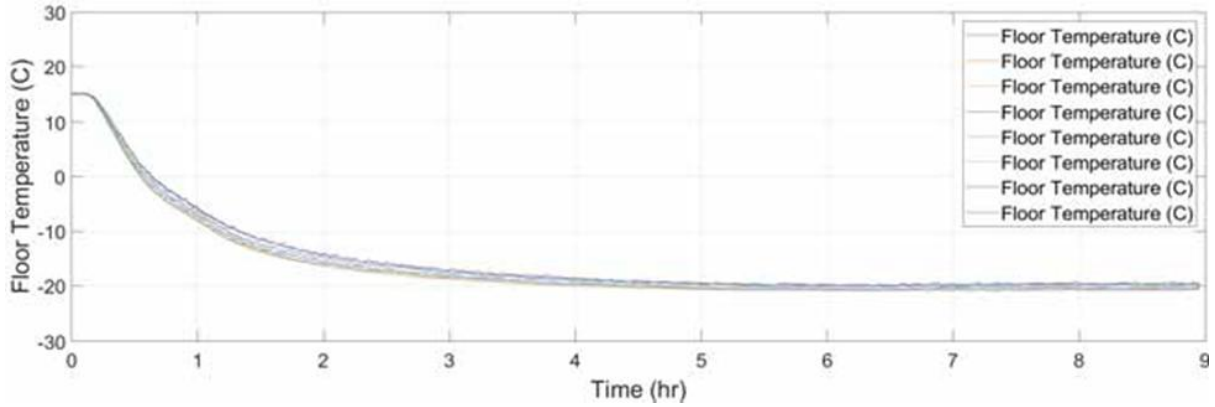

Figure 120619.08: Skin Temperature Slope Time History

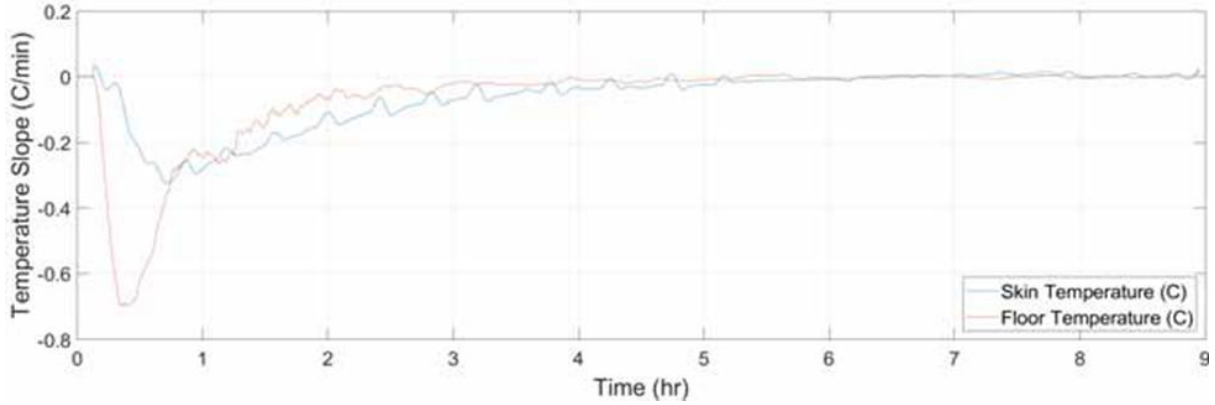

Figure 120619.09: RMS Height Evolution

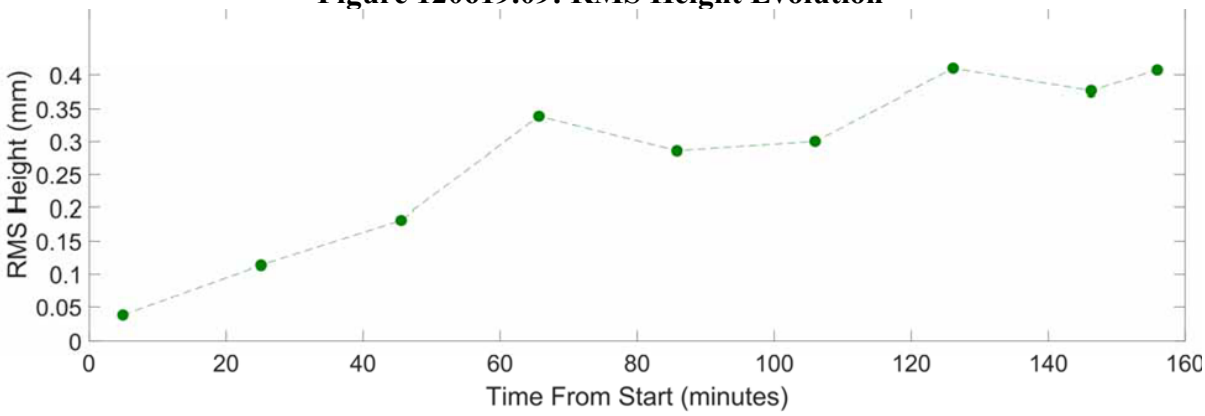

Figure 120619.10: Skewness Evolution

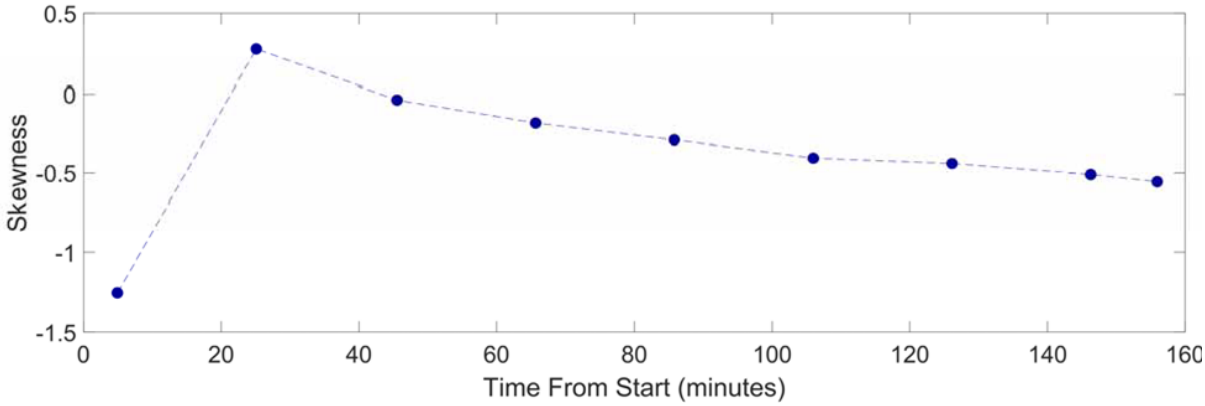

Figure 120619.11: Peak to Valley Evolution

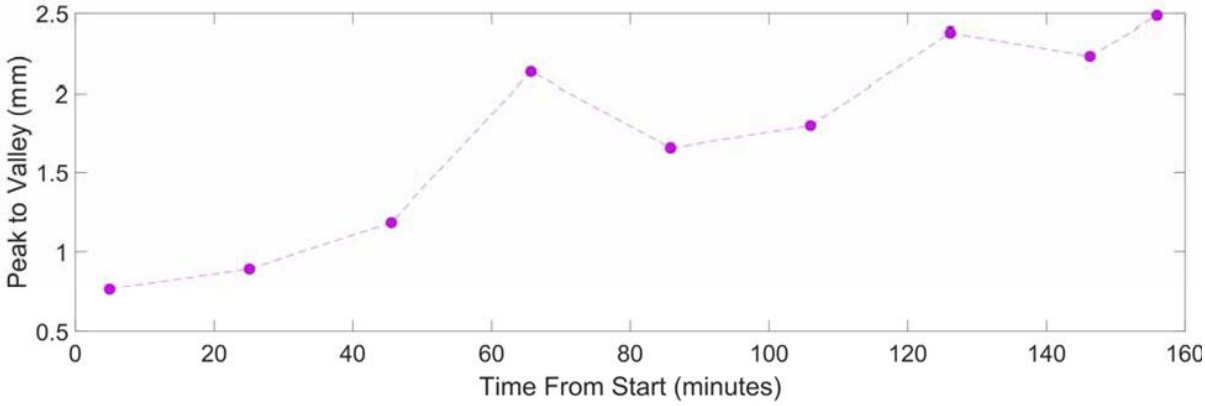

Figure 120619.12: Equivalent Roughness Evolution

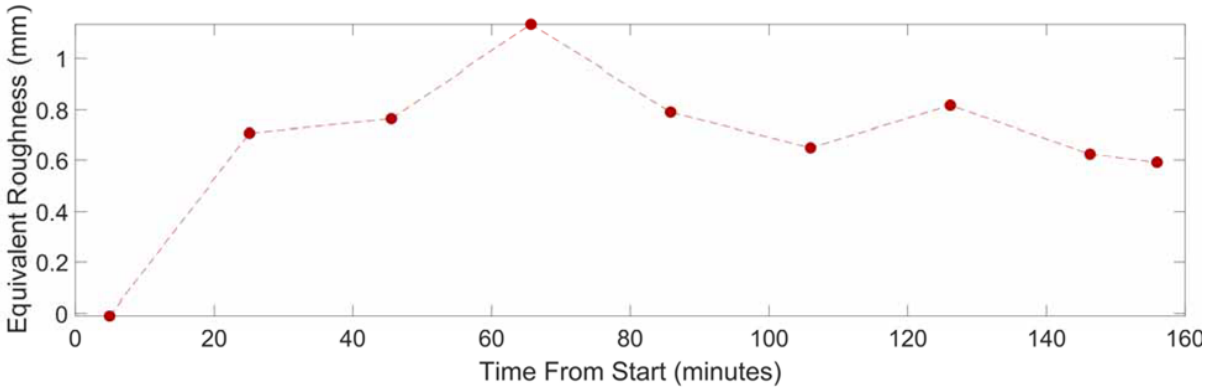

Table 120619.02: Summary of Roughness Parameters

Time (min.)	RMS (mm)	Skewness	Peak to Valley (mm)	ks,Flack-Schultz (mm)
4.9167	0.0375	-1.2589	0.7609	-0.0104
25.0833	0.1136	0.2819	0.8901	0.7075
45.5333	0.1820	-0.0379	1.1859	0.7648
65.6667	0.3389	-0.1836	2.1358	1.1371
85.8000	0.2860	-0.2911	1.6553	0.7909
105.9833	0.3001	-0.4073	1.7974	0.6493
126.1333	0.4100	-0.4411	2.3831	0.8185

Figure 120619.13: Frost Topography at 00:25:05

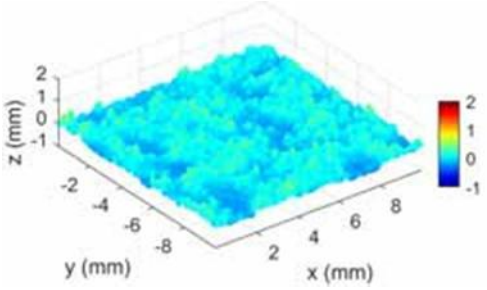

Figure 120619.14: Frost Topography at 00:45:32

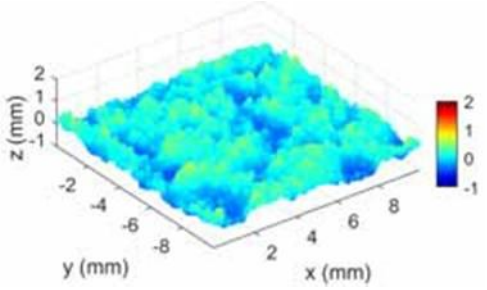

Figure 120619.15: Frost Topography at 01:05:40

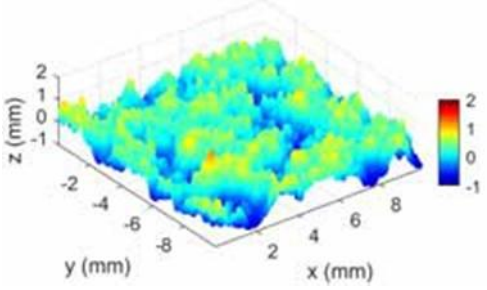

Figure 120619.16: Frost Topography at 01:25:48

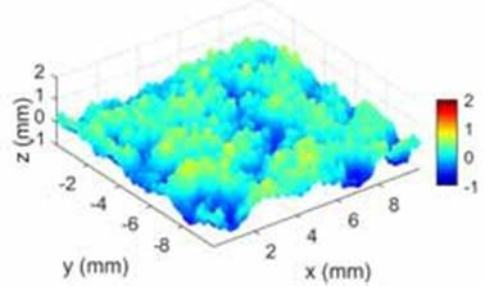

Figure 120619.17: Frost Topography at 01:45:59

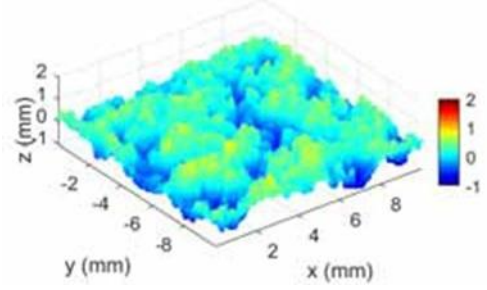

Figure 120619.18: Frost Topography at 02:06:08

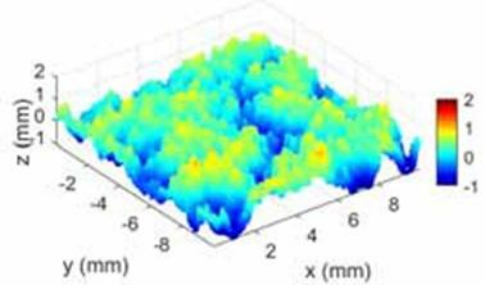

Figure 120619:19: Frost Topography at 02:26:17

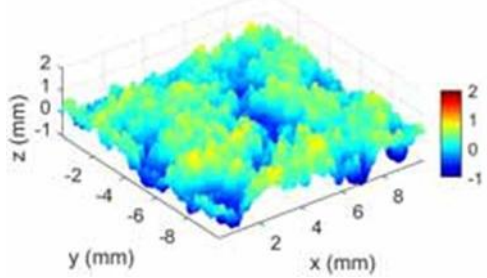

CAFF Conditions Report – Case Date: 121819

Variable	Mean	St. Dev.	Rand. Unc.
T_air (C)	9.0514	0.3643	0.0116
Rh (%)	80.4607	6.2184	0.1983
Omega (kg_v/kg_da)	0.00574626	0.00047155	0.00001504
V_air (m/s)	0.3573	0.1106	0.0035
T_skin (C)	-15.9932	0.1237	0.0039
T_floor (C)	-18.3291	0.0375	0.0012

Figure 121819.01: Temperature and Voltage Control Time History

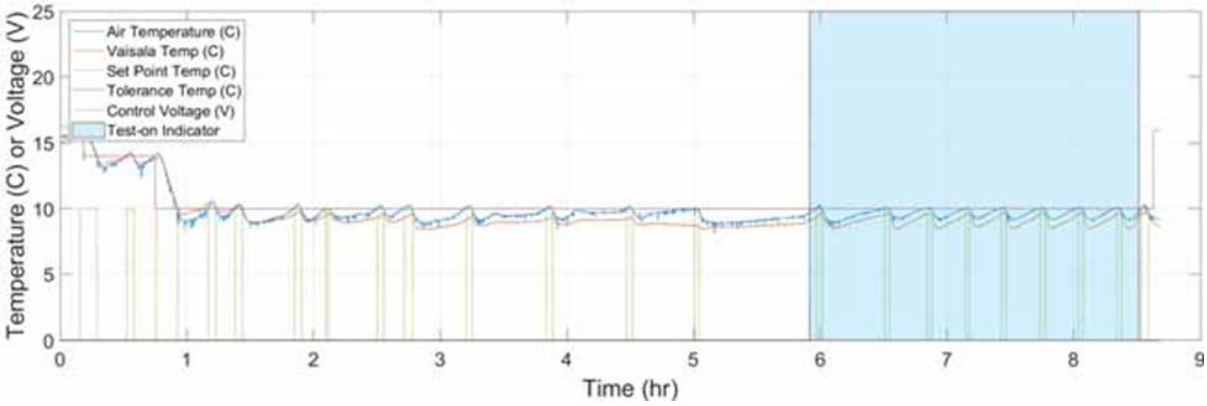

Figure 121819.02: Relative Humidity Time History

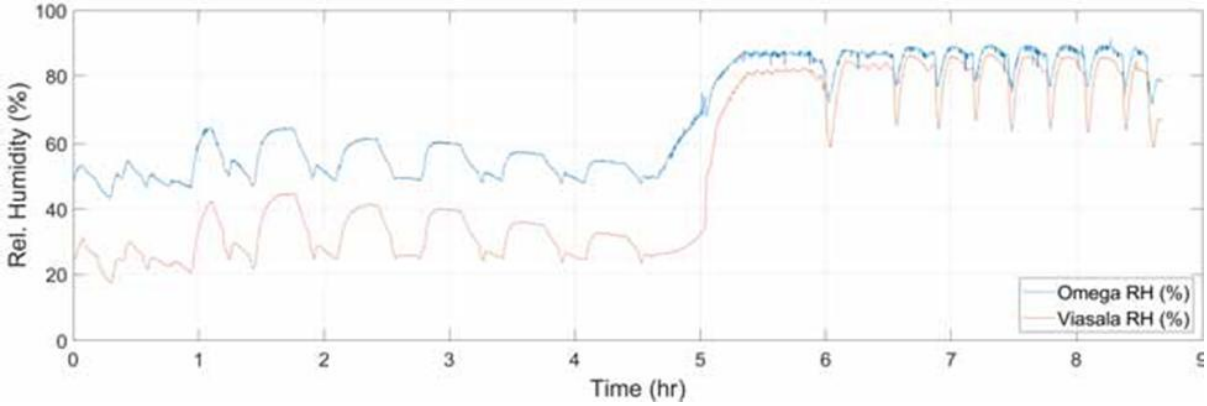

Figure 121819.03: Velocity Time History

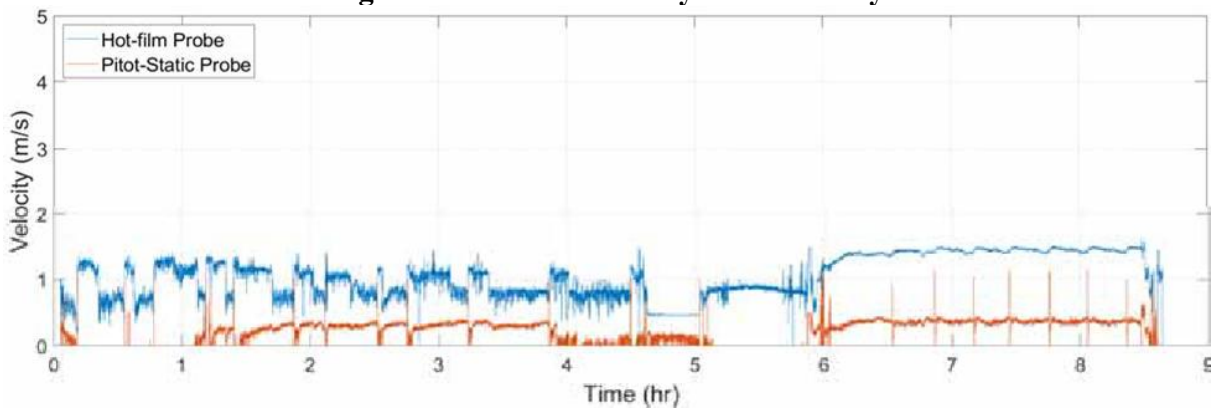

Figure 121819.04: Coolant Return Temperature Time History

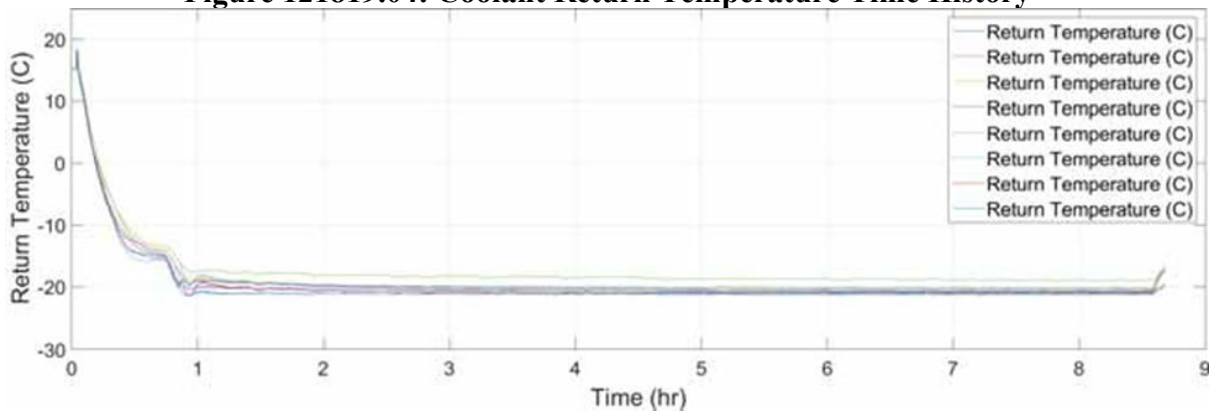

Figure 121819.05: Coolant Supply Temperature Time History

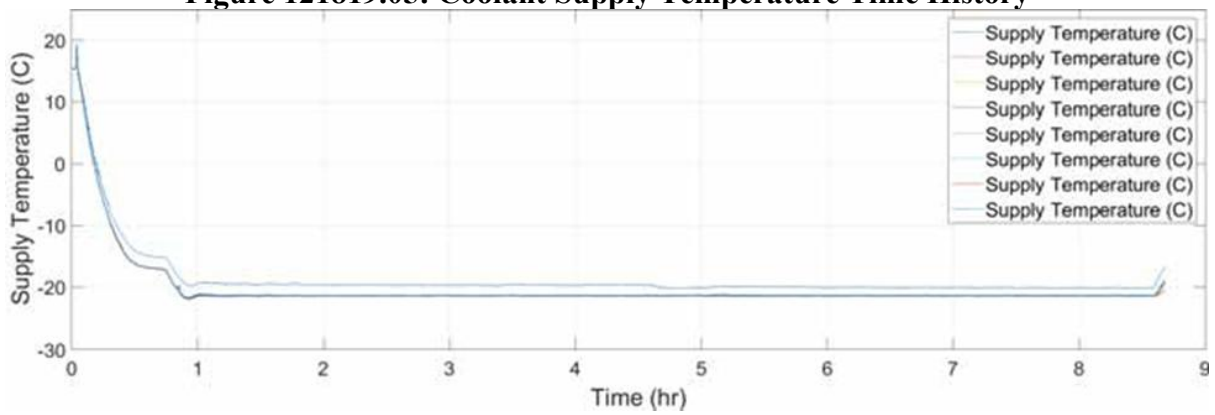

Figure 121819.06: Skin Temperature Time History

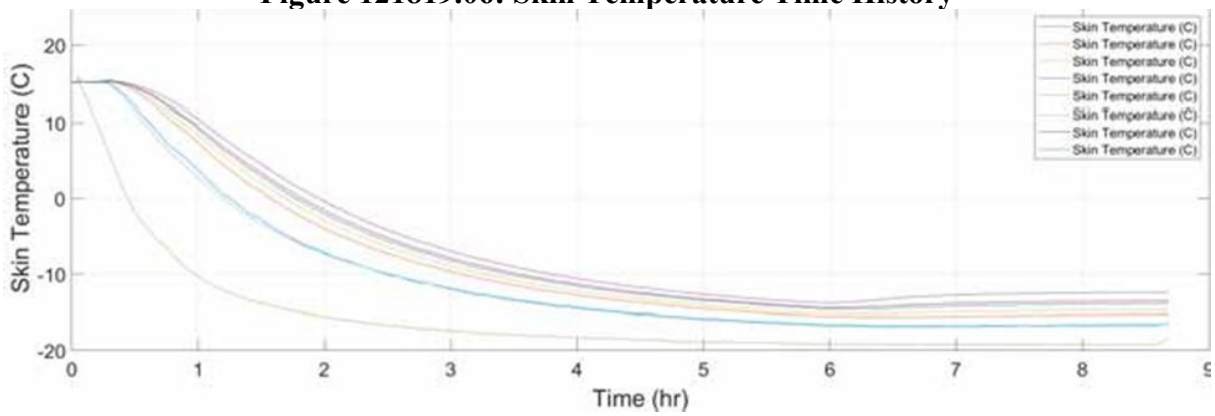

Figure 121819.07: Floor Temperature Time History

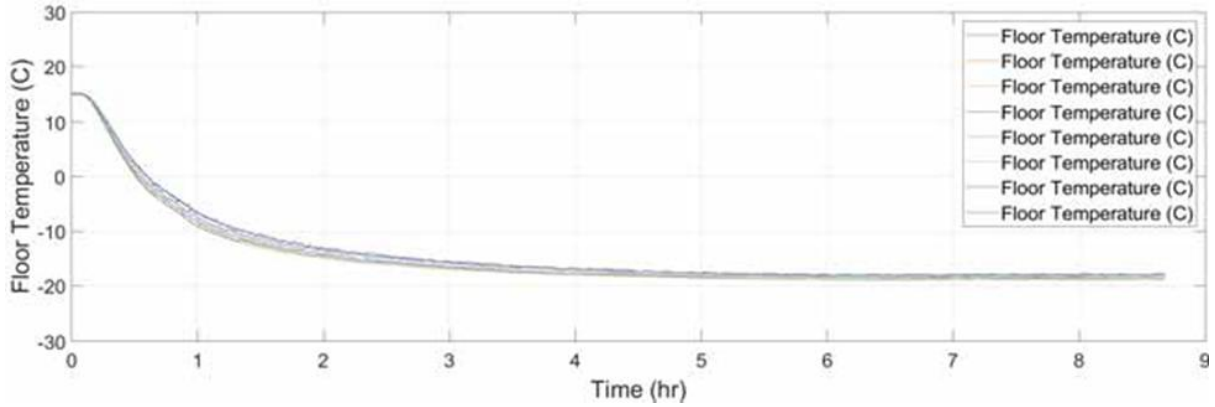

Figure 121819.08: Skin Temperature Slope Time History

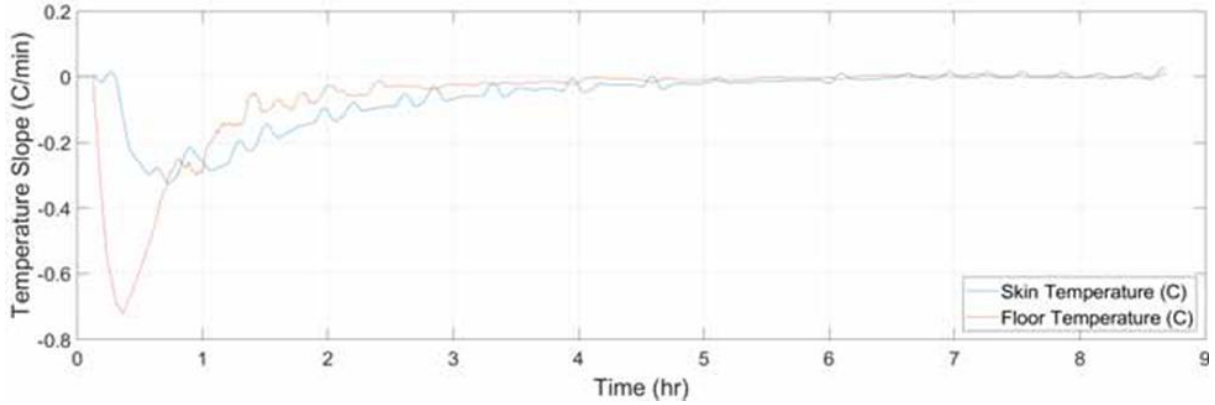

Figure 121819.09: RMS Height Evolution

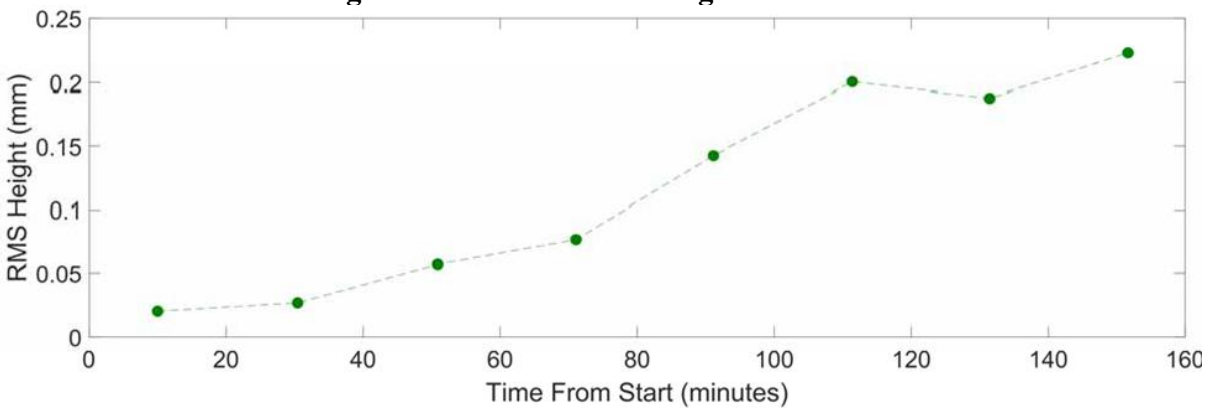

Figure 121819.10: Skewness Evolution

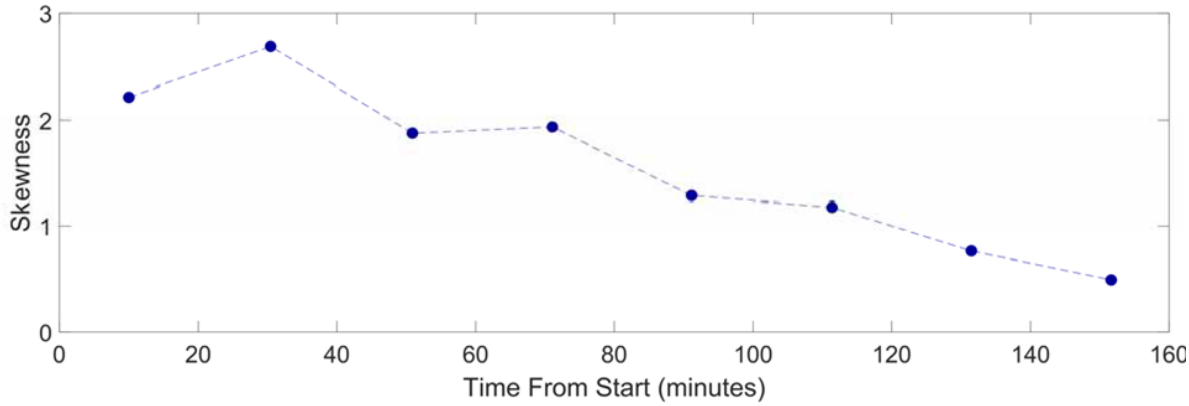

Figure 121819.11: Peak to Valley Evolution

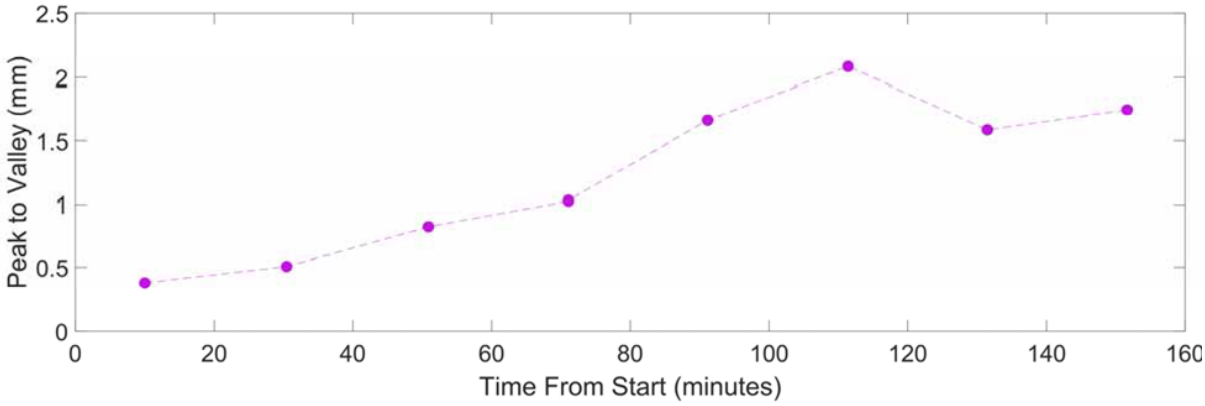

Figure 121819.12: Equivalent Roughness Evolution

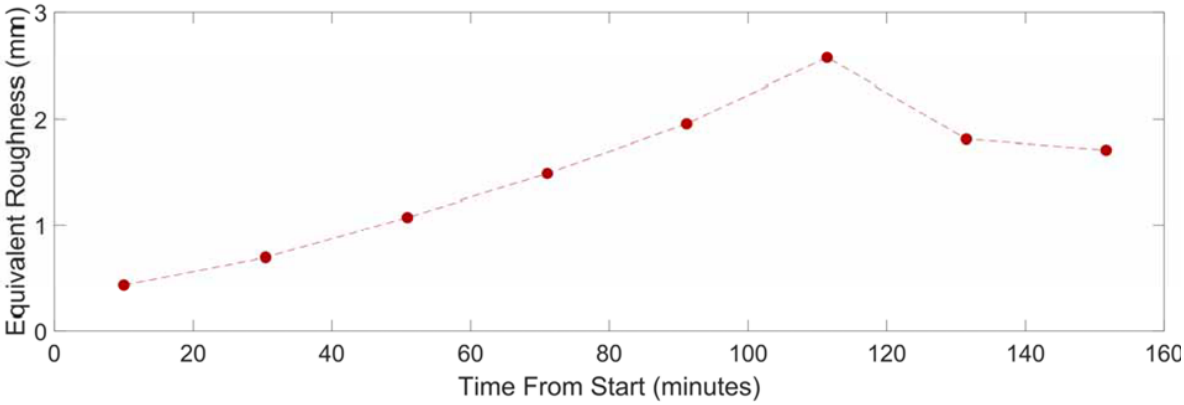

Table 121819.02: Summary of Roughness Parameters

Time (min.)	RMS (mm)	Skewness	Peak to Valley (mm)	ks,Flack-Schultz (mm)
9.9833	0.0194	2.2194	0.3750	0.4267
30.4333	0.0261	2.6967	0.5065	0.6923
50.8833	0.0569	1.8758	0.8236	1.0722
71.0667	0.0765	1.9361	1.0277	1.4829
91.1333	0.1427	1.2819	1.6649	1.9574
111.4000	0.2005	1.1785	2.0873	2.5815
131.4667	0.1881	0.7630	1.5884	1.8118
151.6500	0.2237	0.4864	1.7475	1.7054

Figure 121819.13: Frost Topography at 00:09:59

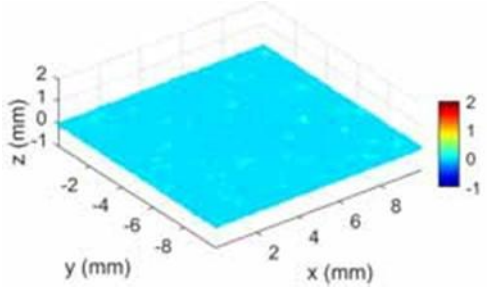

Figure 121819.14: Frost Topography at 00:30:26

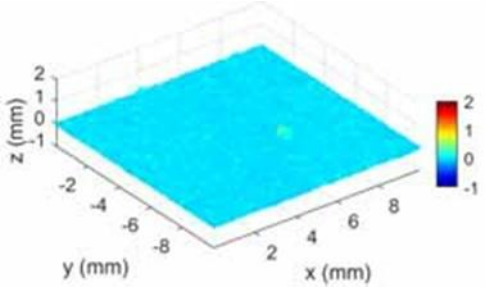

Figure 121819.15: Frost Topography at 00:50:53

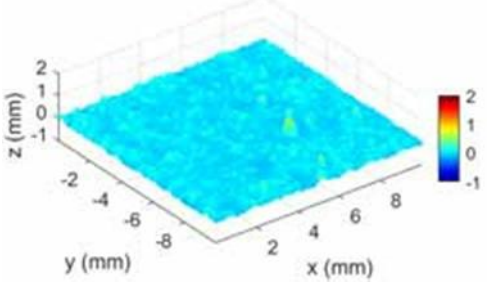

Figure 121819.16: Frost Topography at 01:11:04

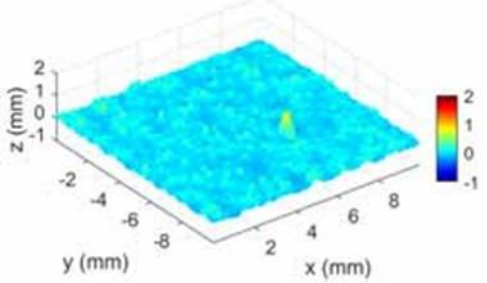

Figure 121819.17: Frost Topography at 01:31:08

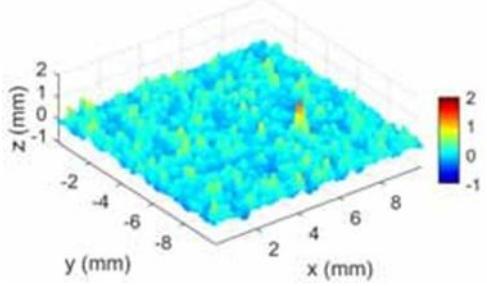

Figure 121819.18: Frost Topography at 01:51:24

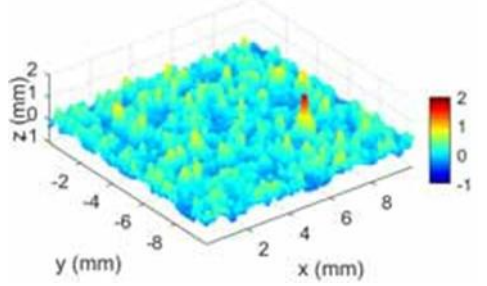

Figure 121819.19: Frost Topography at 02:11:28

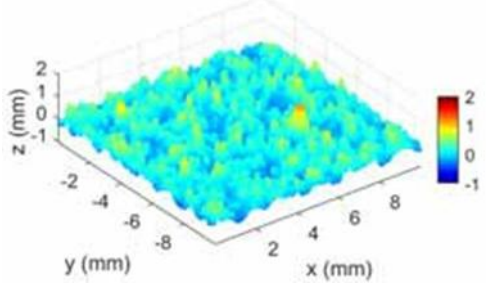

Figure 121819.20: Frost Topography at 02:31:39

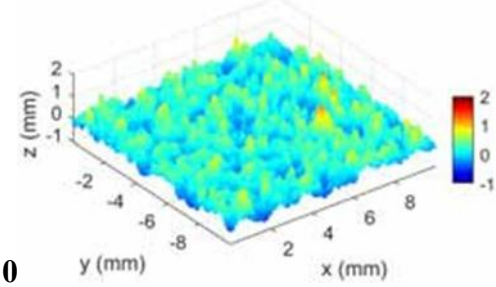

0

CAFF Conditions Report – Case Date: 122019

Table 122019.01: Summary of Measured Test Variables

Variable	Mean	St. Dev.	Rand. Unc.
T_air (C)	5.2595	0.2912	0.0093
Rh (%)	79.7557	6.3373	0.2028
Omega (kg_v/kg_da)	0.00439894	0.00039389	0.00001261
V_air (m/s)	0.2738	0.0850	0.0027
T_skin (C)	-16.5260	0.0269	0.0009
T_floor (C)	-18.6719	0.0321	0.0010

Figure 122019.01: Temperature and Voltage Control Time History

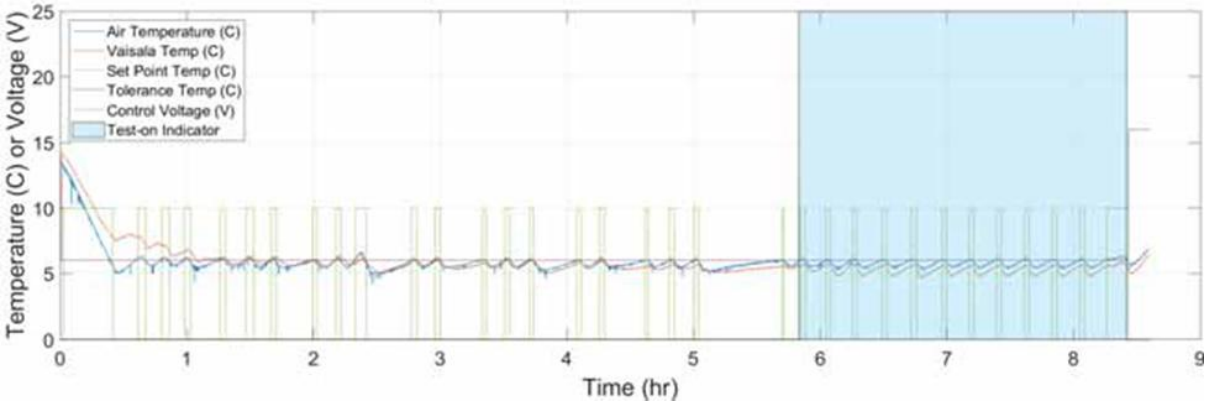

Figure 122019.02: Relative Humidity Time History

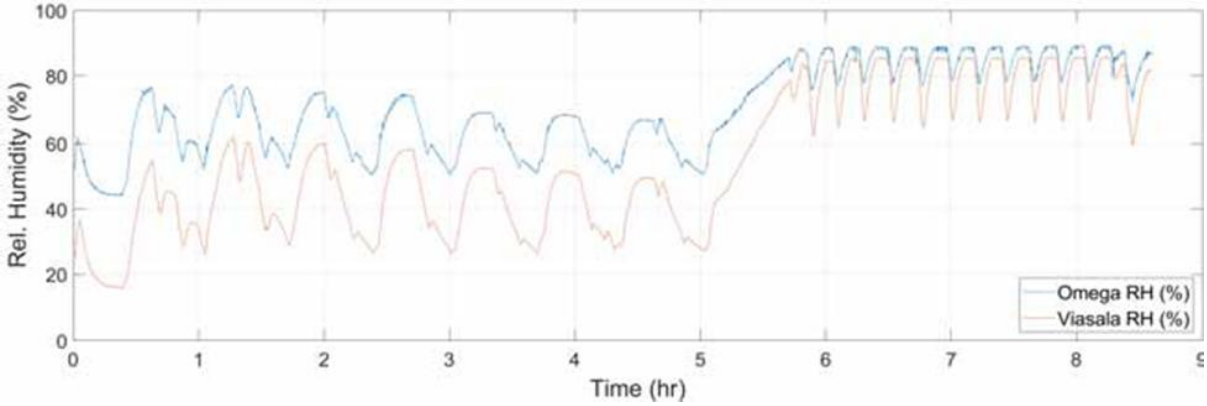

Figure 122019.03: Velocity Time History

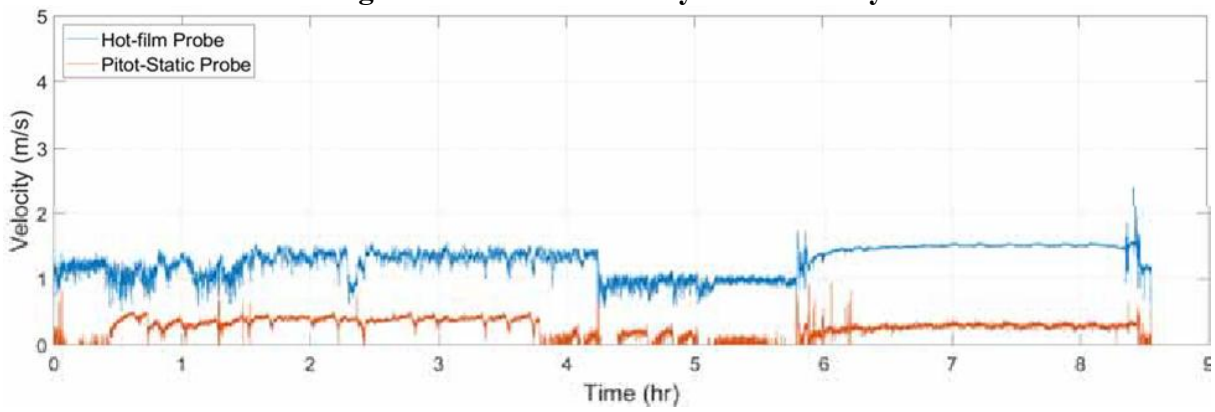

Figure 122019.04: Coolant Return Temperature Time History

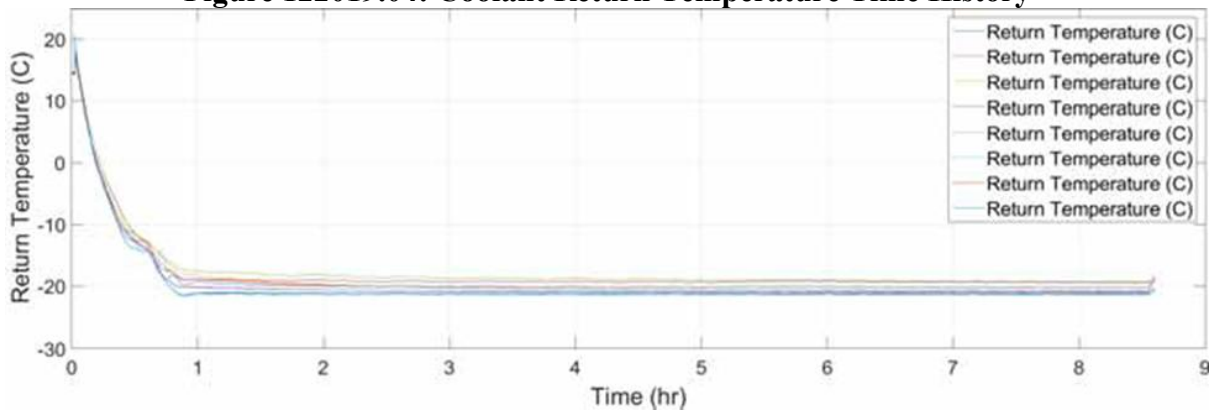

Figure 122019.05: Coolant Supply Temperature Time History

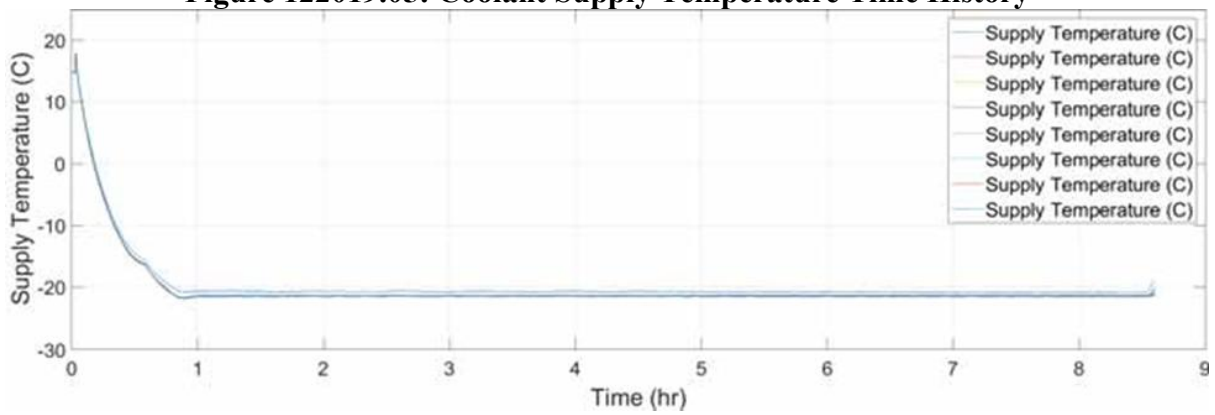

Figure 122019.06: Skin Temperature Time History

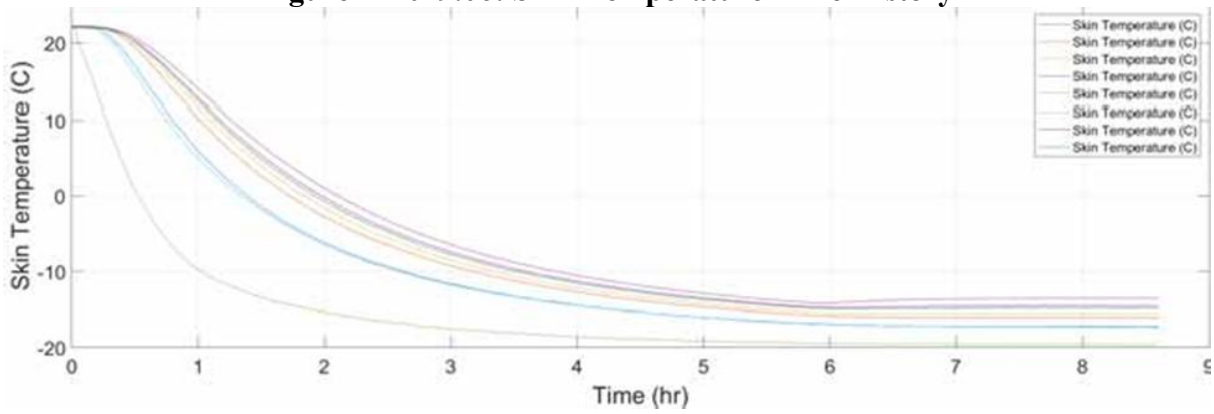

Figure 122019.07: Floor Temperature Time History

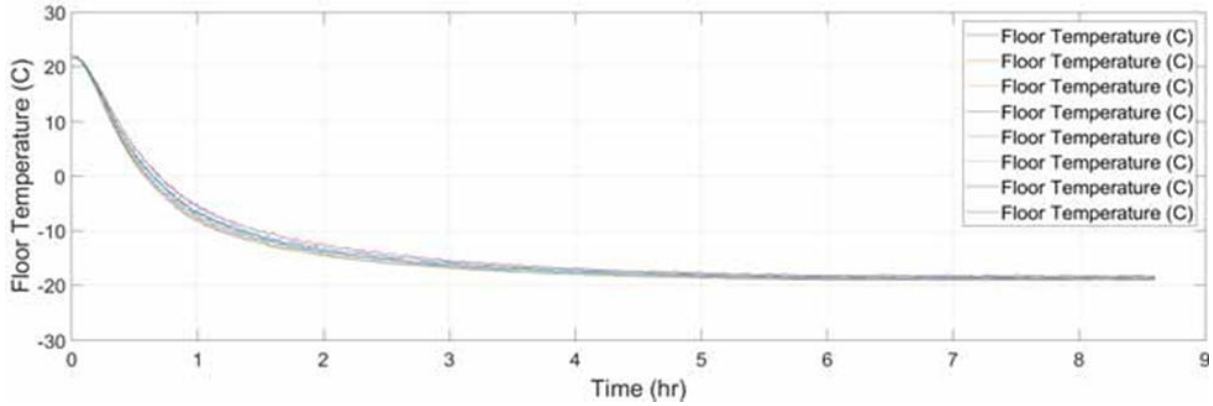

Figure 122019.08: Skin Temperature Slope Time History

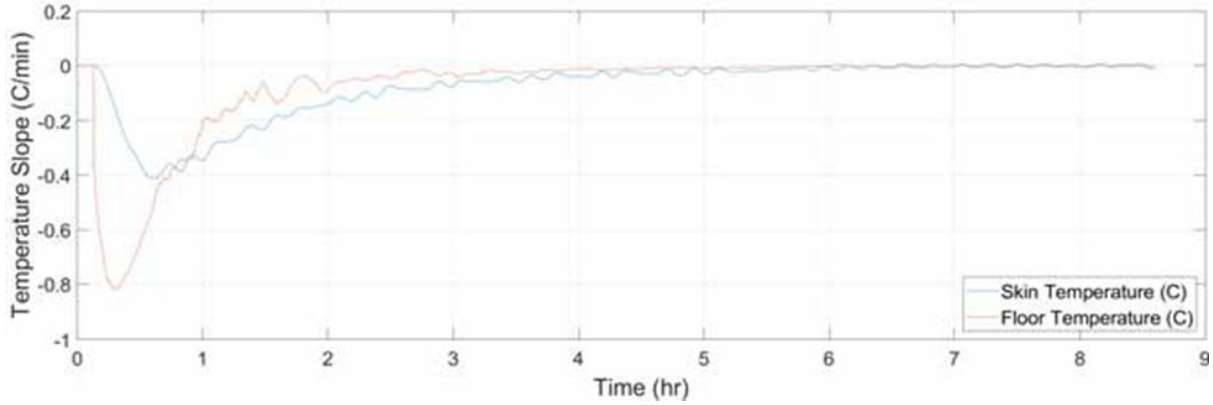

Figure 122019.09: RMS Height Evolution

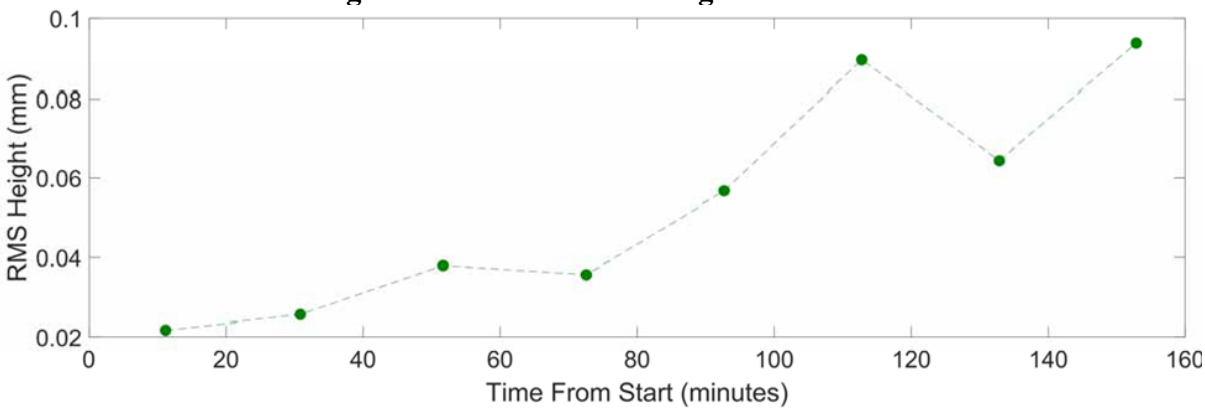

Figure 122019.10: Skewness Evolution

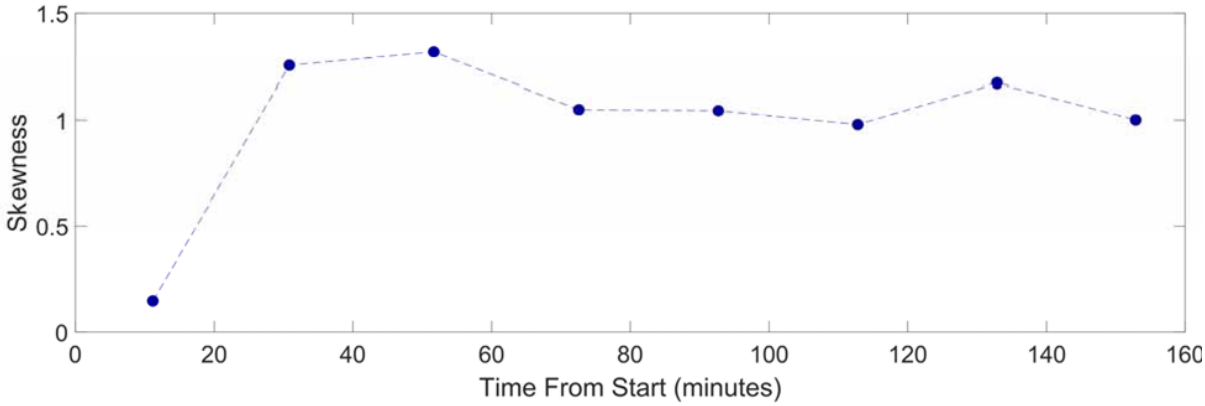

Figure 122019.11: Peak to Valley Evolution

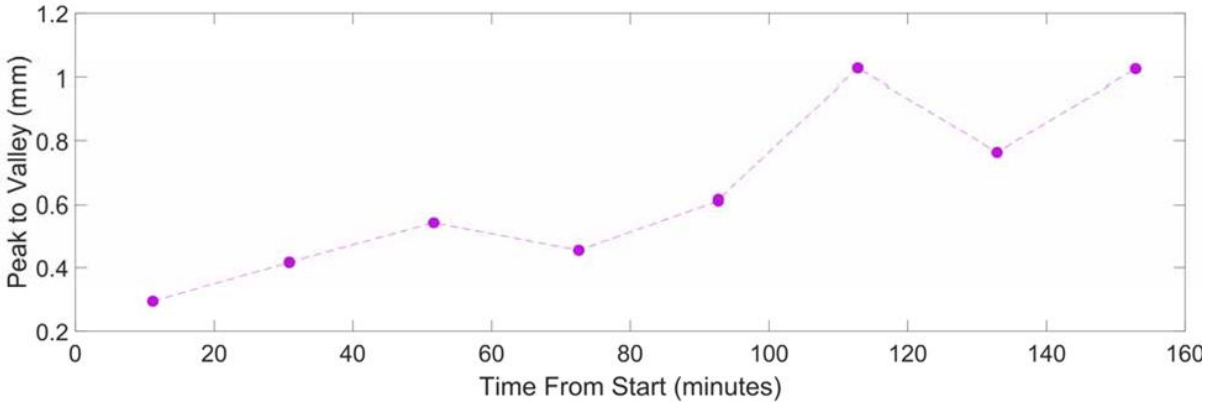

Figure 122019.12: Equivalent Roughness Evolution

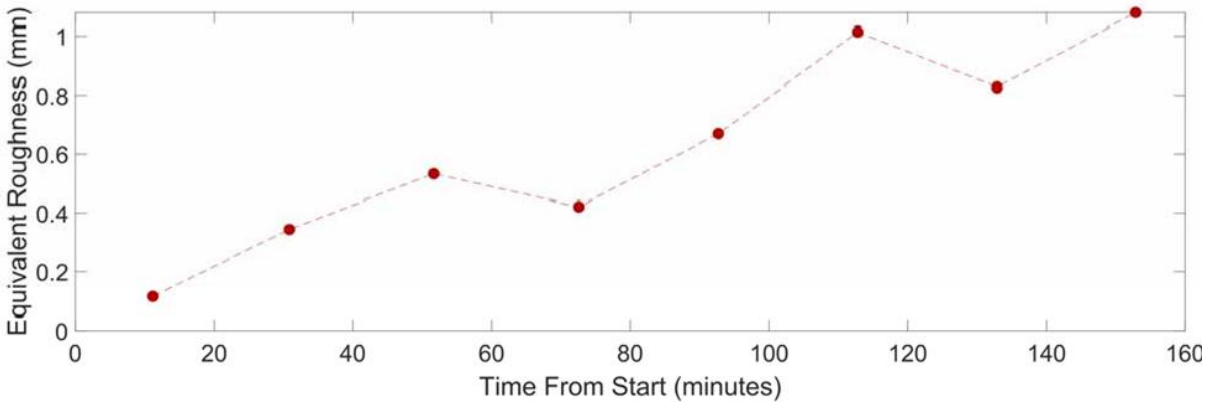

Table 122019.02: Summary of Roughness Parameters

Time (min.)	RMS (mm)	Skewness	Peak to Valley (mm)	ks,Flack-Schultz (mm)
11.1500	0.0217	0.1417	0.2915	0.1153
30.8167	0.0254	1.2586	0.4160	0.3440
51.6667	0.0379	1.3225	0.5426	0.5327
72.5667	0.0355	1.0504	0.4535	0.4212
92.6833	0.0566	1.0460	0.6129	0.6689
112.7833	0.0898	0.9800	1.0294	1.0140
132.8667	0.0644	1.1753	0.7640	0.8268
152.8667	0.0941	1.0016	1.0270	1.0781

Figure 122019.13: Frost Topography at 00:11:09

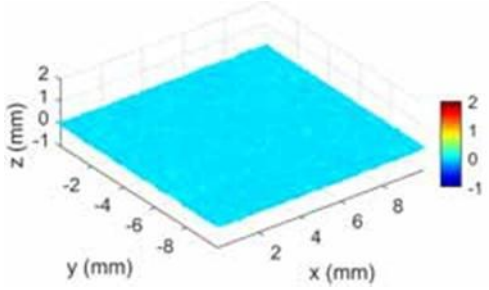

Figure 122019.14: Frost Topography at 00:30:49

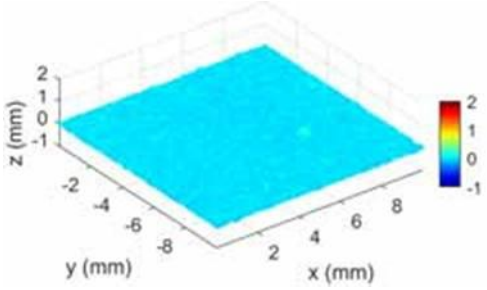

Figure 122019.15: Frost Topography at 00:51:40

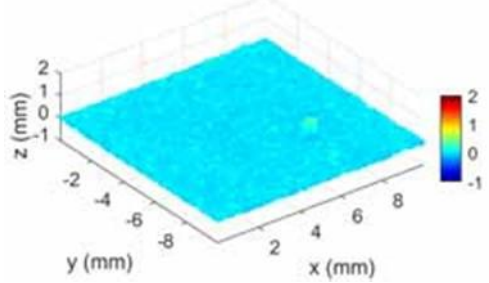

Figure 122019.16: Frost Topography at 01:12:34

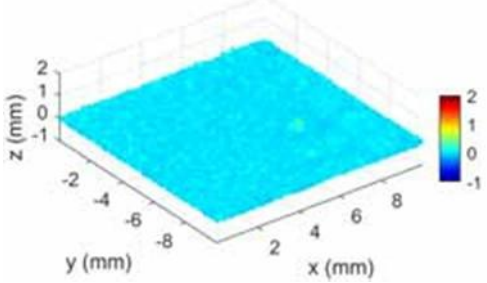

Figure 122019.17: Frost Topography at 01:32:41

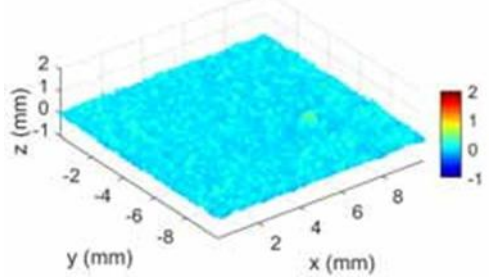

Figure 122019.18: Frost Topography at 01:52:47

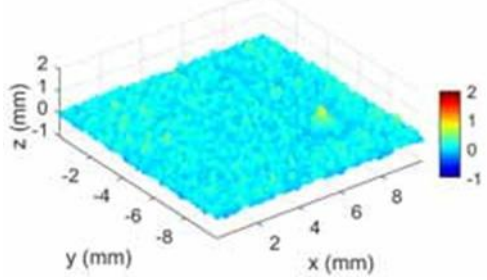

Figure 122019.19: Frost Topography at 02:12:52

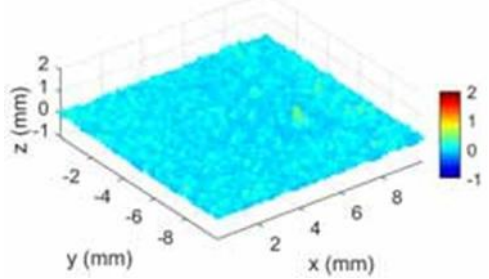

Figure 122019.20: Frost Topography at 02:32:52

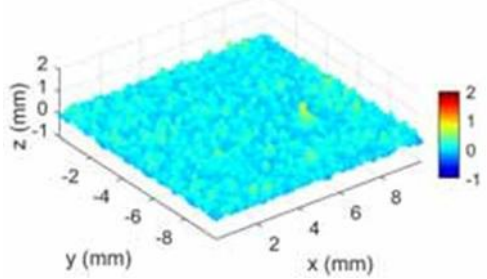

CAFF Conditions Report – Case Date: 122319

Table 122319.01: Summary of Measured Test Variables

Variable	Mean	St. Dev.	Rand. Unc.
T_air (C)	14.0087	0.3411	0.0118
Rh (%)	81.6332	3.1346	0.1084
Omega (kg_v/kg_da)	0.00820870	0.00040265	0.00001392
V_air (m/s)	0.2291	0.1086	0.0038
T_skin (C)	-15.2292	0.2695	0.0093
T_floor (C)	-17.8546	0.0886	0.0031

Figure 122319.01: Temperature and Voltage Control Time History

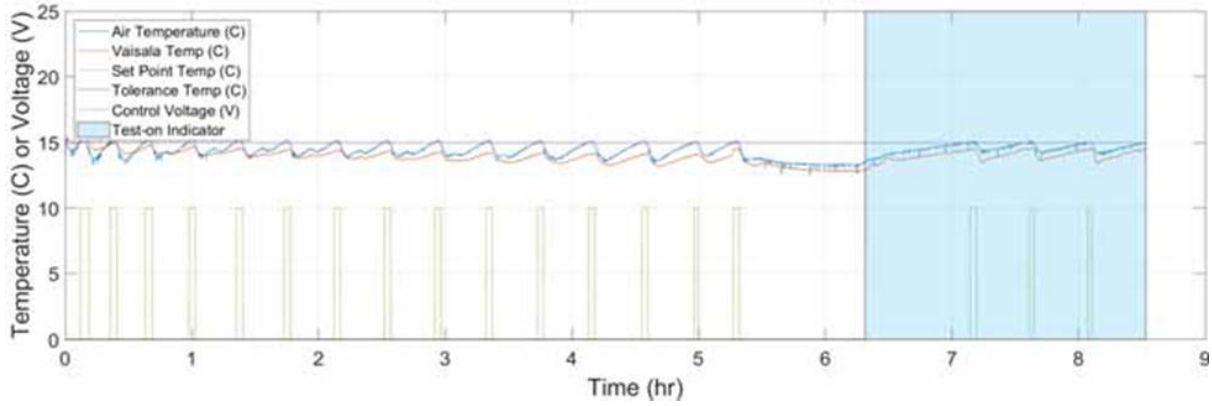

Figure 122319.02: Relative Humidity Time History

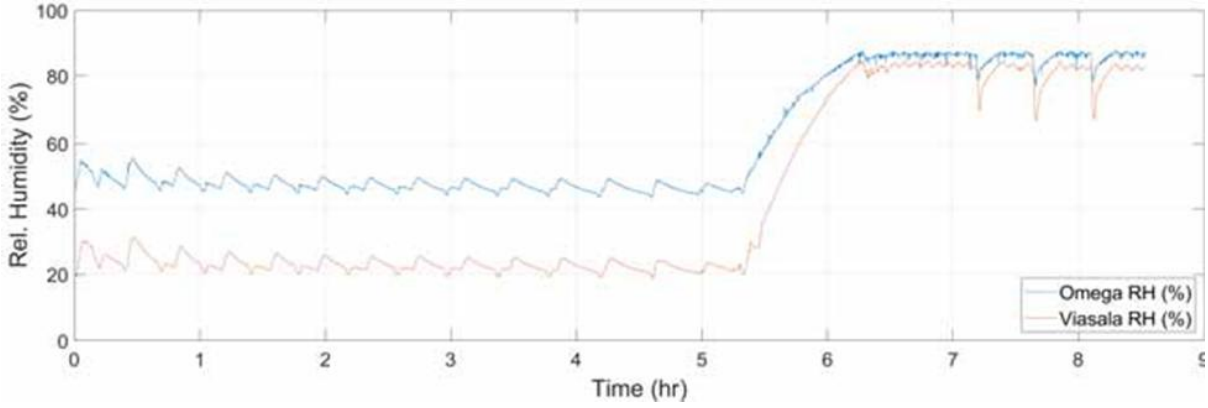

Figure 122319.03: Velocity Time History

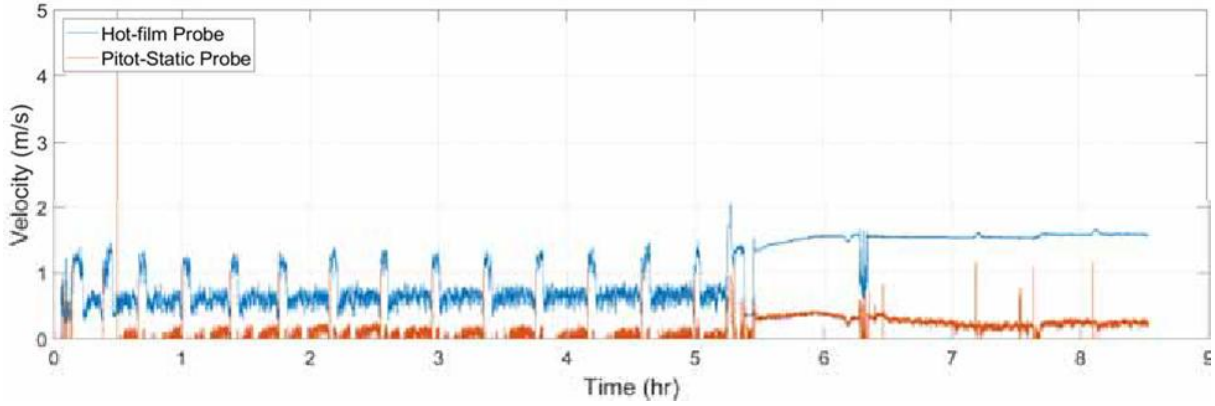

Figure 122319.04: Coolant Return Temperature Time History

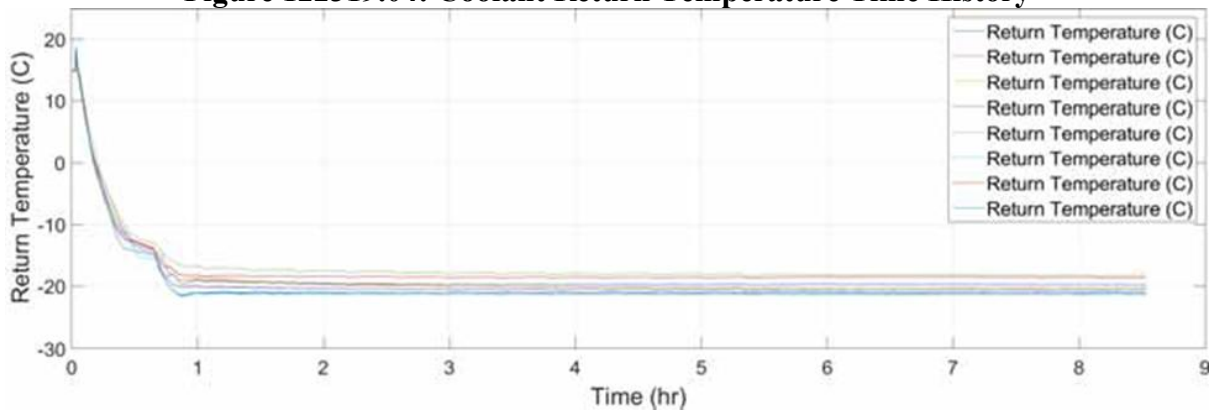

Figure 122319.05: Coolant Supply Temperature Time History

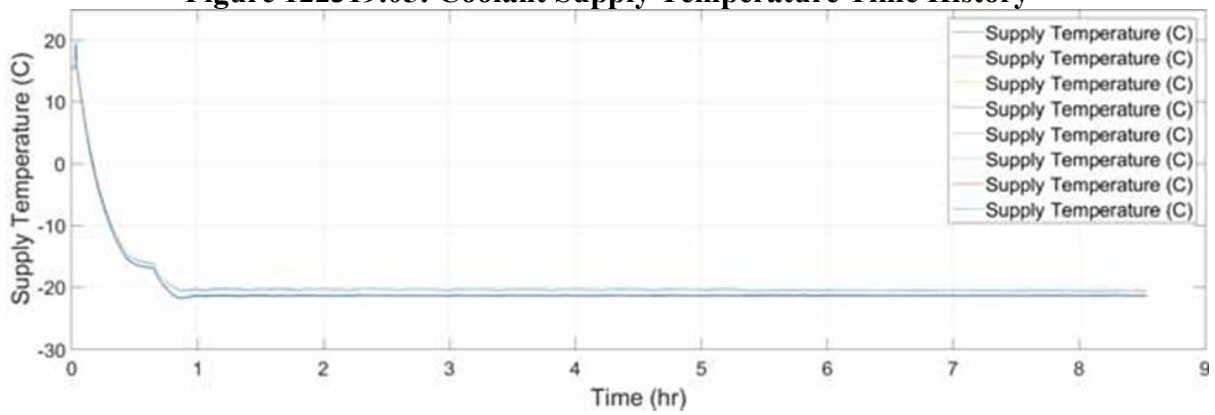

Figure 122319.06: Skin Temperature Time History

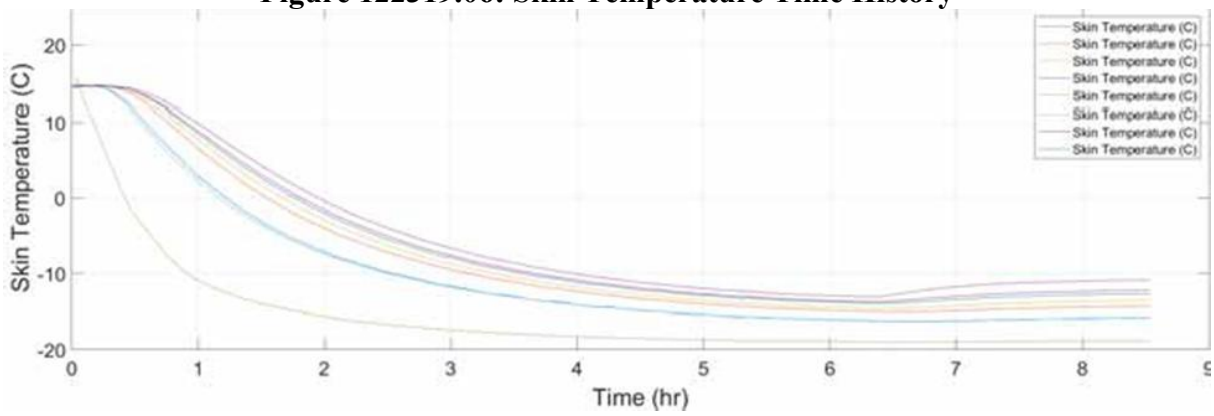

Figure 122319.07: Floor Temperature Time History

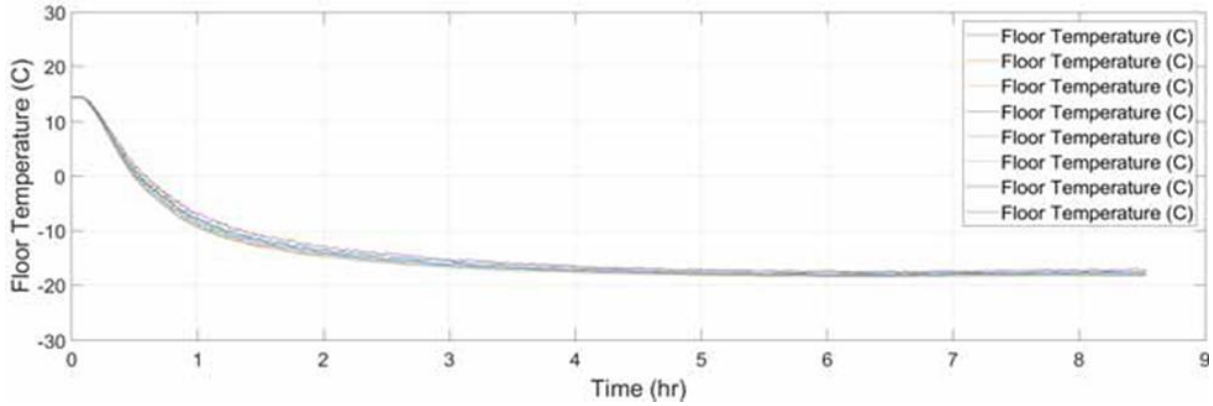

Figure 122319.08: Skin Temperature Slope Time History

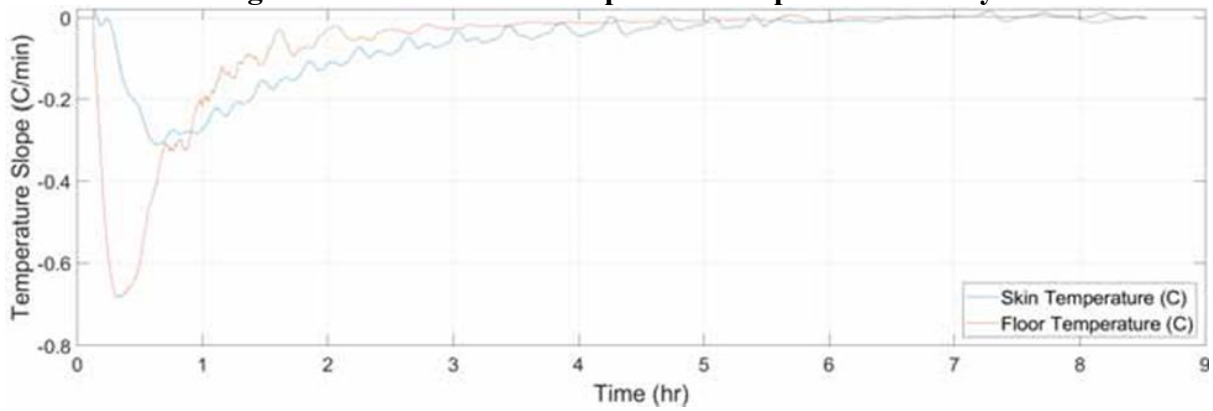

Figure 1223119.09: RMS Height Evolution

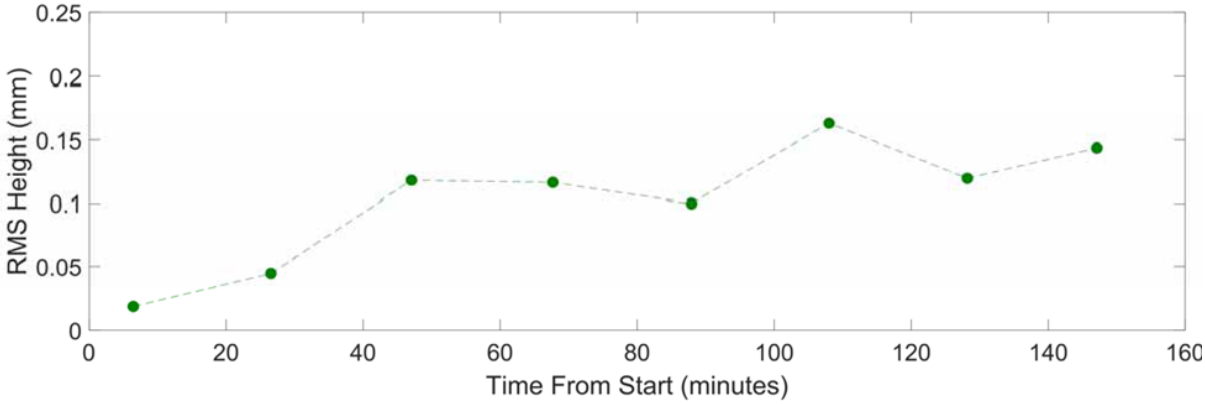

Figure 122319.10: Skewness Evolution

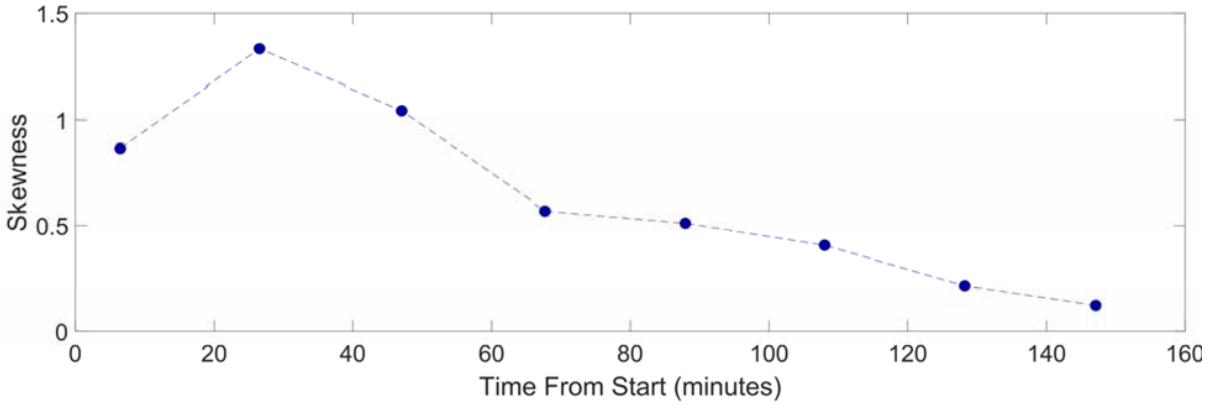

Figure 122319.11: Peak to Valley Evolution

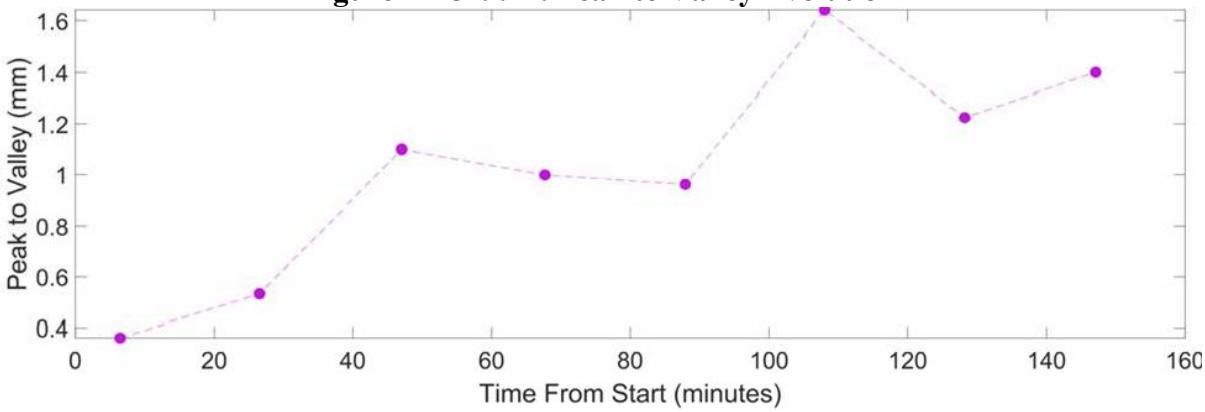

Figure 122319.12: Equivalent Roughness Evolution

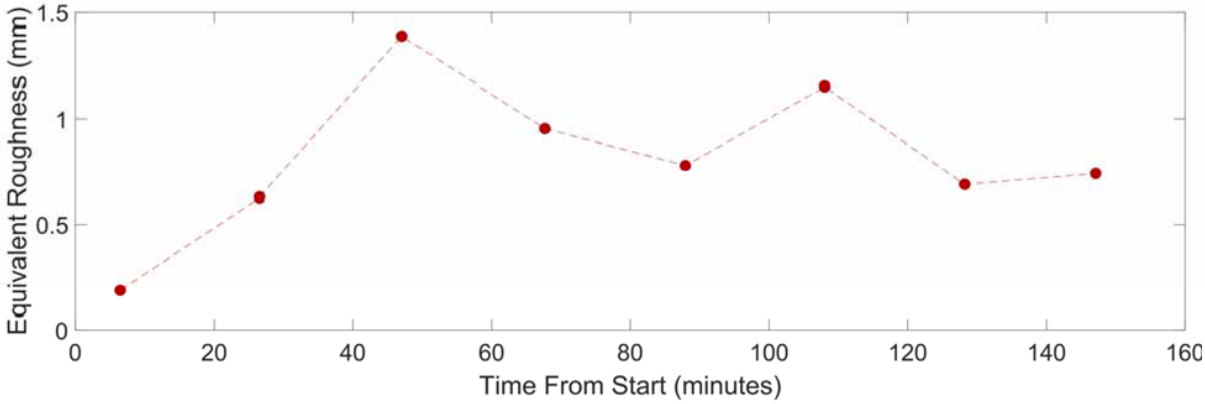

Table 122319.02: Summary of Roughness Parameters

Time (min.)	RMS (mm)	Skewness	Peak to Valley (mm)	ks,Flack-Schultz (mm)
6.4333	0.0178	0.8644	0.3604	0.1850
26.5333	0.0443	1.3372	0.5323	0.6277
47.0333	0.1179	1.0442	1.0995	1.3909
67.6833	0.1162	0.5694	0.9981	0.9542
87.9333	0.0997	0.5107	0.9608	0.7769
108.0167	0.1634	0.4058	1.6425	1.1540
128.2000	0.1194	0.2108	1.2248	0.6872
147.1000	0.1436	0.1166	1.4009	0.7399

Figure 122319.13: Frost Topography at 00:06:26

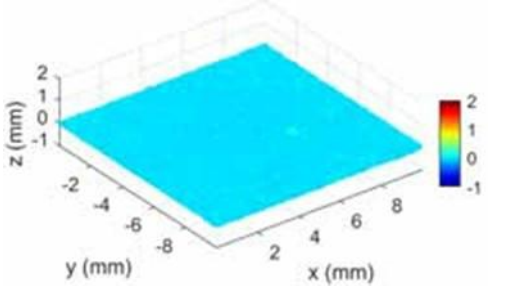

Figure 122319.14: Frost Topography at 00:26:32

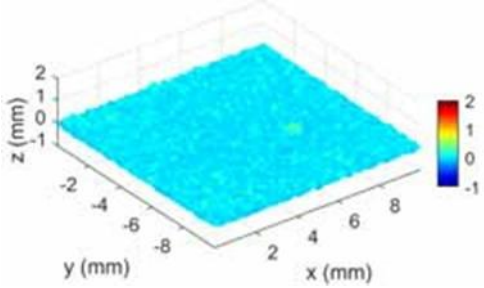

Figure 122319.15: Frost Topography at 00:47:02

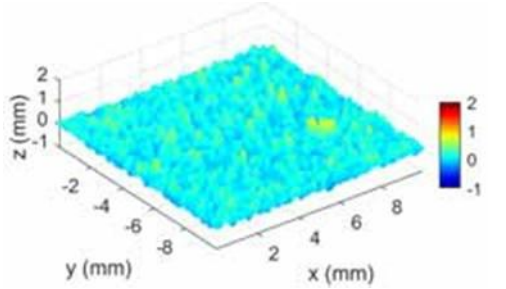

Figure 122319.16: Frost Topography at 01:07:41

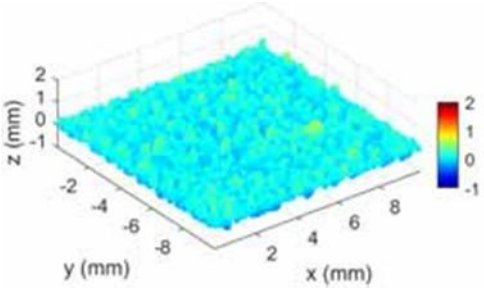

Figure 122319.17: Frost Topography at 01:27:56

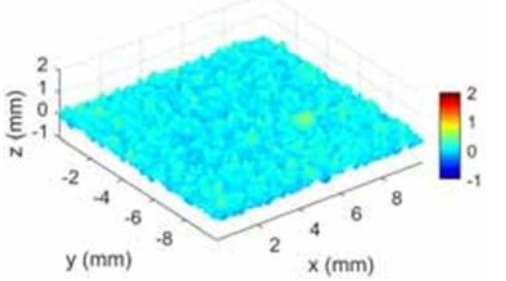

Figure 122319.18: Frost Topography at 01:48:01

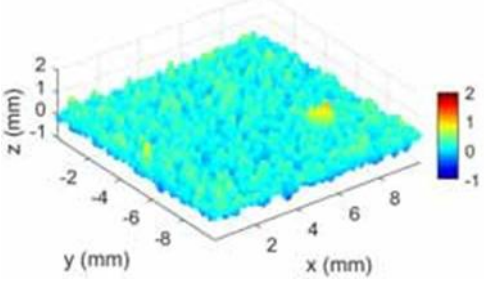

Figure 122319.19: Frost Topography at 02:08:12

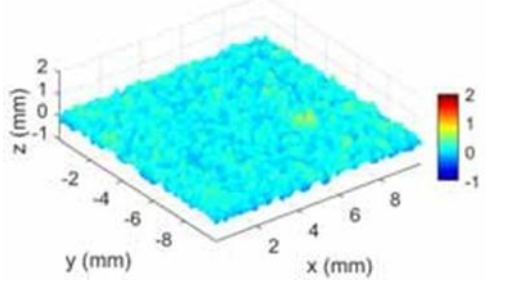

Figure 122319.19: Frost Topography at 02:27:06

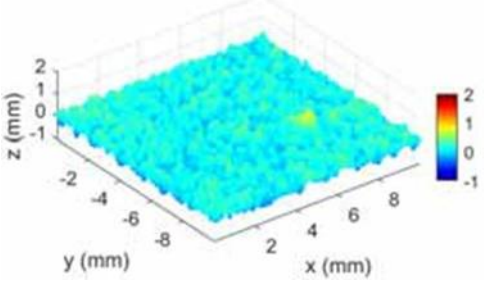

C Appendix C: CAFF test reports using an aluminum skin with structural rib

Table C- 1. Summary of Nominal Test Conditions for Wing Tank Thermal Model with an Aluminum Skin and a Structural Rib

Date	T_{PC} (°C)	$T_{air,set}$ (°C)	RH (%)	V (m/s)	x_{img} (in.)	Notes
2/26/20	-27	16	82	1.3	20.75	20 min. int.
3/04/20	-27	16	82	0.4	20.75	20 min. int.
3/06/20	-27	16	82	0.4	20.75	20 min. int.,repeat
3/09/20	-27	10	82	0.4	20.75	20 min. int.
3/11/20	-27	10	82	0.4	20.75	20 min. int.,repeat
3/18/20	-27	10	82	1.3	20.75	20 min. int.
3/20/20	-27	5	82	1.3	20.75	20 min. int.
3/23/20	-27	5	82	0.4	20.75	20 min. int.
7/29/20	-27	16	82	0.4	11.75	10 min. int.
7/31/20	-27	16	82	1.3	11.75	10 min. int.
8/3/20	-27	16	82	1.3	11.75	10 min. int., repeat
8/5/20	-27	10	82	1.3	11.75	10 min. int.
8/8/20	-27	5	82	1.3	11.75	10 min. int.
8/11/20	-27	10	82	0.4	11.75	10 min. int.
8/14/20	-27	5	82	0.4	11.75	10 min. int.
8/28/20	-27	16	82	1.4	14.75	10 min. int.
9/17/20	-27	16	82	1.4	14.75	10 min. int., repeat
9/24/20	-27	10	82	1.4	14.75	10 min. int.
9/29/20	-27	5	82	1.4	14.75	10 min. int.
10/1/20	-27	10	82	0.4	14.75	10 min. int.
10/6/20	-27	5	82	0.4	14.75	10 min. int.
10/8/20	-27	16	82	0.4	14.75	10 min. int.
9/8/20	-27	16	82	1.4	10.25	10 min. int.
9/10/20	-27	10	82	1.4	10.25	10 min. int.
9/15/20	-27	5	82	1.4	10.25	10 min. int., repeat

CAFF Conditions Report – Case Date: 022620

Table 022620.01: Summary of Measured Test Variables

Variable	Mean	St. Dev.	Rand. Unc.
T_air (C)	15.0011	0.4010	0.0134
Rh (%)	79.8133	3.0415	0.1019
Omega (kg_v/kg_da)	0.00846630	0.00048064	0.00001611
V_air (m/s)	1.0447	0.0706	0.0024
T_skin (C)	-5.9572	1.1511	0.0386
T_floor (C)	-19.1169	0.1876	0.0063

Figure 022620.01: Temperature and Voltage Control Time History

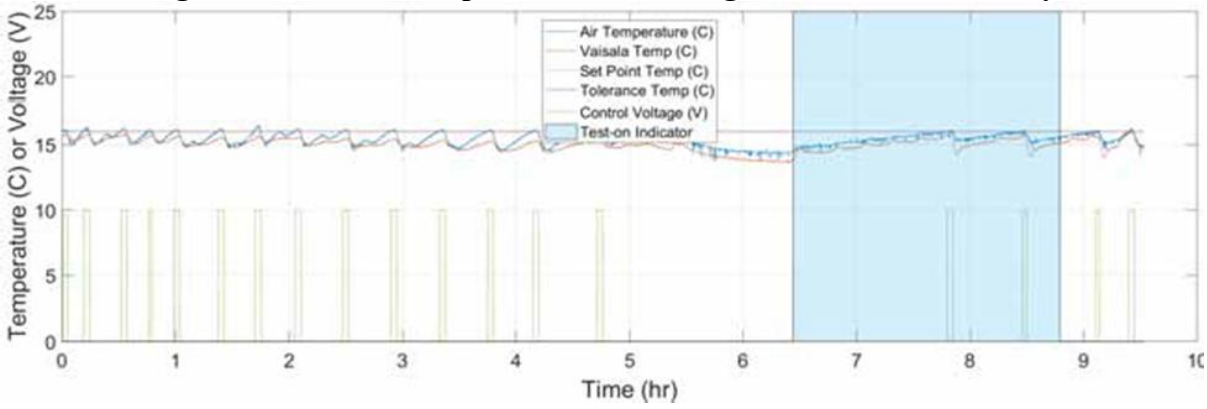

Figure 022620.02: Relative Humidity Time History

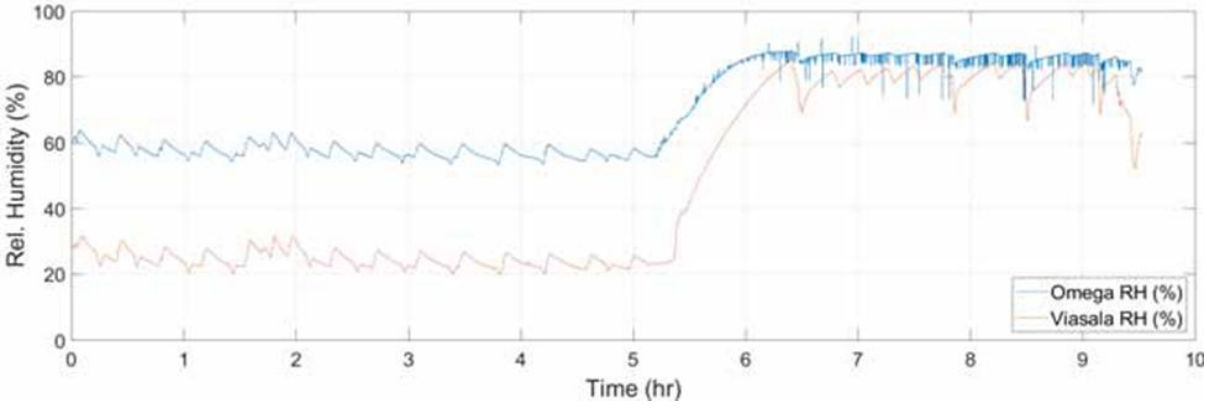

Figure 022620.03: Velocity Time History

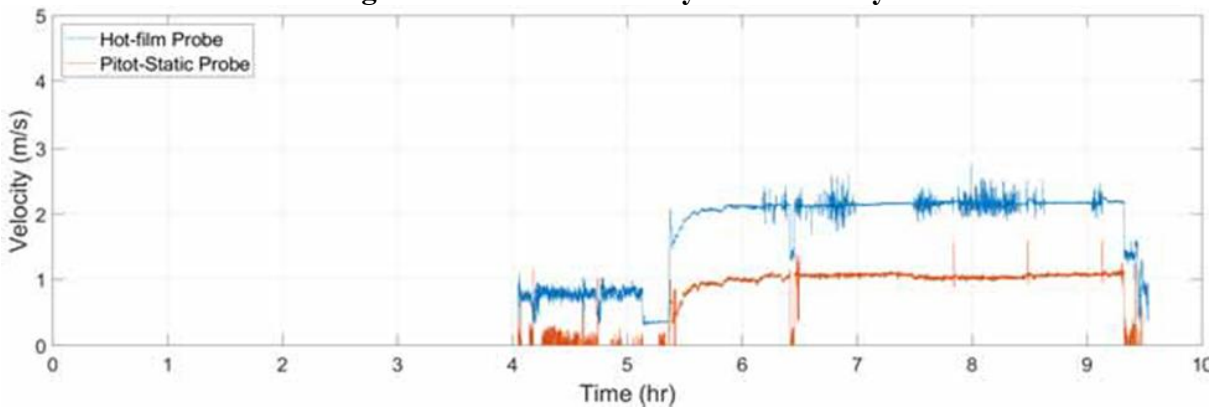

Figure 022620.04: Coolant Return Temperature Time History

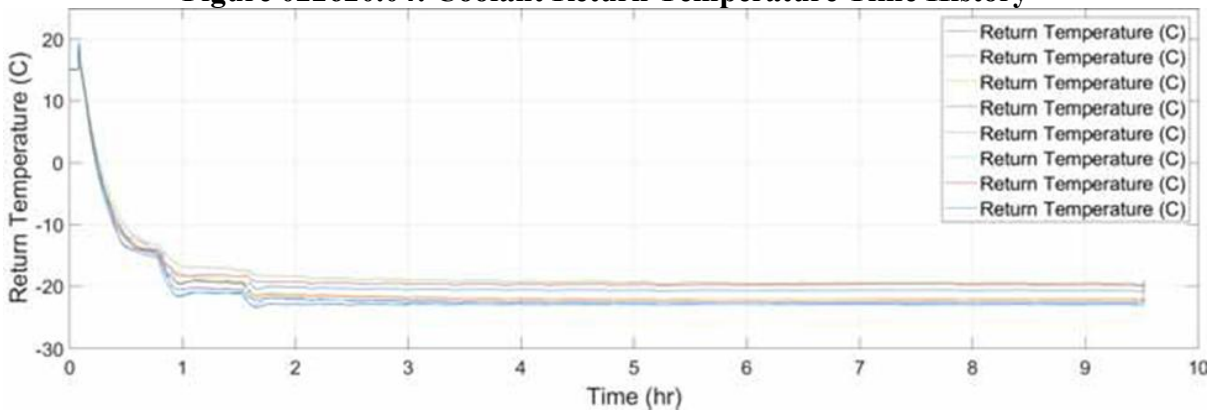

Figure 022620.05: Coolant Supply Temperature Time History

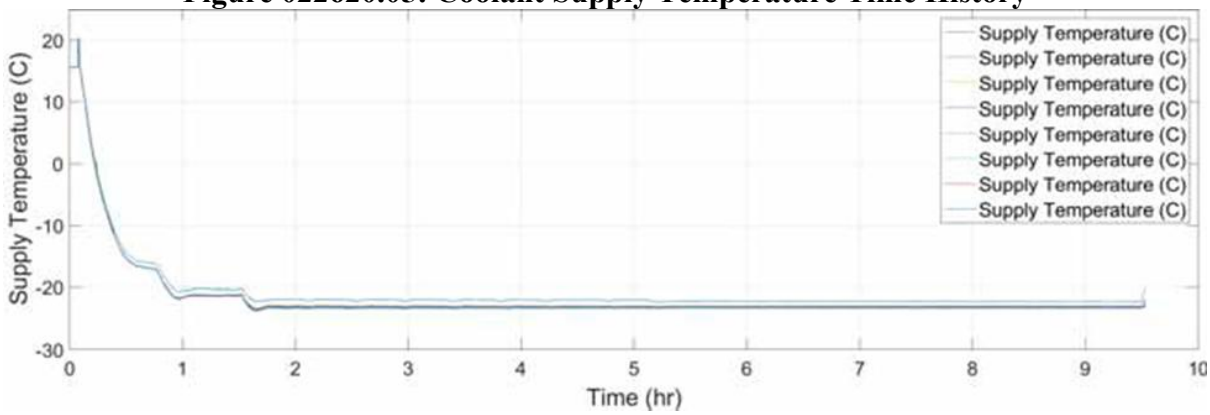

Figure 022620.06: Skin Temperature Time History

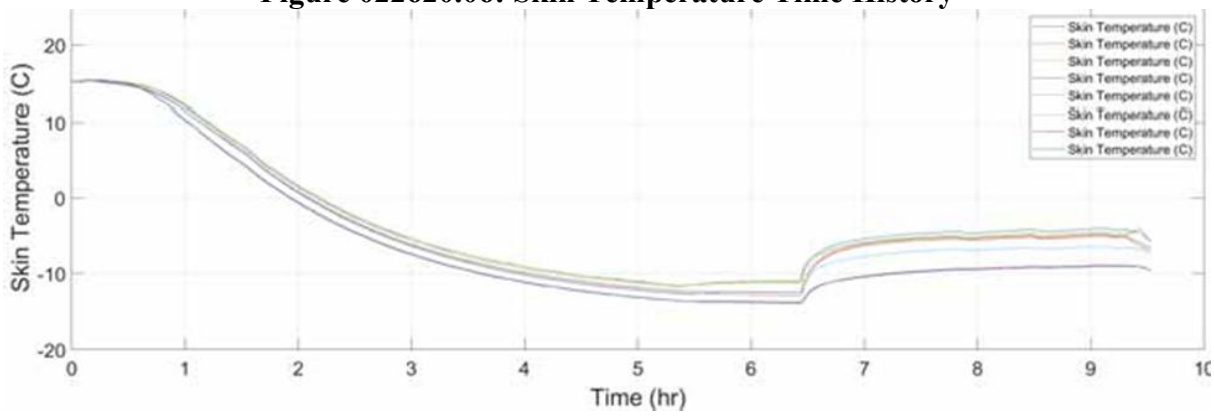

Figure 022620.07: Floor Temperature Time History

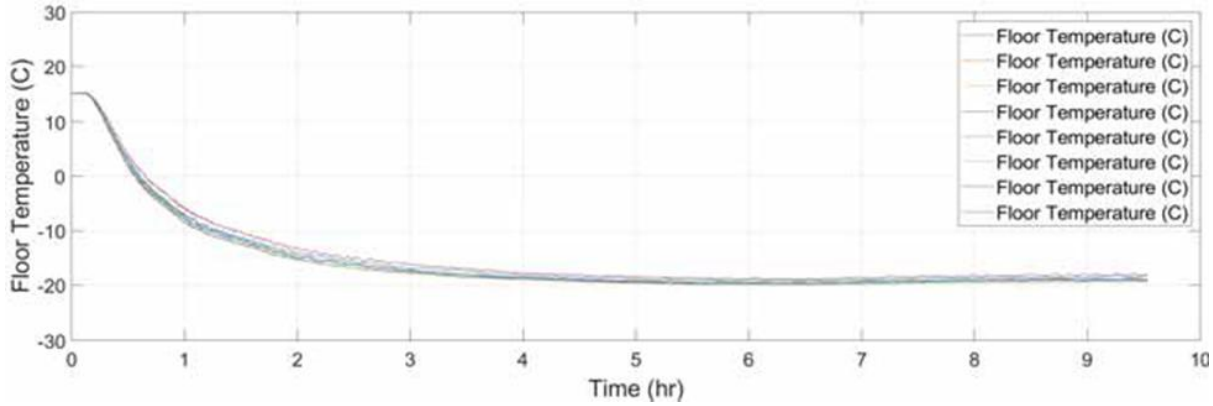

Figure 022620.08: Skin Temperature Slope Time History

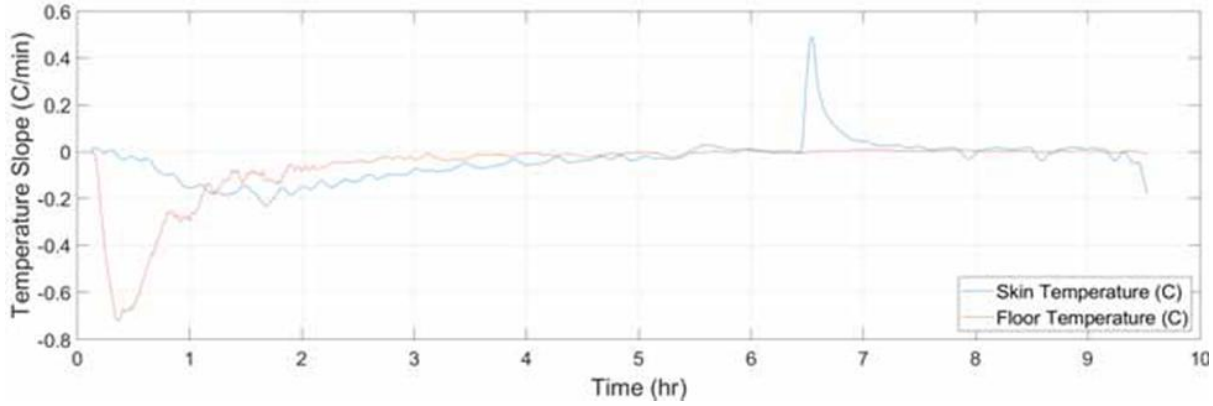

Figure 022620.09: RMS Height Evolution

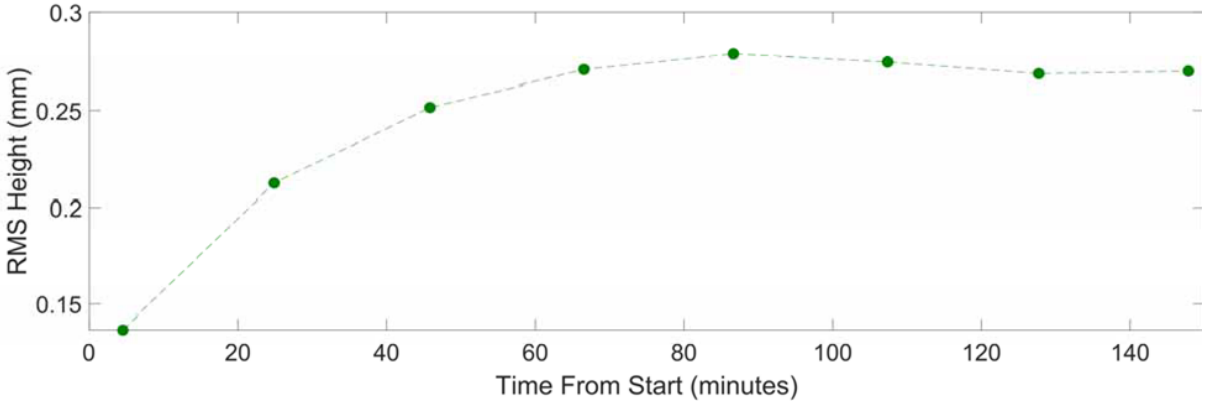

Figure 022620.10: Skewness Evolution

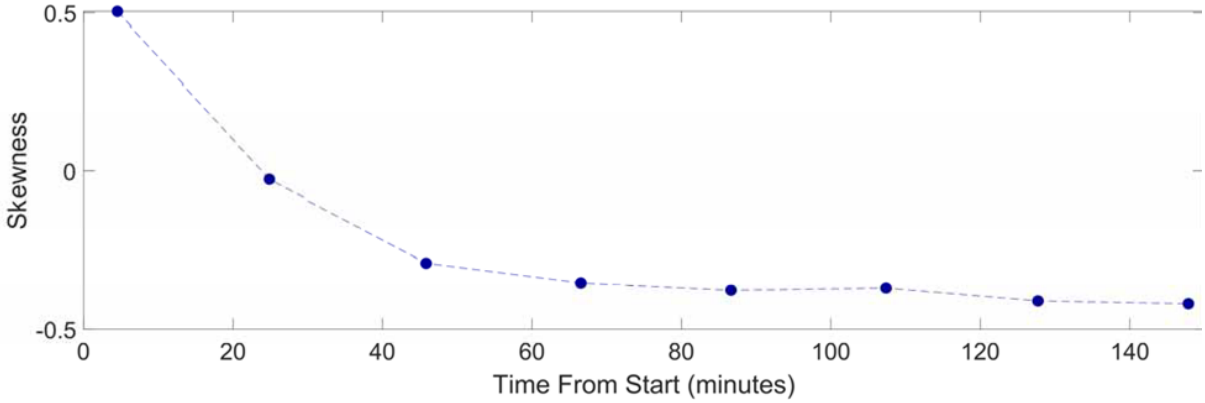

Figure 022620.11: Peak to Valley Evolution

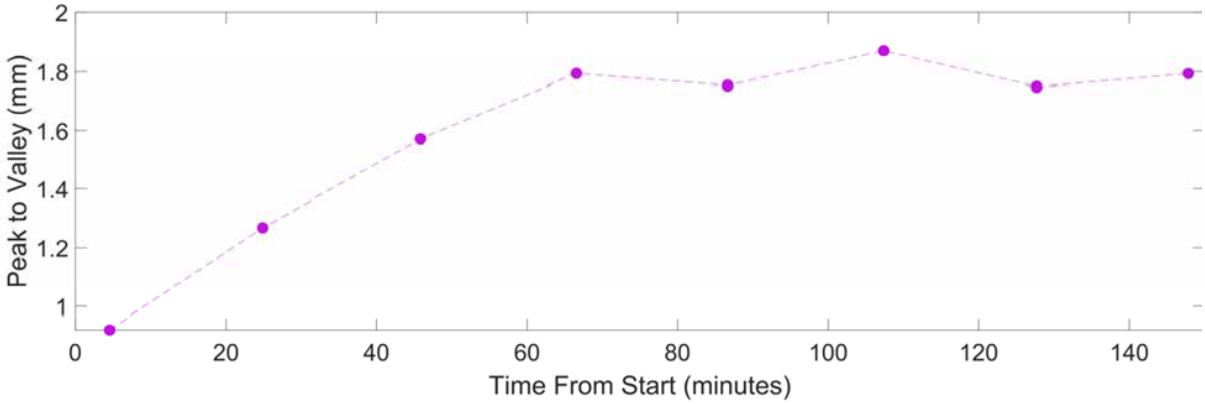

Figure 022620.12: Equivalent Roughness Evolution

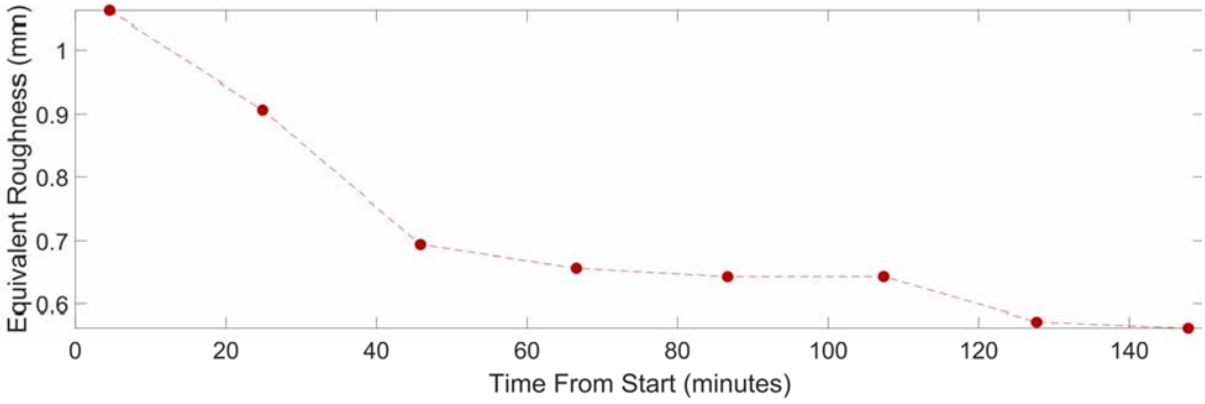

Table 022620.02: Summary of Roughness Parameters

Time (min.)	RMS (mm)	Skewness	Peak to Valley (mm)	ks,Flack-Schultz (mm)
4.5333	0.1369	0.5045	0.9206	1.0616
24.8667	0.2124	-0.0268	1.2687	0.9065
45.8333	0.2516	-0.2923	1.5718	0.6941
66.5500	0.2709	-0.3560	1.7939	0.6568
86.6500	0.2791	-0.3793	1.7535	0.6432
107.3833	0.2748	-0.3721	1.8721	0.6435
127.7167	0.2688	-0.4138	1.7490	0.5728
147.8500	0.2700	-0.4230	1.7935	0.5632

Figure 022620.13: Frost Topography at 00:04:32

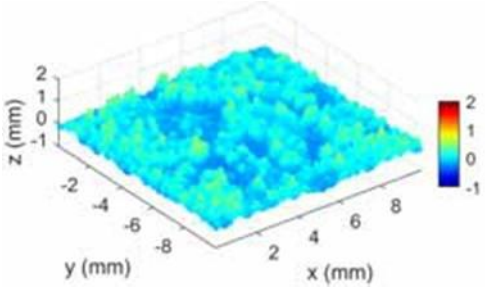

Figure 022620.14: Frost Topography at 00:24:52

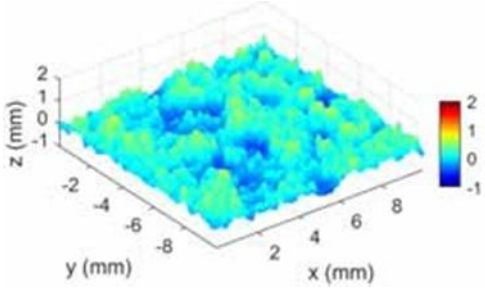

Figure 022620.15: Frost Topography at 00:45:50

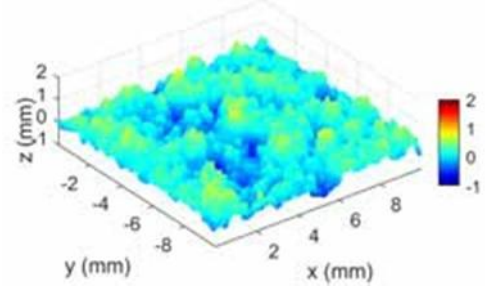

Figure 022620.16: Frost Topography at 01:06:33

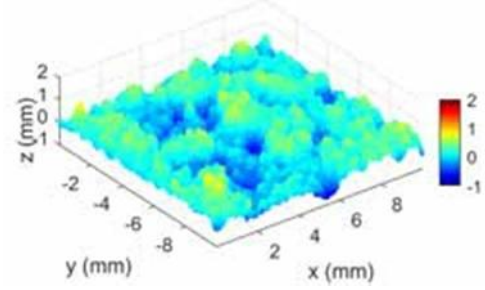

Figure 022620.17: Frost Topography at 01:26:39

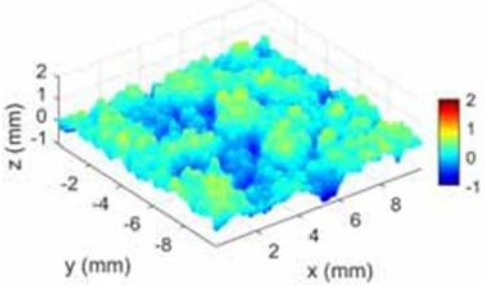

Figure 022620.18: Frost Topography at 01:47:23

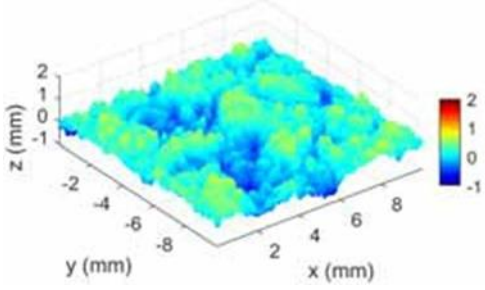

Figure 022620.19: Frost Topography at 02:07:43

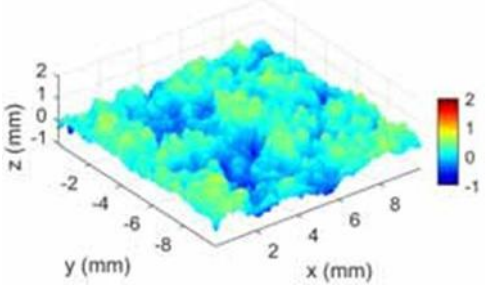

Figure 022620.20: Frost Topography at 02:27:51

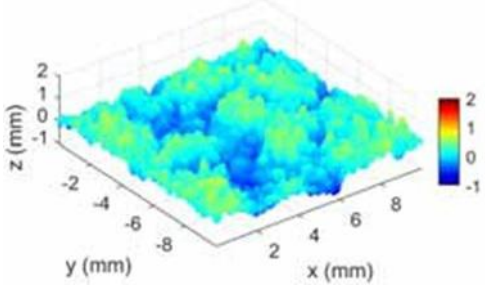

CAFF Conditions Report - Case Date: 030420

Variable	Mean	St. Dev.	Rand. Unc.
T_air (C)	14.8055	0.4411	0.0146
Rh (%)	81.3248	4.1602	0.1382
Omega (kg_v/kg_da)	0.00866932	0.00043181	0.00001434
V_air (m/s)	0.2231	0.1820	0.0060
T_skin (C)	-7.7686	1.0545	0.0350
T_floor (C)	-19.3264	0.1700	0.0056

Figure 030420.01: Temperature and Voltage Control Time History

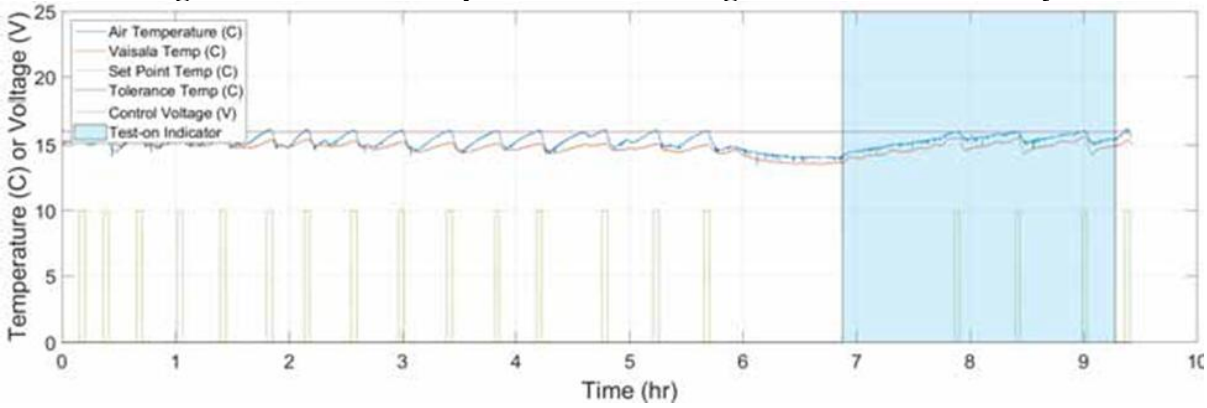

Figure 030420.02: Relative Humidity Time History

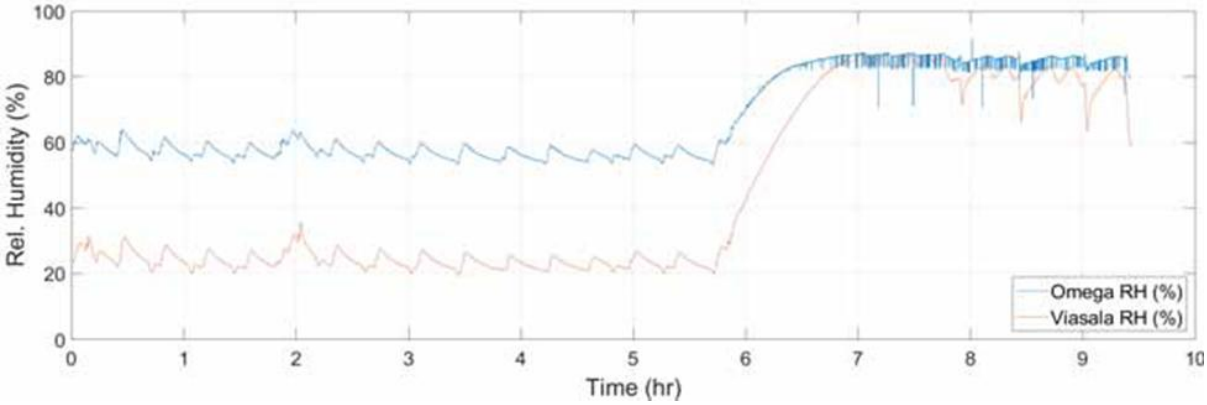

Figure 030420.03: Velocity Time History

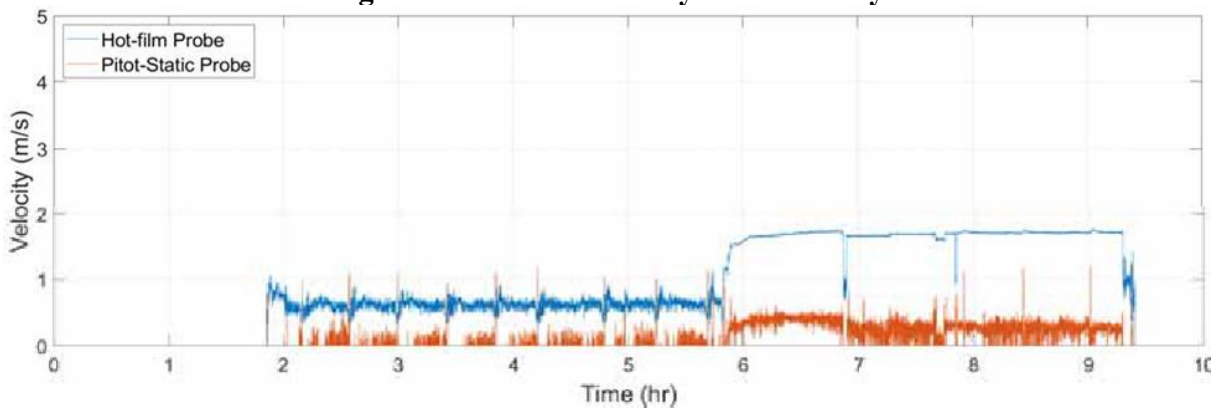

Figure 030420.04: Coolant Return Temperature Time History

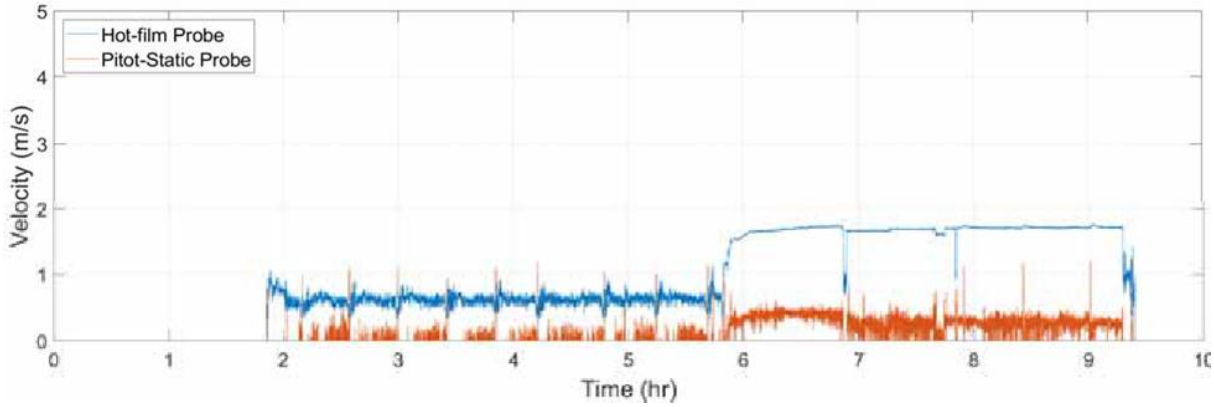

Figure 030420.05: Coolant Supply Temperature Time History

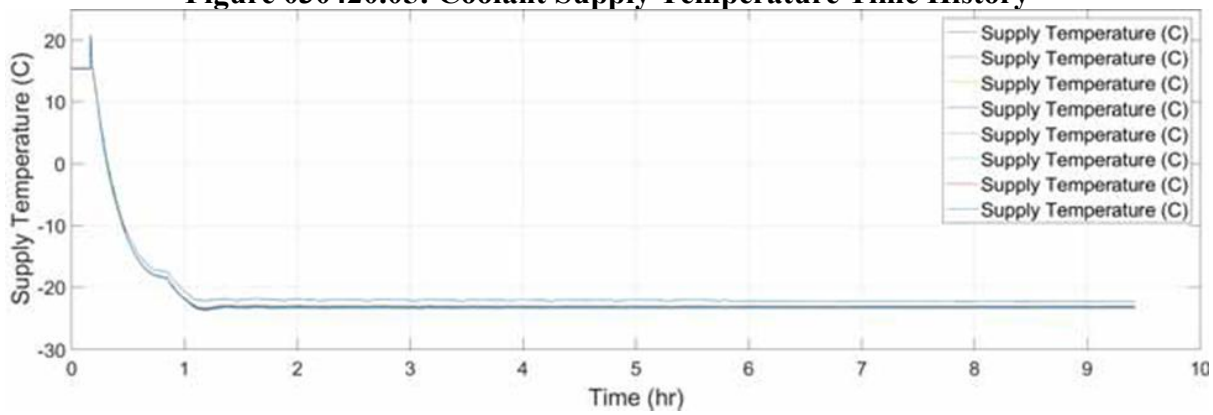

Figure 030420.06: Skin Temperature Time History

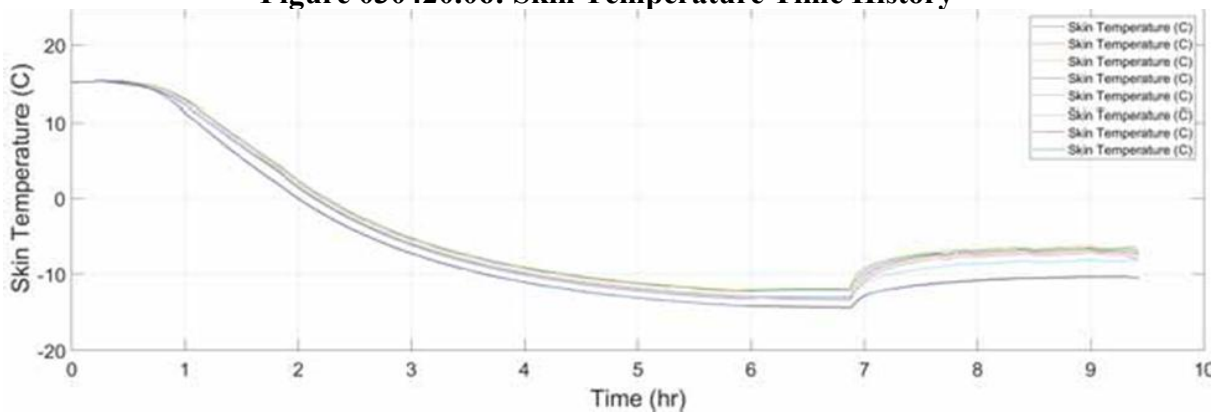

Figure 030420.07: Floor Temperature Time History

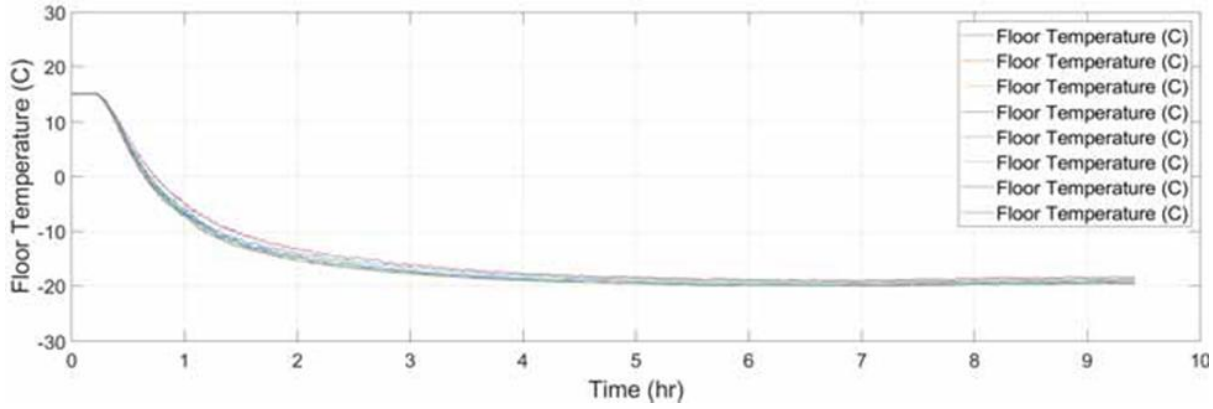

Figure 030420.08: Skin Temperature Slope Time History

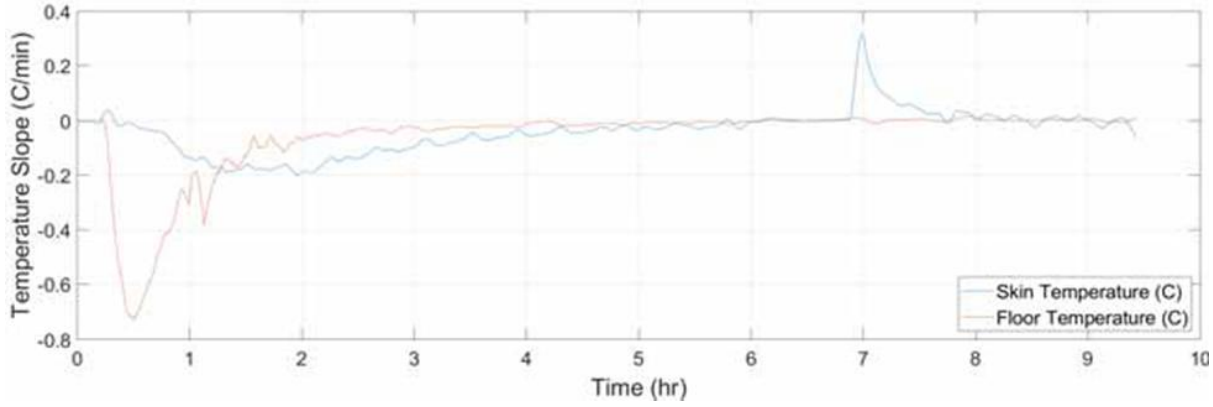

Figure 030420.09: RMS Heigh Evolution

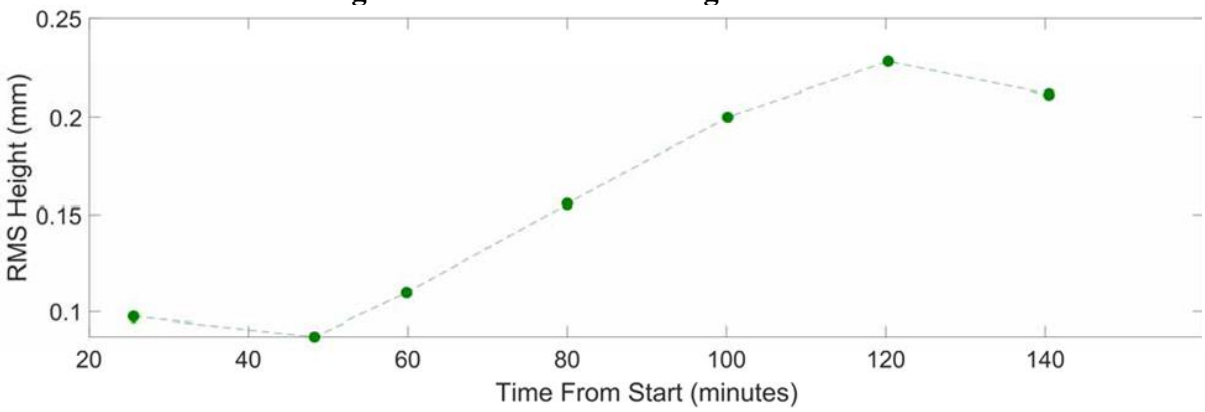

Figure 030420.10: Skewness Evolution

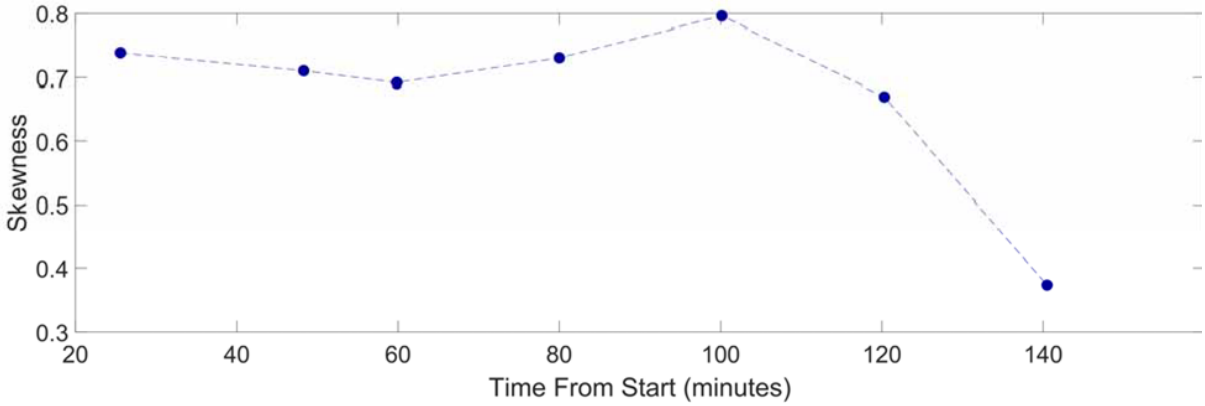

Figure 030420.11: Peak to Valley Evolution

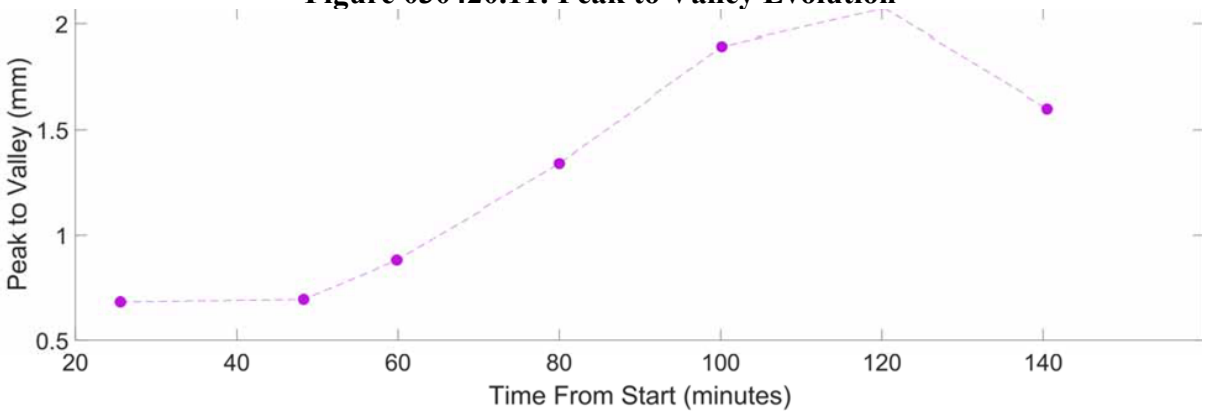

Figure 030420.12: Equivalent Roughness Evolution

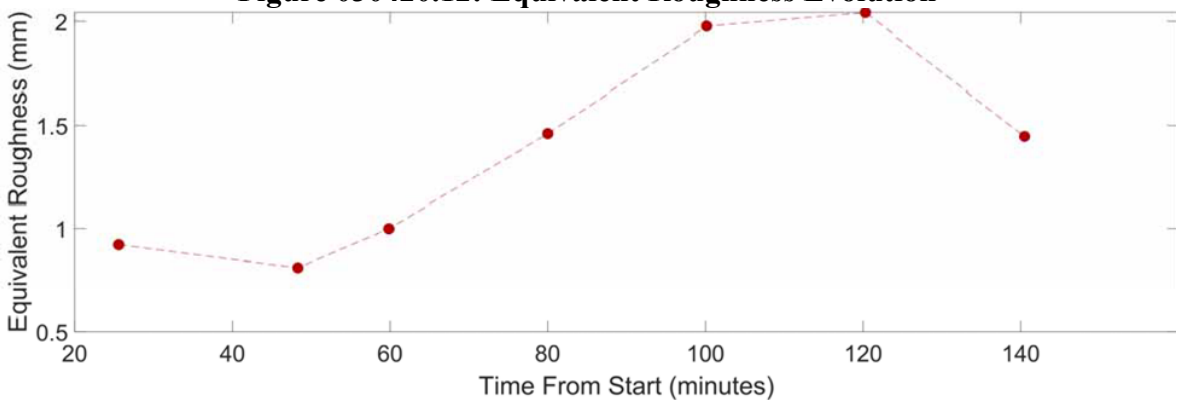

Table 030420.02: Summary of Roughness Parameters

Time (min.)	RMS (mm)	Skewness	Peak to Valley (mm)	ks,Flack-Schultz (mm)
25.5696	0.0975	0.7389	0.6778	0.9213
48.2862	0.0874	0.7106	0.6897	0.8076
59.8362	0.1097	0.6919	0.8785	0.9992
80.0029	0.1554	0.7311	1.3391	1.4601
100.1529	0.2000	0.7964	1.8957	1.9766
120.3029	0.2284	0.6703	2.0754	2.0435
140.4862	0.2115	0.3727	1.6018	1.4460

Figure 030420.13: Frost Topography at 00:25:34

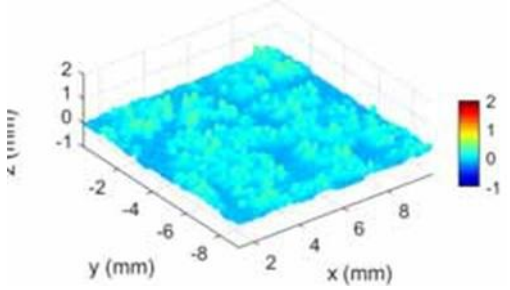

Figure 030420.14: Frost Topography at 00:48:17

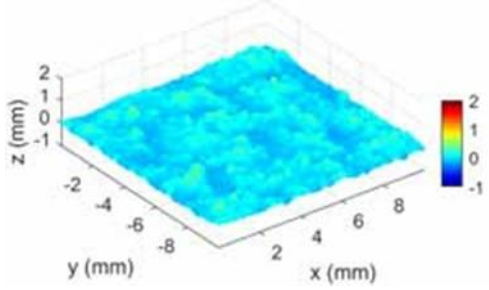

Figure 030420.15: Frost Topography at 00:59:50

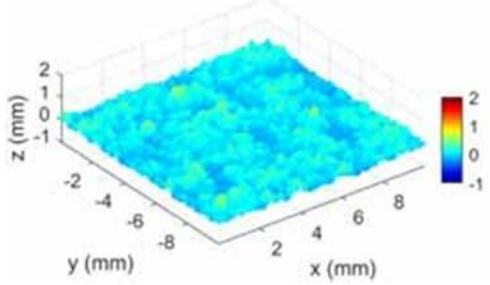

Figure 030420.16: Frost Topography at 01:20:00

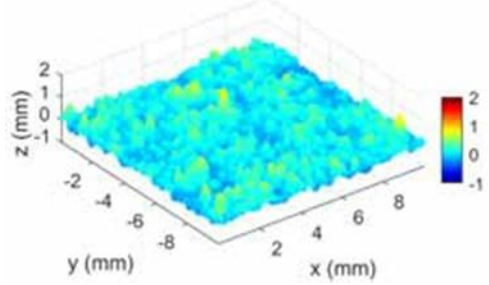

Figure 030420.17: Frost Topography at 01:40:09

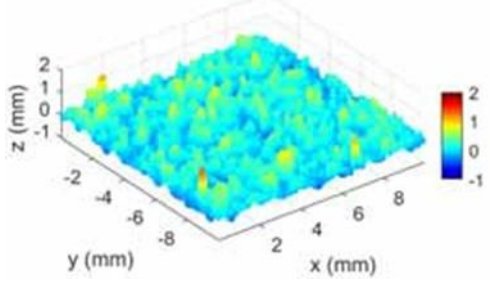

Figure 030420.18: Frost Topography at 02:00:18

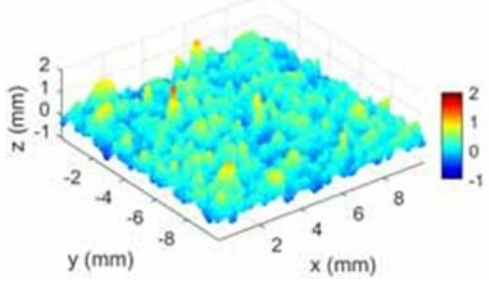

Figure 030420.19: Frost Topography at 2:20:29

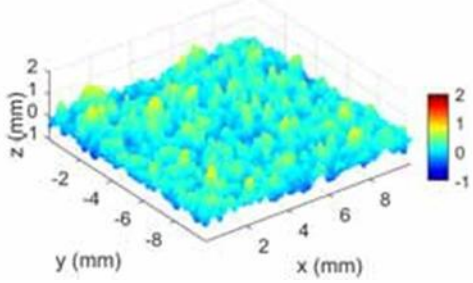

CAFF Conditions Report – Case Date: 030620

Table 030620.01: Summary of Measured Test Variables

Variable	Mean	St. Dev.	Rand. Unc.
T_air (C)	14.8354	0.4616	0.0152
Rh (%)	79.7792	3.6219	0.1191
Omega (kg_v/kg_da)	0.00835330	0.00048100	0.00001582
V_air (m/s)	0.2725	0.1021	0.0034
T_skin (C)	-8.0627	1.0105	0.0332
T_floor (C)	-19.4085	0.1487	0.0049

Figure 030620.01: Temperature and Voltage Control Time History

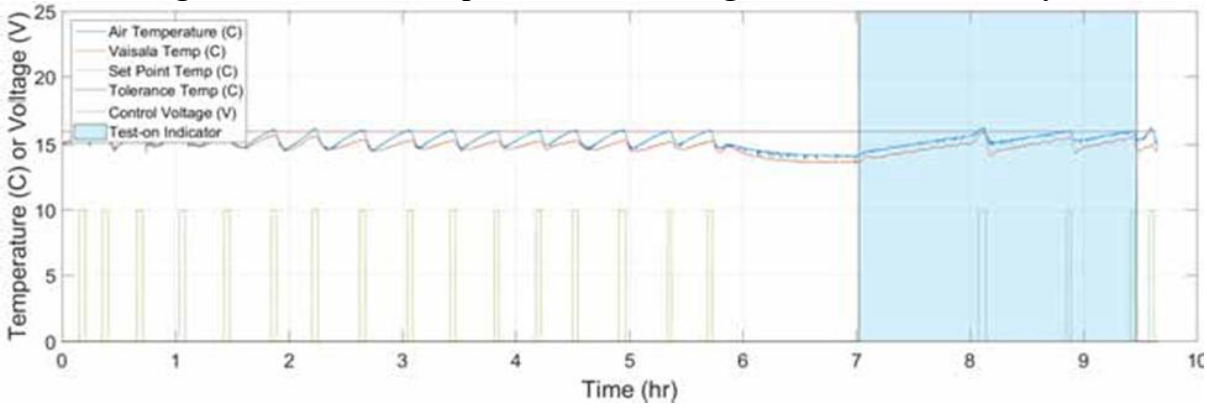

Figure 030620.02: Relative Humidity Time History

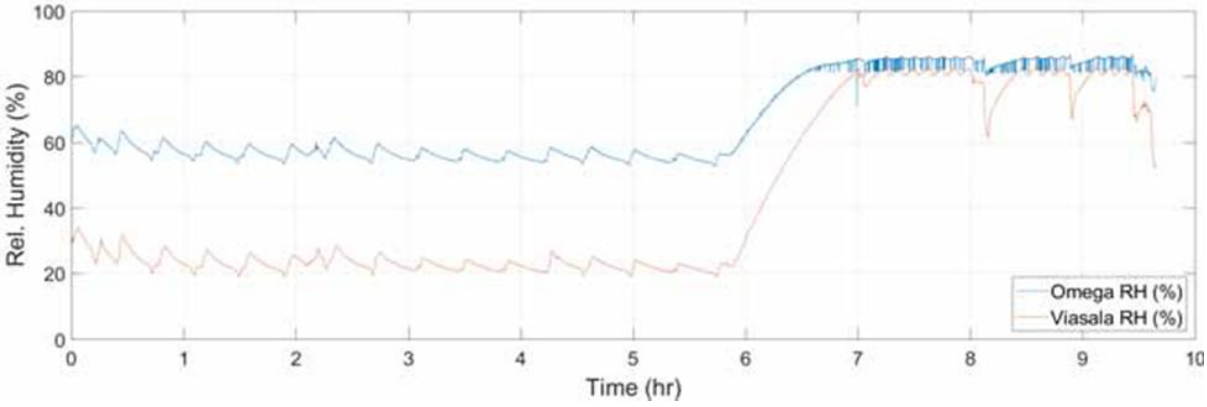

Figure 030620.03: Velocity Time History

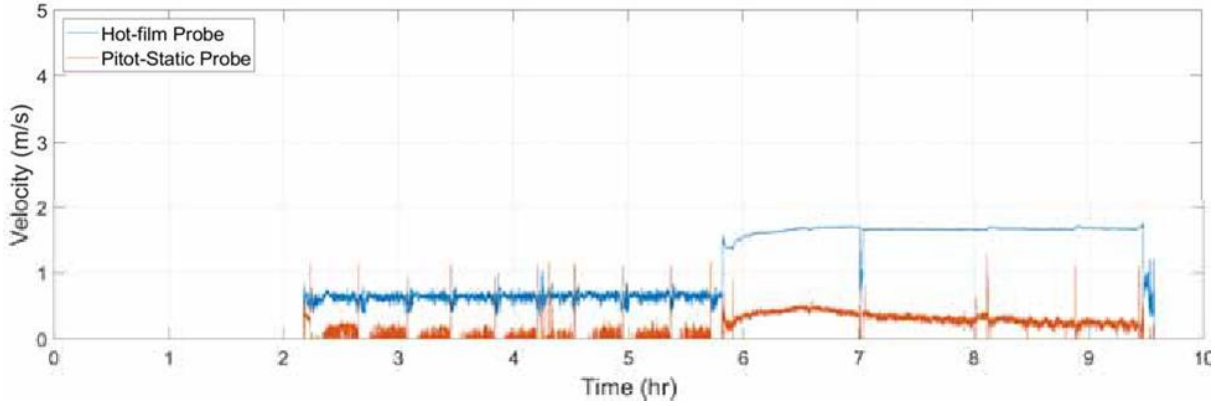

Figure 030620.04: Coolant Return Temperature Time History

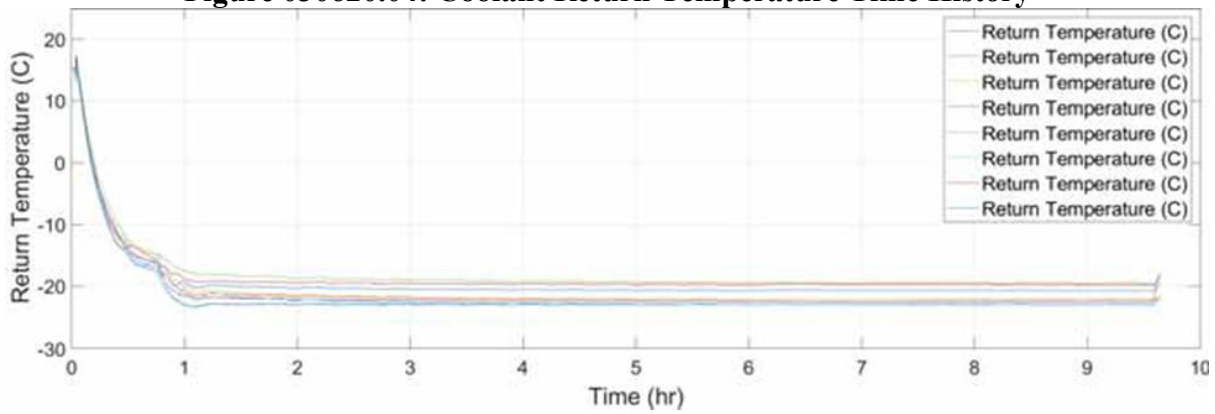

Figure 030620.05: Coolant Supply Temperature Time History

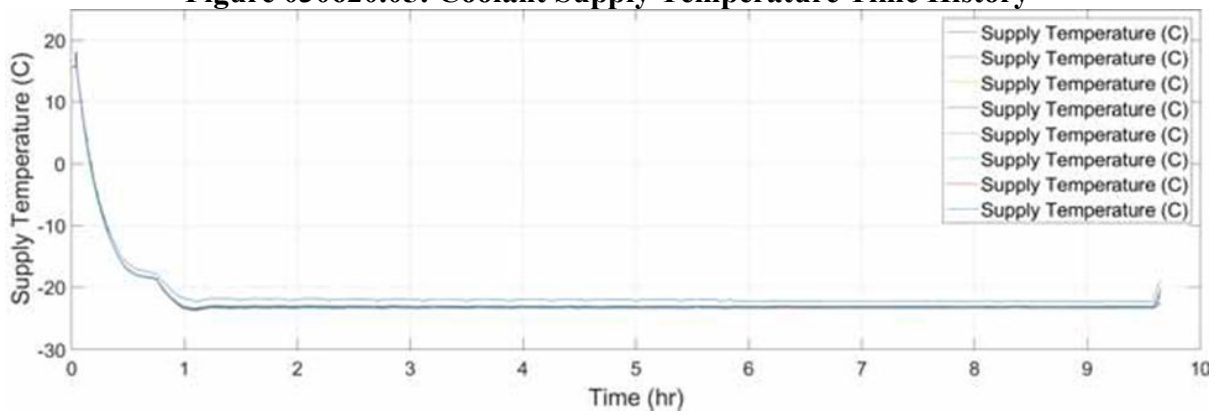

Figure 030620.06: Skin Temperature Time History

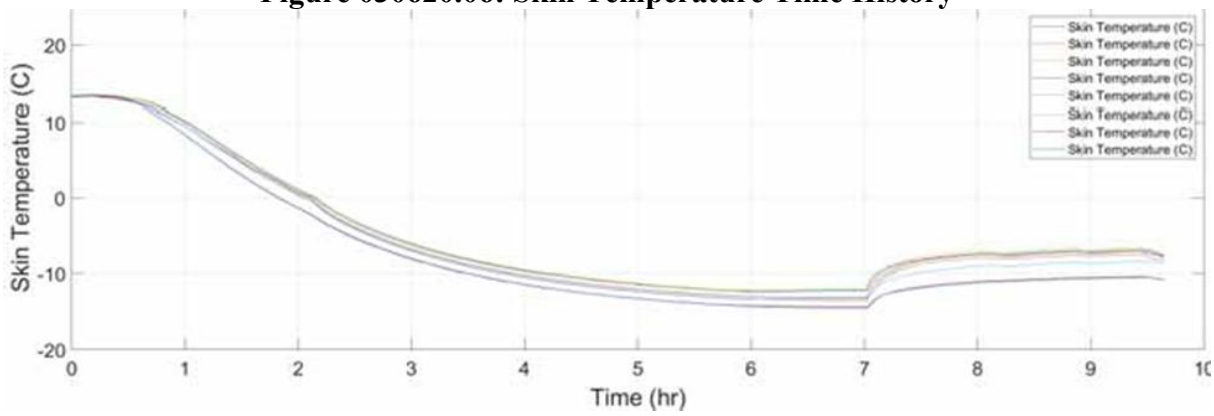

Figure 030620.07: Floor Temperature Time History

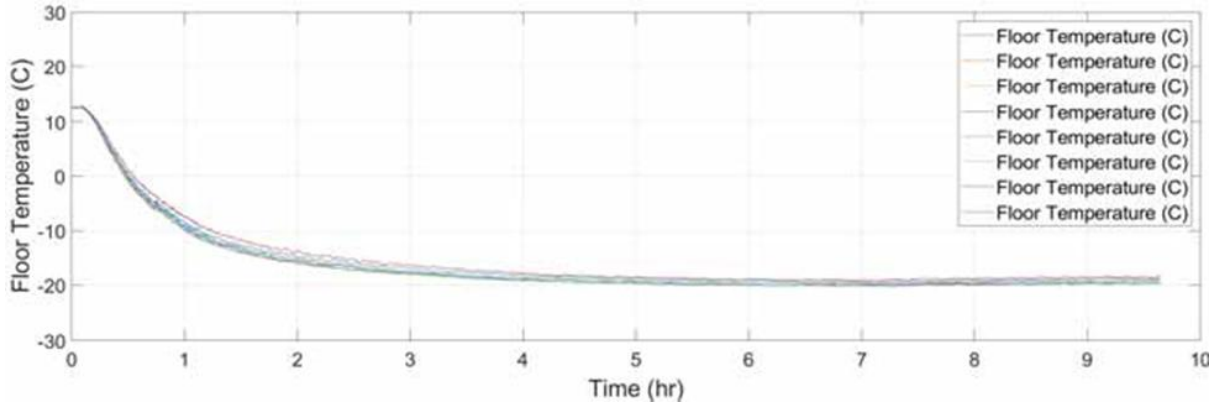

Figure 030620.08: Skin Temperature Slope Time History

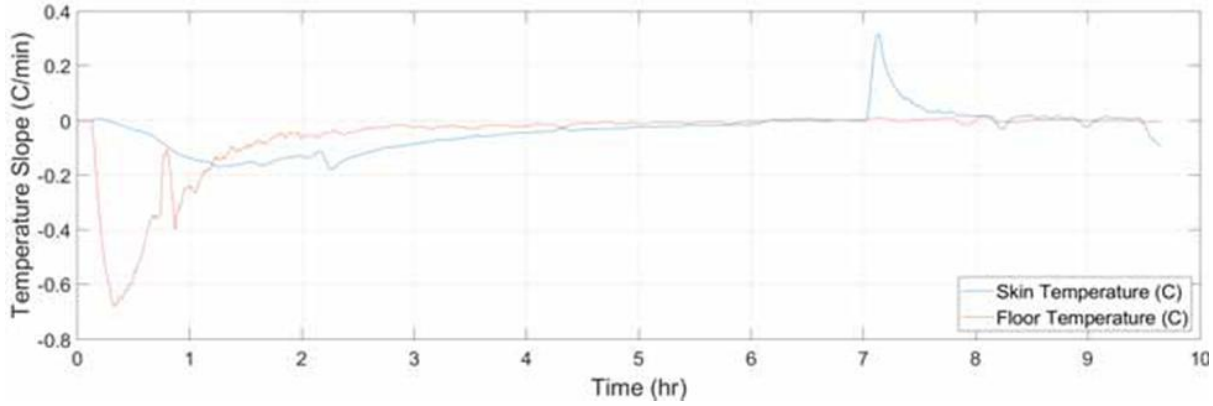

Figure 030620.09: RMS Height Evolution

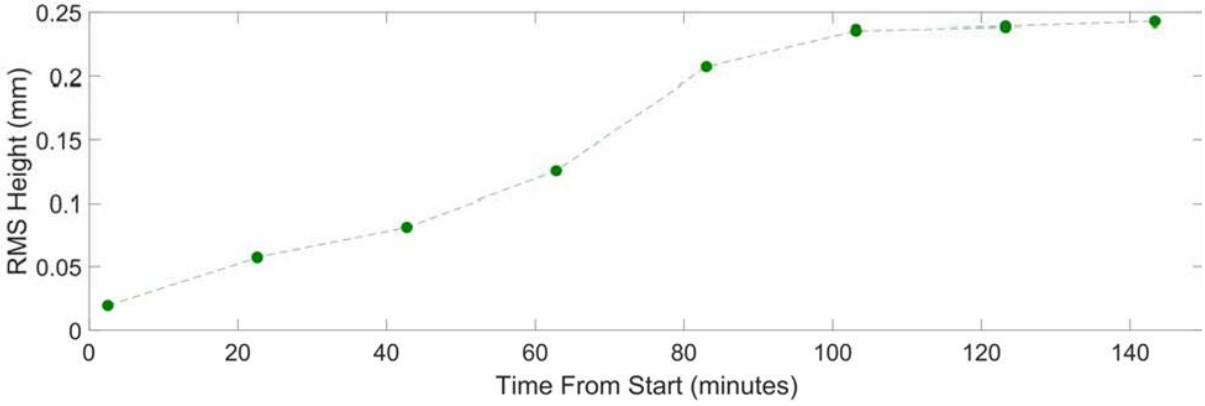

Figure 030620.10: Skewness Evolution

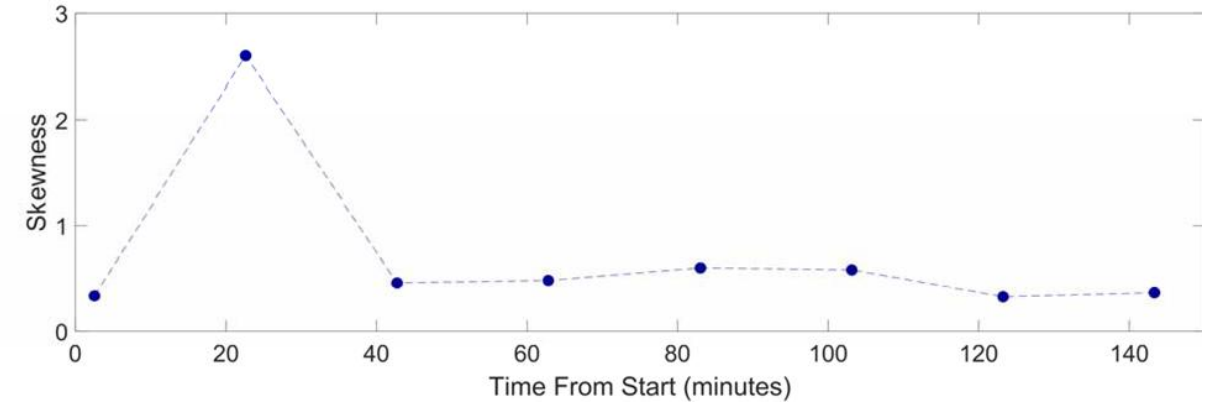

Figure 030620.11: Peak to Valley Evolution

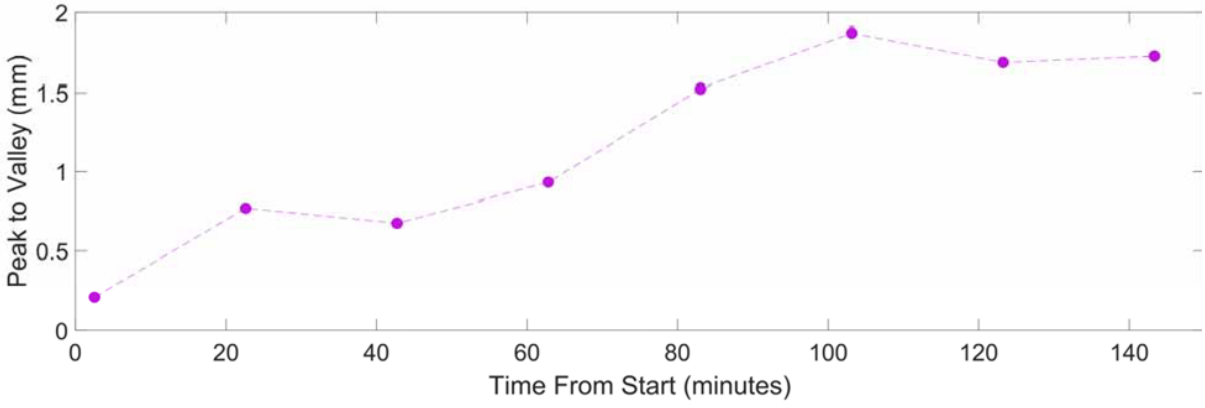

Figure 030620.12: Equivalent Roughness Evolution

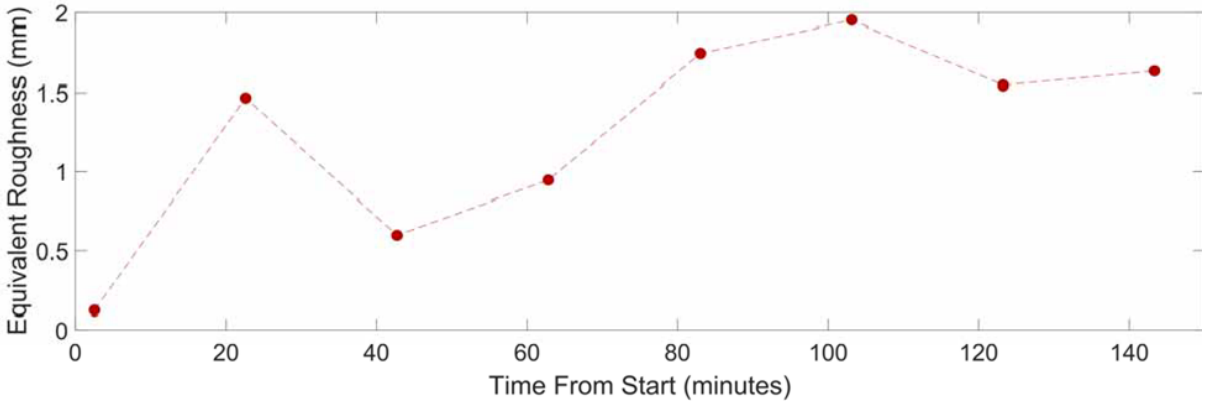

Table 030620.02: Summary of Roughness Parameters

Time (min.)	RMS (mm)	Skewness	Peak to Valley (mm)	ks,Flack-Schultz (mm)
2.5025	0.0186	0.3258	0.2013	0.1210
22.6025	0.0571	2.6079	0.7710	1.4670
42.7192	0.0810	0.4503	0.6747	0.5973
62.8192	0.1254	0.4736	0.9304	0.9449
83.0192	0.2075	0.5958	1.5240	1.7442
103.1358	0.2362	0.5765	1.8746	1.9521
123.2525	0.2390	0.3177	1.6877	1.5449
143.3525	0.2429	0.3563	1.7279	1.6336

Figure 030620.13: Frost Topography at 00:02:30

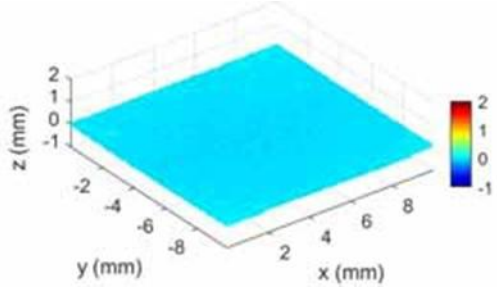

Figure 030620.14: Frost Topography at 00:22:36

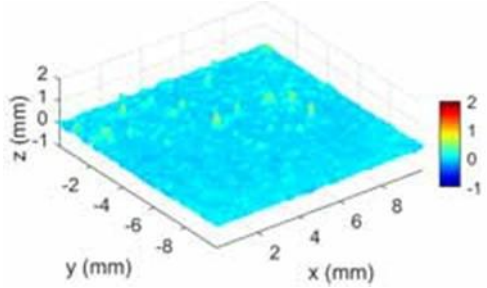

Figure 030620.15: Frost Topography at 00:42:43

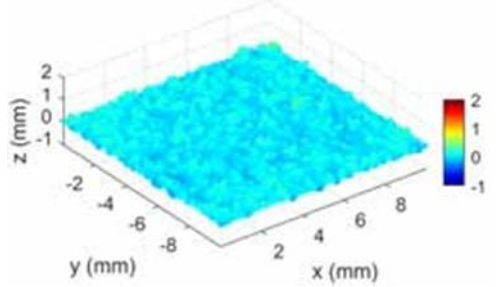

Figure 030620.16: Frost Topography at 01:02:49

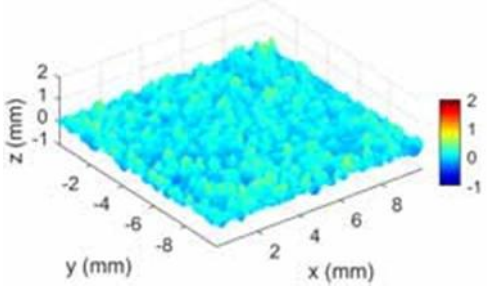

Figure 030620.17: Frost Topography at 01:23:01

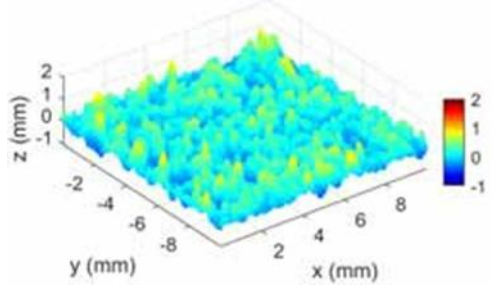

Figure 030620.18: Frost Topography at 01:43:08

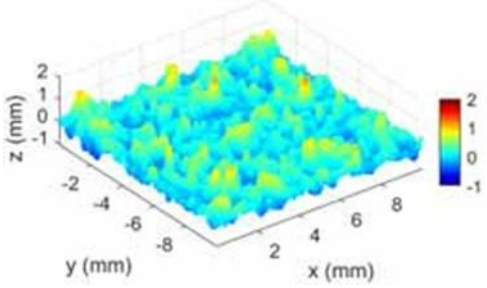

Figure 030620.19: Frost Topography 02:03:15

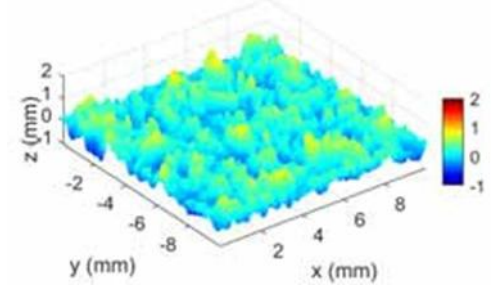

Figure 030620.20: Frost Topography 02:23:21

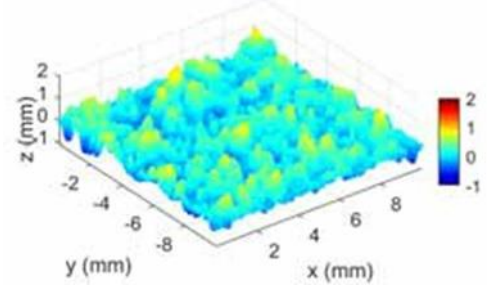

CAFF Conditions Report – Case Date: 030920

Table 030920.01: Summary of Measured Test Variables

Variable	Mean	St. Dev.	Rand. Unc.
T_air (C)	9.0567	0.4309	0.0169
Rh (%)	79.5371	6.7579	0.2643
Omega (kg_v/kg_da)	0.00572434	0.00053174	0.00002080
V_air (m/s)	0.3336	0.1090	0.0043
T_skin (C)	-10.6984	0.7657	0.0299
T_floor (C)	-20.0477	0.0529	0.0021

Figure 030920.01: Temperature and Voltage Control Time History

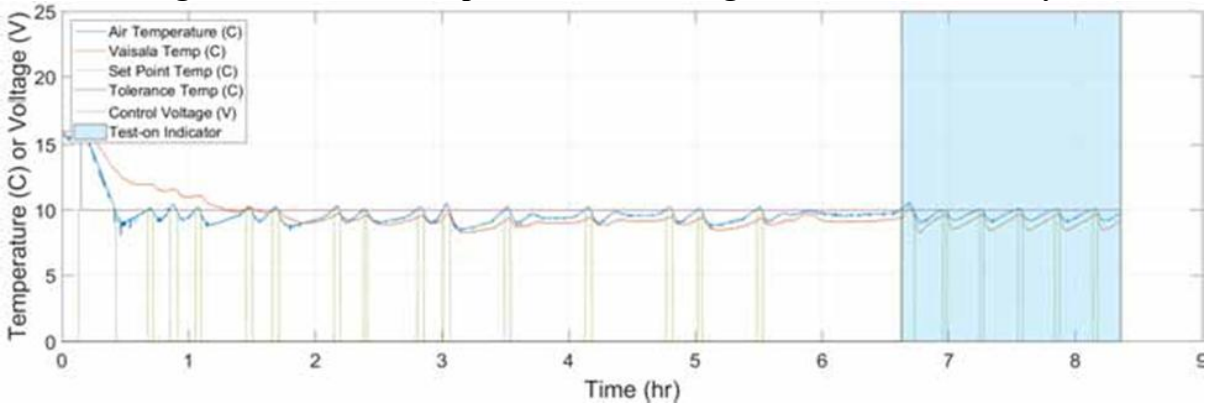

Figure 030920.02: Relative Humidity Time History

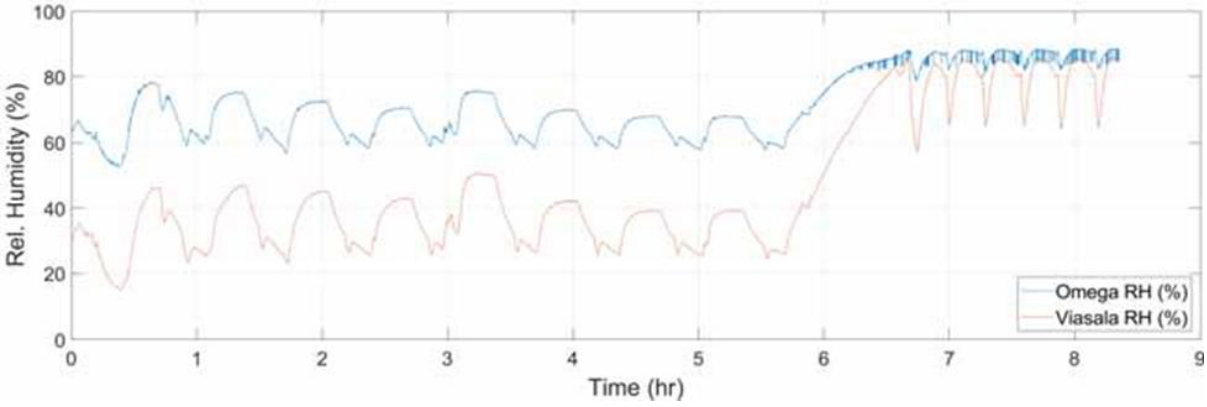

Figure 030920.03: Velocity Time History

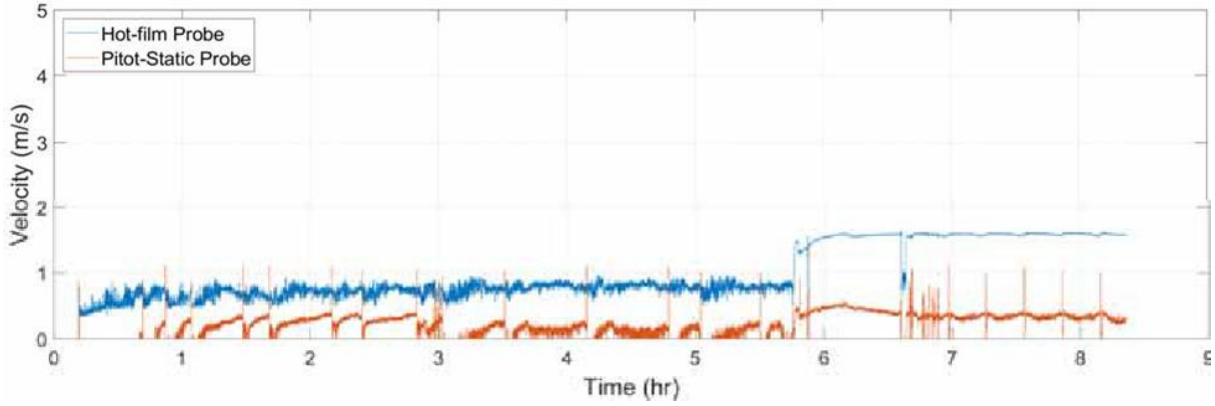

Figure 030920.04: Coolant Return Temperature Time History

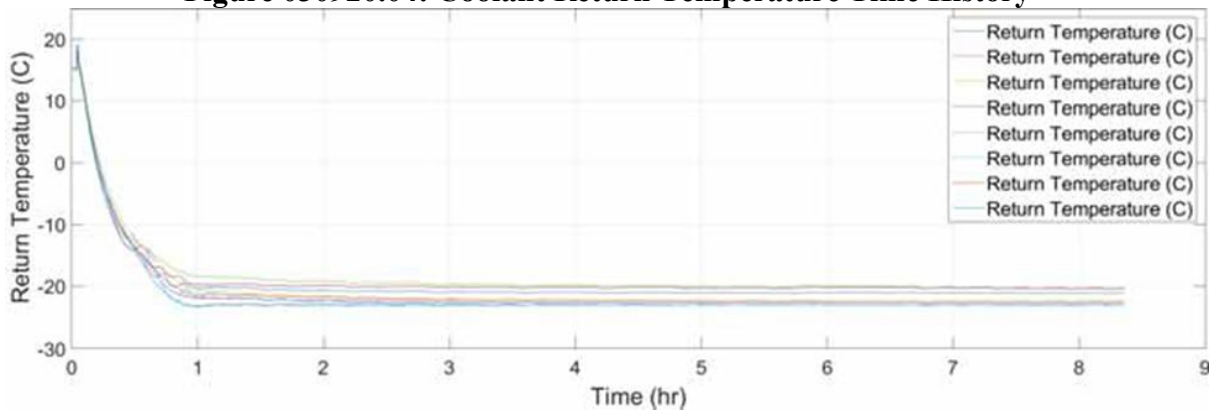

Figure 030920.05: Coolant Supply Temperature Time History

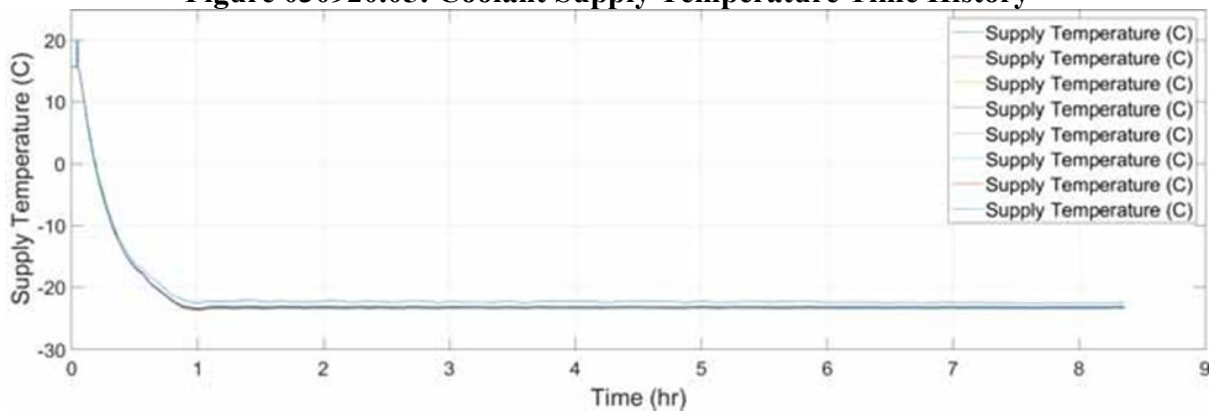

Figure 030920.06: Skin Temperature Time History

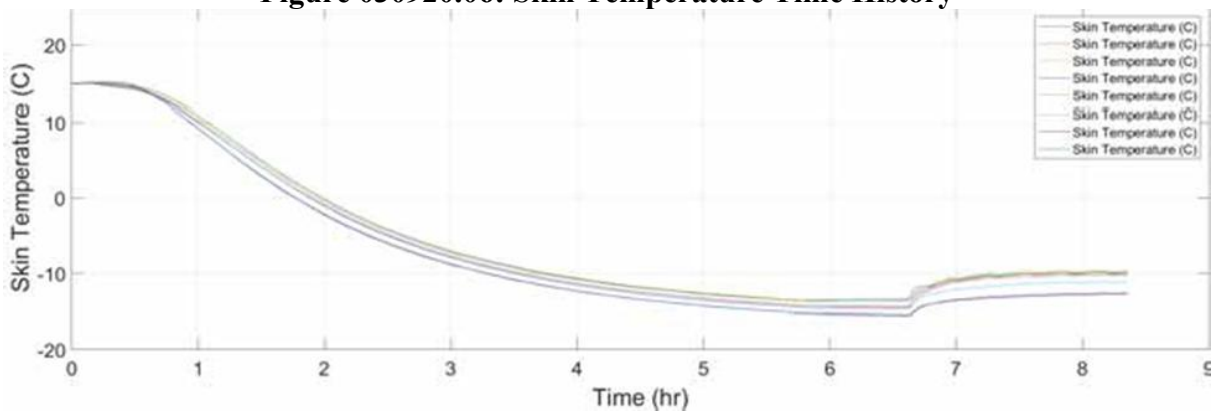

Figure 030920.07: Floor Temperature Time History

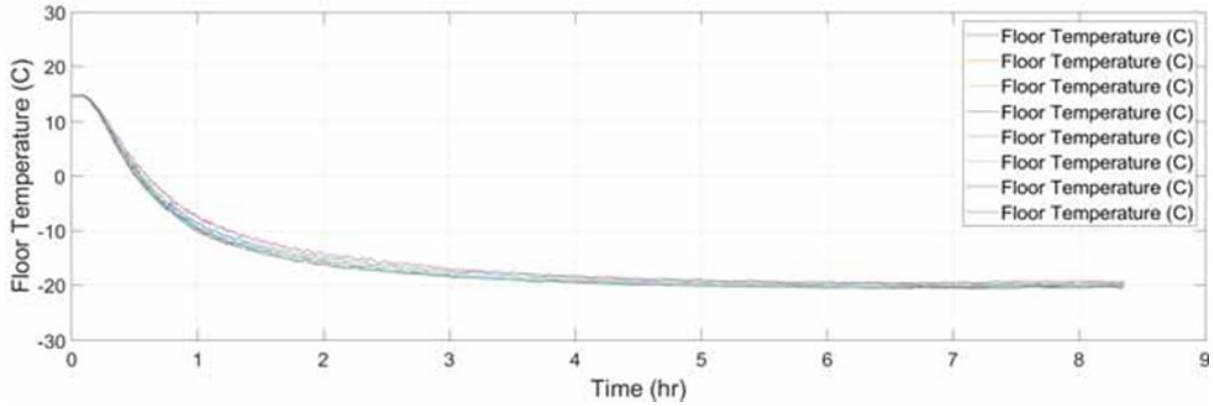

Figure 030920.08: Skin Temperature Slope Time History

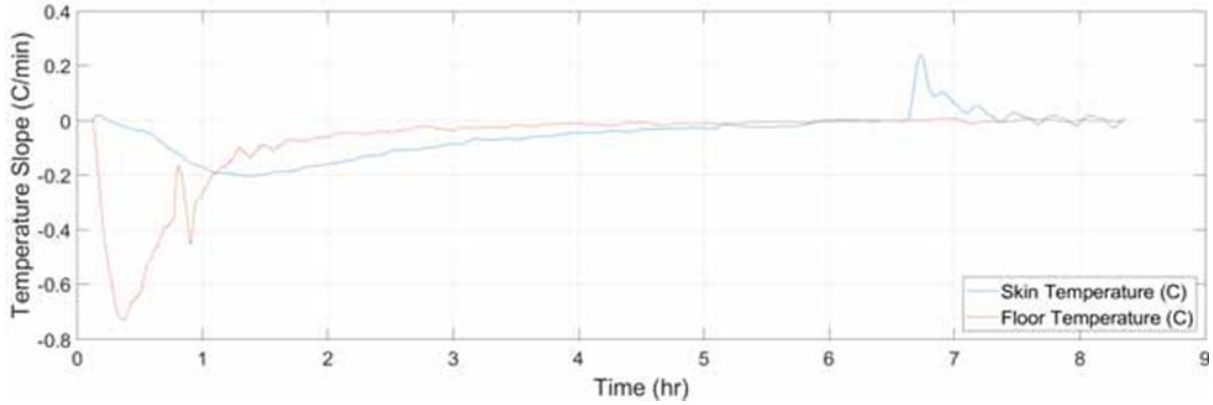

Figure 030920.09: RMS Height Evolution

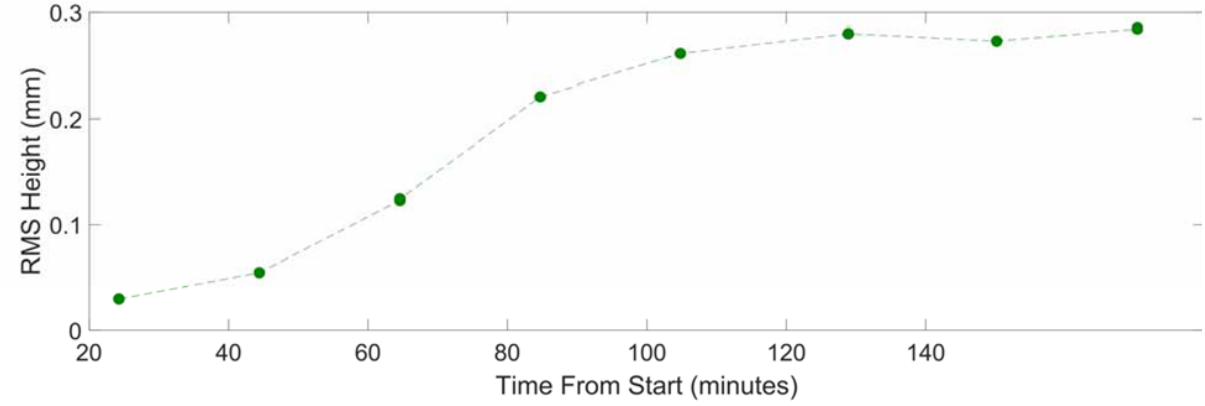

Figure 030920.10: Skewness Evolution

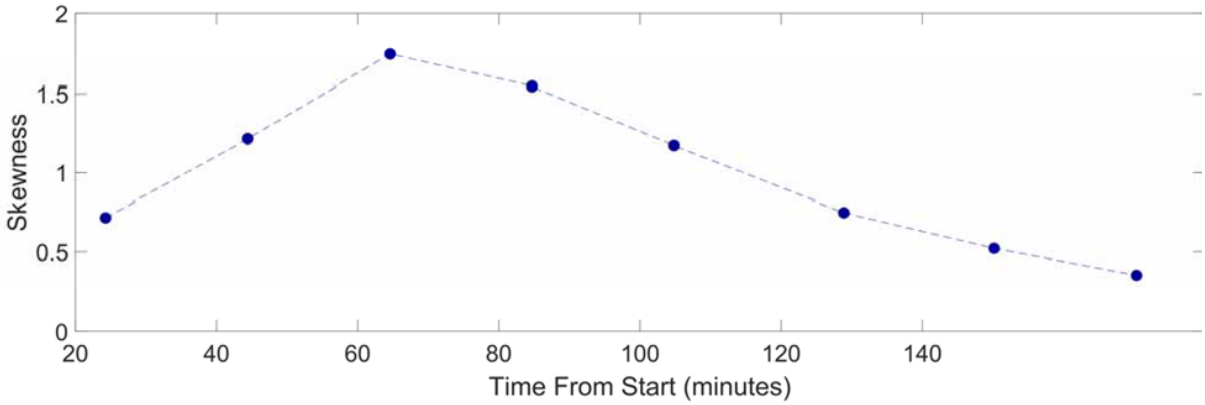

Figure 030920.11: Peak to Valley Evolution

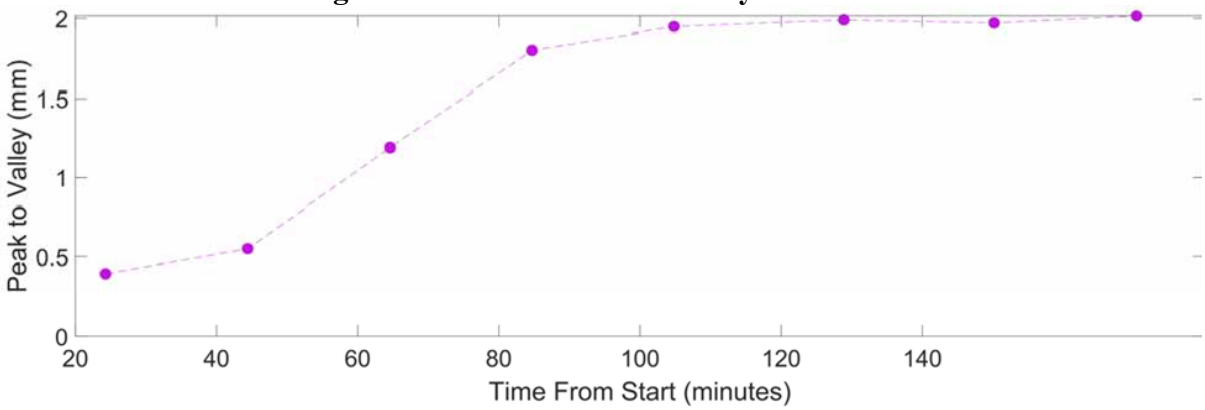

Figure 030920.12: Equivalent Roughness Evolution

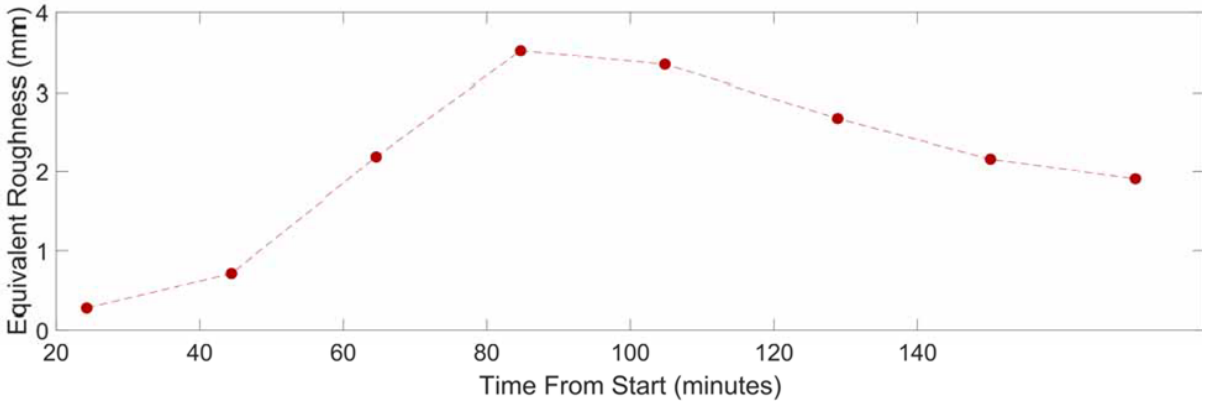

Table 030920.02: Summary of Roughness Parameters

Time (min.)	RMS (mm)	Skewness	Peak to Valley (mm)	ks,Flack-Schultz (mm)
24.2596	0.0285	0.7151	0.3906	0.2647
44.4096	0.0539	1.2132	0.5505	0.7087
64.5762	0.1233	1.7497	1.1895	2.1844
84.7096	0.2214	1.5449	1.8030	3.5257
104.8096	0.2618	1.1707	1.9482	3.3538
128.8929	0.2808	0.7475	1.9894	2.6722
150.1929	0.2737	0.5211	1.9704	2.1537
170.3762	0.2852	0.3485	2.0151	1.9030

Figure 030920.13: Frost Topography at 00:24:15

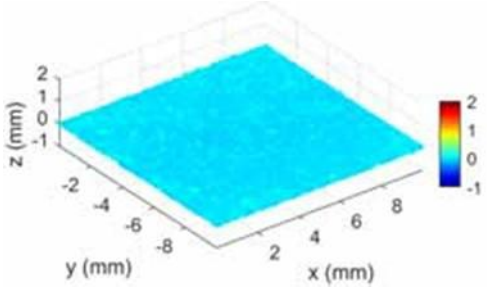

Figure 030920.14: Frost Topography at 00:44:24

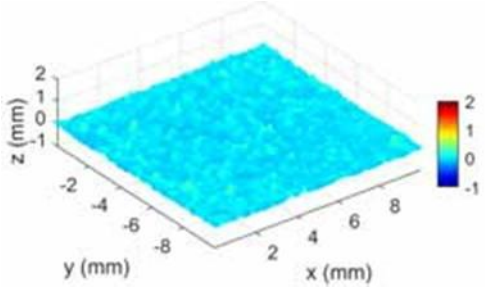

Figure 030920.15: Frost Topography at 01:04:34

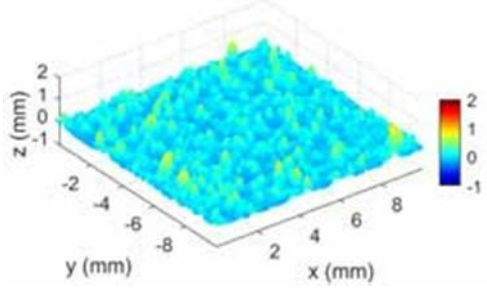

Figure 030920.16: Frost Topography at 01:24:42

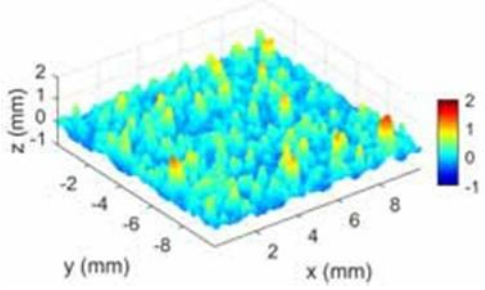

Figure 030920.17: Frost Topography at 01:44:48

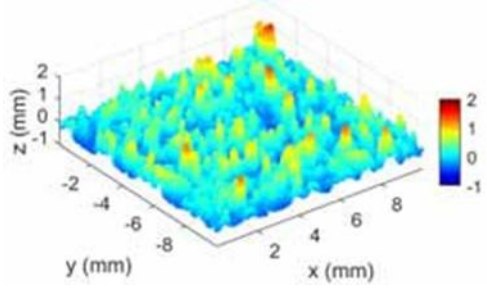

Figure 030920.18: Frost Topography at 02:08:53

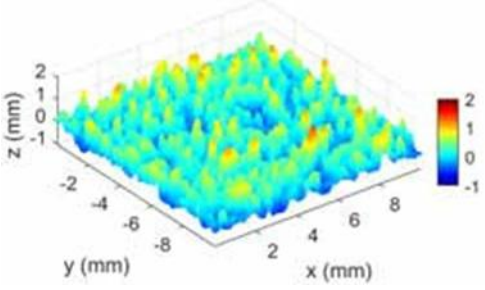

Figure 030920.19: Frost Topography at 02:30:11

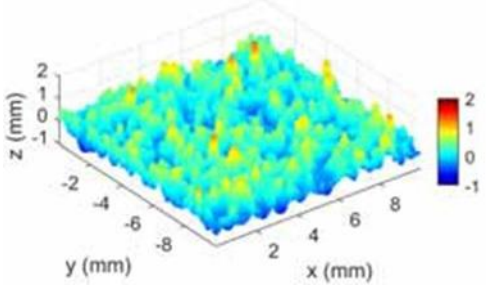

Figure 030920.20: Frost Topography at 02:50:22

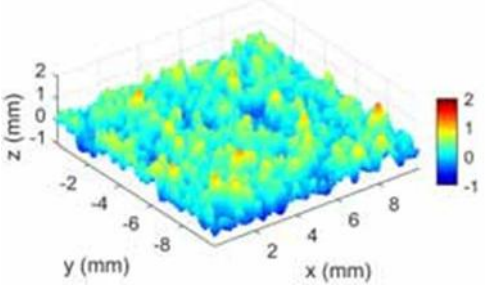

CAFF Conditions Report – Case Date: 031120

Table 031120.01: Summary of Measured Test Variables

Variable	Mean	St. Dev.	Rand. Unc.
T_air (C)	9.0508	0.3952	0.0130
Rh (%)	80.4001	5.5753	0.1828
Omega (kg_v/kg_da)	0.00580731	0.00043881	0.00001439
V_air (m/s)	0.2755	0.1117	0.0037
T_skin (C)	-10.4866	0.6976	0.0229
T_floor (C)	-20.0201	0.0589	0.0019

Figure 031120.01: Temperature and Voltage Control Time History

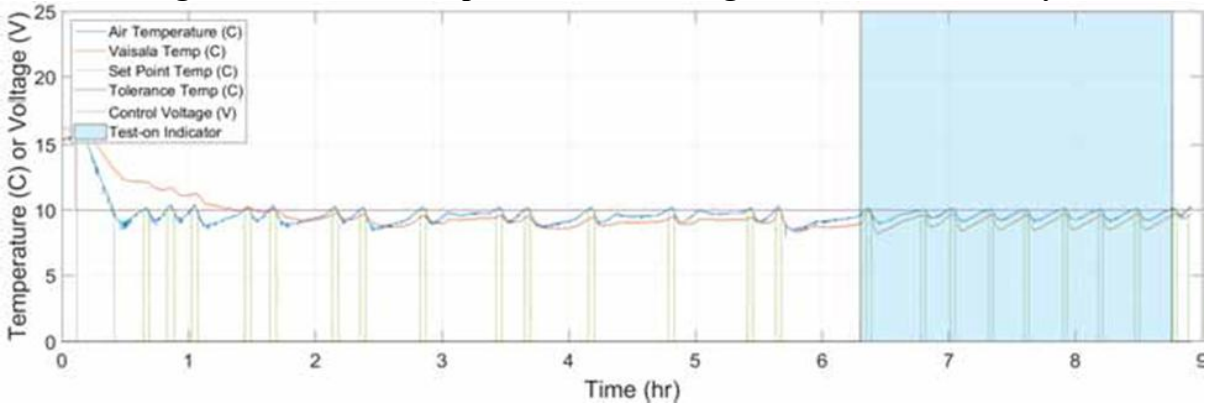

Figure 031120.02: Relative Humidity Time History

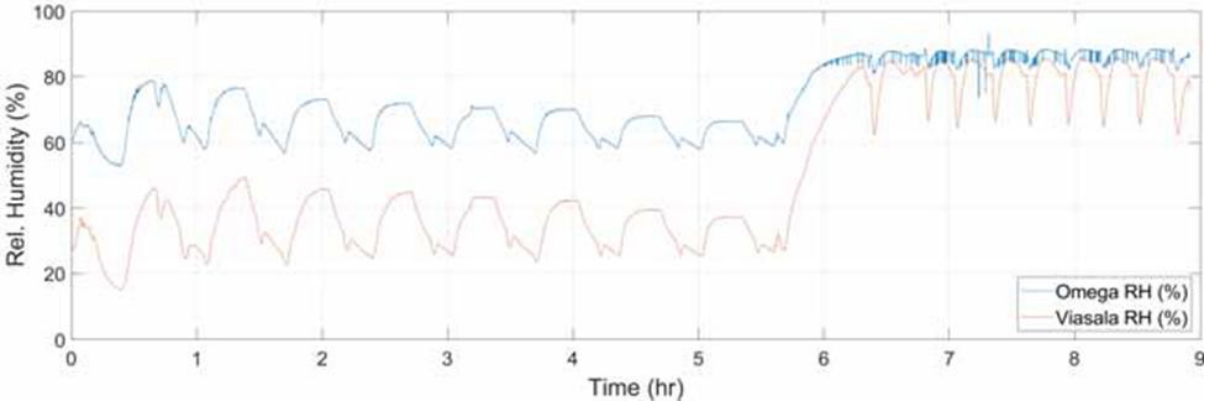

Figure 031120.03: Velocity Time History

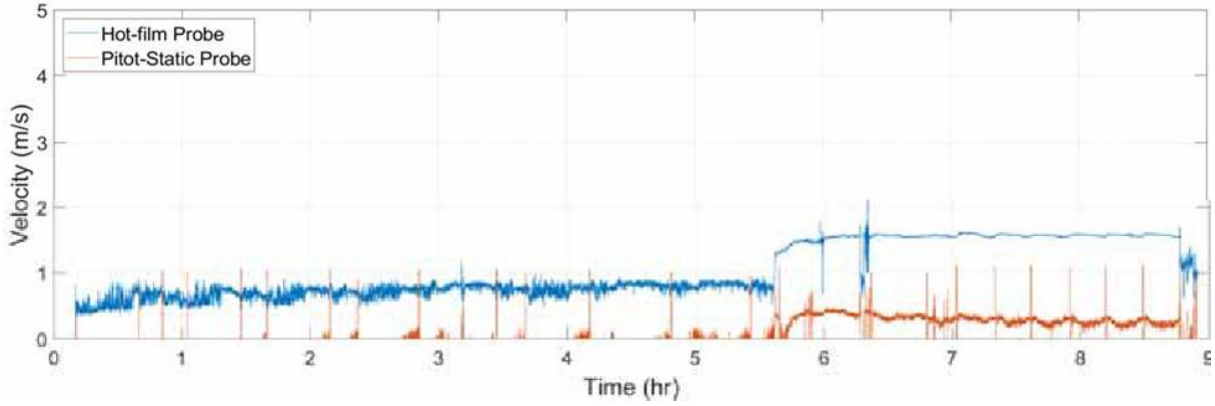

Figure 031120.04: Coolant Return Temperature Time History

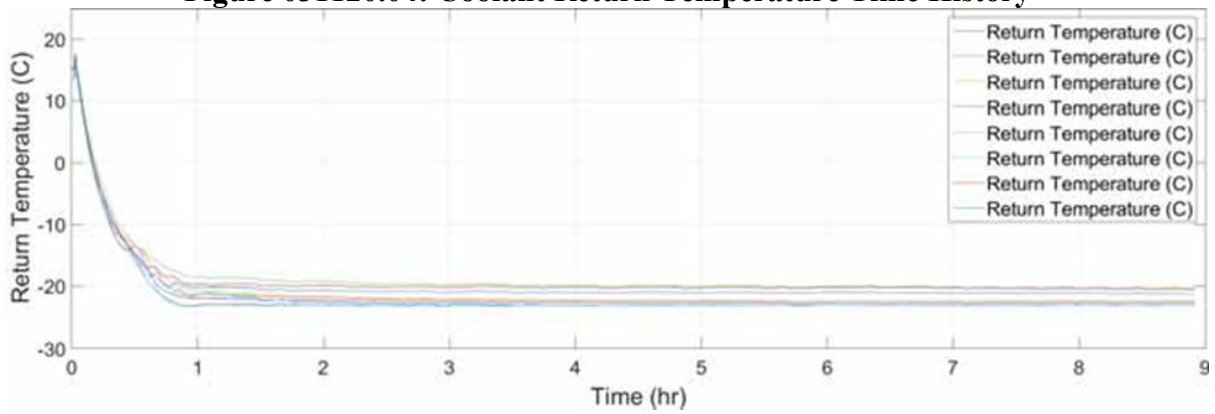

Figure 031120.05: Coolant Supply Temperature Time History

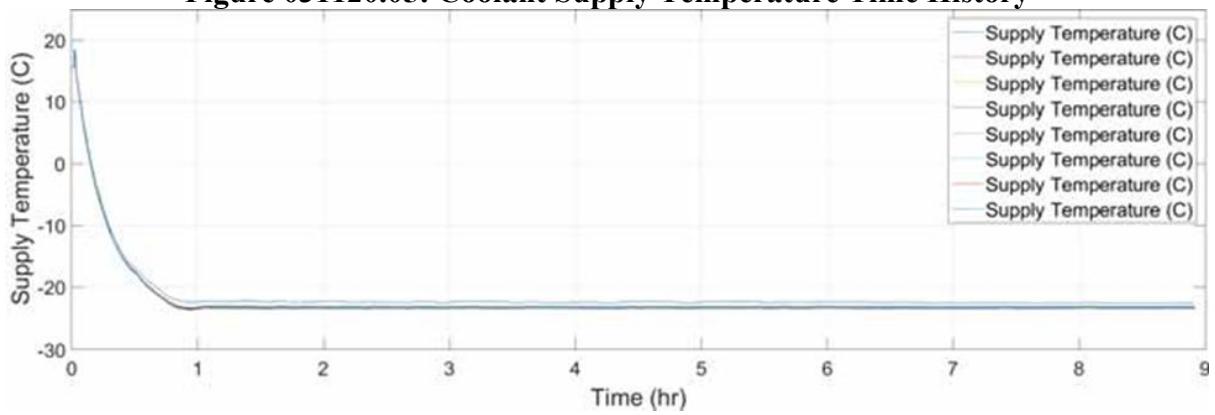

Figure 031120.06: Skin Temperature Time History

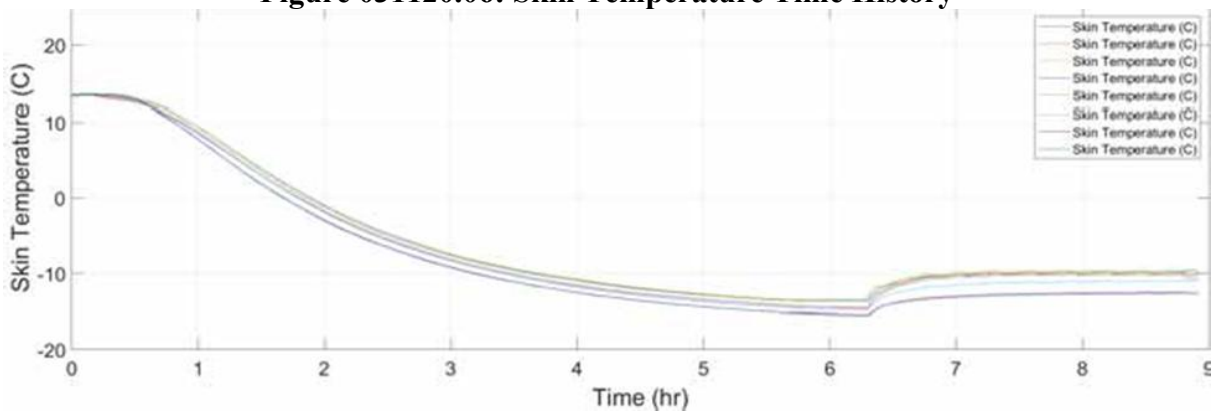

Figure 031120.07: Floor Temperature Time History

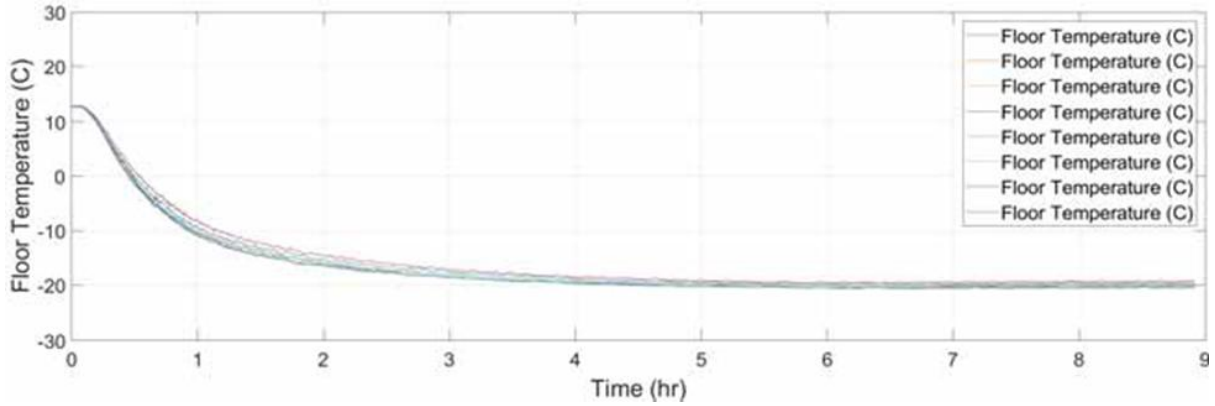

Figure 031120.08: Skin Temperature Slope Time History

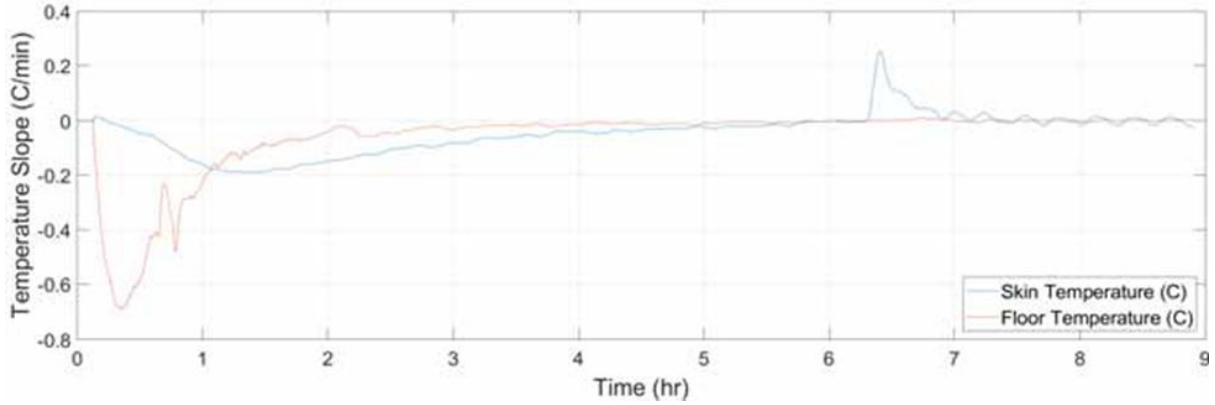

Figure 031120.09: RMS Height Evolution

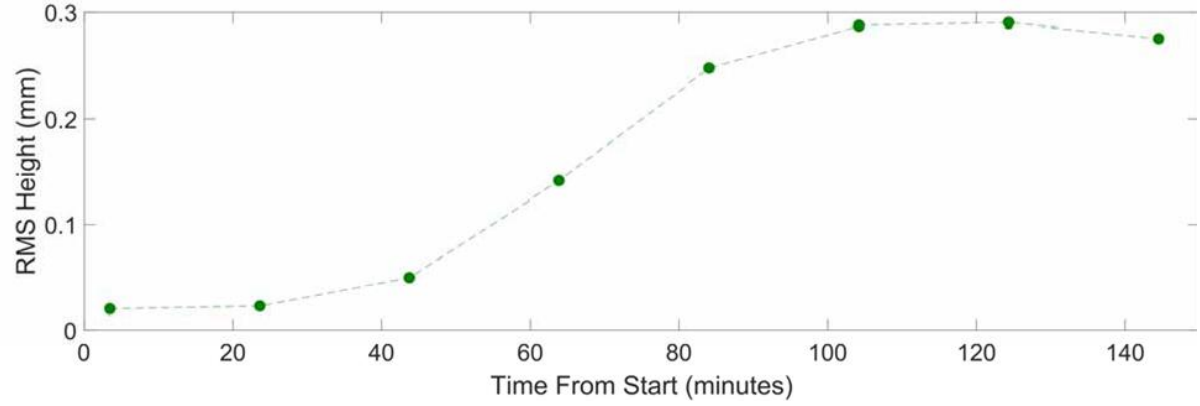

Figure 031120.10: Skewness Evolution

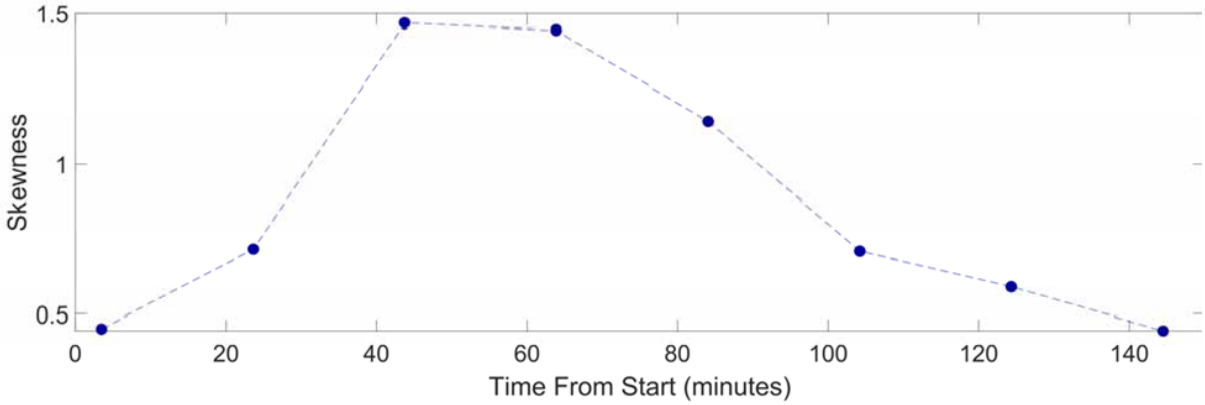

Figure 031120.11: Peak to Valley Evolution

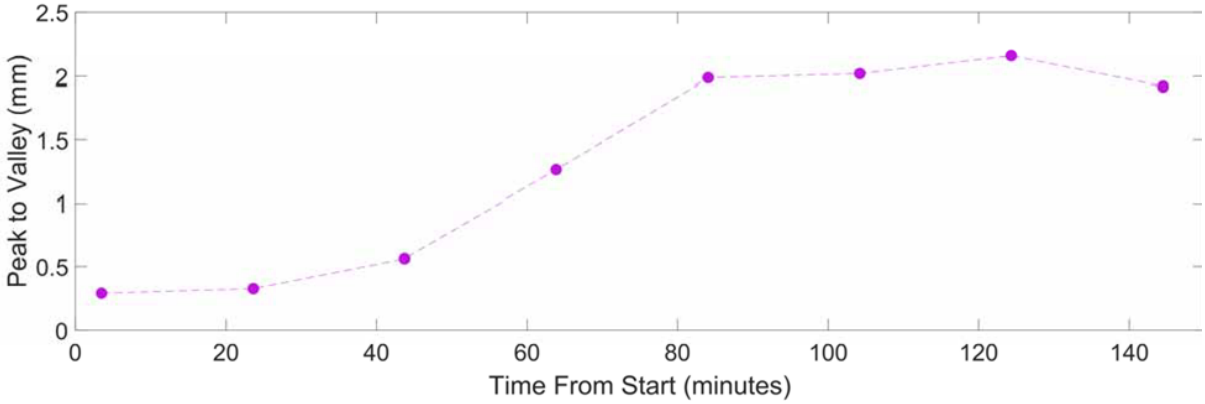

Figure 031120.12: Equivalent Roughness Evolution

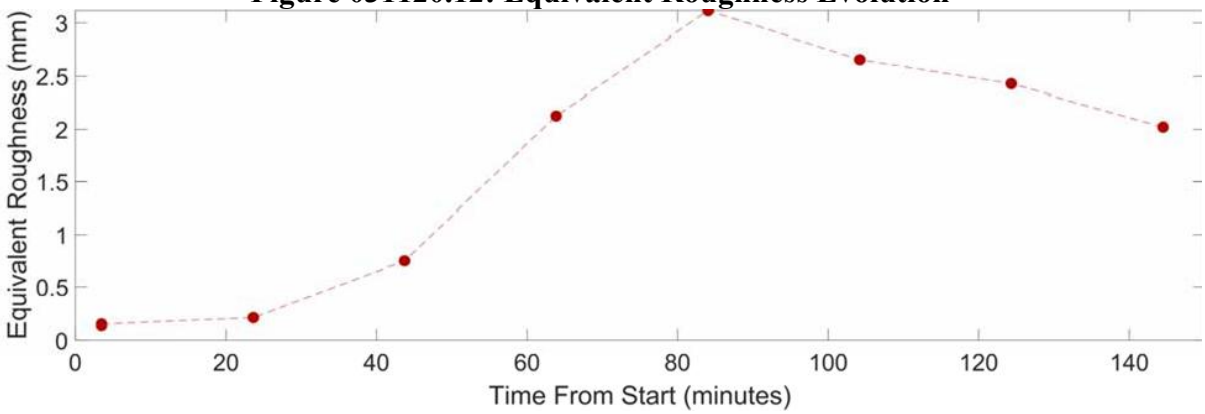

Table 031120.02: Summary of Roughness Parameters

Time (min.)	RMS (mm)	Skewness	Peak to Valley (mm)	ks,Flack-Schultz (mm)
3.4529	0.0193	0.4503	0.2847	0.1423
23.6195	0.0219	0.7158	0.3211	0.2033
43.7195	0.0490	1.4686	0.5609	0.7487
63.8529	0.1411	1.4455	1.2632	2.1279
84.0529	0.2478	1.1433	1.9883	3.1199
104.2029	0.2877	0.7096	2.0205	2.6574
124.3195	0.2904	0.5903	2.1642	2.4295
144.5029	0.2758	0.4440	1.9204	2.0209

Figure 031120.13: Frost Topography at 00:03:27

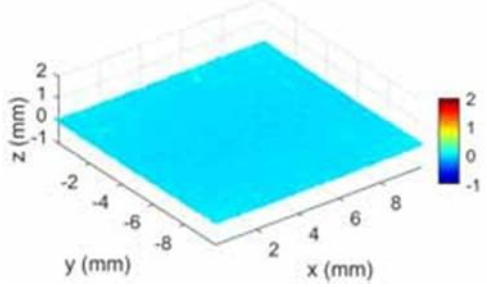

Figure 031120.14: Frost Topography at 00:23:37

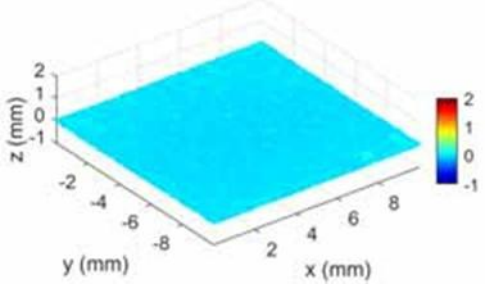

Figure 031120.15: Frost Topography at 00:43:43

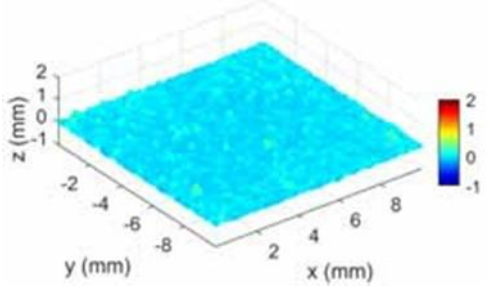

Figure 031120.16: Frost Topography at 01:03:51

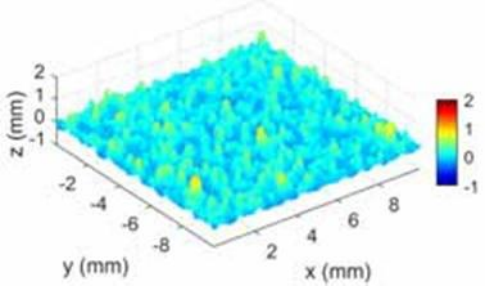

Figure 031120.17: Frost Topography at 01:24:03

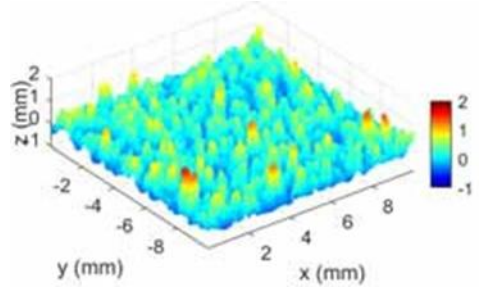

Figure 031120.18: Frost Topography at 01:44:12

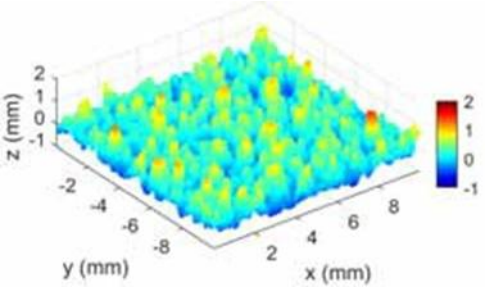

Figure 031120.19: Frost Topography at 02:04:19

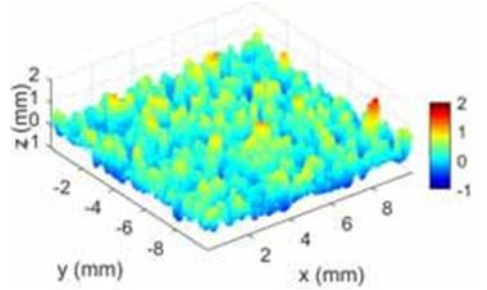

Figure 031120.20: Frost Topography at 02:24:30

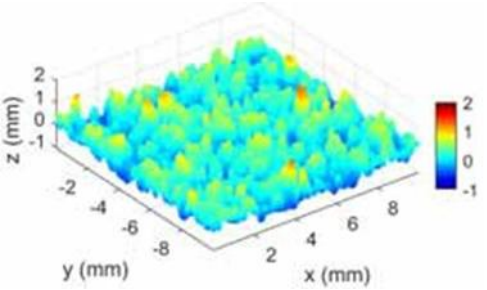

CAFF Conditions Report – Case Date: 031820

Table 031820.01: Summary of Measured Test Variables

Variable	Mean	St. Dev.	Rand. Unc.
T_air (C)	9.0949	0.4846	0.0158
Rh (%)	80.7225	4.6110	0.1504
Omega (kg_v/kg_da)	0.00585972	0.00040942	0.00001335
V_air (m/s)	1.3353	0.1215	0.0040
T_skin (C)	-8.7155	0.9159	0.0299
T_floor (C)	-19.8762	0.1203	0.0039

Figure 031820.01: Temperature and Voltage Control Time History

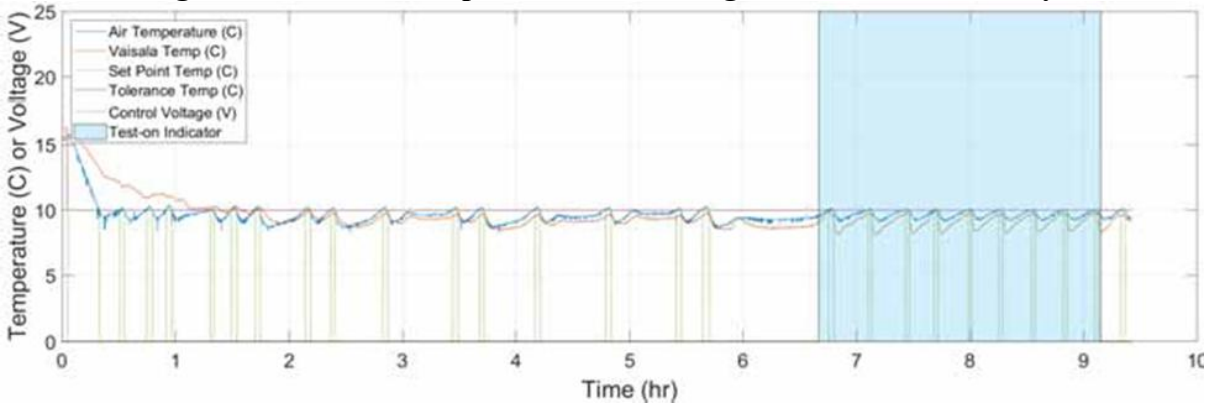

Figure 031820.02: Relative Humidity Time History

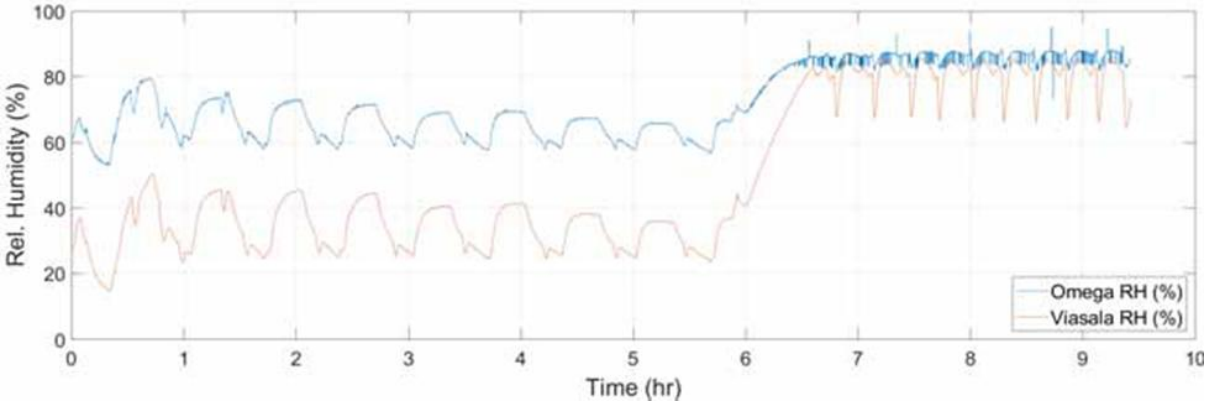

Figure 031820.03: Velocity Time History

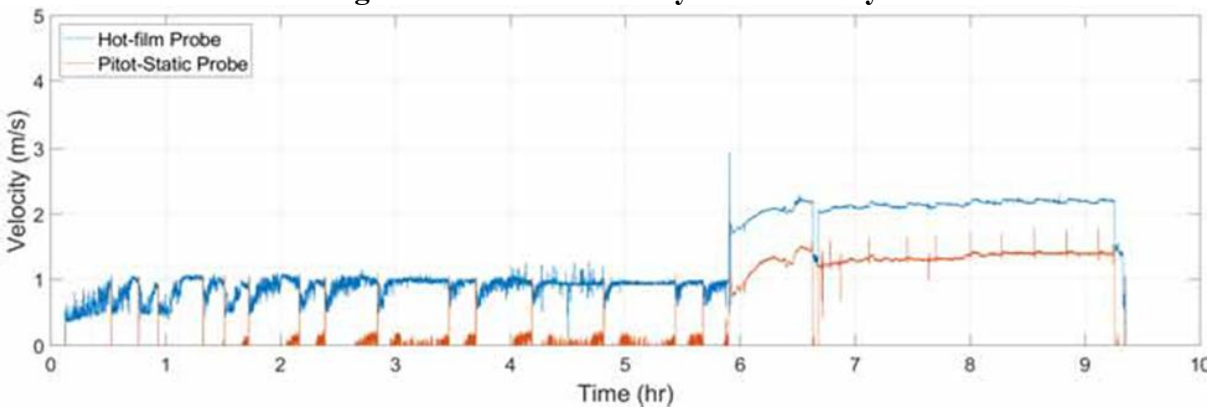

Figure 031820.04: Coolant Return Temperature Time History

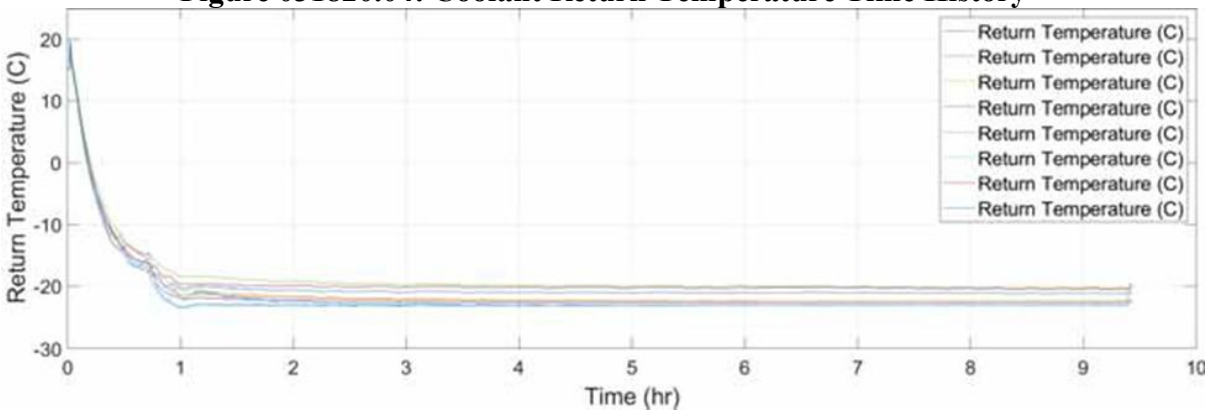

Figure 031820.05: Coolant Supply Temperature Time History

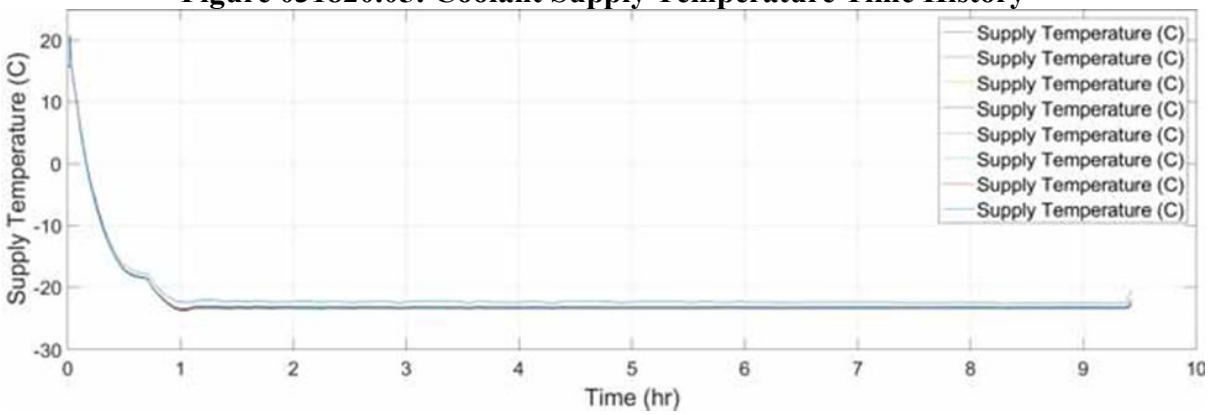

Figure 031820.06: Skin Temperature Time History

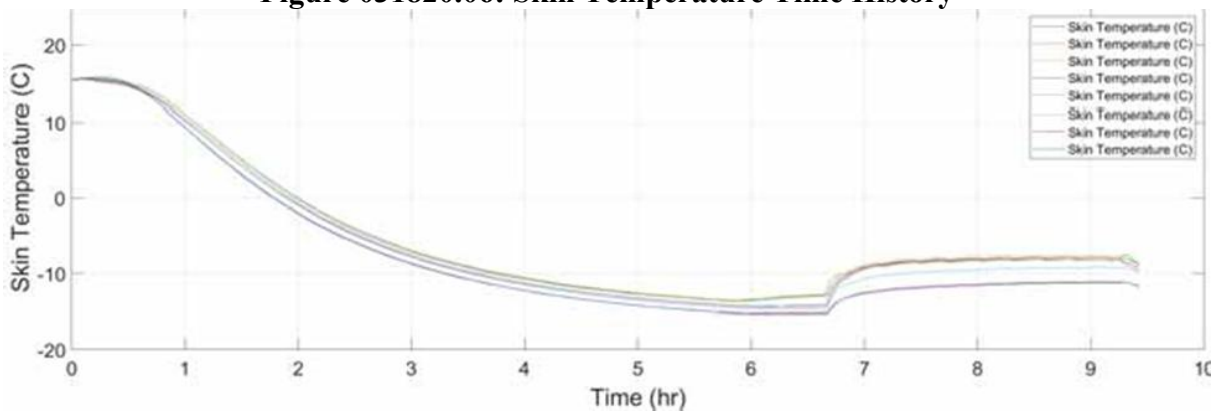

Figure 031820.07: Floor Temperature Time History

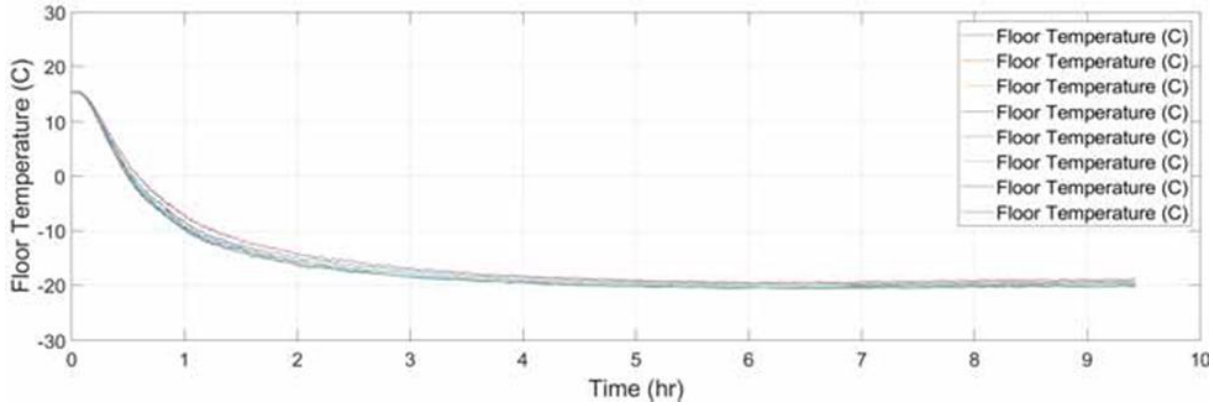

Figure 031820.08: Skin Temperature Slope Time History

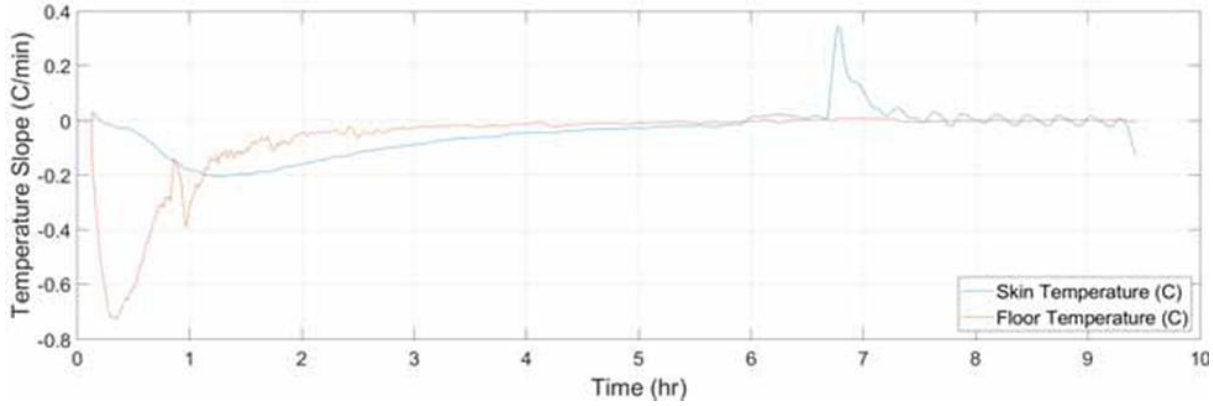

Figure 031820.09: RMS Height Evolution

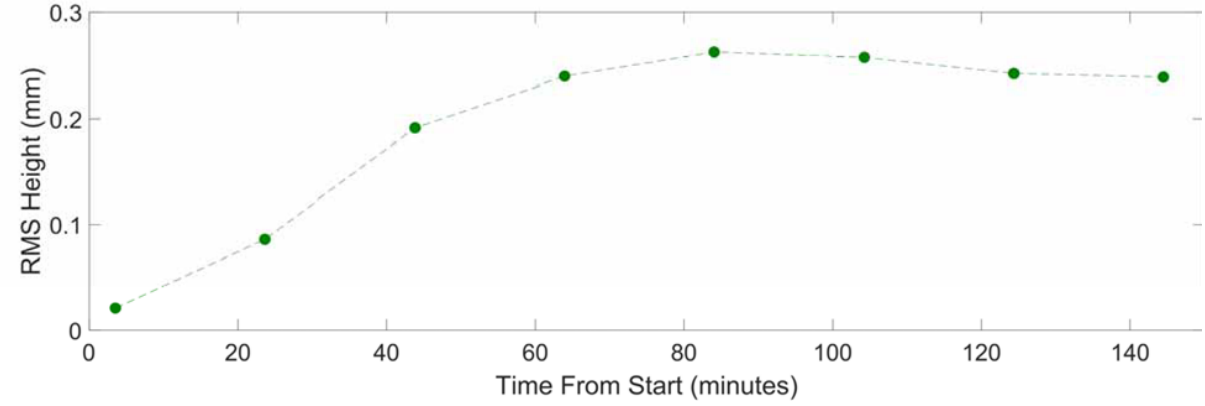

Figure 031820.10: Skewness Evolution

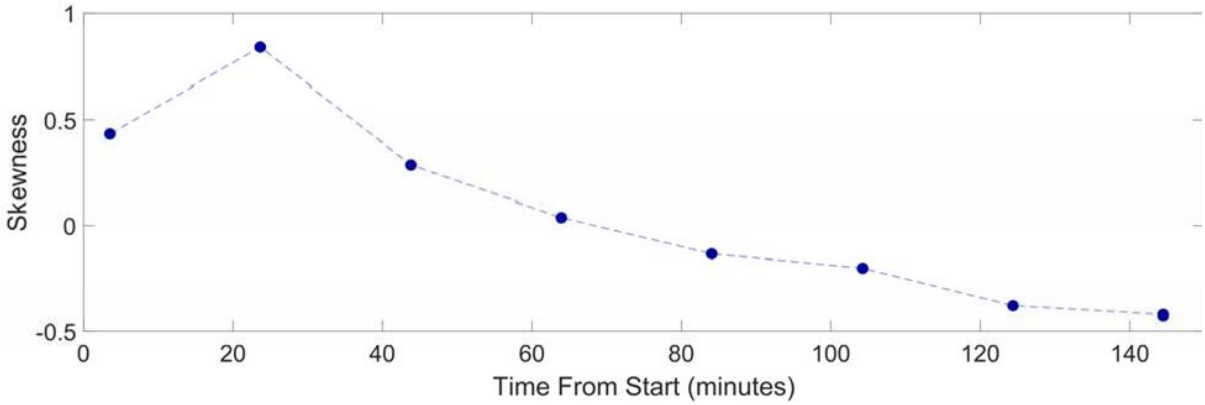

Figure 031820.11: Peak to Valley Evolution

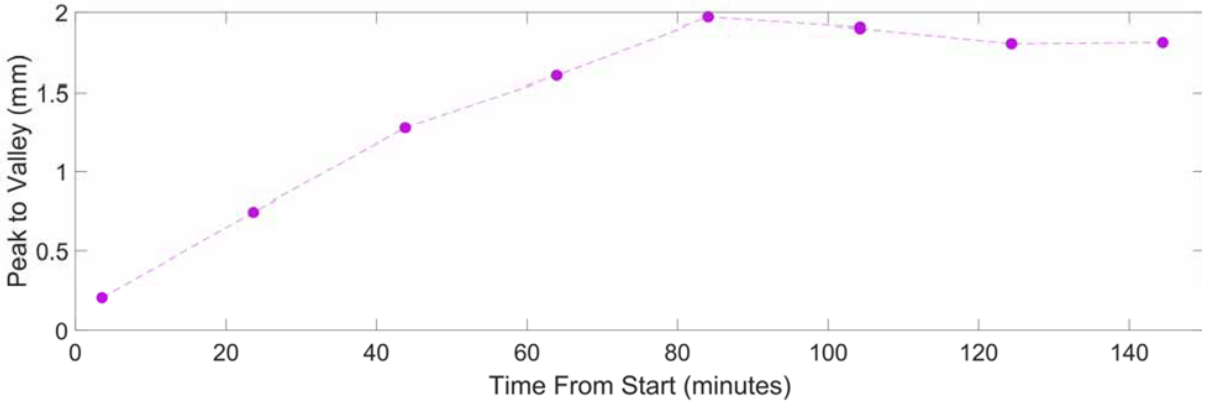

Figure 031820.12: Equivalent Roughness Evolution

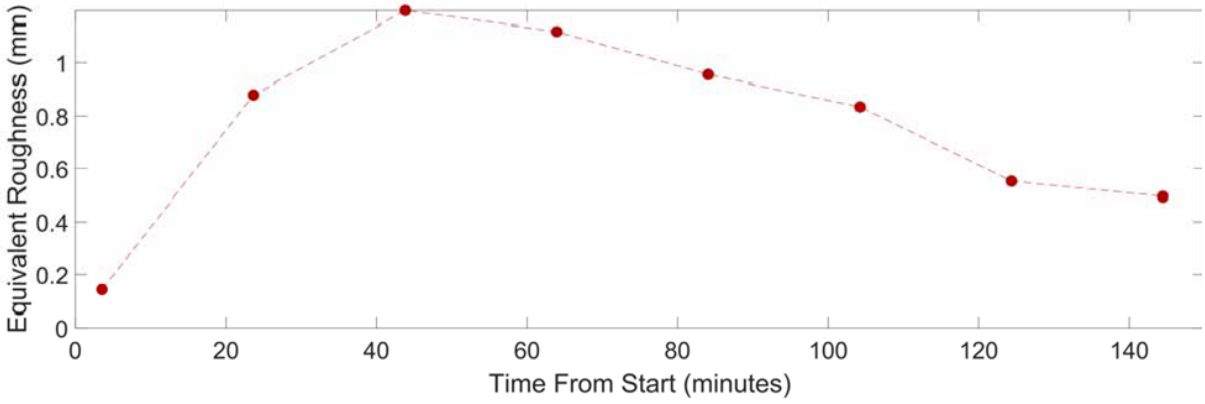

Table 031820.02: Summary of Roughness Parameters

Time (min.)	RMS (mm)	Skewness	Peak to Valley (mm)	ks,Flack-Schultz (mm)
3.5205	0.0197	0.4332	0.1986	0.1431
23.6372	0.0859	0.8454	0.7450	0.8807
43.8205	0.1915	0.2848	1.2777	1.1958
63.9372	0.2399	0.0380	1.6043	1.1185
84.0539	0.2632	-0.1349	1.9705	0.9560
104.2539	0.2580	-0.2044	1.9041	0.8356
124.3705	0.2425	-0.3844	1.8076	0.5527
144.4705	0.2391	-0.4260	1.8164	0.4951

Figure 031820.13: Frost Topography at 00:03:31

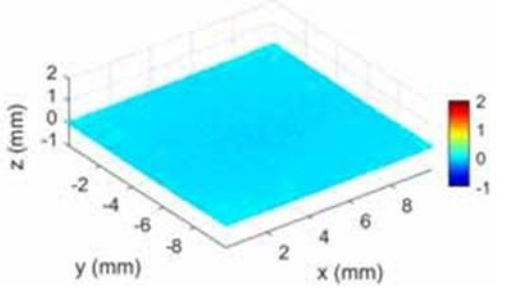

Figure 031820.14: Frost Topography at 00:23:38

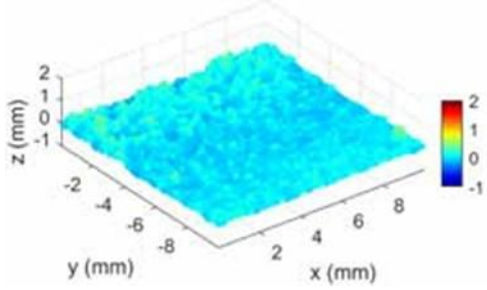

Figure 031820.15: Frost Topography at 00:43:49

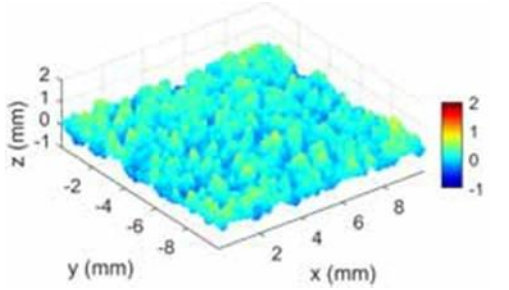

Figure 031820.16: Frost Topography at 01:03:56

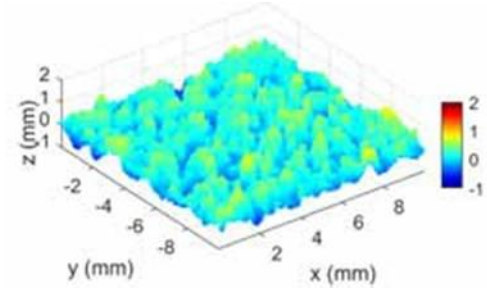

Figure 031820.17: Frost Topography at 01:24:03

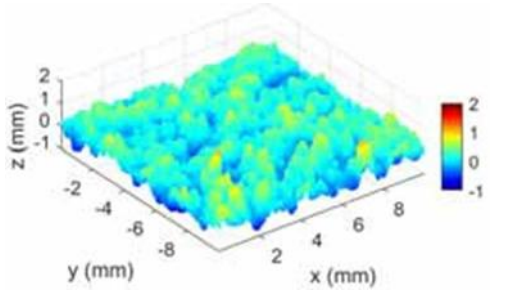

Figure 031820.18: Frost Topography at 01:44:15

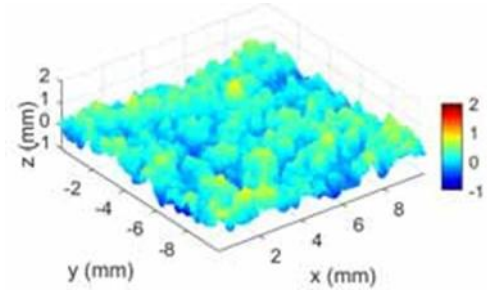

Figure 031820.09: Frost Topography at 02:04:22

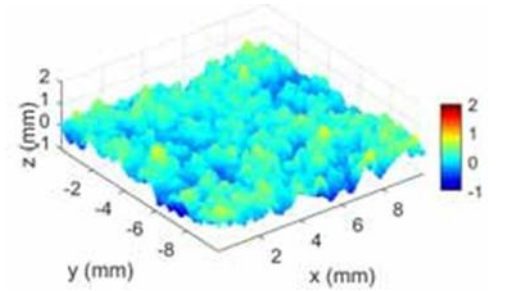

Figure 031820.20: Frost Topography at 02:24:28

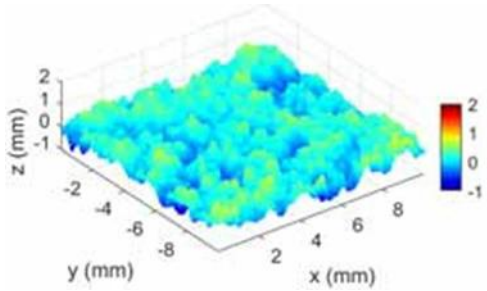

CAFF Conditions Report – Case Date: 032020

Table 032020.01: Summary of Measured Test Variables

Variable	Mean	St. Dev.	Rand. Unc.
T_air (C)	4.2377	0.3224	0.0103
Rh (%)	80.7354	5.0584	0.1620
Omega (kg_v/kg_da)	0.00413747	0.00032933	0.00001055
V_air (m/s)	1.3786	0.0783	0.0025
T_skin (C)	-10.9273	0.7976	0.0255
T_floor (C)	-20.4215	0.1060	0.0034

Figure 032020.01: Temperature and Voltage Control Time History

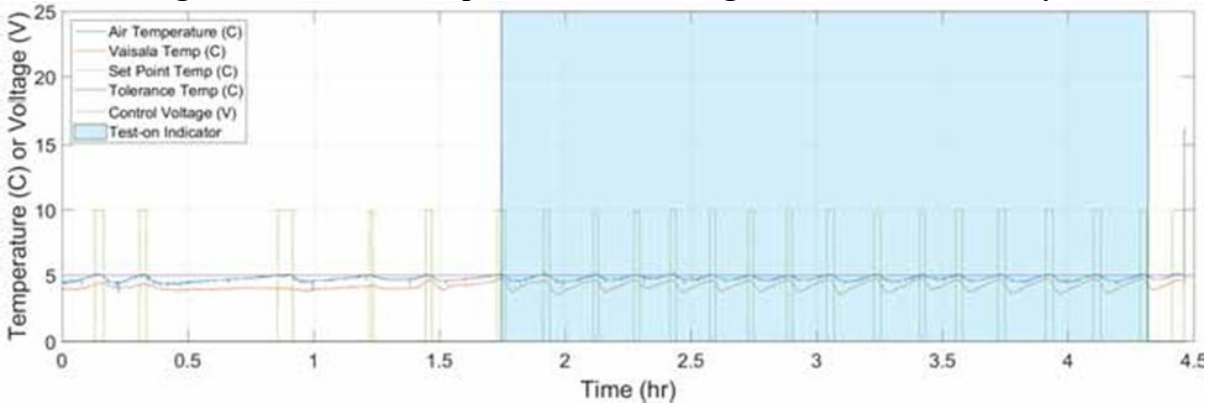

Figure 032020.02: Relative Humidity Time History

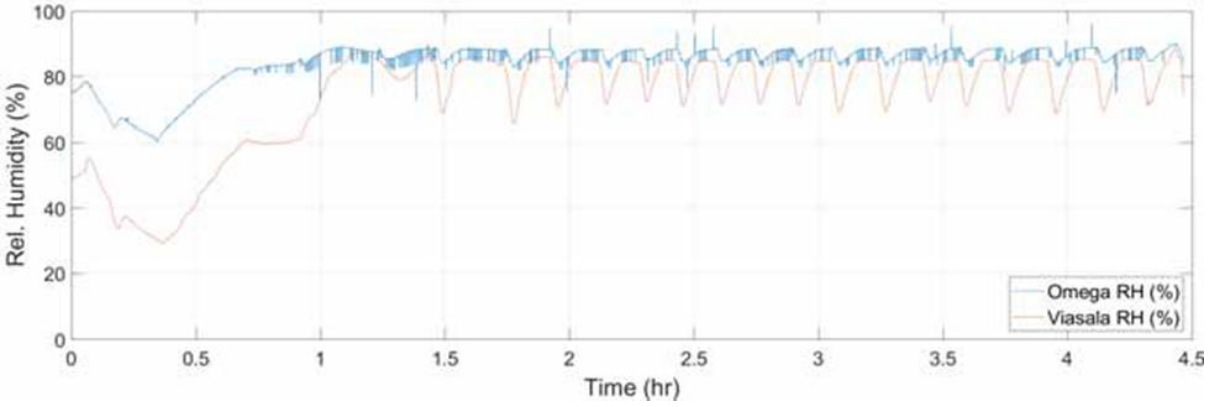

Figure 032020.03: Velocity Time History

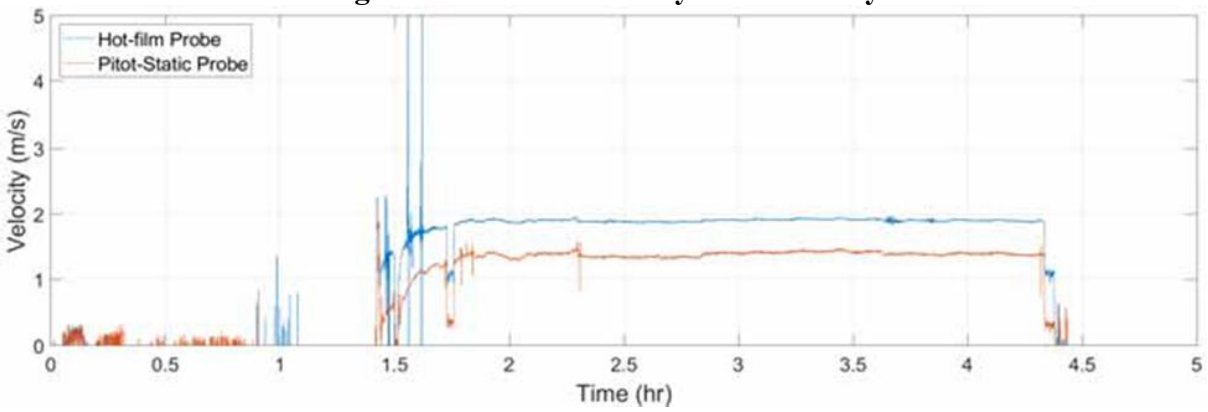

Figure 032020.04: Coolant Return Temperature Time History

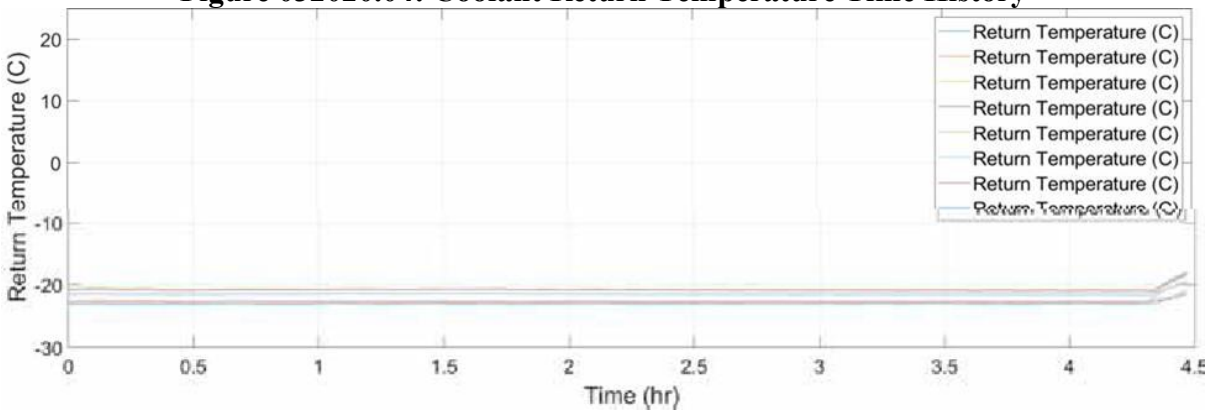

Figure 032020.05: Coolant Supply Temperature Time History

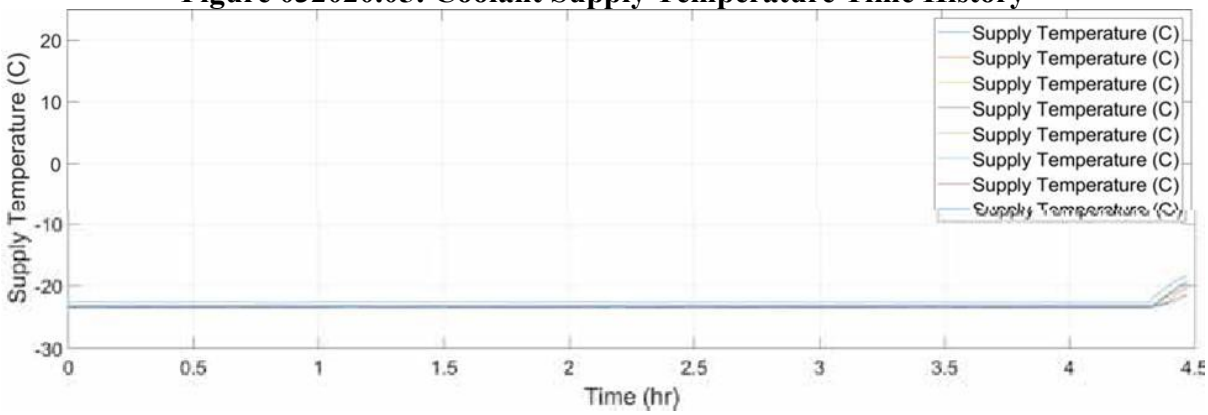

Figure 032020.06: Skin Temperature Time History

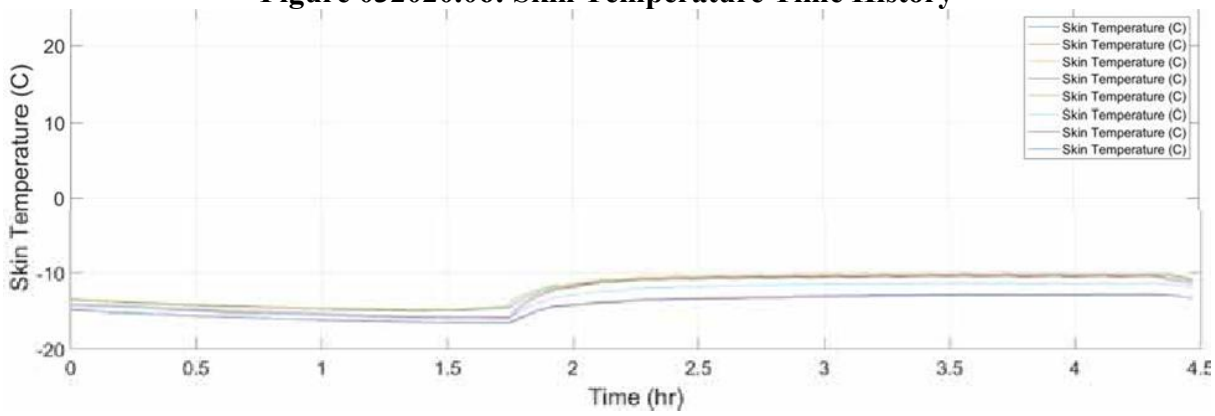

Figure 032020.07: Floor Temperature Time History

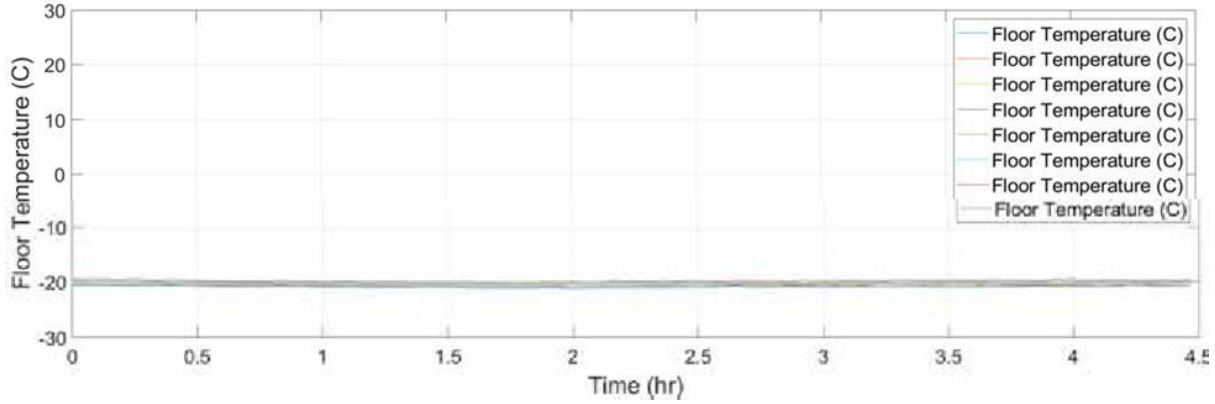

Figure 032020.08: Skin Temperature Slope Time History

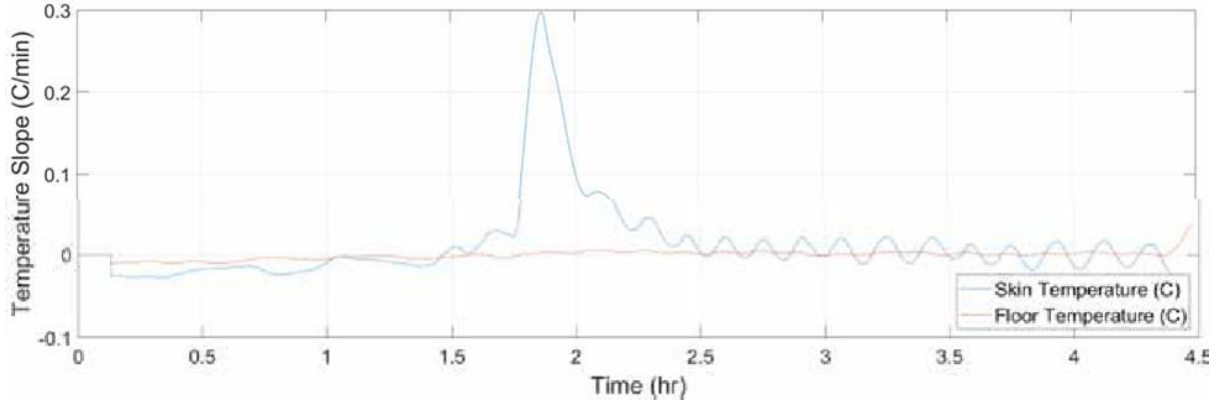

Figure 032020.09: RMS Height Evolution

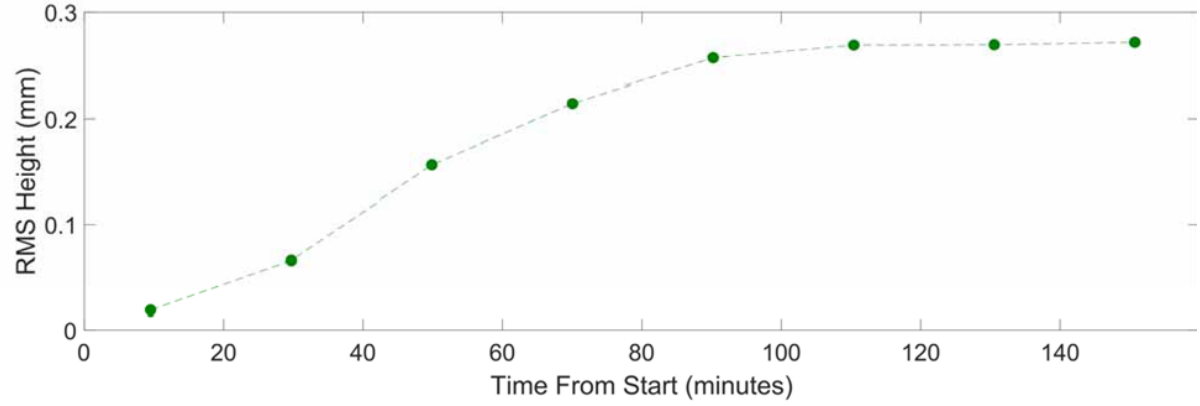

Figure 032020.10: Skewness Evolution

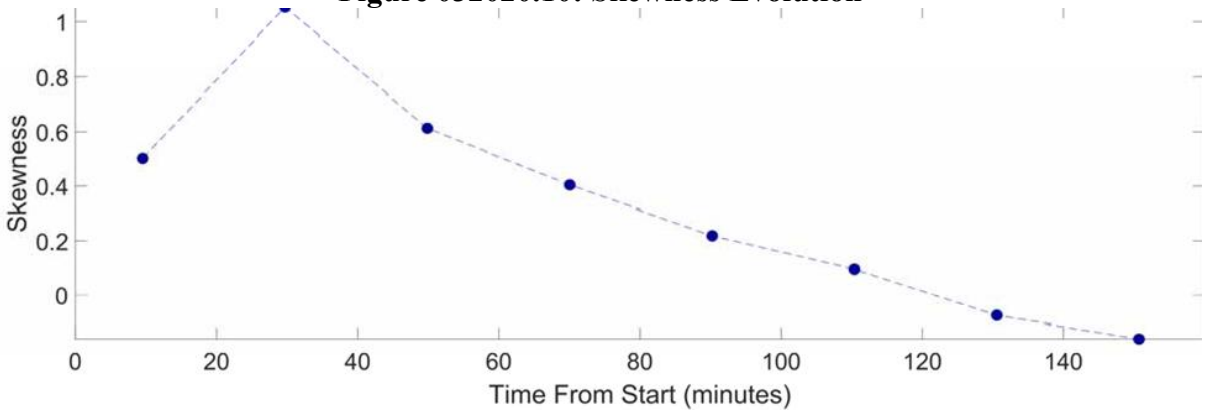

Figure 032020.11: Peak to Valley Evolution

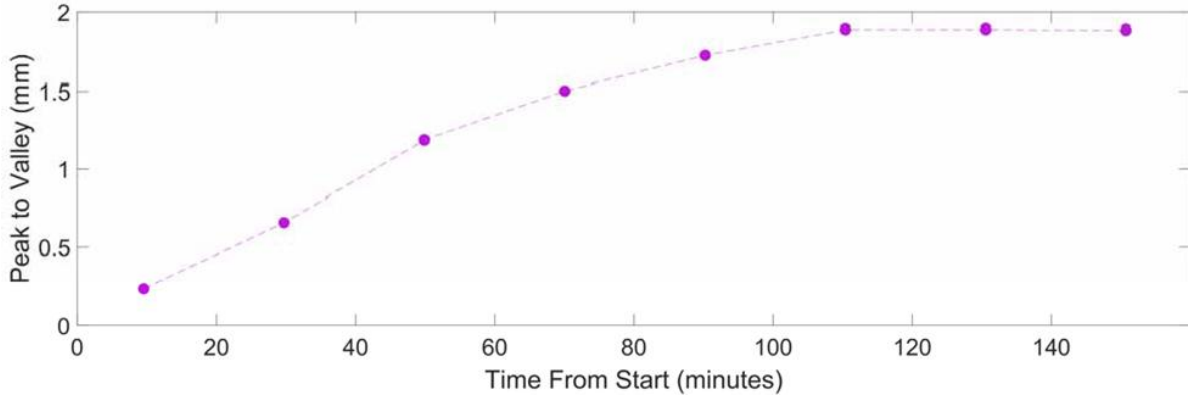

Figure 032020.12: Equivalent Roughness Evolution

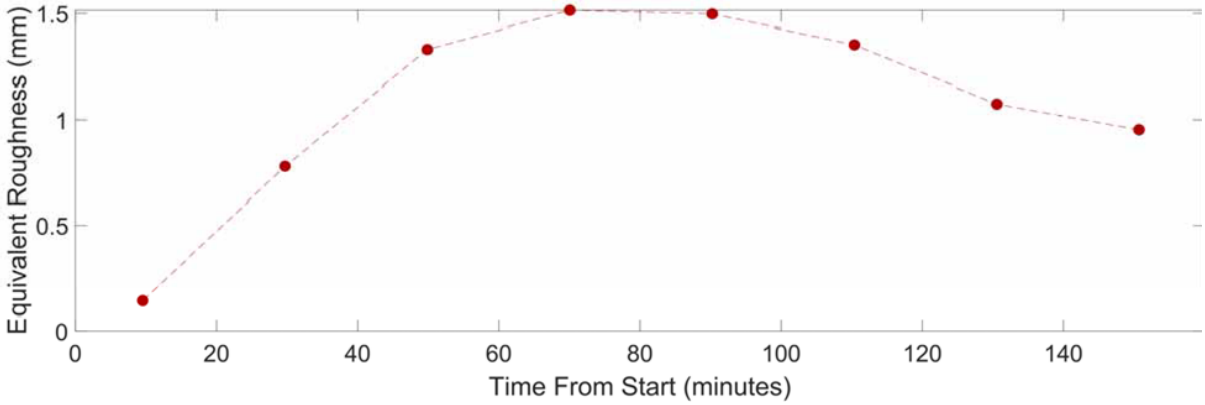

Table 032020.02: Summary of Roughness Parameters

Time (min.)	RMS (mm)	Skewness	Peak to Valley (mm)	ks,Flack-Schultz (mm)
9.5160	0.0181	0.5027	0.2280	0.1402
29.6993	0.0656	1.0543	0.6568	0.7795
49.8660	0.1562	0.6134	1.1857	1.3322
70.0493	0.2148	0.4042	1.5024	1.5153
90.2327	0.2578	0.2188	1.7280	1.4980
110.3993	0.2699	0.0953	1.8934	1.3544
130.5660	0.2703	-0.0751	1.8937	1.0758
150.7327	0.2727	-0.1591	1.8891	0.9527

Figure 032020.13: Frost Topography at 00:09:30

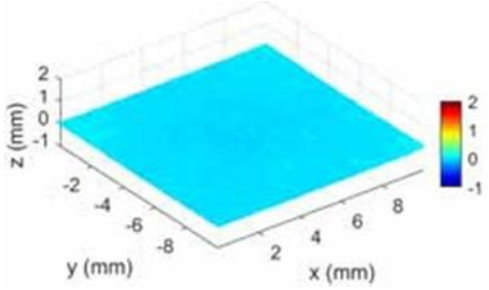

Figure 032020.14: Frost Topography at 00:29:41

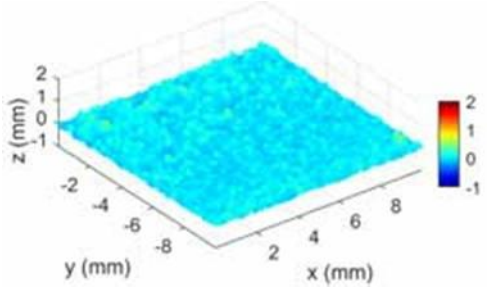

Figure 032020.15: Frost Topography at 00:49:51

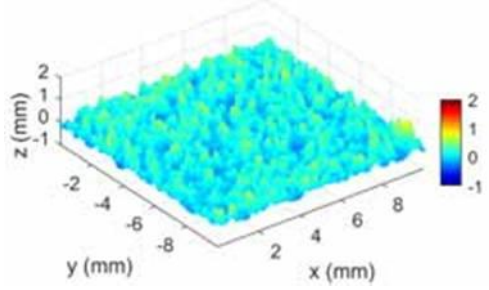

Figure 032020.16: Frost Topography at 01:10:02

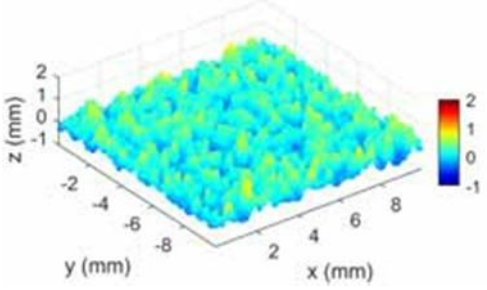

Figure 032020.17: Frost Topography at 01:30:13

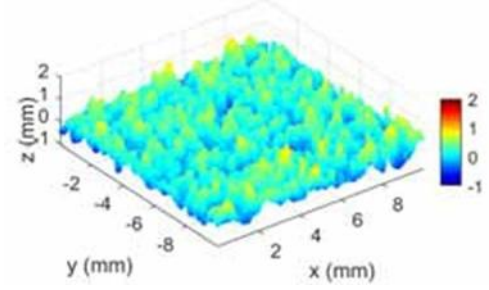

Figure 032020.18: Frost Topography at 01:50:23

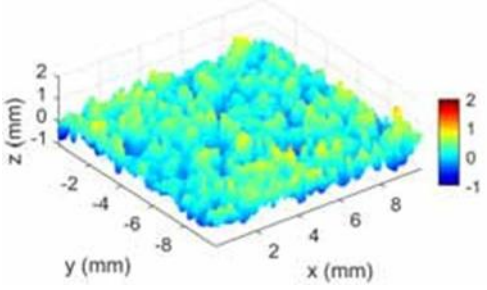

Figure 032020.19: Frost Topography at 02:10:33

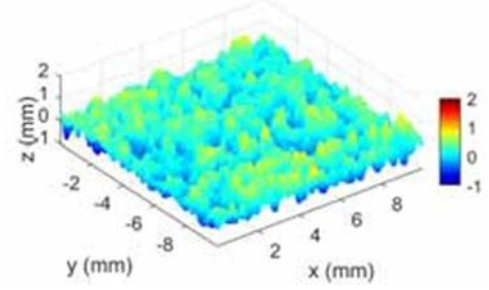

Figure 032020.20: Frost Topography at 02:30:43

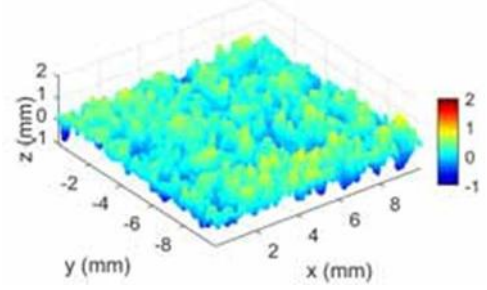

CAFF Conditions Report – Case Date: 032320

Table 032320.01: Summary of Measured Test Variables

Variable	Mean	St. Dev.	Rand. Unc.
T_air (C)	4.1560	0.1877	0.0062
Rh (%)	80.5539	5.2384	0.1717
Omega (kg_v/kg_da)	0.00414327	0.00030758	0.00001008
V_air (m/s)	0.2661	0.0778	0.0026
T_skin (C)	-12.5261	0.5299	0.0174
T_floor (C)	-20.5052	0.0264	0.0009

Figure 032320.01: Temperature and Voltage Control Time History

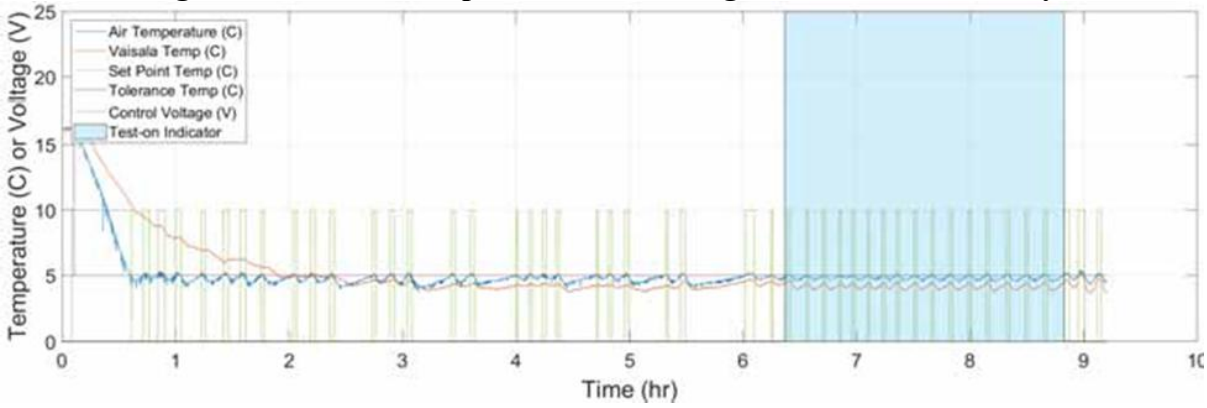

Figure 032320.02: Relative Humidity Time History

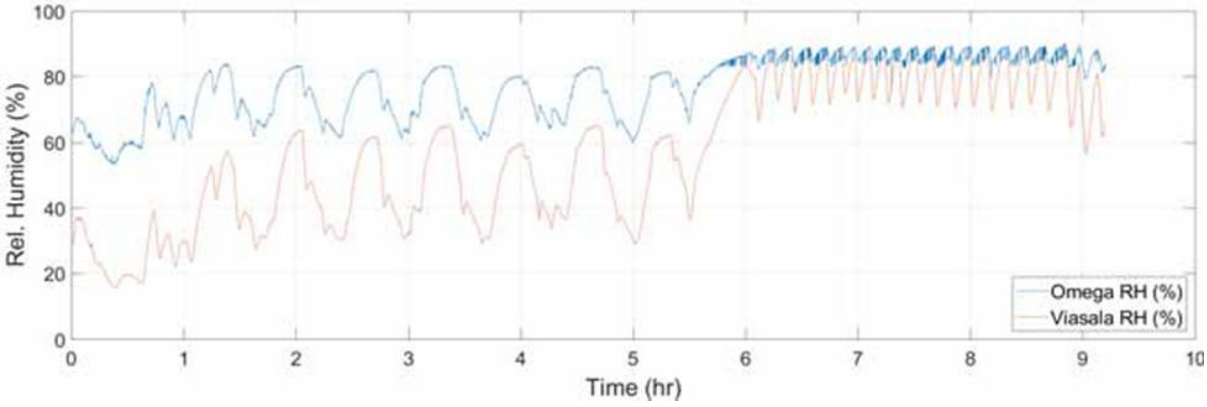

Figure 032320.03: Velocity Time History

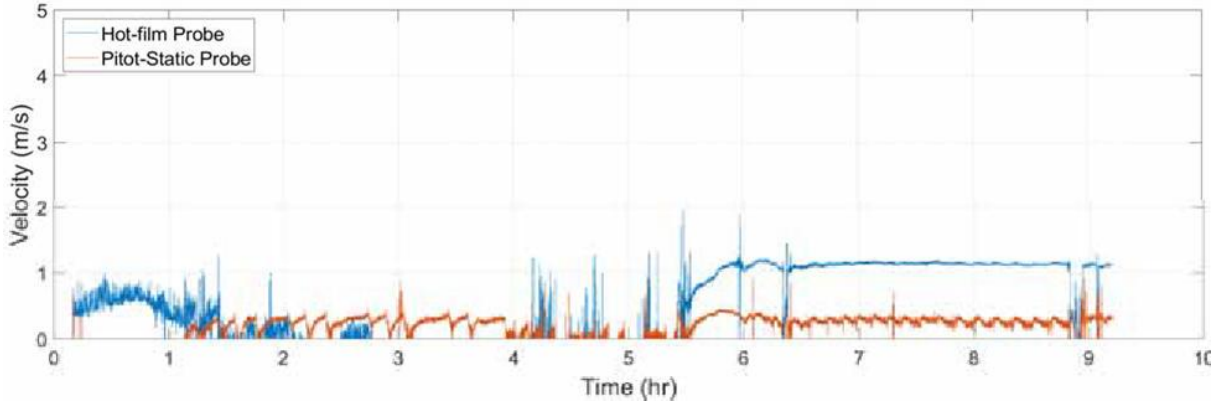

Figure 032320.04: Coolant Return Temperature Time History

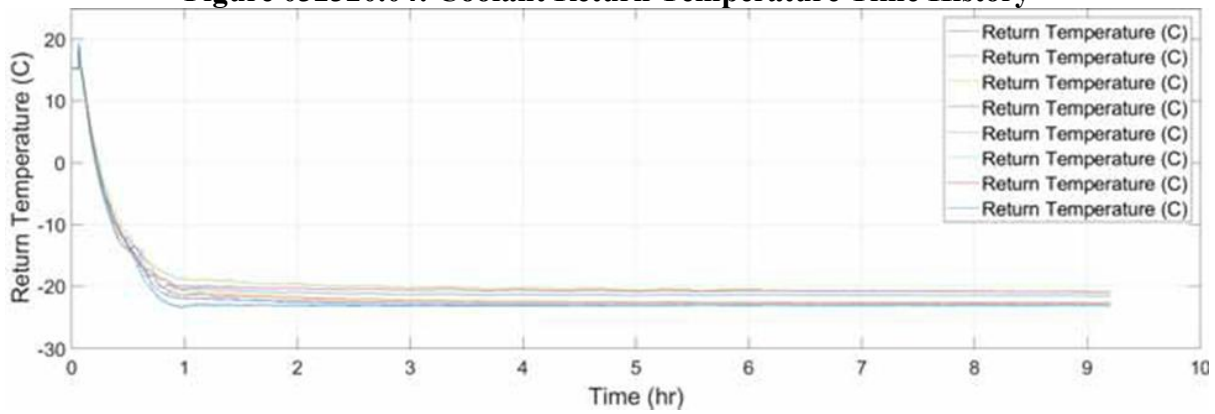

Figure 032320.05: Coolant Supply Temperature Time History

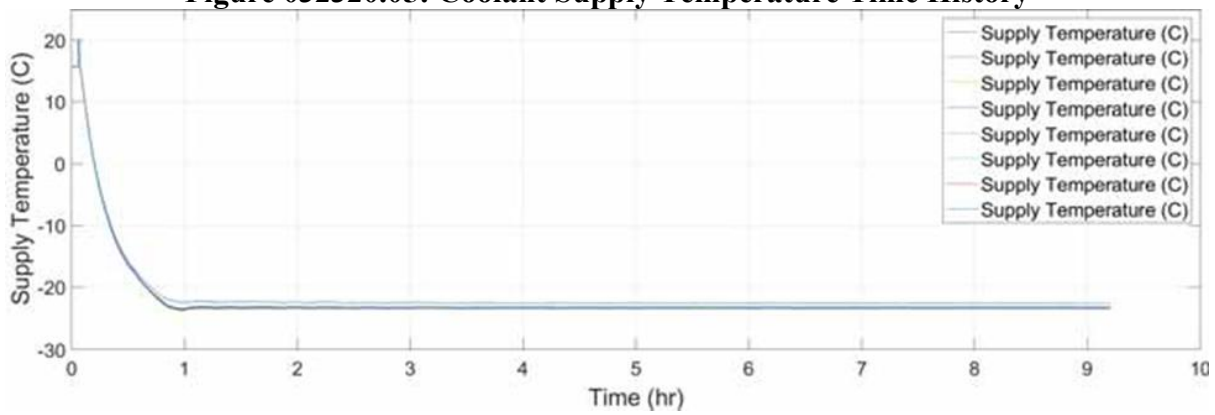

Figure 032320.06: Skin Temperature Time History

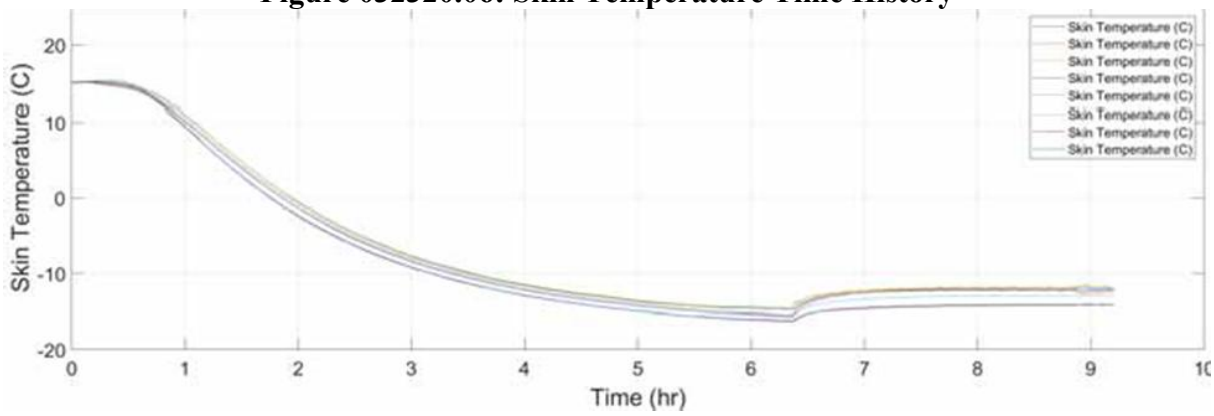

Figure 032320.07: Floor Temperature Time History

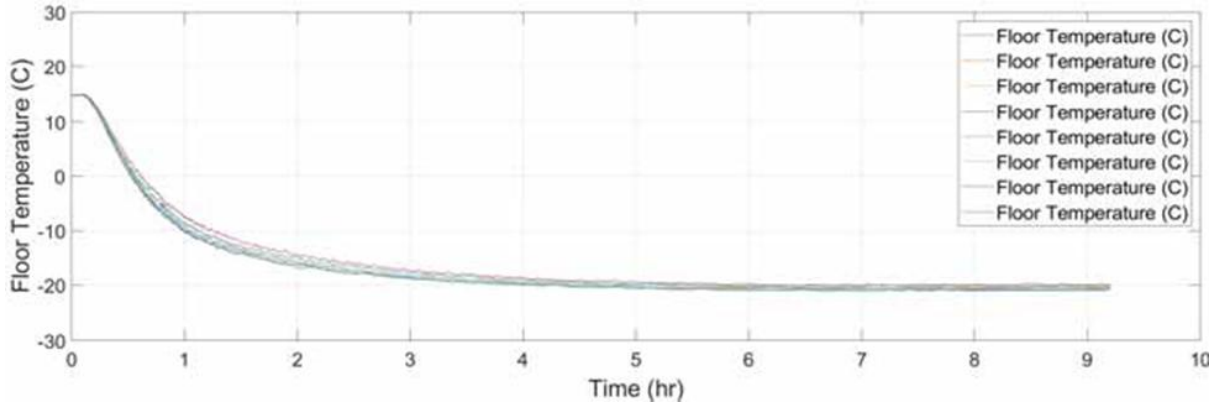

Figure 032320.08: Skin Temperature Slope Time History

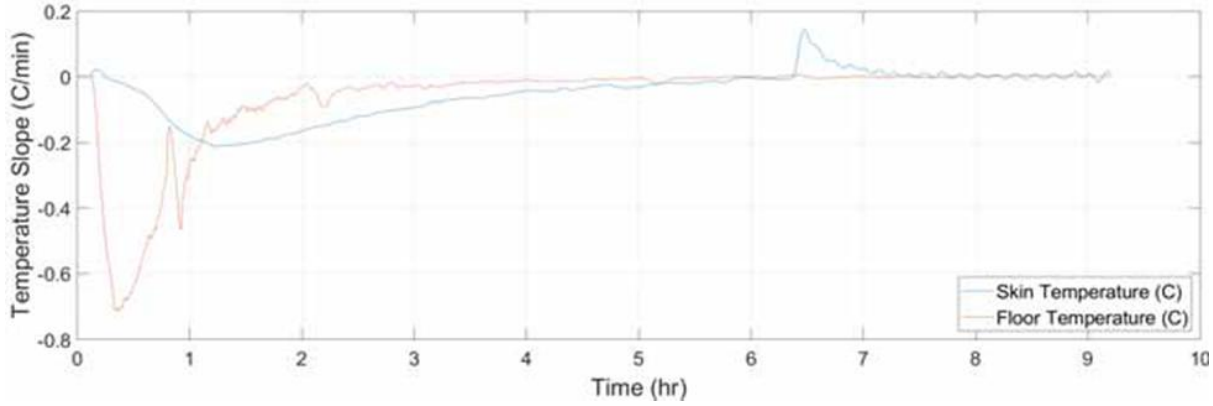

Figure 032320.09: RMS Height Evolution

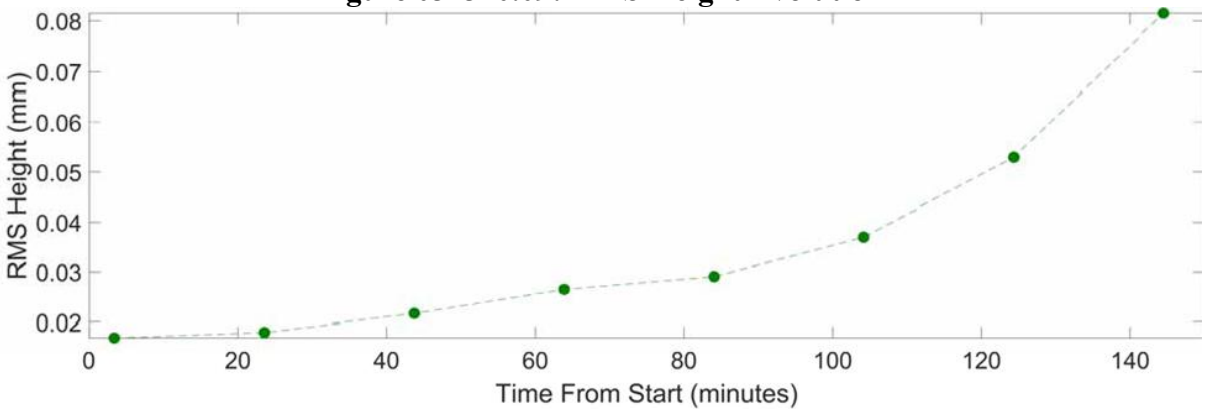

Figure 032320.10: Skewness Evolution

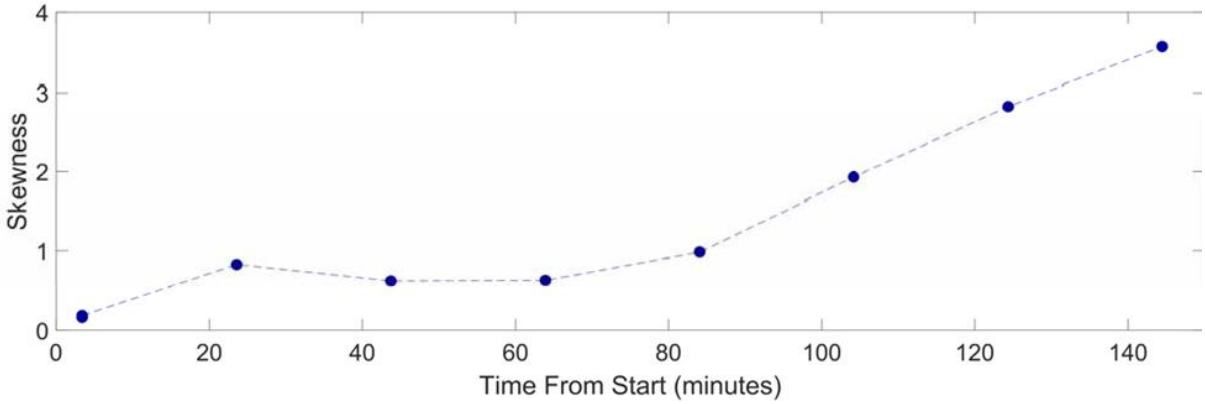

Figure 032320.11: Peak to Valley Evolution

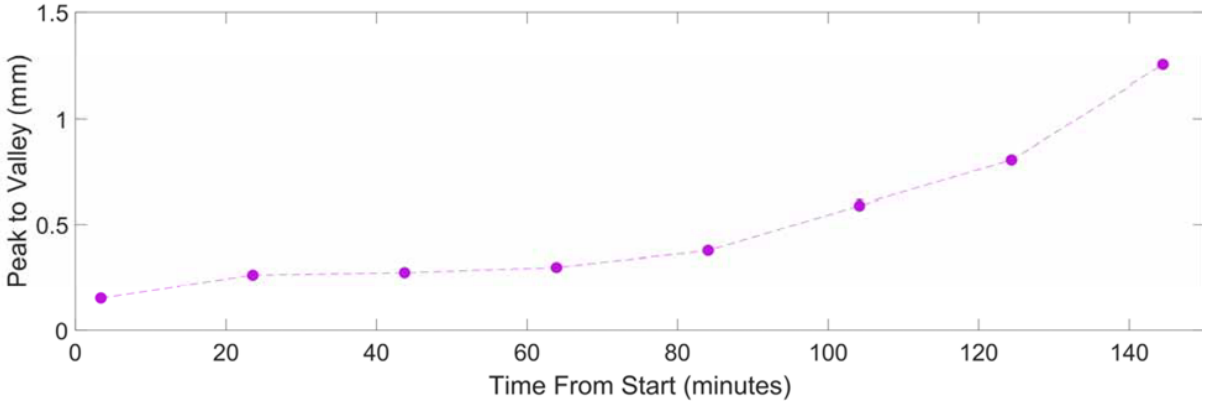

Figure 032320.12: Equivalent Roughness Evolution

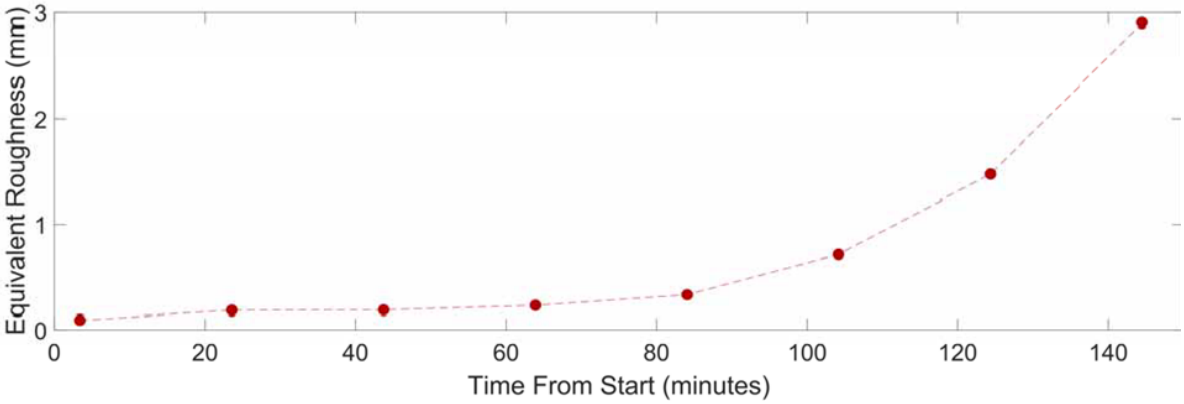

Table 032320.02: Summary of Roughness Parameters

Time (min.)	RMS (mm)	Skewness	Peak to Valley (mm)	ks,Flack-Schultz (mm)
3.3748	0.0169	0.1666	0.1476	0.0923
23.5581	0.0180	0.8236	0.2577	0.1813
43.7248	0.0216	0.6133	0.2693	0.1846
63.8914	0.0265	0.6202	0.2945	0.2272
84.0581	0.0291	0.9811	0.3752	0.3285
104.1581	0.0370	1.9266	0.5901	0.7140
124.3581	0.0530	2.8249	0.8040	1.4747
144.4748	0.0815	3.5796	1.2562	2.9049

Figure 032320.13: Frost Topography at 00:03:22

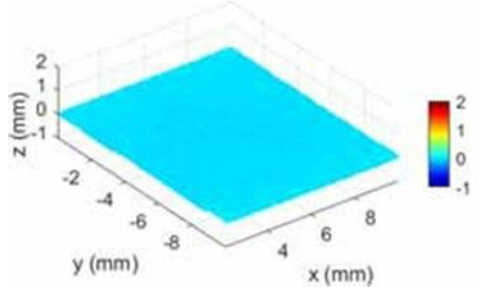

Figure 032320.14: Frost Topography at 00:23:33

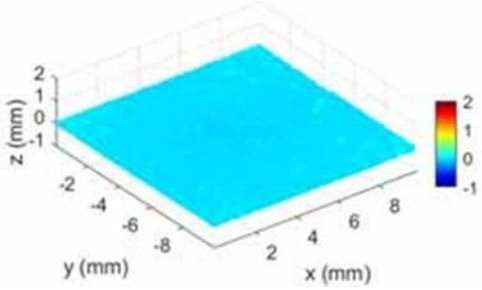

Figure 032320.15: Frost Topography at 00:43:43

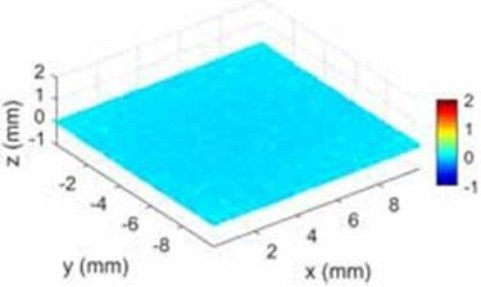

Figure 032320.16: Frost Topography at 01:03:53

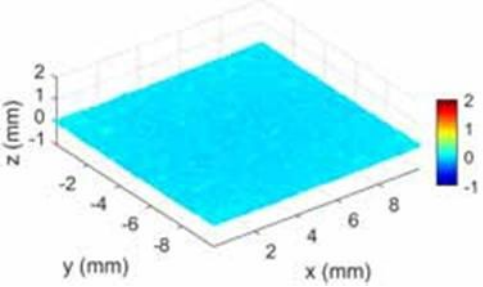

Figure 032320.17: Frost Topography at 01:24:03

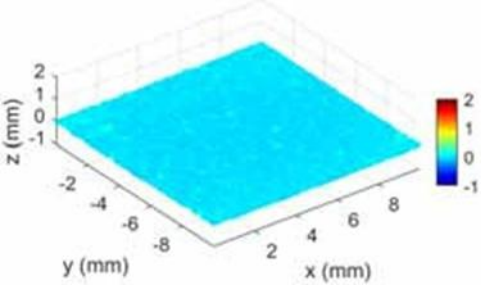

Figure 032320.18: Frost Topography at 01:44:09

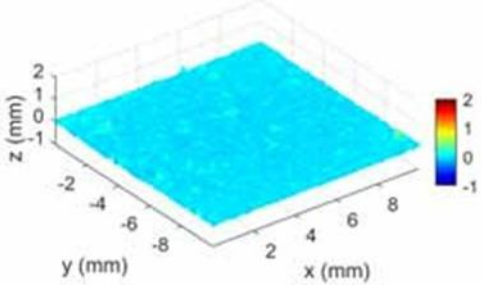

Figure 032320.19: Frost Topography at 02:04:21

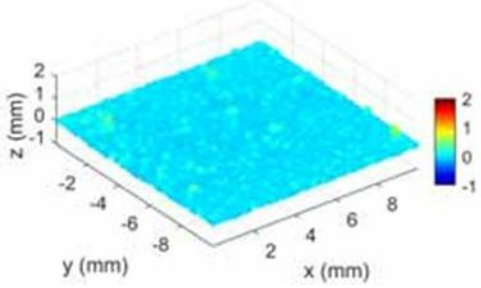

Figure 032320.20: Frost Topography at 02:24:28

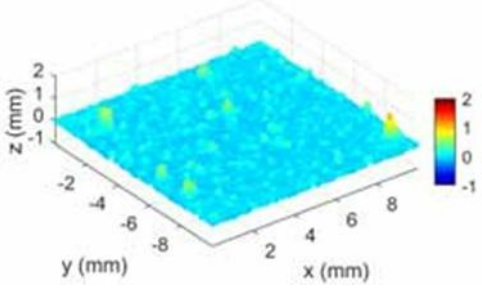

CAFF Conditions Report – Case Date: 072920

Table 072920.01: Summary of Measured Test Variables

Variable	Mean	St. Dev.	Rand. Unc.
T_air (C)	14.9960	0.4070	0.0135
Rh (%)	80.0273	2.4284	0.0803
Omega (kg_v/kg_da)	0.00863373	0.00035212	0.00001165
V_air (m/s)	0.2120	0.1427	0.0047
T_skin (C)	-11.1800	0.8955	0.0296
T_floor (C)	-19.4126	0.1520	0.0050

Figure 072920.01: Temperature and Voltage Control Time History

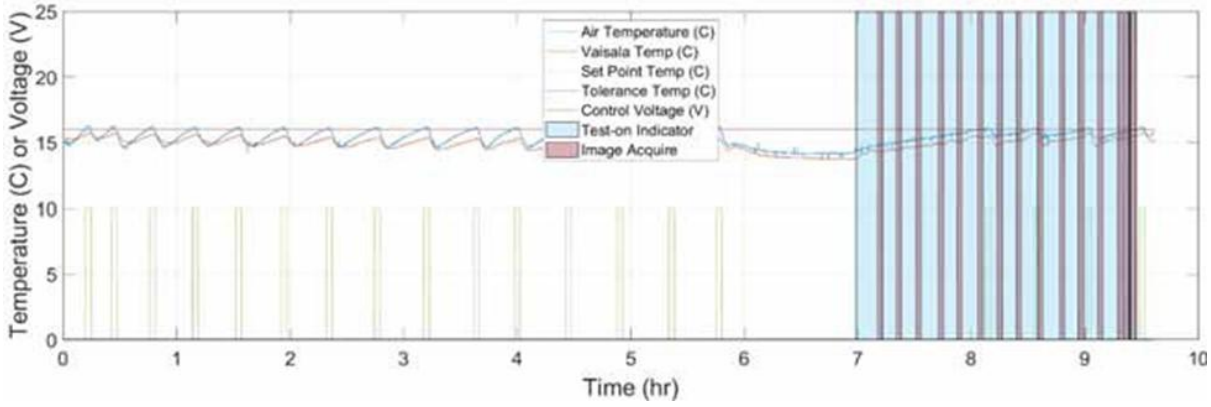

Figure 072920.02: Relative Humidity Time History

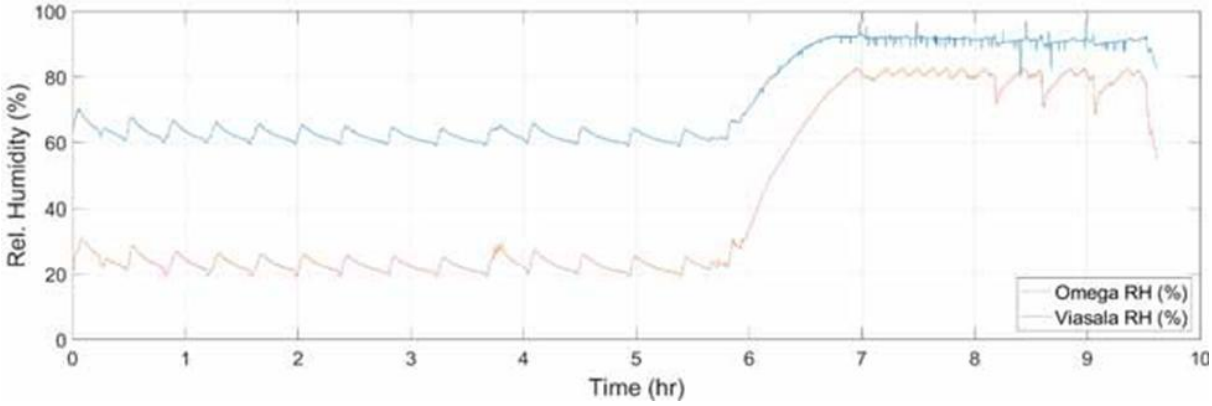

Figure 072920.03: Velocity Time History

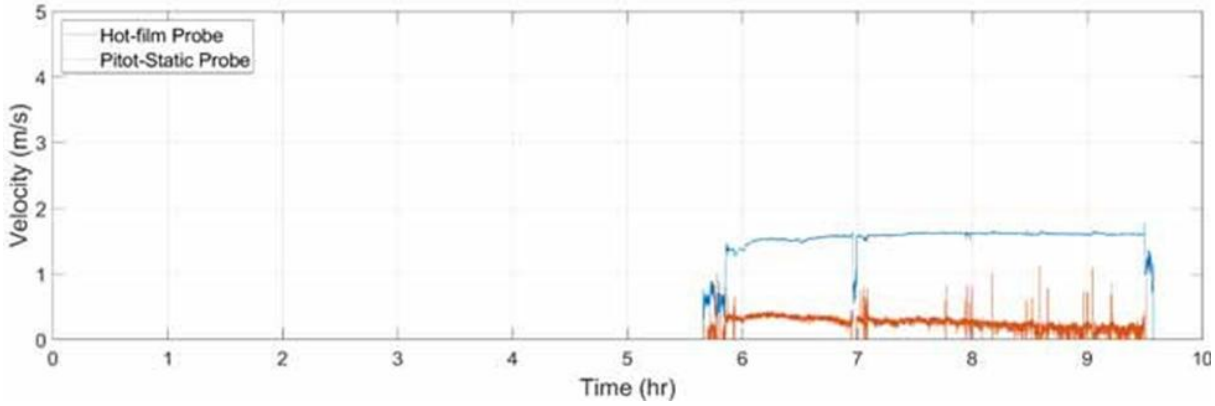

Figure 072920.04: Coolant Return Temperature Time History

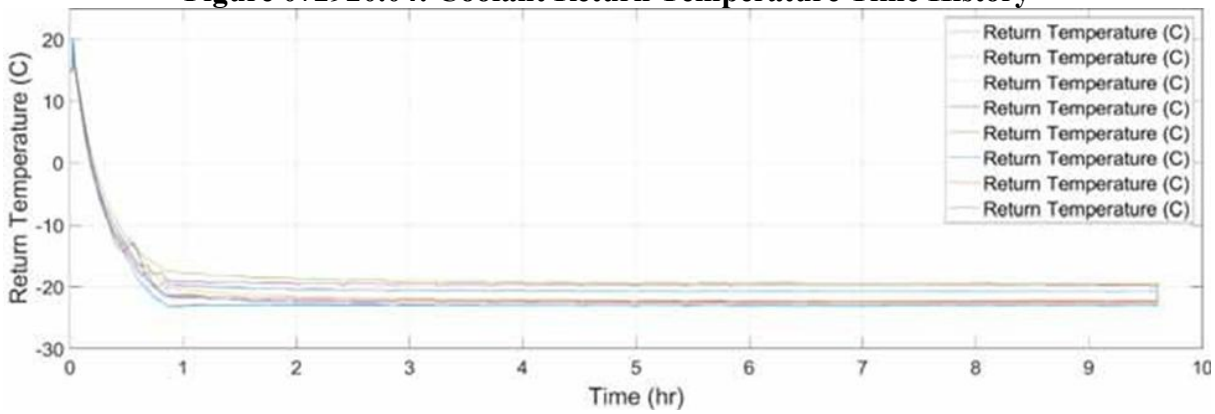

Figure 072920.05: Coolant Supply Temperature Time History

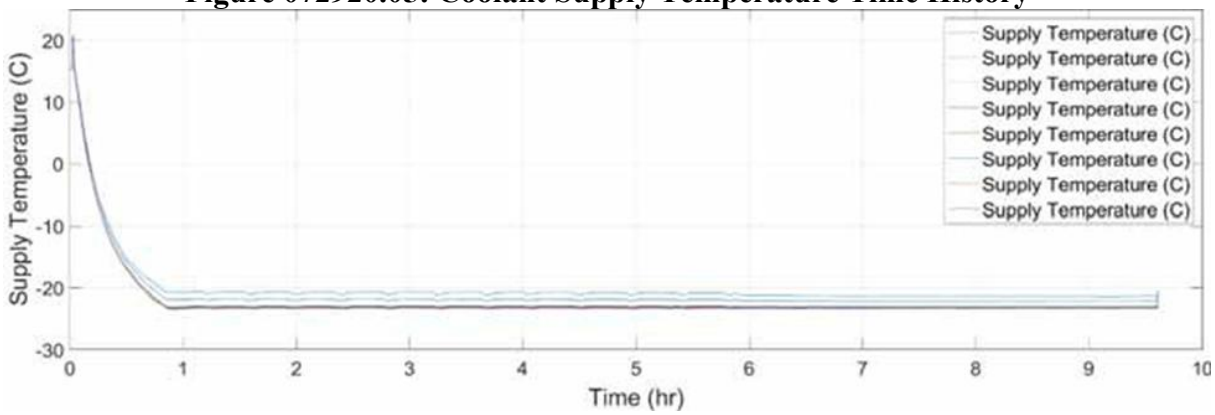

Figure 072920.06: Skin Temperature Time History

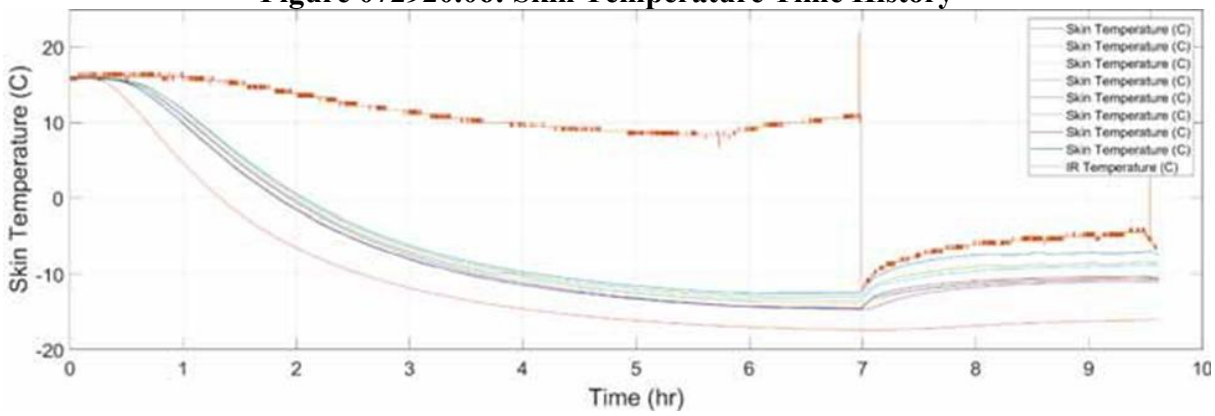

Figure 072920.07: Floor Temperature Time History

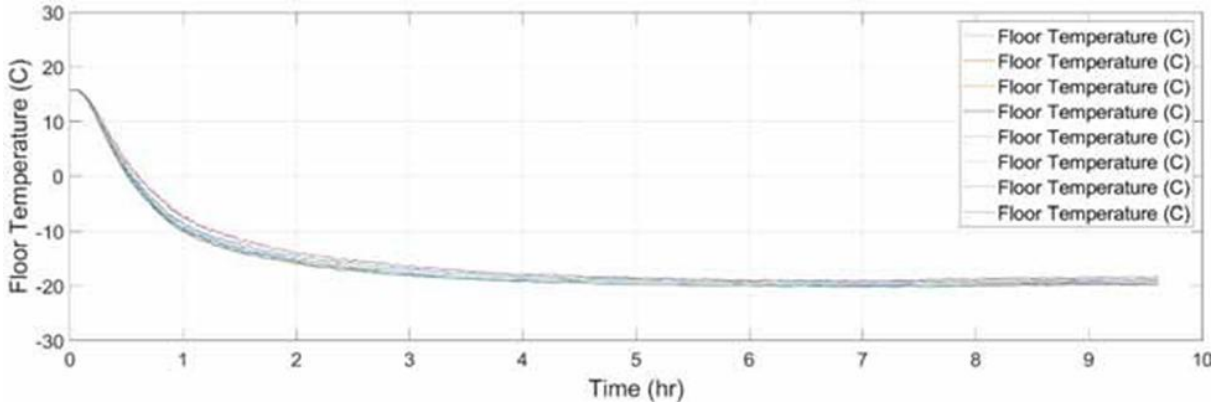

Figure 072920.08: Skin Temperature Slope Time History

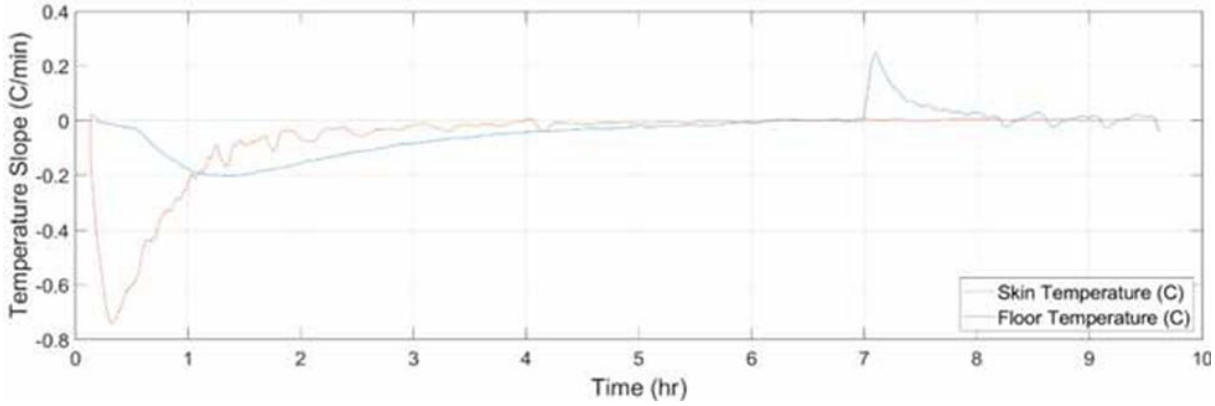

Figure 0729200.09: RMS Height Evolution

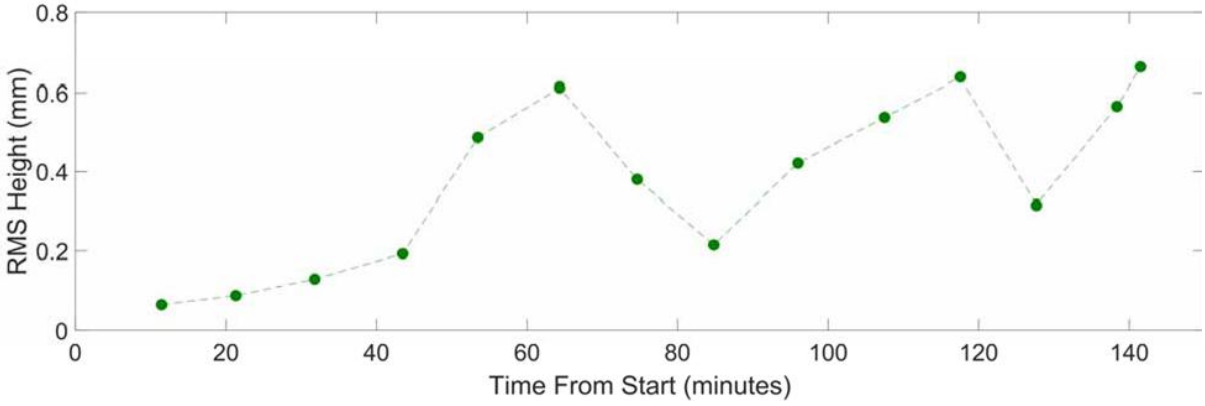

Figure 0729200.10: Skewness Evolution

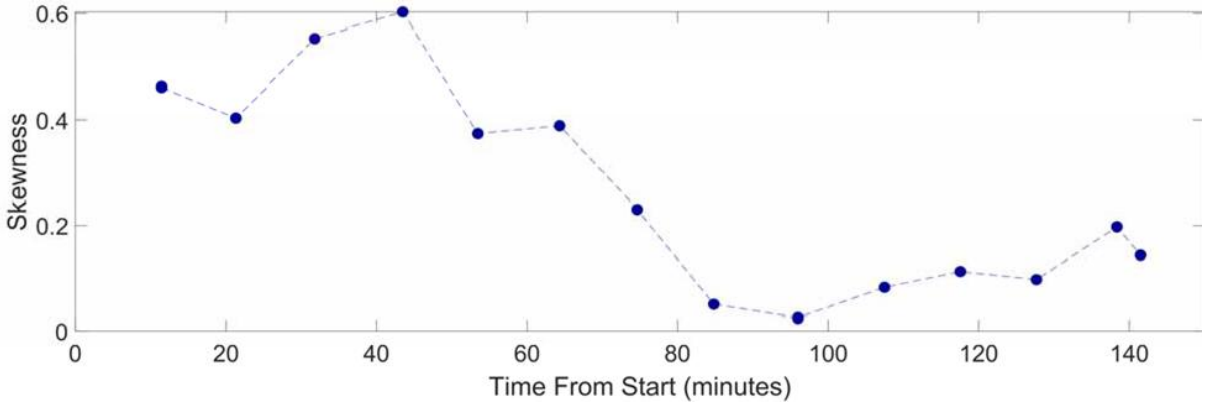

Figure 0729200.11: Peak to Valley Evolution

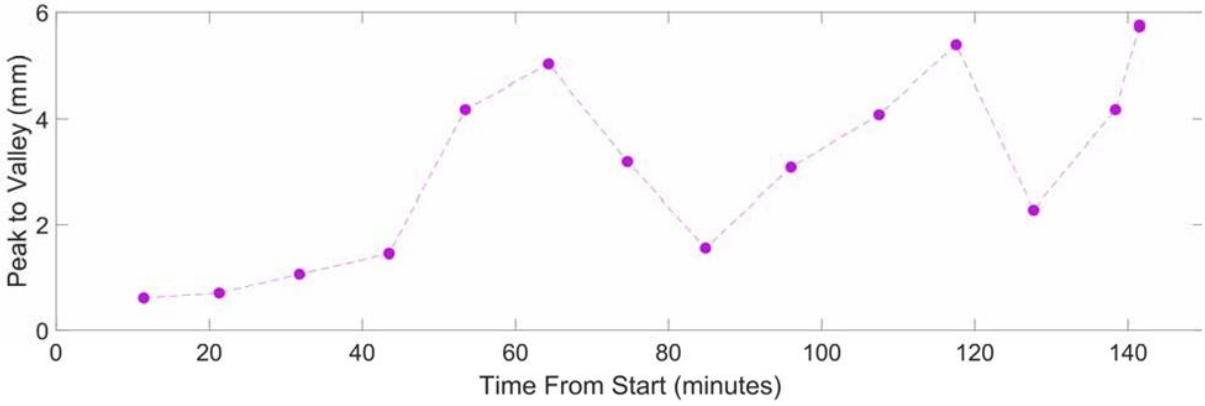

Figure 0729200.12: Equivalent Roughness Evolution

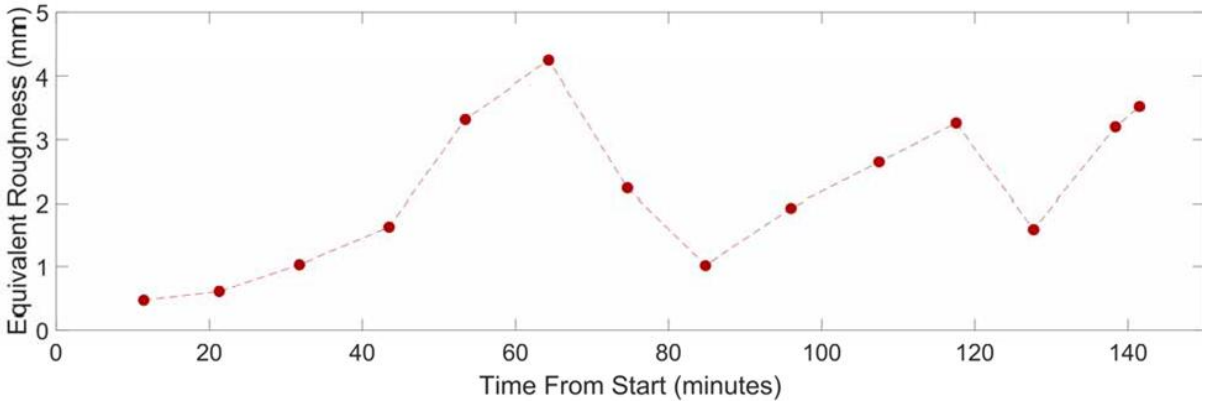

Table 072920.02: Summary of Roughness Parameters

Time (min.)	RMS (mm)	Skewness	Peak to Valley (mm)	ks,Flack-Schultz (mm)
11.4259	0.0613	0.4622	0.5922	0.4573
21.2926	0.0847	0.4035	0.6871	0.5971
31.7759	0.1269	0.5536	1.0515	1.0283
43.4759	0.1922	0.6031	1.4428	1.6255
53.4426	0.4860	0.3739	4.1833	3.3266
64.3259	0.6127	0.3889	5.0353	4.2571
74.6259	0.3796	0.2307	3.1893	2.2347
84.8092	0.2144	0.0492	1.5460	1.0143
95.9926	0.4213	0.0239	3.0819	1.9278
107.4926	0.5374	0.0818	4.0824	2.6512
117.5592	0.6379	0.1120	5.4039	3.2684
127.6759	0.3154	0.0964	2.2758	1.5851
138.3759	0.5656	0.1976	4.1803	3.2075
141.5092	0.6642	0.1434	5.7505	3.5352

Figure 072920.13: Frost Topography at 00:11:18

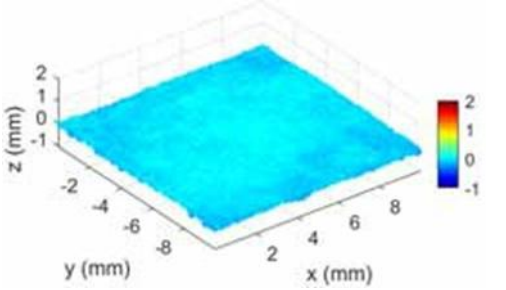

Figure 072920.14: Frost Topography at 00:21:10

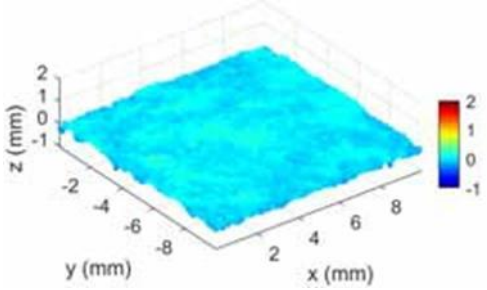

Figure 072920.15: Frost Topography at 00:31:39

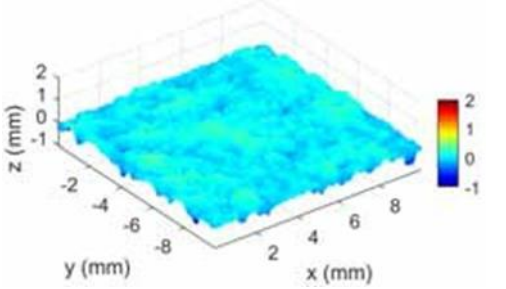

Figure 072920.16: Frost Topography at 00:43:21

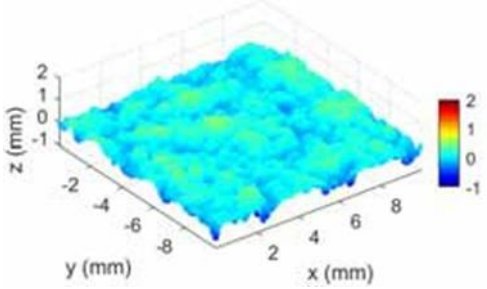

Figure 072920.17: Frost Topography at 00:53:19

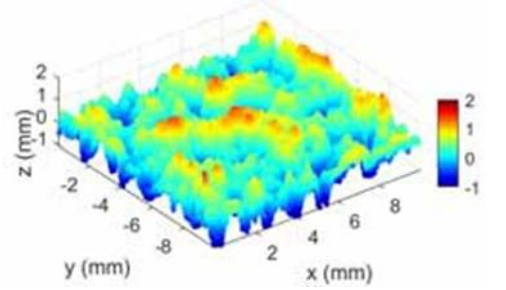

Figure 072920.18: Frost Topography at 01:04:12

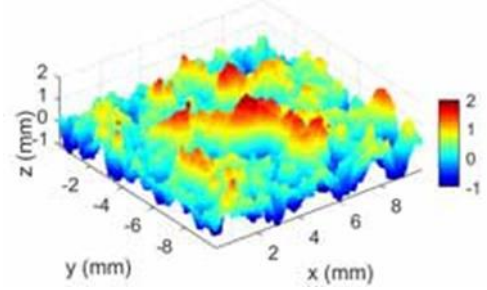

Figure 072920.19: Frost Topography at 01:14:30

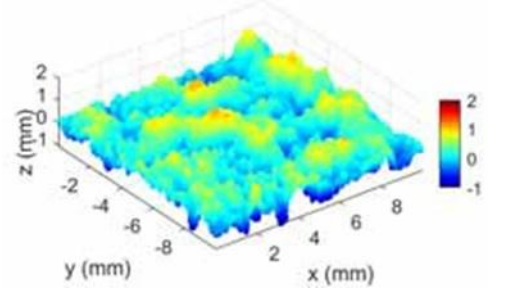

Figure 072920.20: Frost Topography at 01:24:41

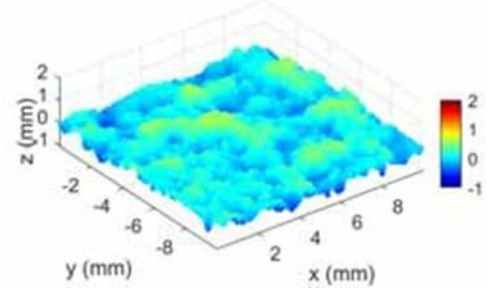

Figure 072920.21: Frost Topography at 01:35:52

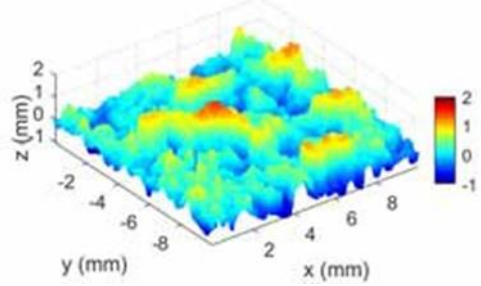

Figure 072920.22: Frost Topography at 01:47:22

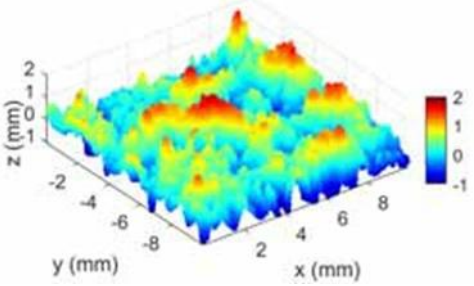

Figure 072920.23: Frost Topography at 01:57:26

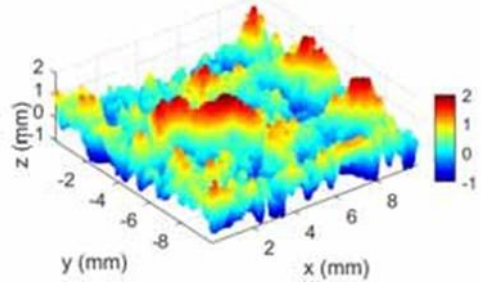

Figure 072920.24: Frost Topography at 02:07:33

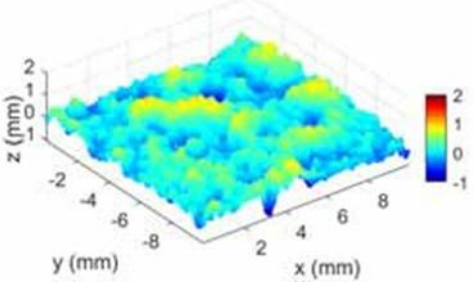

Figure 072920.25: Frost Topography at 02:18:15

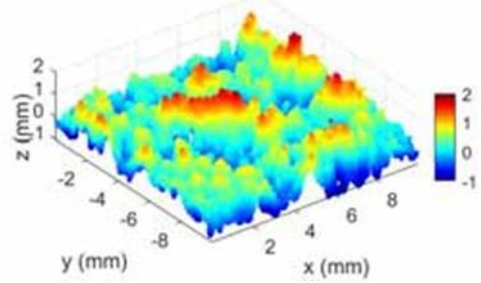

Figure 072920.26: Frost Topography at 02:21:23

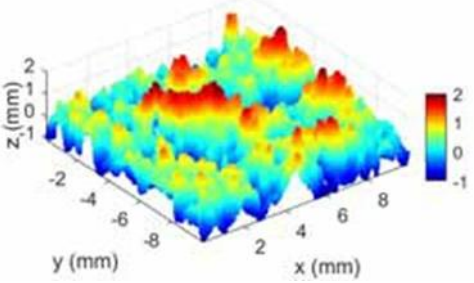

CAFF Conditions Report – Case Date: 080320

Table 080320.01: Summary of Measured Test Variables

Variable	Mean	St. Dev.	Rand. Unc.
T_air (C)	15.0701	0.4586	0.0153
Rh (%)	80.6998	1.8140	0.0605
Omega (kg_v/kg_da)	0.00872572	0.00035400	0.00001180
V_air (m/s)	1.2537	0.1066	0.0036
T_skin (C)	-9.4538	1.1220	0.0374
T_floor (C)	-19.1410	0.2061	0.0069

Figure 080320.01: Temperature and Voltage Control Time History

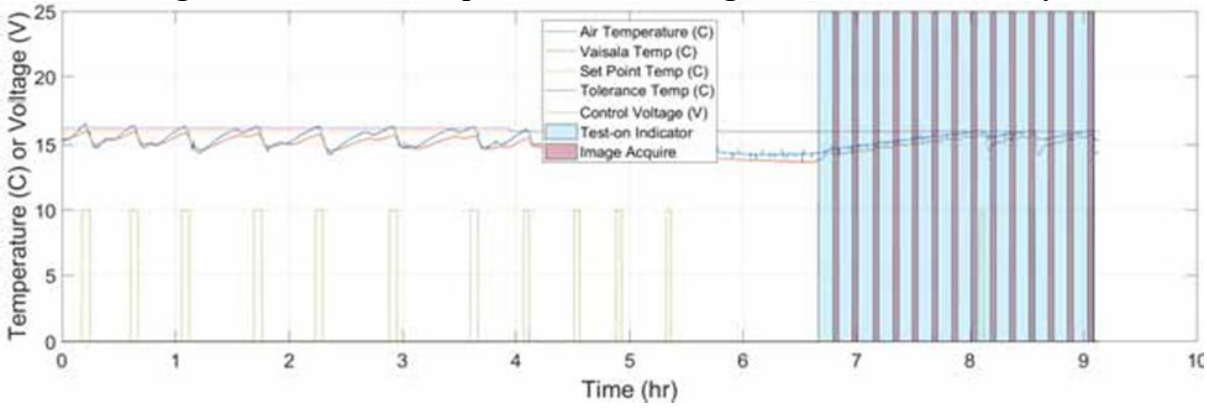

Figure 080320.02: Relative Humidity Time History

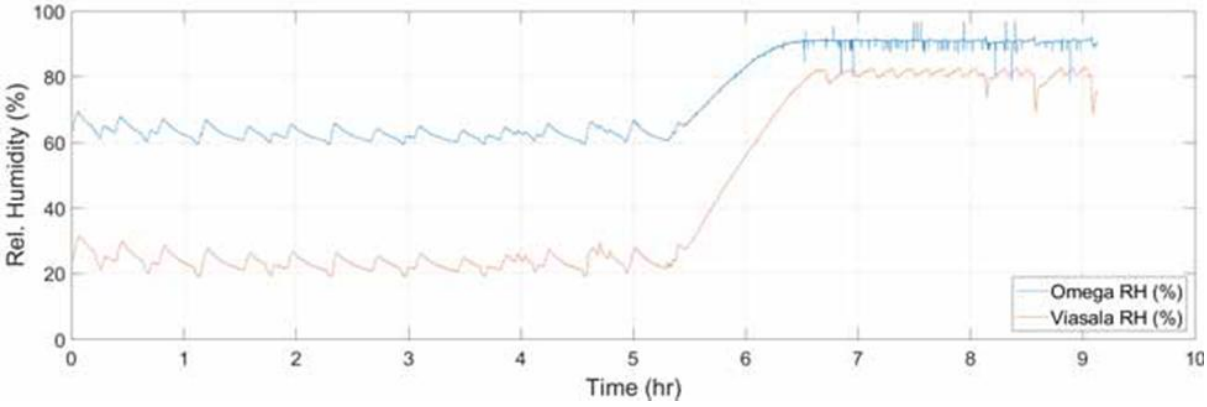

Figure 080320.03: Velocity Time History

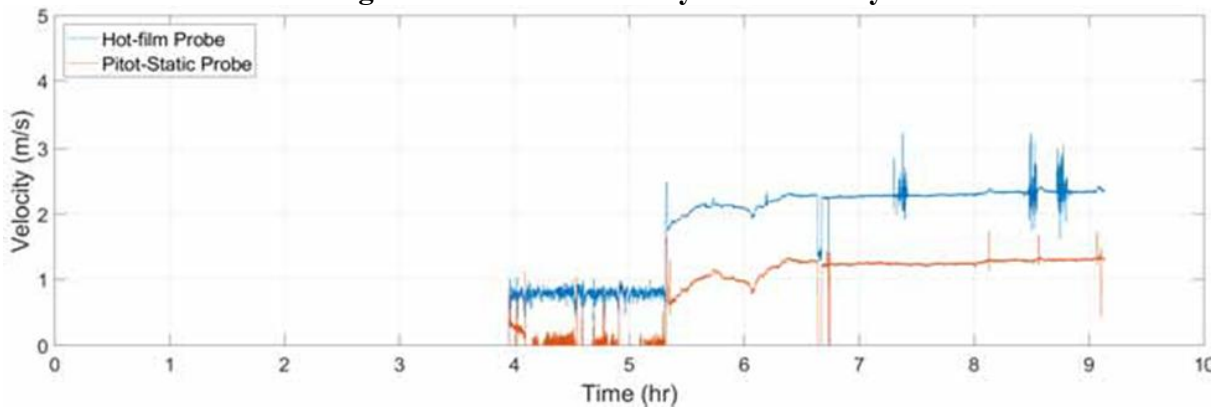

Figure 080320.04: Coolant Return Temperature Time History

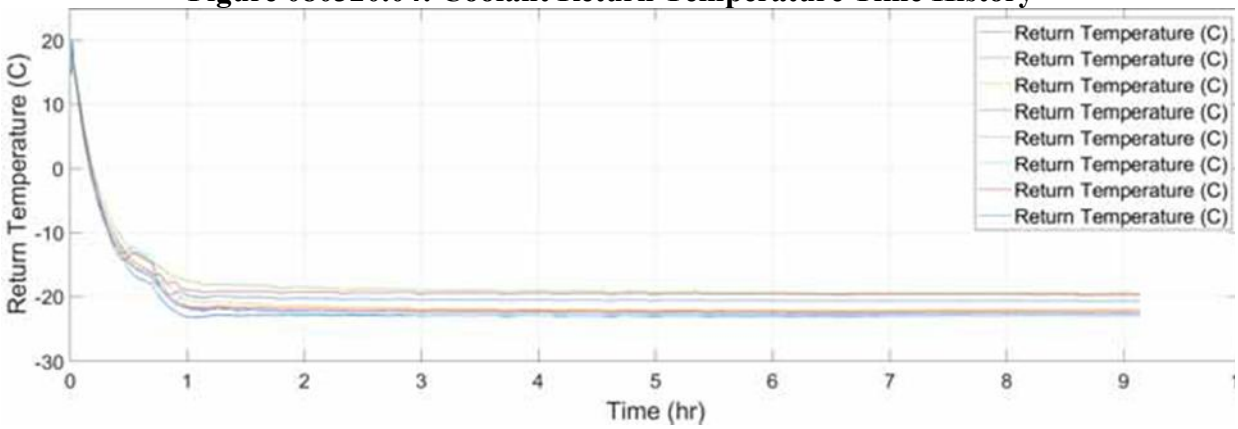

Figure 080320.05: Coolant Supply Temperature Time History

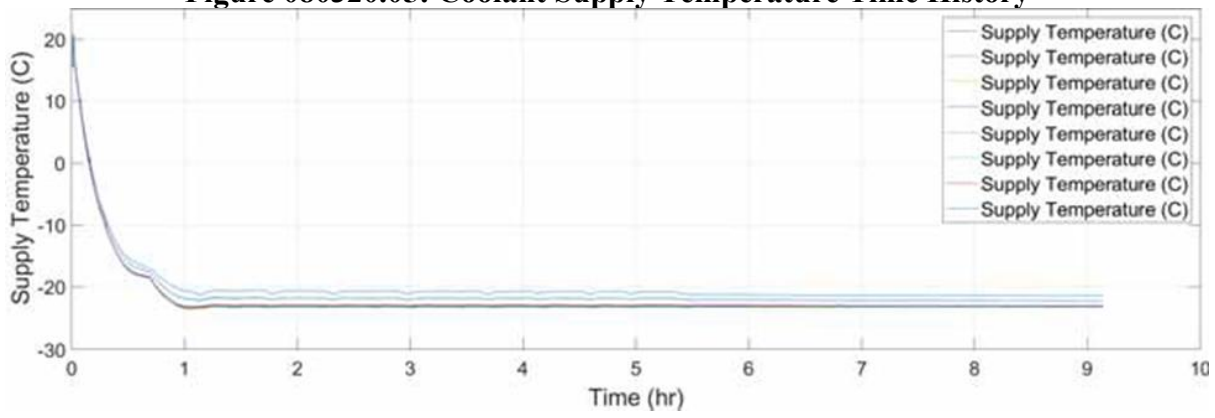

Figure 080320.06: Skin Temperature Time History

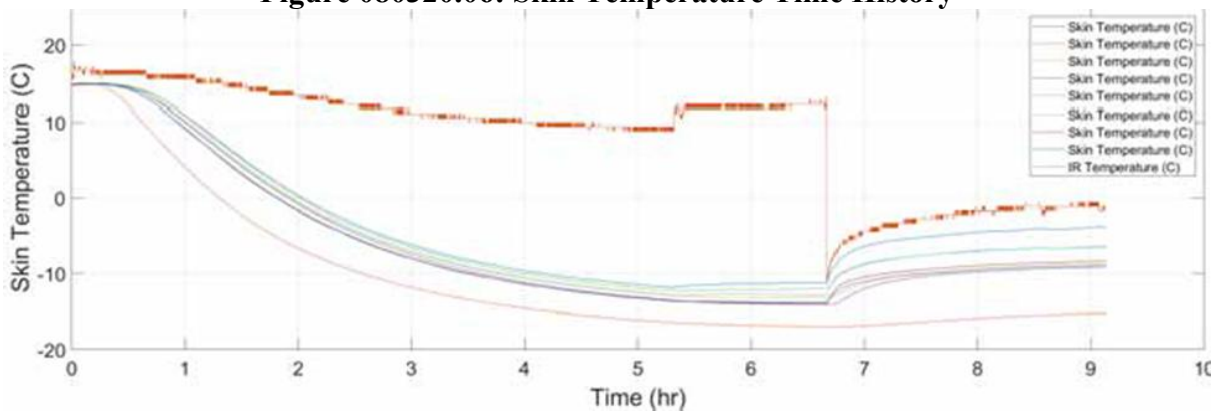

Figure 080320.07: Floor Temperature Time History

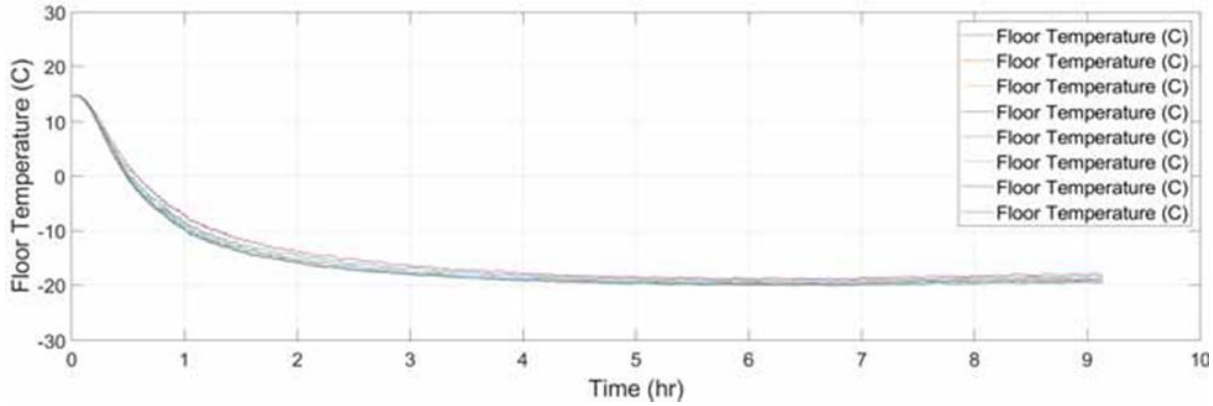

Figure 080320.08: Skin Temperature Slope Time History

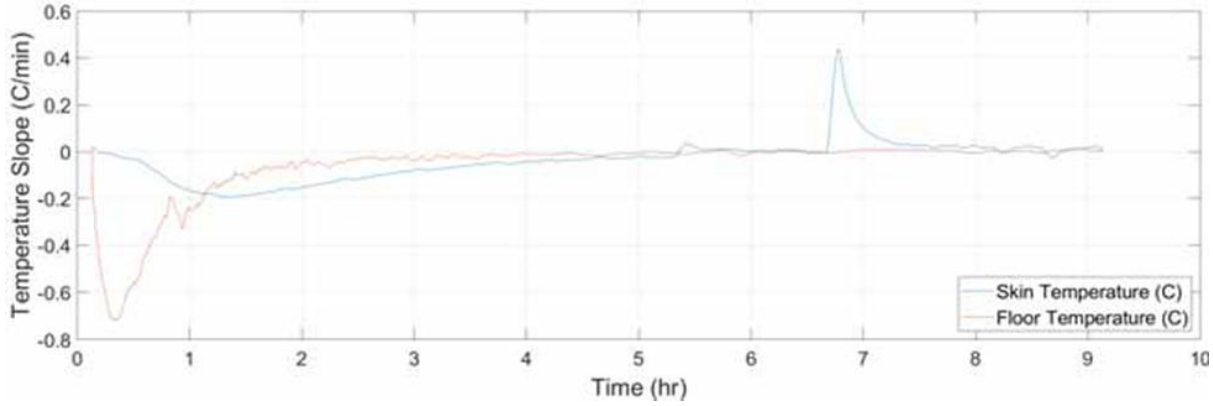

Figure 080320.09: RMS Height Evolution

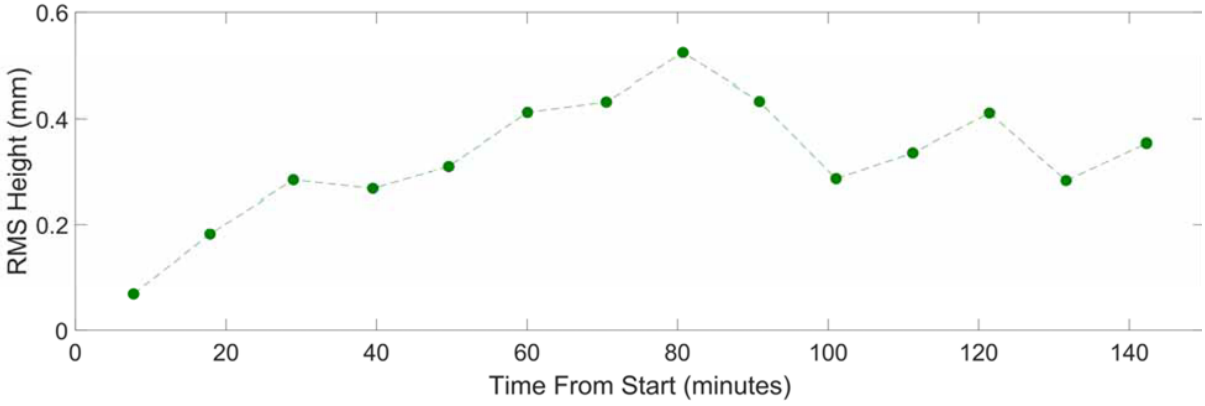

Figure 080320.10: Skewness Evolution

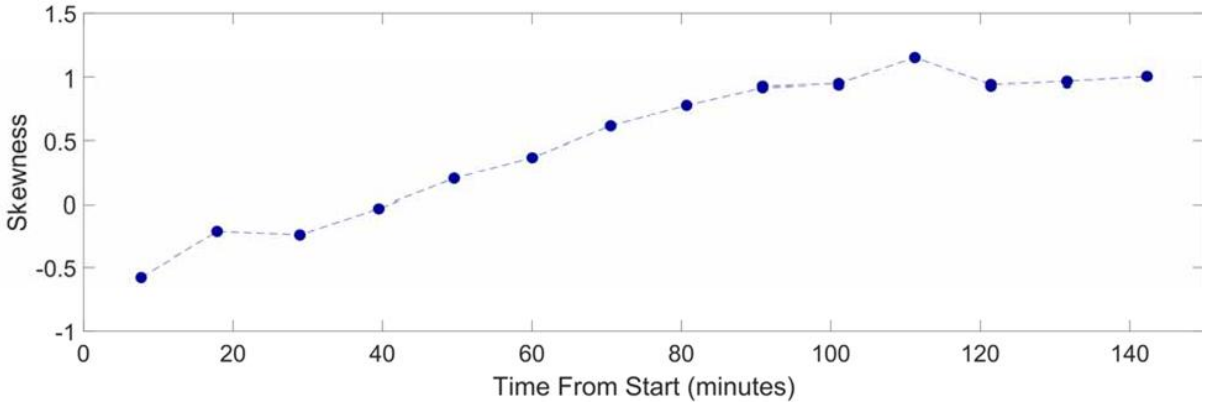

Figure 080320.11: Peak to Valley Evolution

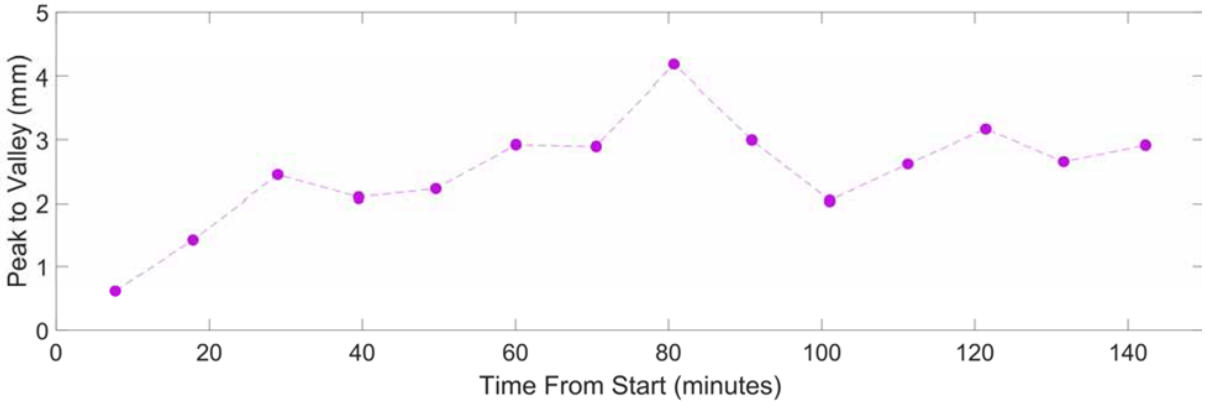

Figure 080320.12: Equivalent Roughness Evolution

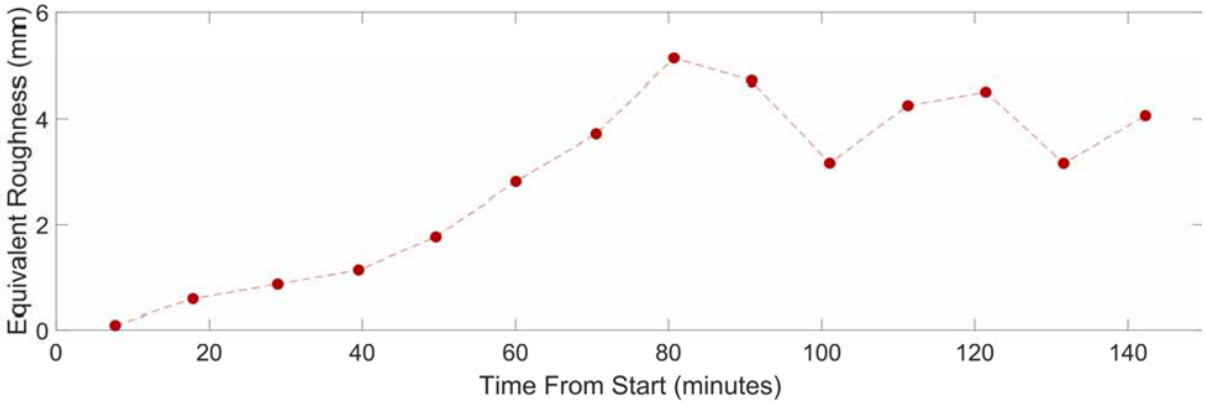

Table 080320.02: Summary of Roughness Parameters

Time (min.)	RMS (mm)	Skewness	Peak to Valley (mm)	ks,Flack-Schultz (mm)
7.7039	0.0669	-0.5805	0.6051	0.0901
17.8706	0.1817	-0.2131	1.4183	0.5798
28.9373	0.2838	-0.2416	2.4480	0.8606
39.5039	0.2670	-0.0316	2.0879	1.1317
49.5873	0.3092	0.2020	2.2229	1.7625
60.0539	0.4128	0.3660	2.9238	2.8038
70.5373	0.4327	0.6209	2.8975	3.7147
80.7039	0.5256	0.7848	4.1928	5.1490
90.8706	0.4336	0.9263	2.9993	4.7160
101.0539	0.2857	0.9482	2.0347	3.1561
111.2539	0.3352	1.1570	2.6182	4.2570
121.4373	0.4116	0.9399	3.1731	4.5201
131.6206	0.2819	0.9657	2.6550	3.1528
142.3039	0.3538	1.0050	2.9176	4.0643

Figure 080320.13: Frost Topography at 00:07:42

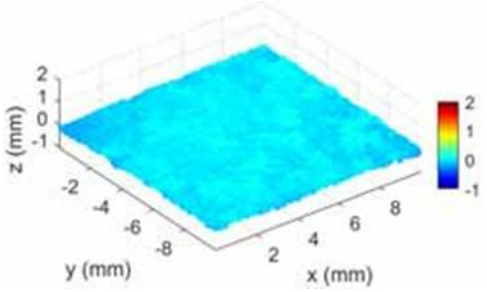

Figure 080320.14: Frost Topography at 00:17:52

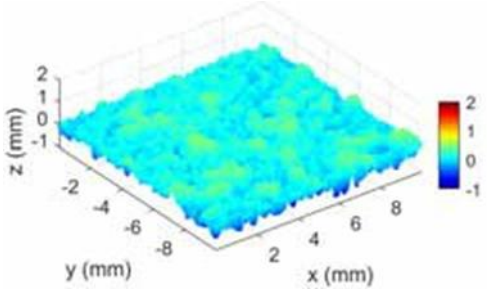

Figure 080320.15: Frost Topography at 00:28:56

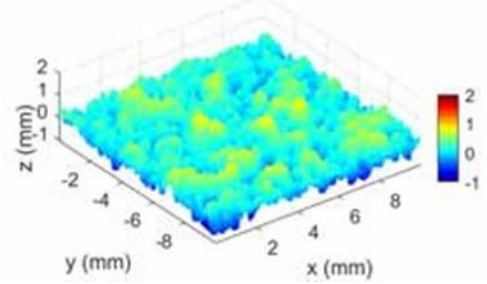

Figure 080320.16: Frost Topography at 00:39:30

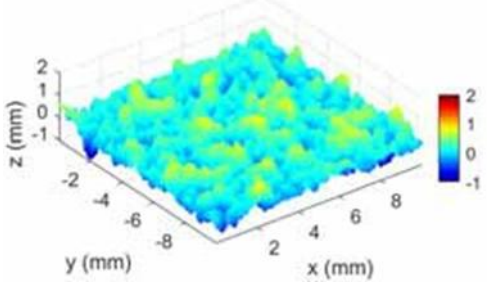

Figure 080320.17: Frost Topography at 00:49:35

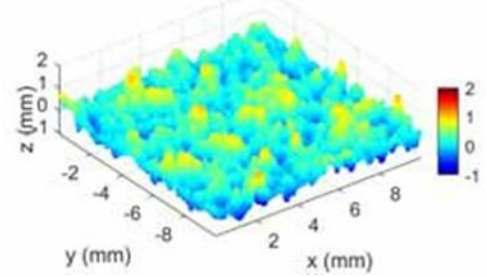

Figure 080320.18: Frost Topography at 01:00:03

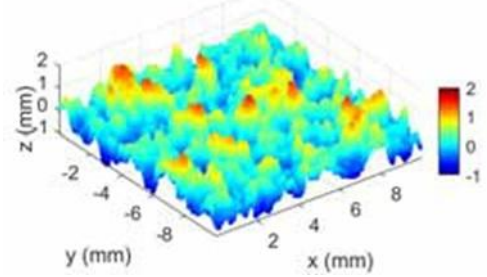

Figure 080320.19: Frost Topography at 01:10:32

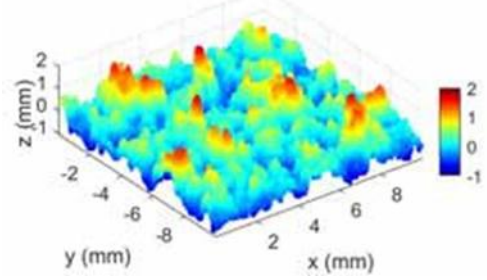

Figure 080320.20: Frost Topography at 01:20:42

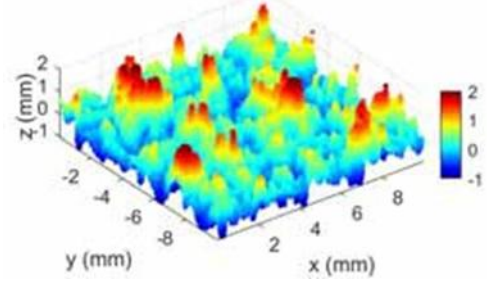

Figure 080320.21: Frost Topography at 01:30:52

Figure 080320.22: Frost Topography at 01:41:03

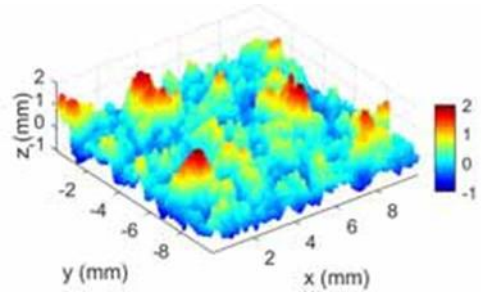

Figure 080320.23: Frost Topography at 01:51:15

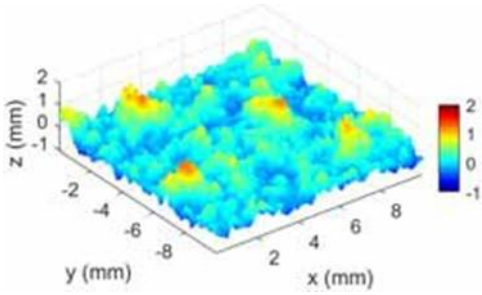

Figure 080320.24: Frost Topography at 02:01:26

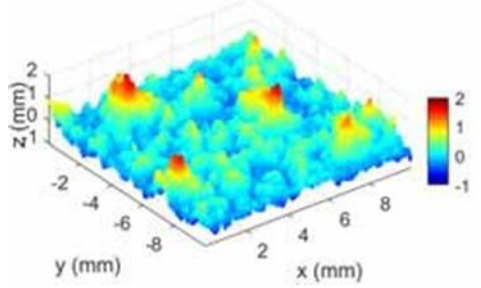

Figure 080320.25: Frost Topography at 02:11:37

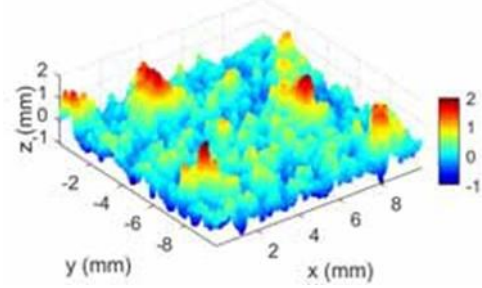

Figure 080320.26: Frost Topography at 02:22:18

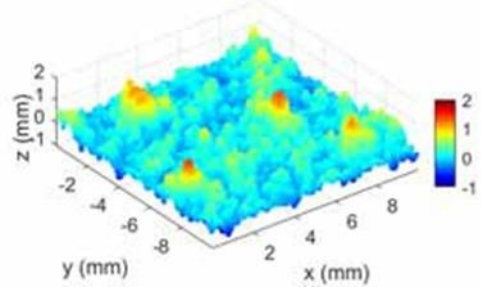

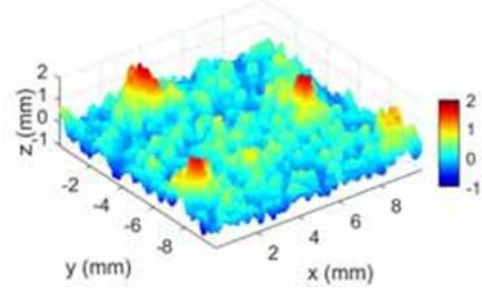

CAFF Conditions Report – Case Date: 080520

Table 080520.01: Summary of Measured Test Variables

Variable	Mean	St. Dev.	Rand. Unc.
T_air (C)	9.1549	0.4136	0.0141
Rh (%)	80.7817	3.8411	0.1305
Omega (kg_v/kg_da)	0.00589940	0.00034450	0.00001171
V_air (m/s)	1.2914	0.1203	0.0041
T_skin (C)	-11.7632	0.8348	0.0284
T_floor (C)	-19.8166	0.1201	0.0041

Figure 080520.01: Temperature and Voltage Control Time History

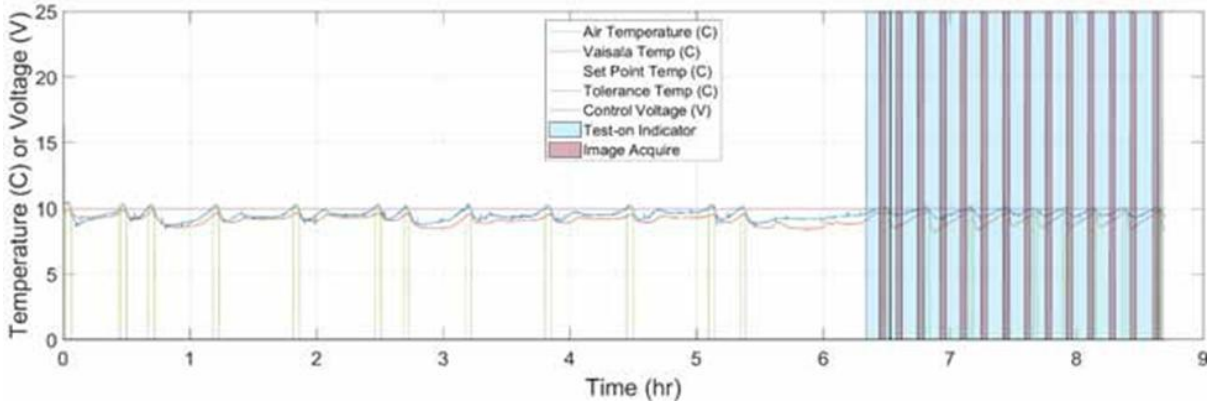

Figure 080520.02: Relative Humidity Time History

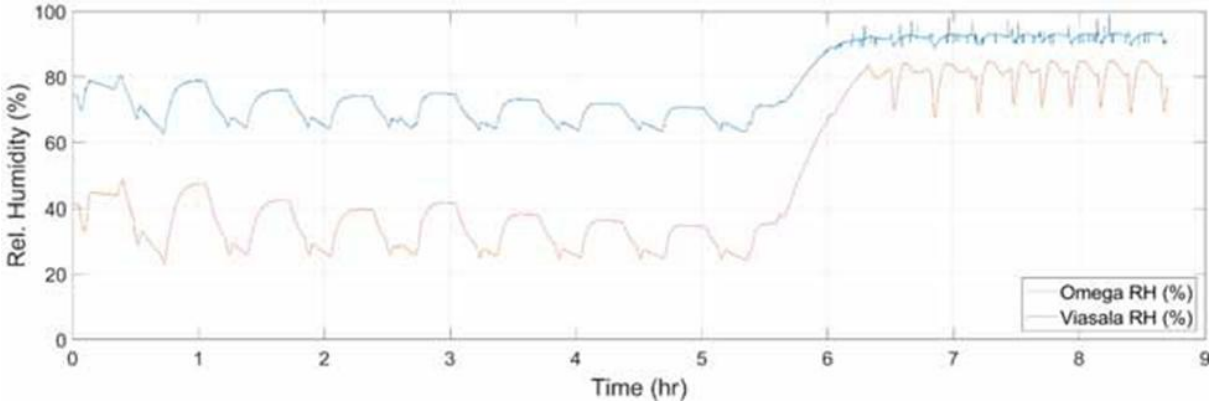

Figure 080520.03: Velocity Time History

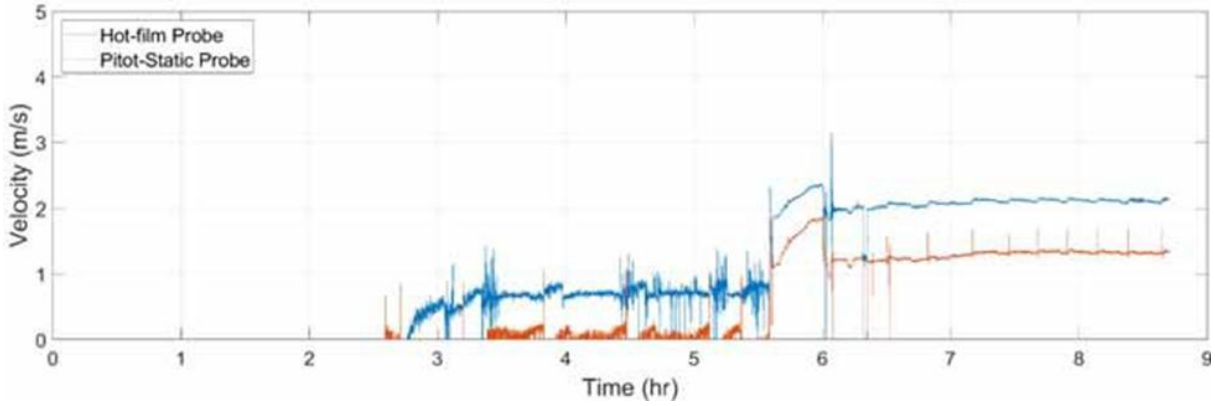

Figure 080520.04: Coolant Return Temperature Time History

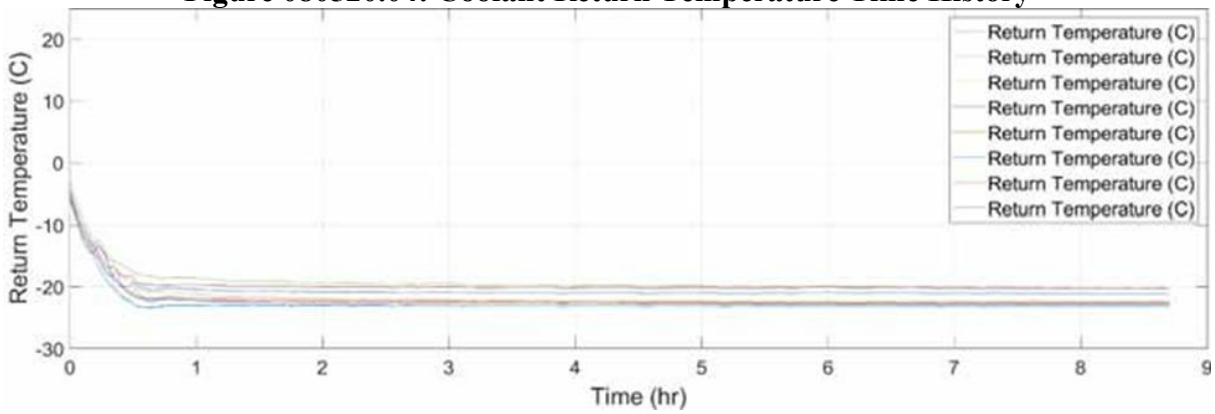

Figure 080520.05: Coolant Supply Temperature Time History

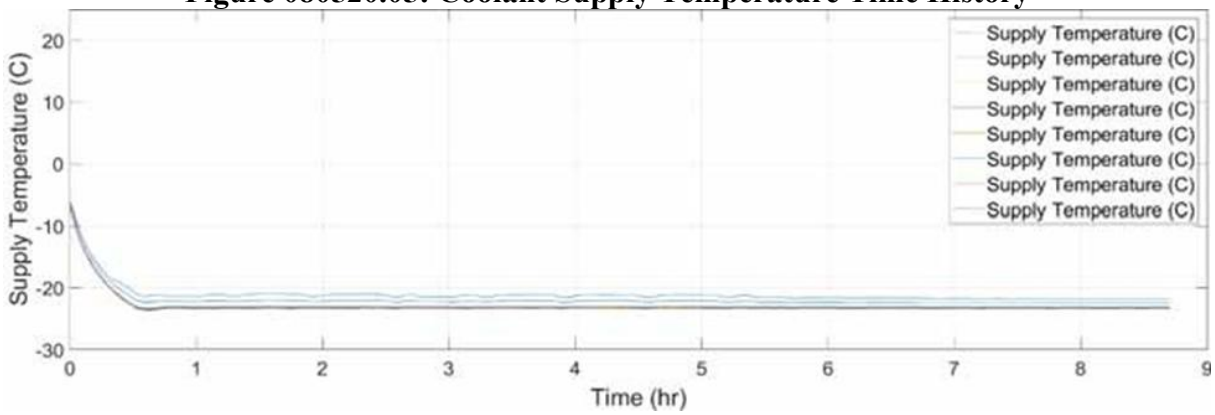

Figure 080520.06: Skin Temperature Time History

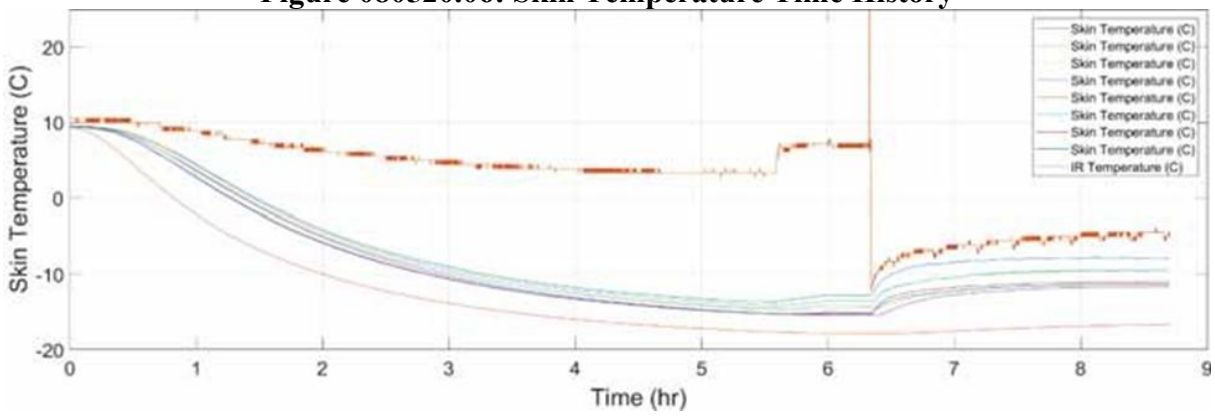

Figure 080520.07: Floor Temperature Time History

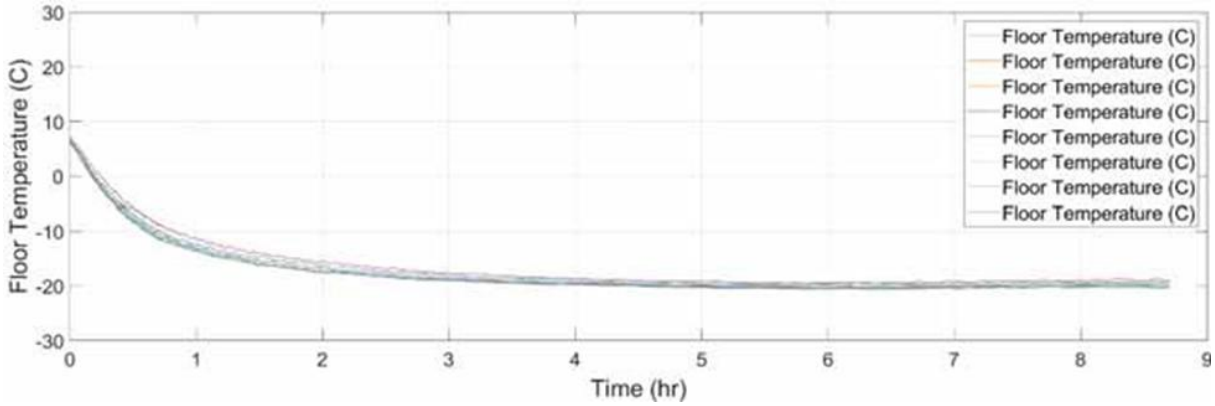

Figure 080520.08: Skin Temperature Slope Time History

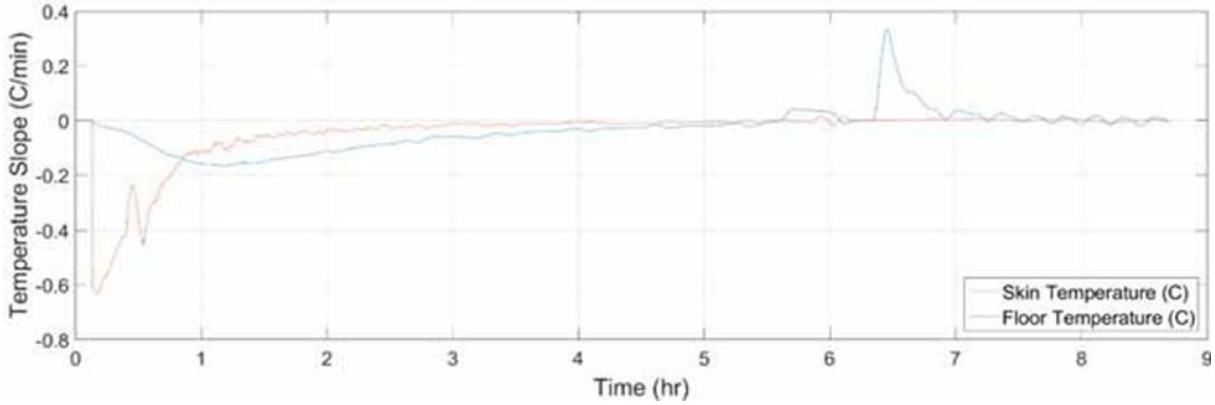

Figure 080520.09: RMS Height Evolution

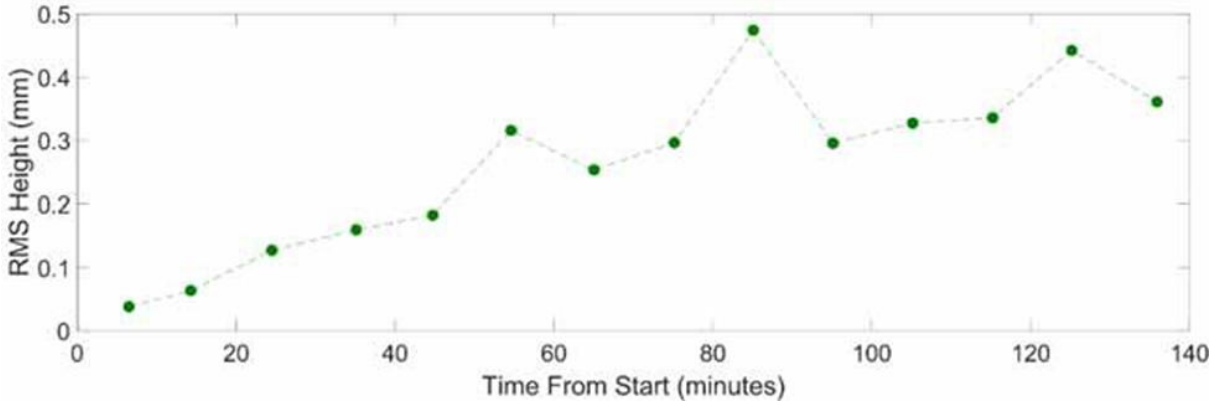

Figure 080520.10: Skewness Evolution

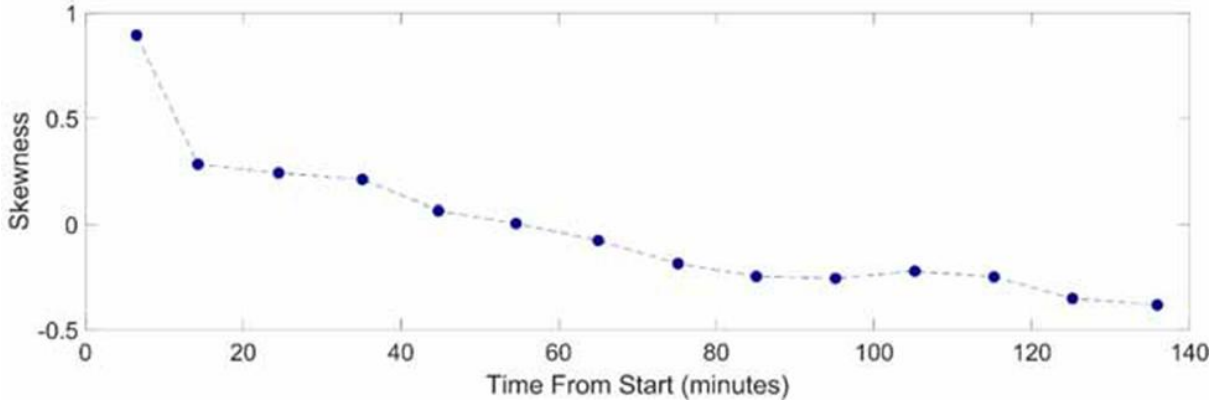

Figure 080520.11: Peak to Valley Evolution

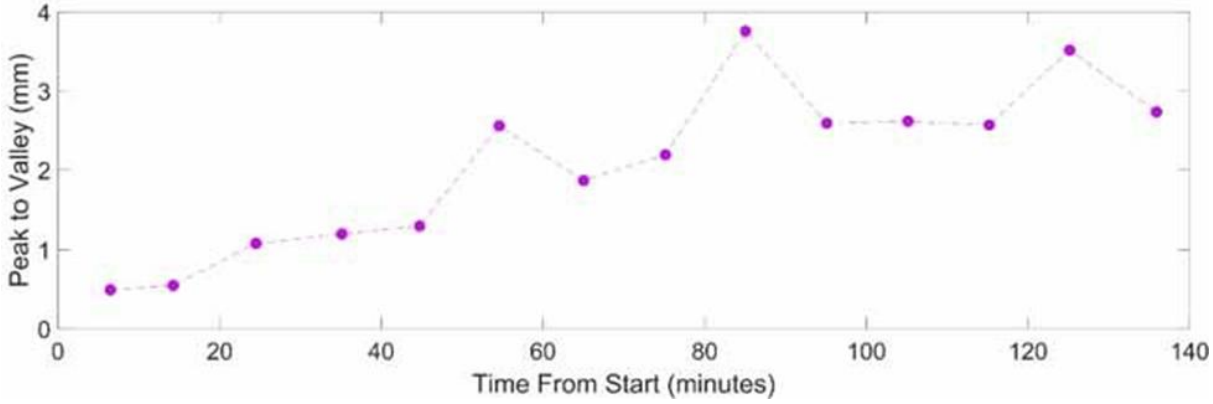

Figure 080520.12: Equivalent Roughness Evolution

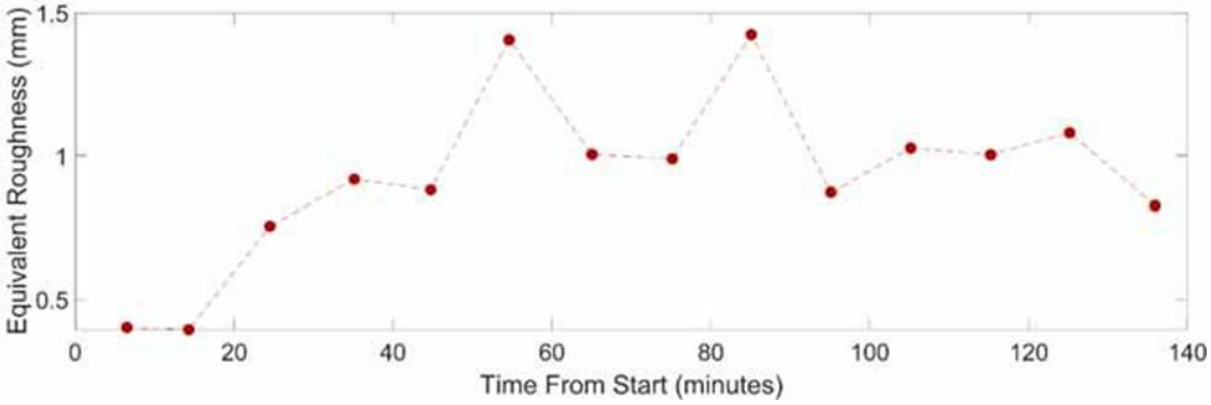

Time (min.)	RMS (mm)	Skewness	Peak to Valley (mm)	ks,Flack-Schultz (mm)
6.4648	0.0378	0.8937	0.4921	0.4016
14.2481	0.0633	0.2815	0.5466	0.3939
24.4815	0.1271	0.2394	1.0788	0.7556
35.0981	0.1597	0.2097	1.2001	0.9181
44.7315	0.1827	0.0636	1.3012	0.8807
54.5815	0.3154	0.0041	2.5576	1.4053
65.0148	0.2529	-0.0767	1.8631	1.0043
75.1315	0.2961	-0.1863	2.1897	0.9890
85.0648	0.4742	-0.2471	3.7563	1.4240
95.0981	0.2953	-0.2564	2.5899	0.8719
105.1481	0.3270	-0.2223	2.6147	1.0264
115.1981	0.3356	-0.2496	2.5681	1.0031
125.1481	0.4424	-0.3525	3.5162	1.0804
135.8981	0.3609	-0.3822	2.7328	0.8265

Figure 080520.13: Frost Topography at 00:06:20

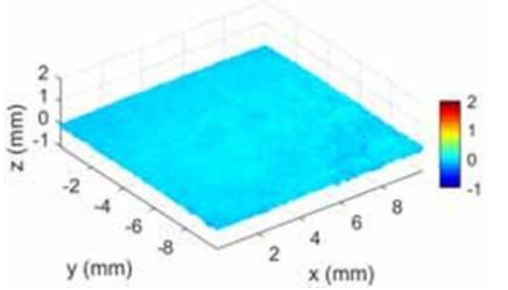

Figure 080520.14: Frost Topography at 00:14:07

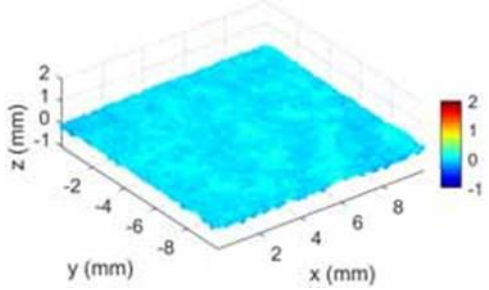

Figure 080520.15: Frost Topography at 00:24:21

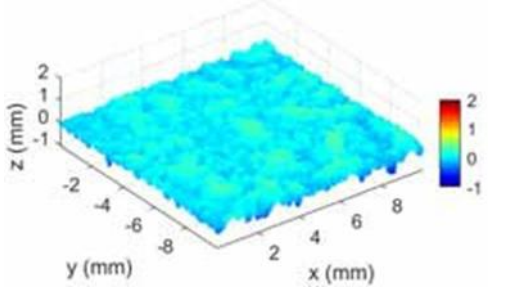

Figure 080520.16: Frost Topography at 00:34:58

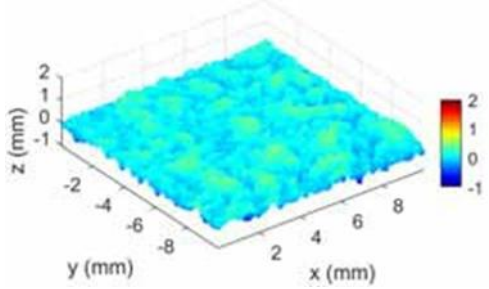

Figure 080520.17: Frost Topography at 00:44:36

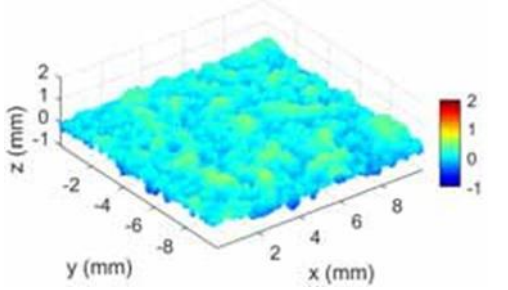

Figure 080520.18: Frost Topography at 00:54:27

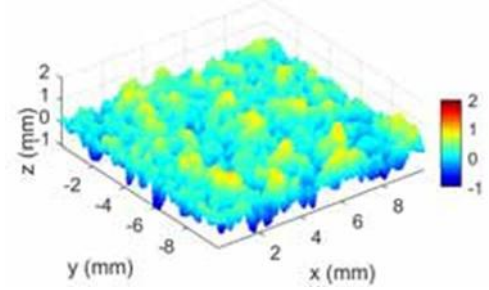

Figure 080520.19: Frost Topography at 01:04:53

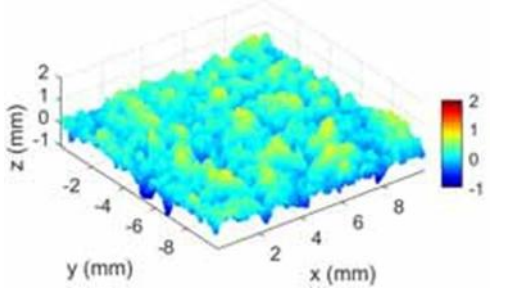

Figure 080520.20: Frost Topography at 01:15:00

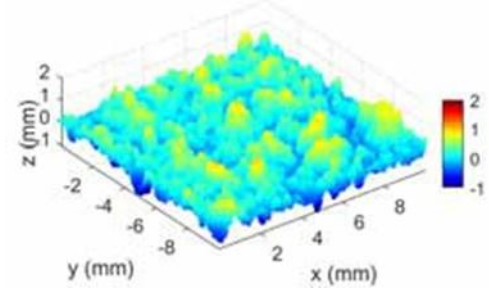

Figure 080520.21: Frost Topography at 01:24:56

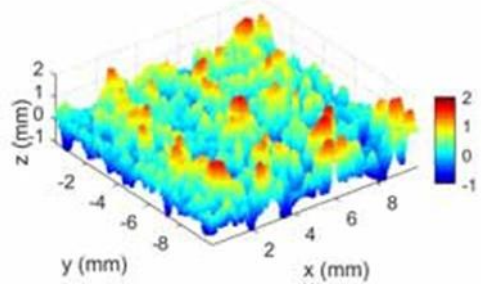

Figure 080520.22: Frost Topography at 01:34:58

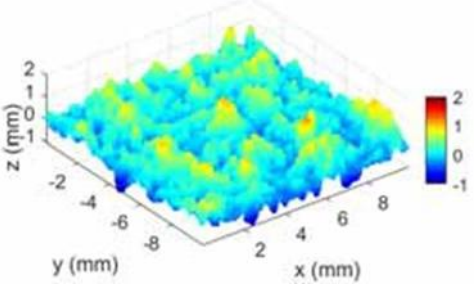

Figure 080520.23: Frost Topography at 01:45:01

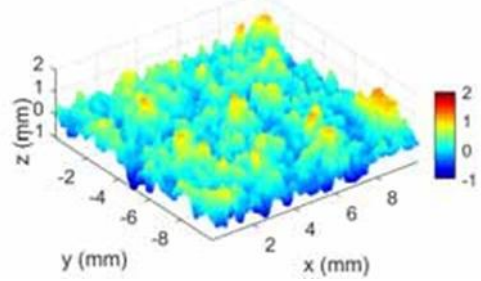

Figure 080520.24: Frost Topography at 01:55:04

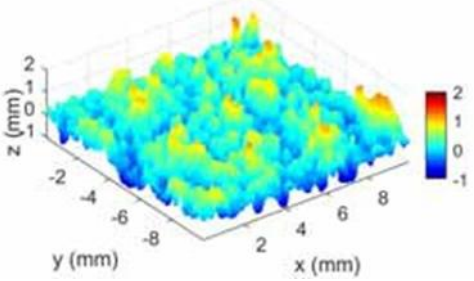

Figure 080520.25: Frost Topography at 02:05:01

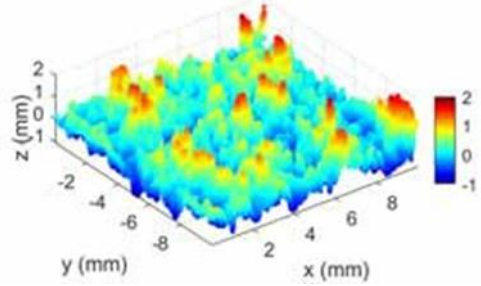

Figure 080520.26: Frost Topography at 02:15:46

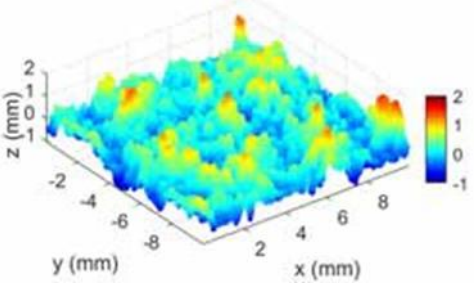

CAFF Conditions Report – Case Date: 080820

Table 080820.01: Summary of Measured Test Variables

Variable	Mean	St. Dev.	Rand. Unc.
T_air (C)	4.2043	0.2689	0.0090
Rh (%)	80.1372	4.7227	0.1584
Omega (kg_v/kg_da)	0.00413653	0.00030693	0.00001029
V_air (m/s)	1.2333	0.1146	0.0038
T_skin (C)	-13.4697	0.6286	0.0211
T_floor (C)	-20.3081	0.0672	0.0023

Figure 080820.01: Temperature and Voltage Control Time History

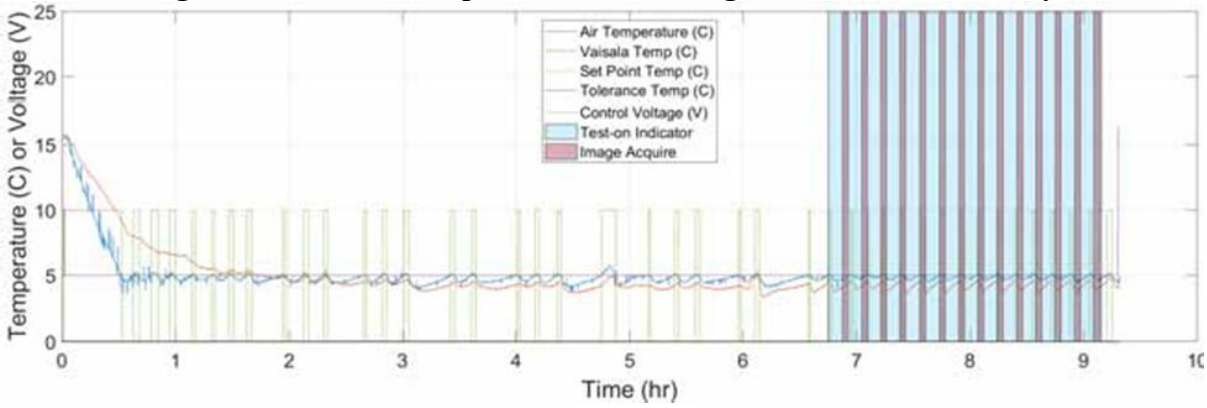

Figure 080820.02: Relative Humidity Time History

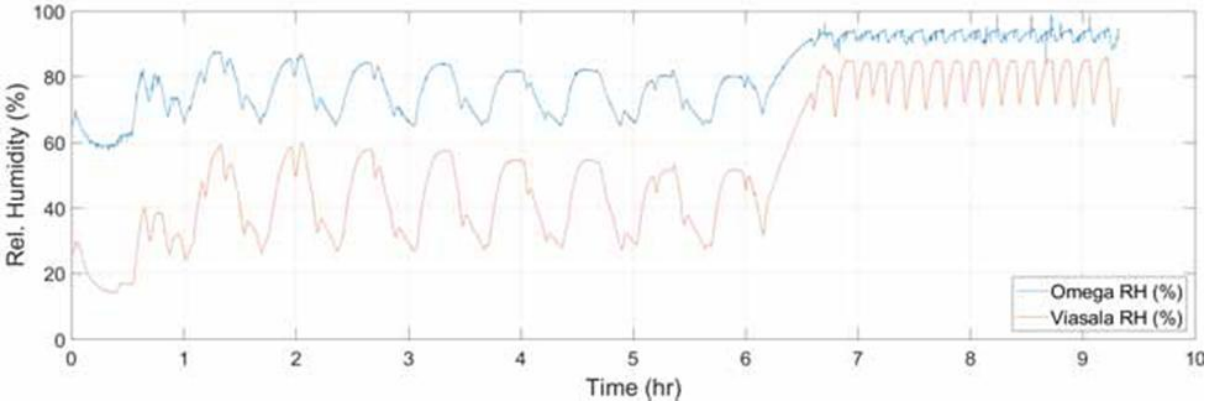

Figure 080820.03: Velocity Time History

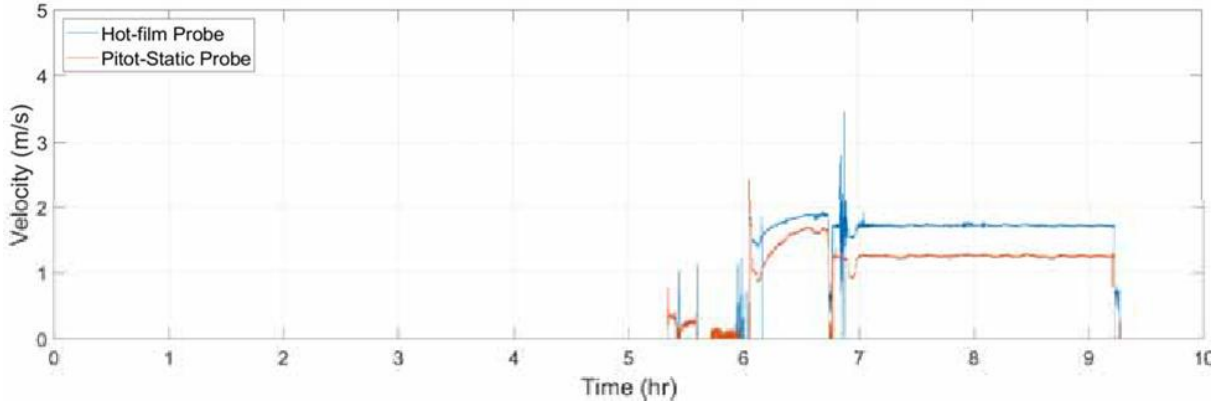

Figure 080820.04: Coolant Return Temperature Time History

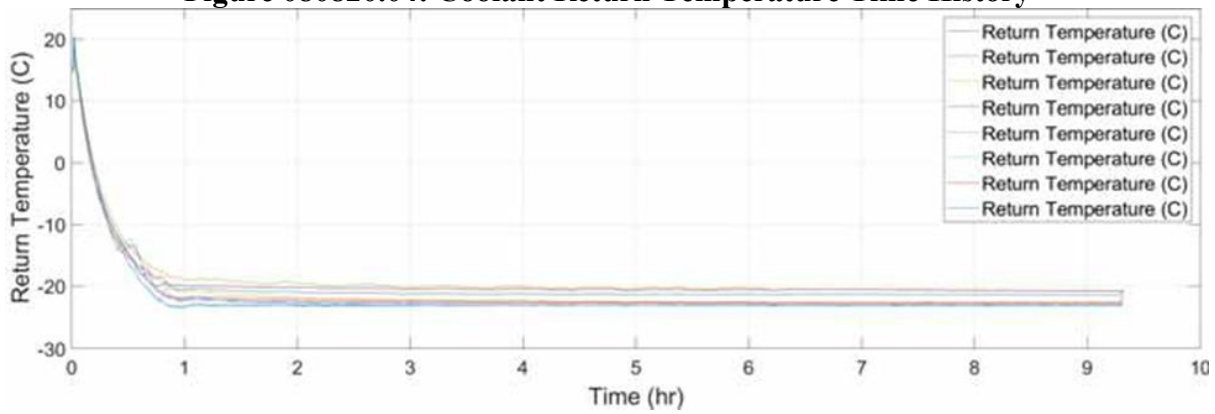

Figure 080820.05: Coolant Supply Temperature Time History

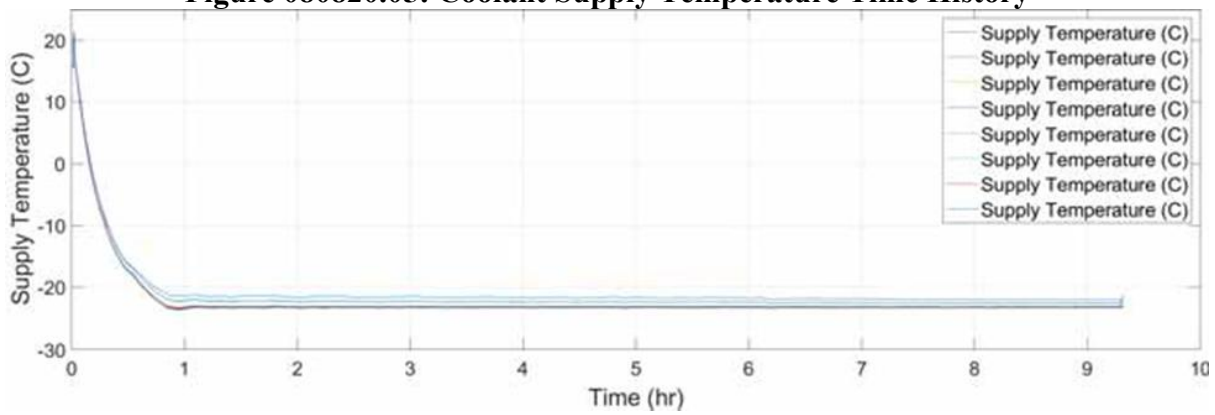

Figure 080820.06: Skin Temperature Time History

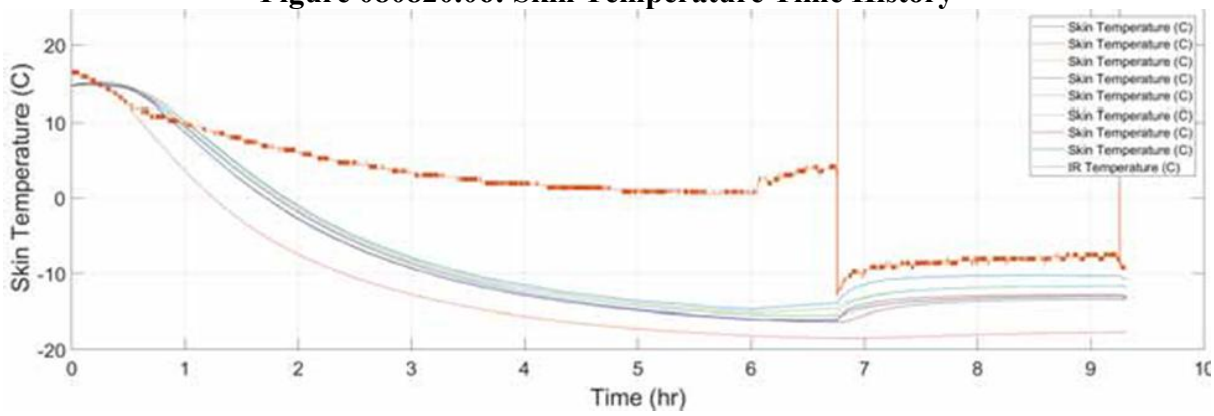

Figure 080820.07: Floor Temperature Time History

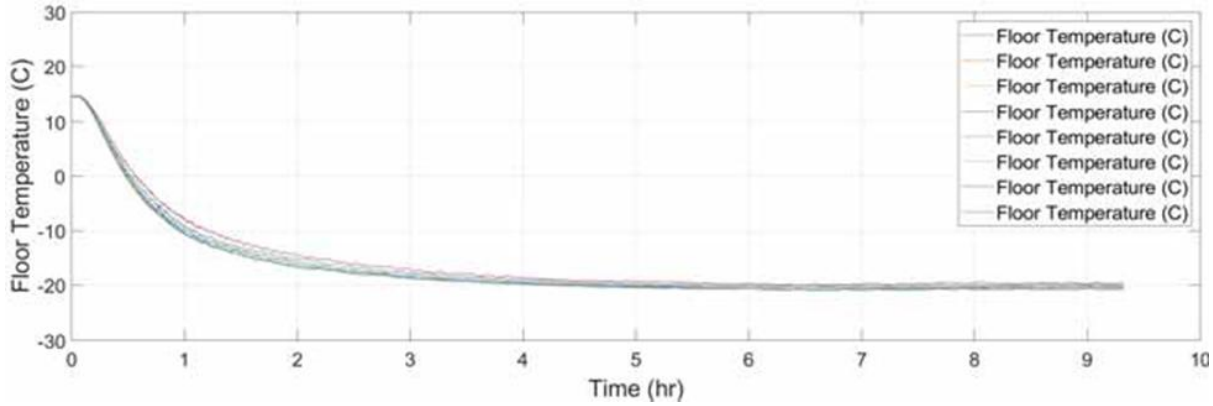

Figure 080820.08: Skin Temperature Slope Time History

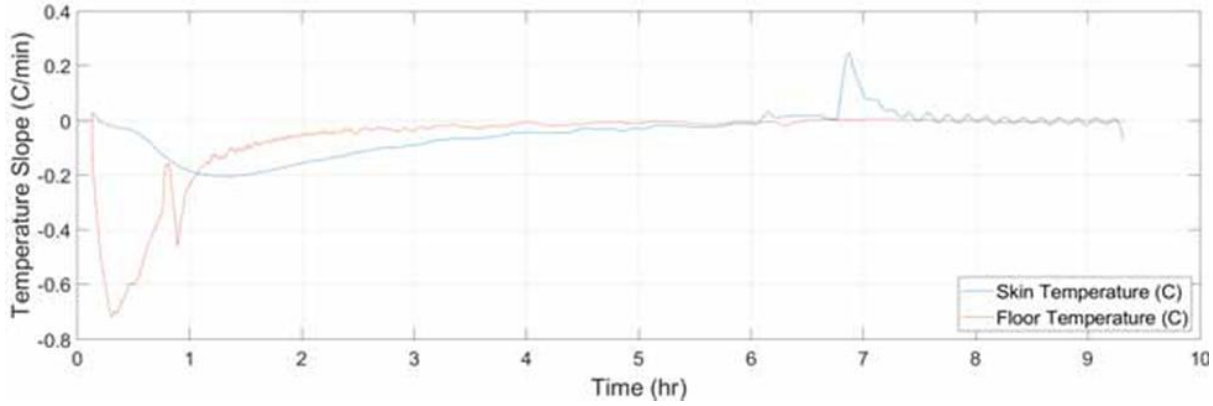

Figure 080820.09: RMS Height Evolution

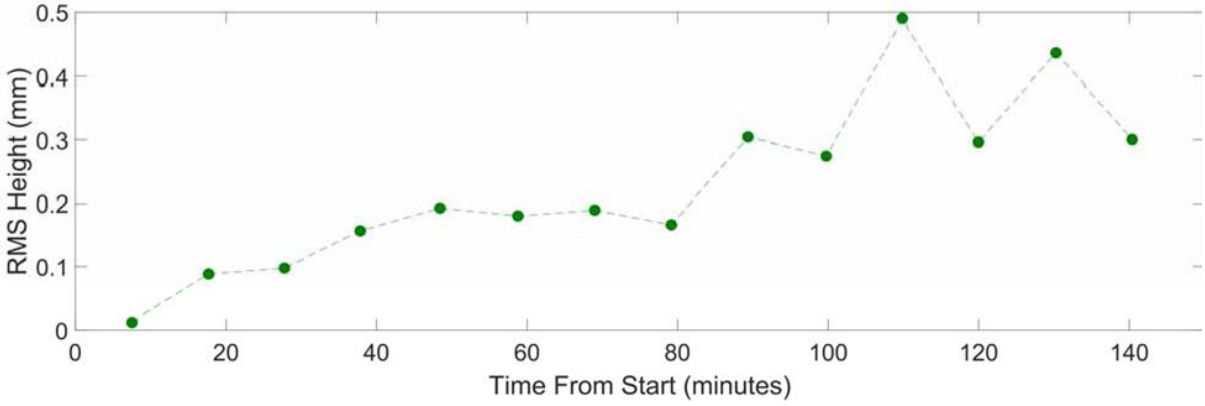

Figure 080820.10: Skewness Evolution

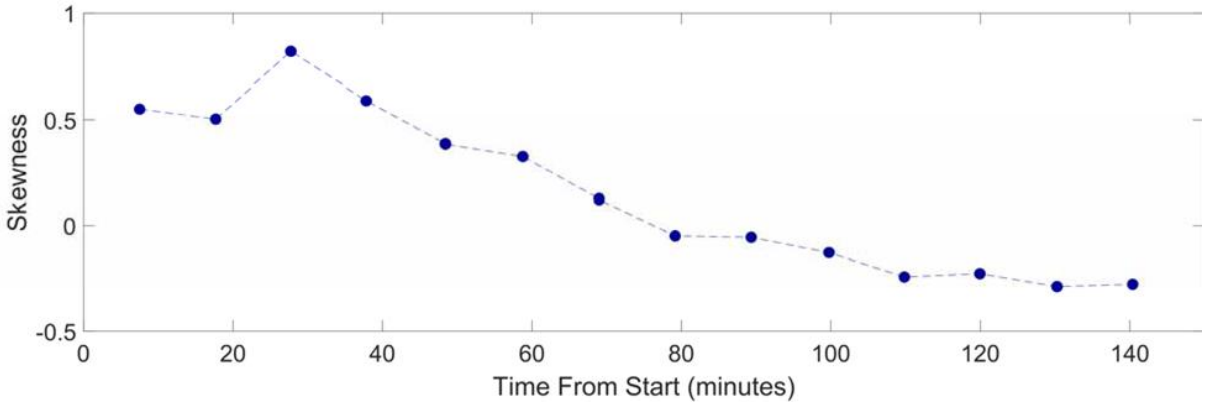

Figure 080820.11: Peak to Valley Evolution

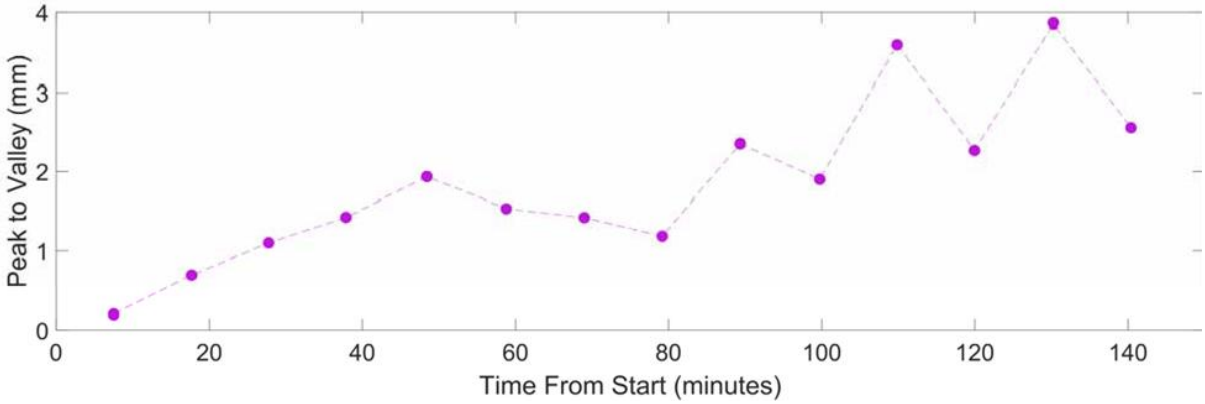

Figure 080820.12; Equivalent Roughness Evolution

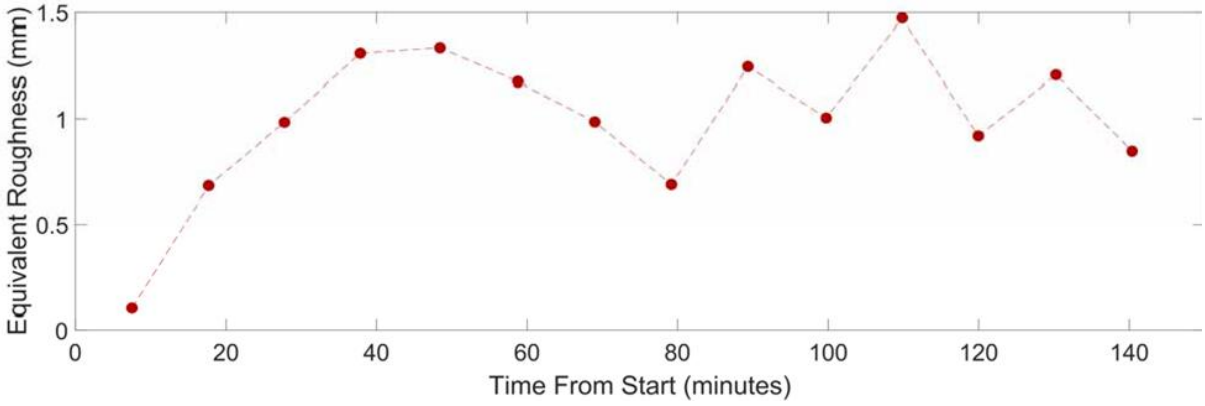

Table 080820.02: Summary of Roughness Parameters

Time (min.)	RMS (mm)	Skewness	Peak to Valley (mm)	ks,Flack-Schultz (mm)
7.4984	0.0123	0.5520	0.1945	0.0997
17.6817	0.0879	0.5038	0.6876	0.6811
27.7484	0.0974	0.8246	1.0982	0.9839
37.8317	0.1564	0.5923	1.4239	1.3103
48.4150	0.1930	0.3856	1.9329	1.3366
58.7817	0.1804	0.3259	1.5344	1.1762
68.9817	0.1896	0.1239	1.4209	0.9858
79.1650	0.1662	-0.0499	1.1827	0.6862
89.3484	0.3046	-0.0563	2.3522	1.2464
99.7484	0.2744	-0.1298	1.8989	1.0046
109.8484	0.4902	-0.2464	3.6037	1.4741
119.9484	0.2965	-0.2301	2.2680	0.9181
130.2650	0.4375	-0.2923	3.8670	1.2069
140.3984	0.3008	-0.2814	2.5543	0.8473

Figure 080820.13: Frost Topography at 00:07:22

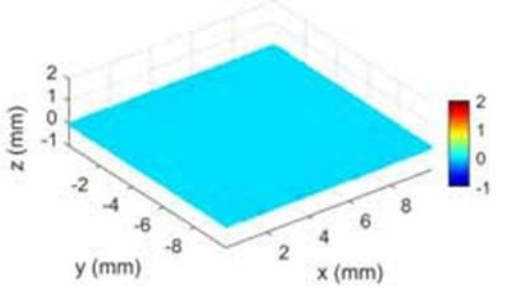

Figure 080820.14: Frost Topography at 00:17:33

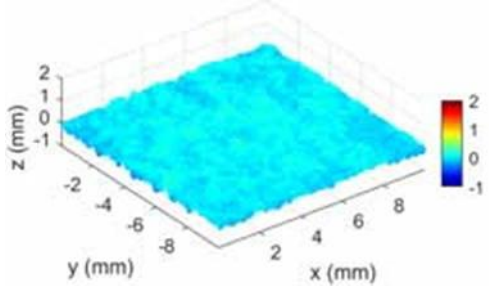

Figure 080820.15: Frost Topography at 00:27:37

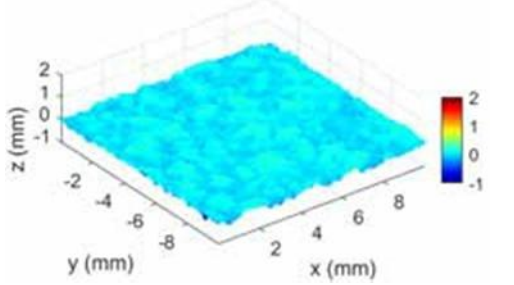

Figure 080820.16: Frost Topography at 00:37:42

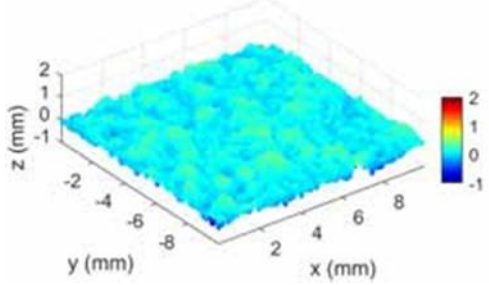

Figure 080820.17: Frost Topography at 00:48:17

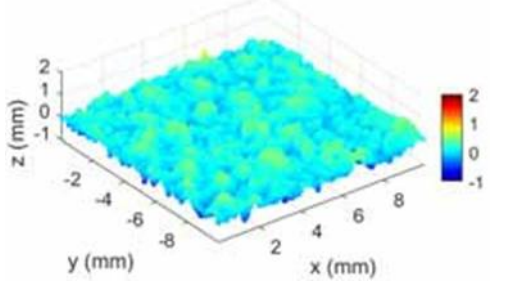

Figur e080820.18: Frost Topography at 00:58:39

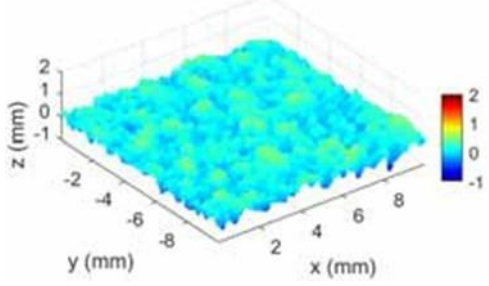

Figure 080820.19: Frost Topography at 01:08:51

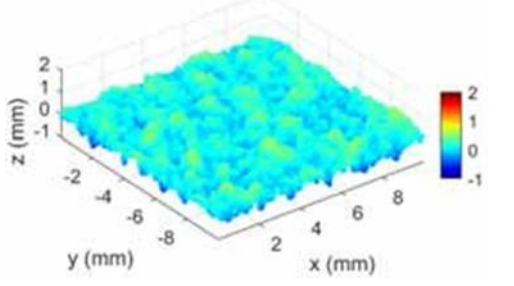

Figure 080820.20: Frost Topography at 01:19:02

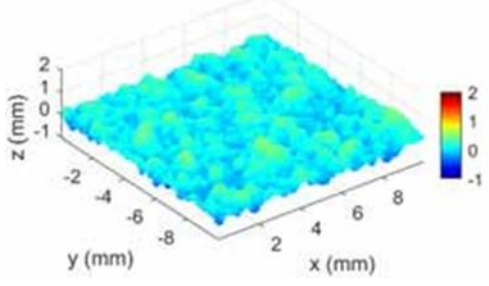

Figure 080820.21: Frost Topography at 01:29:13

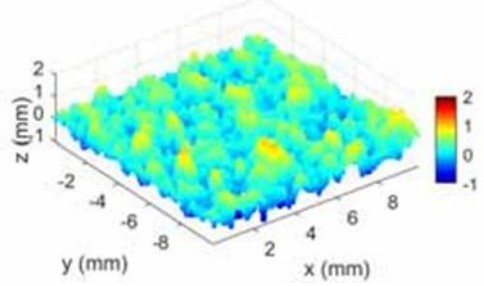

Figure 080820.22: Frost Topography at 01:39:37

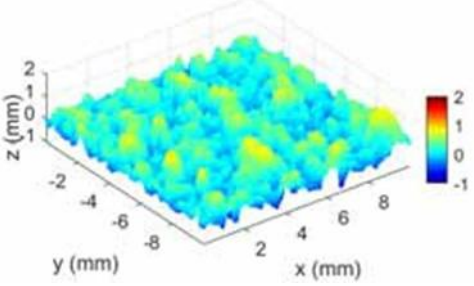

Figure 080820.23: Frost Topography at 01:49:43

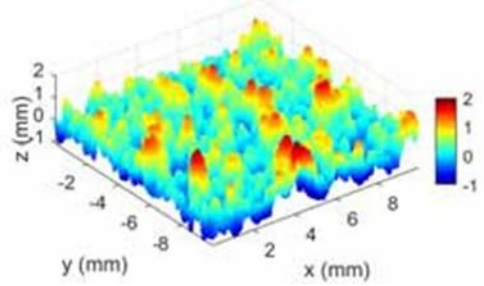

Figure 080820.24: Frost Topography at 01:59:49

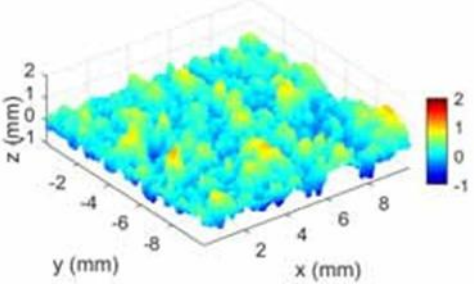

Figure 080820.25: Frost Topography at 02:10:08

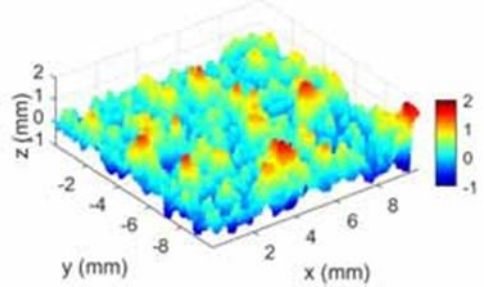

Figure 080820.26: Frost Topography at 02:20:16

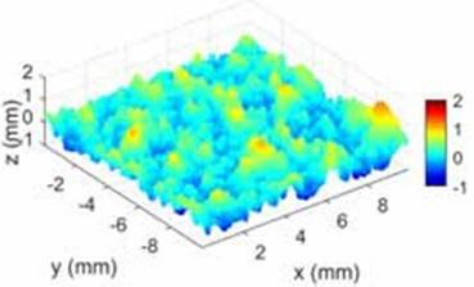

CAFF Conditions Report – Case Date: 081120

Table 081120.01: Summary of Measured Test Variables

Variable	Mean	St. Dev.	Rand. Unc.
T_air (C)	9.1992	0.2834	0.0095
Rh (%)	79.9715	5.5001	0.1837
Omega (kg_v/kg_da)	0.00585808	0.00042109	0.00001406
V_air (m/s)	0.1593	0.1315	0.0044
T_skin (C)	-13.1583	0.5987	0.0200
T_floor (C)	-20.0143	0.0697	0.0023

Figure 081120.01: Temperature and Voltage Control Time History

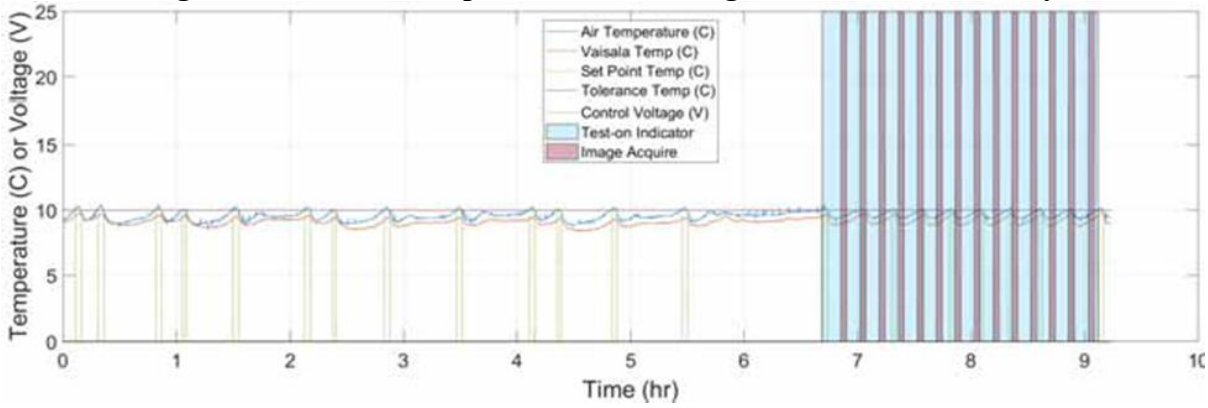

Figure 081120.02: Relative Humidity Time History

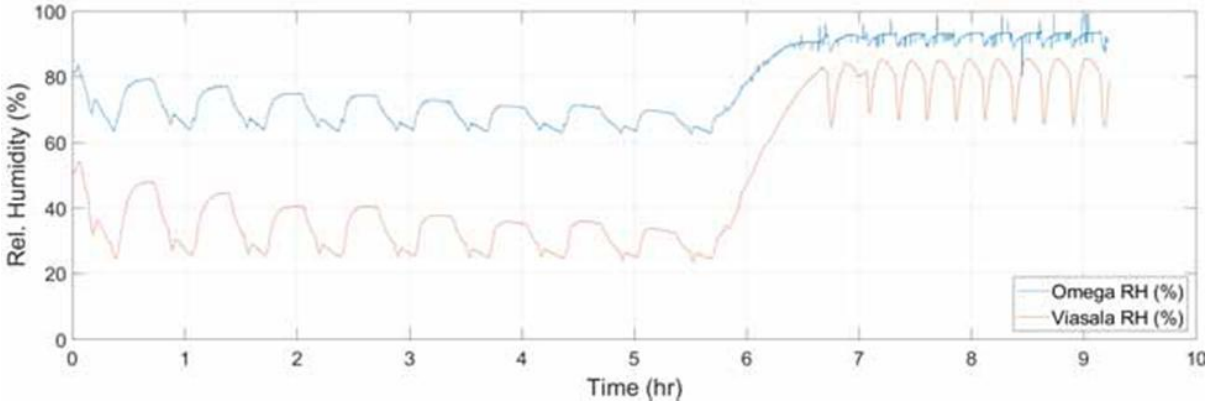

Figure 081120.03: Velocity Time History

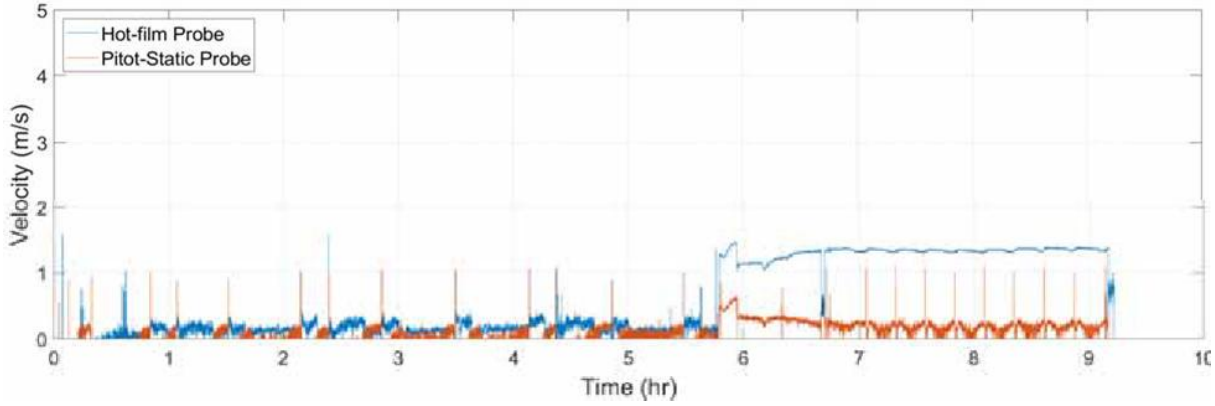

Figure 081120.04: Coolant Return Temperature Time History

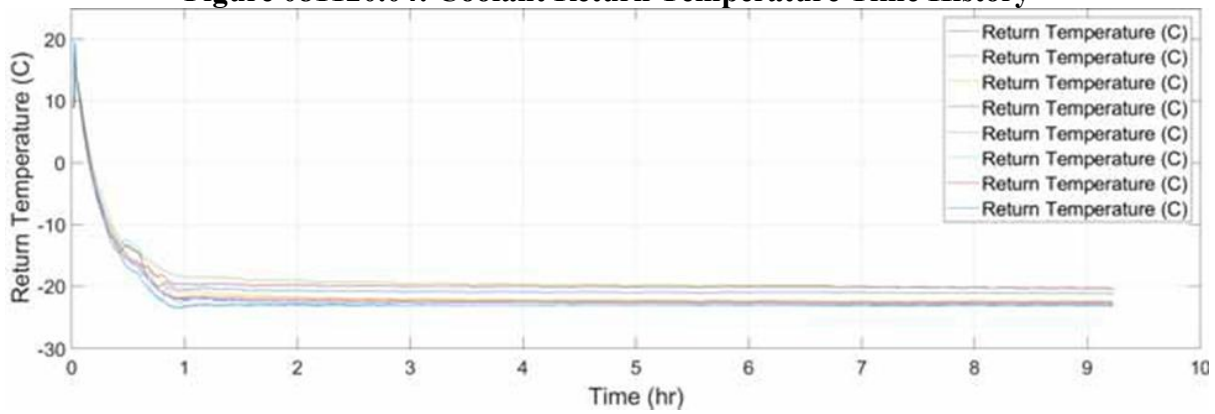

Figure 081120.05: Coolant Supply Temperature Time History

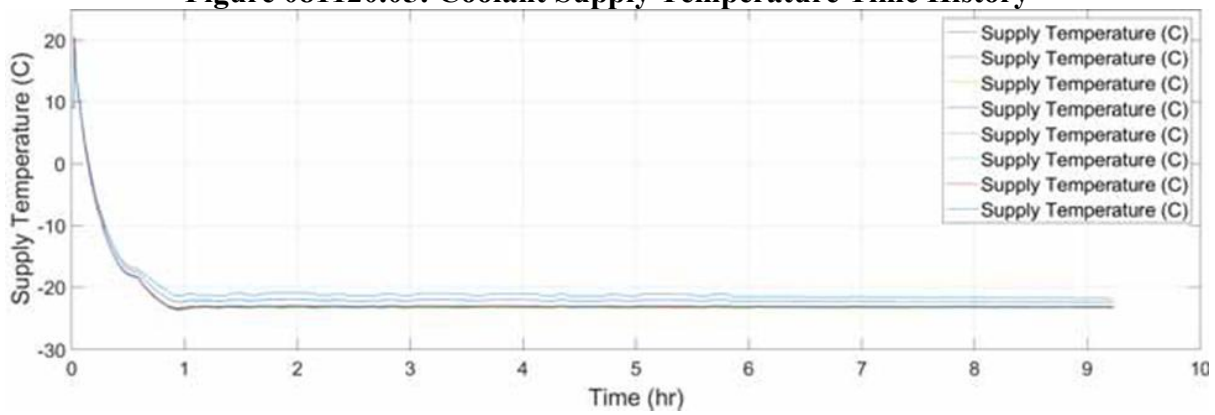

Figure 081120.06: Skin Temperature Time History

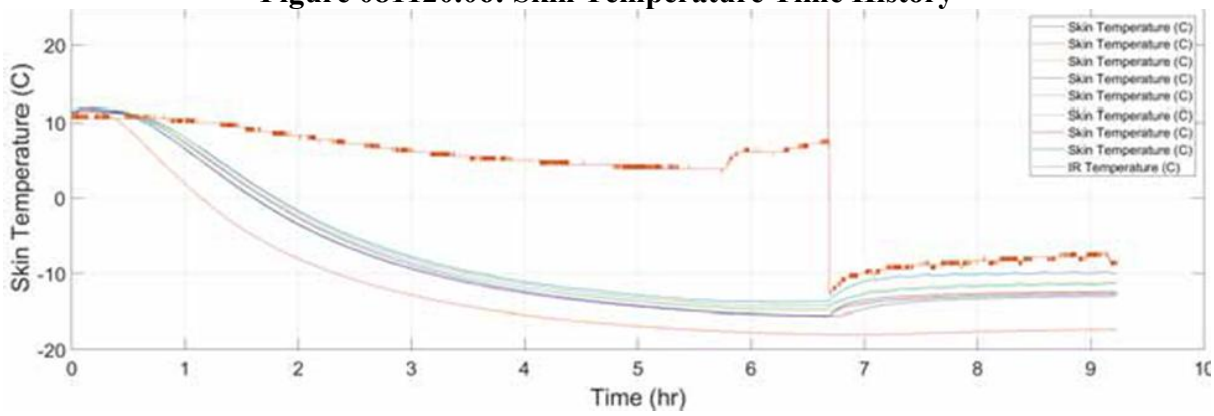

Figure 081120.07: Floor Temperature Time History

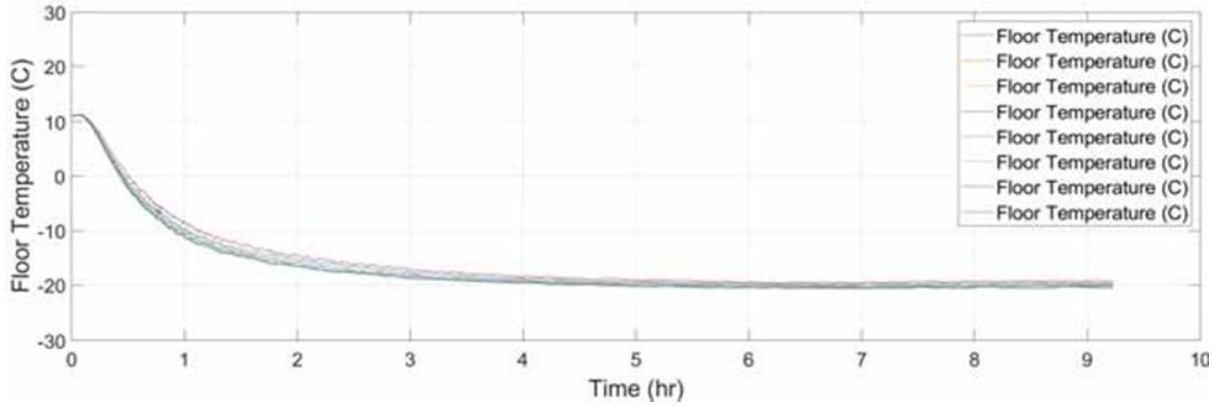

Figure 081120.08: Skin Temperature Slope Time History

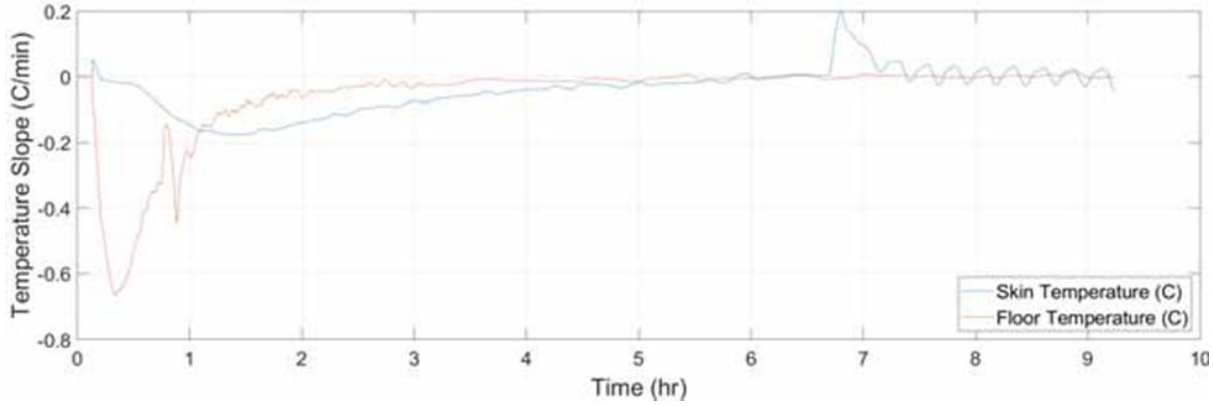

Figure 081120.09: RMS Height Evolution

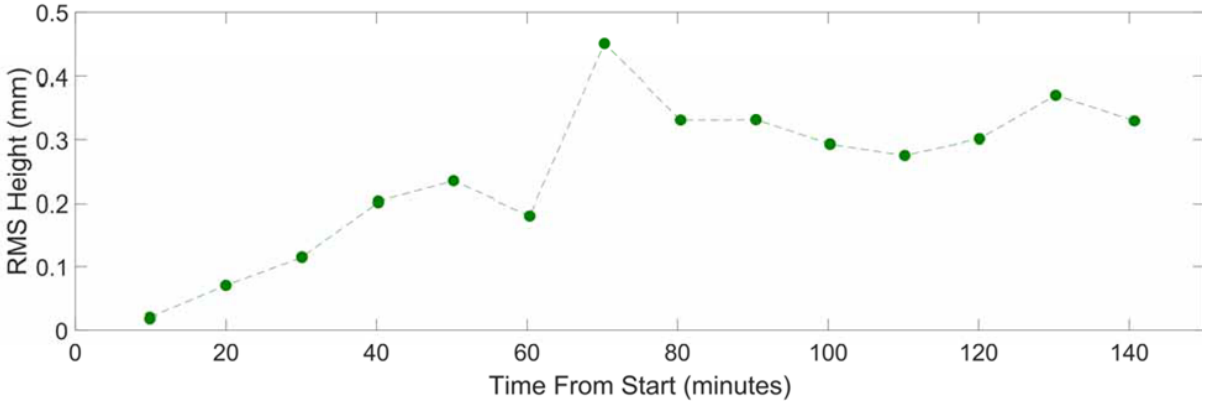

Figure 081120.10: Skewness Evolution

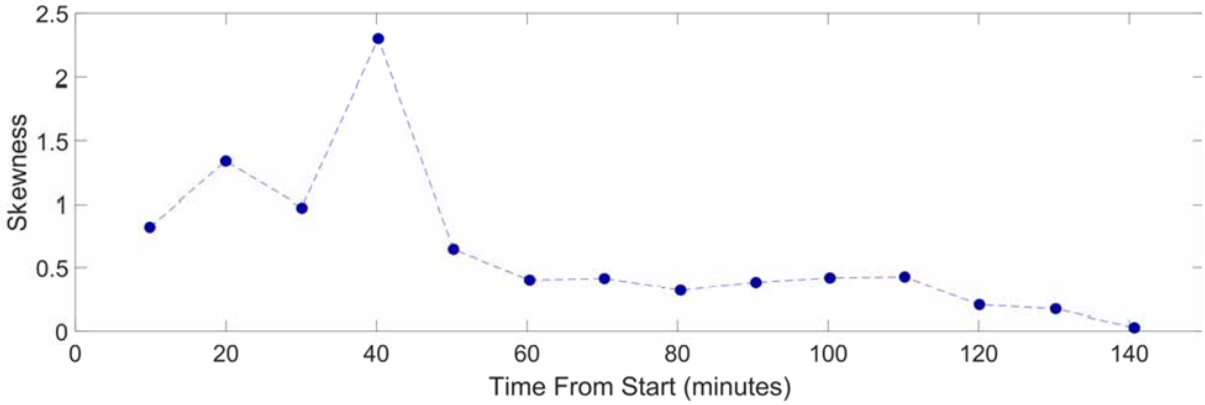

Figure 081120.11: Peak to Valley Evolution

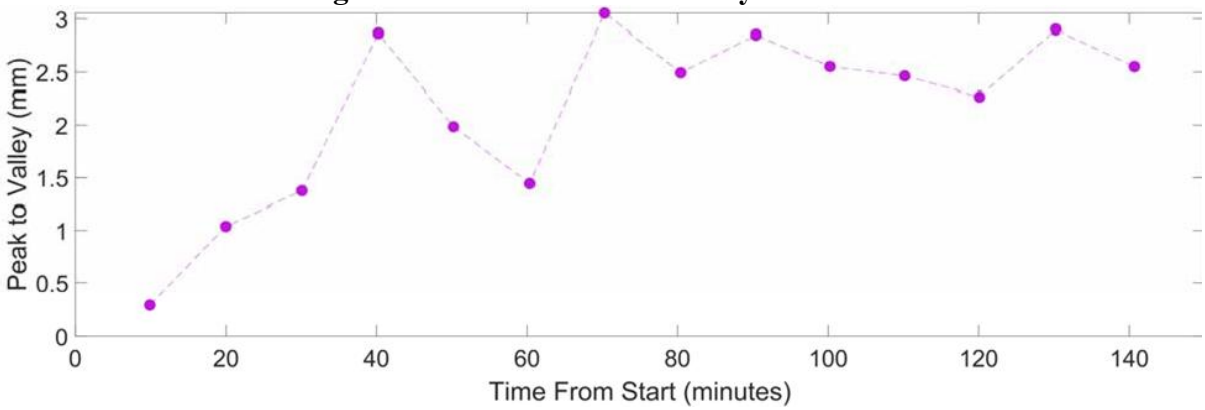

Figure 081120.12: Equivalent Roughness Evolution

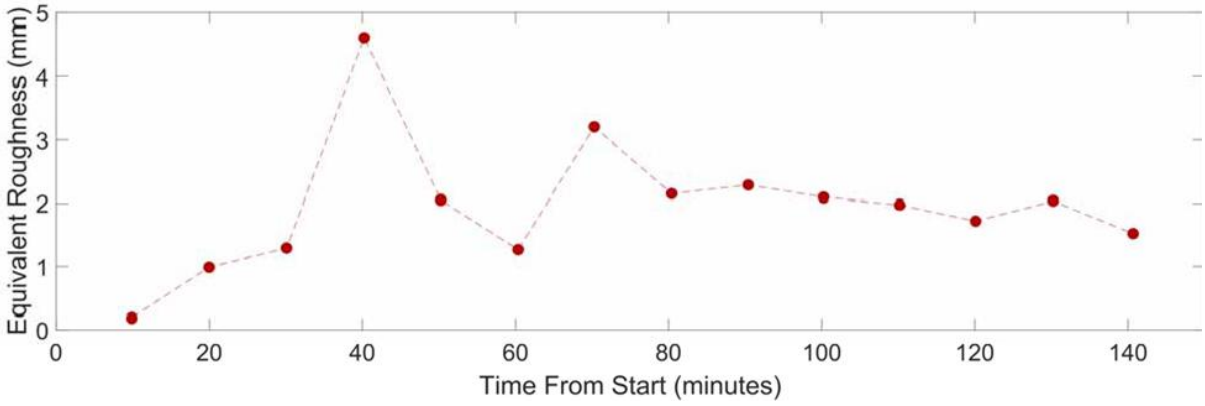

Table 081120.02: Summary of Roughness Parameters

Time (min.)	RMS (mm)	Skewness	Peak to Valley (mm)	ks,Flack-Schultz (mm)
9.8735	0.0183	0.8183	0.2864	0.1836
19.9735	0.0697	1.3407	1.0396	0.9894
30.0902	0.1146	0.9736	1.3738	1.2886
40.2235	0.2021	2.3096	2.8679	4.6131
50.2235	0.2347	0.6425	1.9853	2.0520
60.3402	0.1804	0.3977	1.4427	1.2642
70.2735	0.4524	0.4099	3.0574	3.2088
80.3902	0.3317	0.3184	2.4932	2.1456
90.4069	0.3321	0.3786	2.8515	2.2843
100.2402	0.2933	0.4150	2.5536	2.0908
110.1735	0.2753	0.4224	2.4646	1.9765
120.1069	0.3019	0.2016	2.2695	1.7198
130.2402	0.3717	0.1683	2.9026	2.0377
140.6902	0.3304	0.0277	2.5516	1.5195

Figure 081120.13: Frost Topography at 00:09:45

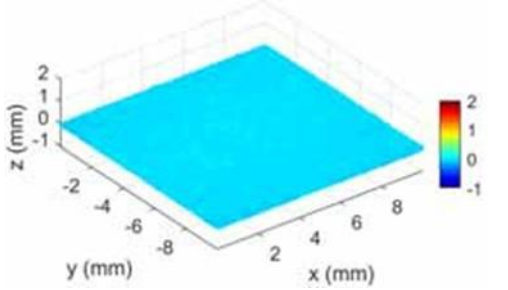

Figure 081120.14: Frost Topography at 00:19:51

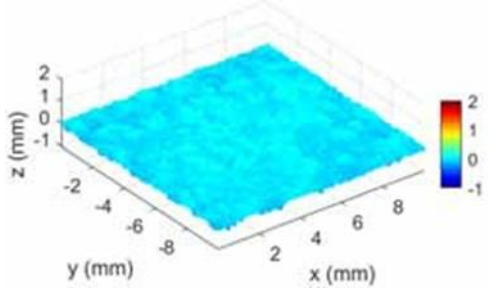

Figure 081120.15: Frost Topography at 00:29:58

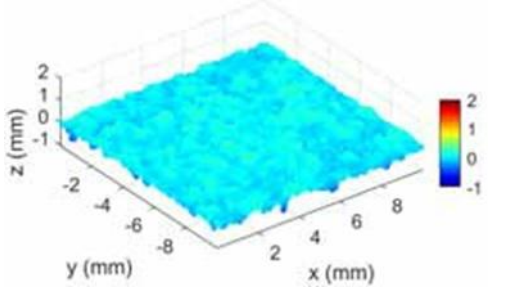

Figure 081120.16: Frost Topography at 00:40:06

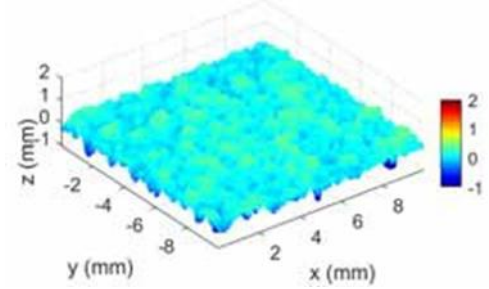

Figure 081120.17: Frost Topography at 00:50:06

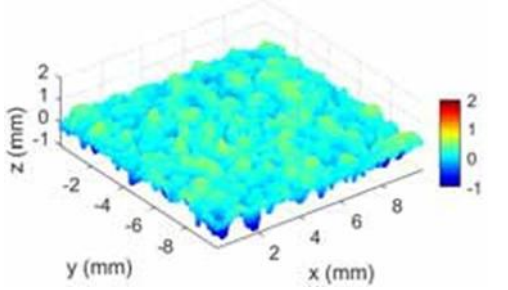

Figure 081120.18: Frost Topography at 01:00:13

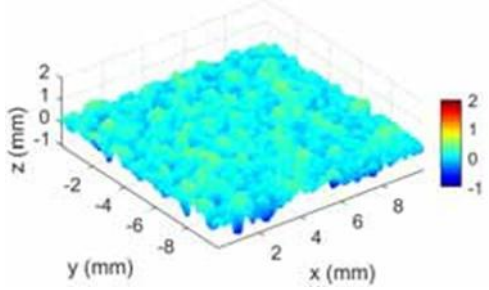

Figure 081120.19: Frost Topography at 01:10:09

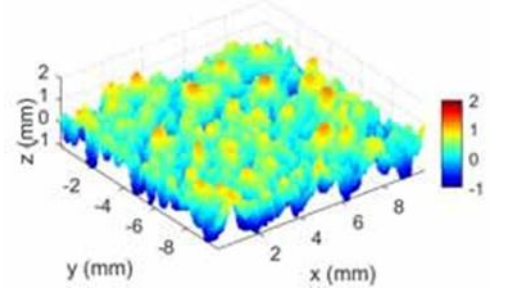

Figure 081120.20: Frost Topography at 01:20:16

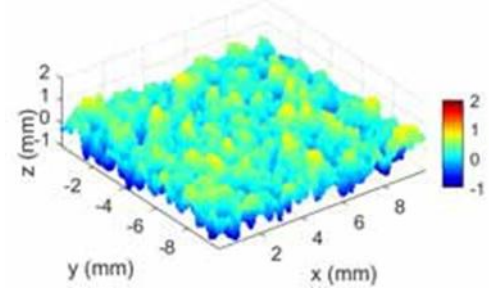

Figure 081120.21: Frost Topography at 01:30:17

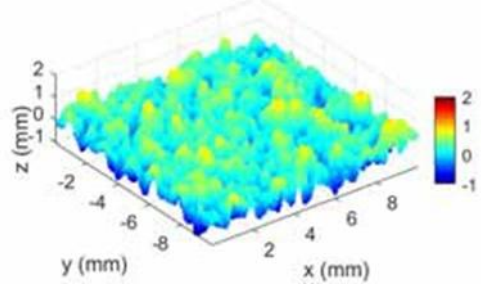

Figure 081120.22: Frost Topography at 01:40:07

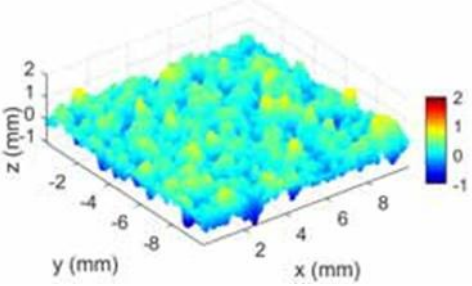

Figure 081120.23: Frost Topography at 01:50:03

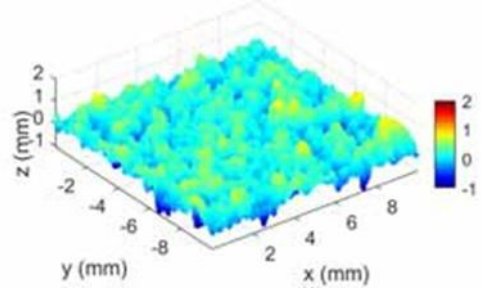

Figure 081120.24: Frost Topography at 01:59:59

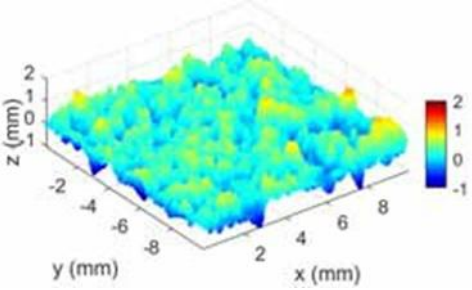

Figure 081120.25: Frost Topography at 02:10:07

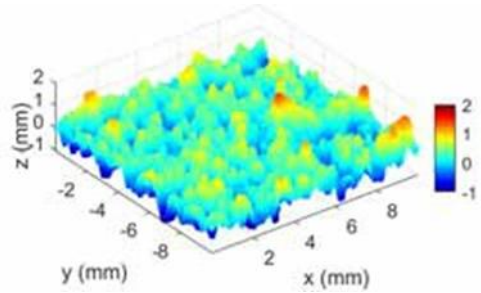

Figure 081120.26: Frost Topography at 02:20:34

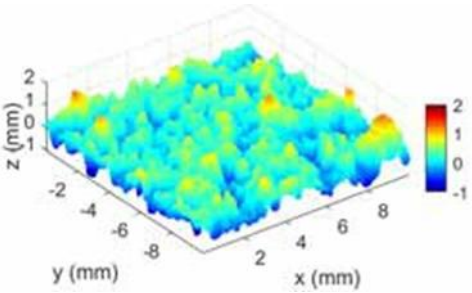

CAFF Conditions Report – Case Date: 081420

Table 081420.01: Summary of Measured Test Variables

Variable	Mean	St. Dev.	Rand. Unc.
T_air (C)	4.2952	0.1473	0.0050
Rh (%)	80.2591	4.7987	0.1614
Omega (kg_v/kg_da)	0.00419765	0.00028513	0.00000959
V_air (m/s)	0.1333	0.1063	0.0036
T_skin (C)	-14.6844	0.3647	0.0123
T_floor (C)	-20.4803	0.0189	0.0006

Figure 081420.01: Temperature and Voltage Control Time History

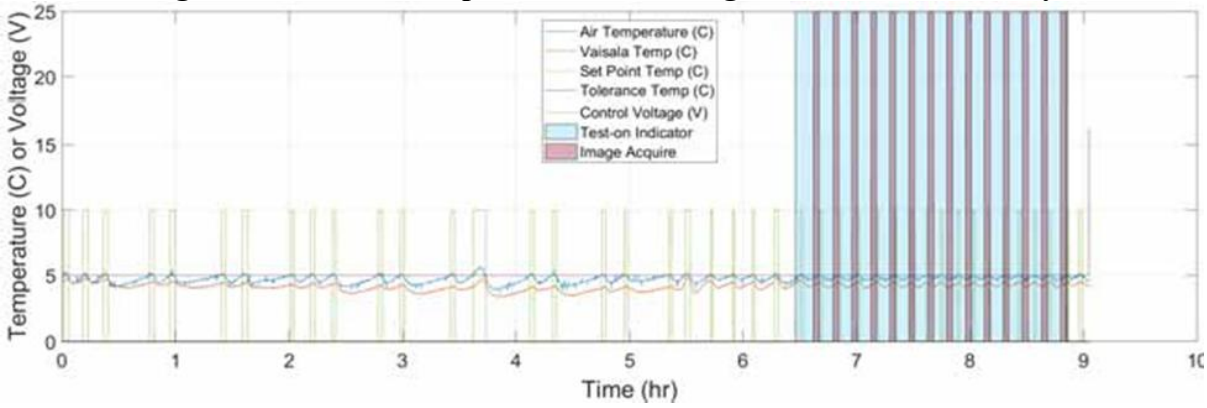

Figure 081420.02: Relative Humidity Time History

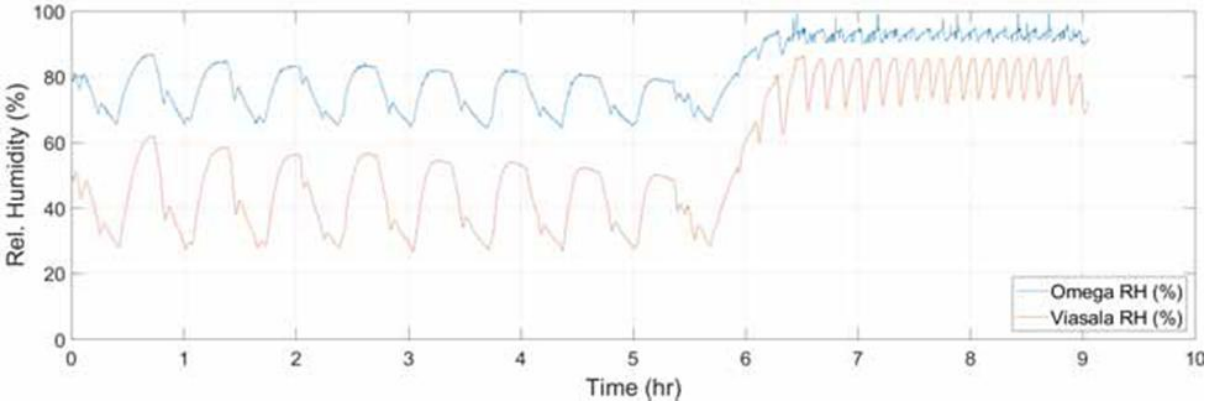

Figure 081420.03: Velocity Time History

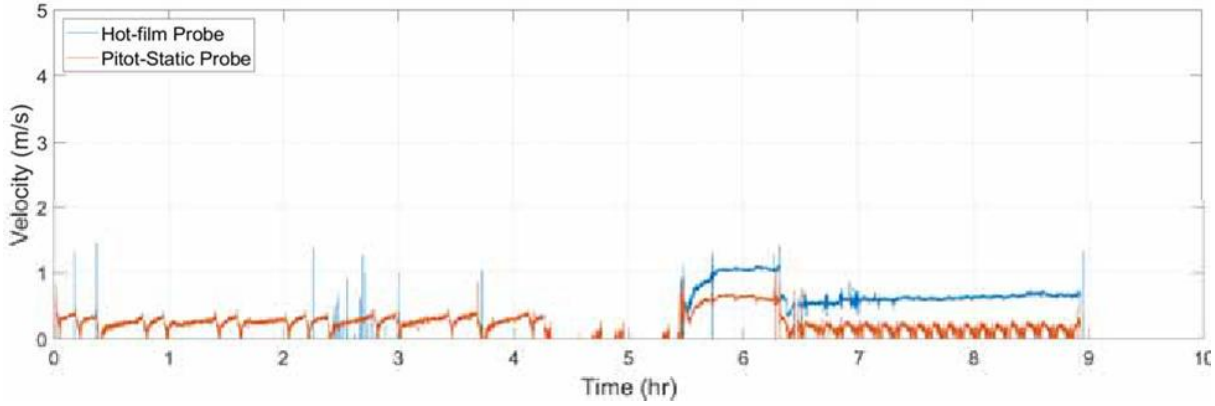

Figure 081420.04: Coolant Return Temperature Time History

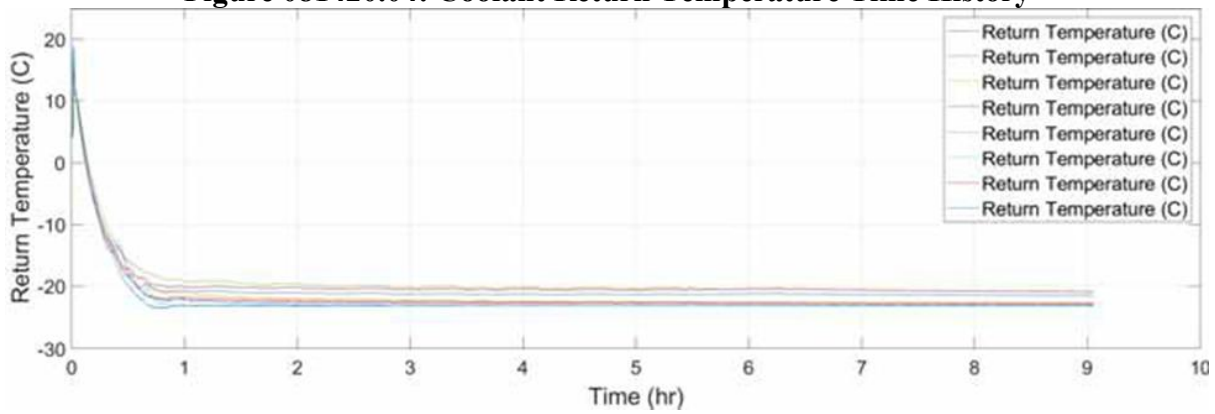

Figure 081420.05: Coolant Supply Temperature Time History

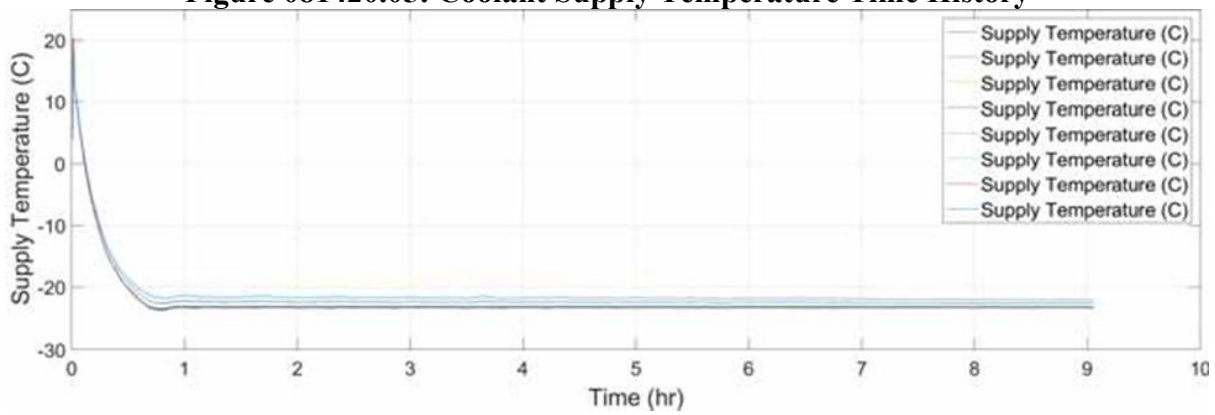

Figure 081420.06: Skin Temperature Time History

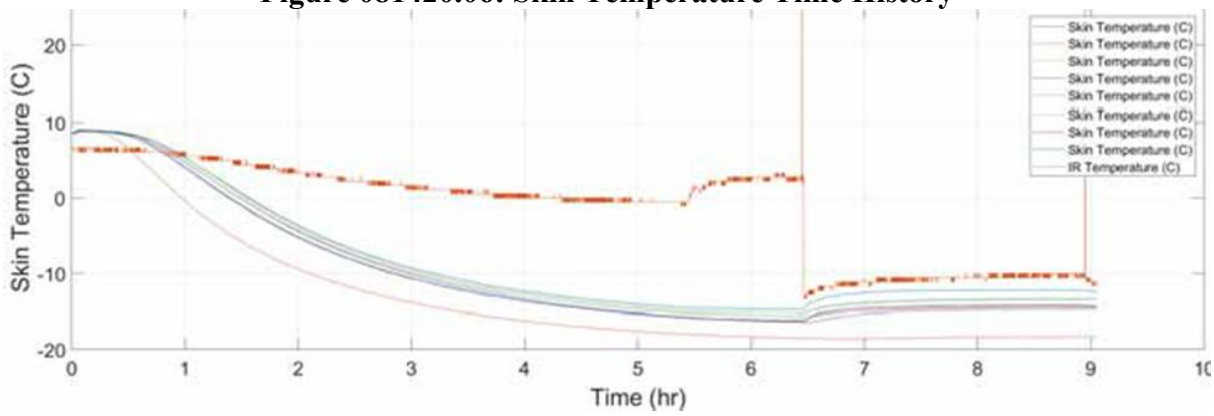

Figure 081420.07: Floor Temperature Time History

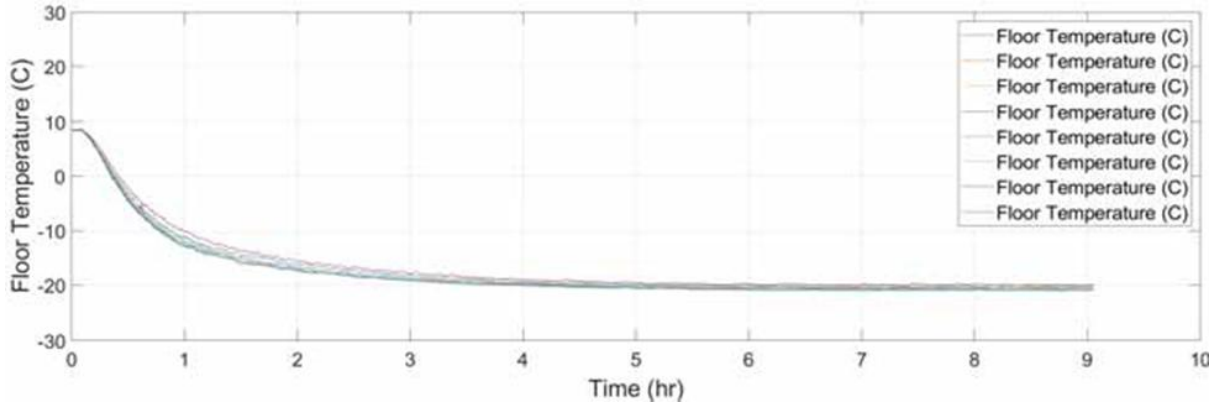

Figure 081420.08: Skin Temperature Slope Time History

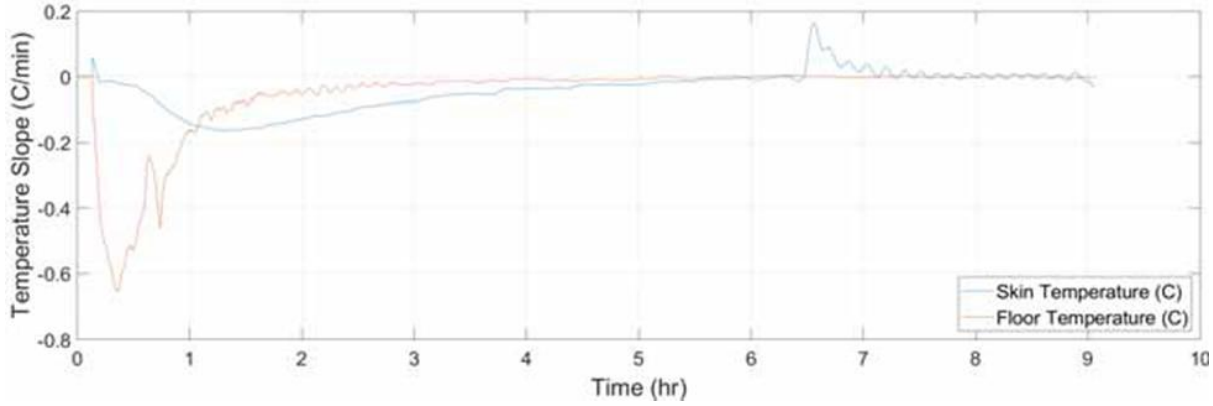

Figure 0814200.09: RMS Height Evolution

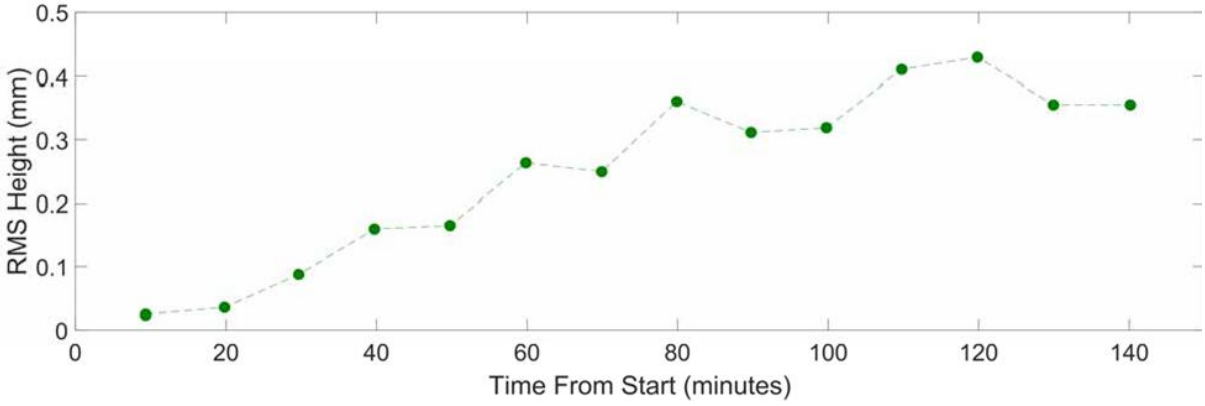

Figure 0814200.10: Skewness Evolution

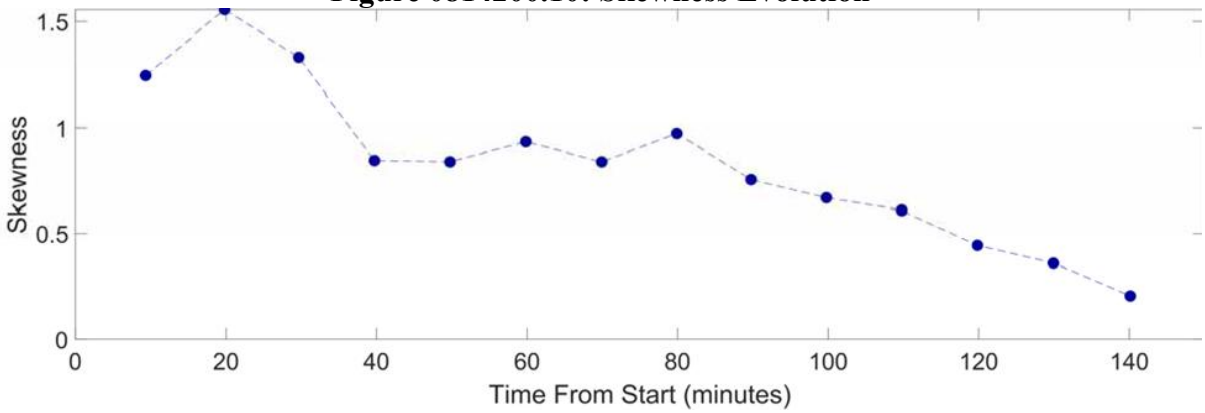

Figure 0814200.11: Peak to Valley Evolution

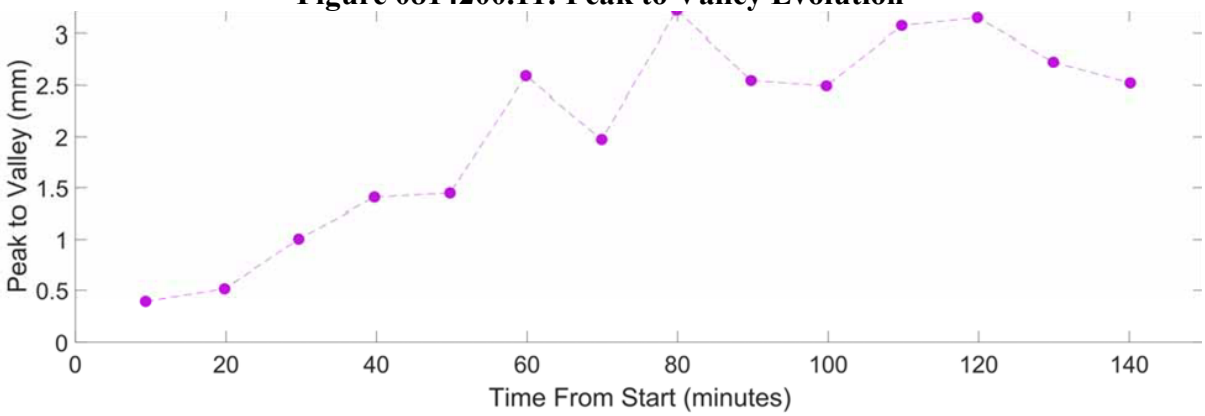

Figure 081420.12: Equivalent Roughness Evolution

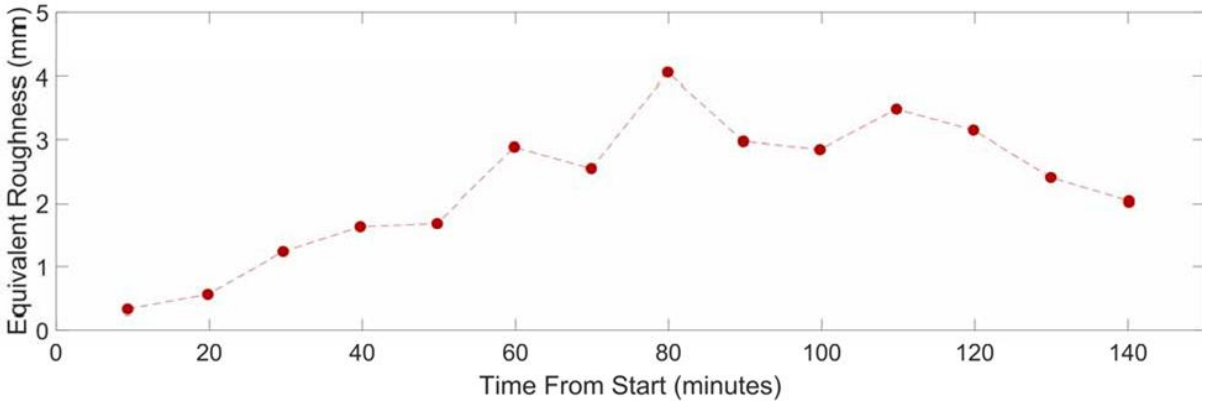

Table 081420.02: Summary of Roughness Parameters

Time (min.)	RMS (mm)	Skewness	Peak to Valley (mm)	ks,Flack-Schultz (mm)
9.3175	0.0235	1.2463	0.3896	0.3157
19.8008	0.0344	1.5573	0.5144	0.5510
29.6508	0.0872	1.3333	1.0042	1.2334
39.7175	0.1593	0.8444	1.4080	1.6323
49.7675	0.1650	0.8388	1.4475	1.6834
59.8342	0.2637	0.9351	2.5937	2.8864
69.9008	0.2492	0.8381	1.9740	2.5423
79.8842	0.3613	0.9740	3.2299	4.0637
89.7675	0.3116	0.7529	2.5455	2.9787
99.7675	0.3193	0.6667	2.4922	2.8480
109.7675	0.4111	0.6089	3.0771	3.4934
119.8342	0.4306	0.4438	3.1553	3.1550
129.9342	0.3558	0.3589	2.7268	2.3993
140.1342	0.3559	0.2006	2.5216	2.0253

Figure 081420.13: Frost Topography at 00:09:21

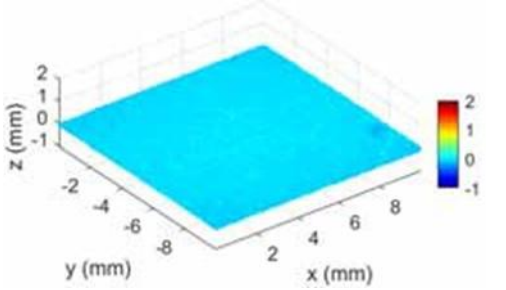

Figure 081420.14: Frost Topography at 00:19:50

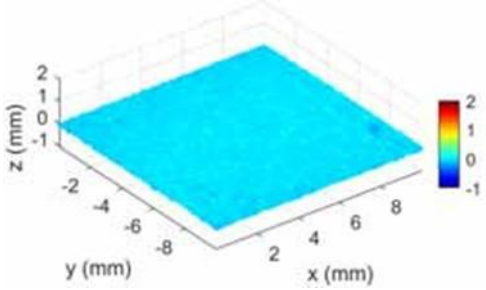

Figure 081420.15: Frost Topography at 00:29:41

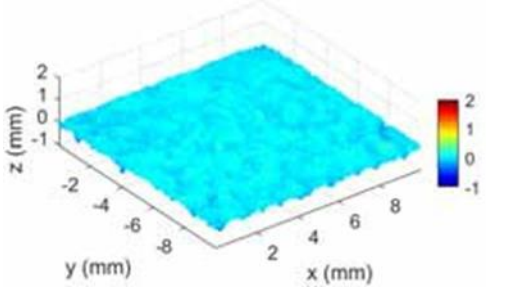

Figure 081420.16: Frost Topography at 00:39:45

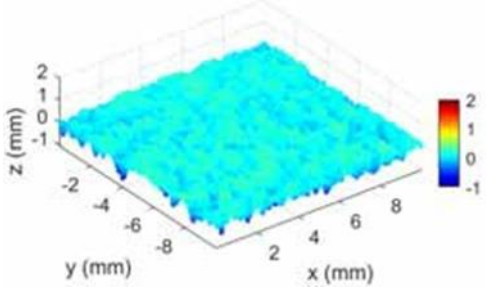

Figure 081420.17: Frost Topography at 00:49:48

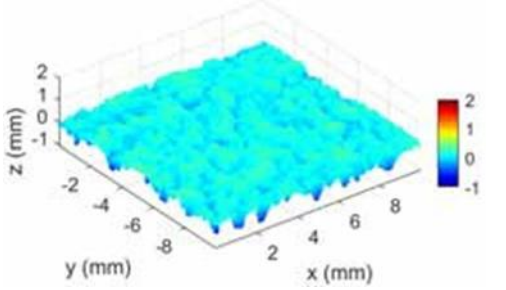

Figure 081420.18: Frost Topography at 00:59:52

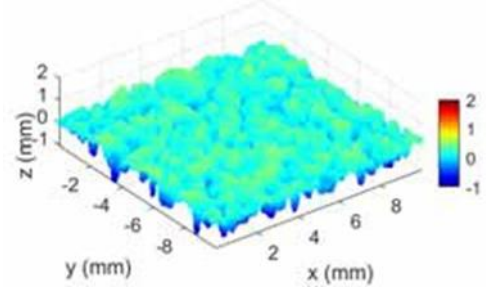

Figure 081420.19: Frost Topography at 01:09:56

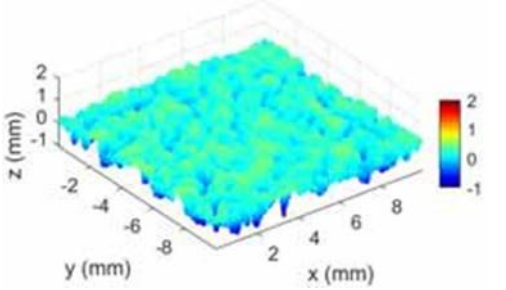

Figure 081420.20: Frost Topography at 01:19:55

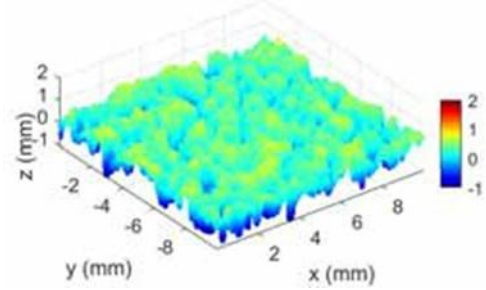

Figure 081420.21: Frost Topography at 01:29:48

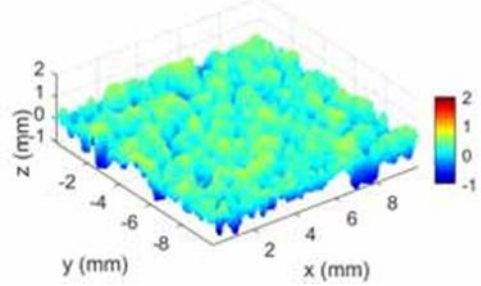

Figure 081420.22: Frost Topography at 01:39:48

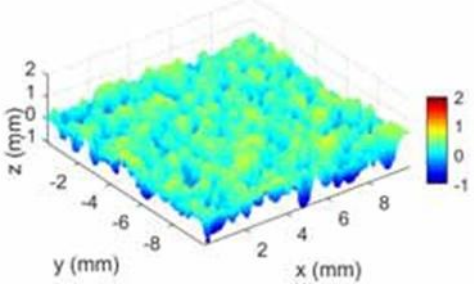

Figure 081420.23: Frost Topography at 01:49:48

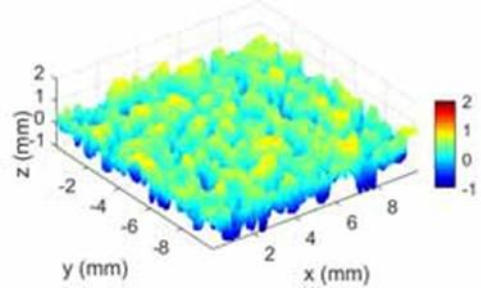

Figure 081420.24: Frost Topography at 01:59:52

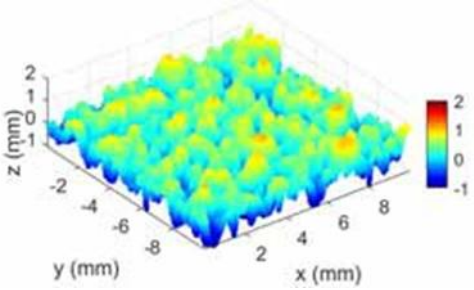

Figure 081420.25: Frost Topography at 02:09:58

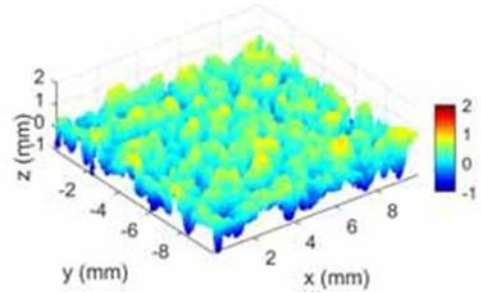

Figure 081420.26: Frost Topography at 02:20:10

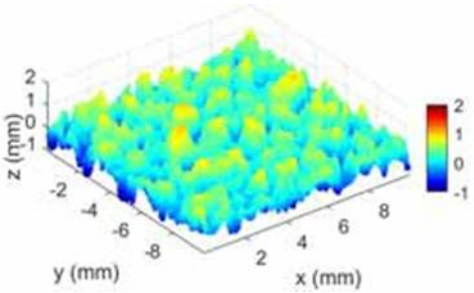

CAFF Conditions Report – Case Date: 090820

Table 090820.01: Summary of Measured Test Variables

Variable	Mean	St. Dev.	Rand. Unc.
T_air (C)	14.9768	0.4919	0.0165
Rh (%)	80.6460	1.8746	0.0630
Omega (kg_v/kg_da)	0.00870914	0.00036151	0.00001214
V_air (m/s)	1.3335	0.1348	0.0045
T_skin (C)	-9.4594	1.1010	0.0370
T_floor (C)	-19.1451	0.1917	0.0064

Figure 090820.01: Temperature and Voltage Control Time History

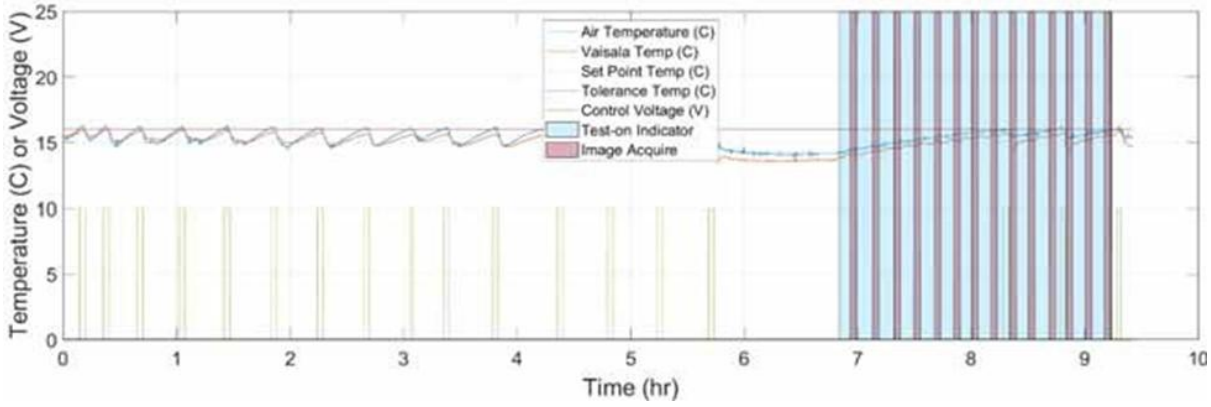

Figure 090820.02: Relative Humidity Time History

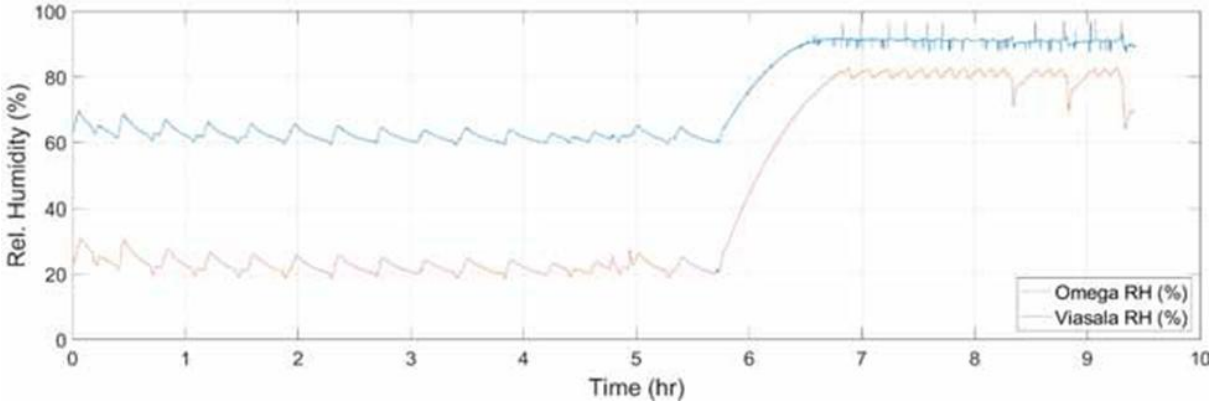

Figure 090820.03: Velocity Time History

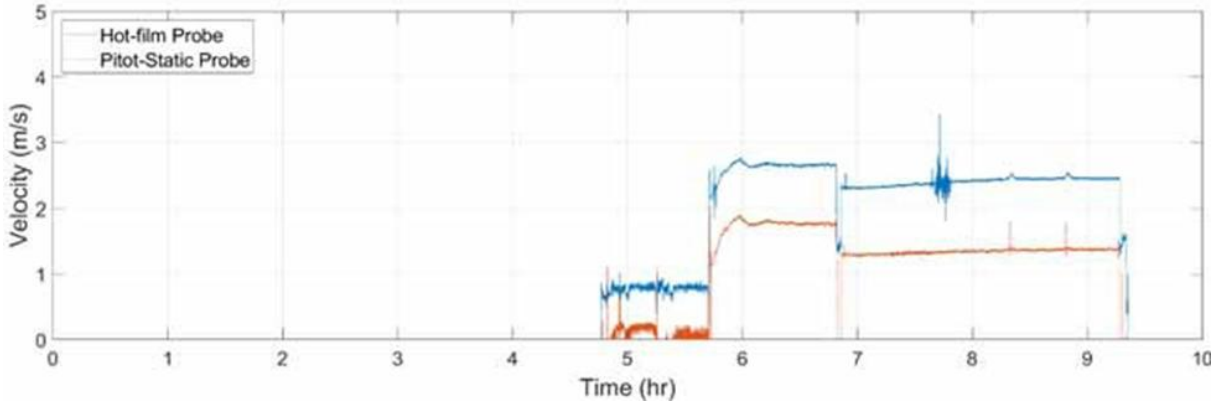

Figure 090820.04: Coolant Return Temperature Time History

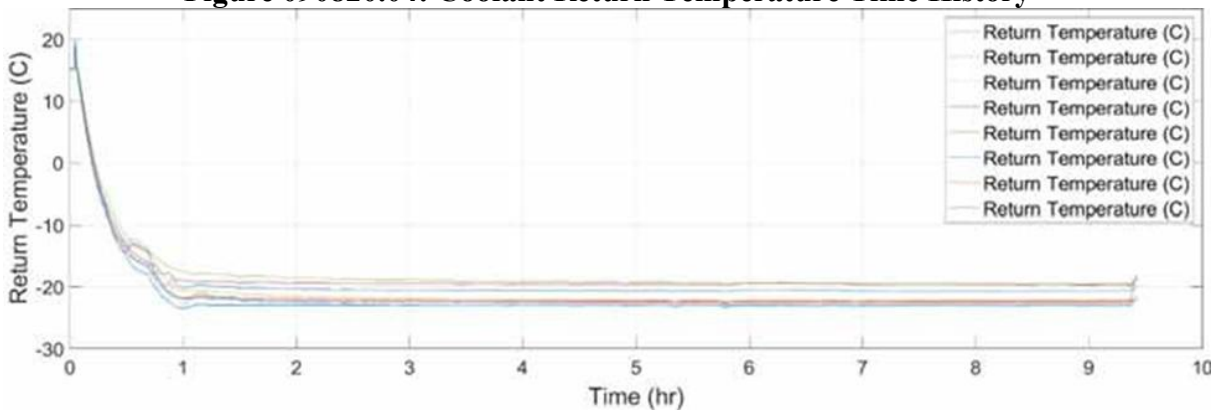

Figure 090820.05: Coolant Supply Temperature Time History

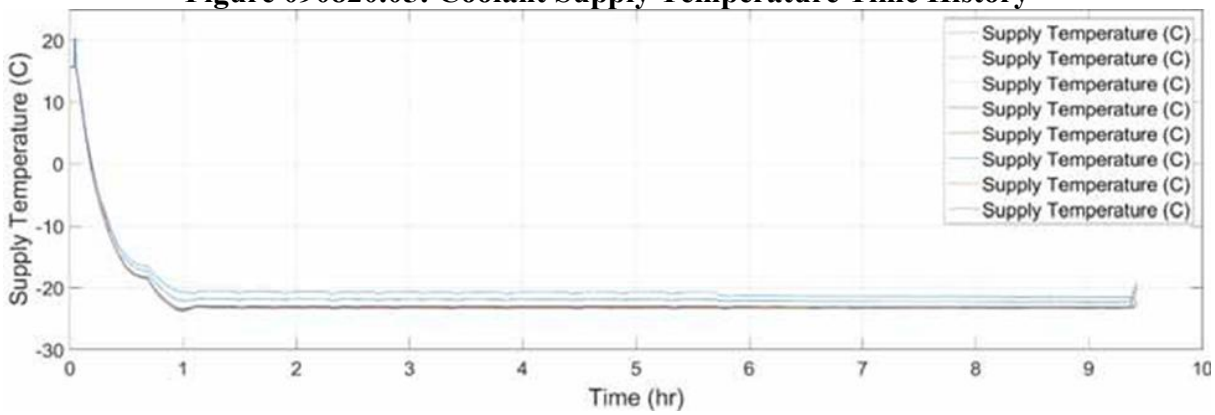

Figure 090820.06: Skin Temperature Time History

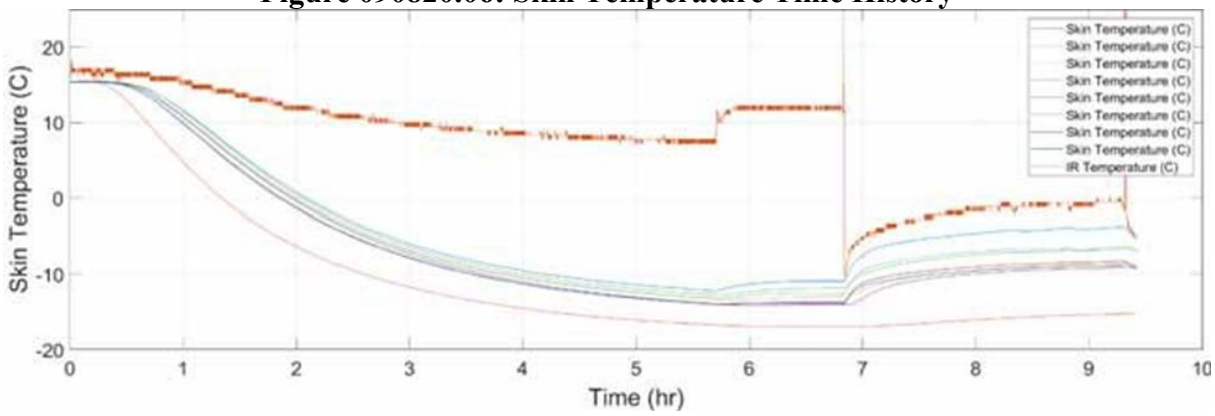

Figure 090820.07: Floor Temperature Time History

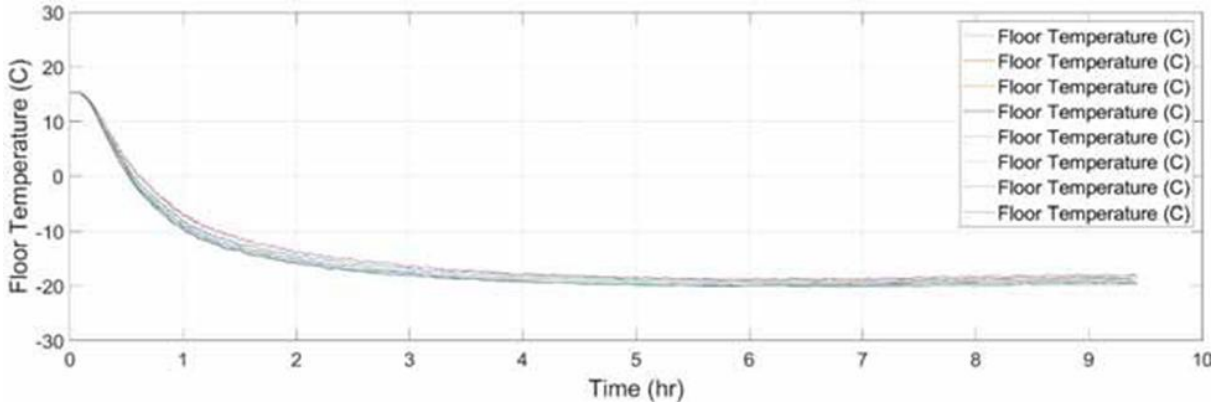

Figure 090820.08: Skin Temperature Slope Time History

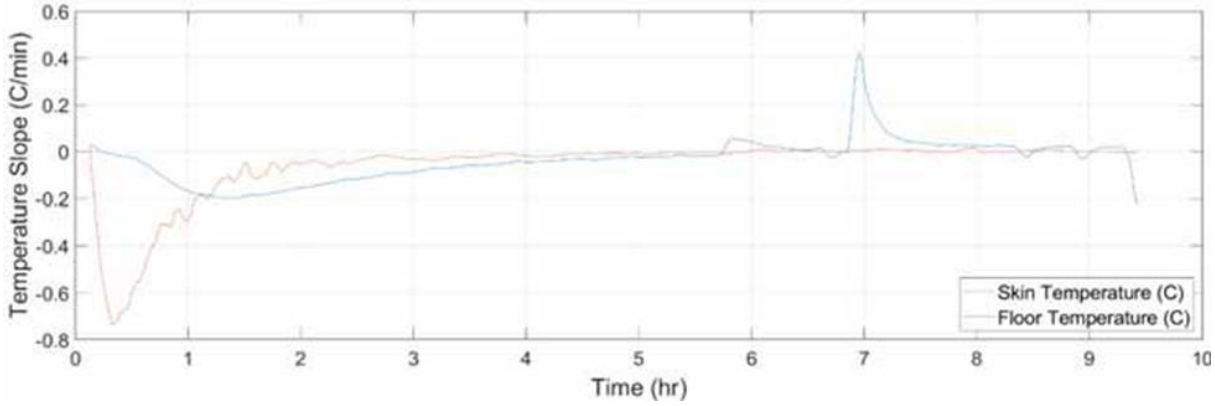

Figure 090820.09: RMS Height Evolution

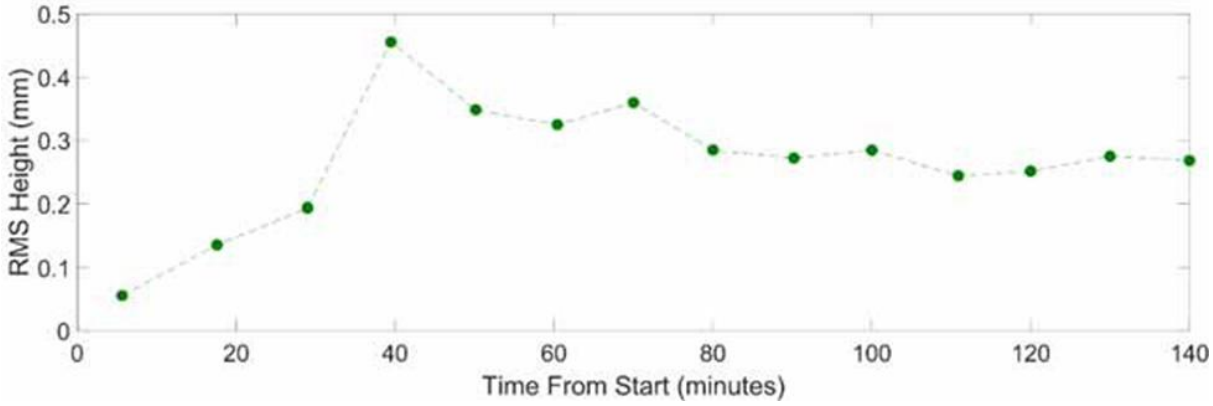

Figure 090820.10: Skewness Evolution

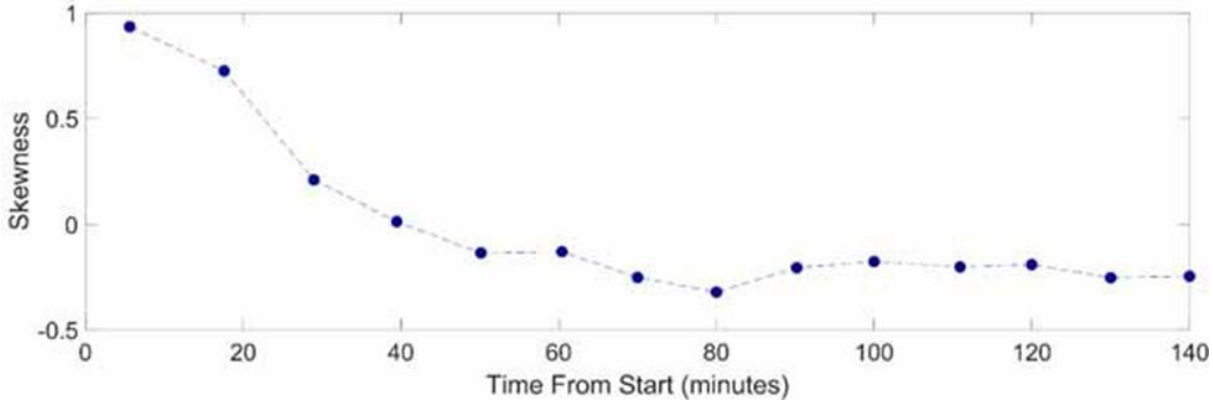

Figure 090820.11: Peak to Valley Evolution

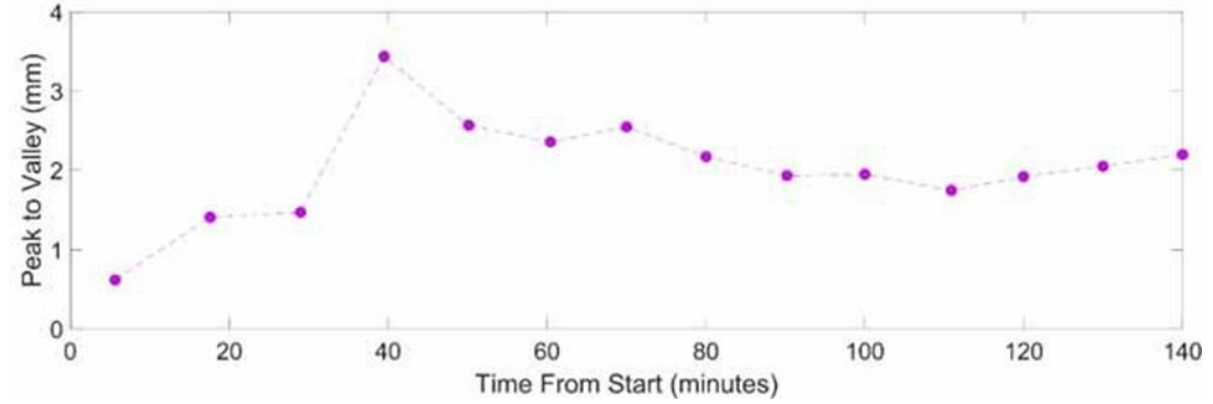

Figure 090820.12: Equivalent Roughness Evolution

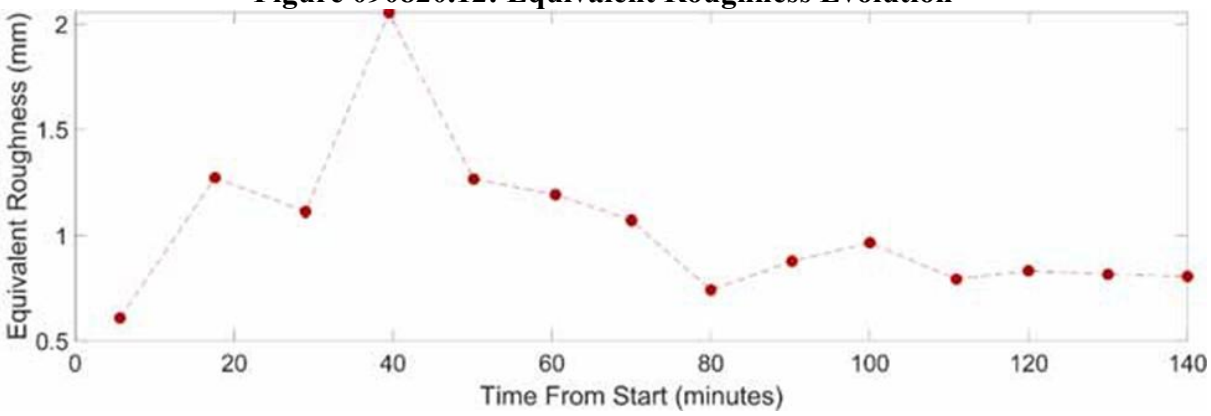

Table 090820.02: Summary of Roughness Parameters

Time (min.)	RMS (mm)	Skewness	Peak to Valley (mm)	ks,Flack-Schultz (mm)
5.5927	0.0556	0.9340	0.6167	0.6076
17.5760	0.1358	0.7246	1.4108	1.2695
28.9593	0.1935	0.2066	1.4738	1.1090
39.4593	0.4555	0.0129	3.4343	2.0535
50.1260	0.3483	-0.1357	2.5640	1.2634
60.4093	0.3248	-0.1300	2.3539	1.1889
69.9927	0.3594	-0.2521	2.5424	1.0693
79.9927	0.2845	-0.3216	2.1660	0.7406
90.1927	0.2717	-0.2064	1.9260	0.8769
99.9927	0.2842	-0.1765	1.9432	0.9650
110.8927	0.2436	-0.2021	1.7384	0.7922
119.9760	0.2510	-0.1910	1.9129	0.8318
129.9760	0.2746	-0.2534	2.0445	0.8150
139.9927	0.2677	-0.2462	2.1946	0.8053

Figure 090820.13: Frost Topography at 00:05:28

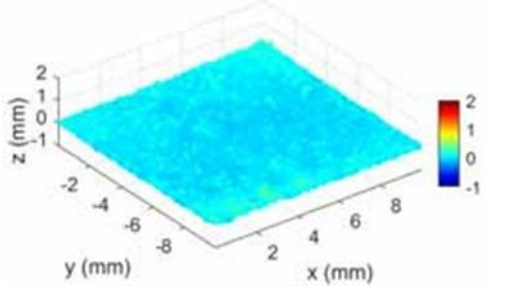

Figure 090820.14: Frost Topography at 00:17:27

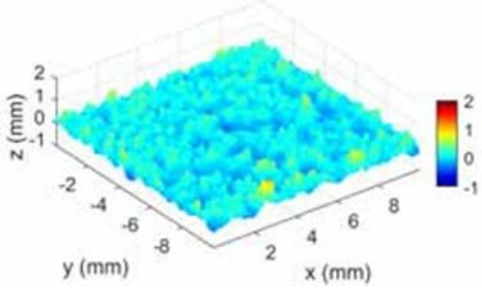

Figure 090820.15: Frost Topography at 00:28:50

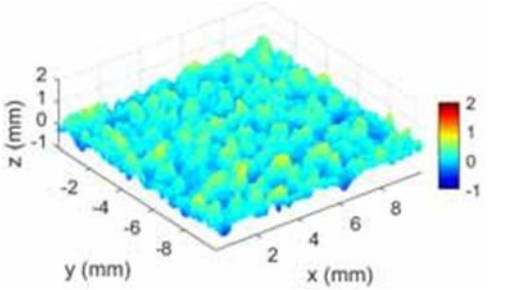

Figure 090820.16: Frost Topography at 00:39:20

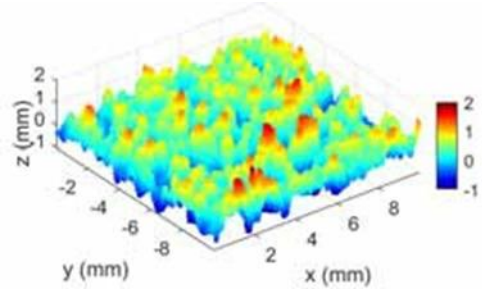

Figure 090820.17: Frost Topography at 00:50:00

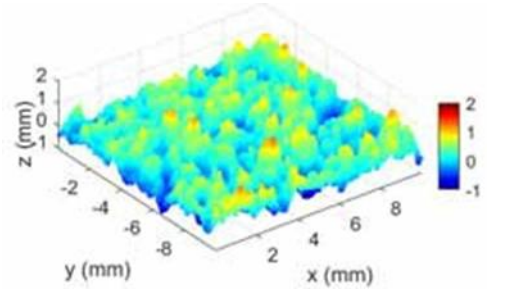

Figure 090820.18: Frost Topography at 01:00:17

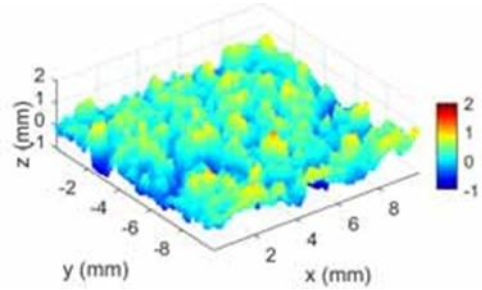

Figure 090820.19: Frost Topography at 01:09:52

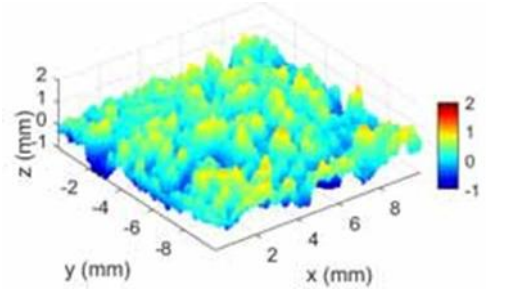

Figure 090820.20: Frost Topography at 01:19:52

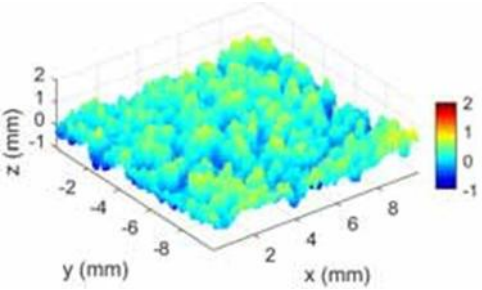

Figure 090820.21: Frost Topography at 01:30:04

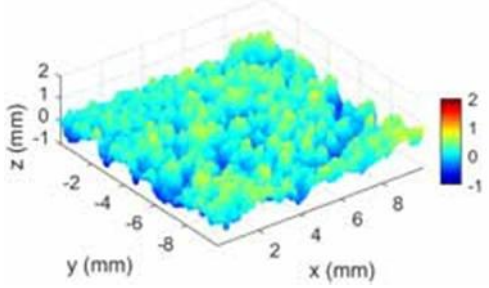

Figure 090820.22: Frost Topography at 01:39:52

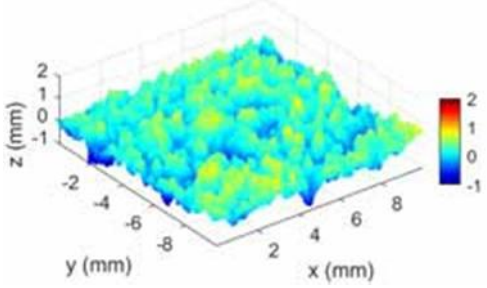

Figure 090820.23: Frost Topography at 01:50:46

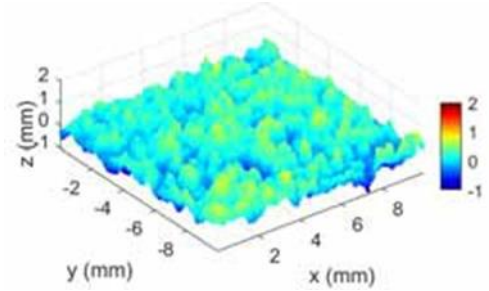

Figure 090820.24: Frost Topography at 01:59:51

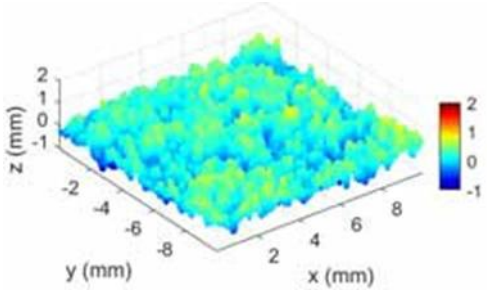

Figure 090820.25: Frost Topography at 02:09:51

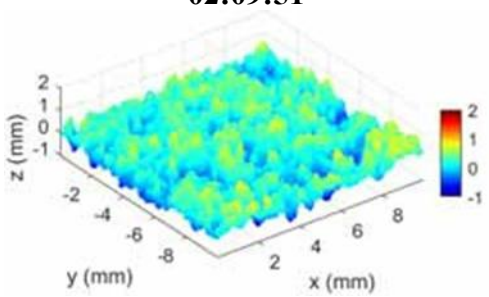

Figure 090820.26: Frost Topography at 02:19:52

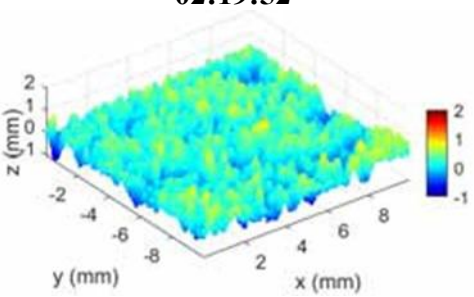

CAFF Conditions Report – Case Date: 091520

Table 091520.01: Summary of Measured Test Variables

Variable	Mean	St. Dev.	Rand. Unc.
T_air (C)	4.1513	0.3174	0.0107
Rh (%)	79.6375	5.3431	0.1794
Omega (kg_v/kg_da)	0.00410181	0.00034963	0.00001174
V_air (m/s)	1.3288	0.0852	0.0029
T_skin (C)	-13.2320	0.5253	0.0176
T_floor (C)	-20.2213	0.0404	0.0014

Figure 091520.01: Temperature and Voltage Control Time History

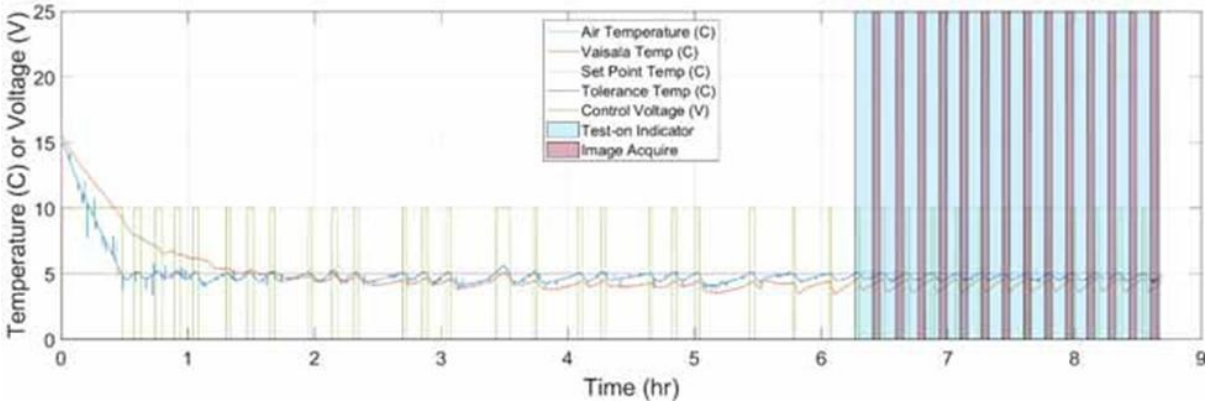

Figure 091520.02: Relative Humidity Time History

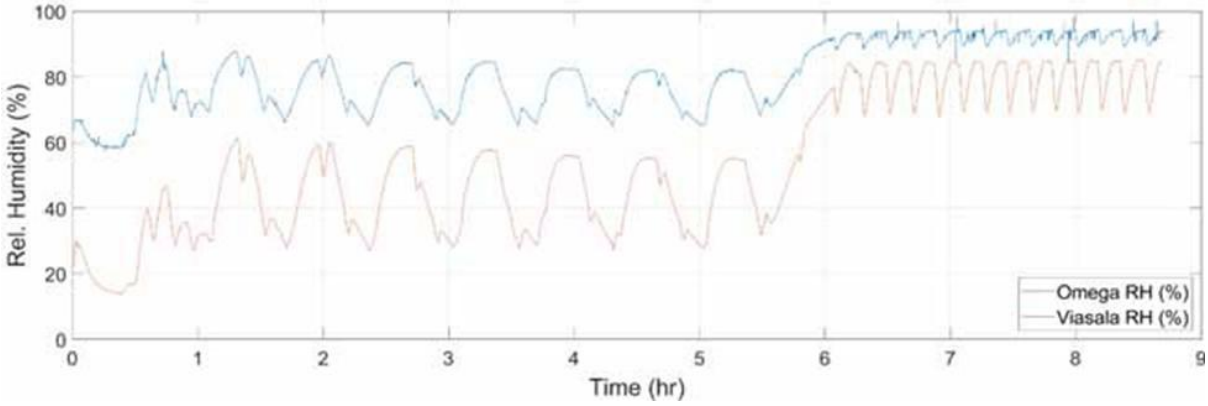

Figure 091520.03: Velocity Time History

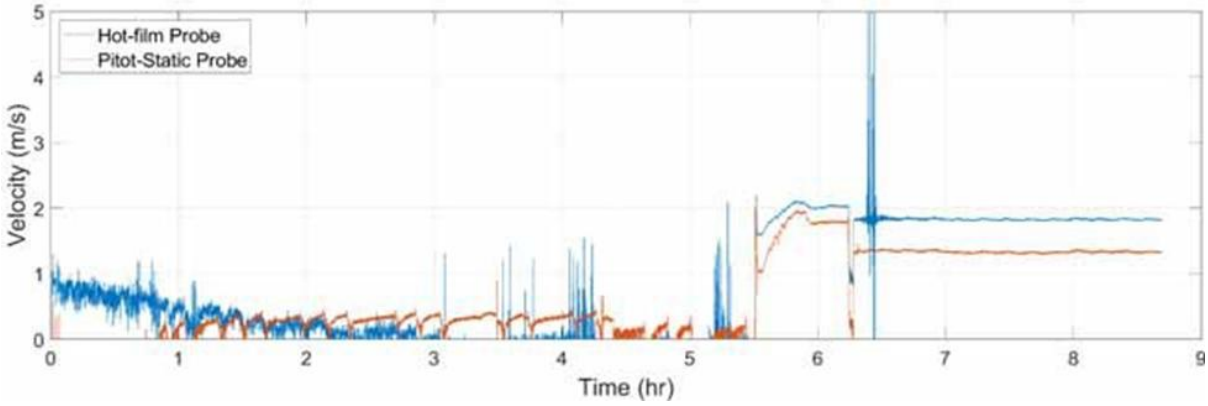

Figure 091520.04: Coolant Return Temperature Time History

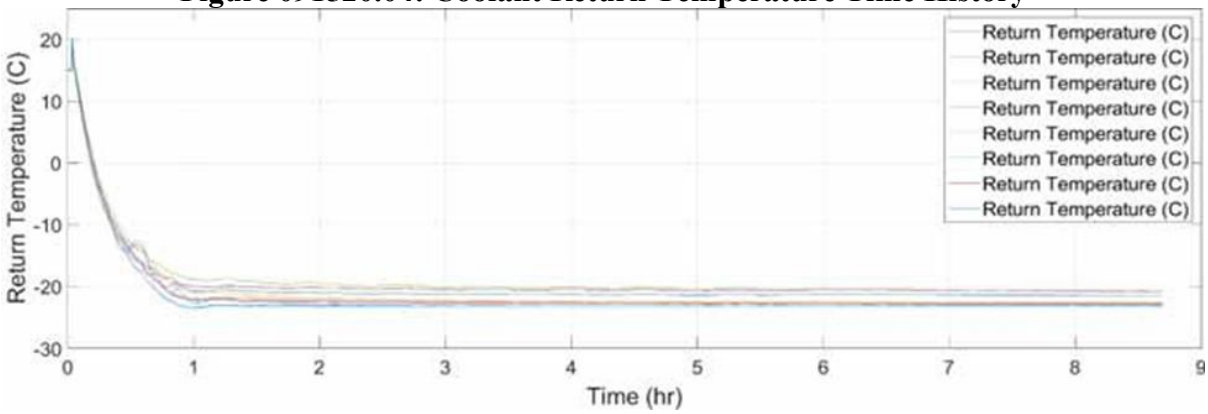

Figure 091520.05: Coolant Supply Temperature Time History

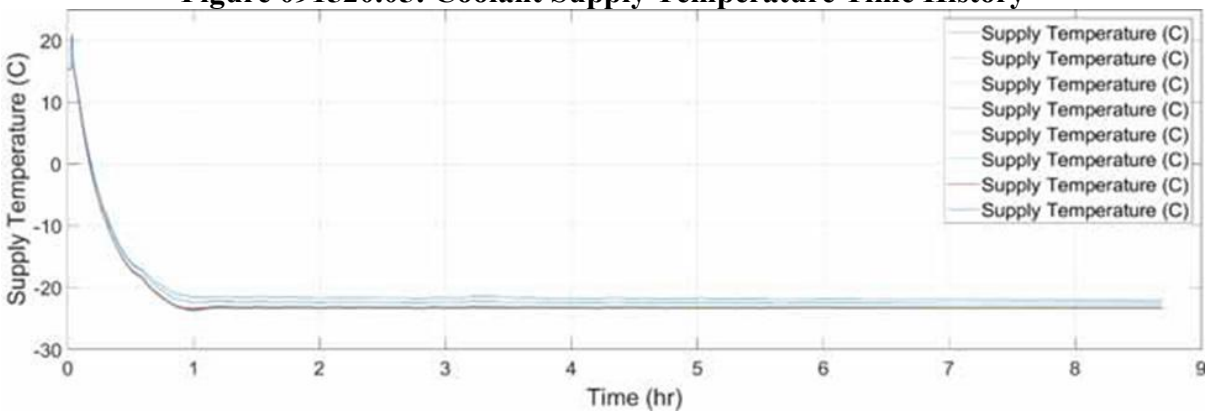

Figure 091520.06: Skin Temperature Time History

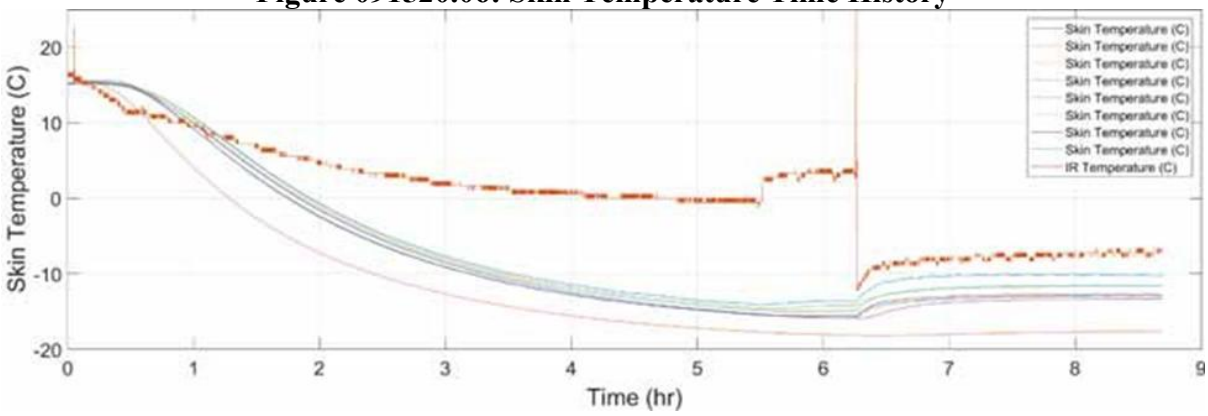

Figure 091520.07: Floor Temperature Time History

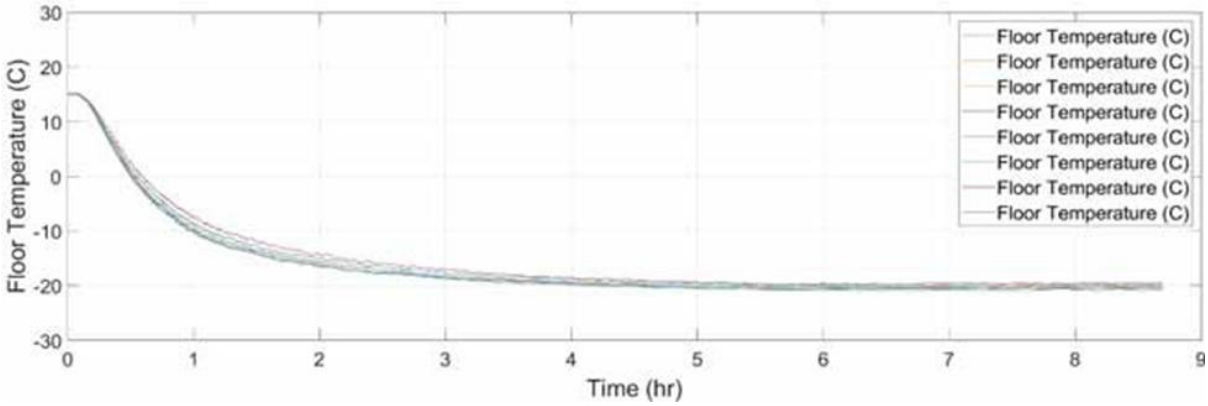

Figure 091520.08: Skin Temperature Slope Time History

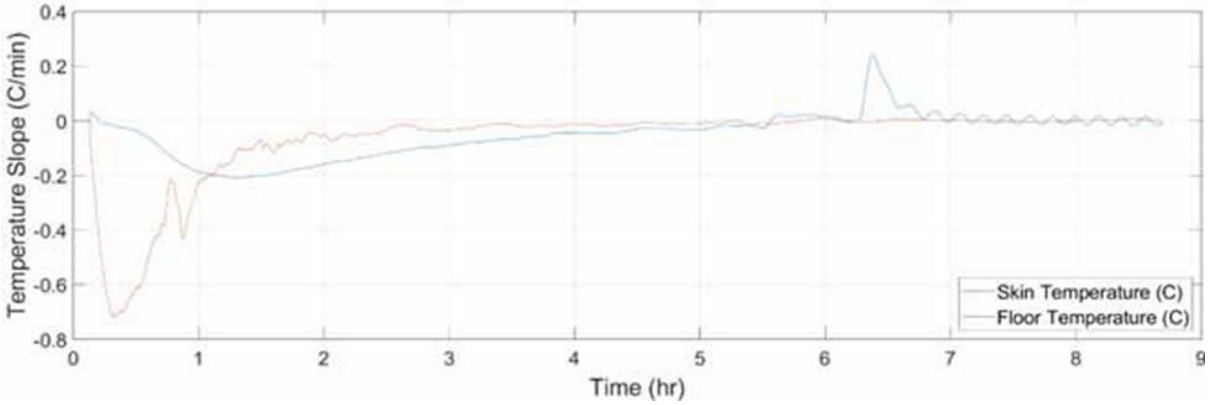

Figure 091520.09: RMS Height Evolution

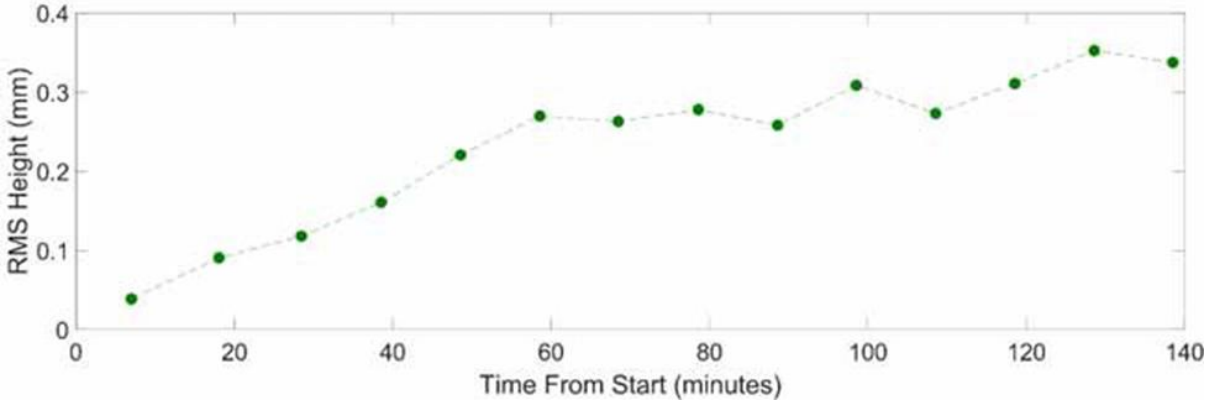

Figure 091520.10: Skewness Evolution

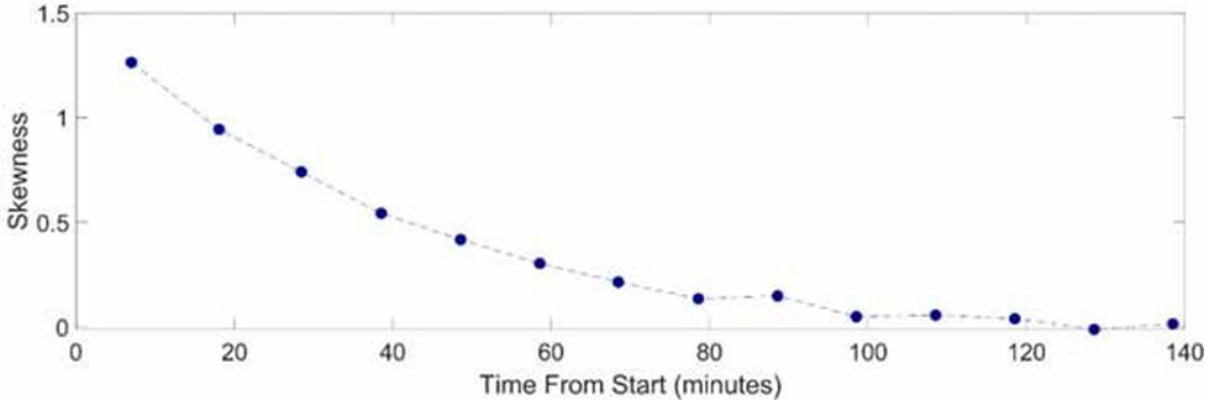

Figure 091520.11: Peak to Valley Evolution

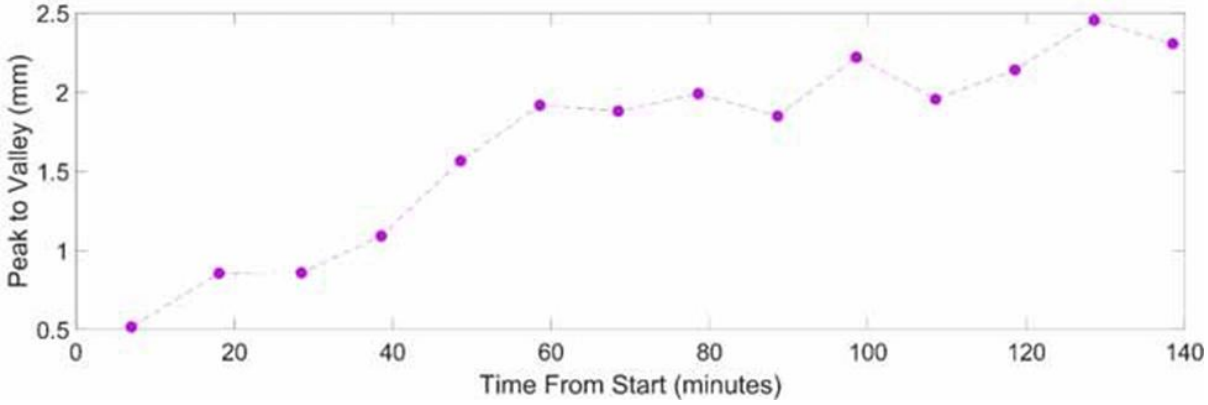

Figure 091520.12: Equivalent Roughness Evolution

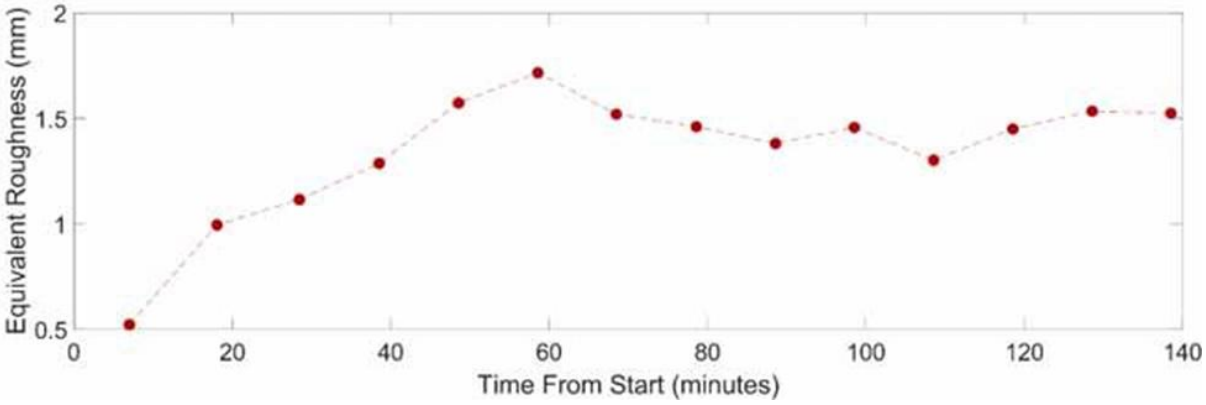

Table 091520.02: Summary of Roughness Parameters

Time (min.)	RMS (mm)	Skewness	Peak to Valley (mm)	ks,Flack-Schultz (mm)
6.9536	0.0385	1.2634	0.5154	0.5227
18.0369	0.0904	0.9435	0.8548	0.9953
28.4369	0.1179	0.7402	0.8576	1.1154
38.5202	0.1605	0.5423	1.0897	1.2874
48.5369	0.2204	0.4165	1.5651	1.5735
58.5536	0.2696	0.3028	1.9160	1.7162
68.4536	0.2629	0.2142	1.8790	1.5196
78.5702	0.2777	0.1335	1.9899	1.4608
88.5869	0.2581	0.1479	1.8475	1.3813
98.5202	0.3085	0.0481	2.2204	1.4573
108.5369	0.2729	0.0556	1.9548	1.3020
118.5536	0.3106	0.0388	2.1401	1.4497
128.5702	0.3523	-0.0125	2.4541	1.5340
138.5036	0.3374	0.0144	2.3053	1.5242

Figure 091520.13: Frost Topography at 00:08:14

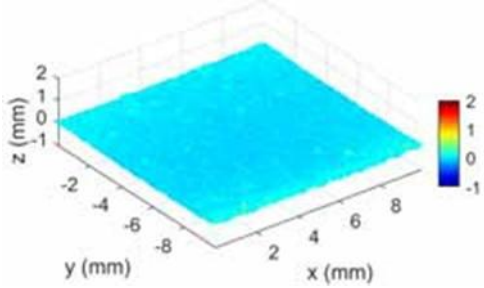

Figure 091520.14: Frost Topography at 00:19:19

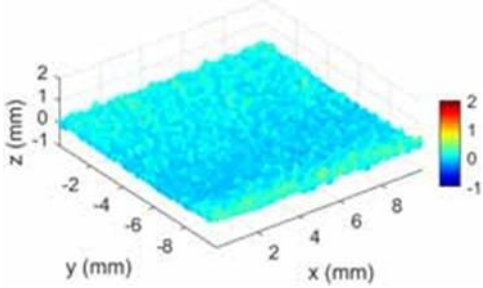

Figure 091520.15: Frost Topography at 00:29:43

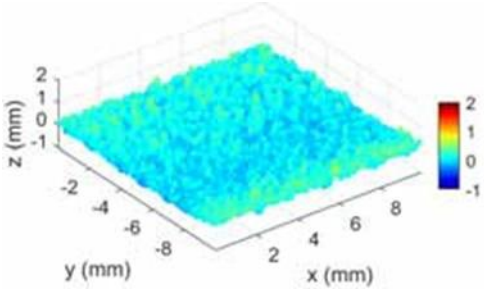

Figure 091520.16: Frost Topography at 00:39:48

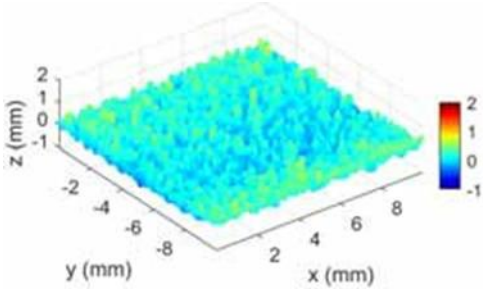

Figure 091520.17: Frost Topography at 00:49:49

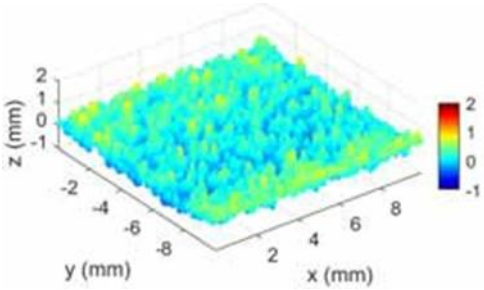

Figure 091520.18: Frost Topography at 00:59:50

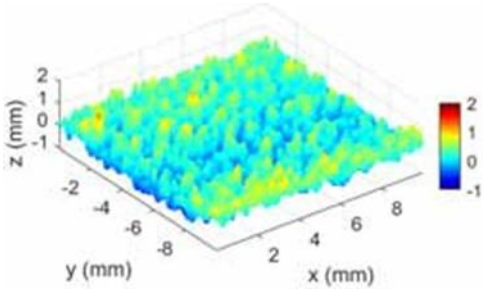

Figure 091520.19: Frost Topography at 01:09:44

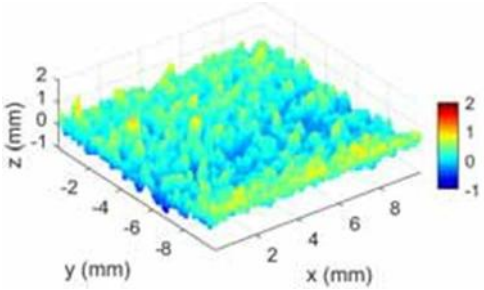

Figure 091520.20: Frost Topography at 01:19:51

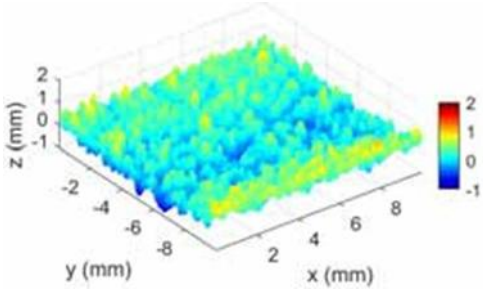

Figure 091520.21: Frost Topography at 01:29:52

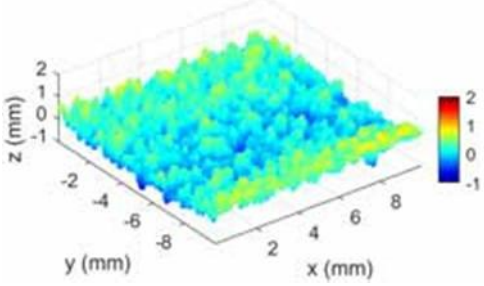

Figure 091520.22: Frost Topography at 01:39:48

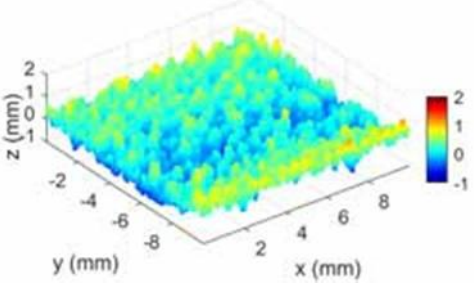

Figure 091520.23: Frost Topography at 01:49:49

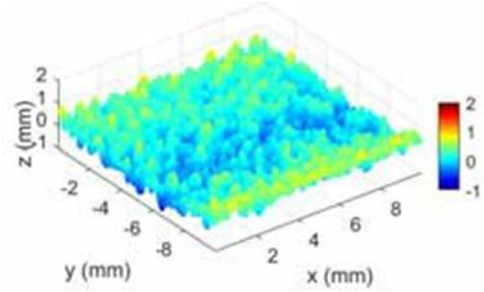

Figure 091520.24: Frost Topography at 01:59:50

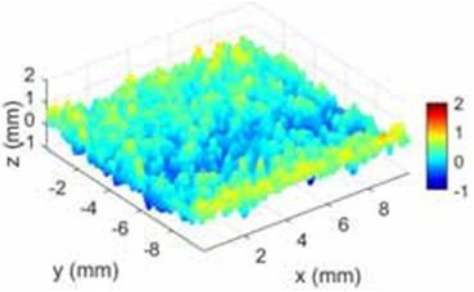

Figure 091520.25: Frost Topography at 02:09:51

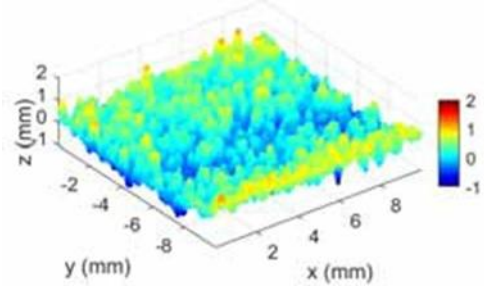

Figure 091520.26: Frost Topography at 02:19:47

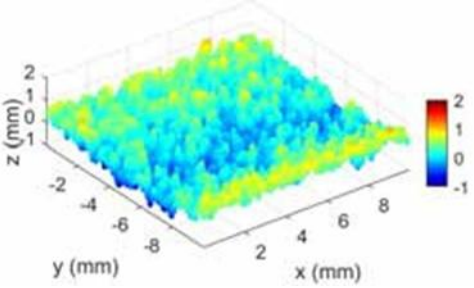

CAFF Conditions Report – Case Date: 091720

Table 091720.01: Summary of Measured Test Variables

Variable	Mean	St. Dev.	Rand. Unc.
T_air (C)	15.2083	0.3511	0.0118
Rh (%)	79.1646	3.1538	0.1060
Omega (kg_v/kg_da)	0.00864396	0.00049287	0.00001657
V_air (m/s)	1.3456	0.1494	0.0050
T_skin (C)	-9.0922	1.0495	0.0353
T_floor (C)	-19.0285	0.1773	0.0060

Figure 091720.01: Temperature and Voltage Control Time History

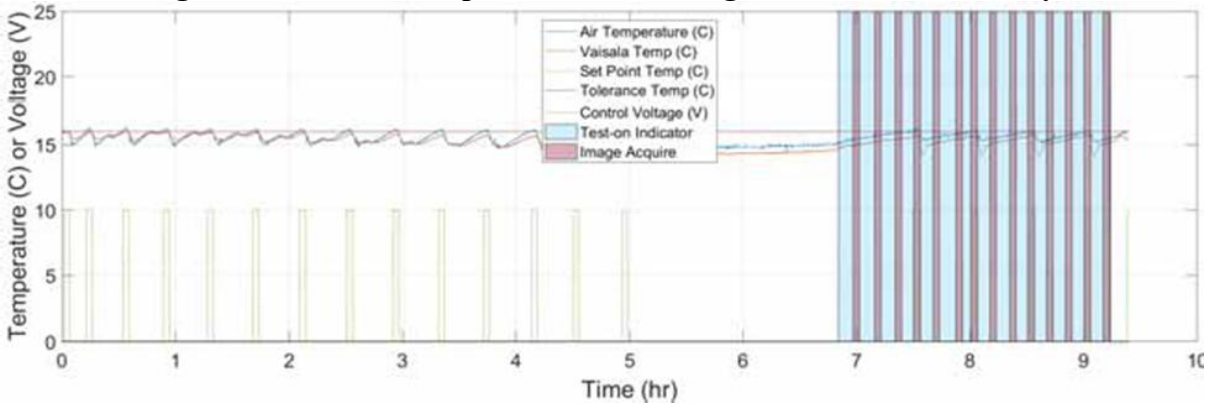

Figure 091720.02: Relative Humidity Time History

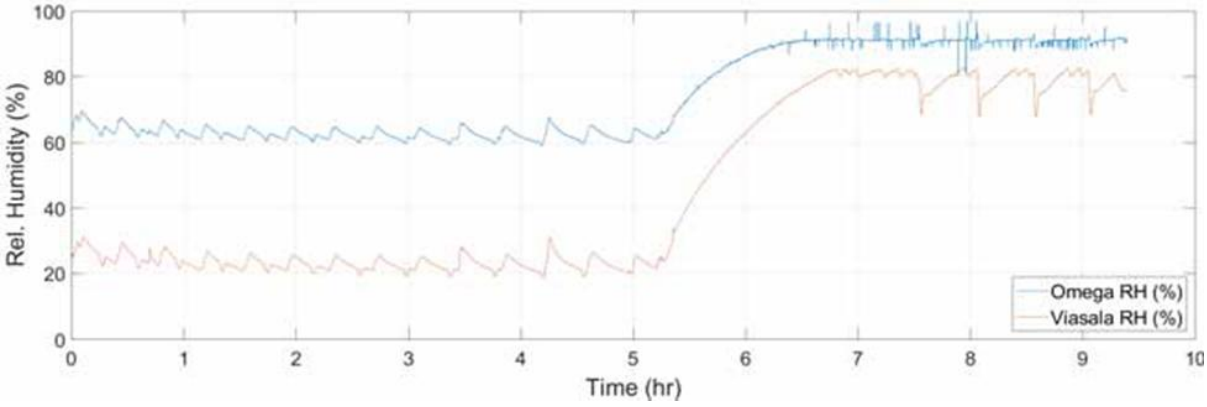

Figure 091720.03: Velocity Time History

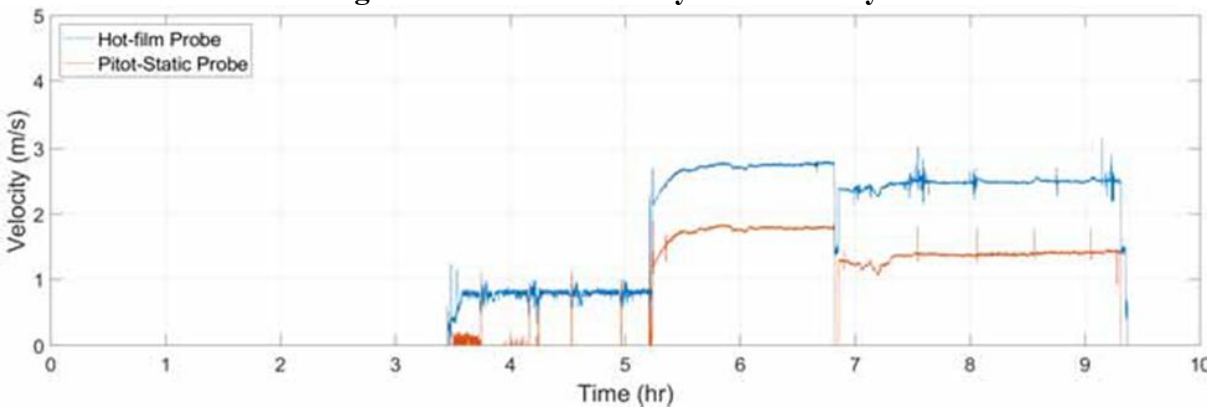

Figure 091720.04: Coolant Return Temperature Time History

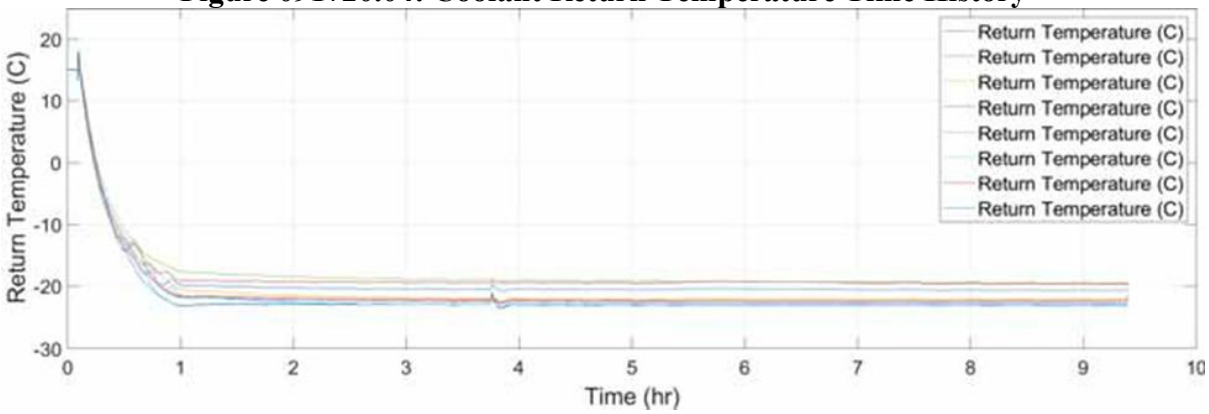

Figure 091720.05: Coolant Supply Temperature Time History

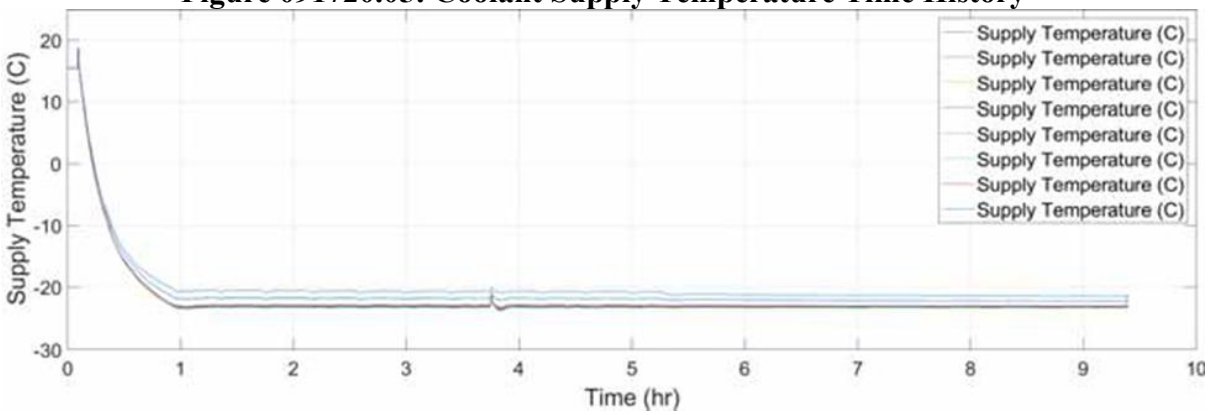

Figure 09170.06: Skin Temperature Time History

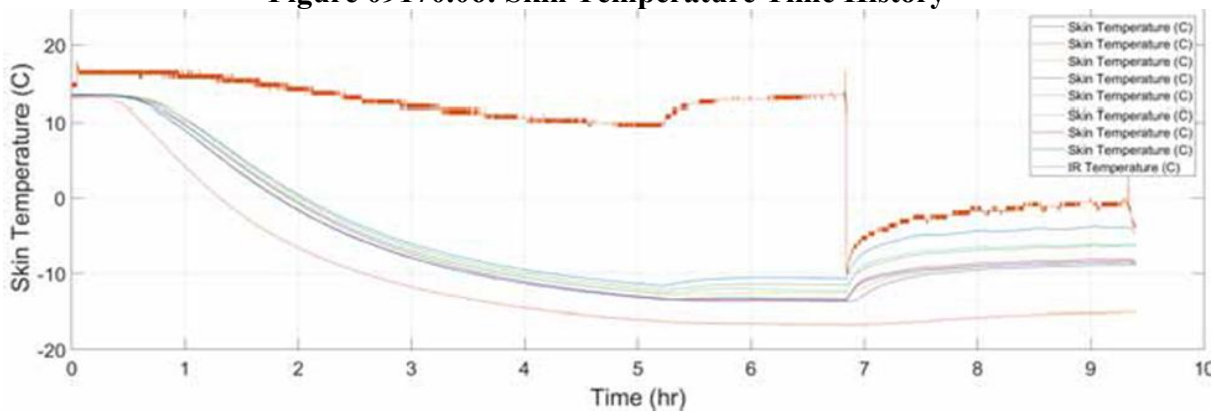

Figure 091720.07: Floor Temperature Time History

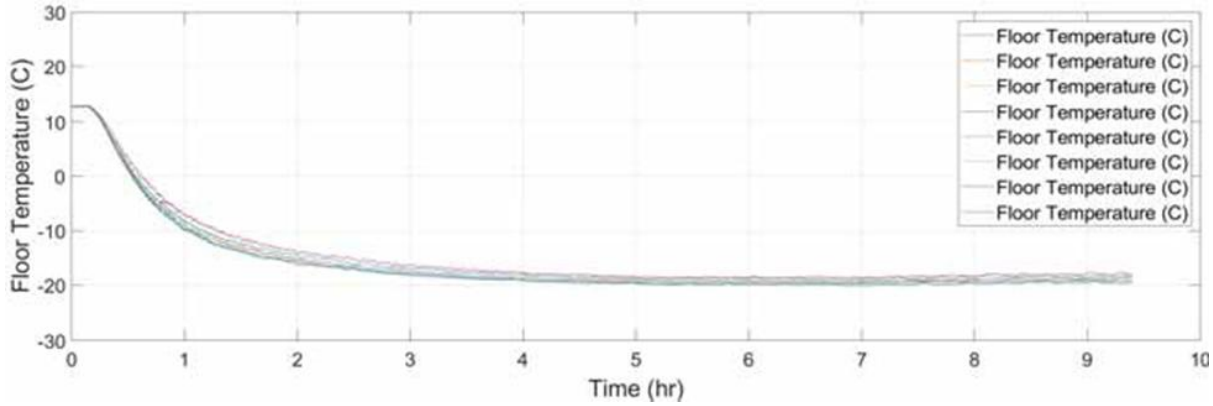

Figure 091720.08: Skin Temperature Slope Time History

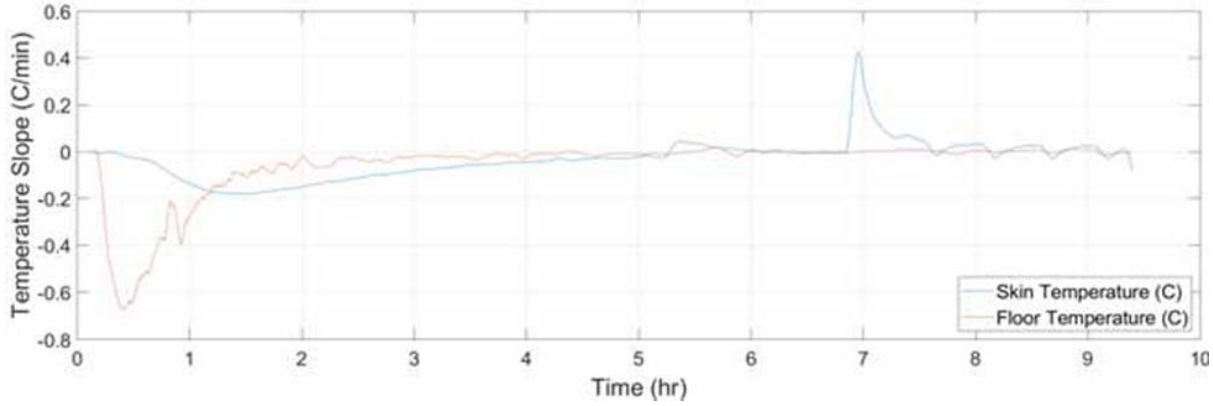

Figure 091720.09: RMS Height Evolution

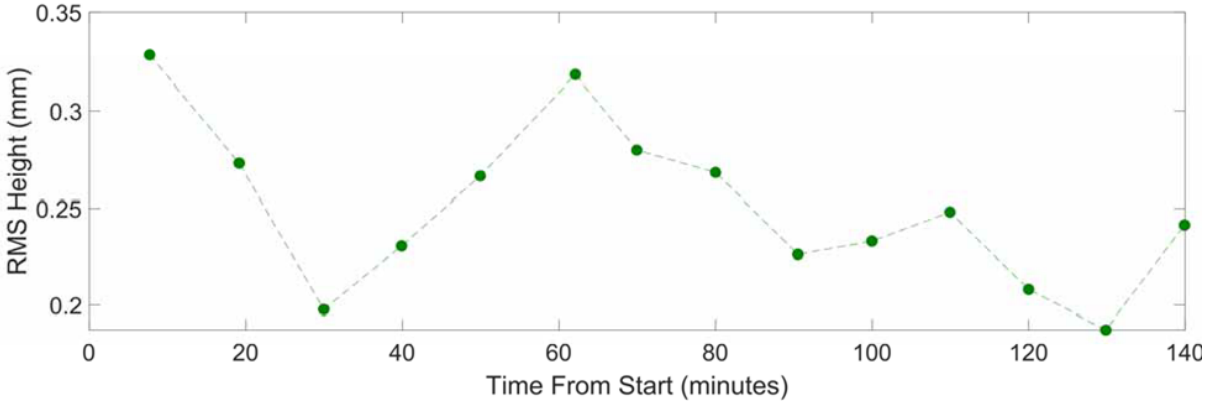

Figure 091720.10: Skewness Evolution

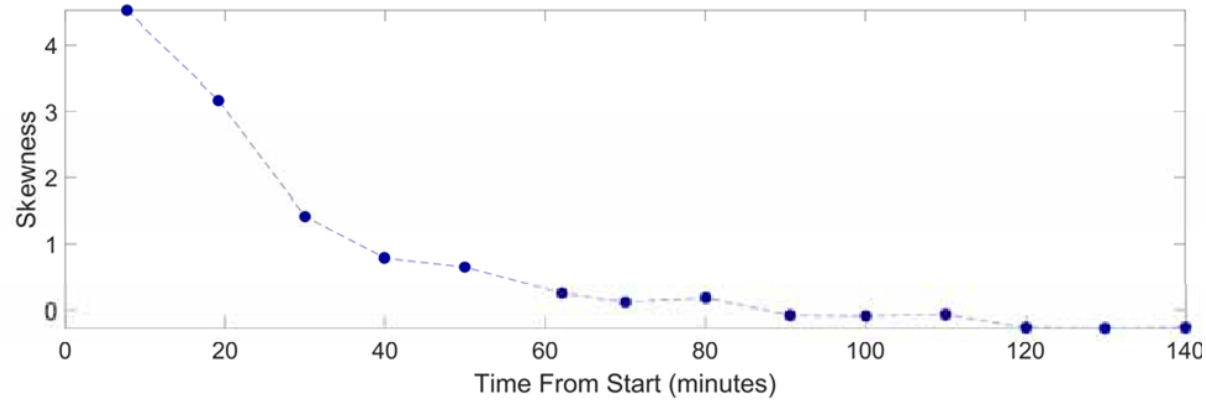

Figure 091720.11: Peak to Valley Evolution

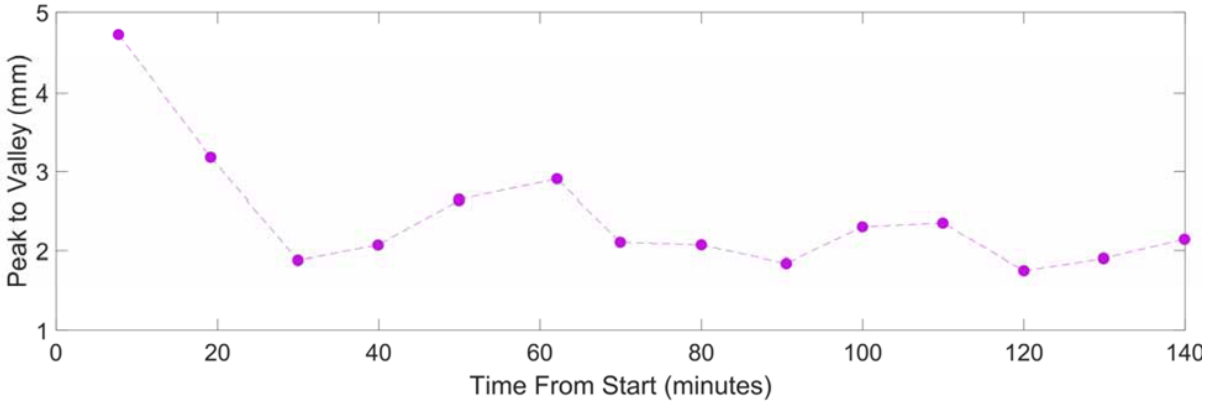

Figure 091720.12: Equivalent Roughness Evolution

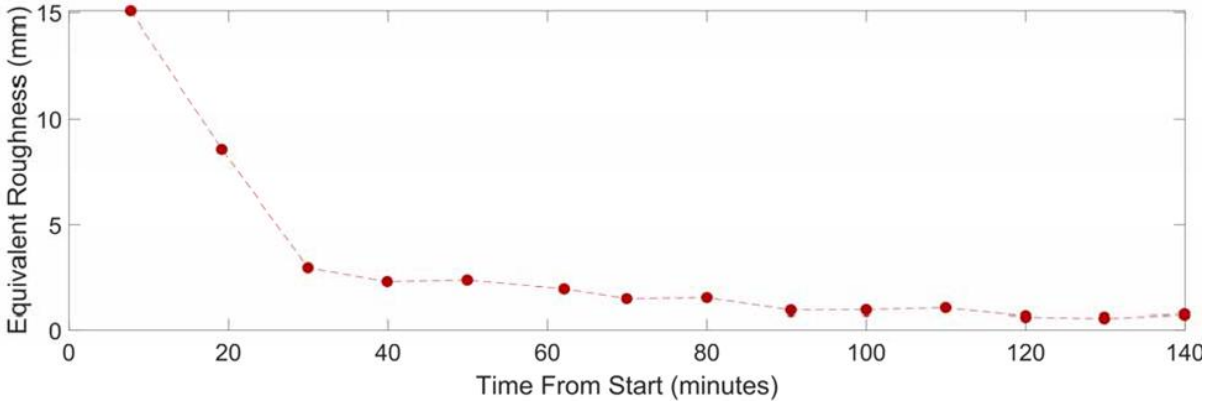

Table 091720.02: Summary of Roughness Parameters

Time (min.)	RMS (mm)	Skewness	Peak to Valley (mm)	ks,Flack-Schultz (mm)
7.7180	0.3286	4.5114	4.7343	15.0890
19.1513	0.2730	3.1747	3.1809	8.5674
29.9680	0.1977	1.4212	1.8769	2.9410
39.9013	0.2306	0.7906	2.0707	2.2692
49.9513	0.2664	0.6524	2.6412	2.3483
62.1013	0.3185	0.2527	2.9037	1.9211
69.9513	0.2798	0.1204	2.1055	1.4485
80.0013	0.2682	0.1844	2.0721	1.4984
90.5347	0.2262	-0.0716	1.8371	0.9052
99.9847	0.2330	-0.0799	2.3048	0.9211
109.9513	0.2481	-0.0579	2.3534	1.0128
120.0013	0.2080	-0.2526	1.7444	0.6185
129.8680	0.1875	-0.2621	1.9007	0.5477
139.9180	0.2414	-0.2522	2.1444	0.7183

Figure 091720.13: Frost Topography at 00:07:35

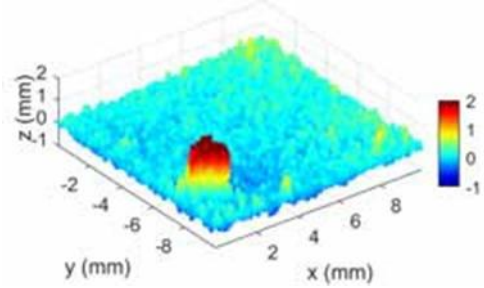

Figure 091720.14: Frost Topography at 00:19:01

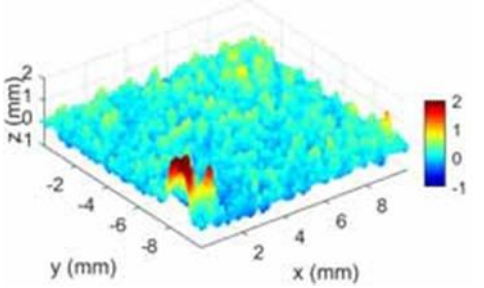

Figure 091720.15: Frost Topography at 00:29:50

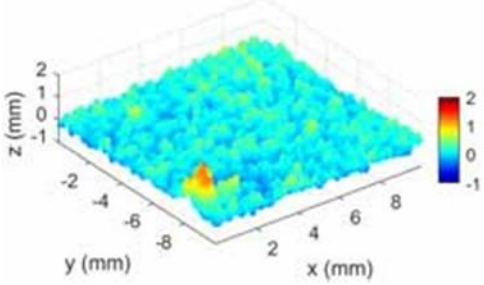

Figure 091720.16: Frost Topography at 00:39:46

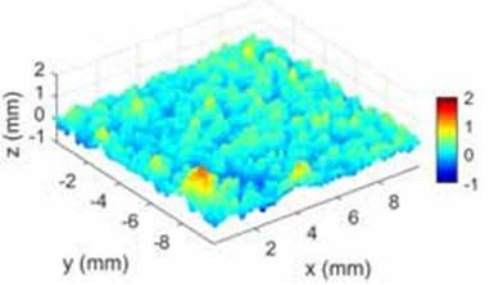

Figure 091720.17: Frost Topography at 00:49:49

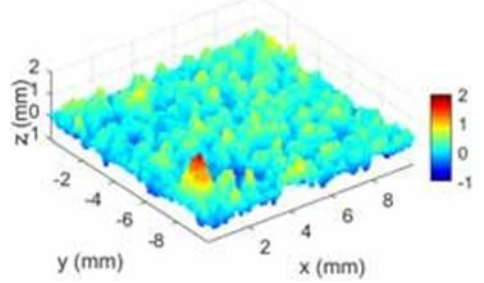

Figure 091720.18: Frost Topography at 01:01:58

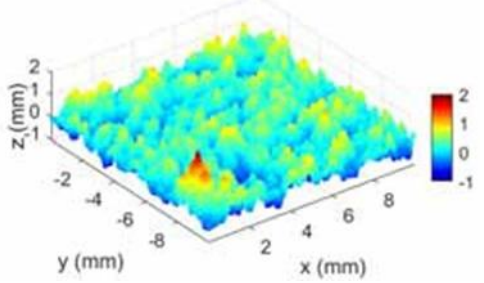

Figure 091720.19: Frost Topography at 01:09:49

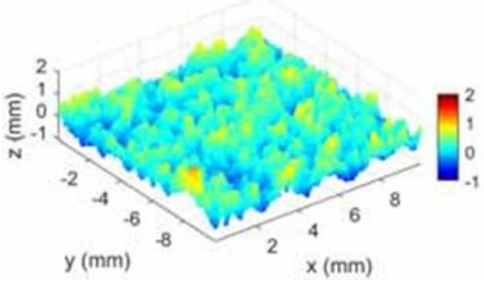

Figure 091720.20: Frost Topography at 01:19:52

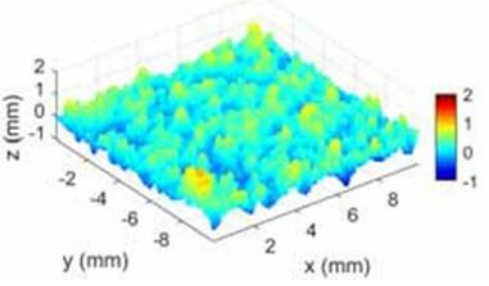

Figure 091720.21: Frost Topography at 01:30:24

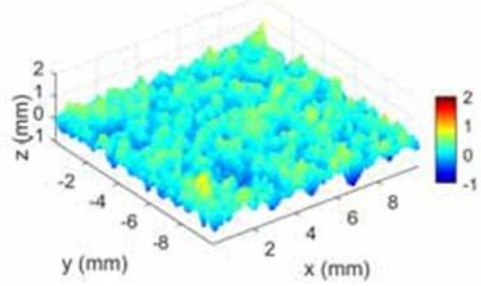

Figure 091720.22: Frost Topography at 01:39:51

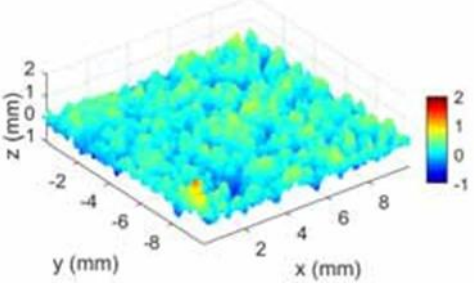

Figure 091720.23: Frost Topography at 01:49:49

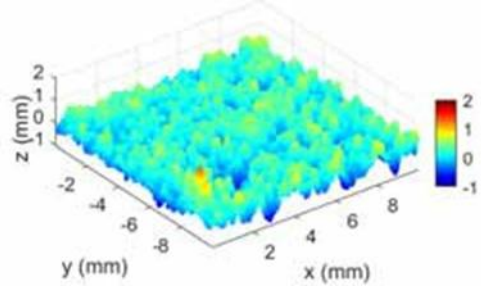

Figure 091720.24: Frost Topography at 01:59:52

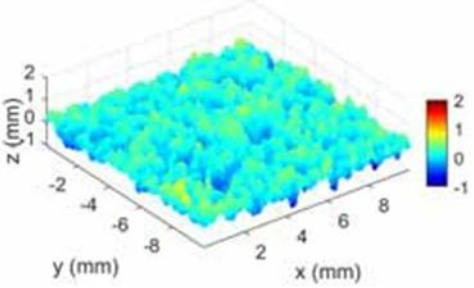

Figure 091720.25: Frost Topography at 02:09:44

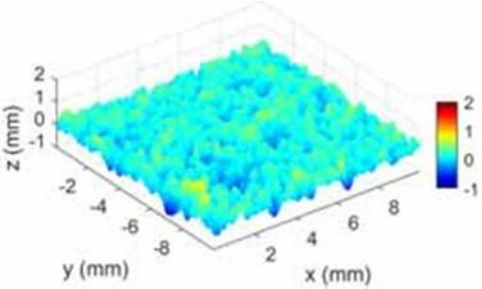

Figure 091720.26: Frost Topography at 02:19:47

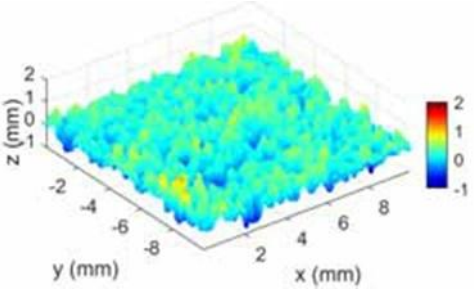

CAFF Conditions Report – Case Date: 092420

Table 092420.01: Summary of Measured Test Variables

Variable	Mean	St. Dev.	Rand. Unc.
T_air (C)	9.1322	0.4825	0.0162
Rh (%)	80.3102	4.8406	0.1623
Omega (kg_v/kg_da)	0.00585897	0.00044599	0.00001496
V_air (m/s)	1.3378	0.1030	0.0035
T_skin (C)	-11.5141	0.7734	0.0259
T_floor (C)	-19.7521	0.0916	0.0031

Figure 092420.01: Temperature and Voltage Control Time History

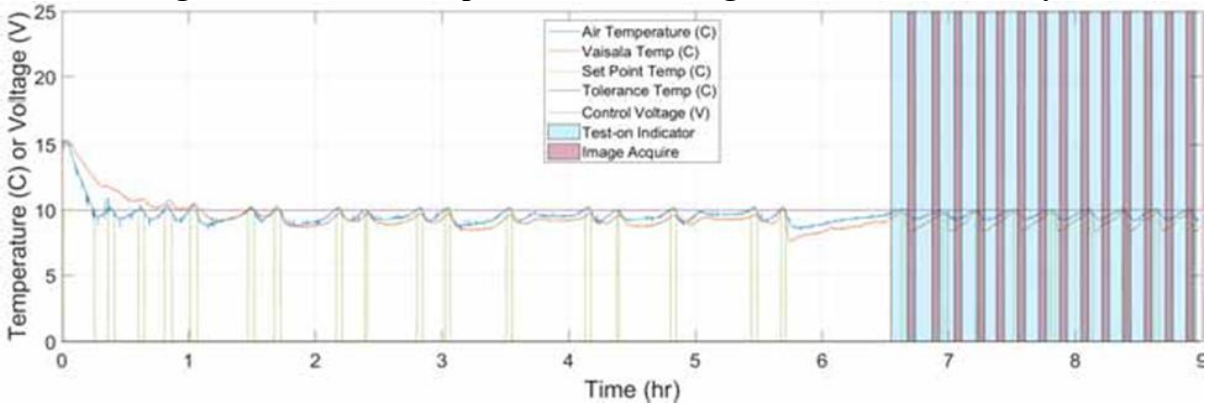

Figure 092420.02: Relative Humidity Time History

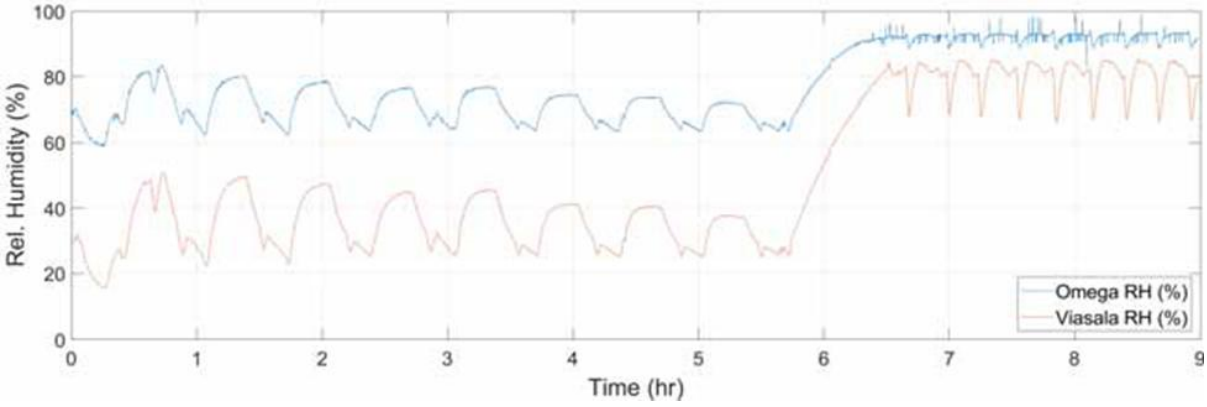

Figure 092420.03: Velocity Time History

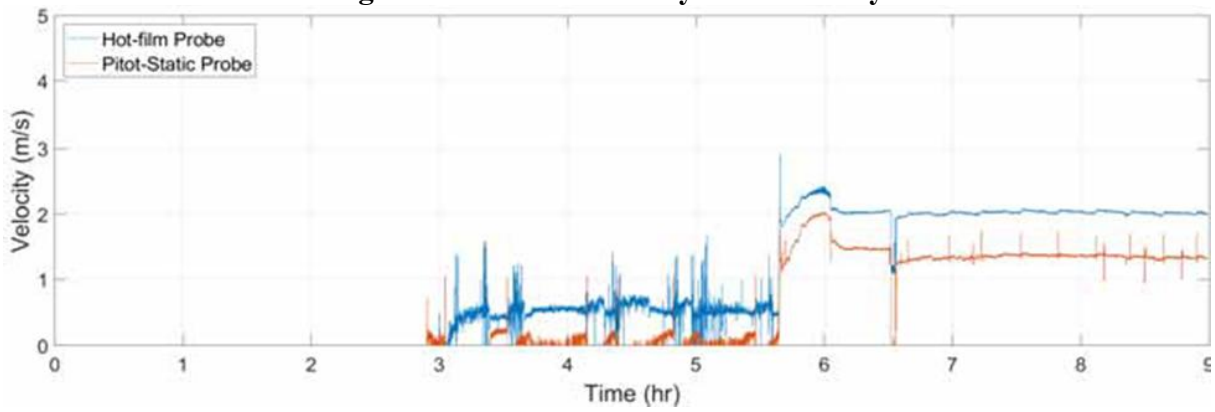

Figure 092420.04: Coolant Return Temperature Time History

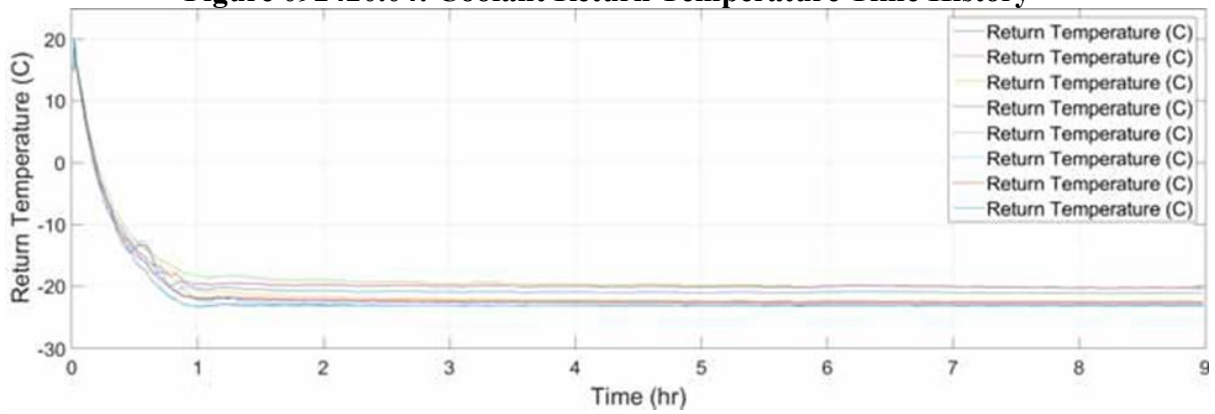

Figure 092420.05: Coolant Supply Temperature Time History

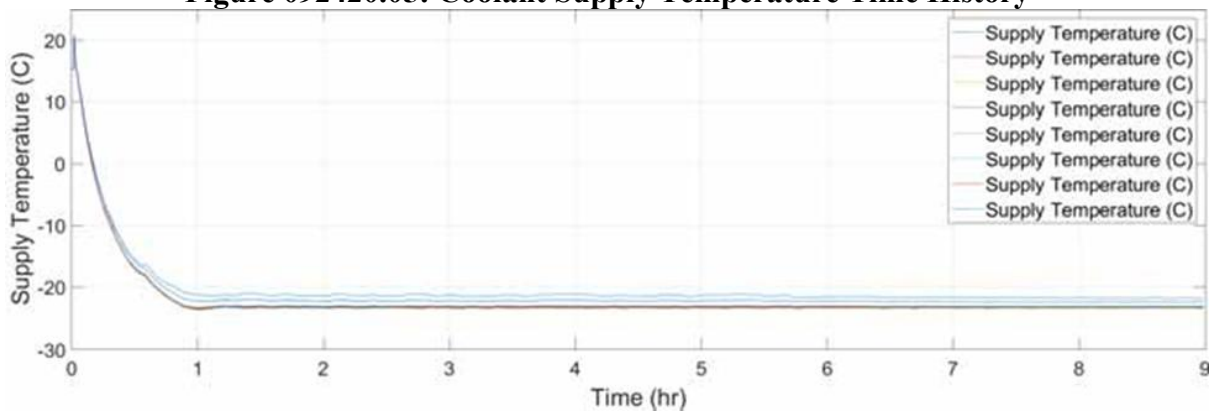

Figure 092420.06: Skin Temperature Time History

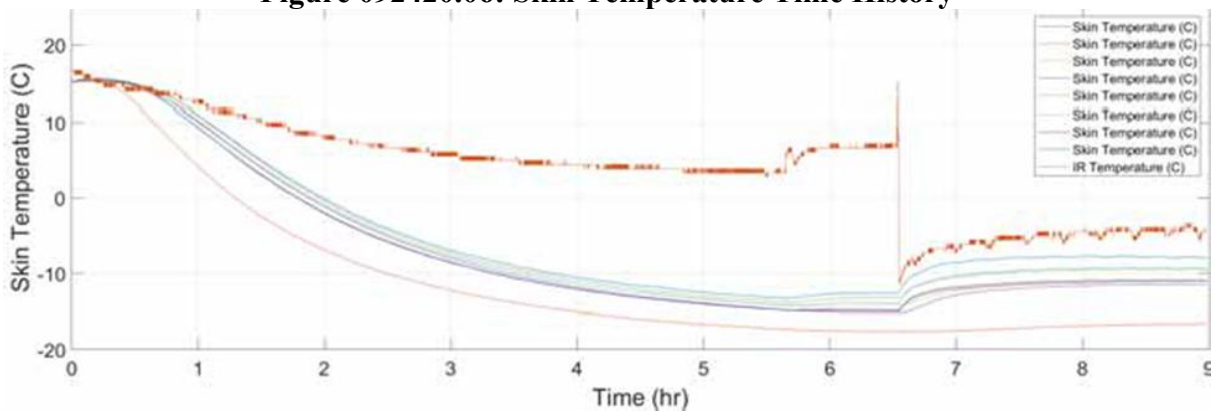

Figure 092420.07: Floor Temperature Time History

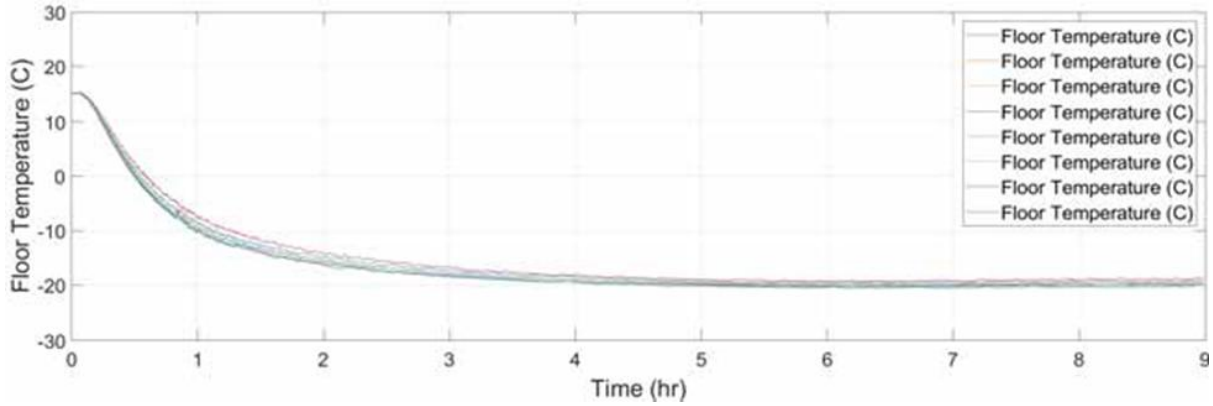

Figure 092420.08: Skin Temperature Slope Time History

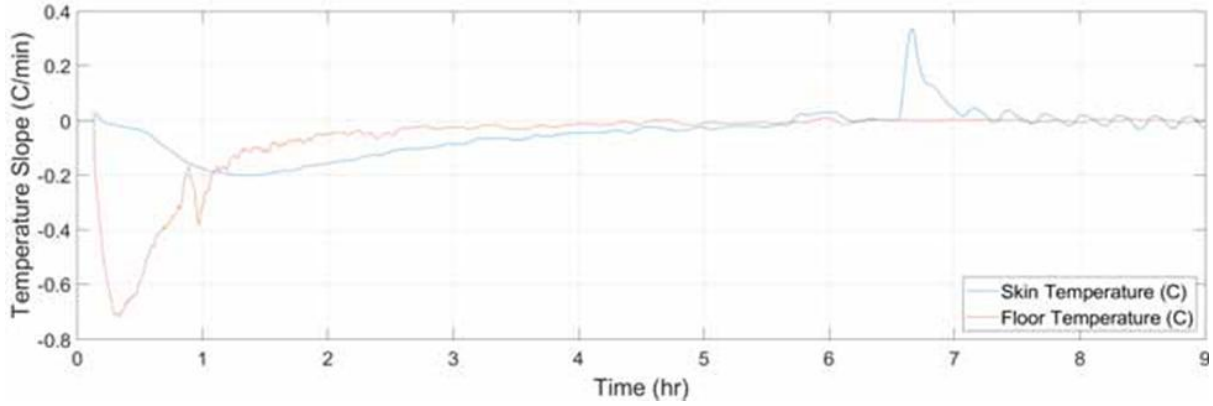

Figure 092420.09: RMS Height Evolution

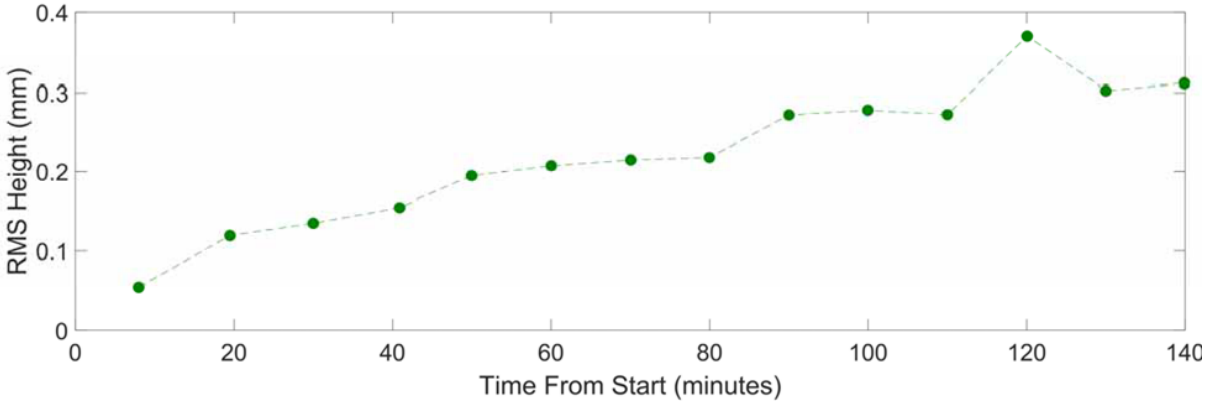

Figure 092420.10: Skewness Evolution

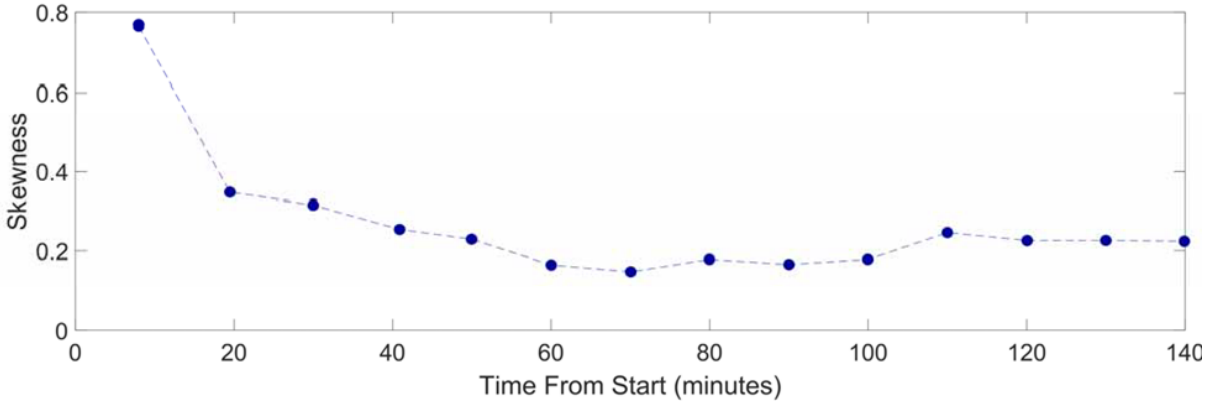

Figure 092420.11: Peak to Valley Evolution

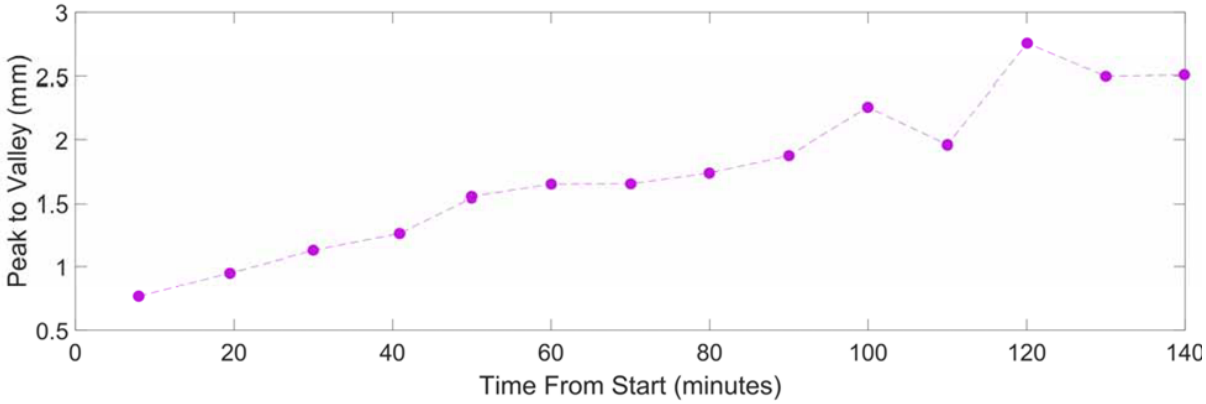

Figure 092420.12: Equivalent Roughness Evolution

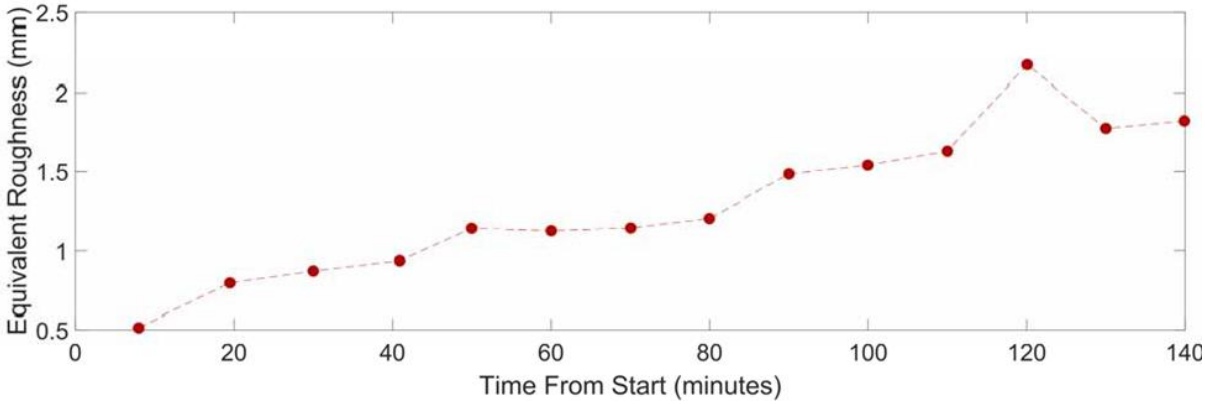

Table 092420.02: Summary of Roughness Parameters

Time (min.)	RMS (mm)	Skewness	Peak to Valley (mm)	ks,Flack-Schultz (mm)
7.9647	0.0532	0.7683	0.7605	0.5142
19.4813	0.1194	0.3467	0.9460	0.7953
29.9980	0.1350	0.3160	1.1268	0.8710
40.8813	0.1549	0.2540	1.2624	0.9358
49.9813	0.1945	0.2292	1.5474	1.1431
60.0147	0.2069	0.1632	1.6466	1.1277
70.0480	0.2144	0.1460	1.6484	1.1447
79.9647	0.2176	0.1774	1.7356	1.2056
90.0147	0.2718	0.1644	1.8757	1.4831
99.9647	0.2778	0.1775	2.2611	1.5393
109.9980	0.2721	0.2461	1.9606	1.6297
120.0647	0.3714	0.2259	2.7648	2.1749
129.9980	0.3026	0.2259	2.4970	1.7717
139.8980	0.3117	0.2238	2.5105	1.8210

Figure 092420.13: Frost Topography at 00:07:50

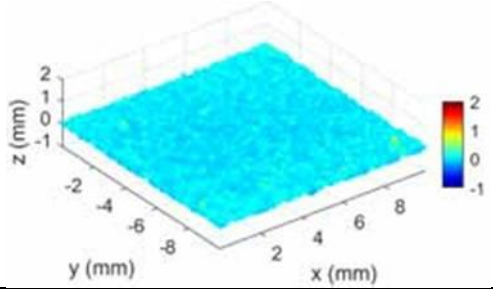

Figure 092420.14: Frost Topography at 00:19:21

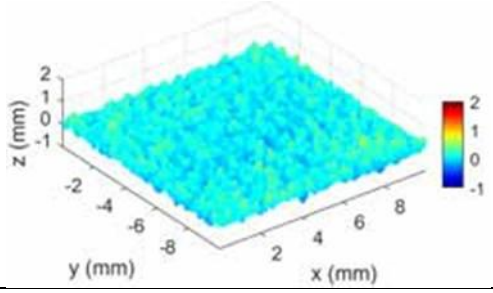

Figure 092420.15: Frost Topography at 00:29:52

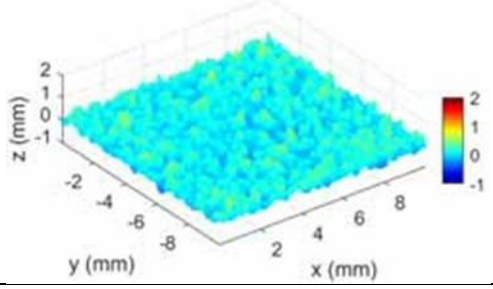

Figure 092420.16: Frost Topography at 00:40:45

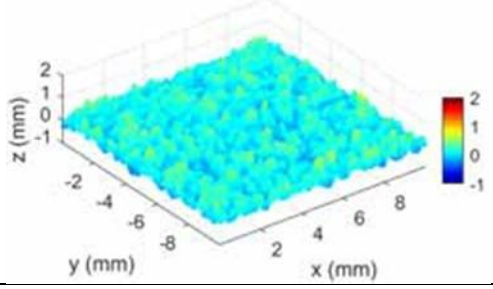

Figure 092420.17: Frost Topography at 00:49:51

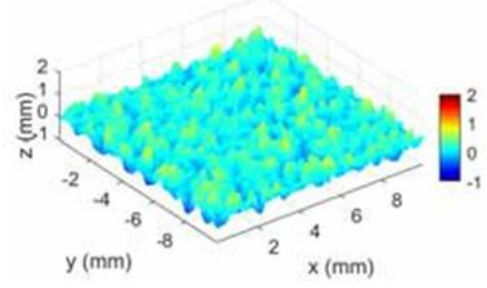

Figure 092420.18: Frost Topography at 00:59:53

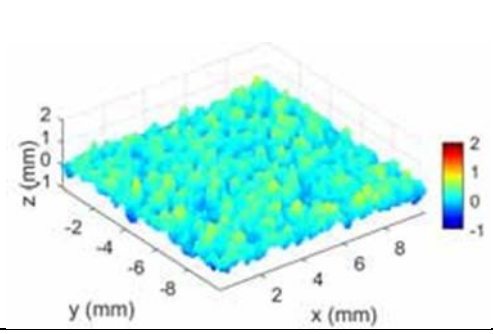

Figure 092420.19: Frost Topography at 01:09:55

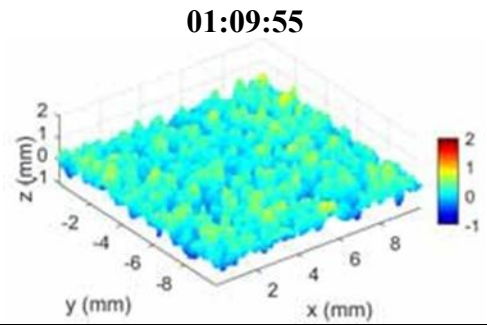

Figure 092420.20: Frost Topography at 01:19:50

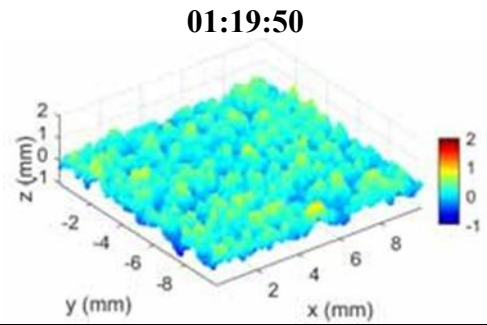

Figure 092420.21: Frost Topography at 01:29:53

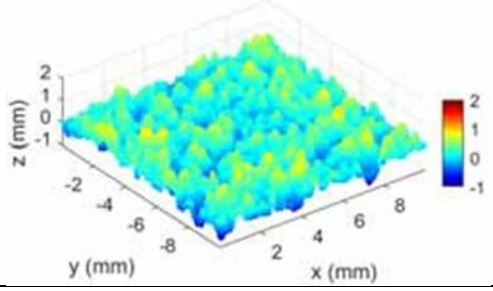

Figure 092420.22: Frost Topography at 01:39:50

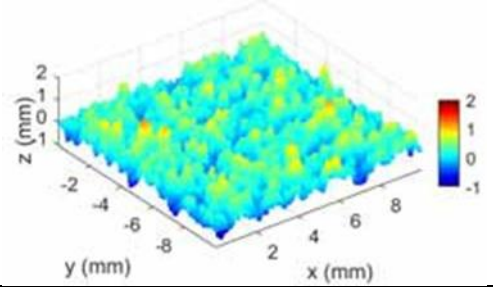

Figure 092420.23: Frost Topography at 01:49:52

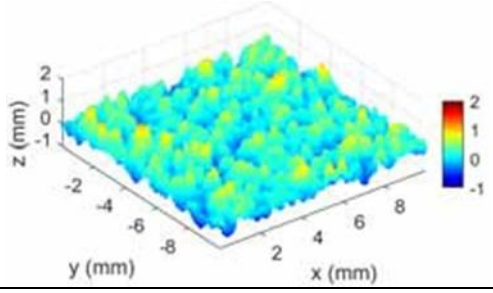

Figure 092420.24: Frost Topography at 01:59:56

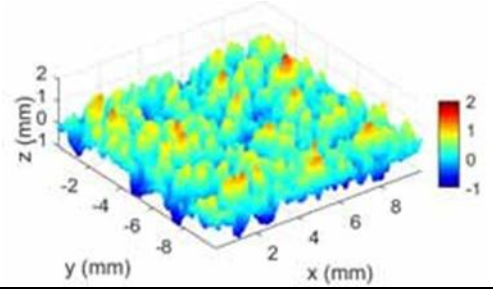

Figure 092420.25: Frost Topography at 02:09:52

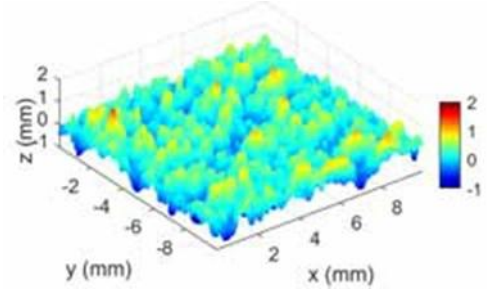

Figure 092420.26: Frost Topography at 02:19:46

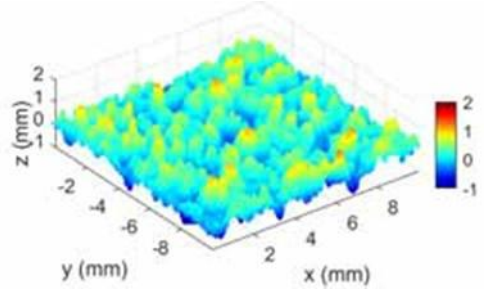

CAFF Conditions Report – Case Date: 092920

Table 092920.01: Summary of Measured Test Variables

Variable	Mean	St. Dev.	Rand. Unc.
T_air (C)	4.2226	0.2461	0.0083
Rh (%)	79.8055	4.5891	0.1541
Omega (kg_v/kg_da)	0.00411373	0.00029619	0.00000995
V_air (m/s)	1.2829	0.1062	0.0036
T_skin (C)	-13.1541	0.5716	0.0192
T_floor (C)	-20.2097	0.0456	0.0015

Figure 092920.01: Temperature and Voltage Control Time History

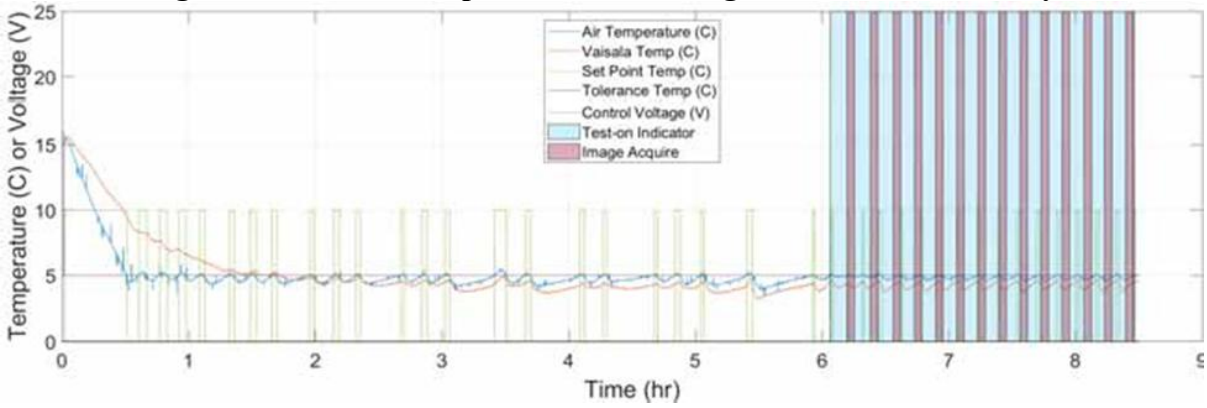

Figure 092920.02: Relative Humidity Time History

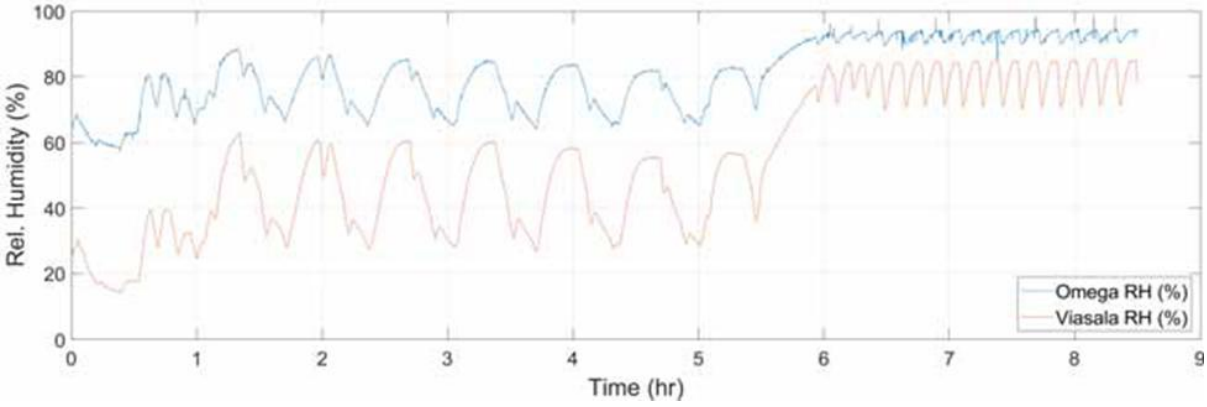

Figure 092920.03: Velocity Time History

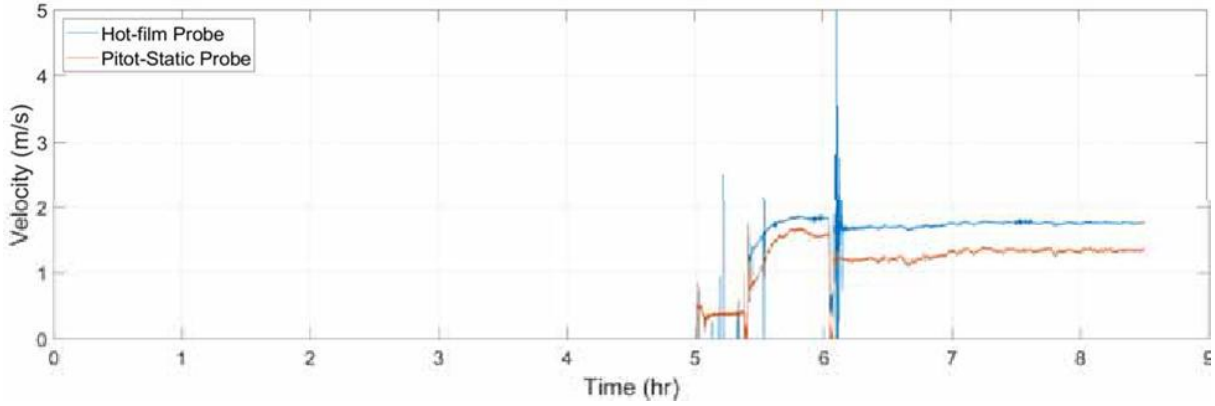

Figure 092920.04: Coolant Return Temperature Time History

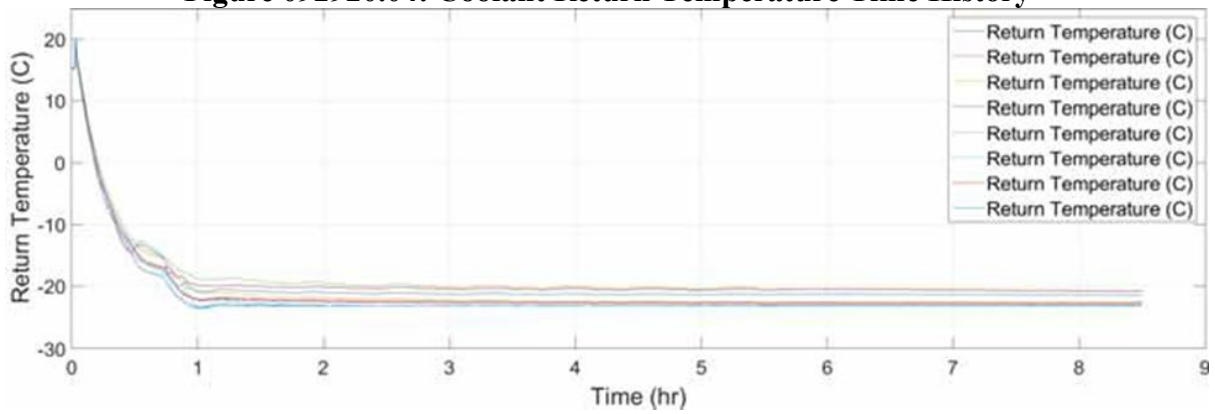

Figure 092920.05: Coolant Supply Temperature Time History

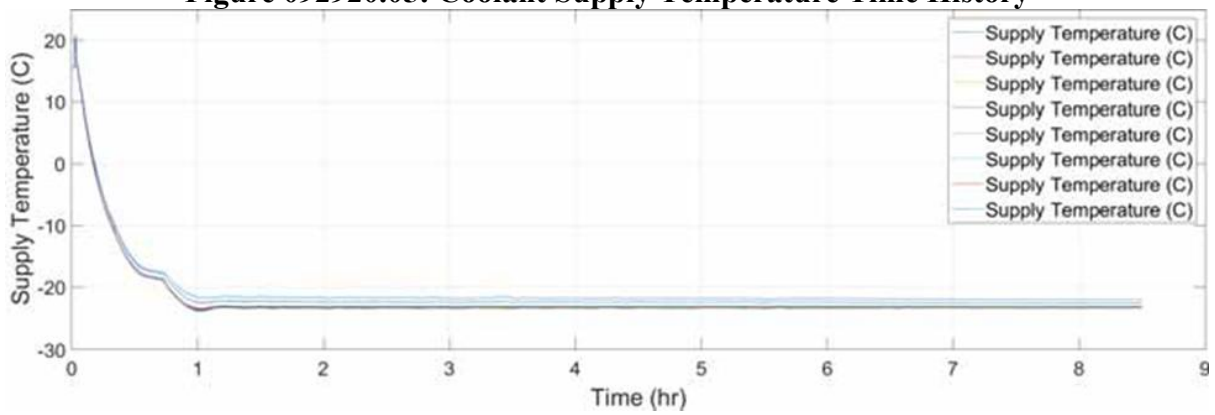

Figure 092920.06: Skin Temperature Time History

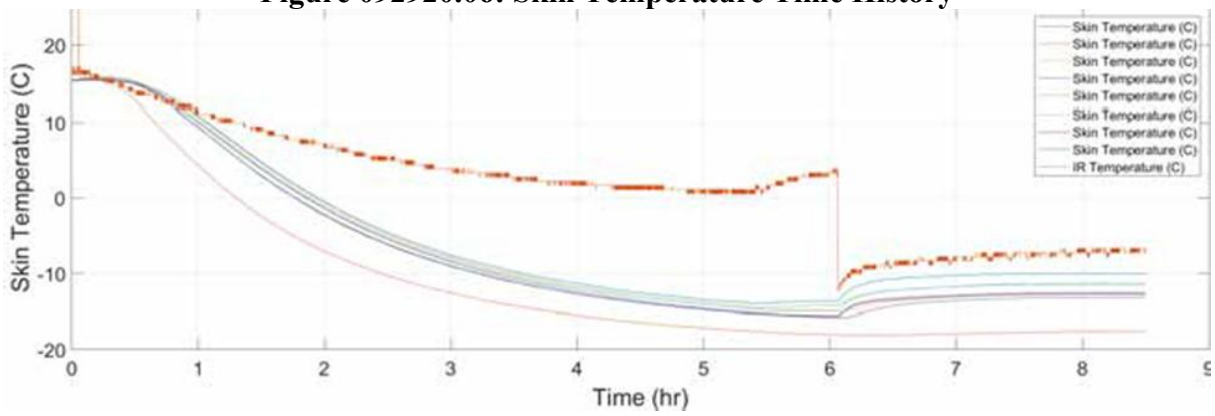

Figure 092920.07: Floor Temperature Time History

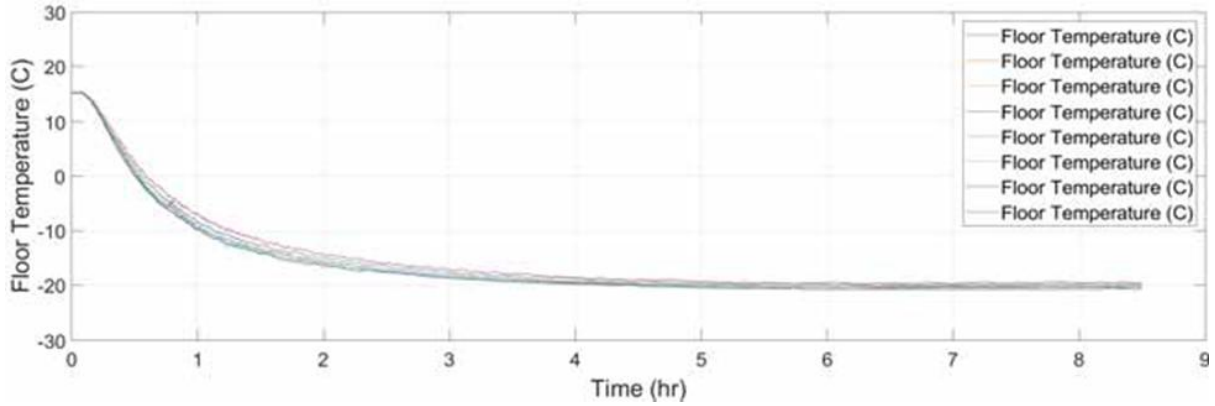

Figure 092920.08: Skin Temperature Slope Time History

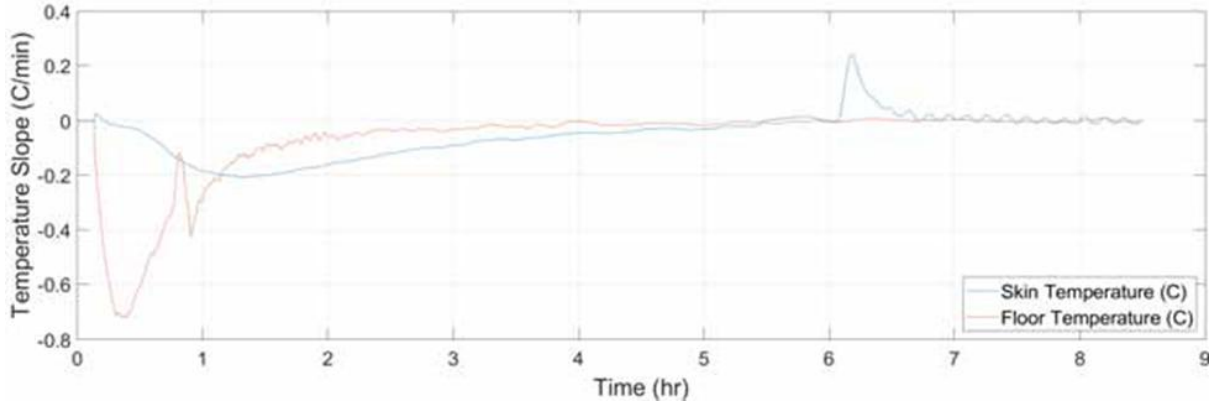

Figure 092920.09: RMS Height Evolution

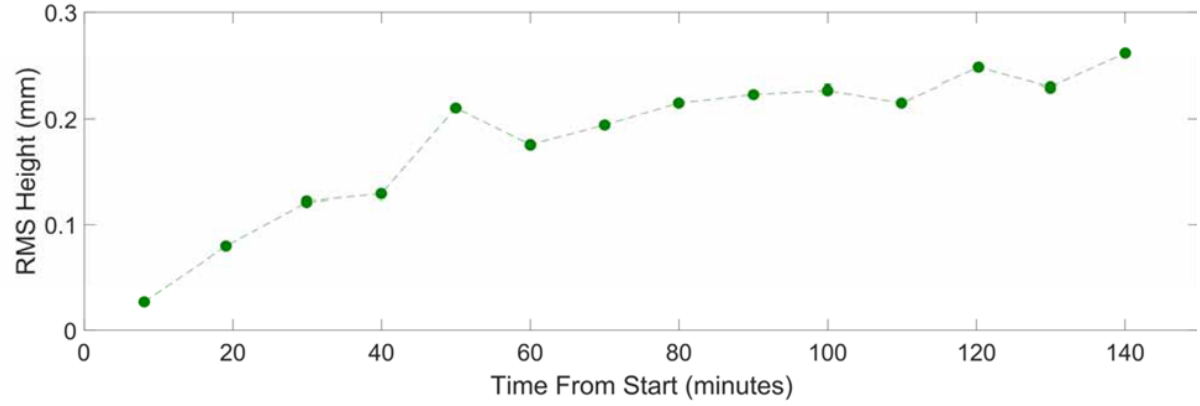

Figure 092920.10: Skewness Evolution

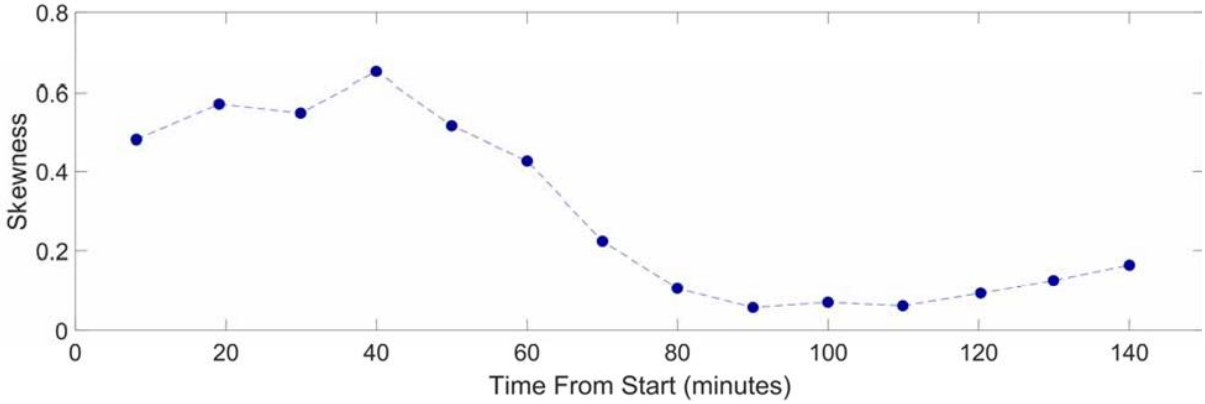

Figure 092920.11: Peak to Valley Evolution

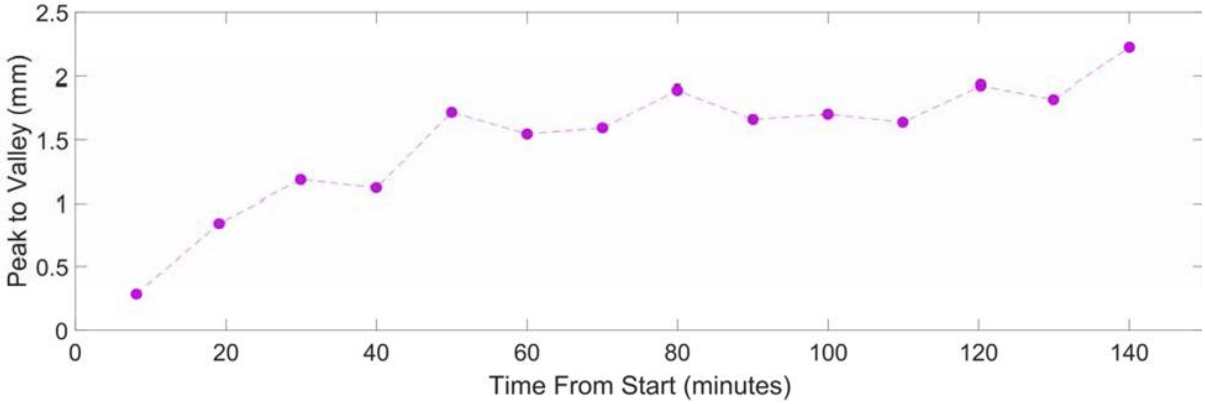

Figure 092920.12: Equivalent Roughness Evolution

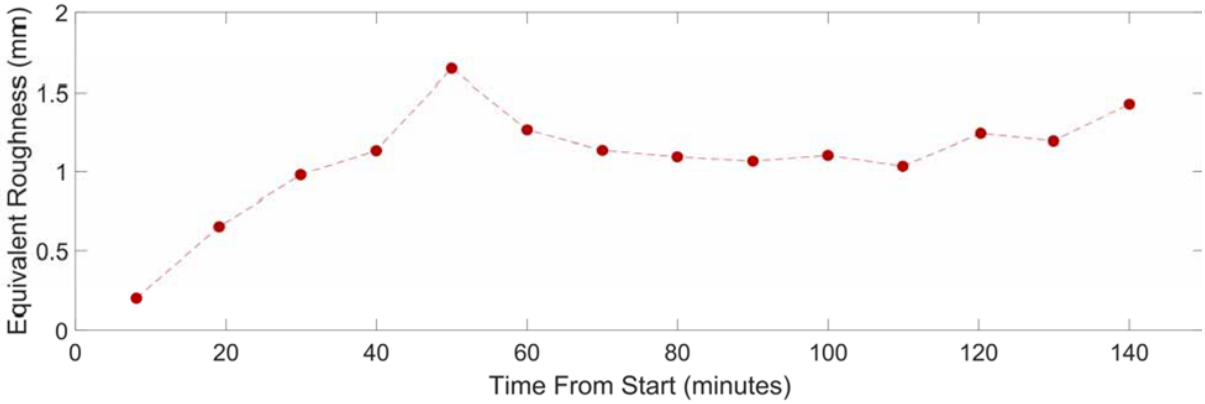

Table 092920.02: Summary of Roughness Parameters

Time (min.)	RMS (mm)	Skewness	Peak to Valley (mm)	ks,Flack-Schultz (mm)
8.0791	0.0258	0.4810	0.2778	0.1957
19.0791	0.0793	0.5719	0.8404	0.6526
29.9125	0.1213	0.5487	1.1843	0.9783
39.9625	0.1285	0.6520	1.1184	1.1325
49.9791	0.2107	0.5161	1.7210	1.6503
60.0125	0.1753	0.4264	1.5461	1.2633
70.0125	0.1943	0.2237	1.5955	1.1349
79.9625	0.2154	0.1040	1.8961	1.0929
90.0125	0.2236	0.0544	1.6634	1.0651
99.9791	0.2274	0.0679	1.7055	1.1024
109.9291	0.2155	0.0587	1.6411	1.0322
120.2791	0.2485	0.0916	1.9326	1.2413
129.9458	0.2297	0.1234	1.8227	1.1932
140.0291	0.2622	0.1634	2.2315	1.4290

Figure 092920.13: Frost Topography at 00:07:57

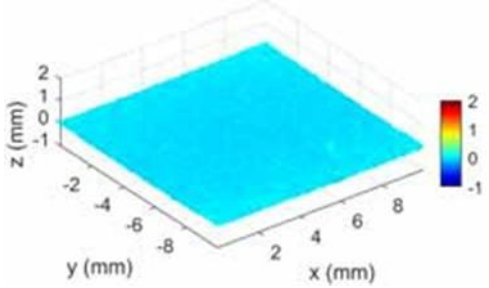

Figure 092920.14: Frost Topography at 00:18:57

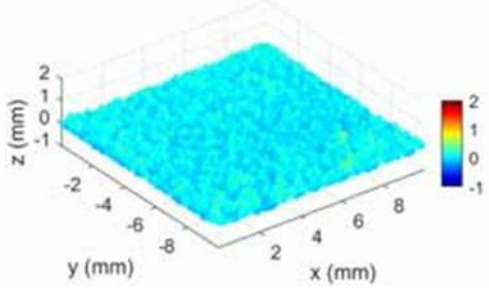

Figure 092920.15: Frost Topography at 00:29:47

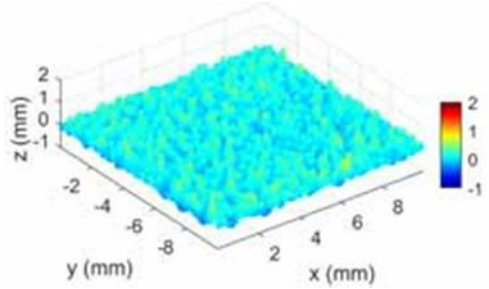

Figure 092920.16: Frost Topography at 00:39:50

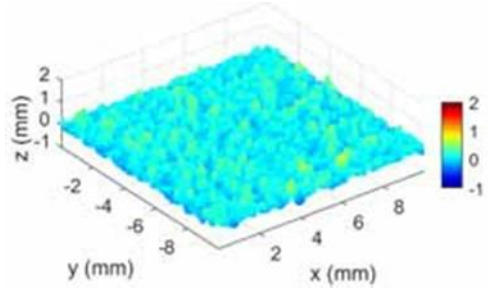

Figure 092920.17: Frost Topography at 00:49:51

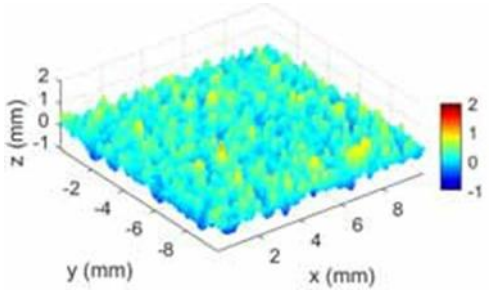

Figure 092920.18: Frost Topography at 00:59:53

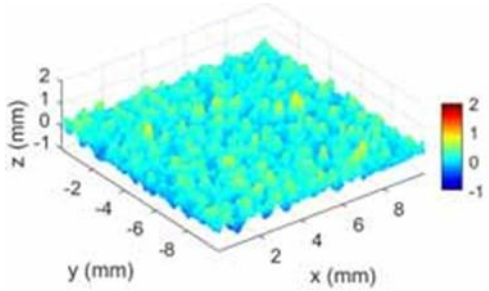

Figure 092920.19: Frost Topography at 01:09:53

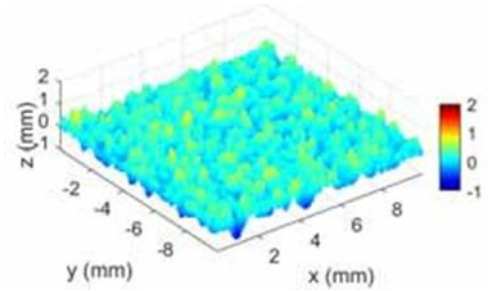

Figure 092920.20: Frost Topography at 01:19:50

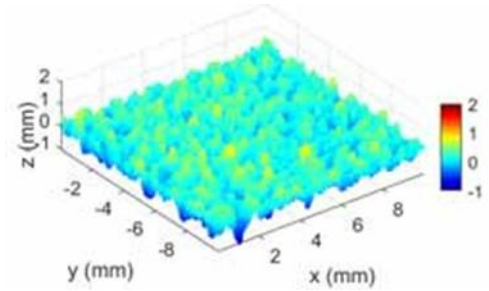

Figure 092920.21: Frost Topography at 01:29:53

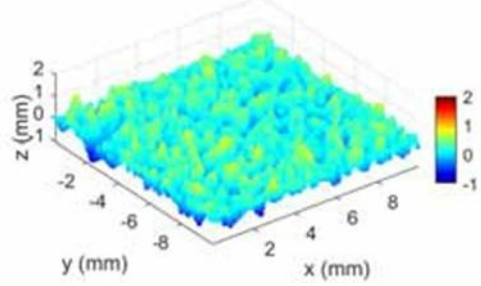

Figure 092920.22: Frost Topography at 01:39:51

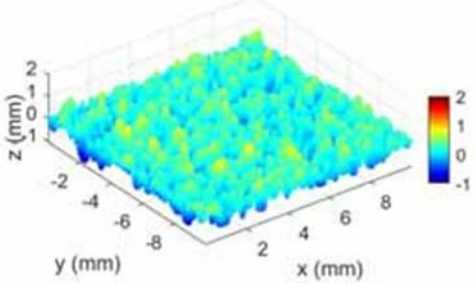

Figure 092920.23: Frost Topography at 01:49:48

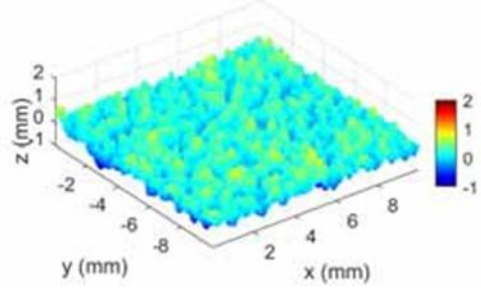

Figure 092920.24: Frost Topography at 02:00:09

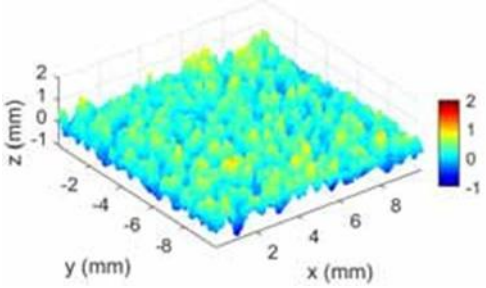

Figure 092920.25: Frost Topography at 02:09:49

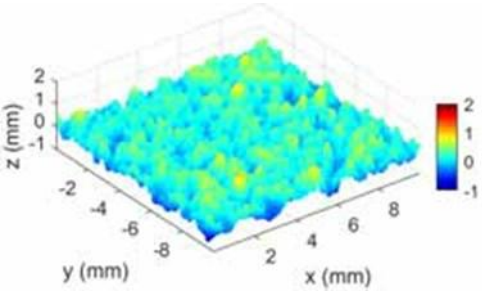

Figure 092920.26: Frost Topography at 02:19:54

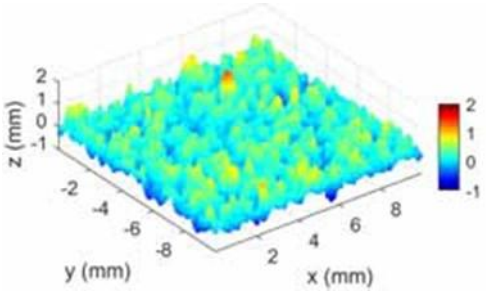

CAFF Conditions Report – Case Date: 100120

Table 100120.01: Summary of Measured Test Variables

Variable	Mean	St. Dev.	Rand. Unc.
T_air (C)	9.2377	0.2873	0.0096
Rh (%)	79.5796	5.7328	0.1925
Omega (kg_v/kg_da)	0.00579852	0.00043718	0.00001468
V_air (m/s)	0.1597	0.0895	0.0030
T_skin (C)	-12.7322	0.3688	0.0124
T_floor (C)	-19.8510	0.0319	0.0011

Figure 100120.01: Temperature and Voltage Control Time History

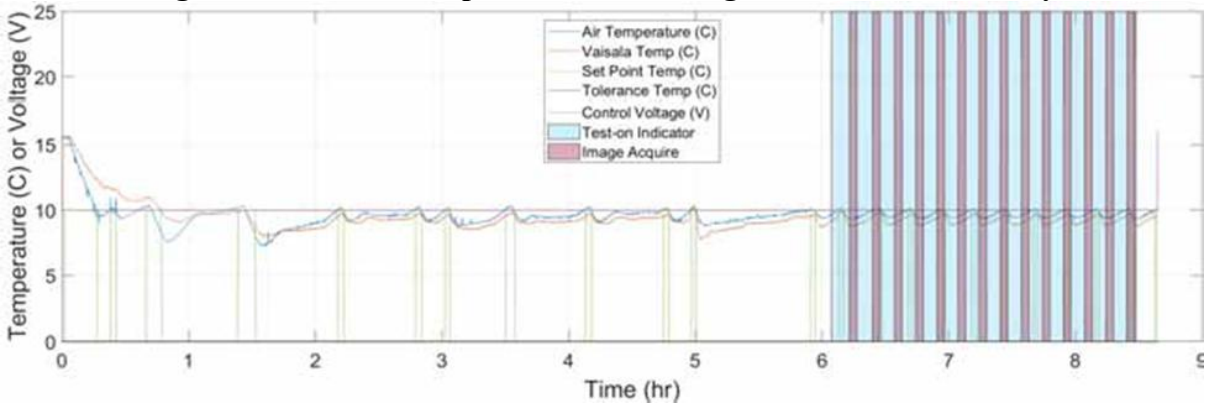

Figure 100120.02: Relative Humidity Time History

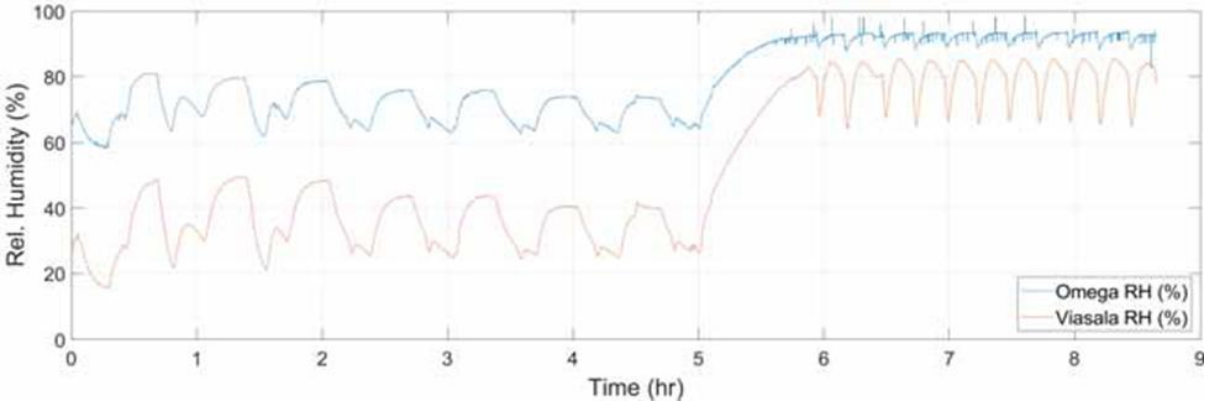

Figure 100120.03: Velocity Time History

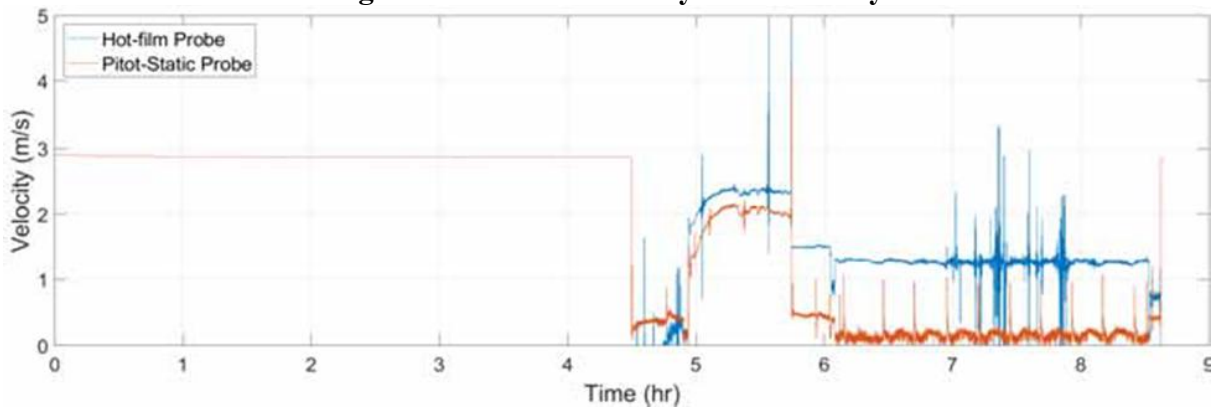

Figure 100120.04: Coolant Return Temperature Time History

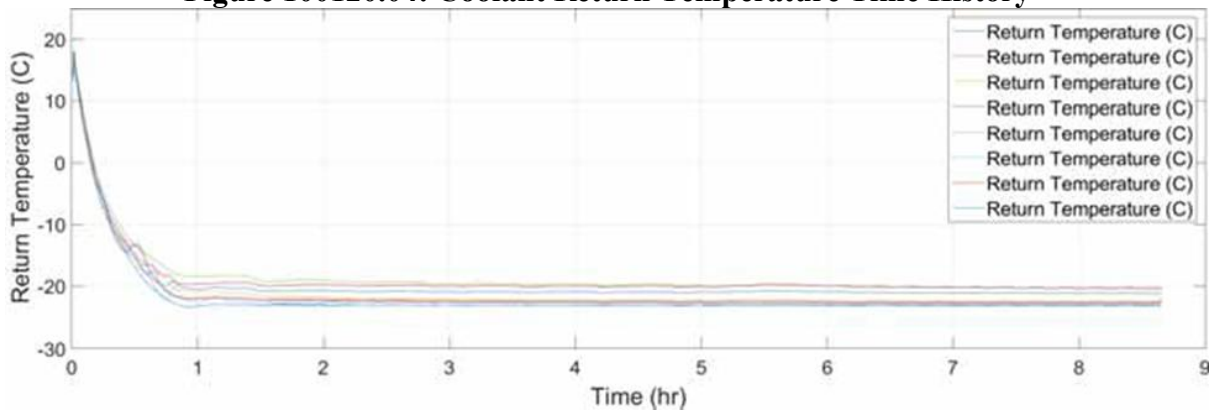

Figure 100120.05: Coolant Supply Temperature Time History

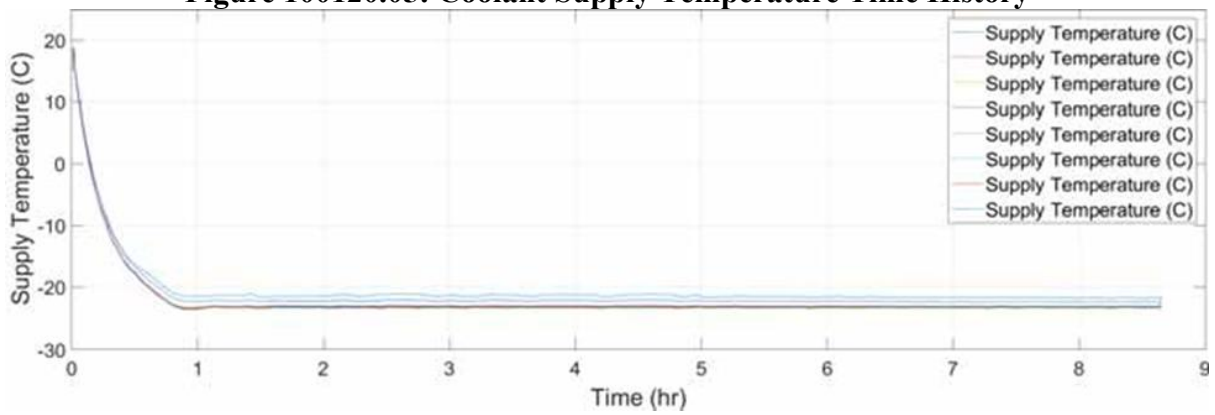

Figure 100120.06: Skin Temperature Time History

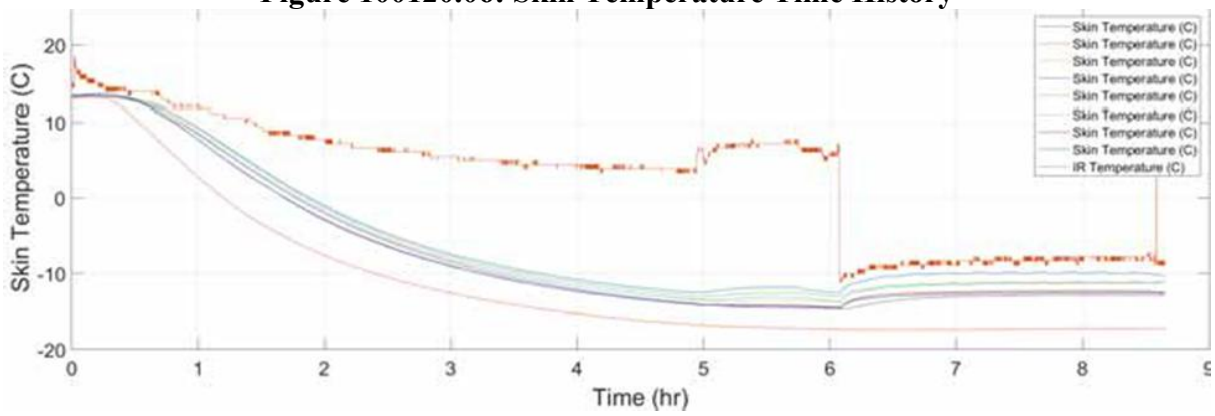

Figure 100120.07: Floor Temperature Time History

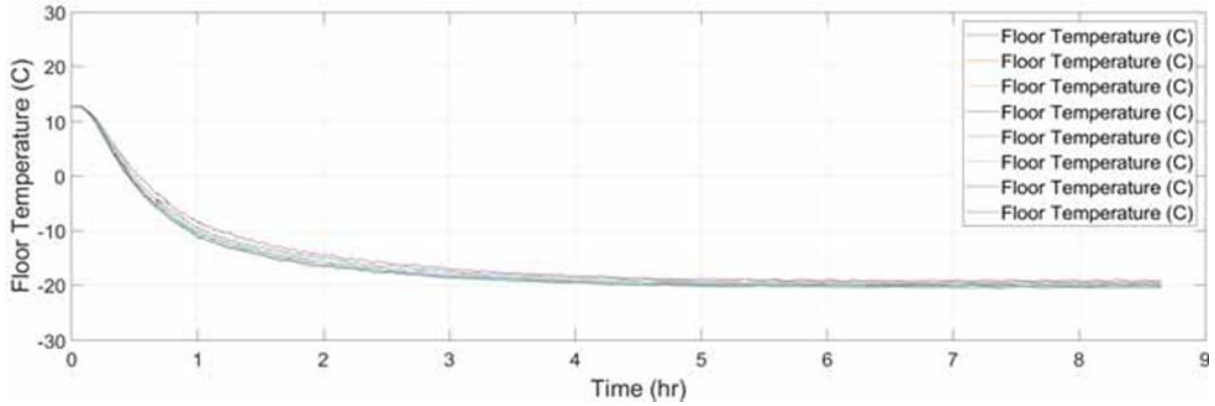

Figure 100120.08: Skin Temperature Slope Time History

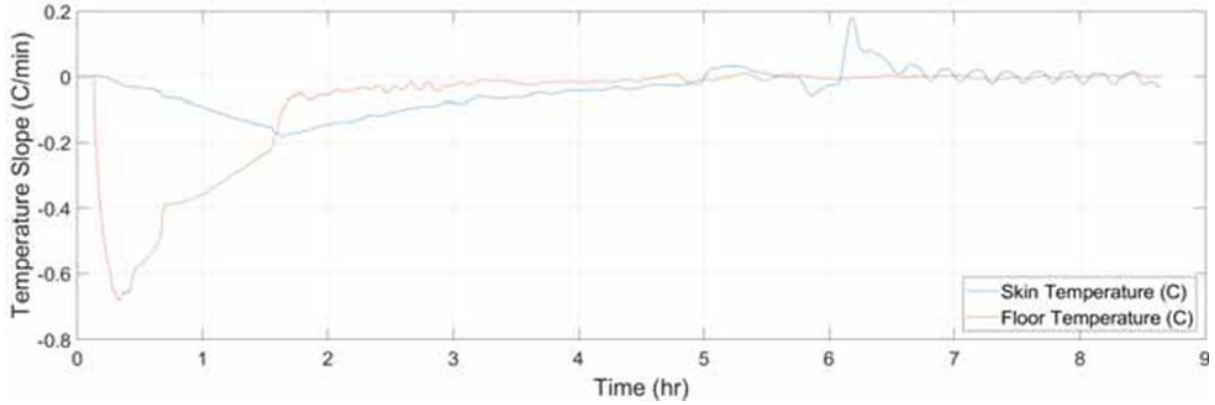

Figure 100120.09: RMS Height Evolution

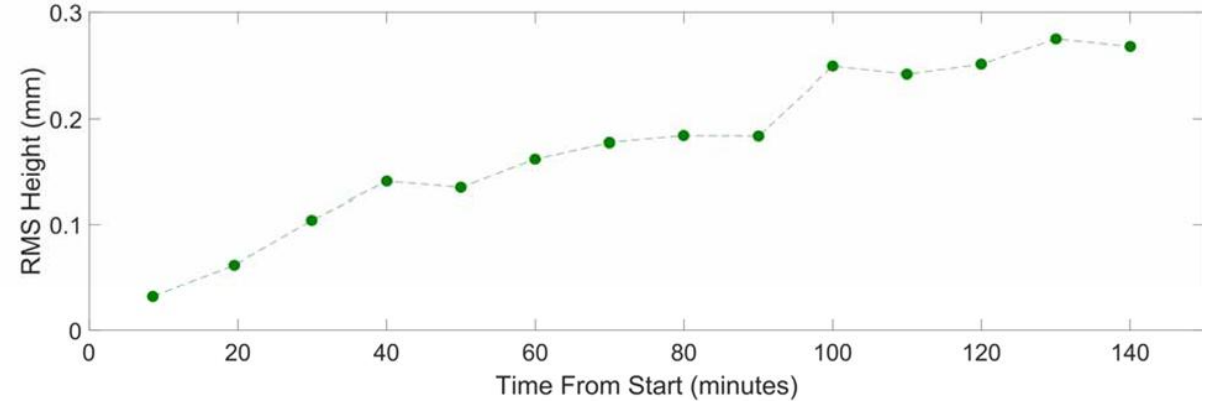

Figure 100120.10: Skewness Evolution

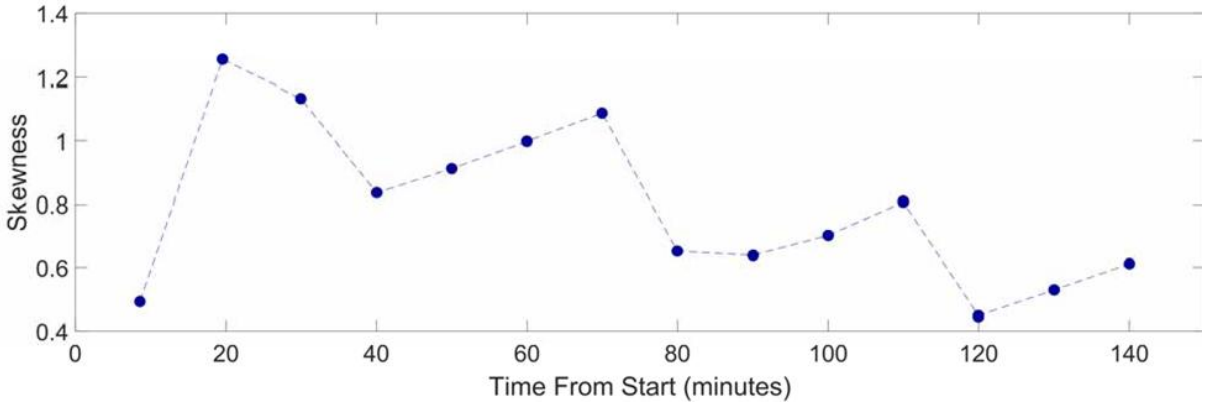

Figure 100120.11: Peak to Valley Evolution

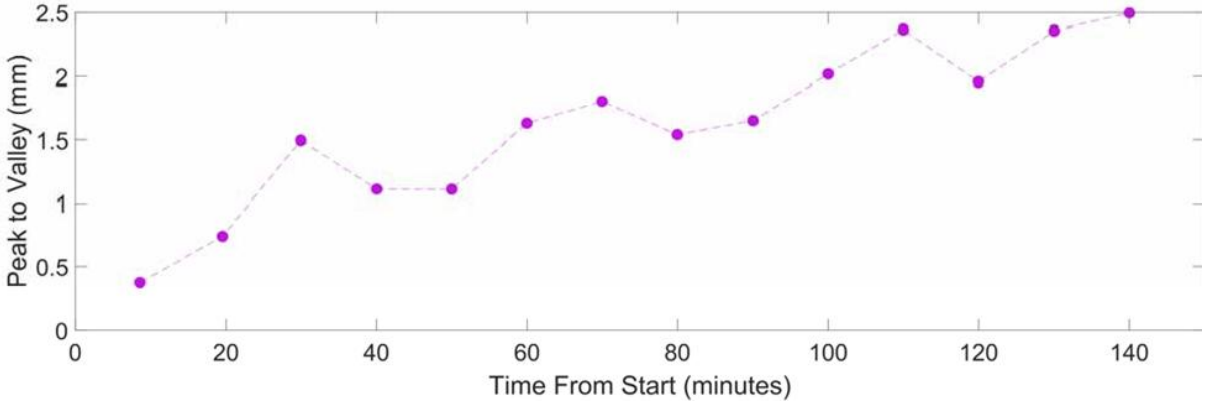

Figure 100120.12: Equivalent Roughness Evolution

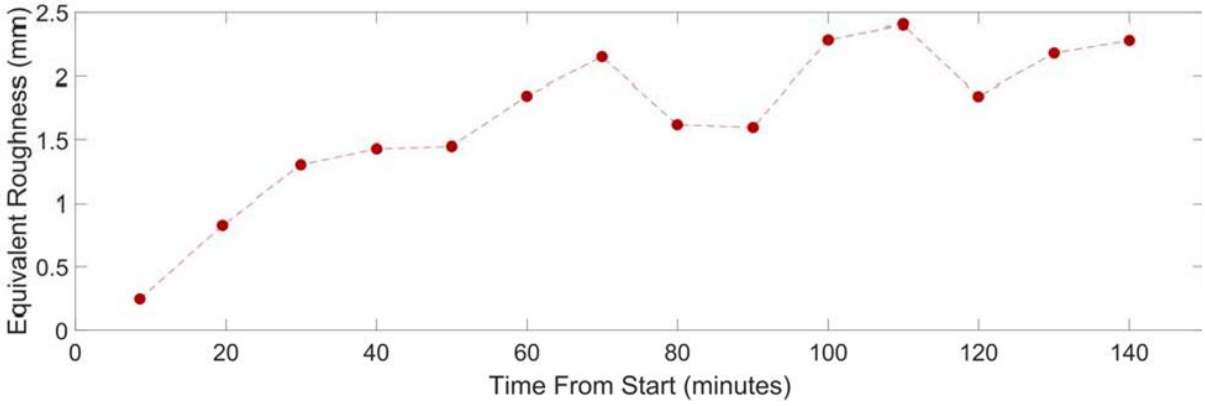

Table 100120.02: Summary of Roughness Parameters

Time (min.)	RMS (mm)	Skewness	Peak to Valley (mm)	ks,Flack-Schultz (mm)
8.5462	0.0310	0.4906	0.3701	0.2377
19.5295	0.0611	1.2577	0.7372	0.8263
29.9295	0.1040	1.1350	1.4973	1.3022
40.0129	0.1405	0.8344	1.1079	1.4295
49.9795	0.1345	0.9118	1.1065	1.4482
59.9795	0.1617	0.9991	1.6333	1.8504
69.9629	0.1775	1.0886	1.8076	2.1566
79.9462	0.1839	0.6515	1.5410	1.6203
90.0295	0.1834	0.6385	1.6534	1.5985
99.9962	0.2496	0.7014	2.0180	2.2902
109.9795	0.2417	0.8078	2.3673	2.4095
119.9629	0.2514	0.4458	1.9574	1.8455
130.0295	0.2759	0.5278	2.3590	2.1845
140.0295	0.2686	0.6112	2.4964	2.2868

Figure 100120.13: Frost Topography at 00:08:25

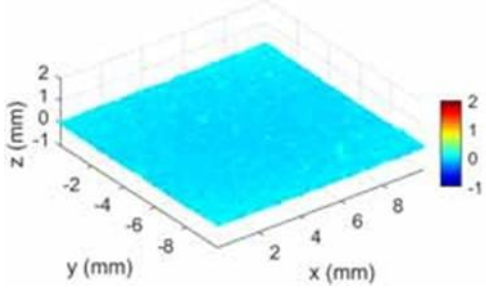

Figure 100120.14: Frost Topography at 00:19:24

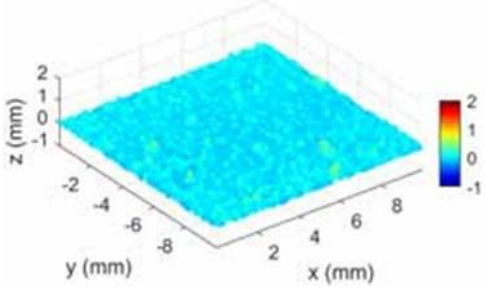

Figure 100120.15: Frost Topography at 00:29:48

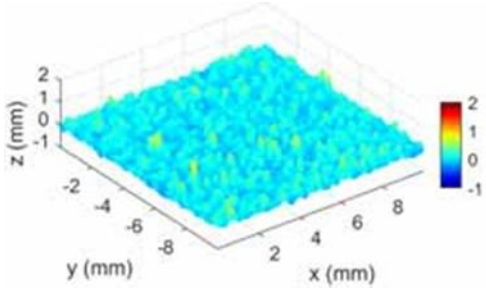

Figure 100120.16: Frost Topography at 00:39:53

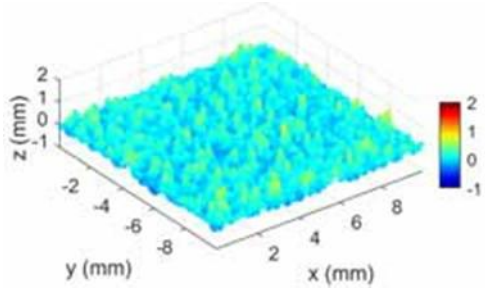

Figure 100120.17: Frost Topography at 00:49:51

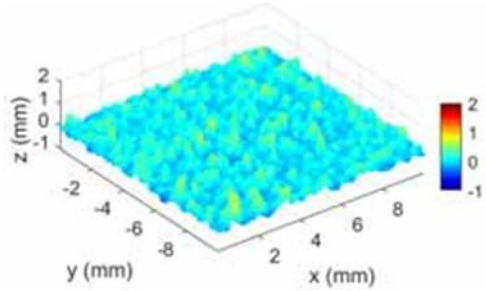

Figure 100120.18: Frost Topography at 00:59:51

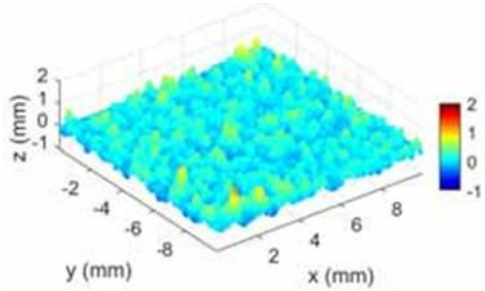

Figure 100120.19: Frost Topography at 01:09:50

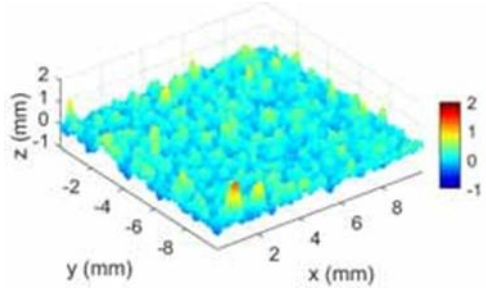

Figure 100120.20: Frost Topography at 01:19:49

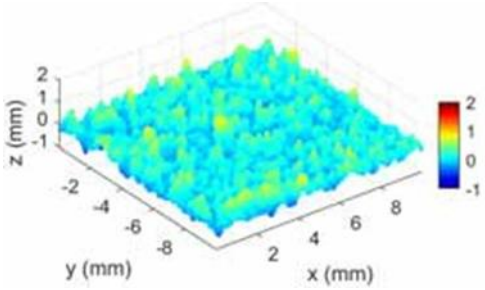

Figure 100120.21: Frost Topography at 01:29:54

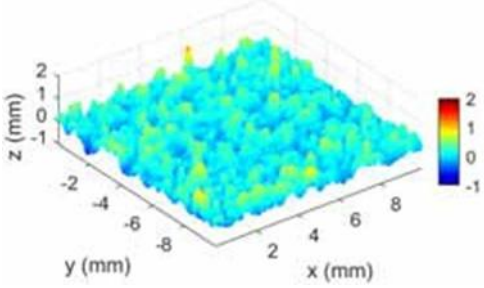

Figure 100120.22: Frost Topography at 01:39:52

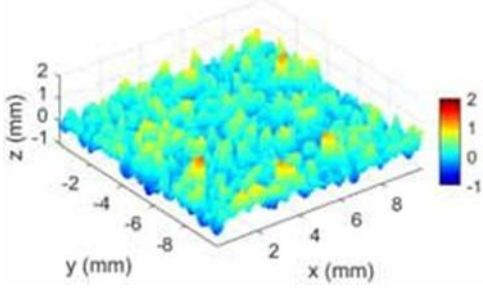

Figure 100120.23: Frost Topography at 01:49:51

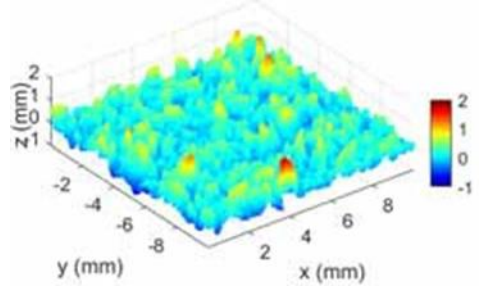

Figure 100120.24: Frost Topography at 01:59:50

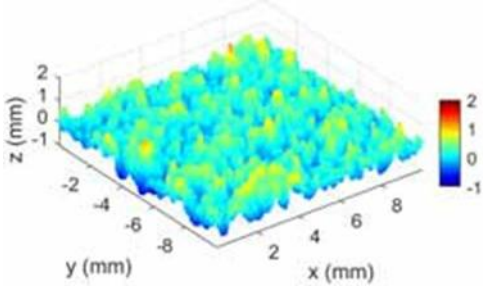

Figure 100120.25: Frost Topography at 02:09:54

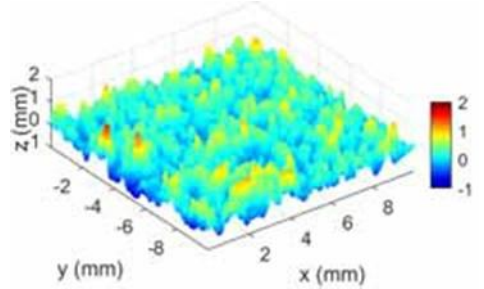

Figure 100120.26: Frost Topography at 02:19:54

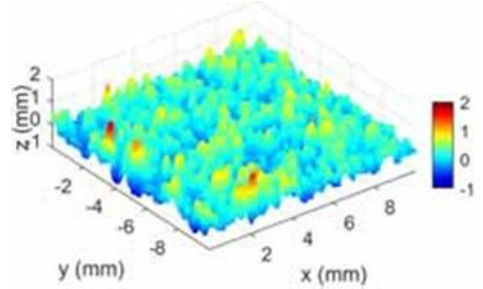

CAFF Conditions Report – Case Date: 100620

Table 100620.01: Summary of Measured Test Variables

Variable	Mean	St. Dev.	Rand. Unc.
T_air (C)	4.2905	0.1613	0.0054
Rh (%)	80.1091	4.9135	0.1642
Omega (kg_v/kg_da)	0.00416315	0.00029178	0.00000975
V_air (m/s)	0.2556	0.0723	0.0024
T_skin (C)	-14.4847	0.3359	0.0112
T_floor (C)	-20.4459	0.0238	0.0008

Figure 100620.01: Temperature and Voltage Control Time History

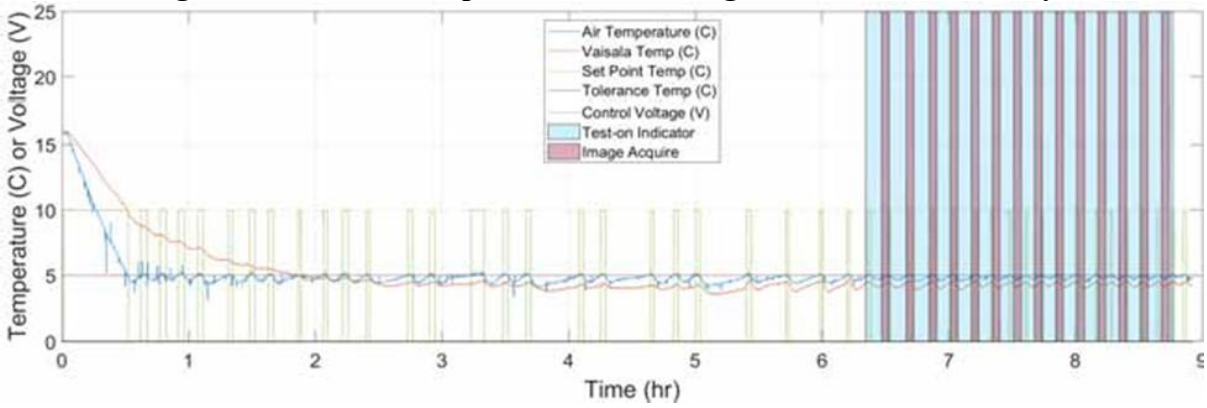

Figure 100620.02: Relative Humidity Time History

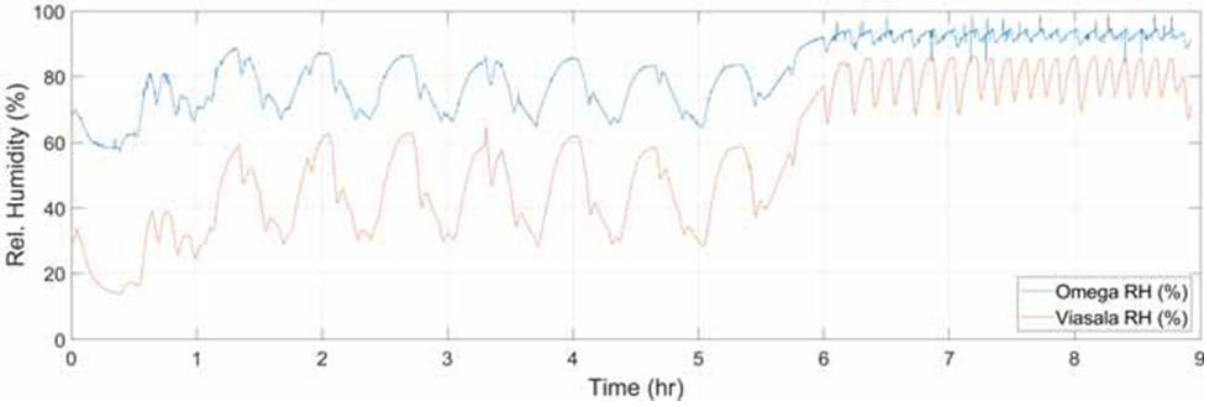

Figure 100620.03: Velocity Time History

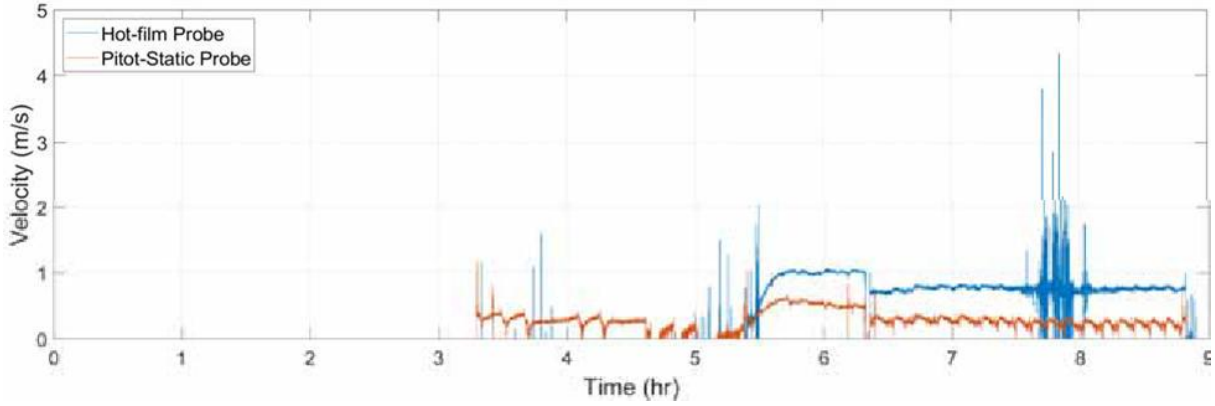

Figure 100620.04: Coolant Return Temperature Time History

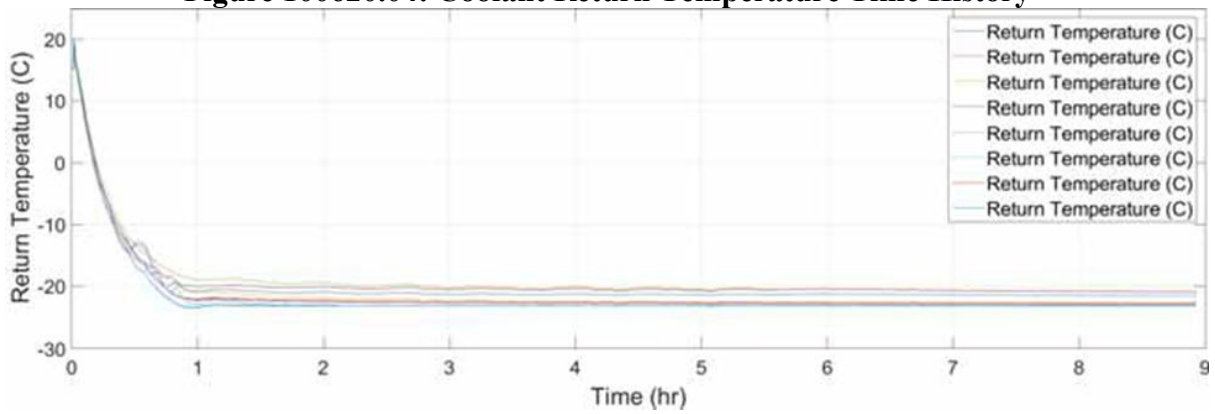

Figure 100620.05: Coolant Supply Temperature Time History

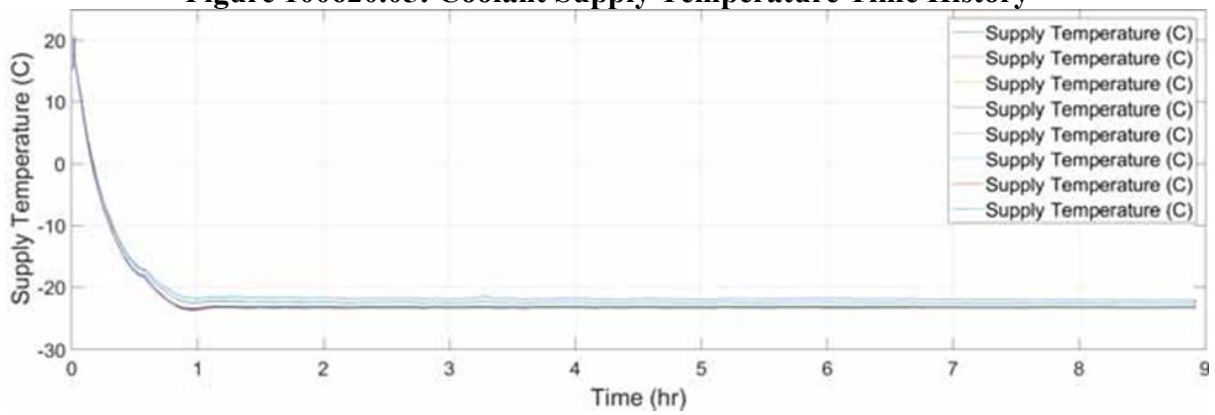

Figure 100620.06: Skin Temperature Time History

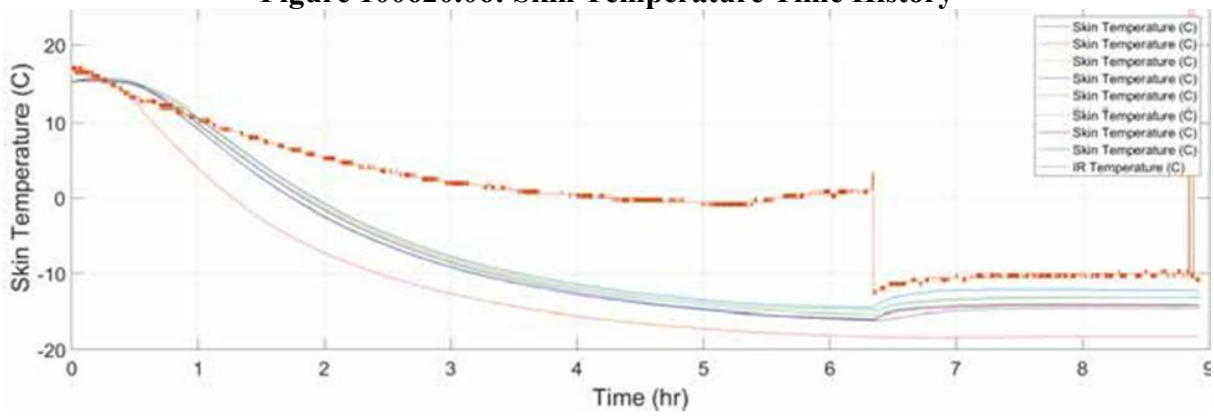

Figure 100620.07: Floor Temperature Time History

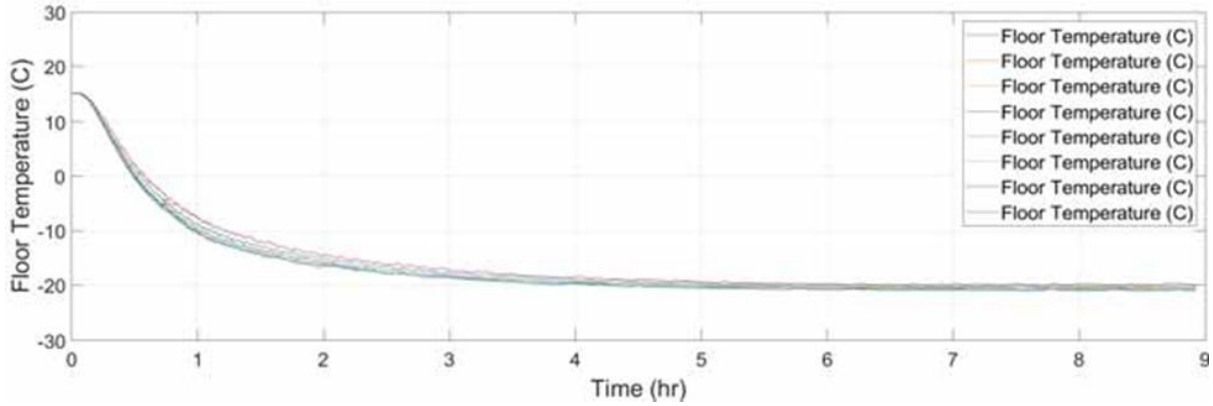

Figure 100620.08: Skin Temperature Slope Time History

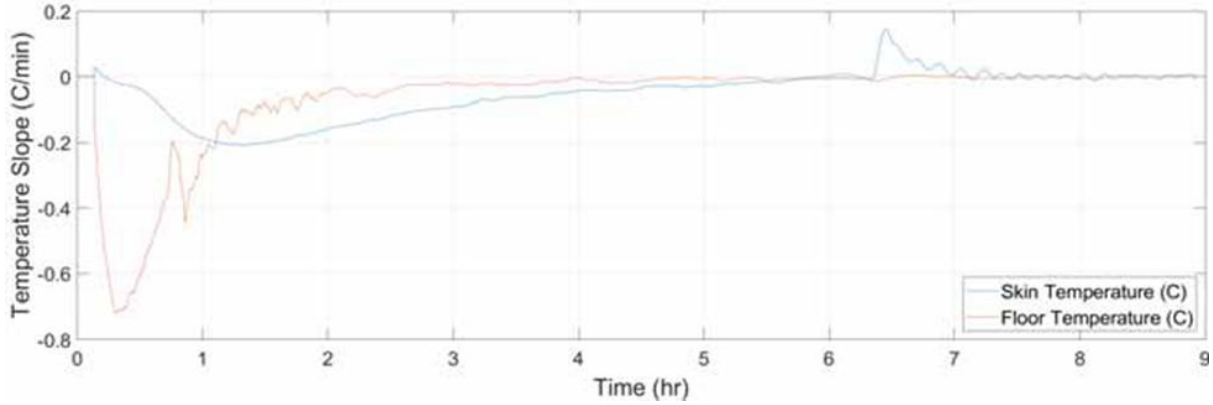

Figure 100620.09: RMS Height Evolution

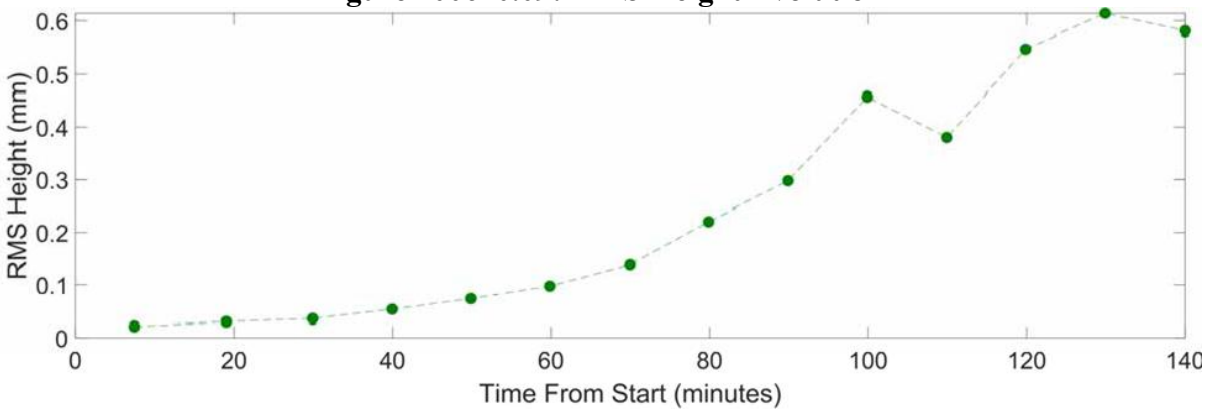

Figure 100620.10: Skewness Evolution

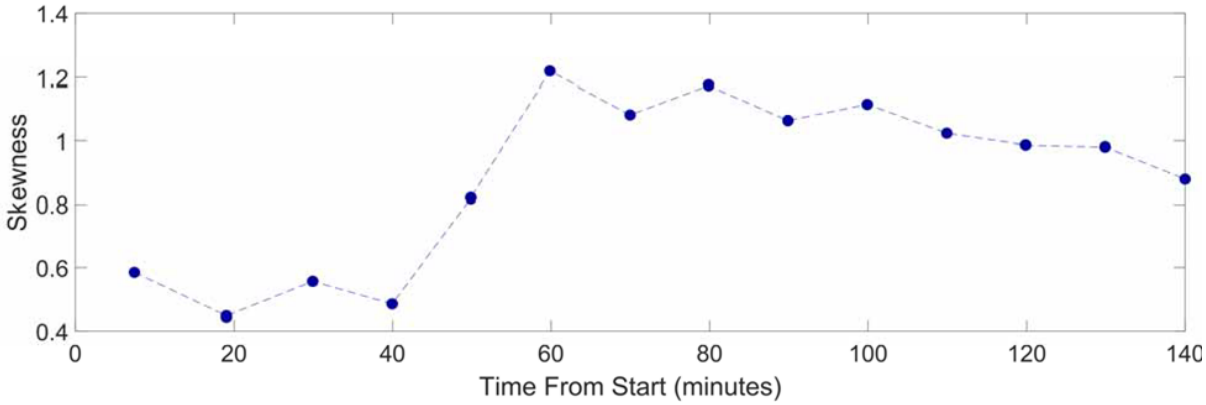

Figure 100620.11: Peak to Valley Evolution

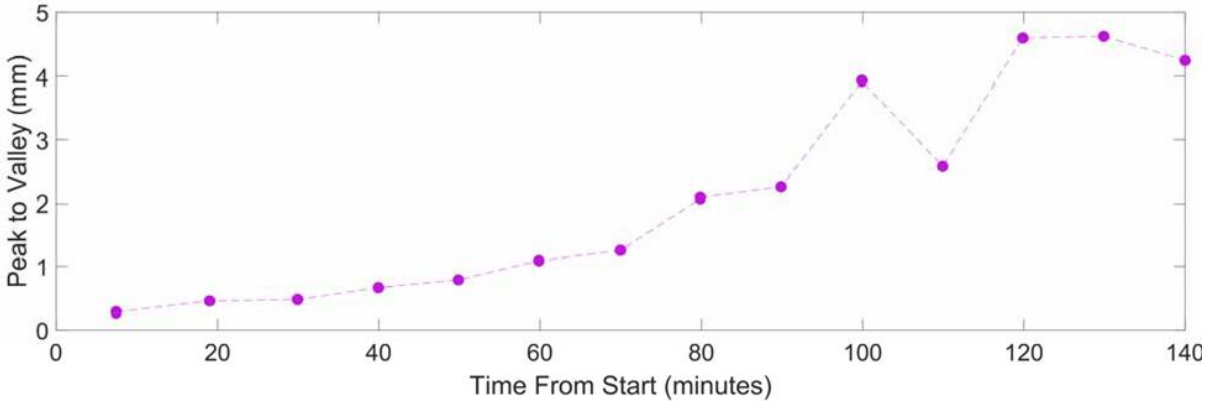

Figure 100620.12: Equivalent Roughness Evolution

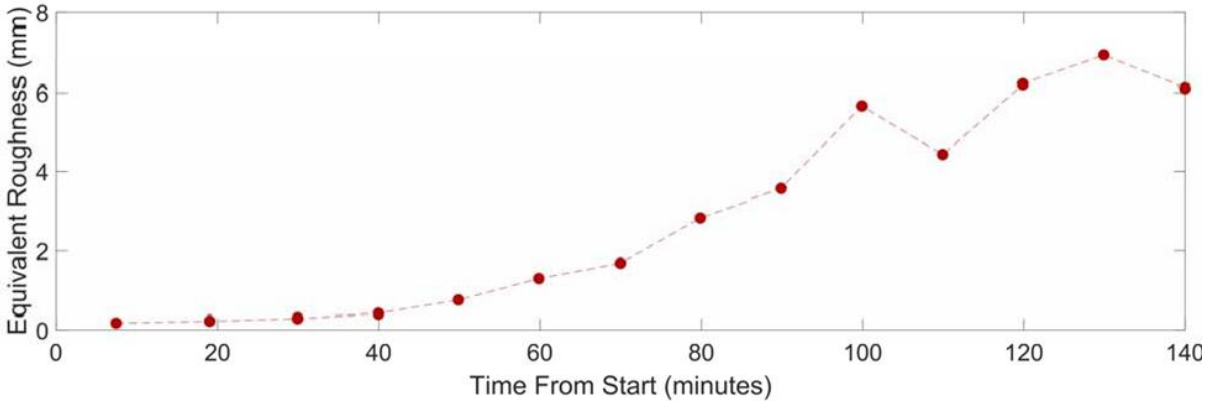

Table 100620.02: Summary of Roughness Parameters

Time (min.)	RMS (mm)	Skewness	Peak to Valley (mm)	ks,Flack-Schultz (mm)
7.4309	0.0213	0.5844	0.2736	0.1774
19.0309	0.0302	0.4450	0.4457	0.2215
29.9309	0.0357	0.5554	0.4688	0.2894
39.9476	0.0535	0.4829	0.6589	0.4066
49.8643	0.0738	0.8194	0.7828	0.7421
59.8476	0.0974	1.2200	1.0886	1.2870
69.9643	0.1388	1.0827	1.2558	1.6798
79.8643	0.2206	1.1762	2.0801	2.8352
89.8809	0.2979	1.0645	2.2486	3.5621
99.8976	0.4579	1.1166	3.9350	5.6656
109.9309	0.3803	1.0242	2.5809	4.4271
119.8643	0.5474	0.9871	4.6130	6.2128
129.8976	0.6145	0.9808	4.6402	6.9433
139.9976	0.5812	0.8781	4.2532	6.1057

Figure 100620.13: Frost Topography at 00:07:23

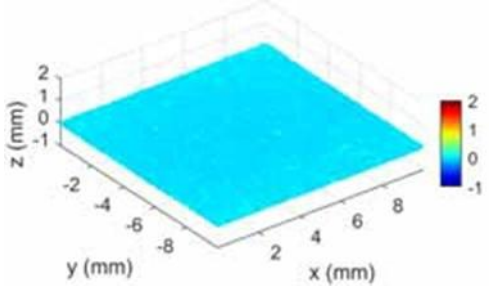

Figure 100620.14: Frost Topography at 00:18:59

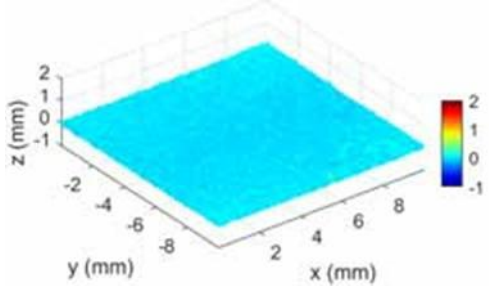

Figure 100620.15: Frost Topography at 00:29:53

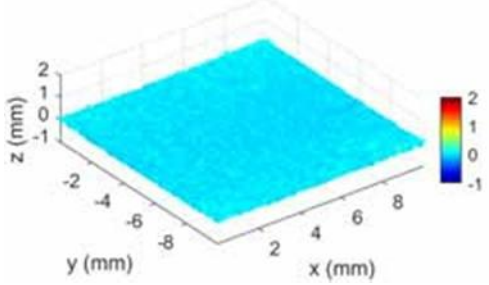

Figure 100620.16: Frost Topography at 00:39:54

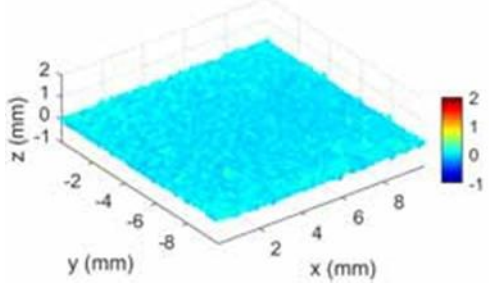

Figure 100620.17: Frost Topography at 00:49:49

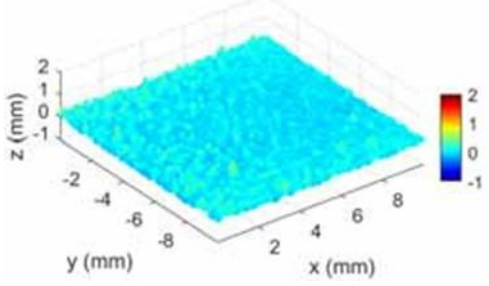

Figure 100620.18: Frost Topography at 00:59:48

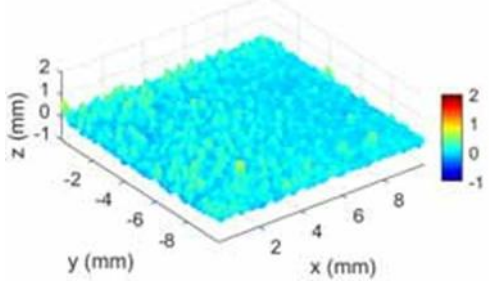

Figure 100620.19: Frost Topography at 01:09:55

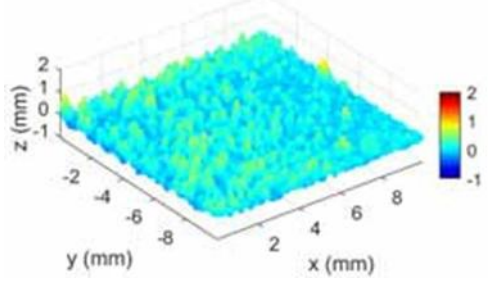

Figure 100620.20: Frost Topography at 01:19:49

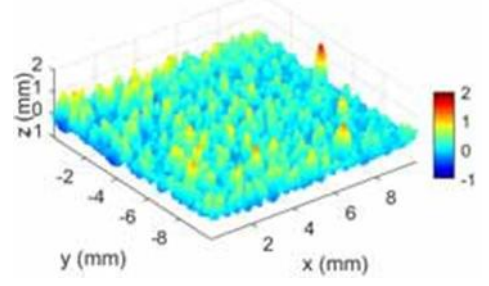

Figure 100620.21: Frost Topography at 01:29:50

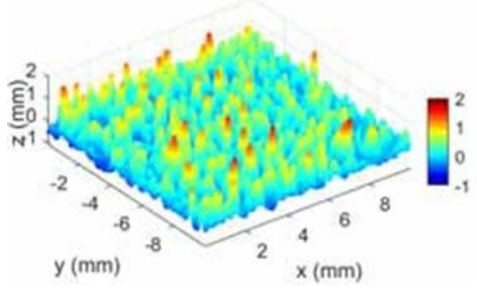

Figure 100620.22: Frost Topography at 01:39:51

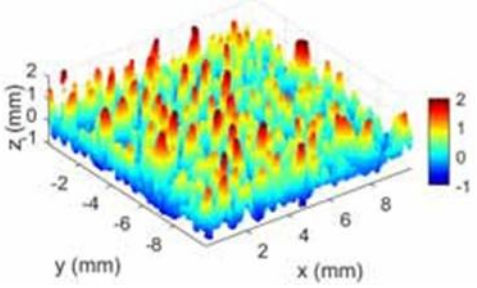

Figure 100620.23: Frost Topography at 01:49:53

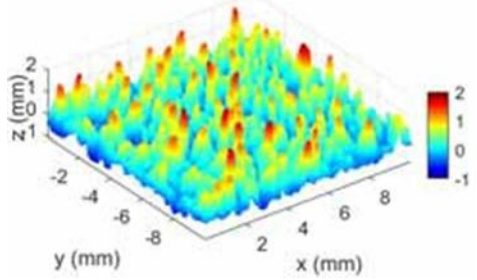

Figure 100620.24: Frost Topography at 01:59:49

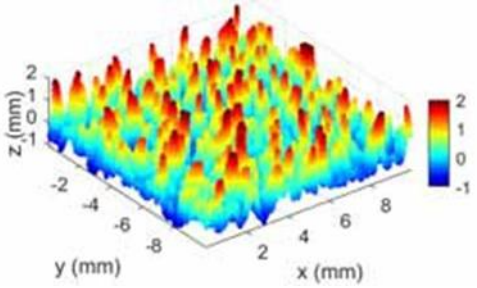

Figure 100620.25: Frost Topography at 02:09:51

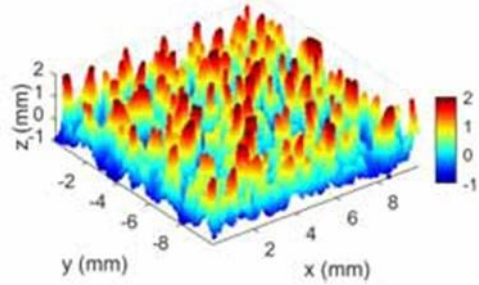

Figure 100620.26: Frost Topography at 02:19:57

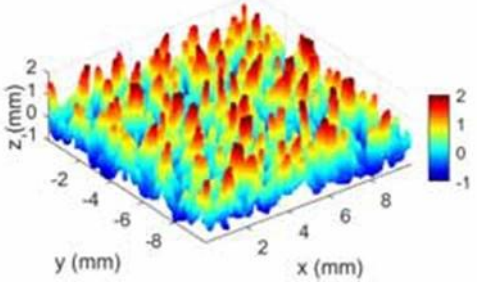

CAFF Conditions Report – Case Date: 100820

Table 100820.01: Summary of Measured Test Variables

Variable	Mean	St. Dev.	Rand. Unc.
T_air (C)	15.1898	0.2912	0.0096
Rh (%)	78.9416	3.3931	0.1115
Omega (kg_v/kg_da)	0.00860599	0.00044494	0.00001463
V_air (m/s)	0.2226	0.1244	0.0041
T_skin (C)	-10.9775	0.8069	0.0265
T_floor (C)	-19.3427	0.1246	0.0041

Figure 100820.01: Temperature and Voltage Control Time History

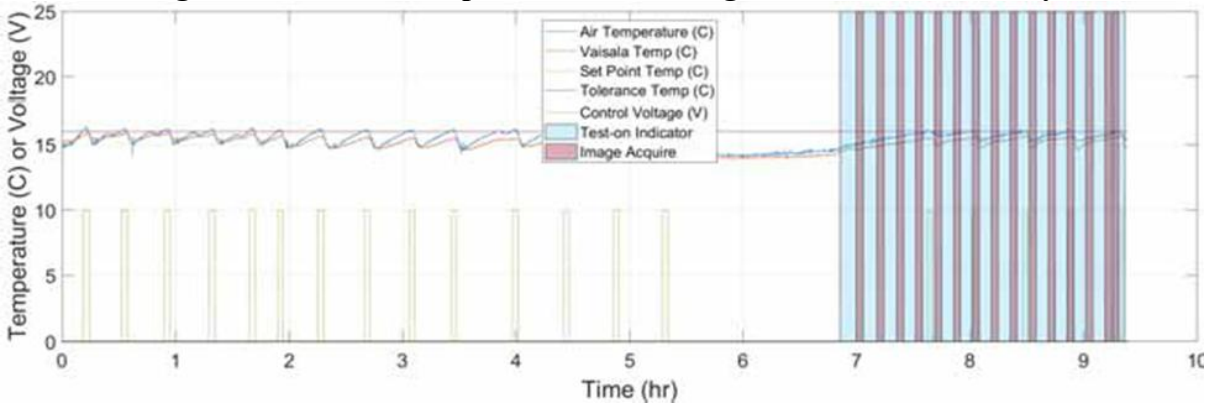

Figure 100820.02: Relative Humidity Time History

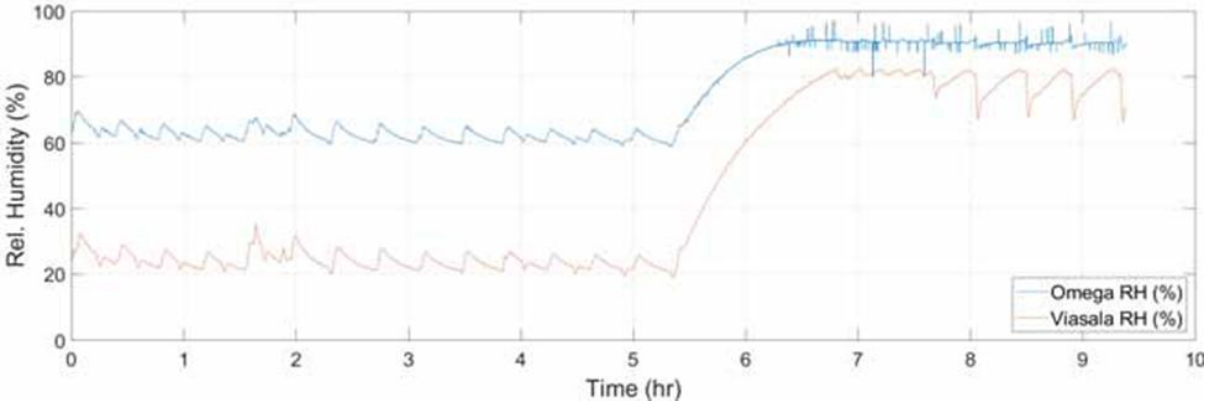

Figure 100820.03: Velocity Time History

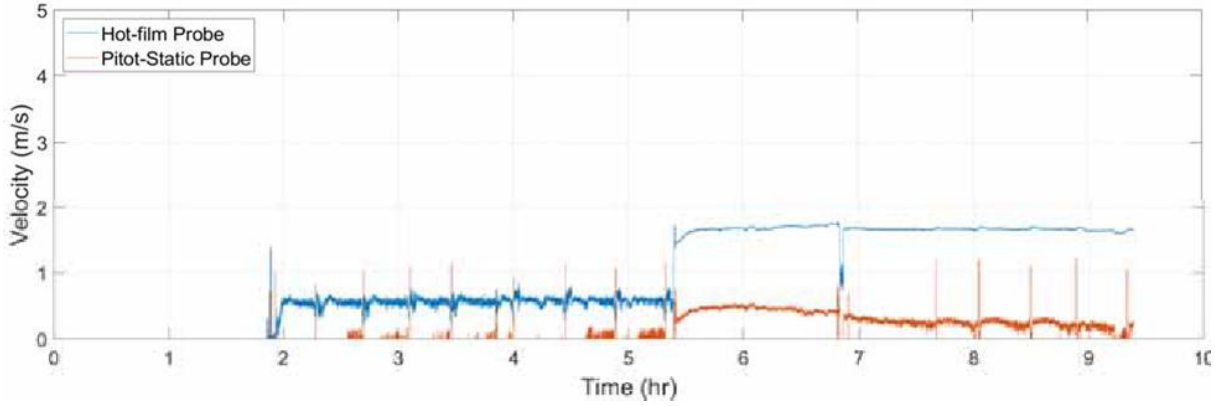

Figure 100820.04: Coolant Return Temperature Time History

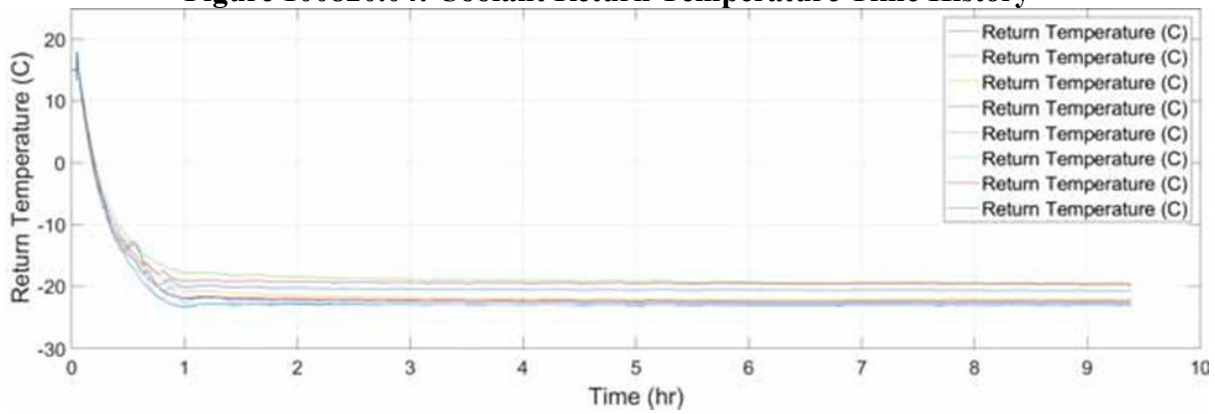

Figure 100820.05: Coolant Supply Temperature Time History

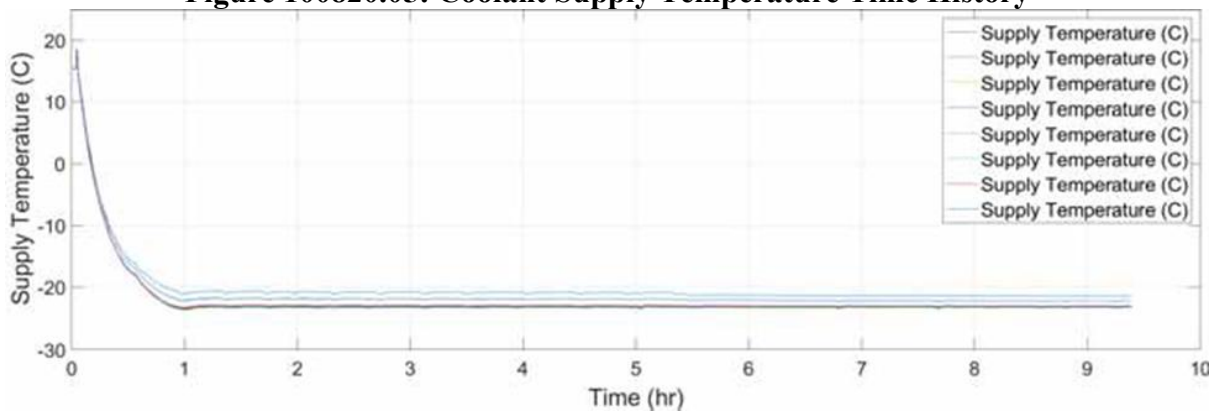

Figure 100820.06: Skin Temperature Time History

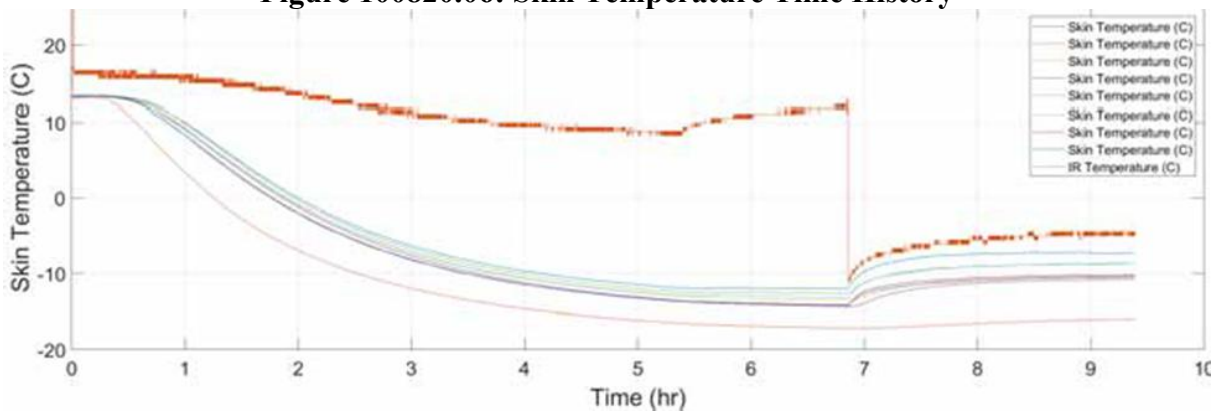

Figure 100820.07: Floor Temperature Time History

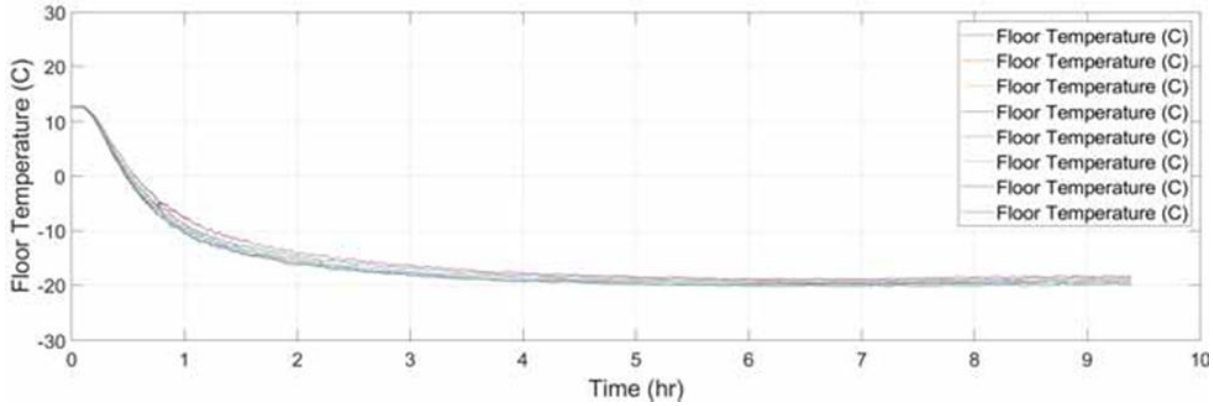

Figure 100820.08: Skin Temperature Slope Time History

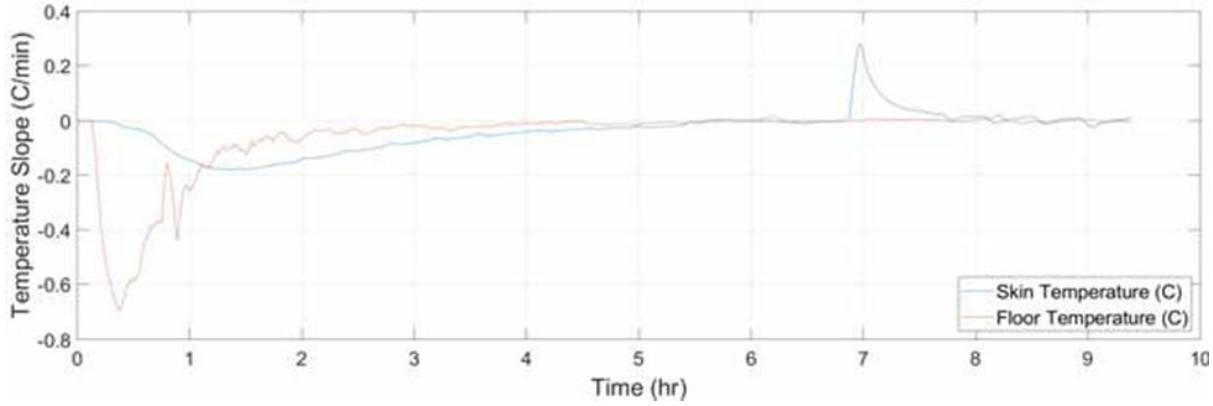

Figure 100820.09: RMS Height Evolution

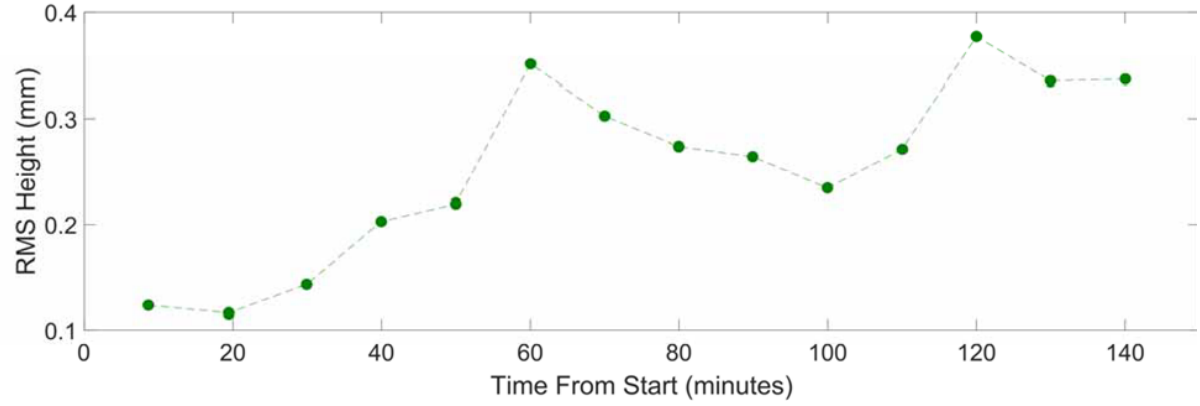

Figure 100820.10: Skewness Evolution

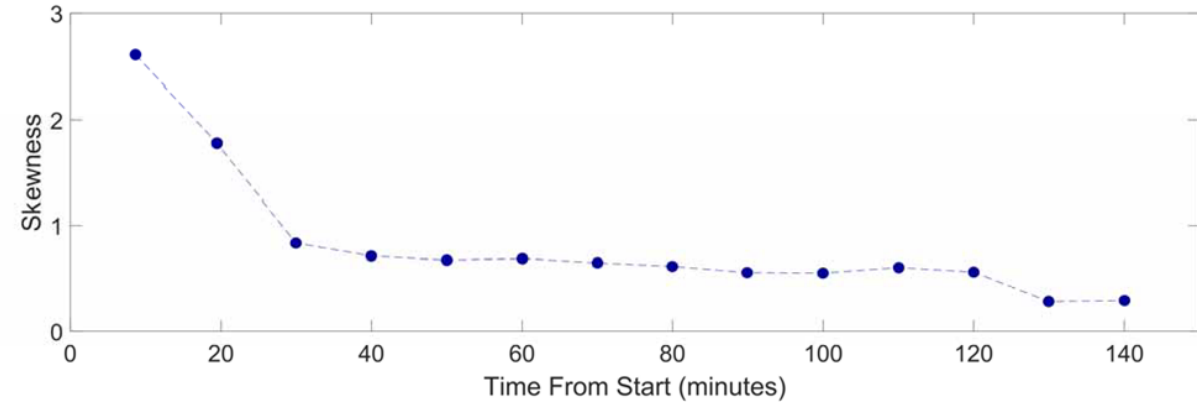

Figure 100820.11: Peak to Valley Evolution

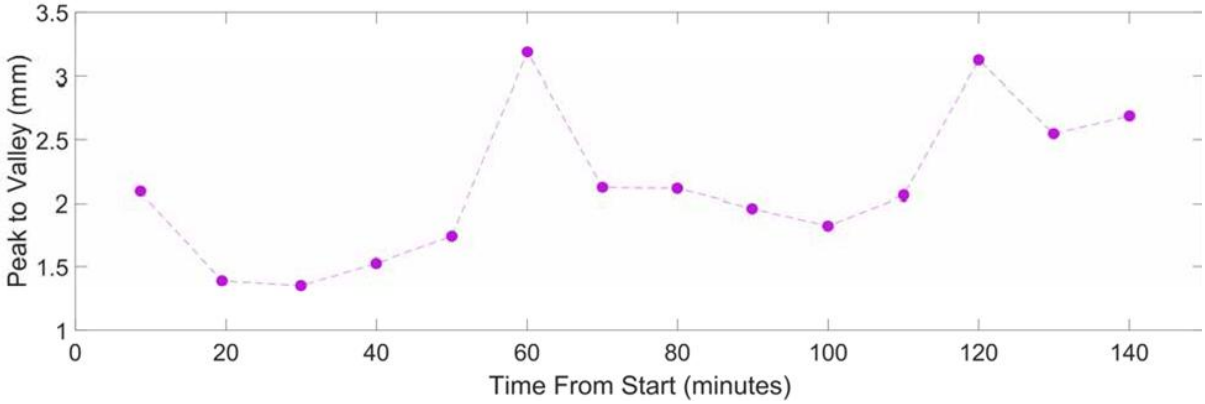

Figure 100820.12: Equivalent Roughness Evolution

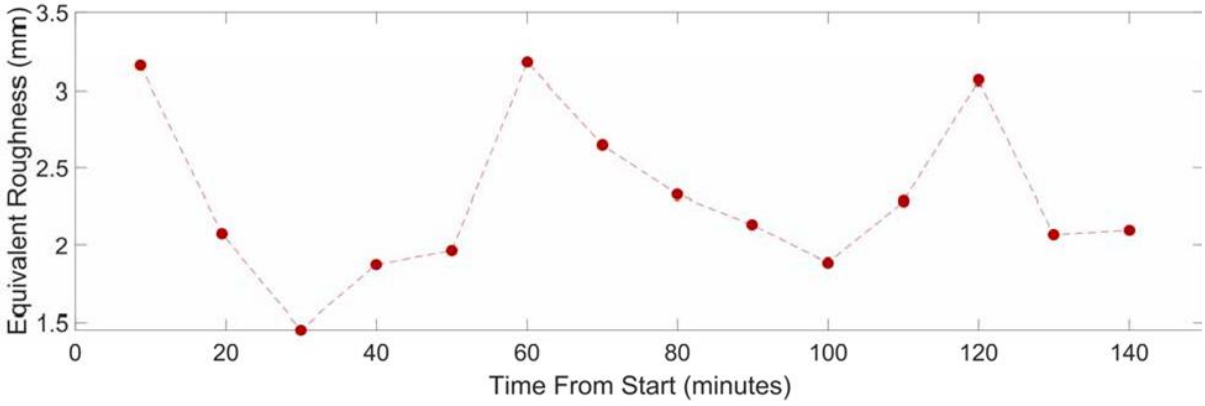

Table 100820.02: Summary of Roughness Parameters

Time (min.)	RMS (mm)	Skewness	Peak to Valley (mm)	ks,Flack-Schultz (mm)
8.6204	0.1226	2.6171	2.0901	3.1623
19.4538	0.1154	1.7781	1.3842	2.0735
29.9371	0.1428	0.8328	1.3453	1.4504
39.9538	0.2029	0.7090	1.5235	1.8731
49.9871	0.2197	0.6681	1.7399	1.9618
60.0371	0.3519	0.6837	3.1943	3.1824
70.0038	0.3028	0.6427	2.1205	2.6473
79.9538	0.2736	0.6089	2.1136	2.3252
89.9038	0.2640	0.5502	1.9614	2.1320
99.9704	0.2341	0.5454	1.8212	1.8824
110.0371	0.2712	0.5982	2.0604	2.2836
120.0038	0.3782	0.5548	3.1296	3.0670
129.9538	0.3357	0.2713	2.5486	2.0666
140.0371	0.3373	0.2800	2.6910	2.0957

Figure 100820.13: Frost Topography at 00:08:29

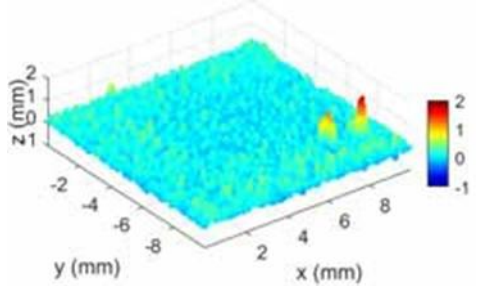

Figure 100820.14: Frost Topography at 00:19:19

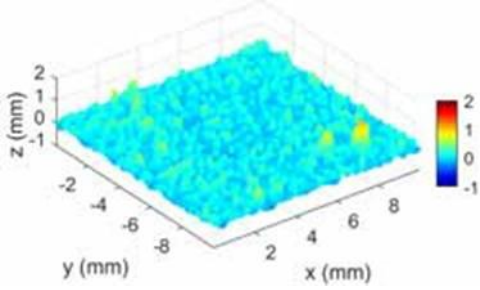

Figure 100820.15: Frost Topography at 00:29:48

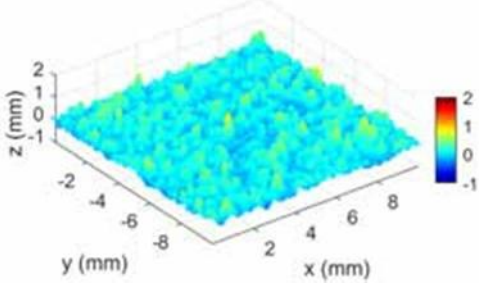

Figure 100820.16: Frost Topography at 00:39:49

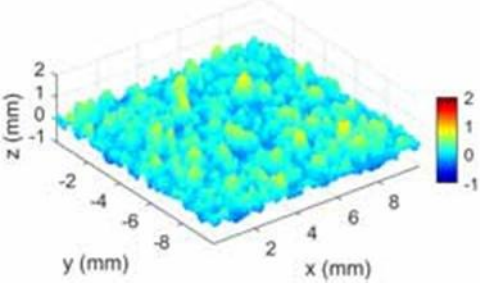

Figure 100820.17: Frost Topography at 00:49:51

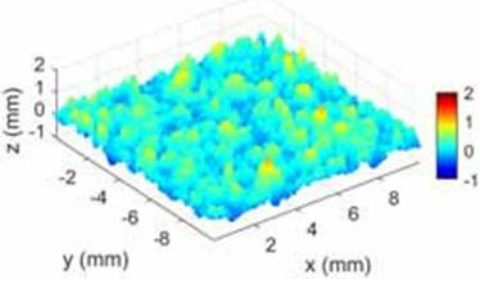

Figure 100820.18: Frost Topography at 00:59:54

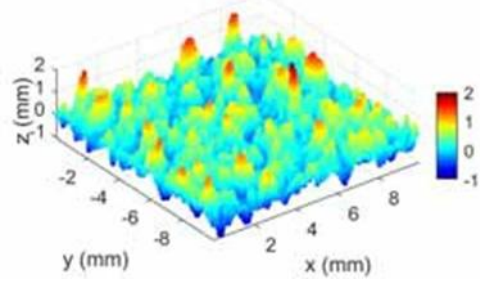

Figure 100820.19: Frost Topography at 01:09:52

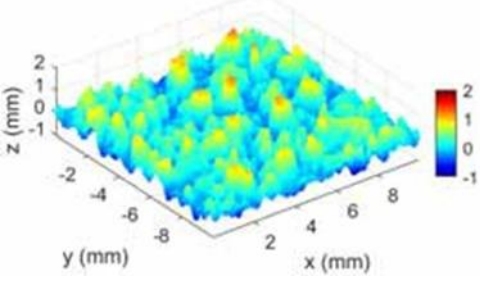

Figure 100820.20: Frost Topography at 01:19:49

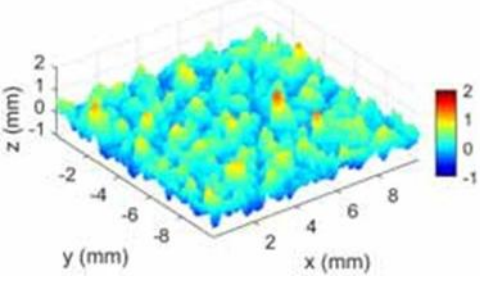

Figure 100820.21: Frost Topography at 01:29:46

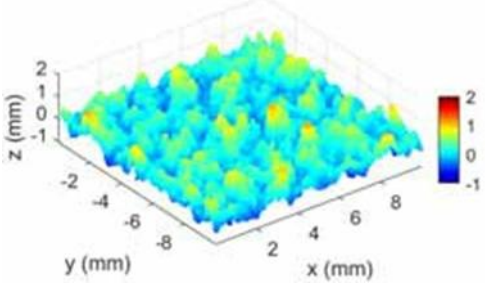

Figure 100820.22: Frost Topography at 01:39:50

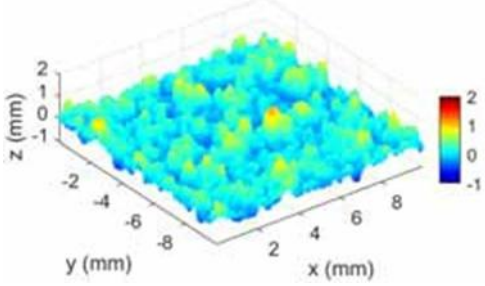

Figure 100820.23: Frost Topography at 01:49:54

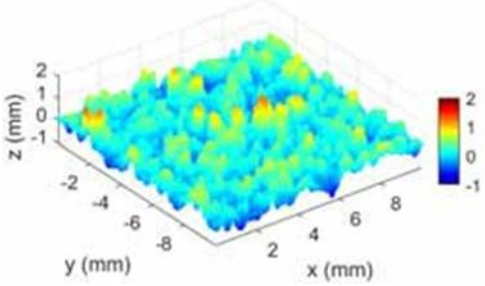

Figure 100820.24: Frost Topography at 01:59:52

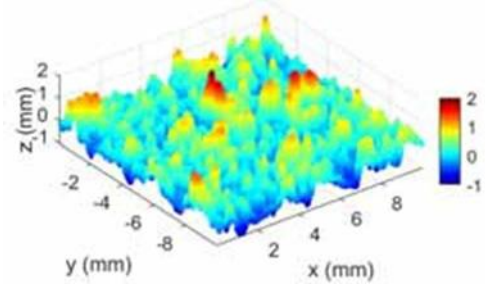

Figure 100820.25: Frost Topography at 02:09:49

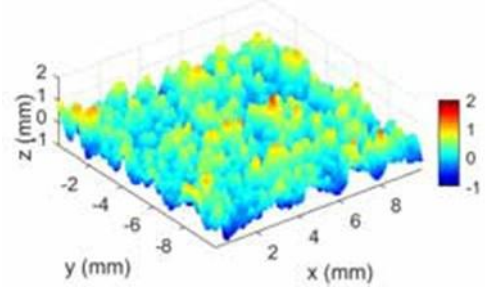

Figure 100820.26: Frost Topography at 02:19:54

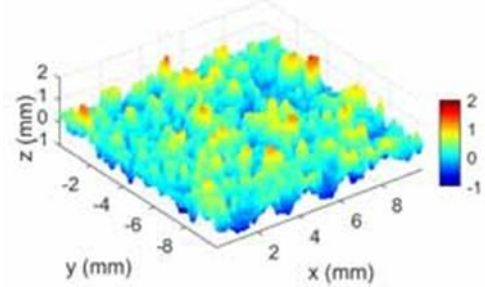

D Appendix D: CAFF test reports using a carbon fiber skin without structural rib

Table D- 1. Summary of Nominal Test Conditions for Wing Tank Thermal Model with a Carbon Fiber Skin and Without a Structural Rib

Date	T_{PC} (°C)	$T_{air,set}$ (°C)	RH (%)	V (m/s)	x_{img} (in.)	Notes
03/03/21	-27	16	82	1.4	17.5	10 min. int., frost formed then quickly melted
03/08/21	-27	10	82	1.4	17.5	10 min. int.
03/10/21	-27	5	82	1.4	17.5	10 min. int.
03/24/21	-27	5	82	0.4	17.5	10 min. int.
03/26/21	-27	10	82	0.4	17.5	10 min. int.
03/31/21	-27	16	82	0.4	17.5	10 min. int., frost formed then melted, test ended at 70 min.
04/12/21	-27	5	82	0.4	12.0	10 min. int.
04/14/21	-27	10	82	0.4	12.0	10 min. int.
04/16/21	-27	5	82	1.4	12.0	10 min. int.
04/19/21	-27	10	82	1.4	12.0	10 min. int.
04/21/21	-27	5	82	1.4	20.8	10 min. int.
04/23/21	-27	10	82	1.4	20.8	10 min. int.
04/26/21	-27	16	82	0.4	20.8	10 min. int.
04/28/21	-27	10	82	0.4	20.8	10 min. int.
04/30/21	-27	5	82	0.4	20.8	10 min. int.

CAFF Conditions Report – Case Date: 030321

Table 030321.01: Summary of Measured Test Variables

Variable	Mean	St. Dev.	Rand. Unc.
T_air (C)	14.9979	0.4356	0.0211
Rh (%)	79.5880	2.8102	0.1364
Omega (kg_v/kg_da)	0.00852845	0.00037646	0.00001827
V_air (m/s)	1.2420	0.2072	0.0101
T_skin (C)	-3.8313	1.4720	0.0714
T_floor (C)	-19.4238	0.0682	0.0033

Figure 030321.01: Temperature and Voltage Control Time History

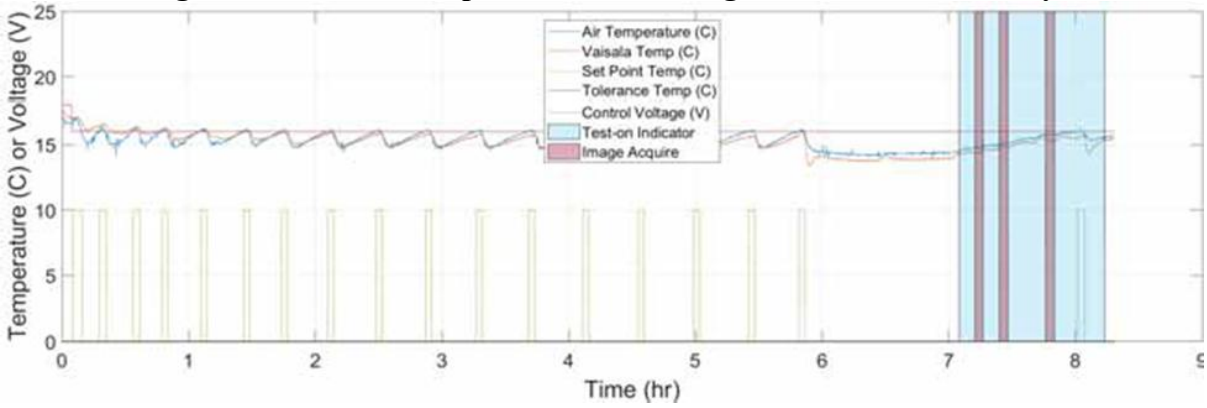

Figure 030321.02: Relative Humidity Time History

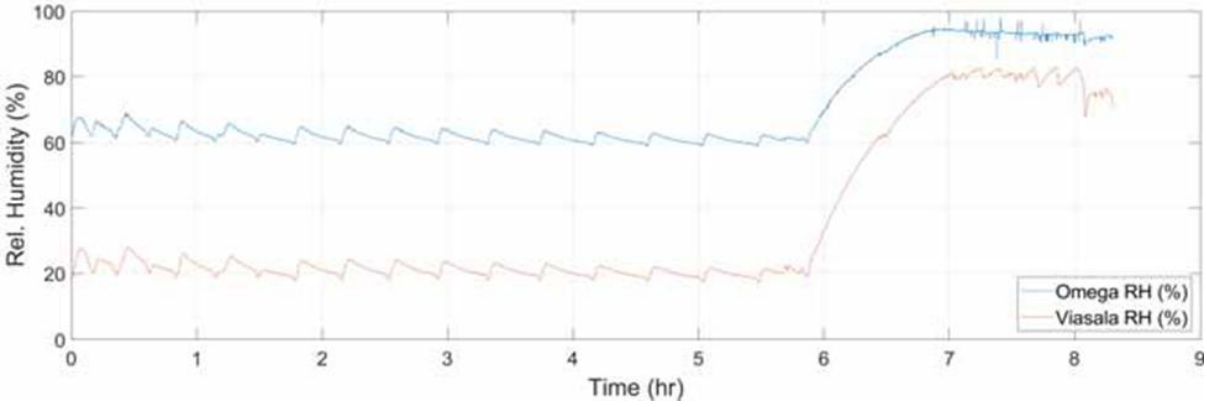

Figure 030321.03: Velocity Time History

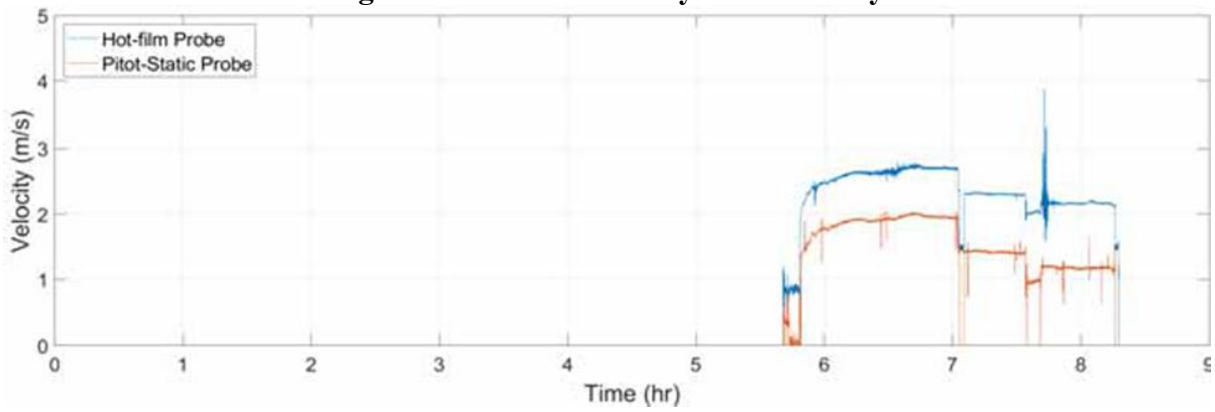

Figure 030321.04: Coolant Return Temperature Time History

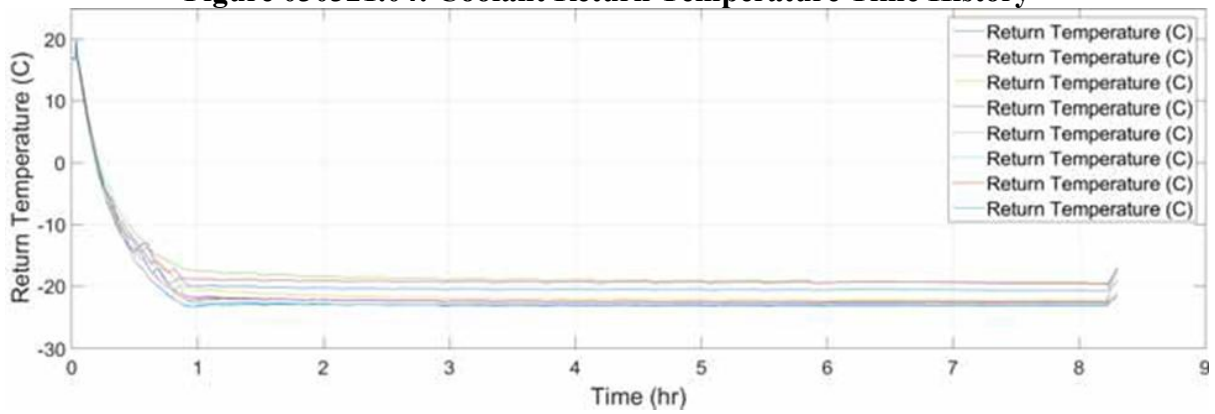

Figure 030321.05: Coolant Supply Temperature Time History

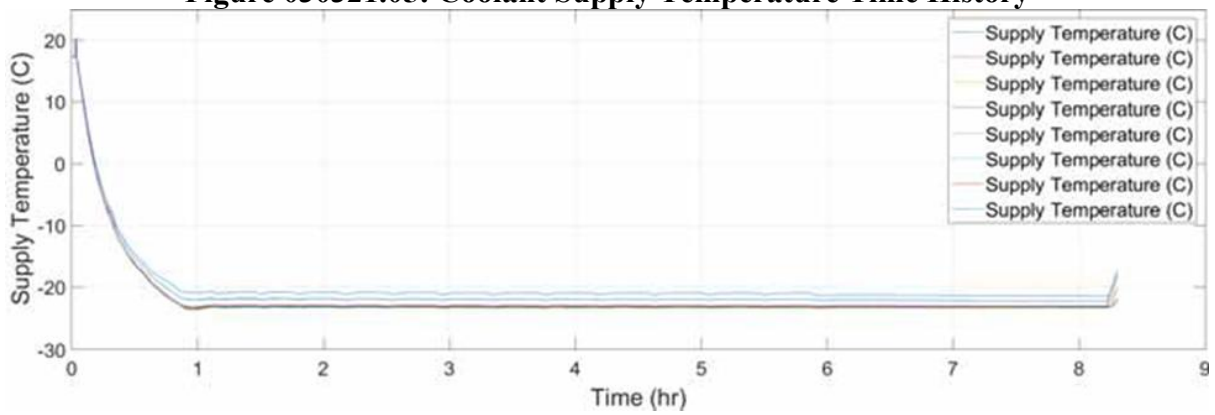

Figure 030321.06: Skin Temperature Time History

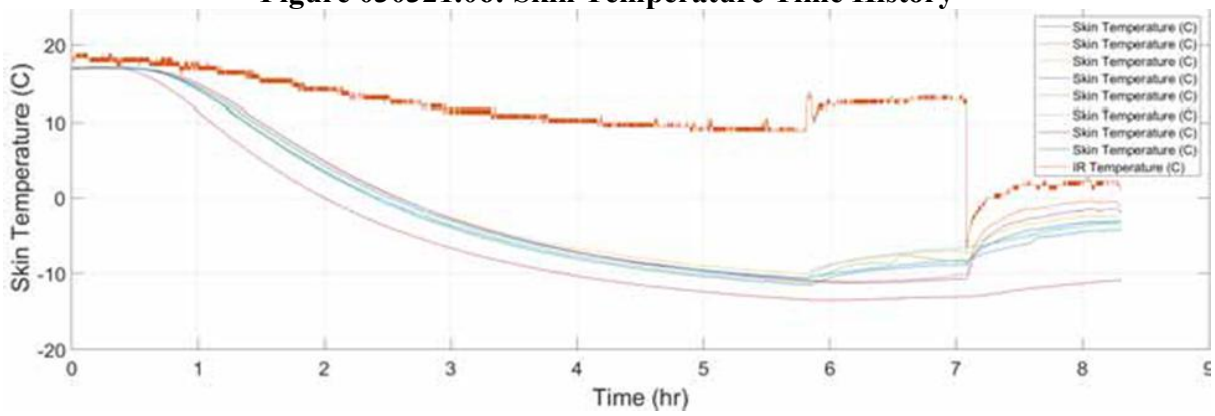

Figure 030321.07: Floor Temperature Time History

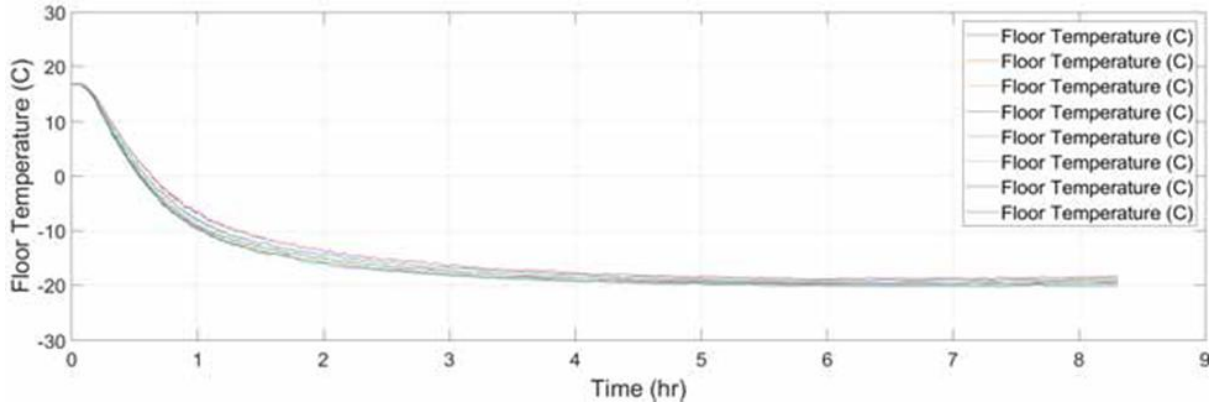

Figure 030321.08: Skin Temperature Slope Time History

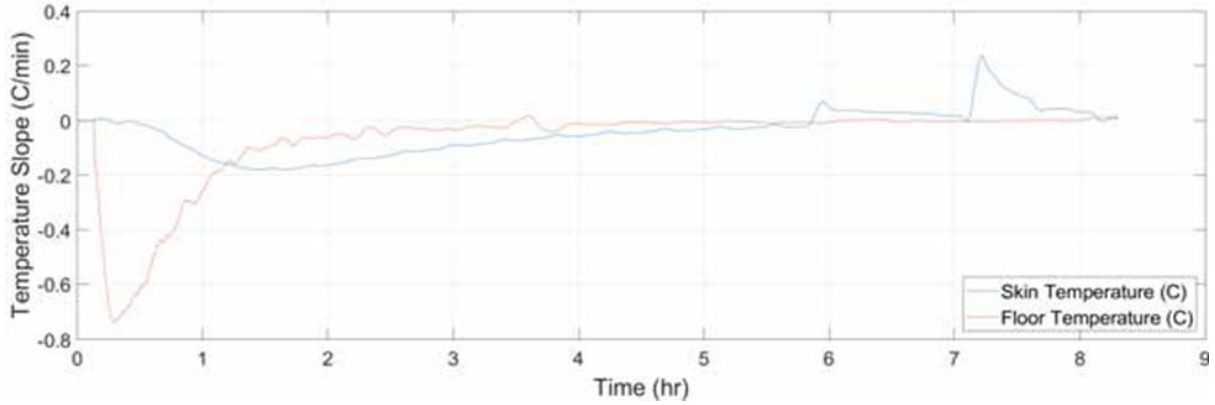

Figure 030321.09: RMS Height Evolution

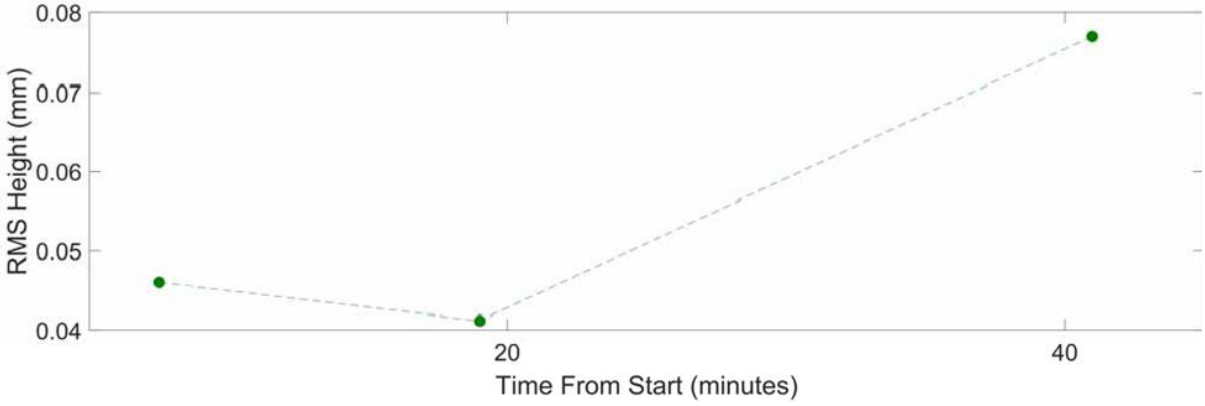

Figure 030321.10: Skewness Evolution

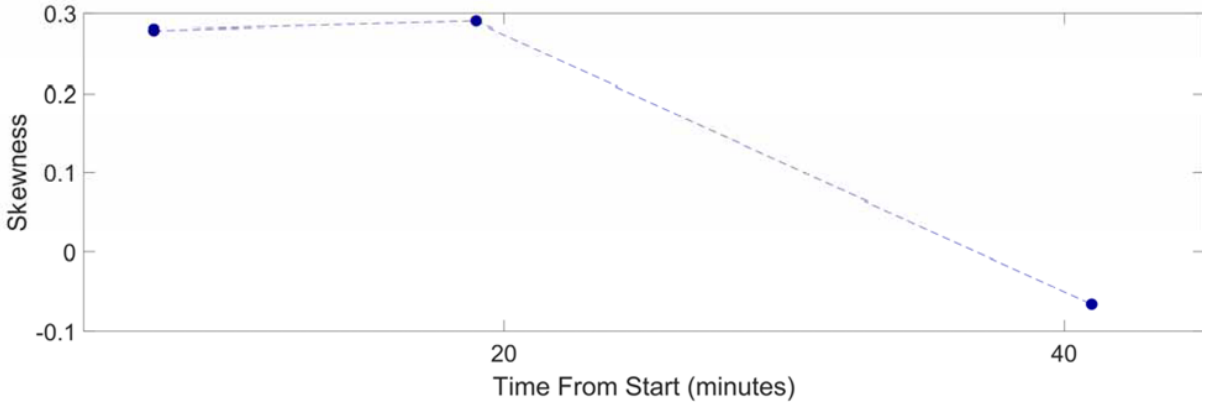

Figure 030321.11: Peak to Valley Evolution

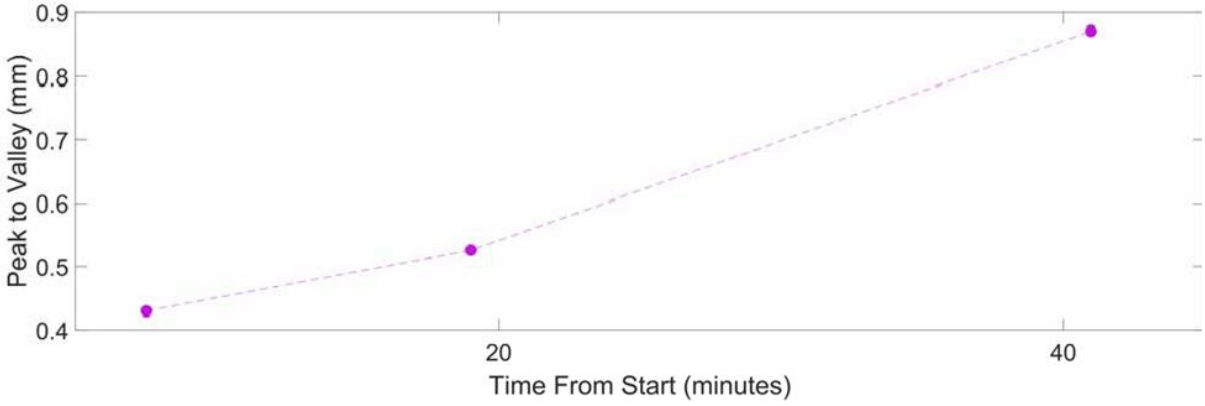

Figure 030321.12: Equivalent Roughness Evolution

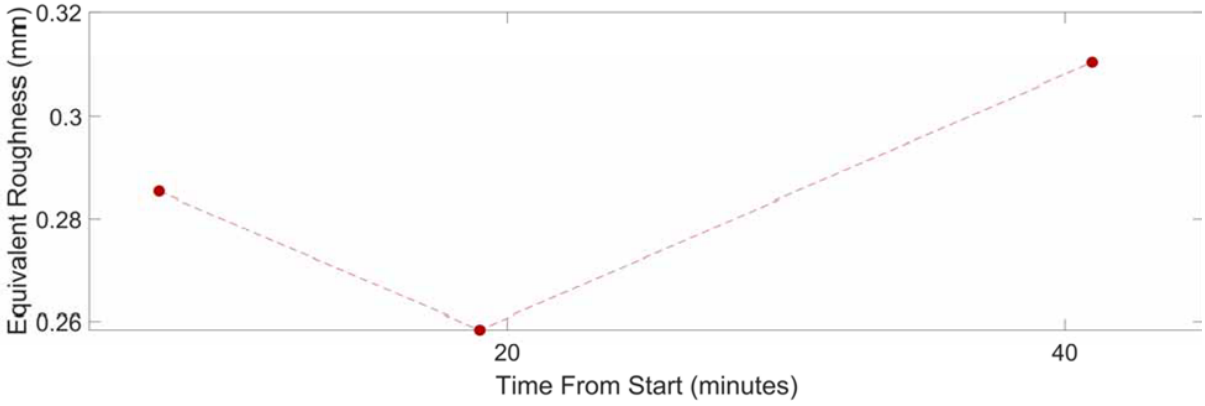

Table 030321.02: Summary of Roughness Parameters

Time (min.)	RMS (mm)	Skewness	Peak to Valley (mm)	ks,Flack-Schultz (mm)
7.5085	0.0459	0.2793	0.4291	0.2853
19.0085	0.0411	0.2902	0.5256	0.2583
40.9752	0.0771	-0.0675	0.8716	0.3104

Figure 030321.13: Frost Topography at 00:07:23

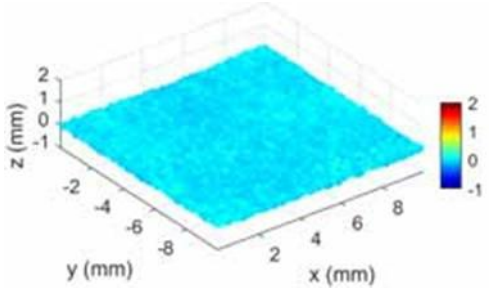

Figure 030321.14: Frost Topography at 00:18:53

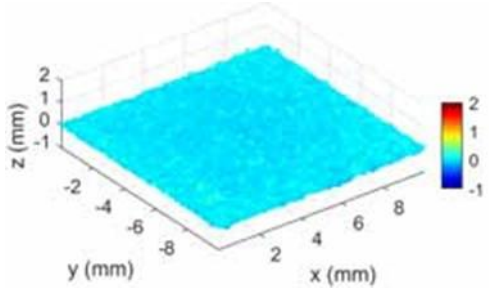

Figure 030321.15: Frost Topography at 00:40:51

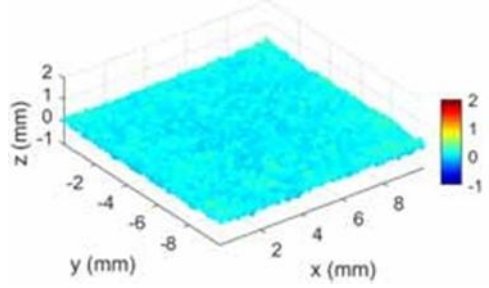

CAFF Conditions Report – Case Date: 030821

Table 030821.01: Summary of Measured Test Variables

Variable	Mean	St. Dev.	Rand. Unc.
T_air (C)	9.2137	0.4399	0.0148
Rh (%)	80.4403	4.5637	0.1533
Omega (kg_v/kg_da)	0.00582328	0.00040539	0.00001362
V_air (m/s)	1.3203	0.0825	0.0028
T_skin (C)	-6.1590	1.1238	0.0378
T_floor (C)	-19.9608	0.0545	0.0018

Figure 030821.01: Temperature and Voltage Control Time History

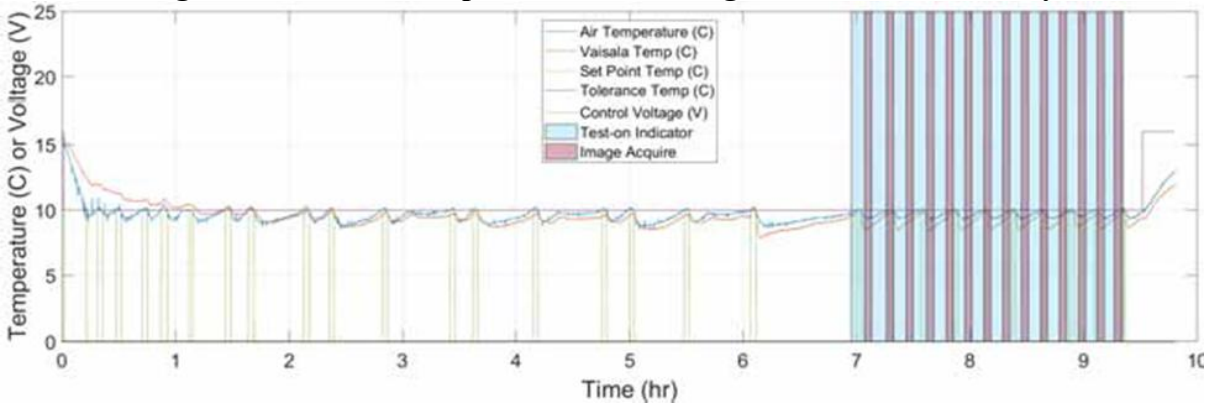

Figure 030821.02: Relative Humidity Time History

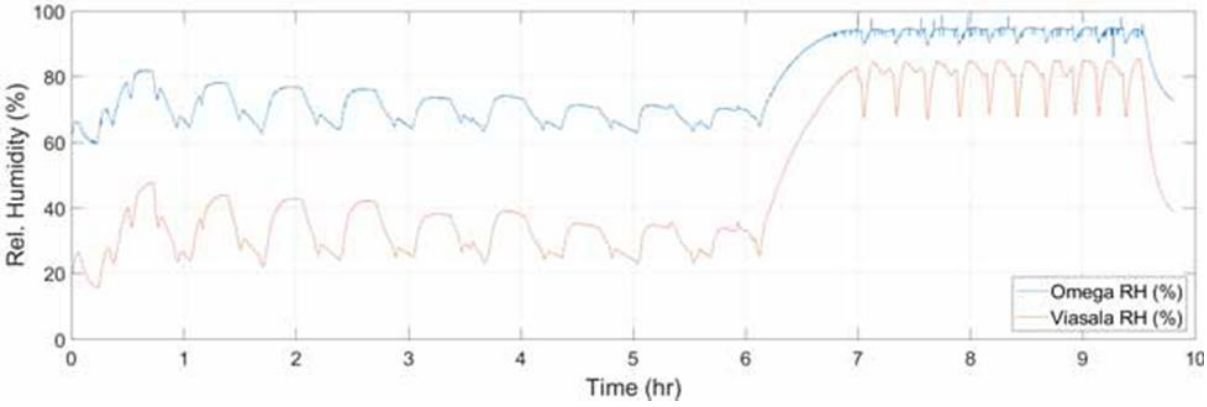

Figure 030821.03: Velocity Time History

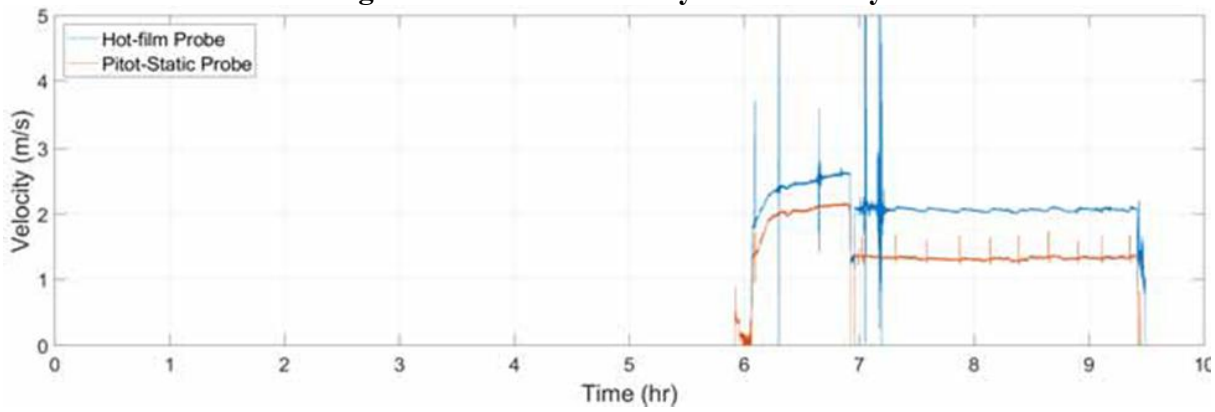

Figure 030821.04: Coolant Return Temperature Time History

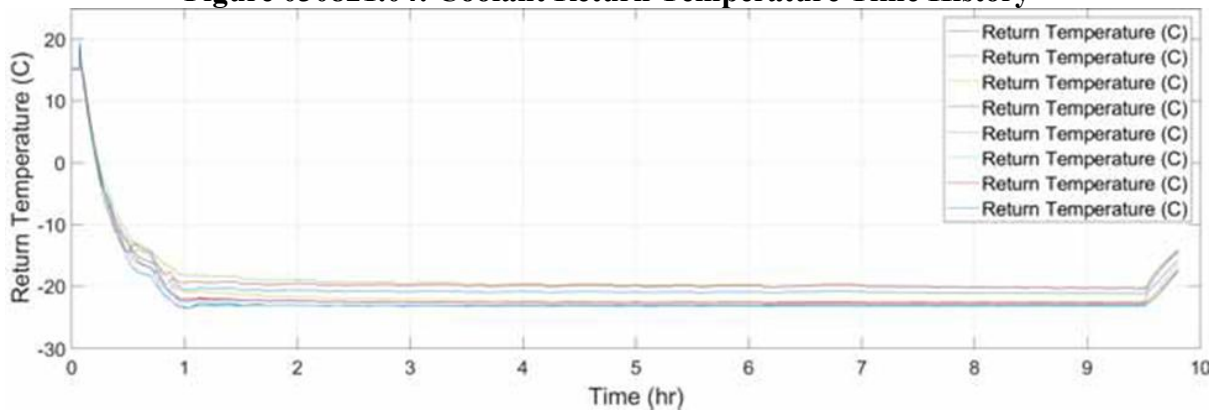

Figure 030821.05: Coolant Supply Temperature Time History

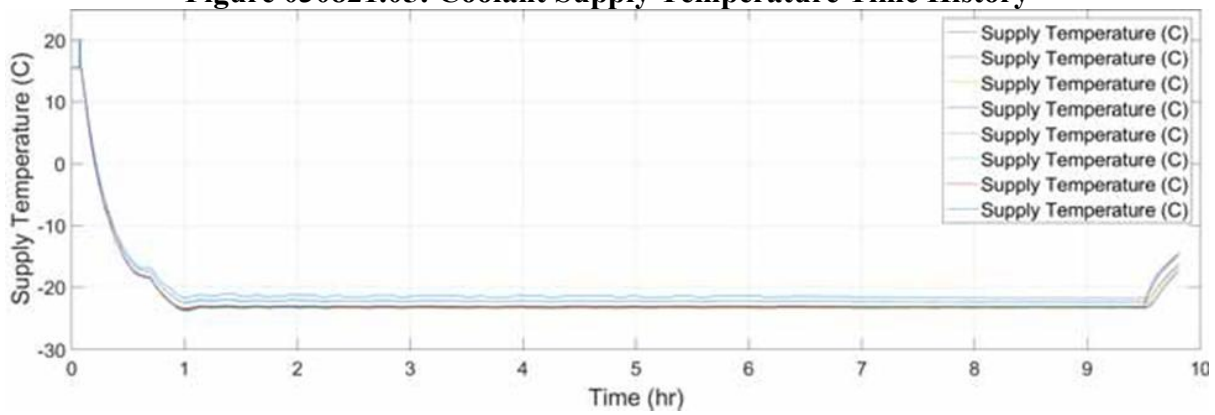

Figure 030821.06: Skin Temperature Time History

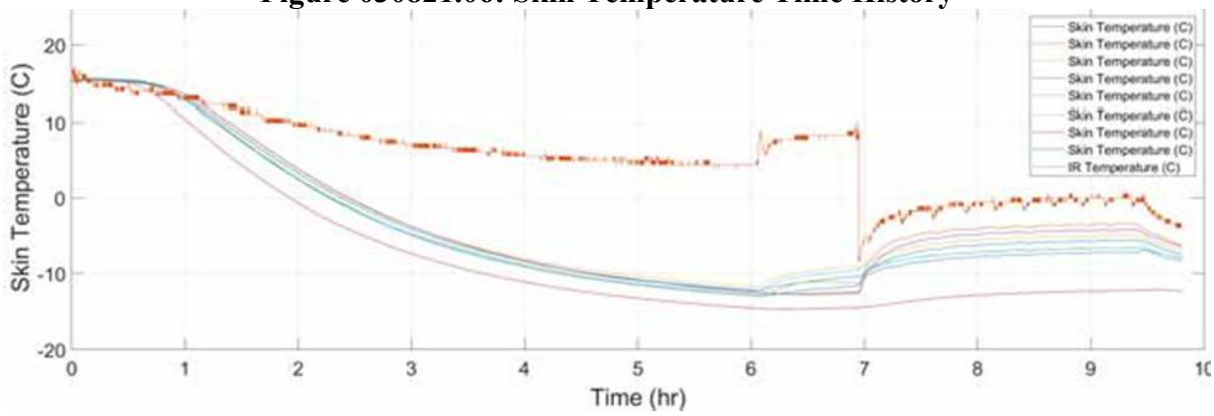

Figure 030821.07: Floor Temperature Time History

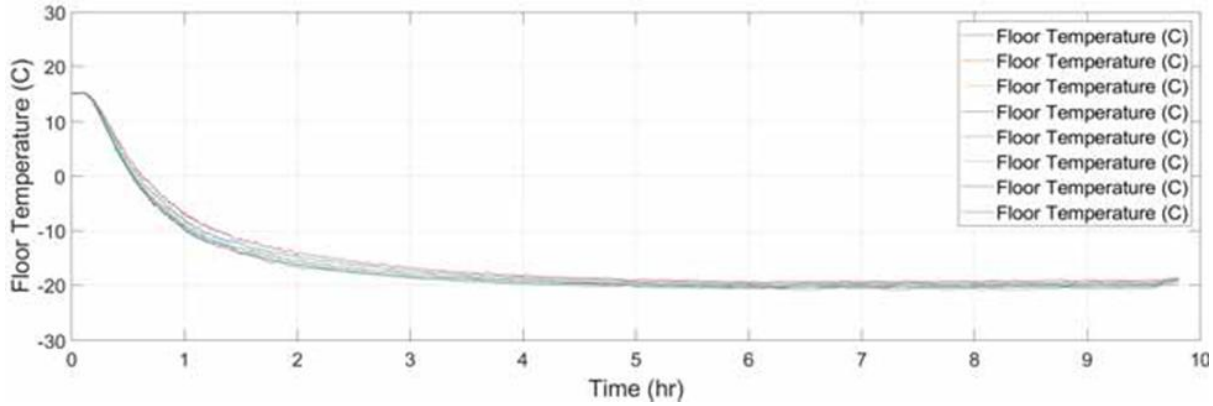

Figure 030821.08: Skin Temperature Slope Time History

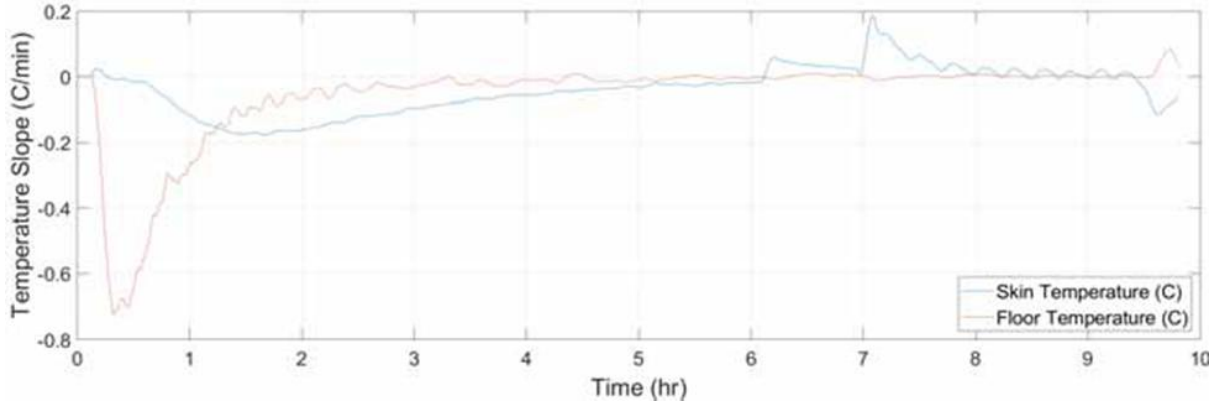

Figure 030821.09: RMS Height Evolution

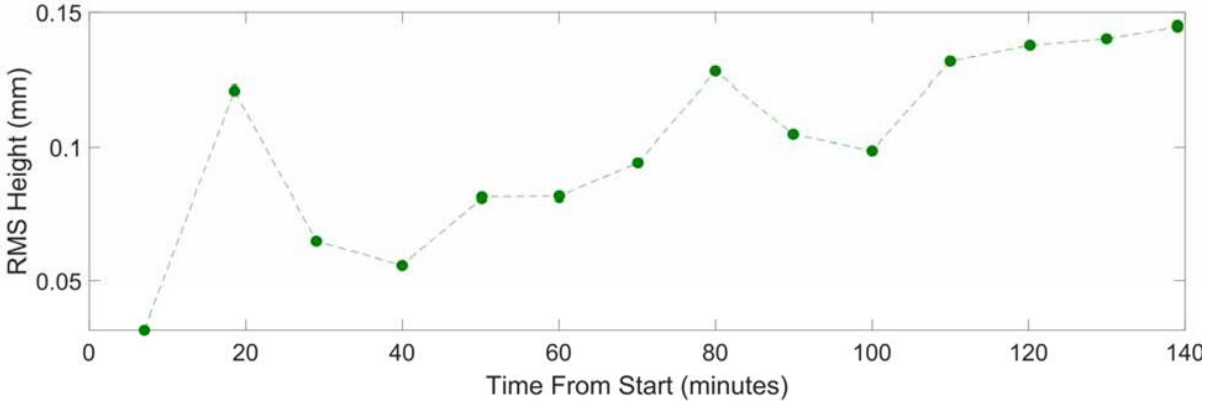

Figure 030821.10: Skewness Evolution

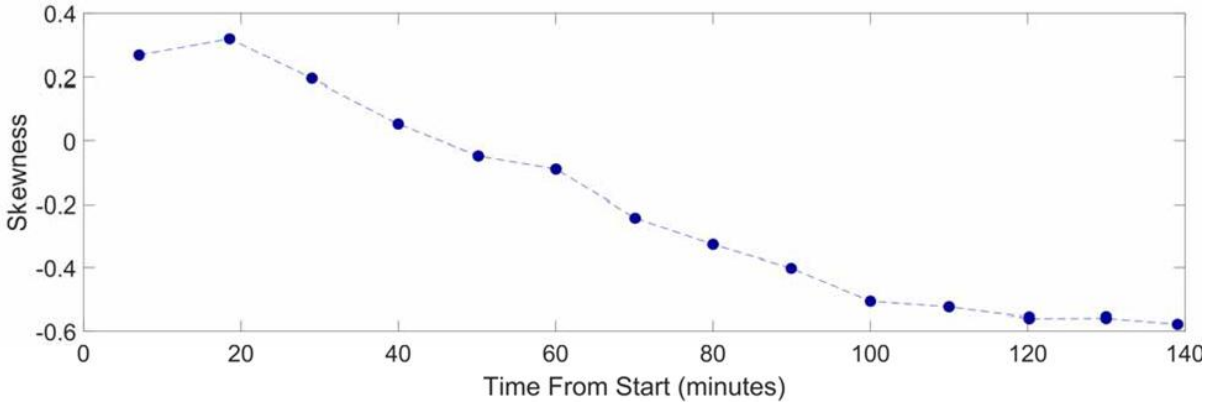

Figure 030821.11: Peak to Valley Evolution

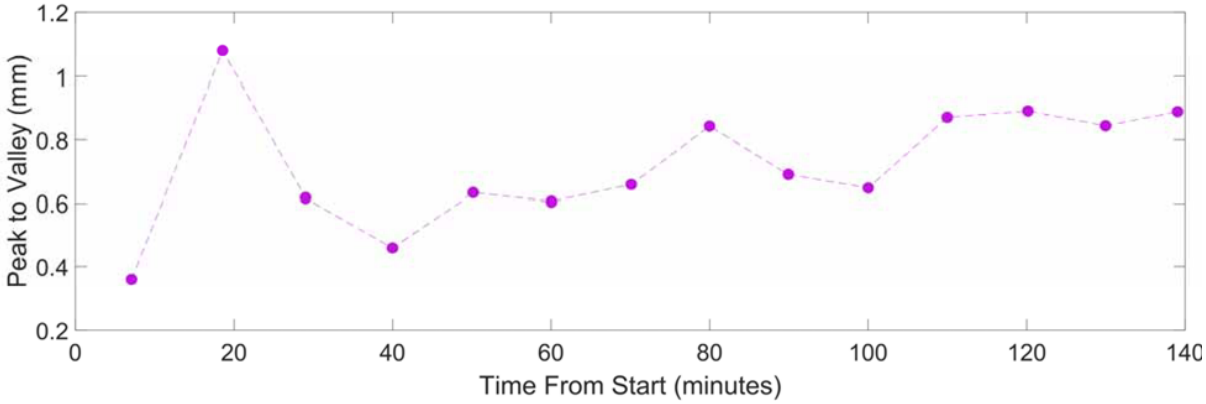

Figure 030821.12: Equivalent Roughness Evolution

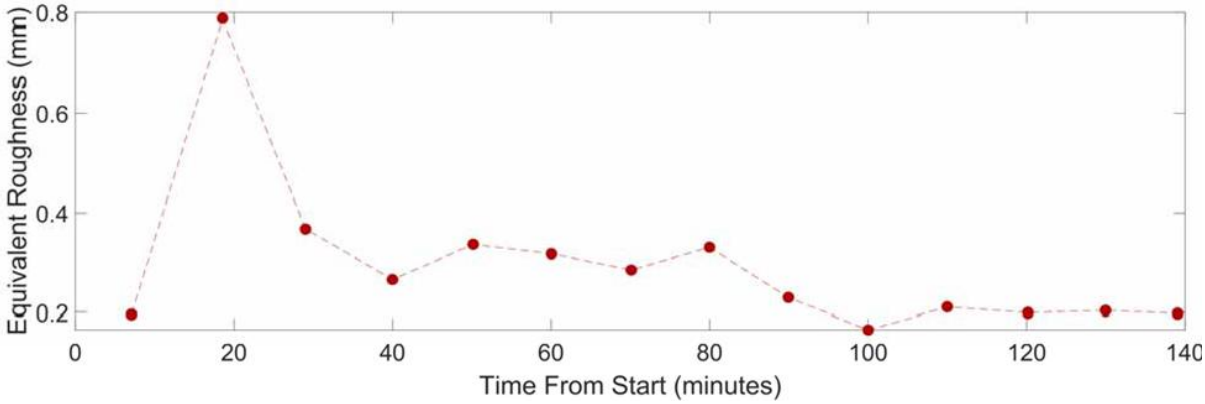

Table 030821.02: Summary of Roughness Parameters

Time (min.)	RMS (mm)	Skewness	Peak to Valley (mm)	ks,Flack-Schultz (mm)
7.0564	0.0318	0.2710	0.3583	0.1954
18.5564	0.1212	0.3231	1.0820	0.7881
29.0230	0.0649	0.1963	0.6165	0.3673
39.9897	0.0558	0.0538	0.4580	0.2655
50.1564	0.0811	-0.0475	0.6321	0.3363
60.0397	0.0815	-0.0897	0.6047	0.3174
70.1064	0.0941	-0.2429	0.6579	0.2846
79.9897	0.1283	-0.3268	0.8438	0.3304
89.9397	0.1048	-0.4029	0.6897	0.2290
100.0064	0.0986	-0.5087	0.6465	0.1650
109.9897	0.1320	-0.5266	0.8717	0.2099
120.1730	0.1381	-0.5600	0.8922	0.1986
129.9564	0.1405	-0.5590	0.8448	0.2028
139.0397	0.1450	-0.5777	0.8901	0.1972

Figure 030821.13: Frost Topography at 00:06:56

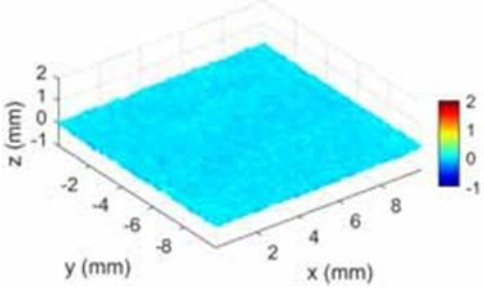

Figure 030821.14: Frost Topography at 00:18:26

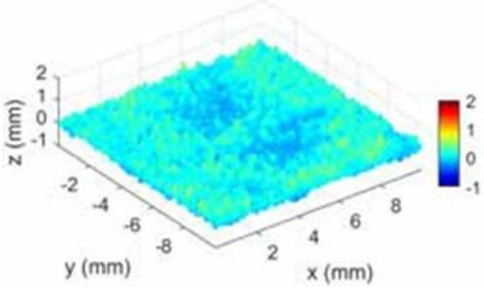

Figure 030821.15: Frost Topography at 00:28:54

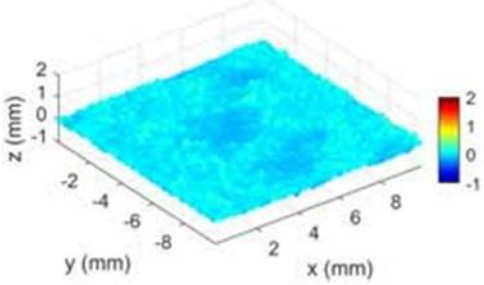

Figure 030821.16: Frost Topography at 00:39:52

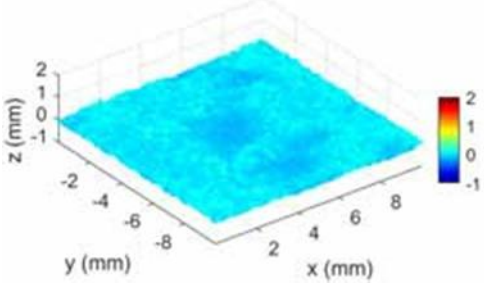

Figure 030821.17: Frost Topography at 00:50:02

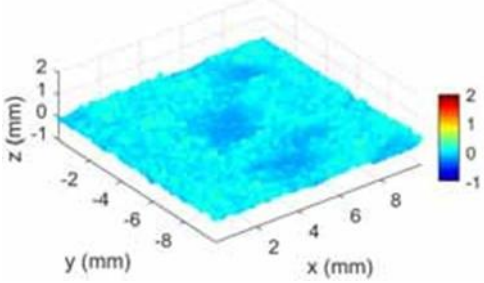

Figure 030821.18: Frost Topography at 00:59:55

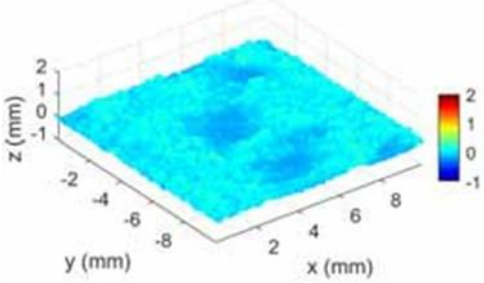

Figure 030821.19: Frost Topography at 01:09:59

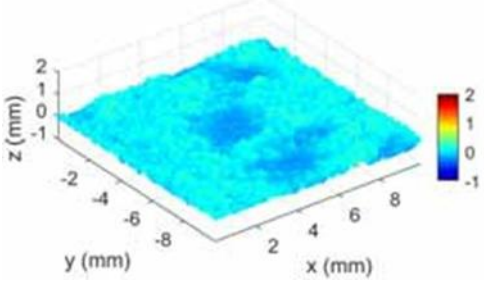

Figure 030821.20: Frost Topography at 01:19:52

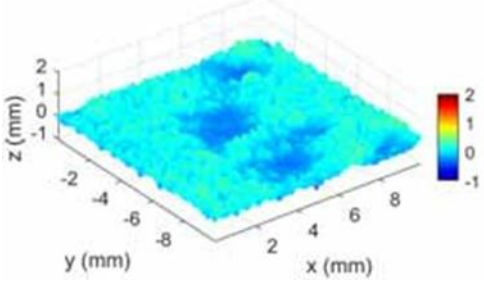

Figure 030821.21: Frost Topography at 01:29:49

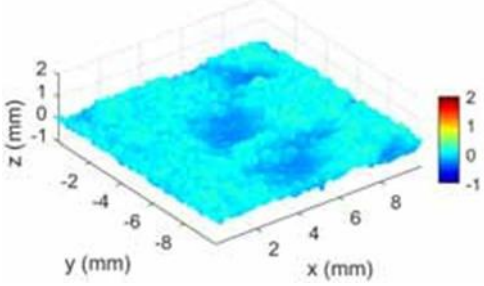

Figure 030821.22: Frost Topography at 01:39:53

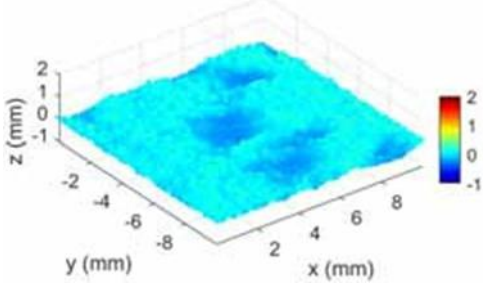

Figure 030821.23: Frost Topography at 01:49:52

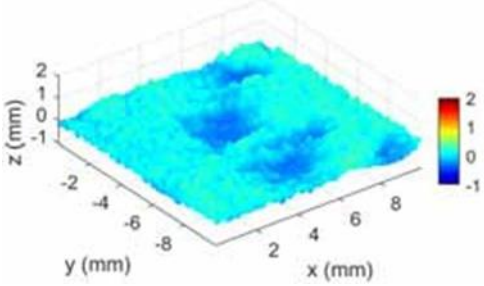

Figure 030821.24: Frost Topography at 02:00:03

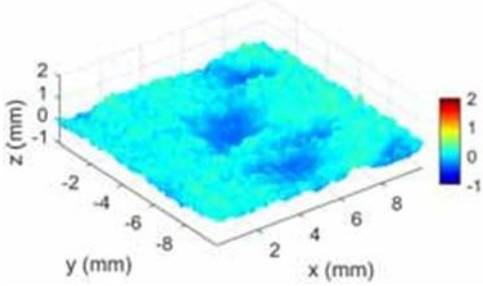

Figure 030821.25: Frost Topography at 02:09:50

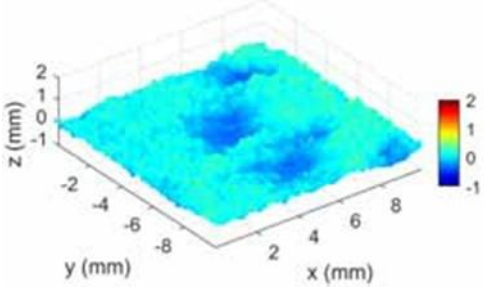

Figure 030821.26: Frost Topography at 02:18:55

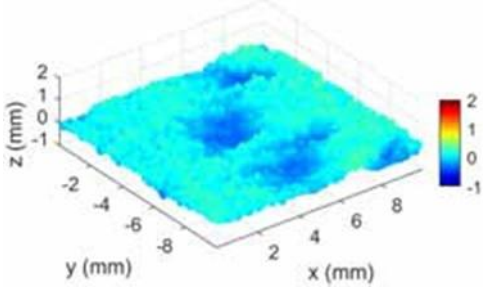

CAFF Conditions Report – Case Date: 031021

Table 031021.01: Summary of Measured Test Variables

Variable	Mean	St. Dev.	Rand. Unc.
T_air (C)	4.2597	0.2866	0.0096
Rh (%)	80.0892	4.9000	0.1644
Omega (kg_v/kg_da)	0.00416099	0.00031938	0.00001072
V_air (m/s)	1.3938	0.1512	0.0051
T_skin (C)	-8.6820	0.9807	0.0329
T_floor (C)	-20.4515	0.0340	0.0011

Figure 031021.01: Temperature and Voltage Control Time History

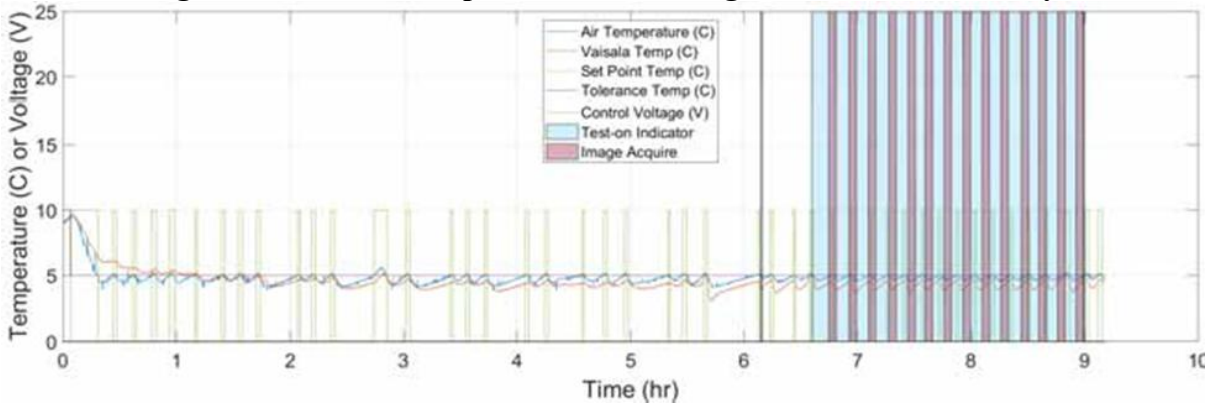

Figure 031021.02: Relative Humidity Time History

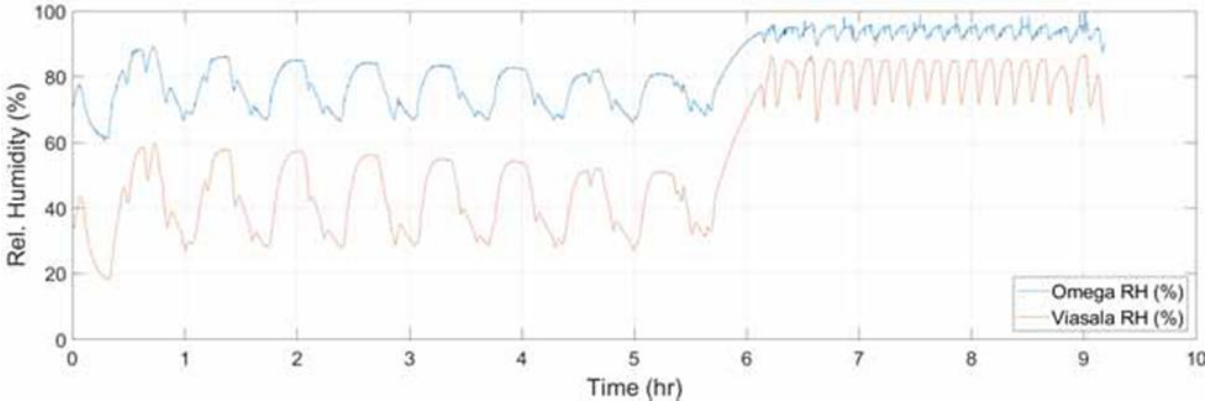

Figure 031021.03: Velocity Time History

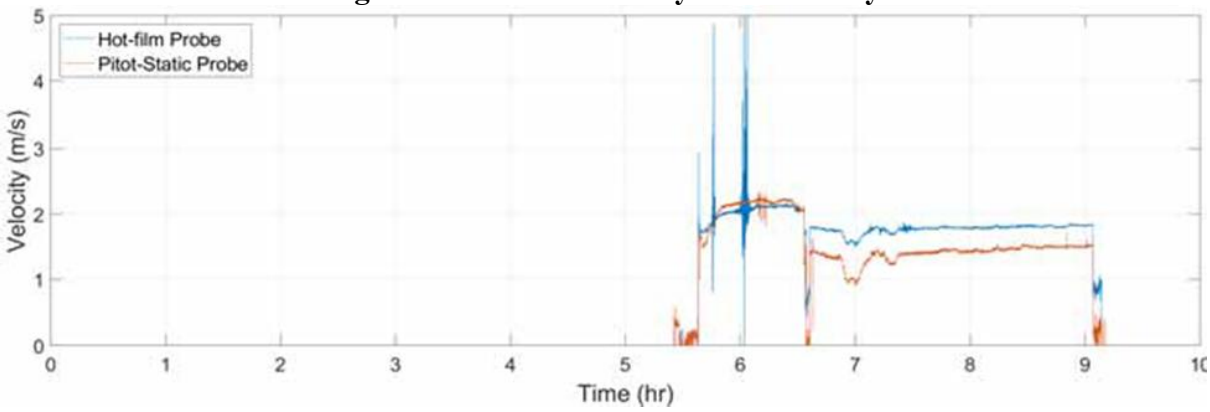

Figure 031021.04: Coolant Return Temperature Time History

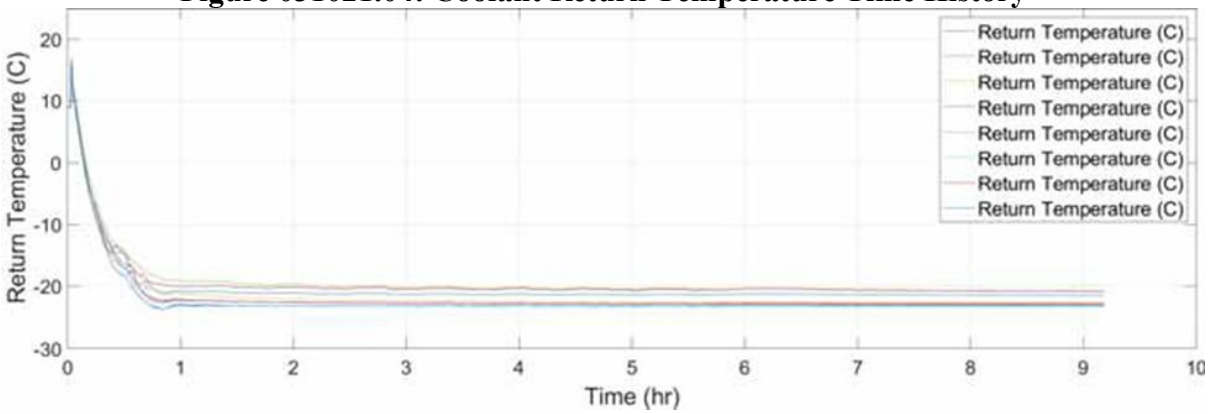

Figure 031021.05: Coolant Supply Temperature Time History

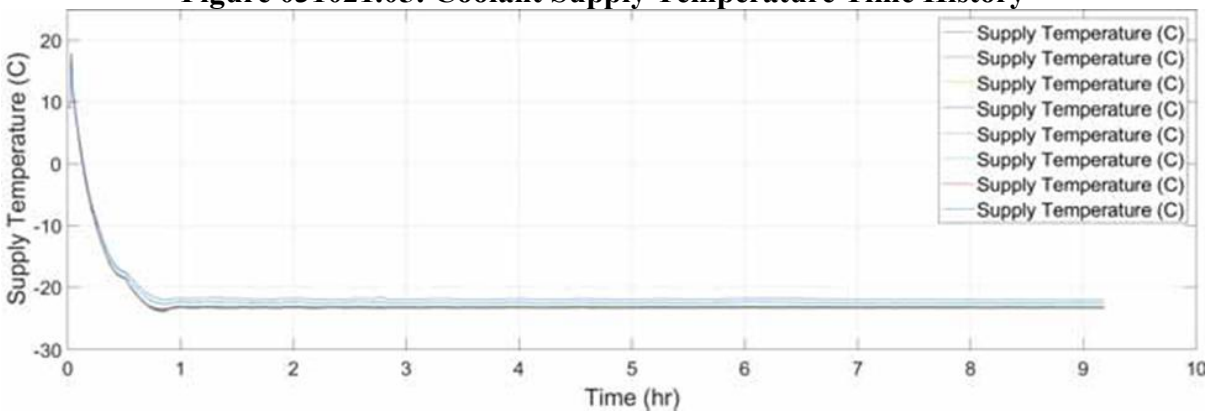

Figure 031021.06: Skin Temperature Time History

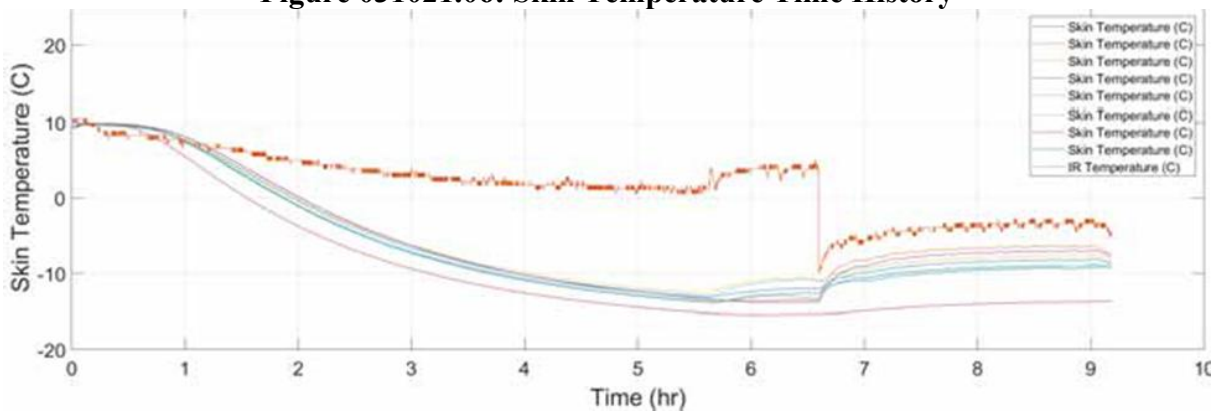

Figure 031021.07: Floor Temperature Time History

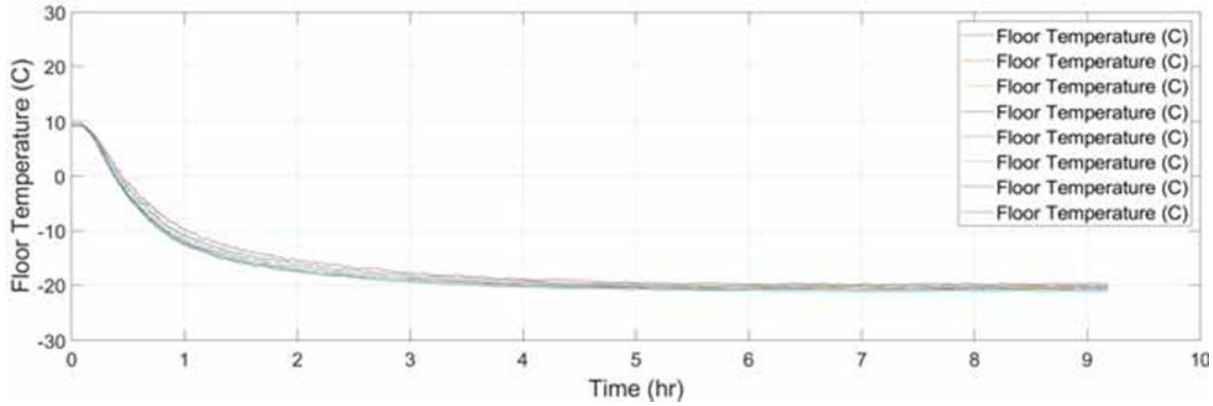

Figure 031021.08: Skin Temperature Slope Time History

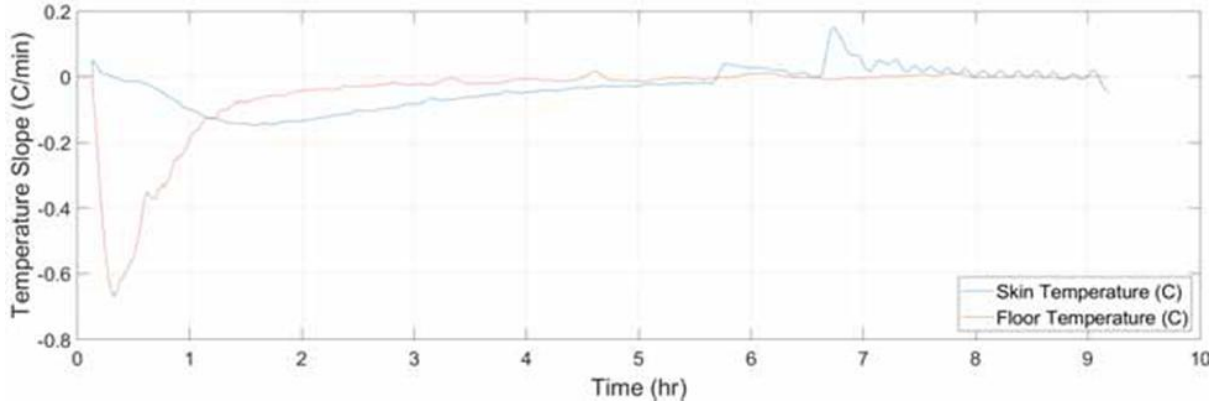

Figure 031021.09: RMS Height Evolution

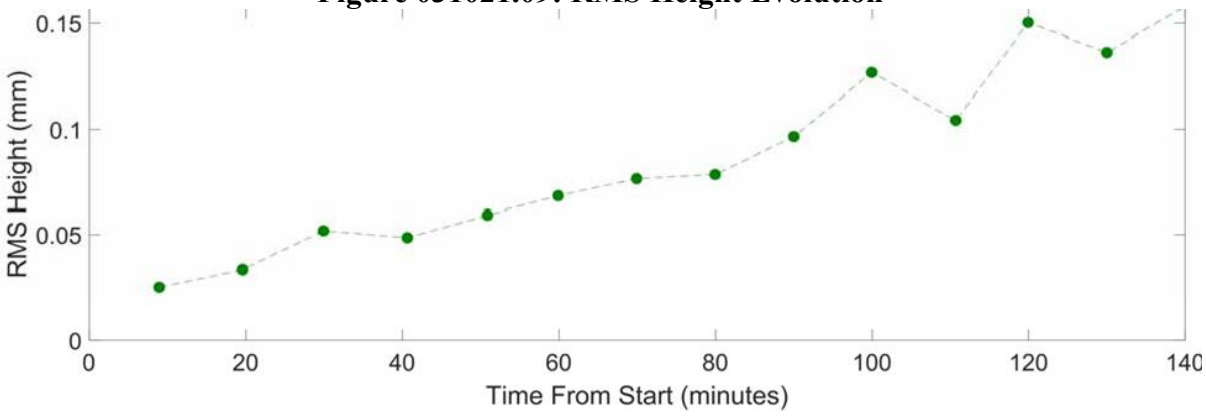

Figure 031021.10: Skewness Evolution

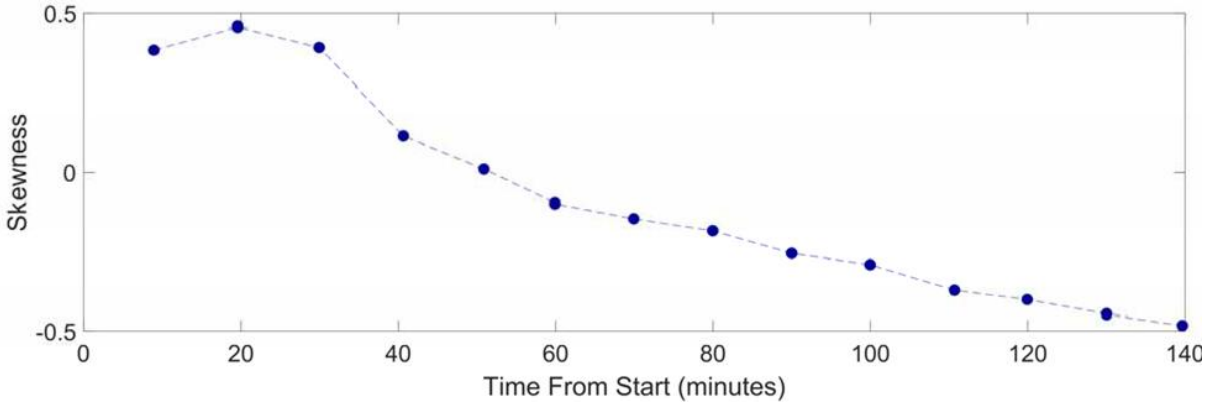

Figure 031021.11: Peak to Valley Evolution

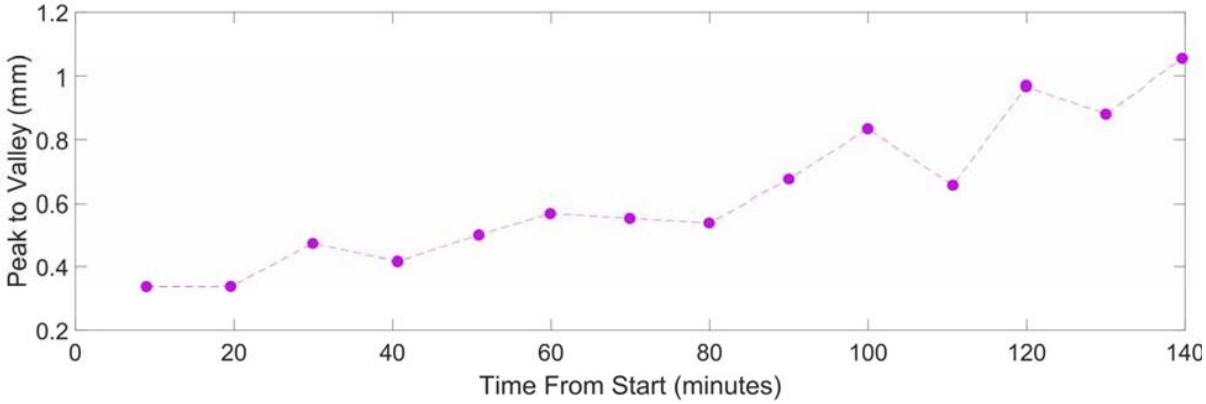

Figure 031021.12: Equivalent Roughness Evolution

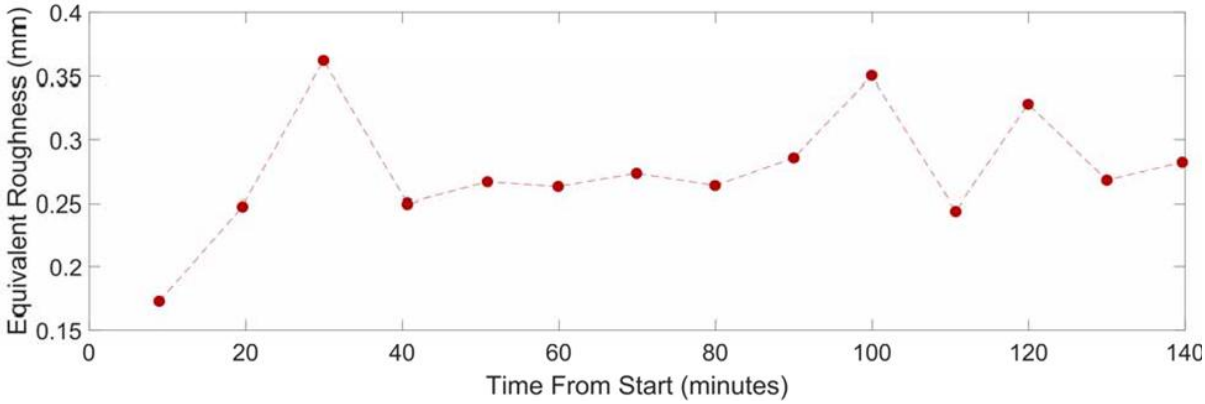

Table 031021.02: Summary of Roughness Parameters

Time (min.)	RMS (mm)	Skewness	Peak to Valley (mm)	ks,Flack-Schultz (mm)
8.9375	0.0248	0.3865	0.3354	0.1720
19.5875	0.0333	0.4594	0.3358	0.2476
29.9375	0.0519	0.3950	0.4726	0.3625
40.6375	0.0485	0.1155	0.4154	0.2496
50.8708	0.0593	0.0104	0.5001	0.2665
59.9041	0.0683	-0.0975	0.5689	0.2627
69.9208	0.0765	-0.1450	0.5537	0.2734
79.9541	0.0785	-0.1832	0.5385	0.2635
90.0041	0.0966	-0.2552	0.6749	0.2857
99.9541	0.1269	-0.2918	0.8353	0.3505
110.6875	0.1044	-0.3732	0.6548	0.2438
119.9375	0.1503	-0.4027	0.9703	0.3286
130.0041	0.1365	-0.4480	0.8826	0.2679
139.6375	0.1572	-0.4828	1.0568	0.2823

Figure 031021.13: Frost Topography at 00:35:36

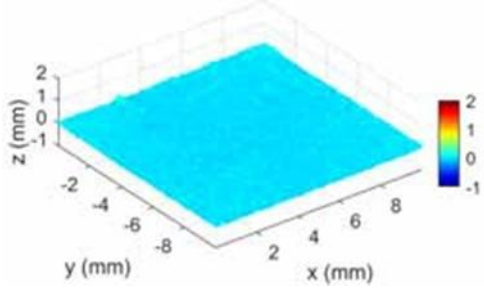

Figure 031021.14: Frost Topography at 00:46:15

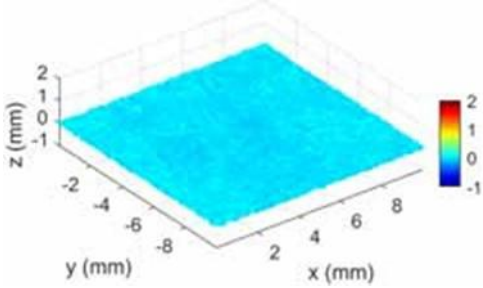

Figure 031021.15: Frost Topography at 00:56:36

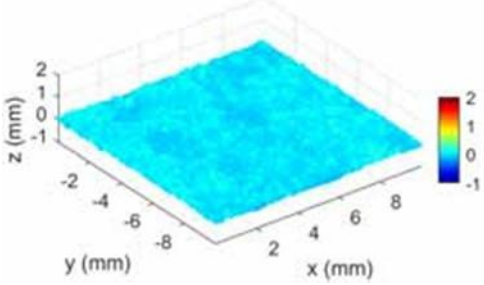

Figure 031021.16: Frost Topography at 01:07:18

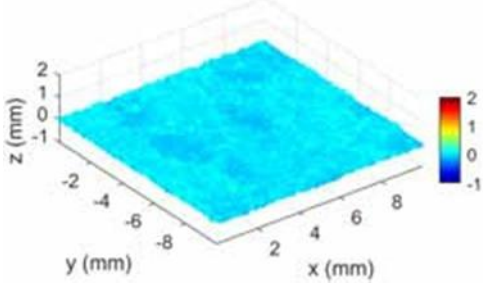

Figure 031021.17: Frost Topography at 01:17:32

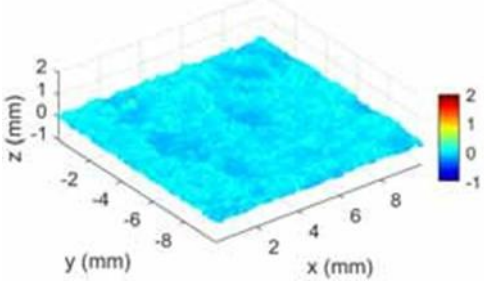

Figure 031021.18: Frost Topography at 01:26:34

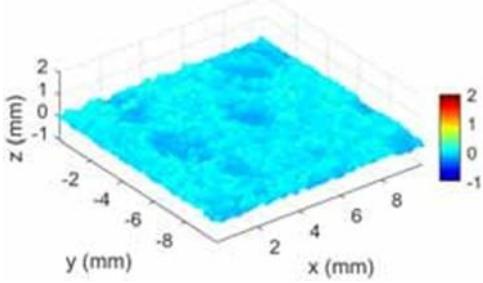

Figure 031021.19: Frost Topography at 01:36:35

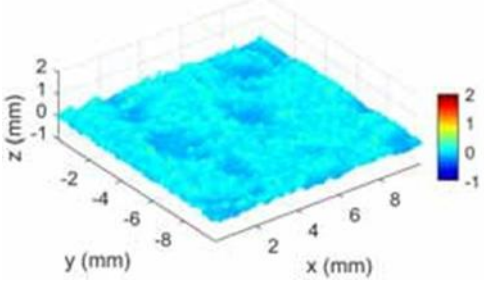

Figure 031021.20: Frost Topography at 01:46:37

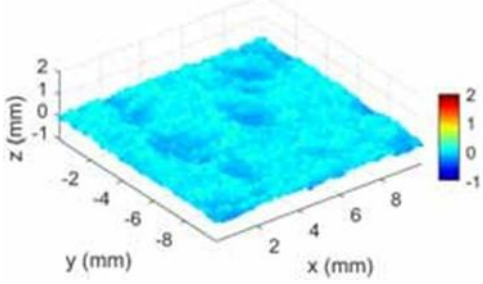

Figure 031021.21: Frost Topography at 01:56:40

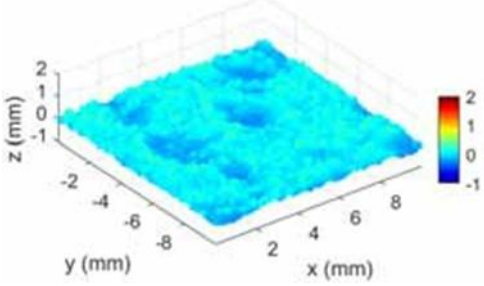

Figure 031021.22: Frost Topography at 02:06:37

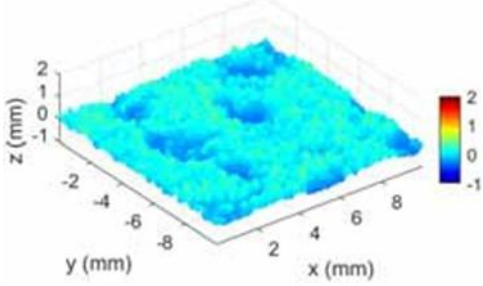

Figure 031021.23: Frost Topography at 02:17:21

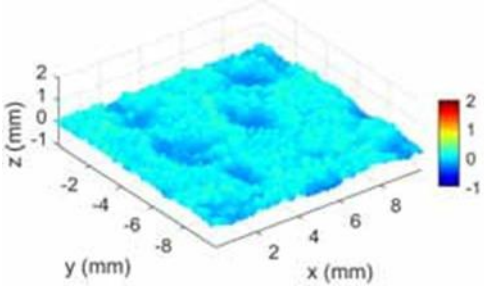

Figure 031021.24: Frost Topography at 02:26:36

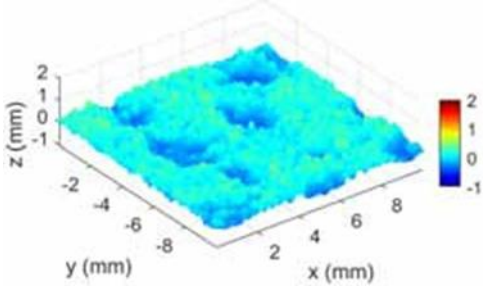

Figure 031021.25: Frost Topography at 02:36:40

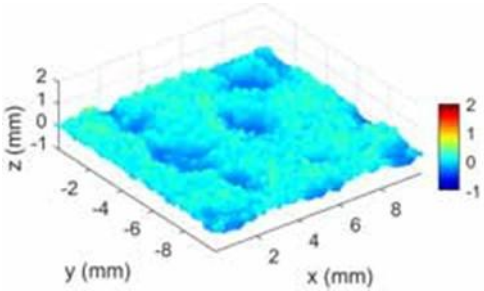

Figure 031021.26: Frost Topography at 02:46:18

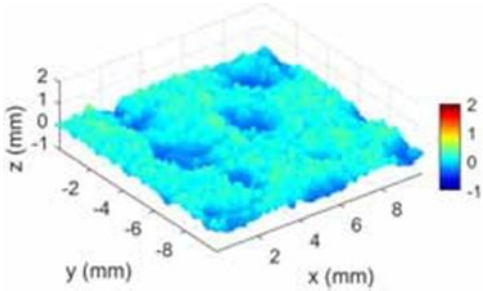

Table 032421.01: Summary of Measured Test Variables

Variable	Mean	St. Dev.	Rand. Unc.
T_air (C)	4.3028	0.1791	0.0060
Rh (%)	79.9919	5.5093	0.1848
Omega (kg_v/kg_da)	0.00420701	0.00032889	0.00001103
V_air (m/s)	0.2455	0.1209	0.0041
T_skin (C)	-10.8736	0.7019	0.0235
T_floor (C)	-20.6363	0.0525	0.0018

Figure 032421.01: Temperature and Voltage Control Time History

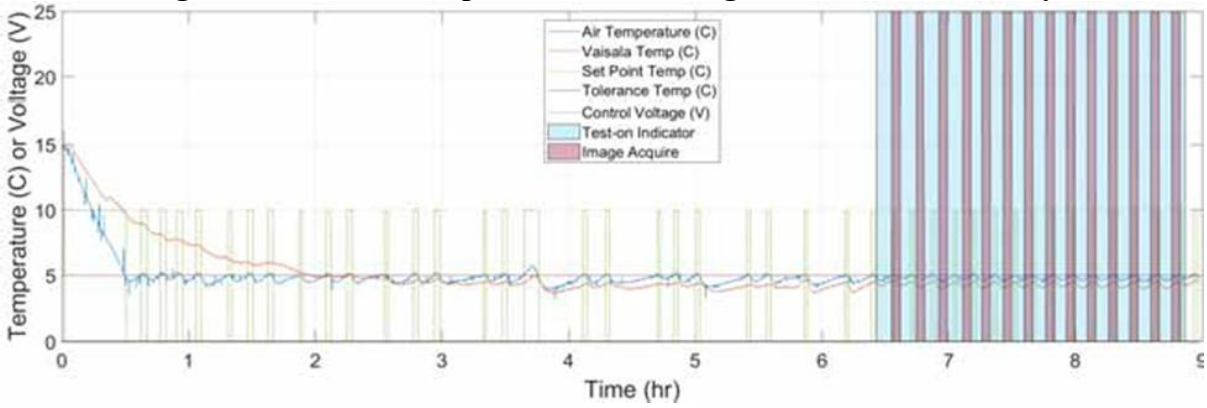

Figure 032421.02: Relative Humidity Time History

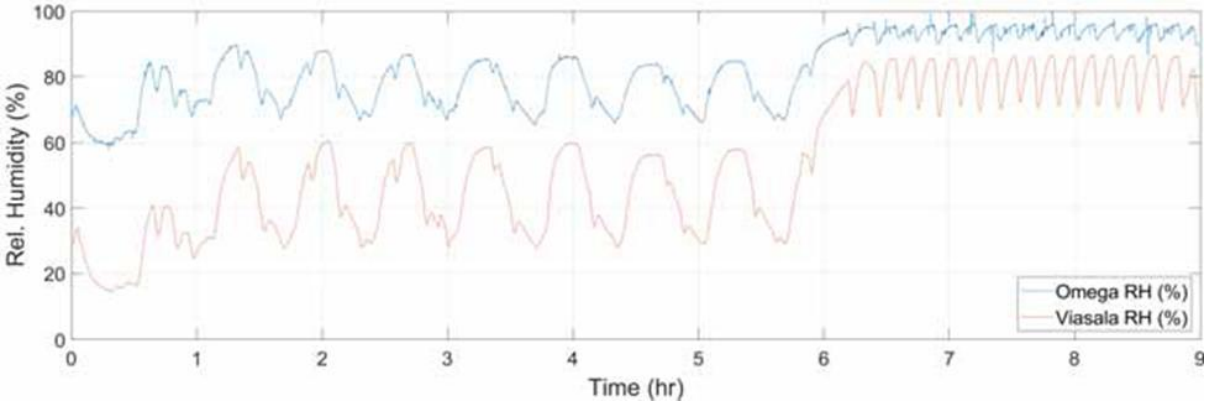

Figure 032421.03: Velocity Time History

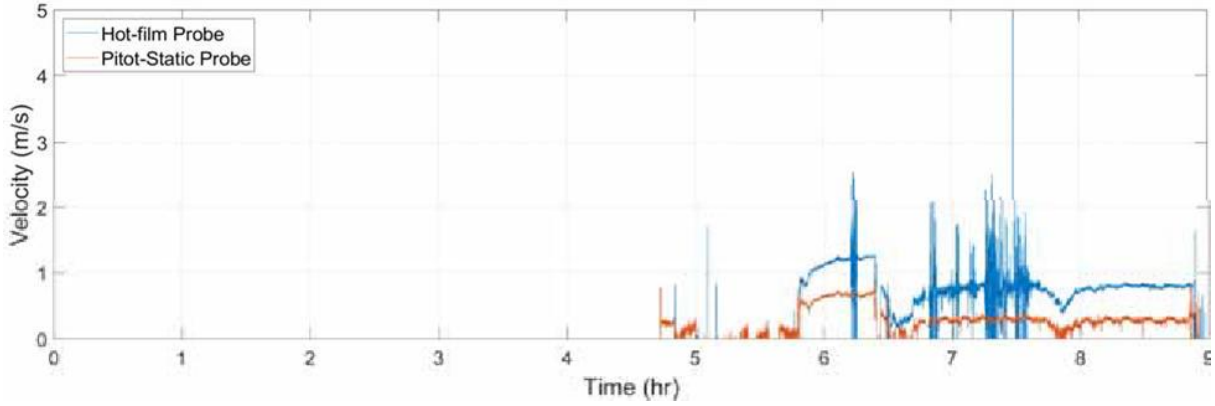

Figure 032421.04: Coolant Return Temperature Time History

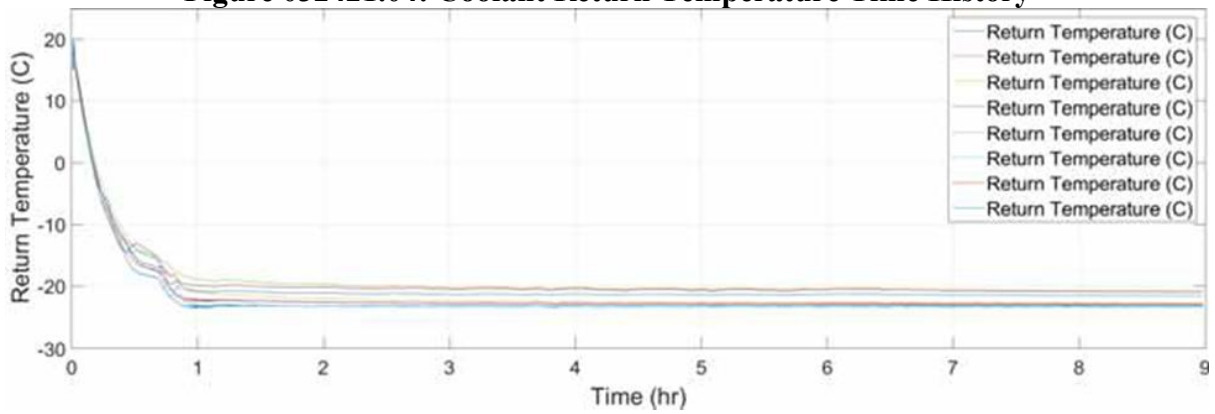

Figure 032421.05: Coolant Supply Temperature Time History

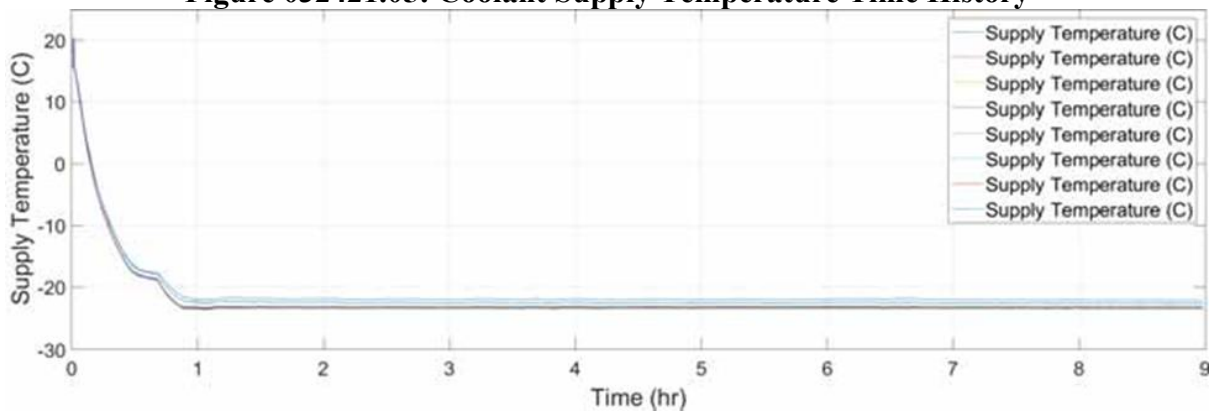

Figure 032421.06: Skin Temperature Time History

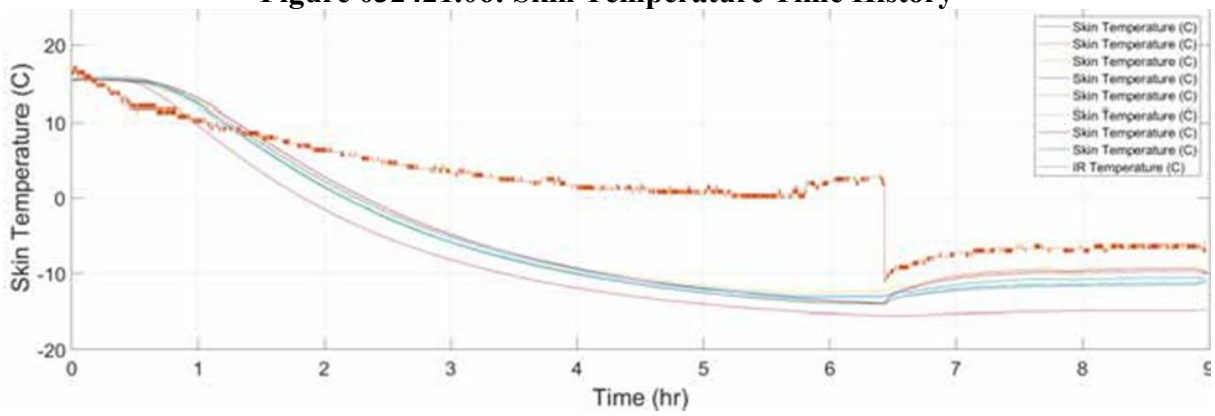

Figure 032421.07: Floor Temperature Time History

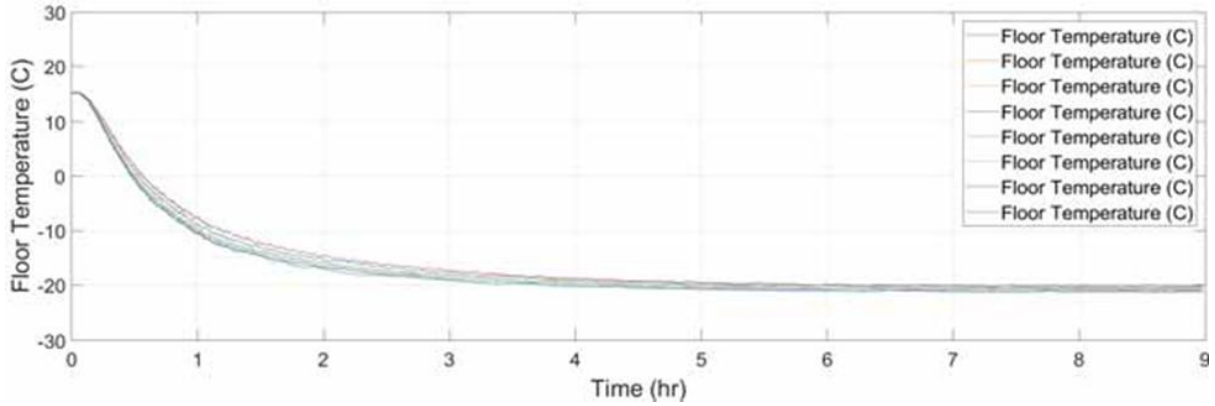

Figure 032421.08: Skin Temperature Slope Time History

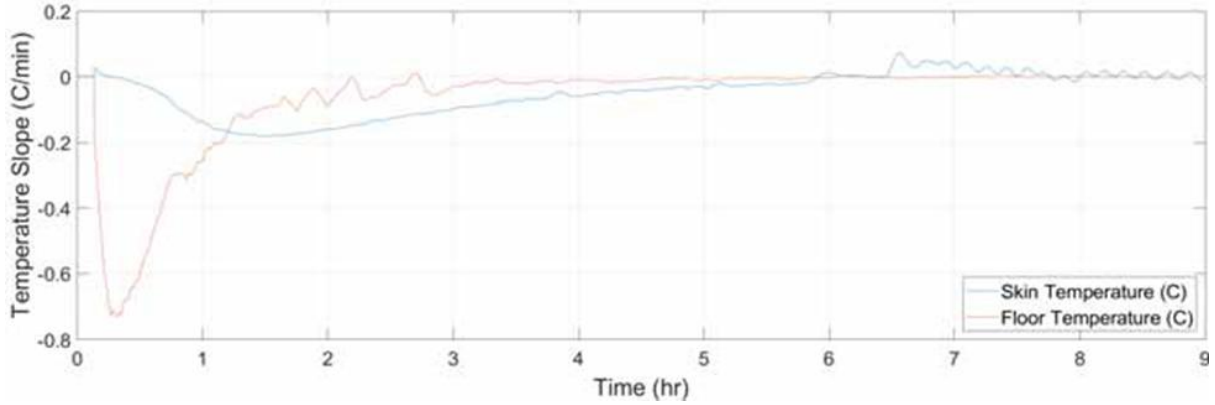

Figure 032421.09: RMS Height Evolution

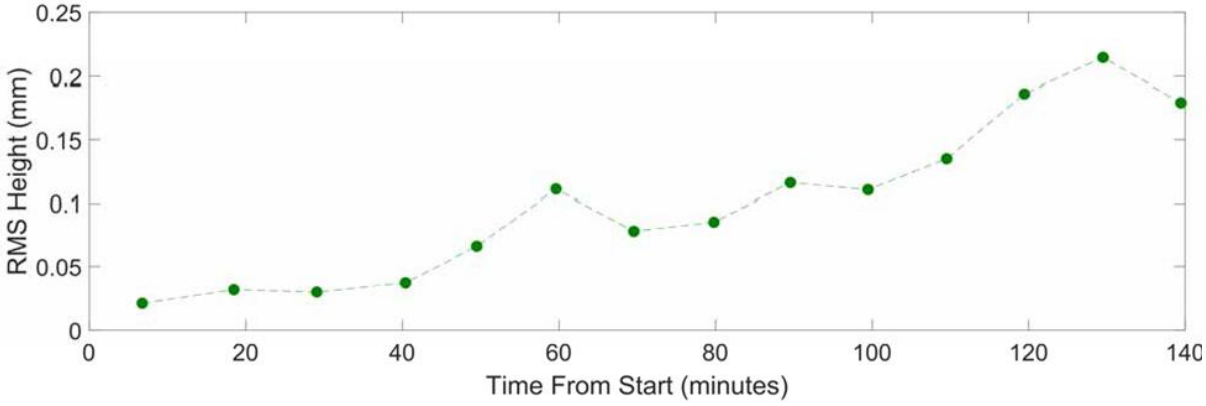

Figure 032421.10: Skewness Evolution

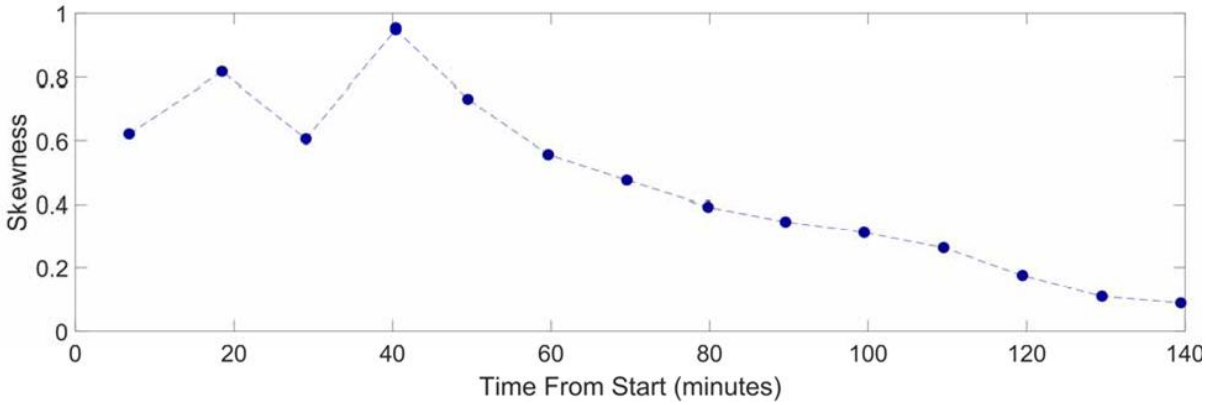

Figure 032421.11: Peak to Valley Evolution

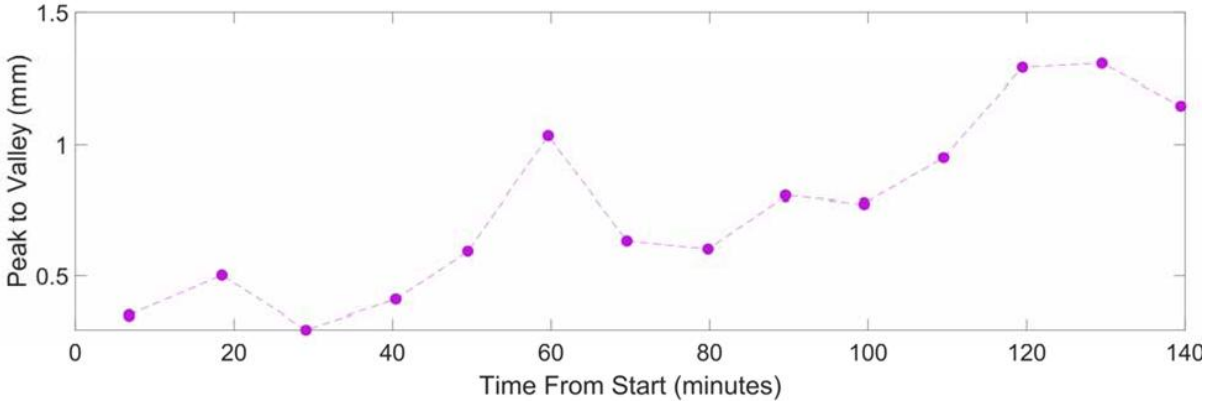

Figure 032421.12: Equivalent Roughness Evolution

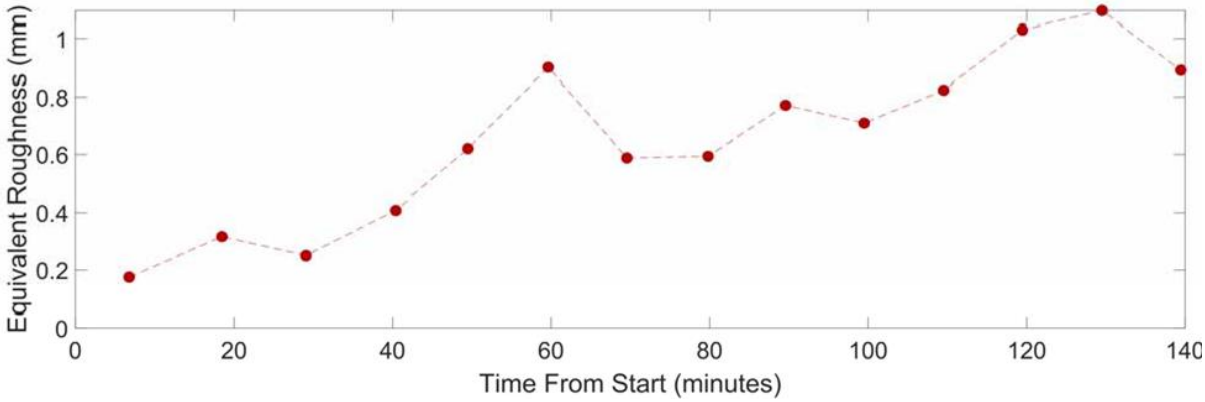

Table 032421.02: Summary of Roughness Parameters

Time (min.)	RMS (mm)	Skewness	Peak to Valley (mm)	ks,Flack-Schultz (mm)
6.7678	0.0203	0.6220	0.3476	0.1748
18.4845	0.0314	0.8184	0.5015	0.3156
29.0678	0.0294	0.6064	0.2936	0.2495
40.4011	0.0368	0.9525	0.4084	0.4081
49.5011	0.0659	0.7332	0.5924	0.6203
59.6345	0.1109	0.5566	1.0335	0.9010
69.5678	0.0779	0.4749	0.6318	0.5875
79.8011	0.0851	0.3921	0.6005	0.5933
89.5678	0.1160	0.3447	0.8046	0.7712
99.5011	0.1103	0.3120	0.7740	0.7088
109.5345	0.1351	0.2626	0.9499	0.8238
119.4678	0.1867	0.1739	1.2932	1.0303
129.5011	0.2150	0.1076	1.3090	1.0956
139.4511	0.1795	0.0861	1.1475	0.8905

Figure 032421.13: Frost Topography at 00:07:05

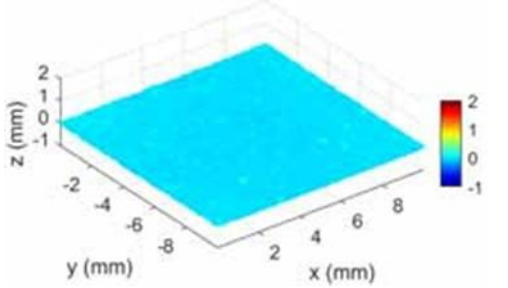

Figure 032421.14: Frost Topography at 00:18:48

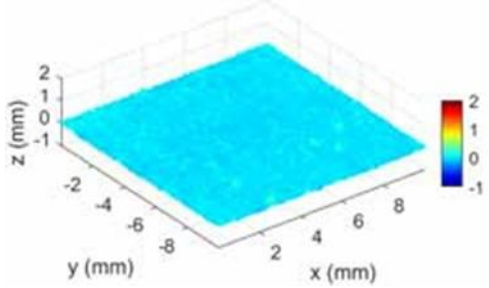

Figure 032421.15: Frost Topography at 00:29:23

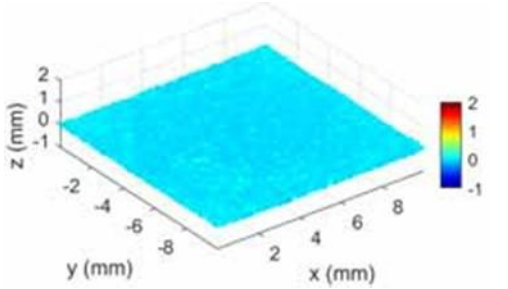

Figure 032421.16: Frost Topography at 00:40:43

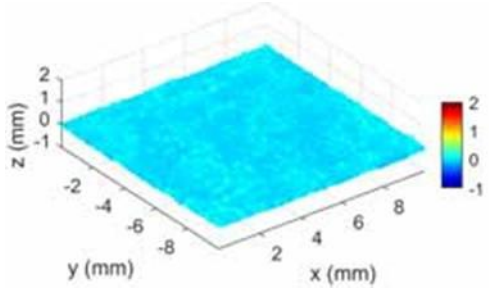

Figure 032421.17: Frost Topography at 00:49:49

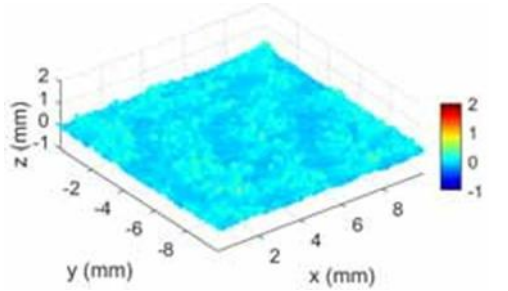

Figure 032421.18: Frost Topography at 00:59:57

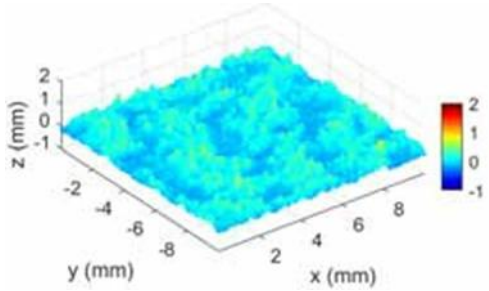

Figure 032421.19: Frost Topography at 01:09:53

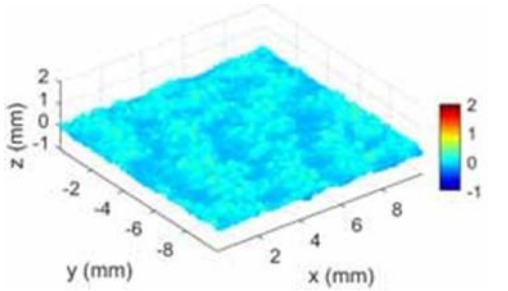

Figure 032421.20: Frost Topography at 01:20:07

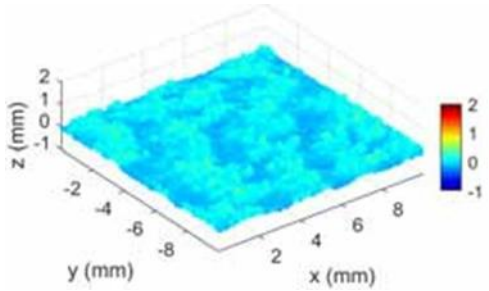

Figure 032421.21: Frost Topography at 01:29:53

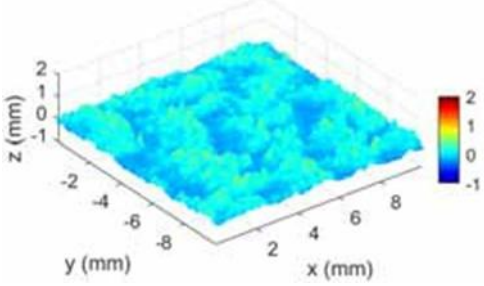

Figure 032421.22: Frost Topography at 01:39:49

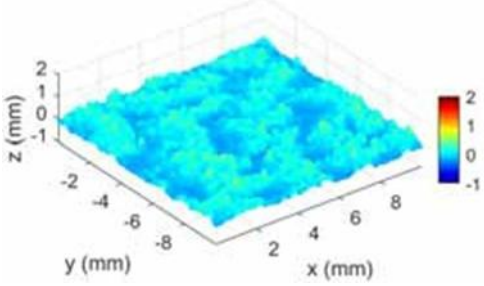

Figure 032421.23: Frost Topography at 01:49:51

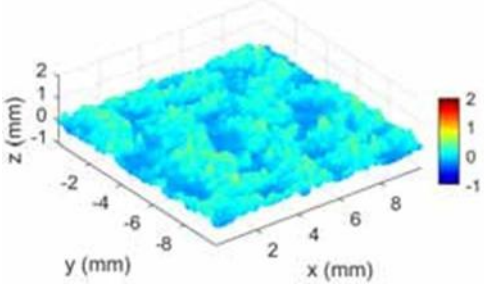

Figure 032421.24: Frost Topography at 01:59:47

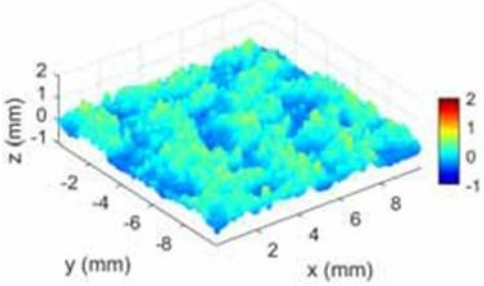

Figure 032421.25: Frost Topography at 02:09:49

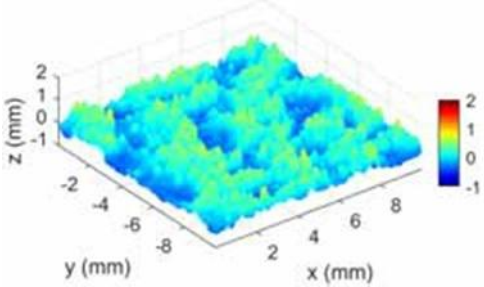

Figure 032421.26: Frost Topography at 02:19:46

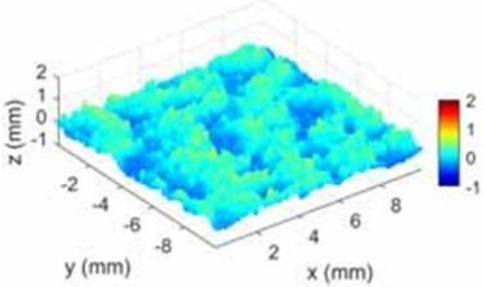

CAFF Conditions Report – Case Date: 032621

Table 032621.01: Summary of Measured Test Variables

Variable	Mean	St. Dev.	Rand. Unc.
T_air (C)	9.2514	0.2882	0.0097
Rh (%)	79.7118	5.7185	0.1923
Omega (kg_v/kg_da)	0.00587047	0.00044406	0.00001493
V_air (m/s)	0.2891	0.1110	0.0037
T_skin (C)	-8.6057	0.9770	0.0328
T_floor (C)	-20.1799	0.0311	0.0010

Figure 032621.01: Temperature and Voltage Control Time History

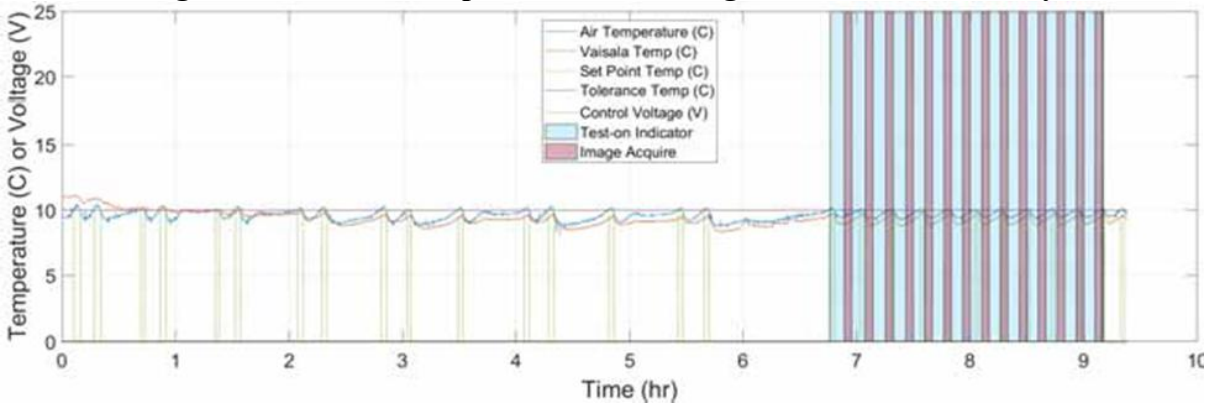

Figure 032621.02: Relative Humidity Time History

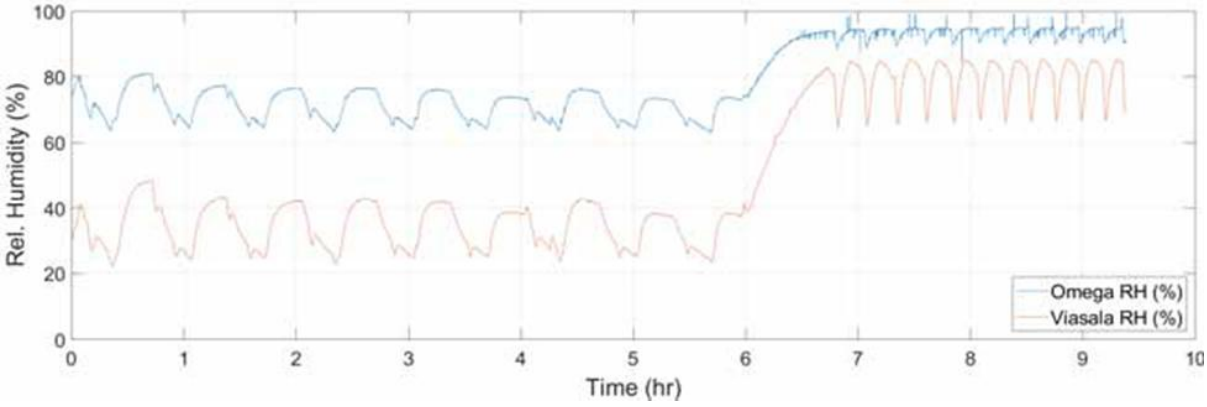

Figure 032621.03: Velocity Time History

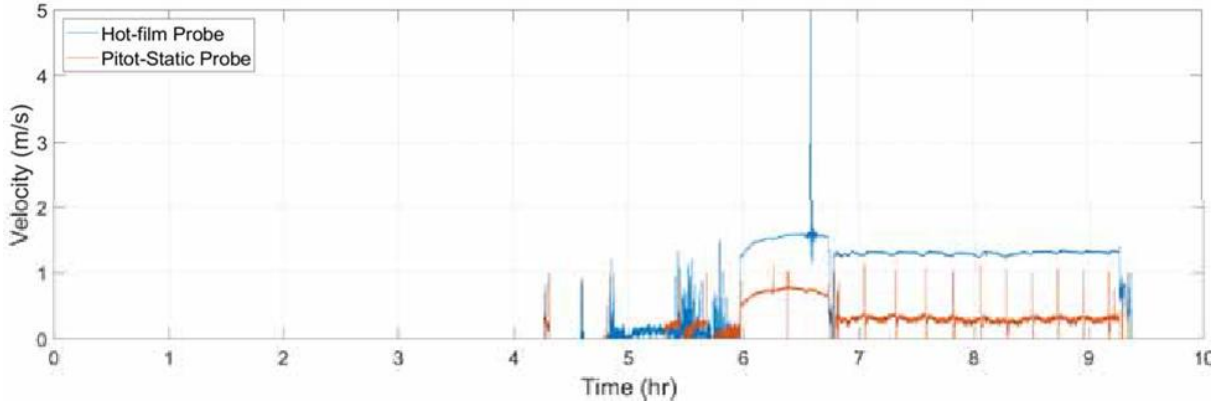

Figure 032621.04: Coolant Return Temperature Time History

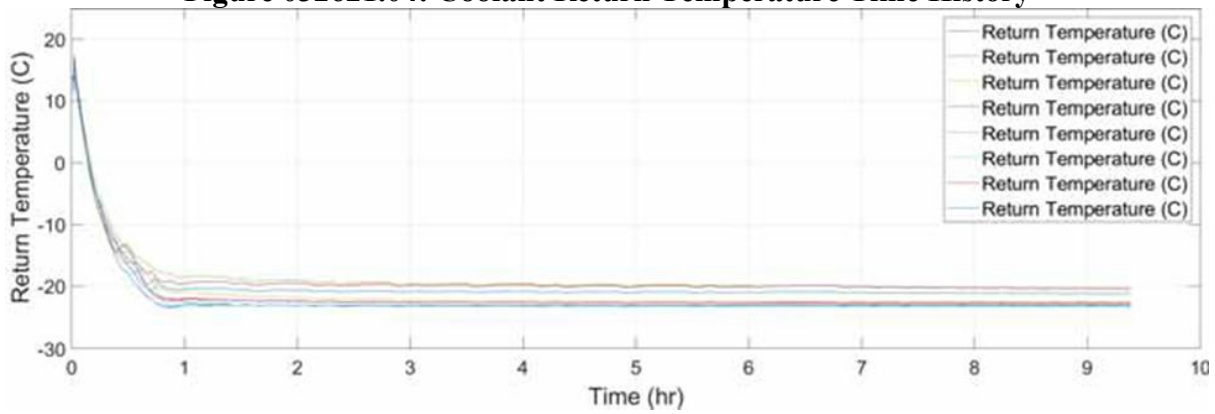

Figure 032621.05: Coolant Supply Temperature Time History

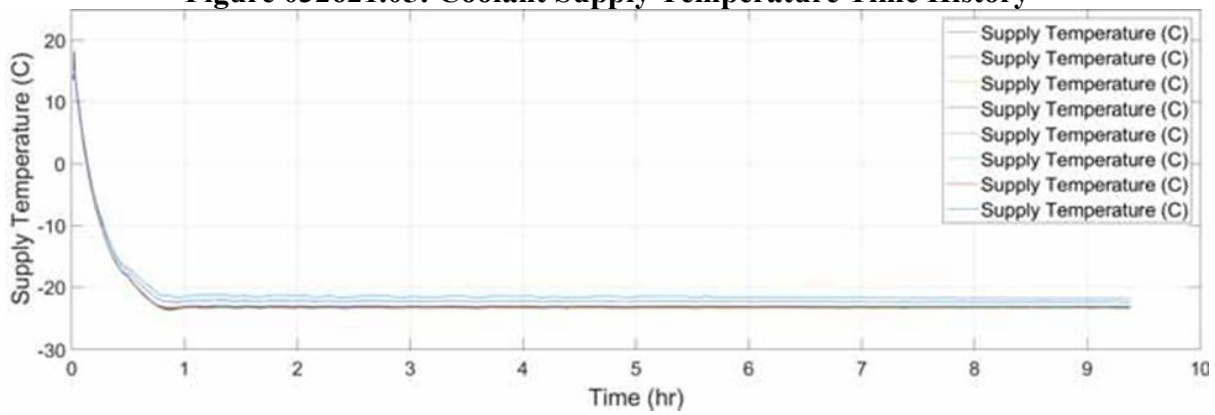

Figure 032621.06: Skin Temperature Time History

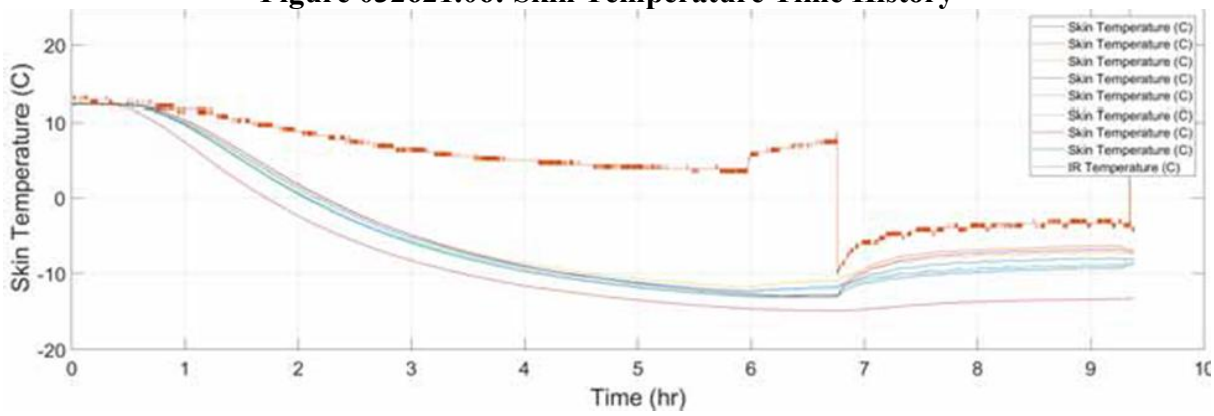

Figure 032621.07: Floor Temperature Time History

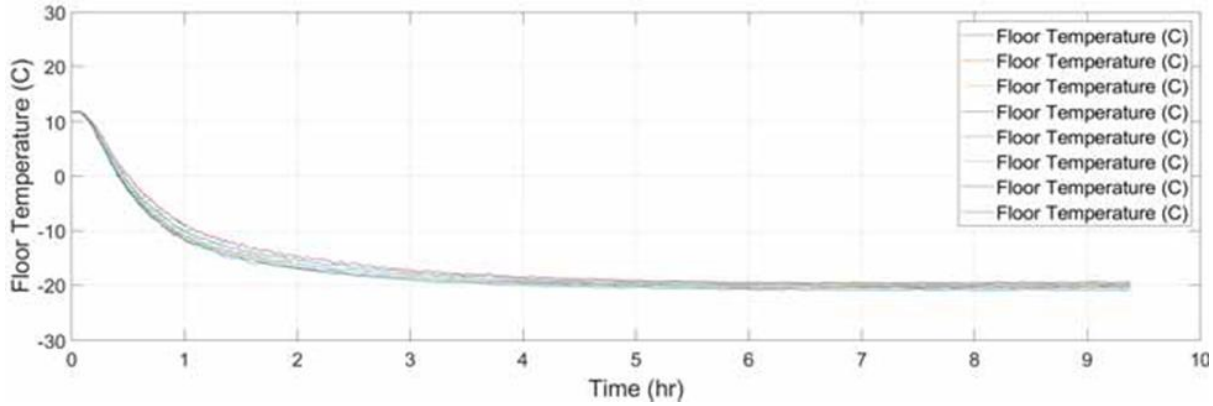

Figure 032621.08: Skin Temperature Slope Time History

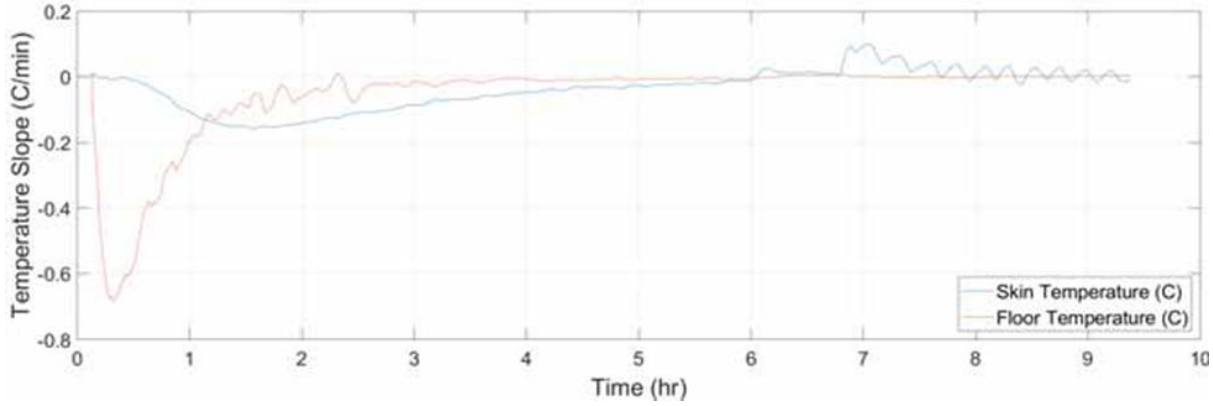

Figure 032621.09: RMS Height Evolution

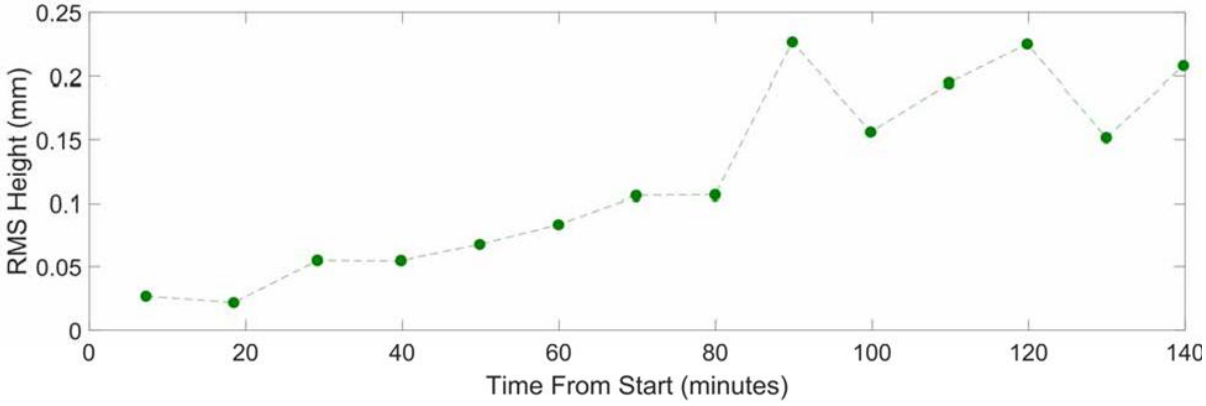

Figure 032621.10: Skewness Evolution

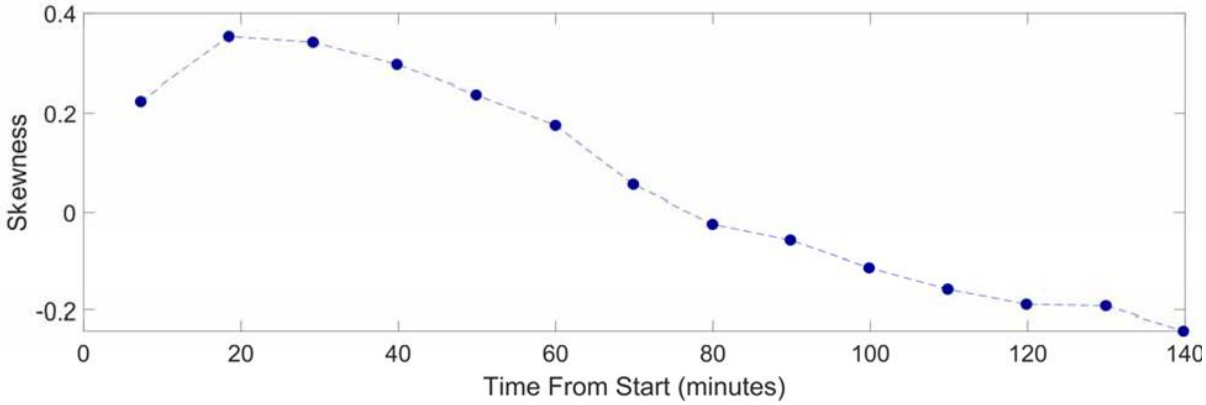

Figure 032621.11: Peak to Valley Evolution

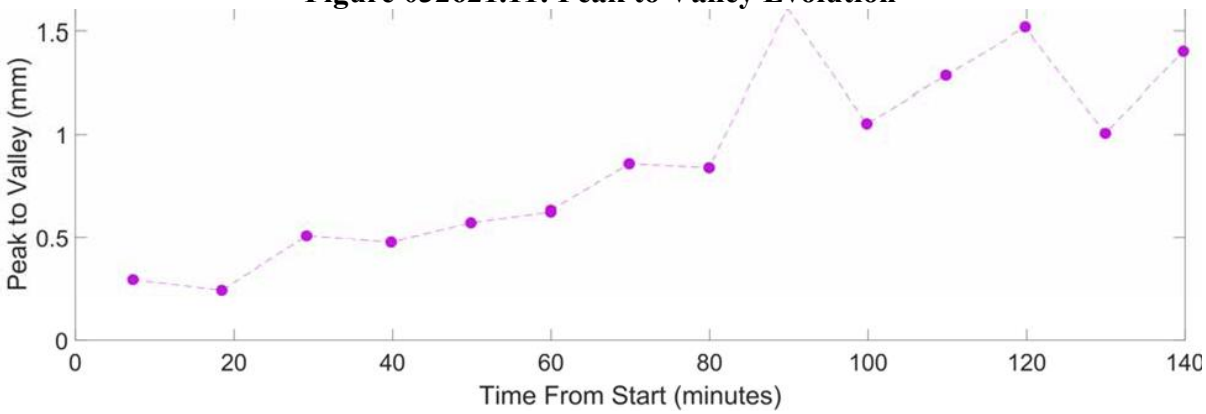

Figure 032621.12: Equivalent Roughness Evolution

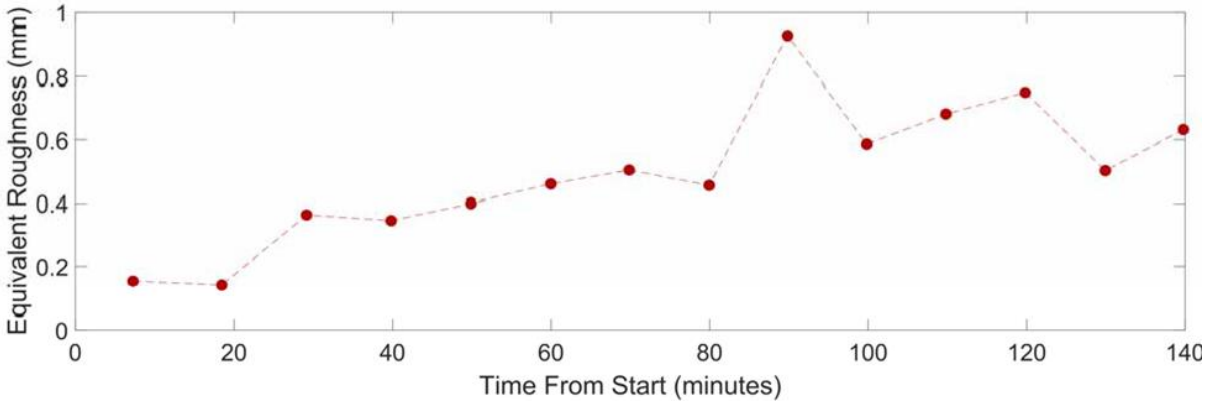

Table 032621.02: Summary of Roughness Parameters

Time (min.)	RMS (mm)	Skewness	Peak to Valley (mm)	ks,Flack-Schultz (mm)
7.2561	0.0261	0.2244	0.2931	0.1525
18.4561	0.0209	0.3555	0.2397	0.1403
29.1561	0.0548	0.3437	0.5082	0.3637
39.8228	0.0546	0.2980	0.4775	0.3455
49.8894	0.0674	0.2382	0.5729	0.4000
59.9561	0.0832	0.1753	0.6267	0.4599
69.8561	0.1058	0.0549	0.8584	0.5041
79.9394	0.1063	-0.0249	0.8388	0.4549
89.8228	0.2275	-0.0573	1.6132	0.9294
99.8228	0.1562	-0.1137	1.0536	0.5865
109.8228	0.1949	-0.1578	1.2879	0.6823
119.8228	0.2258	-0.1888	1.5201	0.7512
129.9228	0.1517	-0.1917	1.0069	0.5021
139.7728	0.2084	-0.2411	1.4073	0.6327

Figure 032621.13: Frost Topography at 00:07:15

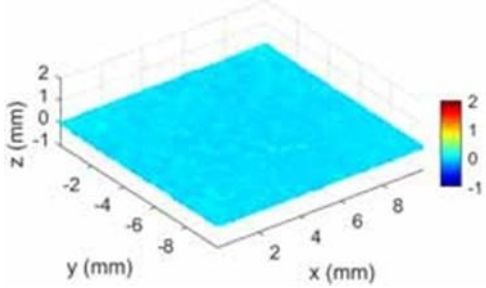

Figure 032621.14: Frost Topography at 00:18:27

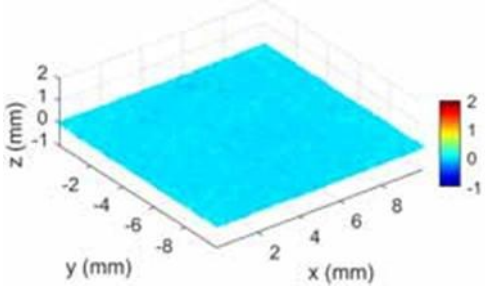

Figure 032621.15: Frost Topography at 00:29:09

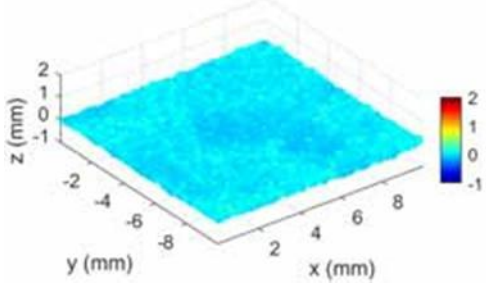

Figure 032621.16: Frost Topography at 00:39:49

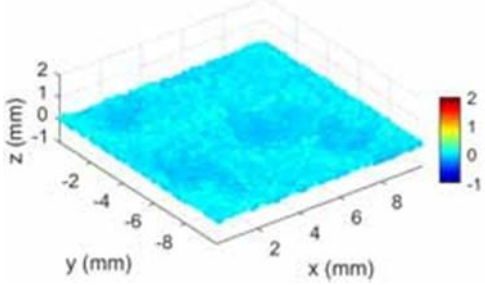

Figure 032621.17: Frost Topography at 00:49:53

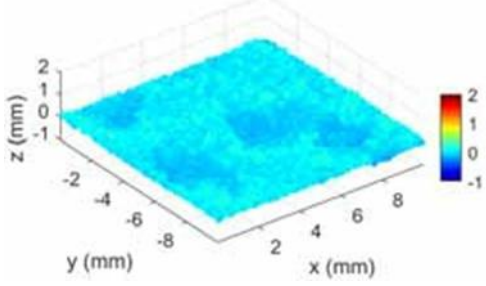

Figure 032621.18: Frost Topography at 00:59:57

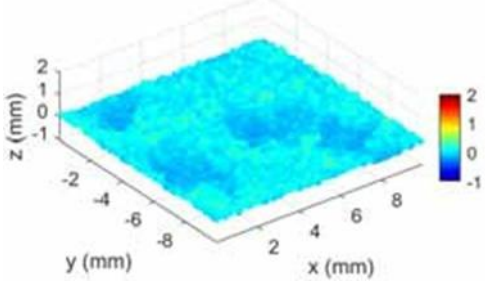

Figure 032621.19: Frost Topography at 01:09:51

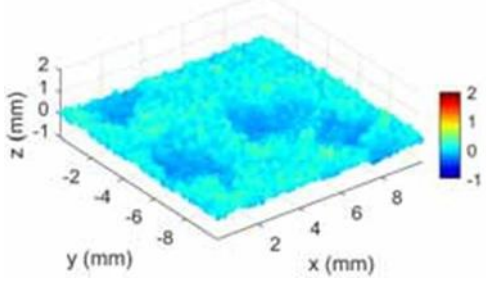

Figure 032621.20: Frost Topography at 01:19:56

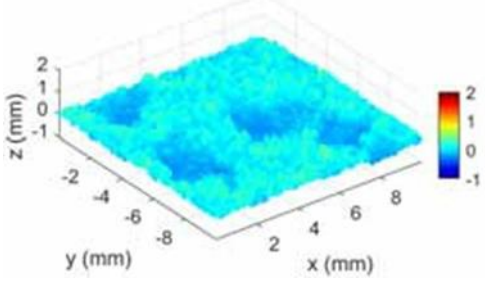

Figure 032621.21: Frost Topography at 01:29:49

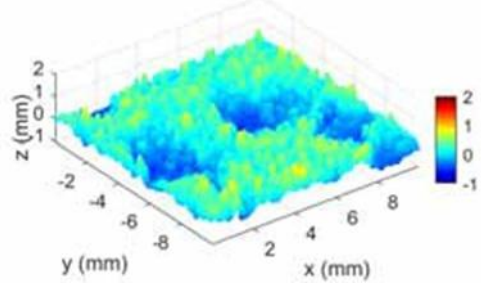

Figure 032621.22: Frost Topography at 01:39:49

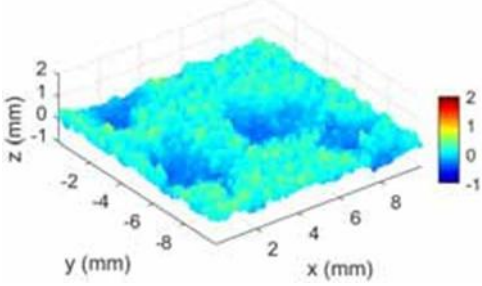

Figure 032621.23: Frost Topography at 01:49:49

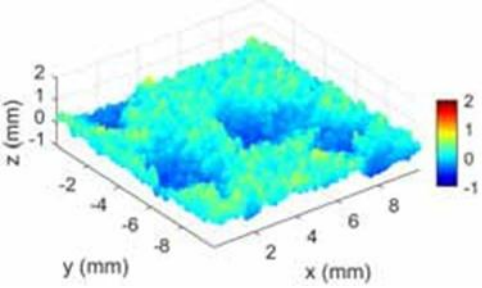

Figure 032621.24: Frost Topography at 01:59:49

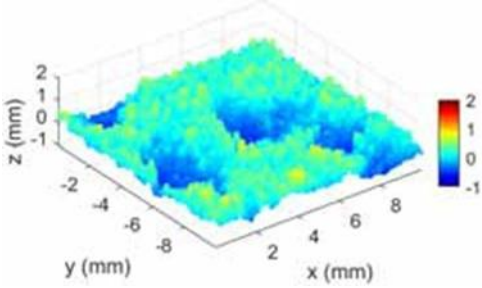

Figure 032621.25: Frost Topography at 02:09:55

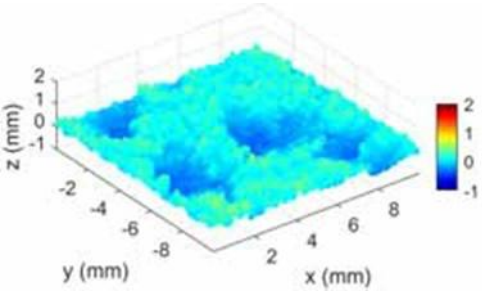

Figure 032621.26: Frost Topography at 02:19:46

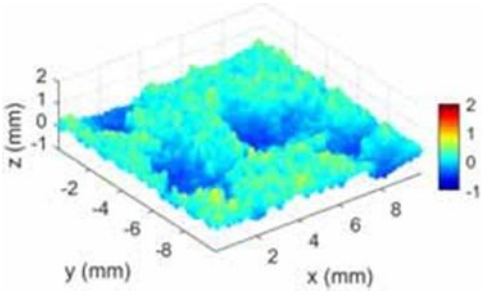

CAFF Conditions Report – Case Date: 033121

Table 033121.01: Summary of Measured Test Variables

Variable	Mean	St. Dev.	Rand. Unc.
T_air (C)	15.2774	0.2579	0.0118
Rh (%)	78.8556	3.7457	0.1709
Omega (kg_v/kg_da)	0.00854526	0.00043407	0.00001981
V_air (m/s)	0.1705	0.1570	0.0072
T_skin (C)	-6.4236	1.2895	0.0588
T_floor (C)	-19.6265	0.0406	0.0019

Figure 033121.01: Temperature and Voltage Control Time History

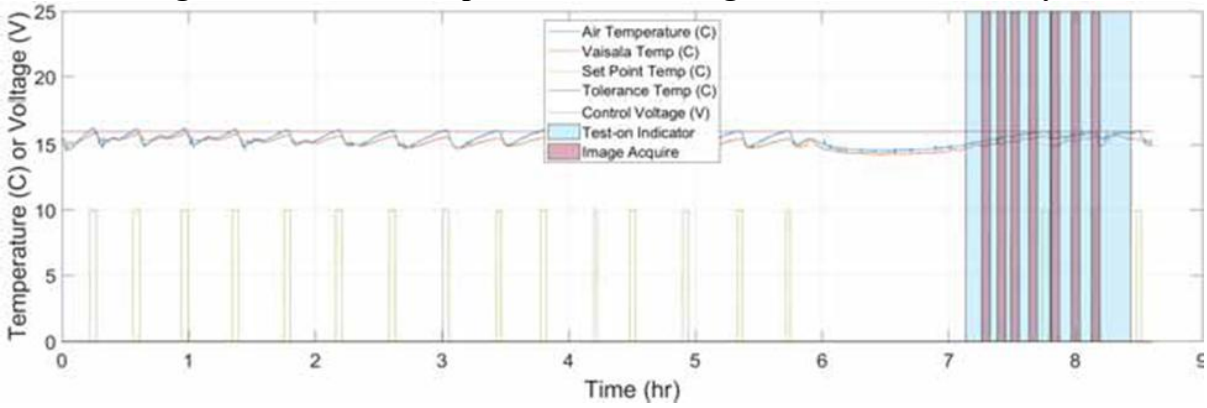

Figure 033121.02: Relative Humidity Time History

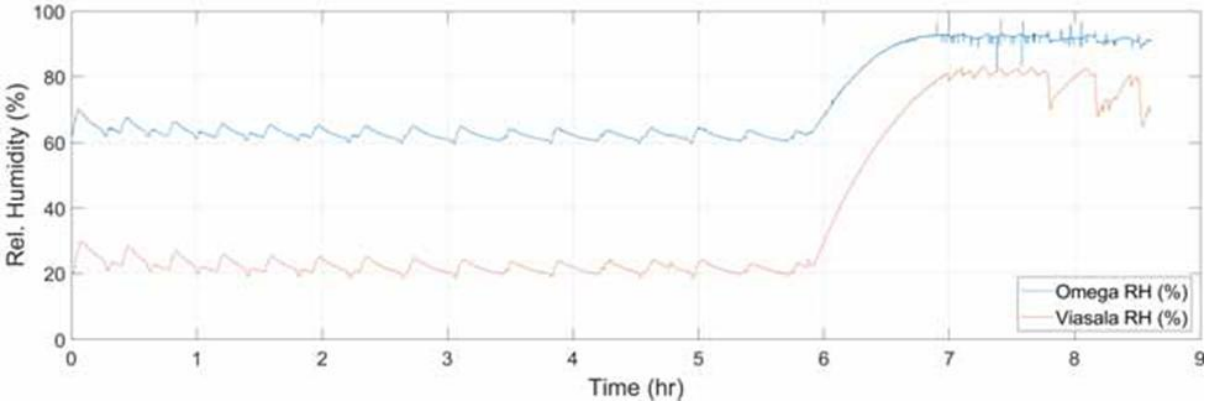

Figure 033121.03: Velocity Time History

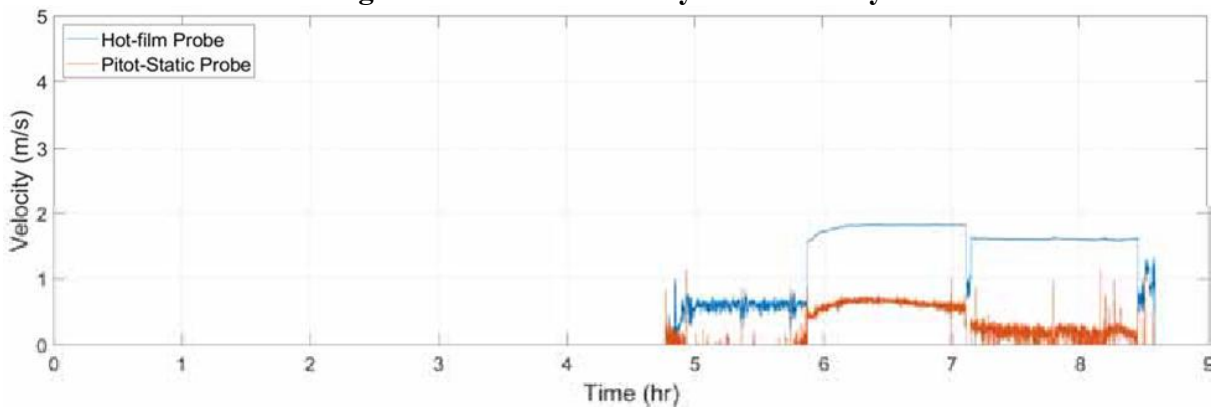

Figure 033121.04: Coolant Return Temperature Time History

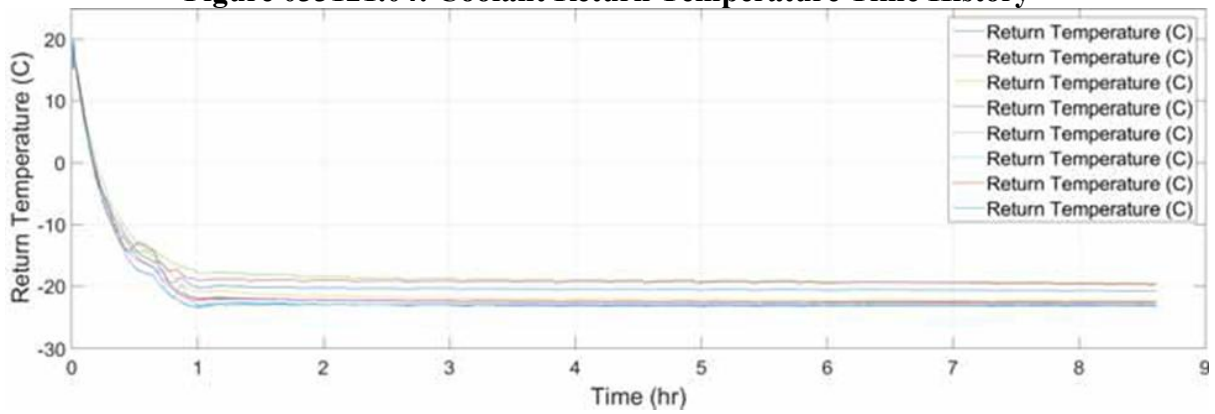

Figure 033121.05: Coolant Supply Temperature Time History

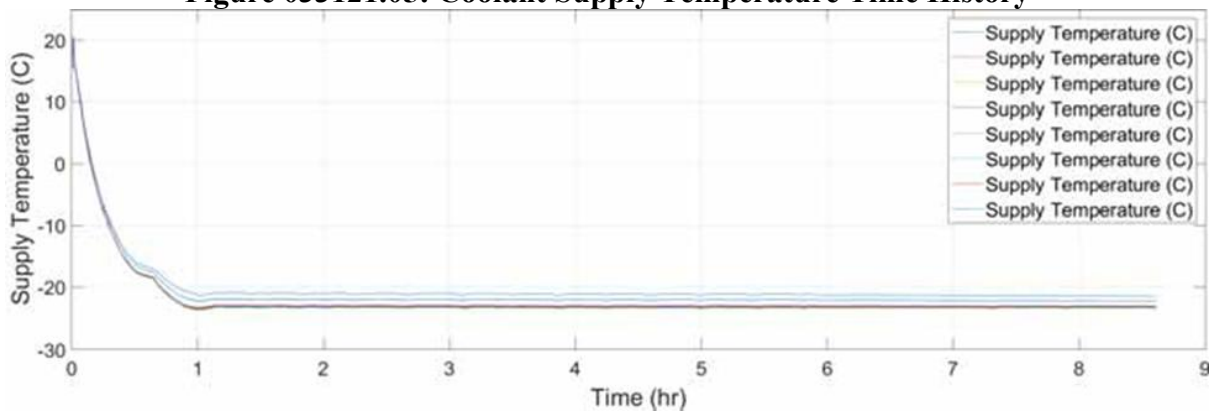

Figure 033121.06: Skin Temperature Time History

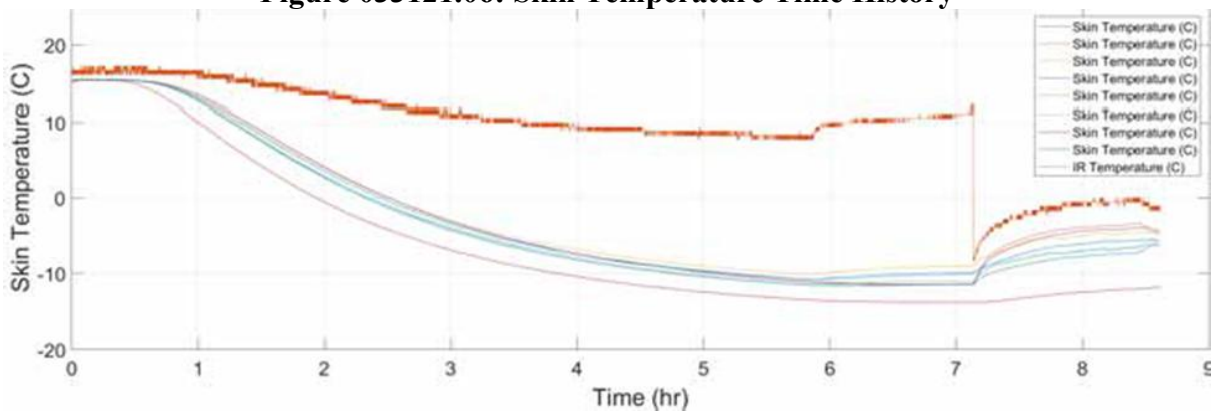

Figure 033121.07: Floor Temperature Time History

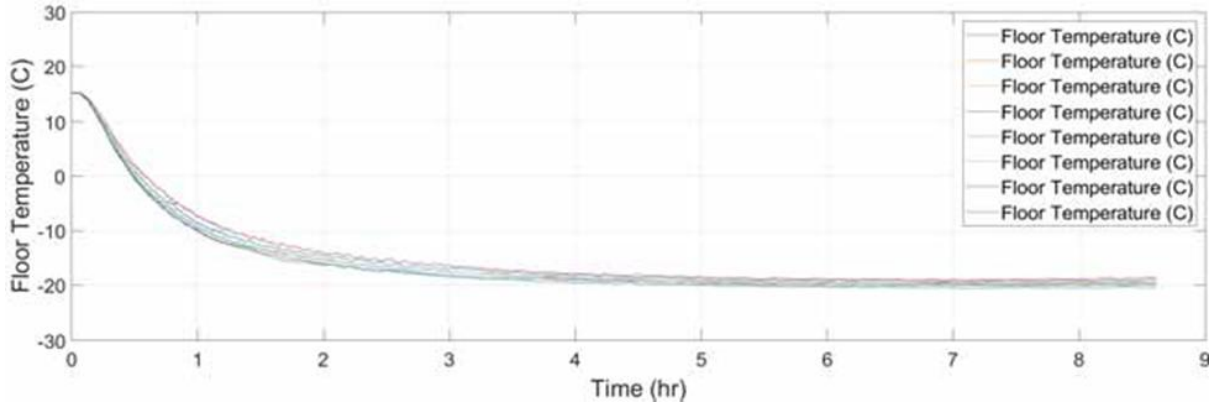

Figure 033121.08: Skin Temperature Slope Time History

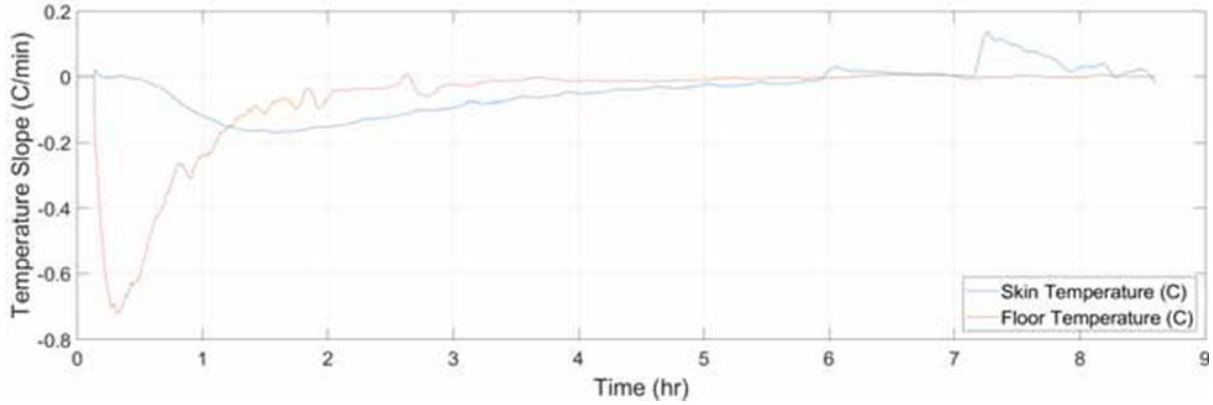

Figure 033121.09: RMS Height Evolution

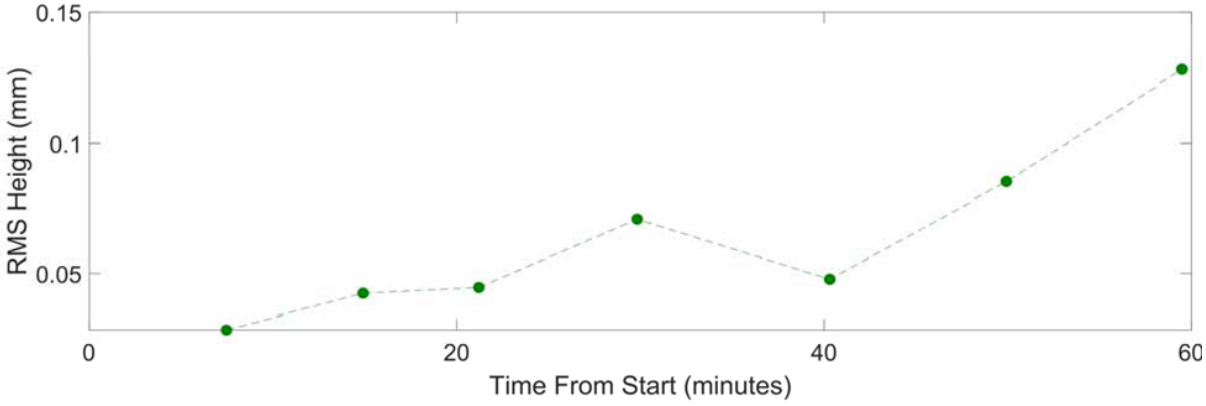

Figure 033121.10: Skewness Evolution

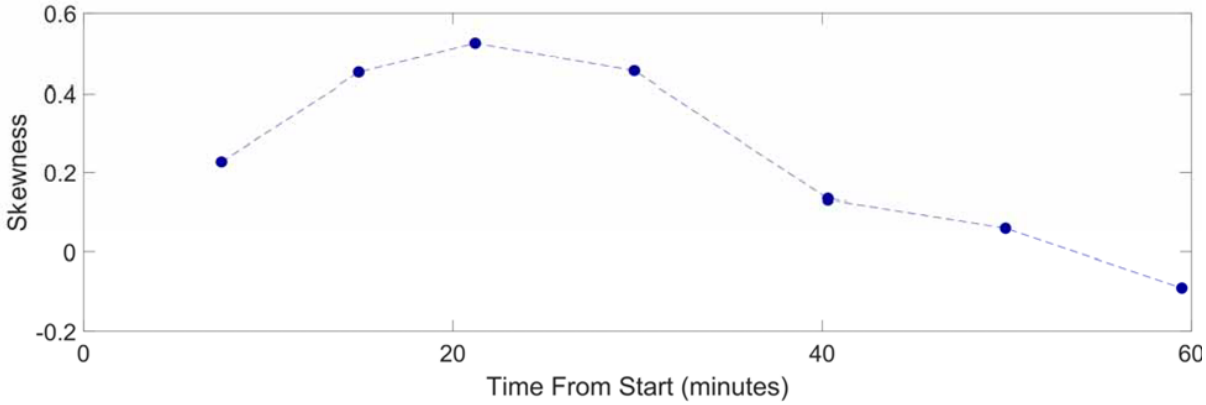

Figure 033121.11: Peak to Valley Evolution

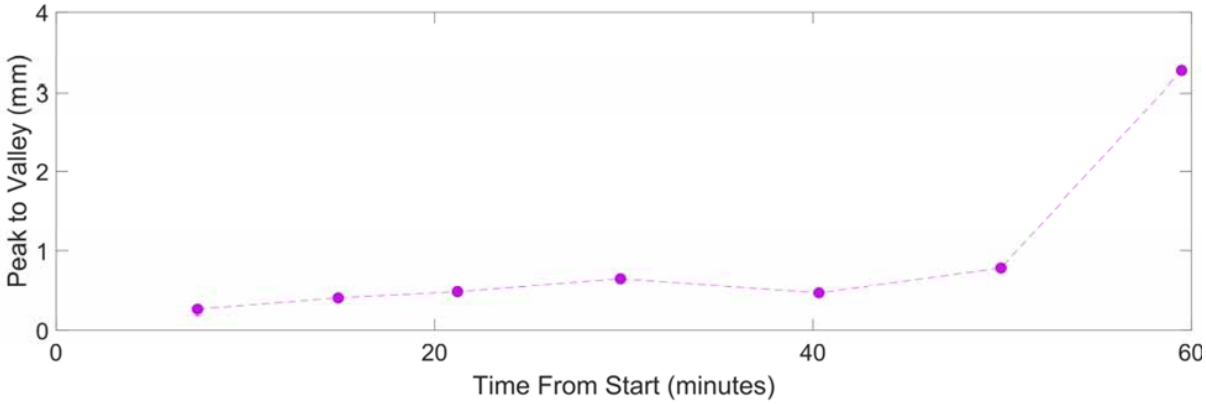

Figure 033121.12: Equivalent Roughness Evolution

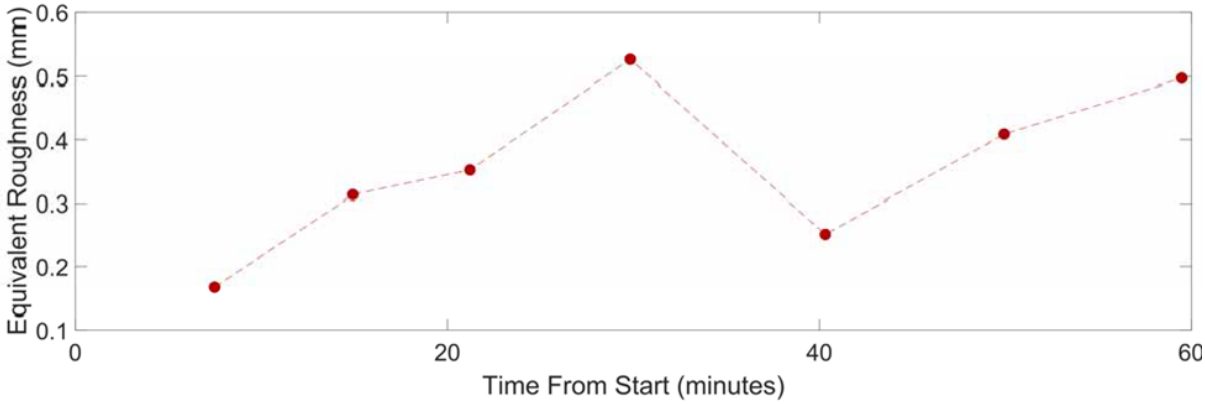

Table 033121.02: Summary of Roughness Parameters

Time (min.)	RMS (mm)	Skewness	Peak to Valley (mm)	ks,Flack-Schultz (mm)
7.4714	0.0285	0.2267	0.2496	0.1668
14.9047	0.0424	0.4530	0.3950	0.3130
21.2047	0.0445	0.5269	0.4757	0.3524
29.8214	0.0711	0.4567	0.6413	0.5272
40.3047	0.0477	0.1327	0.4605	0.2508
49.9214	0.0852	0.0602	0.7799	0.4091
59.4714	0.1283	-0.0934	3.2714	0.4971

Figure 033121.13: Frost Topography at 00:07:28

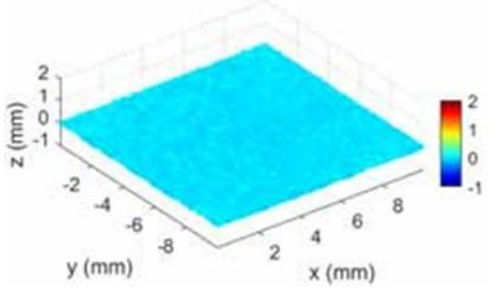

Figure 033121.14: Frost Topography at 00:14:54

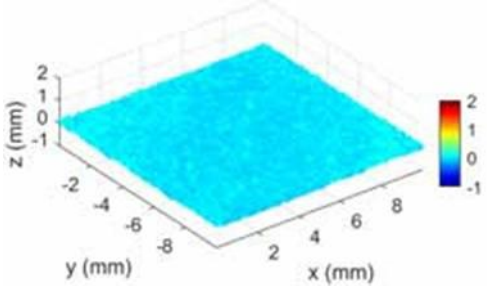

Figure 033121.15: Frost Topography at 00:21:12

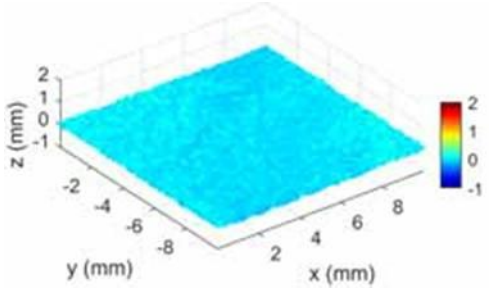

Figure 033121.16: Frost Topography at 00:29:49

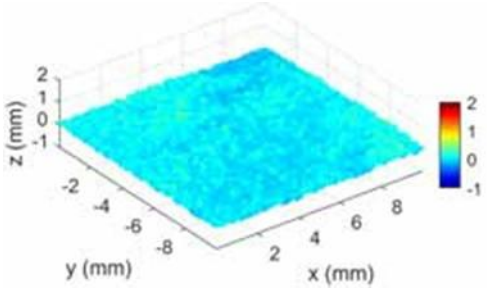

Figure 033121.17: Frost Topography at 00:40:18

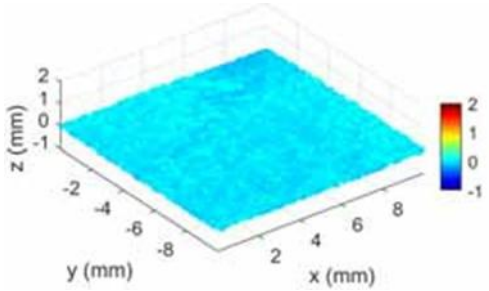

Figure 033121.18: Frost Topography at 00:49:55

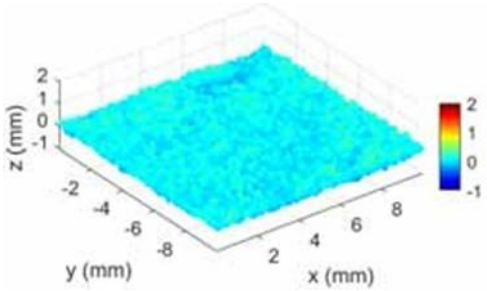

Figure 033121.19: Frost Topography at 00:59:28

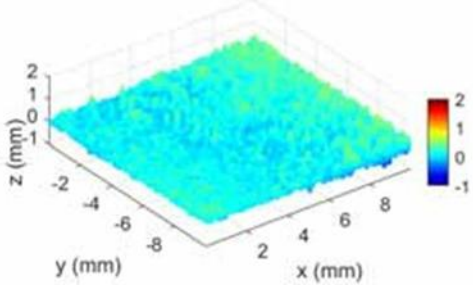

CAFF Conditions Report – Case Date: 041221

Table 041221.01: Summary of Measured Test Variables

Variable	Mean	St. Dev.	Rand. Unc.
T_air (C)	4.3401	0.1618	0.0054
Rh (%)	79.6587	4.9812	0.1670
Omega (kg_v/kg_da)	0.00418649	0.00029966	0.00001005
V_air (m/s)	0.3207	0.0545	0.0018
T_skin (C)	-10.6855	0.6784	0.0227
T_floor (C)	-20.6222	0.0360	0.0012

Figure 041221.01: Temperature and Voltage Control Time History

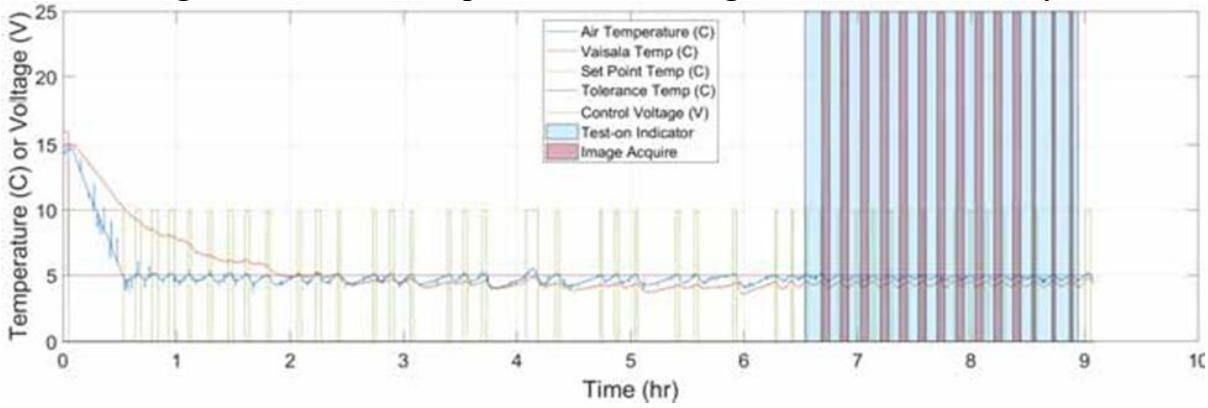

Figure 041221.02: Relative Humidity Time History

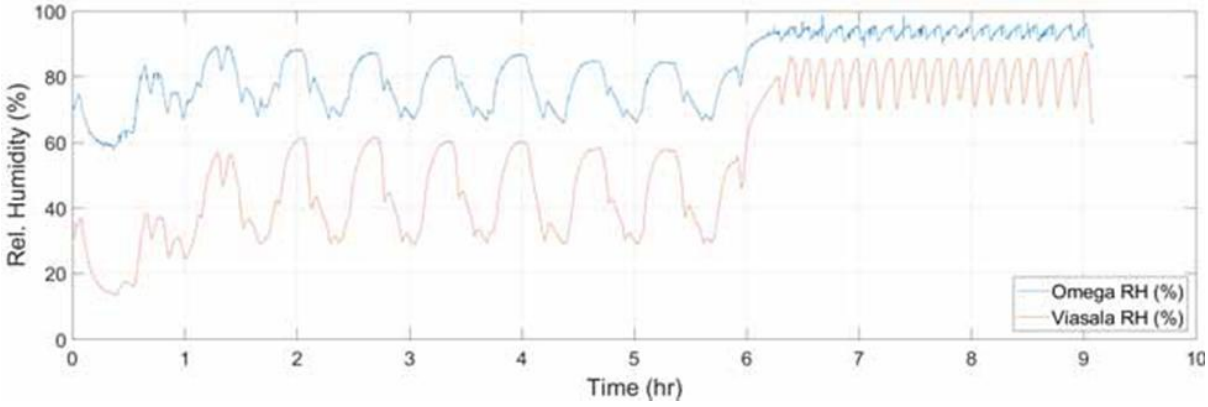

Figure 041221.03: Velocity Time History

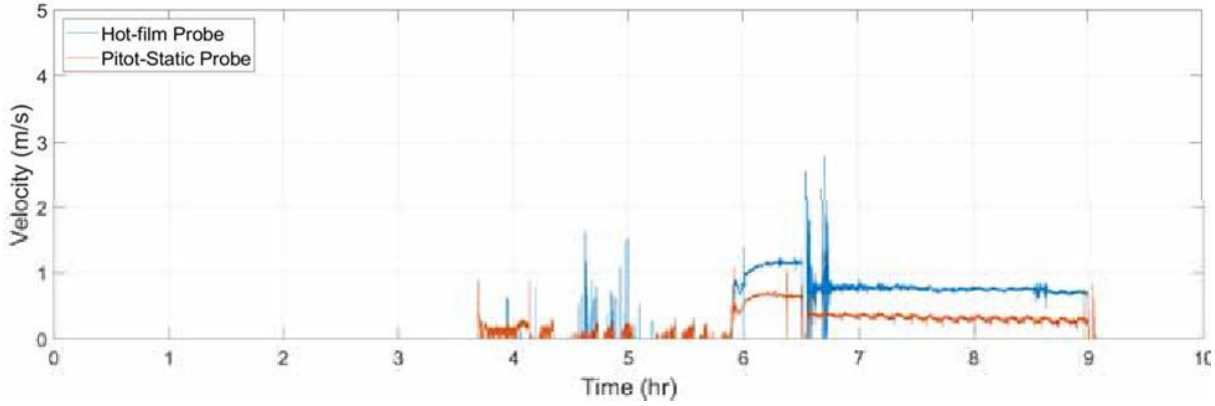

Figure 041221.04: Coolant Return Temperature Time History

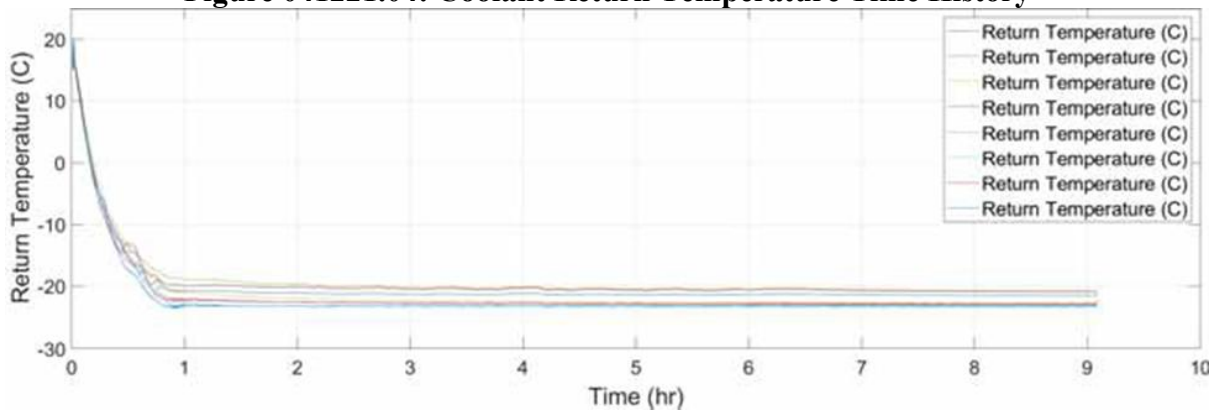

Figure 041221.05: Coolant Supply Temperature Time History

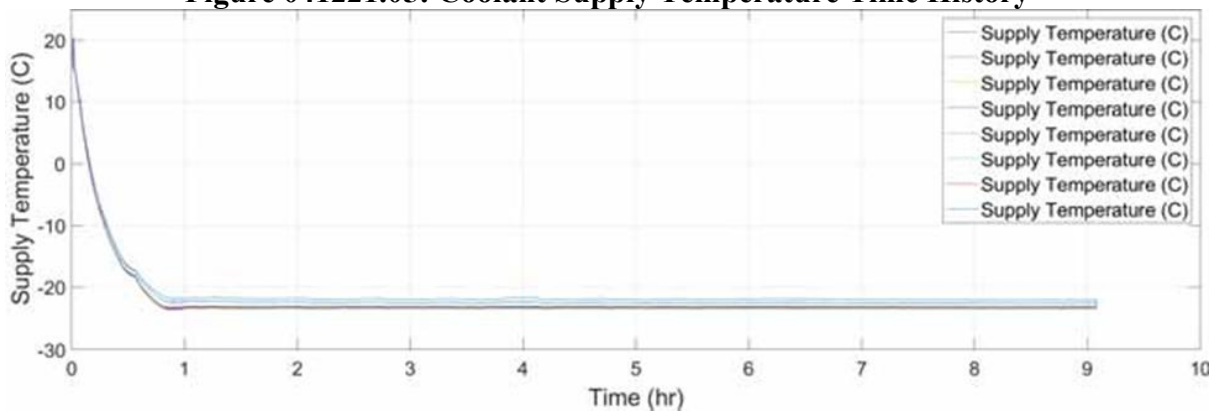

Figure 041221.06: Skin Temperature Time History

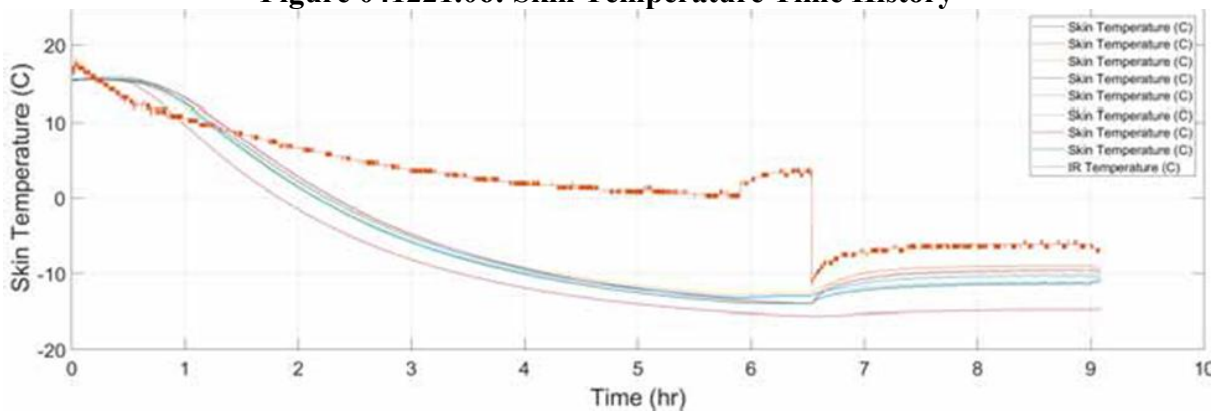

Figure 041221.07: Floor Temperature Time History

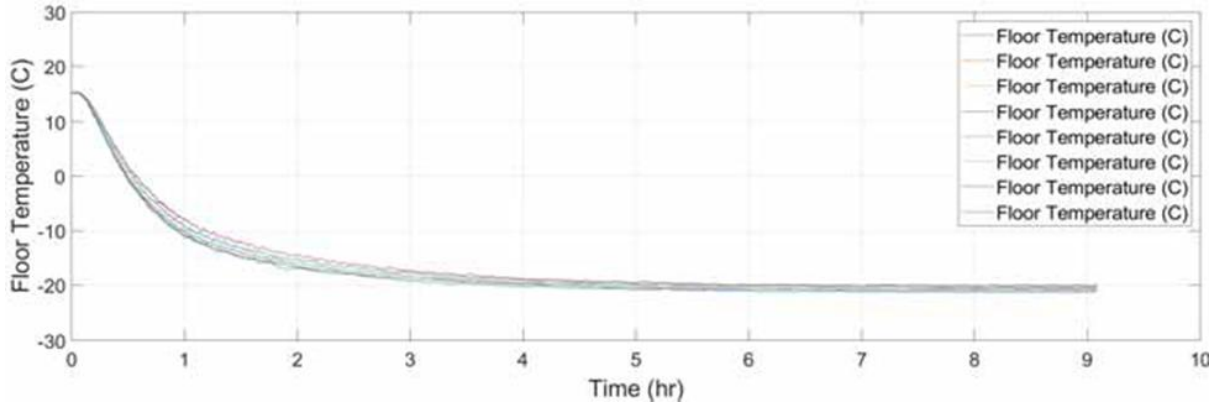

Figure 041221.08: Skin Temperature Slope Time History

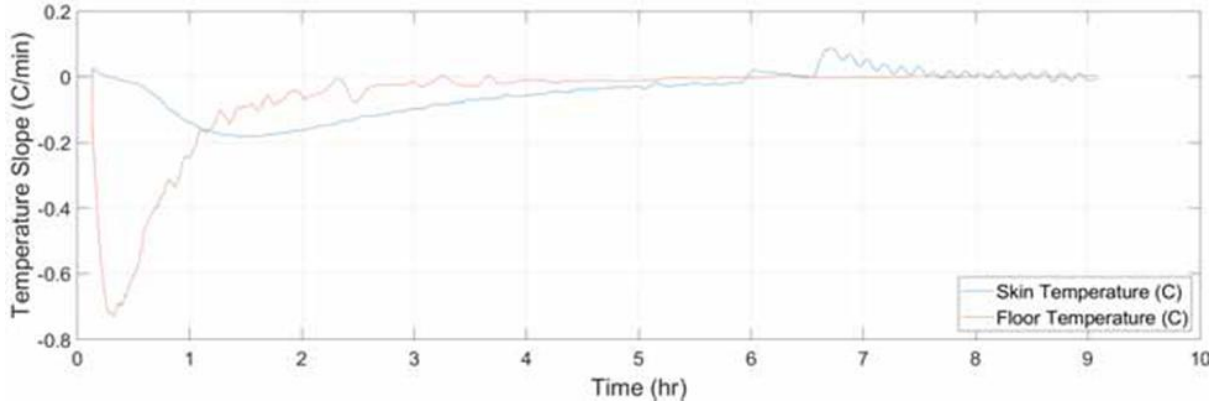

Figure 041221.09: RMS Height Evolution

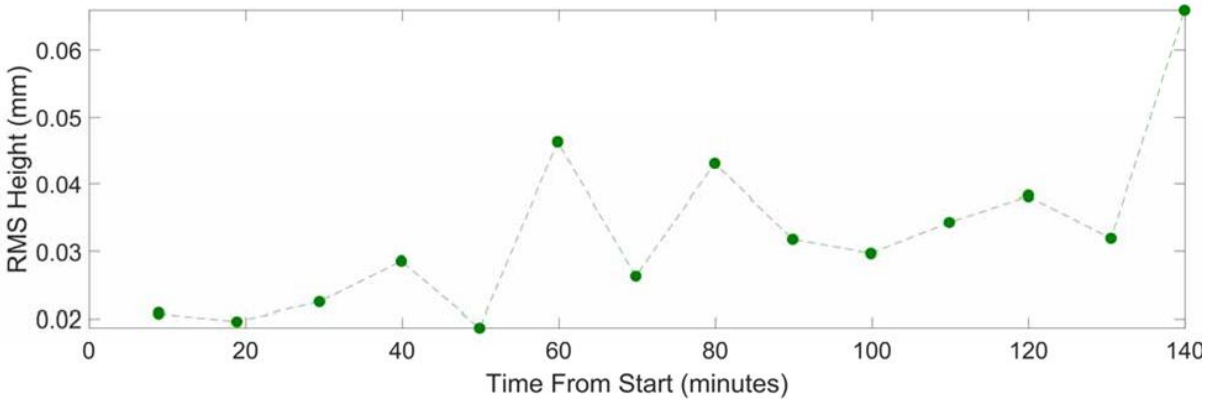

Figure 041221.10: Skewness Evolution

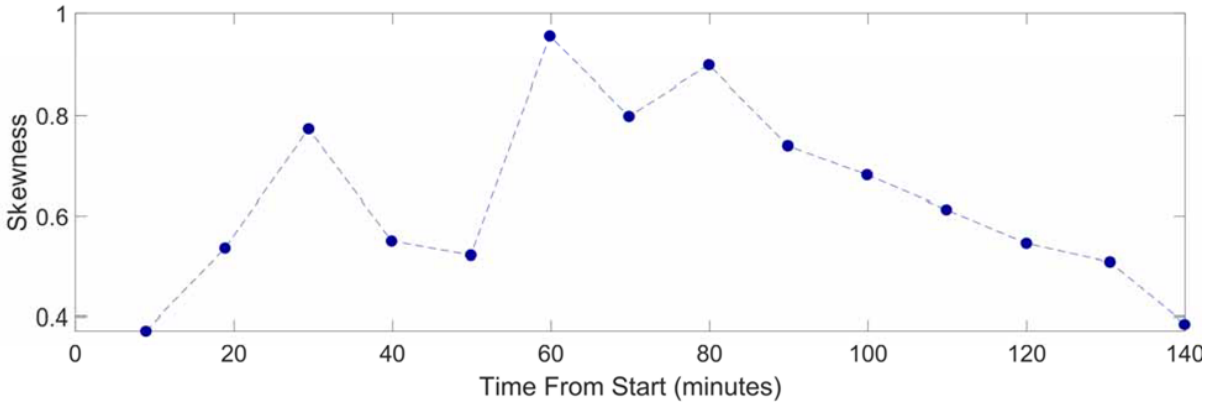

Figure 041221.11: Peak to Valley Evolution

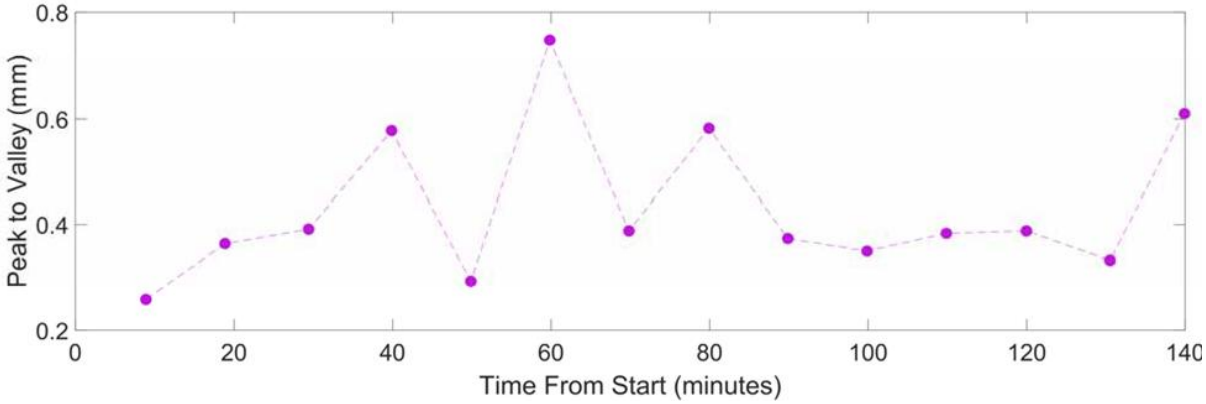

Figure 041221.12: Equivalent Roughness Evolution

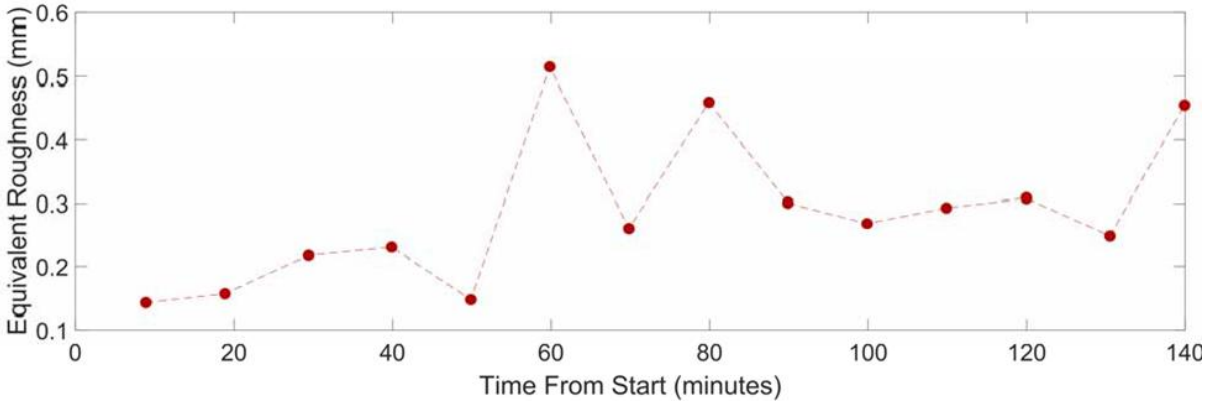

Table 041221.02: Summary of Roughness Parameters

Time (min.)	RMS (mm)	Skewness	Peak to Valley (mm)	ks,Flack-Schultz (mm)
8.8707	0.0208	0.3716	0.2563	0.1419
18.8541	0.0196	0.5355	0.3633	0.1561
29.4041	0.0224	0.7728	0.3910	0.2177
39.8707	0.0286	0.5499	0.5776	0.2307
49.8707	0.0186	0.5217	0.2912	0.1467
59.8374	0.0463	0.9574	0.7494	0.5152
69.8207	0.0263	0.7977	0.3876	0.2601
79.9041	0.0431	0.8993	0.5822	0.4598
89.8707	0.0318	0.7390	0.3731	0.3007
99.8541	0.0297	0.6810	0.3490	0.2680
109.8707	0.0344	0.6129	0.3832	0.2930
119.9707	0.0383	0.5453	0.3879	0.3079
130.5207	0.0320	0.5078	0.3313	0.2485
139.9207	0.0658	0.3852	0.6106	0.4553

Figure 041221.13: Frost Topography at 00:08:52

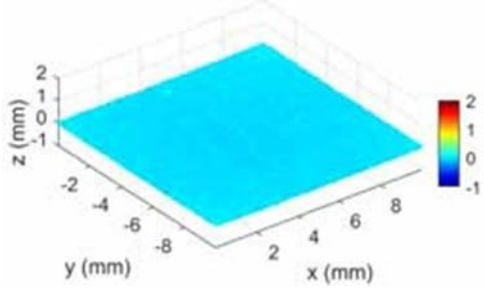

Figure 041221.14: Frost Topography at 00:18:51

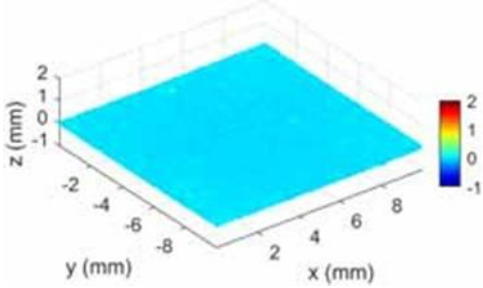

Figure 041221.15: Frost Topography at 00:29:24

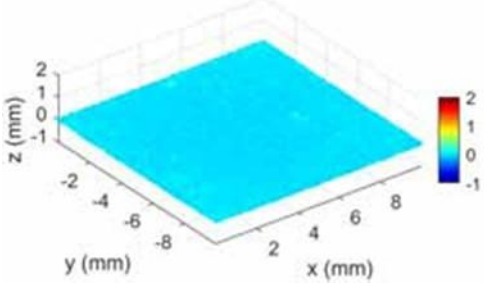

Figure 041221.16: Frost Topography at 00:39:52

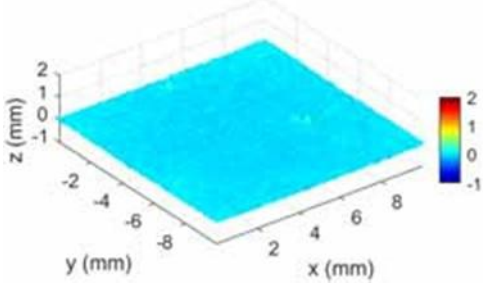

Figure 041221.17: Frost Topography at 00:49:52

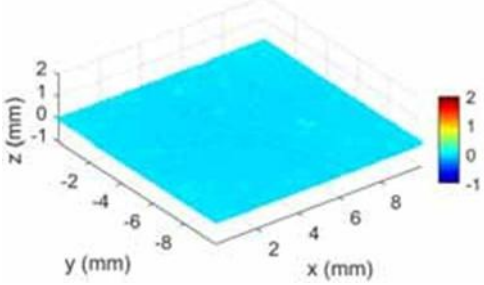

Figure 041221.18: Frost Topography at 00:59:50

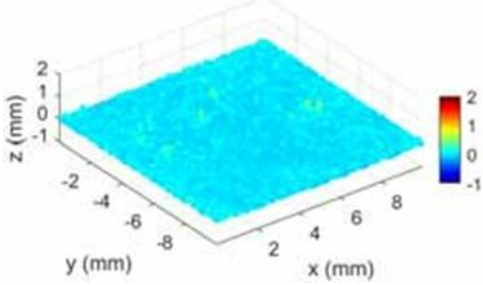

Figure 041221.19: Frost Topography at 01:09:49

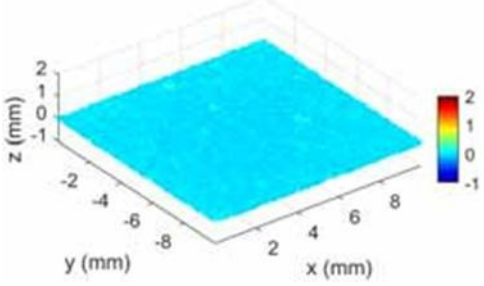

Figure 041221.20: Frost Topography at 01:19:54

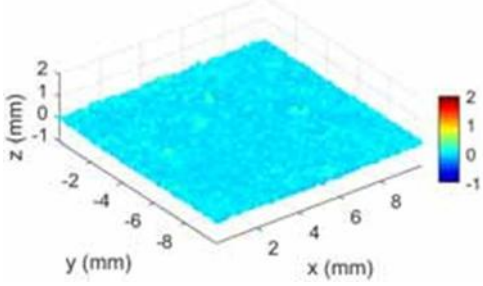

Figure 041221.21: Frost Topography at 01:29:52

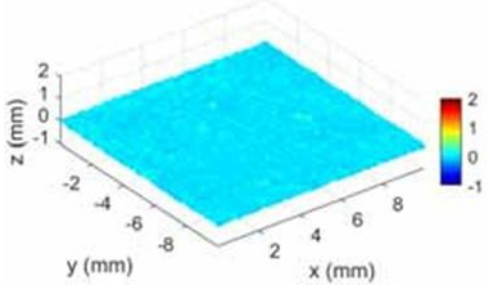

Figure 041221.22: Frost Topography at 01:39:51

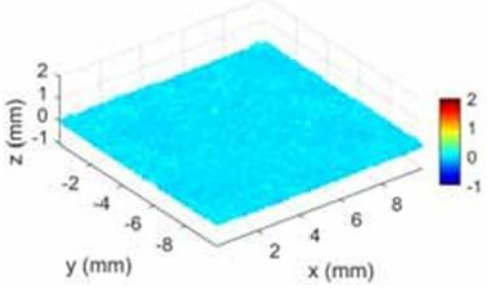

Figure 041221.23: Frost Topography at 01:49:52

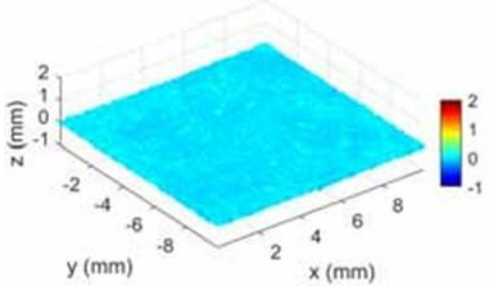

Figure 041221.24: Frost Topography at 01:59:58

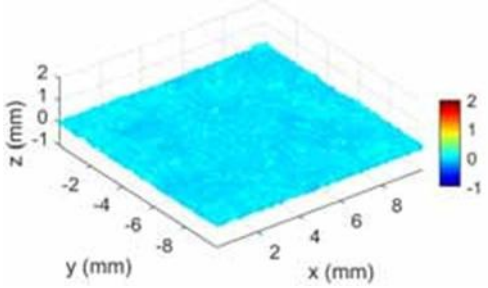

Figure 041221.25: Frost Topography at 02:10:31

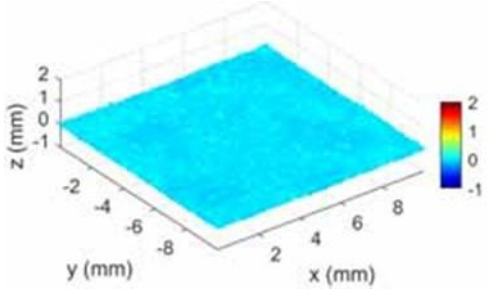

Figure 041221.26: Frost Topography at 02:19:55

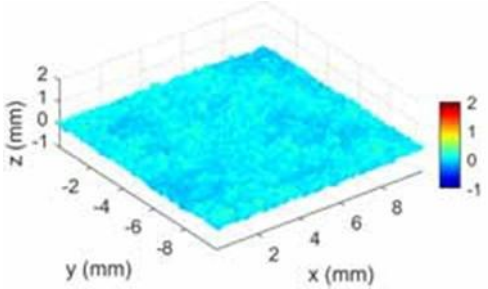

CAFF Conditions Report - Case Date: 041421

Table 041421.01: Summary of Measured Test Variables

Variable	Mean	St. Dev.	Rand. Unc.
T_air (C)	9.2839	0.3010	0.0101
Rh (%)	79.6191	5.8517	0.1973
Omega (kg_v/kg_da)	0.00585999	0.00045897	0.00001548
V_air (m/s)	0.1775	0.1358	0.0046
T_skin (C)	-8.5170	0.9784	0.0330
T_floor (C)	-20.1636	0.0208	0.0007

Figure 041421.01: Temperature and Voltage Control Time History

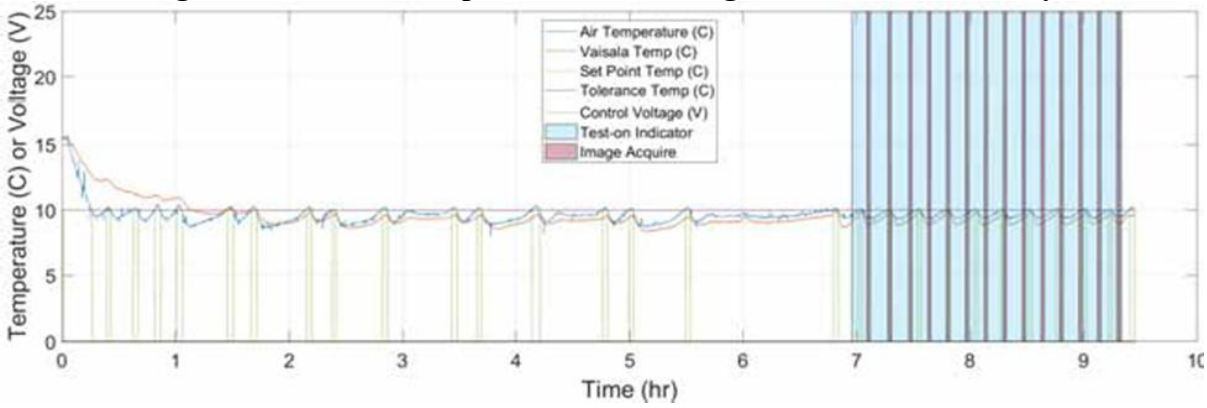

Figure 041421.02: Relative Humidity Time History

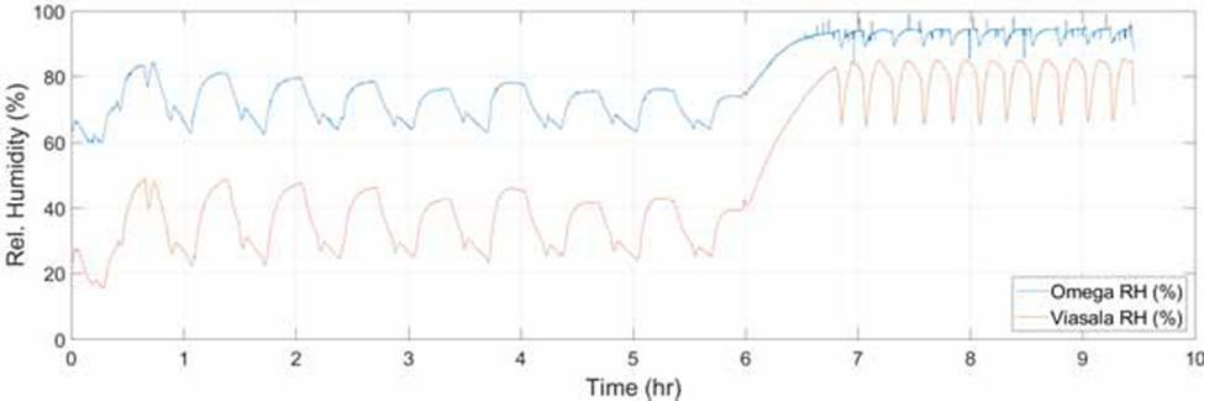

Figure 041421.03: Velocity Time History

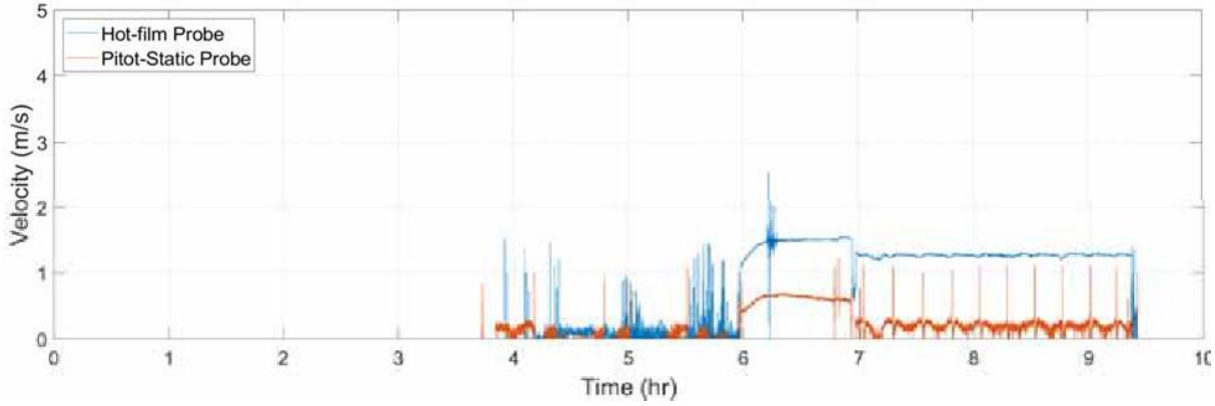

Figure 041421.04: Coolant Return Temperature Time History

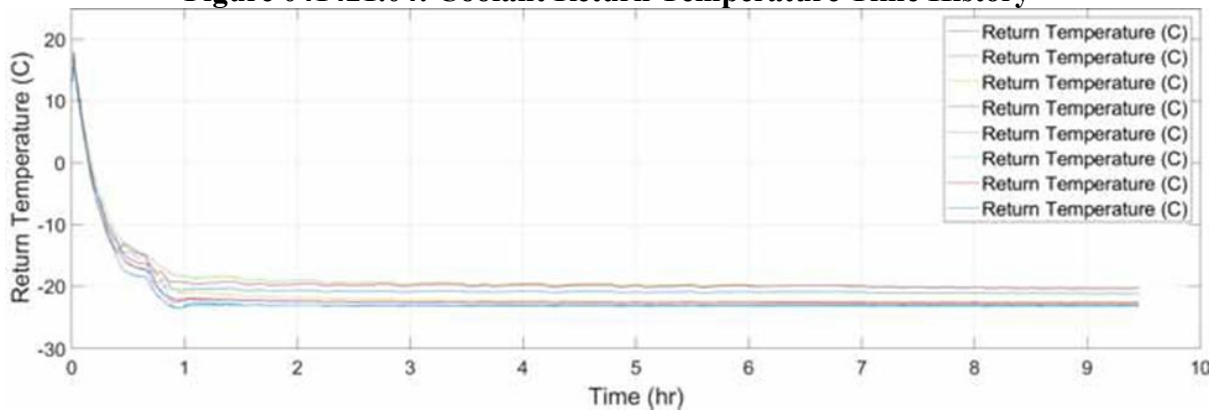

Figure 041421.05: Coolant Supply Temperature Time History

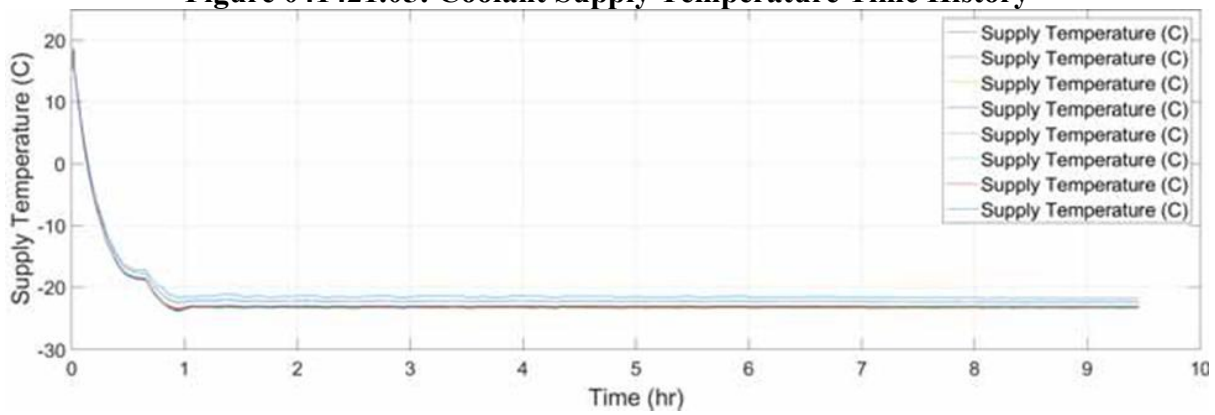

Figure 041421.06: Skin Temperature Time History

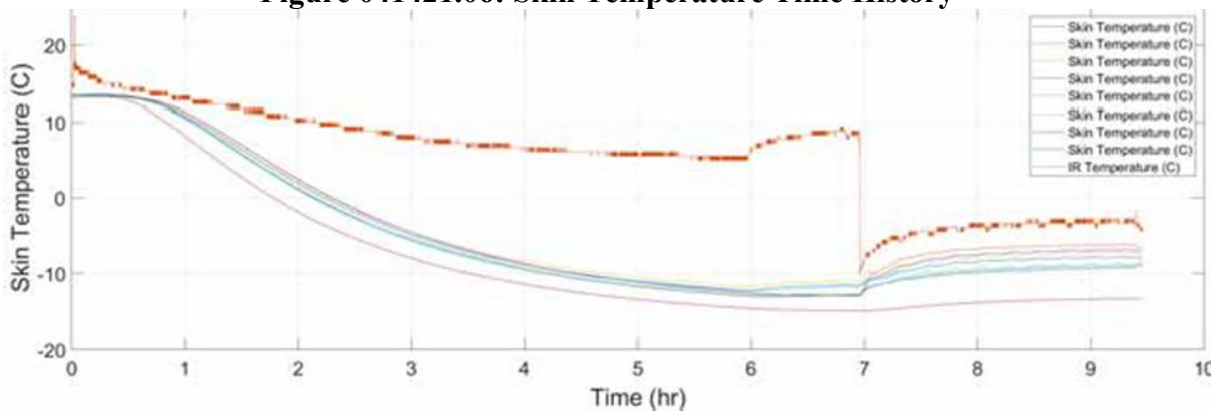

Figure 041421.07: Floor Temperature Time History

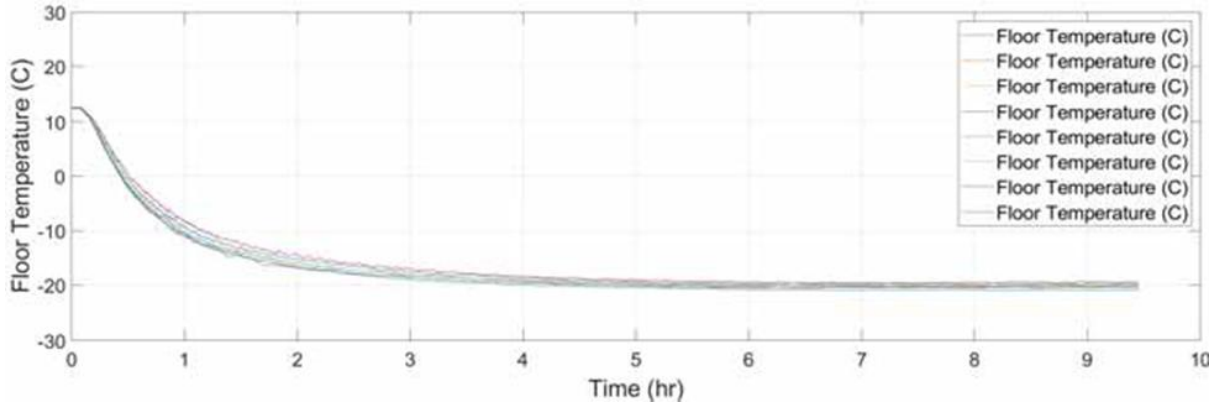

Figure 041421.08: Skin Temperature Slope Time History

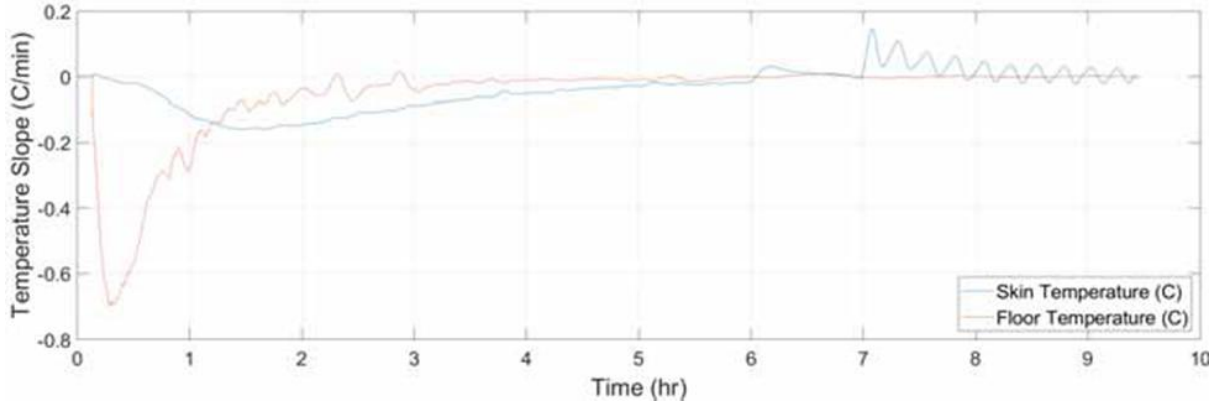

Figure 041421.09: RMS Height Evolution

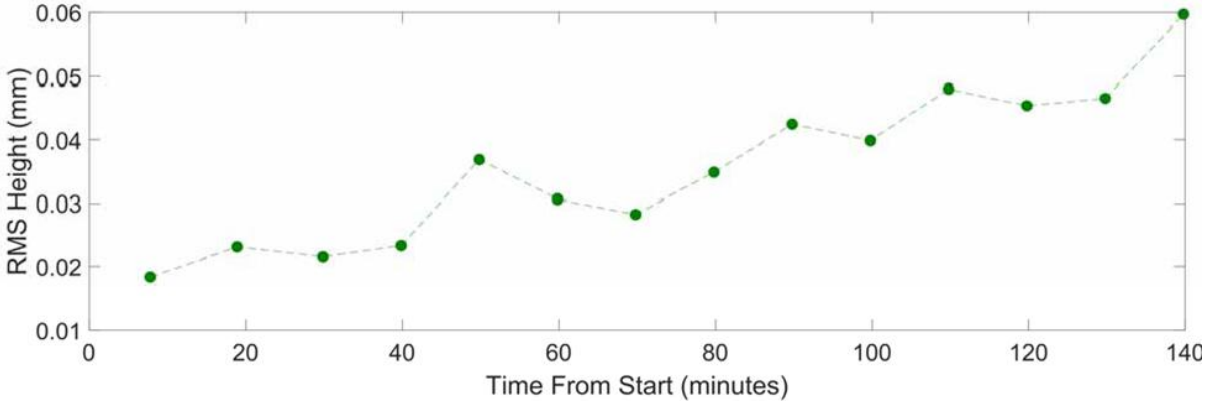

Figure 041421.10: Skewness Evolution

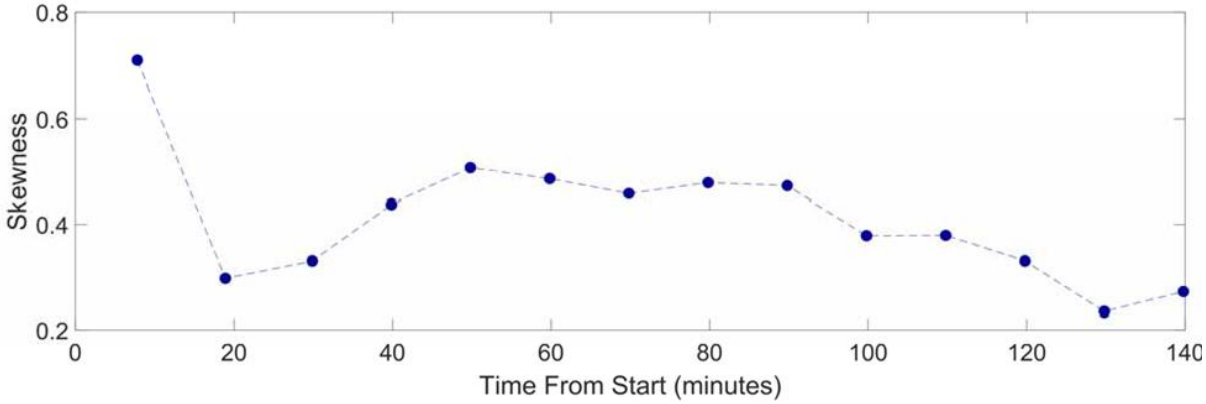

Figure 041421.11: Peak to Valley Evolution

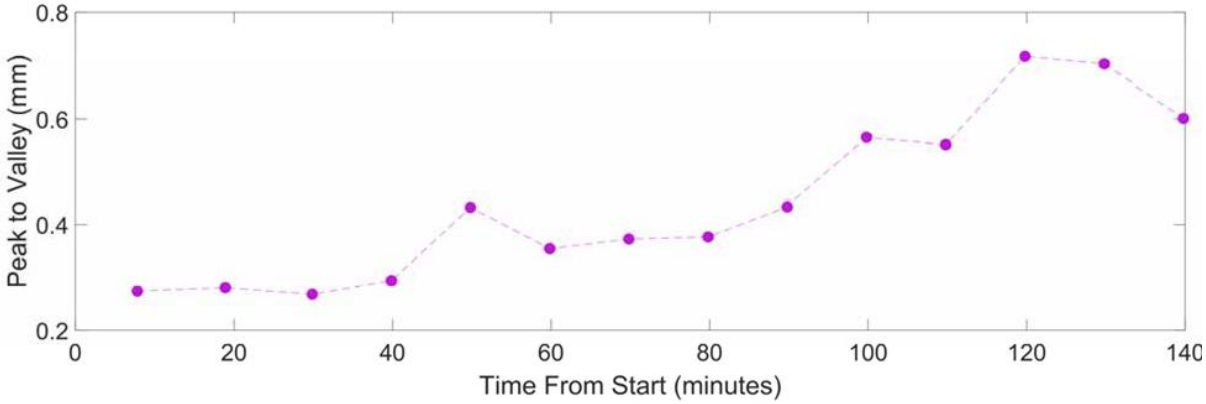

Figure 041421.12: Equivalent Roughness Evolution

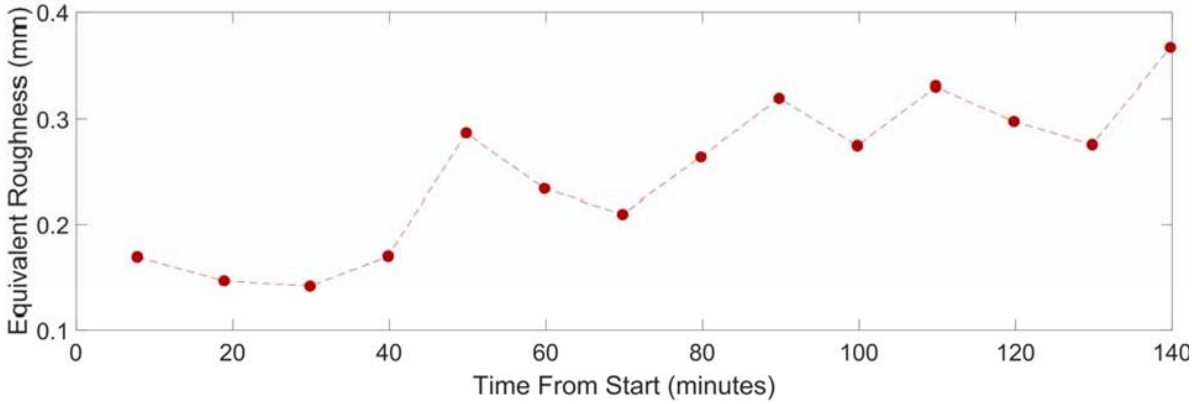

Table 041421.02: Summary of Roughness Parameters

Time (min.)	RMS (mm)	Skewness	Peak to Valley (mm)	ks,Flack-Schultz (mm)
7.7907	0.0183	0.7106	0.2724	0.1690
18.8907	0.0231	0.2972	0.2790	0.1461
29.8740	0.0215	0.3301	0.2664	0.1410
39.8574	0.0233	0.4380	0.2924	0.1697
49.8240	0.0369	0.5070	0.4329	0.2867
59.8240	0.0306	0.4861	0.3537	0.2335
69.8074	0.0283	0.4576	0.3722	0.2097
79.8074	0.0349	0.4785	0.3763	0.2639
89.7907	0.0425	0.4727	0.4339	0.3200
99.7907	0.0399	0.3785	0.5649	0.2745
109.7907	0.0481	0.3792	0.5509	0.3308
119.7907	0.0454	0.3304	0.7179	0.2976
129.7907	0.0466	0.2338	0.7037	0.2754
139.7740	0.0597	0.2716	0.6012	0.3677

Figure 041421.13: Frost Topography at 00:07:47

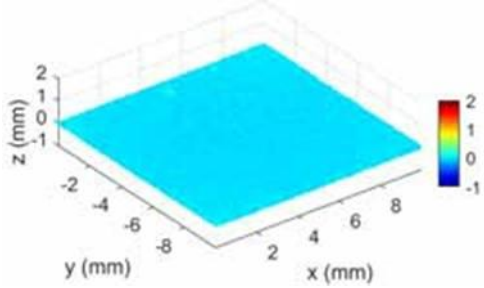

Figure 041421.14: Frost Topography at 00:18:53

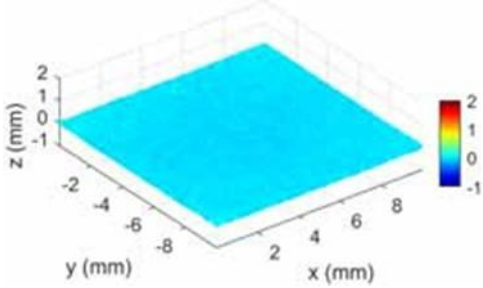

Figure 041421.15: Frost Topography at 00:29:52

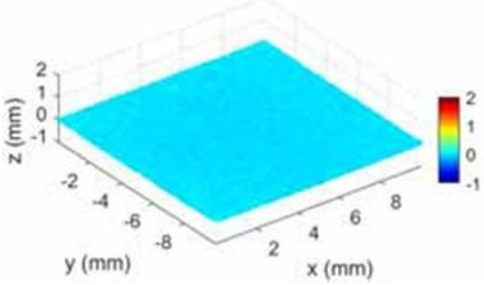

Figure 041421.16: Frost Topography at 00:39:51

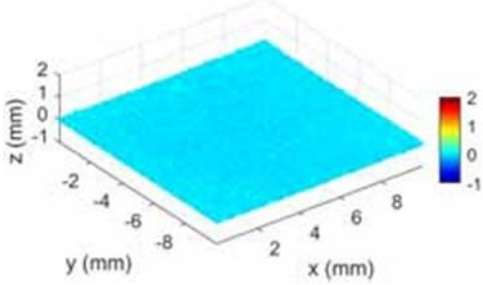

Figure 041421.17: Frost Topography at 00:49:49

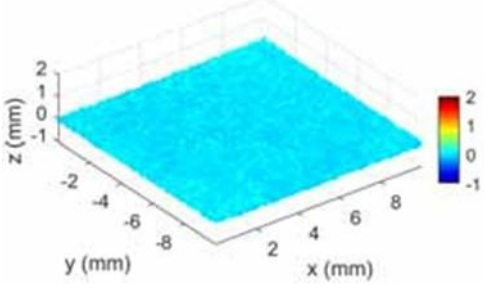

Figure 041421.18: Frost Topography at 00:59:49

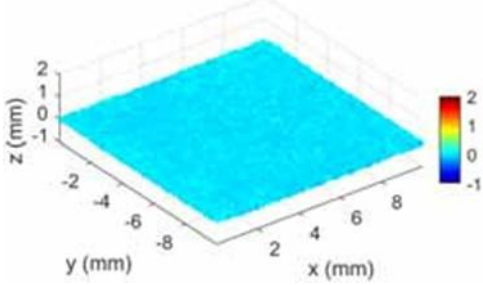

Figure 041421.19: Frost Topography at 01:09:48

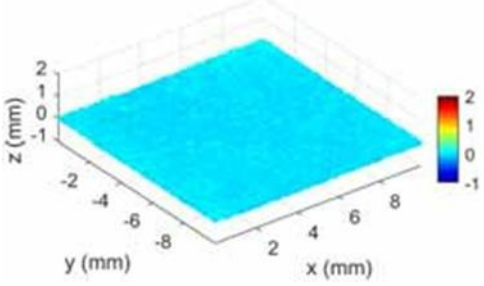

Figure 041421.20: Frost Topography at 01:19:48

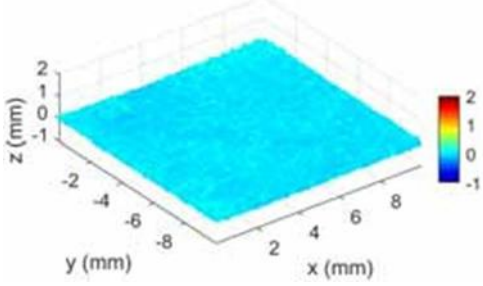

Figure 041421.21: Frost Topography at 01:29:47

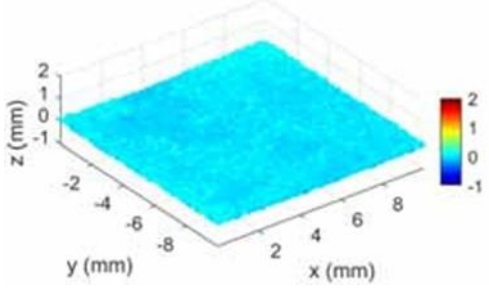

Figure 041421.22: Frost Topography at 01:39:47

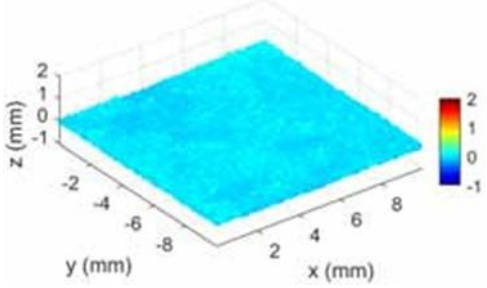

Figure 041421.23: Frost Topography at 01:49:47

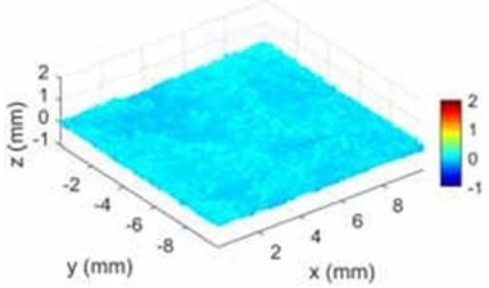

Figure 041421.24: Frost Topography at 01:59:47

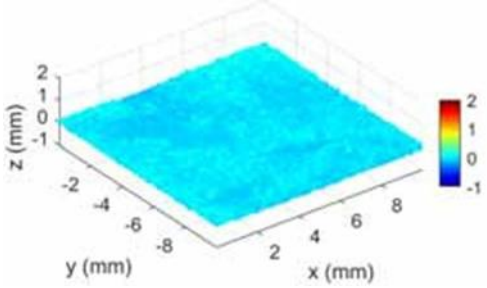

Figure 041421.25: Frost Topography at 02:09:47

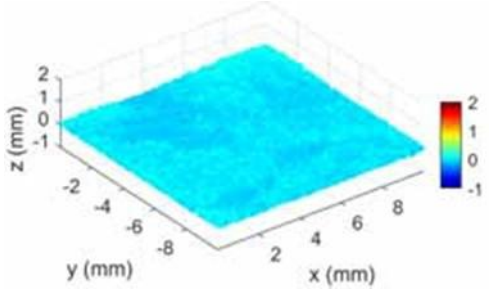

Figure 041421.26: Frost Topography at 02:19:46

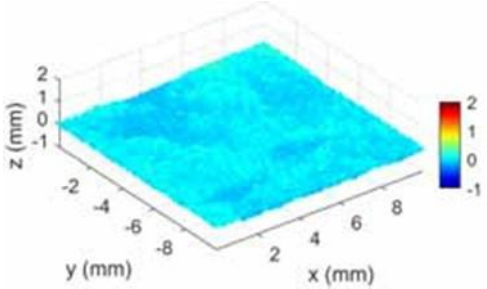

CAFF Conditions Report – Case Date: 041621

Table 041621.01: Summary of Measured Test Variables

Variable	Mean	St. Dev.	Rand. Unc.
T_air (C)	4.2584	0.2742	0.0093
Rh (%)	80.2722	4.7803	0.1615
Omega (kg_v/kg_da)	0.00418396	0.00031703	0.00001071
V_air (m/s)	1.3378	0.1213	0.0041
T_skin (C)	-8.5756	0.8349	0.0282
T_floor (C)	-20.4324	0.0339	0.0011

Figure 041621.01: Temperature and Voltage Control Time History

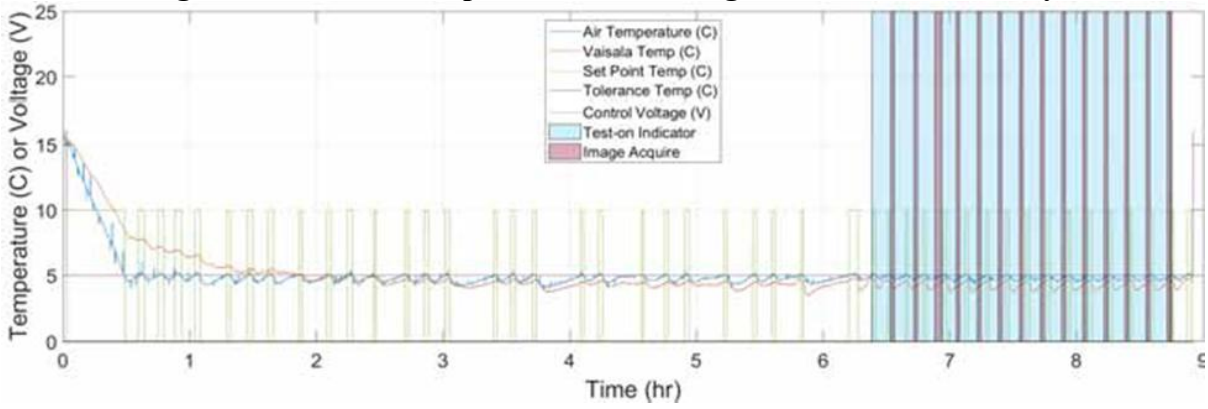

Figure 041621.02: Relative Humidity Time History

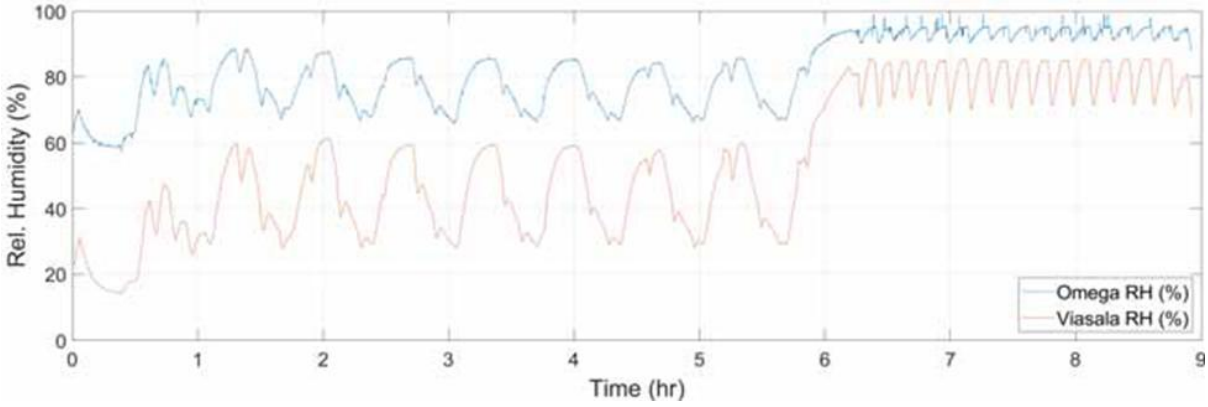

Figure 041621.03: Velocity Time History

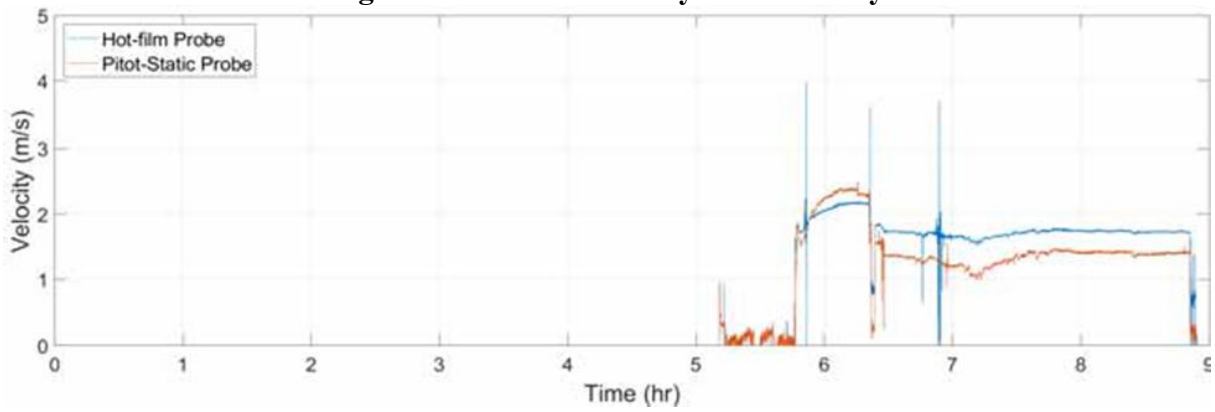

Figure 041621.04: Coolant Return Temperature Time History

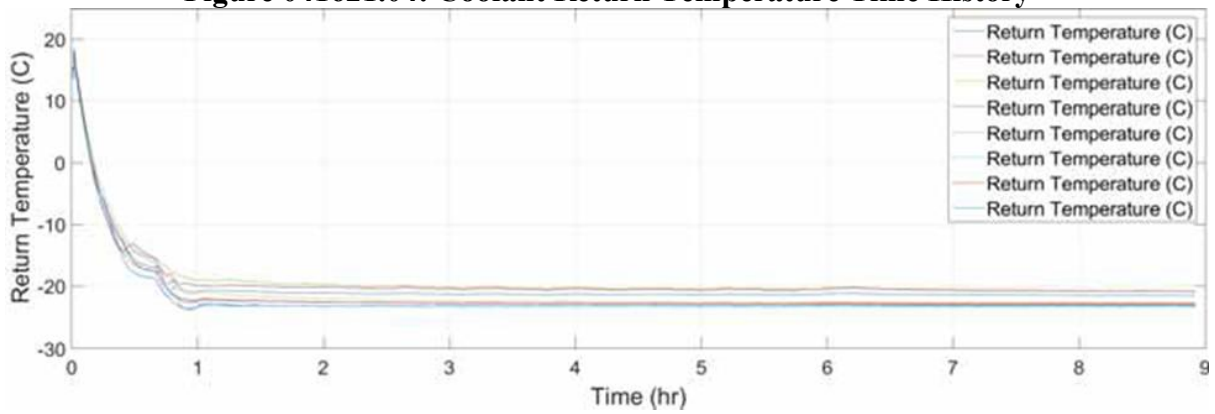

Figure 041621.05: Coolant Supply Temperature Time History

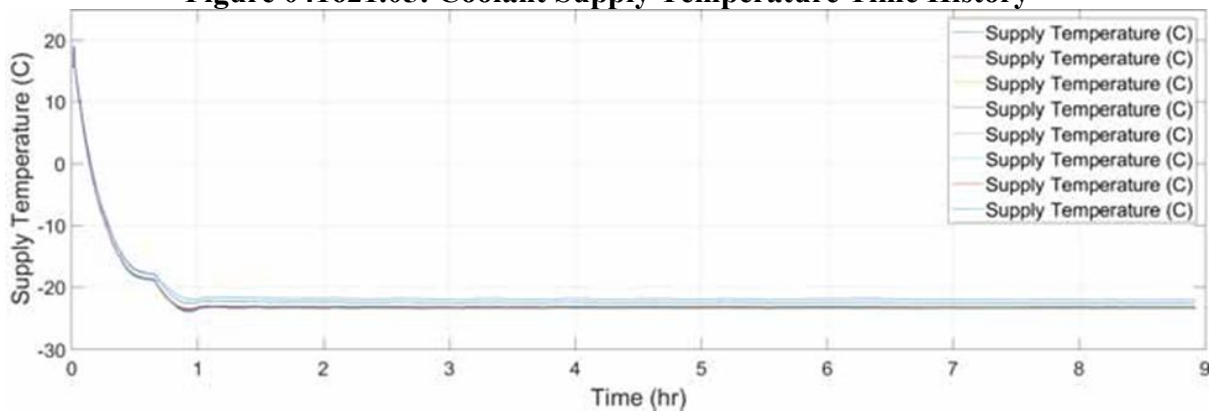

Figure 041621.06: Skin Temperature Time History

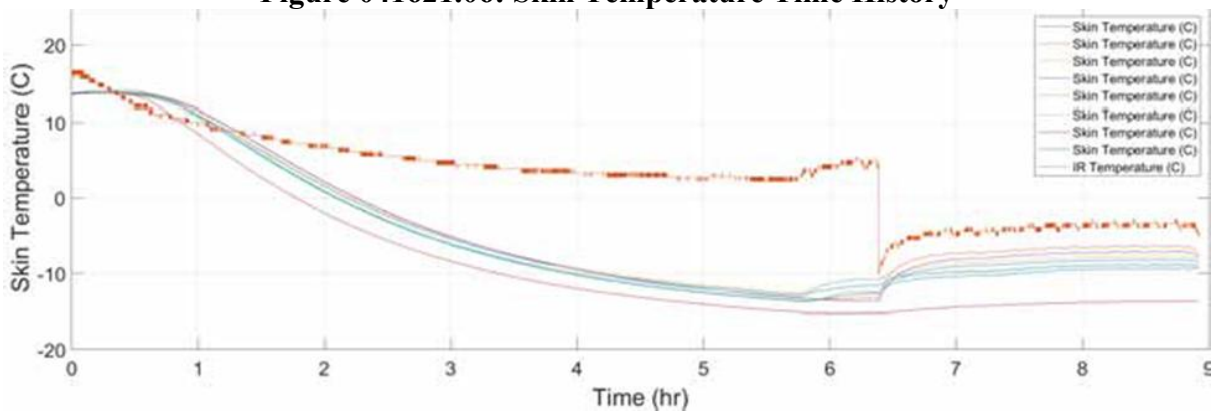

Figure 041621.07: Floor Temperature Time History

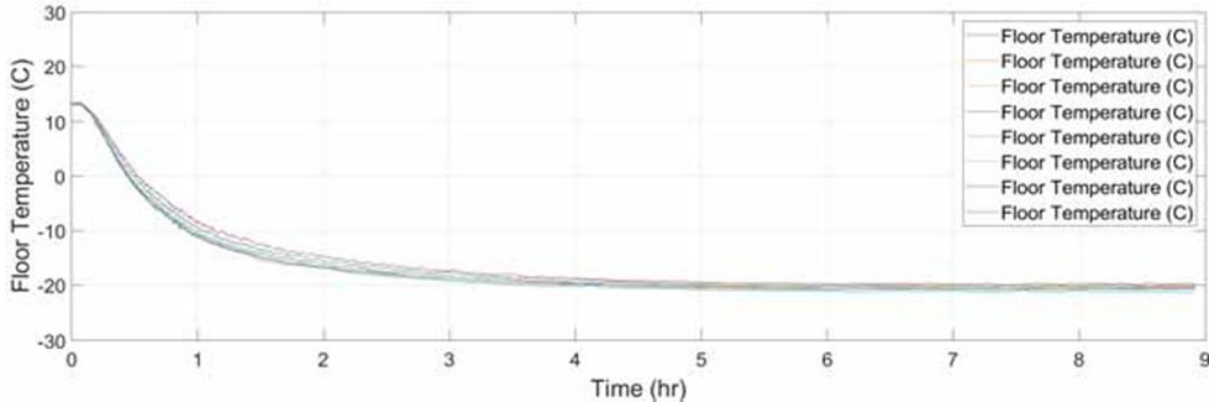

Figure 041621.08: Skin Temperature Slope Time History

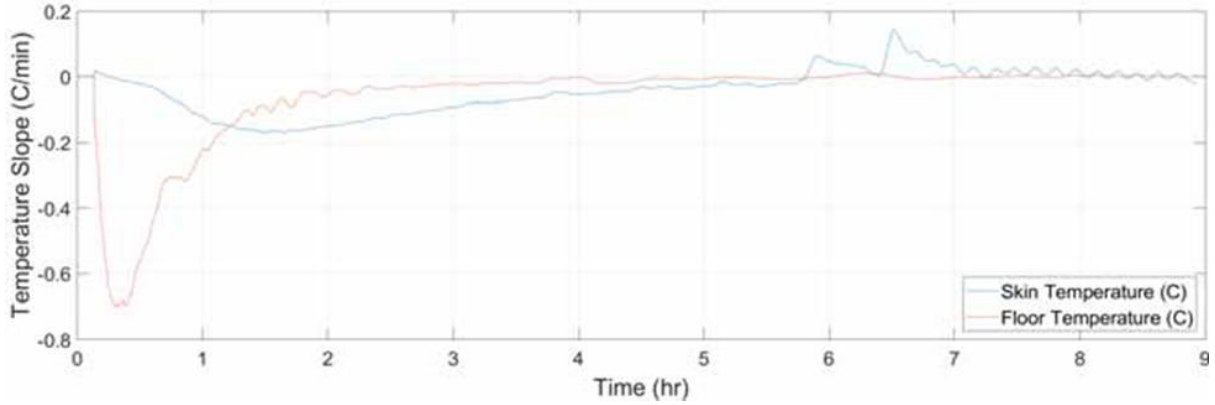

Figure 041621.09: RMS Height Evolution

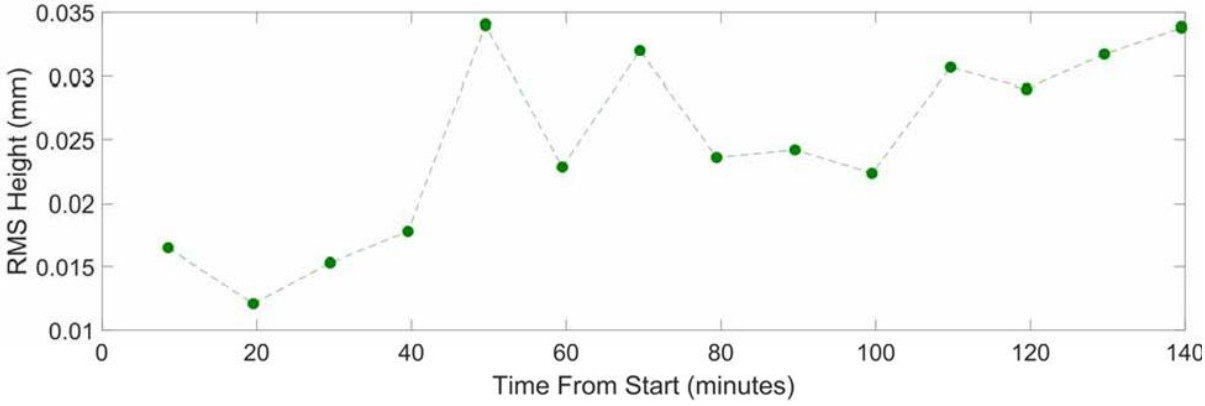

Figure 041621.10: Skewness Evolution

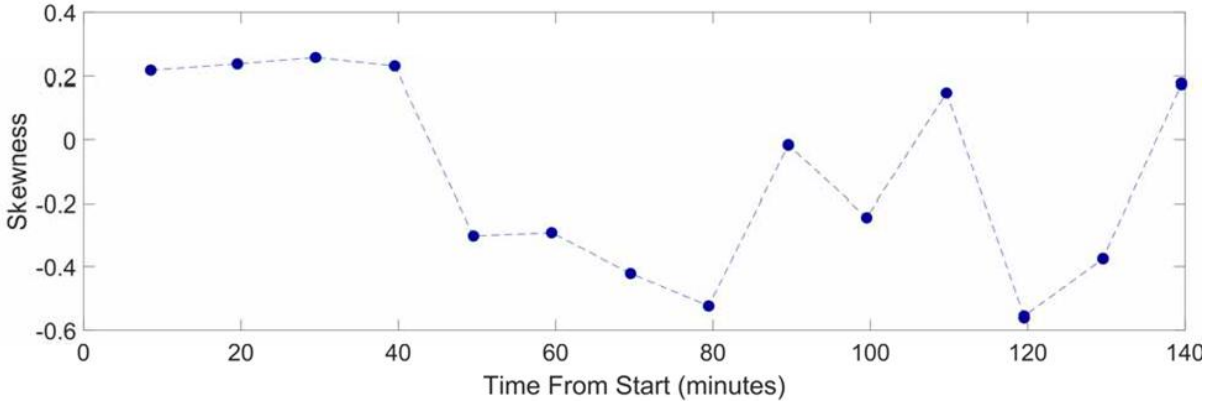

Figure 041621.11: Peak to Valley Evolution

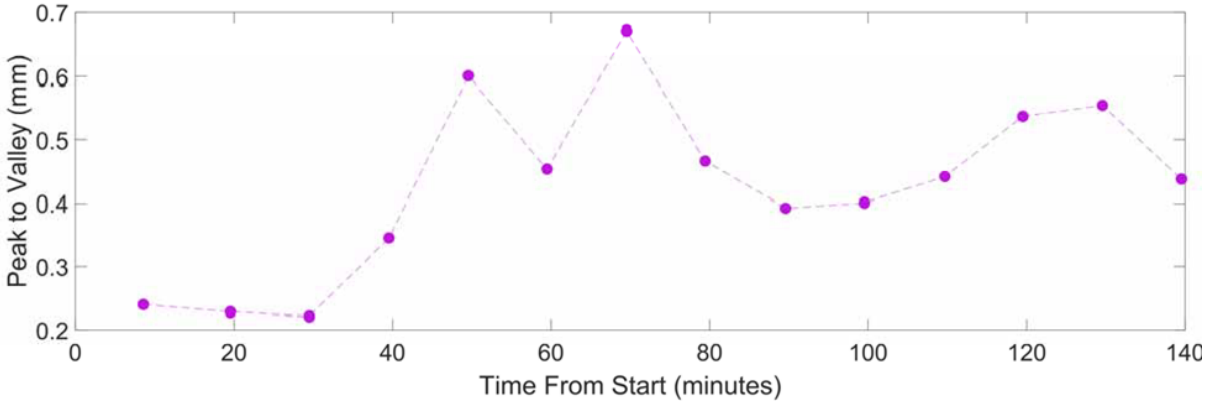

Figure 041621.12: Equivalent Roughness Evolution

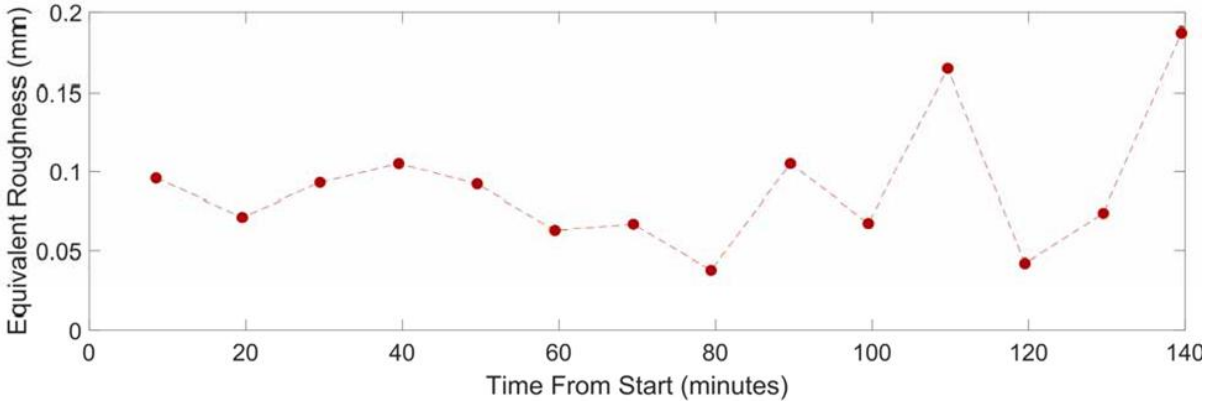

Table 041621.02: Summary of Roughness Parameters

Time (min.)	RMS (mm)	Skewness	Peak to Valley (mm)	ks,Flack-Schultz (mm)
8.5396	0.0165	0.2186	0.2392	0.0957
19.5562	0.0120	0.2389	0.2278	0.0713
29.4896	0.0153	0.2597	0.2208	0.0929
39.5396	0.0178	0.2328	0.3450	0.1049
49.5562	0.0341	-0.3035	0.6008	0.0919
59.4896	0.0228	-0.2929	0.4535	0.0629
69.5229	0.0320	-0.4227	0.6719	0.0669
79.4396	0.0236	-0.5271	0.4665	0.0375
89.5729	0.0242	-0.0156	0.3925	0.1050
99.5229	0.0223	-0.2448	0.4008	0.0673
109.6729	0.0307	0.1508	0.4415	0.1650
119.5229	0.0290	-0.5598	0.5376	0.0418
129.5562	0.0318	-0.3752	0.5550	0.0739
139.5229	0.0339	0.1775	0.4376	0.1877

CAFF Conditions Report – Case Date: 041921

Table 041921.01: Summary of Measured Test Variables

Variable	Mean	St. Dev.	Rand. Unc.
T_air (C)	9.1758	0.4312	0.0203
Rh (%)	80.3115	4.3891	0.2066
Omega (kg_v/kg_da)	0.00586189	0.00039340	0.00001852
V_air (m/s)	1.5362	0.1081	0.0051
T_skin (C)	-6.3577	1.2805	0.0603
T_floor (C)	-19.9862	0.0405	0.0019

Figure 041921.01: Temperature and Voltage Control Time History

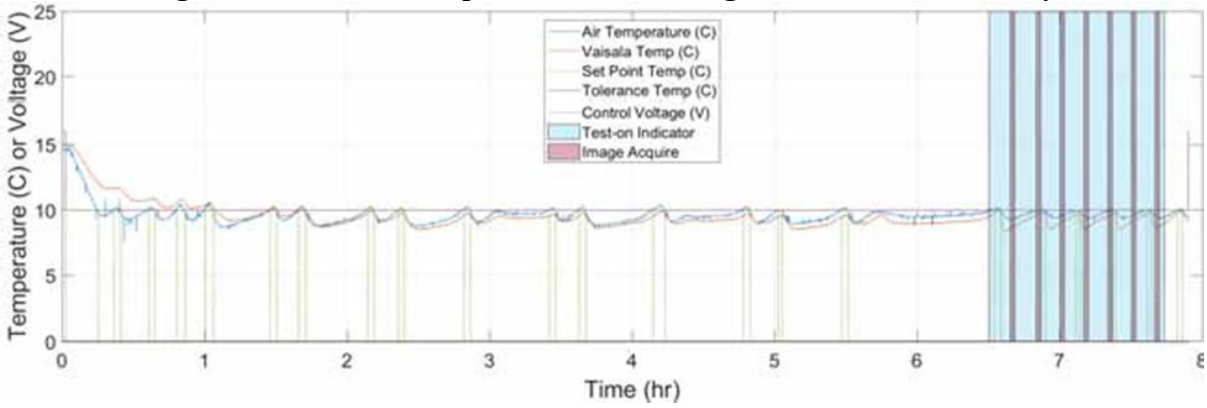

Figure 041921.02: Relative Humidity Time History

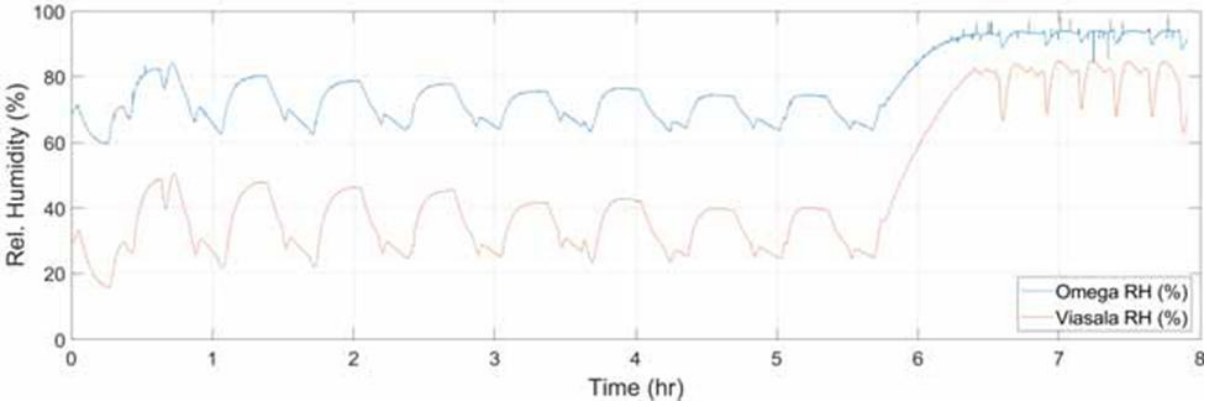

Figure 041921.03: Velocity Time History

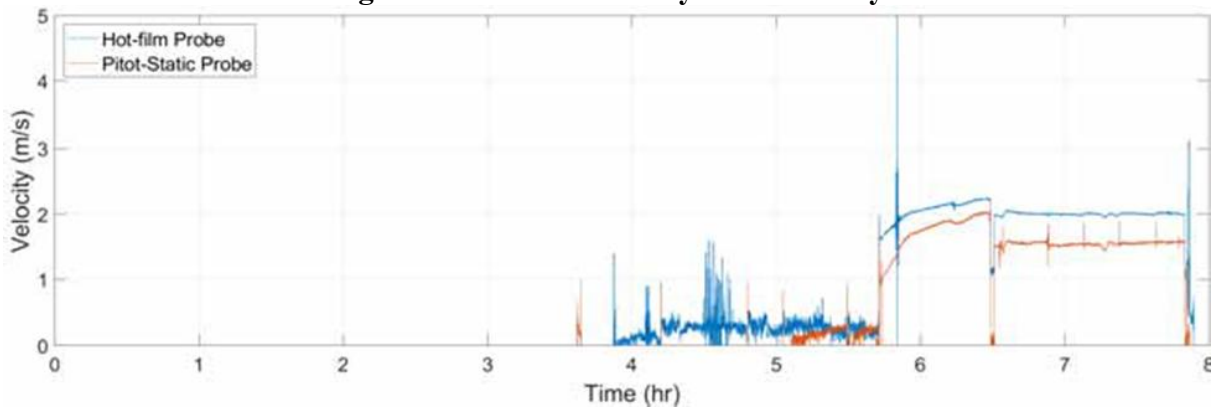

Figure 041921.04: Coolant Return Temperature Time History

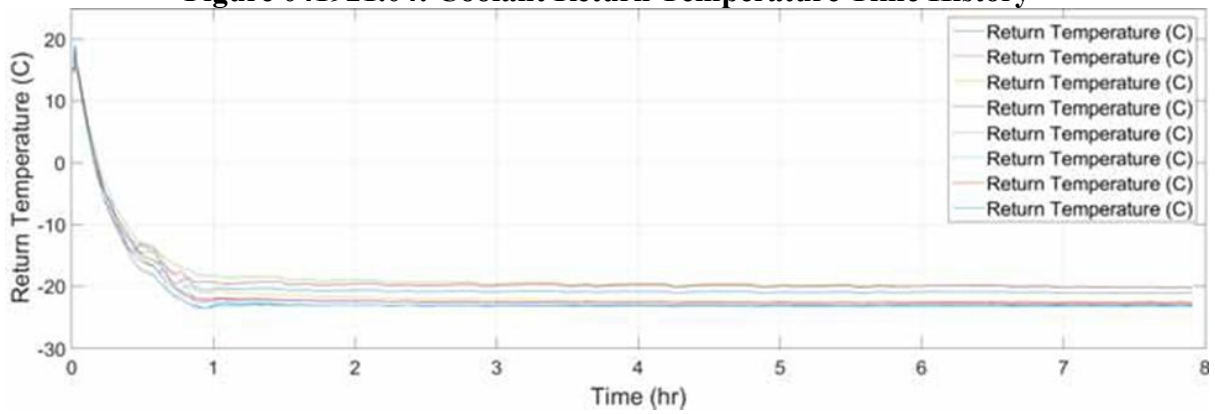

Figure 041921.05: Coolant Supply Temperature Time History

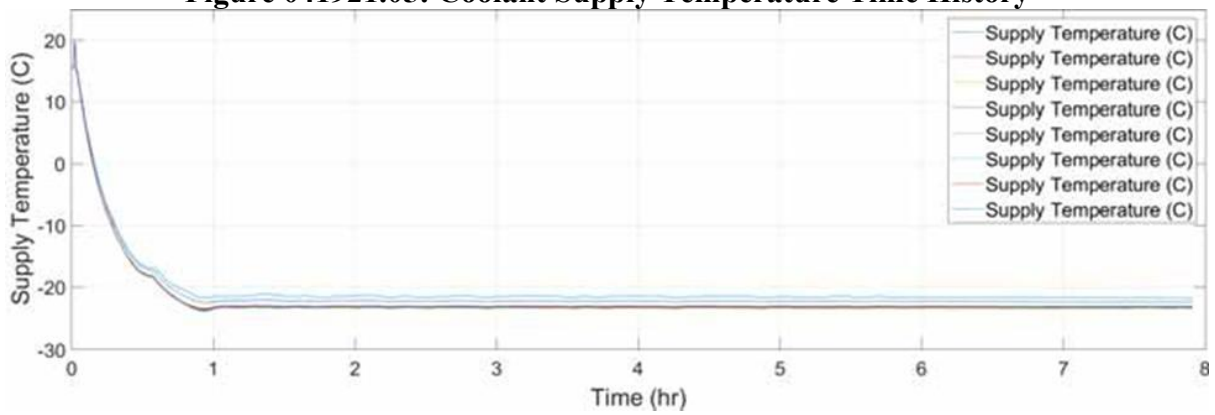

Figure 041921.06: Skin Temperature Time History

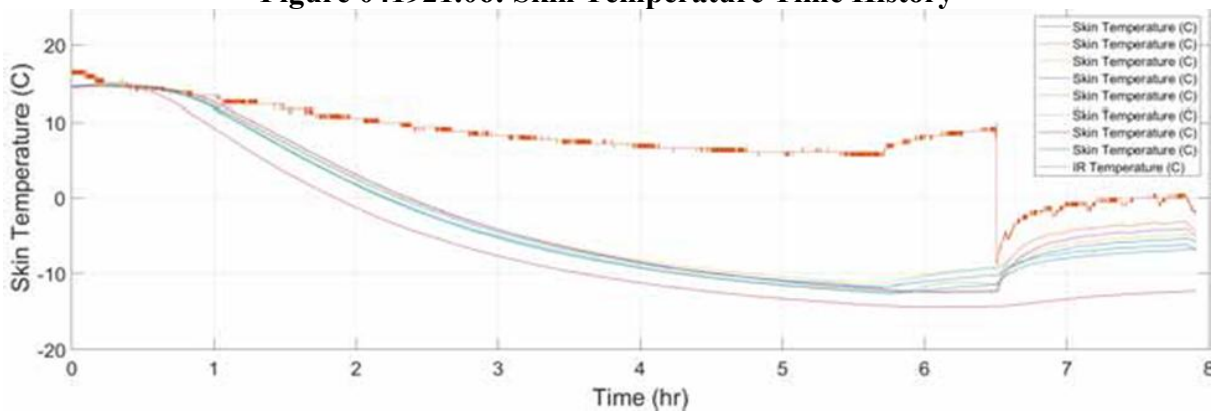

Figure 041921.07: Floor Temperature Time History

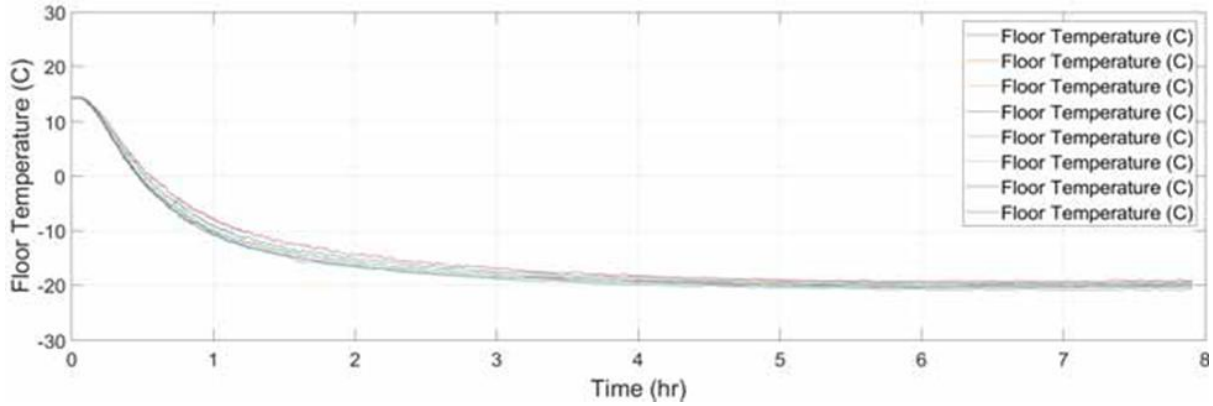

Figure 041921.08: Skin Temperature Slope Time History

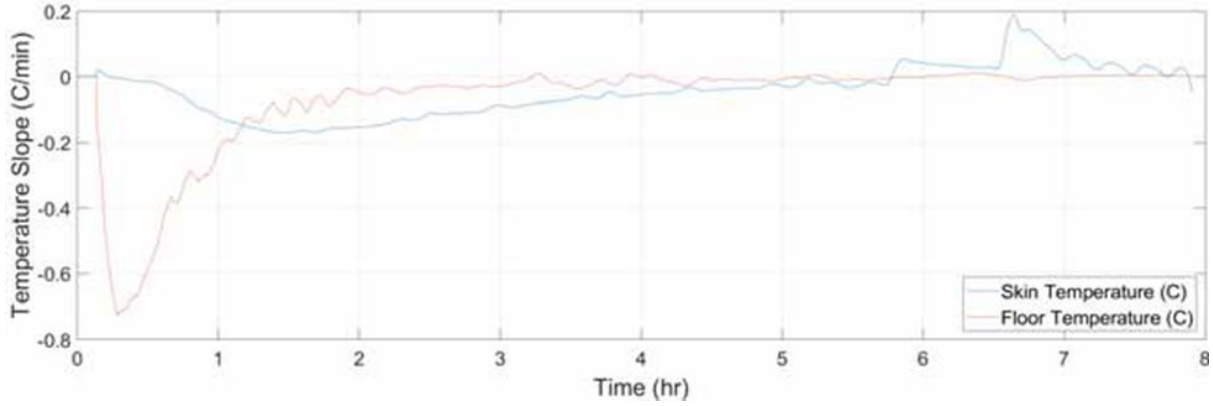

Figure 041921.09: RMS Height Evolution

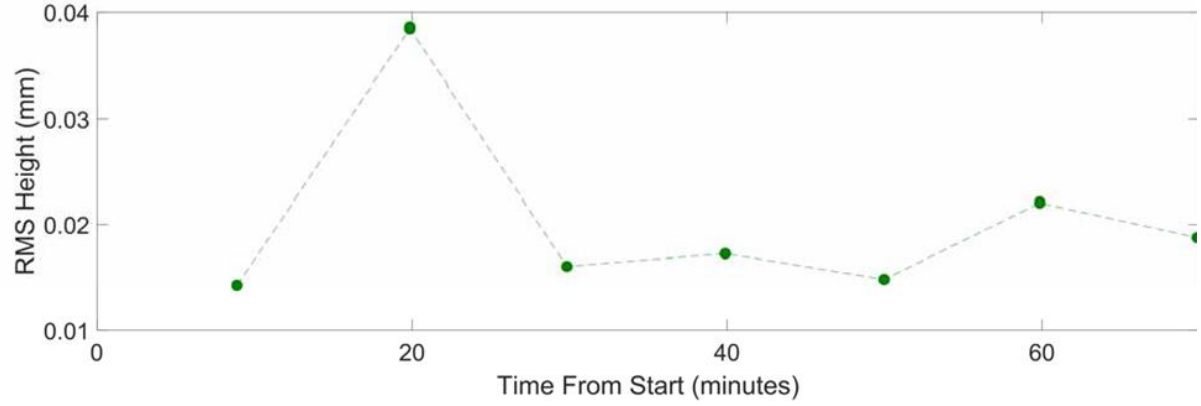

Figure 041921.10: Skewness Evolution

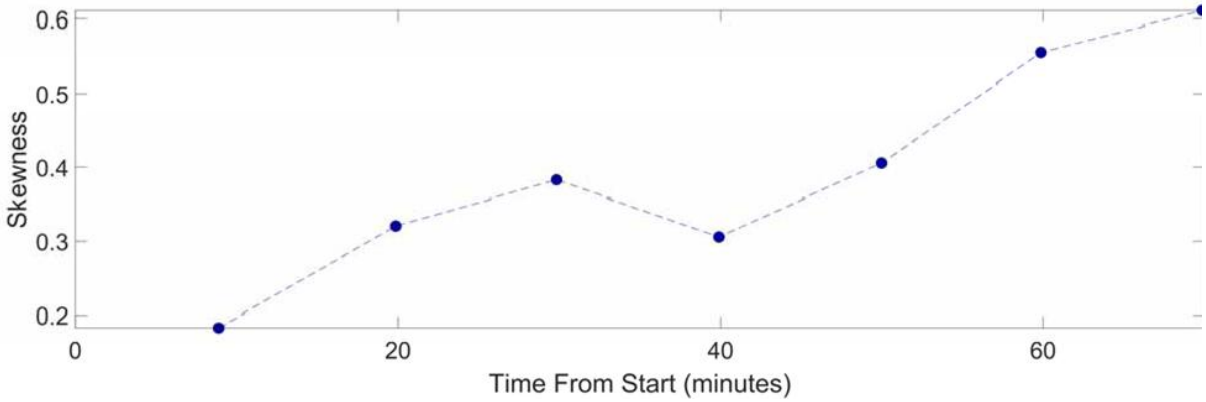

Figure 041921.11: Peak to Valley Evolution

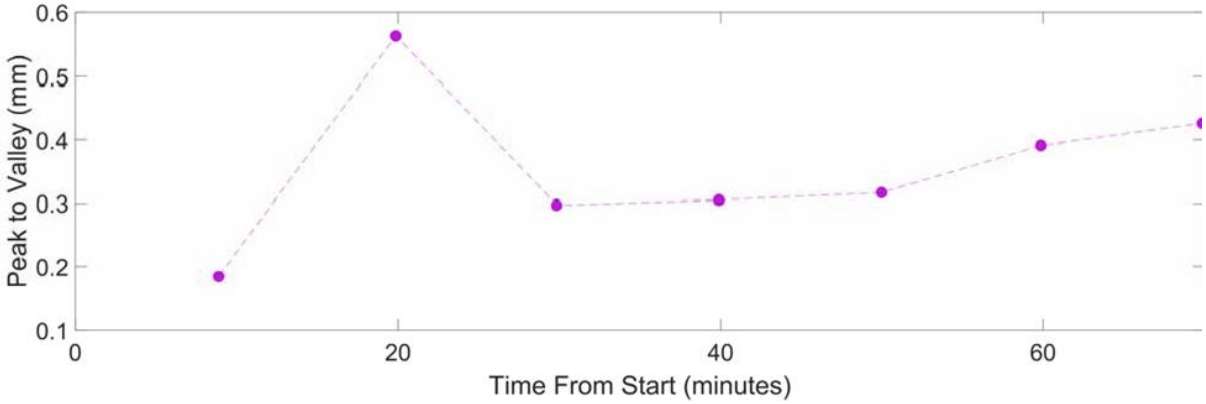

Figure 041921.12: Equivalent Roughness Evolution

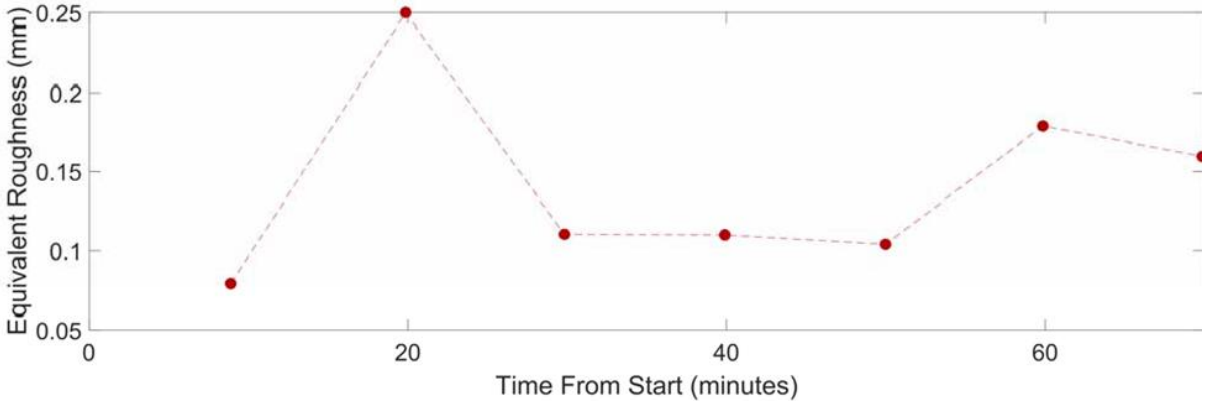

Table 041921.02: Summary of Roughness Parameters

Time (min.)	RMS (mm)	Skewness	Peak to Valley (mm)	ks,Flack-Schultz (mm)
8.8776	0.0142	0.1829	0.1840	0.0790
19.8609	0.0386	0.3208	0.5646	0.2501
29.8276	0.0160	0.3828	0.2971	0.1104
39.8943	0.0172	0.3059	0.3049	0.1100
49.9776	0.0147	0.4056	0.3161	0.1041
59.8609	0.0221	0.5551	0.3913	0.1789
69.8609	0.0187	0.6112	0.4267	0.1596

Figure 041921.13: Frost Topography at 00:08:52

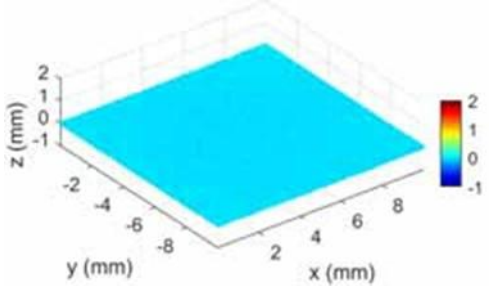

Figure 041921.14: Frost Topography at 00:19:51

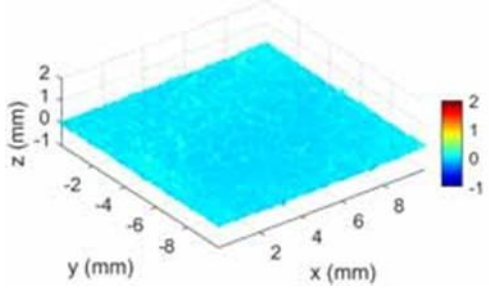

Figure 041921.15: Frost Topography at 00:29:49

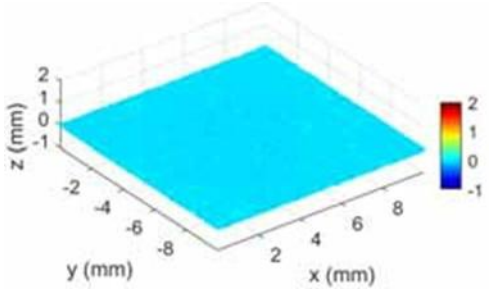

Figure 041921.16: Frost Topography at 00:39:53

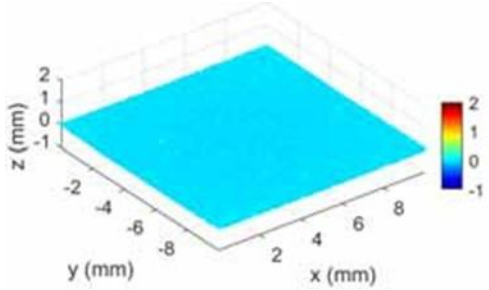

Figure 041921.17: Frost Topography at 00:49:58

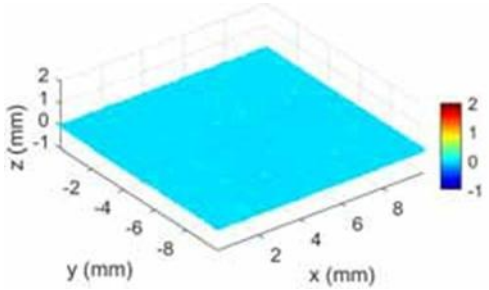

Figure 041921.18: Frost Topography at 00:59:51

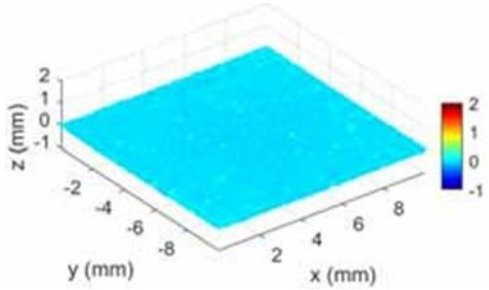

Figure 041921.19: Frost Topography at 01:09:51

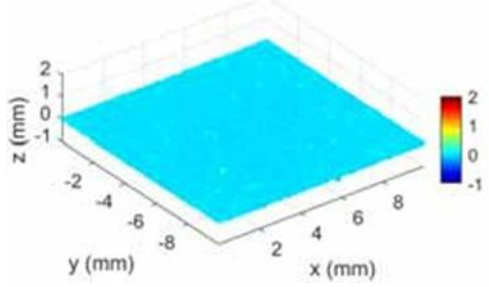

CAFF Conditions Report – Case Date: 042121

Table 042121.01: Summary of Measured Test Variables

Variable	Mean	St. Dev.	Rand. Unc.
T_air (C)	4.2797	0.2824	0.0097
Rh (%)	79.5298	5.0511	0.1734
Omega (kg_v/kg_da)	0.00410203	0.00032543	0.00001117
V_air (m/s)	1.5426	0.1618	0.0056
T_skin (C)	-8.4236	1.0844	0.0372
T_floor (C)	-20.4092	0.0328	0.0011

Figure 042121.01: Temperature and Voltage Control Time History

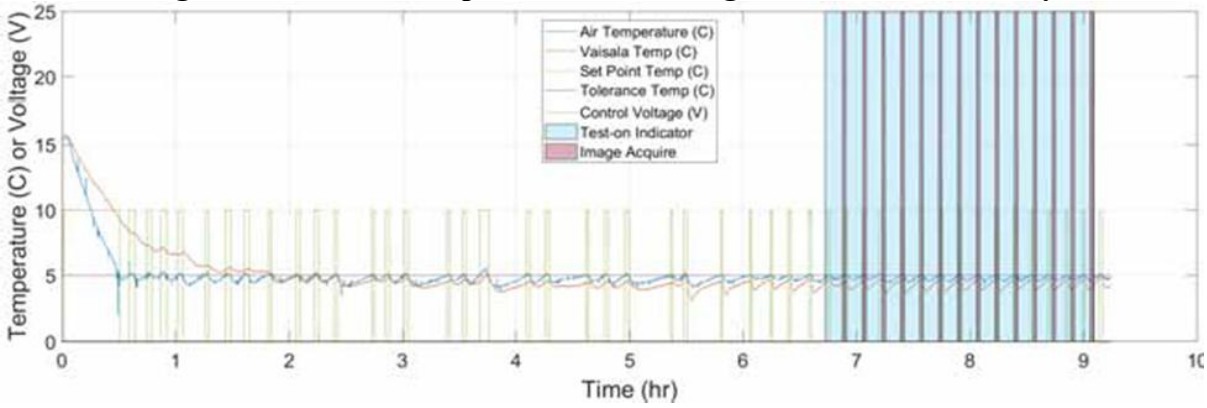

Figure 042121.02: Relative Humidity Time History

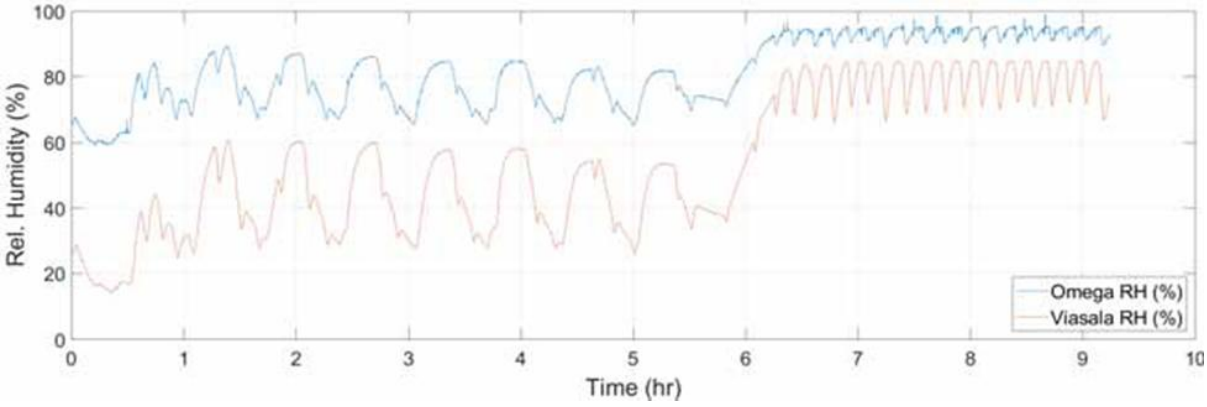

Figure 042121.03: Velocity Time History

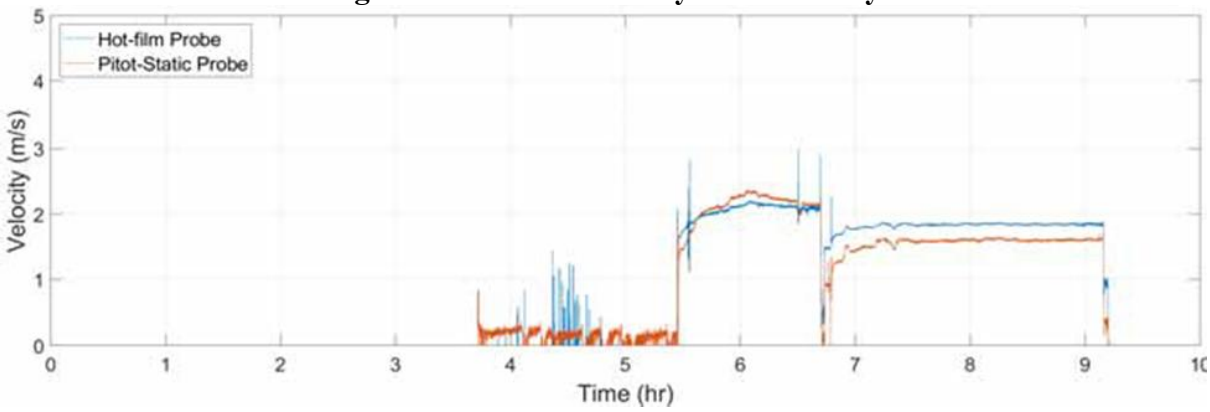

Figure 042121.04: Coolant Return Temperature Time History

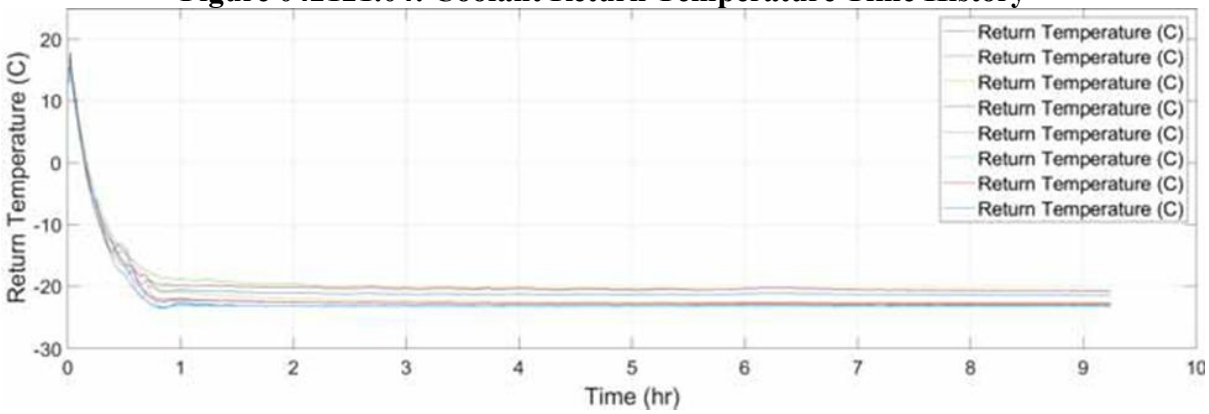

Figure 042121.05: Coolant Supply Temperature Time History

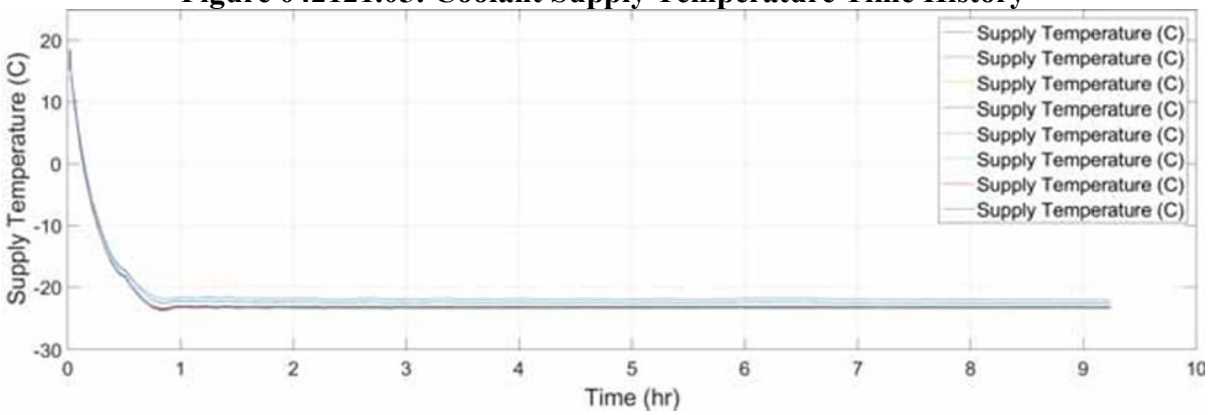

Figure 042121.06: Skin Temperature Time History

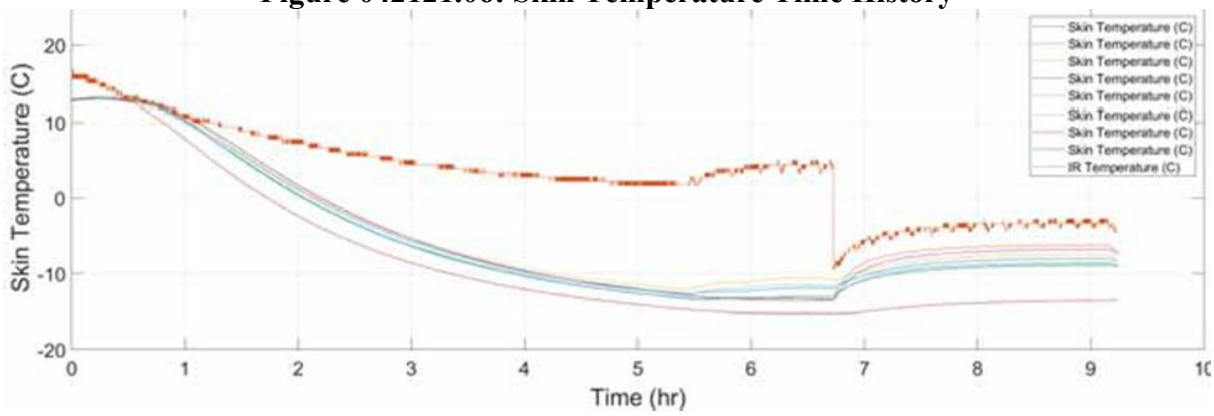

Figure 042121.07: Floor Temperature Time History

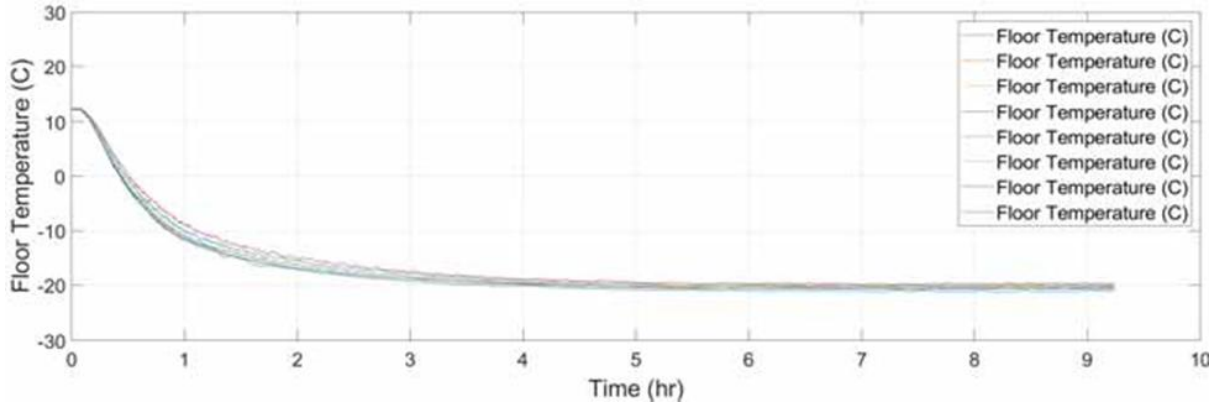

Figure 042121.08: Skin Temperature Slope Time History

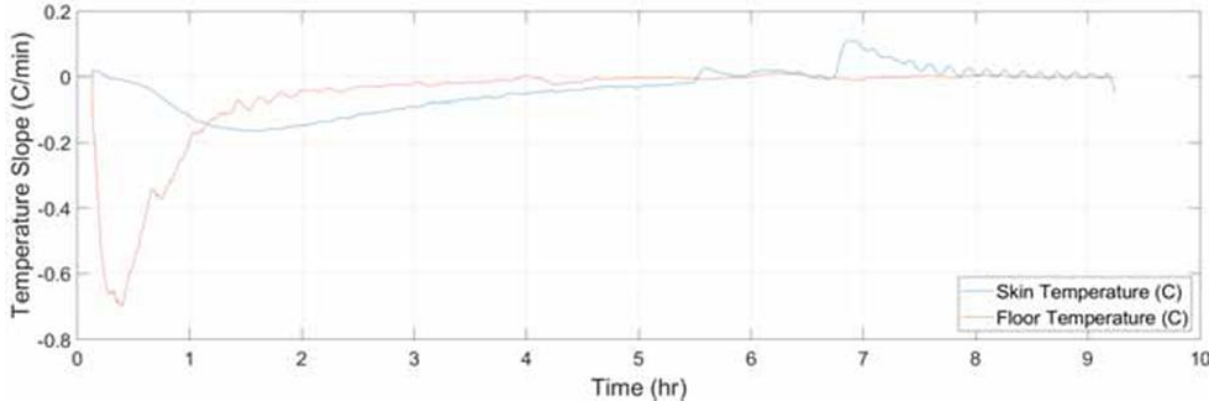

Figure 042121.09: RMS Height Evolution

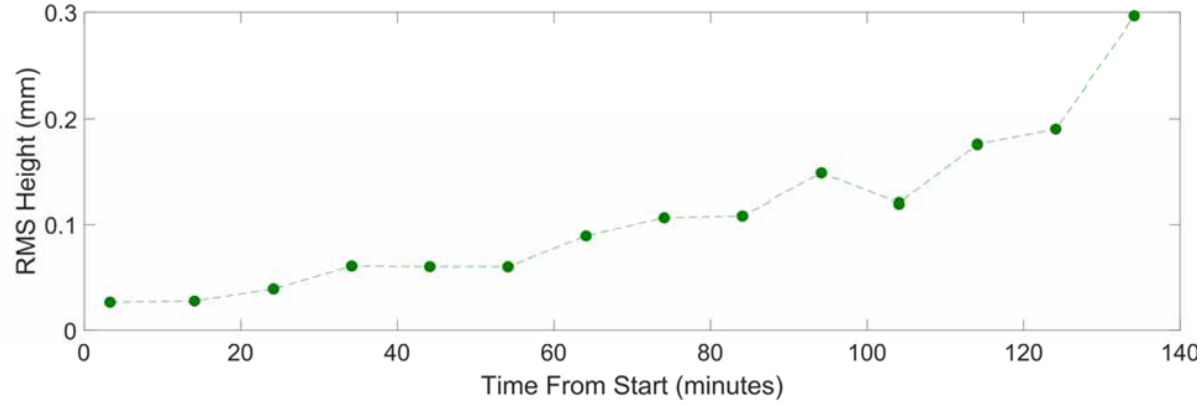

Figure 042121.10: Skewness Evolution

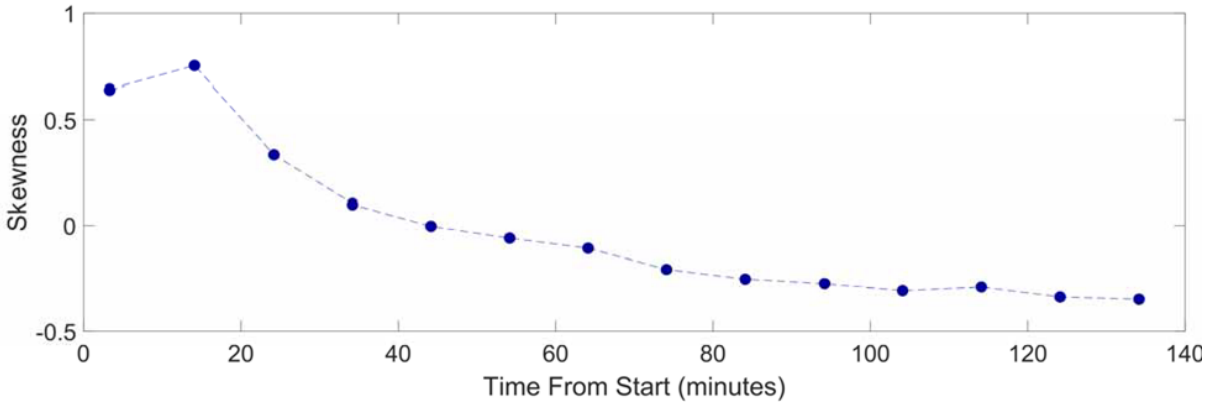

Figure 042121.11: Peak to Valley Evolution

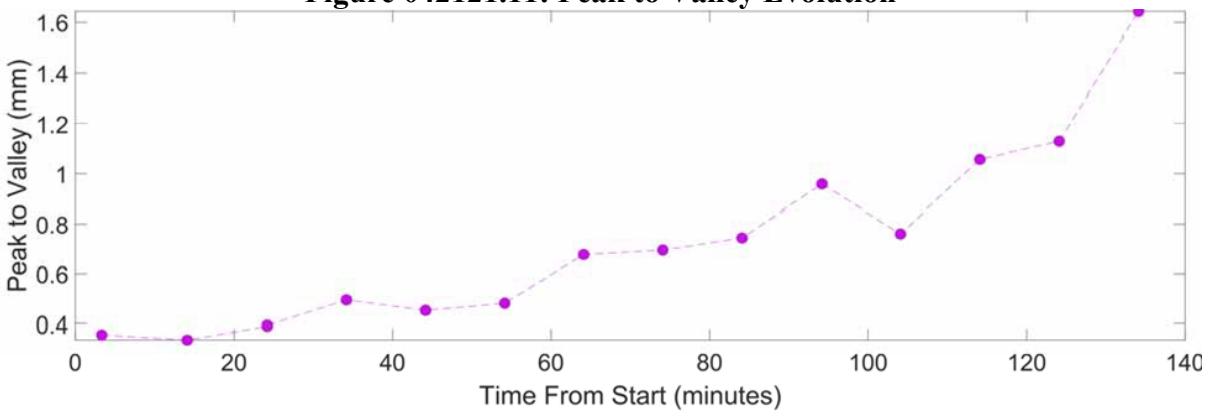

Figure 042121.12: Equivalent Roughness Evolution

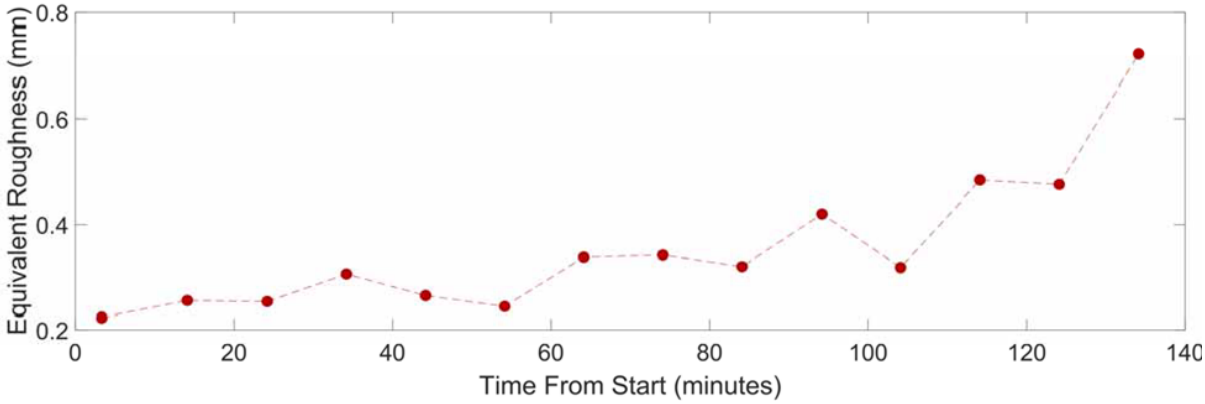

Table 042121.02: Summary of Roughness Parameters

Time (min.)	RMS (mm)	Skewness	Peak to Valley (mm)	ks,Flack-Schultz (mm)
3.3086	0.0255	0.6428	0.3579	0.2228
14.0919	0.0266	0.7563	0.3374	0.2545
24.1919	0.0384	0.3346	0.3928	0.2526
34.1752	0.0605	0.1001	0.4951	0.3052
44.1586	0.0599	-0.0042	0.4530	0.2639
54.1419	0.0598	-0.0600	0.4812	0.2433
64.1086	0.0891	-0.1082	0.6777	0.3375
74.0919	0.1066	-0.2104	0.6956	0.3417
84.0919	0.1082	-0.2567	0.7443	0.3193
94.1752	0.1484	-0.2784	0.9586	0.4205
104.0919	0.1197	-0.3121	0.7599	0.3178
114.0919	0.1757	-0.2941	1.0580	0.4831
124.1086	0.1902	-0.3423	1.1298	0.4747
134.1252	0.2966	-0.3535	1.6451	0.7228

Figure 042121.13: Frost Topography at 00:09:01

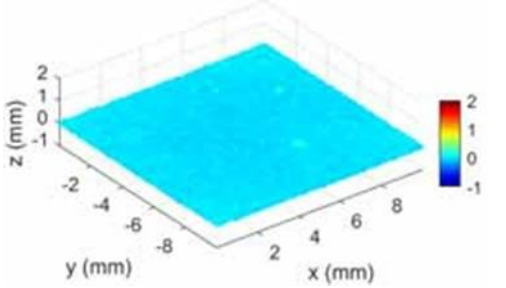

Figure 042121.14: Frost Topography at 00:19:48

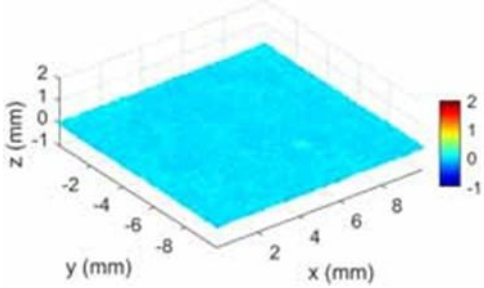

Figure 042121.15: Frost Topography at 00:29:54

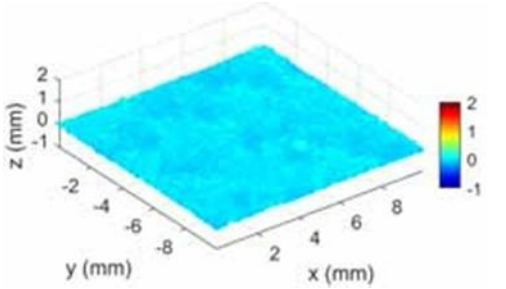

Figure 042121.16: Frost Topography at 00:39:53

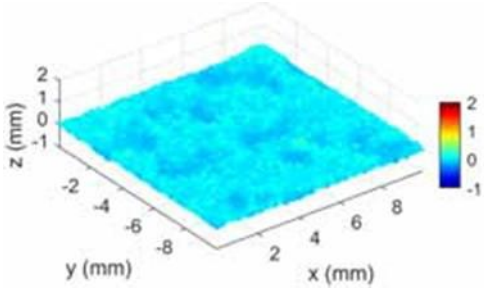

Figure 042121.17: Frost Topography at 00:49:52

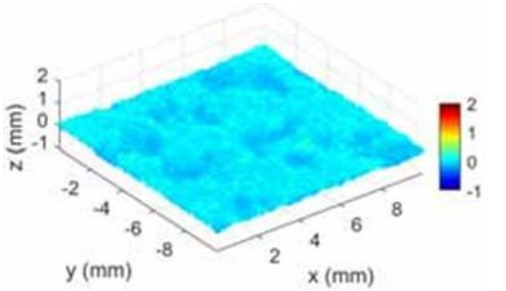

Figure 042121.18: Frost Topography at 00:59:51

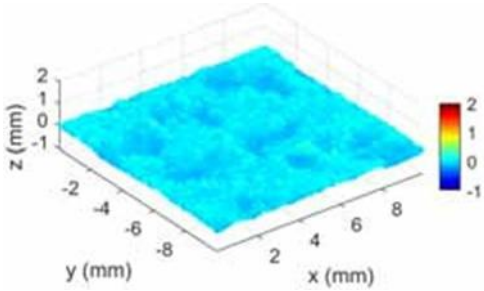

Figure 042121.19: Frost Topography at 01:09:49

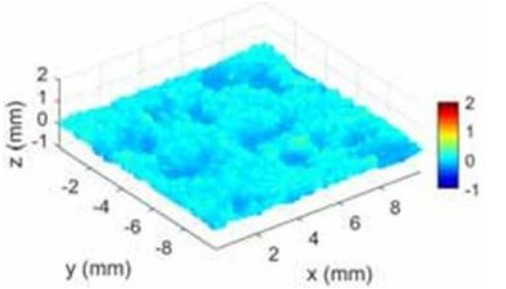

Figure 042121.20: Frost Topography at 01:19:48

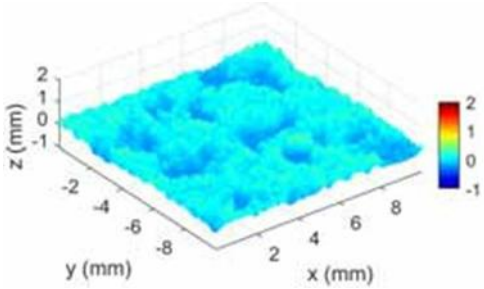

Figure 042121.21: Frost Topography at 01:29:48

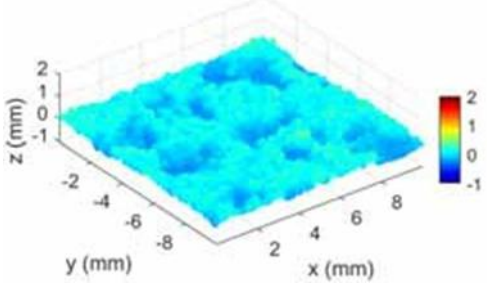

Figure 042121.22: Frost Topography at 01:39:53

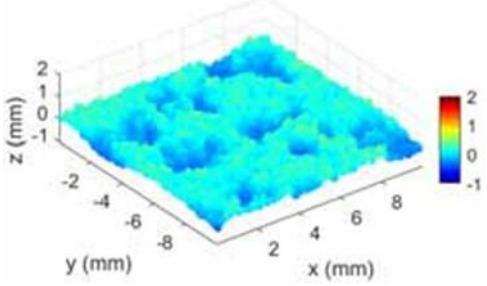

Figure 042121.23: Frost Topography at 01:49:48

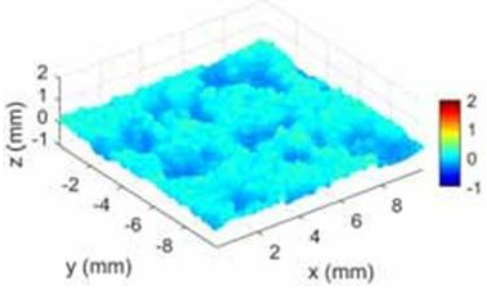

Figure 042121.24: Frost Topography at 01:59:48

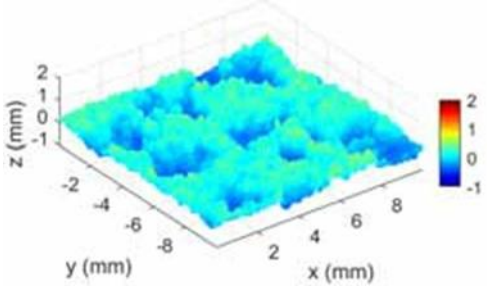

Figure 042121.25: Frost Topography at 02:09:49

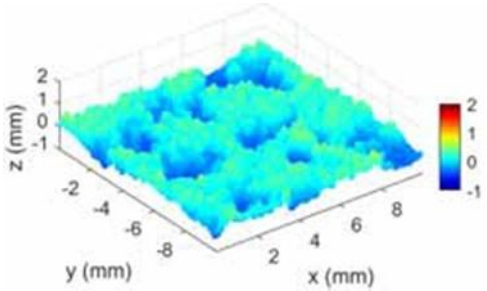

Figure 042121.26: Frost Topography at 02:19:50

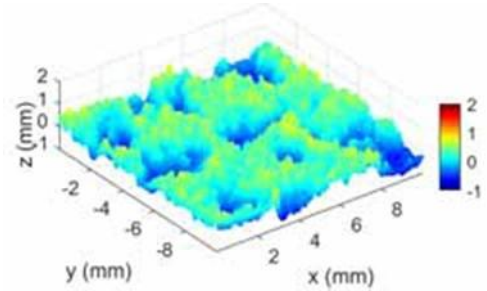

CAFF Conditions Report – Case Date: 042321

Table 042321.01: Summary of Measured Test Variables

Variable	Mean	St. Dev.	Rand. Unc.
T_air (C)	9.2095	0.3906	0.0136
Rh (%)	80.7735	4.0900	0.1425
Omega (kg_v/kg_da)	0.00597330	0.00037449	0.00001304
V_air (m/s)	1.4767	0.0565	0.0020
T_skin (C)	-5.9041	1.0755	0.0375
T_floor (C)	-19.9743	0.0650	0.0023

Figure 042321.01: Temperature and Voltage Control Time History

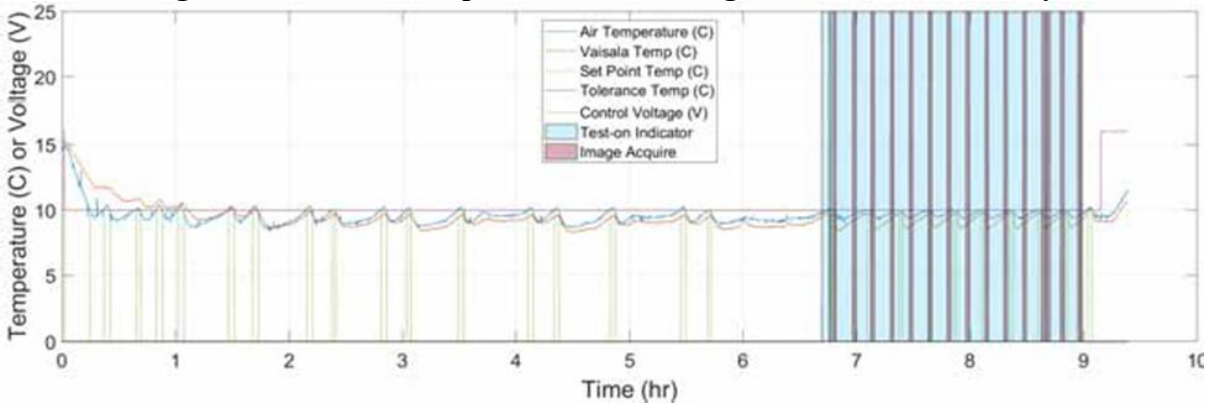

Figure 042321.02: Relative Humidity Time History

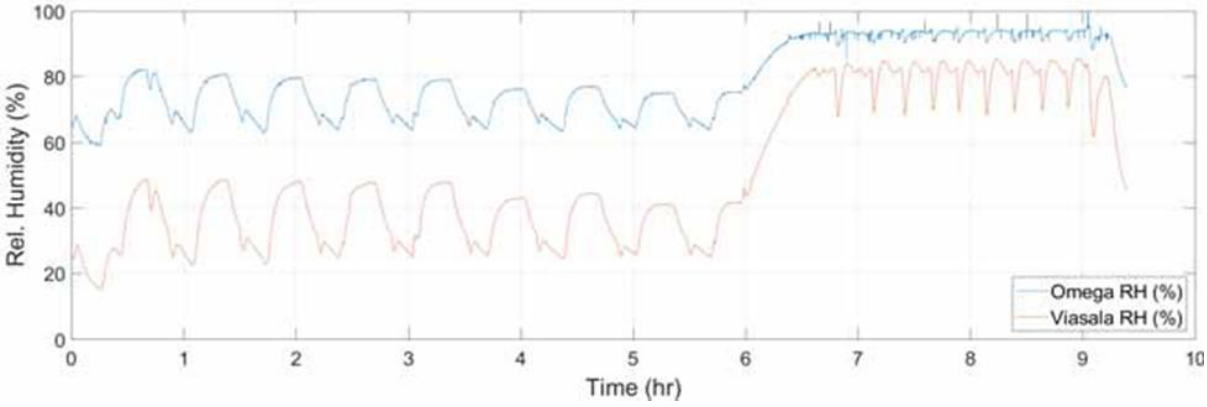

Figure 042321.03: Velocity Time History

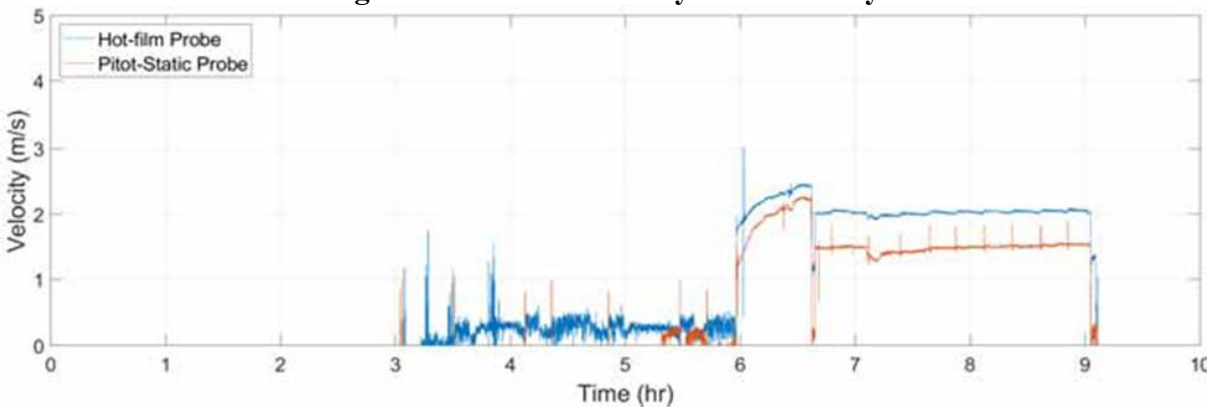

Figure 042321.04: Coolant Return Temperature Time History

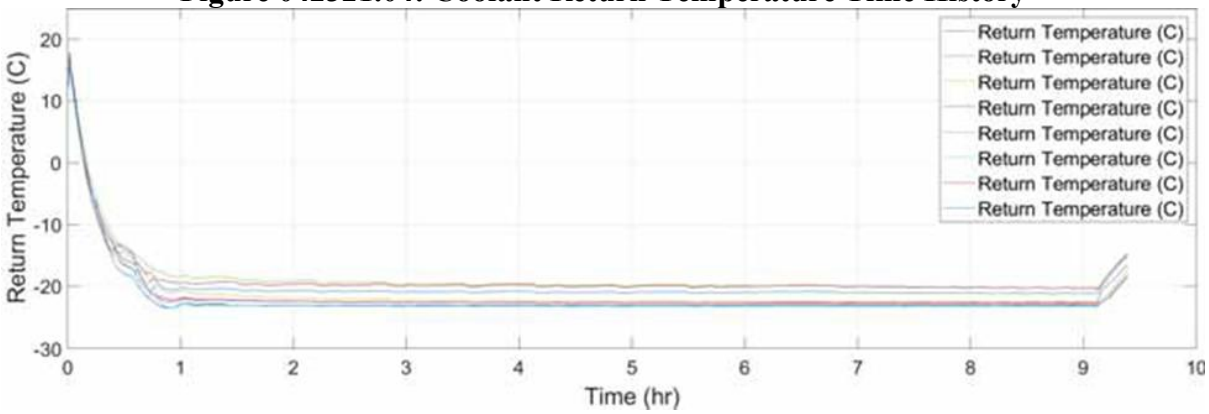

Figure 042321.05: Coolant Supply Temperature Time History

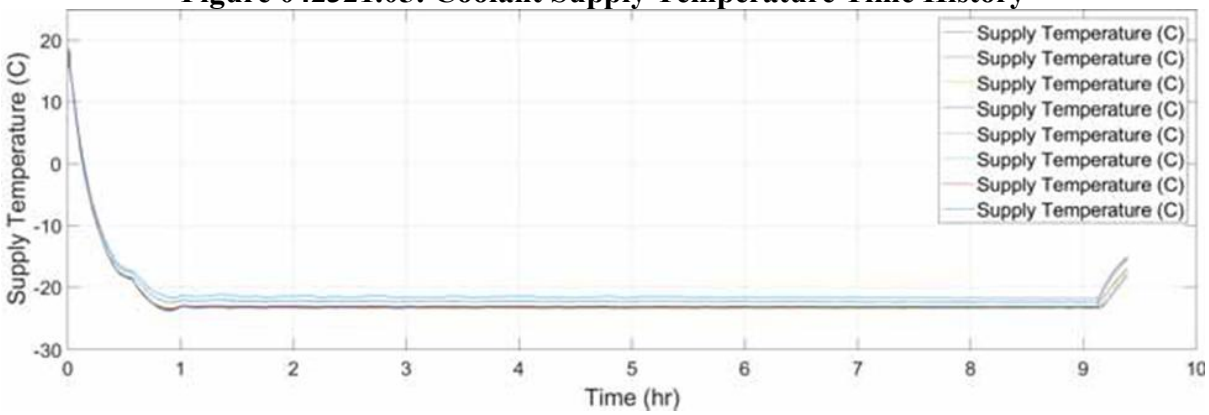

Figure 042321.06: Skin Temperature Time History

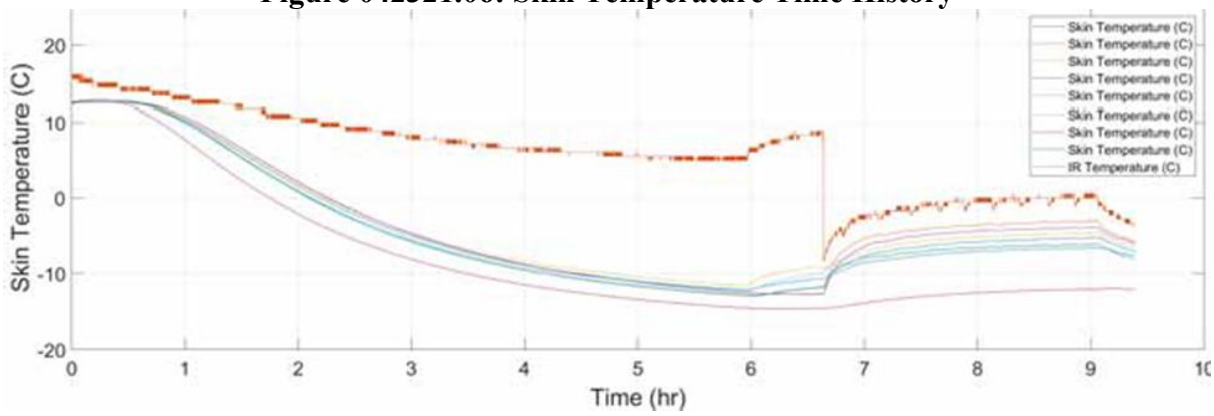

Figure 042321.07: Floor Temperature Time History

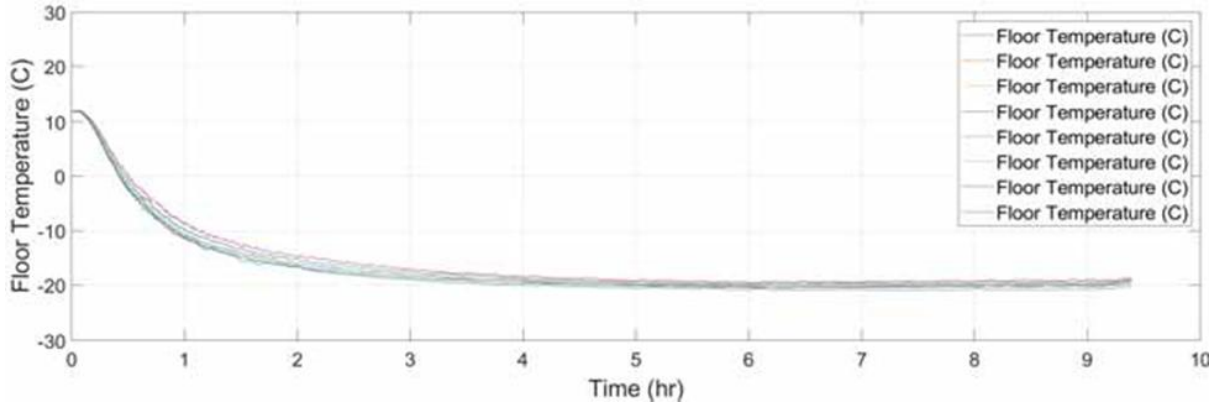

Figure 042321.08: Skin Temperature Slope Time History

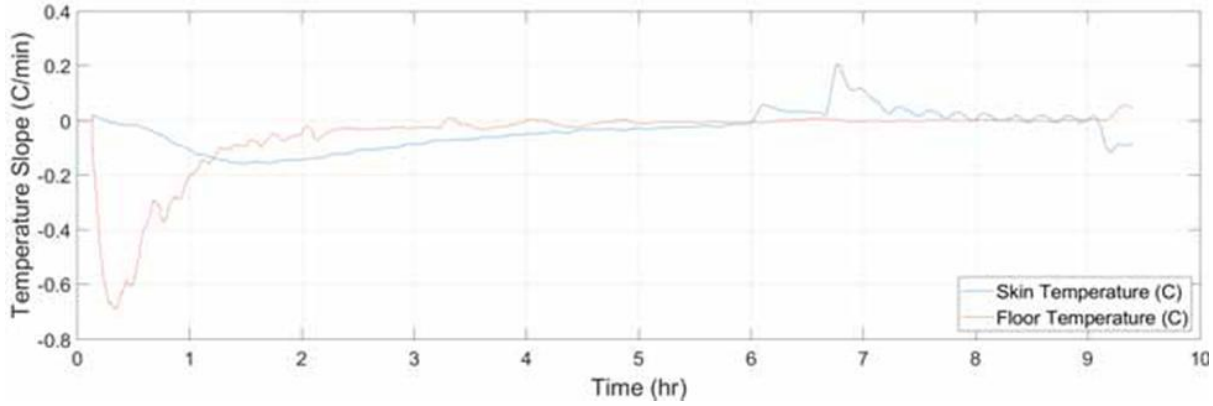

Figure 042321.09: RMS Height Evolution

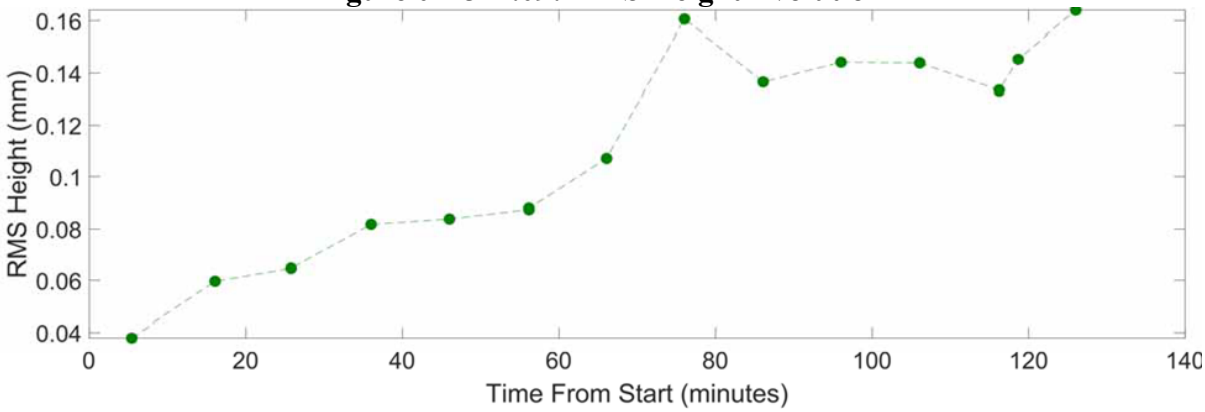

Figure 042321.10: Skewness Evolution

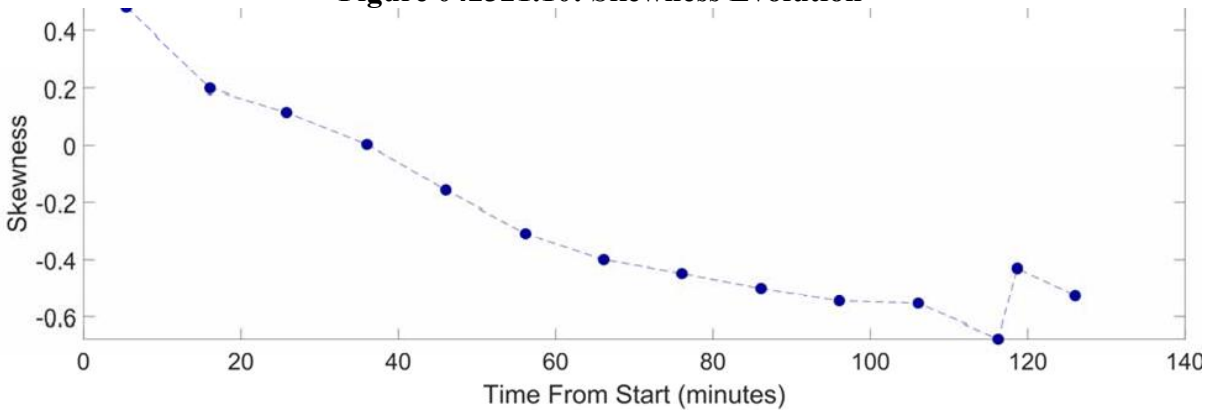

Figure 042321.11: Peak to Valley Evolution

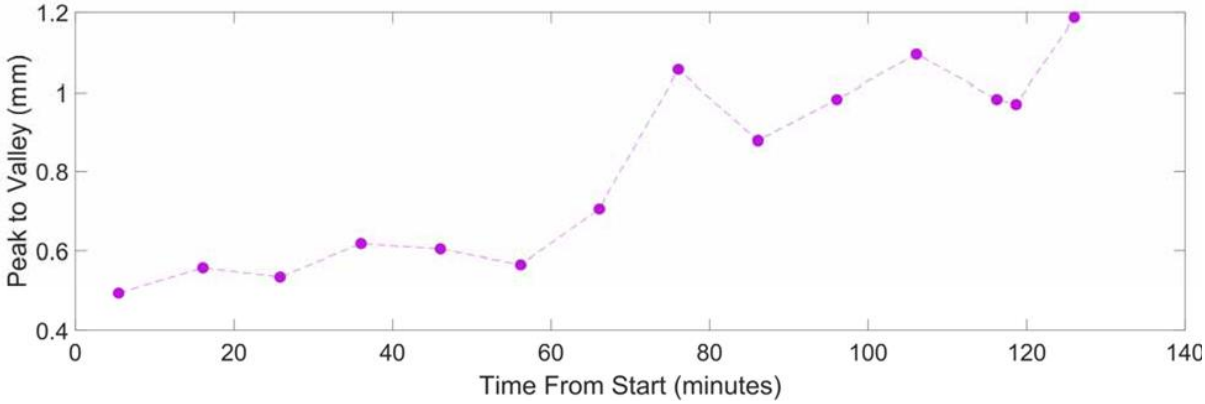

Figure 042321.12: Equivalent Roughness Evolution

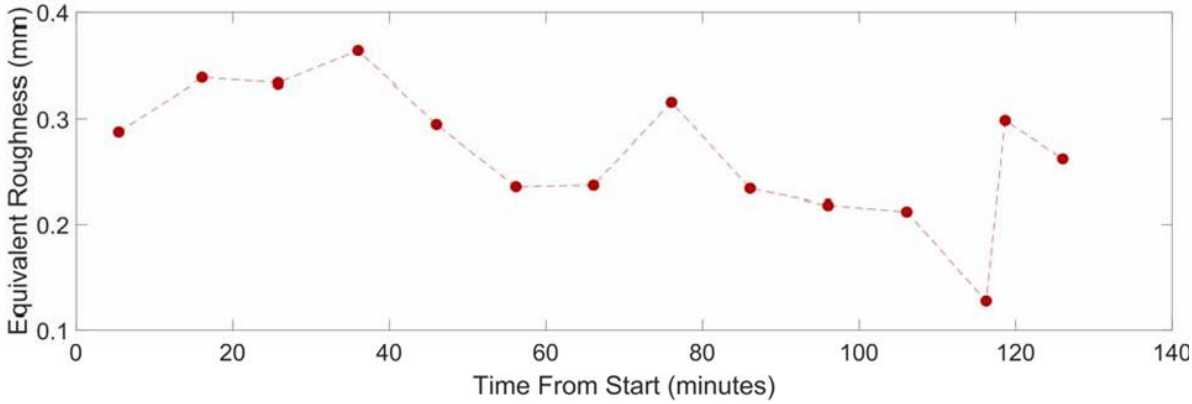

Table 042321.02: Summary of Roughness Parameters

Time (min.)	RMS (mm)	Skewness	Peak to Valley (mm)	ks,Flack-Schultz (mm)
5.4332	0.0378	0.4820	0.4915	0.2874
16.0666	0.0596	0.1996	0.5568	0.3388
25.7999	0.0647	0.1175	0.5329	0.3338
36.0166	0.0818	0.0041	0.6177	0.3646
46.0332	0.0840	-0.1563	0.6041	0.2947
56.1666	0.0876	-0.3069	0.5642	0.2350
66.0999	0.1072	-0.3988	0.7072	0.2365
76.0499	0.1607	-0.4471	1.0573	0.3162
86.0999	0.1365	-0.5006	0.8782	0.2336
96.0499	0.1443	-0.5434	0.9832	0.2183
106.0832	0.1440	-0.5522	1.0968	0.2122
116.2332	0.1334	-0.6751	0.9836	0.1267
118.6666	0.1454	-0.4294	0.9707	0.2986
126.0166	0.1642	-0.5254	1.1869	0.2620

Figure 042321.13: Frost Topography at 00:05:25

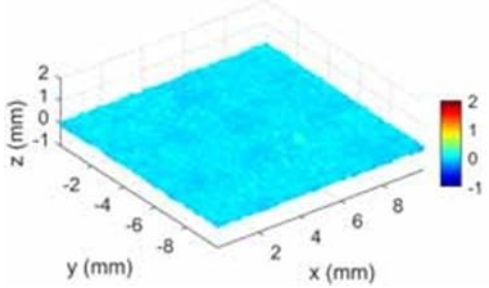

Figure 042321.14: Frost Topography at 00:16:03

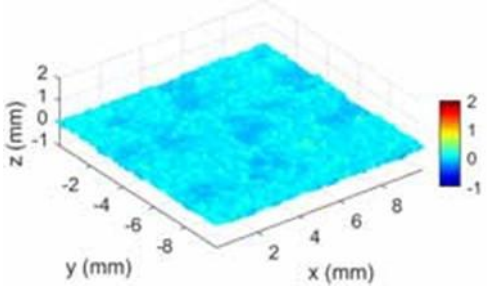

Figure 042321.15: Frost Topography at 00:25:47

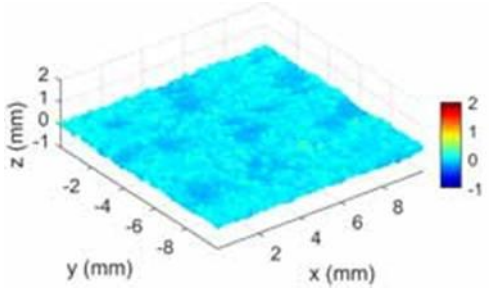

Figure 042321.16: Frost Topography at 00:36:00

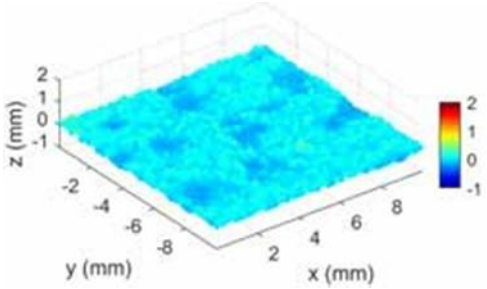

Figure 042321.17: Frost Topography at 00:46:01

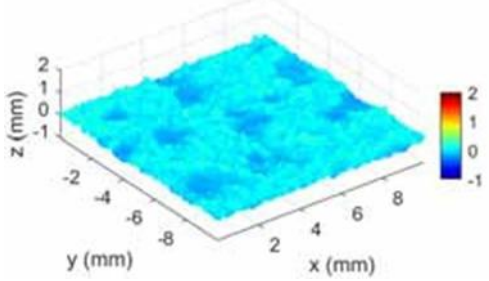

Figure 042321.18: Frost Topography at 00:56:09

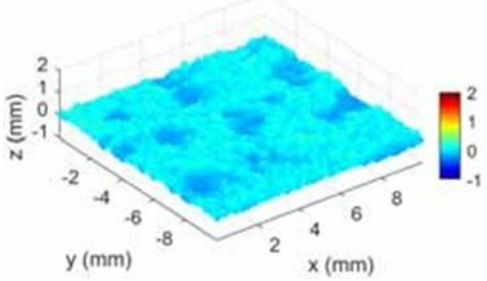

Figure 042321.19: Frost Topography at 01:06:05

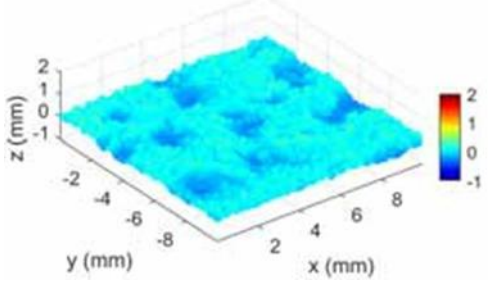

Figure 042321.20: Frost Topography at 01:16:02

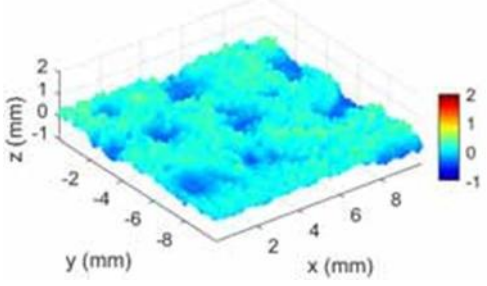

Figure 042321.21: Frost Topography at 01:26:05

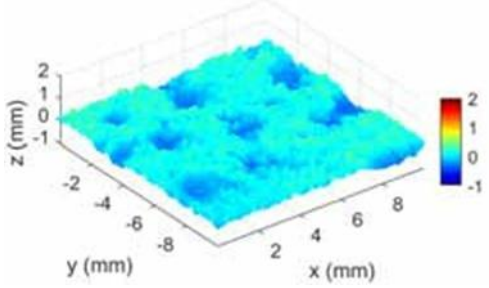

Figure 042321.22: Frost Topography at 01:36:02

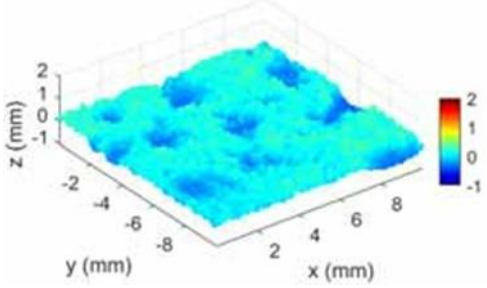

Figure 042321.23: Frost Topography at 01:46:04

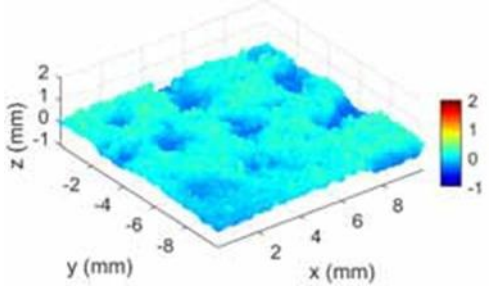

Figure 042321.24: Frost Topography at 01:56:13

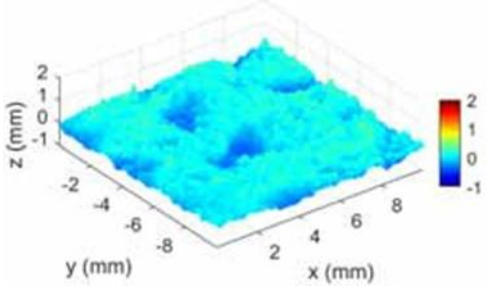

Figure 042321.25: Frost Topography at 01:58:39

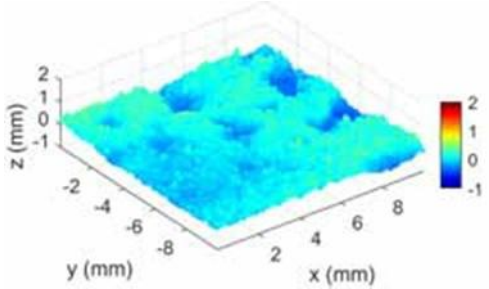

Figure 042321.26: Frost Topography at 02:06:00

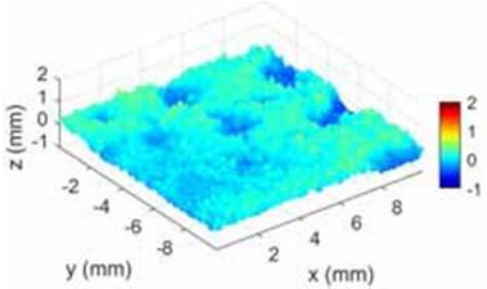

CAFF Conditions Report – Case Date: 042621

Table 042621.01: Summary of Measured Test Variables

Variable	Mean	St. Dev.	Rand. Unc.
T_air (C)	15.2923	0.2463	0.0083
Rh (%)	78.2922	3.8475	0.1299
Omega (kg_v/kg_da)	0.00863022	0.00052626	0.00001777
V_air (m/s)	0.1757	0.0865	0.0029
T_skin (C)	-5.8019	1.1513	0.0389
T_floor (C)	-19.5191	0.0450	0.0015

Figure 042621.01: Temperature and Voltage Control Time History

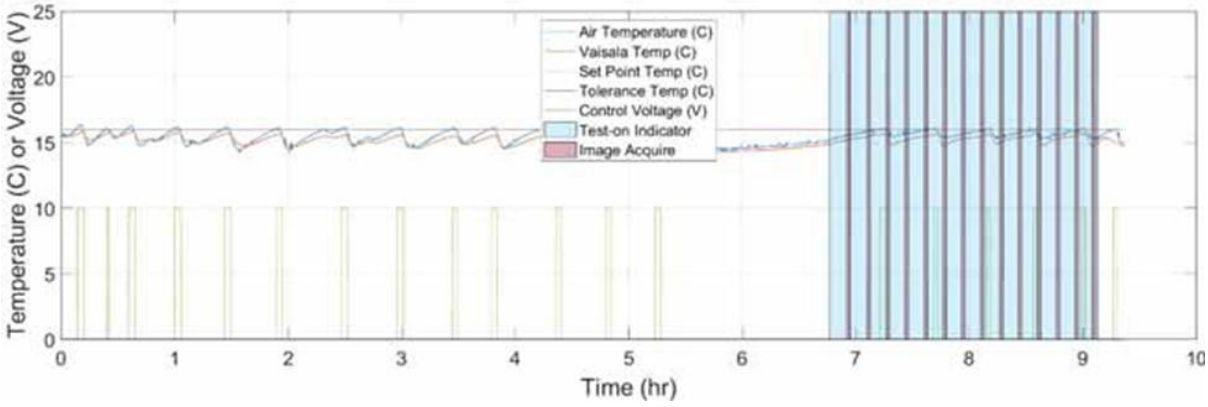

Figure 042621.02: Relative Humidity Time History

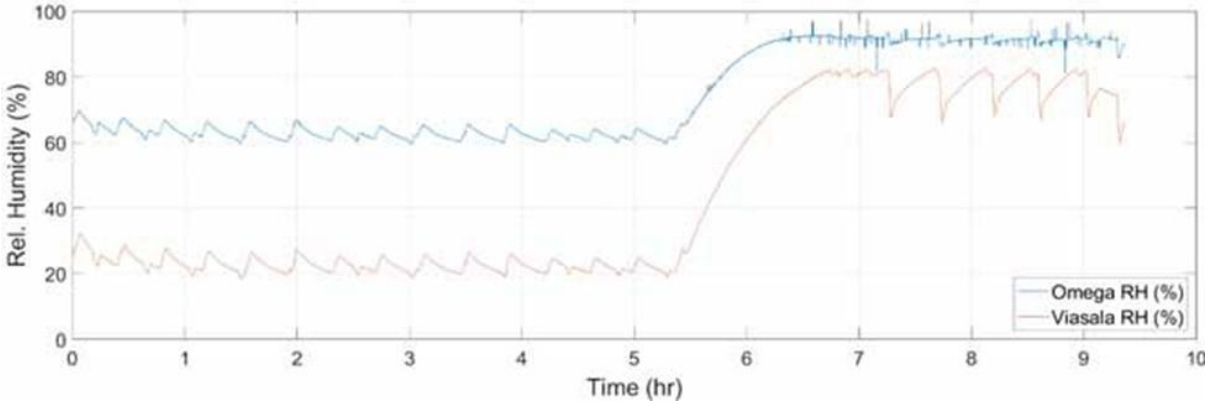

Figure 042621.03: Velocity Time History

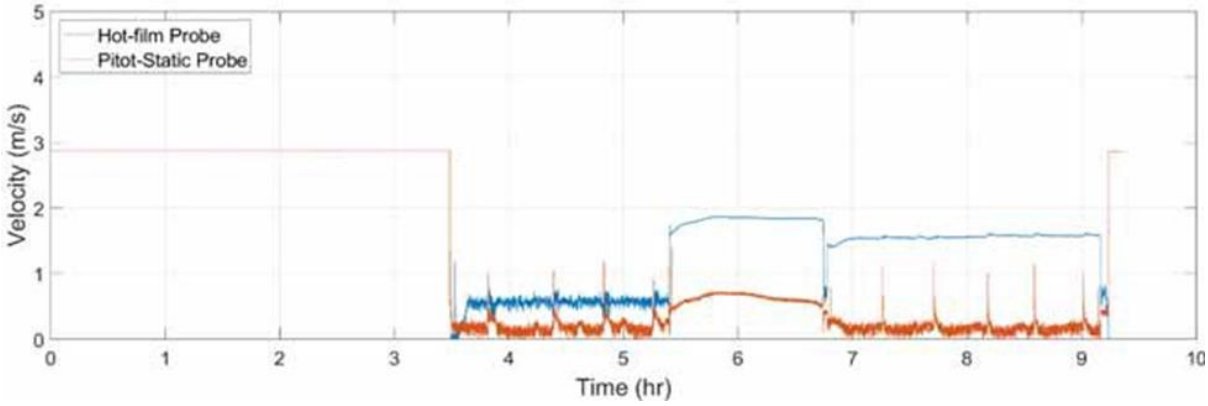

Figure 042621.04: Coolant Return Temperature Time History

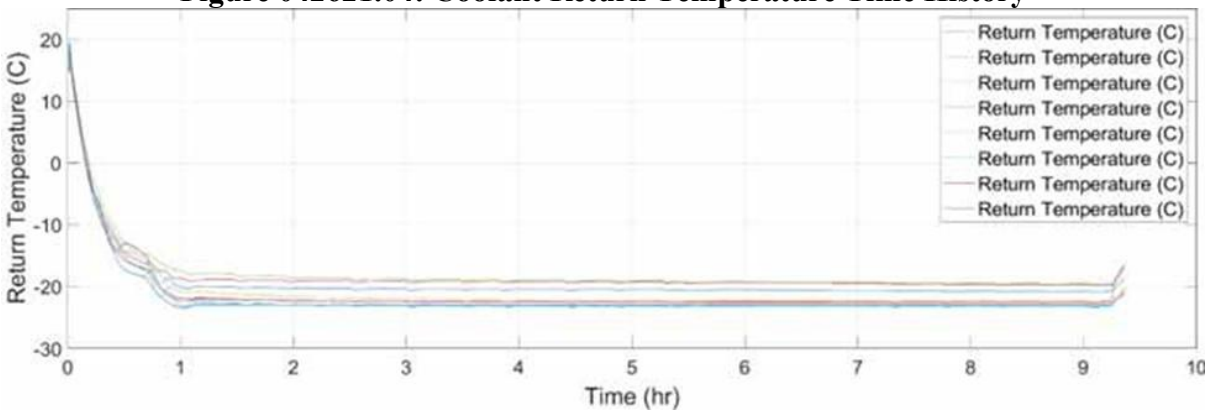

Figure 042621.05: Coolant Supply Temperature Time History

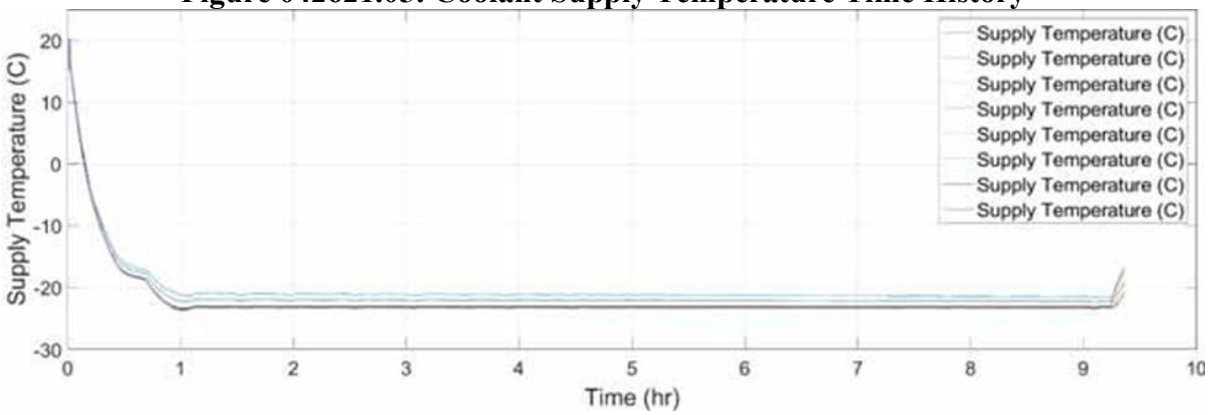

Figure 042621.06: Skin Temperature Time History

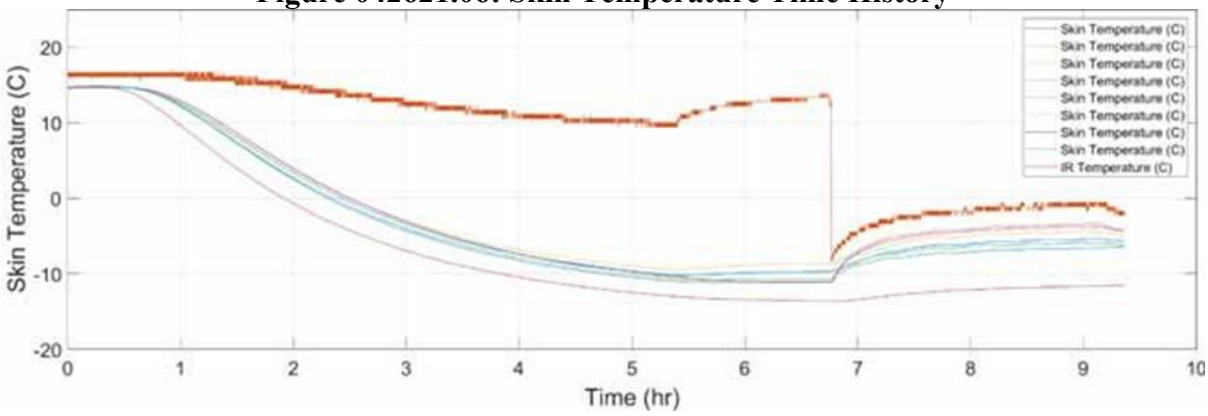

Figure 042621.07: Floor Temperature Time History

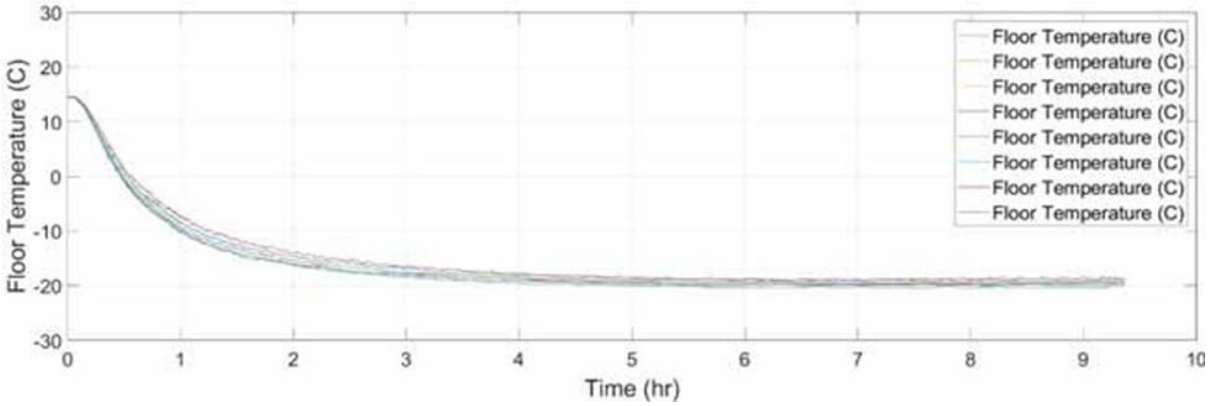

Figure 042621.08: Skin Temperature Slope Time History

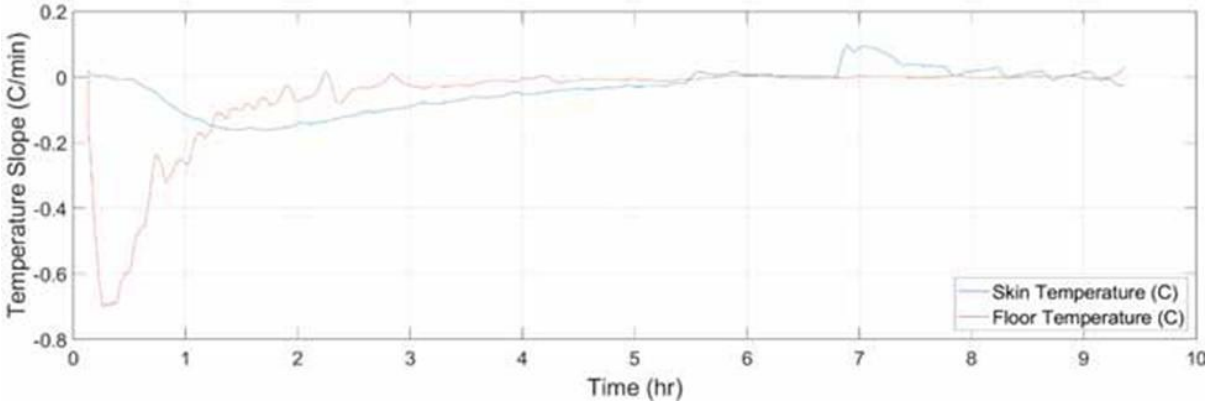

Figure 042621.09: RMS Height Evolution

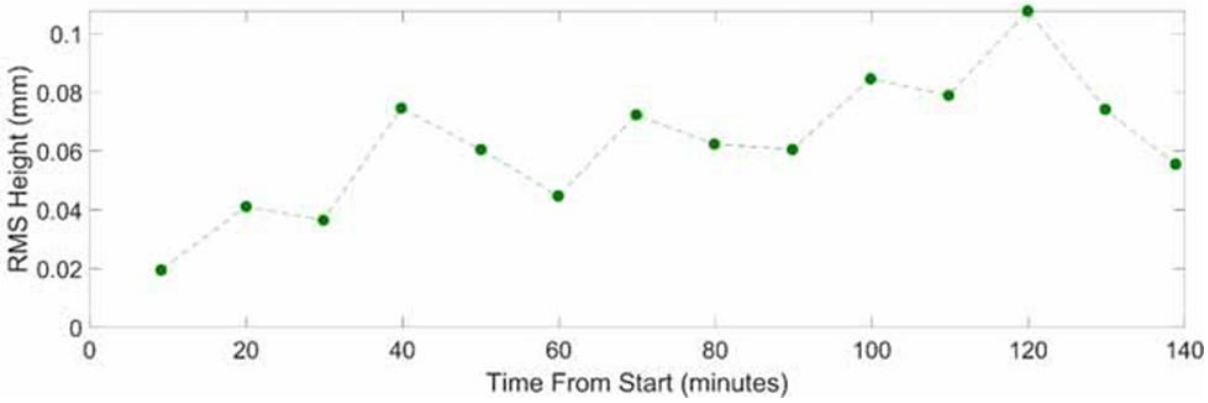

Figure 042621.10: Skewness Evolution

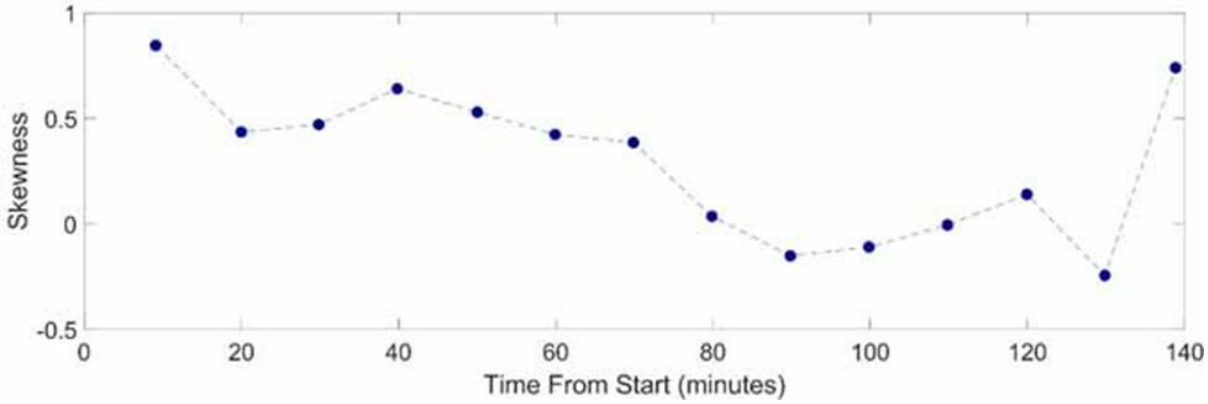

Figure 042621.11: Peak to Valley Evolution

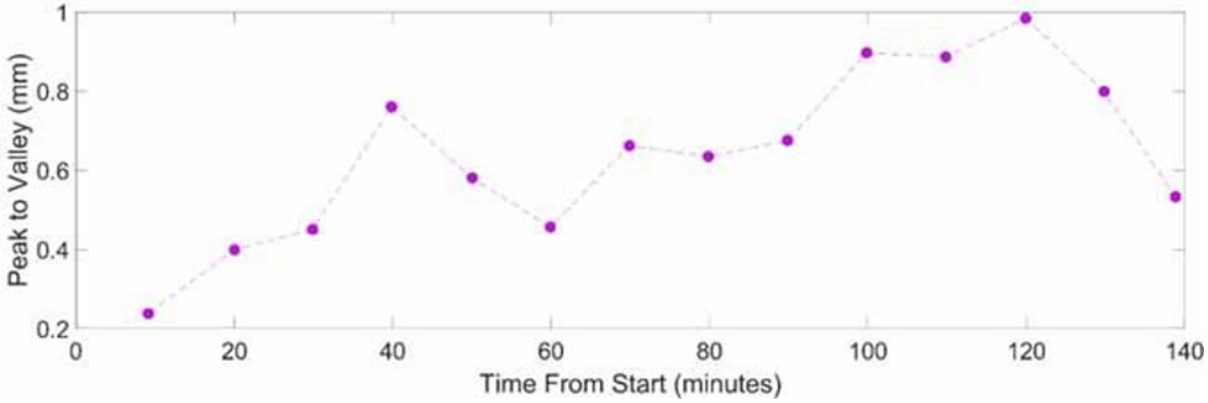

Figure 042621.12: Equivalent Roughness Evolution

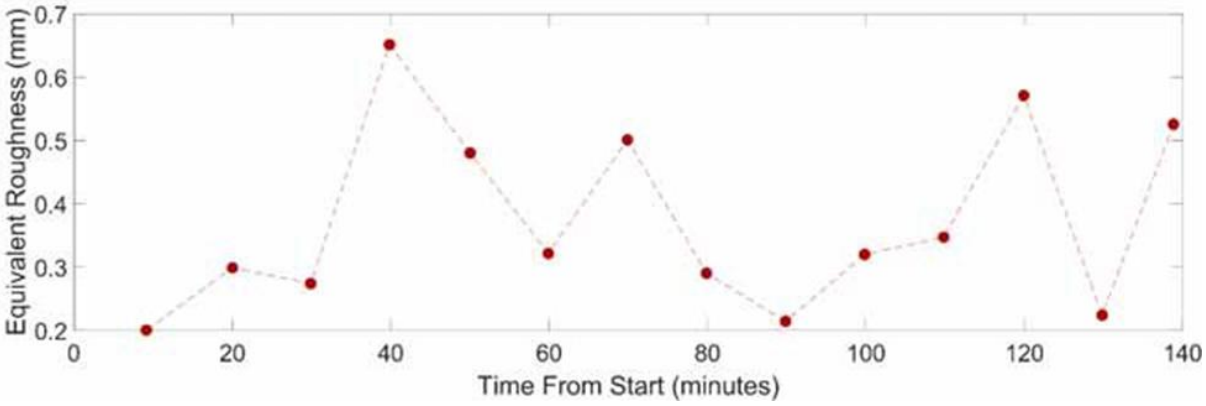

Table 042621.02: Summary of Roughness Parameters

Time (min.)	RMS (mm)	Skewness	Peak to Valley (mm)	ks,Flack-Schultz (mm)
9.1021	0.0195	0.8463	0.2376	0.2004
19.9854	0.0411	0.4353	0.3987	0.2990
29.8521	0.0365	0.4706	0.4500	0.2741
39.8188	0.0746	0.6410	0.7603	0.6514
50.0021	0.0606	0.5296	0.5807	0.4804
59.8854	0.0447	0.4236	0.4559	0.3216
69.8688	0.0723	0.3856	0.6618	0.5011
79.8521	0.0624	0.0358	0.6344	0.2903
89.8354	0.0606	-0.1515	0.6749	0.2143
99.8354	0.0846	-0.1094	0.8968	0.3199
109.8188	0.0790	-0.0052	0.8861	0.3474
119.9188	0.1077	0.1400	0.9839	0.5711
129.8354	0.0742	-0.2439	0.7988	0.2242
138.8354	0.0556	0.7401	0.5328	0.5257

Figure 042621.13: Frost Topography at 00:09:06

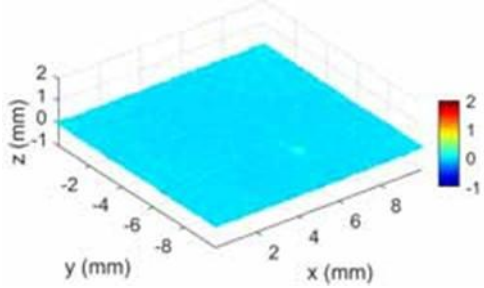

Figure 042621.14: Frost Topography at 00:19:59

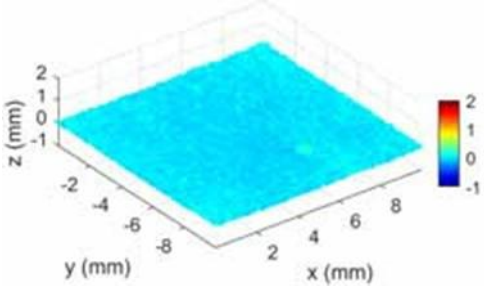

Figure 042621.15: Frost Topography at 00:29:51

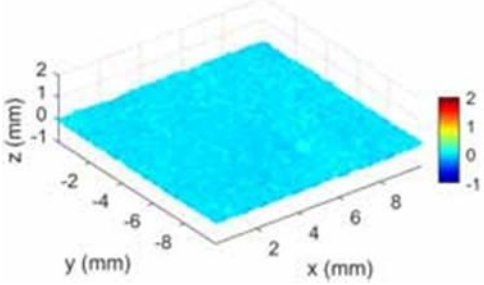

Figure 042621.16: Frost Topography at 00:39:49

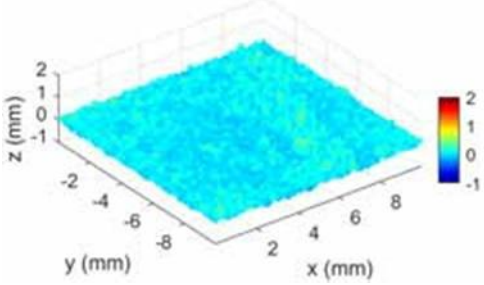

Figure 042621.17: Frost Topography at 00:50:00

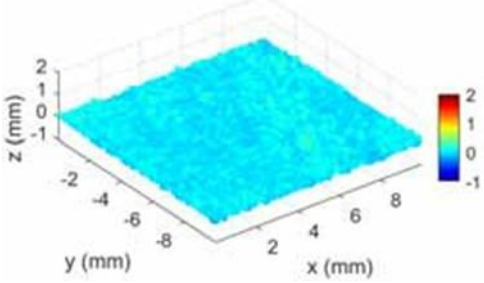

Figure 042621.18: Frost Topography at 00:59:53

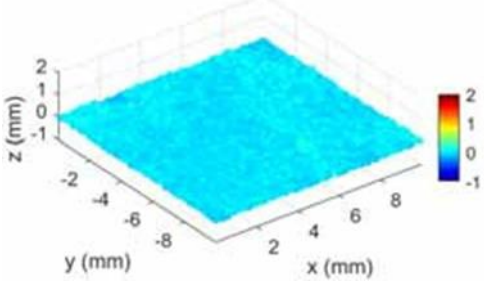

Figure 042621.19: Frost Topography at 01:09:52

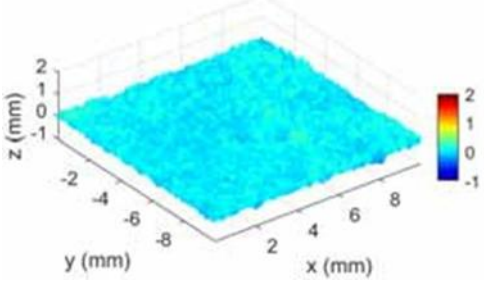

Figure 042621.20: Frost Topography at 01:19:51

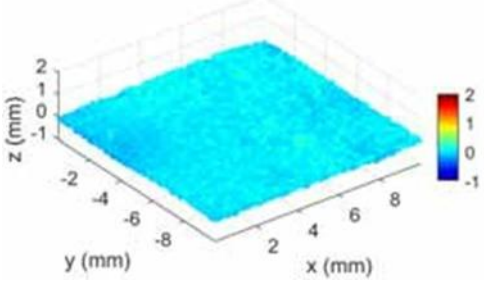

Figure 042621.21: Frost Topography at 01:29:50

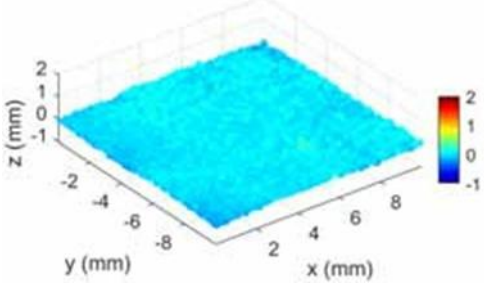

Figure 042621.22: Frost Topography at 01:39:50

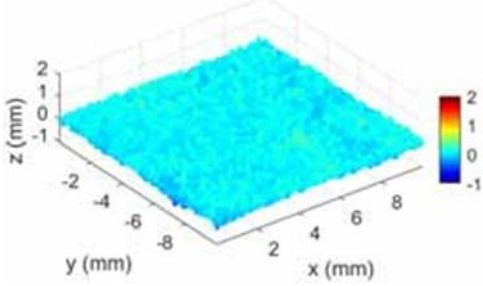

Figure 042621.23: Frost Topography at 01:49:49

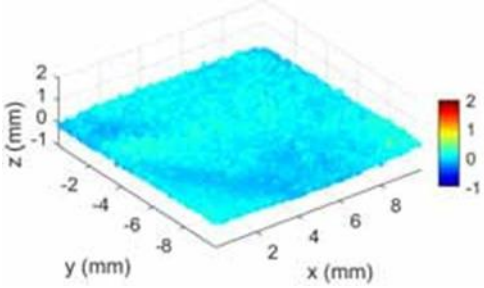

Figure 042621.24: Frost Topography at 01:59:55

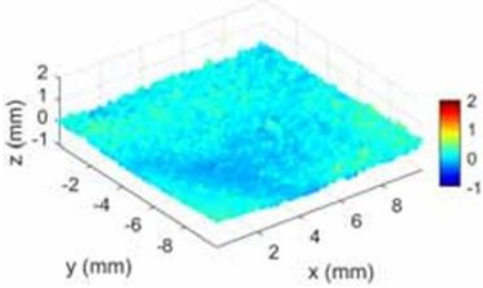

Figure 042621.25: Frost Topography at 02:09:50

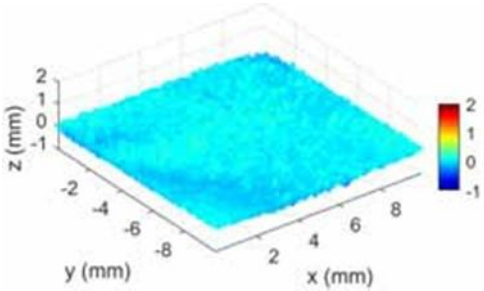

Figure 042621.26: Frost Topography at 02:18:50

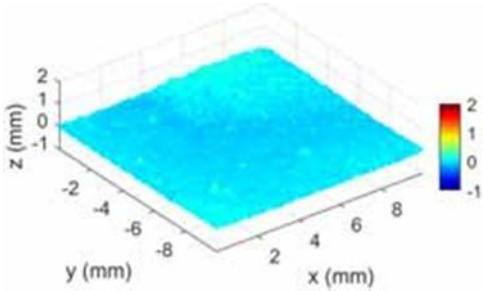

CAFF Conditions Report – Case Date: 0428211

Table 042821.01: Summary of Measured Test Variables

Variable	Mean	St. Dev.	Rand. Unc.
T_air (C)	9.2215	0.2668	0.0090
Rh (%)	79.7679	5.4472	0.1836
Omega (kg_v/kg_da)	0.00589387	0.00043941	0.00001481
V_air (m/s)	0.3340	0.0986	0.0033
T_skin (C)	-8.2119	0.9640	0.0325
T_floor (C)	-20.1105	0.0264	0.0009

Figure 042821.01: Temperature and Voltage Control Time History

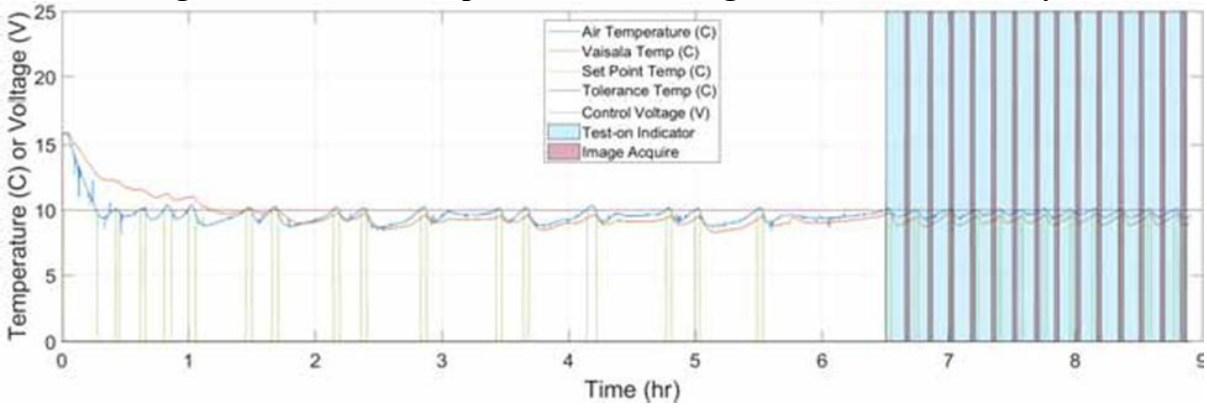

Figure 042821.02: Relative Humidity Time History

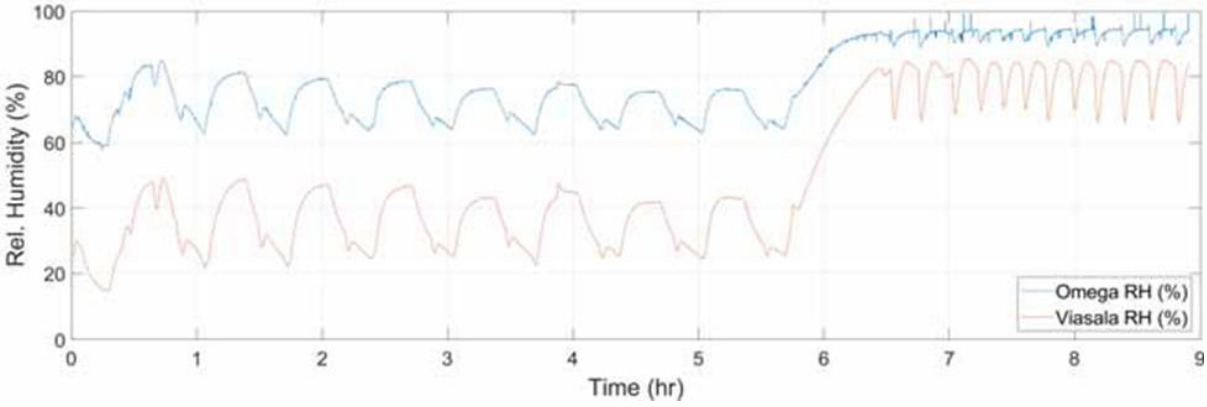

Figure 042821.03: Velocity Time History

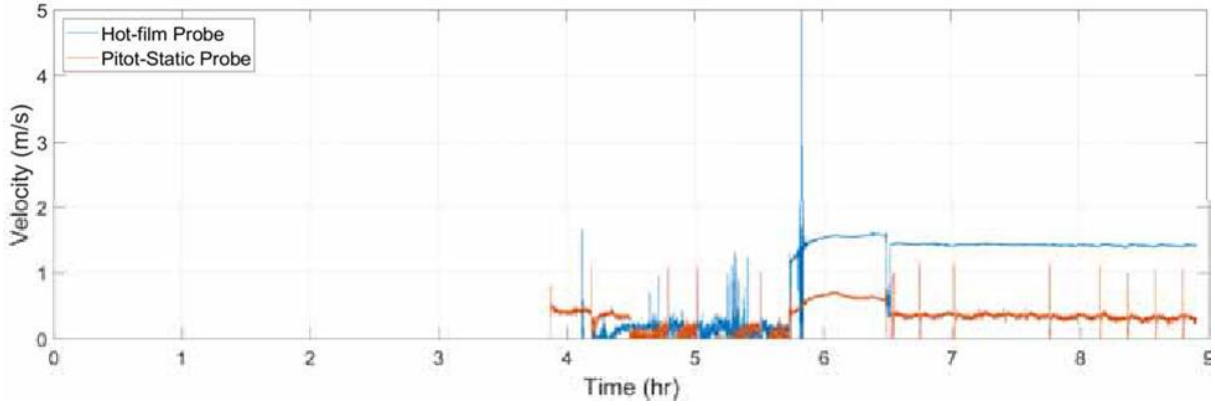

Figure 042821.04: Coolant Return Temperature Time History

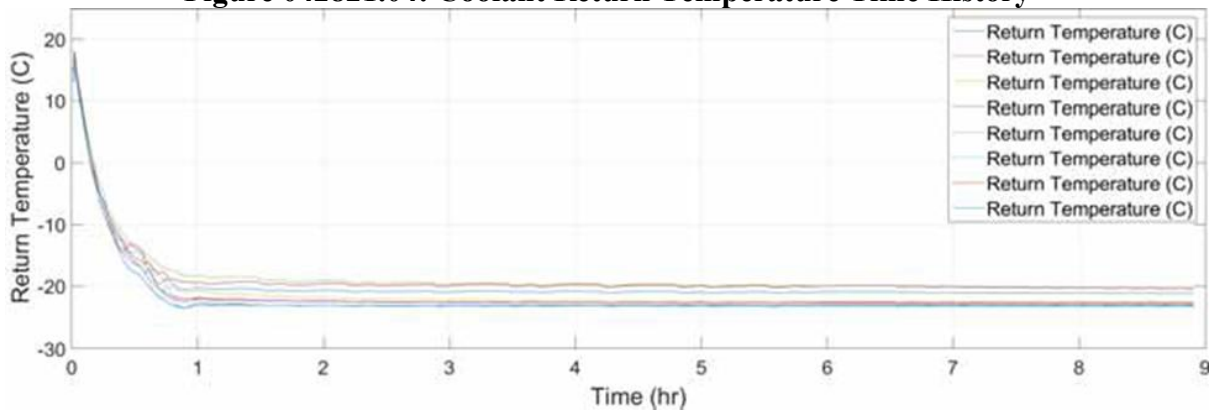

Figure 042821.05: Coolant Supply Temperature Time History

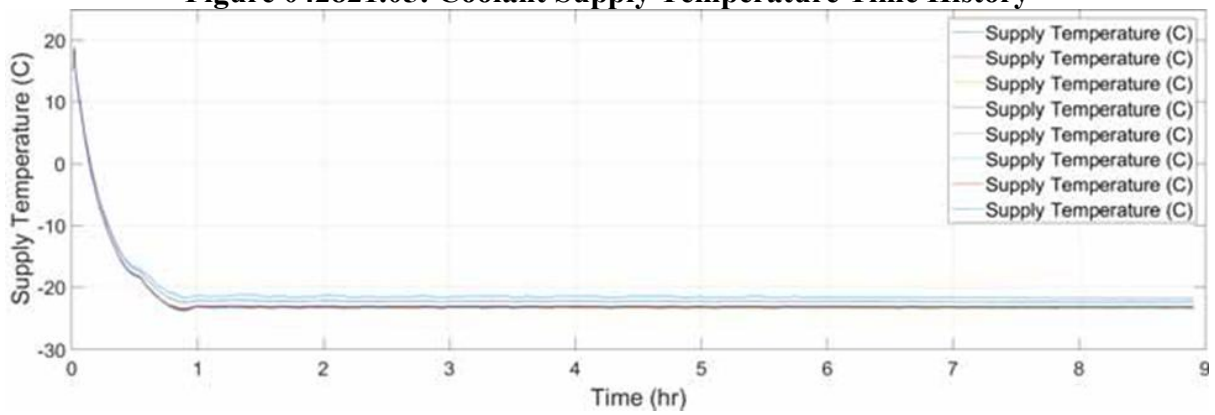

Figure 042821.06: Skin Temperature Time History

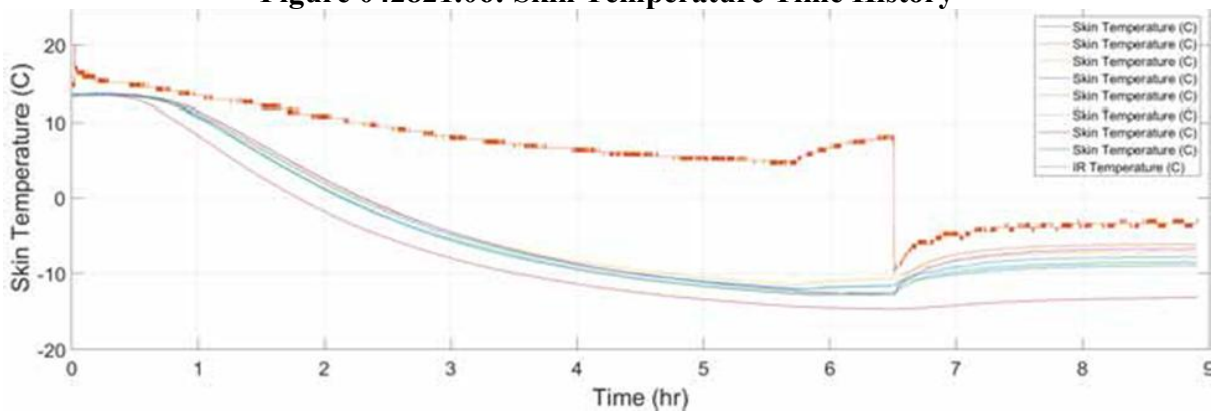

Figure 042821.07: Floor Temperature Time History

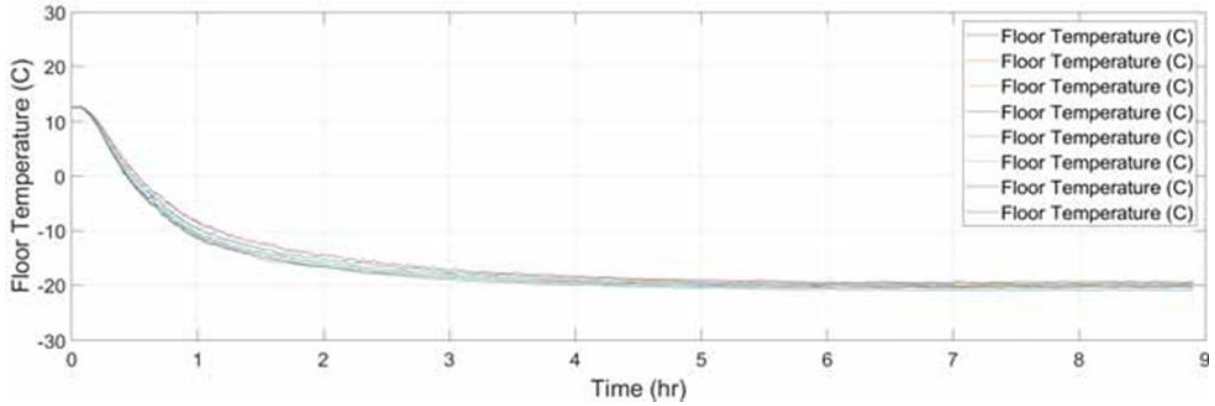

Figure 042821.08: Skin Temperature Slope Time History

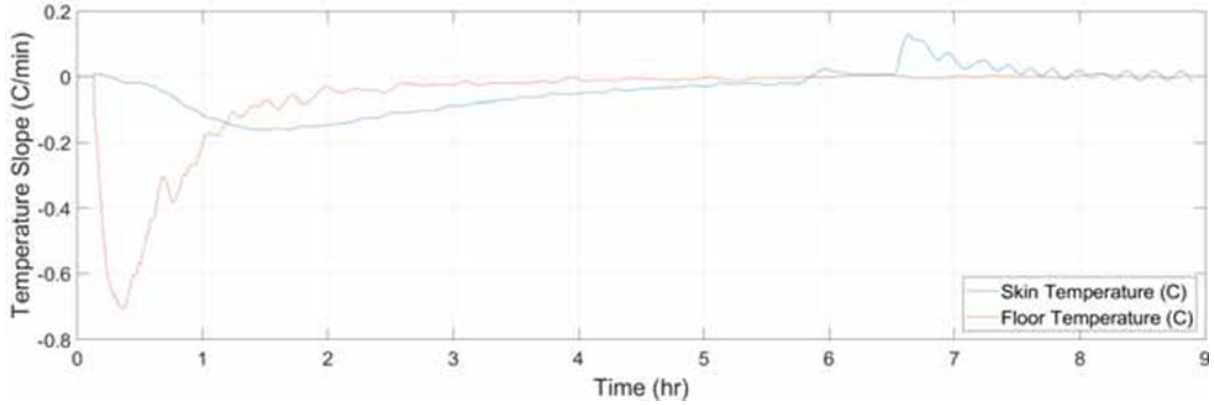

Figure 042821.09: RMS Height Evolution

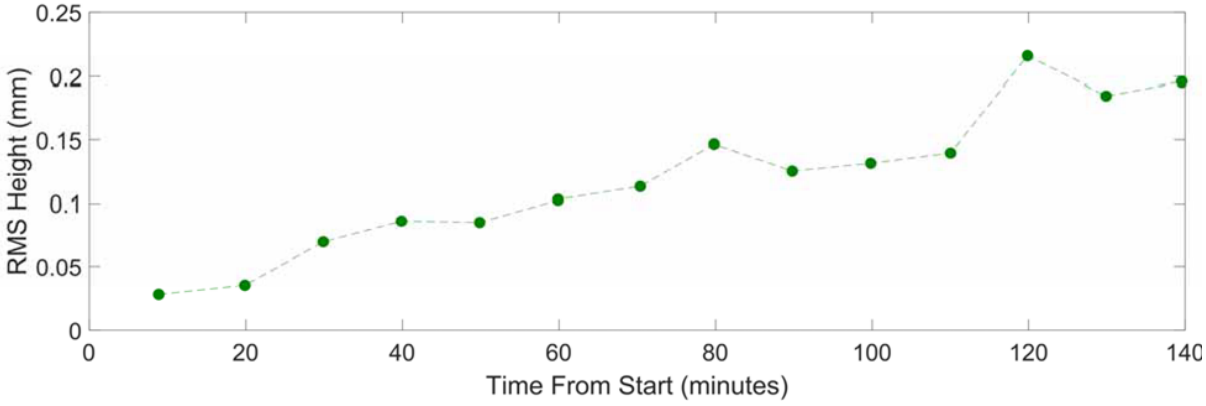

Figure 042821.10: Skewness Evolution

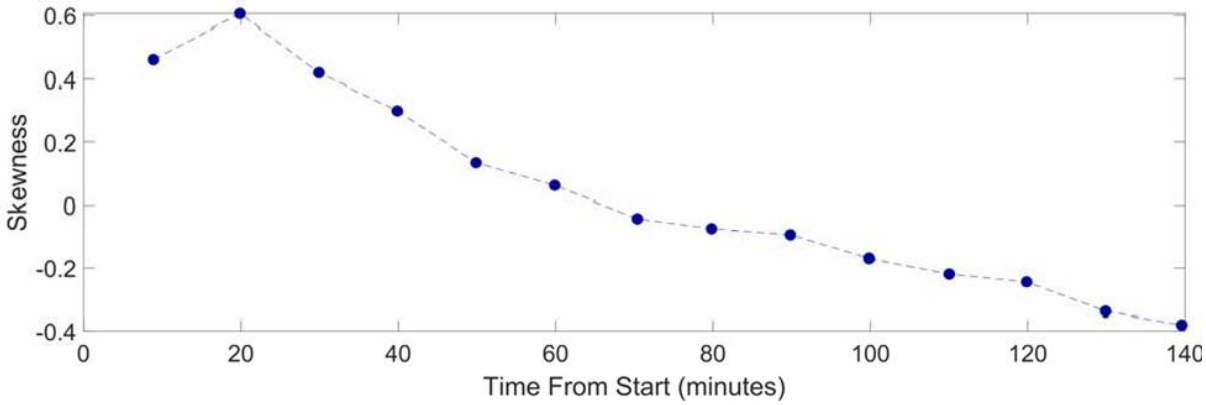

Figure 042821.11: Peak to Valley Evolution

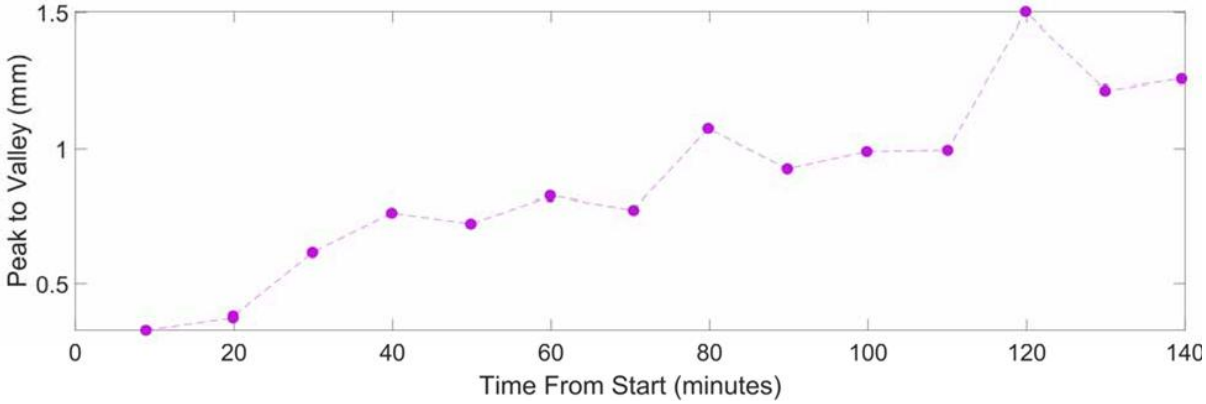

Figure 042821.12: Equivalent Roughness Evolution

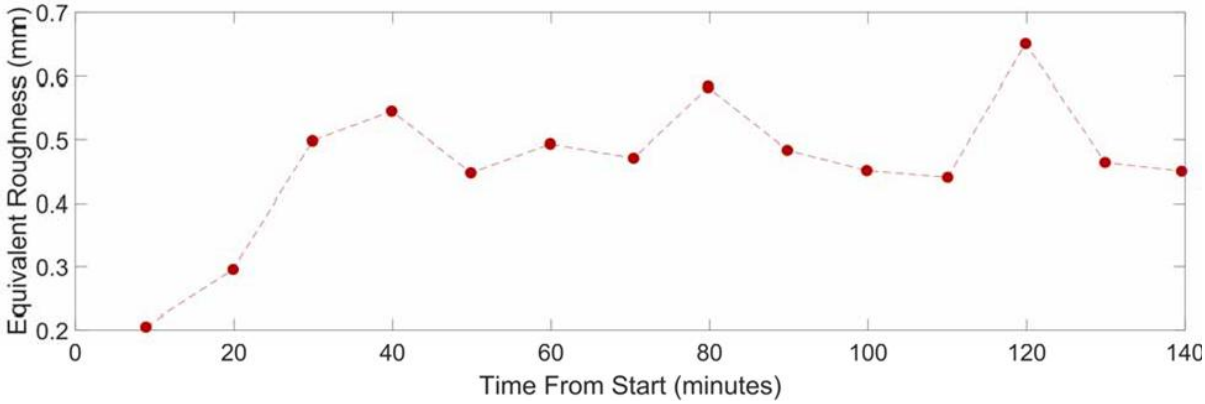

Table 042821.02: Summary of Roughness Parameters

Time (min.)	RMS (mm)	Skewness	Peak to Valley (mm)	ks,Flack-Schultz (mm)
8.8818	0.0275	0.4617	0.3308	0.2051
19.8818	0.0348	0.6068	0.3777	0.2953
29.8985	0.0696	0.4205	0.6165	0.4986
39.8818	0.0860	0.3004	0.7639	0.5461
49.8818	0.0850	0.1344	0.7230	0.4474
59.8818	0.1027	0.0616	0.8257	0.4936
70.3985	0.1130	-0.0434	0.7742	0.4710
79.8152	0.1466	-0.0751	1.0757	0.5837
89.8152	0.1251	-0.0948	0.9251	0.4837
99.8318	0.1314	-0.1699	0.9902	0.4511
110.0318	0.1396	-0.2197	0.9949	0.4403
119.8652	0.2165	-0.2451	1.5041	0.6525
129.8985	0.1849	-0.3394	1.2162	0.4642
139.5485	0.1960	-0.3809	1.2579	0.4501

Figure 042821.13: Frost Topography at 00:08:52

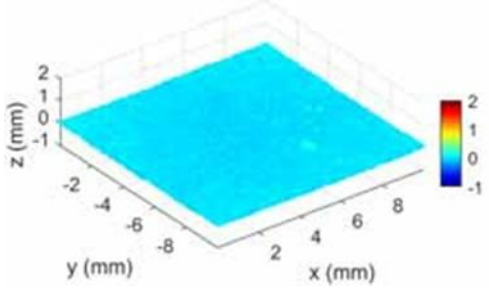

Figure 042821.14: Frost Topography at 00:19:52

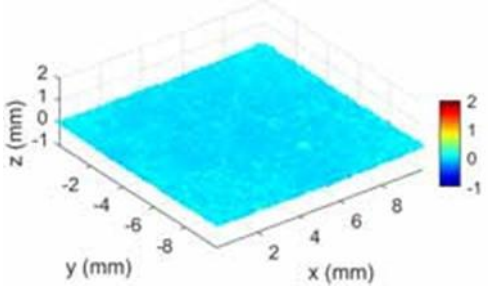

Figure 042821.15: Frost Topography at 00:29:53

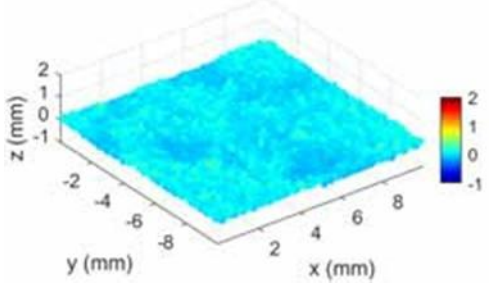

Figure 042821.16: Frost Topography at 00:39:52

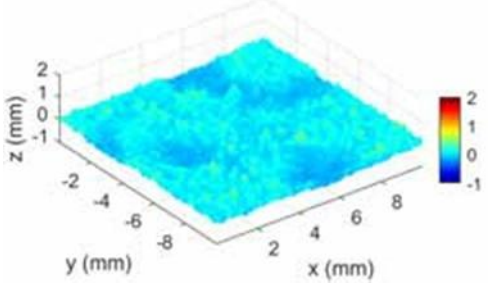

Figure 042821.17: Frost Topography at 00:49:52

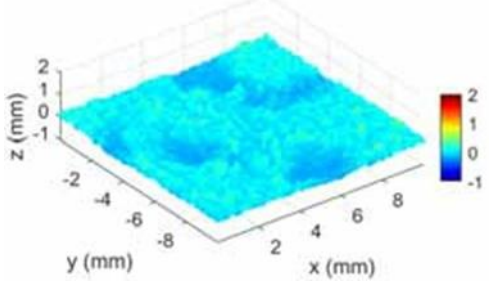

Figure 042821.18: Frost Topography at 00:59:52

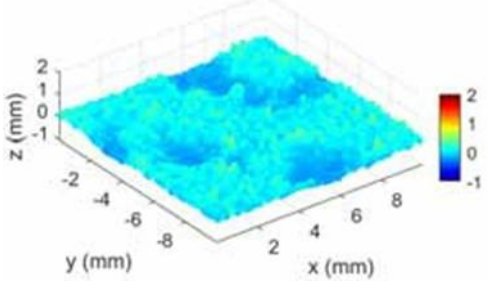

Figure 042821.19: Frost Topography at 01:10:23

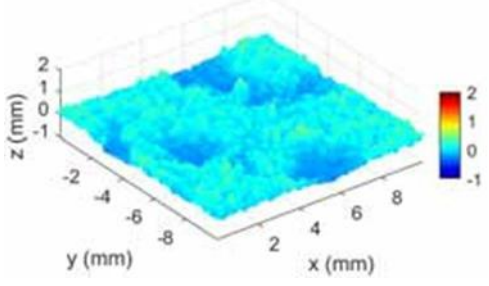

Figure 042821.20: Frost Topography at 01:19:48

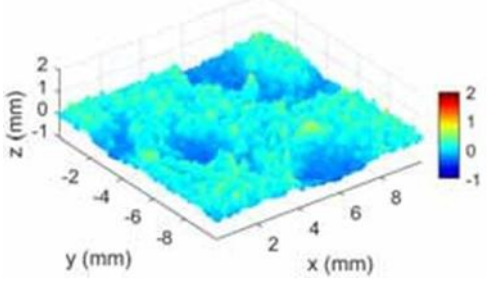

Figure 042821.21: Frost Topography at 01:29:48

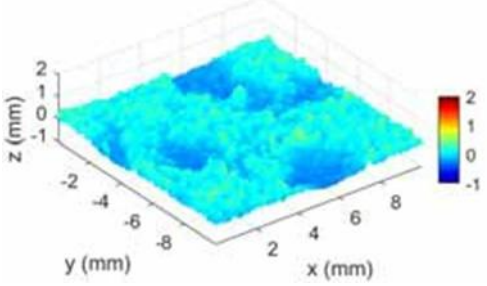

Figure 042821.22: Frost Topography at 01:39:49

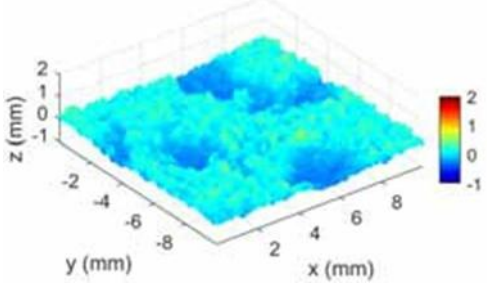

Figure 042821.23: Frost Topography at 01:50:01

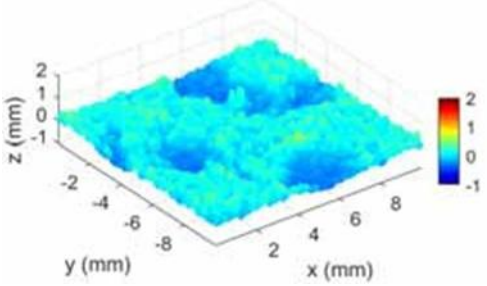

Figure 042821.24: Frost Topography at 01:59:51

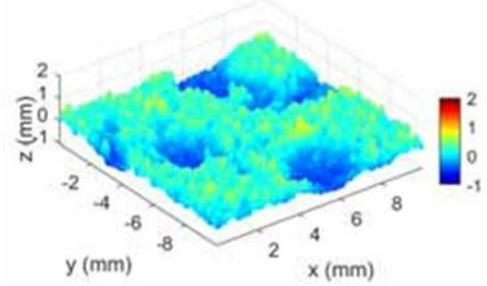

Figure 042821.25: Frost Topography at 02:09:53

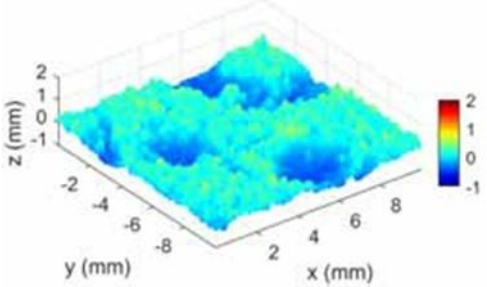

Figure 042821.26: Frost Topography at 02:19:32

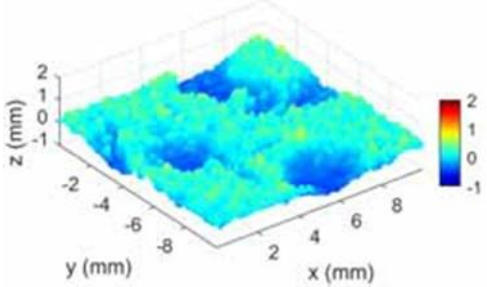

CAFF Conditions Report – Case Date: 043021

Table 043021.01: Summary of Measured Test Variables

Variable	Mean	St. Dev.	Rand. Unc.
T_air (C)	4.2874	0.1914	0.0065
Rh (%)	79.6364	5.4356	0.1841
Omega (kg_v/kg_da)	0.00412649	0.00032386	0.00001097
V_air (m/s)	0.3686	0.0527	0.0018
T_skin (C)	-10.4807	0.7179	0.0243
T_floor (C)	-20.5753	0.0330	0.0011

Figure 043021.01: Temperature and Voltage Control Time History

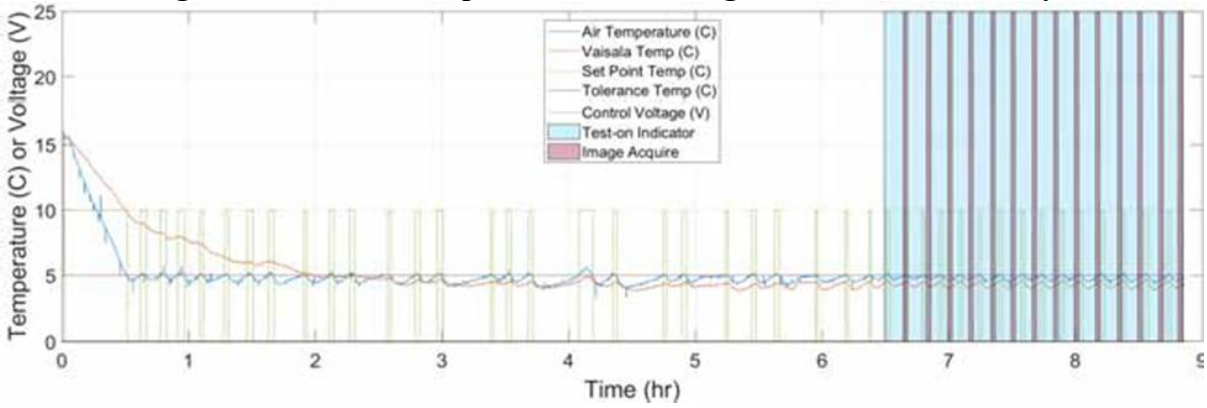

Figure 043021.02: Relative Humidity Time History

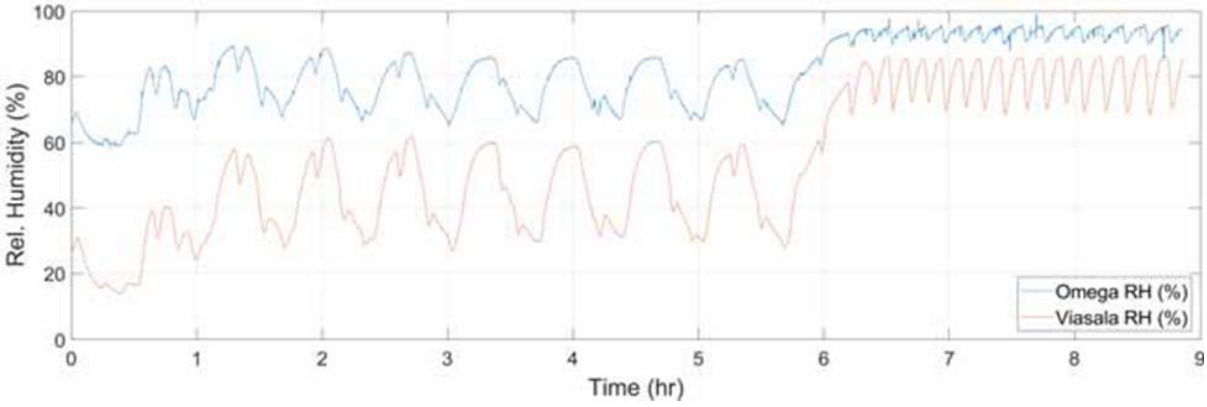

Figure 043021.03: Velocity Time History

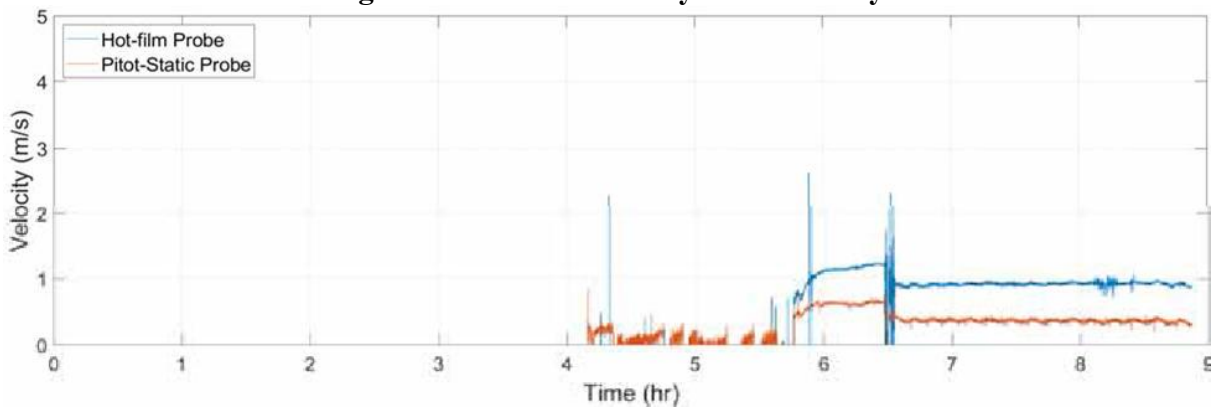

Figure 043021.04: Coolant Return Temperature Time History

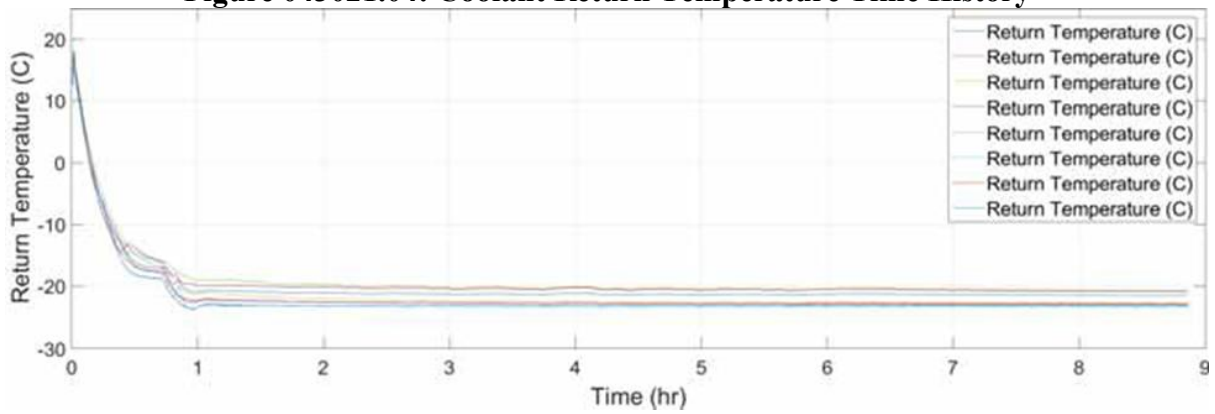

Figure 043021.05: Coolant Supply Temperature Time History

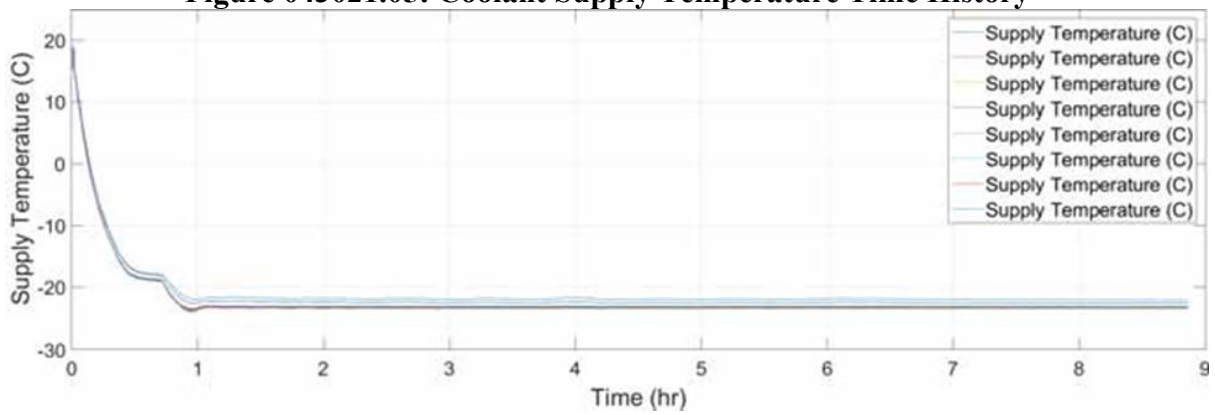

Figure 043021.06: Skin Temperature Time History

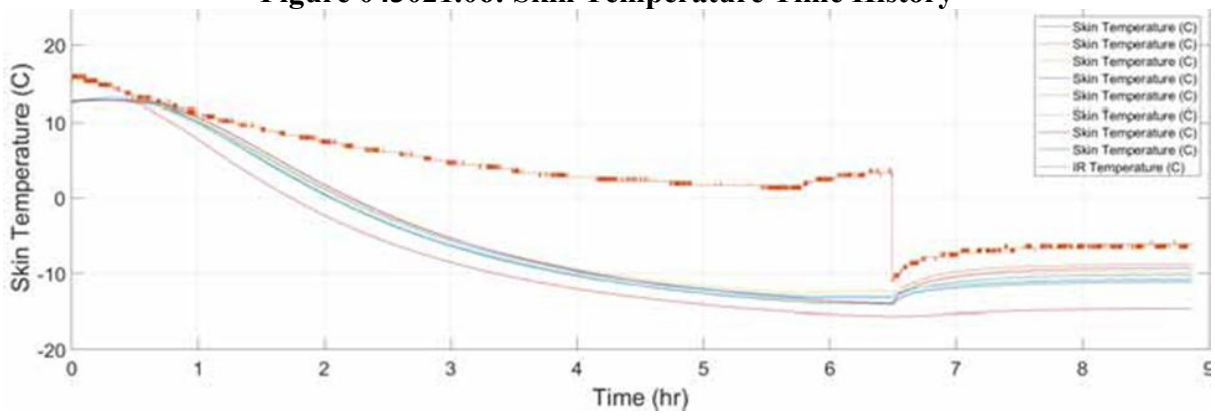

Figure 043021.07: Floor Temperature Time History

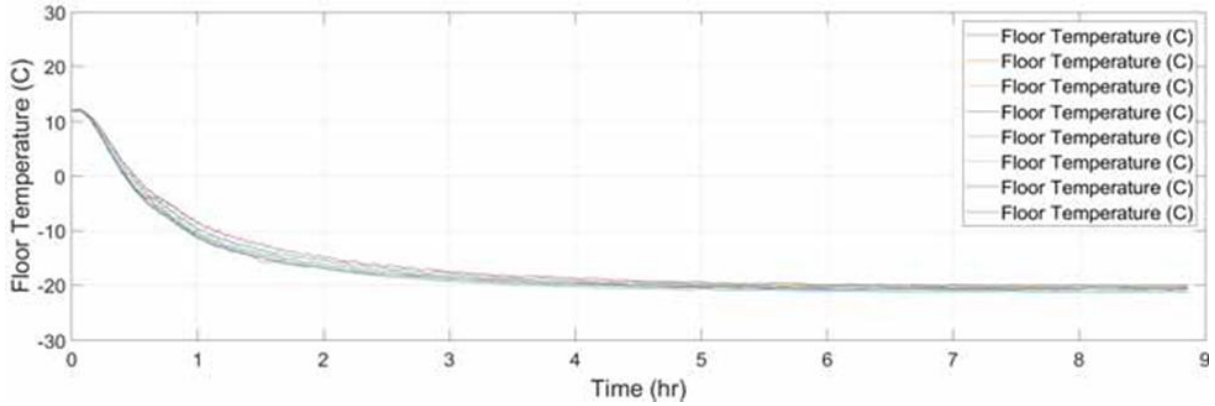

Figure 043021.08: Skin Temperature Slope Time History

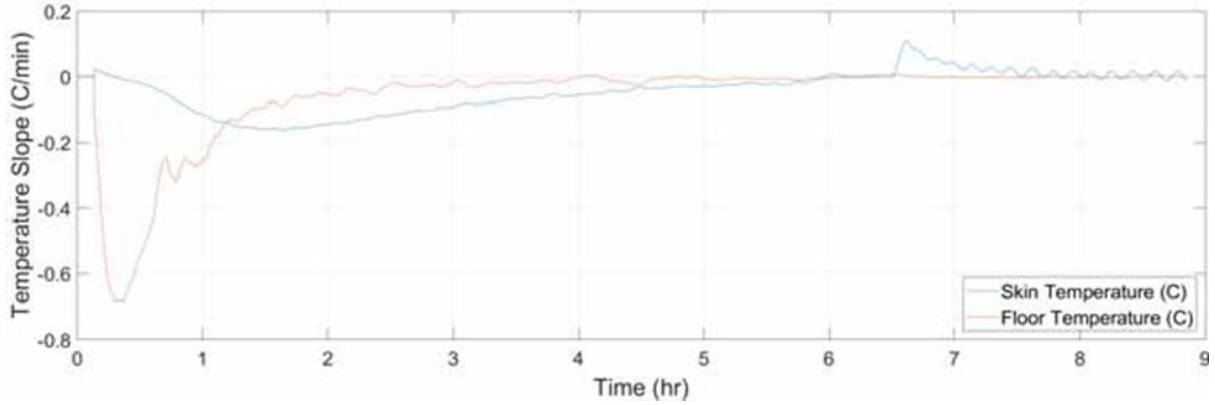

Figure 043021.09: RMS Height Evolution

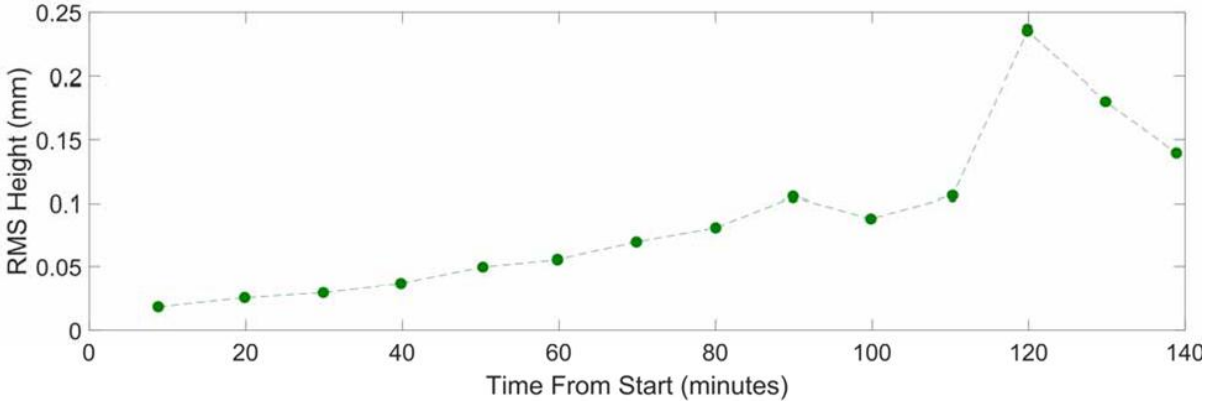

Figure 043021.10: Skewness Evolution

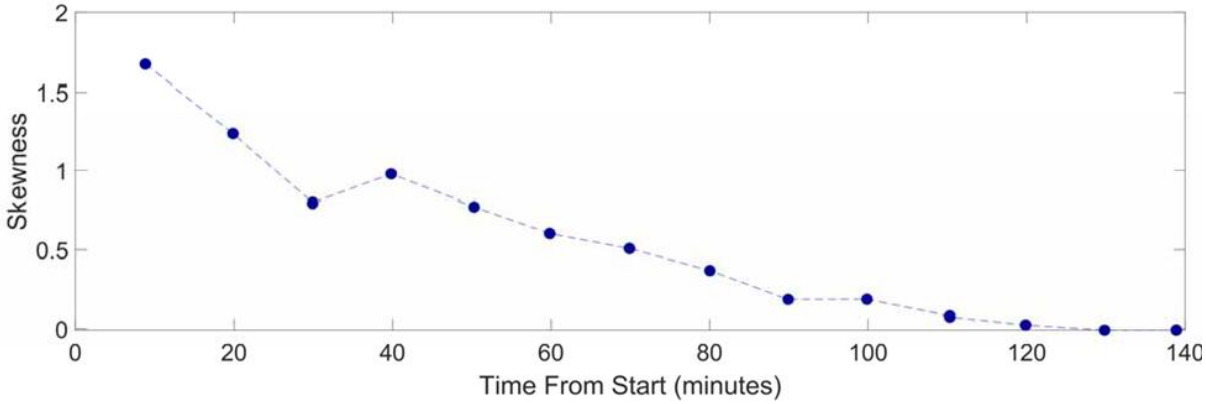

Figure 043021.11: Peak to Valley Evolution

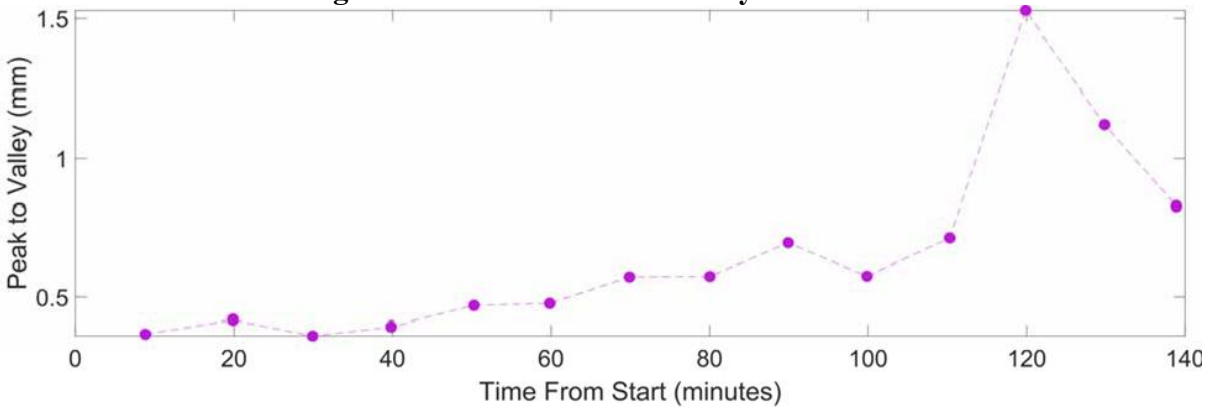

Figure 043021.12: Equivalent Roughness Evolution

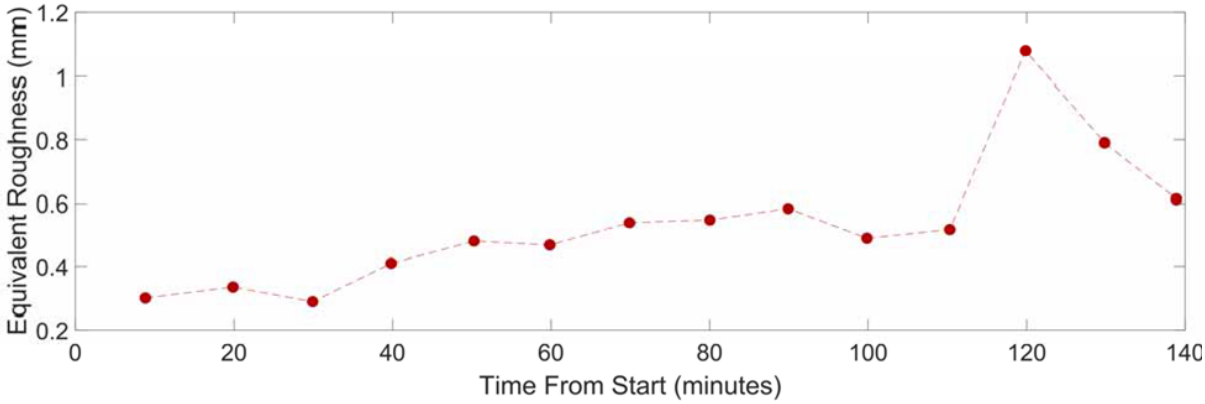

Table 043021.02: Summary of Roughness Parameters

Time (min.)	RMS (mm)	Skewness	Peak to Valley (mm)	ks,Flack-Schultz (mm)
8.8129	0.0175	1.6767	0.3681	0.2986
19.8629	0.0250	1.2367	0.4191	0.3336
29.9129	0.0290	0.7960	0.3616	0.2868
39.8296	0.0363	0.9796	0.3945	0.4094
50.2796	0.0495	0.7736	0.4694	0.4808
59.8296	0.0553	0.6039	0.4767	0.4680
69.8963	0.0694	0.5076	0.5724	0.5392
80.0296	0.0807	0.3658	0.5740	0.5480
89.9129	0.1051	0.1805	0.6970	0.5845
99.8463	0.0879	0.1819	0.5752	0.4894
110.2963	0.1057	0.0750	0.7146	0.5173
119.8629	0.2361	0.0245	1.5288	1.0814
129.8296	0.1806	-0.0084	1.1215	0.7909
138.8796	0.1397	-0.0076	0.8281	0.6124

Figure 043021.13: Frost Topography at 00:08:48

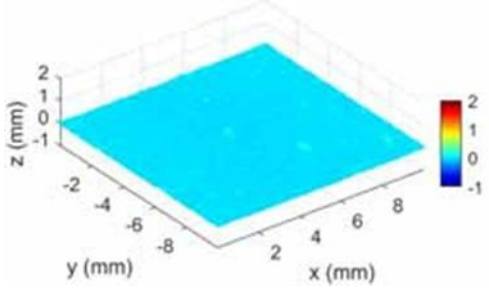

Figure 043021.14: Frost Topography at 00:19:51

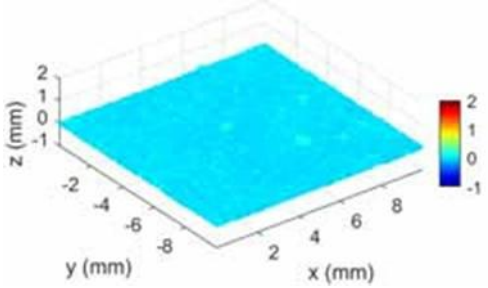

Figure 043021.15: Frost Topography at 00:29:54

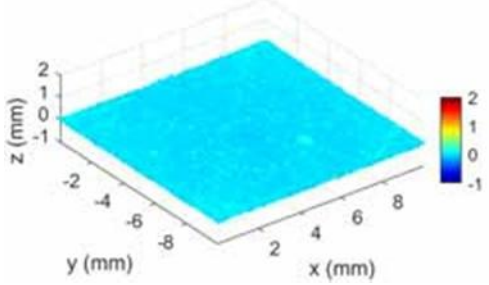

Figure 043021.16: Frost Topography at 00:39:49

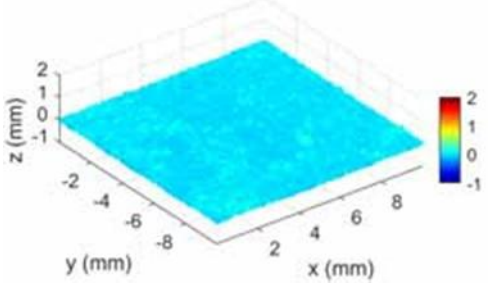

Figure 043021.17: Frost Topography at 00:50:16

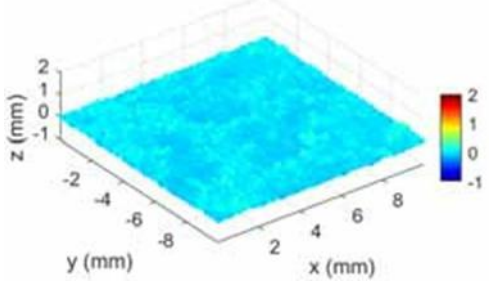

Figure 043021.18: Frost Topography at 00:59:49

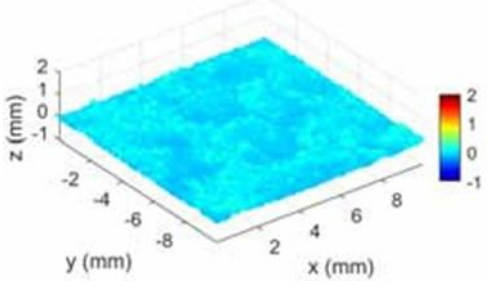

Figure 043021.19: Frost Topography at 01:09:53

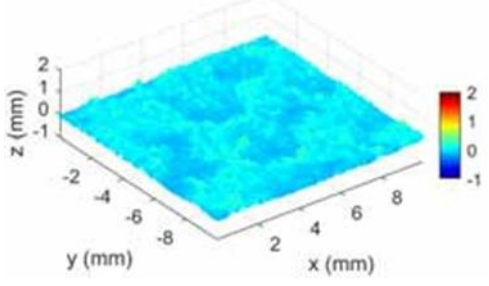

Figure 043021.20: Frost Topography at 01:20:01

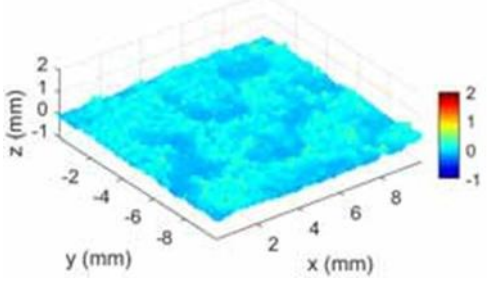

Figure 043021.21: Frost Topography at 01:29:54

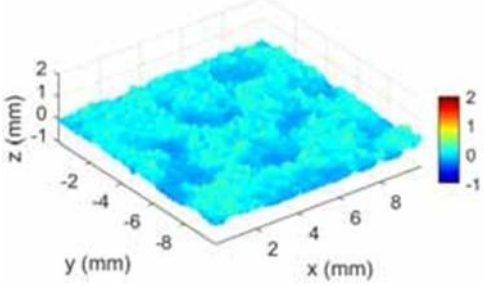

Figure 043021.22: Frost Topography at 01:39:50

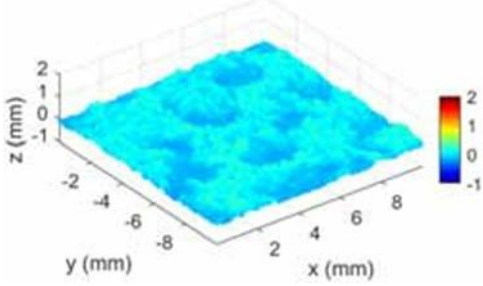

Figure 043021.23: Frost Topography at 01:50:17

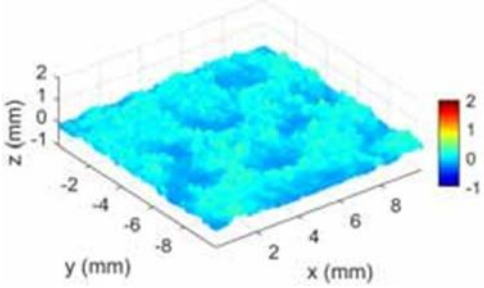

Figure 043021.24: Frost Topography at 01:59:51

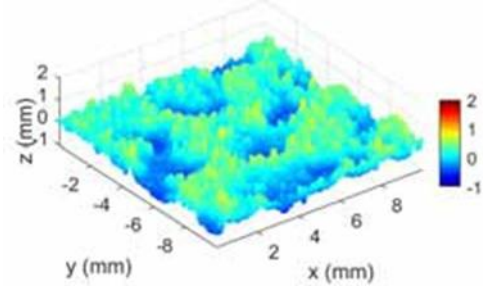

Figure 043021.25: Frost Topography at 02:09:49

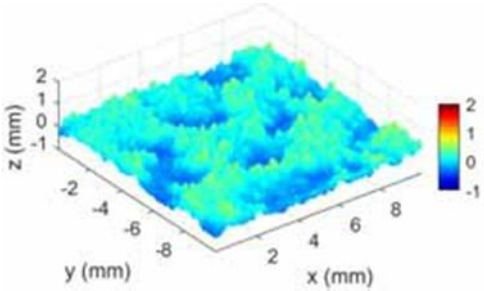

Figure 043021.26: Frost Topography at 02:18:52

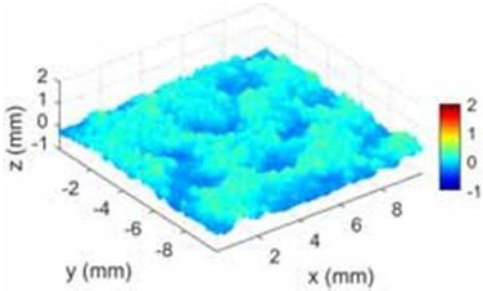

E Appendix E: CAFF test reports using a carbon fiber skin with aluminum structural rib

Table E- 1. Summary of Nominal Test Conditions for Wing Tank Thermal Model with a Carbon Fiber Skin and an Aluminum Structural Rib

Date	T_{PC} (°C)	$T_{air,set}$ (°C)	RH (%)	V (m/s)	x_{img} (in.)	Notes
06/19/21	-27	16	82	1.3	21.0	10 min. int.
06/21/21	-27	10	82	1.3	21.0	10 min. int.
06/23/21	-27	5	82	1.3	21.0	10 min. int.
06/25/21	-27	5	82	1.5	21.0	10 min. int.
06/28/21	-27	16	82	0.3	21.0	10 min. int.
06/30/21	-27	10	82	0.3	21.0	10 min. int.
07/02/21	-27	5	82	0.3	21.0	10 min. int.
07/06/21	-27	5	82	0.3	12.0	10 min. int.
07/30/21	-27	16	82	0.3	12.0	10 min. int.
08/03/21	-27	10	82	0.3	12.0	10 min. int.
08/12/21	-27	5	82	0.3	12.0	10 min. int.
08/16/21	-27	5	82	1.4	12.0	10 min. int.
08/18/21	-27	10	82	1.4	12.0	10 min. int.
08/21/21	-27	16	82	1.4	12.0	10 min. int.
09/04/21	-27	5	82	1.4	17.0	10 min. int.
09/07/21	-27	10	82	1.4	17.0	10 min. int.
09/10/21	-27	16	82	1.4	17.0	10 min. int.
09/14/21	-27	5	82	0.3	17.0	10 min. int.
09/16/21	-27	10	82	0.3	17.0	10 min. int.
08/18/21	-27	16	82	0.3	17.0	10 min. int.

CAFF Conditions Report – Case Date: 061921

Table 061921.01: Summary of Measured Test Variables

Variable	Mean	St. Dev.	Rand. Unc.
T_air (C)	15.1931	0.3386	0.0119
Rh (%)	79.1098	3.1608	0.1110
Omega (kg_v/kg_da)	0.00867026	0.00047751	0.00001677
V_air (m/s)	1.2766	0.1200	0.0042
T_skin (C)	-2.7001	1.6969	0.0596
T_floor (C)	-19.2333	0.1798	0.0063

Figure 061921.01: Temperature and Voltage Control Time History

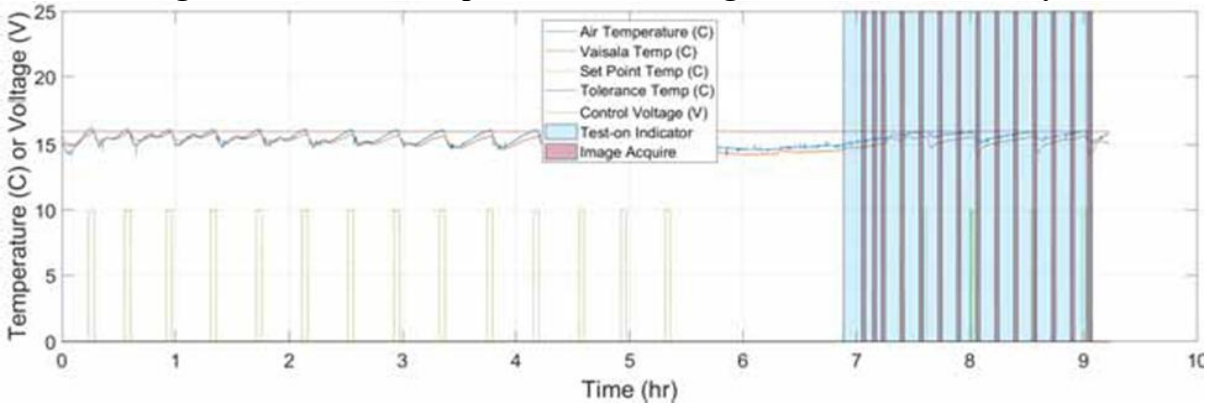

Figure 061921.02: Relative Humidity Time History

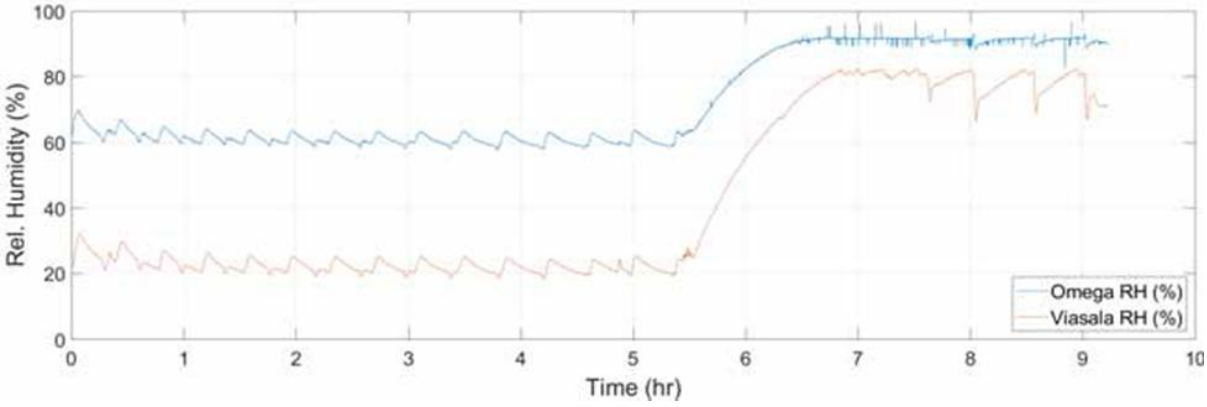

Figure 061921.03: Velocity Time History

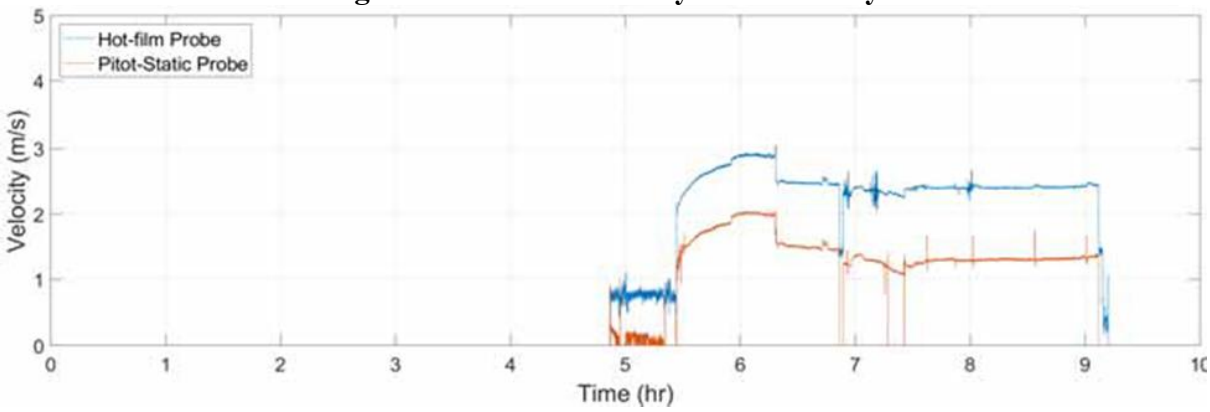

Figure 061921.04: Coolant Return Temperature Time History

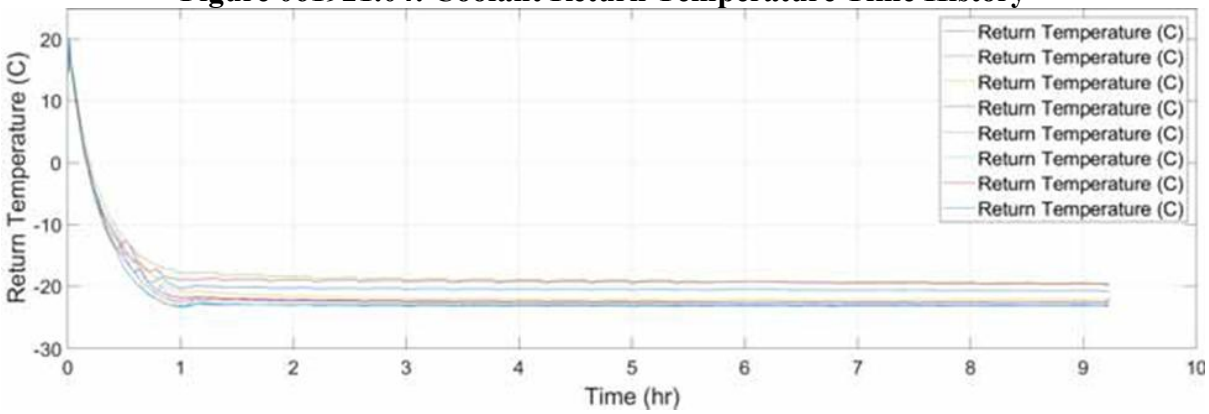

Figure 061921.05: Coolant Supply Temperature Time History

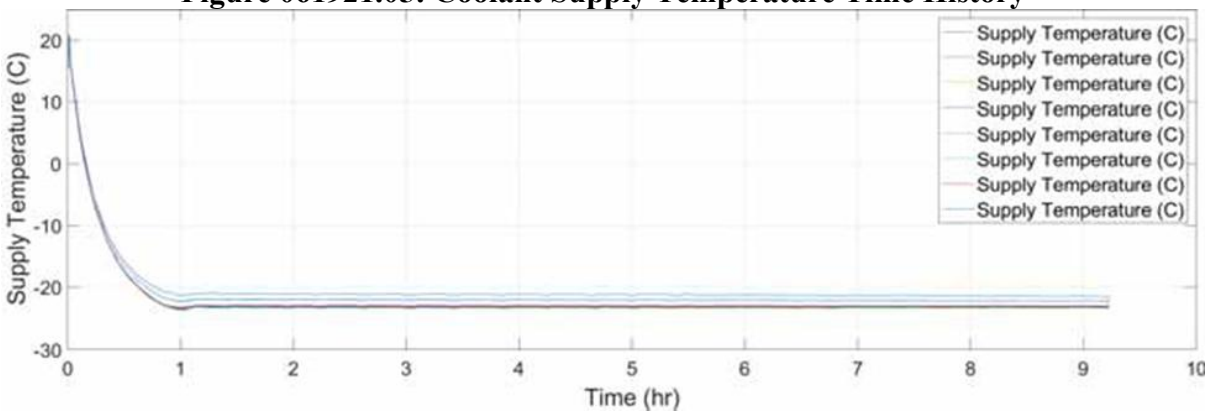

Figure 061921.06: Skin Temperature Time History

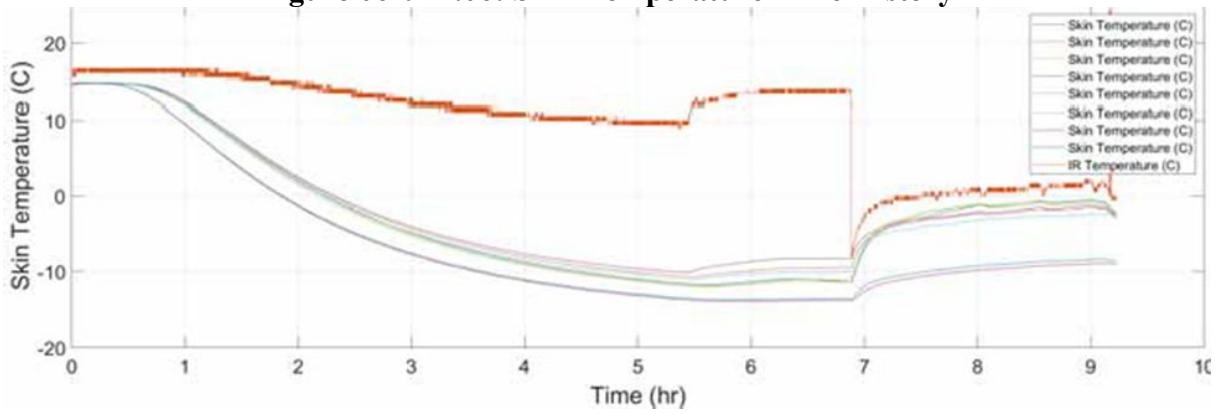

Figure 061921.07: Floor Temperature Time History

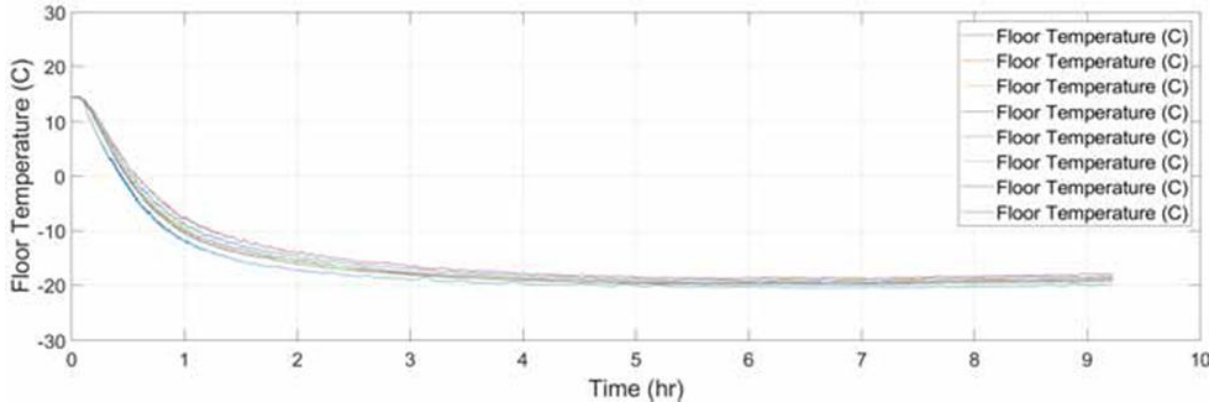

Figure 061921.08: Skin Temperature Slope Time History

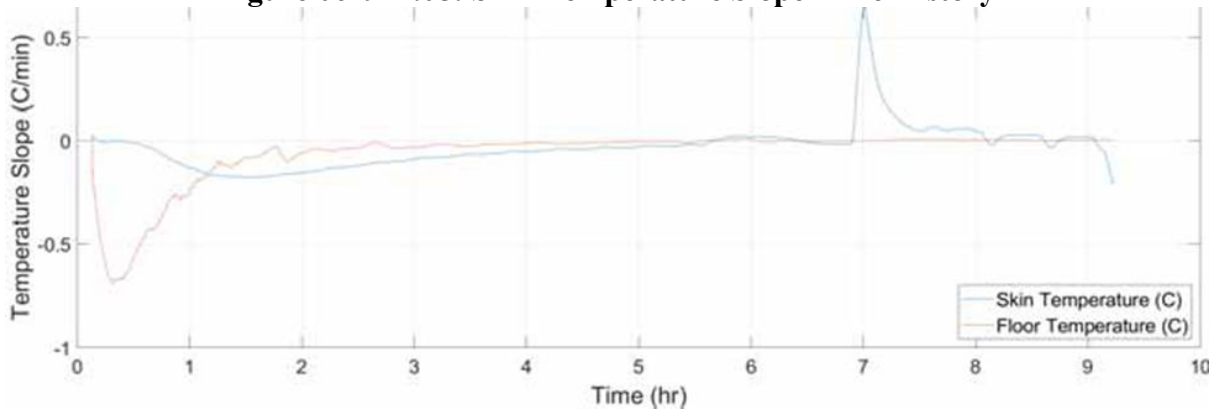

Figure 061921.09: RMS Height Evolution

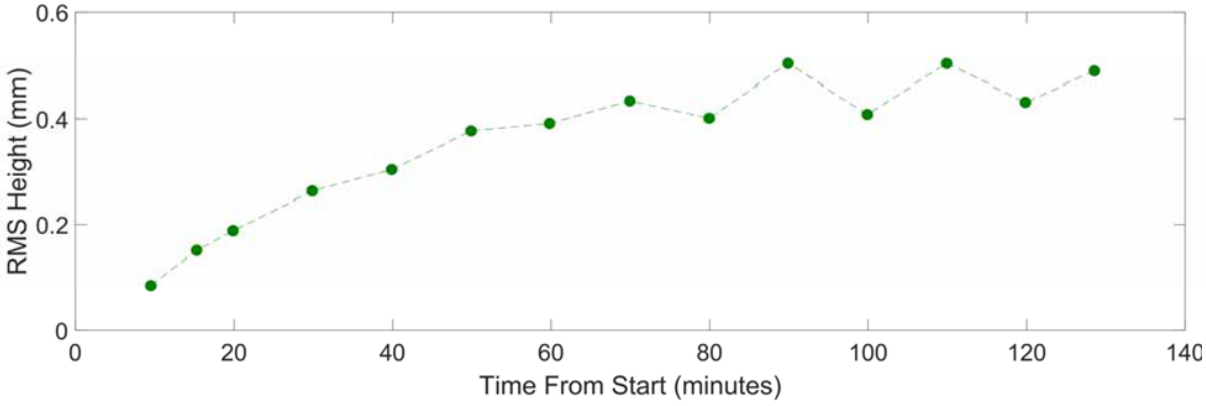

Figure 061921.10: Skewness Evolution

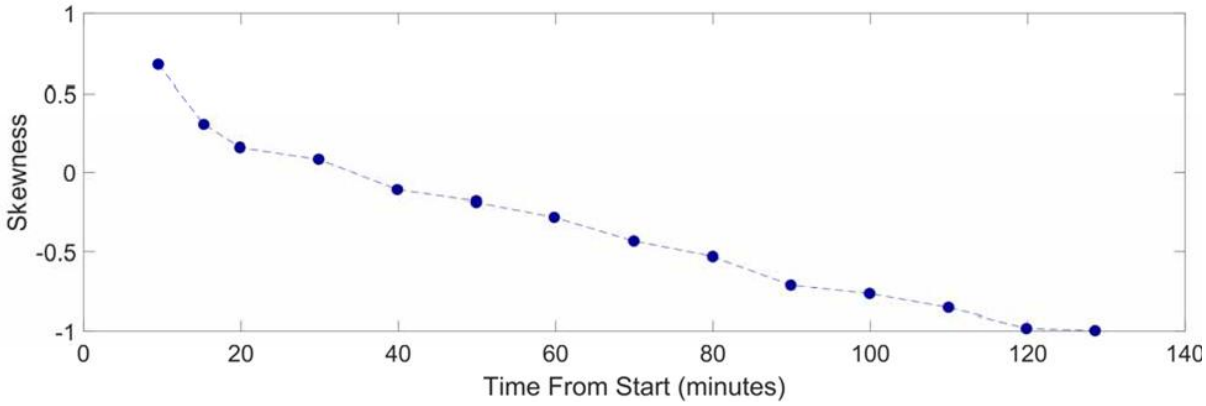

Figure 061921.11: Peak to Valley Evolution

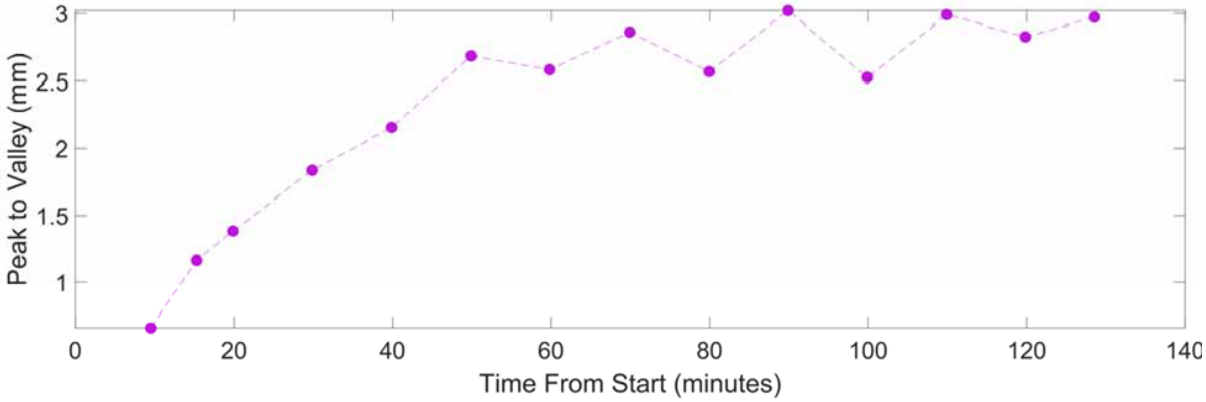

Figure 061921.12: Equivalent Roughness Evolution

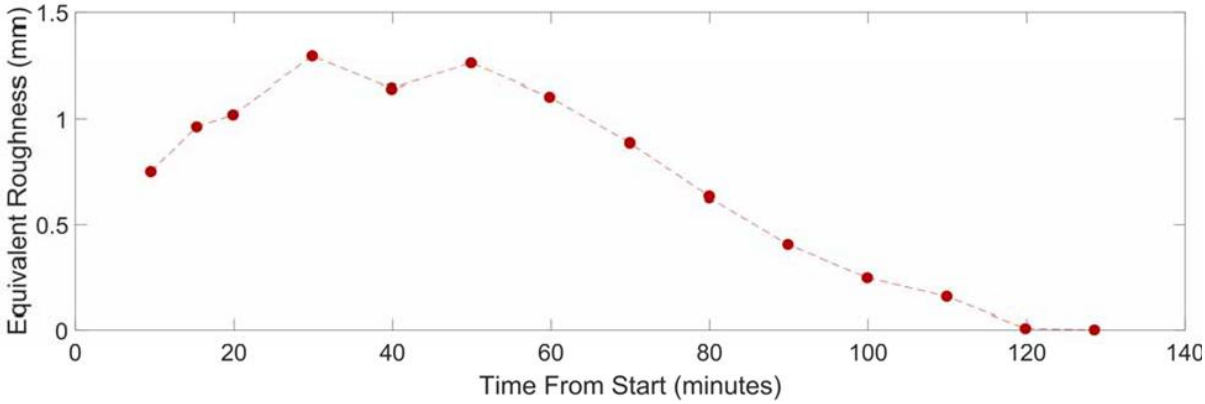

Table 061921.02: Summary of Roughness Parameters

Time (min.)	RMS (mm)	Skewness	Peak to Valley (mm)	ks,Flack-Schultz (mm)
9.4822	0.0828	0.6834	0.6611	0.7485
15.2822	0.1507	0.3054	1.1631	0.9621
19.8655	0.1882	0.1586	1.3829	1.0200
29.8655	0.2624	0.0833	1.8348	1.2972
39.8822	0.3034	-0.1119	2.1550	1.1424
49.8988	0.3770	-0.1840	2.6870	1.2639
59.8155	0.3913	-0.2802	2.5834	1.1049
69.9322	0.4348	-0.4327	2.8646	0.8859
79.9488	0.4013	-0.5309	2.5689	0.6303
89.8822	0.5050	-0.7132	3.0207	0.4042
99.8988	0.4087	-0.7672	2.5254	0.2458
109.9155	0.5047	-0.8567	2.9899	0.1561
119.8322	0.4318	-0.9828	2.8281	0.0073
128.5488	0.4903	-0.9959	2.9705	0.0012

Figure 061921.13: Frost Topography at 00:09:28

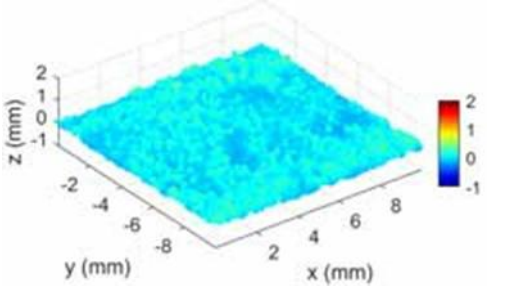

Figure 061921.14: Frost Topography at 00:15:16

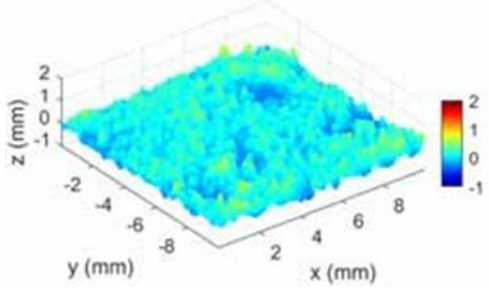

Figure 061921.15: Frost Topography at 00:19:51

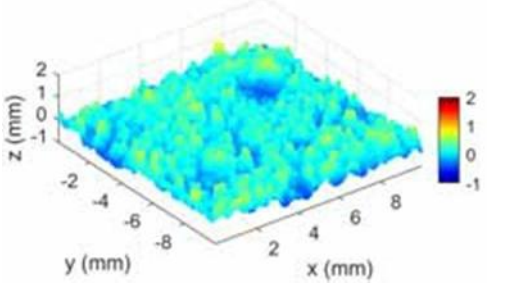

Figure 061921.16: Frost Topography at 00:29:51

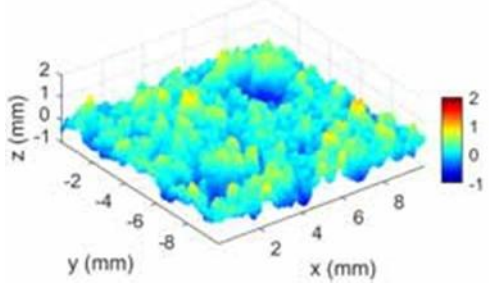

Figure 061921.17: Frost Topography at 00:39:52

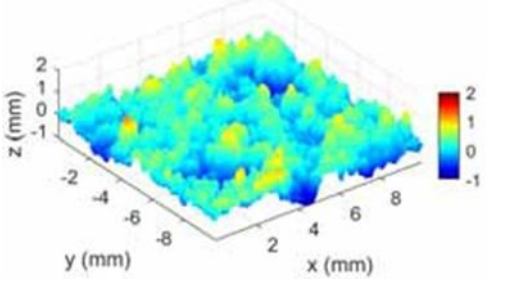

Figure 061921.18: Frost Topography at 00:49:53

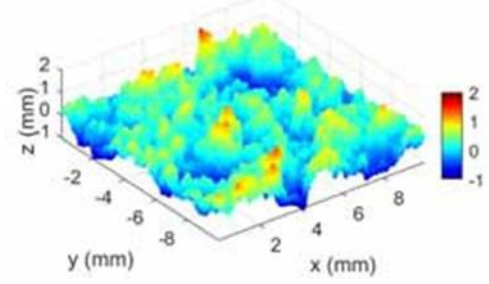

Figure 061921.19: Frost Topography at 00:59:48

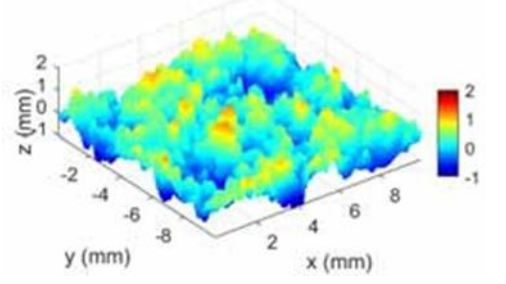

Figure 061921.20: Frost Topography at 01:09:55

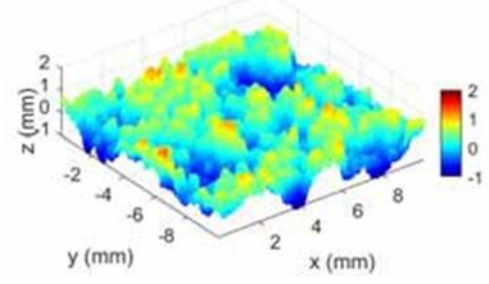

Figure 061921.21: Frost Topography at 01:19:56

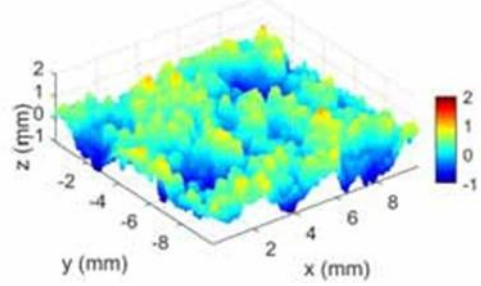

Figure 061921.22: Frost Topography at 01:29:52

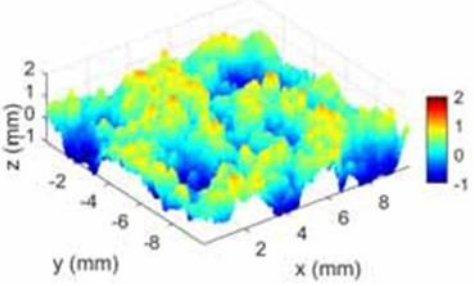

Figure 061921.23: Frost Topography at 01:39:53

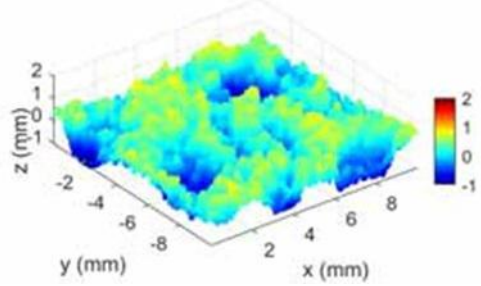

Figure 061921.24: Frost Topography at 01:49:54

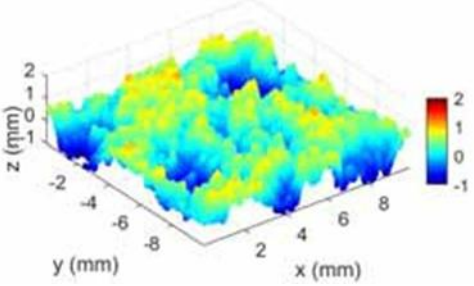

Figure 061921.25: Frost Topography at 01:59:49

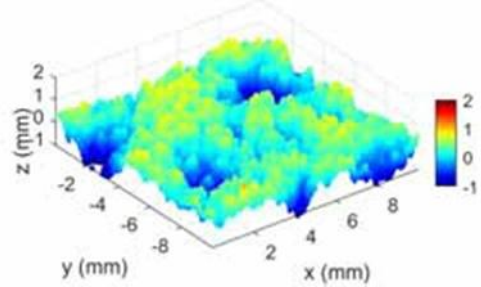

Figure 061921.26: Frost Topography at 02:08:32

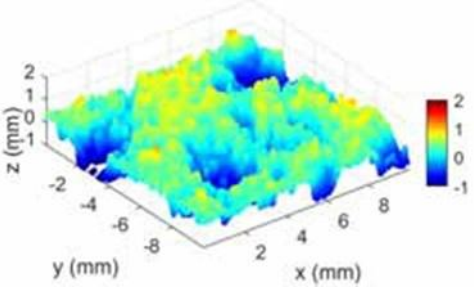

CAFF Conditions Report – Case Date: 062121

Table 062121.01: Summary of Measured Test Variables

Variable	Mean	St. Dev.	Rand. Unc.
T_air (C)	9.1842	0.3752	0.0127
Rh (%)	80.5918	4.0263	0.1363
Omega (kg_v/kg_da)	0.00592673	0.00036749	0.00001244
V_air (m/s)	1.3314	0.0849	0.0029
T_skin (C)	-6.1494	1.1913	0.0403
T_floor (C)	-19.8831	0.0910	0.0031

Figure 062121.01: Temperature and Voltage Control Time History

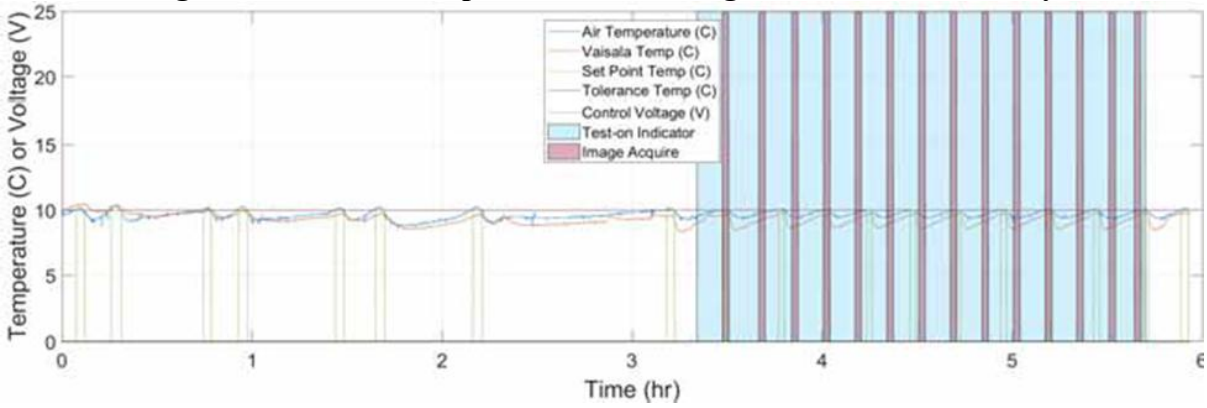

Figure 062121.02: Relative Humidity Time History

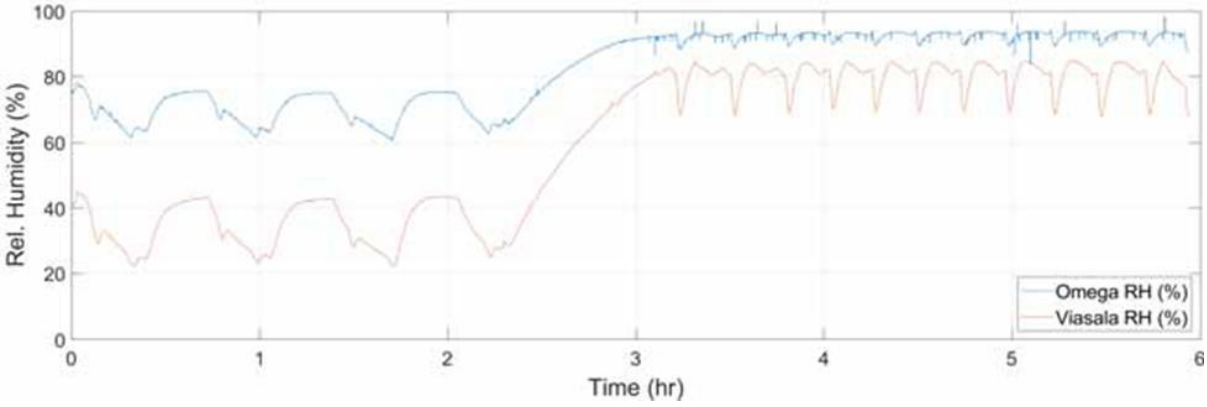

Figure 062121.03: Velocity Time History

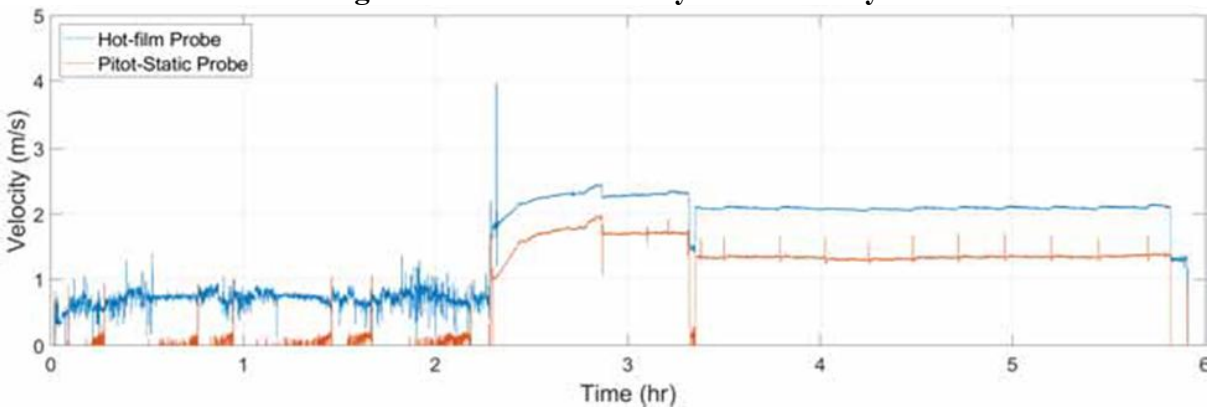

Figure 062121.04: Coolant Return Temperature Time History

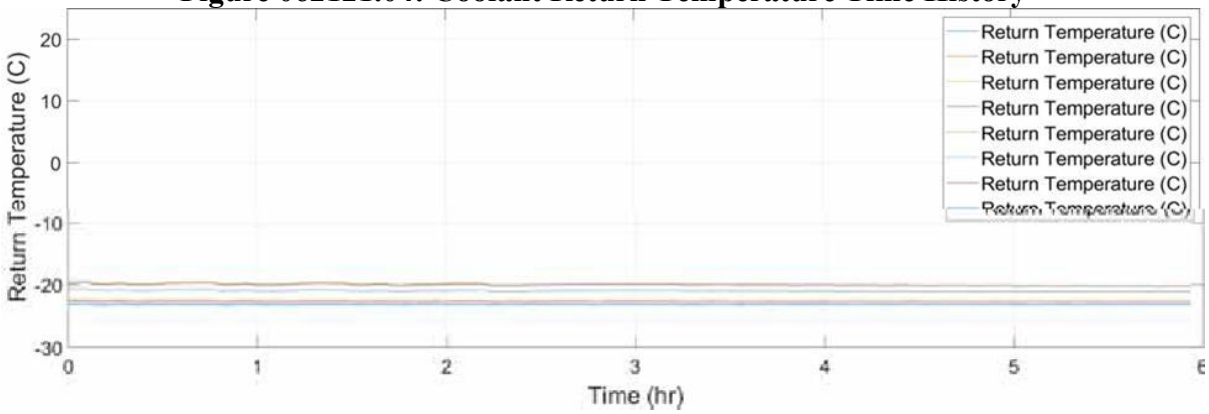

Figure 062121.05: Coolant Supply Temperature Time History

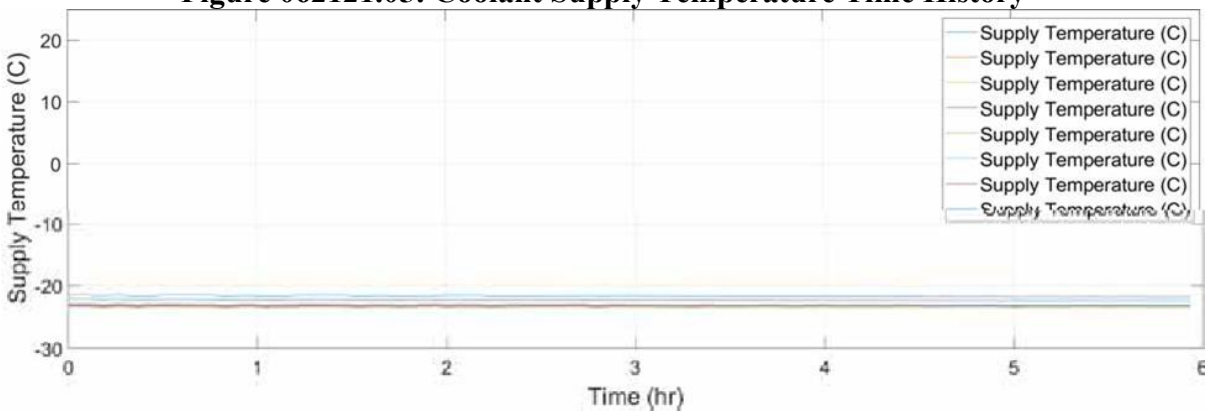

Figure 062121.06: Skin Temperature Time History

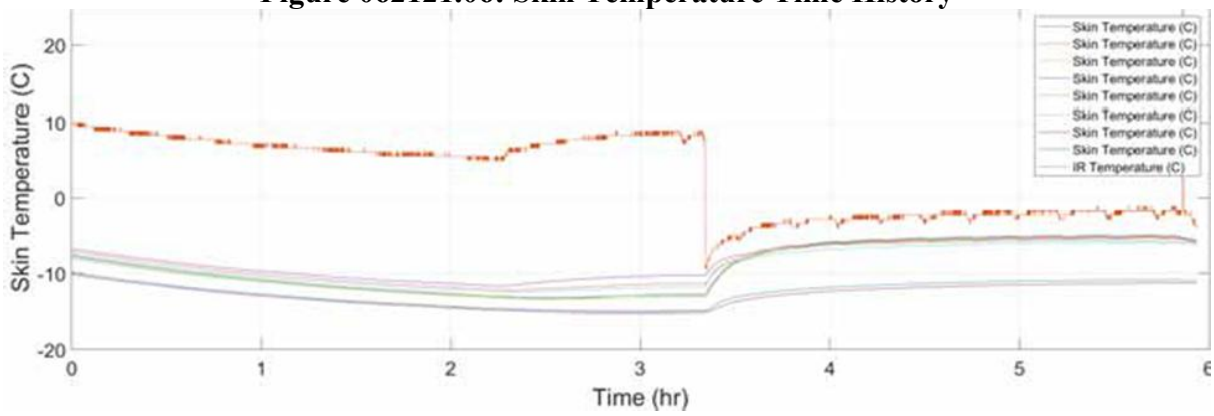

Figure 062121.07: Floor Temperature Time History

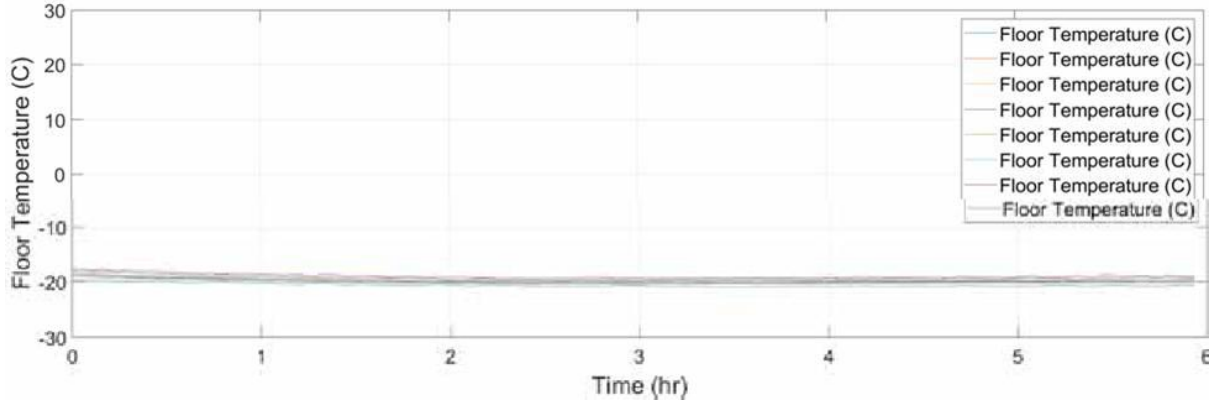

Figure 062121.08: Skin Temperature Slope Time History

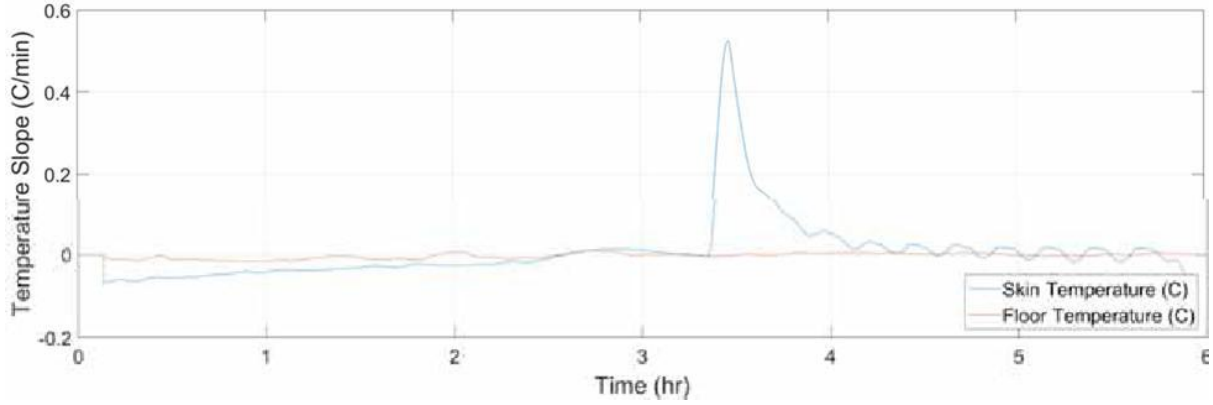

Figure 062121.09: RMS Height Evolution

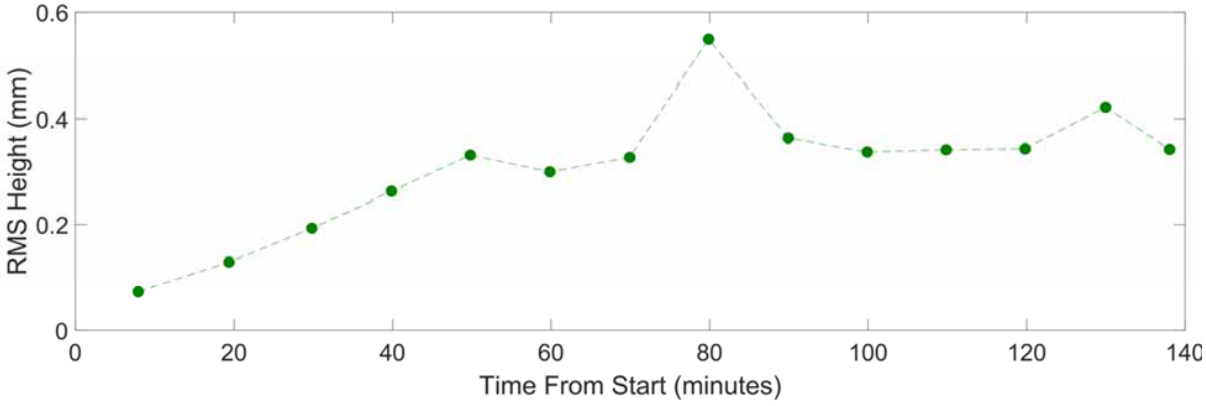

Figure 062121.10: Skewness Evolution

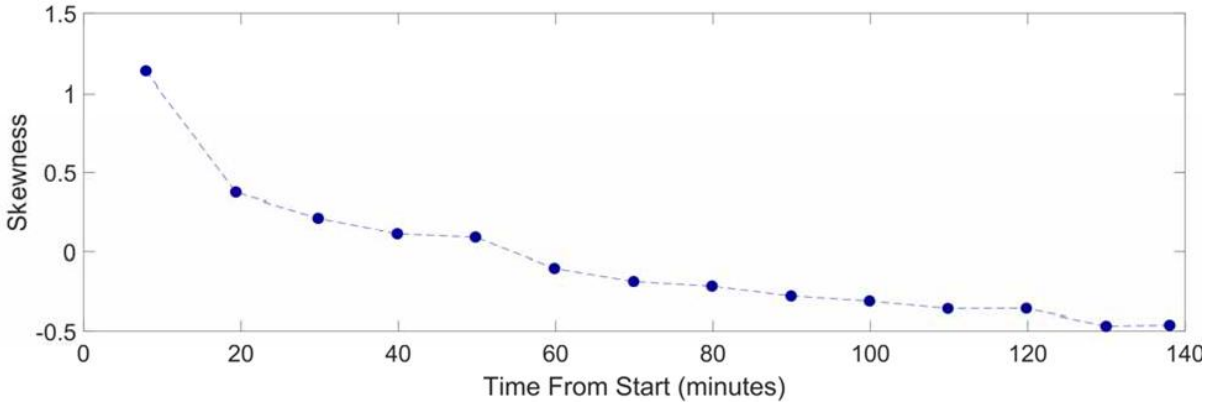

Figure 062121.11: Peak to Valley Evolution

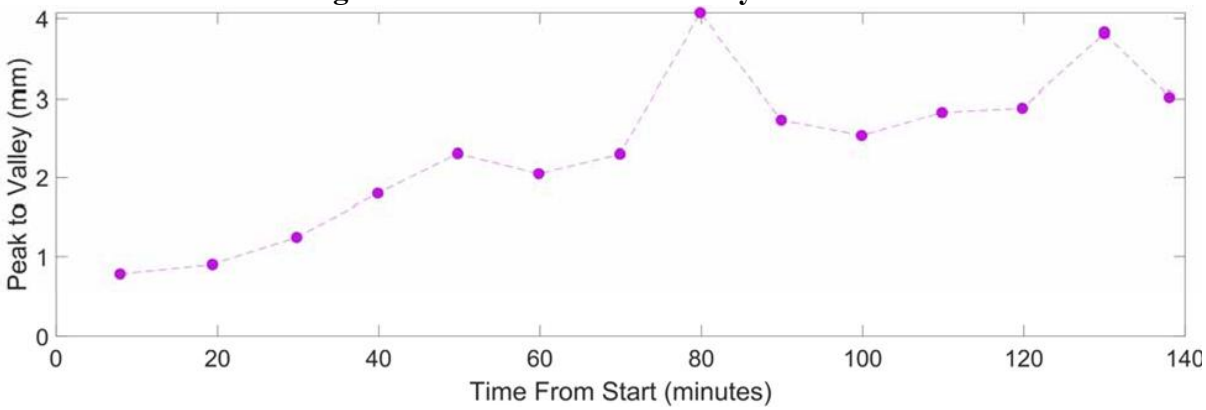

Figure 062121.12: Equivalent Roughness Evolution

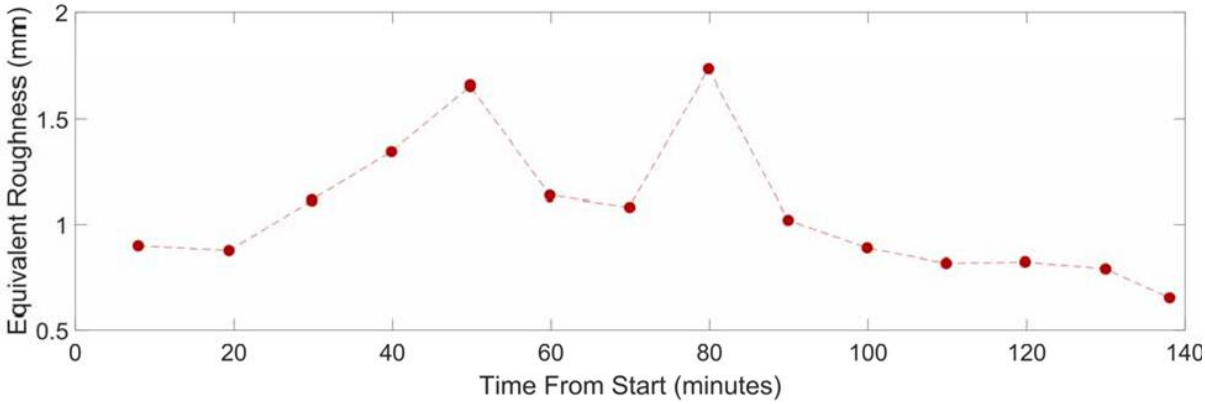

Table 062121.02: Summary of Roughness Parameters

Time (min.)	RMS (mm)	Skewness	Peak to Valley (mm)	ks,Flack-Schultz (mm)
7.9134	0.0715	1.1397	0.7822	0.8975
19.3634	0.1280	0.3722	0.9002	0.8748
29.8134	0.1929	0.2130	1.2461	1.1136
39.8634	0.2617	0.1144	1.7968	1.3451
49.7967	0.3312	0.0930	2.3060	1.6574
59.8467	0.2990	-0.1065	2.0476	1.1353
69.9134	0.3268	-0.1910	2.2981	1.0830
79.8634	0.5511	-0.2204	4.0740	1.7357
89.9134	0.3634	-0.2831	2.7320	1.0204
99.8800	0.3373	-0.3161	2.5342	0.8878
109.8467	0.3414	-0.3636	2.8288	0.8144
119.8134	0.3433	-0.3622	2.8849	0.8212
129.9634	0.4226	-0.4683	3.8259	0.7880
138.0300	0.3421	-0.4619	3.0224	0.6485

Figure 062121.13: Frost Topography at 00:07:54

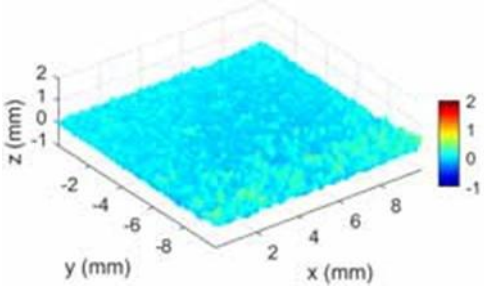

Figure 062121.14: Frost Topography at 00:19:21

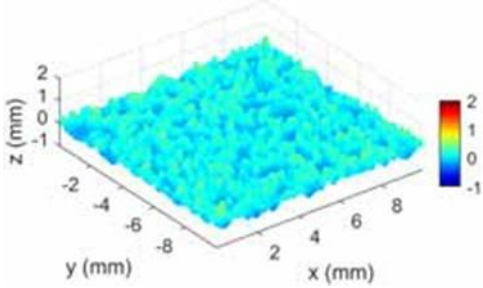

Figure 062121.15: Frost Topography at 00:29:48

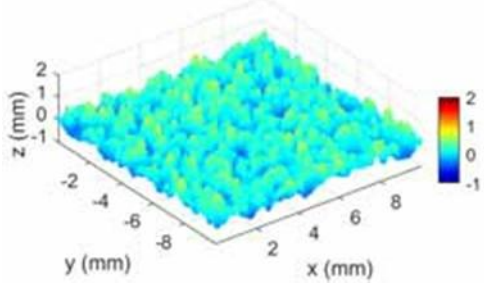

Figure 062121.16: Frost Topography at 00:39:51

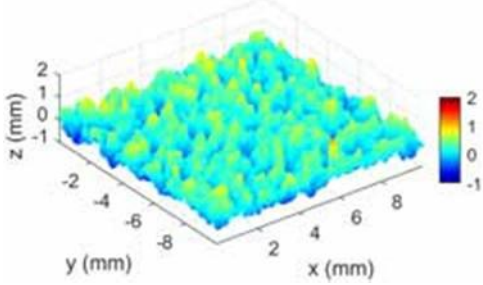

Figure 062121.17: Frost Topography at 00:49:47

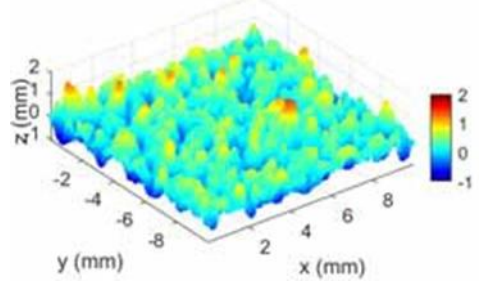

Figure 062121.18: Frost Topography at 00:59:50

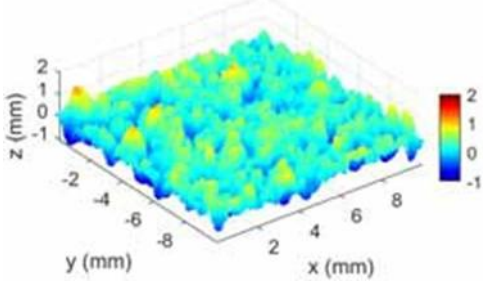

Figure 062121.19: Frost Topography at 01:09:54

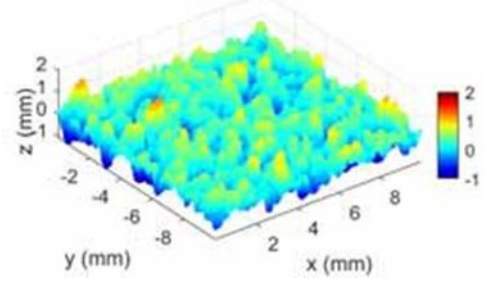

Figure 062121.20: Frost Topography at 01:19:51

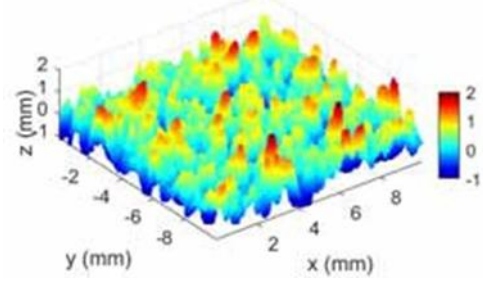

Figure 062121.21: Frost Topography at 01:29:54

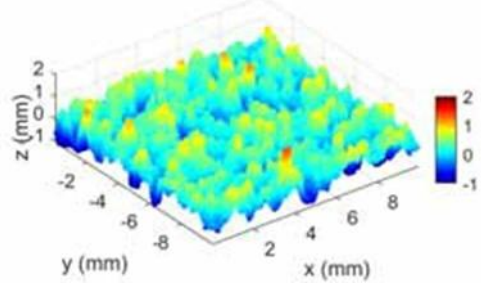

Figure 062121.22: Frost Topography at 01:39:52

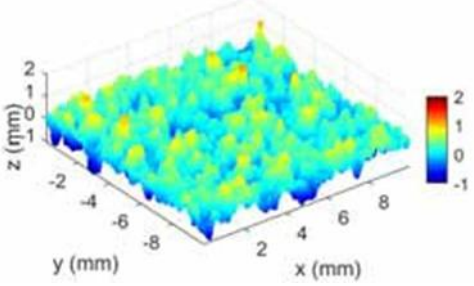

Figure 062121.23: Frost Topography at 01:49:50

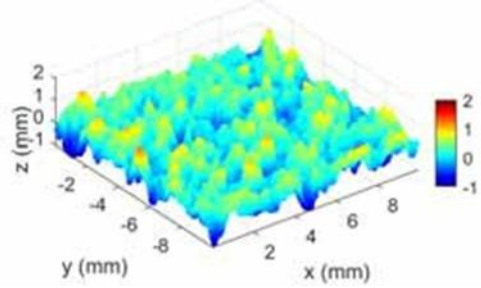

Figure 062121.24: Frost Topography at 01:59:48

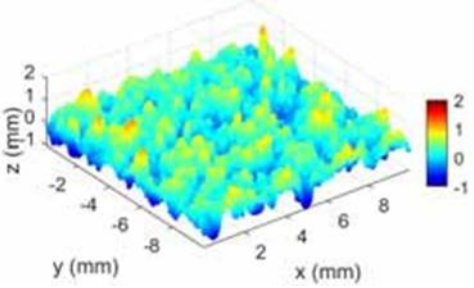

Figure 062121.25: Frost Topography at 02:09:57

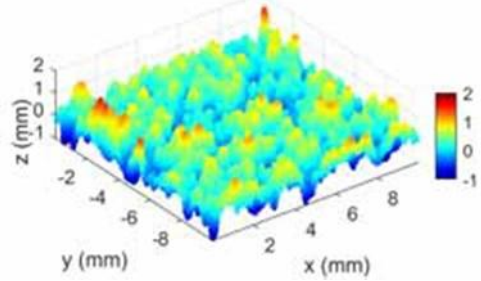

Figure 062121.26: Frost Topography at 02:18:01

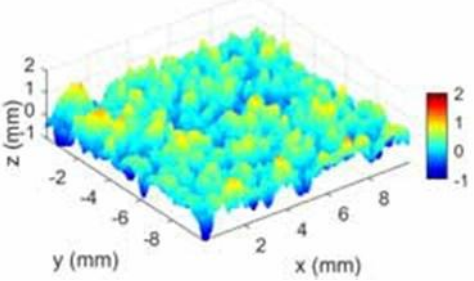

CAFF Conditions Report – Case Date: 062521

Table 062521.01: Summary of Measured Test Variables

Variable	Mean	St. Dev.	Rand. Unc.
T_air (C)	4.2533	0.2725	0.0092
Rh (%)	79.5749	5.0087	0.1695
Omega (kg_v/kg_da)	0.00414550	0.00032428	0.00001097
V_air (m/s)	1.4800	0.1224	0.0041
T_skin (C)	-8.5113	1.1387	0.0385
T_floor (C)	-20.3682	0.0630	0.0021

Figure 062521.01: Temperature and Voltage Control Time History

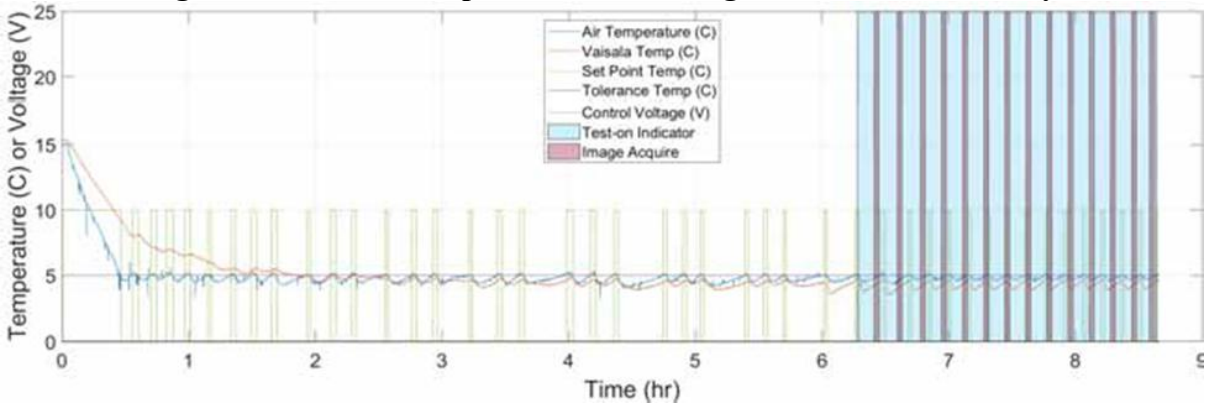

Figure 062521.02: Relative Humidity Time History

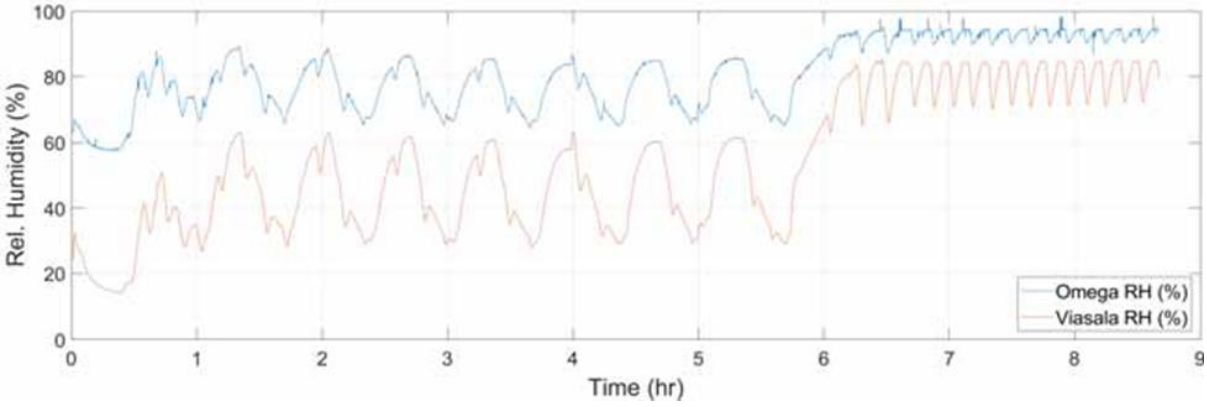

Figure 062521.03: Velocity Time History

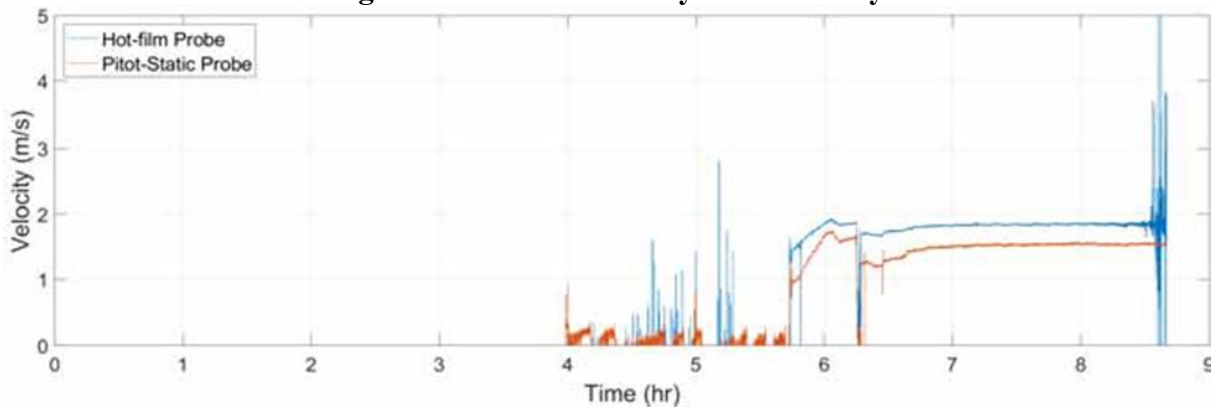

Figure 062521.04: Coolant Return Temperature Time History

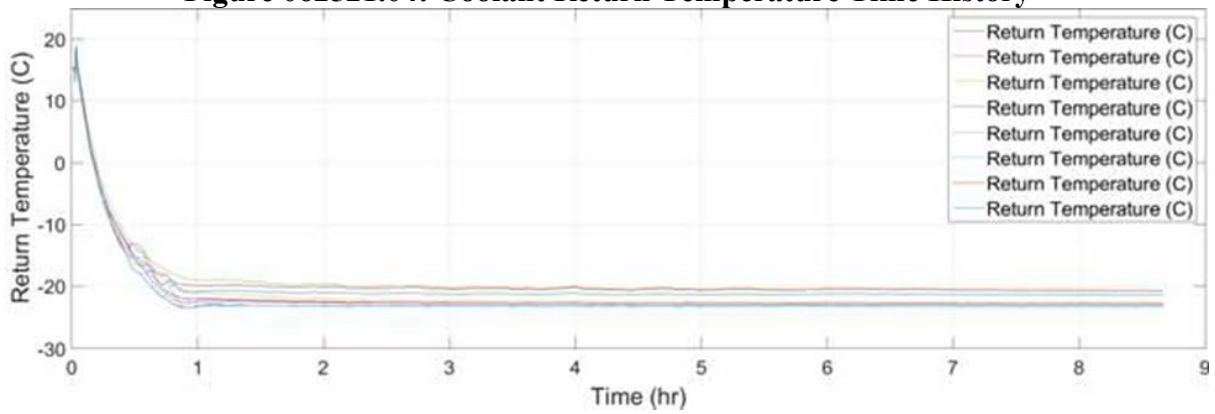

Figure 062521.05: Coolant Supply Temperature Time History

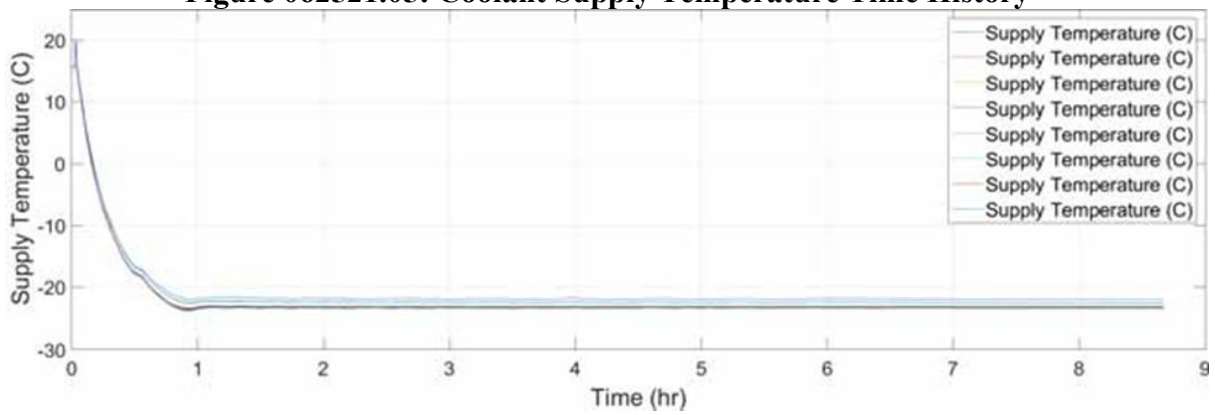

Figure 062521.06: Skin Temperature Time History

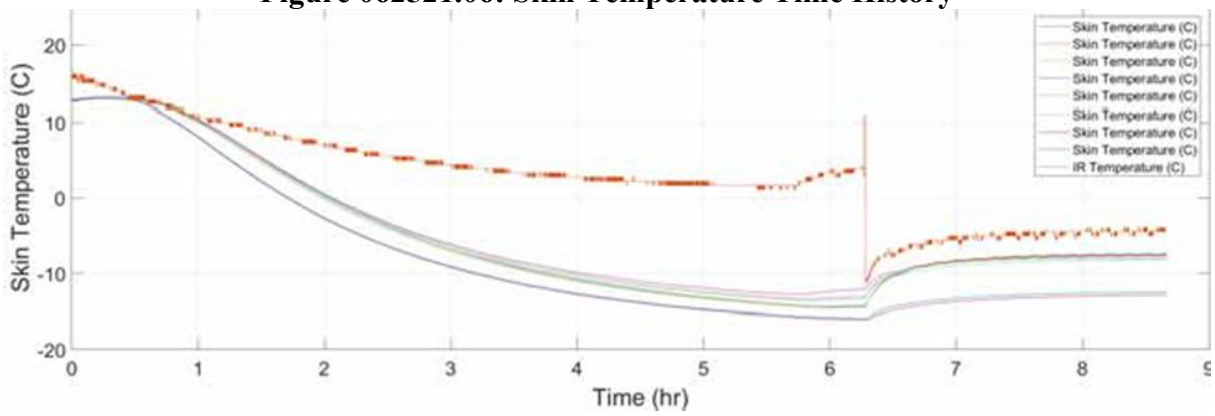

Figure 062521.07: Floor Temperature Time History

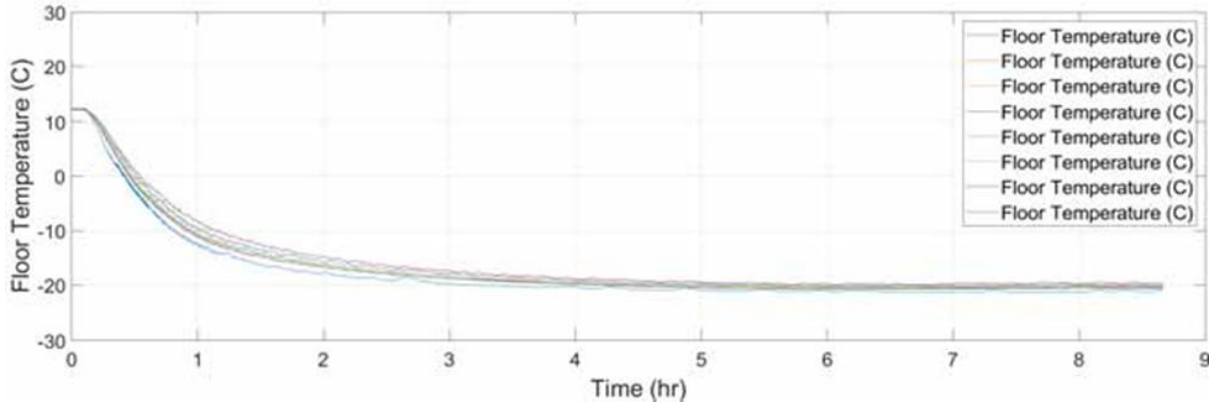

Figure 062521.08: Skin Temperature Slope Time History

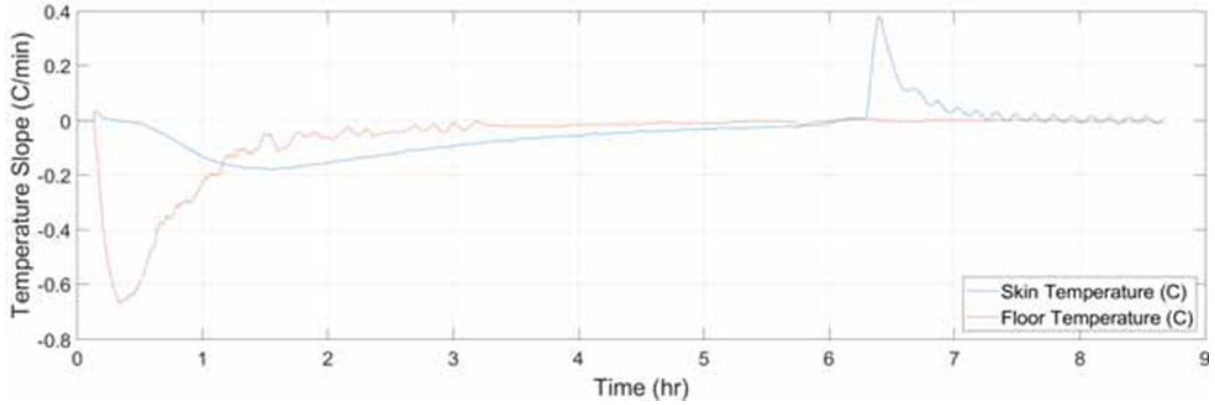

Figure 062521.09: RMS Height Evolution

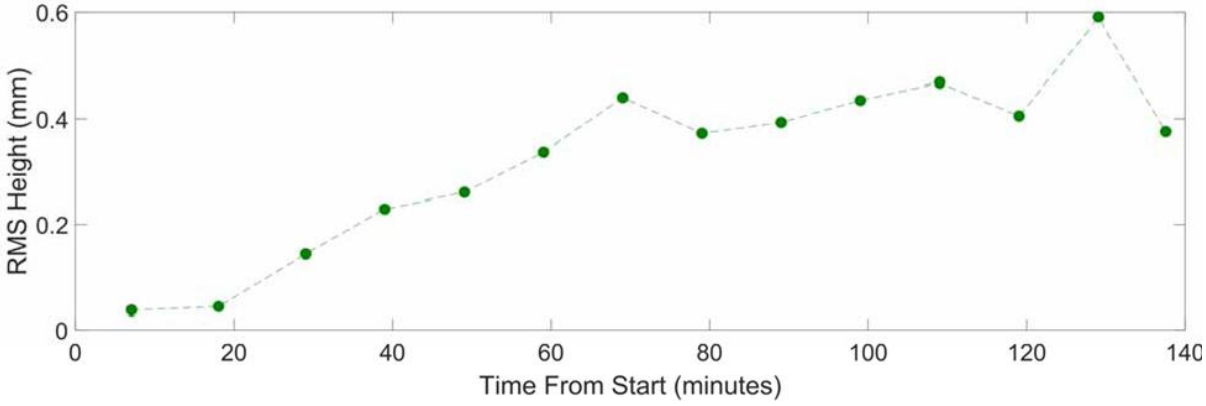

Figure 062521.10: Skewness Evolution

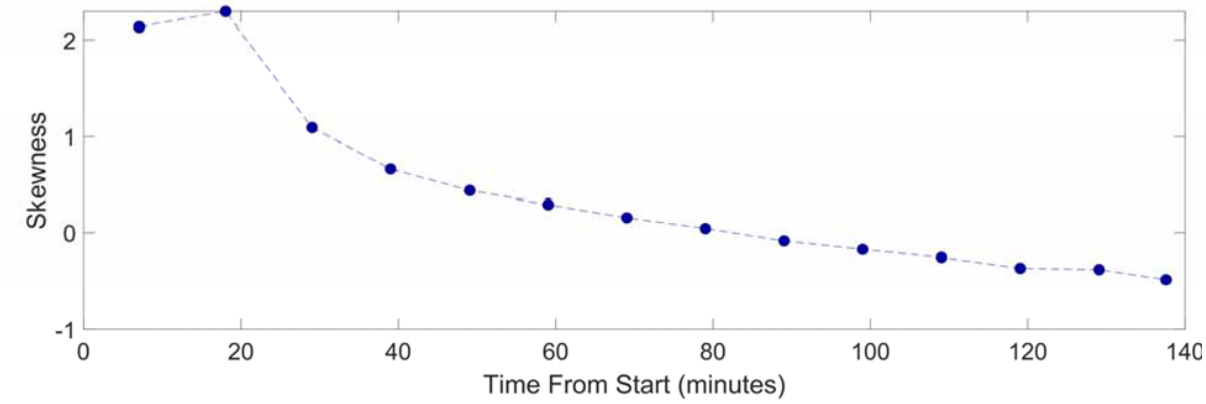

Figure 062521.11: Peak to Valley Evolution

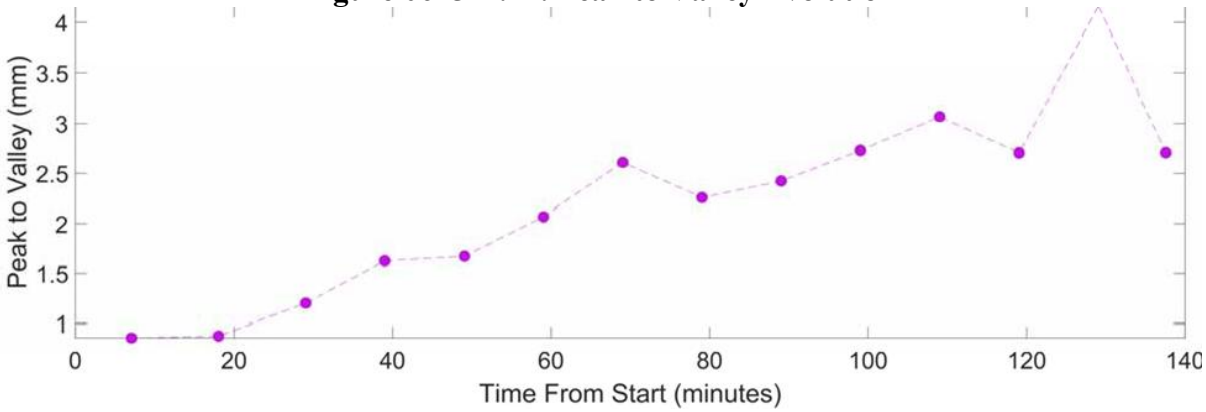

Figure 062521.12: Equivalent Roughness Evolution

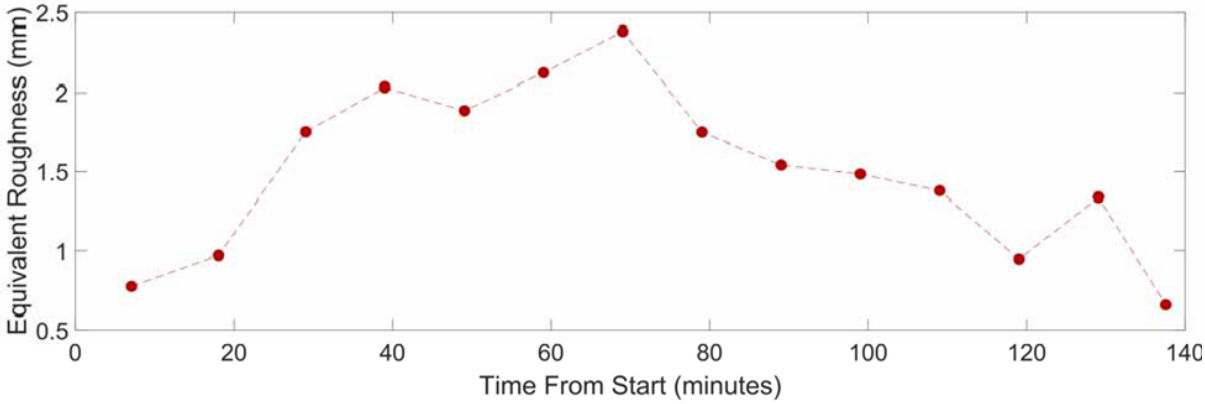

Table 062521.02: Summary of Roughness Parameters

Time (min.)	RMS (mm)	Skewness	Peak to Valley (mm)	ks,Flack-Schultz (mm)
7.0598	0.0365	2.1303	0.8577	0.7726
18.0431	0.0429	2.2897	0.8767	0.9705
29.0431	0.1437	1.0926	1.1997	1.7507
39.0098	0.2295	0.6587	1.6262	2.0333
49.0764	0.2599	0.4336	1.6726	1.8857
59.0431	0.3367	0.2938	2.0704	2.1229
69.0431	0.4411	0.1564	2.6107	2.3845
79.0264	0.3724	0.0437	2.2550	1.7494
89.0264	0.3933	-0.0864	2.4213	1.5394
99.0098	0.4355	-0.1749	2.7299	1.4825
109.0264	0.4689	-0.2594	3.0684	1.3766
119.0431	0.4055	-0.3744	2.7053	0.9448
129.0598	0.5909	-0.3874	4.1639	1.3378
137.5598	0.3757	-0.4943	2.7064	0.6541

Figure 062521.13: Frost Topography at 00:07:52

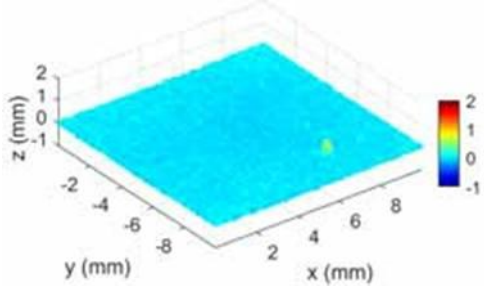

Figure 062521.14: Frost Topography at 00:18:51

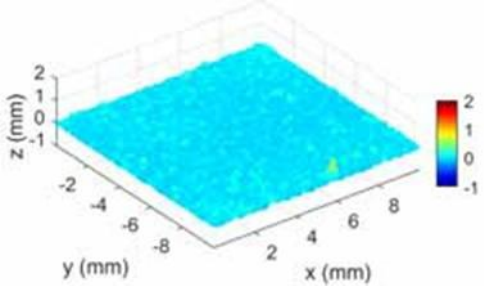

Figure 062521.15: Frost Topography at 00:29:51

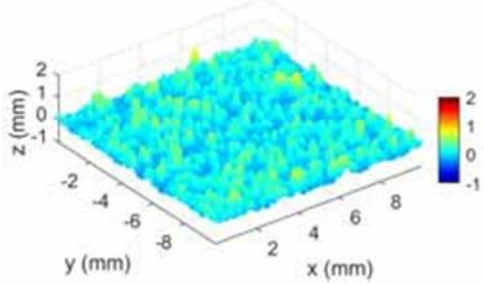

Figure 062521.16: Frost Topography at 00:39:49

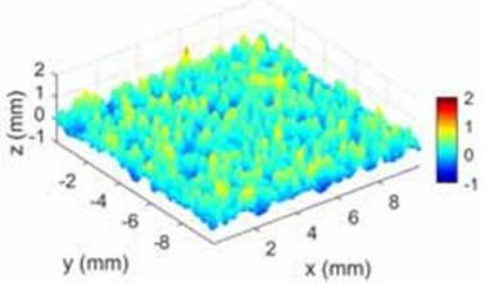

Figure 062521.17: Frost Topography at 00:49:53

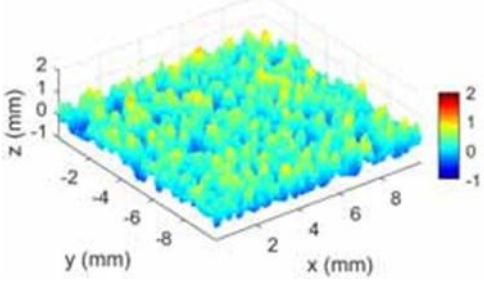

Figure 062521.18: Frost Topography at 00:59:51

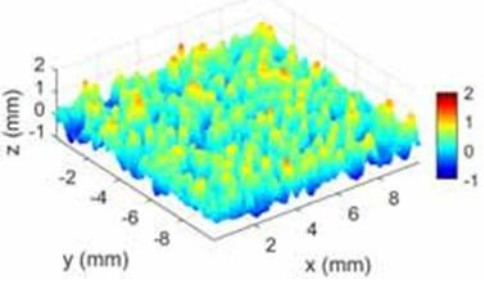

Figure 062521.19: Frost Topography at 01:09:51

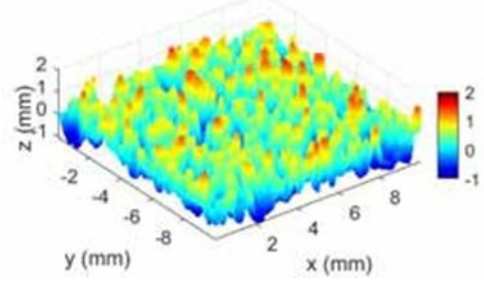

Figure 062521.20: Frost Topography at 01:19:50

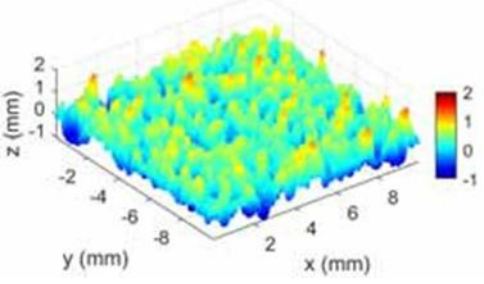

Figure 062521.21: Frost Topography at 01:29:50

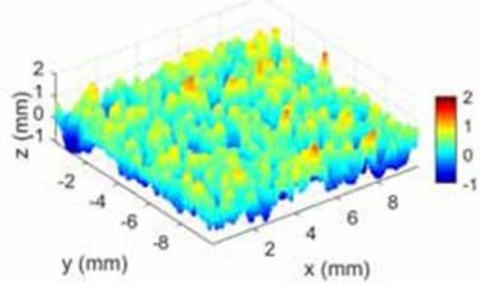

Figure 062521.22: Frost Topography at 01:39:49

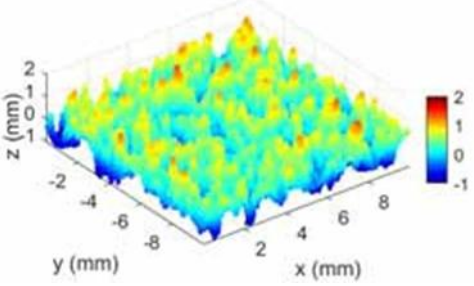

Figure 062521.23: Frost Topography at 01:49:50

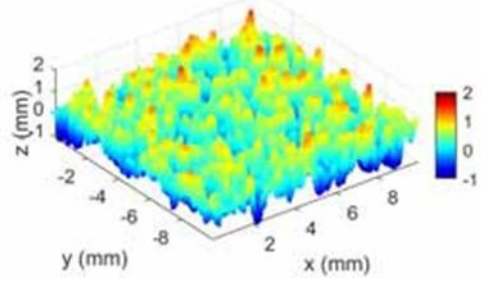

Figure 062521.24: Frost Topography at 01:59:51

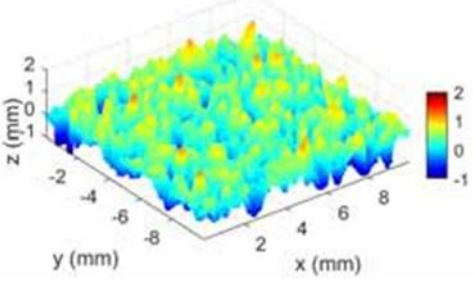

Figure 062521.25: Frost Topography at 02:09:52

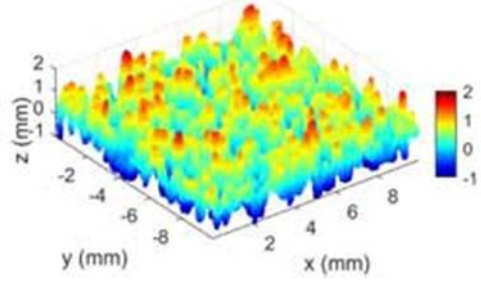

Figure 062521.26: Frost Topography at 02:18:22

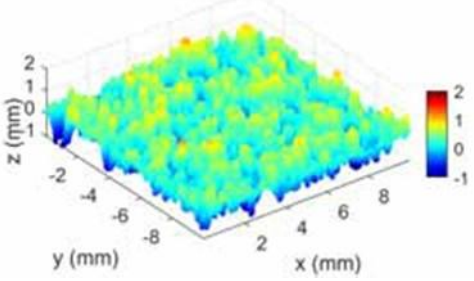

CAFF Conditions Report – Case Date: 062821

Table 062821.01: Summary of Measured Test Variables

Variable	Mean	St. Dev.	Rand. Unc.
T_air (C)	15.2212	0.2233	0.0076
Rh (%)	78.6477	3.5085	0.1191
Omega (kg_v/kg_da)	0.00859625	0.00047297	0.00001605
V_air (m/s)	0.2556	0.1044	0.0035
T_skin (C)	-5.7015	1.2768	0.0433
T_floor (C)	-19.4718	0.0992	0.0034

Figure 062821.01: Temperature and Voltage Control Time History

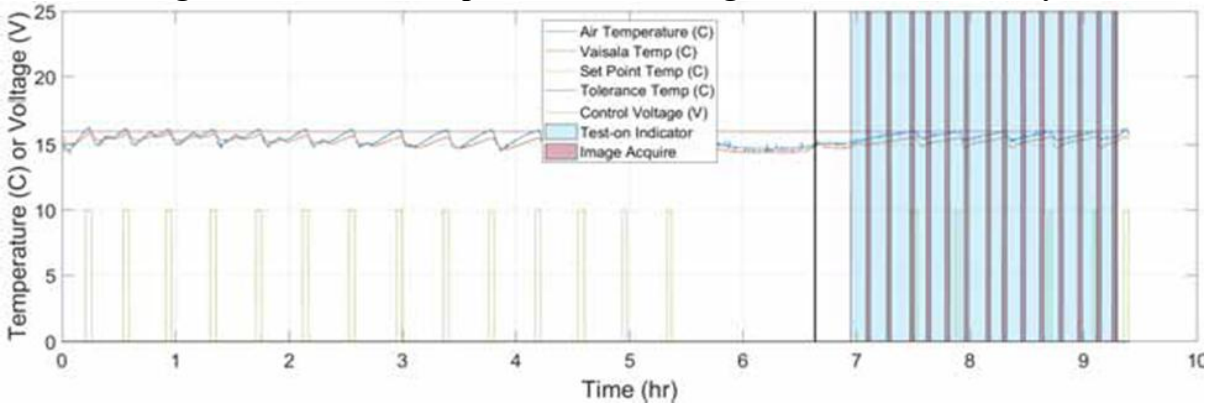

Figure 062821.02: Relative Humidity Time History

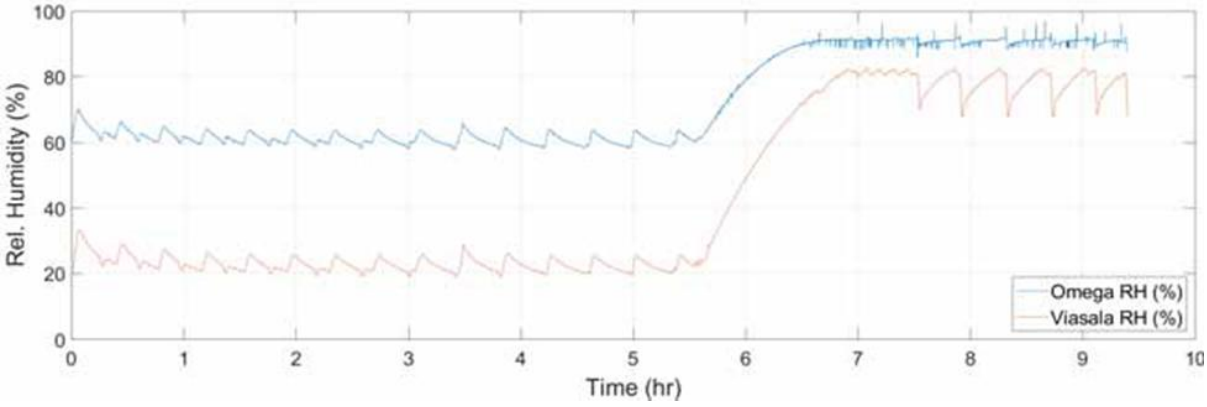

Figure 062821.03: Velocity Time History

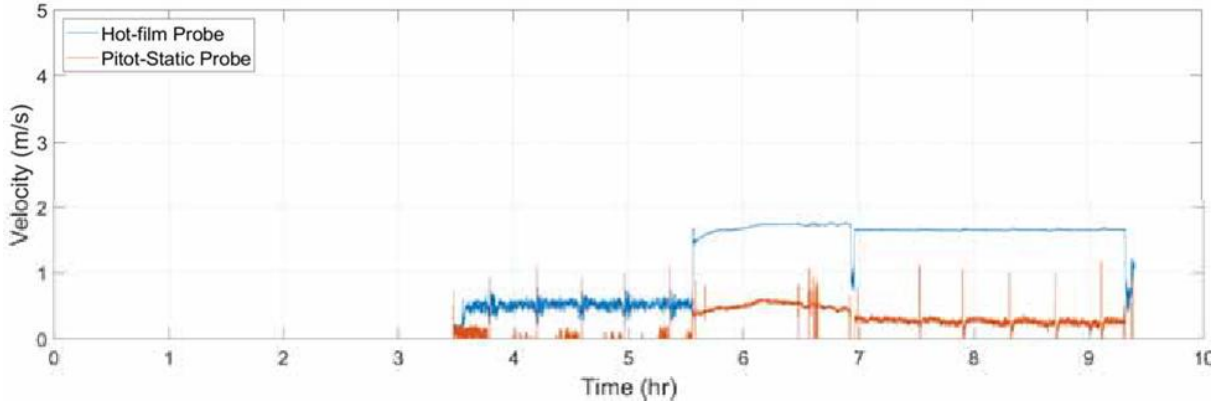

Figure 062821.04: Coolant Return Temperature Time History

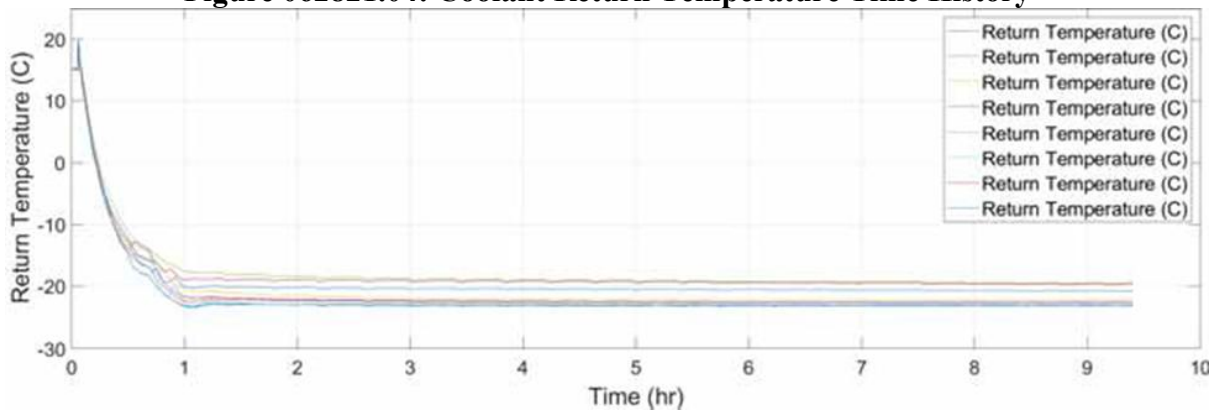

Figure 062821.05: Coolant Supply Temperature Time History

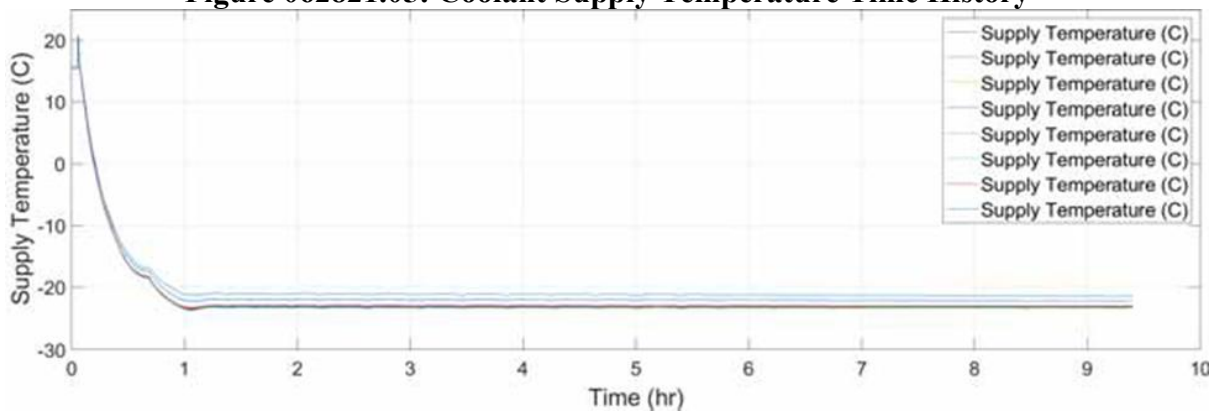

Figure 062821.06: Skin Temperature Time History

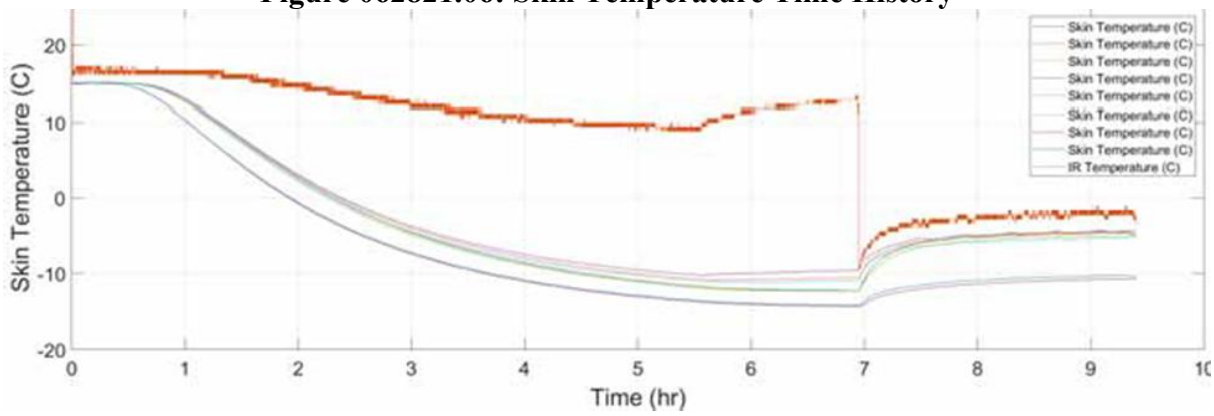

Figure 062821.07: Floor Temperature Time History

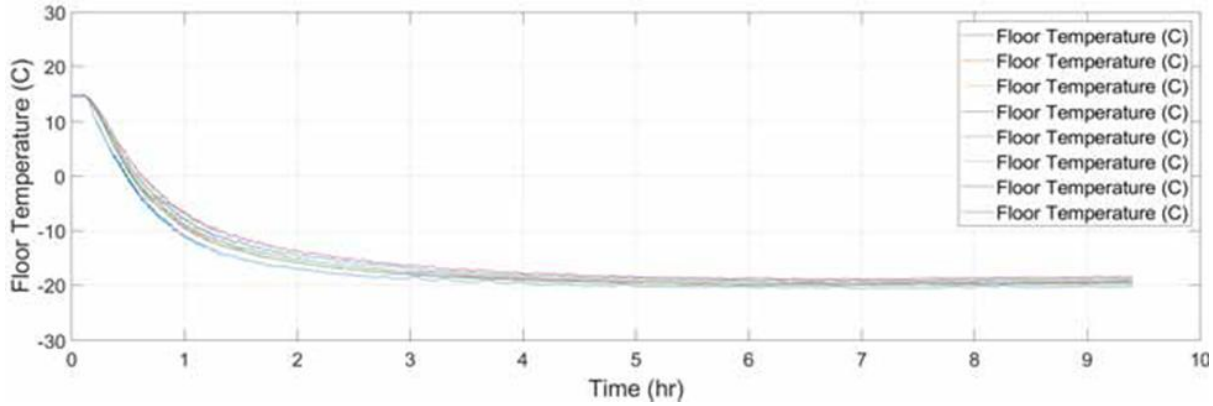

Figure 062821.08: Skin Temperature Slope Time History

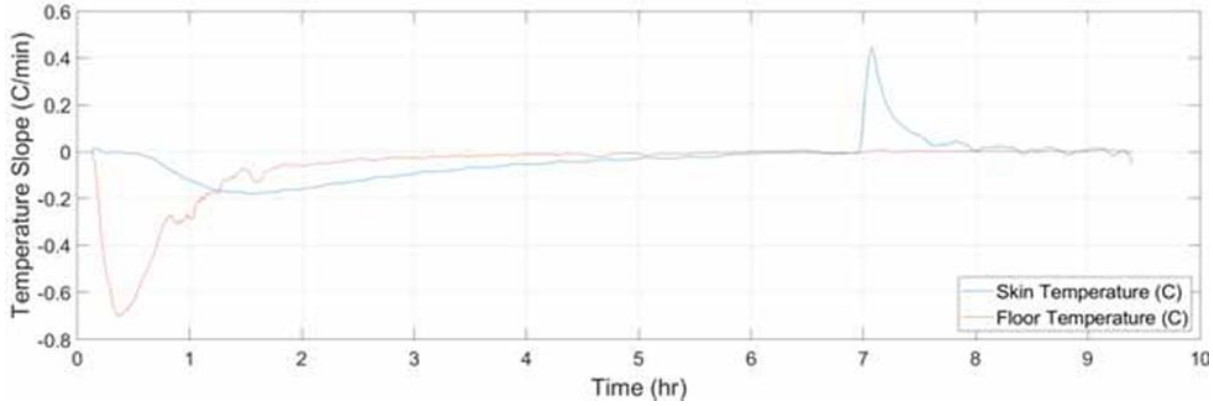

Figure 062821.09: RMS Height Evolution

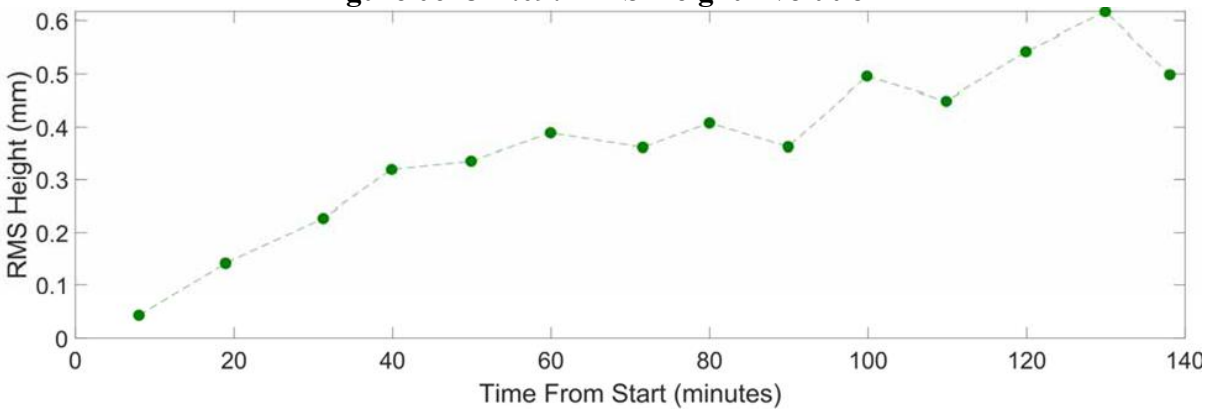

Figure 062821.10: Skewness Evolution

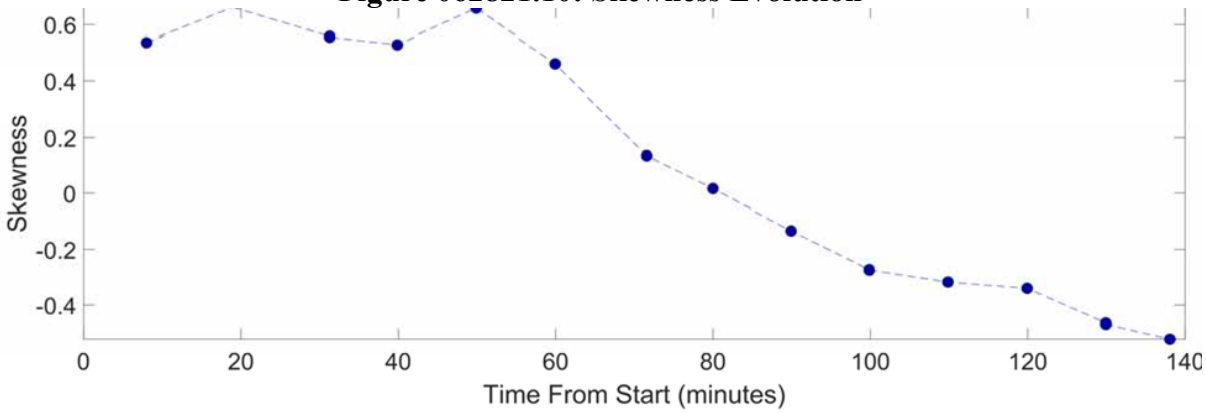

Figure 062821.11: Peak to Valley Evolution

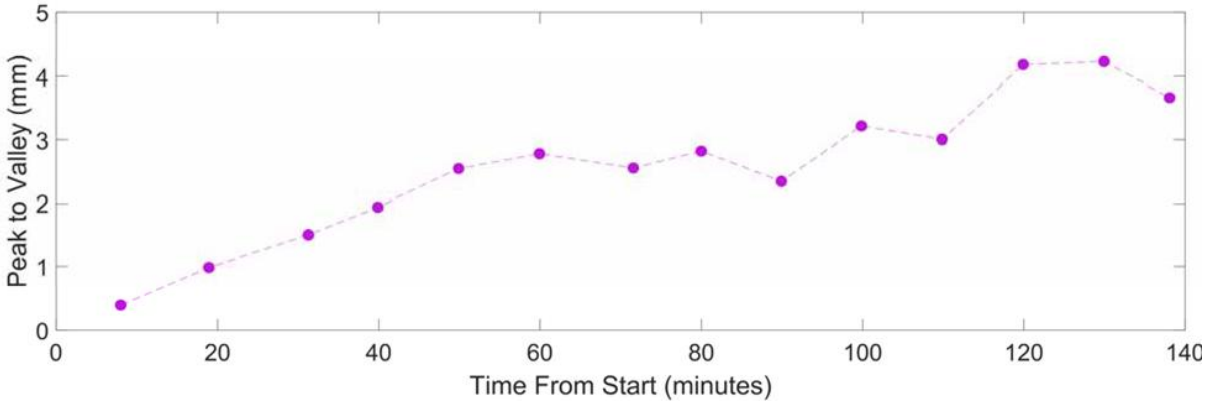

Figure 062821.12: Equivalent Roughness Evolution

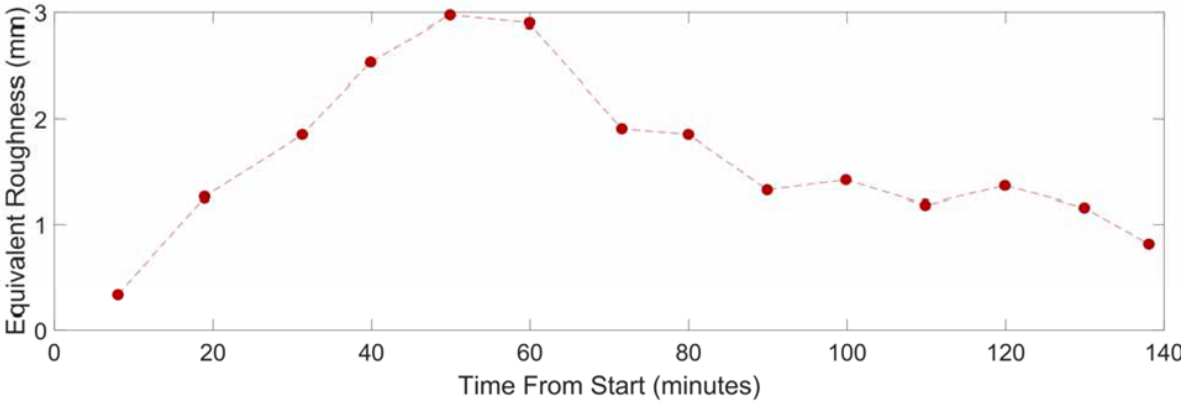

Table 062821.02: Summary of Roughness Parameters

Time (min.)	RMS (mm)	Skewness	Peak to Valley (mm)	ks,Flack-Schultz (mm)
7.9974	0.0410	0.5386	0.3772	0.3278
18.9308	0.1414	0.6633	0.9824	1.2580
31.2641	0.2276	0.5583	1.5009	1.8512
39.8808	0.3194	0.5307	1.9417	2.5354
49.8974	0.3353	0.6603	2.5450	2.9750
59.9308	0.3893	0.4616	2.7826	2.9009
71.5641	0.3616	0.1351	2.5531	1.9056
79.9808	0.4084	0.0169	2.8248	1.8513
89.9141	0.3626	-0.1327	2.3406	1.3218
99.8474	0.4959	-0.2729	3.2225	1.4196
109.8641	0.4501	-0.3166	3.0098	1.1838
119.9141	0.5431	-0.3392	4.1859	1.3638
129.9308	0.6174	-0.4650	4.2370	1.1609
138.0641	0.4984	-0.5186	3.6738	0.8111

Figure 062821.13: Frost Topography at 00:08:02

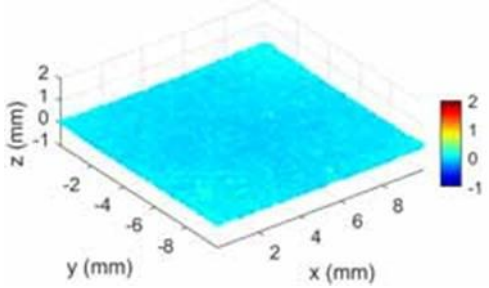

Figure 062821.14: Frost Topography at 00:18:58

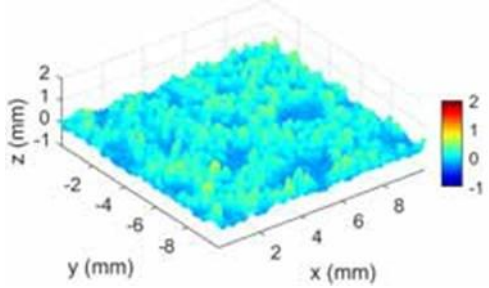

Figure 062821.15: Frost Topography at 00:31:18

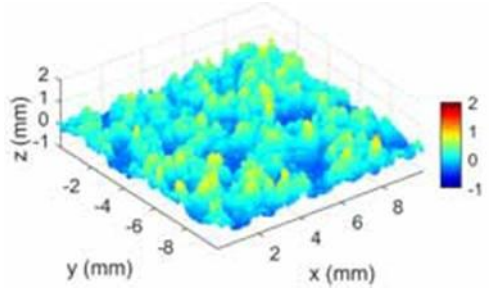

Figure 062821.16: Frost Topography at 00:39:55

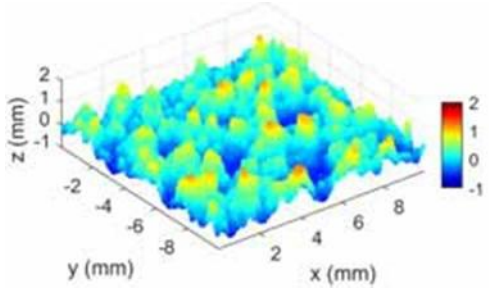

Figure 062821.17: Frost Topography at 00:49:56

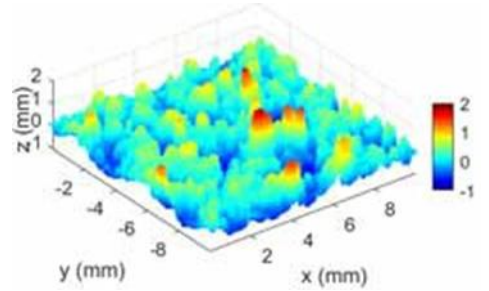

Figure 062821.18: Frost Topography at 00:59:58

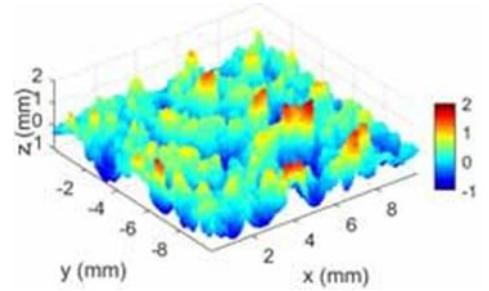

Figure 062821.19: Frost Topography at 01:11:36

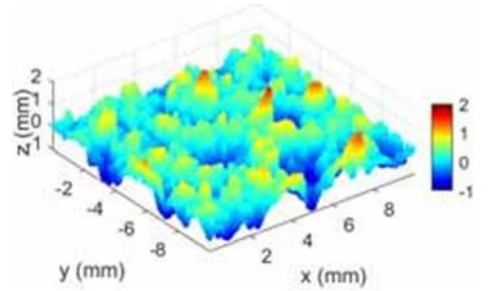

Figure 062821.20: Frost Topography at 01:20:01

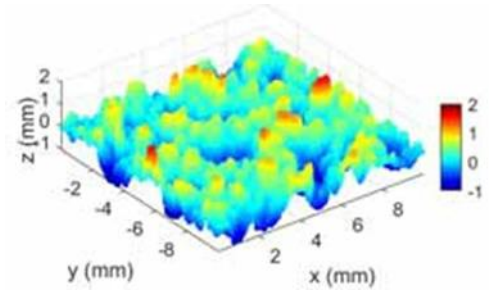

Figure 062821.21: Frost Topography at 01:29:57

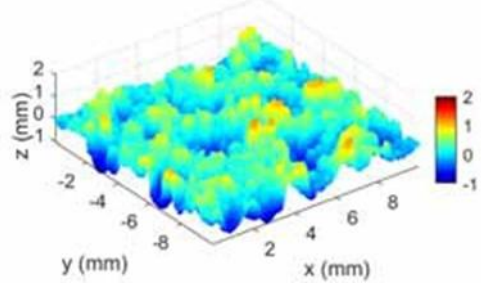

Figure 062821.22: Frost Topography at 01:39:53

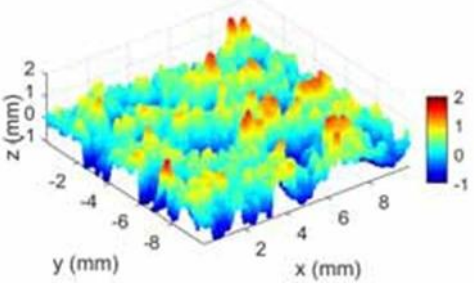

Figure 062821.23: Frost Topography at 01:49:54

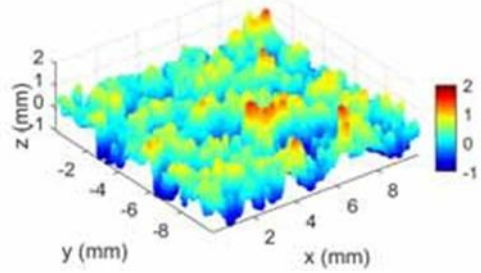

Figure 062821.24: Frost Topography at 01:59:57

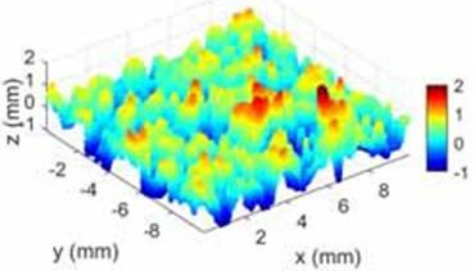

Figure 062821.25: Frost Topography at 02:09:58

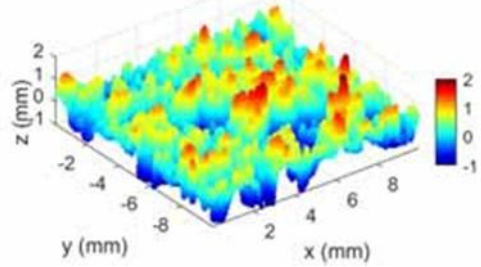

Figure 062821.26: Frost Topography at 02:18:06

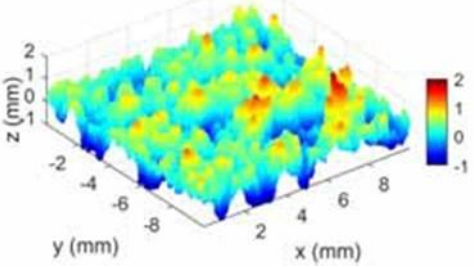

CAFF Conditions Report – Case Date: 063021

Table 063021.01: Summary of Measured Test Variables

Variable	Mean	St. Dev.	Rand. Unc.
T_air (C)	9.2170	0.3170	0.0108
Rh (%)	79.6242	5.6857	0.1933
Omega (kg_v/kg_da)	0.00581739	0.00045088	0.00001533
V_air (m/s)	0.3097	0.1070	0.0036
T_skin (C)	-8.7448	1.0831	0.0368
T_floor (C)	-20.1618	0.0575	0.0020

Figure 063021.01: Temperature and Voltage Control Time History

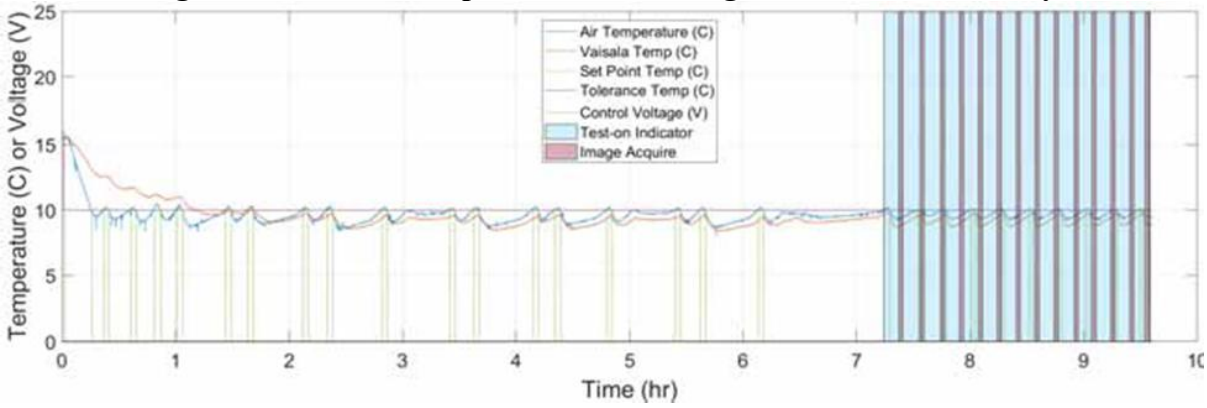

Figure 063021.02: Relative Humidity Time History

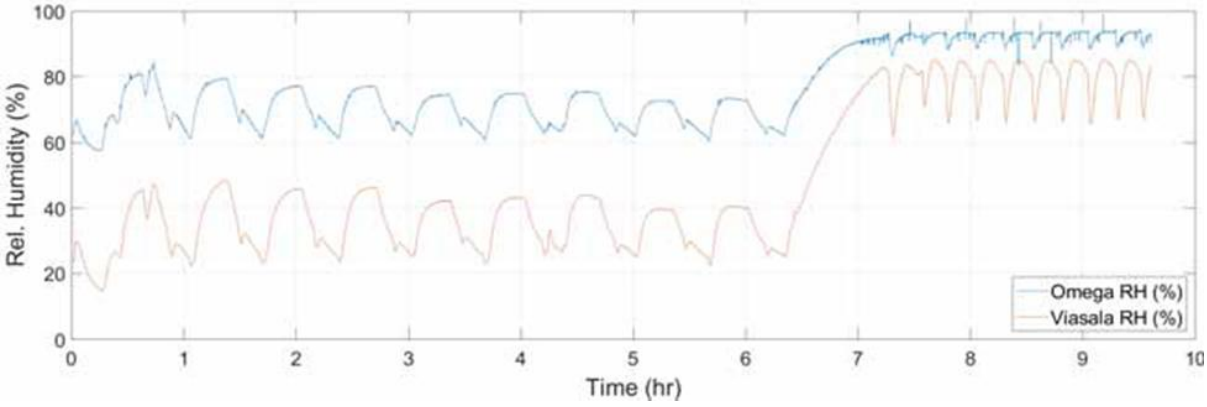

Figure 063021.03: Velocity Time History

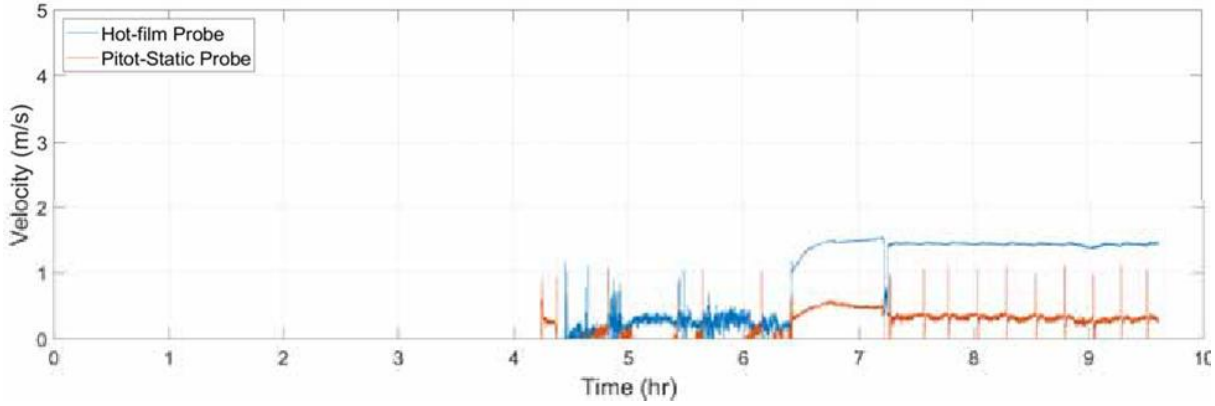

Figure 063021.04: Coolant Return Temperature Time History

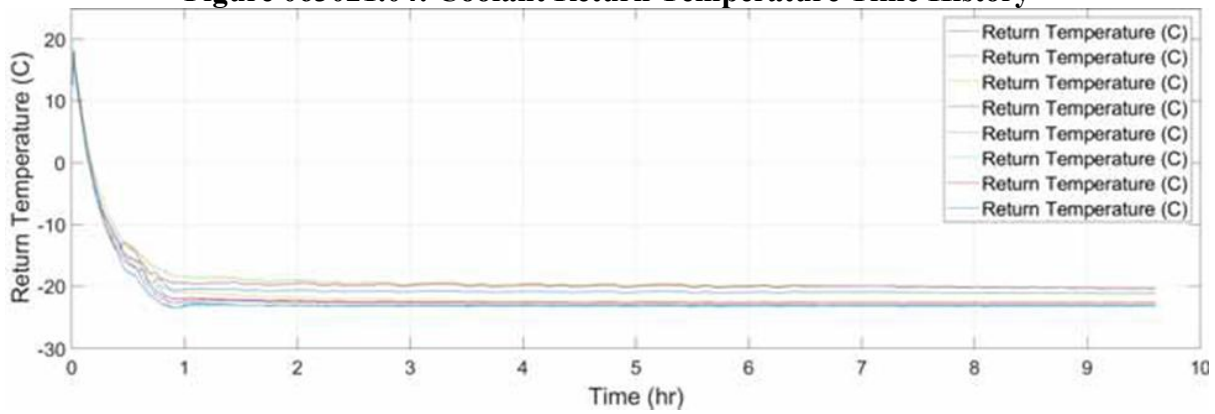

Figure 063021.05: Coolant Supply Temperature Time History

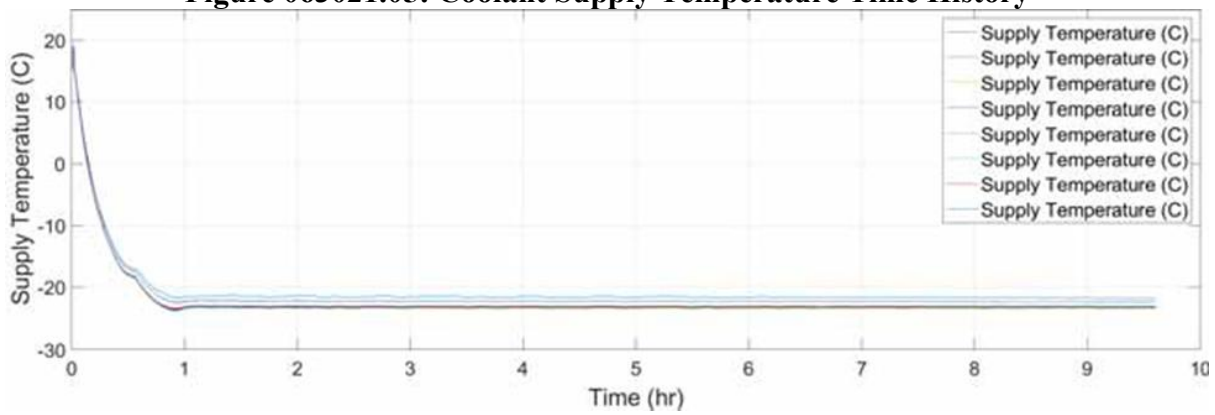

Figure 063021.06: Skin Temperature Time History

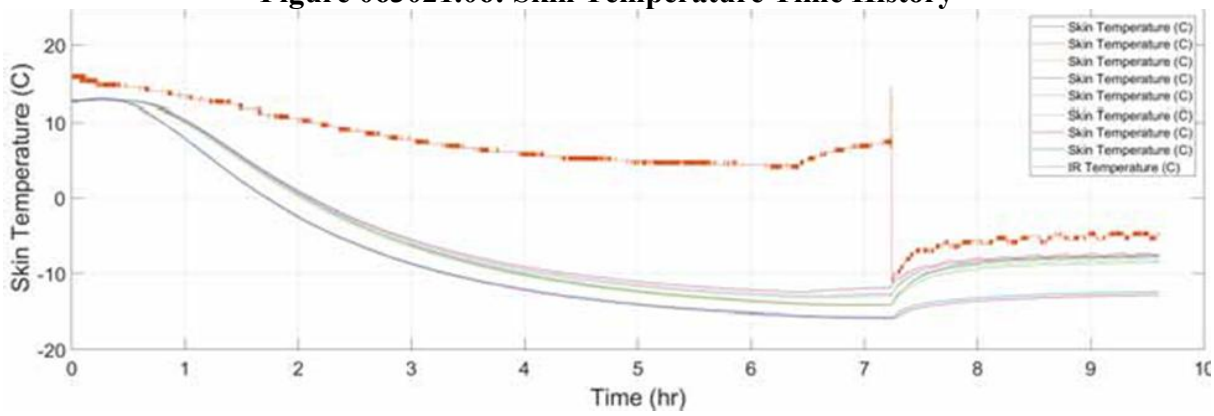

Figure 063021.07: Floor Temperature Time History

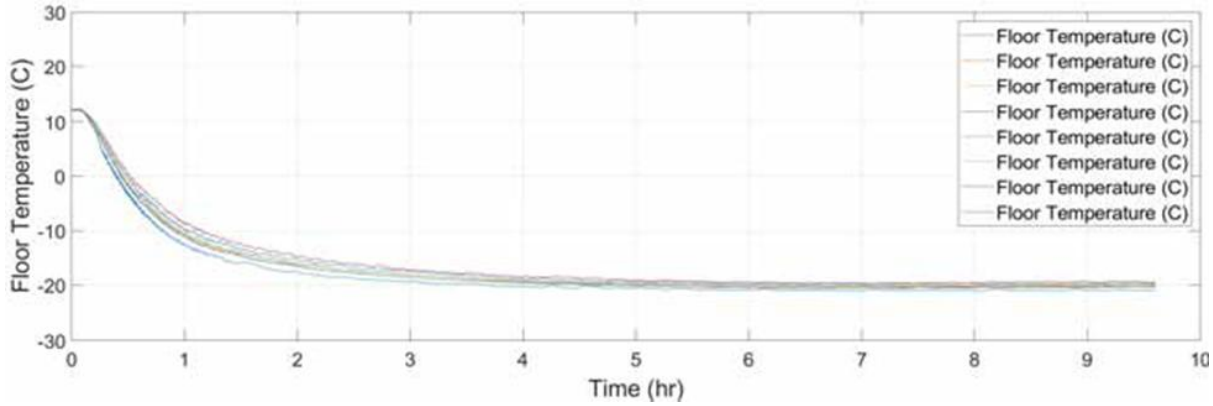

Figure 063021.08: Skin Temperature Slope Time History

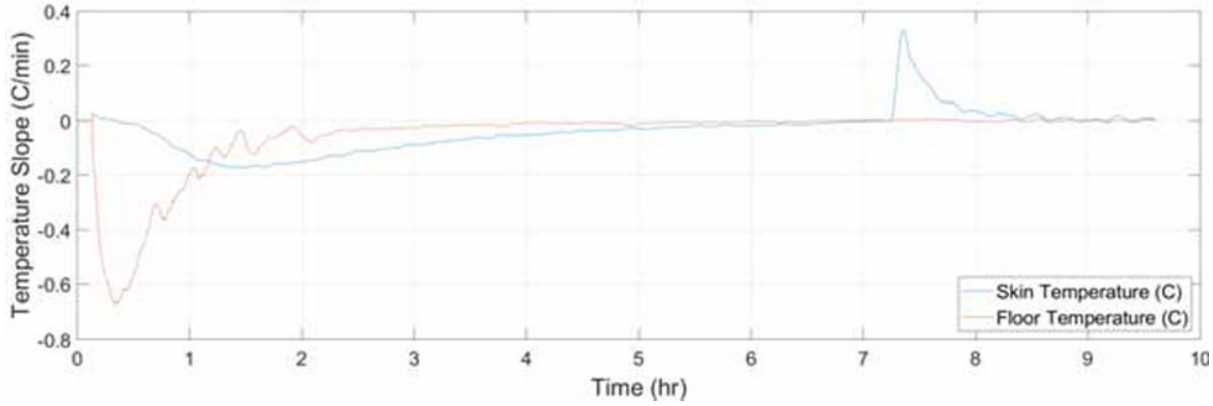

Figure 063021.09: RMS Height Evolution

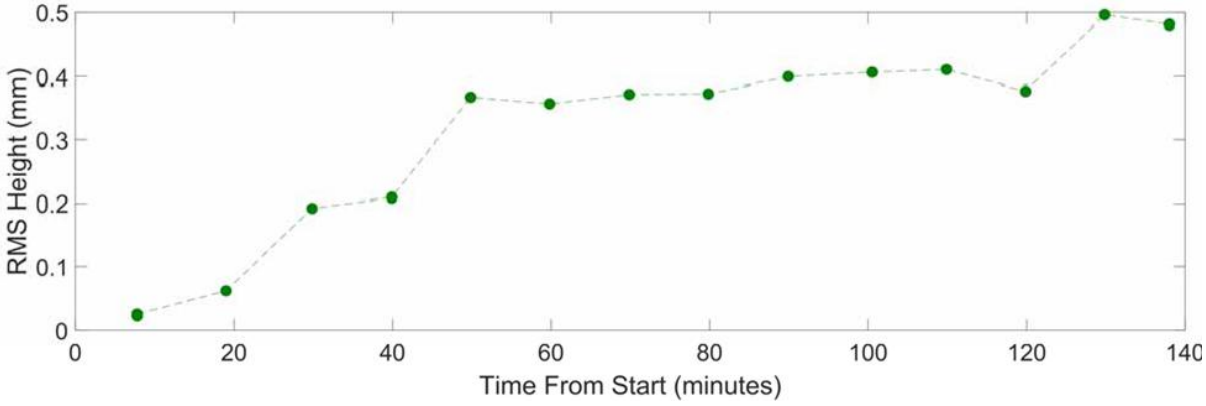

Figure 063021.10: Skewness Evolution

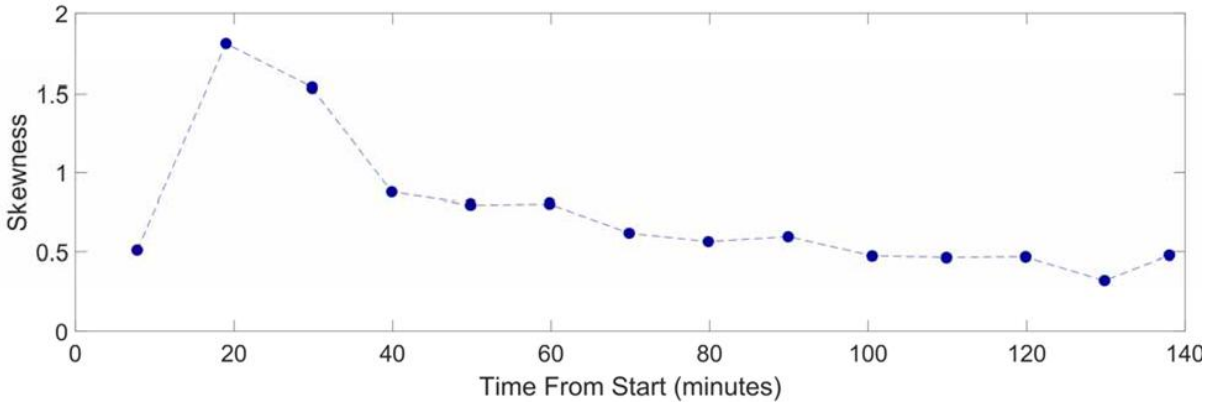

Figure 063021.11: Peak to Valley Evolution

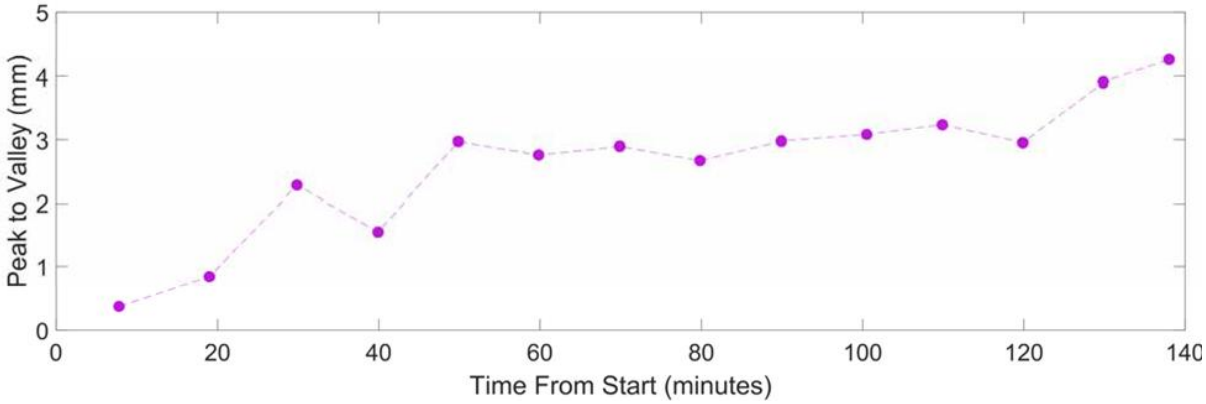

Figure 063021.12: Equivalent Roughness Evolution

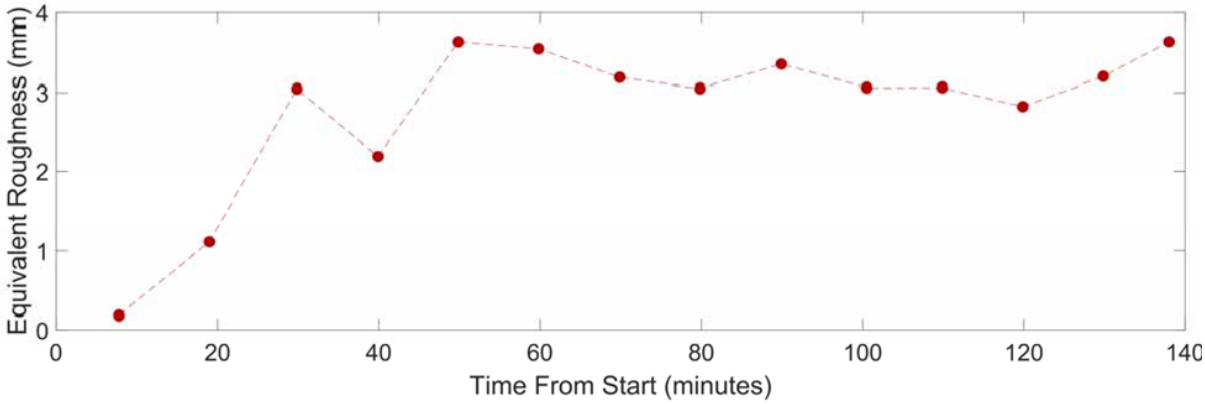

Table 063021.02: Summary of Roughness Parameters

Time (min.)	RMS (mm)	Skewness	Peak to Valley (mm)	ks,Flack-Schultz (mm)
7.7825	0.0233	0.5090	0.3567	0.1810
18.9825	0.0609	1.8156	0.8354	1.1132
29.8491	0.1923	1.5361	2.2801	3.0486
39.8991	0.2089	0.8748	1.5452	2.1889
49.8491	0.3680	0.7970	2.9757	3.6389
59.8158	0.3573	0.8036	2.7609	3.5510
69.8658	0.3724	0.6170	2.8985	3.1865
79.8325	0.3733	0.5634	2.6731	3.0506
89.9158	0.3996	0.5955	2.9811	3.3574
100.4991	0.4066	0.4722	3.0844	3.0598
109.8825	0.4108	0.4623	3.2422	3.0632
119.8658	0.3772	0.4663	2.9554	2.8230
129.8325	0.4963	0.3152	3.9119	3.2001
138.0158	0.4814	0.4774	4.2674	3.6399

Figure 063021.13: Frost Topography at 00:07:46

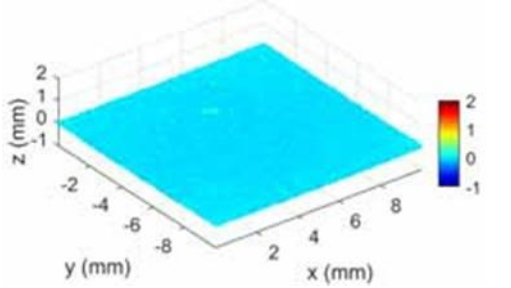

Figure 063021.14: Frost Topography at 00:18:58

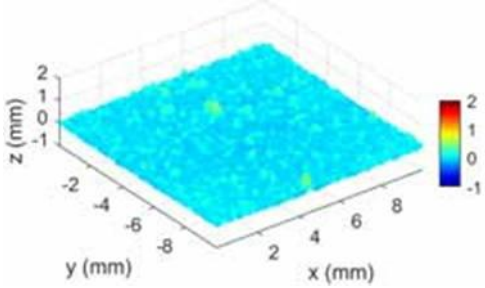

Figure 063021.15: Frost Topography at 00:29:50

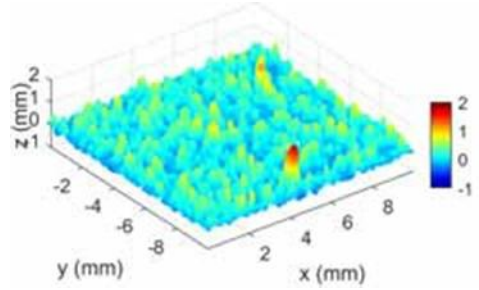

Figure 063021.16: Frost Topography at 00:39:53

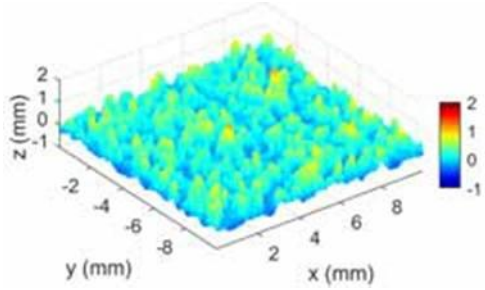

Figure 063021.17: Frost Topography at 00:49:50

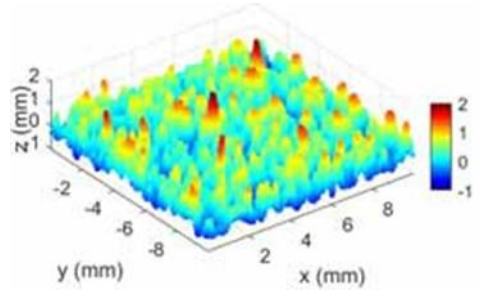

Figure 063021.18: Frost Topography at 00:59:48

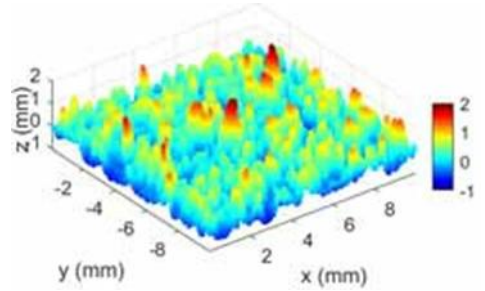

Figure 063021.19: Frost Topography at 01:09:51

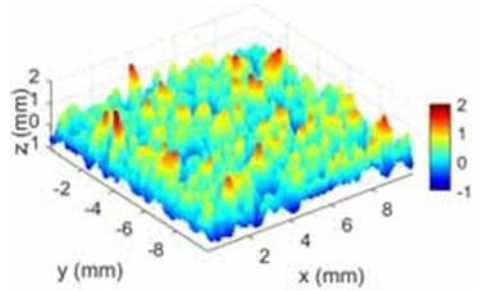

Figure 063021.20: Frost Topography at 01:19:49

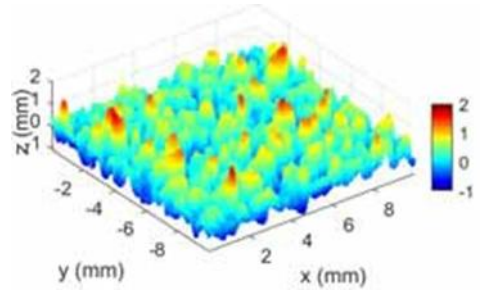

Figure 063021.21: Frost Topography at 01:29:54

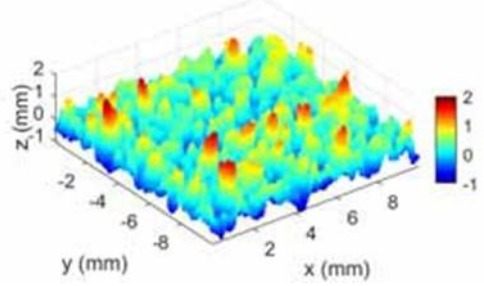

Figure 063021.22: Frost Topography at 01:40:29

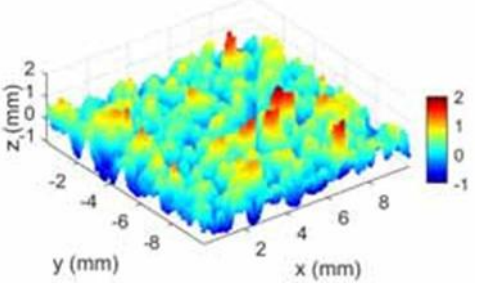

Figure 063021.23: Frost Topography at 01:49:52

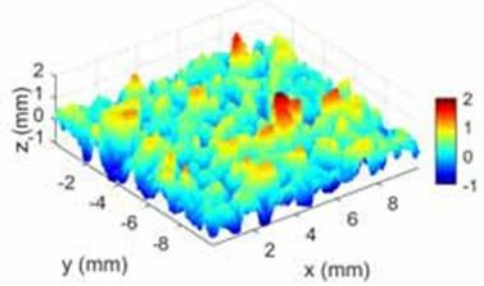

Figure 063021.24: Frost Topography at 01:59:51

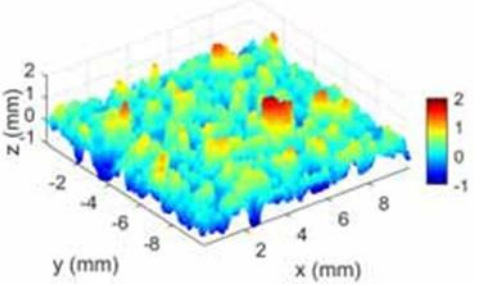

Figure 063021.25: Frost Topography at 02:09:49

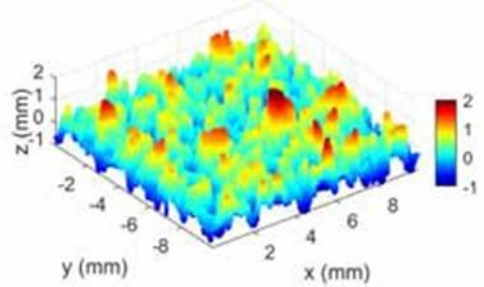

Figure 063021.26: Frost Topography at 02:18:00

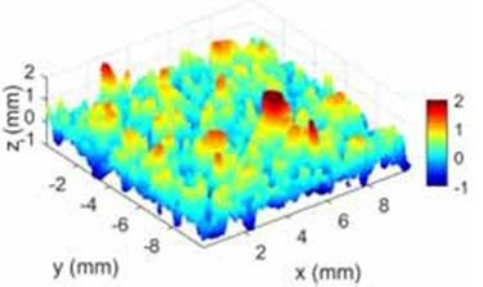

CAFF Conditions Report – Case Date: 070221

Table 070221.01: Summary of Measured Test Variables

Variable	Mean	St. Dev.	Rand. Unc.
T_air (C)	4.2635	0.1795	0.0061
Rh (%)	79.7435	5.0375	0.1715
Omega (kg_v/kg_da)	0.00414491	0.00030197	0.00001028
V_air (m/s)	0.4023	0.0554	0.0019
T_skin (C)	-10.7346	0.8201	0.0279
T_floor (C)	-20.5662	0.0290	0.0010

Figure 070221.01: Temperature and Voltage Control Time History

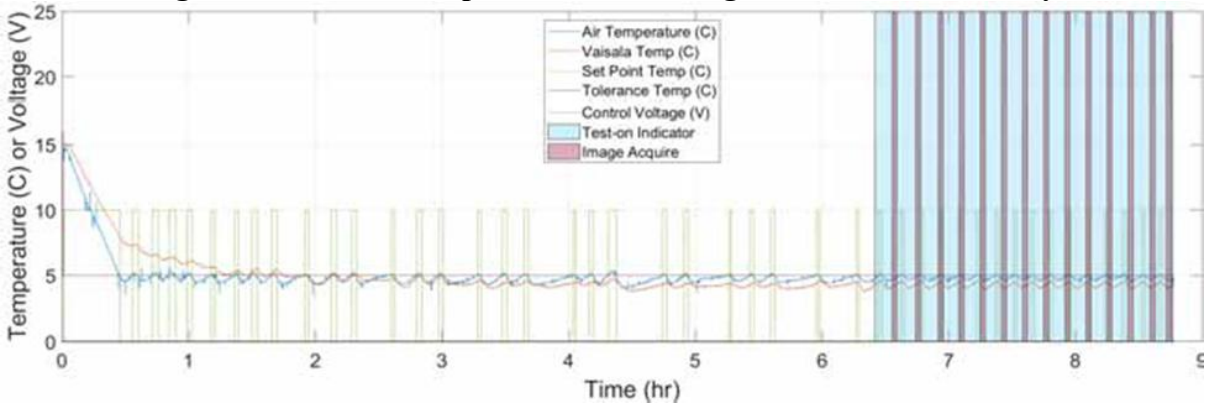

Figure 070221.02: Relative Humidity Time History

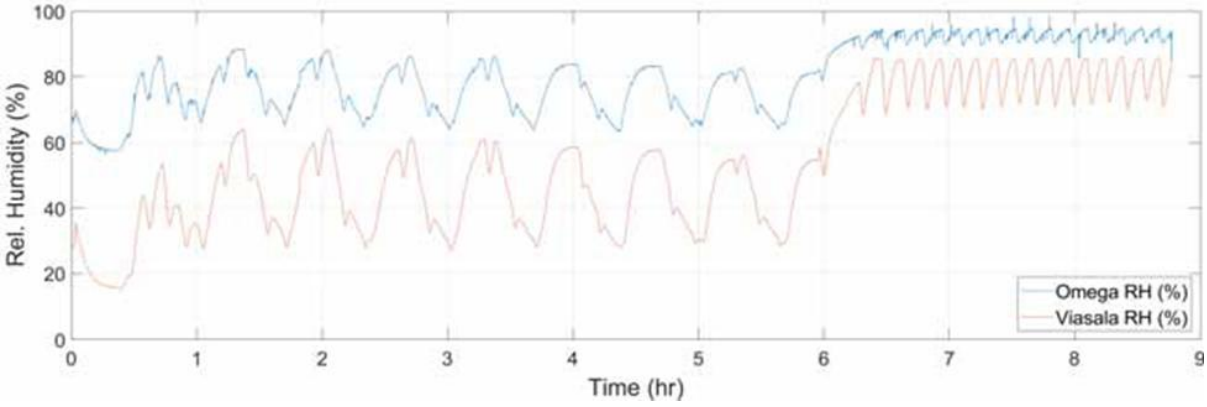

Figure 070221.03: Velocity Time History

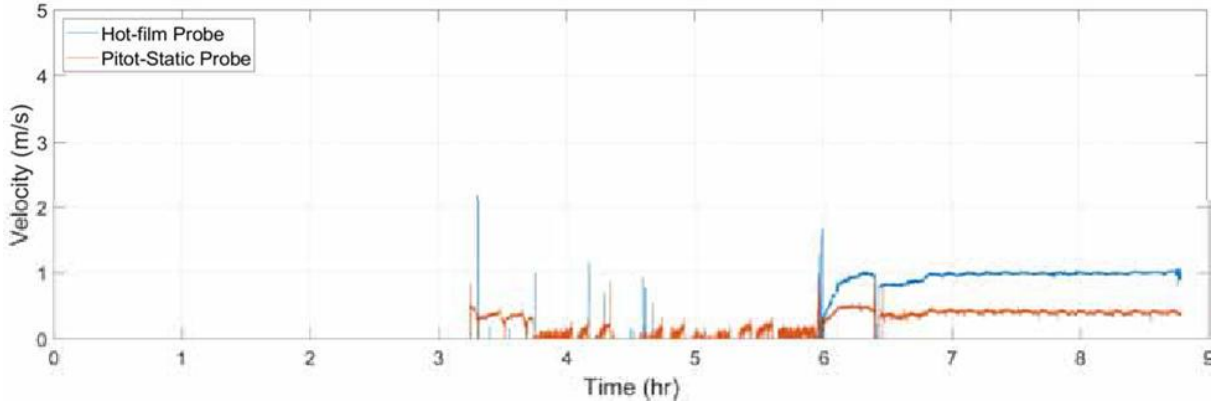

Figure 070221.04: Coolant Return Temperature Time History

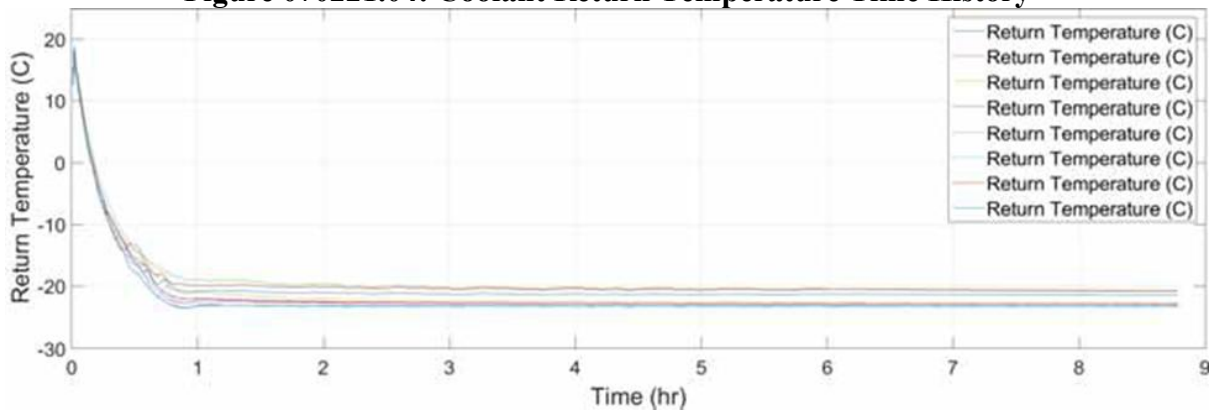

Figure 070221.05: Coolant Supply Temperature Time History

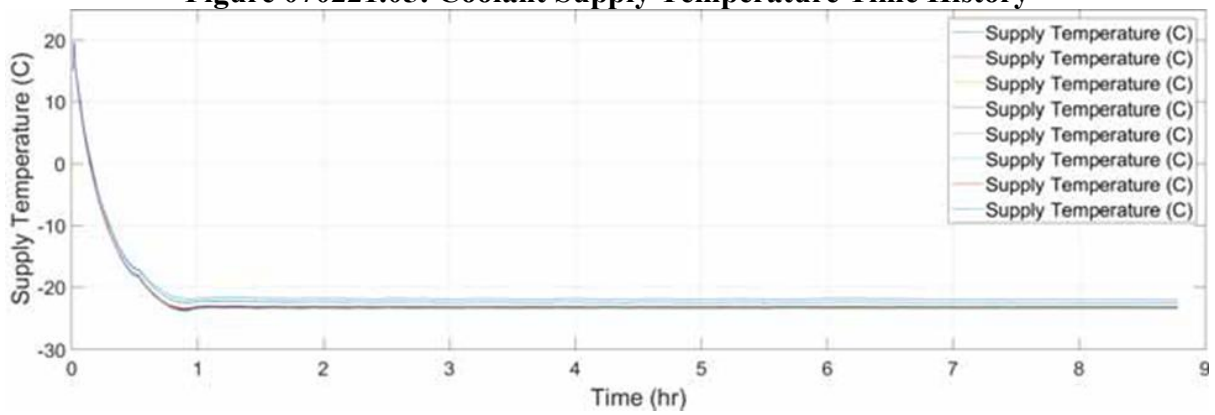

Figure 070221.06: Skin Temperature Time History

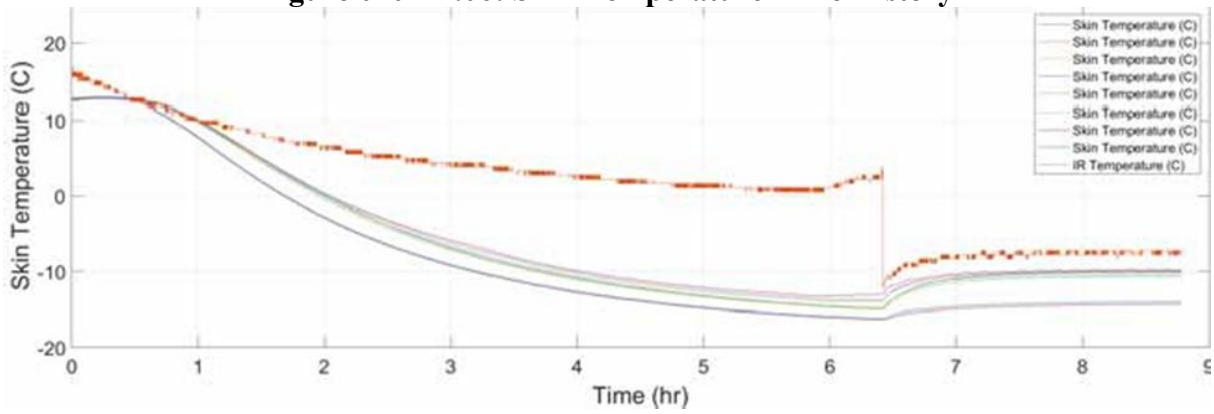

Figure 070221.07: Floor Temperature Time History

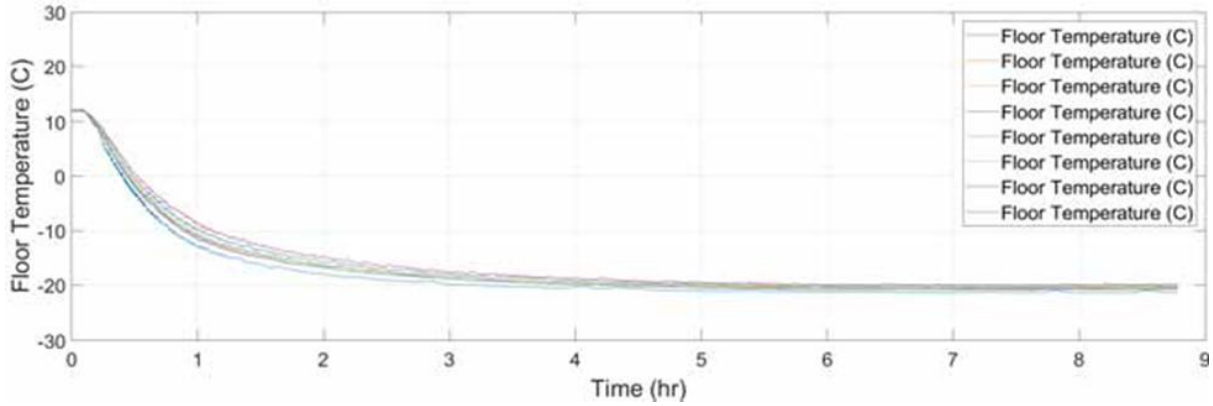

Figure 070221.08: Skin Temperature Slope Time History

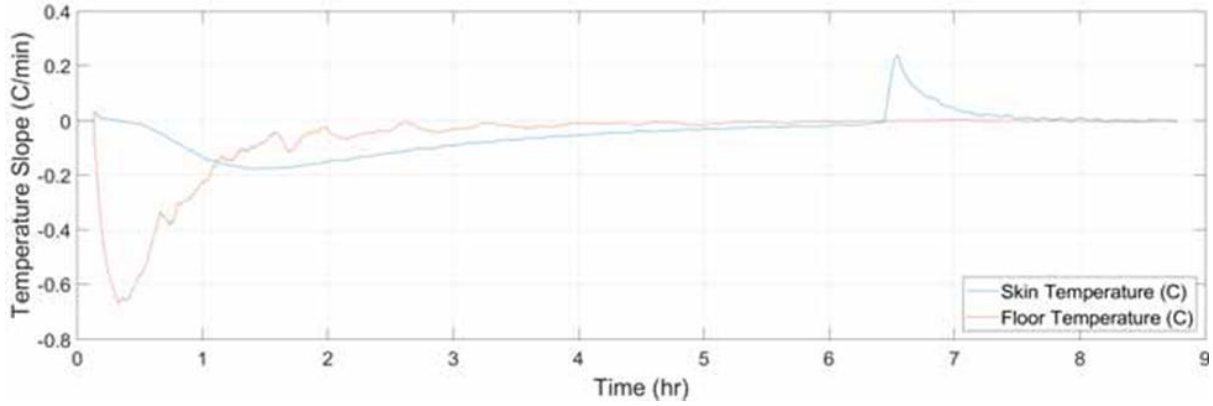

Figure 070221.09: RMS Height Evolution

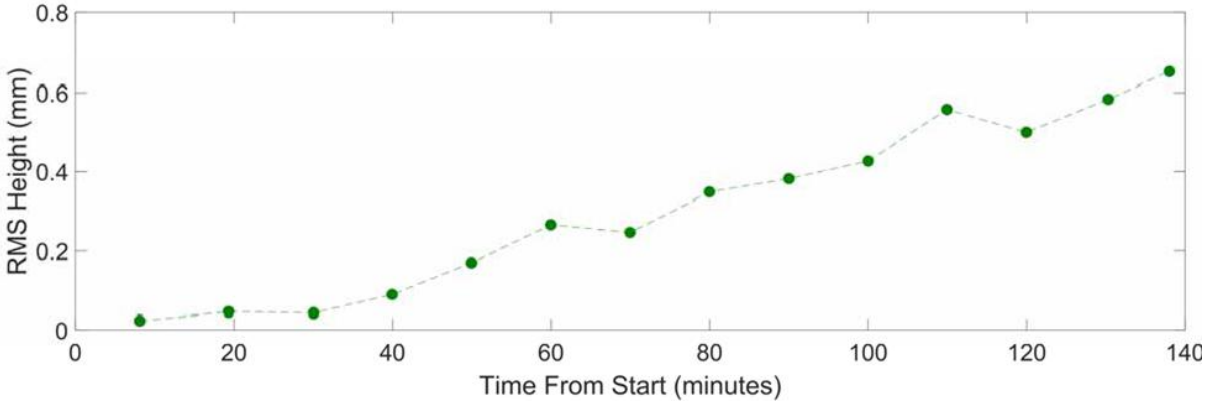

Figure 070221.10: Skewness Evolution

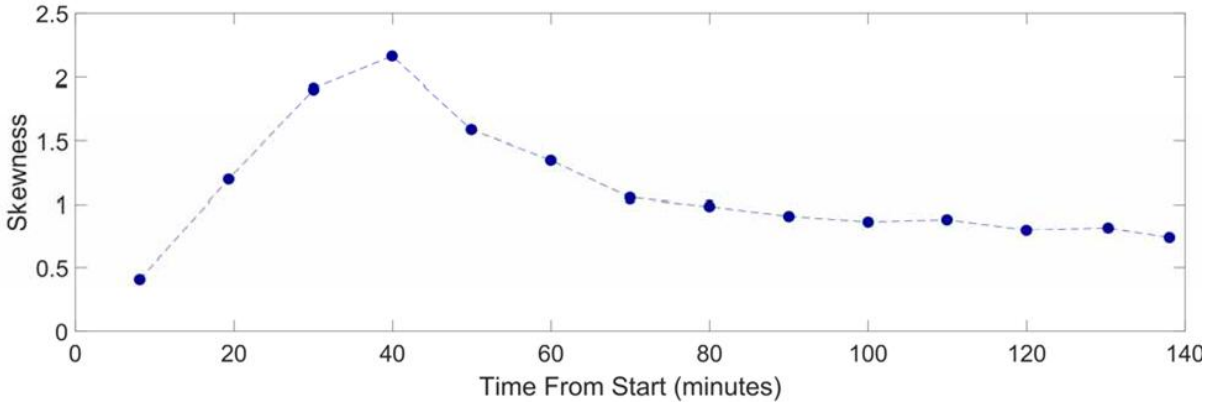

Figure 070221.11: Peak to Valley Evolution

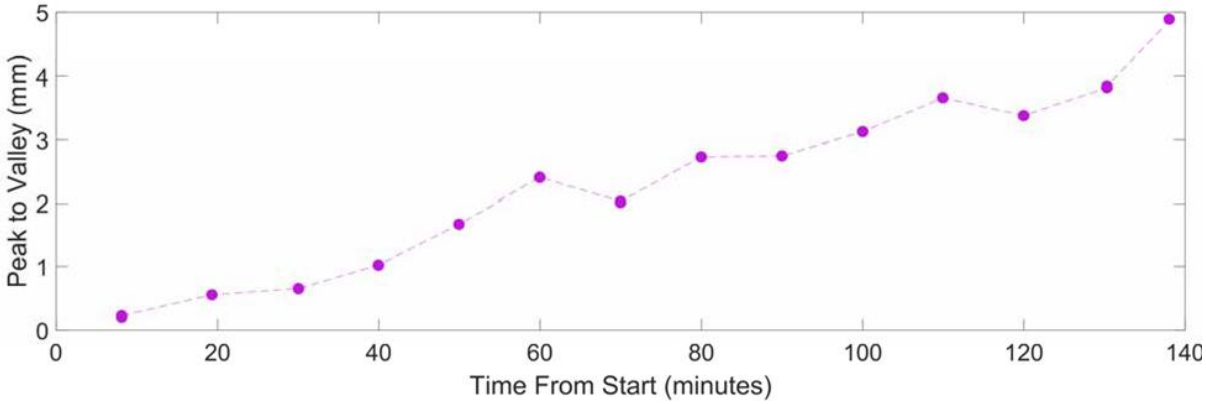

Figure 070221.12: Equivalent Roughness Evolution

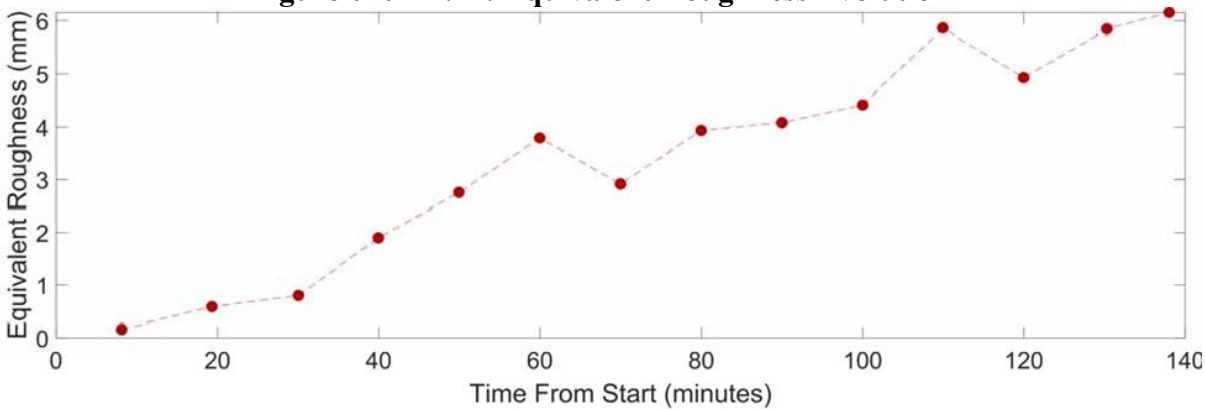

Table 070221.02: Summary of Roughness Parameters

Time (min.)	RMS (mm)	Skewness	Peak to Valley (mm)	ks,Flack-Schultz (mm)
8.1019	0.0231	0.4027	0.2081	0.1625
19.3186	0.0448	1.1956	0.5442	0.5825
30.0352	0.0416	1.9093	0.6442	0.7964
39.9352	0.0882	2.1694	1.0204	1.8972
49.9352	0.1686	1.5896	1.6694	2.7505
59.9519	0.2660	1.3471	2.4059	3.7927
69.9686	0.2462	1.0490	2.0202	2.9135
79.9852	0.3475	0.9847	2.7302	3.9379
90.0019	0.3812	0.9066	2.7454	4.0885
100.0019	0.4265	0.8621	3.1308	4.4278
109.9519	0.5574	0.8798	3.6748	5.8630
119.9686	0.4989	0.7958	3.3889	4.9289
130.2852	0.5836	0.8137	3.8363	5.8441
138.0186	0.6524	0.7371	4.8878	6.1581

Figure 070221.13: Frost Topography at 00:07:58

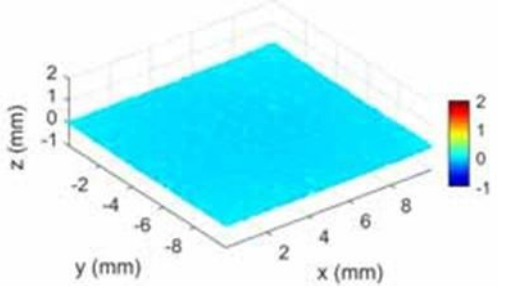

Figure 070221.14: Frost Topography at 00:19:11

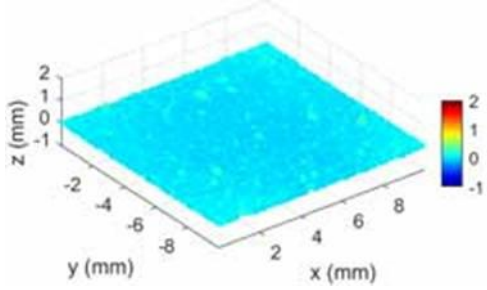

Figure 070221.15: Frost Topography at 00:29:54

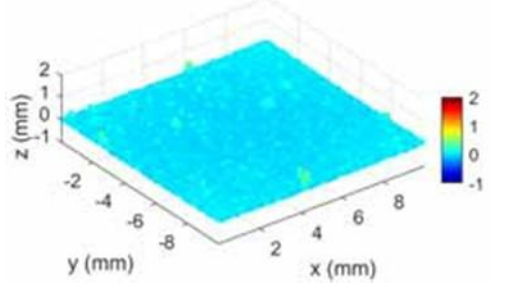

Figure 070221.16: Frost Topography at 00:39:48

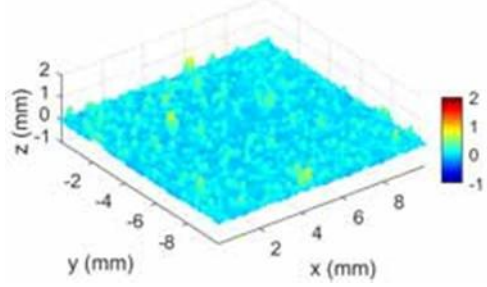

Figure 070221.17: Frost Topography at 00:49:48

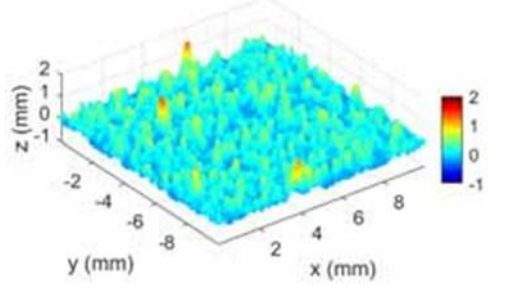

Figure 070221.18: Frost Topography at 00:59:49

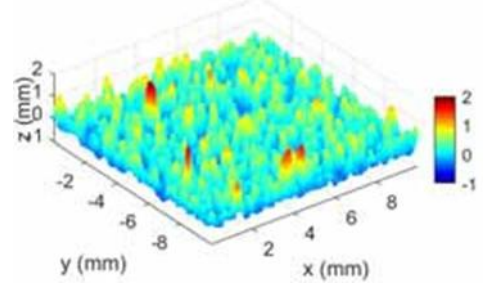

Figure 070221.19: Frost Topography at 01:09:50

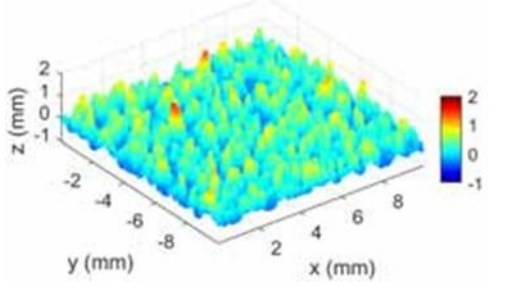

Figure 070221.20: Frost Topography at 01:19:51

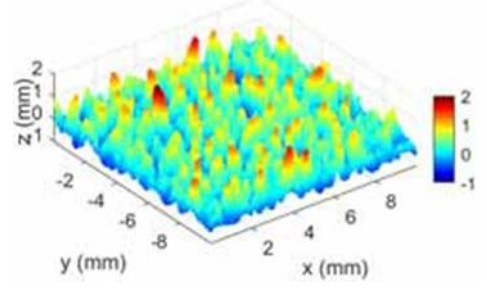

Figure 070221.21: Frost Topography at 01:29:52

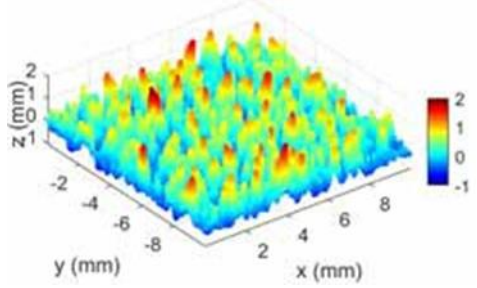

Figure 070221.22: Frost Topography at 01:39:52

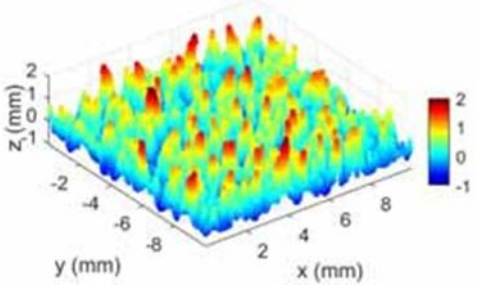

Figure 070221.23: Frost Topography at 01:49:49

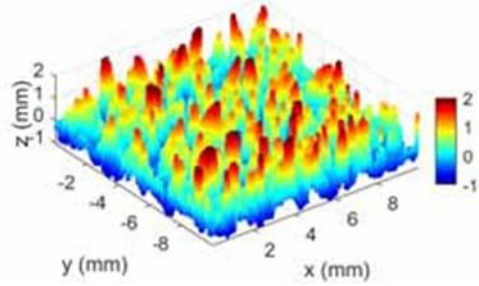

Figure 070221.24: Frost Topography at 01:59:50

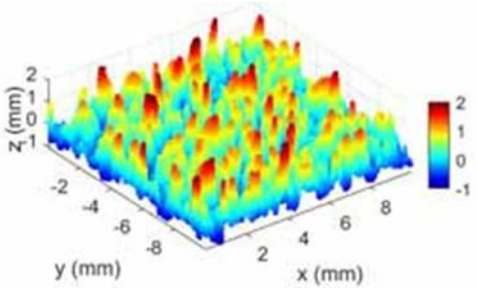

Figure 070221.25: Frost Topography at 02:10:09

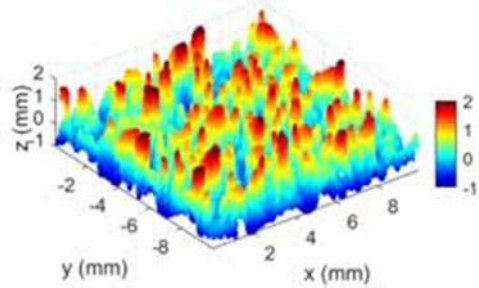

Figure 070221.26: Frost Topography at 02:17:53

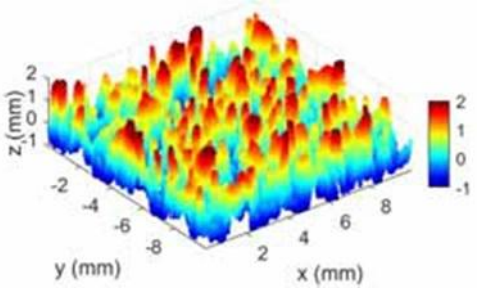

CAFF Conditions Report – Case Date: 070621

Table 070621.01: Summary of Measured Test Variables

Variable	Mean	St. Dev.	Rand. Unc.
T_air (C)	4.3178	0.2030	0.0069
Rh (%)	79.6928	5.5090	0.1870
Omega (kg_v/kg_da)	0.00416532	0.00033388	0.00001133
V_air (m/s)	0.3533	0.0496	0.0017
T_skin (C)	-10.8351	0.7567	0.0257
T_floor (C)	-20.6229	0.0193	0.0007

Figure 070621.01: Temperature and Voltage Control Time History

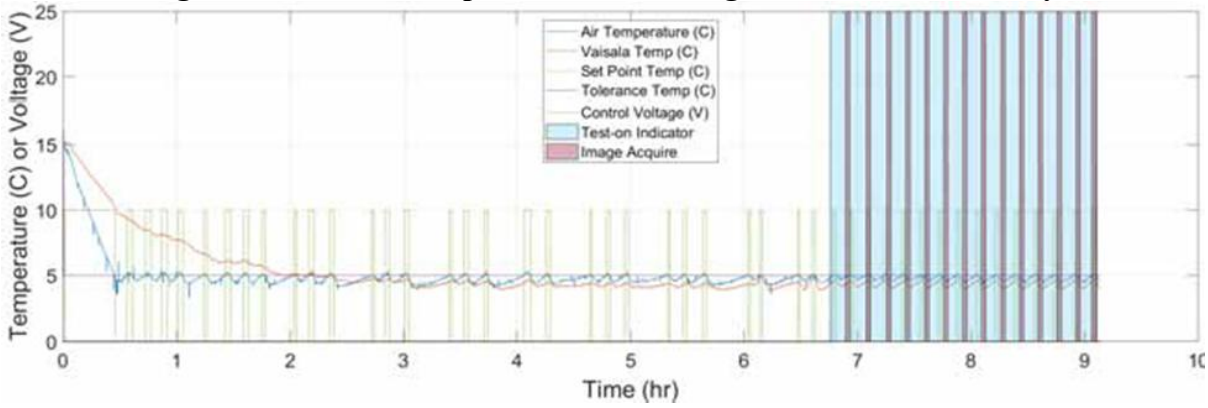

Figure 070621.02: Relative Humidity Time History

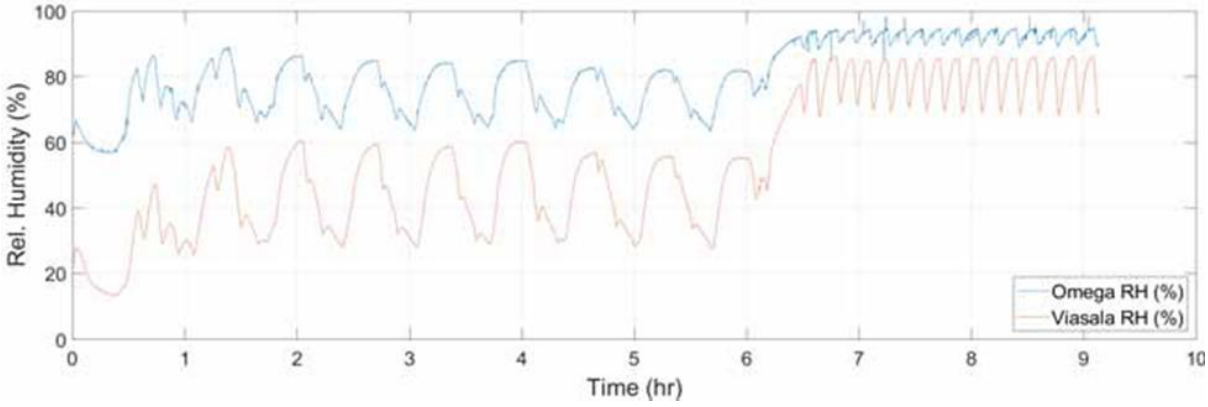

Figure 070621.03: Velocity Time History

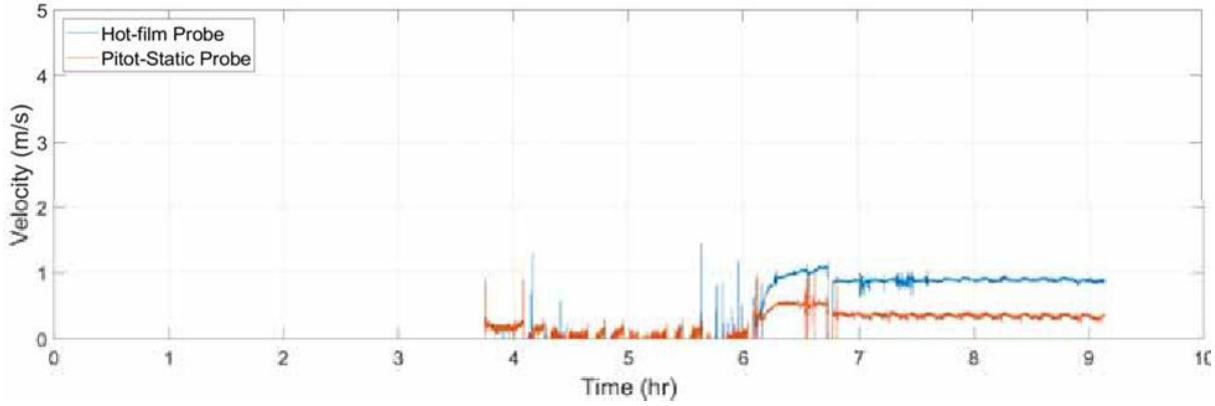

Figure 070621.04: Coolant Return Temperature Time History

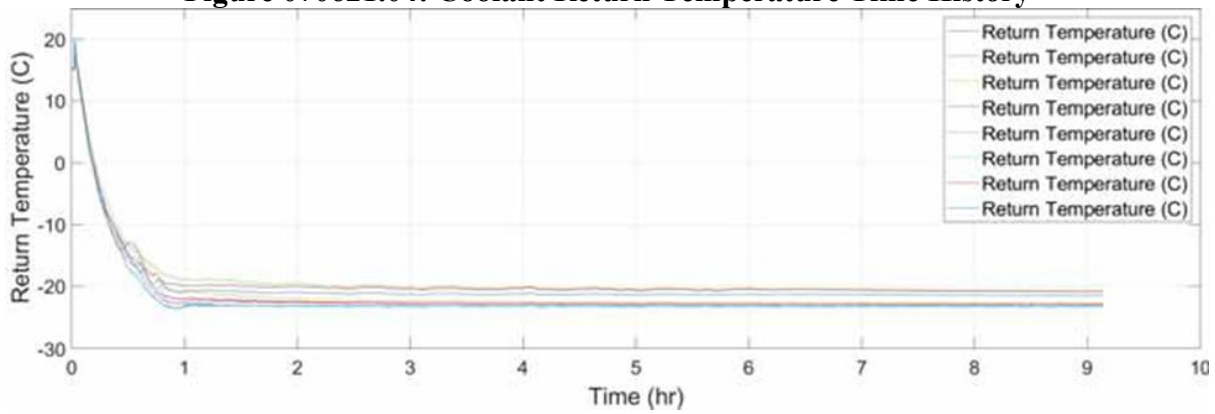

Figure 070621.05: Coolant Supply Temperature Time History

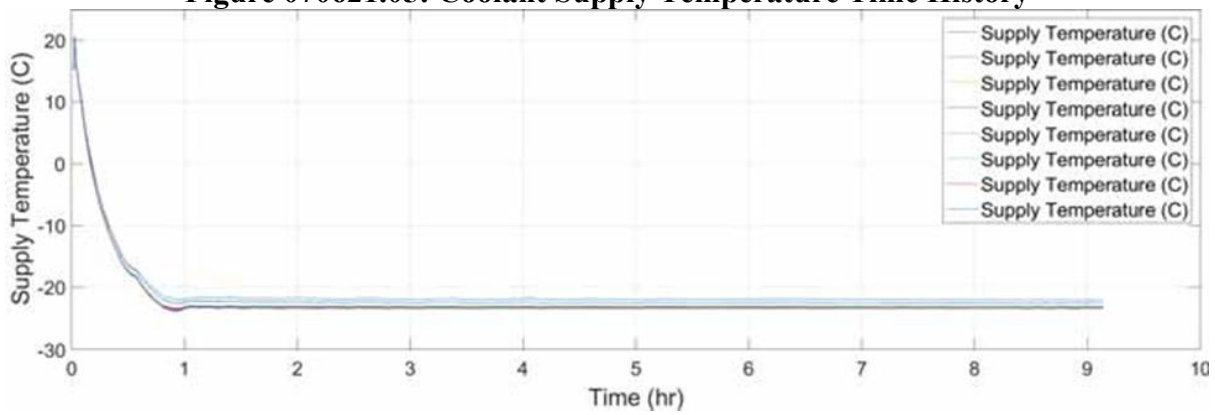

Figure 070621.06: Skin Temperature Time History

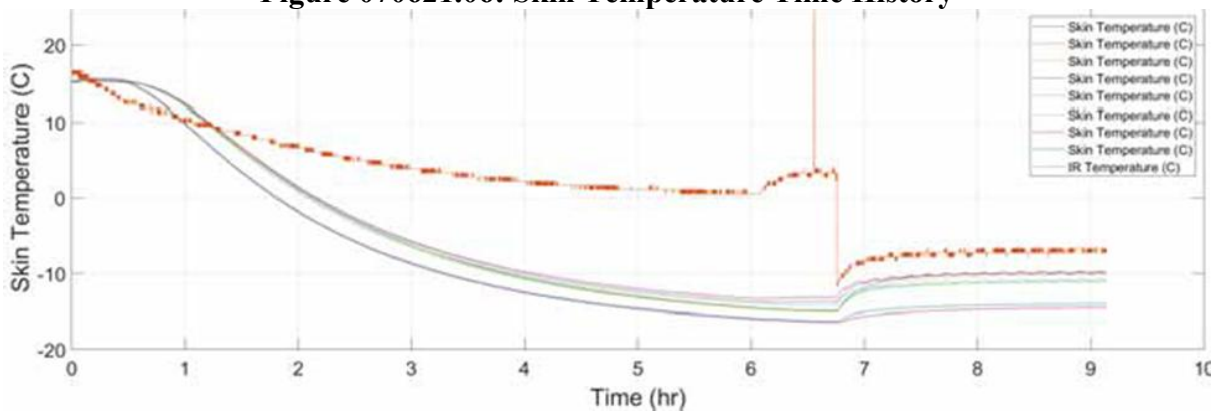

Figure 070621.07: Floor Temperature Time History

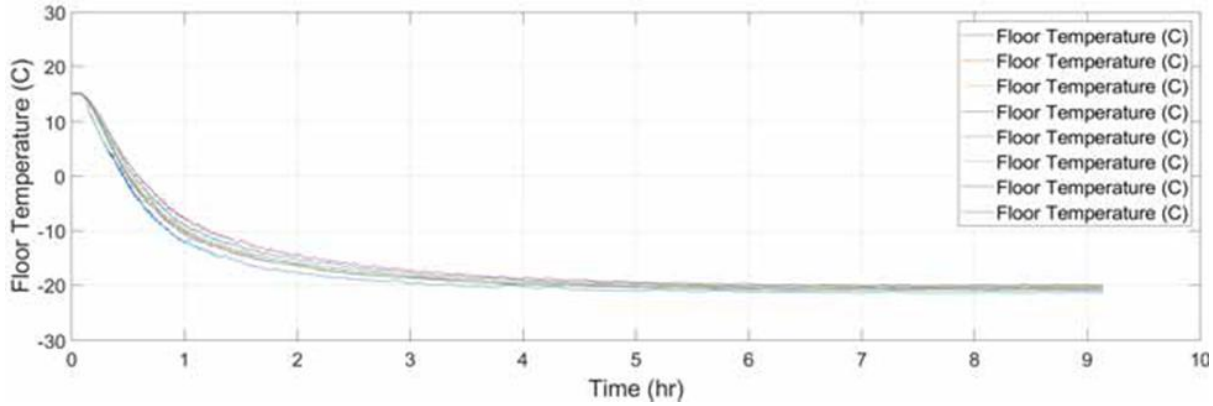

Figure 070621.08: Skin Temperature Slope Time History

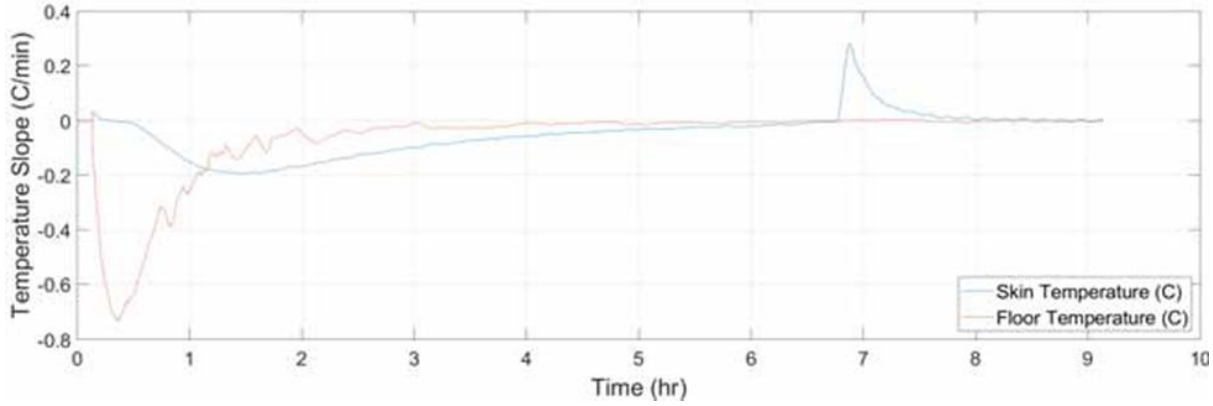

Figure 070621.09: RMS Height Evolution

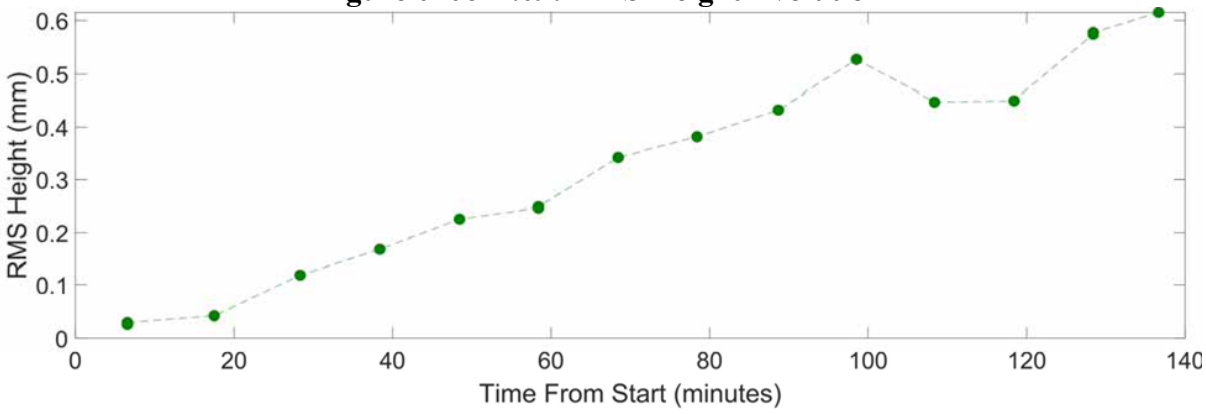

Figure 070621.10: Skewness Evolution

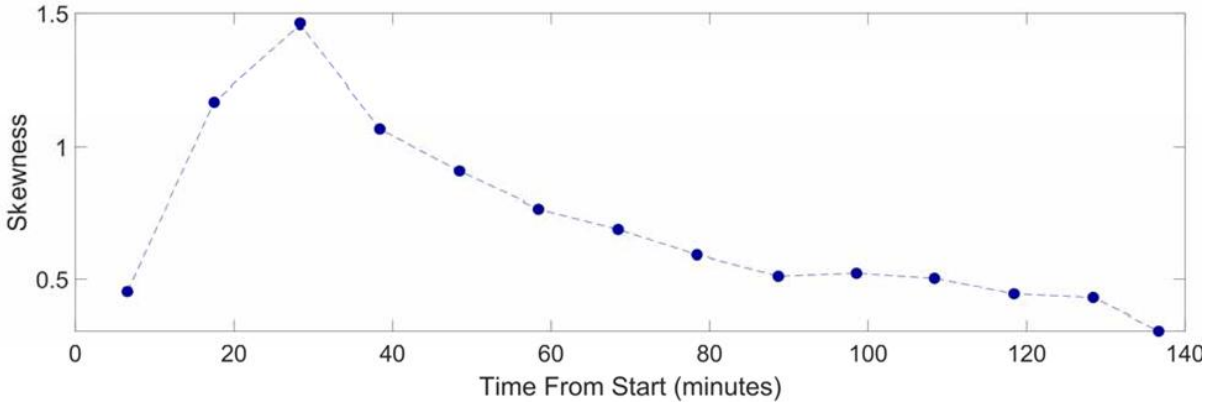

Figure 070621.11: Peak to Valley Evolution

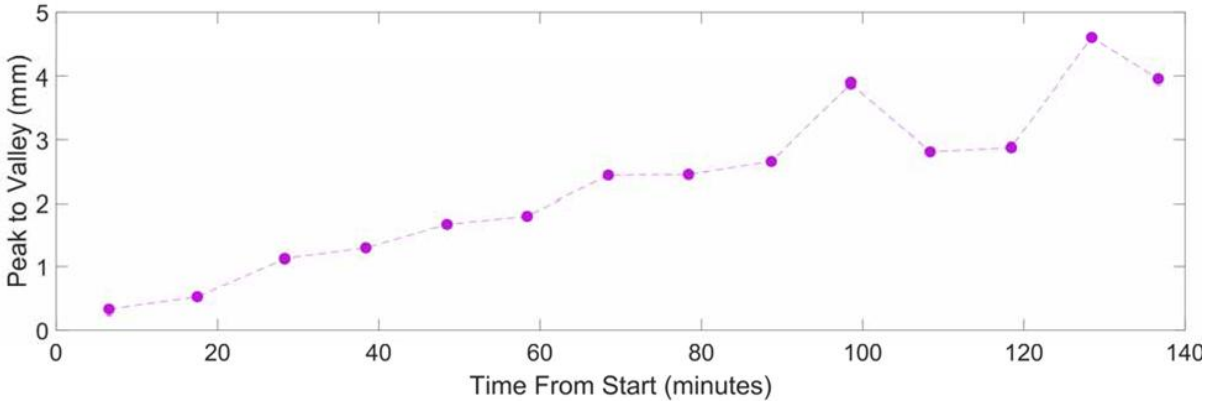

Figure 070621.12: Equivalent Roughness Evolution

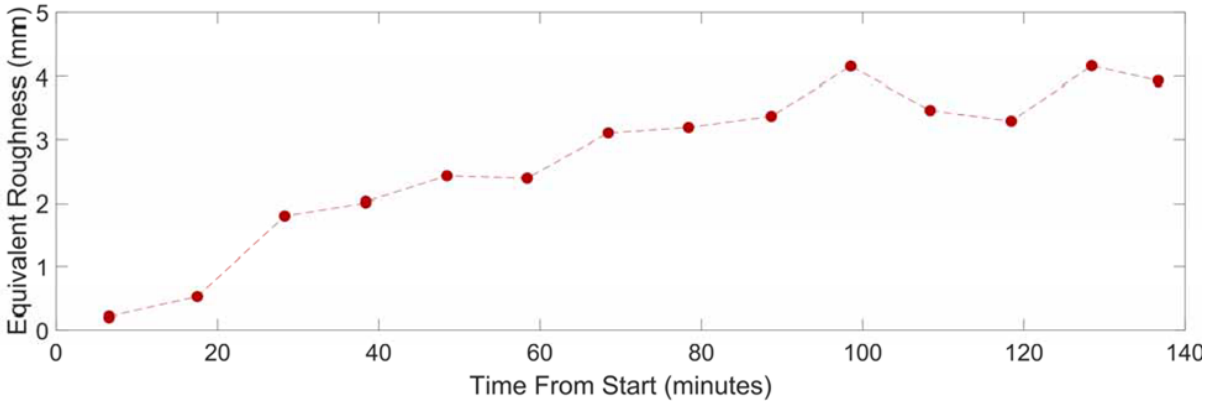

Table 070621.02: Summary of Roughness Parameters

Time (min.)	RMS (mm)	Skewness	Peak to Valley (mm)	ks,Flack-Schultz (mm)
6.5394	0.0272	0.4517	0.3123	0.2006
17.4894	0.0403	1.1700	0.5122	0.5154
28.3394	0.1185	1.4625	1.1232	1.8042
38.3894	0.1681	1.0671	1.2918	2.0140
48.4394	0.2261	0.9078	1.6690	2.4272
58.4061	0.2473	0.7665	1.8003	2.3891
68.4561	0.3423	0.6889	2.4394	3.1093
78.4061	0.3815	0.5923	2.4493	3.1969
88.6728	0.4330	0.5108	2.6586	3.3757
98.5394	0.5281	0.5222	3.8988	4.1603
108.3728	0.4481	0.5027	2.8134	3.4678
118.4228	0.4505	0.4432	2.8794	3.2985
128.4061	0.5766	0.4290	4.6216	4.1658
136.6561	0.6157	0.3055	3.9558	3.9299

Figure 070621.13: Frost Topography at 00:07:59

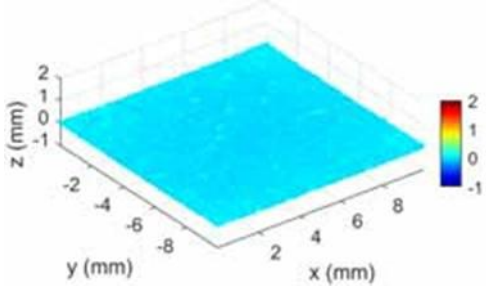

Figure 070621.14: Frost Topography at 00:18:56

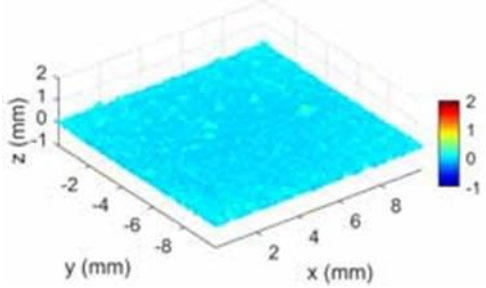

Figure 070621.15: Frost Topography at 00:29:47

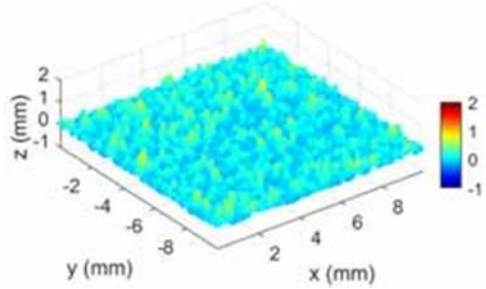

Figure 070621.16: Frost Topography at 00:39:50

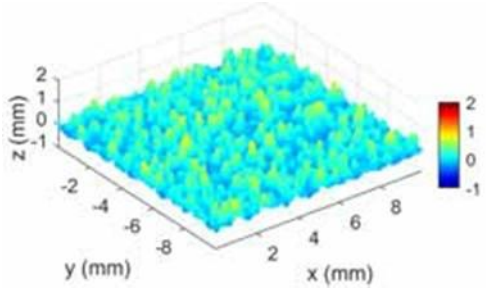

Figure 070621.17: Frost Topography at 00:49:53

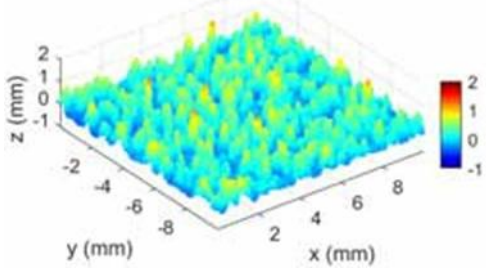

Figure 070621.18: Frost Topography at 00:59:51

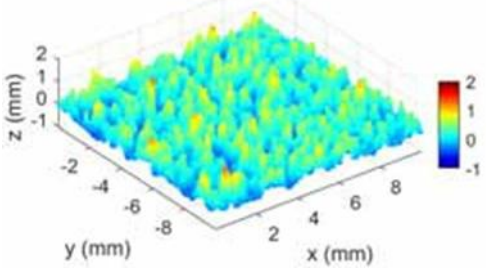

Figure 070621.19: Frost Topography at 01:09:54

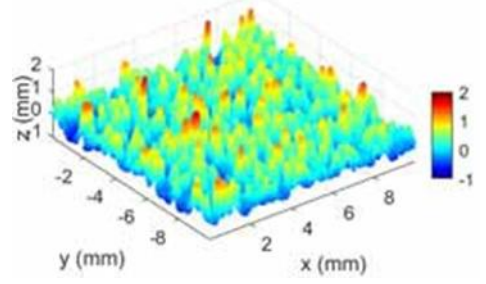

Figure 070621.20: Frost Topography at 01:19:51

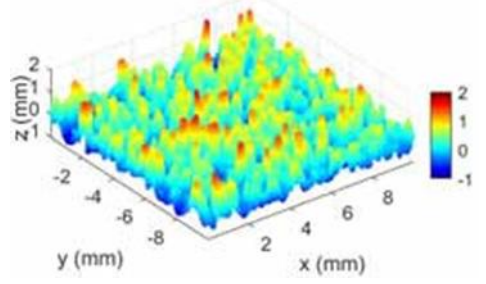

Figure 070621.21: Frost Topography at 01:30:07

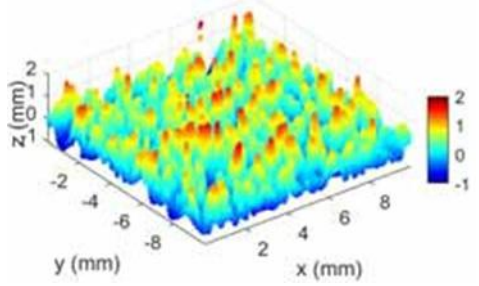

Figure 070621.22: Frost Topography at 01:39:59

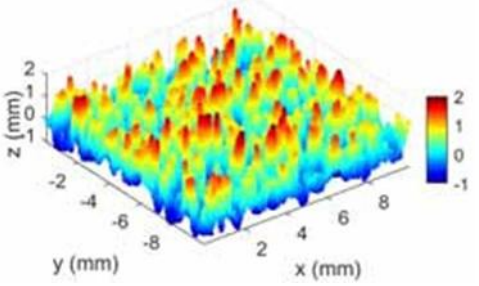

Figure 070621.23: Frost Topography at 01:49:49

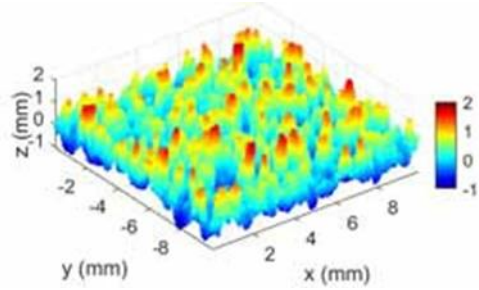

Figure 070621.24: Frost Topography at 01:59:52

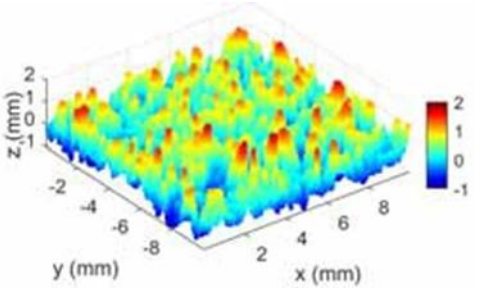

Figure 070621.25: Frost Topography at 02:09:51

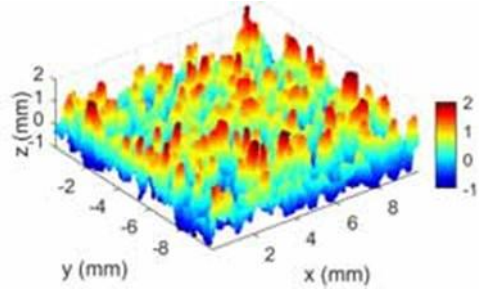

Figure 070621.26: Frost Topography at 02:18:06

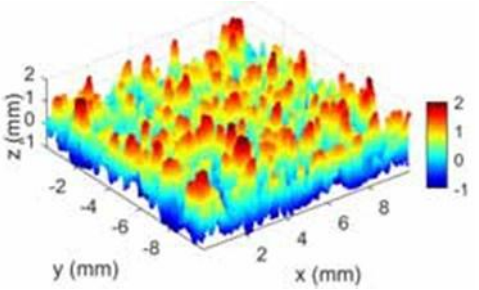

CAFF Conditions Report – Case Date: 073021

Table 073021.01: Summary of Measured Test Variables

Variable	Mean	St. Dev.	Rand. Unc.
T_air (C)	15.2862	0.3025	0.0103
Rh (%)	78.2765	3.8586	0.1312
Omega (kg_v/kg_da)	0.00856859	0.00051383	0.00001748
V_air (m/s)	0.2702	0.1006	0.0034
T_skin (C)	-5.7370	1.3404	0.0456
T_floor (C)	-19.4863	0.1235	0.0042

Figure 073021.01: Temperature and Voltage Control Time History

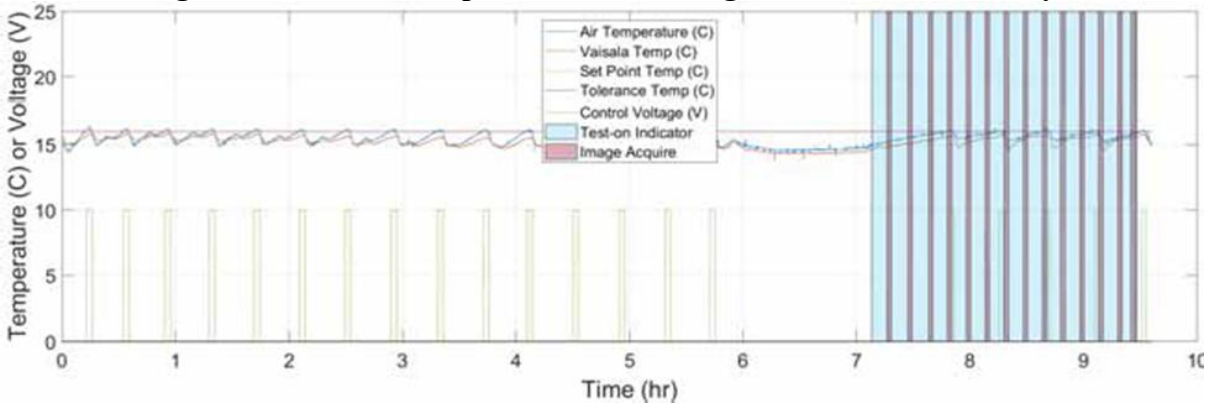

Figure 073021.02: Relative Humidity Time History

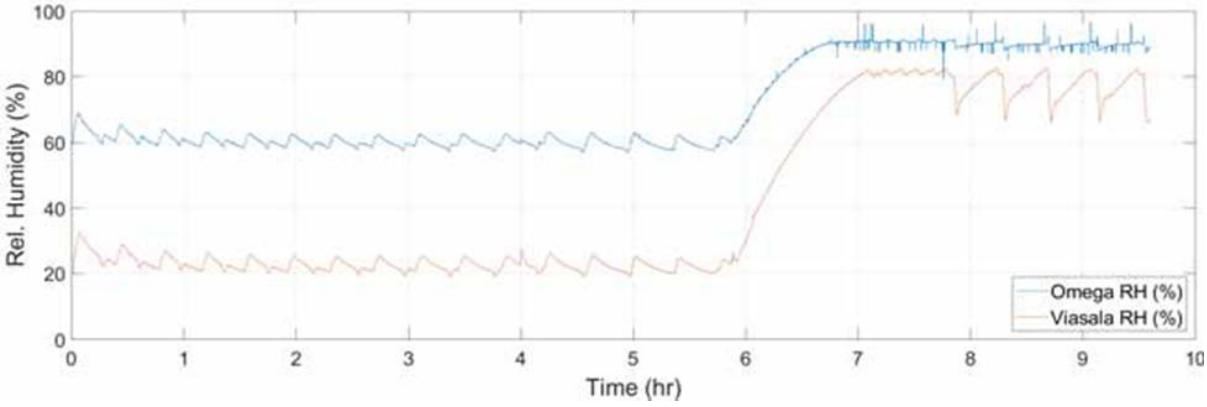

Figure 073021.03: Velocity Time History

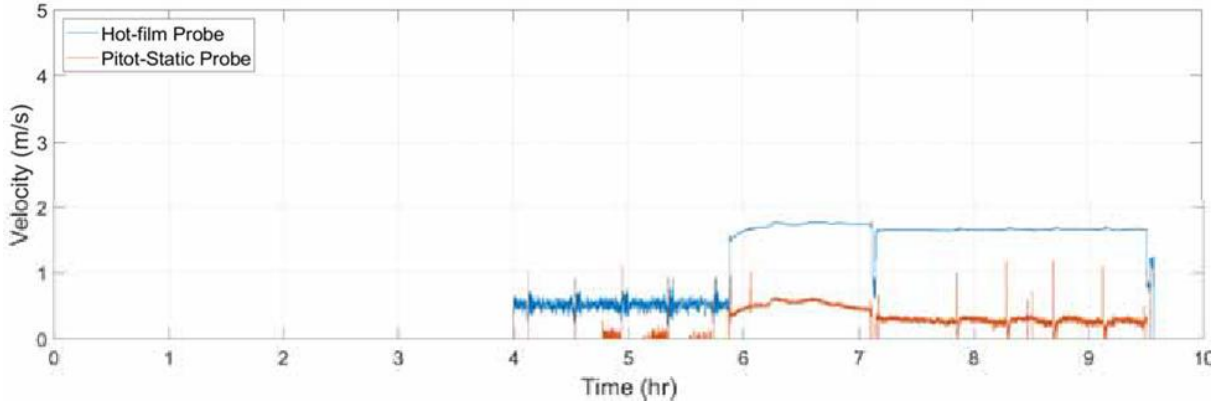

Figure 073021.04: Coolant Return Temperature Time History

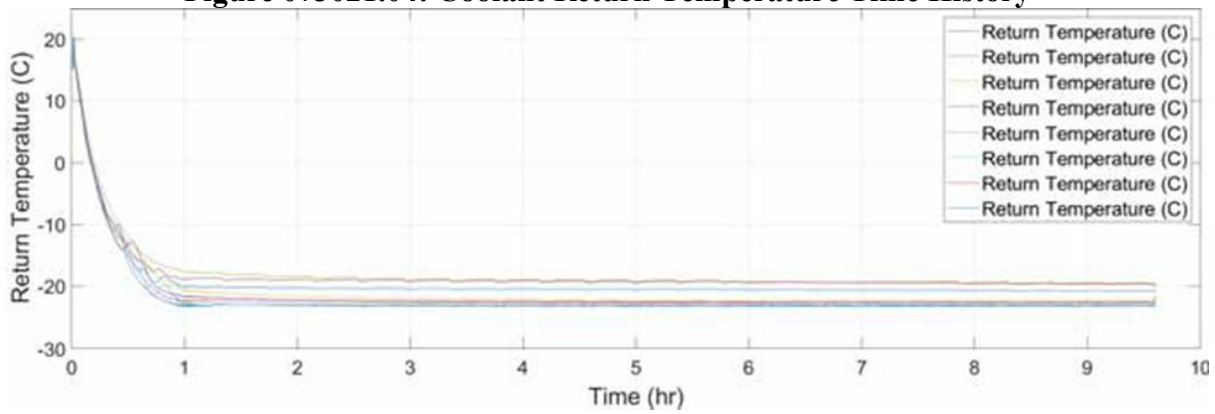

Figure 073021.05: Coolant Supply Temperature Time History

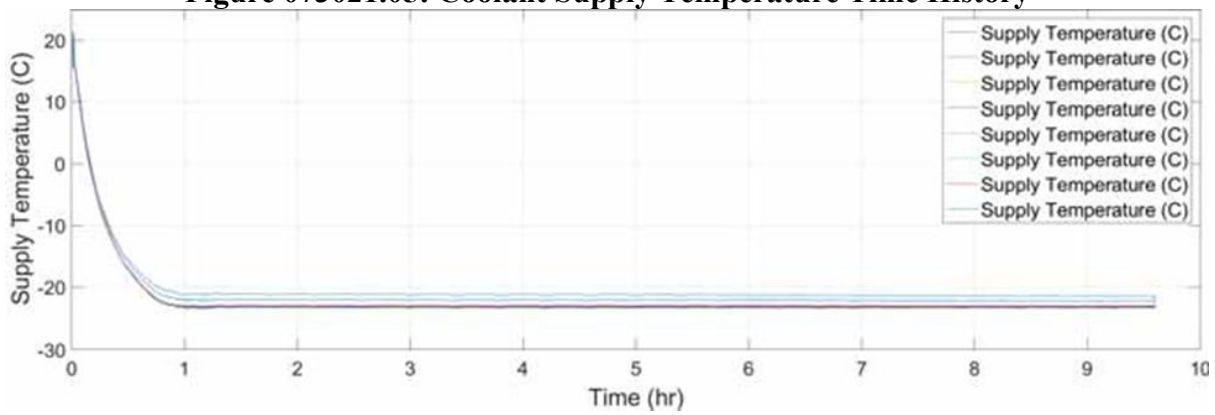

Figure 073021.06: Skin Temperature Time History

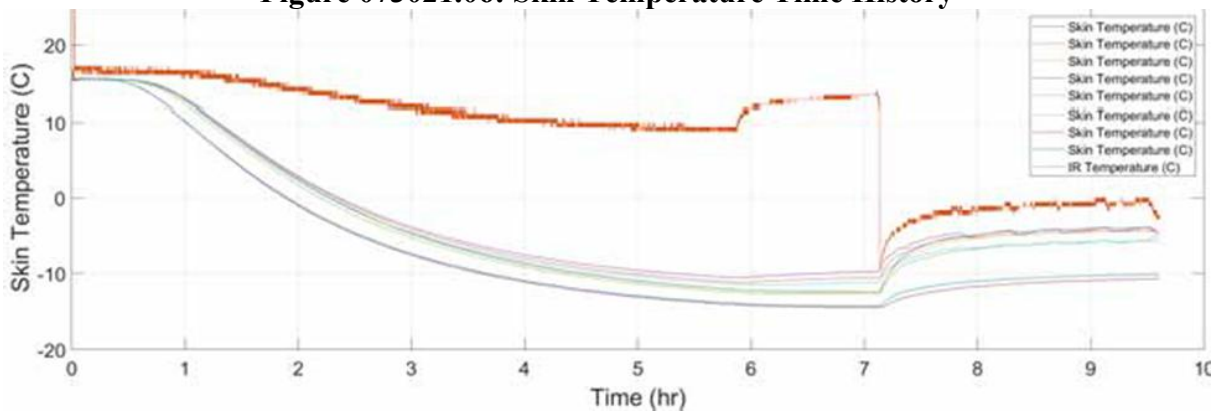

Figure 073021.07: Floor Temperature Time History

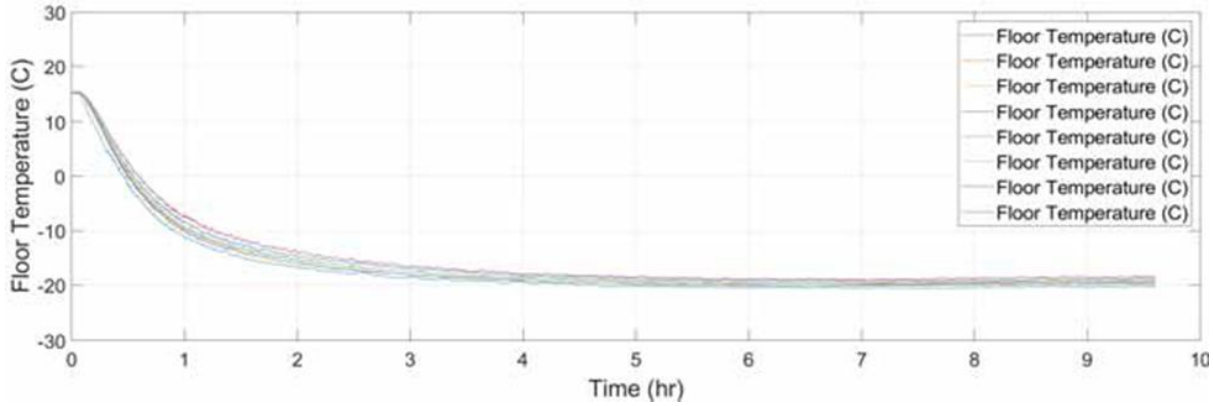

Figure 073021.08: Skin Temperature Slope Time History

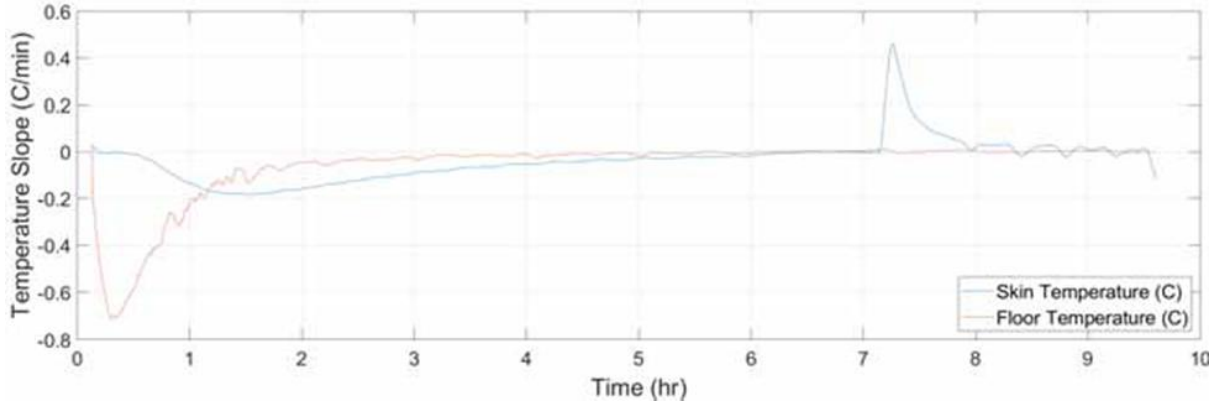

Figure 073021.09: RMS Height Evolution

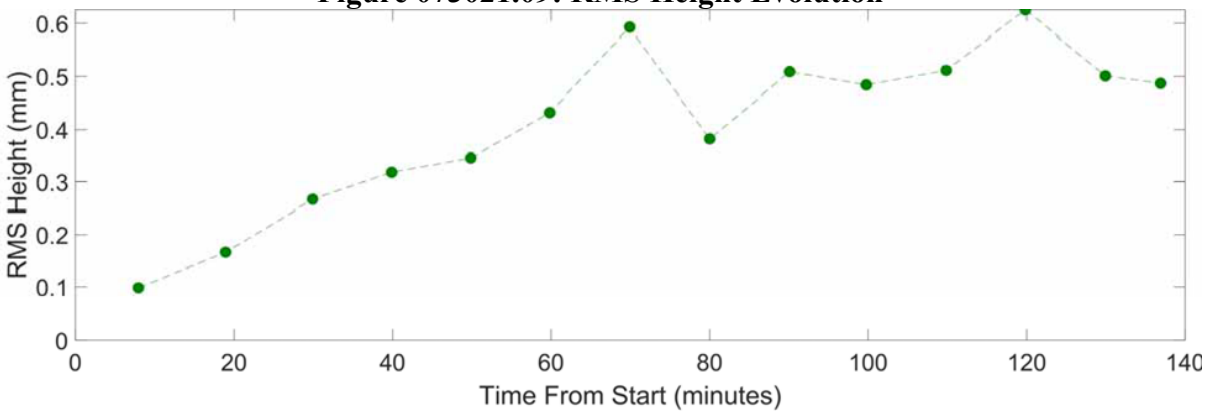

Figure 073021.10: Skewness Evolution

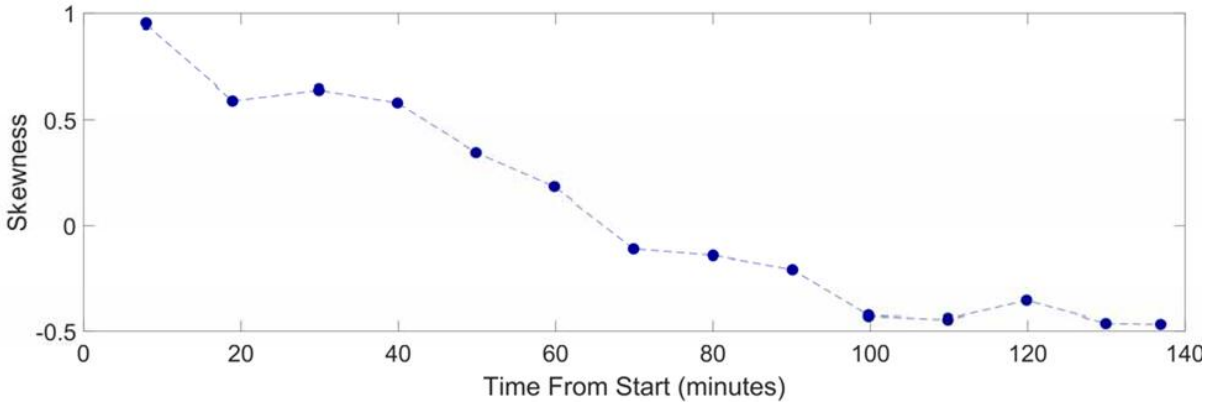

Figure 073021.11: Peak to Valley Evolution

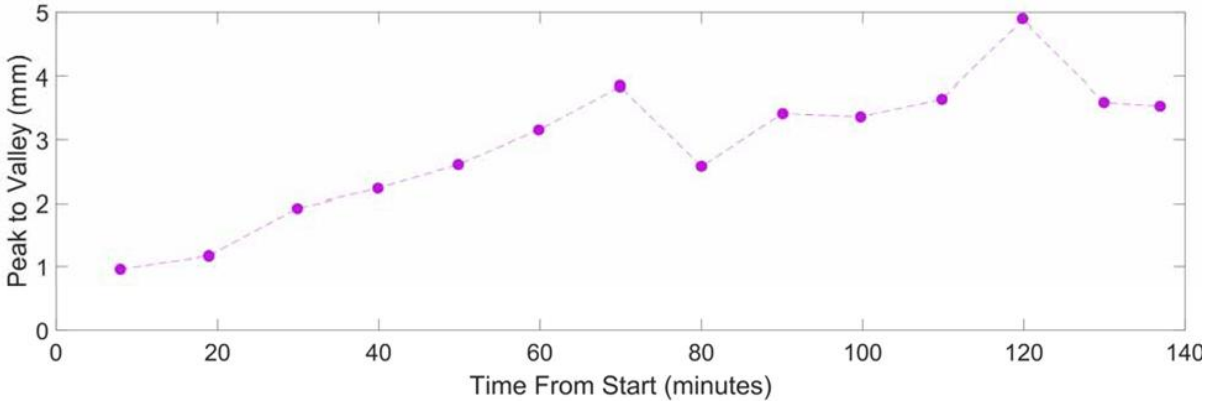

Figure 073021.12: Equivalent Roughness Evolution

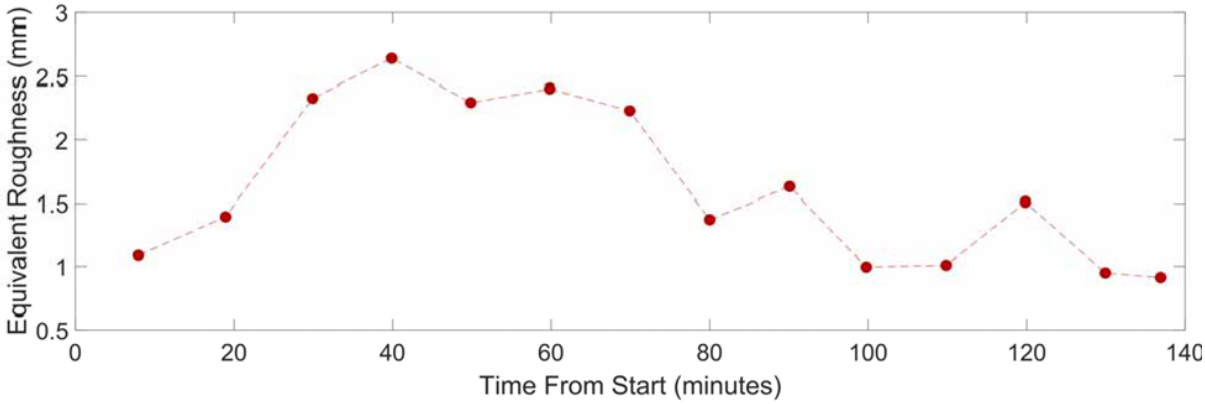

Table 073021.02: Summary of Roughness Parameters

Time (min.)	RMS (mm)	Skewness	Peak to Valley (mm)	ks,Flack-Schultz (mm)
7.9431	0.0982	0.9531	0.9552	1.0886
18.9265	0.1665	0.5915	1.1664	1.3944
29.9098	0.2665	0.6431	1.9244	2.3309
39.8931	0.3183	0.5824	2.2280	2.6444
49.8598	0.3454	0.3449	2.6081	2.2965
59.8431	0.4326	0.1807	3.1576	2.4061
69.9098	0.5927	-0.1119	3.8508	2.2315
80.0098	0.3822	-0.1425	2.5783	1.3715
90.0931	0.5090	-0.2112	3.4208	1.6291
99.7598	0.4838	-0.4290	3.3678	0.9947
109.8431	0.5114	-0.4463	3.6523	1.0080
119.8431	0.6260	-0.3586	4.8983	1.5094
129.9265	0.5009	-0.4628	3.5981	0.9472
136.8931	0.4868	-0.4671	3.5391	0.9104

Figure 073021.13: Frost Topography at 00:07:56

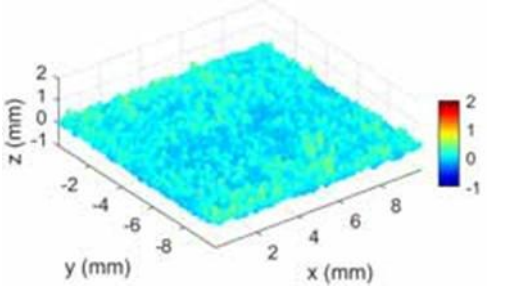

Figure 073021.14: Frost Topography at 00:18:55

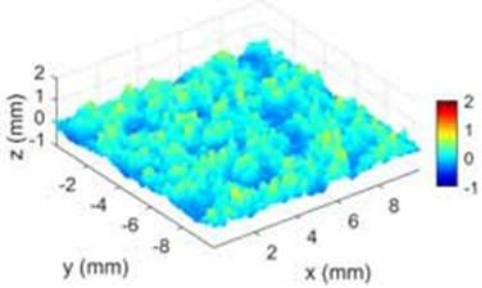

Figure 073021.15: Frost Topography at 00:29:54

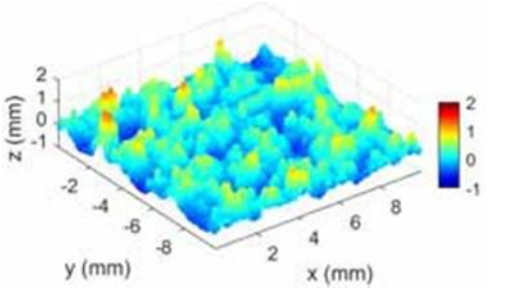

Figure 073021.16: Frost Topography at 00:39:53

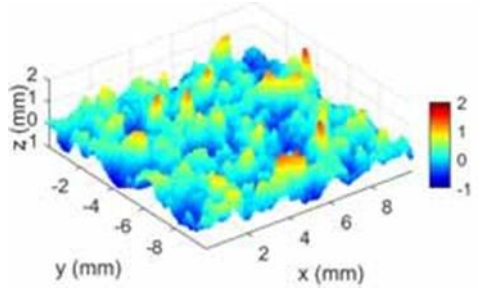

Figure 073021.17: Frost Topography at 00:49:51

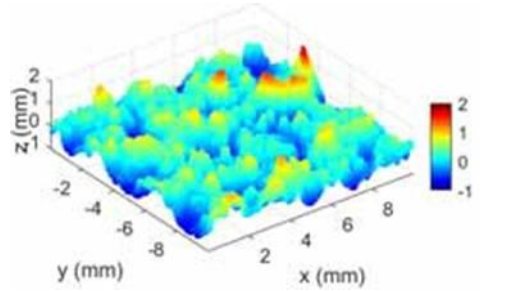

Figure 073021.18: Frost Topography at 00:59:50

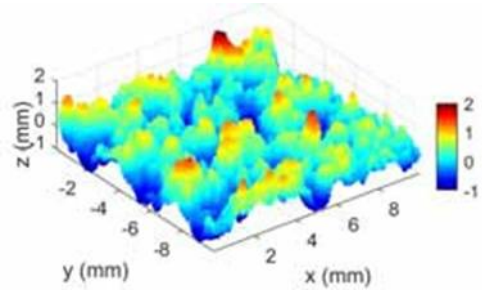

Figure 073021.19: Frost Topography at 01:09:54

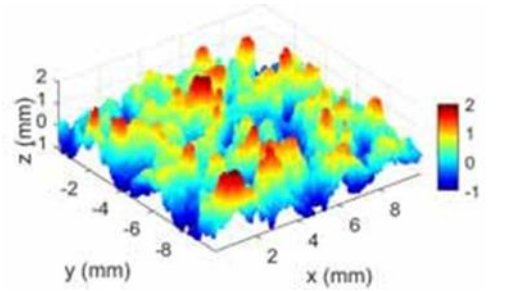

Figure 073021.20: Frost Topography at 01:20:00

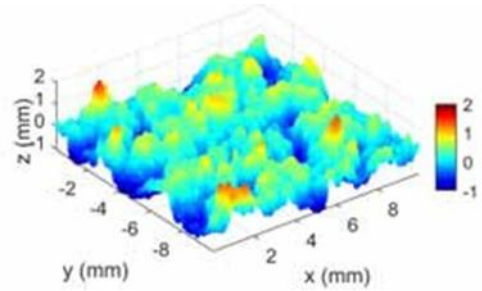

Figure 073021.21: Frost Topography at 01:30:05

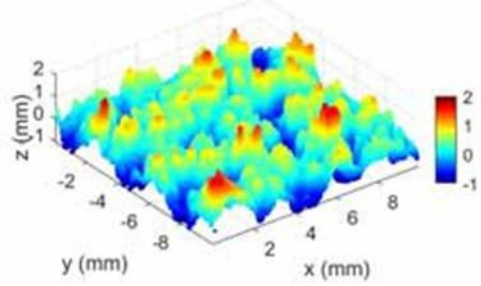

Figure 073021.22: Frost Topography at 01:39:45

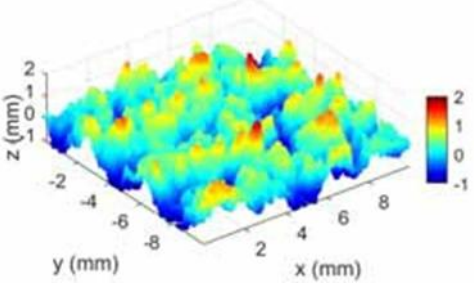

Figure 073021.23: Frost Topography at 01:49:50

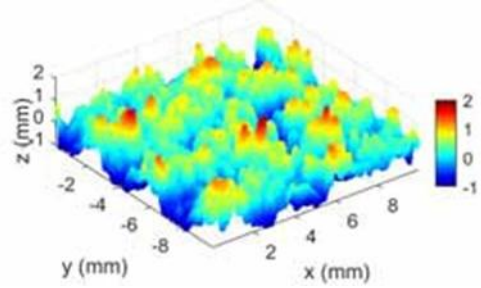

Figure 073021.24: Frost Topography at 01:59:50

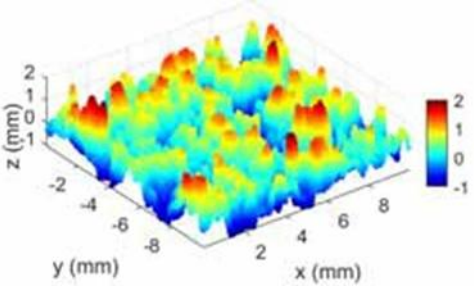

Figure 073021.25: Frost Topography at 02:09:55

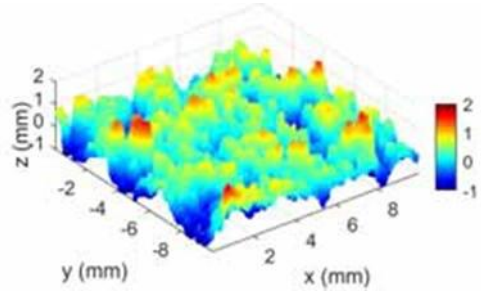

Figure 073021.26: Frost Topography at 02:16:53

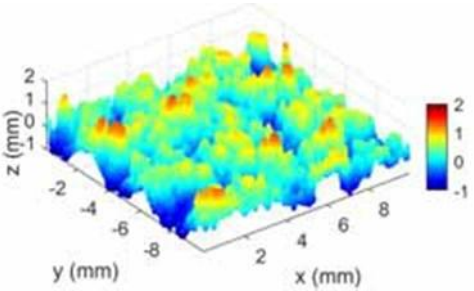

CAFF Conditions Report – Case Date: 080321

Table 080321.01: Summary of Measured Test Variables

Variable	Mean	St. Dev.	Rand. Unc.
T_air (C)	9.3031	0.2506	0.0086
Rh (%)	79.9994	5.0836	0.1736
Omega (kg_v/kg_da)	0.00589844	0.00041090	0.00001403
V_air (m/s)	0.3144	0.0821	0.0028
T_skin (C)	-8.7443	1.0109	0.0345
T_floor (C)	-20.1671	0.0695	0.0024

Figure 080321.01: Temperature and Voltage Control Time History

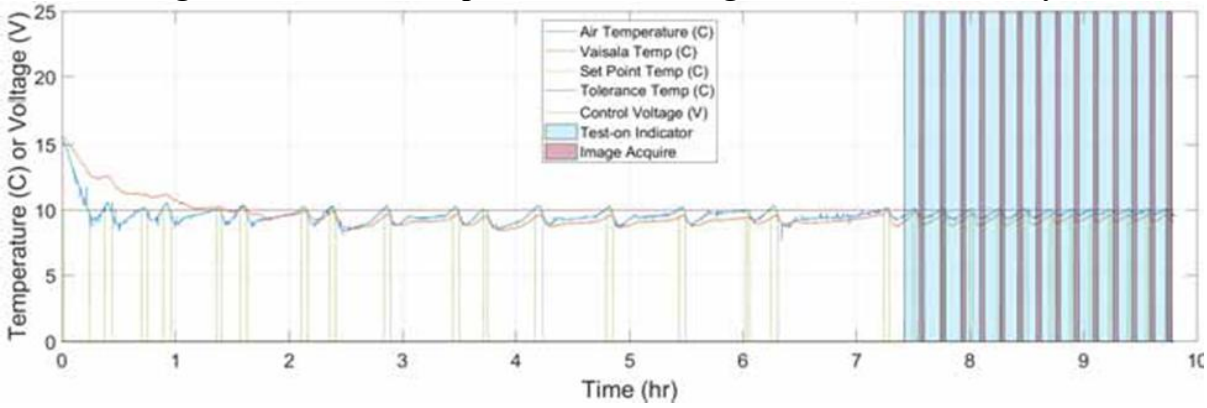

Figure 080321.02: Relative Humidity Time History

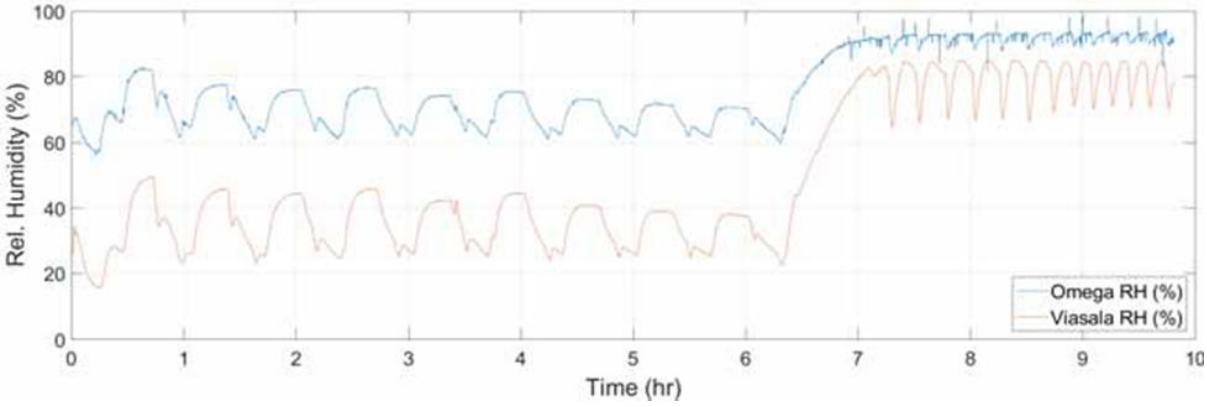

Figure 080321.03: Velocity Time History

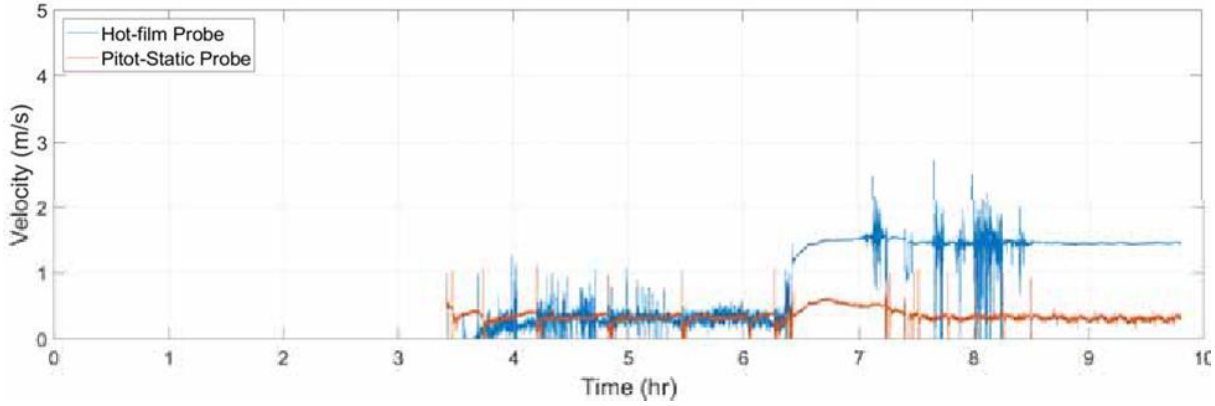

Figure 080321.04: Coolant Return Temperature Time History

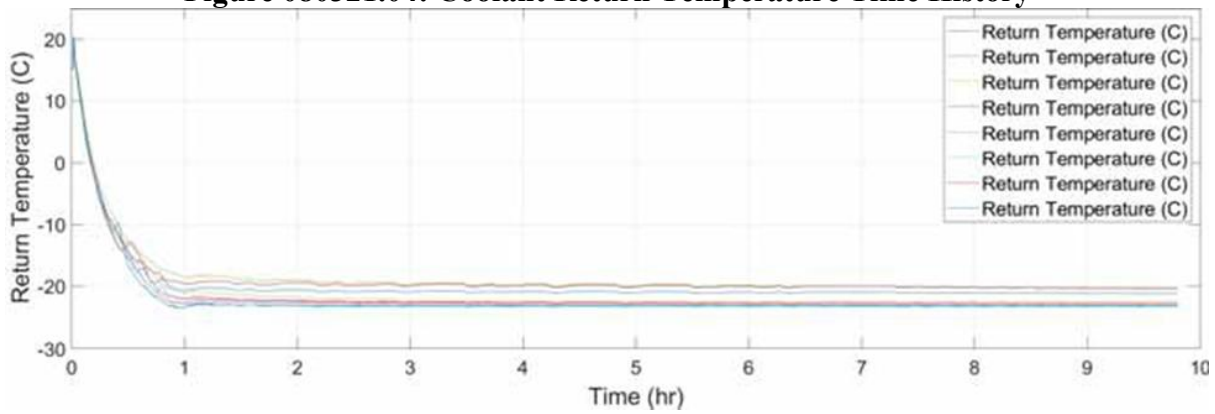

Figure 080321.05: Coolant Supply Temperature Time History

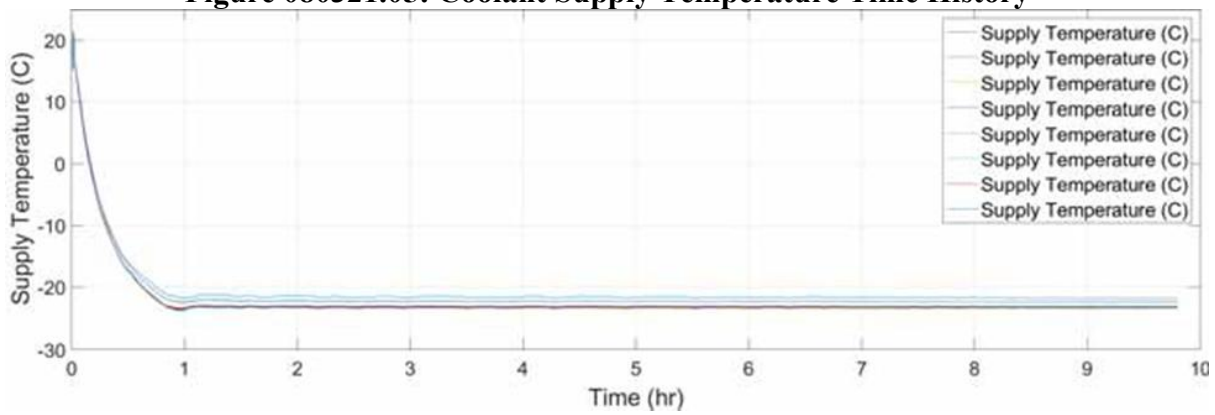

Figure 080321.06: Skin Temperature Time History

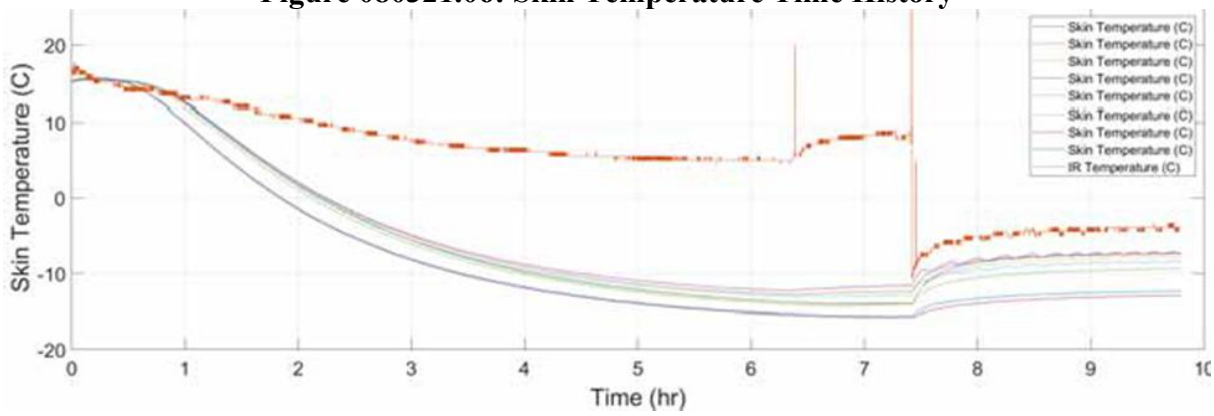

Figure 080321.07: Floor Temperature Time History

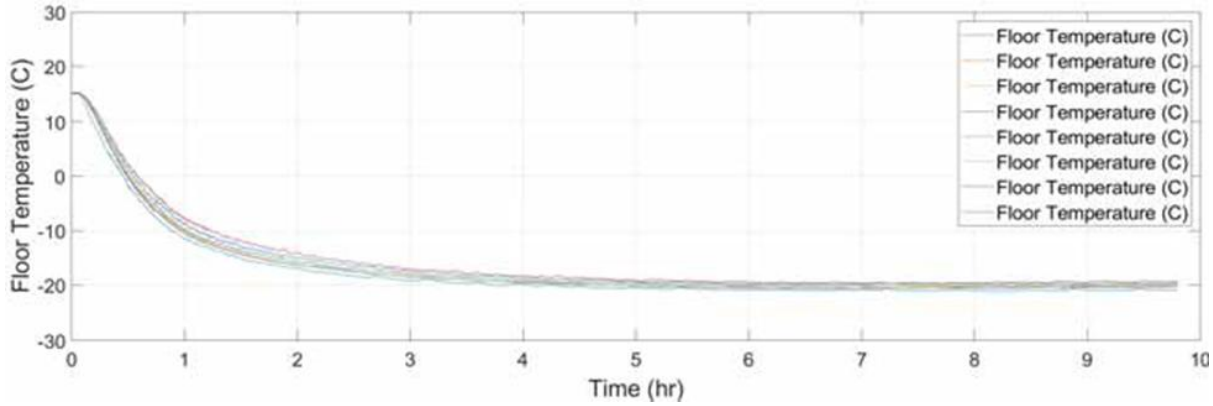

Figure 080321.08: Skin Temperature Slope Time History

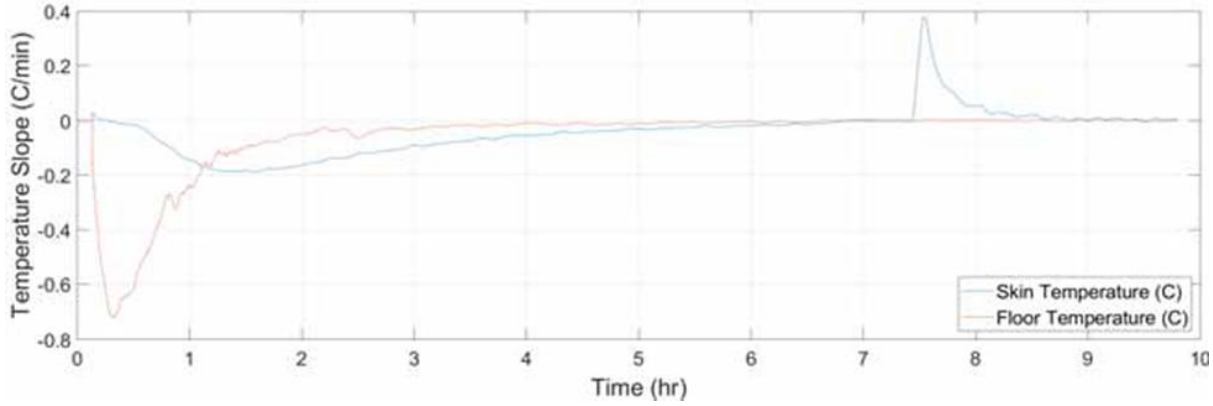

Figure 080321.09: RMS Height Evolution

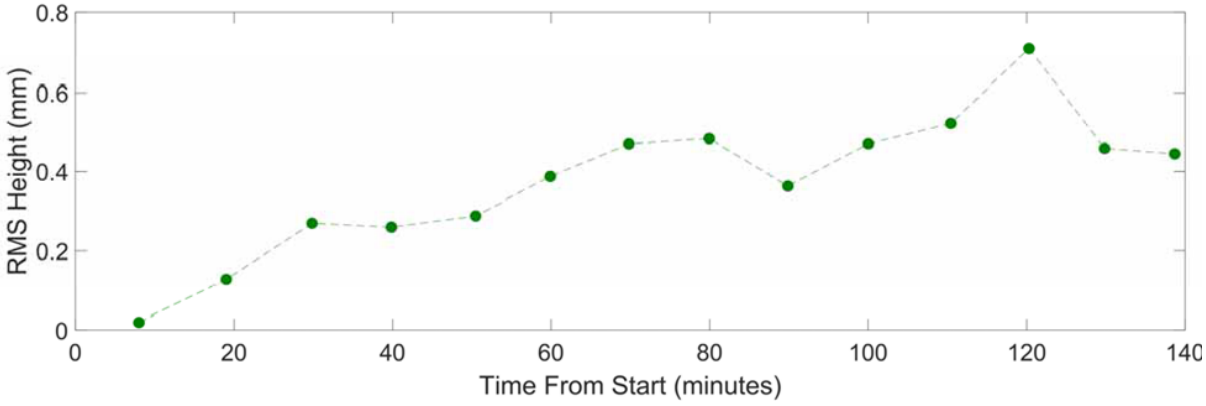

Figure 080321.10: Skewness Evolution

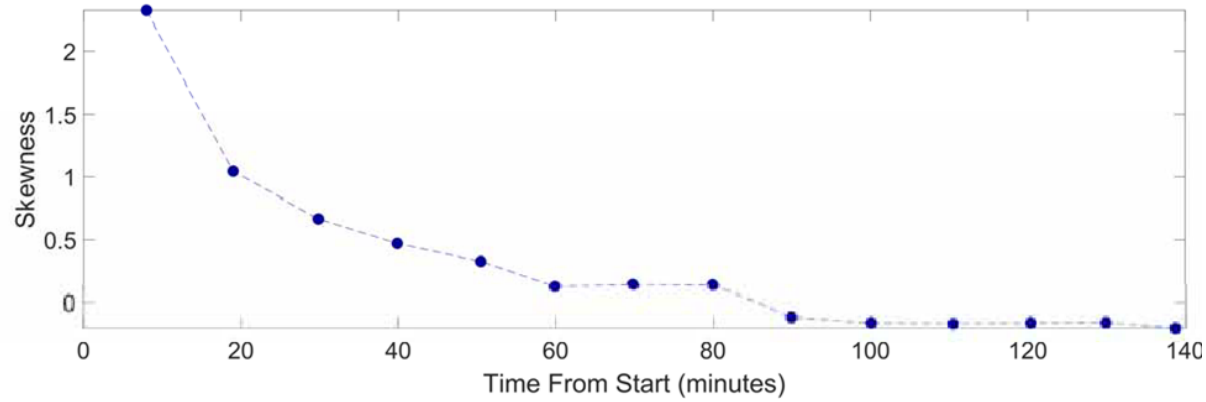

Figure 080321.11: Peak to Valley Evolution

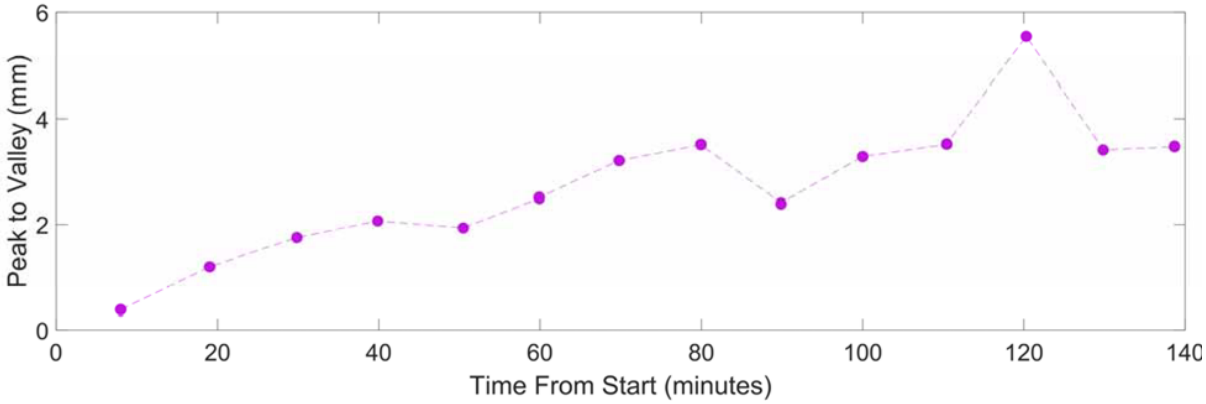

Figure 080321.12: Equivalent Roughness Evolution

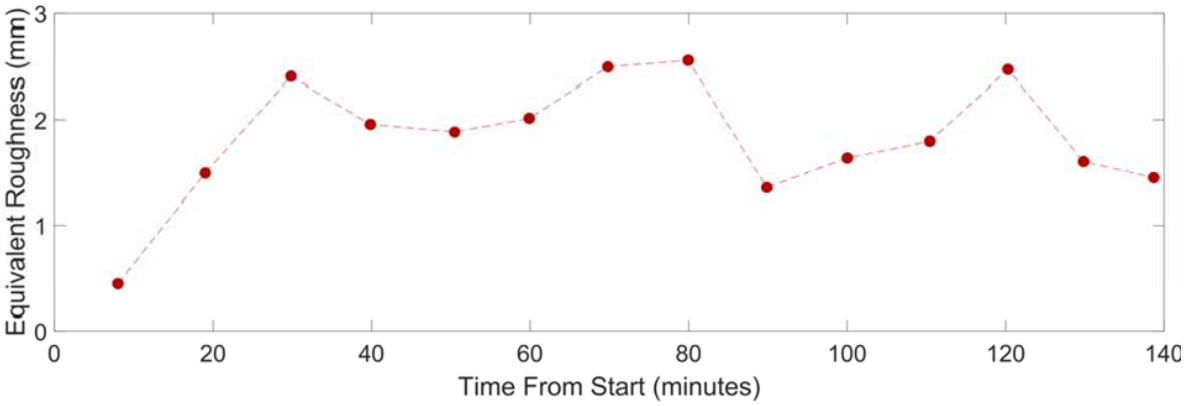

Table 080321.02: Summary of Roughness Parameters

Time (min.)	RMS (mm)	Skewness	Peak to Valley (mm)	ks,Flack-Schultz (mm)
7.9948	0.0194	2.3195	0.3707	0.4436
19.0115	0.1267	1.0438	1.1938	1.4943
29.8448	0.2701	0.6670	1.7507	2.4095
39.8615	0.2601	0.4716	2.0694	1.9561
50.4781	0.2886	0.3265	1.9341	1.8829
59.8948	0.3866	0.1260	2.5006	2.0147
69.8115	0.4700	0.1431	3.2073	2.5008
79.9448	0.4837	0.1395	3.5121	2.5627
89.8781	0.3623	-0.1166	2.3923	1.3540
100.0115	0.4702	-0.1608	3.2849	1.6381
110.4281	0.5221	-0.1682	3.5217	1.7973
120.2948	0.7110	-0.1612	5.5674	2.4757
129.8281	0.4585	-0.1585	3.4133	1.6035
138.6781	0.4448	-0.2008	3.4747	1.4494

Figure 080321.13: Frost Topography at 00:07:59

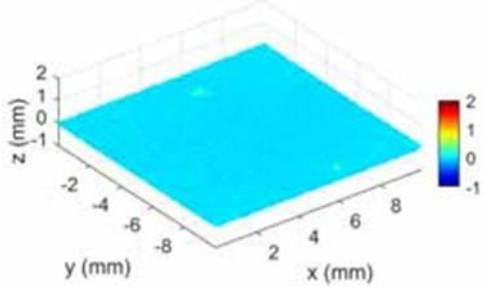

Figure 080321.14: Frost Topography at 00:19:00

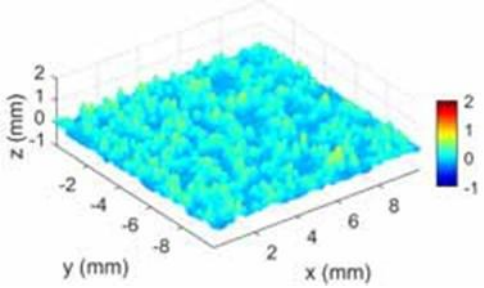

Figure 080321.15: Frost Topography at 00:29:50

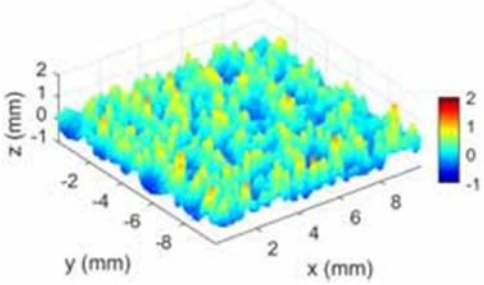

Figure 080321.16: Frost Topography at 00:39:51

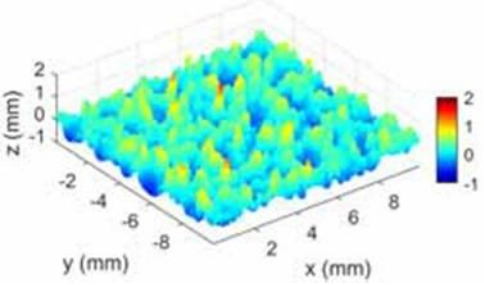

Figure 080321.17: Frost Topography at 00:50:28

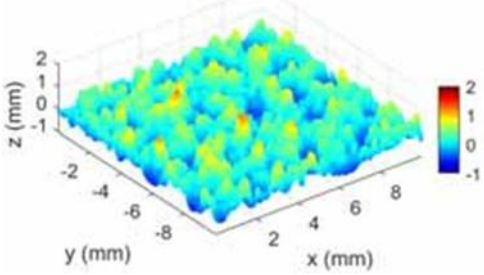

Figure 080321.18: Frost Topography at 00:59:53

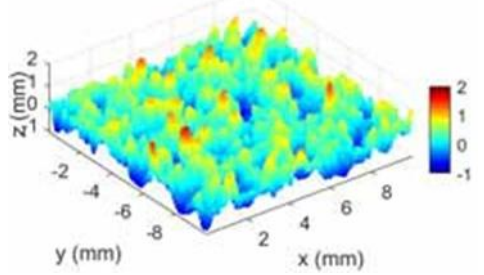

Figure 080321.19: Frost Topography at 01:09:48

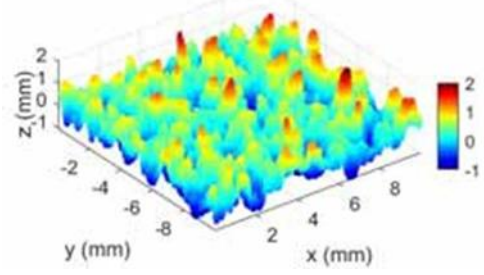

Figure 080321.20: Frost Topography at 01:19:56

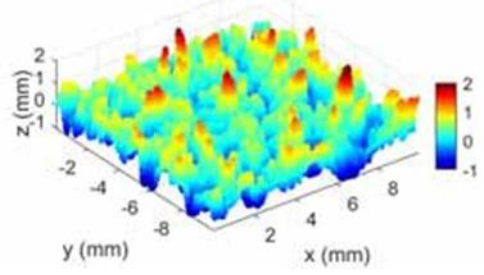

Figure 080321.21: Frost Topography at 01:29:52

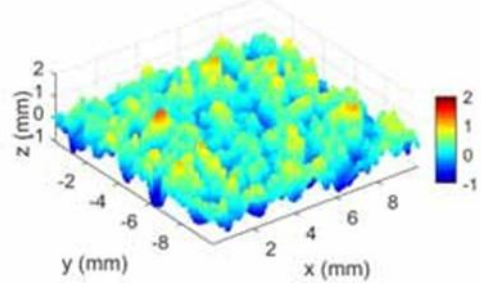

Figure 080321.22: Frost Topography at 01:40:00

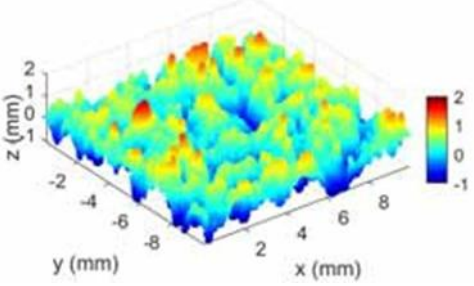

Figure 080321.23: Frost Topography at 01:50:25

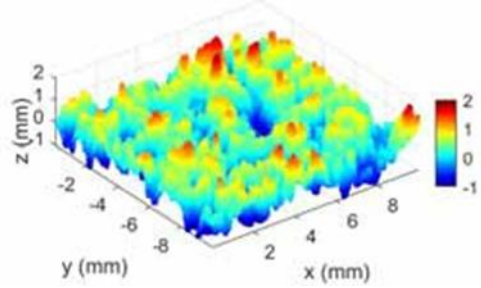

Figure 080321.24: Frost Topography at 02:00:17

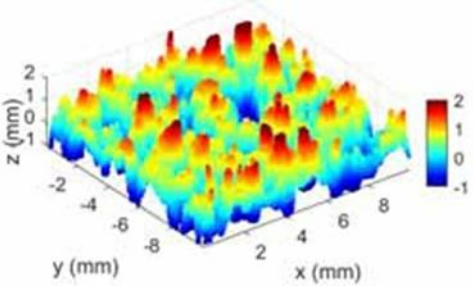

Figure 080321.25: Frost Topography at 02:09:49

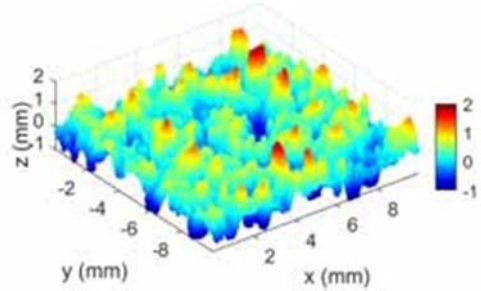

Figure 080321.26: Frost Topography at 02:18:40

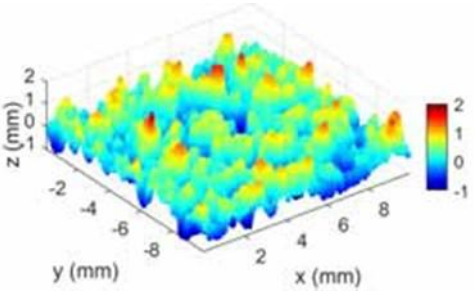

CAFF Conditions Report – Case Date: 081221

Table 081221.01: Summary of Measured Test Variables

Variable	Mean	St. Dev.	Rand. Unc.
T_air (C)	4.2520	0.2496	0.0084
Rh (%)	79.1902	6.3160	0.2129
Omega (kg_v/kg_da)	0.00410540	0.00038056	0.00001283
V_air (m/s)	0.3603	0.0528	0.0018
T_skin (C)	-10.7960	0.7259	0.0245
T_floor (C)	-20.5565	0.0205	0.0007

Figure 081221.01: Temperature and Voltage Control Time History

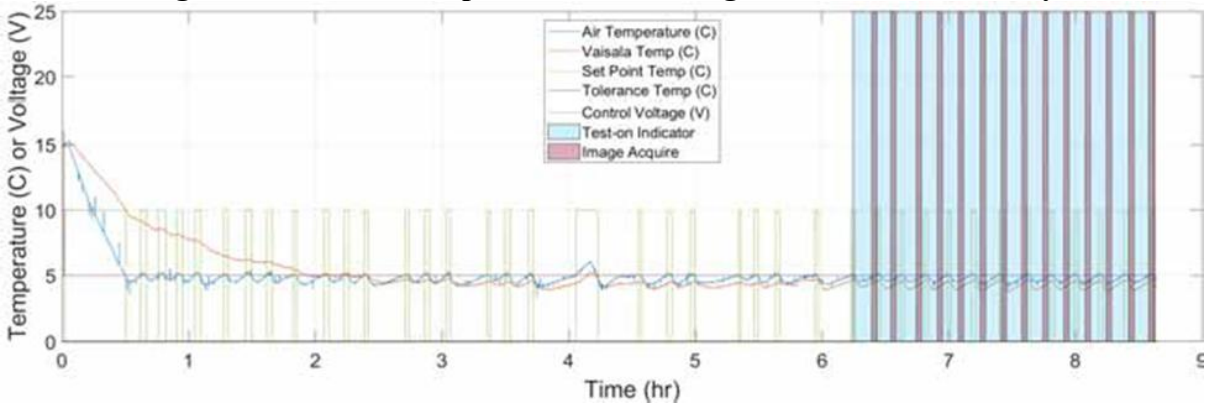

Figure 081221.02: Relative Humidity Time History

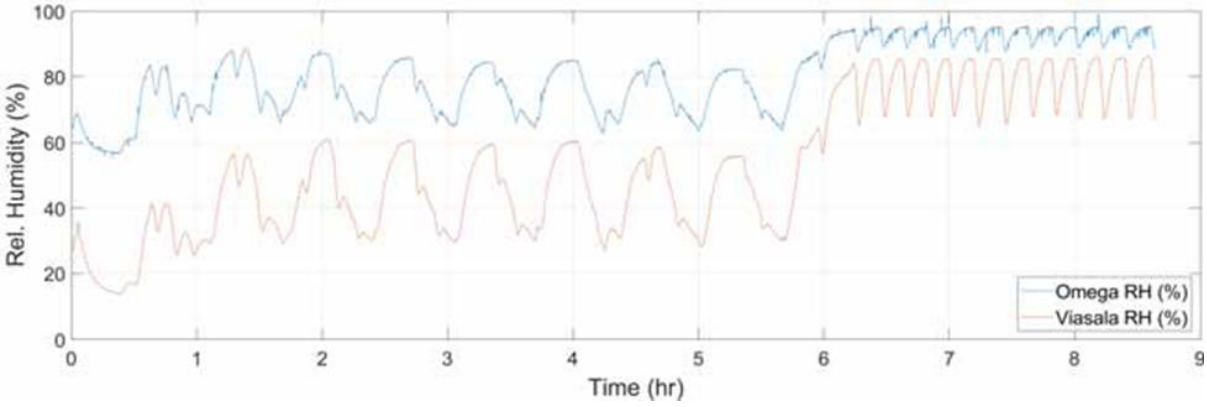

Figure 081221.03: Velocity Time History

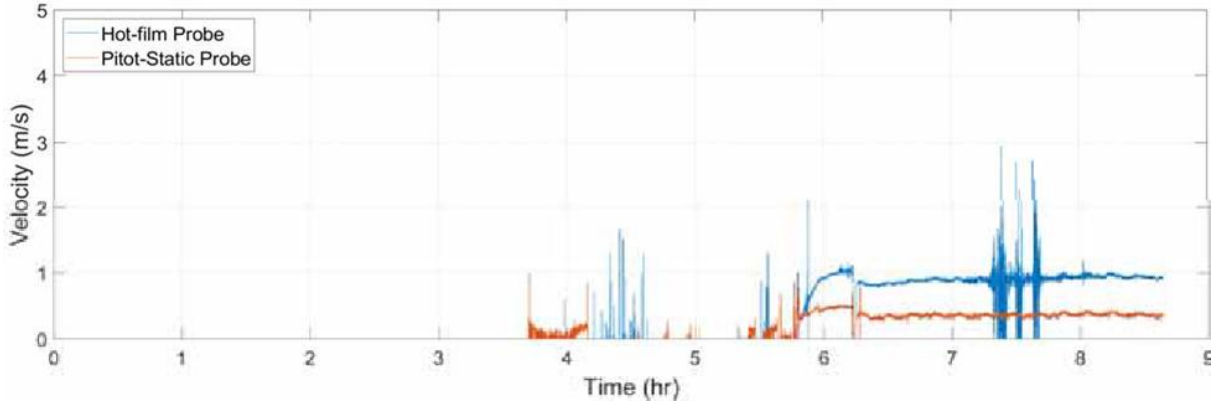

Figure 081221.04: Coolant Return Temperature Time History

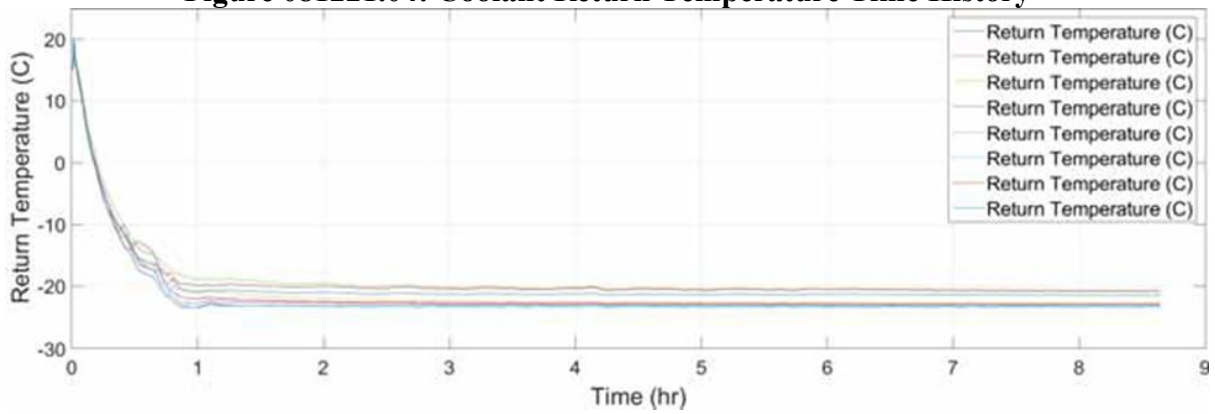

Figure 081221.05: Coolant Supply Temperature Time History

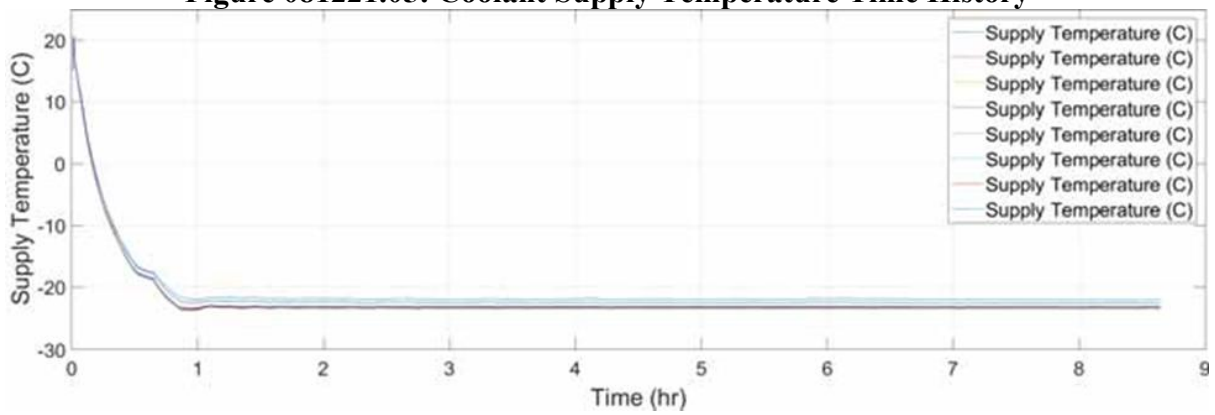

Figure 081221.06: Skin Temperature Time History

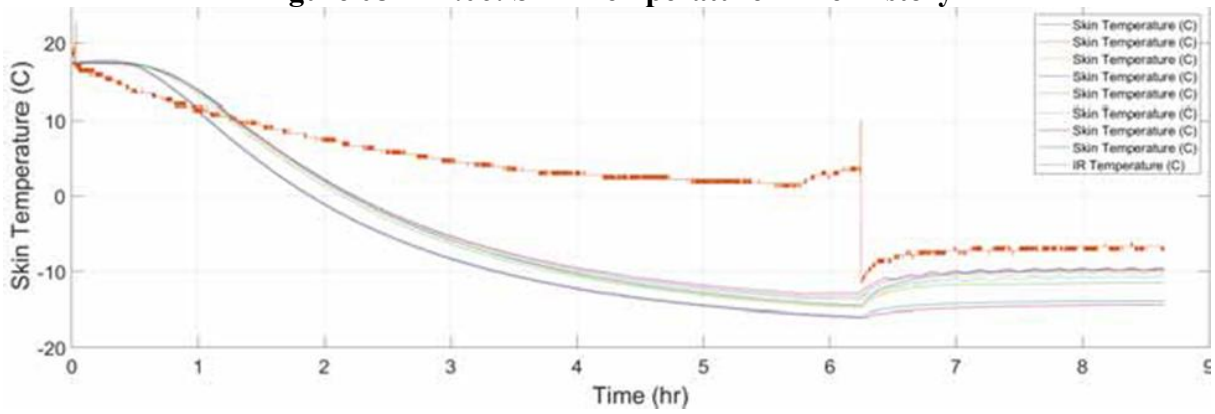

Figure 081221.07: Floor Temperature Time History

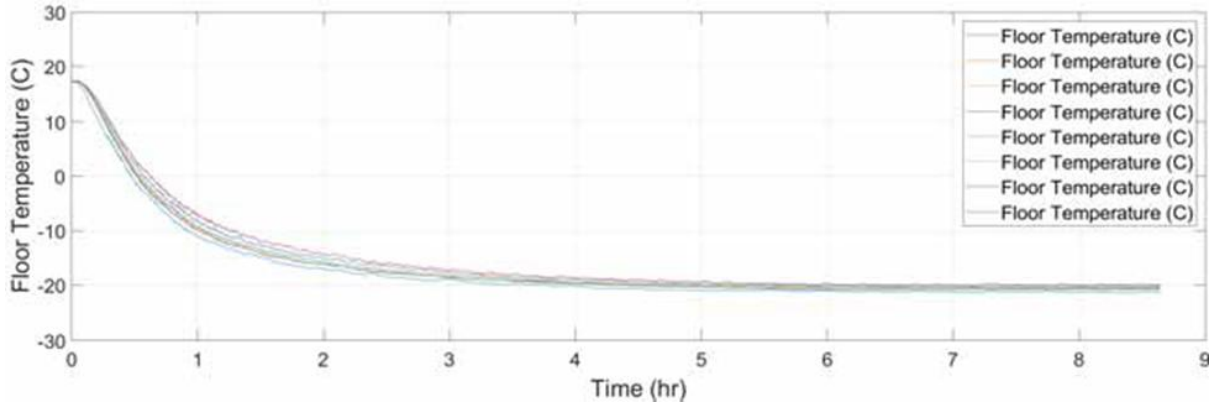

Figure 081221.08: Skin Temperature Slope Time History

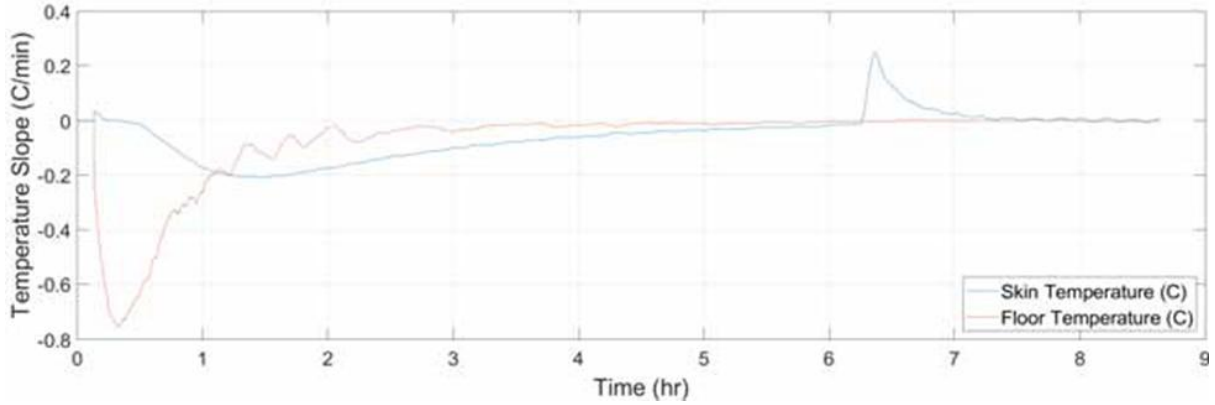

Figure 081221.09: RMS Height Evolution

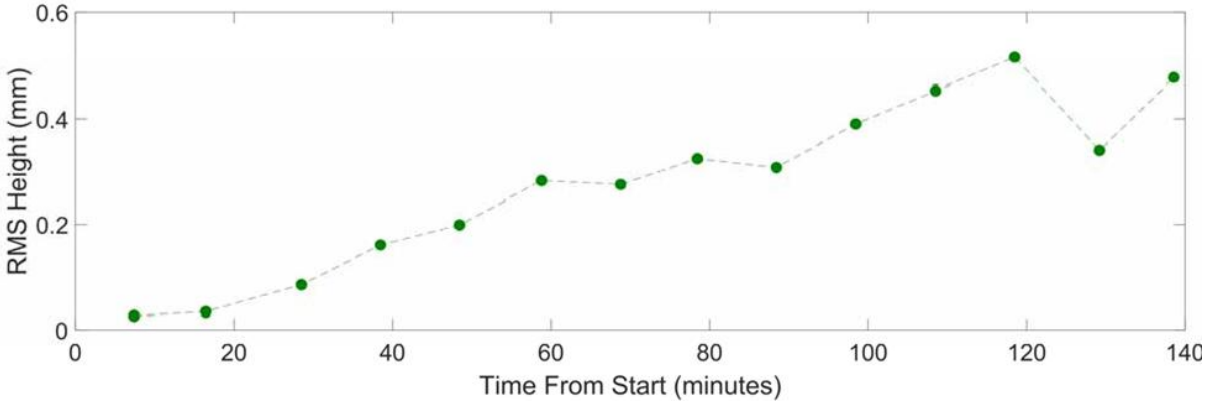

Figure 081221.10: Skewness Evolution

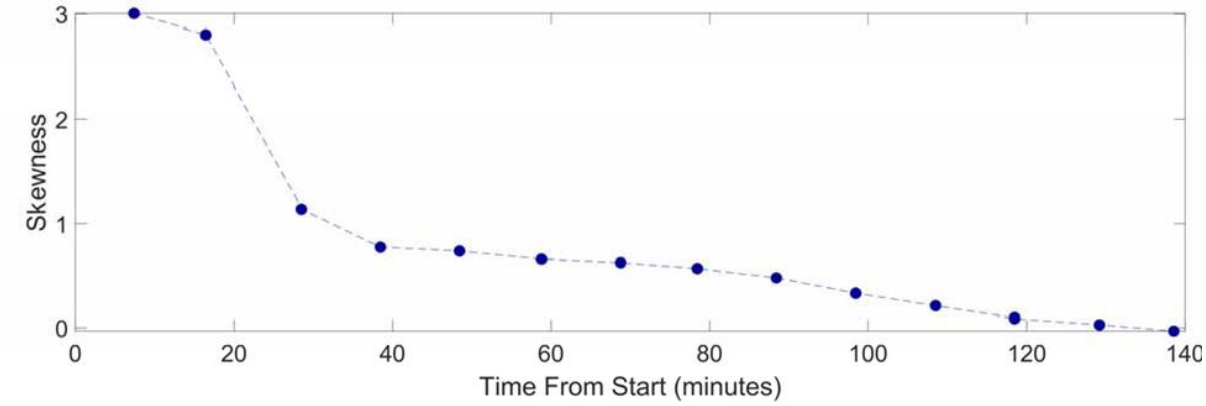

Figure 081221.11: Peak to Valley Evolution

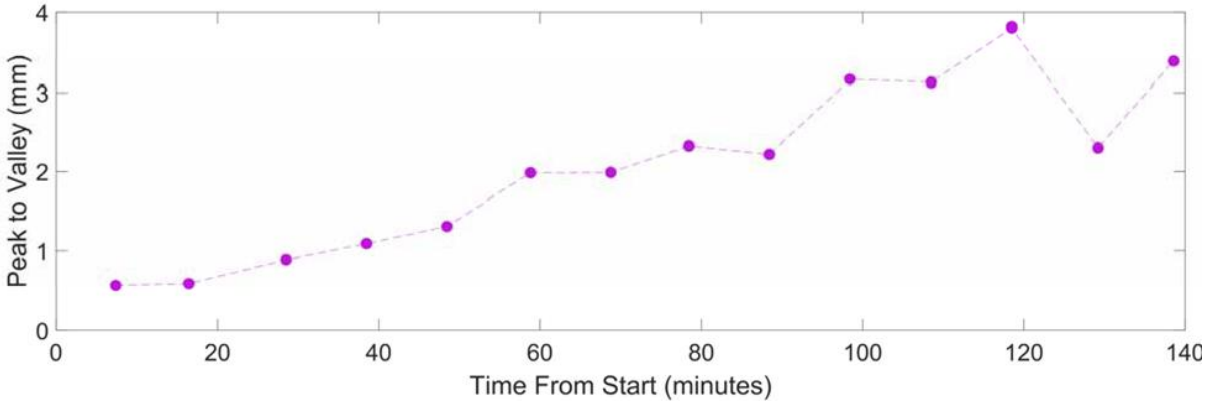

Figure 081221.12: Equivalent Roughness Evolution

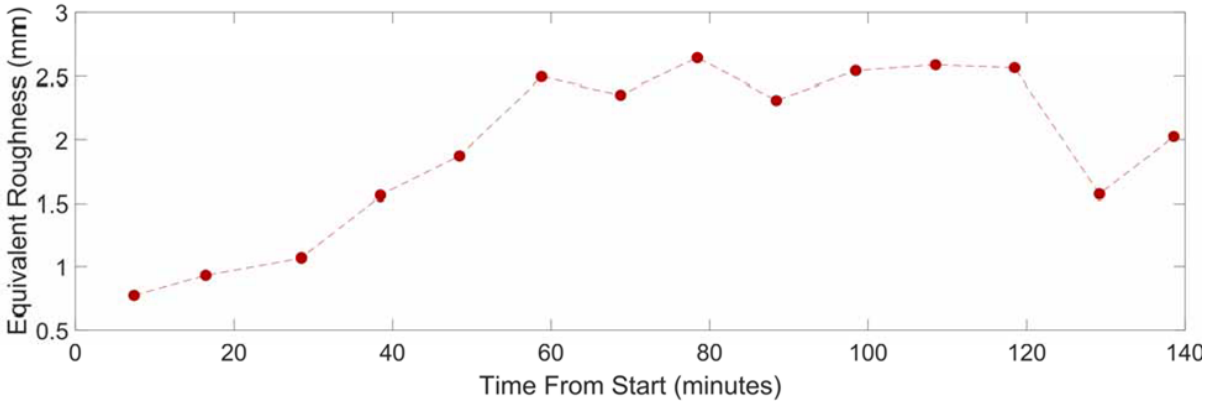

Table 081221.02: Summary of Roughness Parameters

Time (min.)	RMS (mm)	Skewness	Peak to Valley (mm)	ks,Flack-Schultz (mm)
7.3719	0.0259	3.0050	0.5551	0.7665
16.4386	0.0336	2.8074	0.5779	0.9290
28.5052	0.0850	1.1408	0.8837	1.0677
38.4719	0.1608	0.7713	1.0896	1.5588
48.4386	0.1989	0.7346	1.3082	1.8735
58.8052	0.2823	0.6561	1.9819	2.4965
68.7719	0.2748	0.6202	1.9860	2.3576
78.4552	0.3242	0.5634	2.3245	2.6488
88.4219	0.3072	0.4736	2.2153	2.3145
98.4219	0.3905	0.3253	3.1633	2.5442
108.5052	0.4537	0.2036	3.1271	2.5908
118.4886	0.5168	0.0875	3.8161	2.5682
129.1886	0.3402	0.0296	2.2980	1.5687
138.5719	0.4778	-0.0314	3.3952	2.0262

Figure 081221.13: Frost Topography at 00:08:44

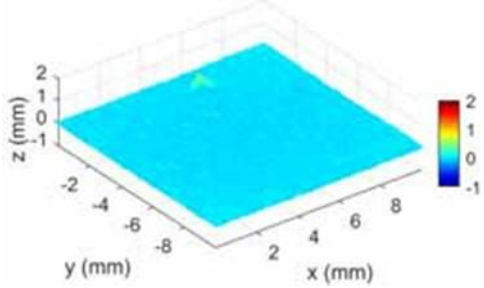

Figure 081221.14: Frost Topography at 00:17:48

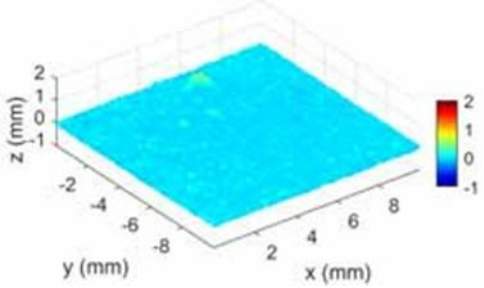

Figure 081221.15: Frost Topography at 00:29:52

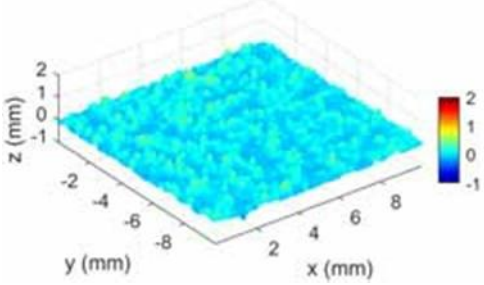

Figure 081221.16: Frost Topography at 00:39:50

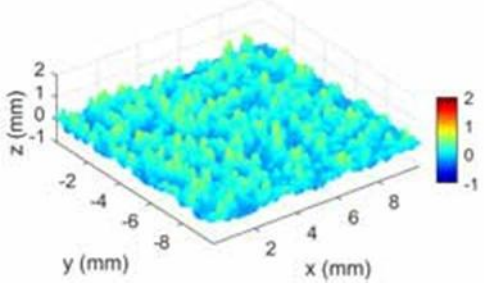

Figure 081221.17: Frost Topography at 00:49:48

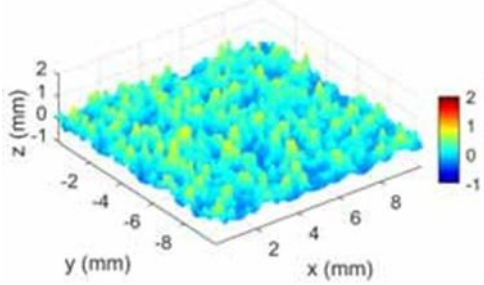

Figure 081221.18: Frost Topography at 01:00:10

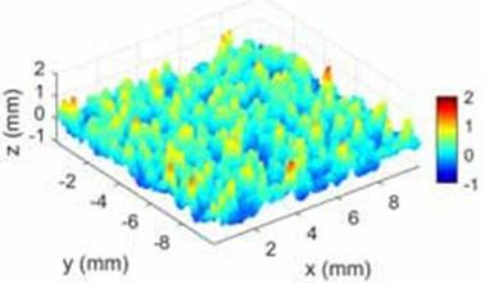

Figure 081221.19: Frost Topography at 01:10:08

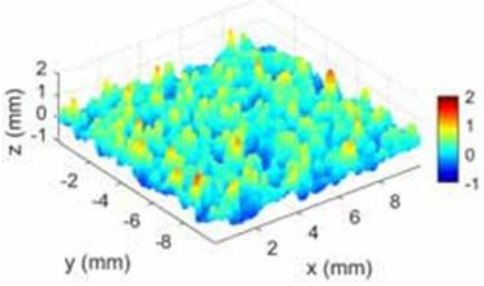

Figure 081221.20: Frost Topography at 01:19:49

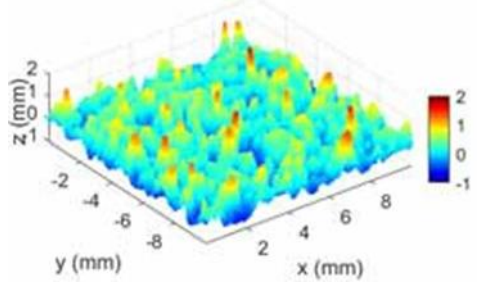

Figure 081221.21: Frost Topography at 01:29:47

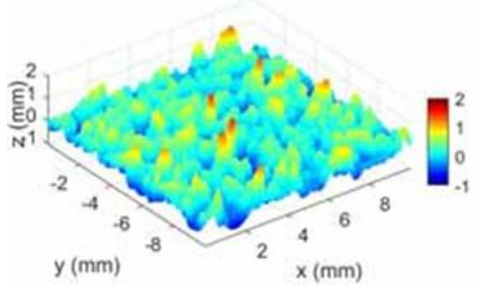

Figure 081221.22: Frost Topography at 01:39:47

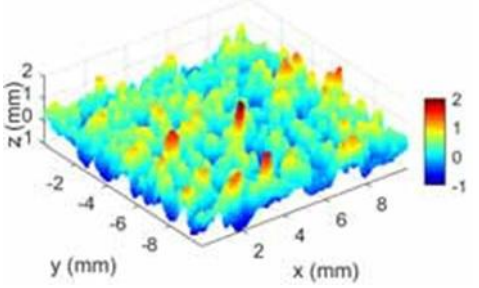

Figure 081221.23: Frost Topography at 01:49:52

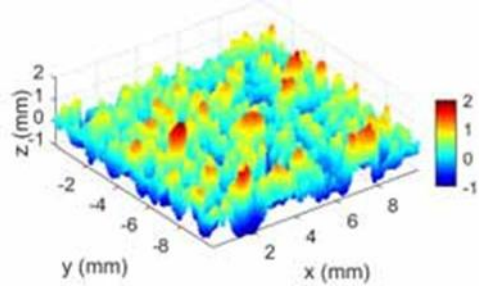

Figure 081221.24: Frost Topography at 01:59:51

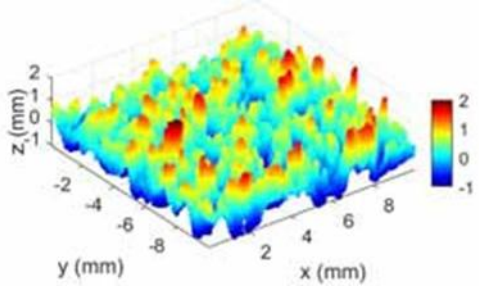

Figure 081221.25: Frost Topography at 02:10:33

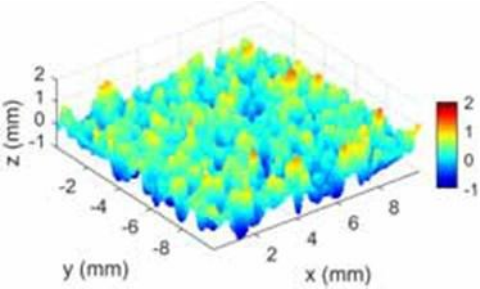

Figure 081221.26: Frost Topography at 02:19:56

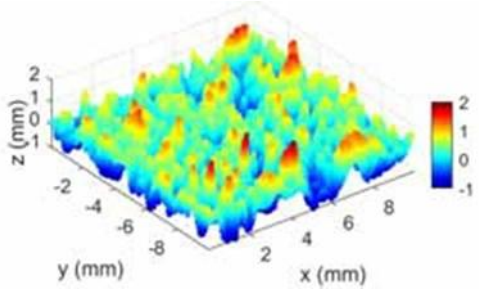

CAFF Conditions Report – Case Date: 081621

Table 081621.01: Summary of Measured Test Variables

Variable	Mean	St. Dev.	Rand. Unc.
T_air (C)	4.2813	0.2699	0.0091
Rh (%)	79.5172	4.7663	0.1614
Omega (kg_v/kg_da)	0.00415160	0.00031465	0.00001065
V_air (m/s)	1.4693	0.0914	0.0031
T_skin (C)	-8.4056	1.0184	0.0345
T_floor (C)	-20.3819	0.0577	0.0020

Figure 081621.01: Temperature and Voltage Control Time History

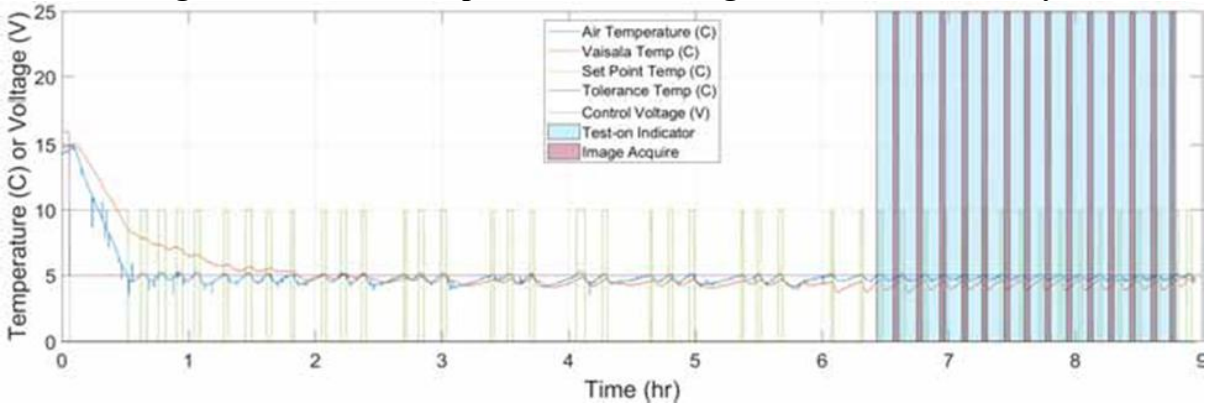

Figure 081621.02: Relative Humidity Time History

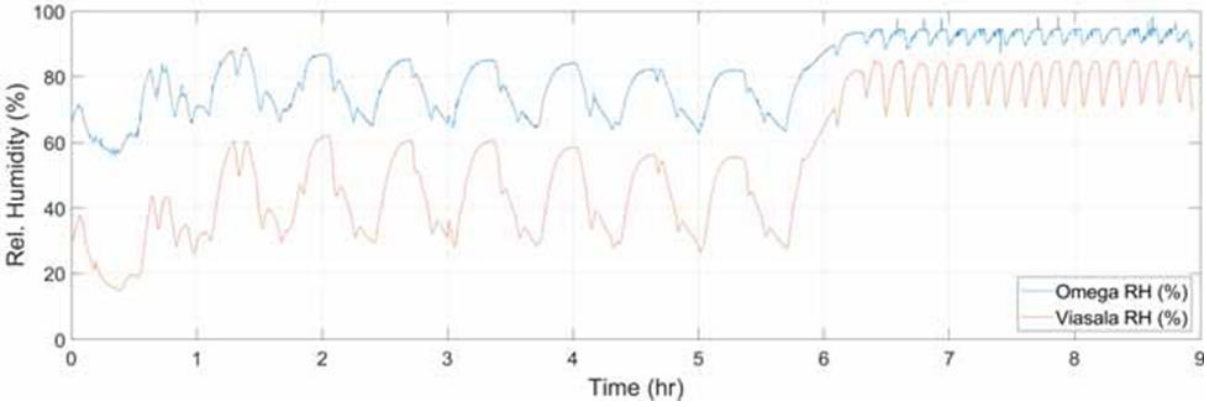

Figure 081621.03: Velocity Time History

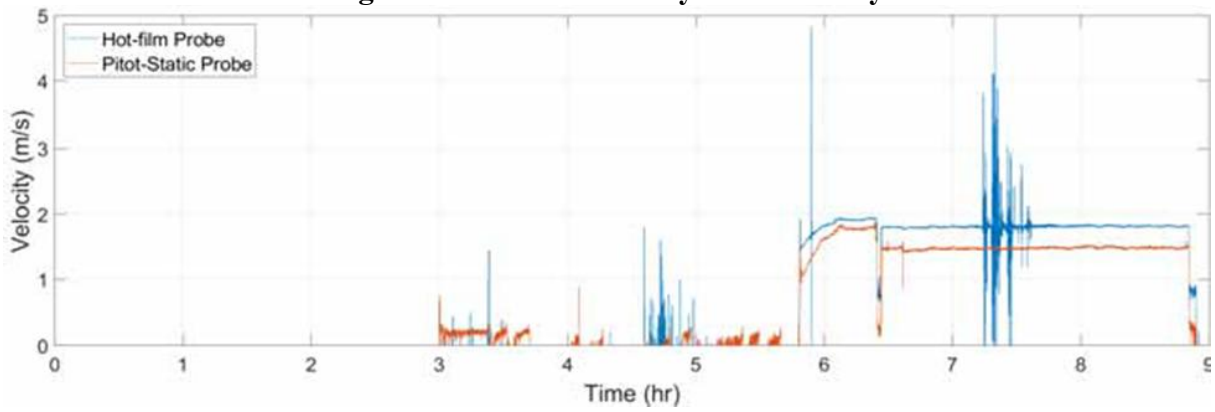

Figure 081621.04: Coolant Return Temperature Time History

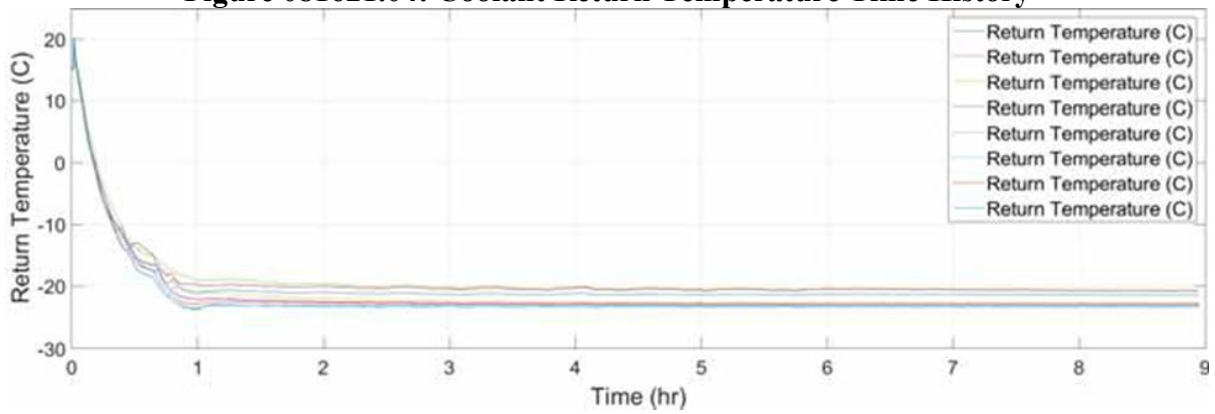

Figure 081621.05: Coolant Supply Temperature Time History

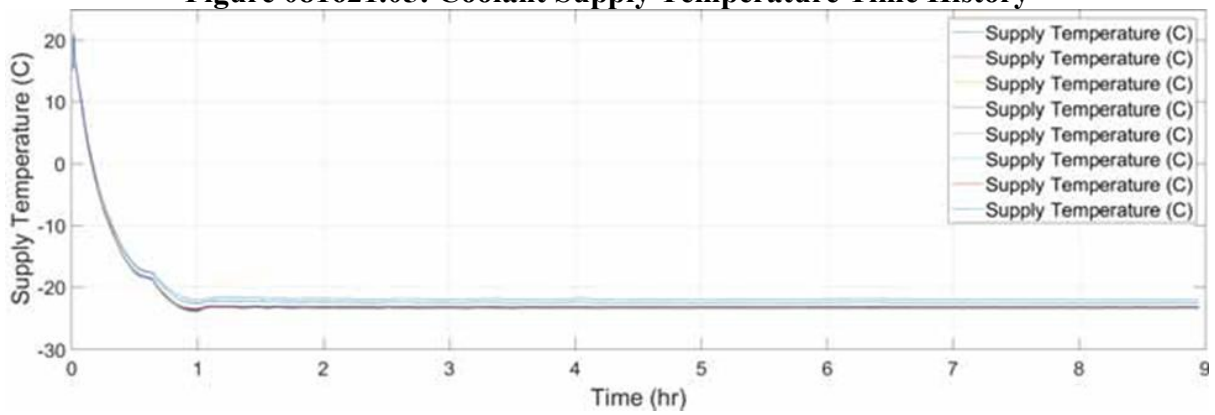

Figure 081621.06: Skin Temperature Time History

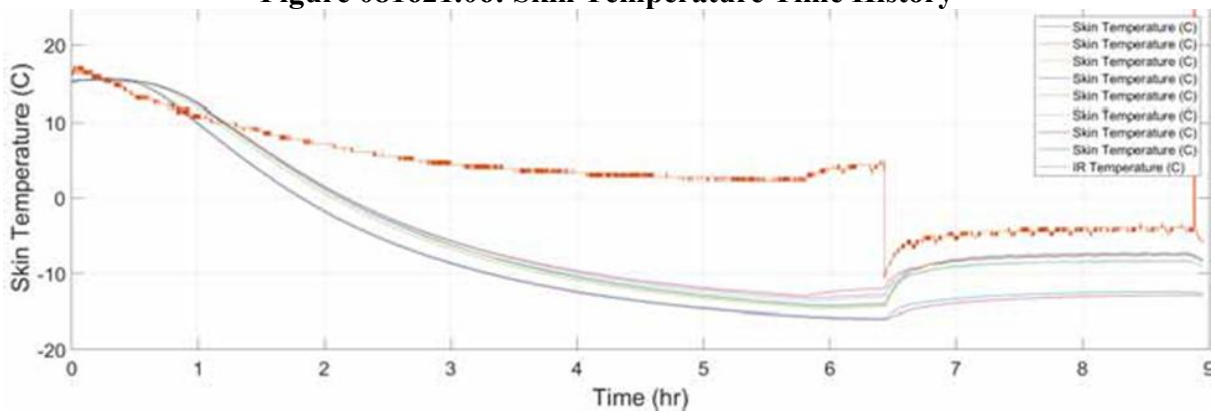

Figure 081621.07: Floor Temperature Time History

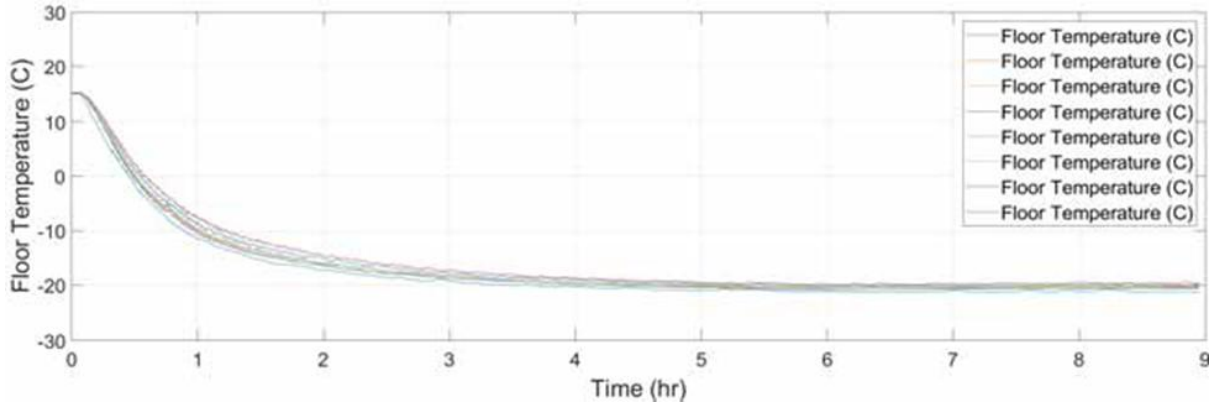

Figure 081621.08: Skin Temperature Slope Time History

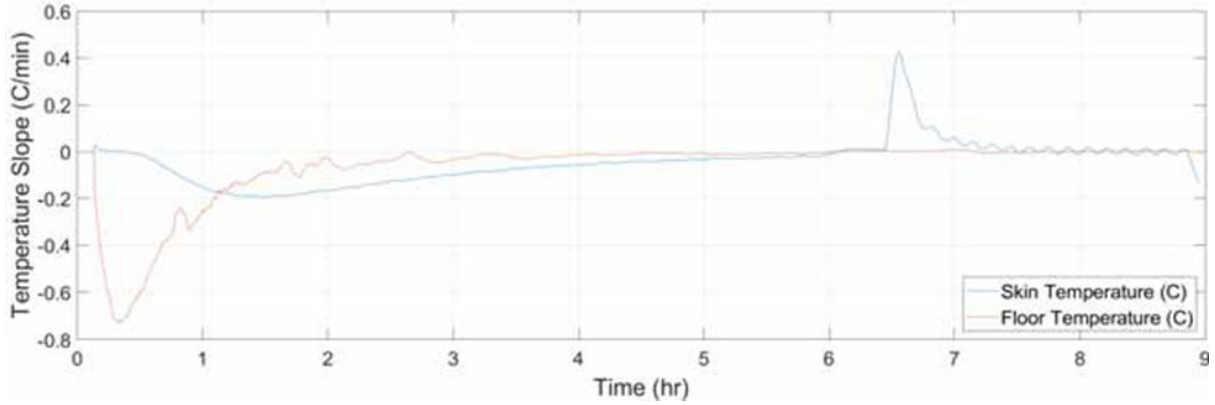

Figure 081621.09: RMS Height Evolution

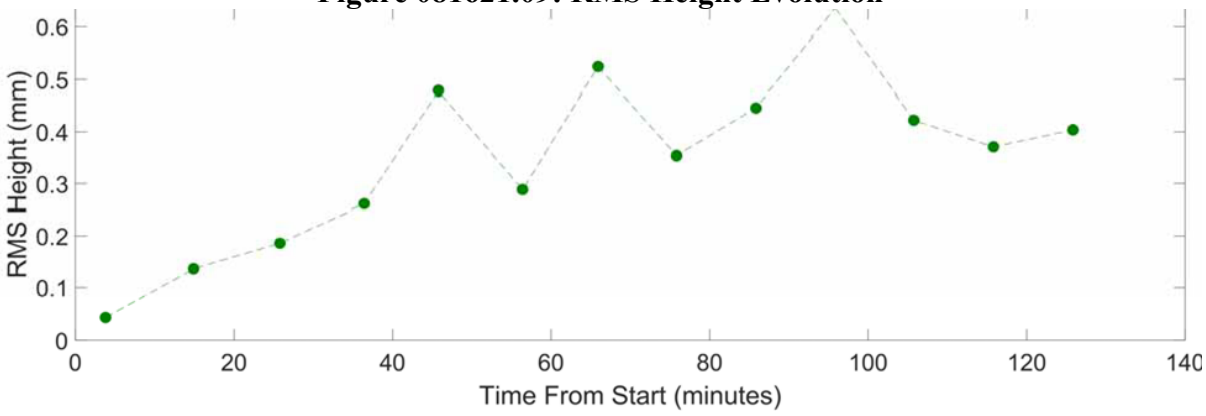

Figure 081621.10: Skewness Evolution

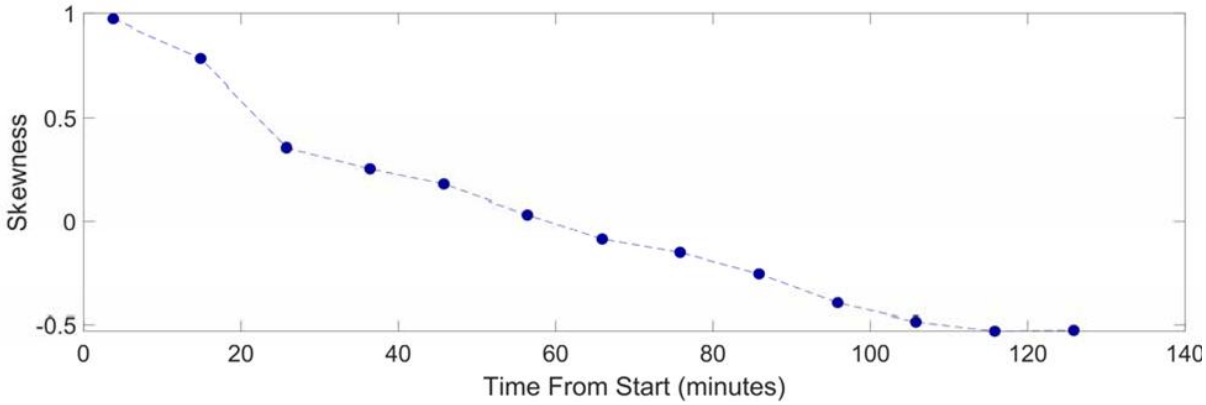

Figure 081621.11: Peak to Valley Evolution

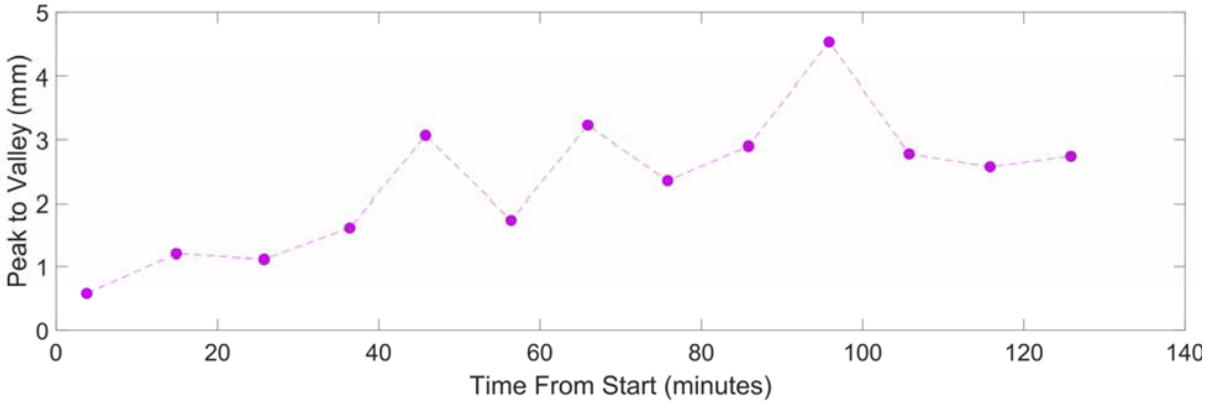

Figure 081621.12: Equivalent Roughness Evolution

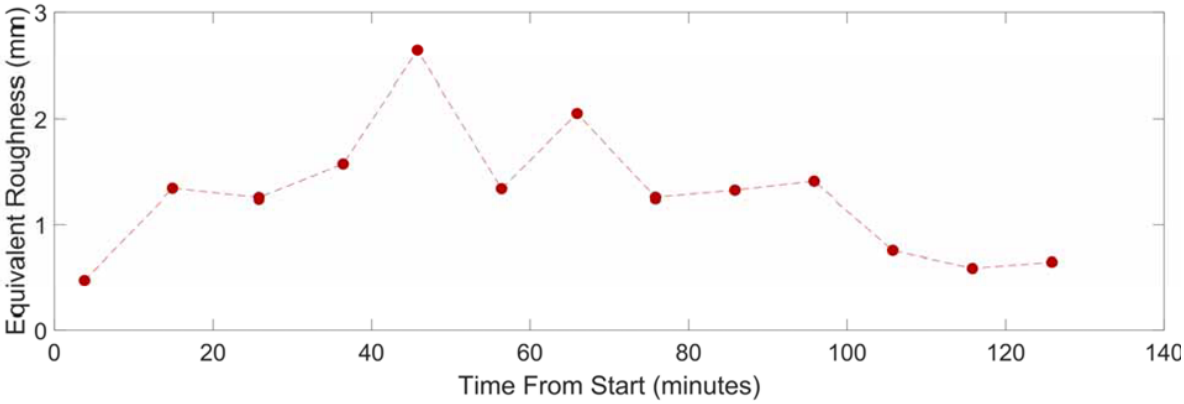

Table 081621.02: Summary of Roughness Parameters

Time (min.)	RMS (mm)	Skewness	Peak to Valley (mm)	ks,Flack-Schultz (mm)
3.7713	0.0412	0.9730	0.5668	0.4630
14.8880	0.1363	0.7851	1.2015	1.3358
25.7880	0.1857	0.3540	1.1106	1.2462
36.4046	0.2608	0.2508	1.6109	1.5697
45.7880	0.4787	0.1766	3.0707	2.6502
56.4046	0.2881	0.0308	1.7336	1.3305
65.9213	0.5252	-0.0871	3.2352	2.0534
75.8213	0.3541	-0.1532	2.3472	1.2490
85.8380	0.4464	-0.2568	2.8998	1.3171
95.8380	0.6362	-0.3986	4.5495	1.4043
105.7713	0.4226	-0.4868	2.7781	0.7506
115.8046	0.3706	-0.5315	2.5705	0.5809
125.8380	0.4038	-0.5276	2.7421	0.6403

Figure 081621.13: Frost Topography at 00:07:49

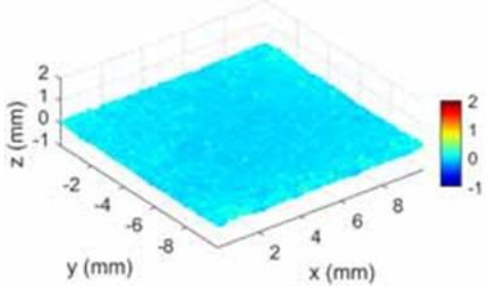

Figure 081621.14: Frost Topography at 00:18:56

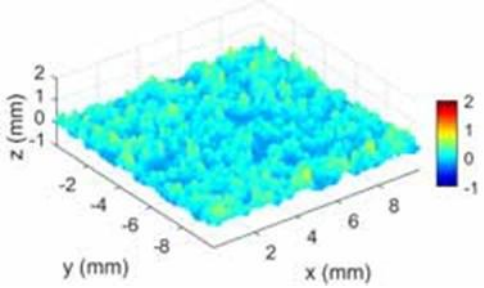

Figure 081621.15: Frost Topography at 00:29:50

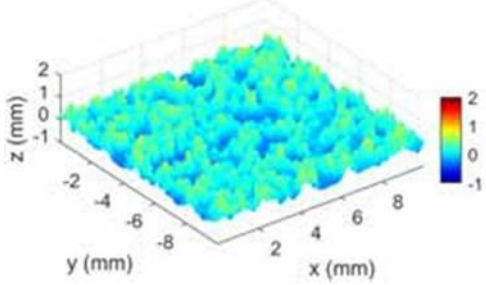

Figure 081621.16: Frost Topography at 00:40:27

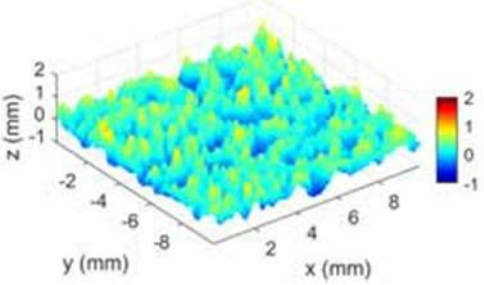

Figure 081621.17: Frost Topography at 00:49:50

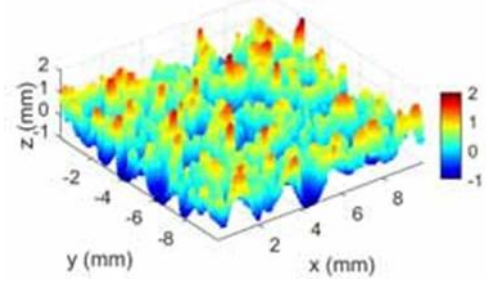

Figure 081621.18: Frost Topography at 01:00:27

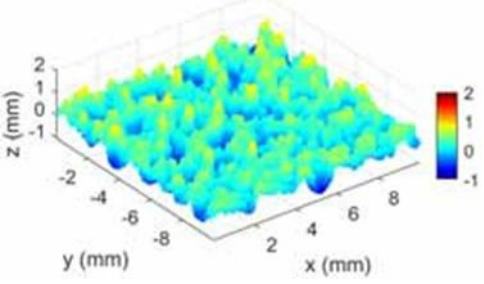

Figure 081621.19: Frost Topography at 01:09:55

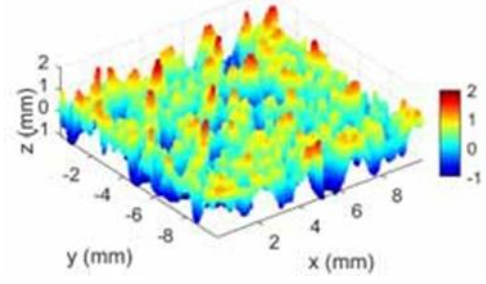

Figure 081621.20: Frost Topography at 01:19:52

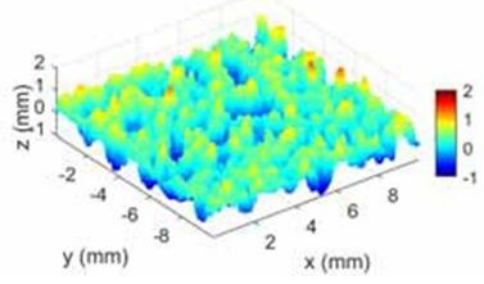

Figure 081621.21: Frost Topography at 01:29:53

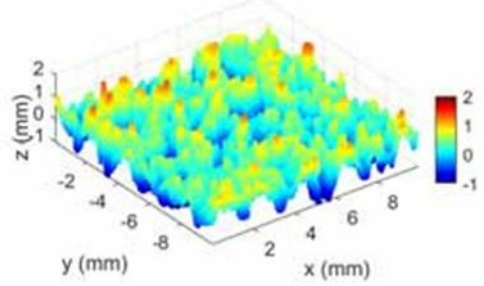

Figure 081621.22: Frost Topography at 01:39:53

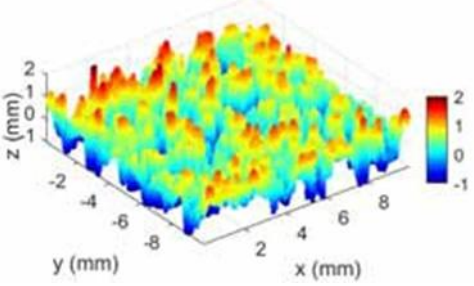

Figure 081621.23: Frost Topography at 01:49:49

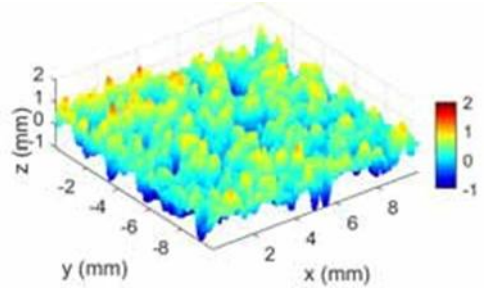

Figure 081621.24: Frost Topography at 01:59:51

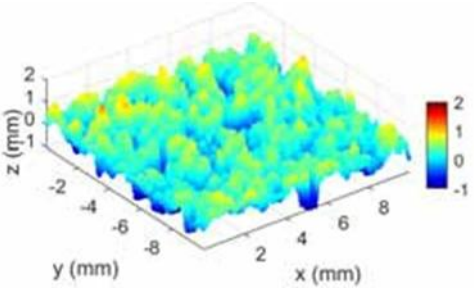

Figure 081621.25: Frost Topography at 02:09:53

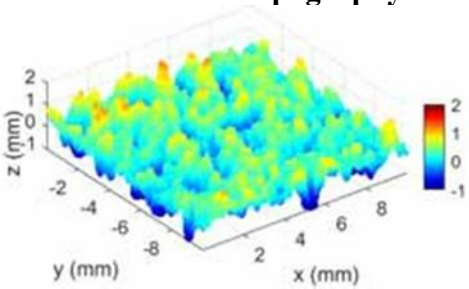

CAFF Conditions Report – Case Date: 081821

Table 081821.01: Summary of Measured Test Variables

Variable	Mean	St. Dev.	Rand. Unc.
T_air (C)	9.2065	0.3919	0.0132
Rh (%)	80.6562	3.9630	0.1337
Omega (kg_v/kg_da)	0.00590626	0.00036727	0.00001239
V_air (m/s)	1.4151	0.1208	0.0041
T_skin (C)	-6.0261	1.4143	0.0477
T_floor (C)	-19.9413	0.1443	0.0049

Figure 081821.01: Temperature and Voltage Control Time History

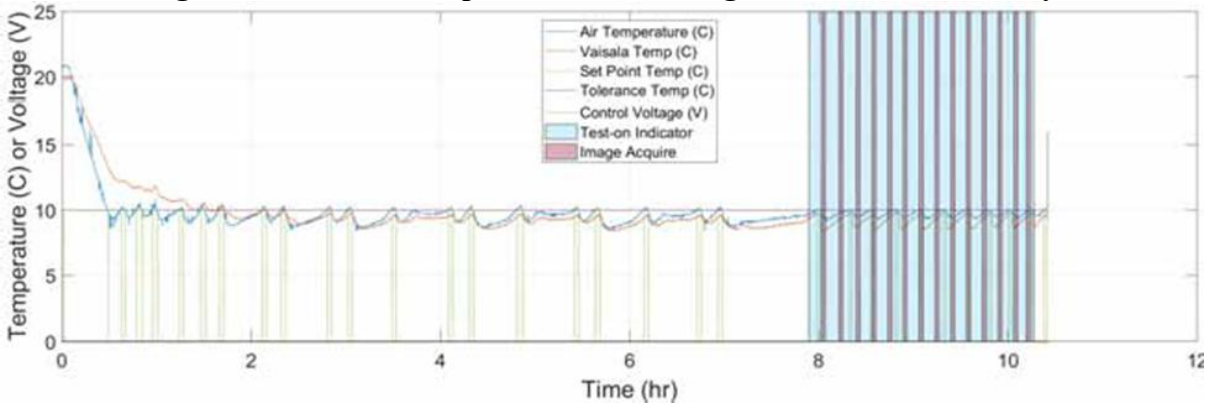

Figure 081821.02: Relative Humidity Time History

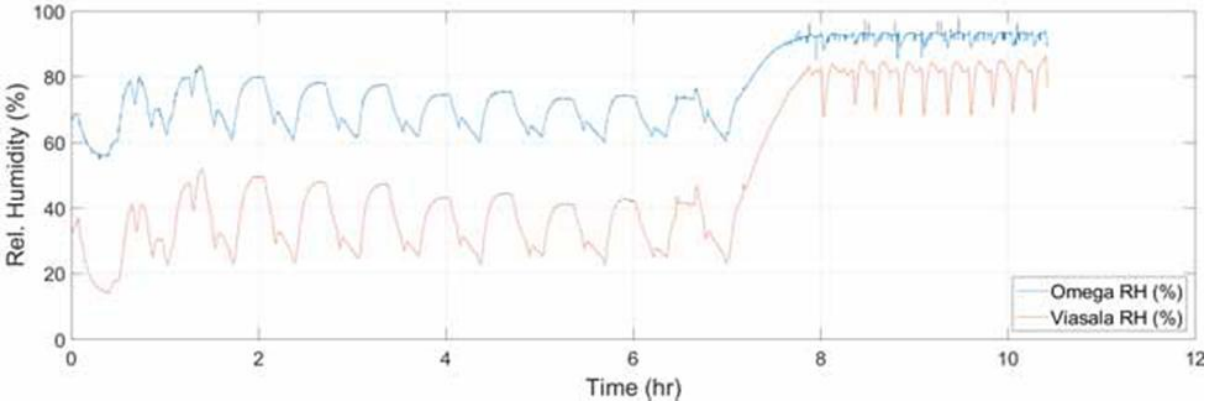

Figure 081821.03: Velocity Time History

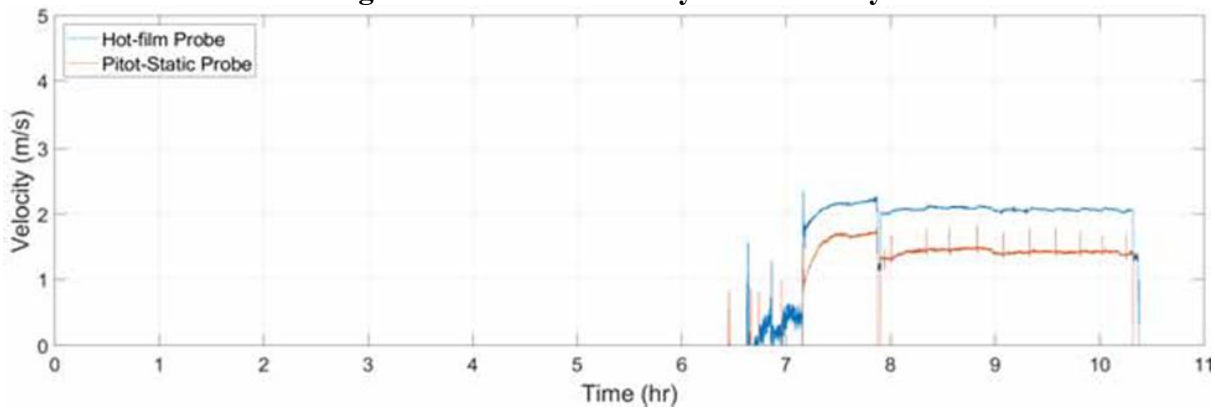

Figure 081821.04: Coolant Return Temperature Time History

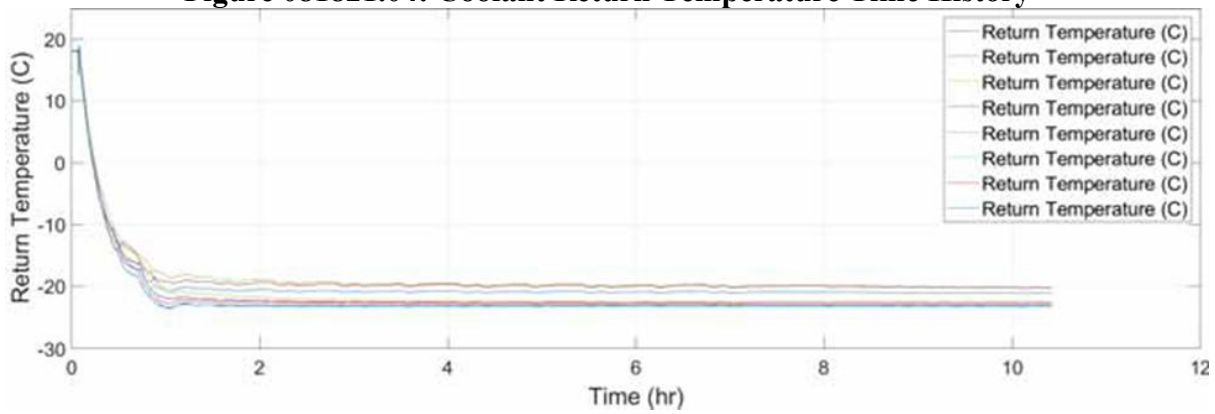

Figure 081821.05: Coolant Supply Temperature Time History

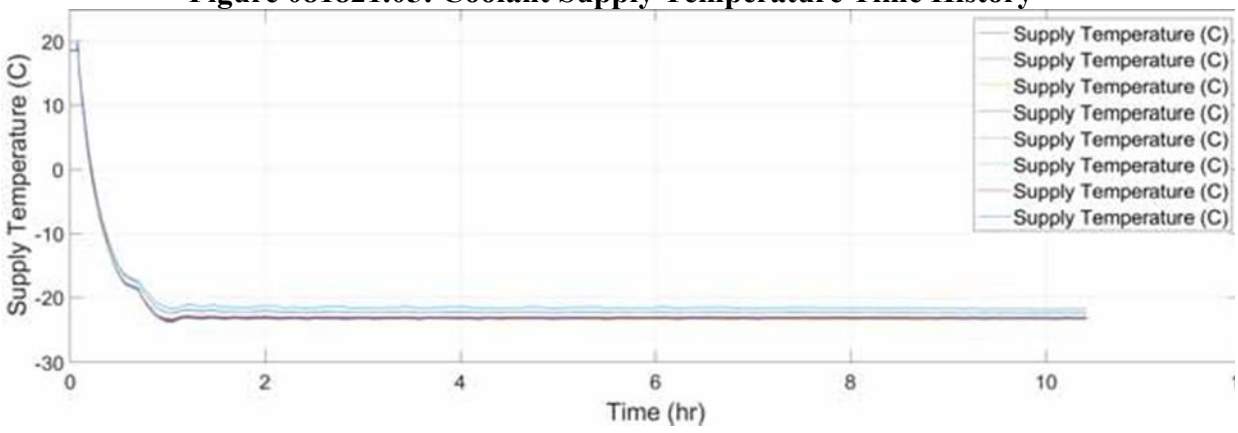

Figure 081821.06: Skin Temperature Time History

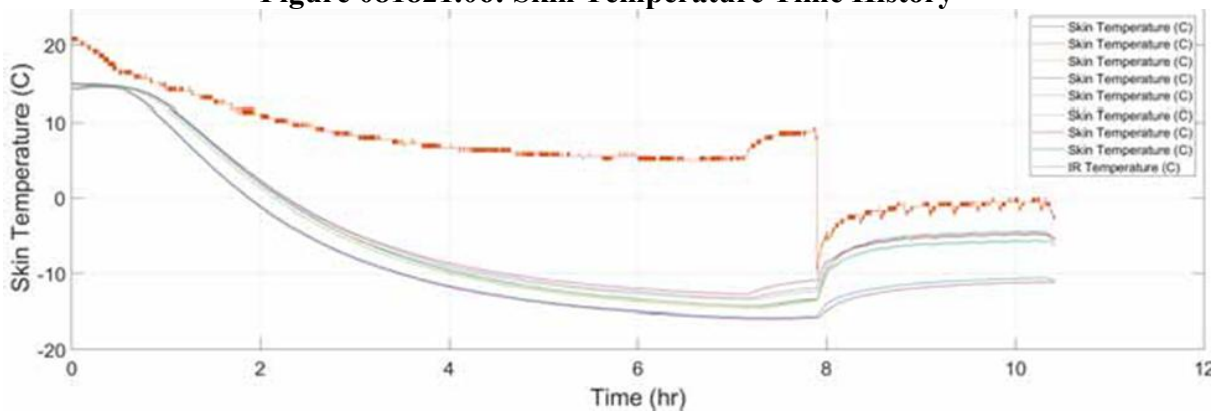

Figure 081821.07: Floor Temperature Time History

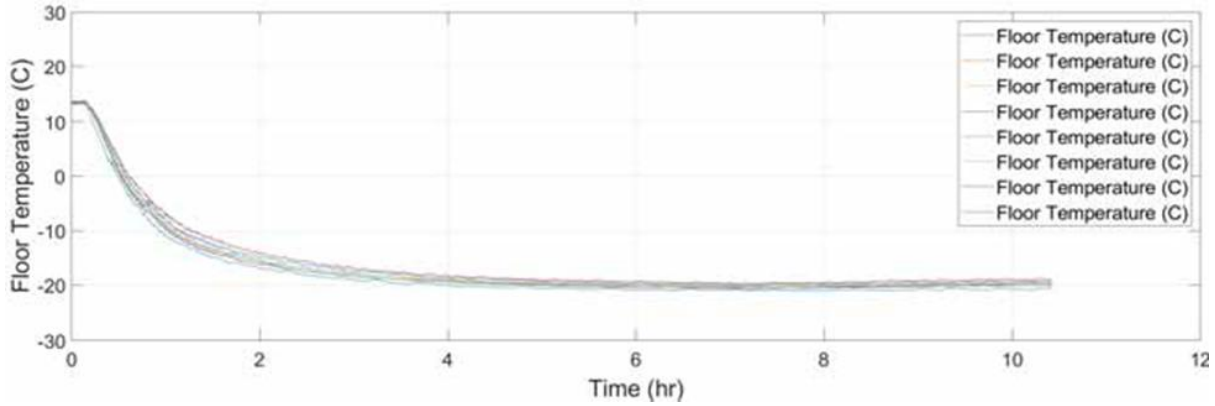

Figure 081821.08: Skin Temperature Slope Time History

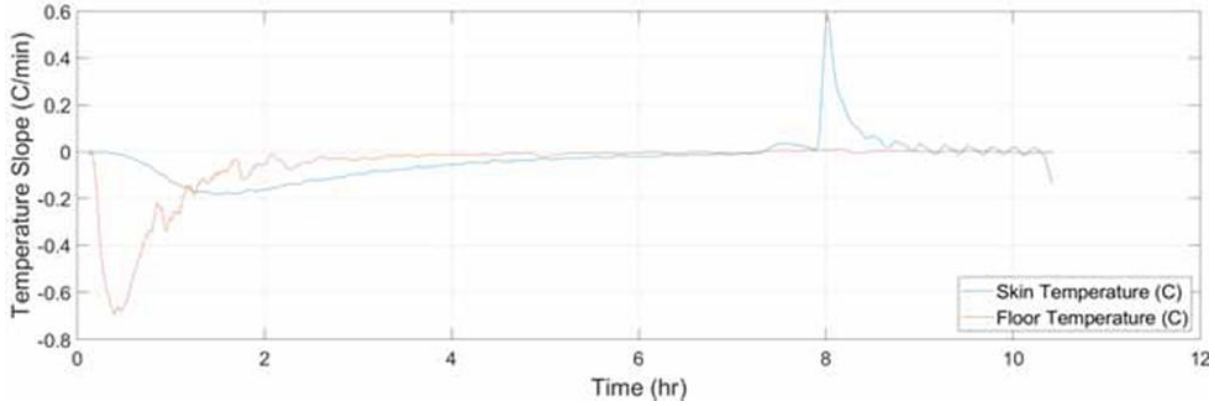

Figure 081821.09: RMS Height Evolution

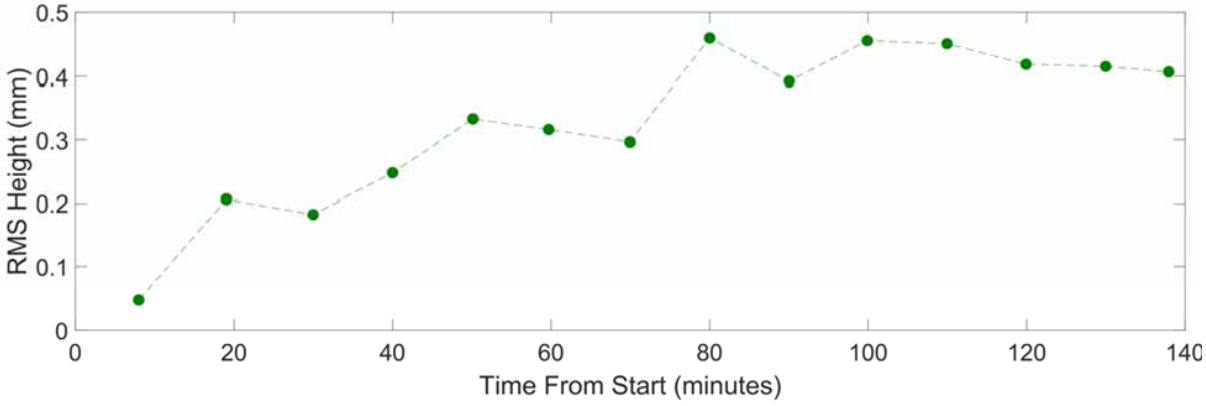

Figure 081821.10: Skewness Evolution

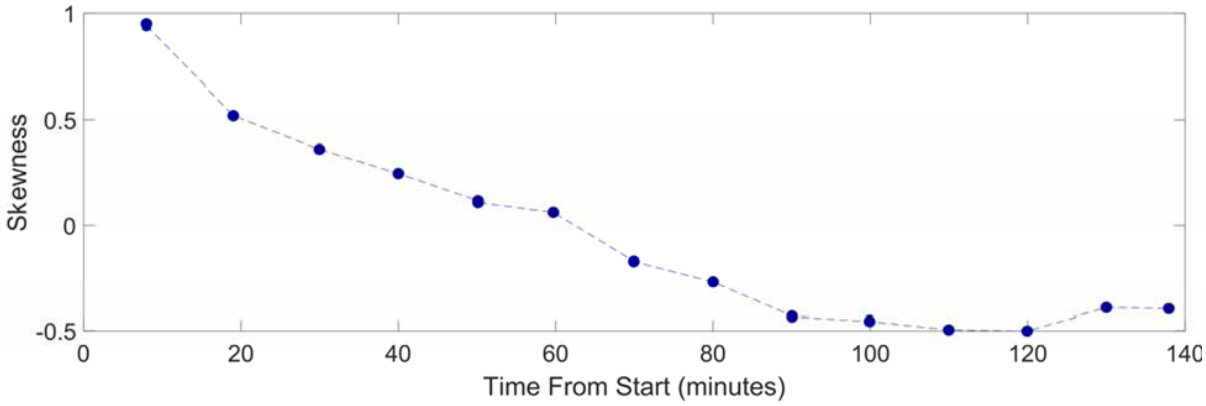

Figure 081821.11: Peak to Valley Evolution

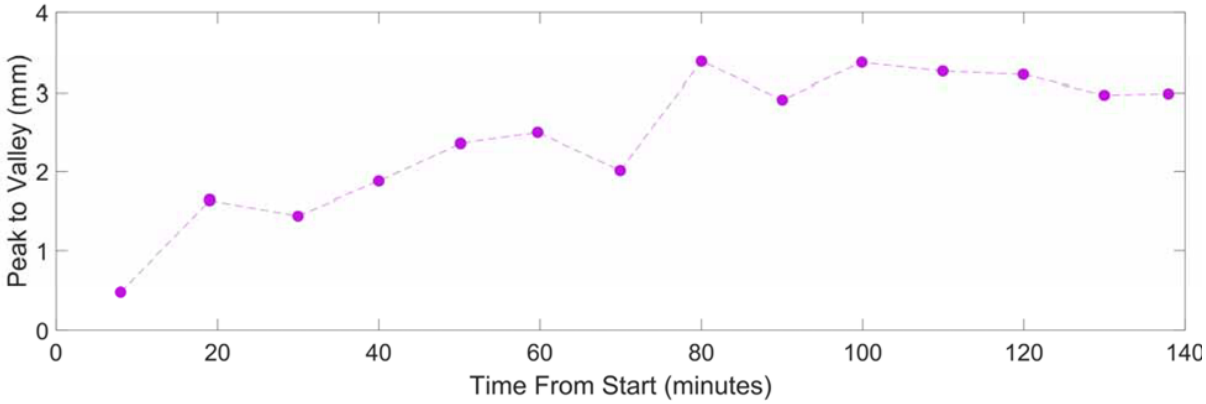

Figure 081821.12: Equivalent Roughness Evolution

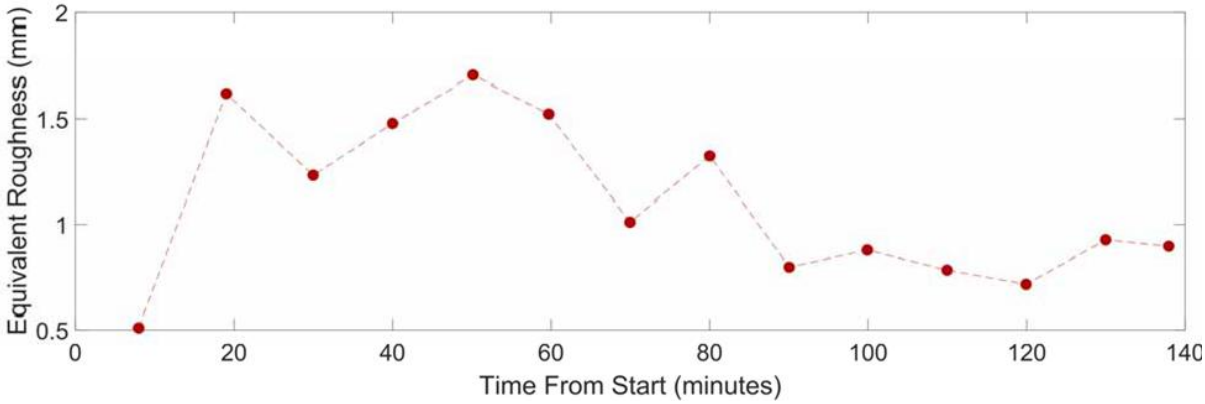

Table 081821.02: Summary of Roughness Parameters

Time (min.)	RMS (mm)	Skewness	Peak to Valley (mm)	ks,Flack-Schultz (mm)
7.9759	0.0462	0.9486	0.4680	0.5100
19.0259	0.2062	0.5203	1.6398	1.6218
29.9759	0.1826	0.3588	1.4422	1.2310
39.9926	0.2478	0.2424	1.8747	1.4781
50.1426	0.3334	0.1109	2.3558	1.7061
59.7093	0.3164	0.0629	2.4945	1.5239
69.9426	0.2965	-0.1739	2.0094	1.0110
80.0093	0.4614	-0.2714	3.3919	1.3245
90.0426	0.3924	-0.4345	2.9120	0.7960
99.8926	0.4570	-0.4565	3.3780	0.8781
109.9593	0.4522	-0.4969	3.2651	0.7817
119.9259	0.4190	-0.5022	3.2223	0.7139
129.9759	0.4157	-0.3943	2.9717	0.9265
137.9259	0.4068	-0.3996	2.9892	0.8959

Figure 081821.13: Frost Topography at 00:07:51

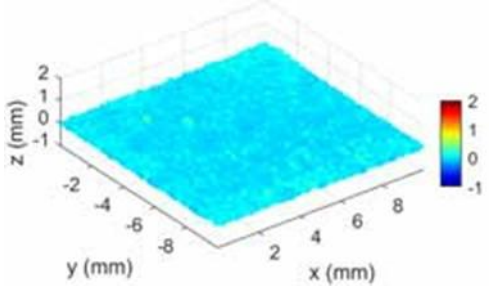

Figure 081821.14: Frost Topography at 00:18:54

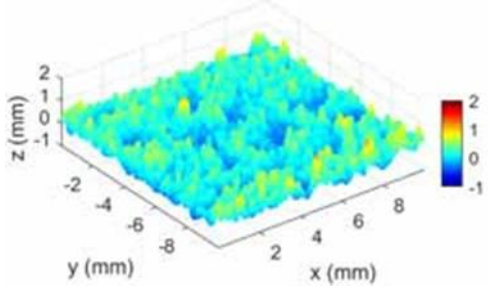

Figure 081821.15: Frost Topography at 00:29:51

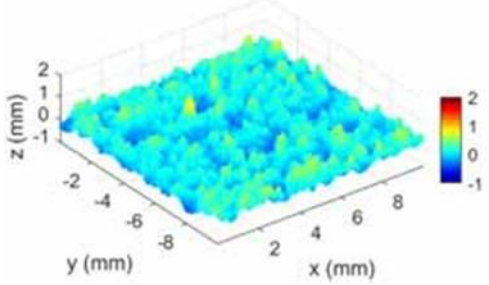

Figure 081821.16: Frost Topography at 00:39:52

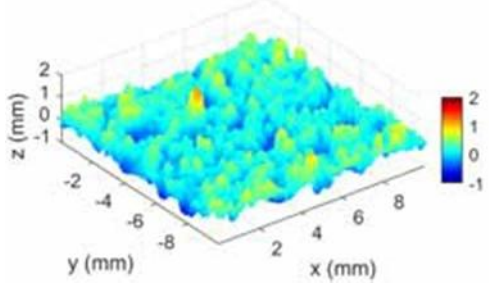

Figure 081821.17: Frost Topography at 00:50:01

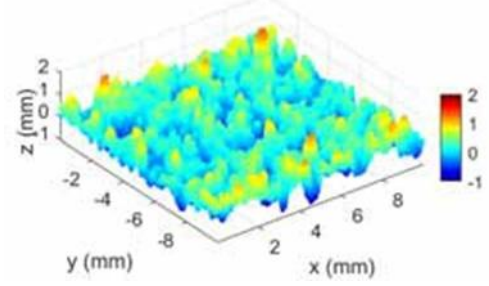

Figure 081821.18: Frost Topography at 00:59:35

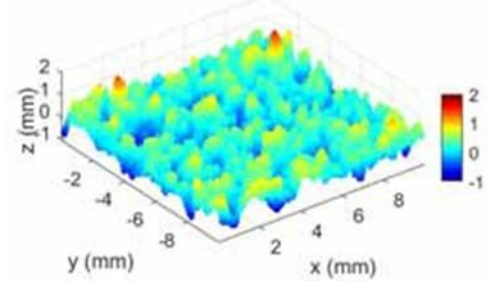

Figure 081821.19: Frost Topography at 01:09:49

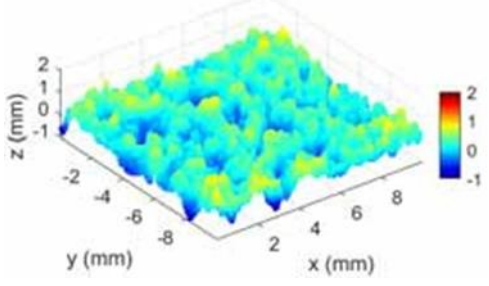

Figure 081821.20: Frost Topography at 01:19:53

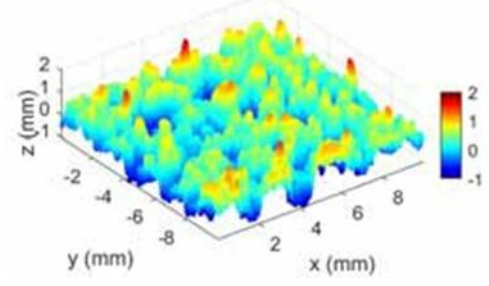

Figure 081821.21: Frost Topography at 01:29:55

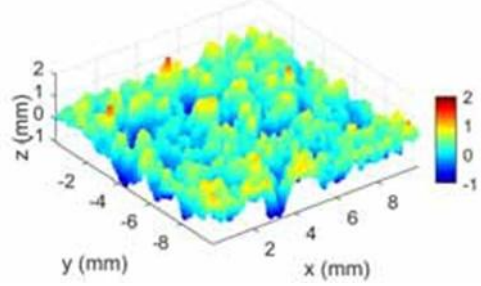

Figure 081821.22: Frost Topography at 01:39:46

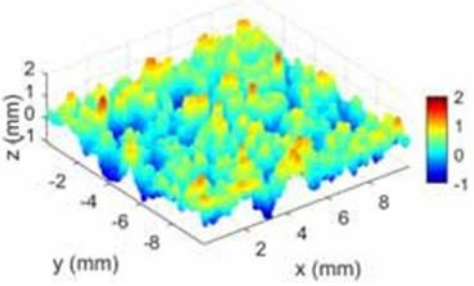

Figure 081821.23: Frost Topography at 01:49:50

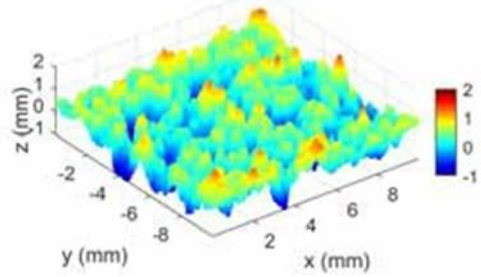

Figure 081821.24: Frost Topography at 01:59:48

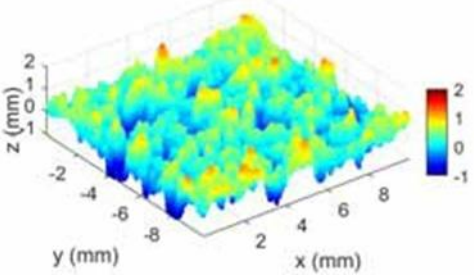

Figure 081821.25: Frost Topography at 02:09:51

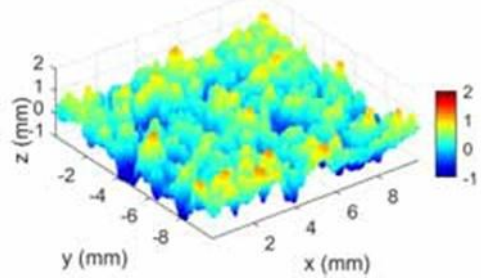

Figure 081821.26: Frost Topography at 02:17:48

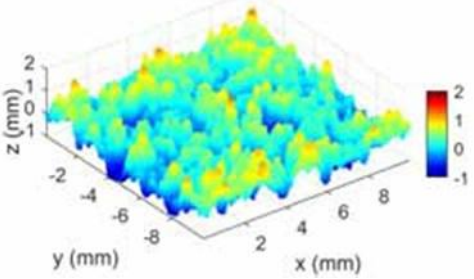

CAFF Conditions Report – Case Date: 082121

Table 082121.01: Summary of Measured Test Variables

Variable	Mean	St. Dev.	Rand. Unc.
T_air (C)	15.1814	0.3200	0.0108
Rh (%)	79.8793	2.5090	0.0847
Omega (kg_v/kg_da)	0.00871894	0.00036752	0.00001241
V_air (m/s)	1.3956	0.0962	0.0032
T_skin (C)	-2.2118	1.8196	0.0614
T_floor (C)	-19.1472	0.2272	0.0077

Figure 082121.01: Temperature and Voltage Control Time History

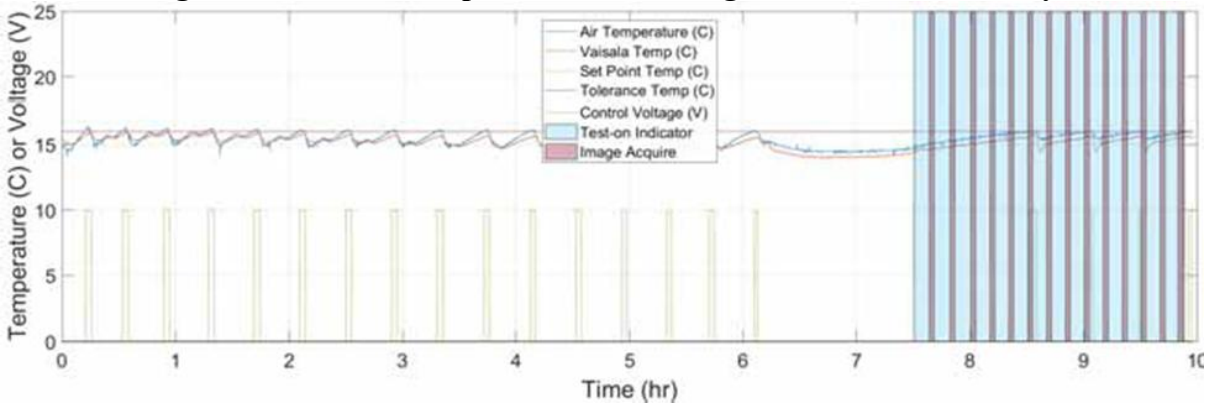

Figure 082121.02: Relative Humidity Time History

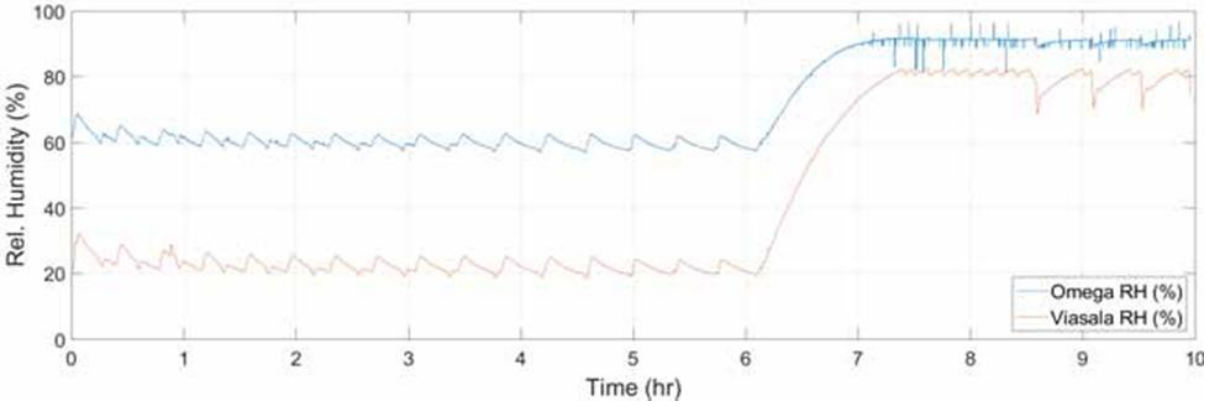

Figure 082121.03: Velocity Time History

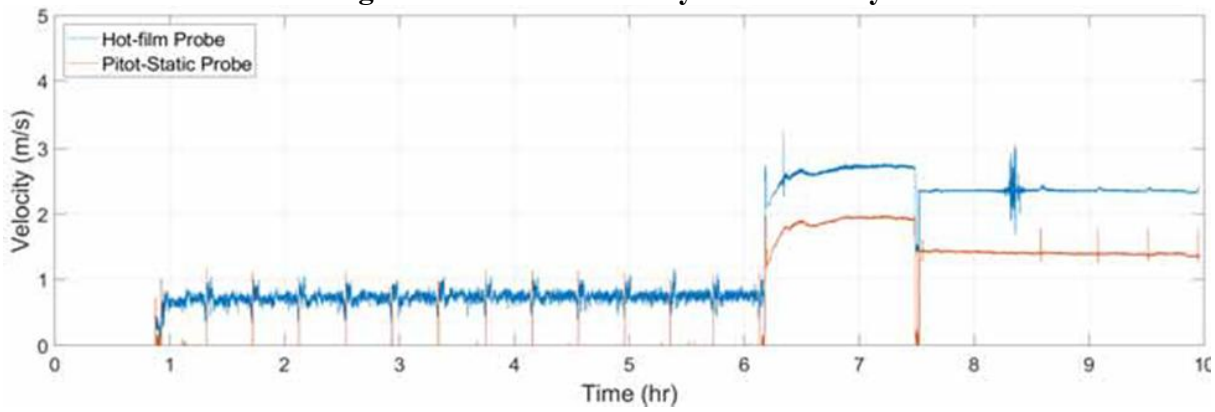

Figure 082121.04: Coolant Return Temperature Time History

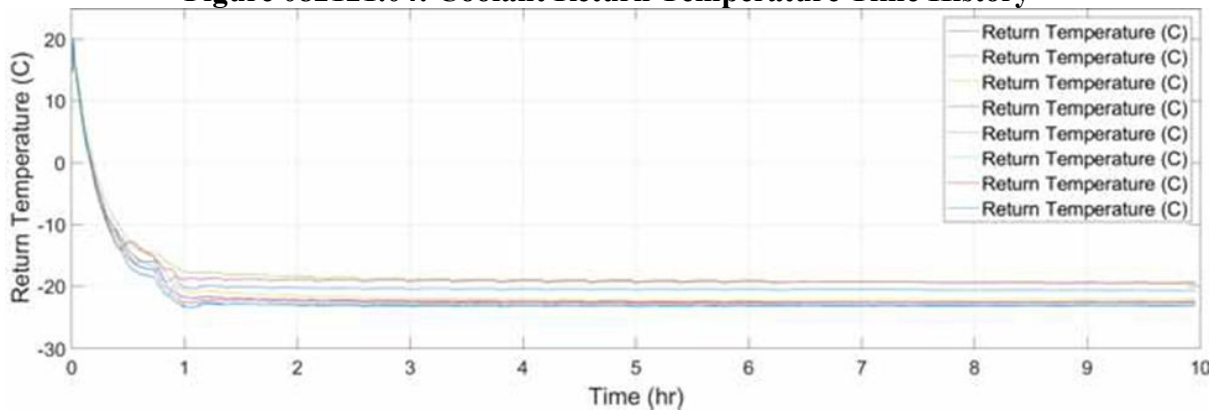

Figure 082121.05: Coolant Supply Temperature Time History

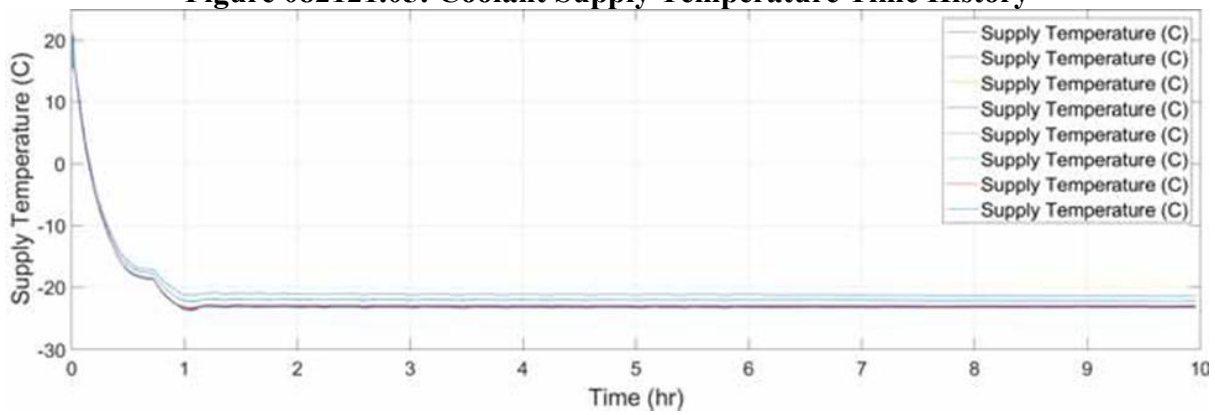

Figure 082121.06: Skin Temperature Time History

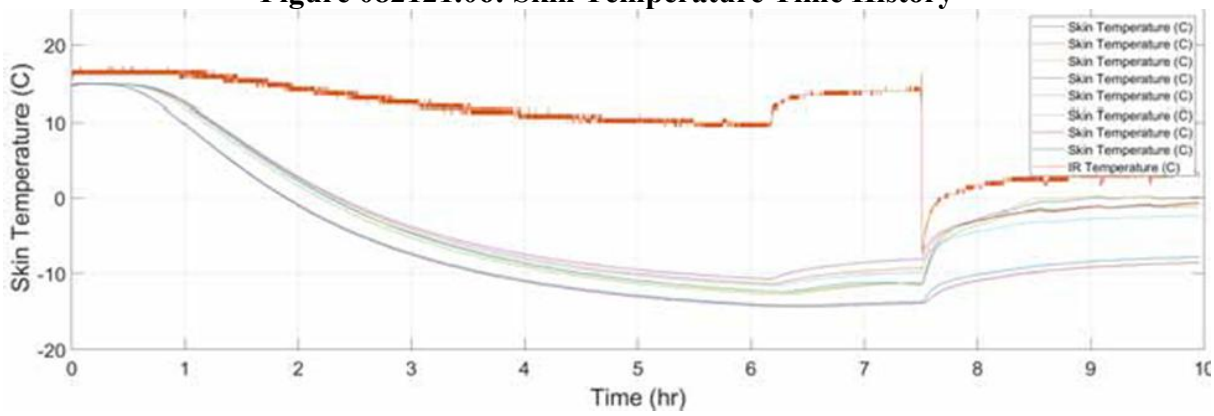

Figure 082121.07: Floor Temperature Time History

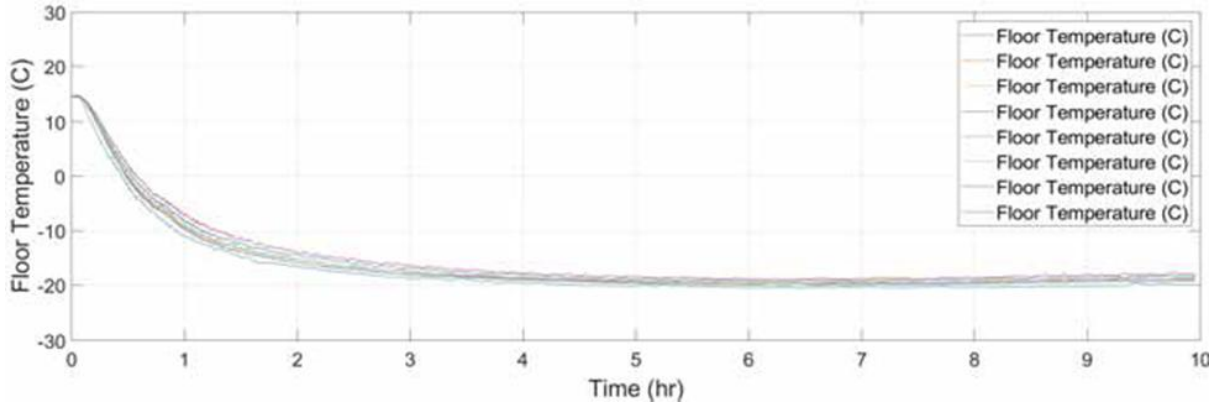

Figure 082121.08: Skin Temperature Slope Time History

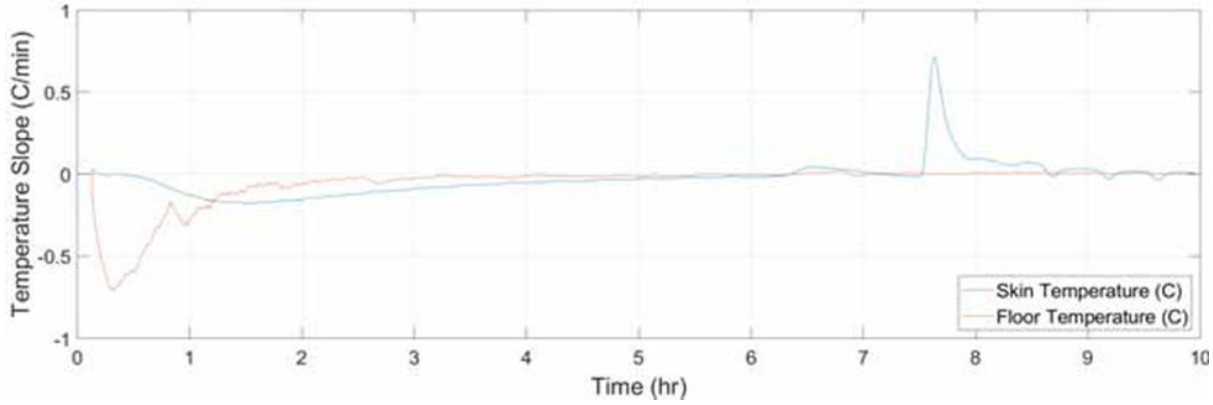

Figure 082121.09: RMS Height Evolution

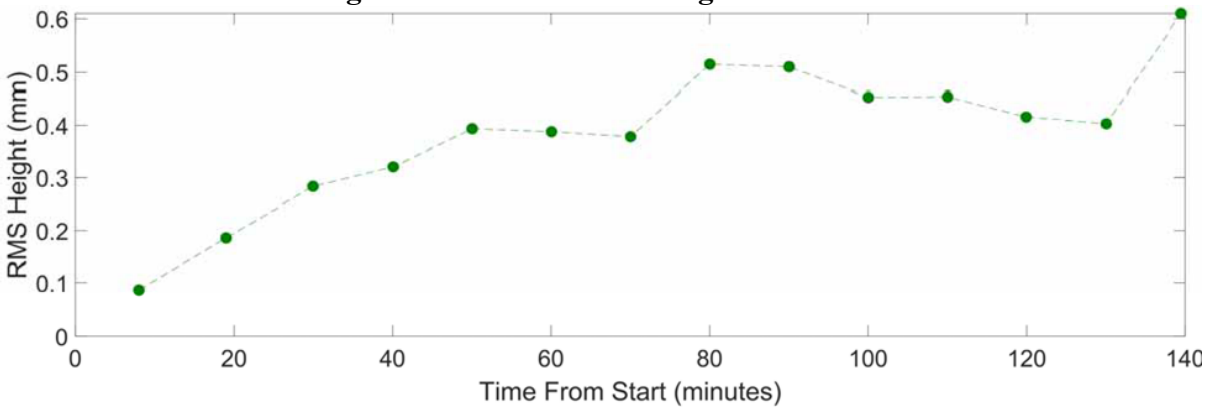

Figure 082121.10: Skewness Evolution

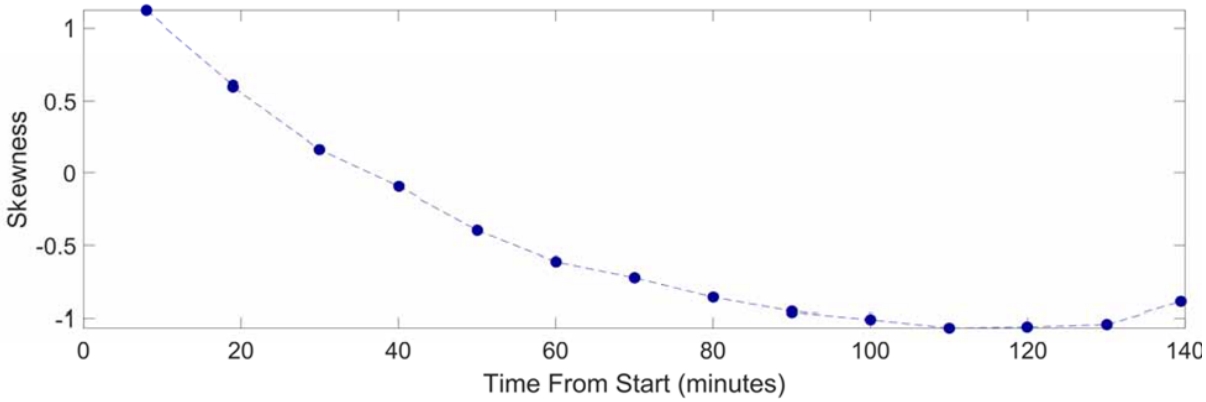

Figure 082121.11: Peak to Valley Evolution

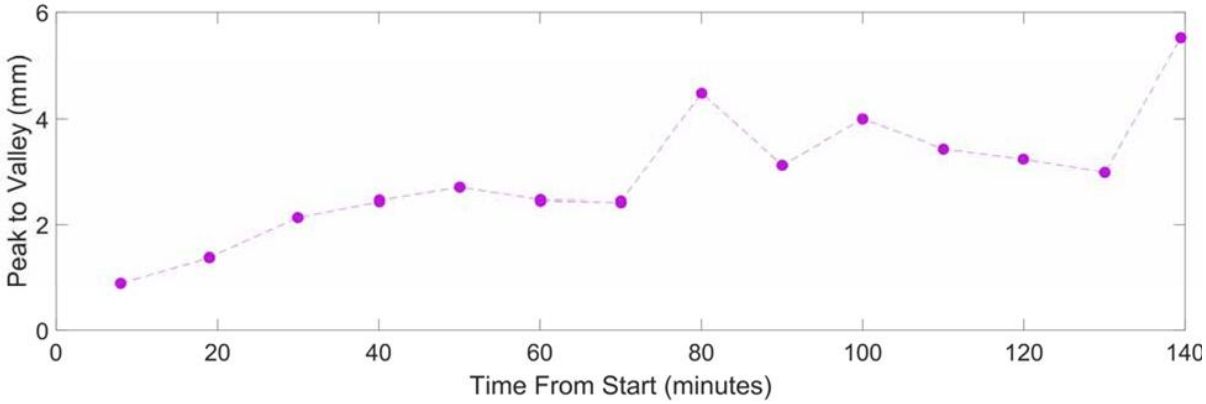

Figure 082121.12: Equivalent Roughness Evolution

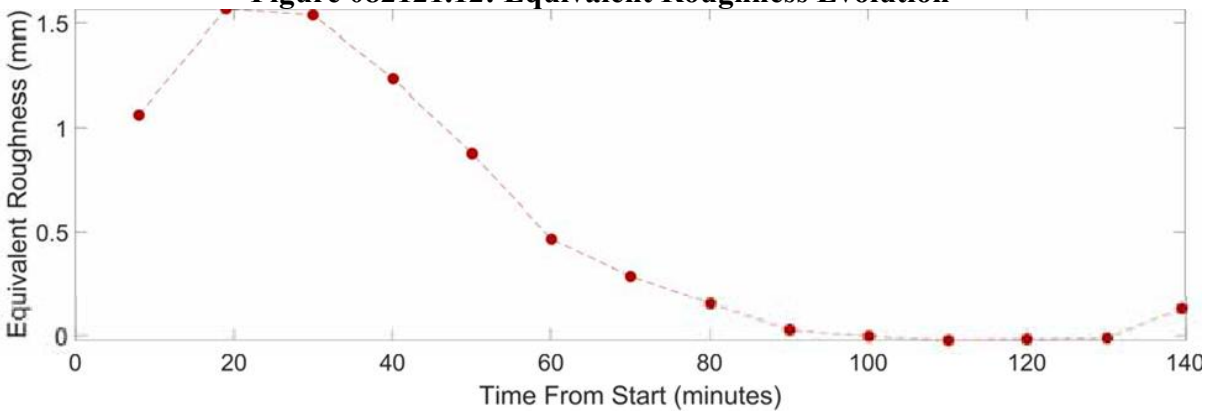

Table 082121.02: Summary of Roughness Parameters

Time (min.)	RMS (mm)	Skewness	Peak to Valley (mm)	ks,Flack-Schultz (mm)
7.9964	0.0861	1.1148	0.8730	1.0636
18.9964	0.1862	0.5985	1.3681	1.5687
29.9631	0.2830	0.1614	2.1363	1.5392
40.0797	0.3205	-0.0972	2.4416	1.2343
50.0464	0.3934	-0.3947	2.6913	0.8760
60.0464	0.3876	-0.6147	2.4540	0.4648
70.0297	0.3780	-0.7257	2.4229	0.2846
80.0297	0.5156	-0.8613	4.5004	0.1526
90.0297	0.5105	-0.9592	3.1153	0.0282
100.0131	0.4534	-1.0103	4.0020	-0.0015
110.0297	0.4546	-1.0688	3.4279	-0.0204
119.9297	0.4157	-1.0607	3.2341	-0.0157
130.0464	0.4029	-1.0435	2.9774	-0.0097
139.4631	0.6100	-0.8916	5.5415	0.1288

Figure 082121.13: Frost Topography at 00:07:59

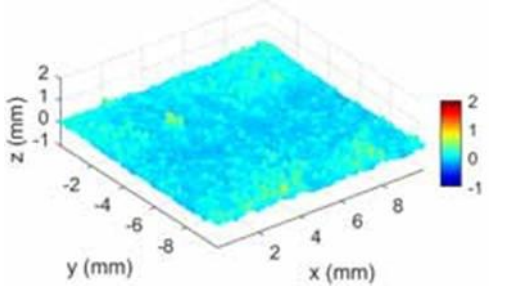

Figure 082121.14: Frost Topography at 00:18:59

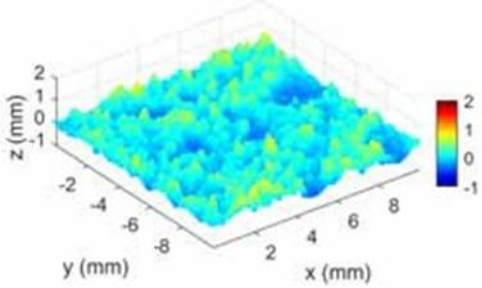

Figure 082121.15: Frost Topography at 00:29:57

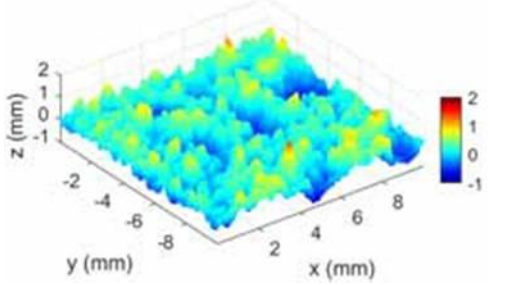

Figure 082121.16: Frost Topography at 00:40:04

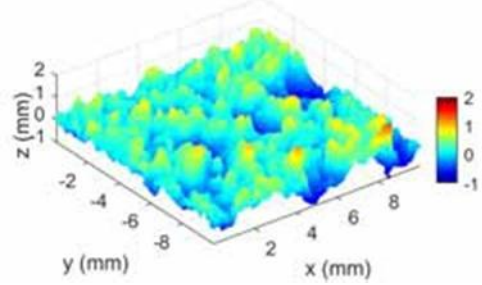

Figure 082121.17: Frost Topography at 00:50:02

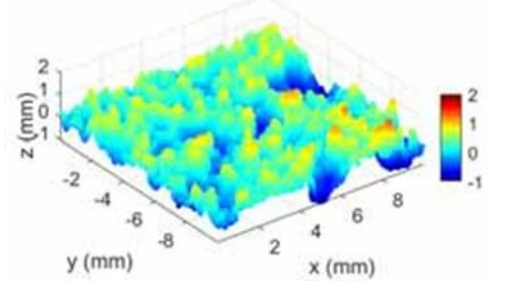

Figure 082121.18: Frost Topography at 01:00:02

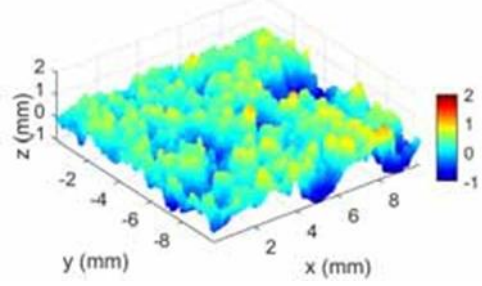

Figure 082121.19: Frost Topography at 01:10:01

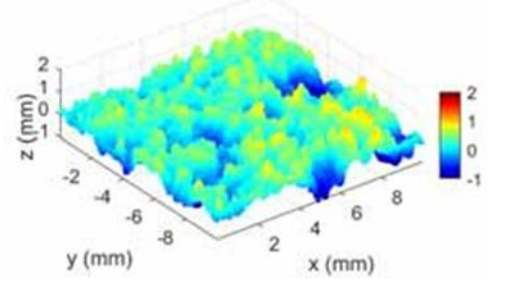

Figure 082121.20: Frost Topography at 01:20:01

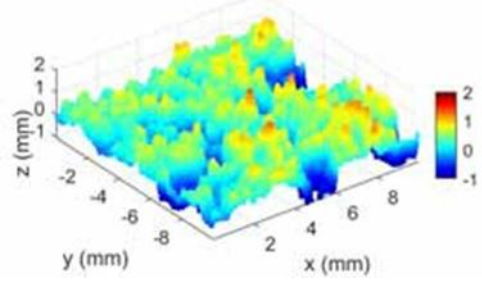

Figure 082121.21: Frost Topography at 01:30:01

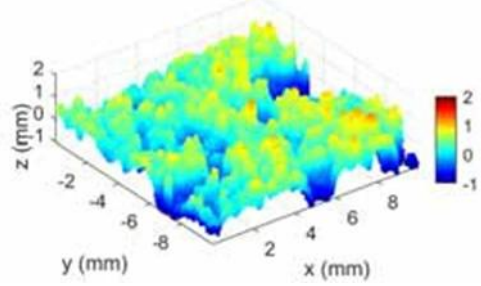

Figure 082121.22: Frost Topography at 01:40:00

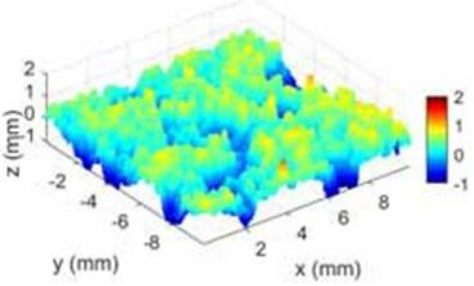

Figure 082121.23: Frost Topography at 01:50:01

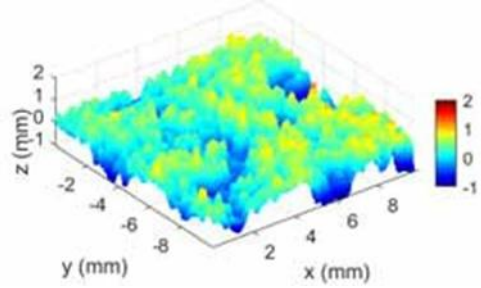

Figure 082121.24: Frost Topography at 01:59:55

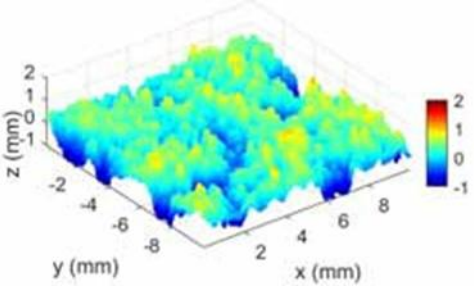

Figure 082121.25: Frost Topography at 02:10:02

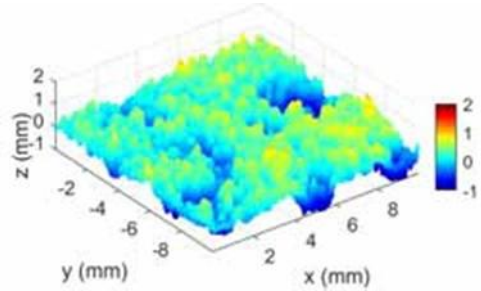

Figure 082121.26: Frost Topography at 02:19:27

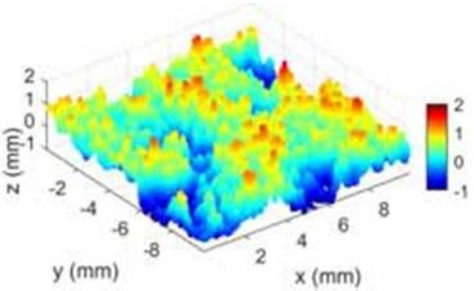

CAFF Conditions Report – Case Date: 090421

Table 090421.01: Summary of Measured Test Variables

Variable	Mean	St. Dev.	Rand. Unc.
T_air (C)	4.2703	0.2661	0.0090
Rh (%)	79.4658	4.8974	0.1656
Omega (kg_v/kg_da)	0.00414230	0.00031784	0.00001075
V_air (m/s)	1.4416	0.0852	0.0029
T_skin (C)	-8.4931	1.0511	0.0355
T_floor (C)	-20.4203	0.0583	0.0020

Figure 090421.01: Temperature and Voltage Control Time History

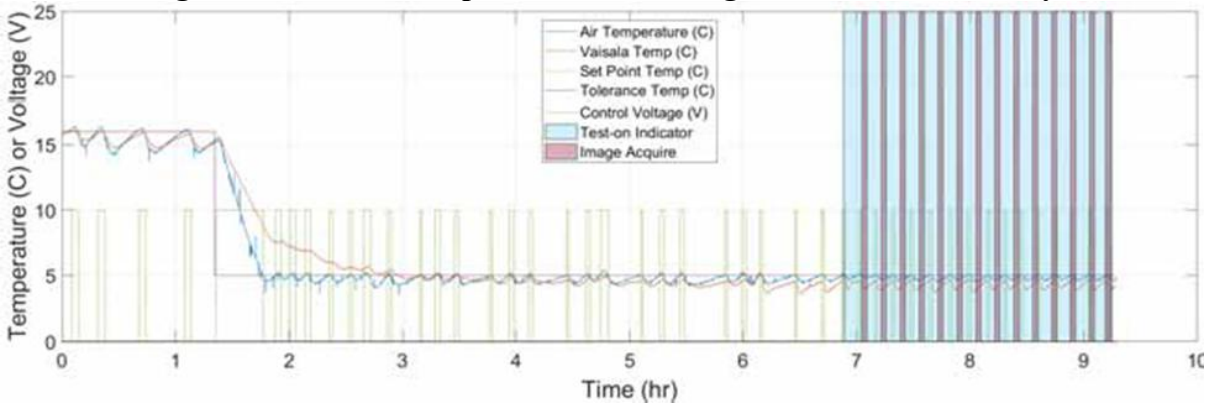

Figure 090421.02: Relative Humidity Time History

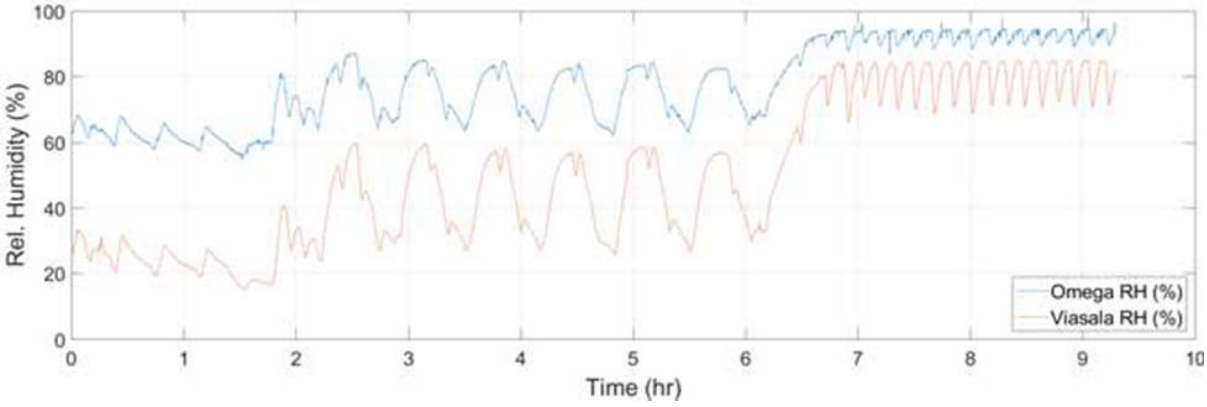

Figure 090421.03: Velocity Time History

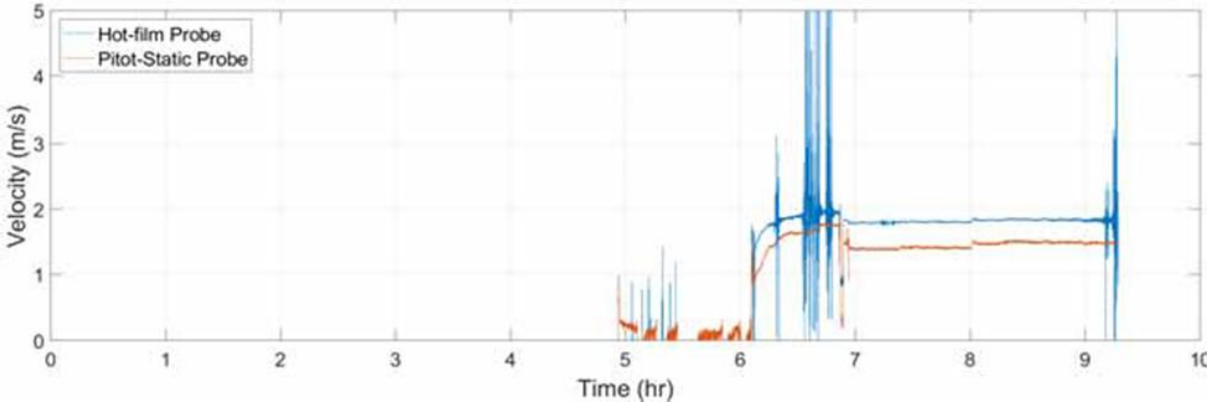

Figure 090421.04: Coolant Return Temperature Time History

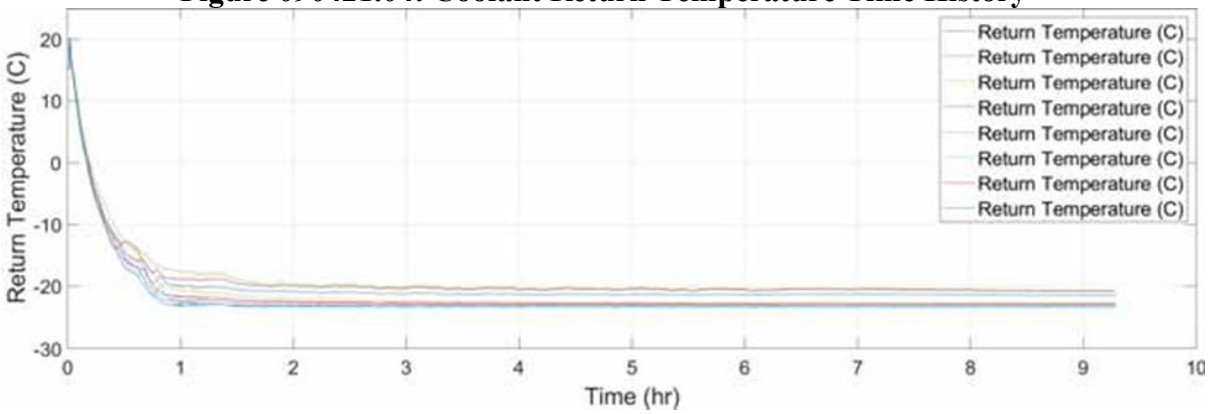

Figure 090421.05: Coolant Supply Temperature Time History

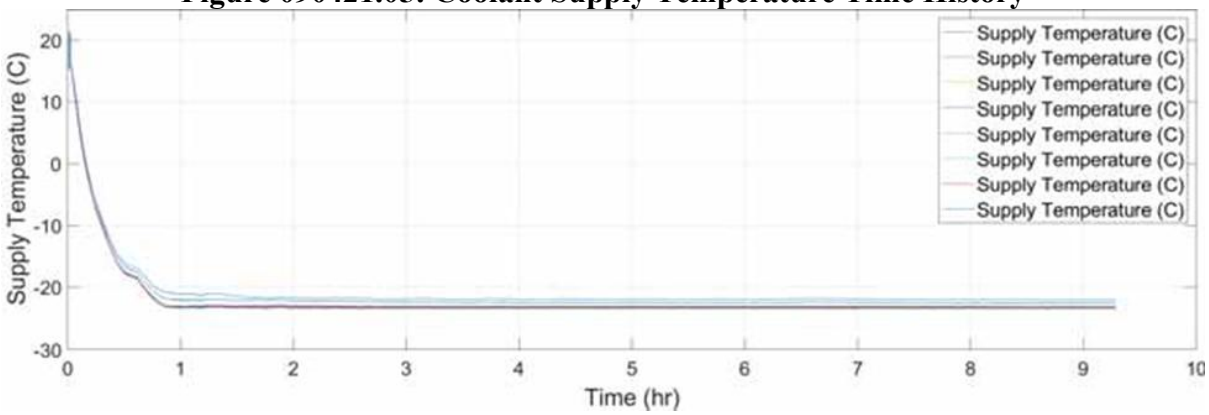

Figure 090421.06: Skin Temperature Time History

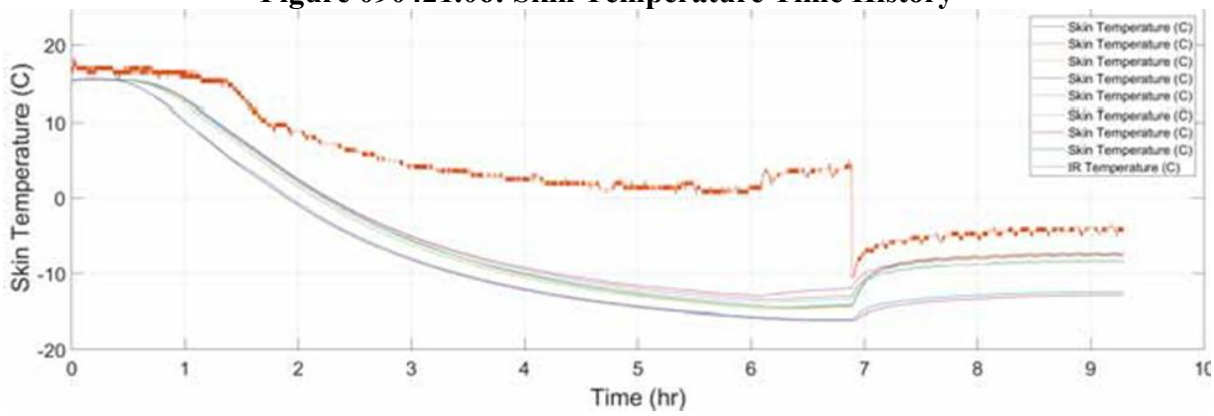

Figure 090421.07: Floor Temperature Time History

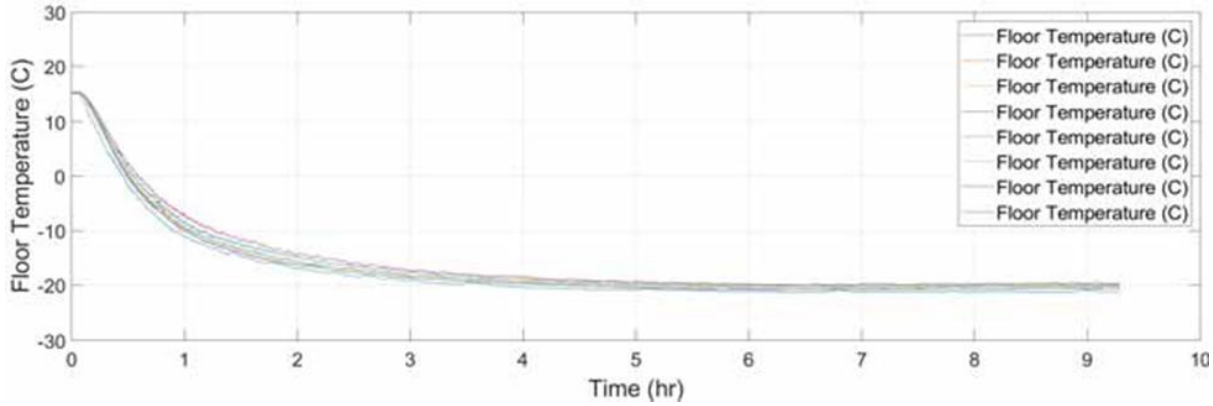

Figure 090421.08: Skin Temperature Slope Time History

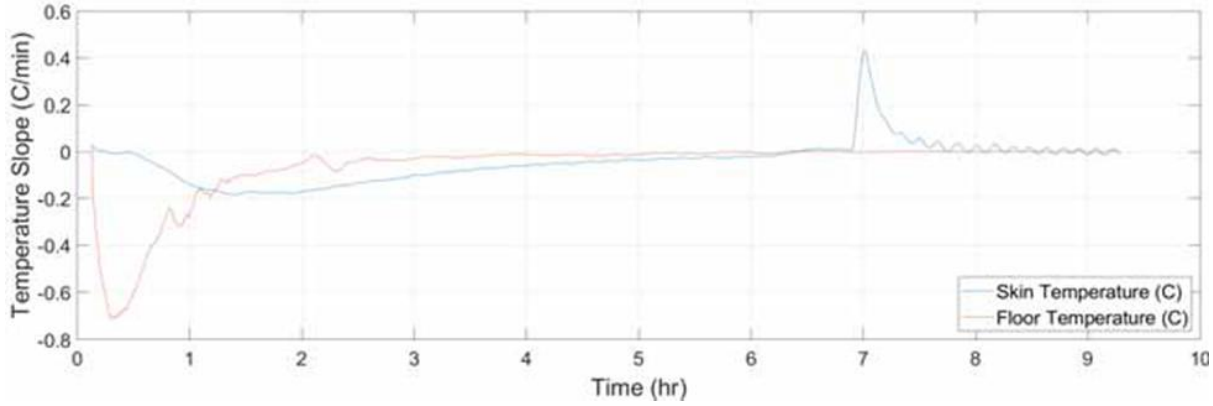

Figure 090421.09: RMS Height Evolution

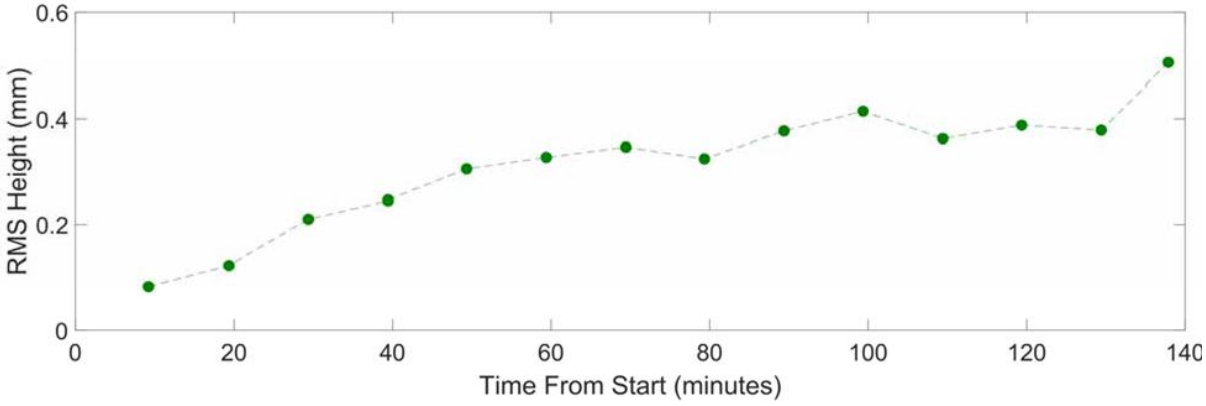

Figure 090421.10: Skewness Evolution

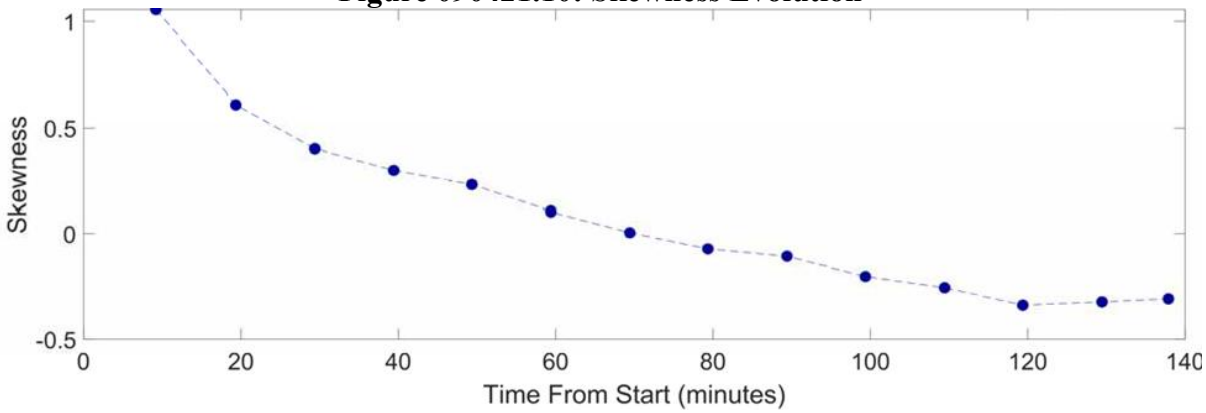

Figure 090421.11: Peak to Valley Evolution

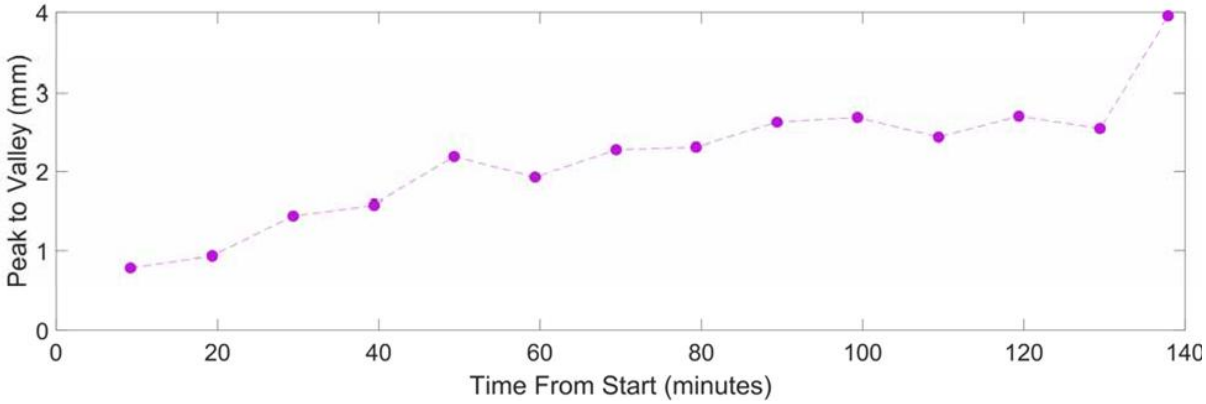

Figure 090421.12: Equivalent Roughness Evolution

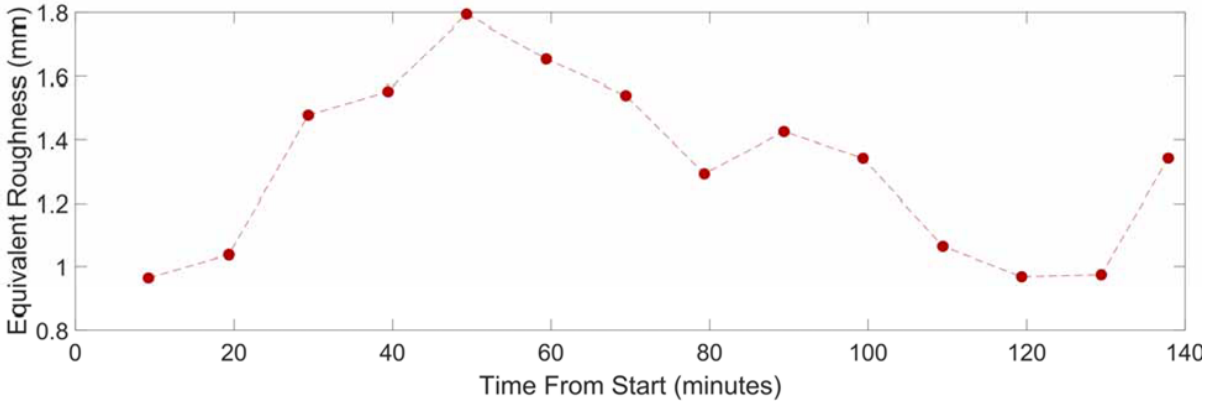

Table 090421.02: Summary of Roughness Parameters

Time (min.)	RMS (mm)	Skewness	Peak to Valley (mm)	ks,Flack-Schultz (mm)
9.1909	0.0809	1.0579	0.7819	0.9630
19.3409	0.1217	0.6121	0.9329	1.0373
29.3742	0.2103	0.4014	1.4426	1.4790
39.4242	0.2455	0.2979	1.5804	1.5543
49.3409	0.3047	0.2308	2.1896	1.7941
59.3909	0.3265	0.1036	1.9243	1.6553
69.4242	0.3462	0.0037	2.2774	1.5415
79.3409	0.3238	-0.0735	2.3085	1.2918
89.3909	0.3771	-0.1089	2.6268	1.4265
99.3575	0.4150	-0.2054	2.6863	1.3418
109.4242	0.3624	-0.2596	2.4345	1.0635
119.3742	0.3883	-0.3432	2.7024	0.9670
129.4242	0.3786	-0.3278	2.5442	0.9733
137.8742	0.5066	-0.3128	3.9541	1.3424

Figure 090421.13: Frost Topography at 00:09:40

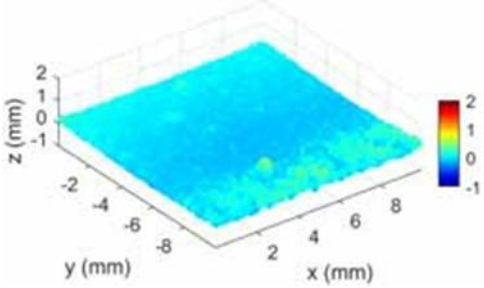

Figure 090421.14: Frost Topography at 00:19:49

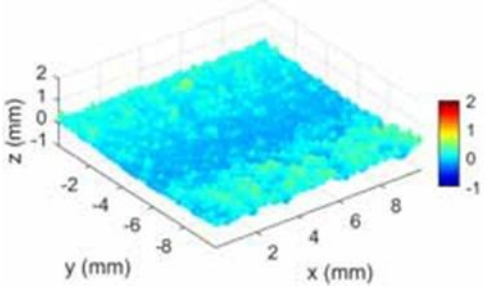

Figure 090421.15: Frost Topography at 00:29:51

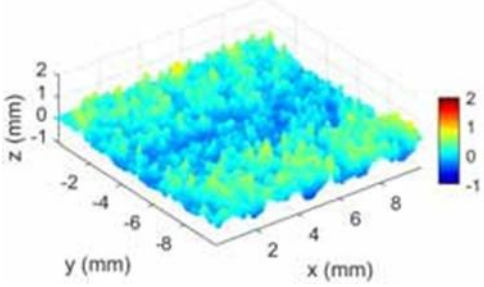

Figure 090421.16: Frost Topography at 00:39:54

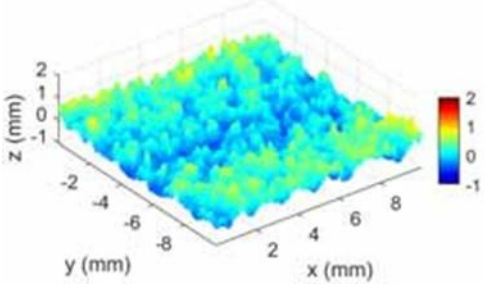

Figure 090421.17: Frost Topography at 00:49:49

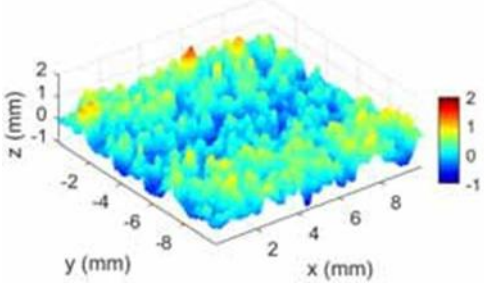

Figure 090421.18: Frost Topography at 00:59:52

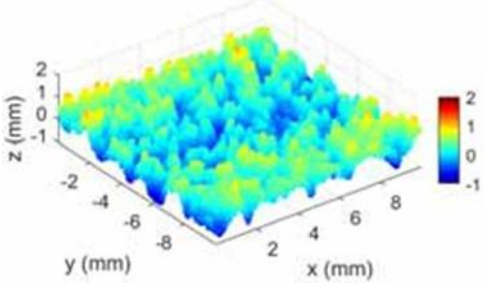

Figure 090421.19: Frost Topography at 01:09:54

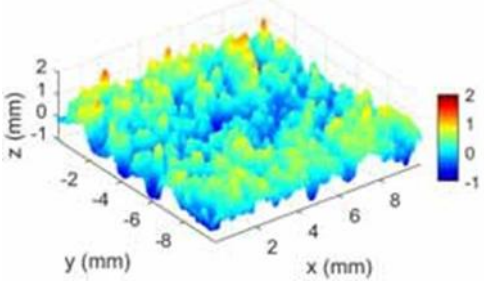

Figure 090421.20: Frost Topography at 01:19:49

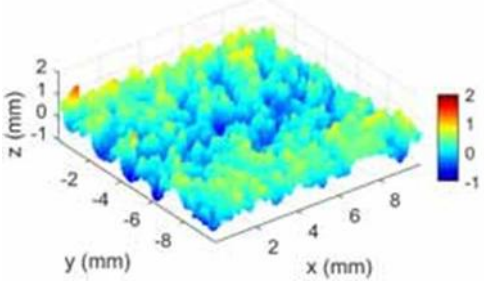

Figure 090421.21: Frost Topography at 01:29:52

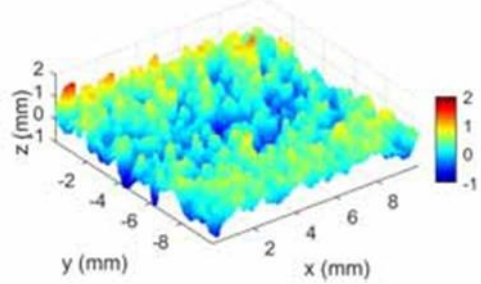

Figure 090421.22: Frost Topography at 01:39:50

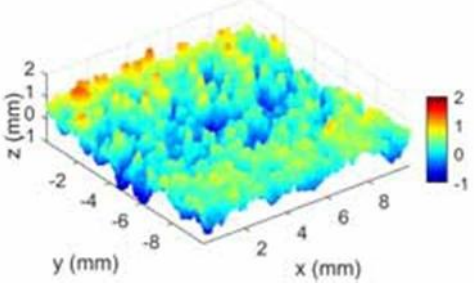

Figure 090421.23: Frost Topography at 01:49:54

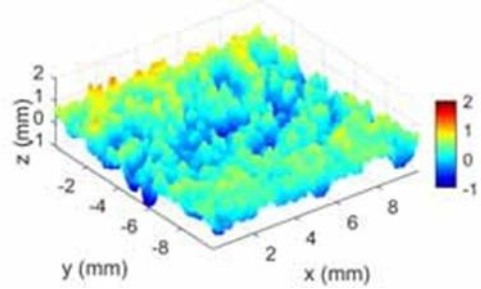

Figure 090421.24: Frost Topography at 01:59:51

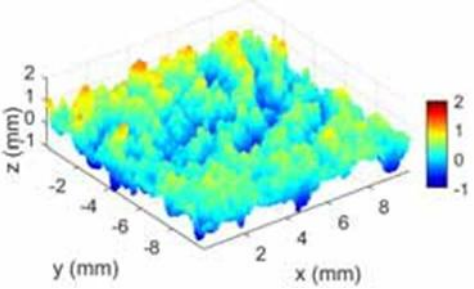

Figure 090421.25: Frost Topography at 02:09:54

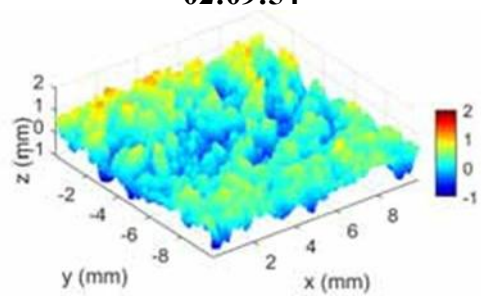

Figure 090421.26: Frost Topography at 02:18:21

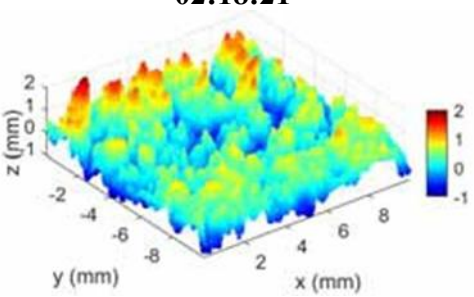

CAFF Conditions Report – Case Date: 090721

Table 090721.01: Summary of Measured Test Variables

Variable	Mean	St. Dev.	Rand. Unc.
T_air (C)	9.1527	0.3417	0.0123
Rh (%)	79.3799	4.6005	0.1653
Omega (kg_v/kg_da)	0.00580779	0.00042893	0.00001541
V_air (m/s)	1.4343	0.0858	0.0031
T_skin (C)	-5.8362	1.2613	0.0453
T_floor (C)	-19.8396	0.0992	0.0036

Figure 090721.01: Temperature and Voltage Control Time History

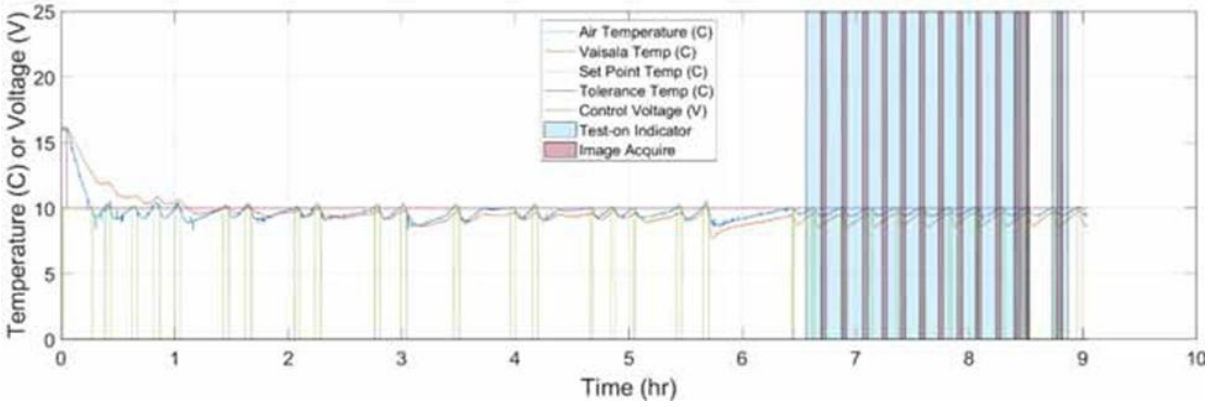

Figure 090721.02: Relative Humidity Time History

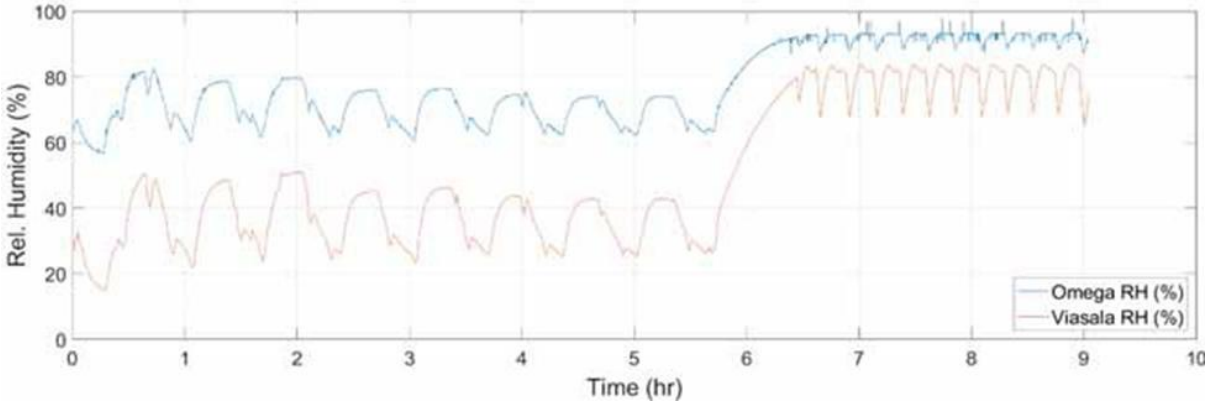

Figure 090721.03: Velocity Time History

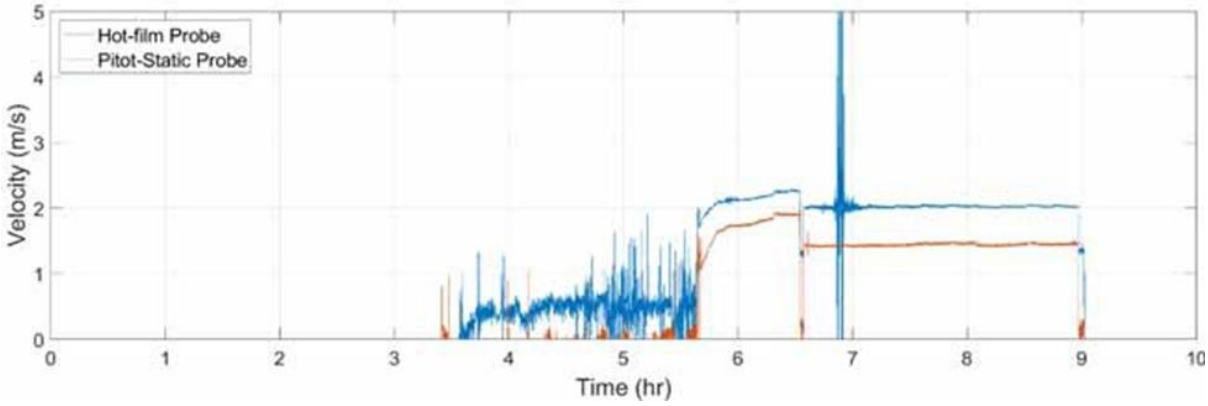

Figure 090721.04: Coolant Return Temperature Time History

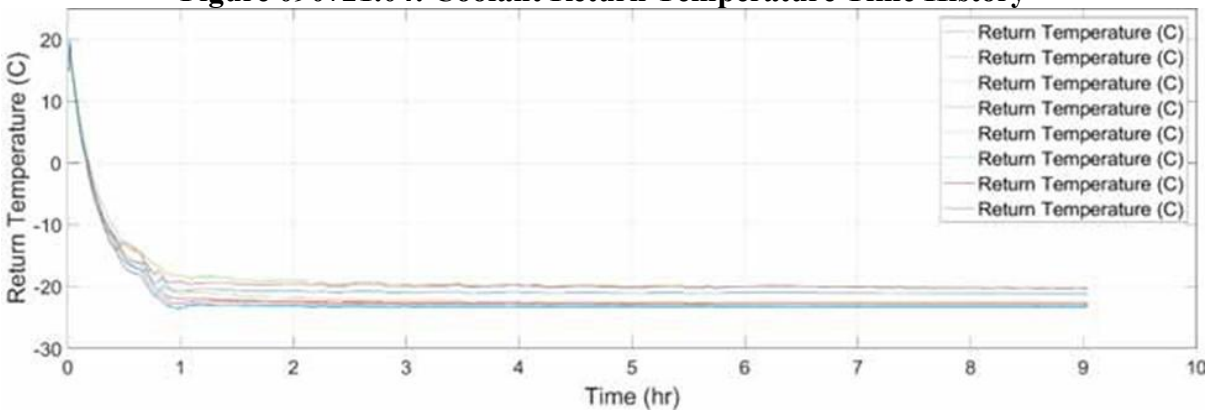

Figure 090721.05: Coolant Supply Temperature Time History

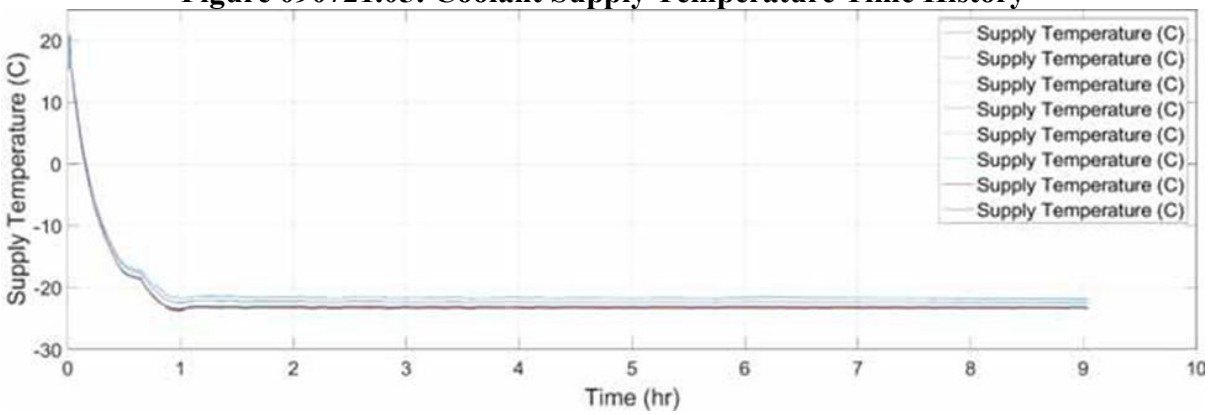

Figure 090721.06: Skin Temperature Time History

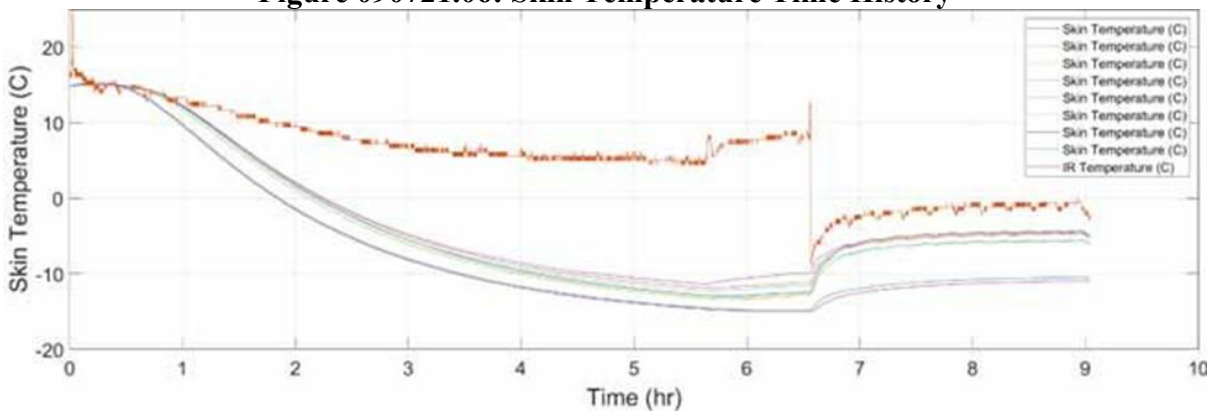

Figure 090721.07: Floor Temperature Time History

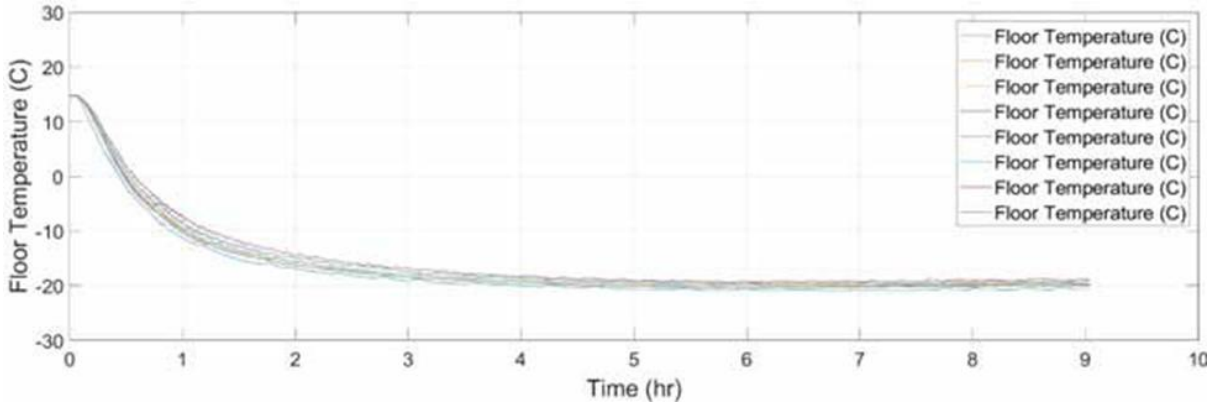

Figure 090721.08: Skin Temperature Slope Time History

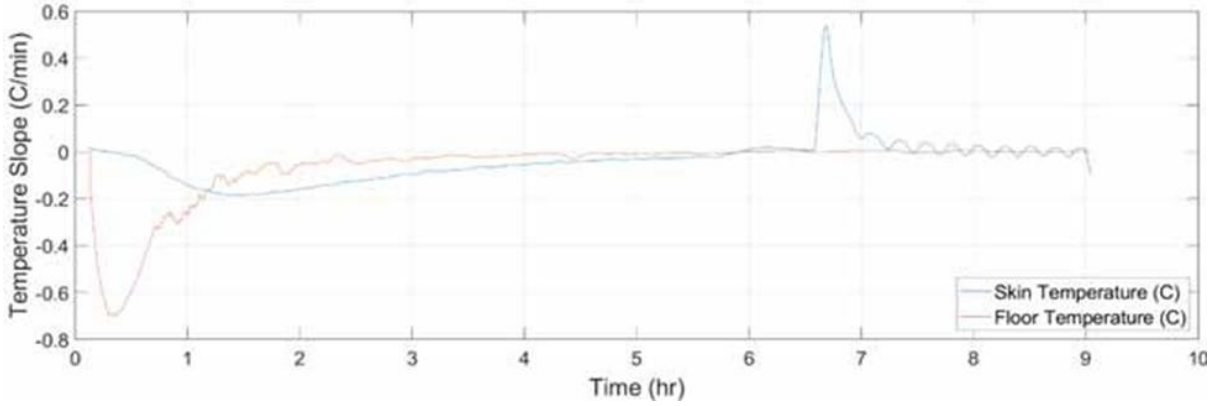

Figure 090721.09: RMS Height Evolution

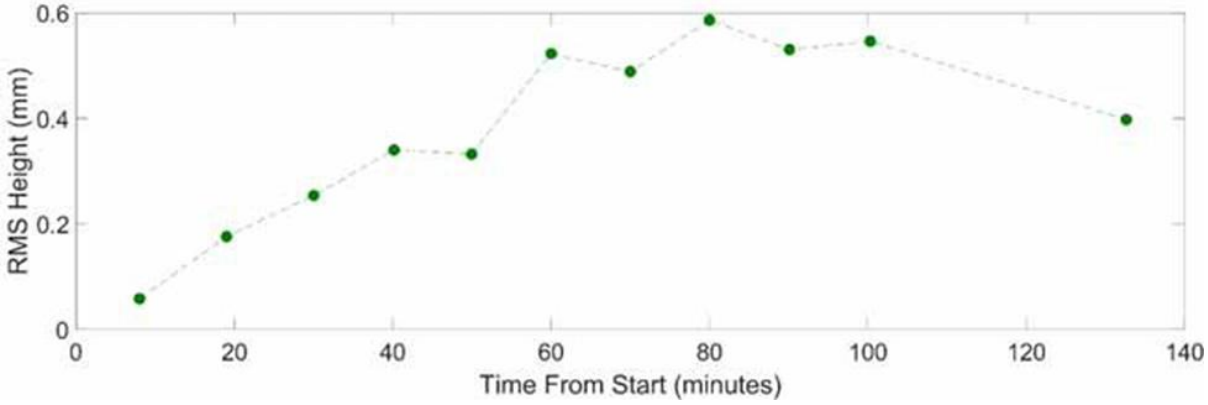

Figure 090721.10: Skewness Evolution

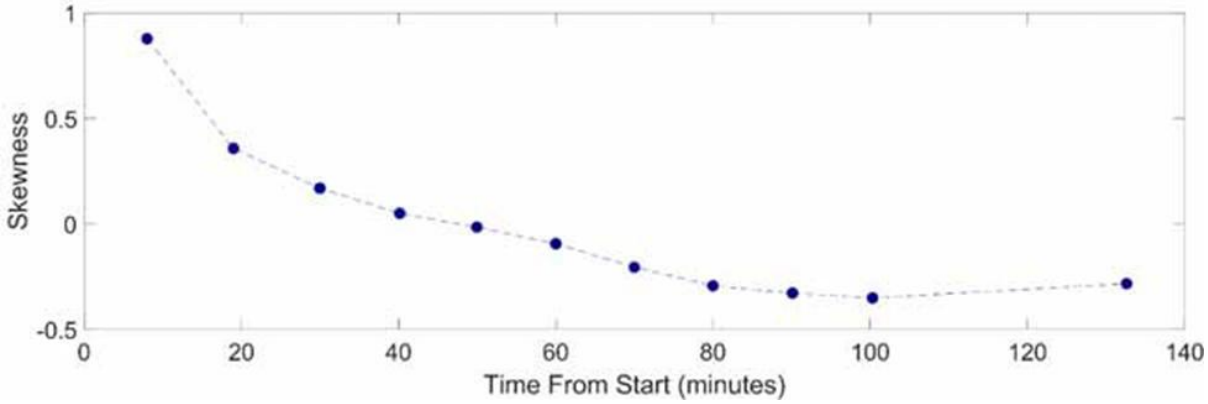

Figure 090721.11: Peak to Valley Evolution

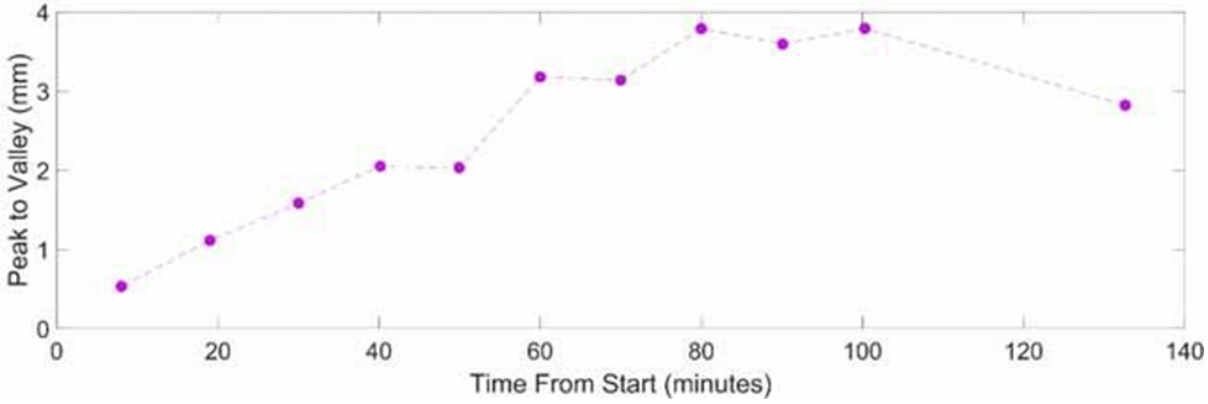

Figure 090721.12: Equivalent Roughness Evolution

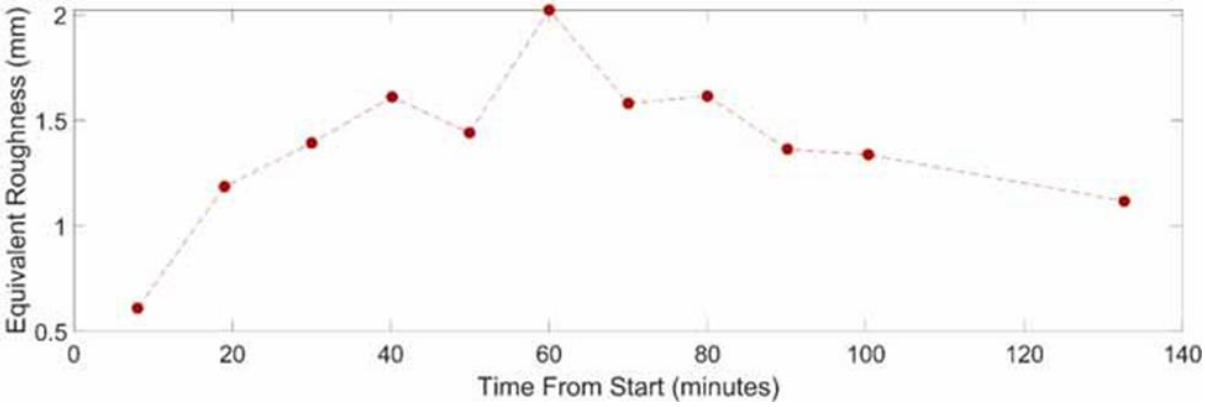

Table 090721.02: Summary of Roughness Parameters

Time (min.)	RMS (mm)	Skewness	Peak to Valley (mm)	ks,Flack-Schultz (mm)
7.9977	0.0581	0.8779	0.5306	0.6099
18.9811	0.1760	0.3578	1.1106	1.1857
29.9811	0.2538	0.1693	1.5830	1.3931
40.1477	0.3403	0.0497	2.0490	1.6110
49.9311	0.3323	-0.0153	2.0311	1.4412
59.9977	0.5227	-0.0940	3.1780	2.0226
69.9811	0.4888	-0.2052	3.1373	1.5809
79.9811	0.5863	-0.2931	3.7884	1.6149
90.0811	0.5307	-0.3280	3.5935	1.3638
100.2811	0.5461	-0.3511	3.7913	1.3378
132.6144	0.3978	-0.2832	2.8210	1.1168

Figure 090721.13: Frost Topography at 00:07:52

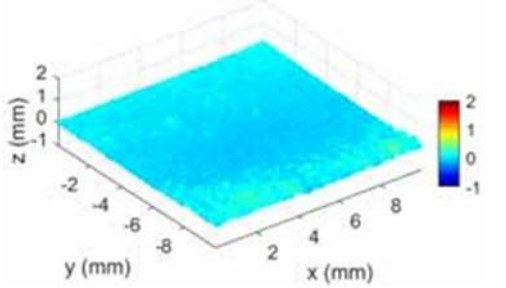

Figure 090721.14: Frost Topography at 00:18:51

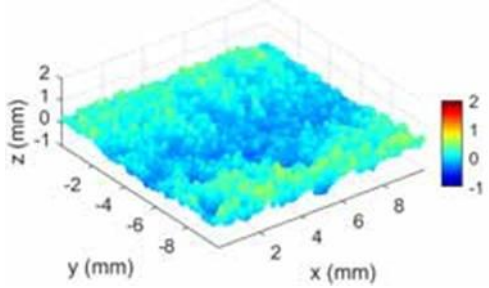

Figure 090721.15: Frost Topography at 00:29:51

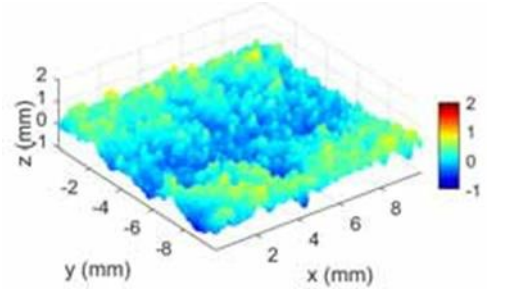

Figure 090721.16: Frost Topography at 00:40:01

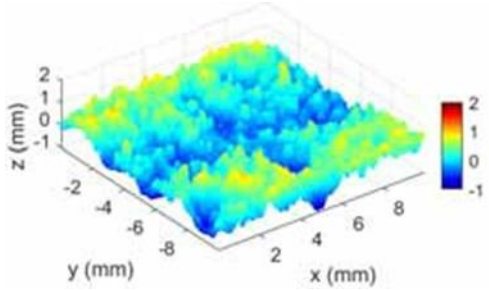

Figure 090721.17: Frost Topography at 00:49:48

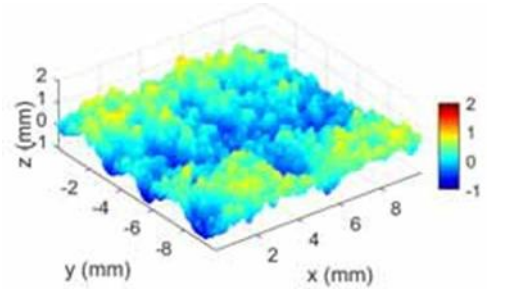

Figure 090721.18: Frost Topography at 00:59:52

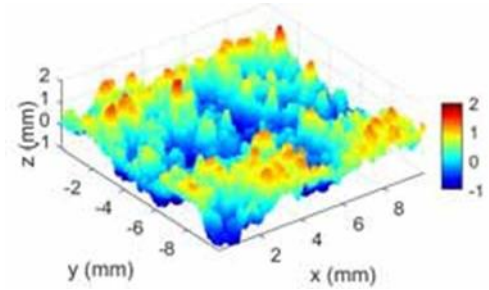

Figure 090721.19: Frost Topography at 01:09:51

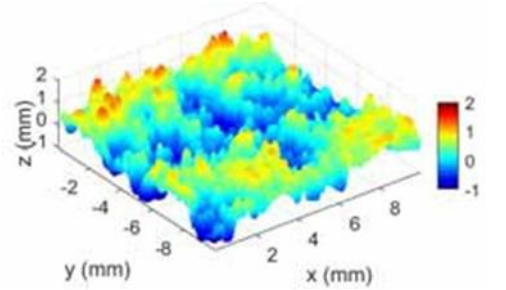

Figure 090721.20: Frost Topography at 01:19:51

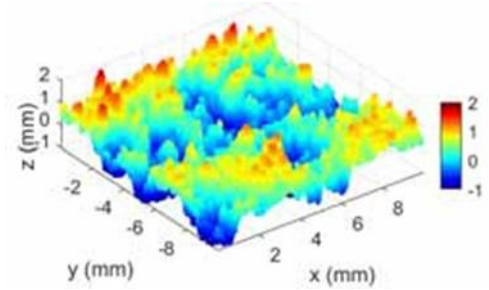

Figure 090721.21: Frost Topography at 01:29:57

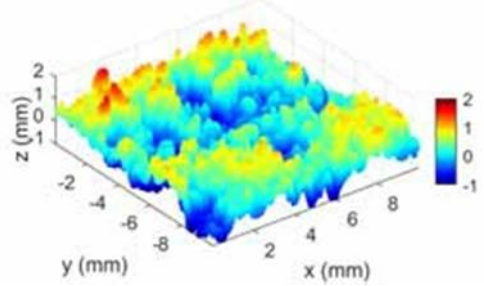

Figure 090721.22: Frost Topography at 01:40:09

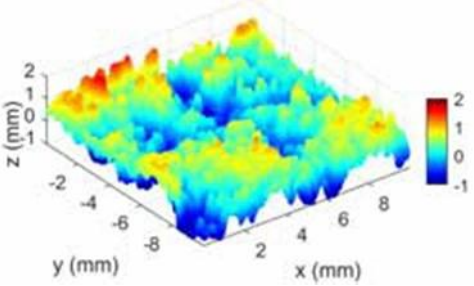

Figure 090721.23: Frost Topography at 02:12:29

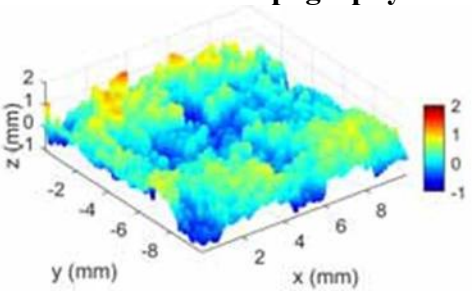

CAFF Conditions Report – Case Date: 091021

Table 091021.01: Summary of Measured Test Variables

Variable	Mean	St. Dev.	Rand. Unc.
T_air (C)	15.1844	0.3247	0.0112
Rh (%)	79.7324	2.7769	0.0955
Omega (kg_v/kg_da)	0.00866135	0.00041769	0.00001436
V_air (m/s)	1.3740	0.1130	0.0039
T_skin (C)	-2.0886	1.8037	0.0620
T_floor (C)	-19.1056	0.2151	0.0074

Figure 091021.01: Temperature and Voltage Control Time History

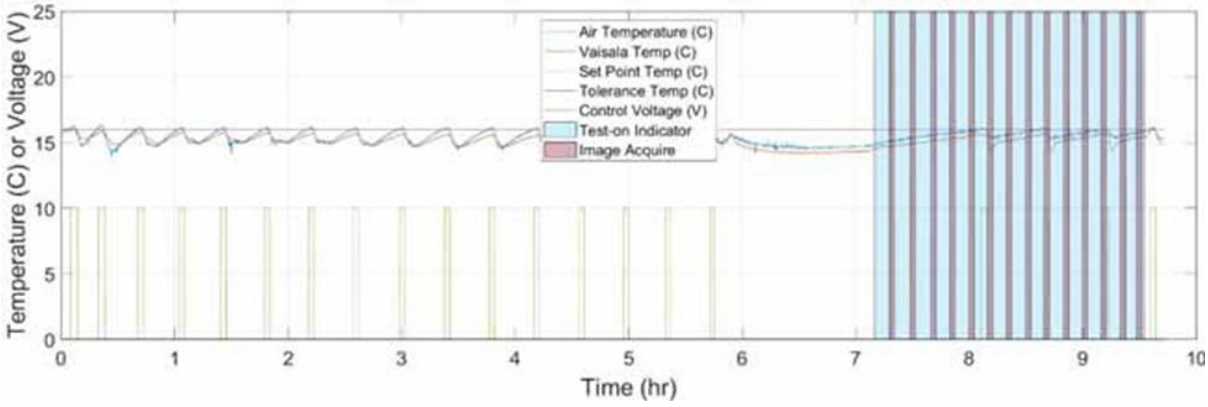

Figure 091021.02: Relative Humidity Time History

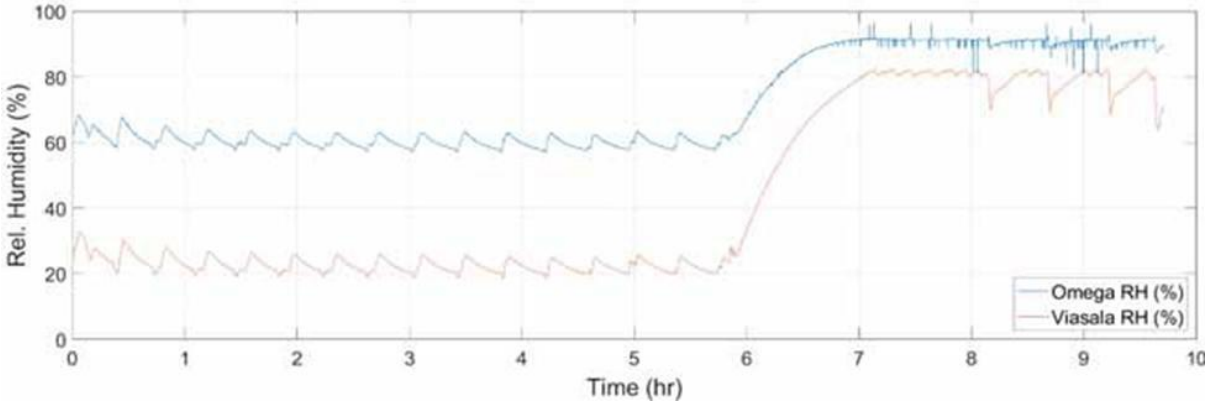

Figure 091021.03: Velocity Time History

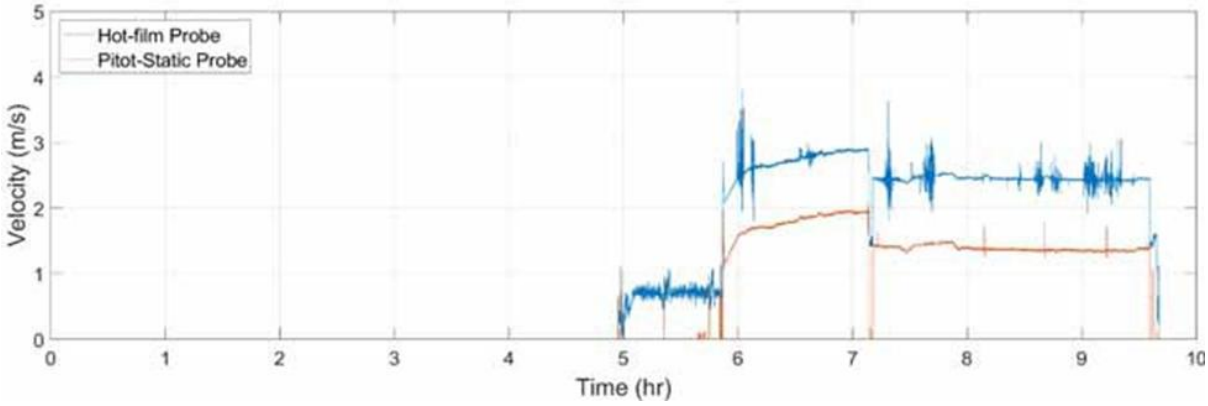

Figure 091021.04: Coolant Return Temperature Time History

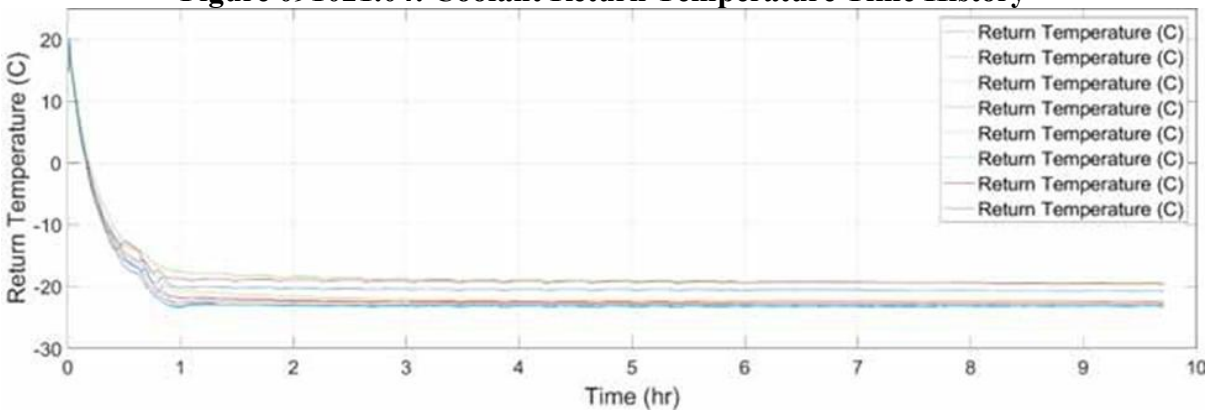

Figure 091021.05: Coolant Supply Temperature Time History

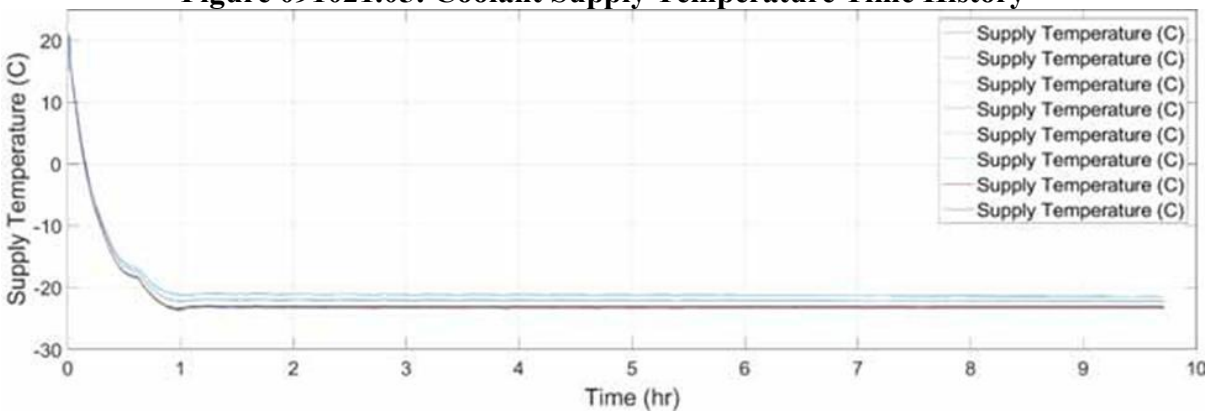

Figure 091021.06: Skin Temperature Time History

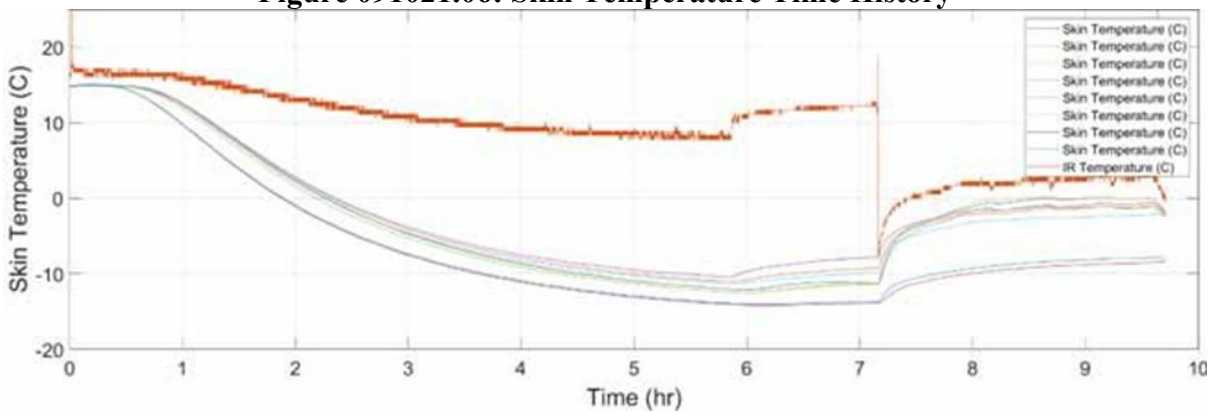

Figure 091021.07: Floor Temperature Time History

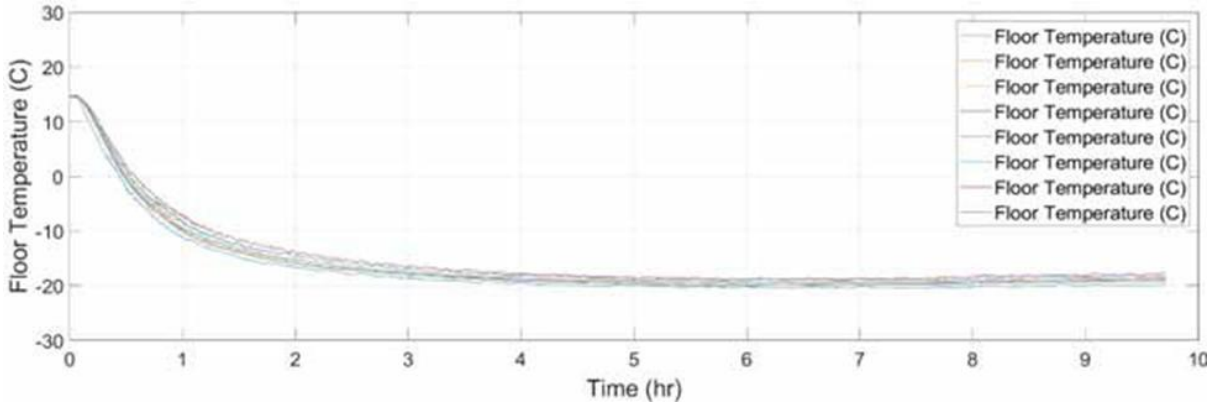

Figure 091021.08: Skin Temperature Slope Time History

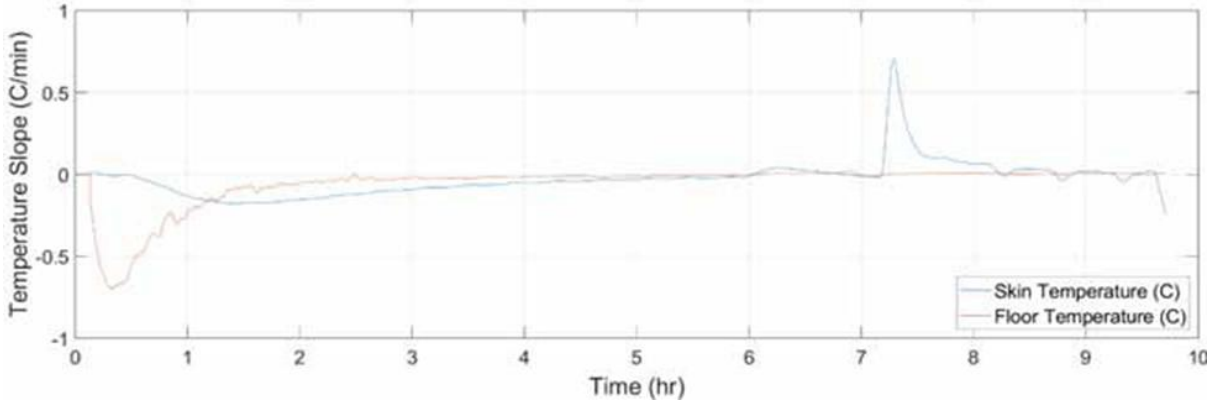

Figure 091021.09: RMS Height Evolution

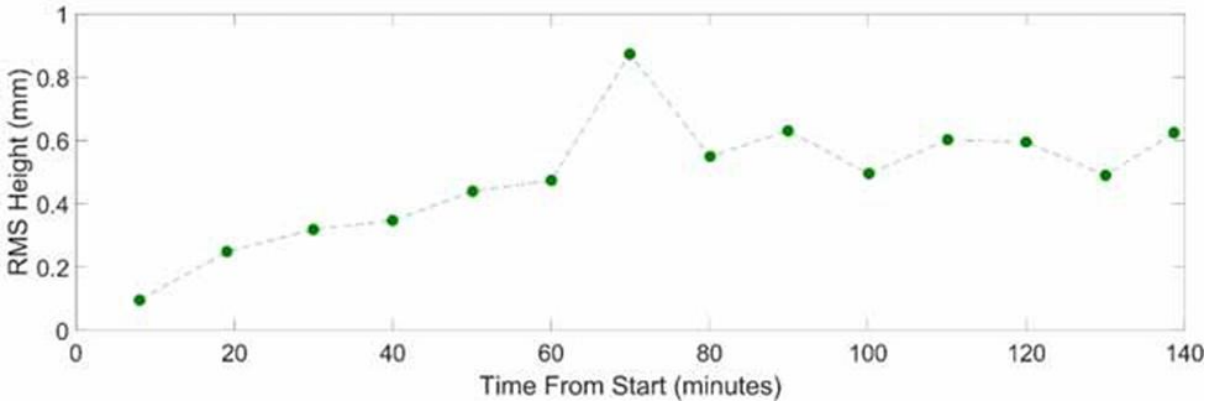

Figure 091021.10: Skewness Evolution

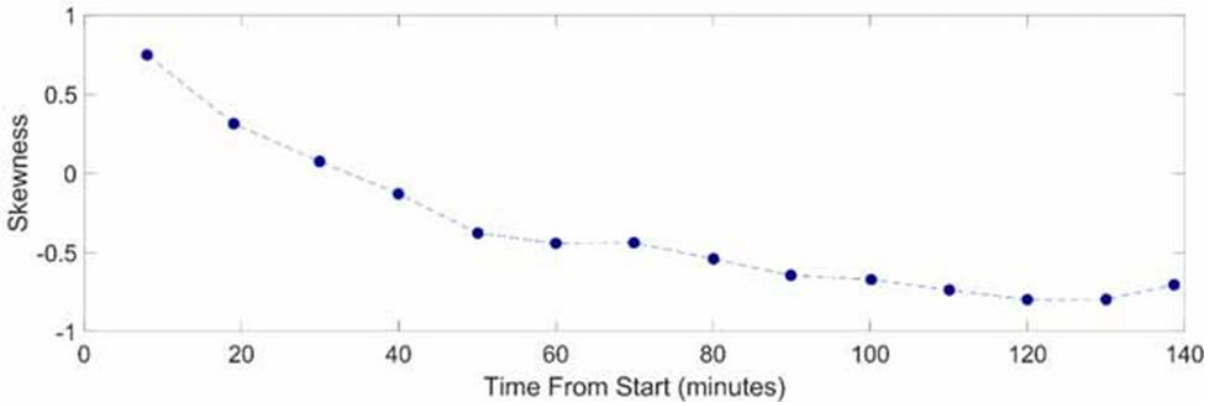

Figure 091021.11: Peak to Valley Evolution

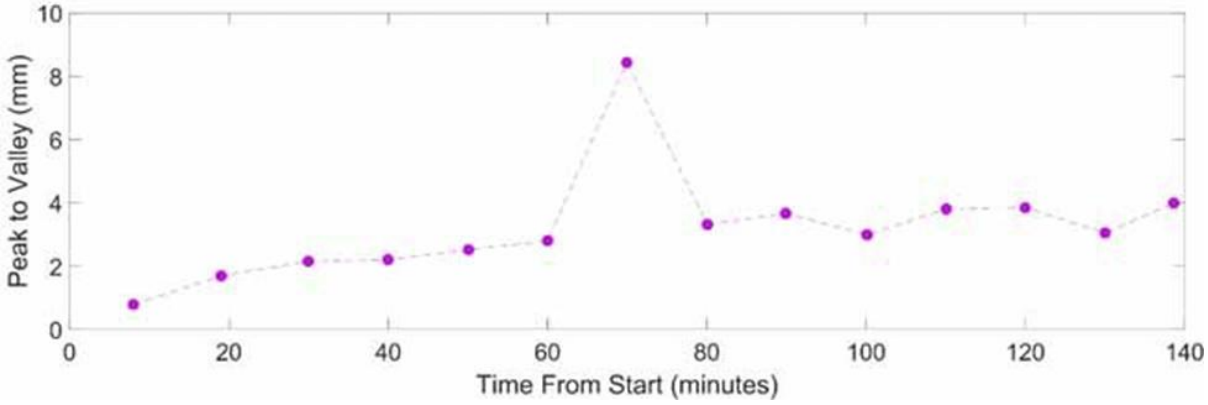

Figure 091021.12: Equivalent Roughness Evolution

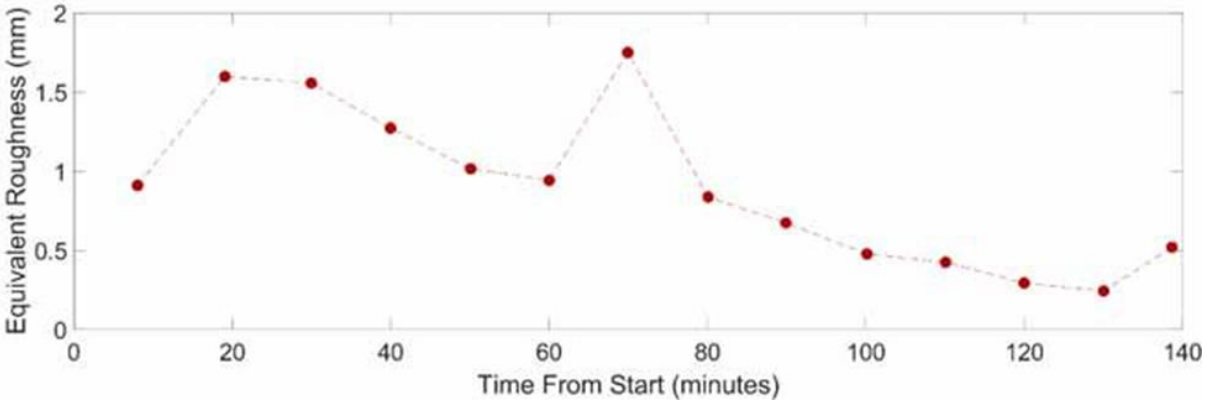

Table 091021.02: Summary of Roughness Parameters

Time (min.)	RMS (mm)	Skewness	Peak to Valley (mm)	ks,Flack-Schultz (mm)
7.9900	0.0957	0.7469	0.7866	0.9100
19.0233	0.2485	0.3123	1.6915	1.5976
29.9400	0.3187	0.0739	2.1512	1.5568
39.9567	0.3474	-0.1300	2.2045	1.2717
50.0733	0.4398	-0.3788	2.5163	1.0148
59.9900	0.4740	-0.4432	2.8026	0.9415
69.9233	0.8730	-0.4396	8.4349	1.7494
80.0567	0.5496	-0.5415	3.3171	0.8366
89.8900	0.6304	-0.6459	3.6631	0.6735
100.1233	0.4954	-0.6721	2.9939	0.4762
110.0567	0.6026	-0.7386	3.8025	0.4246
119.9733	0.5951	-0.7990	3.8476	0.2926
130.0067	0.4901	-0.7978	3.0503	0.2430
138.6400	0.6248	-0.7051	3.9916	0.5196

Figure 091021.13: Frost Topography at 00:07:52

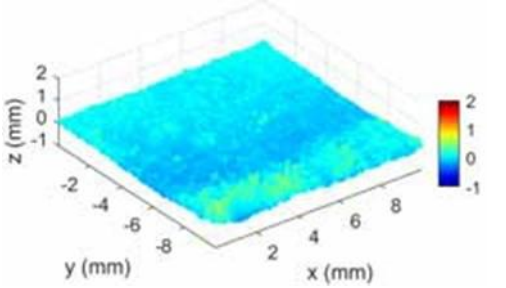

Figure 091021.14: Frost Topography at 00:18:54

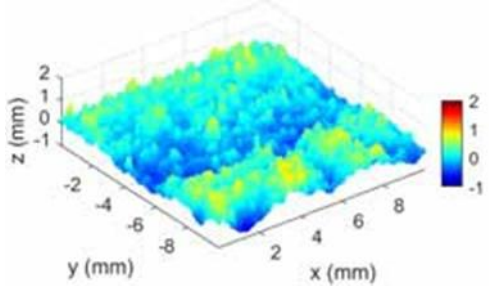

Figure 091021.15: Frost Topography at 00:29:49

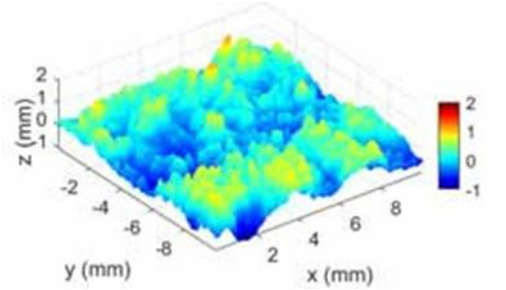

Figure 091021.16: Frost Topography at 00:39:50

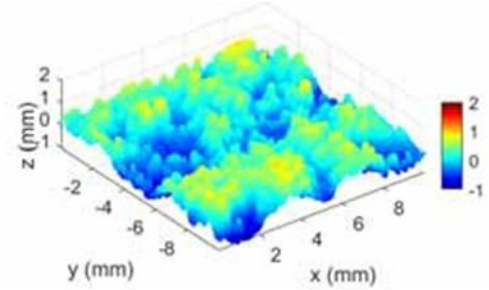

Figure 091021.17: Frost Topography at 00:49:57

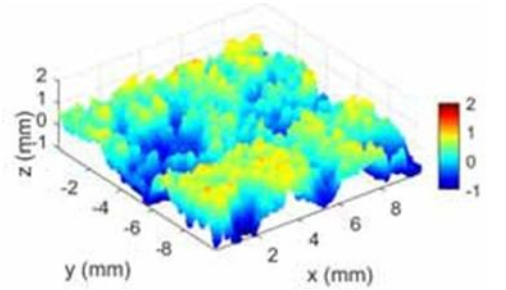

Figure 091021.18: Frost Topography at 00:59:52

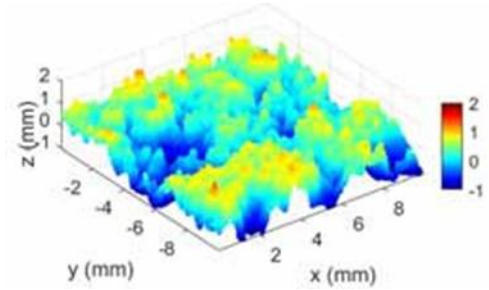

Figure 091021.19: Frost Topography at 01:09:48

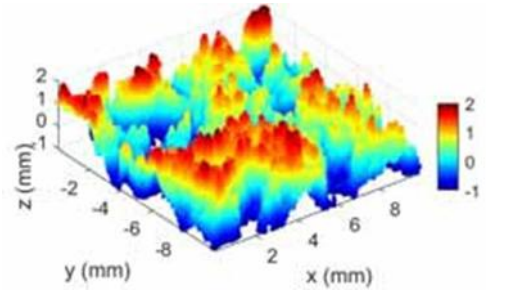

Figure 091021.20: Frost Topography at 01:19:56

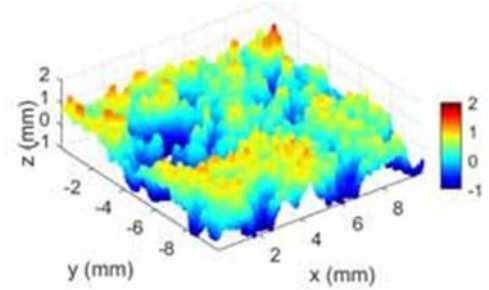

Figure 091021.21: Frost Topography at 01:29:46

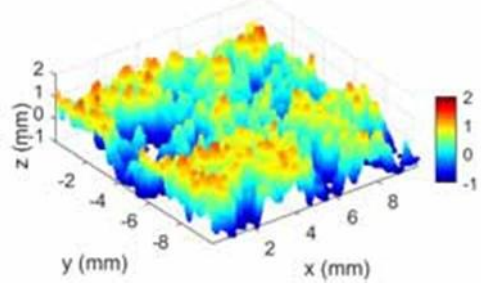

Figure 091021.22: Frost Topography at 01:40:00

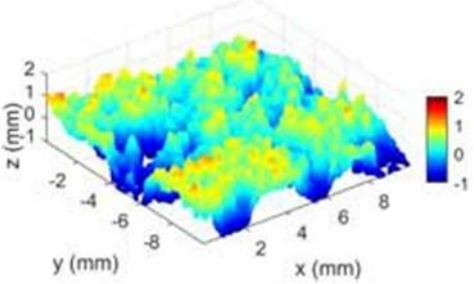

Figure 091021.23: Frost Topography at 01:49:56

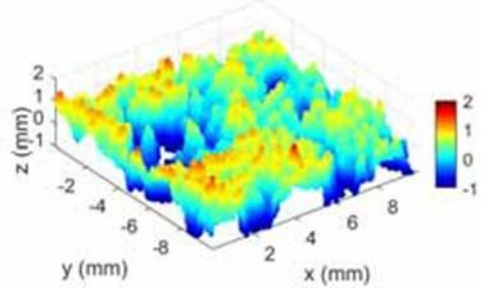

Figure 091021.24: Frost Topography at 01:59:51

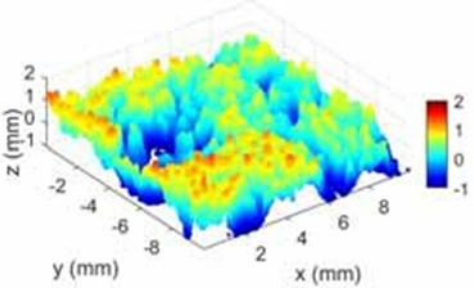

Figure 091021.25: Frost Topography at 02:09:53

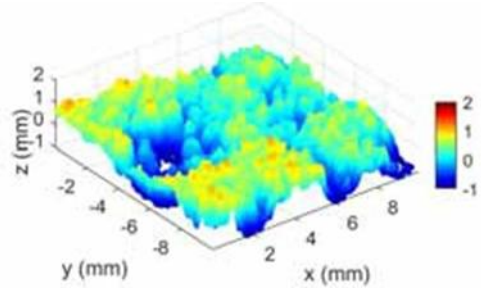

Figure 091021.26: Frost Topography at 02:18:31

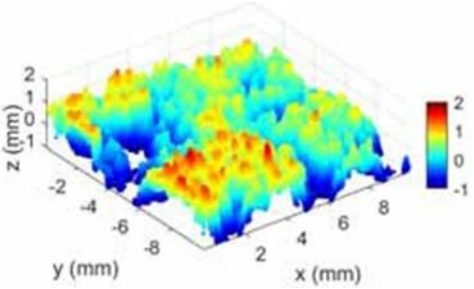

CAFF Conditions Report – Case Date: 091421

Table 091421.01: Summary of Measured Test Variables

Variable	Mean	St. Dev.	Rand. Unc.
T_air (C)	4.2748	0.2339	0.0080
Rh (%)	79.4047	5.9470	0.2044
Omega (kg_v/kg_da)	0.00414485	0.00036034	0.00001239
V_air (m/s)	0.3659	0.0520	0.0018
T_skin (C)	-10.8656	0.8045	0.0277
T_floor (C)	-20.6238	0.0220	0.0008

Figure 091421.01: Temperature and Voltage Control Time History

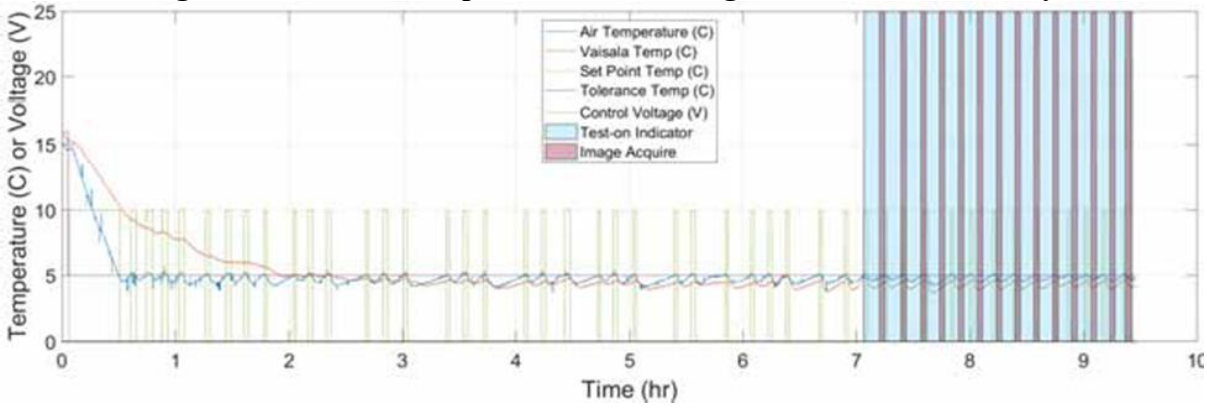

Figure 091421.02: Relative Humidity Time History

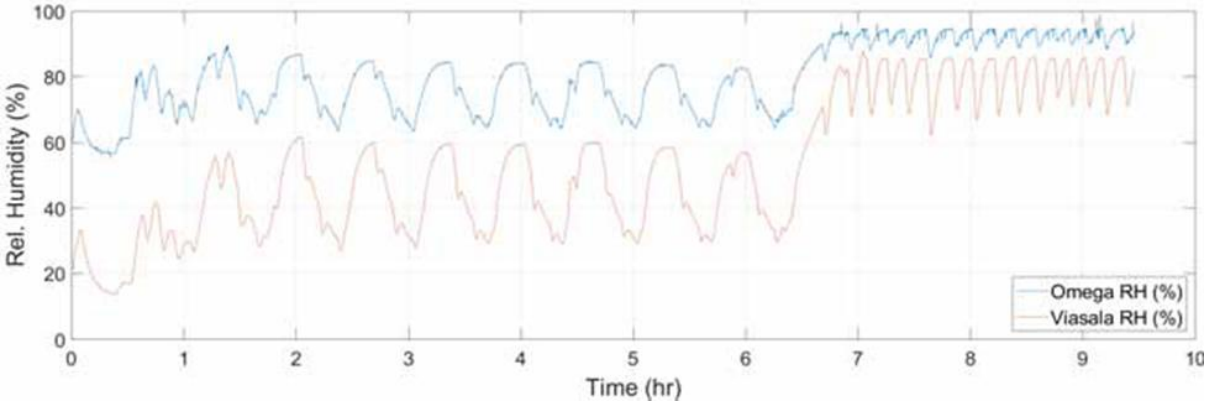

Figure 091421.03: Velocity Time History

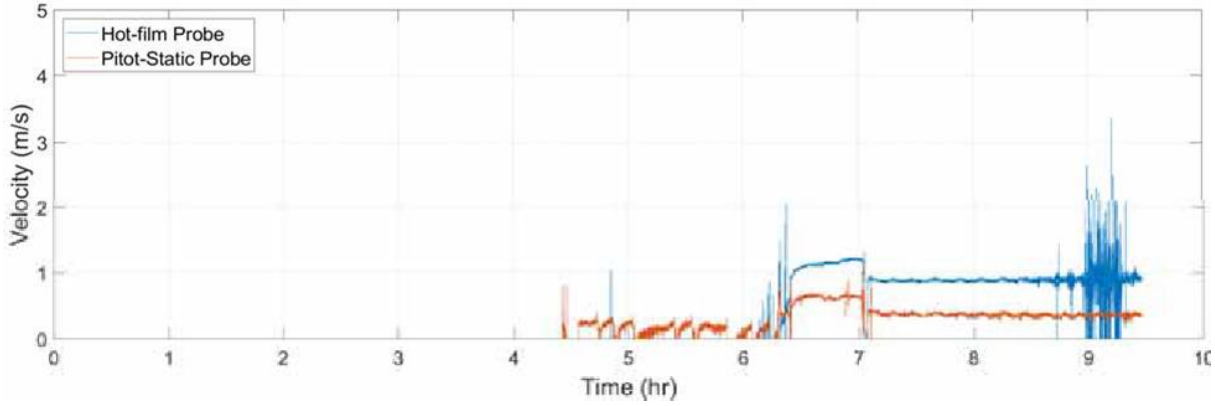

Figure 091421.04: Coolant Return Temperature Time History

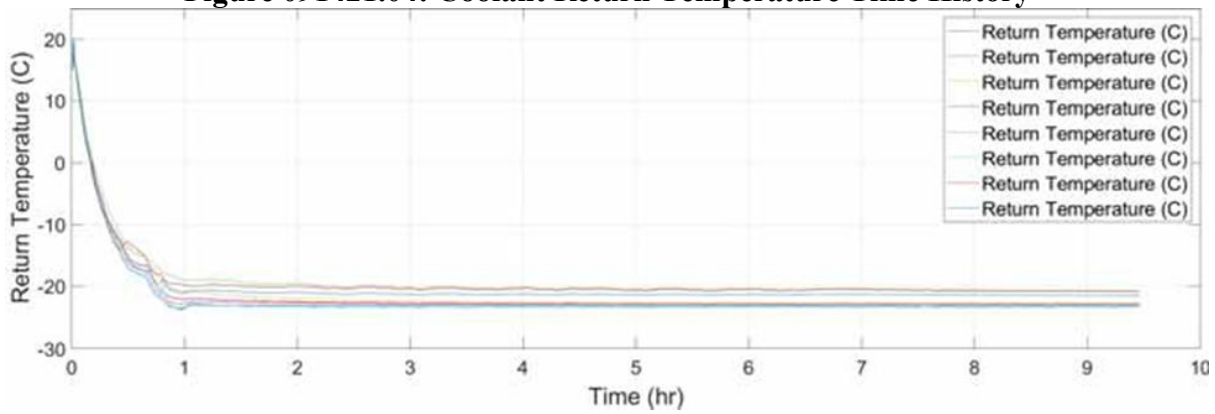

Figure 091421.05: Coolant Supply Temperature Time History

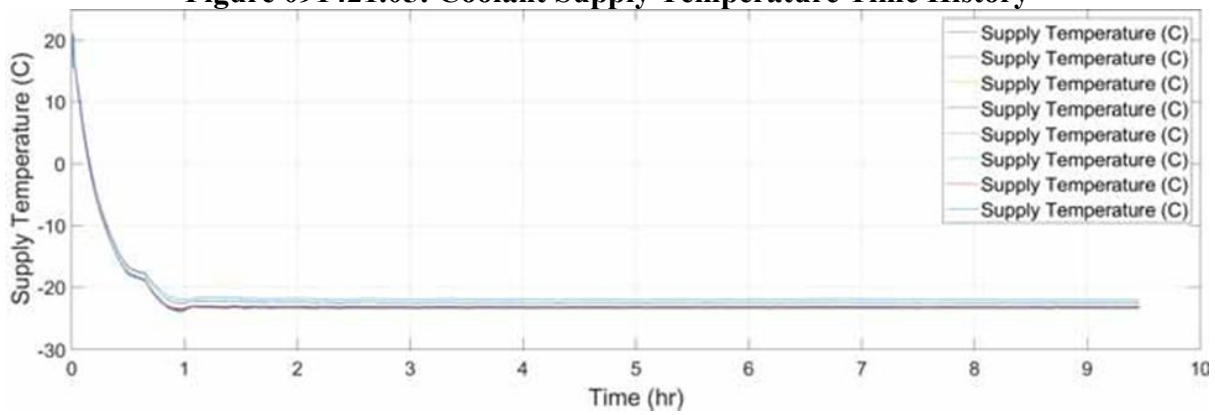

Figure 091421.06: Skin Temperature Time History

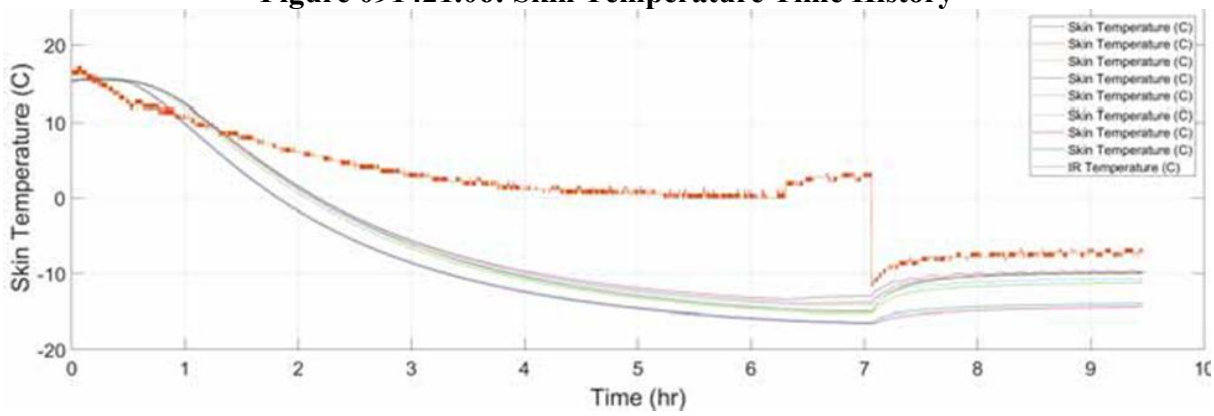

Figure 091421.07: Floor Temperature Time History

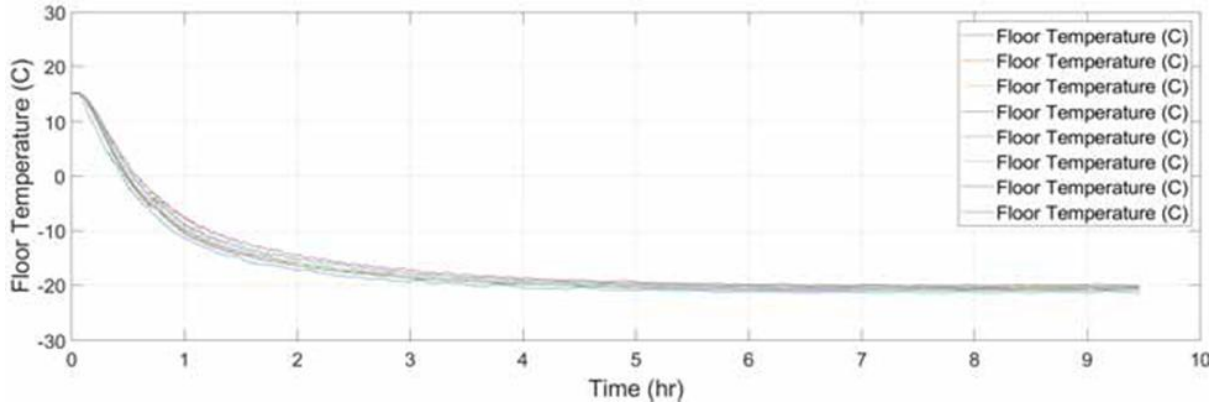

Figure 091421.08: Skin Temperature Slope Time History

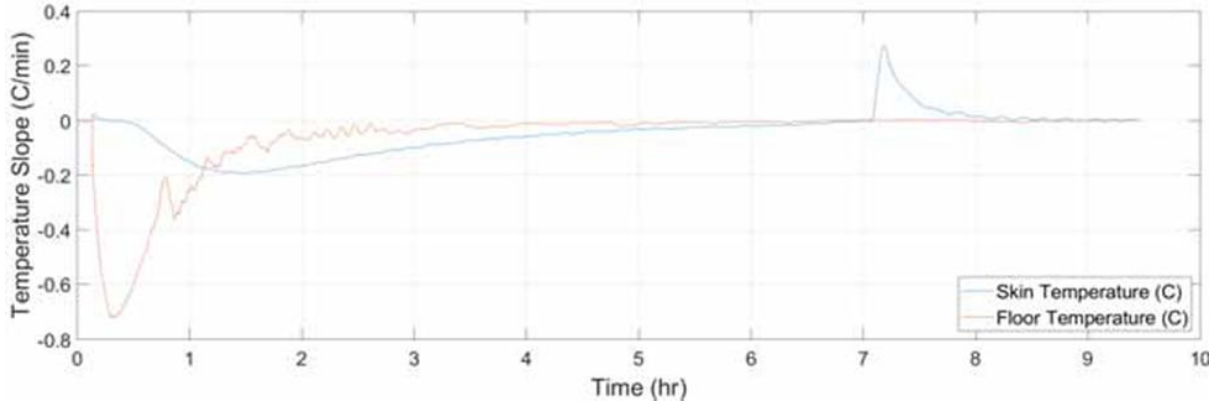

Figure 091421.09: RMS Height Evolution

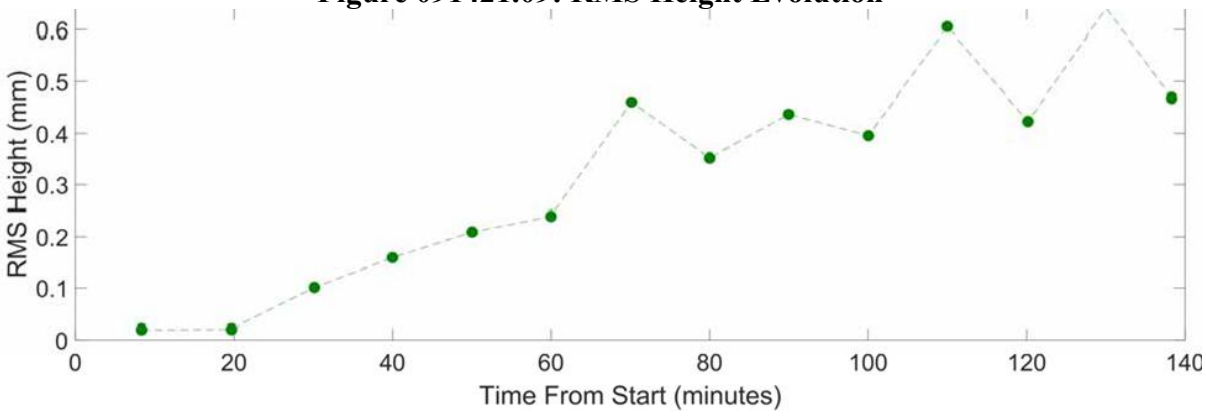

Figure 091421.10: Skewness Evolution

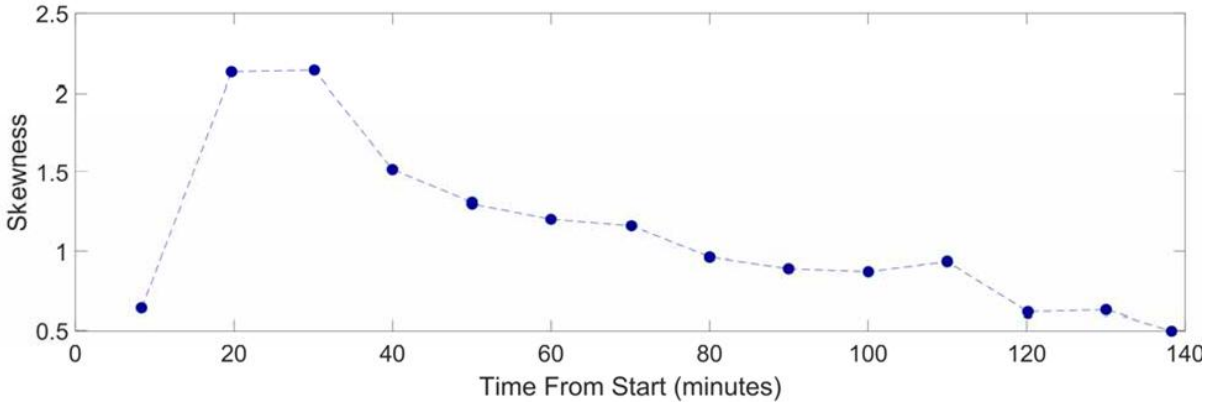

Figure 091421.11: Peak to Valley Evolution

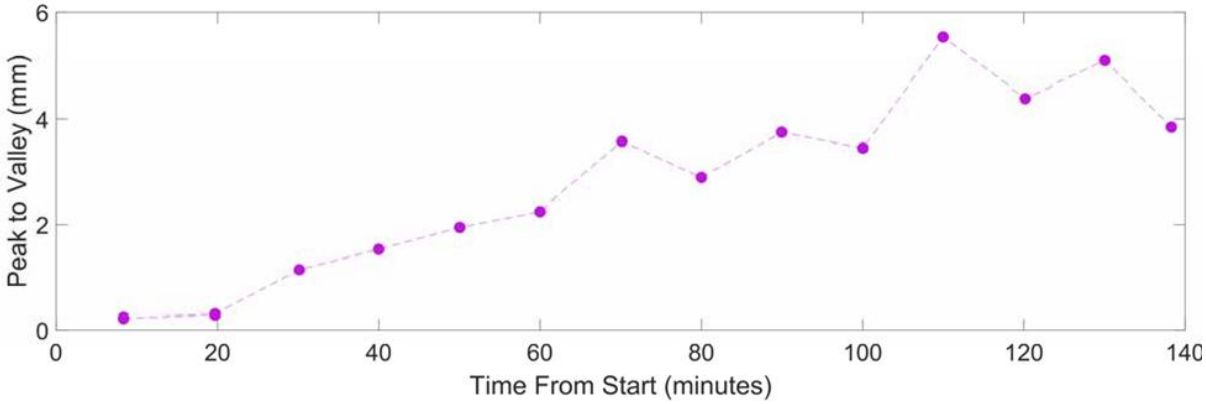

Figure 091421.12: Equivalent Roughness Evolution

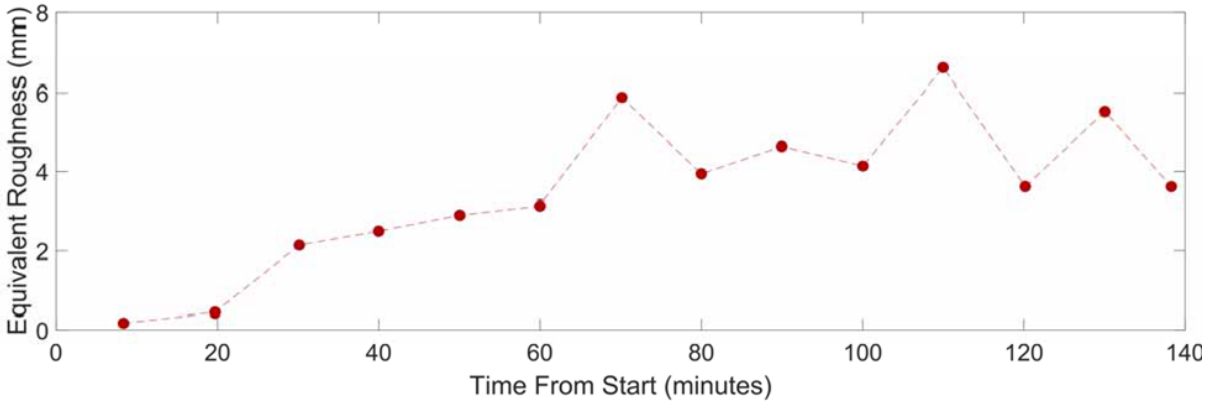

Table 091421.02: Summary of Roughness Parameters

Time (min.)	RMS (mm)	Skewness	Peak to Valley (mm)	ks,Flack-Schultz (mm)
8.3333	0.0200	0.6361	0.2224	0.1742
19.6833	0.0204	2.1338	0.2904	0.4325
30.1333	0.1007	2.1441	1.1341	2.1424
39.9833	0.1594	1.5154	1.5271	2.4983
50.0333	0.2092	1.3039	1.9448	2.9078
59.9833	0.2399	1.2050	2.2480	3.1395
70.1500	0.4616	1.1628	3.5740	5.8843
80.0000	0.3524	0.9626	2.8800	3.9323
89.9667	0.4377	0.8883	3.7470	4.6325
100.0333	0.3958	0.8691	3.4419	4.1309
109.9833	0.6055	0.9346	5.5540	6.6240
120.1667	0.4233	0.6117	4.3907	3.6062
130.0333	0.6413	0.6249	5.1023	5.5247
138.2833	0.4687	0.4957	3.8459	3.6045

Figure 091421.13: Frost Topography at 00:08:12

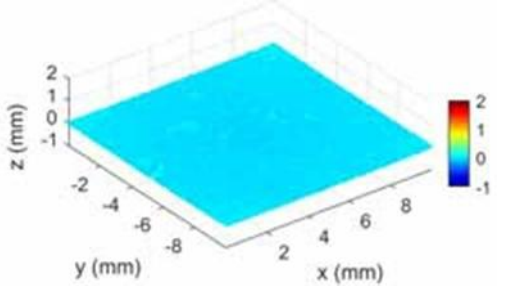

Figure 091421.14: Frost Topography at 00:19:33

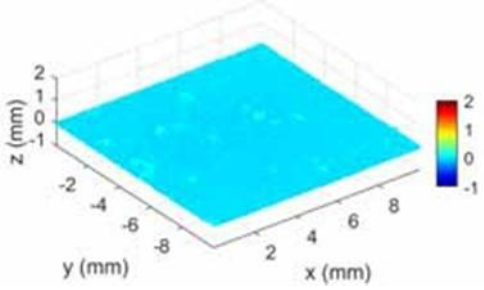

Figure 091421.15: Frost Topography at 00:30:00

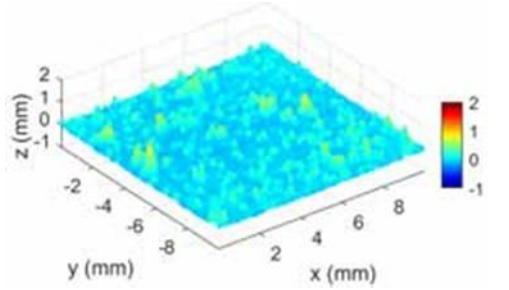

Figure 091421.16: Frost Topography at 00:39:51

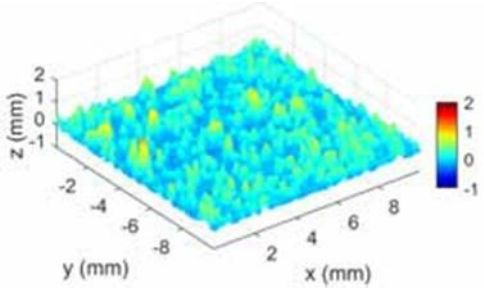

Figure 091421.17: Frost Topography at 00:49:54

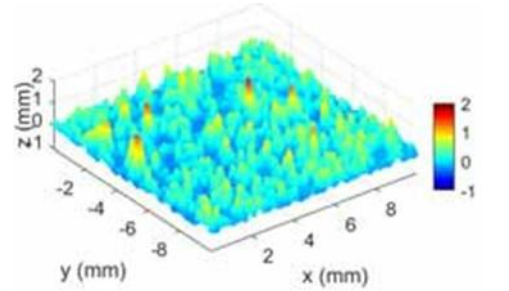

Figure 091421.18: Frost Topography at 00:59:51

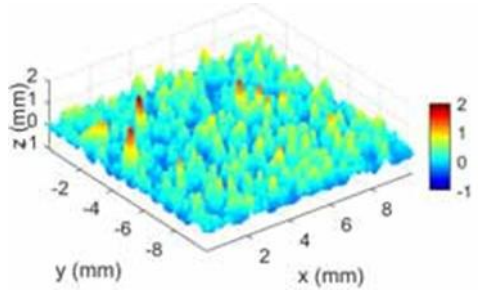

Figure 091421.19: Frost Topography at 01:10:01

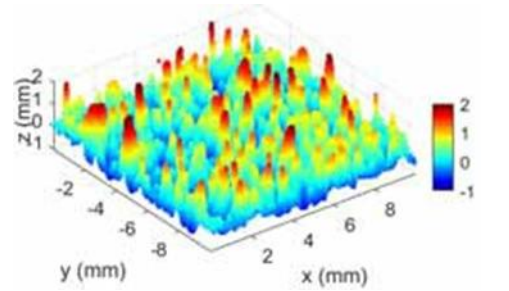

Figure 091421.20: Frost Topography at 01:19:52

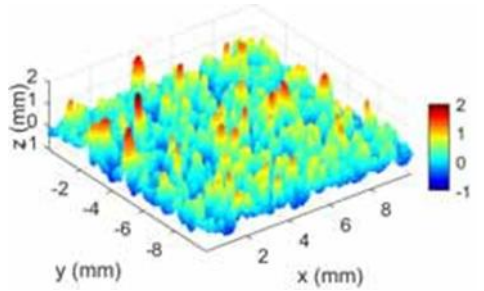

Figure 091421.21: Frost Topography at 01:29:50

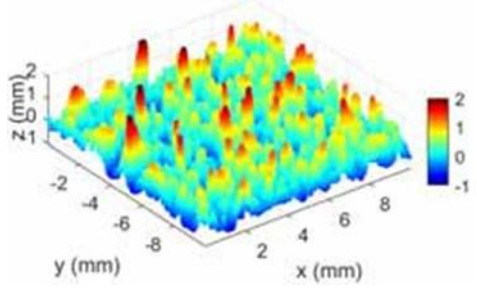

Figure 091421.22: Frost Topography at 01:39:54

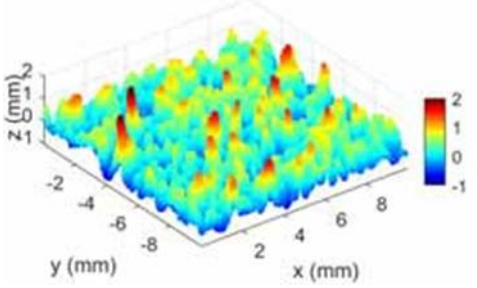

Figure 091421.23: Frost Topography at 01:49:51

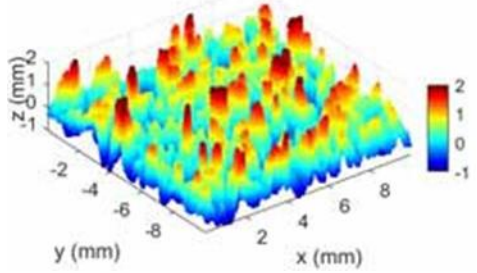

Figure 091421.24: Frost Topography at 02:00:02

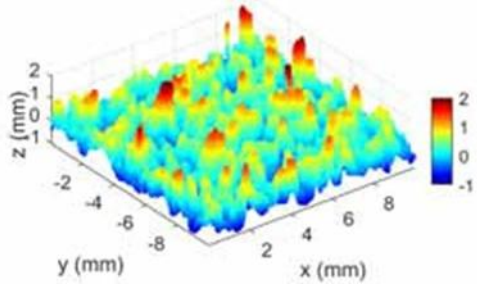

Figure 091421.25: Frost Topography at 02:09:54

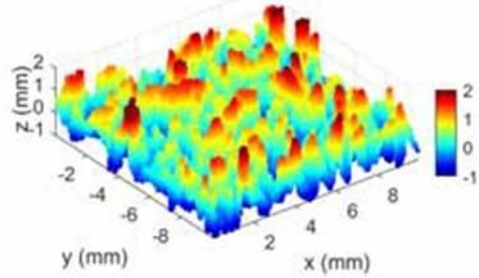

Figure 091421.26: Frost Topography at 02:18:09

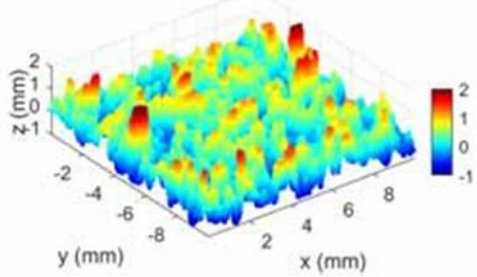

CAFF Conditions Report – Case Date: 091621

Table 091621.01: Summary of Measured Test Variables

Variable	Mean	St. Dev.	Rand. Unc.
T_air (C)	9.2497	0.3192	0.0110
Rh (%)	79.6128	5.6052	0.1928
Omega (kg_v/kg_da)	0.00586888	0.00044915	0.00001545
V_air (m/s)	0.2899	0.1122	0.0039
T_skin (C)	-8.7184	1.0829	0.0372
T_floor (C)	-20.1297	0.0675	0.0023

Figure 091621.01: Temperature and Voltage Control Time History

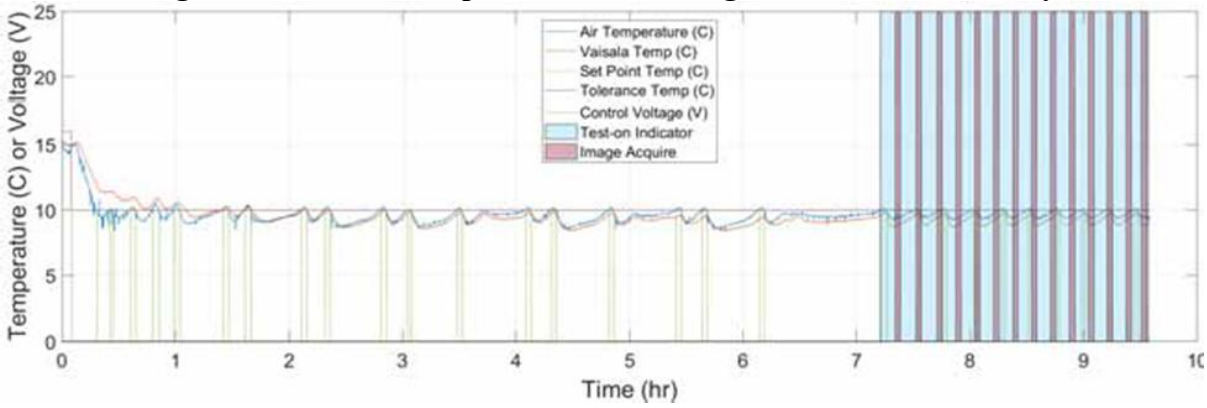

Figure 091621.02: Relative Humidity Time History

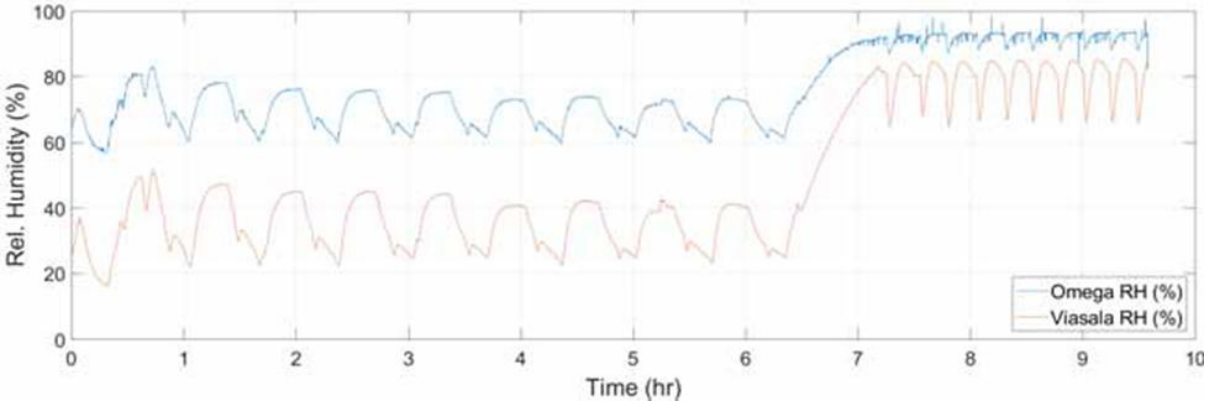

Figure 091621.03: Velocity Time History

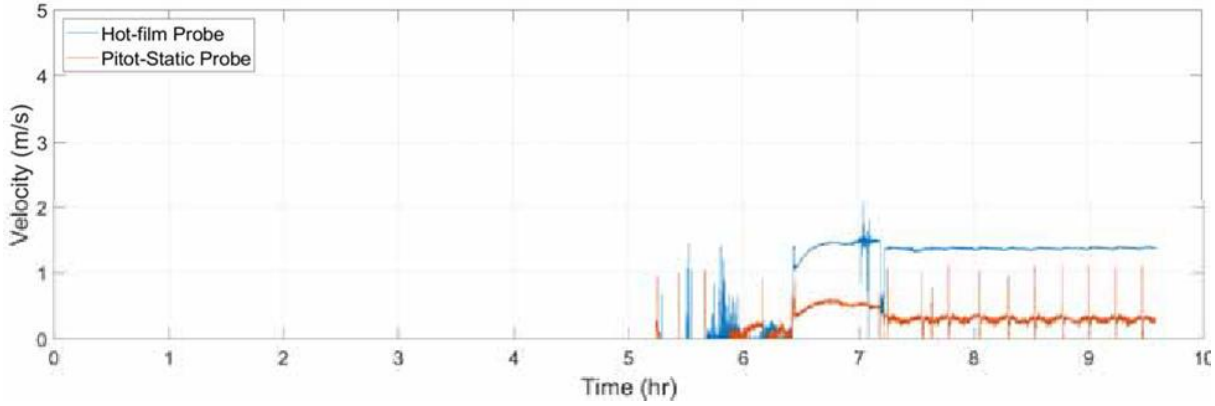

Figure 091621.04: Coolant Return Temperature Time History

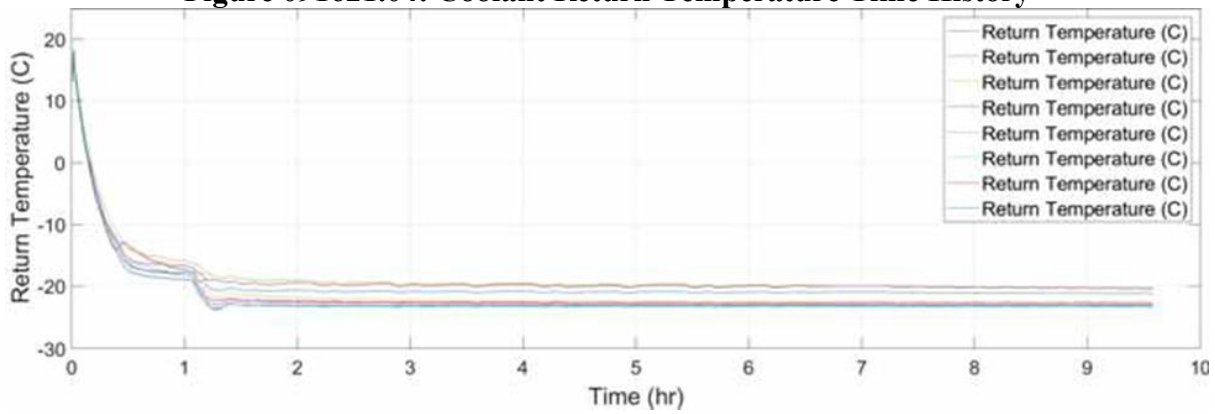

Figure 091621.05: Coolant Supply Temperature Time History

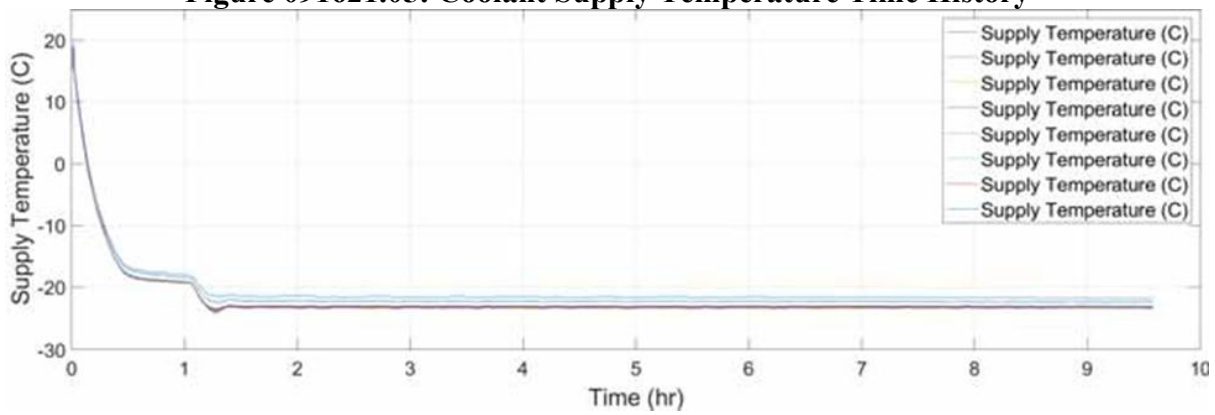

Figure 091621.06: Skin Temperature Time History

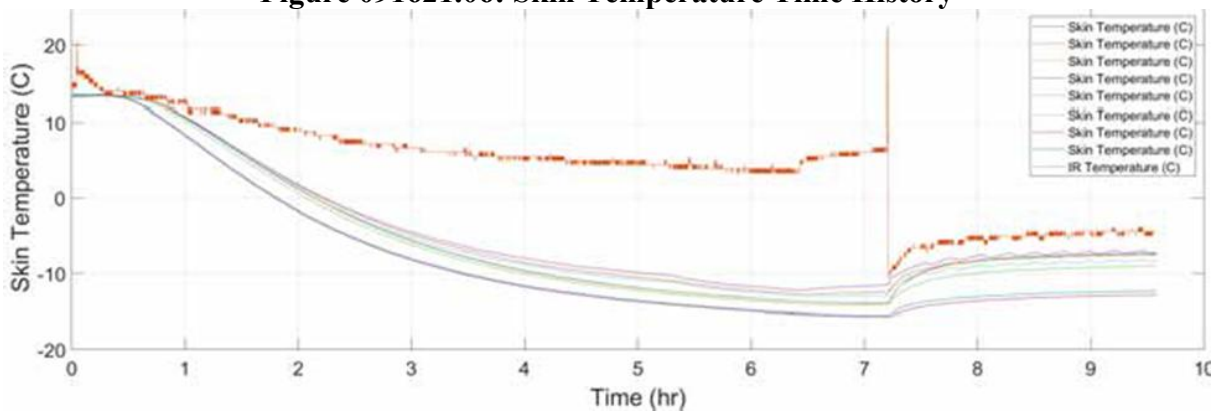

Figure 091621.07: Floor Temperature Time History

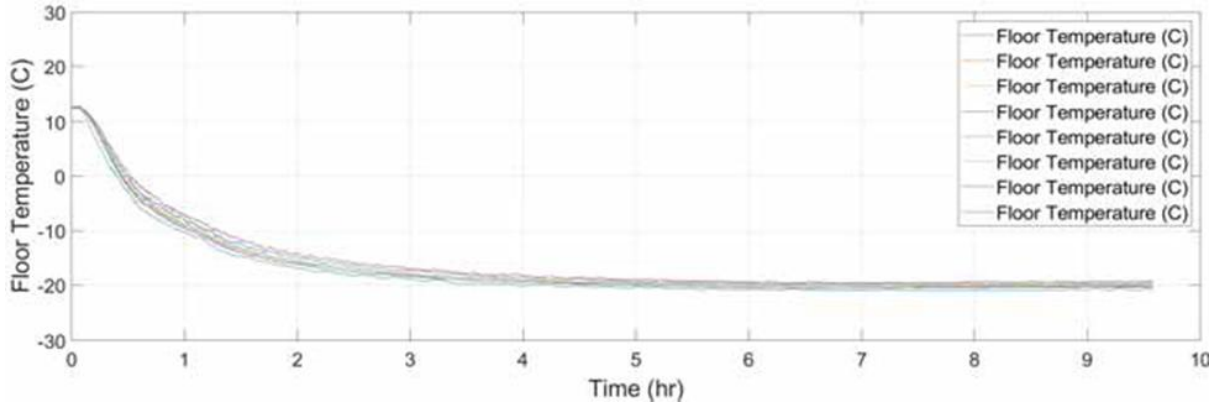

Figure 091621.08: Skin Temperature Slope Time History

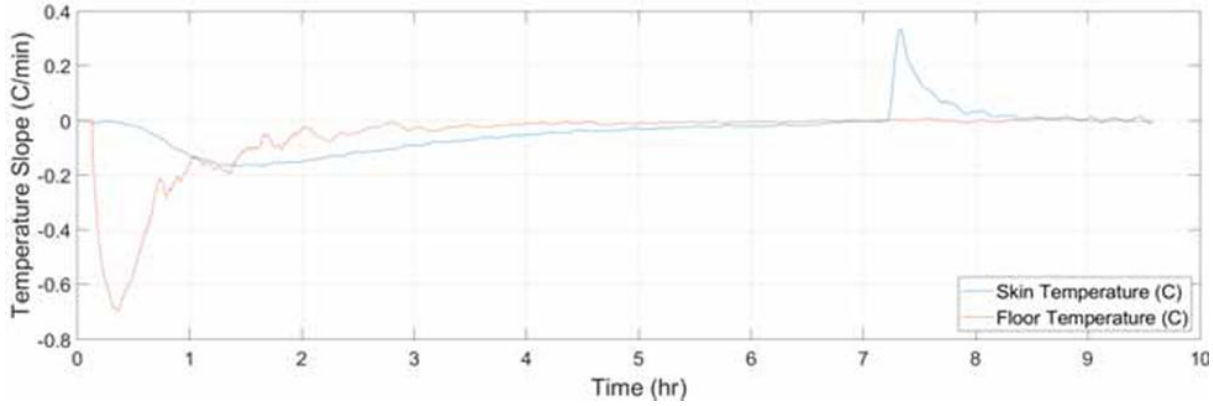

Figure 091621.09: RMS Height Evolution

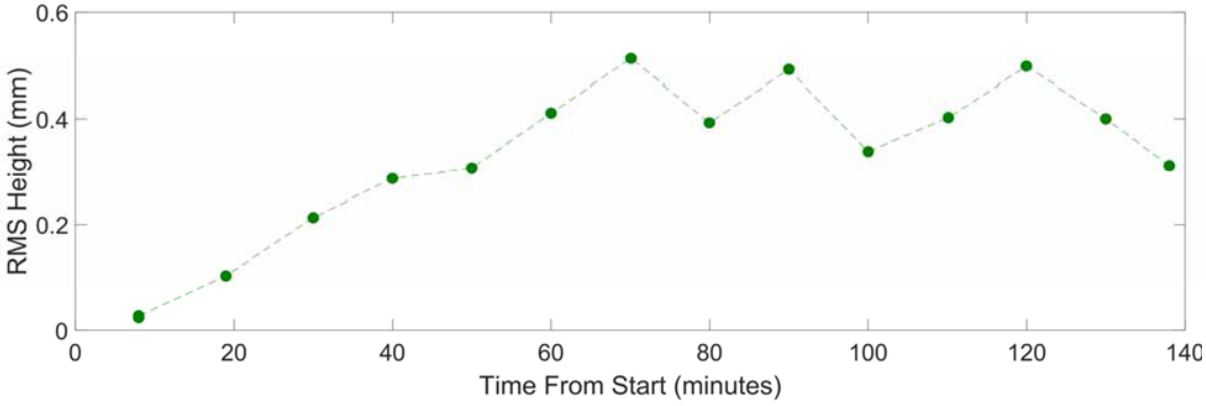

Figure 091621.10: Skewness Evolution

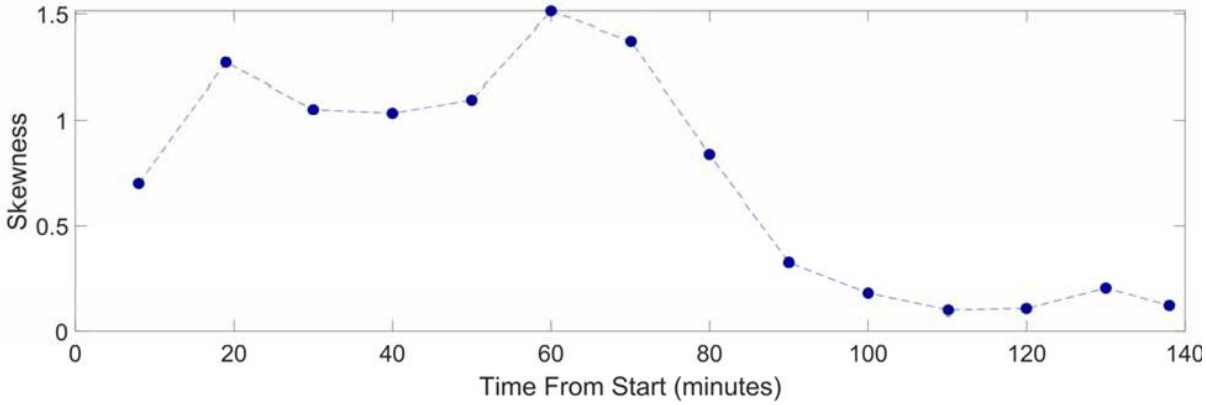

Figure 091621.11: Peak to Valley Evolution

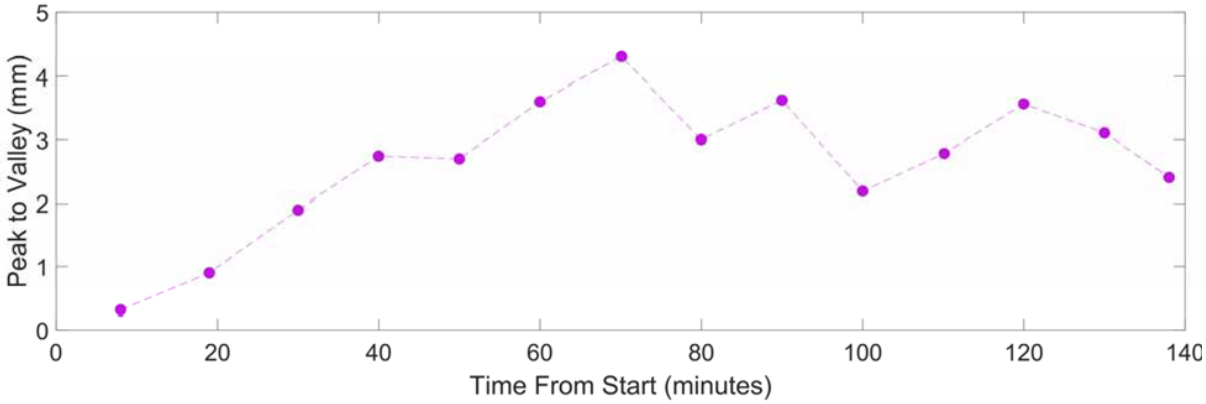

Figure 091621.12: Equivalent Roughness Evolution

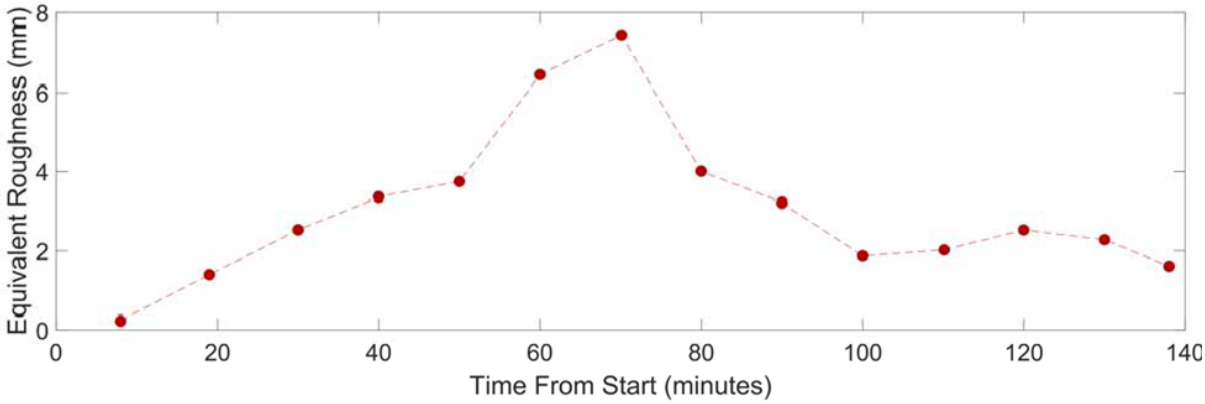

Table 091621.02: Summary of Roughness Parameters

Time (min.)	RMS (mm)	Skewness	Peak to Valley (mm)	ks,Flack-Schultz (mm)
7.9751	0.0246	0.6975	0.3051	0.2254
18.9751	0.1016	1.2743	0.8986	1.3867
29.9918	0.2132	1.0517	1.8968	2.5284
39.9751	0.2864	1.0345	2.7431	3.3575
49.9918	0.3060	1.0978	2.6983	3.7400
59.9918	0.4111	1.5145	3.6114	6.4420
70.0918	0.5144	1.3743	4.3158	7.4504
79.9751	0.3926	0.8374	3.0059	4.0025
89.9918	0.4931	0.3245	3.6361	3.2103
100.0084	0.3379	0.1766	2.1817	1.8705
110.1251	0.4026	0.0950	2.7850	2.0195
119.9751	0.4993	0.1019	3.5765	2.5264
129.9918	0.4003	0.2009	3.1126	2.2788
138.0084	0.3106	0.1162	2.4007	1.5999

Figure 091621.13: Frost Topography at 00:07:51

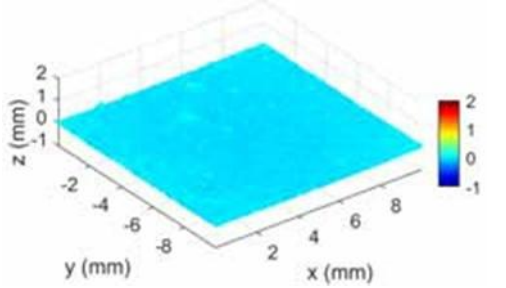

Figure 091621.14: Frost Topography at 00:18:51

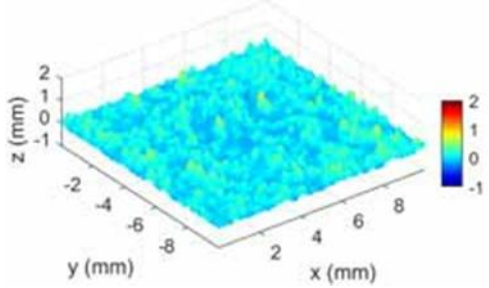

Figure 091621.15: Frost Topography at 00:29:52

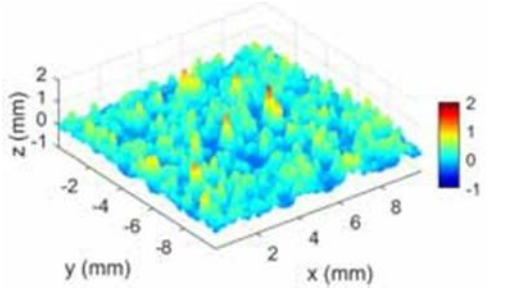

Figure 091621.16: Frost Topography at 00:39:51

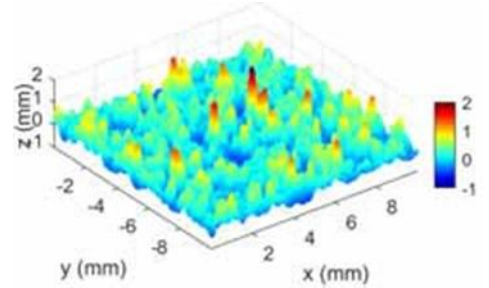

Figure 091621.17: Frost Topography at 00:49:52

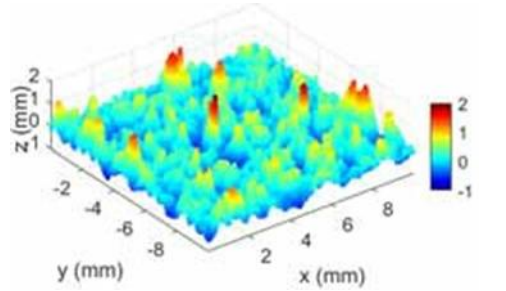

Figure 091621.18: Frost Topography at 00:59:52

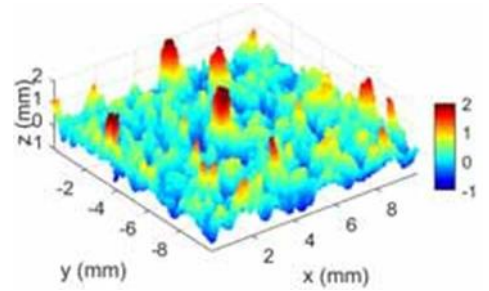

Figure 091621.19: Frost Topography at 01:09:58

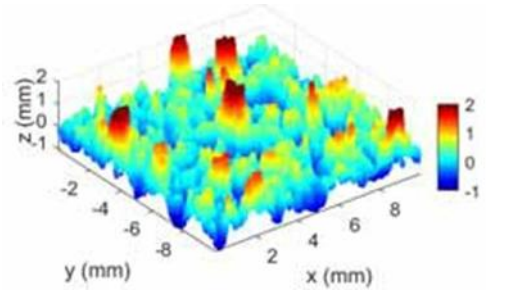

Figure 091621.20: Frost Topography at 01:19:51

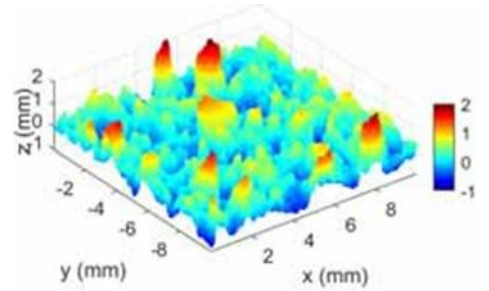

Figure 091621.21: Frost Topography at 01:29:52

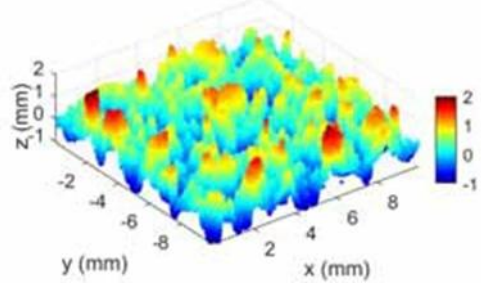

Figure 091621.22: Frost Topography at 01:39:53

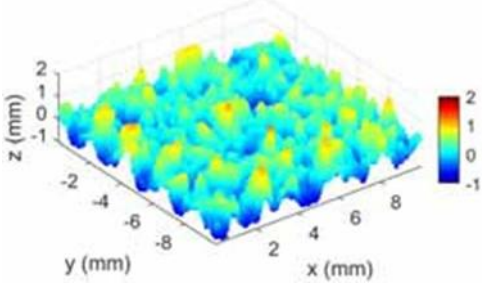

Figure 091621.23: Frost Topography at 01:50:00

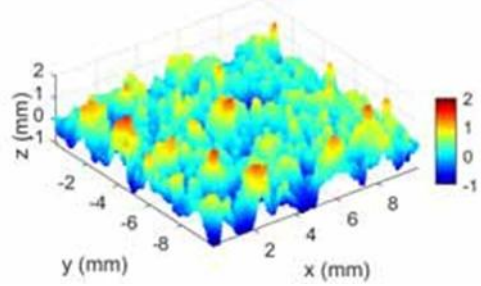

Figure 091621.24: Frost Topography at 01:59:51

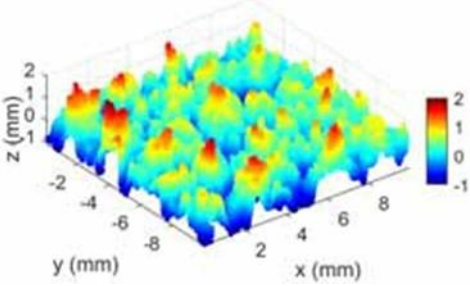

Figure 091621.25: Frost Topography at 02:09:52

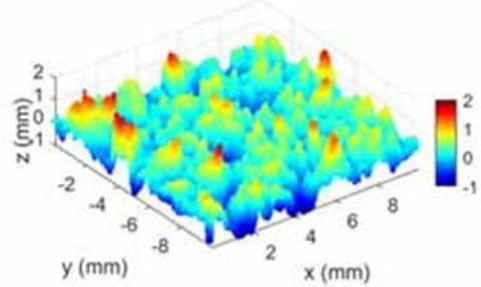

Figure 091621.26: Frost Topography at 02:17:53

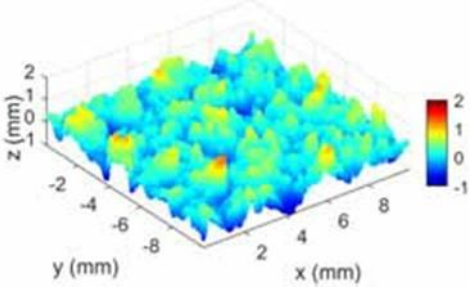

CAFF Conditions Report – Case Date: 091821

Table 091821.01: Summary of Measured Test Variables

Variable	Mean	St. Dev.	Rand. Unc.
T_air (C)	15.3140	0.2923	0.0099
Rh (%)	78.3381	3.4736	0.1174
Omega (kg_v/kg_da)	0.00861387	0.00048429	0.00001636
V_air (m/s)	0.2884	0.0969	0.0033
T_skin (C)	-5.4613	1.2863	0.0435
T_floor (C)	-19.4248	0.1028	0.0035

Figure 091821.01: Temperature and Voltage Control Time History

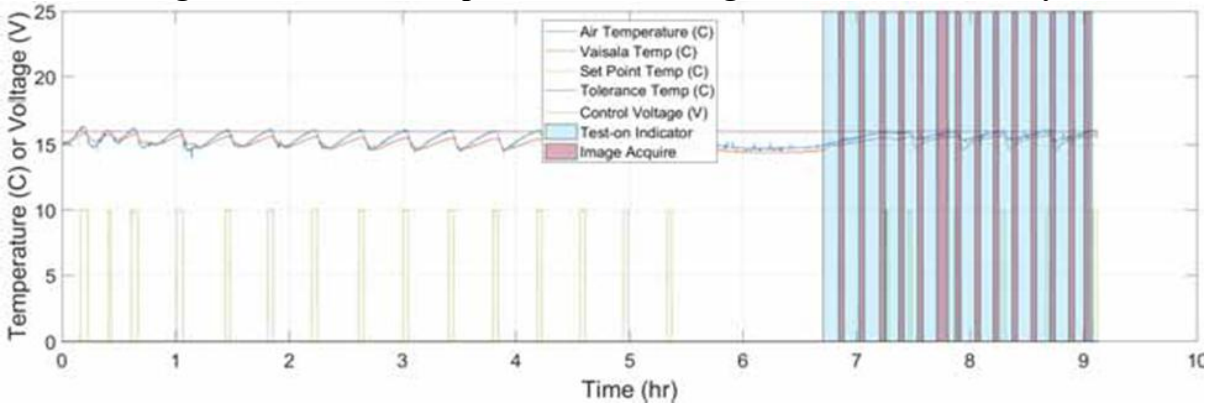

Figure 091821.02: Relative Humidity Time History

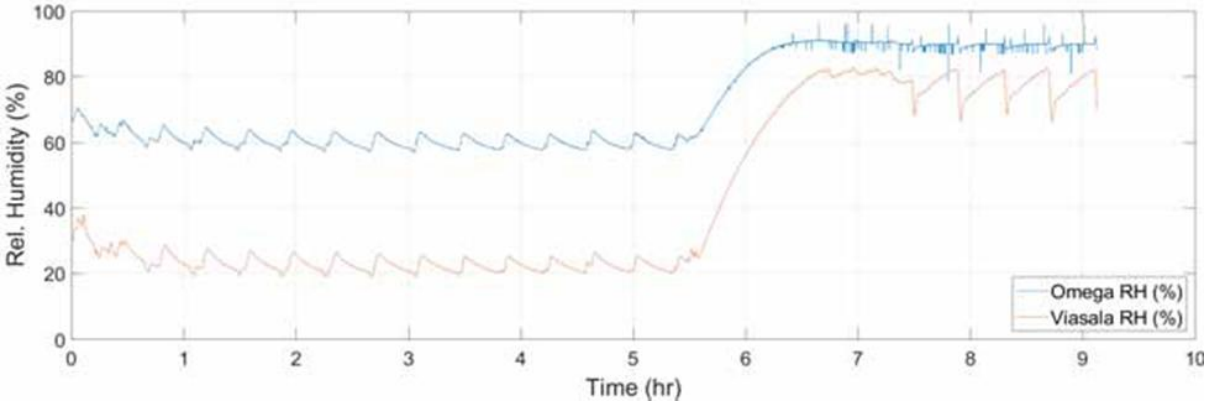

Figure 091821.03: Velocity Time History

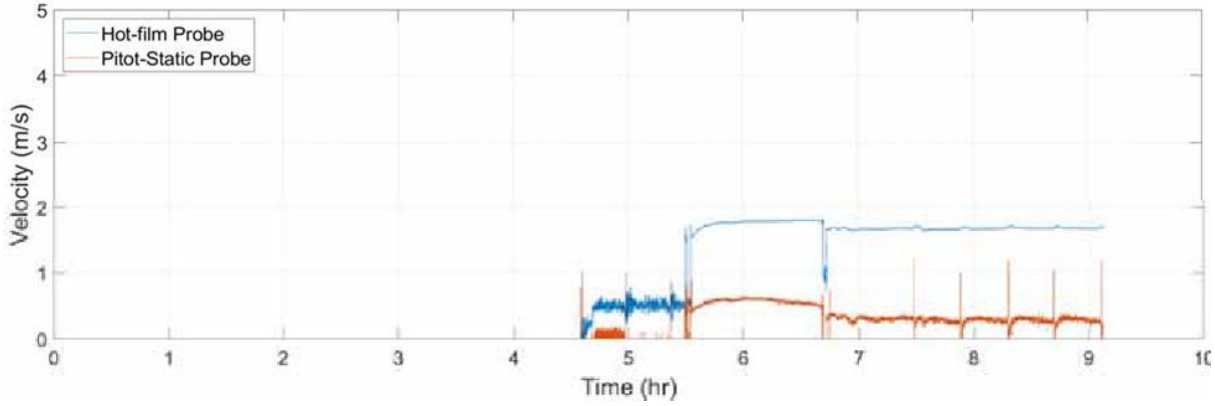

Figure 091821.04: Coolant Return Temperature Time History

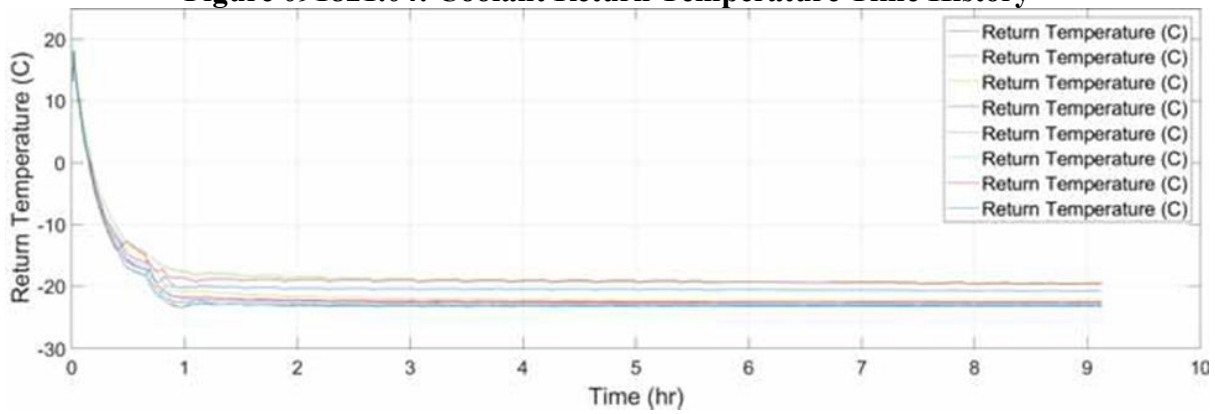

Figure 091821.05: Coolant Supply Temperature Time History

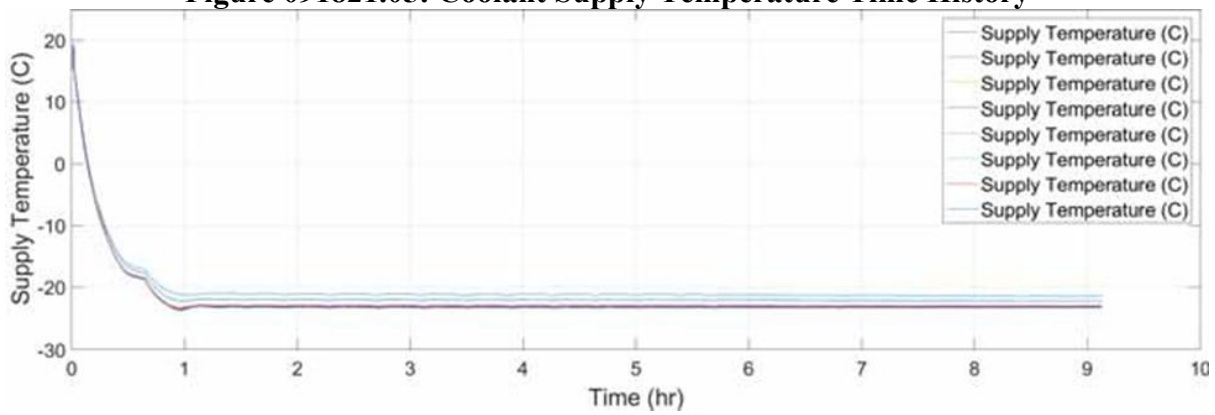

Figure 091821.06: Skin Temperature Time History

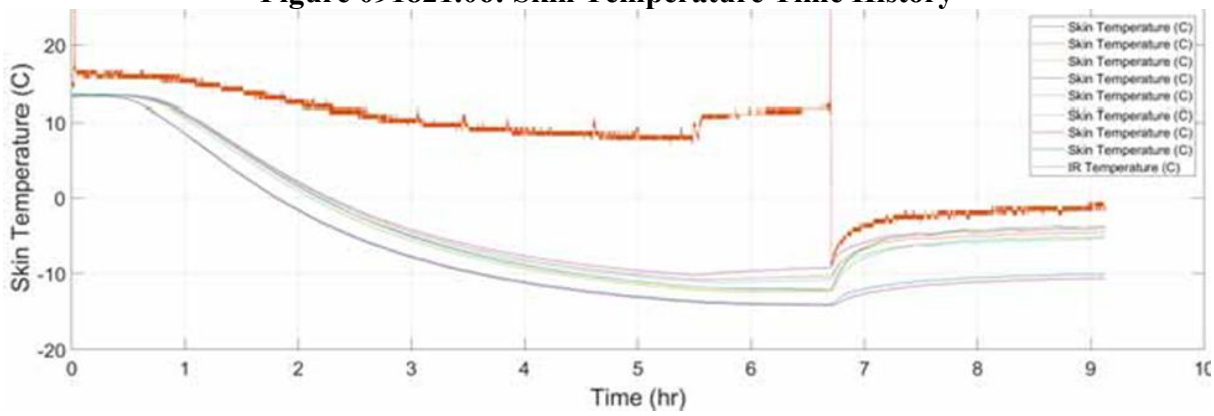

Figure 091821.07: Floor Temperature Time History

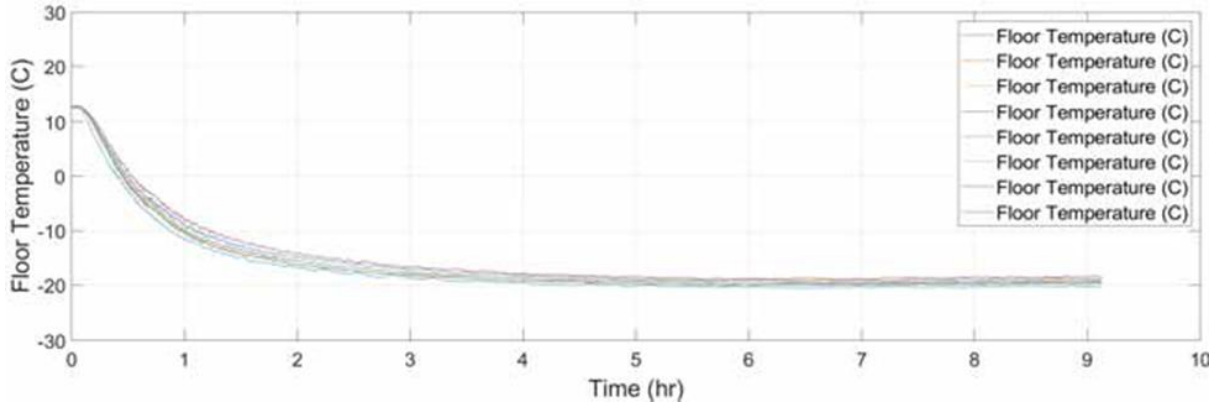

Figure 091821.08: Skin Temperature Slope Time History

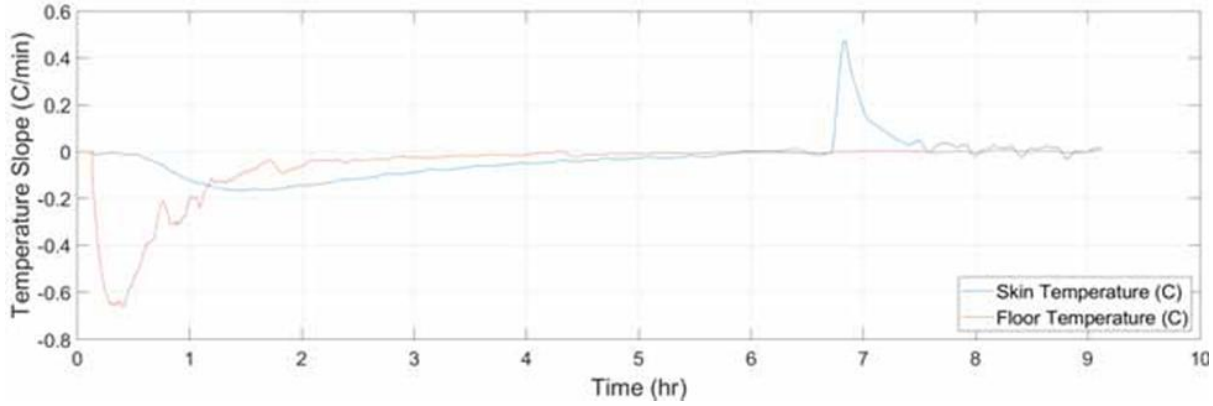

Figure 091821.09: RMS Height Evolution

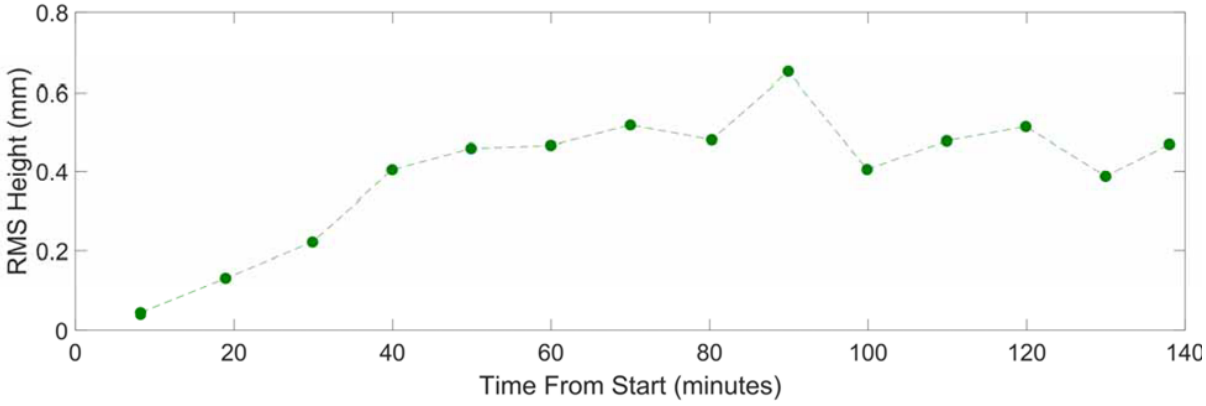

Figure 091821.10: Skewness Evolution

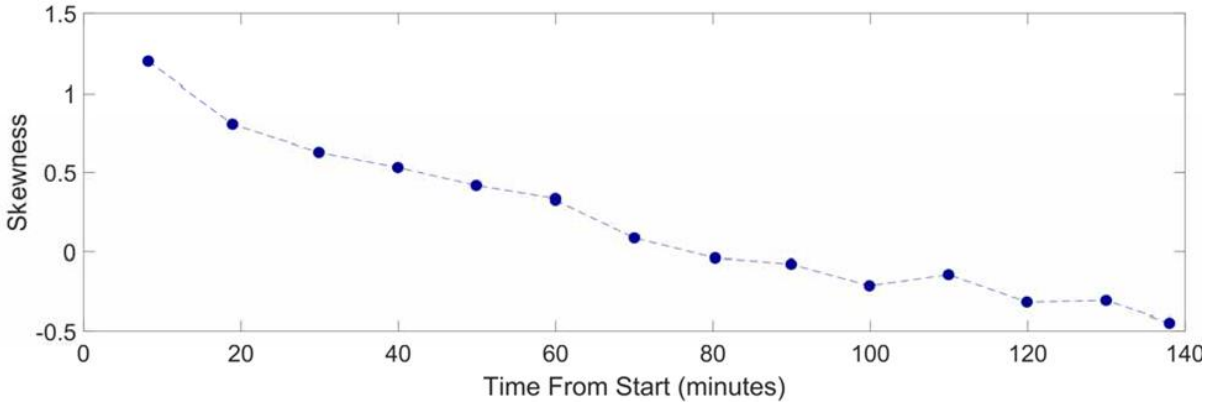

Figure 091821.11: Peak to Valley Evolution

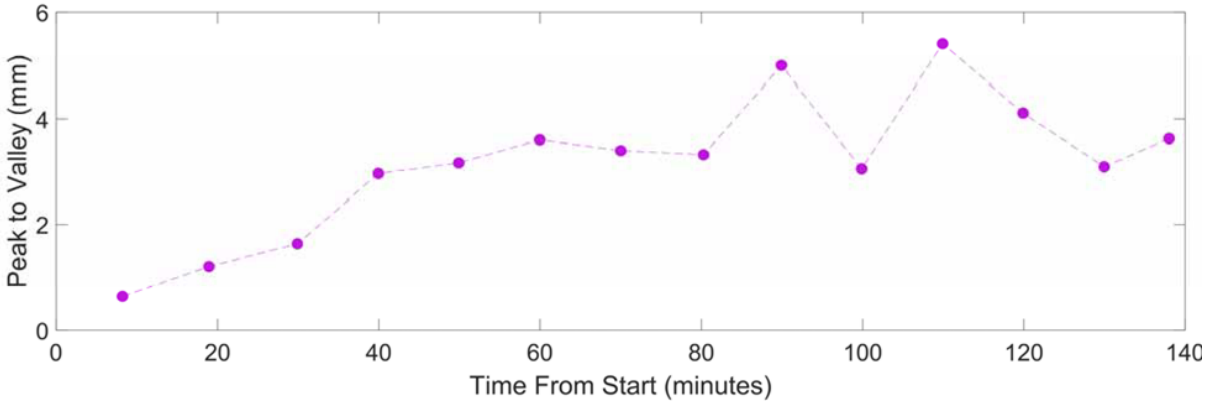

Figure 091821.12: Equivalent Roughness Evolution

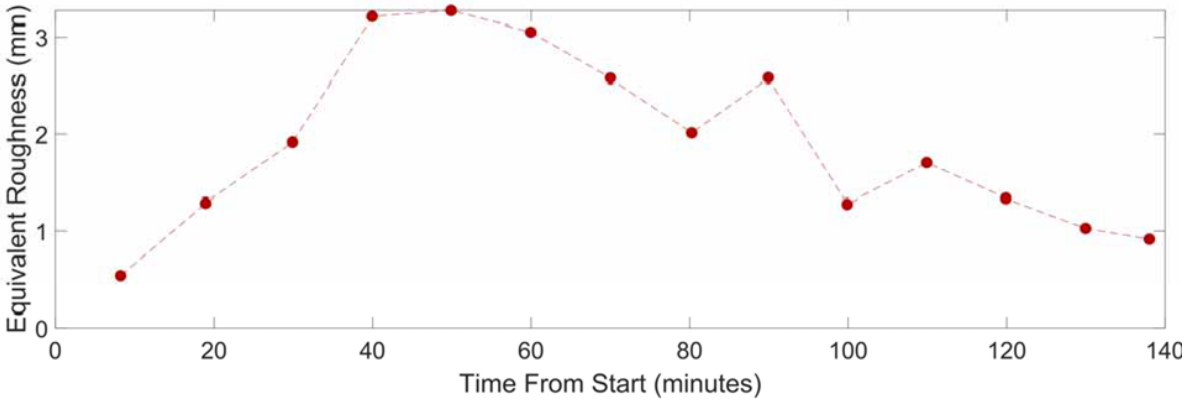

Table 091821.02: Summary of Roughness Parameters

Time (min.)	RMS (mm)	Skewness	Peak to Valley (mm)	ks,Flack-Schultz (mm)
8.2064	0.0410	1.2021	0.6228	0.5351
18.9397	0.1294	0.8062	1.1982	1.2889
29.9064	0.2220	0.6271	1.6287	1.9156
39.9397	0.4039	0.5305	2.9585	3.2055
49.9064	0.4583	0.4153	3.1605	3.2674
59.9564	0.4657	0.3305	3.6014	3.0509
70.0064	0.5182	0.0877	3.3944	2.5759
80.2731	0.4805	-0.0403	3.3177	2.0122
89.9231	0.6525	-0.0798	5.0075	2.5793
99.8731	0.4042	-0.2183	3.0456	1.2778
109.9231	0.4778	-0.1463	5.4257	1.7042
119.8897	0.5142	-0.3225	4.1124	1.3365
129.9564	0.3869	-0.3119	3.0859	1.0271
138.0064	0.4685	-0.4492	3.6271	0.9168

Figure 091821.13: Frost Topography at 00:08:07

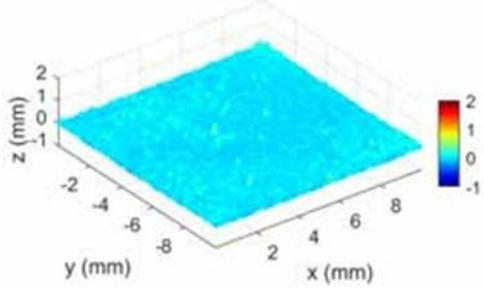

Figure 091821.14: Frost Topography at 00:18:51

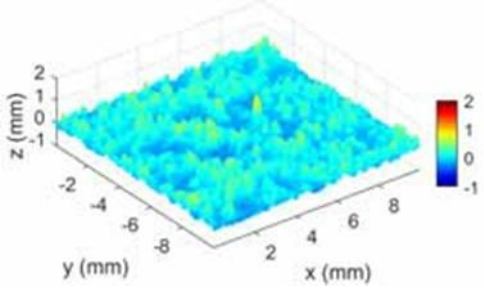

Figure 091821.15: Frost Topography at 00:29:49

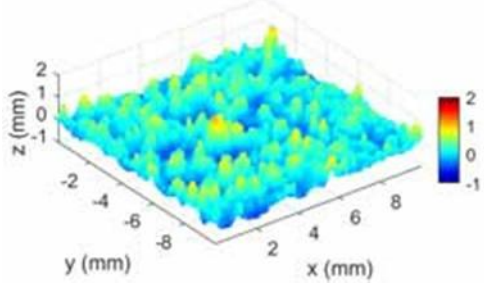

Figure 091821.16: Frost Topography at 00:39:51

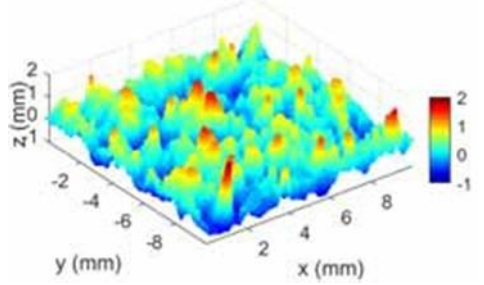

Figure 091821.17: Frost Topography at 00:49:49

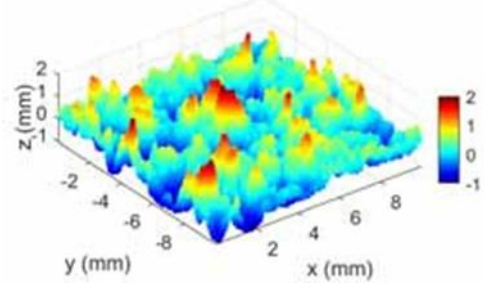

Figure 091821.18: Frost Topography at 00:59:52

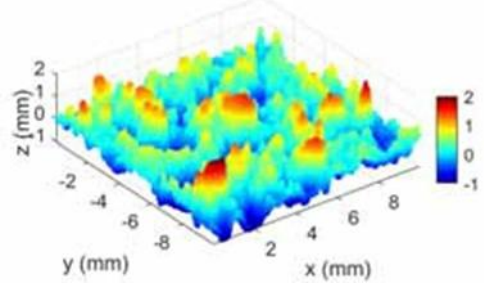

Figure 091821.19: Frost Topography at 01:09:55

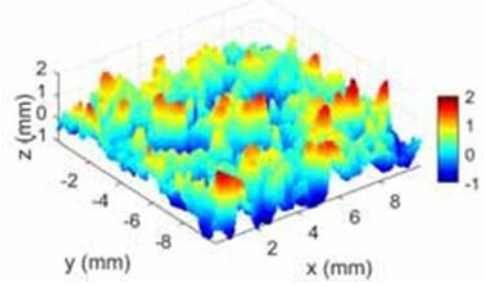

Figure 091821.20: Frost Topography at 01:20:11

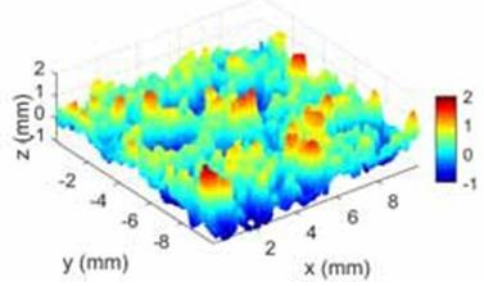

Figure 091821.21: Frost Topography at 01:29:50

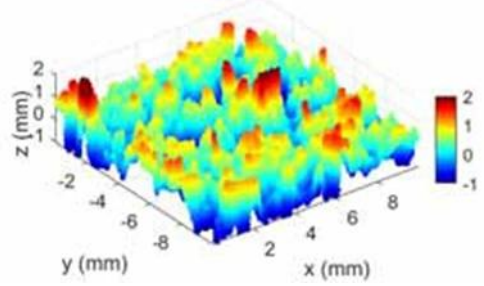

Figure 091821.22: Frost Topography at 01:39:47

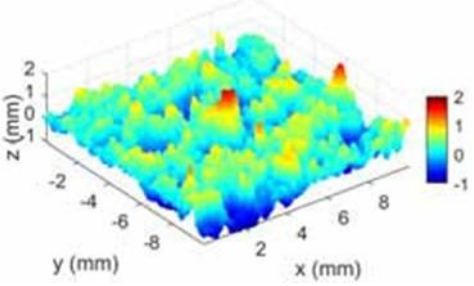

Figure 091821.23: Frost Topography at 01:49:50

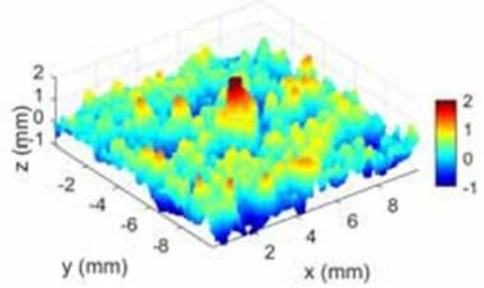

Figure 091821.24: Frost Topography at 01:59:48

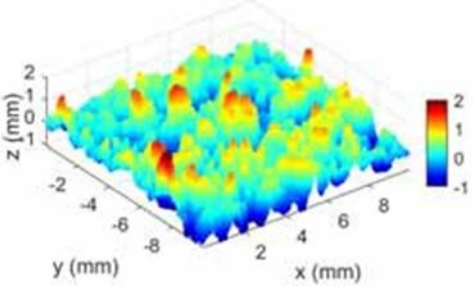

Figure 091821.25: Frost Topography at 02:09:52

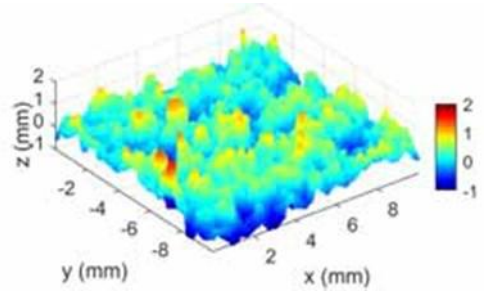

Figure 091821.26: Frost Topography at 02:17:55